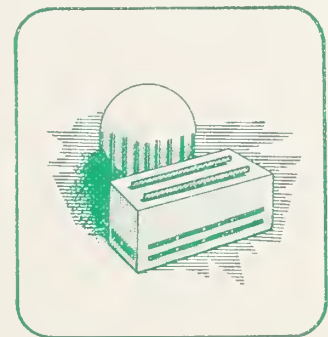
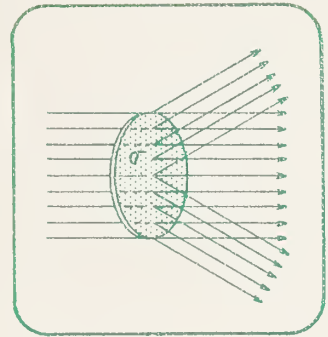




A11107 263358

NBS
PUBLICATIONS



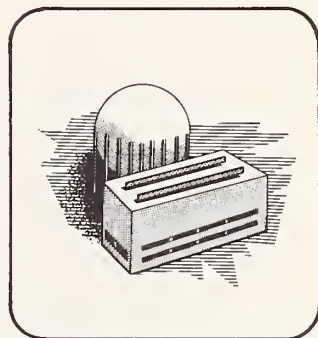
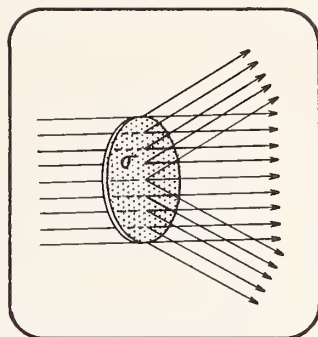
Neutron Cross Sections and Technology

Proceedings of a Conference

Washington, D.C.
March 4-7, 1968

NBS Special Publication 299
Volume II

U.S. DEPARTMENT OF COMMERCE
C. R. Smith, Secretary
NATIONAL BUREAU OF STANDARDS
A. V. Astin, Director



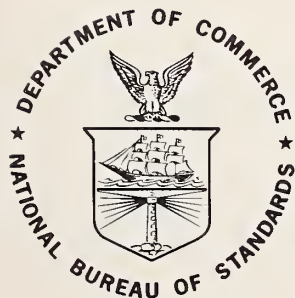
Neutron Cross Sections and Technology

Proceedings of a Conference

Washington, D.C.
March 4-7, 1968

Edited by
D. T. Goldman
Center for
Radiation
Research

National Bureau of Standards
Washington, D.C., 20234



U.S. National Bureau of Standards. Special Publication 299, - Issued ^{t.} SEPT. 1968
0 0 0

Volume II, Sessions E-H, Pages 641-1341

For sale by the Superintendent of Documents, U.S. Government
Printing Office, Washington, D.C. 20402 - Price \$10.50 per
set of 2 volumes

DEC 3 1968

142558

QC 100

U57

No. 299

V. 2

1968

Abstract

The Second Conference on Neutron Cross Sections and Technology was held in Washington, D. C. on March 4-7, 1968. Papers from this Conference have been published in two volumes, as follows: Volume I, Sessions A-D, pages 1-640; Volume II, Sessions E-H, pages 641-1337. These volumes contain the texts of the invited and contributed papers of the Conference. Topics covered include: The need for neutron data in fields of science and technology; standard data and flux measurements; the determination of neutron cross sections by theoretical and experimental techniques; a presentation of recently measured data and their utilization in a variety of applications.

Key words: cross sections, neutrons, nuclear data, nuclear technology, reactors.

Library of Congress Catalog Card Number: 68-60083

Foreword

The National Bureau of Standards, along with the other sponsoring institutions, has been most gratified with the conduct of this second in a series of conferences designed to bring neutron cross section measurers and users together. The first conference was entitled "Neutron Cross Section Technology," and was held in Washington, D. C., March 22-24, 1966. Its success prompted the "Second Conference on Neutron Cross Sections and Technology," held in Washington, D. C., on March 4-7, 1968.

The sponsors generally, and the Center for Radiation Research particularly, are keenly interested in promoting effective coupling between basic and applied radiation research. These conferences have proved to be a most successful exercise in the transfer of technology. We look forward to more of these symposia in the future. For this recent one, we wish to acknowledge the very capable manner in which the General Chairman, Dr. David T. Goldman, of the Center for Radiation Research, conducted the conference.

Carl O. Muehlhause, Director
Center for Radiation Research
National Bureau of Standards

Preface

These are the proceedings of the Second Conference on Neutron Cross Sections and Technology held at the Shoreham Hotel in Washington, D. C., 1968. The meeting was sponsored by the Atomic Energy Commission, the National Bureau of Standards, the American Physical Society, and the Reactor Physics and Shielding Divisions of the American Nuclear Society. There were 320 registrants, of whom approximately 20 percent came from outside the United States.

The purpose of this conference, as elucidated in its prospectus, was to provide a common meeting area for the exchange of information among nuclear scientists and engineers interested in neutron cross sections. The program was designed to consider aspects of neutron cross sections in the following sequence: the need for accurate measurements; their determination by theoretical and experimental techniques; and their applications. As indicated in the Table of Contents, the conference was divided into eight sessions, each lasting half a day. Each session consisted of two or three invited talks, which are distinguishable in these pages by their greater length, and contributed papers. No attempt was made to record the comments and questions following each oral presentation in order to retain informality at the meeting. By requesting one speaker to summarize several papers dealing with a single topic, it was possible to avoid simultaneous sessions and yet present over half of the more than one hundred contributed papers. There is, however, no distinction made between those presented orally and those accepted for publication only. The report of the panel summarizing the contents of the meeting was recorded verbatim and subsequently edited. It is suggested that the reader turn to these pages first to receive an impression of the general flavor of the meeting, prior to turning to specific research contributions.

Following a well established custom for the rapid dissemination of the proceedings of scientific conferences, it was decided to publish this volume by direct photoreproduction of manuscripts provided by the authors. The editor would like to acknowledge the cooperation of the authors who provided a suitable copy promptly, thereby assisting the speedy publication of these proceedings. Any errors appearing herein are, however, the responsibility of the editor, though effort was made to avoid them by retyping where necessary.

The editor, who also functioned as Conference Chairman, would like to thank the members of the Program Committee who were responsible for arranging the choice of speakers, the selection of contributed papers, and an initial review of the manuscripts. They responded immediately to any request from the chairman. The success of the conference was due to the Committee members, many of whom also functioned as session chairmen, to the speakers, and, most important of all, to the attendees who provided well attended sessions

complete with stimulating discussions. The experience provided by the initial conference and its Chairman, Professor W. W. Havens, Jr., and the example of its Proceedings, CONF-660303 (1966) edited by P. Hemmig were of extreme value. The most delightful and informative speech delivered by Congressman Craig Hosmer of California, ranking minority member on the Joint Committee on Atomic Energy, following the Conference banquet, was one of the high points of the meeting. The talk entitled, "The Scientific Establishment, Where Is It Headed?" provided many points for future discussions and will be published in PHYSICS TODAY.

Appreciation is expressed to the sponsoring organizations without whose encouragement and financial assistance this Conference would not have taken place.

The editor gratefully acknowledges the assistance of the NBS Office of Technical Information and Publications and secretarial assistance of Mrs. Sue Damron and Miss Wanda Hein in the preparation of these proceedings.

March 1968

David T. Goldman
National Bureau of Standards

Contents, Volume I

Foreword.	III
Preface	IV
Conference Personnel.	XVII
Papers from Sessions A, B, C, and D - Pages 1 through 640	
Session A. The Need for and Use of Neutron Data in Fields of Basic and Applied Science, Chairman: J. R. Beyster, Gulf General Atomic	
The Role of Neutrons in Astrophysical Phenomena, W. A. Fowler, California Institute of Technology.	1
Cosmic Abundances and the Extrapolation of Nuclear Systematics, P. A. Seeger, Los Alamos Scientific Laboratory.	25
The Field of Shielding Technology, H. Goldstein, Columbia University.	37
Sensitivity of Gamma-Ray Dose Calculations to the Energy Dependence of Gamma-Ray Production Cross Sections, K. J. Yost and M. Solomito, Oak Ridge National Laboratory.	53
Temperature Dependence of the Average Transmission of Tungsten Between 2 keV and 2 MeV Neutron Energy, F. H. Fröhner, J. L. Russell, Jr., and J. C. Young, Gulf General Atomic.	61
Neutron Cross Sections: The Field of Radiation Damage, M. S. Wechsler, Oak Ridge National Laboratory	67
Production of s-Nuclei from e- and r-Seed Nuclei by a Fixed Neutron Flux, J. P. Amiet and H. D. Zeh, Universität Heidelberg .	85
Session B. Standard Data Flux Measurements, and Analysis, Chairman: R. S. Caswell, National Bureau of Standards	
Neutron Flux Measurements, R. Batchelor, AWRE, Aldermaston. . . .	89
Developments in Standard Neutron Cross Sections, J. H. Gibbons, Oak Ridge National Laboratory	111
Helium Production Cross Section Measurements, J. Weitman and N. Däverhög, AB Atomenergi, Studsvik.	125
Measurement of Gamma-Ray Production Cross Sections Using a LINAC, V. J. Orphan, A. D. Carlson, and C. G. Hoot, Gulf General Atomic.	139

Neutron Cross Sections of ${}^6\text{Li}$ in the Kilovolt Region, J. A. Farrell, Los Alamos Scientific Laboratory, and W. F. E. Pineo, Duke University.	153
Total Neutron Cross Sections of ${}^6\text{Li}$, ${}^7\text{Li}$, and Lithium from 10 to 1236 keV, C. T. Hibdon and F. P. Mooring, Argonne National Laboratory	159
The Non-Elastic Cross-Section of Beryllium for Neutrons from 2.3 to 5.2 MeV, J. R. P. Eaton and J. Walker, University of Birmingham, England.	169
Fast Neutron Energy Measurements, J. C. Davis and F. T. Noda, University of Wisconsin.	177
Experimental Techniques in Absolute Measurements of the Fission Neutron Yield, A. De Volpi, Argonne National Laboratory.	183
Review of Some Fast Neutron Cross Section Data, Y. Kanda, Tokyo Institute of Technology, and R. Nakasima, Hosei University	193
Characteristics of Various Isotopes for Sandwich Foil Measurements of Neutron Spectra, T. J. Connolly, and F. De Kruijf, Institut für Angewandte Reaktorphysik, Karlsruhe, Germany	201
Advances in Accurate Fast Neutron Detection, A. De Volpi and K. G. Porges, Argonne National Laboratory.	213
Nonelastic and Some Inelastic Cross Sections in C^{12} and N^{14} at 15.3 MeV, L. F. Hansen, J. D. Anderson, M. L. Stelts, and C. Wong, Lawrence Radiation Laboratory, Livermore, California	225
Neutron Differential Cross Section Evaluation by a Multiple Foil Activation Iterative Method, W. N. McElroy and J. A. Ulseth, Battelle - PNL, S. Berg, TRW Systems, Inc., G. Gigas and T. B. Crockett, Atomics International.	235
Spatially Continuous Neutron Flux Plotting with Spark Chambers, K. G. Porges, W. W. Managan, and W. C. Kaiser, Argonne National Laboratory	247
The Manganese-55 Resonance Activation Integral, R. Sher, Brookhaven National Laboratory	253

Session C. The Need for and Use of Neutron Data in Reactor Design Applications, Chairman: D. R. Harris, Bettis Atomic Power Laboratory	
Use of Neutron Data in Thermal Reactor Power Plant Design, R. J. French, Westinghouse	259
Sensitivity of Reactivity Characteristics to Cross Section Uncertainties for Plutonium-Fueled Thermal Systems, U. P. Jenquin, V. O. Uotinen, and C. M. Heeb, Battelle-PNL.	273
Significance of Neutron Data to Fast Reactor Power Plant Design, P. Greebler, B. A. Hutchins, and B. Wolfe, General Electric-Advanced Products Operations	291
Fission Product Cross-Section and Poisoning in Fast Reactors, V. Benzi, Centro di Calcolo, CNEN, Bologna, Italy.	311
The $(n, \gamma n')$ and Fission Reactions as Possible Sources of Low Energy Neutrons in Fast Critical Assemblies, K. Parker, E. D. Pendlebury, J. P. Shepherd, and P. Stanley, AWRE, Aldermaston	315
Fissile Doppler Effect Measurement Data and Techniques, C. E. Till and R. A. Lewis, Argonne National Laboratory.	323
An Examination of Methods for Calculating the Doppler Coefficient in Fast Breeder Reactors, M. W. Dyos, C. R. Adkins, and T. E. Murley, Westinghouse - Advanced Reactors Division.	337
Influence of Neutron Data in the Design of Other Types of Power Reactors, A. M. Perry, Oak Ridge National Laboratory	345
Effects of Cross-Section Uncertainties in Compact Space Power Reactors, P. S. Brown, J. L. Watts, and R. J. Doyas, Lawrence Radiation Laboratory, Livermore, California.	363
New Cross Section Needs for Zirconium Hydride SNAP Reactors, E. H. Ottewitte, Atomics International	371
FISSPROD, A, Fission Product Program for Thermal Reactor Calculations, F. E. Lane and W. H. Walker, Atomic Energy of Canada, Ltd..	381
Effects of Uncertainties in Nuclear Data on Experimental and Calculated Reactor Burnup, D. E. Christensen, R. C. Liikala, R. P. Matsen, and D. L. Prezbindowski, Battelle - PNL.	389

	Page
Ratio of Photon to Neutron Fission Rates in Fast Reactors, E. J. Dowdy, W. H. Kohler, R. T. Perry, and N. B. Poulsen, Texas A & M University	401
Criticality and Central Reactivity Calculations Using ENDF/B Data, R. J. LaBauve and M. E. Battat, Los Alamos Scientific Laboratory .	407
Transuranium Cross Sections Which Influence FBR Economics, E. H. Ottewitte, Atomics International	415
Session D. Measurement and Analysis of Total and Partial Cross Sections for Fissile and Fertile Nuclei, Chairman: A. Hemmendinger, Los Alamos Scientific Laboratory	
Measurements on Fissile Nuclei: Experimental Results and Inter- pretation, A. Michaudon, Centre d'Etudes Nucleaires de Saclay. . .	427
Normalization of Relative ^{235}U Fission Cross-Section in the Resonance Region, A. J. Deruytter and C. Wagemans, Central Bureau for Nuclear Measurements, EURATOM, Geel, and Studiecentrum voor Kernenergi, Mol.	475
Fission Cross-Section Measurement on U^{235} , M. G. Cao, E. Migneco, J. P. Theobald, J. A. Wartena, and J. Winter, Central Bureau for Nuclear Measurements, EURATOM, Geel.	481
Precise 2200 m/s Fission Cross-Section of U^{235} , A. J. Deruytter, J. Spaepen, and P. Pelfer, Central Bureau for Nuclear Measurements, EURATOM, Geel.	491
Measurement of the U^{235} Fission Cross-Section in the keV Energy Range, W. P. Poenitz, Argonne National Laboratory.	503
Scattering Cross-Section of Pu^{240} , M. G. Cao, E. Migneco, J. P. Theobald, and J. A. Wartena, Central Bureau for Nuclear Measure- ments, EURATOM, Geel	513
Final Results on the Neutron Total Cross Section of Pu^{240} , W. Kolar and K. H. Böckhoff, Central Bureau for Nuclear Measurements, EURATOM, Geel.	519
Resonance Grouping Structure in the Neutron Induced Subthreshold Fission of Pu^{240} , E. Migneco and J. P. Theobald, Central Bureau for Nuclear Measurements, EURATOM, Geel.	527
Neutron Capture Measurements in the Resonance Region: Cu and Pu^{240} , H. Weigmann, J. Winter, and H. Schmid, Central Bureau for Nuclear Measurements, EURATOM, Geel.	533

Neutron Scattering Cross-Section of U^{233} , U^{235} , and Pu^{241} from 1 to 30 eV, G. D. Sauter, University of California, Davis, and C. D. Bowman, Lawrence Radiation Laboratory, Livermore	541
Fission Cross Section Measurements: Present and Potential Capabilities, J. A. Farrell, Los Alamos Scientific Laboratory. . .	553
Neutron Induced Fission Cross-Section Measurements in ^{244}Cm , R. R. Fullwood, J. H. McNally, and E. R. Shunk, Los Alamos Scientific Laboratory.	567
U^{238} Neutron Capture Results from Bomb Source Neutrons, N. W. Glass, A. D. Schelberg, L. D. Tatro, and J. H. Warren, Los Alamos Scientific Laboratory.	573
Measurement of the Absolute Value of Eta for Pu^{241} by the Manganese Bath Method, J. R. Smith and S. D. Reeder, Idaho Nuclear Corporation.	589
Techniques for Fission Cross-Section Measurements for Elements with High α and Spontaneous Fission Activity, P. G. Koontz and D. M. Barton, Los Alamos Scientific Laboratory	597
Fragment Angular Distributions for Monoenergetic Neutron-Induced Fission of Pu^{239} , J. R. Huizenga and A. N. Behkami, University of Rochester and Argonne National Laboratory, J. W. Meadows, Jr., Argonne National Laboratory, and E. D. Klema, Northwestern University	603
Fission Cross-Section of ^{232}Th for Thermal Neutrons, M. Neve De Mevergnies and P. Del Marmol, C.E.N.-S.C.K., Mol	611
A Single Level Analysis of U^{233} Cross Sections, M. J. Schneider, Westinghouse Astronuclear Laboratory	615
Relative Fission Cross Sections of U^{236} , U^{238} , Np^{237} , and U^{235} , W. E. Stein, R. K. Smith, and H. L. Smith, Los Alamos Scientific Laboratory	627
Low Energy $U-235$ $\bar{\nu}$ Measurements, S. Weinstein and R. C. Block, Rensselaer Polytechnic Institute	635

Contents, Volume II

Papers from Sessions E, F, G, and H - Pages 641 through 1341

	Page
Session E. The Measurement and Analysis of Total and Partial Cross Sections for Non-Fissile Nuclei, Chairman: R. C. Block, Rensselaer Polytechnic Institute	
Neutron Cross Section Measurements in the Resonance Region, M. C. Moxon, AERE, Harwell.	641
A Study of Partial Radiative Widths at and Between Neutron Resonances, C. Samour, R. Alves, H. E. Jackson, J. Julien and J. Morgenstern, Centre d'Etudes Nucleaires de Saclay.	669
Gamma Rays Following Neutron Capture in Iron, Sodium, and Thorium, O. A. Wasson, J. B. Garg, R. E. Chrien, and M. R. Bhat, Brookhaven National Laboratory	675
Total Neutron Cross Section and Resonance Parameters for Pm^{147} , G. J. Kirouac, H. M. Eiland, R. E. Slovacek, C. A. Conrad, and K. W. Seemann, Knolls Atomic Power Laboratory	687
Radiation Width of the 2.85-keV Resonance in Na^{23} , S. J. Friesenhahn, W. M. Lopez, F. H. Fröhner, A. D. Carlson, and D. G. Costello, Gulf General Atomic	695
Fast Neutron Cross Sections: keV to MeV, S. A. Cox, Argonne National Laboratory	701
Neutron Radiative Capture in the keV Region, R. W. Hockenbury, Z. M. Bartolome, W. R. Moyer, J. R. Tatarczuk, and R. C. Block, Rensselaer Polytechnic Institute.	729
Neutron Scattering Measurements in Low Energy Cd and Rh Resonances, T. J. King and R. C. Block, Rensselaer Polytechnic Institute. . .	735
High Resolution Total Fast Neutron Cross Sections on Some Non-Fissible Nuclei in the Energy Range $0.5 \leq E_n \leq 30$ MeV, S. Cierjacks, P. Forti, D. Kopsch, L. Kropp, and J. Nebe, Institut für Angewandte Kernphysik, Karlsruhe.	743
Elastic Scattering of Fast Neutrons by Praseodymium and Lanthanum, D. L. Bernard, G. H. Lenz, and J. D. Reber, University of Virginia	755
Gamma Rays from Inelastic Neutron Scattering in Nitrogen, H. Condé and I. Bergqvist, Research Institute of National Defense, Stockholm, and G. Nystrom, AB Atomenergi, Studsvik	763

Total Neutron Cross-Sections of Carbon, Iron, and Lead in the MeV Region, R. B. Schwartz, R. A. Schrack, and H. T. Heaton, II, National Bureau of Standards.	771
Nuclear Level Schemes from Resonance Neutron Capture (^{196}Pt , ^{184}W , ^{200}Hg , ^{64}Cu , ^{68}Cu , ^{36}Cl , ^{198}Au , ^{60}Co), R. N. Alves, C. Samour, J. M. Kuchly, J. Julien, and J. Morgenstern, Centre d'Etudes Nucleaires de Saclay.	783
Neutron-Resonance Parameters of Cadmium and Antimony, A. Asami, M. Okubo, Y. Nakajima, and T. Fuketa, Japan Atomic Energy Research Institute, Tokai-mura.	789
Neutron Capture Resonances of Tungsten in the Range 150 eV to 100 keV, Z. M. Bartolome, W. R. Moyer, R. W. Hockenbury, J. R. Tatarczuk, and R. C. Block, Rensselaer Polytechnic Institute.	795
The Neutron Inelastic Cross-Section for the Production of $^{103\text{m}}\text{Rh}$, J. P. Butler and D. C. Santry, Chalk River Nuclear Laboratories	803
The ^{14}N ($n, n'\gamma$) Reaction for $5.8 \leq E_n \leq 8.6$ MeV, J. K. Dickens, E. Eichler, F. G. Perey, P. H. Stelson, J. Ashe, and D. O. Nellis, Oak Ridge National Laboratory	811
Measurements of Absorption Resonance Integrals for ^{176}Hf , ^{177}Hf , ^{178}Hf , ^{179}Hf , and ^{180}Hf , R. H. Fulmer, L. J. Esch, F. Feiner, and T. F. Ruane, Knolls Atomic Power Laboratory	821
Measurements of Neutron Scattering from ^7Li , H.-H. Knitter and M. Coppola, Central Bureau for Nuclear Measurements, EURATOM, Geel.	827
Capture Cross-Section Measurements for Lu, ^{151}Eu , and ^{153}Eu and the Total Cross-Section of Eu, M. V. Harlow, A. D. Schelberg, L. D. Tatro, J. H. Warren, and N. W. Glass, Los Alamos Scientific Laboratory.	837
A Systematic Investigation of Fast Neutron Elastic Scattering, B. Holmqvist and T. Wielding, AB Atomenergi, Studsvik	845
Total Neutron Cross-Sections of ^9Be , ^{14}N , and ^{16}O , C. H. Johnson, F. X. Haas, J. L. Fowler, F. D. Martin, R. L. Kernell, and H. O. Cohn, Oak Ridge National Laboratory	851
Cross-Section Measurements of Zirconium, W. M. Lopez, F. H. Fröhner, S. J. Friesenhahn, and A. D. Carlson, Gulf General Atomic.	857

The Strength Functions S_0 and S_1 , The Total Radiative Width Γ_γ and the Mean Level Spacing \bar{D} as a Function of Mass Number and Spin Value, J. Morgenstern, R. Alves, S. de Barros, J. Julien, and C. Samour, Centre d'Etudes Nucleaires de Saclay.	867
The Thermal Cross-Sections and Paramagnetic Scattering Cross-Sections of the Yb Isotopes, S. F. Mughabghab and R. E. Chrien, Brookhaven National Laboratory	875
Cross-Section Measurements for the Reaction $^{152}\text{Eu} (n,\gamma) ^{152m}\text{Eu}$ Between 0.02 eV and 0.5 eV, F. Poortmans, A. Fabry, and I. Girlea, S.C.K. - C.E.N., Mol	883
Precision Measurements of Excitation Functions of (n,p) , (n,α) , and $(n,2n)$ Reactions Induced by 13.5 - 14.7 MeV Neutrons, H. K. Vonach and W. G. Vonach, Technische Hochschule München, H. Munzer, Universität München, and P. Schramel, Ges. Für Strahlenforschung, Neuherberg	885
Total Neutron Cross-Section of ^{204}Tl from 0.2 eV to 1000 eV, T. Watanabe, G. E. Stokes, and R. P. Schuman, Idaho Nuclear Corporation.	893
Detection of a Spin Dependent Effect in the Gamma Spectrum Following Neutron Capture, C. Coceva, F. Corvi, D. Giacobbe, and G. Carraro, CBNM, EURATOM, Geel, and CNEN Centro di Calcolo, Bologna.	897
Session F. The Theory of Nuclear Cross-Sections and the Analysis of Neutron Interactions, Chairman: M. H. Kalos, New York University	
Nuclear Theory and Neutron Cross-Sections, E. W. Vogt, University of British Columbia.	903
Correlations in Positions of Single-Particle Levels on Complex Nuclei, S. I. Sukchoruchkin, Institute for Theoretical and Experimental Physics, Moscow	923
Calculations of Elastic Scattering and Inelastic Direct Processes of Fast Neutrons by U-238, F. Bühler, Institut für Strahlenphysik, Stuttgart.	933
Determination of the Optical Potential Depth from a Many Body Approach, N. Azziz, Westinghouse Atomic Power Divisions.	943
Thermal Neutron Cross-Sections and Resonance Integrals for Transuranium Isotopes, A. Prince, Brookhaven National Laboratory .	951

Interpretation of the Correlated Analysis of Fission, Total and Capture Cross-Section Data, F. T. Adler and D. B. Adler, University of Illinois	967
Gerade - Ungerade Symmetry and the Nuclear Mass Division in Fission, J. J. Griffin, University of Maryland.	975
Calculation of Photon Production Cross-Sections and Spectra from 4 to 15 MeV Neutron Induced Reactions, R. J. Howerton, Lawrence Radiation Laboratory, Livermore	1013
Theory of Doppler Broadening of Neutron Resonances, S. N. Purohit, T. Shea and S. Kang, Rensselaer Polytechnic Institute.	1021
The Neutron Cross-Section and Resonance Integrals of Holmium, T. E. Stephenson, Brookhaven National Laboratory	1031
Session G. Data Storage, Retrieval, and Evaluation, Chairman: P. Hemmig, Atomic Energy Commission	
Recent Developments in the Automated Compilation and Publication of Neutron Data, S. Pearlstein, Brookhaven National Laboratory . .	1041
Automated Evaluation of Experimental Data, H. A. Alter, Atomics International.	1049
Principles of Cross-Section Evaluation, J. J. Schmidt, Kernforschungs-zentrum, Karlsruhe	1067
Neutron Data Compilation at the International Atomic Energy Agency, H. D. Lemmel, P. M. Attree, T. A. Byer, W. M. Good, L. Hjaerne, V. A. Konshin, and A. Lorenz, IAEA Nuclear Data Unit, Vienna . . .	1083
The ENEA Neutron Data Compilation Centre, V. I. Bell, ENEA Neutron Data Compilation Centre, Gif-Sur-Yvette.	1089
An Integrated System for Producing Computational Constants for Neutronics and Photonics Codes, R. J. Howerton, Lawrence Radiation Laboratory, Livermore.	1093
A Computer File of Resonance Data, T. Fuketa, Y. Nakajima, and K. Okamoto, Japan Atomic Energy Research Institute, Tokaimura. . .	1097
Storage and Retrieval of Photon Production and Interaction Data in the ENDF/B System, D. J. Dudziak and R. J. LaBauve, Los Alamos Scientific Laboratory.	1101

A Mathematical Scheme for Evaluating Cross-Section Data on the Fissile Isotopes U ²³³ , U ²³⁵ , and Pu ²³⁹ in the Energy Range 10 keV - 10 MeV, P. C. Young and K. B. Cady, Cornell University.	1109
On Line Computer System for Cross-Section Evaluation, L. E. Beghian and J. Tardelli, Lowell Technological Institute.	1117
Data Reduction with a Small Remote Computer Linked to a CDC-6600, W. R. Moyer, Rensselaer Polytechnic Institute, and R. P. Bianchini and E. Franceschini, New York University	1123
Evaluation of Uranium 238 Neutron Data in the Energy Range .0001 eV to 15 MeV, M. Vaste, Electricité de France, and J. Ravier, Association EURATOM-CEA, Cadarache	1129
Session H. Use of Differential Data in Analyzing Integral Experiments, Chairman: D. Bogart, NASA-Lewis	
Neutronic Measurements in Non-Critical Media, C. A. Stevens, Gulf General Atomic.	1143
The Use of Integral Spectrum Measurements to Improve Neutron Cross-Section Data, E. D. Pendlebury, AWRE, Aldermaston.	1177
Fast Neutron Spectra in Multiplying and Non-Multiplying Media, J. M. Neill, J. L. Russell, Jr., R. A. Moore, and C. A. Preskitt, Gulf General Atomic.	1183
Studies of the Angular Distribution of Fast Neutrons in Depleted Uranium, E. Greenspan, B. K. Malaviya, N. N. Kaushal, E. R. Gaerttner, and A. Mallen, Rensselaer Polytechnic Institute	1193
Adequacy of Fast and Intermediate Cross-Section Data From Neutron Spectrum Measurements in Bulk Media, B. K. Malaviya, E. Greenspan, E. R. Gaerttner, and A. Mallen, Rensselaer Polytechnic Institute.	1203
Differential Data and the Interpretation of Large, Fast Reactor, Critical Experiments, W. G. Davey, Argonne-Idaho	1211
Calculations of Fast Critical Experiments Using ENDF/B Data and a Modified ENDF/B Data File, T. A. Pitterle, E. M. Page, and M. Yamamoto, Atomic Power Development Associates	1243
A Comparison of Pu-240 Cross-Section Evaluations by Calculations of ZPR-III Assemblies 48 and 48B, T. A. Pitterle and M. Yamamoto, Atomic Power Development Associates.	1253

Integral Test of Capture Cross-Sections in the Energy Range 0.1 - 2 MeV, A. Fabry and M. De Coster, C.E.N. - S.C.K., Mol	1263
^{238}Pu Production Predictions from Available Neutron Cross-Sections, E. J. Hennelly, W. R. Cornman, N. P. Baumann, DuPont, Savannah River Laboratory	1271
Foil Measurements of Integral Cross-Sections of Higher Mass Actinides, R. L. Folger, J. A. Smith, L. C. Brown, R. F. Overman, and H. P. Holcomb, DuPont, Savannah River Laboratory	1279
Reactor Cross-Sections for ^{242}Pu - ^{252}Cf , J. A. Smith, C. J. Banick, R. L. Folger, H. P. Holcomb, and I. B. Richter, DuPont, Savannah River Laboratory	1285
Thermal Reactor Absorption Cross-Sections of Radioactive Nuclides, R. S. Mowatt and W. H. Walker, Atomic Energy of Canada, Ltd.	1291
The Decay of a Neutron Pulse in a Fast Nonmultiplying System as an Integral Check on the High Energy Inelastic Scattering, T. Gozani and P. d'Oultremont, Gulf General Atomic	1301
Panel Discussion Summarizing the Conference, Chairman: W. W. Havens, Columbia University.	1309
Participants: H. Goldstein, Columbia University	
H. Kouts, Brookhaven National Laboratory	
A. Radkowsky, Naval Reactors Branch, AEC	
R. Taschek, Los Alamos Scientific Laboratory	
List of Registrants.	1321
Author Index	1339

CONFERENCE CHAIRMAN

David T. Goldman, National Bureau of Standards

PROGRAM COMMITTEE

J. R. Beyster, Gulf General Atomic
R. C. Block, Rensselaer Polytechnic Institute
D. Bogart, National Aeronautics and Space Administration
R. S. Caswell, National Bureau of Standards
F. Feiner, Cornell University
J. L. Fowler, Oak Ridge National Laboratory
D. T. Goldman, National Bureau of Standards
H. Goldstein, Columbia University
P. Greebler, General Electric--Advanced Products Operations
E. Haddad, Atomic Energy Commission
D. R. Harris, Bettis Atomic Power Laboratory
W. W. Havens, Columbia University
A. Hemmendinger, Los Alamos Scientific Laboratory
P. B. Hemmig, Atomic Energy Commission
J. C. Hopkins, Los Alamos Scientific Laboratory
M. H. Kalos, New York University
S. Pearlstein, Brookhaven National Laboratory
J. L. Russell, Gulf General Atomic
A. B. Smith, Argonne National Laboratory

ARRANGEMENTS COMMITTEE

E. H. Eisenhower, National Bureau of Standards
F. J. Shorten, National Bureau of Standards

Session E

THE MEASUREMENT AND ANALYSIS OF
TOTAL AND PARTIAL CROSS SECTIONS
FOR NON-FISSILE NUCLEI

Chairman

R. C. BLOCK

Rensselaer Polytechnic Institute

NEUTRON CROSS SECTION MEASUREMENTS IN THE
RESONANCE REGION

M. C. Moxon

Atomic Energy Research Establishment, Harwell,
Didcot, Berks.,
United Kingdom

ABSTRACT

The measurement of total, capture and scattering cross-sections can now be made with high resolution and accuracy up to neutron energies of several kilovolts. These measurements can be analysed by the shape and area techniques to give accurate values of the resonance parameters for all but the very small resonances. Some of the problems, advantages and disadvantages of the various techniques used in the measurements and analysis will be discussed together with some recent measurements of neutron cross-sections in the resonance region.

1. Introduction

To the various experimenters carrying out neutron cross-section measurements, the "Resonance Region" means different neutron energy regions according to the elements they are examining. It can cover many MeV for the low masses while for the rare earth region it may only cover a few kilovolts. We shall take it to mean the energy region covering from about 1 eV to about 100 keV, the region where, if we had good enough energy resolution, individual resonances could be observed in most of the nuclei.

Although measurements of neutron cross-sections in the resonance region cover only a small fraction of the field of neutron physics, they have contributed a great deal to our knowledge of the properties of the compound nucleus at energies corresponding to the neutron separation energy. These include the individual resonance parameters and their distribution functions, and the average values all as a function of the target mass and the spins and parities of the resonances.

2. Neutron Spectrometers Used in the Resonance Region

The neutron sources used for measurements in the resonance region can be divided into two main groups, first the continuous sources such as nuclear reactors and secondly the sources giving short intense pulses of neutrons where time of flight techniques are employed to determine the neutron energy.

2.1 Continuous Sources

These sources can again be divided up into groups (a) nuclear reactors with their wide energy spectrum of neutrons, (b) crystal monochromators giving nearly mono-energetic neutrons and (c) charged particle reactions producing nearly mono-energetic neutrons in the energy region above about 20 keV.

The resonance integral (1,2) has been measured for many nuclei in the well moderated neutron flux of a nuclear reactor where the intensity of the neutron flux in the resonance region is assumed to be inversely proportional to the neutron energy. The data are often difficult to interpret, involving corrections both for finite size of the samples and departures from the $1/E$ law of the neutron spectrum.

More detailed data on neutron cross-sections have been obtained from narrow beams of reactor neutrons incident on a single crystal (3,4) (e.g. beryllium) which can produce nearly mono-energetic neutrons with an energy spread $\Delta E(\text{eV}) \sim 5 \times 10^{-3} E^{3/2}(\text{eV})$. The crystal spectrometer has been used to measure all types of neutron cross-sections and many accurate resonance parameters below about 20 eV have been obtained from the data (6,7,8,9).

Charged particle reactions with light elements can give intense

sources of nearly mono-energetic neutrons above neutron energies of about a few keV. A general discussion of these types of neutron sources will be found in references 10 and 11. The neutron energy resolution using continuous beams of particles has been pushed close to its limit by Newson who achieved a resolution of $\lesssim 1$ keV. These continuous sources have been used mainly to measure average cross-sections for medium and heavy nuclei and only in the light nuclei are they the main source of the resonance data.

2.2 Pulsed Sources of Neutrons

In the neutron energy range 10 eV to 100 keV time of flight techniques using intense pulsed neutron sources are superior to any other method of carrying out neutron cross-section measurements.

Fast choppers (12) with a burst width of ~ 1 μ s are used with neutron beams emerging from nuclear reactors to measure neutron cross-sections, but are being superseded by pulsed accelerator sources.

These pulsed accelerator sources can be divided into two main groups: firstly those giving a white neutron spectrum and secondly those using charged particle reactions to give neutrons with a finite energy band.

Electron linear accelerators (13) and proton cyclotrons(14) with pulse lengths less than 100 nS are used to produce intense pulsed white sources of neutrons for use in time of flight measurements and are superior to choppers for all neutron measurements in excess of 100 eV.

The Van de Graaff accelerator used with top terminal pulsing and pulse compression magnets, can be used to produce pulses of 10 mA of protons of duration 1 nsec. They have been used to measure neutron cross-sections in the neutron energy region above a few kilovolts. Time of flight is used to determine both the neutron energy and the background. The background can be measured at times when no neutrons coming directly from the target can interact either with the detector or the sample.

The IBR pulsed reactor at Dubna (16) is another pulsed source which has been extensively used for neutron time of flight spectroscopy. The long pulse (40 μ sec at half height) requires the use of very long flight paths in order to obtain good resolution. In fact flight paths of up to 1 km in length are employed, giving a timing resolution at best 40 nsec/m which is very poor except at low neutron energies. In 1965 however the IBR was successfully operated in a sub-critical state being driven by a 30 MeV electron microtron giving a pulse length of 2 μ sec, 50 times a second. Used in this way the neutron pulse lengths at half maximum were 4 μ sec giving a time of flight resolution with the 1000 m flight path of 4 nsec/m which is intermediate between chopper and pulsed accelerator performance.

Nuclear explosions (16) can produce very much larger fluxes of pulsed neutrons in the resonance region than any other presently known source. The atomic explosion produces $\sim 10^{24}$ neutrons in a burst with a repetition frequency of about one every two years. This is a factor of

about 100 more than any of the present accelerator sources, which produce at most 10^{22} neutrons per year (i.e. $\sim 10^{12}$ neutrons/pulse at ~ 200 bursts/second).

The atomic explosion takes place underground, an evacuated flight path some 200 metres long allowing the neutrons to escape to the surface. The duration of the primary pulse is less than 100 nsec. These intense neutron beams are used for measurements of cross-sections which are not easily carried out with other sources, e.g. the measurement of the partial cross-sections of very radioactive isotopes when only small amounts of material are available.

The lead slowing down spectrometer (17) does not compete in resolution with modern time of flight spectrometers. It consists of a large cube of lead into which a pulse of fast (14 MeV) neutrons from the T(d,n) reaction is introduced from a 300 keV Cockcroft Walton Set. It utilizes the fact that fast neutrons slow down by many collisions with lead nuclei so that they remain as a nearly homogeneous energy group, allowing the energy at which neutrons are captured in a small sample placed in the cube to be determined from the time interval between the initial pulse and the detection of the prompt capture γ -rays. This device has good enough resolution to allow some individual resonances to be observed and has mainly been used for measurements of capture cross-section up to 50 keV.

3. Measurements

3.1 The Total Cross-sections

The measurements of the total cross-section are reasonably easy to perform. Any type of neutron detector can be used to determine the neutron count rate, with and without a uniformly thick sample, of the element under investigation in the neutron beam. Figure 1 shows the arrangement used on the Harwell 45 MeV linear accelerator neutron time of flight spectrometer to measure transmissions in the energy region ~ 100 eV to ~ 10 MeV. Here two ^{10}B -NaI detectors are used to detect the neutrons. The ^{10}B plug at the 120 metres station acts both as a neutron detector for that station and an overlap filter, (i.e. to absorb the slow neutrons from previous machine cycles) for the 300 metre station. Similar arrangements are used on other pulsed neutron sources using ^6Li -glass scintillators and boron loaded liquid scintillators as neutron detectors as well as the ^{10}B -NaI system.

The Harwell measurements (18) of the total cross-section of ^{232}Th using the 120 metre flight path are shown in figure 2 and clearly illustrate the presence of well-separated narrow resonances, typical of non-fissile heavy elements. In contrast to the thorium data figure 3 shows the total cross-section of vanadium in the tens of kilovolts region measured at Karlsruhe by Rohr et al (19) on the pulsed Van de Graaff. The resonances here have widths comparable with the level spacing and only shape analysis will produce meaningful parameters.

The transmission of polarised neutrons through a polarised sample is one of the most positive means of identifying the spin of a resonance. The groups headed by Stolovy (20,21) and Sailor (22, 23, 24) have published many articles in this field. Polarisation of the neutrons in these experiments is achieved by means of Bragg reflection from a magnetised

cobalt-iron crystal. In a paper presented at the Antwerp Conference (1965) (25) Shapiro describes a method of producing polarised neutrons by their transmission through a polarised proton target. By this method one can produce polarised neutrons up to 10 keV whereas the other method mentioned is only applicable up to 10 or 20 eV.

Figure 4 illustrates this technique as used by Alfimenkov et al (26) to obtain data on holmium (Fig. 5). This clearly shows the separation of the resolved resonances into two sets. The negative sign of ϵ for the 3.92 eV and 12.6 eV resonances indicates that these resonances have spin 4 while the positive sign of ϵ for these at 18.1 and 8.1 eV indicates spin 3. The small neutron width (~ 0.5 MeV) of the 8.1 eV resonance makes it nearly impossible to determine its spin by any other technique.

It is hoped that this technique can be used with better energy resolution and on more elements to enable the spins of more resonances to be definitely assigned but at present there appears to be many technical difficulties associated with the polarisation of nuclei other than holmium.

3.2 The Capture Cross-section

The accurate measurement of the components of the total cross-section are much more difficult to perform than that of measuring the total itself. This is due to the necessity of knowing the number of neutrons incident on the sample and the efficiency of detecting the resultant reactions, together with the problems of calculating the corrections used to obtain meaningful cross-sections from the raw data.

Some of these difficulties can be minimised by carrying out the measurements relative to a "known" standard. This can reduce the effects of uncertainties in the measurements of the neutron spectrum, the solid angle and efficiency of the detecting system.

In the case of capture cross-section measurements, the smoothly varying cross-section for the $^{10}\text{B}(n,\alpha)^7\text{Li}$ reaction is ideally suited as a standard, but at present the cross-section in the region above about 10 keV is not known with sufficient accuracy ($\sim 5\%$ at ~ 100 keV).

This cross-section has been used by many workers as a standard, often making the following assumptions:-

- (a) the cross-section for the $^{10}\text{B}(n,\alpha)^7\text{Li}$ reaction in the energy range 1 to 105 eV is inversely proportional to the neutron velocity
- (b) the ratio of the alpha particles going to the ground state of ^7Li to those going to the first excited state at 578 keV in ^7Li remains constant over the same energy range.

The first assumption comes from the fact that the total cross-section of ^{10}B below 10 keV can be fitted to the form $\sigma_T = aE^{1/2} + \beta$. The best fitting curve as evaluated by Diment (27) on his data

was $\sigma_{nT} = (610.3 \pm 3.1)E^{1/2} + (1.95 \pm 0.1)$ barns. The values of the absorption cross-section above 10 keV obtained by subtracting Moorings (28) scattering data from the total cross-section data follow the $E^{-1/2}$ law up to about 300 keV to within experimental errors which vary from about $\pm 3\%$ at 100 keV to $\pm 7\%$ at 500 keV.

Recent more accurate measurements of the ^{10}B scattering cross-section by Asami (29) indicate a value of 2.20 ± 0.06 barns, suggesting from Diment's data that there is a constant term of -0.25 ± 0.12 in the reaction cross-section. This will have little effect on the capture cross-section measurements below a few keV but above 10 keV it will have an increasing effect on the measured values, with increasing neutron energy.

The second assumption was recently confirmed at Harwell by Sowerby (30) and by Macklin and Gibbons (31) at Oak Ridge who measured the ratio (α_0 to α_1) of the two alpha groups using a BF_3 counter in the neutron energy range 1 eV to 200 keV and found it to be constant up to about 10 keV followed by a slow increase up to about 100 keV and then a more rapid rise up to 200 keV.

The advantages of ^{10}B as a standard over other nuclei are not only nuclear but also physical. It can be used as the filling gas BF_3 in a proportional counter or as a thick slab, detecting the 478 keV gamma ray which is emitted in most of the neutron reaction events ($93.5 \pm 0.5\%$).

Neutron capture measurements can be divided into two main sections, firstly the determination of the total capture cross-section and secondly the measurement of the variation with neutron energy of the intensity of individual γ -rays following neutron capture events.

Two basic types of detector have been developed to measure the total capture cross-section. These have been designed to overcome the problems associated with the variation of the γ -ray cascade following a neutron capture event. The large liquid scintillator (L.L.S.) overcomes this problem by absorbing a large fraction of the emitted γ -ray energy. The General Atomics 4000 litre L.L.S. (32) at San Diego is the largest example of this type of detector (See fig. 6) most of the others used for neutron capture cross-section measurements having been somewhat smaller (100-500 l) (33,34).

The detectors based on the Moxon-Rae type (35, 36, 37) (See fig. 7) have an efficiency proportional to the total γ -ray energy emitted which minimises the effects of changes in the γ -ray cascade scheme following the neutron capture event.

Very weak resonances can be observed more clearly in capture measurements than in total or scattering data due to the absence of a large potential cross-section. The total cross-section in figure 8 was taken from BNL 325 and is mainly from the Columbia data, which has an energy resolution some 10 times better than that used to obtain the capture results. Even so, many weak resonances are observed in the capture data (38) that do not appear in the total cross-section data. The presence of numerous weak capturing resonances in light and medium mass nuclei could possibly explain some of the discrepancies between the resonance integrals calculated from only resonances observed in total

cross-section data when compared with the resonance integrals obtained from reactor measurements.

Early measurements (39) on the variation with neutron energy of the cross-section for the production of "groups" of γ -rays were carried out with NaI crystals, but the development of Ge(Li) γ -ray detectors with superior γ -ray energy resolution ($\sim 8 \rightarrow 15$ keV at 8 MeV) has enabled many laboratories (40, 41) to carry out studies of the variation with neutron energy of the production of many single γ -rays following neutron capture. Several reports on this subject are presented to this conference.

The group at Brookhaven have carried out measurements on several nuclei and in reference 41 there is presented experimental evidence for the direct capture processes in cobalt, using data obtained with a Ge(Li) γ -ray detector. They have also carried out measurements on uranium (42) and tin (43). In the case of tin the angular distribution of γ -rays from capture in P-wave resonances was measured for several γ -rays in order to determine the spins and parities of the initial and final states in the reaction.

It should be principle be possible to infer the spin of the capturing state from the observed γ -ray spectra but in practice they are generally unreliable owing to the Porter-Thomas distribution in reduced strengths which gives a high probability of very weak transitions. The spin of the capturing state will affect the multiplicity of the decay scheme. A recent measurement by Coceva et al (44) at Ispra of the ratio of coincidences to single events (where the higher multiplicity of the γ -rays from the higher spin state augments the coincidence count rate) enabled them to determine the spins of 17 resonances in $^{105}\text{Pd} + n$.

3.3 The Scattering Cross-section

The scattering cross-section in the resonance region is more difficult to measure accurately than the capture due to the possibility of strong absorption of the emerging neutron near the resonance energies and the possible presence of anisotropic distribution of the scattered neutrons. As in the case of the capture measurements the effects of uncertainties in solid angles and efficiencies of the neutron detectors are minimised by carrying out measurements against a known standard. Lead and carbon have been used as standards, since for these materials the capture cross-section is negligible and the total cross-sections are smooth and have been measured with reasonable accuracy by transmission techniques. The presence of small resonances above 1 keV in natural lead and its possibly uncertain isotopic content do not make it a good candidate for a standard cross-section, and it has been suggested that lead highly enriched in ^{208}Pb would be a better choice for a standard for use in scattering cross-section measurements for the heavy elements.

When using the area analysis techniques the measured value of the scattering area of a resonance is essential in order to determine the spin and radiation width with some degree of certainty. This is especially true when the neutron width is smaller than the radiation width, and the capture and total cross-section data both give the neutron width multiplied by the spin weighting factor.

Early scattering measurements (45) were carried out with BF₃ counters but the development of more efficient detectors such as boron

loaded liquid scintillators and lithium glass scintillators has made it possible to carry out measurements with better energy and angular resolution and over much wider neutron energy ranges.

At Harwell on the linear accelerator time of flight spectrometer, Li glass scintillators (46) have been used for some time to carry out scattering measurements. Recently this detector system was rebuilt, so that the angular distribution of the scattered neutrons could be studied. This was mainly for studies on the scattering cross-section of ^{10}B and angular distribution of the scattered neutrons from resonances.

It may be possible to determine the parity of a resonance from observation of the sign of the interference terms as a function of angle and neutron energy.

The parity of the resonance at 1.15 keV in iron has long been a subject of controversy but the scattering results (47) shown in figure 11 suggest it is not due to s-wave neutrons, since there exists an interference effect in the scattering cross-section which alters in sign when going from a forward scattering angle to a backward one. This indicates that the neutron wave has odd parity and the resonance is almost certainly due to p-wave neutrons. f and higher wave neutrons can be excluded due to the exceedingly large neutron width which would be quoted. Pulse shape methods have been tried to reduce the sensitivity of the Li glass scintillators to γ -rays with varying degrees of success. At R.P.I. (48) the group using the large liquid scintillator have reduced the sensitivity to γ -rays by observing the pulses from a Li glass detector placed inside the L.L.S., in anti-coincidence with those from the L.L.S. This gives a large reduction in the sensitivity to γ -rays and enables them to make accurate measurements on resonances with small neutron widths.

4. Analysis of Neutron Cross-section Measurements

The measured values of the neutron cross-sections are distorted due to the effects of finite energy resolution and the thermal motion of the target nucleus (Doppler effect). Various analysis techniques have been developed to minimise the effects of these on the required parameters.

These analysis techniques can be divided into three sections. Firstly, shape analysis can be used where the resolution width is smaller than the width of the resonances. Secondly, area analysis can be used over the energy region in which resonances are well separated and thirdly average parameters can be determined from data which have been averaged over many resonances or in the region where the resolution is so poor that each datum point covers many resonances.

4.1 The Effects of Doppler and Resolution Broadening

Before going on to consider the merits of the various methods of analysis let us examine the expressions for the total and partial cross-sections for a non-fissile nucleus.

At energies below the first inelastic scattering level only scattering and capture can take place. The total cross-section $\sigma_T(E)$ at energy E is thus the sum of the cross-section for scattering $\sigma_{nn}(E)$ and for capture $\sigma_{nR}(E)$ where both can be expressed in a variety of forms, the simplest of which is given by the sum of several single level

Breit-Wigner terms and is applicable where the resonances are well separated. Where appreciable overlapping occurs the more complicated multilevel formalism must be applied.

The thermal motion of the atoms in the sample must be taken into account and this is carried out by convoluting the nuclear cross-section with the Doppler broadening function. The Doppler broadening is assumed to follow a Gaussian function which neglects the effects of the crystal lattice on the motion of the atoms (63) and may have to be taken into account in very accurate measurements.

The Doppler broadened cross-section $\sigma_{\Delta}(E)$ is given as follows:

$$\sigma_{\Delta}(E) = \frac{1}{\Delta\sqrt{\pi}} \int_0^{\infty} \sigma(E') \text{Exp} \left\{ - \left(\frac{E-E'}{\Delta} \right)^2 \right\} dE'$$

where Δ is the Doppler width given by

$$\Delta = 2 \left\{ \frac{k \tau_{\text{eff}} E}{M} \right\}^{1/2}$$

τ_{eff} is the effective temperature of the sample obtained from the Debye temperature, k is Boltzmann's constant and M is the mass of the target nucleus.

Before we can compare the calculated transmission and yields with the observed data they must be convoluted with the instrumental resolution function:

$$T(E) = \int_0^{\infty} \exp(-n\sigma_{\Delta T}(E')) \phi(E') dE'$$

$$Y_p(E) = \int_0^{\infty} \left\{ (1 - \exp(-n\sigma_{\Delta T}(E'))) \frac{\sigma_{\Delta p}(E')}{\sigma_{\Delta T}(E')} + Y_{ms}(E') \right\} \phi(E') dE'$$

where n is the thickness of the sample (atoms/barn), $Y_{ms}(E')$ is the correction to the yield for neutrons initially scattered and then captured on subsequent collisions and $\phi(E')$ is the resolution function. For time of flight spectrometers using moderated pulsed neutron sources $\phi(E')$ is made up of several factors:-

- (a) the pulse shape of the incident particles
- (b) the relaxation time of the neutrons in the target
- (c) the width of the timing pulses
- (d) the time jitter introduced by the electronics
- (e) the moderation time spread
- (f) distance uncertainties in the neutron source and detector

The first four are assumed to be independent of the neutron energy and their resultant time spread divided by the flight path length is often quoted as the time resolving power of the spectrometer.

The latter two are functions of the neutron energy. An

expression for the moderation time spread for an infinite slab moderator has been calculated by Groenwold and Gröendijk (49). Patrick et al (50) at Harwell have carried out measurements of the effects of different moderator thicknesses on both the resolution and the flux at neutron energies of 10^3 and 10^2 eV. It was found that the shape of the moderation time distribution could be fitted to the form given by Groenwold and Gröendijk but the mean free path used in the calculation was dependent on the moderator thickness.

4.2 Shape Analysis of the Data

Shape analysis of neutron cross-section data makes full use of all the available data and can be used successfully even when data on only one sample thickness are available. An accurate knowledge of the resolution and Doppler broadening functions is however required. Several computer programs (19, 51, 52, 53) have been written using a variety of formalisms and techniques to determine the resonance and other necessary parameters by fitting the observed data. Some of the most widely used programs for shape analysis of transmission data are based on the Atta-Harvey (52) program from O.R.N.L. This uses a complex probability integral to represent the Doppler broadened single level Breit-Wigner formula. One of the disadvantages of this is that it does not take into account multilevel interference effects and erroneous results can be obtained when it is used where resonance-resonance interference effects are seen to be present (e.g. in light nuclei and thick samples).

The group at Karlsruhe (19) have developed a shape fitting program using the R matrix formalism. This program can accommodate 50 resonances of each spin for three different isotopes considering s and p-waves only. A fit to a set of vanadium data is shown in figure 3.

The use of a shape fitting program to fit data from several sample thicknesses and different types of measurements may possibly reveal unknown systematic errors in the data and assist in obtaining better cross-section values with more meaningful errors from the data. Another advantage of using a shape analysis program is that the study of the cross-section between large resonances can reveal small resonances and resonance-resonance interference effects can lead to spin assignments once the spin of one resonance has been determined.

4.3 Area Analysis Techniques

This was one of the first methods (54) used to determine resonance parameters and the majority of the values of Γ_n and Γ have been obtained using this technique. This method is based on the assumption that the area under a resonance curve is almost independent of the resolution function depending only on the resonance parameters, the Doppler width Δ and the sample thickness. The limiting area for thin samples is almost independent of Δ being given as follows:

$$\begin{array}{ll}
 \text{Transmission} & A_T n\sigma_0 \rightarrow 0 = \frac{\pi}{2} n\sigma_0 \Gamma \propto g \Gamma_n \\
 \text{Capture} & A_Y = \frac{\pi}{2} n\sigma_0 \Gamma_Y \propto g \frac{\Gamma_n \Gamma_Y}{\Gamma} \\
 \text{Scattering} & A_S = \frac{\pi}{2} n\sigma_0 \Gamma_n \propto g \frac{\Gamma_n^2}{\Gamma}
 \end{array}$$

where σ_0 is the peak cross-section equal to $4\pi \lambda^2 g \Gamma_n / \Gamma$, Γ , Γ_n and Γ_γ are respectively the total, scattering and capture widths of the resonance and g is the spin weighting factor = $(2J + 1)/2(2I + 1)$. Figure 12 shows the determination of the resonance parameters for uranium using thin sample data from capture and scattering measurements.

For thicker samples Doppler broadening becomes important and for very thick samples ($n\sigma_0 \sim 100$) the interference terms, particularly resonance-potential scattering interference, become very important. In an area analysis method developed by Lynn (55) these interference terms are taken into account and it is possible to determine with reasonable accuracy the neutron and total width of a resonance from transmission data alone provided the value of the scattering length in the region of the resonance can be determined from the data.

In the case of capture and scattering the effects of neutrons initially scattered and captured on subsequent collisions can be very large even when the samples are thin (i.e. $n\sigma_0 < 1$) so that the interpretation of thick sample data is much more difficult.

One of the techniques developed at Harwell (56) to analyse capture and scattering data is to use a Monte Carlo program to calculate an experimental area, taking into account the secondary and high order interactions, from a given set of resonance parameters. This calculated area is compared with the measured value and one of the input parameters altered until there is agreement between the measured and calculated areas; then the other parameter is altered and the process repeated. In this way a plot of Γ_n versus Γ_γ can be built up for that resonance. A least square fit to the intersection of the curves for the different sample thicknesses and for both sets of measurements gives the best set of parameters for that resonance.

4.4 Average Cross-section Analysis

The observed average total and capture cross-sections have been used to determine average values of resonance parameters, particularly the strength functions, and like area analysis this technique has been in use for some time.

The most accurate values of the strength function are obtained from total cross-section data but to make full use of this technique the measurements (55) have to extend to an energy of several MeV which really puts them beyond the scope of this talk.

Some of the first determinations (58, 59, 60) of the P-wave strength functions near mass 100 were made from average capture cross-section data. These results varied rather widely among themselves, and there was strong disagreement with the results obtained from transmission data. These discrepancies are not very surprising when it is considered that most of these measurements were carried out in the energy region 10 to 100 keV, where, as can be seen from figure 13, the average capture cross-section is insensitive to the strength function and has almost a linear dependence on the ratio of the average radiation width to the average level spacing for resonances of spin $J = 0$. This suggests that a better use of capture data would be to determine $\overline{\Gamma_\gamma}/\overline{D_0}$ utilising the values of the strength functions obtained from transmission experiments. As an example of this technique the following information has been

obtained from an analysis of the capture cross-section of ^{103}Rh . A value of $\overline{\Gamma}_{\gamma}/\overline{D}_0$ for s-, p- and d-wave neutrons was obtained from the fit, using values of the strength function determined from total cross-section data. This gives an average level spacing of 32.2 ± 8 eV assuming an average radiation width of 155 MeV as obtained from the data on individual resonances. The group at Saclay (61) obtained a lower limit of 26.6 eV for this average level spacing by observing the discrepancies between the distribution of the reduced neutron widths of 274 resonances in the energy region 0 to 4145 eV and an assumed Porter-Thomas distribution. This lower limit involves a correction of a factor of 2 being applied to the observed level spacing. We would suggest that the analysis of the capture data can give level spacings with considerably greater accuracy than can be obtained by application of such large corrections to the observed low energy level spacing.

5. Results of Measurements

There are numerous examples of cross-section data and their analysis in terms of resonance parameters in the published literature, a large amount of which has been collected together in various compilations notably the Brookhaven publication BNL 325. It is clear from these that the comparison of cross-section data in the resonance region from the various laboratories is complicated by the effects of the different energy resolutions with which the measurements were made.

In the case of total cross-section data, comparisons can most easily be made in the regions where the resolution has little effect such as the effective potential scattering between resonances and at higher energies in the average cross-section region where resonance self-screening becomes less important. These data often indicate the presence of systematic differences of several per cent in measurements from different laboratories. This is illustrated by the spread in the data on the smooth total cross-section of carbon and the region between resonances in the heavy elements as shown in BNL 325.

In the case of capture data the cross-section is usually very small between resonances and there are very few published measurements (62). From the comparisons of the average capture cross-section data above 1 keV it is apparent that at least in this region there are still many problems that have to be solved before accurate neutron capture cross-sections can be obtained. This is best illustrated by the average capture cross-section of gold where there are numerous experimental determinations of the cross-section covering wide energy ranges. The spread among these is about +25% but there is now better agreement both in magnitude and shape in the more recent measurements.

In the resolved resonance region the value obtained for the comparison of the various resonance parameters is probably the best method of comparing the data from different laboratories. There is general agreement between most laboratories on the energies of the resonances and any disagreements that did exist are gradually disappearing as measurements with better resolutions are superceding the older data.

The accuracy with which neutron and radiation widths can be determined depends on several factors, such as the strength of the resonance as well as the statistical accuracy of the data. In general, using area

analysis techniques, the smaller the neutron width the greater are the fractional uncertainties on the resulting parameters. But in the case of resonances in the energy region where both the Doppler and resolution effects are small, both parameters can be obtained with reasonable accuracy by using shape fitting techniques on the data.

The distribution function for the reduced neutron width is reasonably well understood to be a Porter-Thomas distribution. The divergences from this distribution are frequently used to estimate the number of p-wave resonances that have been observed in a given energy region and to make corrections for these in the values of the strength function and average s-wave level spacing.

The distribution function for the total radiation width is not as well understood as that for the reduced neutron width. The radiation width is often assumed to be constant from resonance to resonance (e.g. in order to determine the neutron width from transmission data alone) but there is mounting evidence that this is not true. In the case of the lighter elements variations are to be expected and the observed (38, 64) spread is consistent with the number of channels for radiative decay corresponding to the number of strong transitions observed in the thermal neutron capture spectrum (assuming a Porter-Thomas distribution for the partial widths). Determinations of the radiation width distribution (18, 65, 66) for the heavy nuclei appear to be consistent with known features of the capture gamma ray spectra. In reference 66 there appears to be some evidence for possible structure in the way the radiation width varies with energy. This is possibly not inconsistent with the recent discovery of sub-threshold fission in well-separated groups of resonances by Migneco and Theobald (67) at Geel in ^{240}Pu , by Paya et al (68) at Saclay in ^{237}Np and by James (69) at Harwell in ^{234}U . This sub-threshold fission (70, 71, 72) is explained in terms of the formation of a shape isomer with a binding energy some 1-3 MeV less than the more stable configuration of the nucleus. The existence of similar shape isomers in non-fissile nuclei could possibly give rise to the observation of structure in the radiation widths and it would be interesting to see if any anomalies in the capture γ -ray spectra are in phase with the observation of such structure. The observed level spacing depends on the statistical accuracy of the data, the resolution and the type of measurement. In capture cross-section measurements small capturing resonances (38, 73) are enhanced relative to larger scattering resonances giving a smaller observed level spacing. The Saclay (61) and Columbia (73) data in figure 17 on thorium clearly illustrates the variation in level spacing that can be obtained as the sensitivity of the measuring equipment is improved. But great care must be taken to ensure that the samples are very pure; if not some of the small resonances observed may be due to large resonances in small amounts of impurities present in the sample. The capture data (74) in figure 18 is an illustration of this point. The iron sample was supposed to be 99.999% pure, but the resonances observed at 4.2, 18.9 and 28 eV indicate the presence of about 70 ppm of tungsten in the sample. The peaks at 5.8 and 14.5 eV have not been positively identified with the presence of any other impurity. This possibly indicates that it might be better to carry out accurate cross-section measurements on the actual materials that are used in the fabrication of a nuclear reactor rather than supposedly pure samples of the components.

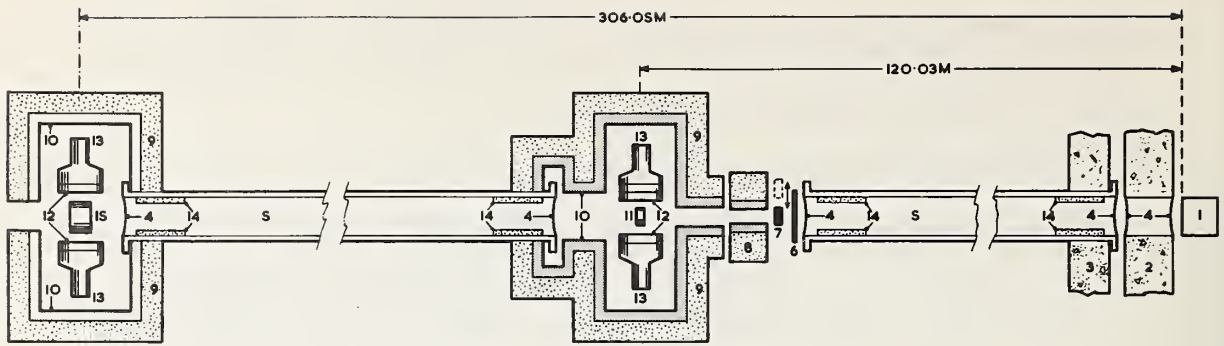
6. References

- (1) S. P. Harris, C. O. Muelhause and G. E. Thomas, Phys. Rev., 79 (1950) 11.
- (2) R. L. Macklin and H. S. Pomerance, Proc. Geneva Conf. (1955) Vol. 5, P/833 page 96.
- (3) W. M. Zinn, Phys. Rev. 70 (1946) 102.
- (4) Borst, Ulrich, Osborne and Hasbrouck, Phys. Rev. 70 (1966) 108.
- (5) R. L. Zimmerman, L. Q. Amaral, R. Fulfaro, M. C. Mattes, M. Abreu and R. Stasculevicius, Conf. Proc. Nuclear Data for Reactors, Paris (1966), IAEA Vienna (1967) 63.
- (6) F. J. Shore and V. L. Sailor, Phys. Rev., 112 (1958) 191.
- (7) B. B. Bernabei, L. B. Borst and V. L. Sailor, Nuclear Sci. Eng. 12 (1962) 63.
- (8) M. Ceulemans and P. Poortmans, Bull. Am. Phys. Soc. 8 (1963) 70.
- (9) H. B. Møller, F. J. Shore and J. L. Sailor, Nuclear Sci. Eng. 8 (1960) 183.
- (10) J. B. Bralley and J. L. Fowler, Fast Neutron Physics Part I page 73 Interscience publishers.
- (11) J. B. Marion, Fast Neutron Physics Part I, page 113, Interscience publishers.
- (12) P. A. Egelstaff, Neutron Time of Flight Methods (Spaepen J., Ed.) EANDC Brussels (1961) 261.
- (13) M. J. Poole and E. R. Wiblin, Proc. 2nd U.N. Int. Conf. PUAE 14 (1958) 266.
- (14) S. Cierjacks, Proc. Santa Fe Seminar on Intense Neutron Sources, (1966).
- (15) G. E. Blokmin et al, Physics of Fast and Intermediate Reactors III IAEA Vienna (1962) 399.
- (16) B. Diven, Nuclear Structure Study with Neutrons (M. Neve et al Eds) North-Holland Publishing Co., Amsterdam
- (17) A. A. Bergman et al, Proc. U.N. Int. Conf. PUAE 4 (1958) 135.
- (18) M. Asghar et al., Nucl. Phys. 76 (1966) 196.
- (19) G. Rohr, E. Friedland and J. Nebe, Int. Conf. on Nuclear Data for Reactors, Paris (1966) paper CN-23/9.
- (20) A. Stoloy, Phys. Rev. 118 (1960) 211.
- (21) A. Stoloy, Phys. Rev. 134 (1964) B68.

- (22) H. Postma et al, Phys. Rev. 126 (1962) 979.
- (23) H. Postma et al, Phys. Rev. 127 (1962) 1124.
- (24) H. Postma et al, Phys. Rev. 128 (1962) 1287.
- (25) F. L. Shapiro, Nuclear Study with Neutrons (M. Neve et al, Eds) North Holland Publishing Co., Amsterdam (1966) 223.
- (26) V. P. Alfimenkov et al, Yadern Fiz. 3 (1966) 55.
- (27) K. M. Diment - private communication.
- (28) F. P. Mooring, J. E. Monahan and C. M. Huddleston, Nuc. Phys. 82 (1966) 16.
- (29) A. Asami - private communication.
- (30) M. G. Sowerby, J. Nucl. Eng. 20 (1966) 135.
- (31) R. L. Macklin and J. H. Gibbons, Phys. Rev. 140 (1965) B324.
- (32) E. Haddod et al, Nuc. Insts. and Methods, 31 (1965) 125.
- (33) B. G. Diven, J. Terrell and A. Hemmendinger, Phys. Rev. 120 (1960) 556.
- (34) D. Kompe, Conf. Proc. Nuclear Data for Reactors Paris (1966) IAEA Vienna (1967) 513.
- (35) M. C. Moxon and E. R. Rae, Nuc. Inst., 24 (1963) 445.
- (36) R. L. Macklin, J. H. Gibbons and T. Inada, Nuc. Phys. 43 (1963) 353.
- (37) H. Weigmann, G. Carrano and K. H. Bockhoff, Nucl. Instr. and Methods 50 (1967) 265.
- (38) M. C. Moxon, Nuclear Study with Neutrons (M. Neve et al, Eds) North Holland Publishing Co., Amsterdam (1966) 531.
- (39) L. M. Bollinger, R. E. Cote, R. T. Carpenter, and J. P. Marion, Phys. Rev. 132 (1963) 1640.
- (40) E. R. Rae, W. Moyer, R. R. Fullwood and J. L. Andrews, Phys. Rev. 155 (1967) No. 4, 1301.
- (41) O. A. Wasson, M. R. Bhat, R. E. Chrien, M. A. Lone, and M. Beer, Phys. Rev. Lett., 17 (1966) 1220.
- (42) R. E. Chrien et al, Phys. Letters 25B (1967) 195.
- (43) M. R. Bhat et al - private communication and report BNL 11797 (1967).
- (44) C. Coceva, F. Corvi, P. Giacobbe and M. Stefano, Phys. Letters 16 (1965) 159.

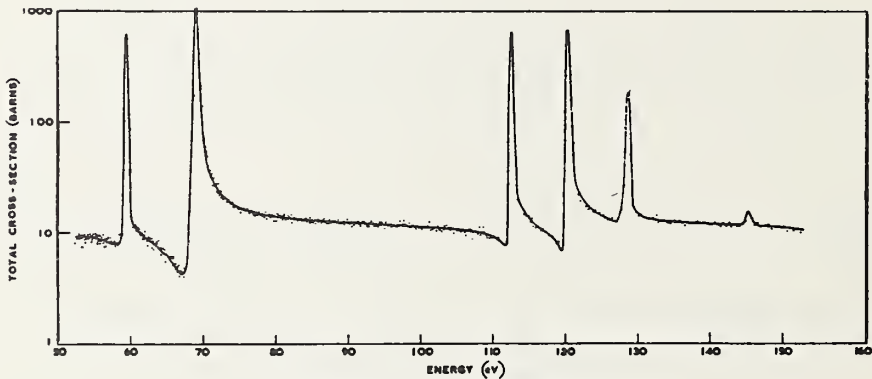
- (45) E. R. Rae, E. R. Collins, B. B. Kinsey, J. E. Lynn and E. R. Wiblin, Nucl. Phys. 5 (1958) 89.
- (46) M. Asghar and F. D. Brooks, Nucl. Instr. and Methods 39 (1966) 68.
- (47) A. Asami, M. C. Moxon and W. E. Stein - private communication
- (48) T. J. King, R. R. Fullwood and R. C. Block - private communication and submitted for publication in Nuc. Instr. and Methods (1967).
- (49) Groenwold and Groendijk, Physica 13 (1947) 141.
- (50) B. H. Patrick et al - private communication
- (51) T. Fuketa et al, Proc. Conf. on Nuclear Data for Reactors Paris (1966) IAEA Vienna (1967) 147.
- (52) S. E. Atta, J. A. Harvey, ORNL-3205 (1961) and its addendum (1963).
- (53) Ribon et al - private communication
- (54) D. J. Hughes, J. Nucl. Energy 1 (1955) 237.
- (55) J. E. Lynn, Nucl. Instr. and Methods, 91 (1960) 315.
- (56) M. C. Moxon and J. E. Lynn - private communication
- (57) C. A. Uttley, C. M. Newstead and K. M. Diment, Conf. Proc. Nuclear Data for Reactors, Paris (1966) IAEA Vienna (1967) 165.
- (58) E. G. Bilpuch, L. W. Weston and N. W. Newson, ANN Phys. 10 (1960) 455.
- (59) J. H. Gibbons, R. L. Macklin, P. D. Miller and J. M. Neiler, Phys. Rev. 122 (1961) 182.
- (60) Yu. Y. Popov and Yu. I. Fenin, J.E.T.P. 16 (1963) 1409.
- (61) Data from Saclay - private communication.
- (62) S. J. Friesenhohm et al, Nucl. Sci. Eng. 26 (1966) 487.
- (63) K. Drittler, Conf. Proc. Nuclear Data for Reactors Paris (1966) IAEA Vienna (1967) 155.
- (64) R. W. Hockenbury, Z. M. Bartolome, W. R. Moyer, J. R. Tatarezuk and R. C. Block - private communication (1968)
- (65) M. Asghar, M. C. Moxon and C. H. Chaffey
- (66) N. W. Glass, A. D. Schebberg, L. D. Tatro and J. H. Warren - private communication (1968)
- (67) E. Migneco and J. P. Theobald - private communication (1968)

- (68) D. Paya, H. Derrien, A. Fubini, A. Michaudon and P. Ribon,
Conf. Proc. Nuclear Data for Reactors II, IAEA Vienna (1967) 128.
- (69) G. D. James - private communication
- (70) J. E. Lynn - private communication
- (71) V. M. Strutinsky, Nuc. Phys. A95 (1967) 420.
- (72) R. C. Block, R. W. Hockenbury, Z. Bartolome and R. R. Fullwood,
Conf. Proc. Nuclear Data for Reactors (Paris 1966) IAEA Vienna
(1967) 565.
- (73) J. B. Gorg, J. Rainwater, J. S. Petersen and W. W. Havens, Phys.
Rev. P34 (1964) B985.
- (74) M. G. Noxon and F. B. Horsman - private communication.

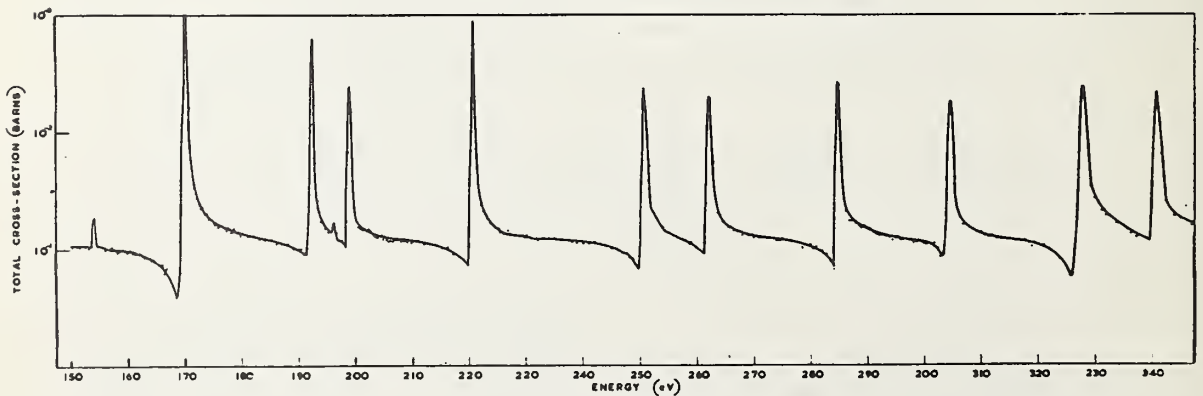


- | | |
|----------------------------------|--|
| 1 NEUTRON BOOSTER | 8 MASTER COLLIMATOR (Pb, NI & WAX PLUS BORIC ACID) |
| 2 6' CONCRETE SHIELD | 9 PARAFFIN WAX/BORIC ACID SHIELDING |
| 3 4' CONCRETE SHIELD | 10 LEAD SHIELDING |
| 4 MELINEX WINDOW | 11 ^{10}B PLUG |
| 5 EVACUATED FLIGHT PATH | 12 NaI (TI) CRYSTALS |
| 6 NATURAL BORON OVERLAP FILTER | 13 PHOTOMULTIPLIER TUBES |
| 7 TRANSMISSION SAMPLE & CARRIAGE | 14 COLLIMATORS (PARAFFIN WAX/BORIC ACID) |
| | 15 ^{10}B & VASELINE PLUG |

Figure 1 Layout of the Harwell 120-300 metre system used to measure by transmission and time of flight techniques total neutron cross-sections in the energy region 100 eV to ~ 10 MeV.



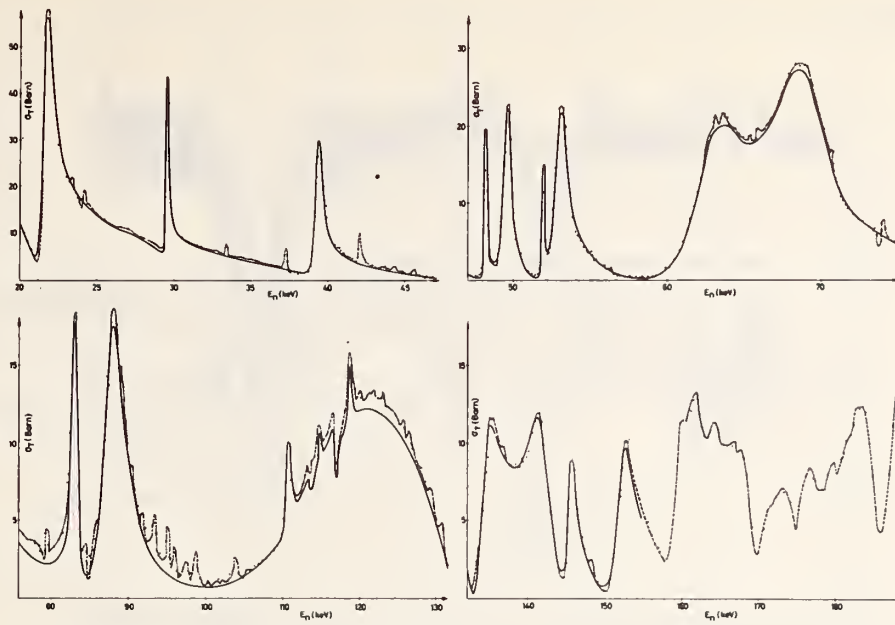
THE NEUTRON TOTAL CROSS-SECTION OF Th^{232}



THE NEUTRON TOTAL CROSS-SECTION OF Th^{232}

FIG 2.

THE TOTAL CROSS SECTION OF THORIUM IN THE NEUTRON ENERGY REGION 50 to 350 eV MEASURED ON THE 120 METRE FLIGHT PATH AT HARWELL



Total neutron cross section curve for ⁵¹V. The solid line represents the multilevel fit.

Figure 3

THE TOTAL CROSS SECTION OF VANADIUM IN THE KILOVOLT REGION MEASURED AT KARLSRUHE ON A PULSED VAN DE GRAAF TIME OF FLIGHT SPECTROMETER (ref. 17)

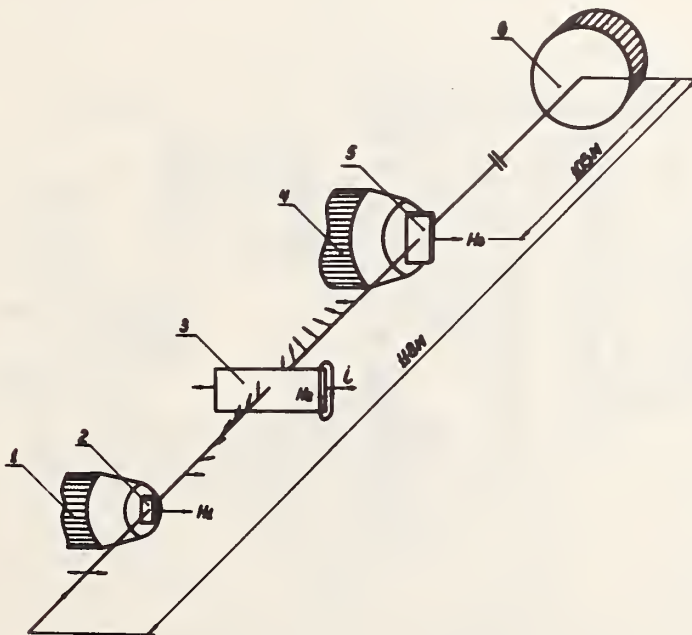


Figure 4

THE SCHEMATIC PLAN OF THE EQUIPMENT USED TO MEASURE THE TRANSMISSION OF POLARISED NEUTRONS (1) and (4) are magnets, (2) is a proton polarised target, (3) is the neutron spin rotator (5) is the cooled Ho sample and (6) the neutron detector (ref. 23)

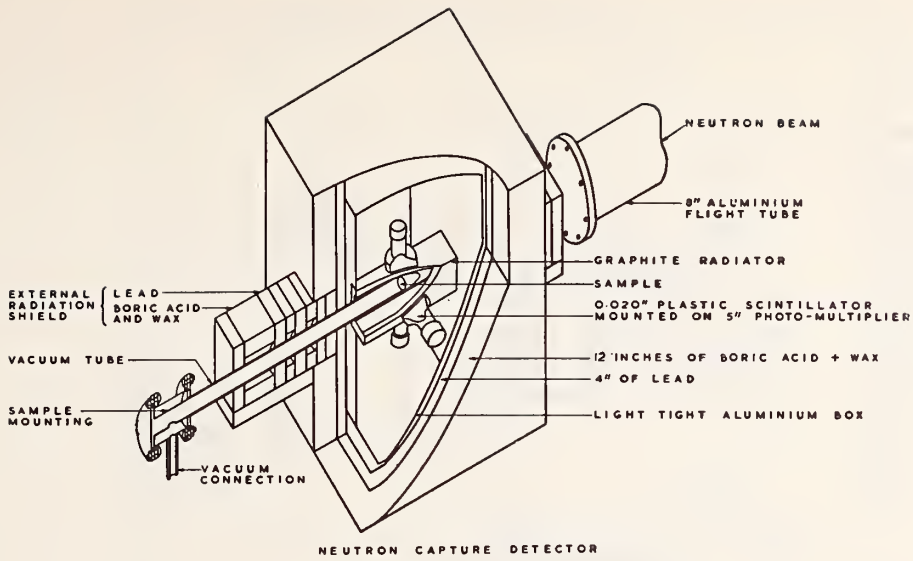


FIGURE 7

THE γ RAY DETECTOR USED AT HARWELL TO MEASURE NEUTRON CAPTURE CROSS SECTIONS

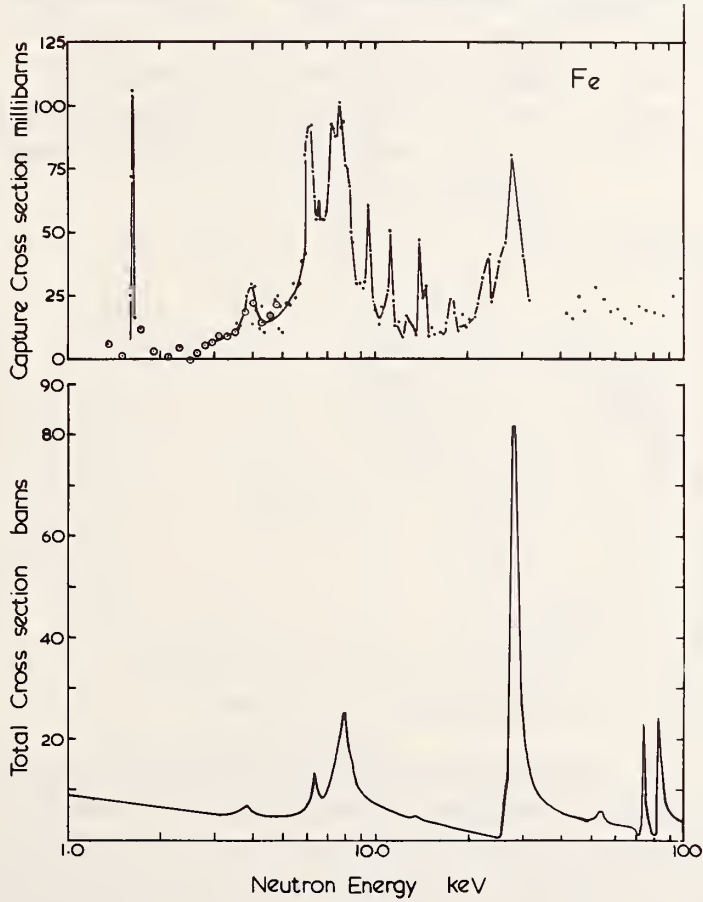


Figure 8

LOWER CURVE - TOTAL CROSS SECTION OF IRON FROM BNL 325

UPPER CURVE - CAPTURE CROSS SECTION OF IRON MEASURED AT HARWELL
(ref. 33)

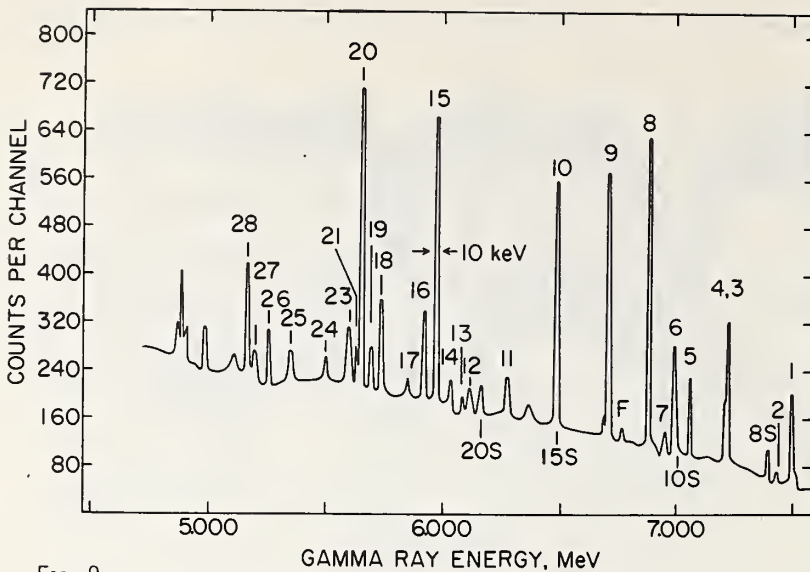


FIG. 9

The $\text{Co}^{59}(n, \gamma)\text{Co}^{60}$ γ -ray spectrum from 2.2- to 5.5-eV incident neutron energy. The peaks shown are mostly two-escape peaks, except for peaks labeled *F* and *S*, which correspond to full energy and single escape. The line numbering is chosen to agree with the thermal capture work of Shera and Hafemeister.

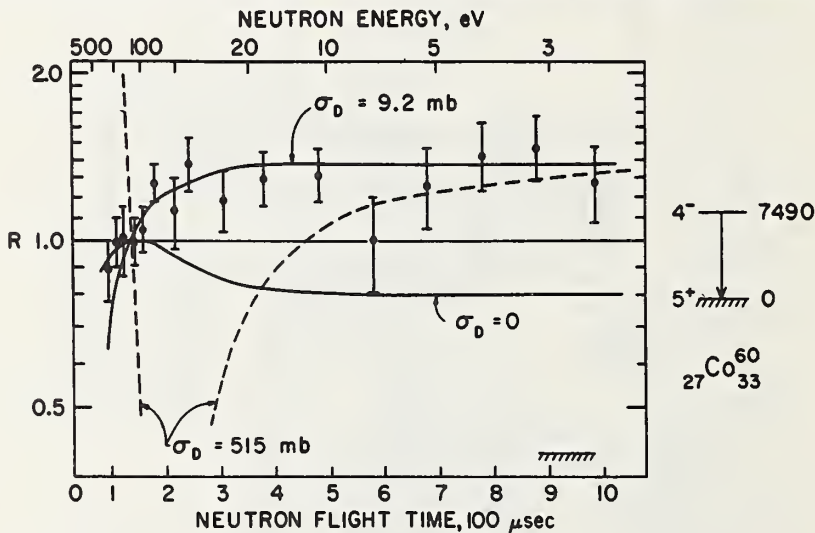


FIG. 10

The energy variation of $R \propto \sigma_{n\gamma f} / \sigma_{n\gamma}$ for the ground-state transition. The curve $\sigma_D = 0$ would be the expected variation after correction for the presence of the 3^- bound state, with no interference assumed between the resonance and direct reaction amplitudes. The curves $\sigma_D = 9.2$ mb and $\sigma_D = 515$ mb result from constructive and destructive interference below the 132-eV resonance.

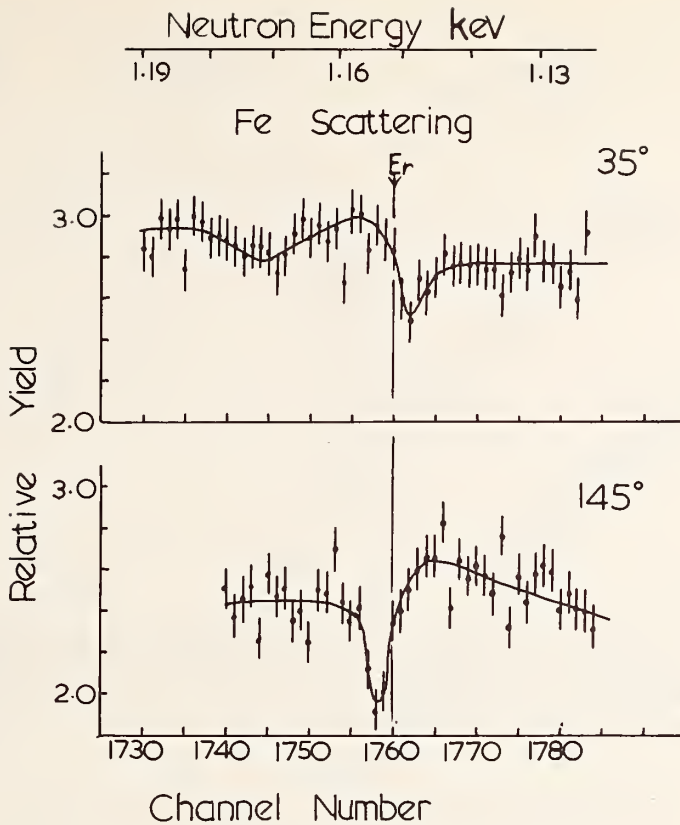


Figure 11 The relative scattering cross-section of iron near the 1.15 keV resonance at angles of 35° and 145°.

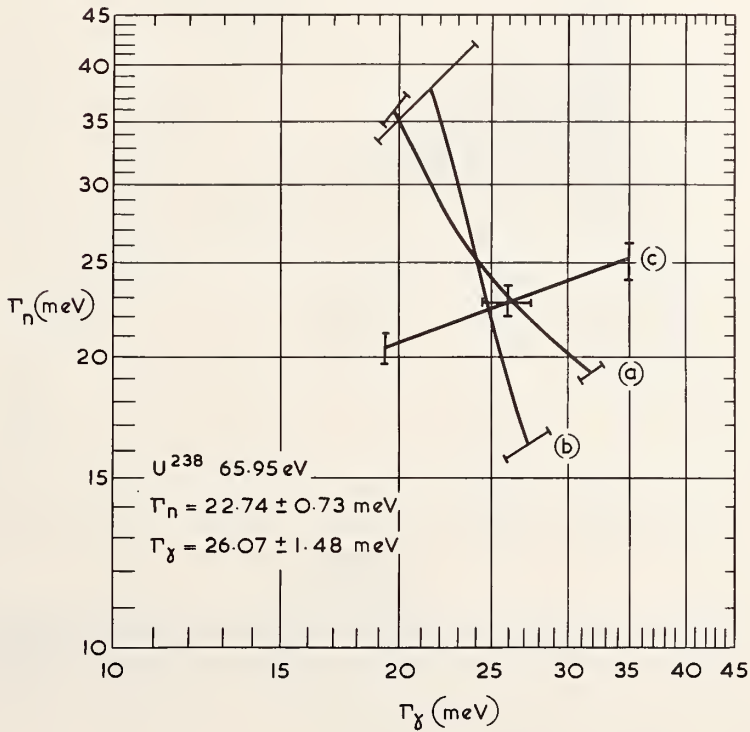
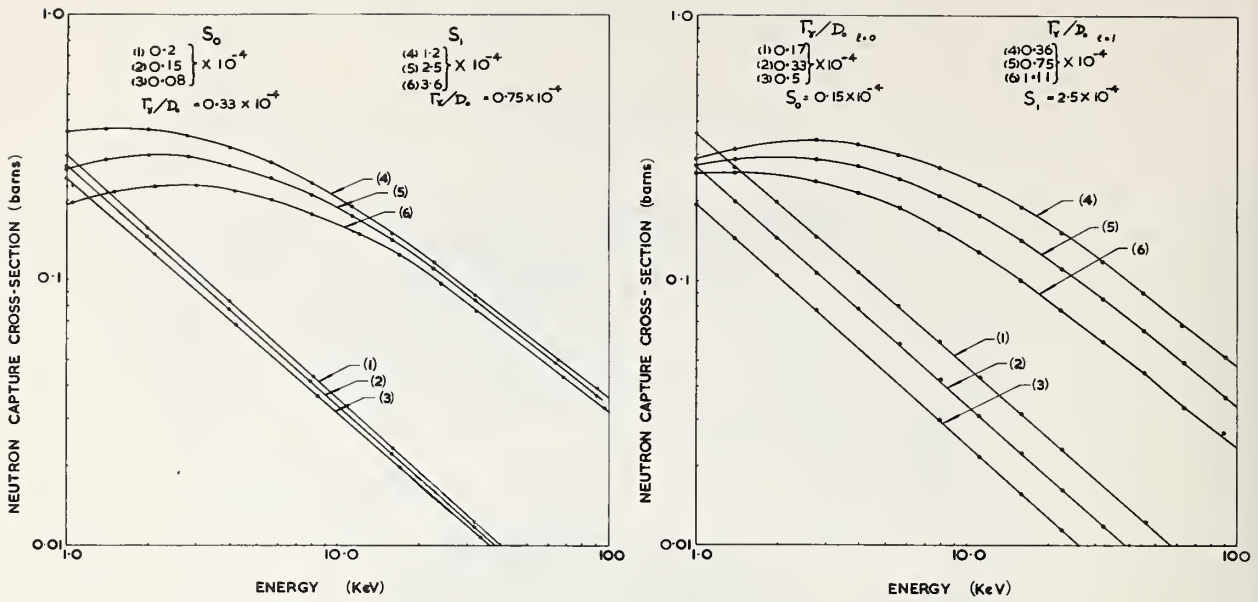


Figure 12 The determination of the parameters for the 65.95 eV resonance in uranium using capture and scattering data on thin samples.



THE DEPENDENCE OF THE S AND P WAVE COMPONENTS OF THE NEUTRON AVERAGE CAPTURE CROSS SECTION ON THE NEUTRON STRENGTH FUNCTION AND Γ_γ/D_0

Figure 13

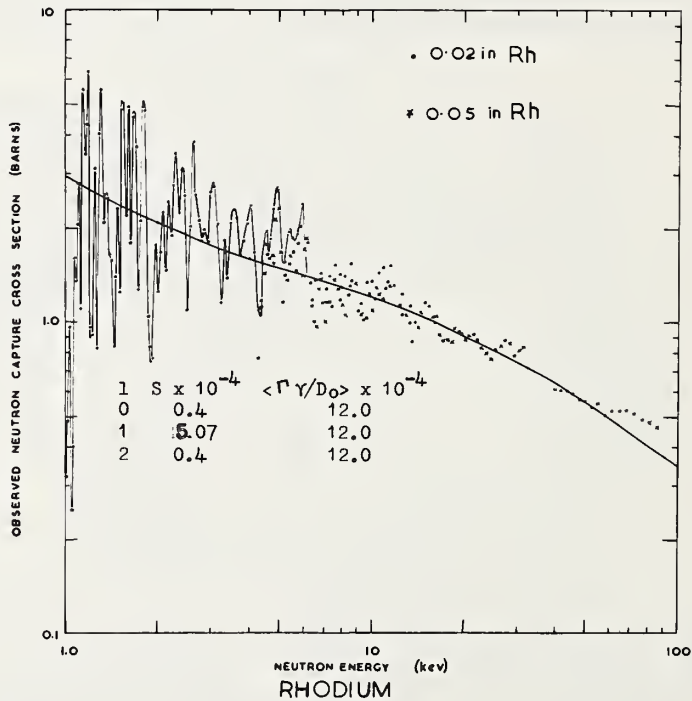


FIGURE 14

A FIT TO THE AVERAGE CAPTURE CROSS SECTION OF RHODIUM IN THE NEUTRON ENERGY RANGE 1 TO 100 keV DETERMINING THE AVERAGE VALUE OF Γ_γ/D_0

Rh 103

DISTRIBUTION OF $2g\Gamma_n^0$ FOR ALL RESONANCES
FROM 0 TO 4145 eV

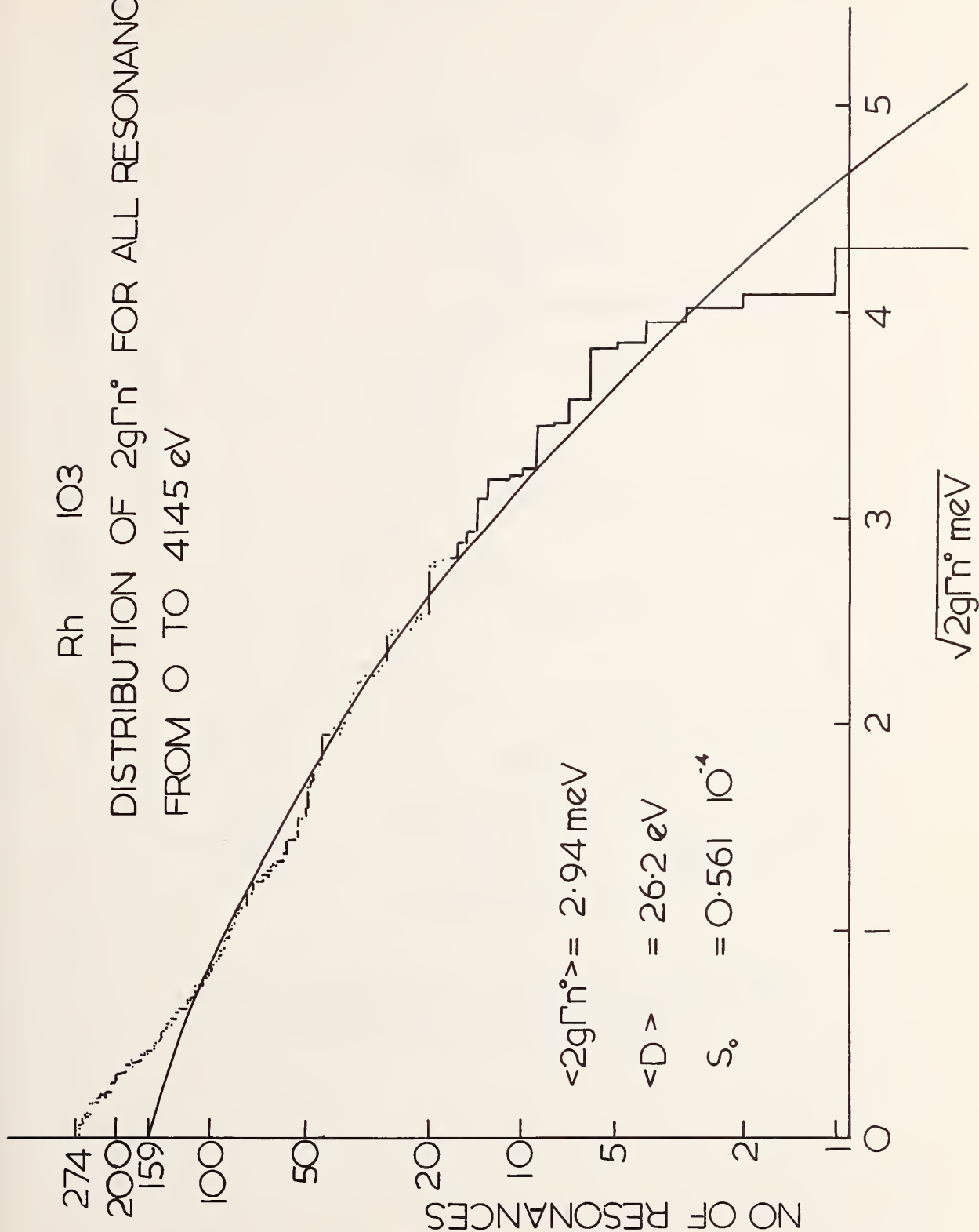


Figure 15 The comparison of the integral distribution of reduced neutron width of ^{103}Rh in the energy range 0-4145 eV with the Porter-Thomas distribution (ref. 59)

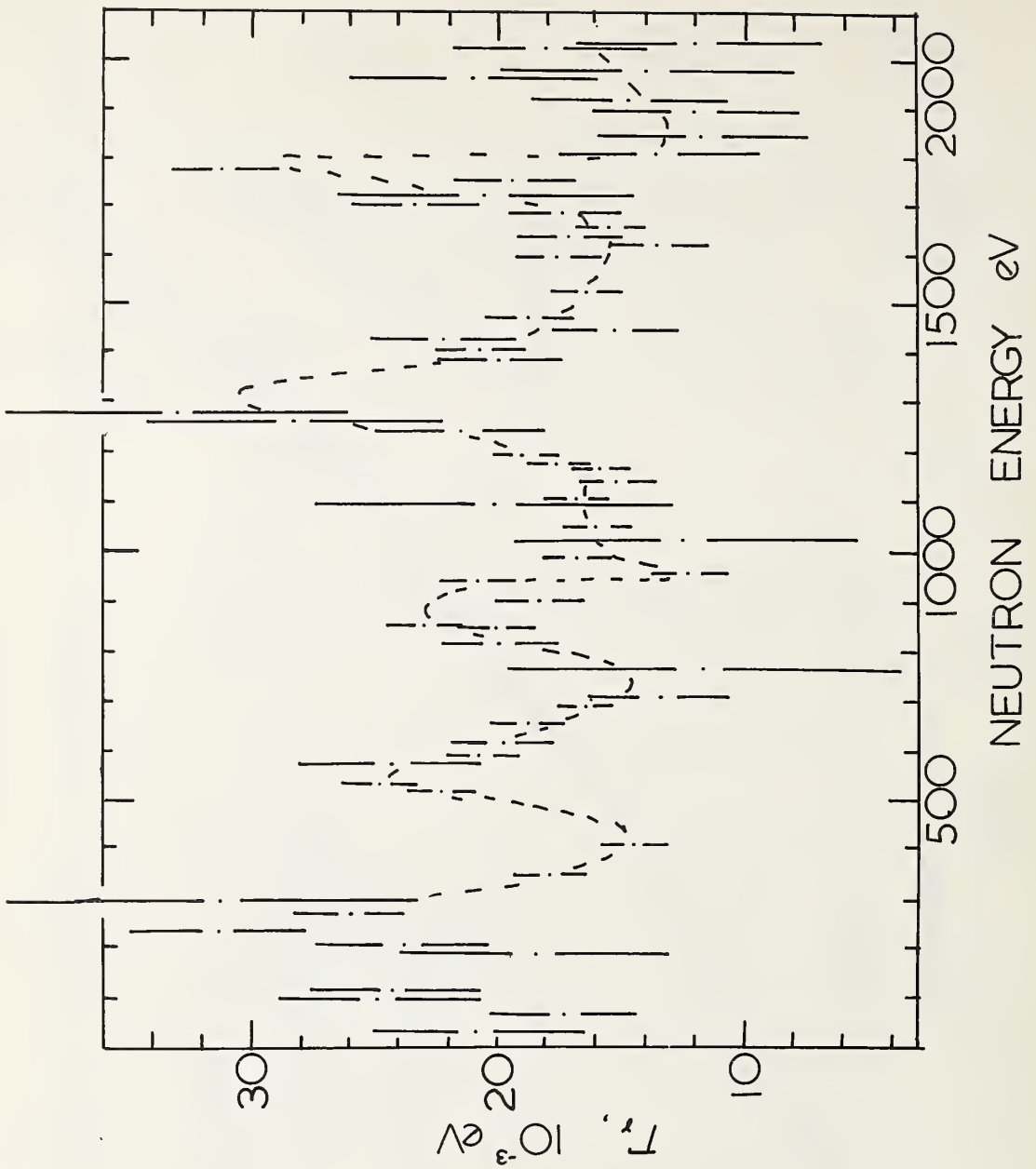


Figure 16 Radiation width versus neutron energy. The dashed line is a guide to the eye to emphasize possible structure. Error bars are statistical only (ref. 66)

Thorium Level Spacing

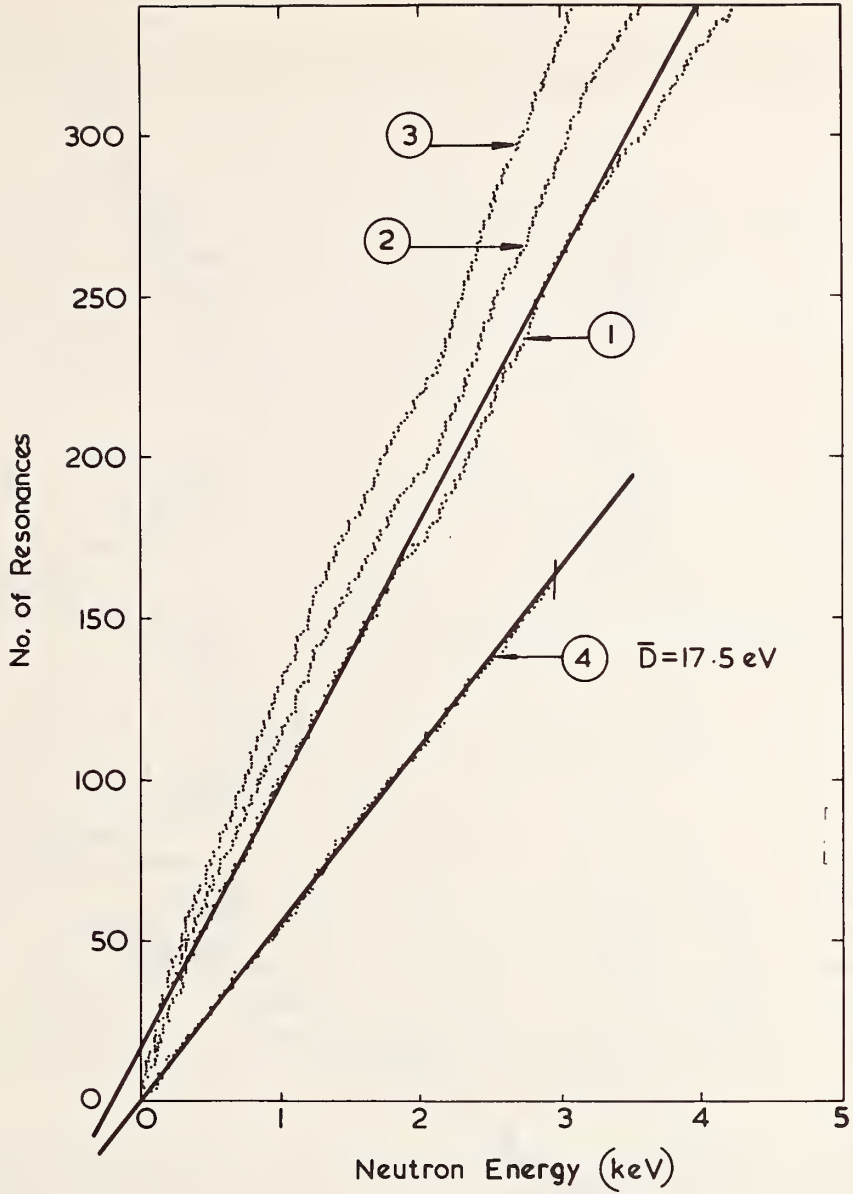


Figure 17 The observed number of resonances up to the given neutron energy. Curves 1, 2, 3 date from ref. 61 and 4 dates from ref. 73.

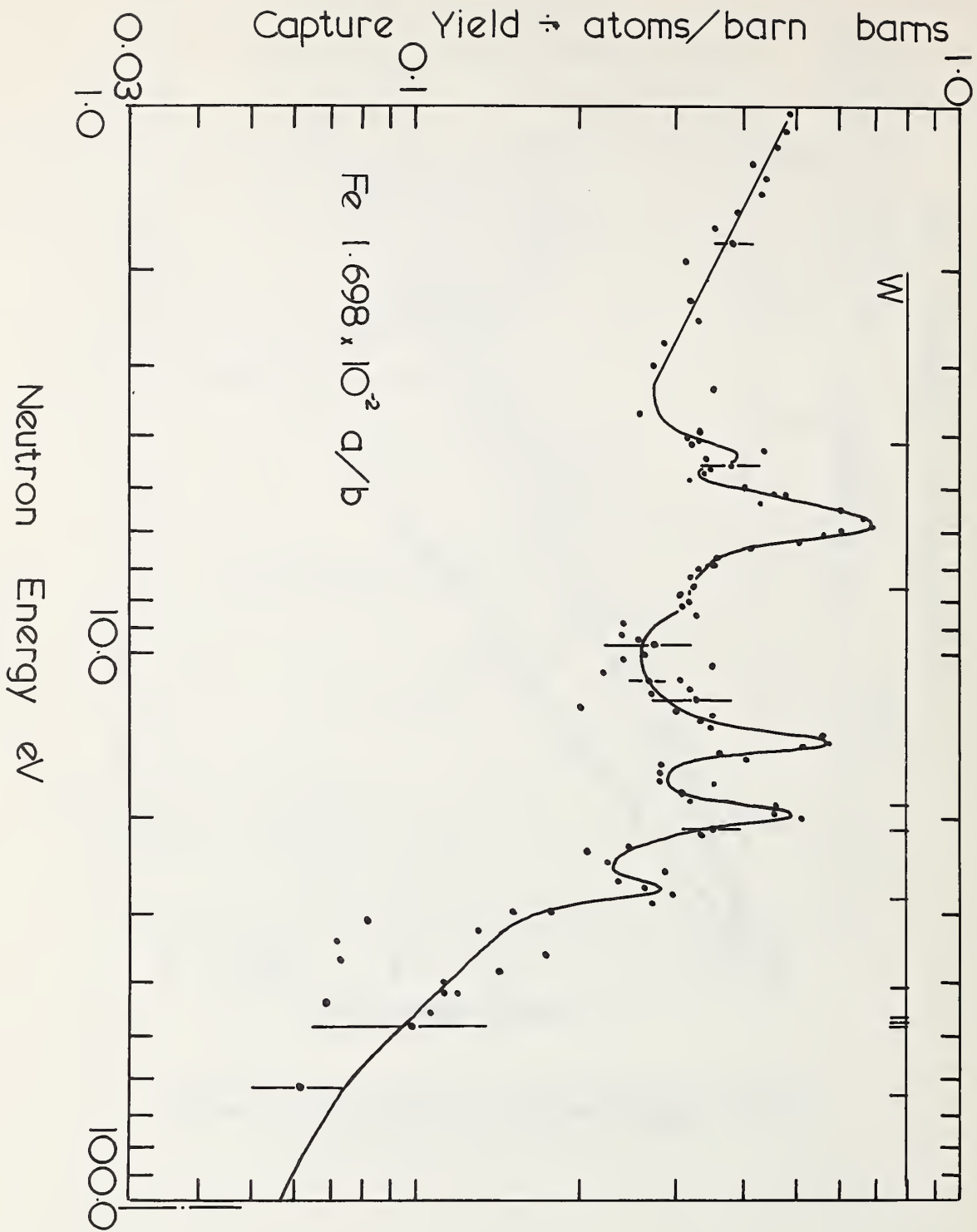


Figure 18 The capture cross-section of a sample of "pure" iron in the neutron energy region 1 to 100 eV (ref. 74)

C. Samour, R. Alves[†], H. E. Jackson^{††}, J. Julien and J. Morgenstern

Centre d'Etudes Nucléaires de Saclay, France

91 Gif-sur-Yvette, France

The improvements made to experimental apparatus at Saclay allow detailed examination of resonance neutron capture gamma ray spectra.⁽¹⁾ These gamma rays were detected in an 8 cc Ge(Li) detector. Time-of-flight experiments were performed around the 2 kW Saclay linear electron accelerator with two flight paths (28.7 m or 14.7 m); spectra were recorded with Intertechnique 24 digit two parameter tape-recording system.

The distribution of partial radiative widths $\Gamma_{\gamma i}$ was determined in the framework of Porter-Thomas description.⁽²⁾ Such a distribution is given by the χ^2 distribution function for ν degrees of freedom. The ν parameter may be interpreted as the reaction channel number. Then the distribution of $\Gamma_{\gamma i}$, which corresponds to only one exit channel, should be expected to have $\nu = 1$. The ¹⁹⁶Pt compound nucleus is a very favorable case for such a study: a large number of $J = 1$ resonances is available (22 resonances from 10 to 700 eV) and there are 3 distinct intense transitions to the ground state and two first excited states, giving an experimental sample of 66 widths. The experimental distribution of $x_i = \Gamma_{\gamma i} / \langle \Gamma_{\gamma i} \rangle$ is shown in figure 1. χ^2 distributions for $\nu = 1$ and 2 are also drawn. Our data appear consistent with $\nu = 1$ rather than an exponential function ($\nu = 2$). A statistical treatment based on a two dimensional Monte Carlo method,⁽¹⁾ in which the experimental threshold is introduced, gives the best estimate^(1,3) $\nu = 1.25 \pm 0.35$. Then partial radiative capture can be considered as a one exit channel reaction and we have an a posteriori justification of the extension of the channel notion to reactions with photon emission.

To investigate the possibility of correlation between two partial radiative widths relative to transitions going to very close energy states, one may examine the distribution of their sum, which must be a χ^2 distribution with $\nu = 2$ if the two transitions are to be independent. We have investigated the two dipolar electric transitions going to fundamental state and first excited state of ¹⁸⁴W. Figure 2 shows the experimental distribution. Our data are consistent with χ^2 functions for $\nu = 2$. The Monte Carlo method gives⁽¹⁾ $\nu = 2.5 \pm 1.6$, in agreement with previous values and we conclude there is no appreciable correlation between these two transitions.

[†] Nuclear Engineering Institute, Sao Paulo, Brazil

^{††} On leave from Argonne National Laboratory, Argonne, Illinois 60439

Variation of partial capture cross-section with neutron energy allows the demonstration of interference or direct capture effects. We have found⁽¹⁾ two interference effects in $^{195}\text{Pt} + n$, for 7920 and 6516 keV transitions between 12 and 19 eV resonances. Figure 3 gives an example. Positive interference between 4.9 and 60 eV resonances of $^{197}\text{Au} + n$ has been found⁽¹⁾ for three transitions (6510, 6455 and 6313 keV); experimental data for 6245 keV transition can be explained if a direct capture effect is taken into account, the cross-section at 1 eV being about 2 mb.⁽¹⁾ For $^{59}\text{Co} + n$ we have studied eight transitions; a direct capture cross-sections of 10 ± 2 mb fits experimental data for the 7490 keV transition, but it is necessary to introduce the bound state at - 320 eV to get a suitable fit. For the other transitions, direct capture is not necessary but may exist. Interference effects are also found in Tm and Hg.⁽⁴⁾

Such studies allow the mean value of many transitions intensities to be determined. The energy dependence versus E can be checked. If M1 and E1 transitions are detected one can compare the ratio of their mean intensities value with the theoretical predictions. In platinum and wolfram data seem to be consistent with an E^5 law⁽⁵⁾ rather than with an E^3 law.⁽⁶⁾ On the other hand, an analysis of 12 E1 and 12 M1 transitions in several tin isotopes showed very strong M1 transitions far in excess of the single particle estimate.⁽¹⁾ We have calculated experimental reduced widths k introduced by Bartholomew⁽⁷⁾:

$$k(E1) = \Gamma_{\gamma i}(E1) / [E_{\gamma i}^3 A^{2/3} D]$$

$$k(M1) = \Gamma_{\gamma i}(M1) / [E_{\gamma i}^3 D]$$

and compared them with the Blatt-Weisskopf estimate. For E1 transitions, the ratio of mean values $k_{\text{exp}}/k_{\text{BW}}$ is 1.53, whereas it is 113 for M1 transitions. On the other hand, BW estimation gives a ratio $\langle k(E1) \rangle / \langle k(M1) \rangle$ equal to 3.5, whereas our data give 0.055, that is about 60 times less. A similar result is found in ^{35}Cl resonance located at 405 eV.⁽⁴⁾ The M1 transitions are enhanced by a factor of the same order of magnitude as in Sn.

REFERENCES

1. C. Samour, Thesis, 1968.
2. C. E. Porter and R. G. Thomas, Phys. Rev., 1956, 104, 483.
3. C. Samour et al., to be published.
4. R. N. Alves, Thesis, 1968.
5. P. Axel, Phys. Rev., 1962, 126, 671.
6. J. M. Blatt and V. F. Weisskopf, Theoretical Nuclear Physics, Chap. XII (J. Wiley, New York, 1952).
7. G. A. Bartholomew, Ann. Rev. Nucl. Sci., 1961, 11, 259.

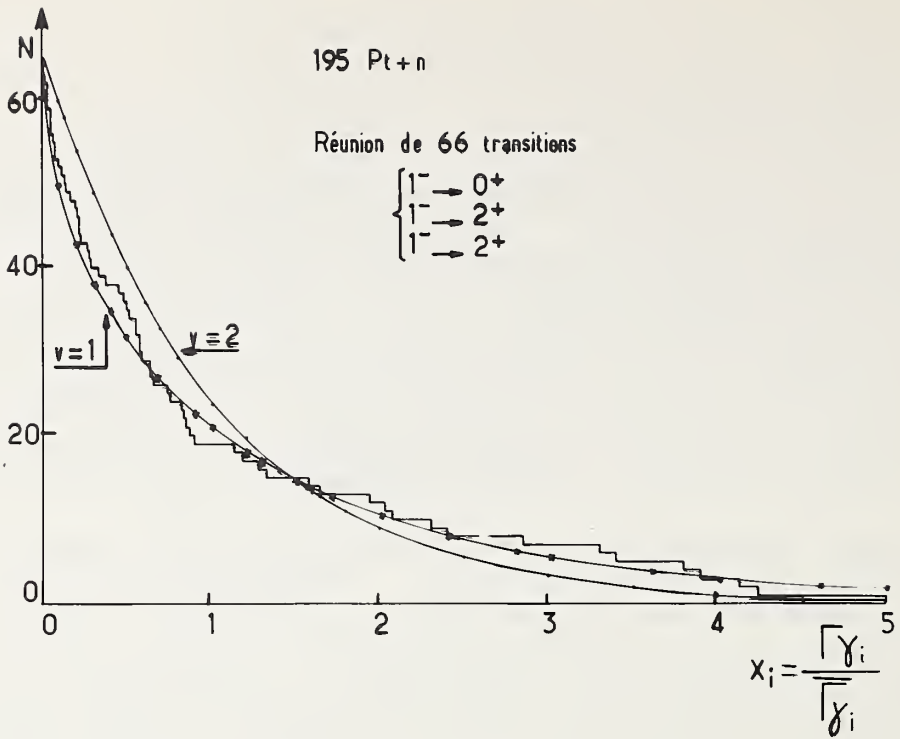


Fig. 1 - Partial radiative width distribution for $^{195}\text{Pt} + n$.

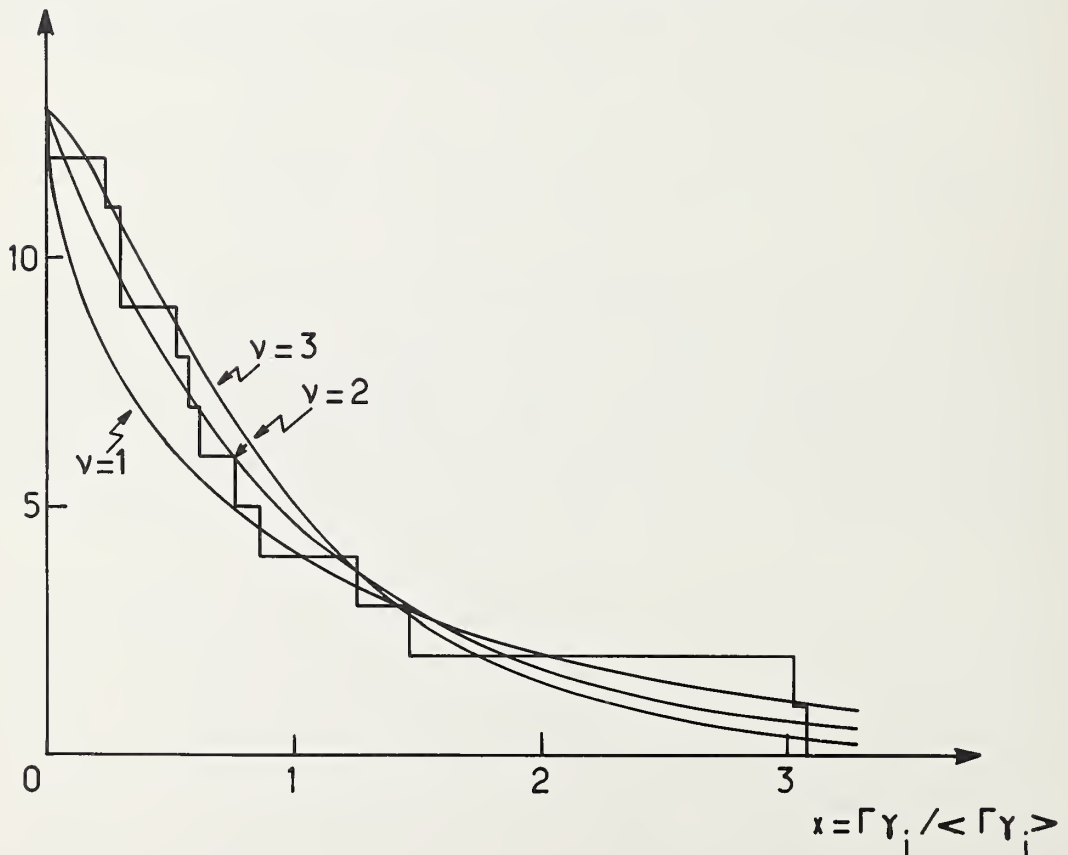


Fig. 2 - Distribution of the sum of 7413 and 7302 keV transition relative intensities for $^{183}\text{W} + n$.

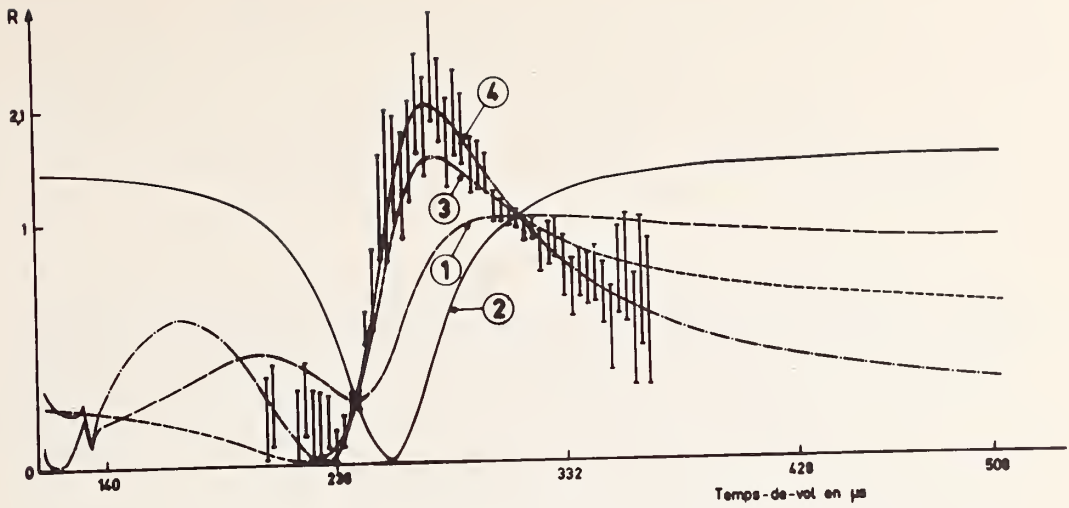


Fig. 3 - Interference effect for $^{195}\text{Pt} + n$ 7920 keV transition. For curve number 1 there is no interference effect. Curves 2 and 3 mean respectively constructive and destructive interferences between the 12 and 19 eV resonances. Curve 4 takes into account effects of 67, 68, 110 and 120 eV resonances.

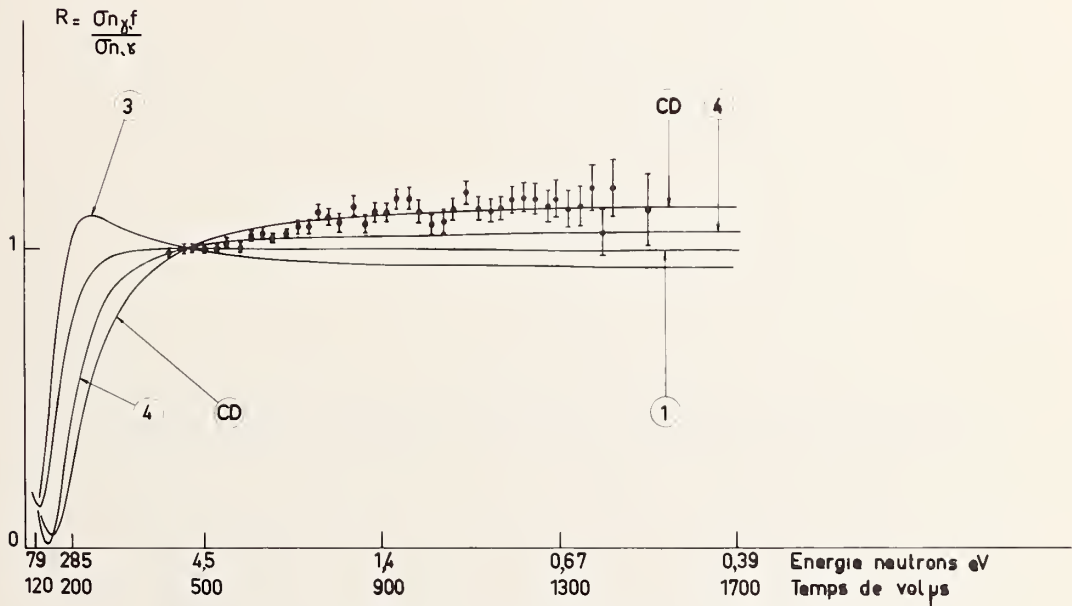


Fig. 4 - Interference effect for $^{197}\text{Au} + n$ 6245 keV transition. Curve 1 is calculated without interference and direct capture effects. In curves 3 and 4, the 4.9 and 60 eV resonances interfere with negative and positive signs. Curve noted CD is calculated like curve 4, but with a direct capture cross-section of 2 mb at 1 eV; direct capture and resonant capture processes interfere positively.

Gamma Rays Following Neutron Capture in Iron,
Sodium, and Thorium^{*}

O. A. Wasson, J. B. Garg,[†] R. E. Chrien,
and M. R. Bhat

Brookhaven National Laboratory, Upton, New York 11973

The intensities of prominent γ rays from neutron capture in iron, sodium, and thorium have been measured as a function of incident neutron energy at the HFBR fast chopper facility at Brookhaven. The partial capture cross section of 27 γ rays in iron was measured from thermal to 5 keV neutron energies. Additional γ rays were observed in the 1167 eV resonance and at thermal energy. In sodium, the observation of a ground state γ ray in the thermal spectrum ($E_\gamma = 6960 \pm 2.0$ keV) with an intensity of ~ 0.1 photons/100 captures supports the 2+ assignment of the 2.85 keV resonance. The γ -ray spectra from capture at thermal and in the four lowest energy S-wave resonances in Th^{232} exhibit large fluctuations in the partial radiation widths.

* This work was supported by the U. S. Atomic Energy Commission.

† State University of New York at Albany, Albany, New York. 12203

The nuclear properties of iron, sodium, and thorium are of considerable interest because of their use in the nuclear power field. Of prime interest is the measurement of the capture cross section and the resulting γ -ray spectrum as a function of neutron energy. We report the results of such measurements which have been performed at the HFBR fast chopper facility^[1] at Brookhaven National Laboratory. Using the 22-meter flight path, neutron capture γ -ray spectra have been obtained from thermal to 5 keV neutron energies. The γ rays were detected by lithium-drifted Ge diodes of various volumes, yielding a γ -ray energy resolution of ~ 8 keV for 7.6 MeV γ rays in iron. Experimental events were recorded on magnetic tape and subsequently analyzed at the central computer.

Since for iron the average capture cross section is small, $\sigma(0.0025 \text{ eV}) \sim 2.7$ barns, the measurement of the cross section is difficult with the conventional capture tank technique. On the other hand, the γ -ray spectrum produced in neutron capture is characterized by a relatively small number of relatively strong lines. It is therefore feasible to measure the cross sections of individual γ rays in the epithermal neutron energy region. Figure 1 shows the resulting time-of-flight spectrum for γ -ray events above 3.2 MeV ($E_\gamma > 3.2 \text{ MeV}$). The spectrum is dominated by the resonance at 1167 eV.^[2] The structure in the region from 0.1 to 1.0 keV is due to neutrons scattered from the 1/4 in. iron target and captured in the germanium detector, which was shielded with Lithium-6 and polyethylene. The weak germanium capture γ rays presented little difficulty in the analysis of the data.

Structure in the γ -ray yield near 46 eV is observable in Figure 1. Contrary to the higher energy structure, this bump is definitely attributable to iron since it does not appear in a control experiment using an equivalent thickness lead scatterer. A neutron width of $9 \times 10^{-8} \text{ eV}$ is obtained for this resonance by comparison to the area observed for the 1167 eV resonance. This width is subject to a large uncertainty because of spectrum differences and multiple scattering near the 1167 eV resonance. Nevertheless, it is acceptable as an order of magnitude estimate and is most likely to be a P-wave resonance.

The work of Groshev^[3] demonstrates that $\sim 80\%$ of the primary γ -ray transitions have an energy greater than 3.2 MeV. We have used the figure of 83% to normalize our relative thermal intensities to an absolute basis. The presence of several secondary transitions in this region^[4] does not appreciably alter this figure since it is probable that their presence is balanced by primary transitions too weak to be detected and therefore not included in the normalization.

The intensity variation of 27 of the stronger γ rays has been measured in the epithermal region by use of a flux monitor based on the $B^{10}(n, \alpha, \gamma)$ reaction, detecting the 478 keV γ ray. A correction has been applied for neutron absorption in the boron. We have used the fact that the iron capture cross section is proportional to v^{-1} near thermal to normalize our thermal capture run to the data recorded in the epithermal region.

The results of the experiment are given in Table I which lists the partial cross sections of 27 lines from Fe^{56} . The partial radiation widths of the 1167 eV resonance are listed in Table II. It was assumed that 83% of the primary transitions had energies greater than 3.2 MeV and

that the total radiation width was 0.6 eV.

Most of the γ rays follow the $1/v$ cross section rather closely from thermal to 1 keV neutron energies. The partial cross section of a few representative γ rays are shown in Figures 2 and 3. Figure 2 shows the quantity $\sqrt{E} \sigma$ as a function of neutron energy for three γ rays. The region near the 1167 eV resonance has been excluded. The hatched regions indicate the $1/v$ behavior including the uncertainty in the thermal cross section. The 5922 keV γ ray follows the $1/v$ trend quite accurately while ground state doublet at 7645 and 7631 keV shows small variations. Figure 3 shows a similar plot. The point at 2.6 keV may be affected by events associated with the 1167 eV resonance due to the relatively poor neutron energy resolution and is considered less reliable than the other points. The 6382 γ ray follows the $1/v$ law, while the 4463 keV γ ray shows a slight departure from $1/v$.

Portions of the typical γ -ray spectra are shown in Figures 4-6 for the neutron energy regions of Table I. Differences in the spectrum associated with the 1167 eV resonance are clearly seen. Figure 4 shows the variation in γ -ray intensity of the ground state doublet between thermal and the 1167 eV resonance. Of particular interest is the γ ray at 7511.4 keV which feeds a $5/2^-$ level in Fe^{57} at 134 keV excitation energy.^[4] This line is weakly seen in the resonance but is not seen at thermal or in the off-resonance region. The isotropic angular distribution of γ rays from the 1167 eV resonance indicates a spin of $1/2$ and therefore, we believe this to be an E-2 transition. Figure 5 demonstrates the large variation for the 7279 and 6382 keV γ rays between thermal and the resonance. The strongest γ ray in the germanium spectrum at 7259 keV is observed in the 100 eV region. Figure 6 compares the thermal spectrum with the off-resonance regions at 54 eV and 2600 eV to establish the cross-sectional variation of the 3268, 3358, 3416, and 3439 keV γ rays.

The implications of the γ -ray intensities observed in the off-resonance region and in the 1167 eV resonance are now under study.

Sodium. The γ -ray spectra produced by capture of thermal and 100 eV neutrons in sodium were found to be similar. However, a weak 6961 keV ground state transition was observed with an intensity of < 0.1 photons per 100 neutrons captured, which has previously been unreported.^[5] If thermal capture is dominated by the 2.9 keV resonance with spin $2+$, as is likely from the known resonance parameters, then the multipolarity of this ground state transition is E-2. The partial radiation width is ~ 600 μeV , which is $\sim .01$ Weisskopf units.

Thorium. In spite of the importance of thorium, little is known of the nuclear properties of the isotope thorium-233. Even its neutron binding energy and ground state spin and parity have not been measured. No excitation energies have been deduced. Only a few weak high energy γ rays have previously been observed in thermal capture by Groshev^[6] and Greenwood.^[7] The neutron time-of-flight spectrum for a $1/4$ in. thorium sample is shown in Figure 7. The γ -ray energies were limited to the region above 2.8 MeV in order to be above the full energy peak of the Th^{232} back-ground γ ray at 2614 keV. The γ -ray spectra produced in the four $1/2+$ S-wave resonances at 21.8, 23.4, 59.5, and 69.1 eV are shown in Figure 8.

The γ -ray energy scale which extends from 3.8 to 5.0 MeV refers to the double-escape peaks, although the full energy peaks of lower energy γ rays are also included. The most striking feature of these spectra are the variations in γ -ray intensities from resonance to resonance. These variations are not due to angular momentum selection rules since the resonance spins are $1/2^+$ for all the spectra. This large variation in partial radiation widths is characteristic of the Porter-Thomas distribution which is expected for a complicated nucleus whose properties vary statistically.

The results of various calculations of the neutron binding energy vary between 4779 and 4983 keV as shown by the bar labelled B_n . Groshev^[6] has reported a 4920 keV transition in thermal capture which was not confirmed in this experiment. Weak γ -ray peaks are observed at 4889 and 4862 keV in the 23.4 and 21.8 eV resonances, respectively. Unfortunately, these peaks are only partially resolved from the full energy peaks of other γ rays, and a definite statement that the neutron binding energy exceeds 4889 keV is not justified at this time.

A total of 30 γ rays with energies greater than 2.9 MeV were observed in the various spectra and are listed in Table III along with the deduced partial radiation widths. The γ -ray energies labelled with the symbol F were determined from the full energy peaks; the unlabelled from the double escape peaks. The partial widths were determined by normalizing the relative intensity of the 3.94 MeV γ ray observed in thermal capture to absolute intensity of 0.5 photons per 100 captures given by Groshev.^[6] The total radiation width of each resonance was taken to be 26 meV. The listed errors contain only the statistical uncertainty in the γ -ray peak areas. The absolute error is probably a factor of 2. The strongest γ ray has a width of 400 μ eV.

The ground state spin and parity of thorium-233 is expected to be $1/2^+$ or $7/2^-$ ^[8] based on the Nilsson Model. The $1/2^+$ states would be populated by primary M-1 transitions from the capturing state while the $7/2^-$ states require E-3 transitions. The observation of weak γ rays near the expected neutron binding energy is evidence for the $1/2^+$ assignment. No strong γ rays are observed within ~ 500 keV of the expected ground state transition. If the observed strong γ rays are electric dipole, then the negative parity $1/2^-$ and $3/2^-$ states are located above 500 keV excitation energy. This is similar to the situation observed in U-239.

Asghar, et al.^[9] have measured the total radiation width of the 23.4 eV resonance to be 29.9 meV, which is 39% larger than the mean width of 21.5 meV. This difference was attributed to the Porter-Thomas fluctuation of a few high energy γ rays. Our measurements indicate that the high energy γ rays contribute only 5% of the required increase in the total radiation width of the 23.4 eV resonance, thus supporting the value of 22 meV for the total radiation width of this resonance as measured by Bhat and Chrien.^[10]

In summary, we have measured the partial capture cross section of 27 γ rays in iron and found most of them to follow a $1/v$ dependence. In thorium the γ -ray spectra for the 4 lowest energy S-wave resonances demonstrated large fluctuations in the partial radiation widths.

References

1. R. E. Chrien and M. Reich, Nucl. Instr. and Methods 53, 93 (1967).
2. J. A. Moore, H. Palevsky, and R. E. Chrien, Phys. Rev. 132, 801 (1963).
3. L. V. Groshev, A. M. Demidov, G. A. Kotel'nikov, and V. N. Lutsenko, Izv. ANSSSR ser. fiz. 28, 1234 (1964), transl. Bull. Acad. Sci. Phys. Ser., p. 1132.
4. G. A. Bartholomew, A. Doveika, K. M. Eastwood, S. Monaro, L. V. Groshev, A. M. Demidov, V. I. Pelekhov, and L. L. Sokolovskii, Nuclear Data, Section A, 3, 502 (1967).
5. R. C. Greenwood (private communication).
6. L. V. Groshev, A. M. Demidov, V. N. Lutsenko, V. I. Pelekhov, Atlas of γ -Ray Spectra from Radiative Capture of Thermal Neutrons, Pergamon Press, New York, 1959.
7. R. C. Greenwood and J. H. Reed, IITR1-1193-53, Vol. I (1965).
8. E. K. Hyde, I. Perlman, and G. T. Seaborg, The Nuclear Properties of the Heavy Elements, Vol. 1, p. 168, Prentice-Hall, Inc., Englewood Cliffs, New Jersey, 1967.
9. M. Asghar, C. M. Chaffey, M. C. Moxon, N. J. Pattenden, E. R. Rae, and C. A. Uttley, Nucl. Phys. 76, 196 (1966).
10. M. R. Bhat and R. E. Chrien, Phys. Rev. 155, No. 4, 1362 (1967).

Table I
Iron Partial Capture Cross Sections (mb)

E_{γ} , keV	Neutron Energy Range (eV)						
	Thermal	5.67	53.6	136	243	540	2700
7645.4	571 + 19	38.5 + 1	11.7 + 0.3	6.8 + 0.4	4.3 + 0.3	3.0 + 0.2	1.2 + 0.14
7631.0	666 + 21	44.8 + 1	13.9 + 0.3	8.2 + 0.4	6.5 + 0.3	3.6 + 0.2	1.9 + 0.18
7511.4	< 1	< 0.1	< 0.05	< 0.10	< 0.10	< 0.10	0.22 + 0.10
7279.2	128 + 6	8.0 + 0.5	2.5 + 0.15	1.6 + 0.3	1.0 + 0.2	0.7 + 0.1	0.18 + 0.06
6507.0	3 + 1	0.67 + 0.18	< 0.1	< 0.10	< 0.10	< 0.10	< 0.10
6382.2	14 + 2	1.0 + 0.2	0.3 + 0.06	0.16 + 0.12	0.15 + 0.10	< 0.10	0.41 + 0.11
6020.0	193 + 4	12.7 + 0.35	4 + 0.1	2.4 + 0.2	1.6 + 0.2	1.1 + 0.2	0.32 + 0.09
5922.0	184 + 4	12.5 + 0.35	3.9 + 0.1	2.2 + 0.2	1.5 + 0.2	1.2 + 0.2	0.58 + 0.12
4950.8	16 + 2	1.3 + 0.2	0.33 + 0.05	0.30 + 0.12	0.22 + 0.11	0.2 + 0.1	0.12 + 0.05
4811.7	30 + 3	2.0 + 0.3	0.69 + 0.08	0.38 + 0.14	0.41 + 0.15	0.08 + 0.07	0.07 + 0.06
* 4676.4	7.2 + 1.5	0.4 + 0.15	0.16 + 0.05	0.27 + 0.12	< 0.10	0.22 + 0.11	< 0.10
4463.0	13 + 2	1.0 + 0.2	0.28 + 0.04	0.31 + 0.13	< 0.10	0.16 + 0.09	0.09 + 0.06
4408.0	32 + 2	1.8 + 0.2	0.58 + 0.05	0.65 + 0.16	0.26 + 0.10	0.27 + 0.09	< 0.10
4276.8	7 + 2	0.35 + 0.15	0.24 + 0.04	< 0.10	< 0.10	0.25 + 0.10	< 0.10
4220.0	76 + 4	5.0 + 0.3	1.5 + 0.08	1.05 + 0.21	0.59 + 0.16	0.48 + 0.10	0.06 + 0.06
* 4014.2	8 + 2	0.48 + 0.17	0.14 + 0.05	0.15 + 0.14	< 0.2	< 0.15	< 0.10
3856.6	26 + 4	2.3 + 0.3	0.60 + 0.08	0.23 + 0.13	0.32 + 0.14	< 0.15	< 0.10
* 3794.6	5 + 2	.58 + 0.2	0.14 + 0.05	< 0.15	0.2 + 0.2	< 0.15	0.09 + 0.07
* 3780.0	6.4 + 1.5	.81 + 0.2	0.18 + 0.05	0.13 + 0.14	< 0.2	< 0.15	< 0.10
3745.3	7 + 2	0.49 + 0.19	0.17 + 0.05	< 0.15	< 0.2	< 0.15	< 0.10
3721.3	3.4 + 1.4	2.0 + 0.2	0.08 + 0.05	0.18 + 0.15	0.25 + 0.20	< 0.15	< 0.10
3508.4	4.7 + 1.6	< 0.2	< 0.05	< 0.15	< 0.2	< 0.15	< 0.10
* 3490.0	11 + 2	0.5 + 0.2	0.22 + 0.06	< 0.15	< 0.2	0.20 + 0.13	< 0.10
3439.0	35 + 3	2.1 + 0.25	0.75 + 0.10	< 0.15	< 0.2	< 0.15	< 0.10
* 3415.7	35 + 3	1.7 + 0.2	0.54 + 0.09	0.53 + 0.15	< 0.2	0.21 + 0.14	< 0.10
* 3358.0	7.6 + 1.7	0.58 + 0.18	< 0.05	< 0.15	< 0.2	0.14 + 0.14	0.22 + 0.09
3267.7	23 + 14	1.35 + 0.3	0.51 + 0.14	< 0.15	0.4 + 0.2	0.16 + 0.12	0.16 + 0.10

* Non-primary γ ray.

Table II

Partial Radiation Widths of 1167 eV Resonance

E_{γ} , keV	Width (meV) $\Gamma_{\gamma i}$
7645.4	106 ± 7
7631.0	208 ± 9
7511.4	14.5 ± 3.0
7279.2	4.6 ± 1.7
6507.0	5.5 ± 1.0
6382.2	76.0 ± 2.4
6020.0	7.5 ± 1.6
5922.0	16.2 ± 2.3
4950.8	12.3 ± 2.1
4811.7	< 1.0
* 4676.4	(3.2 ± 1.2)
4463	12.1 ± 2.3
4408	3.6 ± 1.4
4276.8	2.8 ± 1.4
4220.0	2.8 ± 1.4
* 4014.2	(< 1.0)
3856.6	2.6 ± 1.9
* 3794.6	(< 1.0)
* 3780.0	(4.7 ± 2.0)
3745.3	< 1.0
3721.3	3.9 ± 2.1
3508.4	< 1.0
* 3490.0	(< 1.0)
3439.0	< 1.0
* 3415.7	(2.2 ± 1.6)
* 3358.0	(2.9 ± 1.6)
3267.0	3.9 ± 2.5

* Non-primary γ ray.

Table III

Thorium γ -ray Energies and Partial Radiation Widths for
the Indicated Neutron Energies

E_{γ}, keV^c	$\Gamma_{\gamma j}, \mu\text{eV}$				
	$< 1 \text{ eV}^b$	21.8 eV	23.4 eV	59.5 eV	69.1 eV
2965.0 F	< 8	49 ± 20	47 ± 20	< 20	< 20
2979.2 F	< 8	122 ± 22	< 8	< 25	< 20
a 3113.4 F or 4135.4	< 8	55 ± 21	42 ± 20	130 ± 22	< 25
3145.0 F	55 ± 10	< 18	< 18	< 25	< 22
a 3261.7 F or 4283.7	15 ± 8	39 ± 26	88 ± 20	< 28	52 ± 26
3305.6 F	< 13	39 ± 26	78 ± 22	< 40	< 20
a 3319.8 F or 4341.8	< 13	50 ± 26	< 20	< 28	52 ± 26
3336.6 F	17 ± 10	29 ± 26	166 ± 25	< 28	< 18
a 3349.5 F or 4371.5	< 10	50 ± 25	55 ± 20	177 ± 30	< 20
a 3393.3 F or 4415.3	20 ± 10	< 20	44 ± 20	88 ± 30	< 18
3430.0 F	75 ± 10	< 20	42 ± 20	< 28	< 18
3459.1 F	< 10	< 25	< 20	148 ± 30	52 ± 20
3473.3 F	135 ± 20	< 20	< 20	< 16	70 ± 20
a 3501.3 F or 4523.3	36 ± 10	< 20	42 ± 20	< 16	< 18
3525.0 F	67 ± 12	60 ± 26	20 ± 20	< 31	< 18
3733.9 F	< 8	< 20	< 18	88 ± 30	< 20
3833.0	88 ± 13	< 39	< 20	117 ± 50	208 ± 40
3856.7	82 ± 13	122 ± 30	166 ± 25	116 ± 50	205 ± 45
3877.4	77 ± 13	< 20	122 ± 25	< 30	< 25
3891.6	< 10	31 ± 20	122 ± 25	< 28	< 25
3951.0	130 ± 15	143 ± 26	< 20	< 28	< 25
3967.7	< 8	39 ± 20	88 ± 26	< 28	< 20
4033.5	< 8	42 ± 26	120 ± 25	< 28	52 ± 20
4043.8	60 ± 15	123 ± 26	167 ± 25	88 ± 45	52 ± 20
4069.6	55 ± 12	20 ± 20	80 ± 26	< 30	78 ± 26
4103.1	20 ± 10	151 ± 20	400 ± 40	< 28	34 ± 26
4198.6	78 ± 10	50 ± 26	55 ± 28	90 ± 30	< 26
4212.8	81 ± 15	180 ± 30	275 ± 30	57 ± 30	310 ± 30
4243.8	78 ± 20	112 ± 26	55 ± 26	90 ± 30	104 ± 26
4861.7	< 8	60 ± 29	< 10	< 15	< 20
4888.8	< 8	30 ± 26	31 ± 20	29 ± 20	< 20

^a Either a full energy peak or a double escape peak.

^b "Effective" width

^c $\pm 2.0 \text{ keV}$

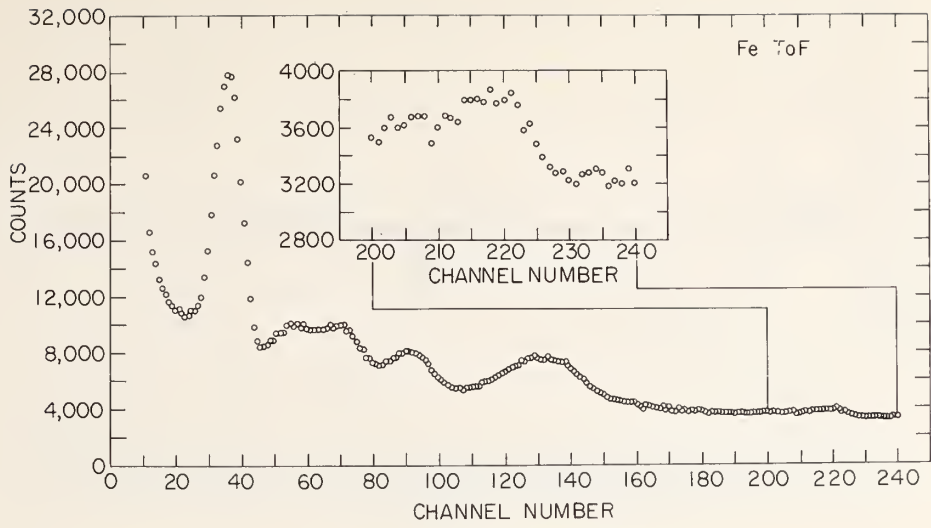


Figure 1. Iron time-of-flight spectrum.

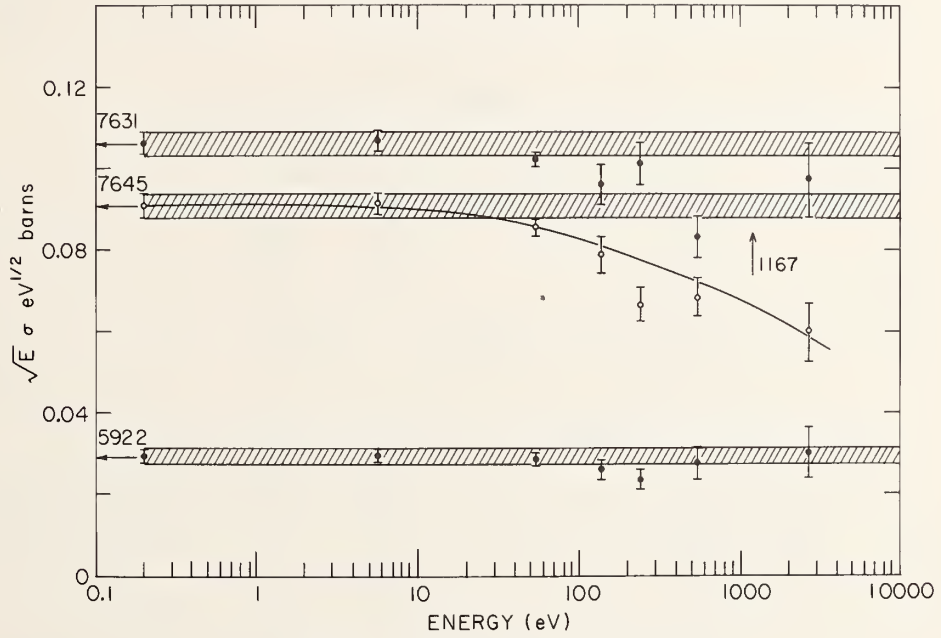


Figure 2. Iron partial capture cross sections.

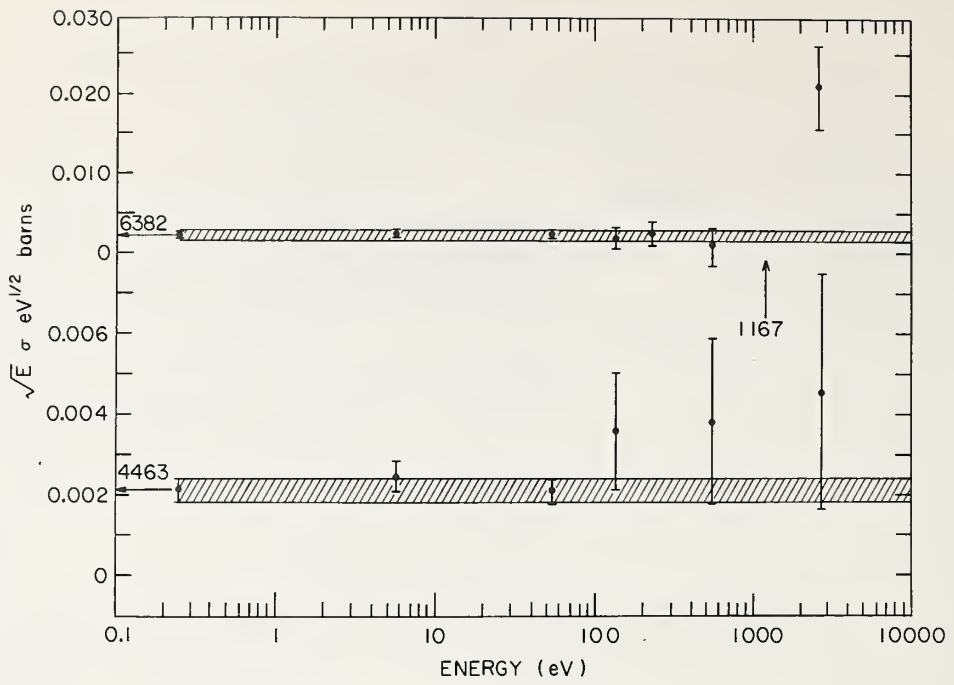


Figure 3. Iron partial capture cross sections.

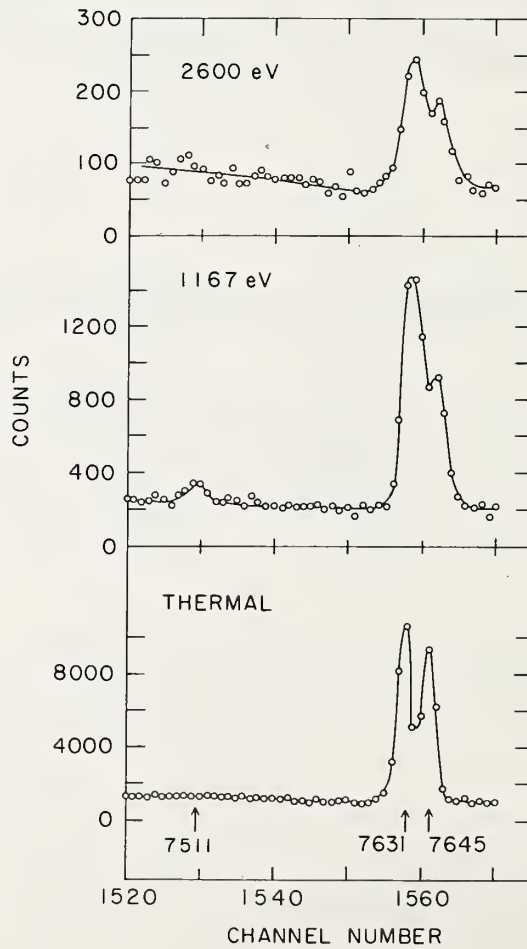


Figure 4. Iron γ -ray spectra.

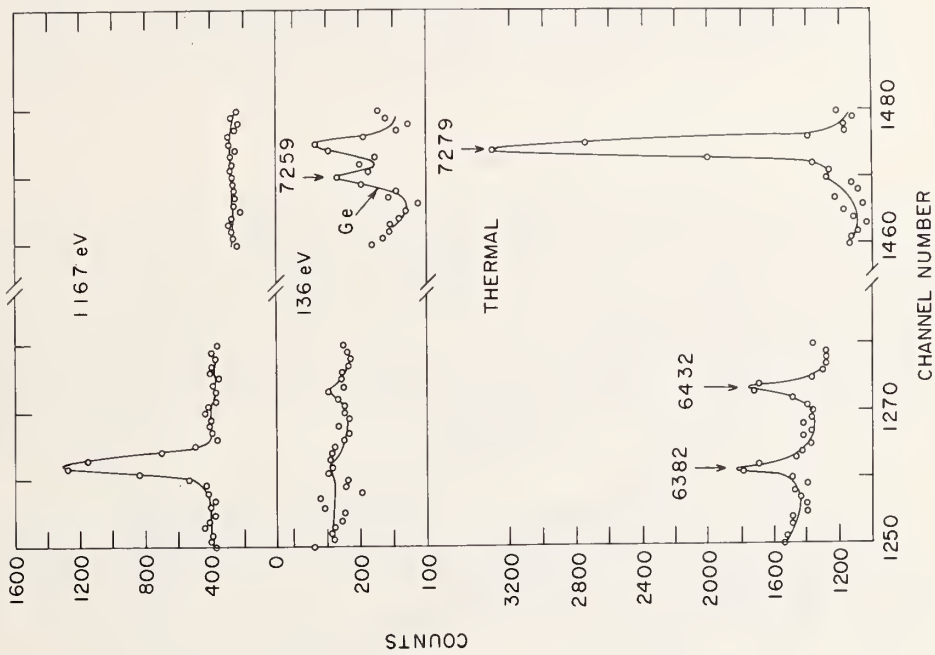


Figure 5. Iron Y-ray spectra.

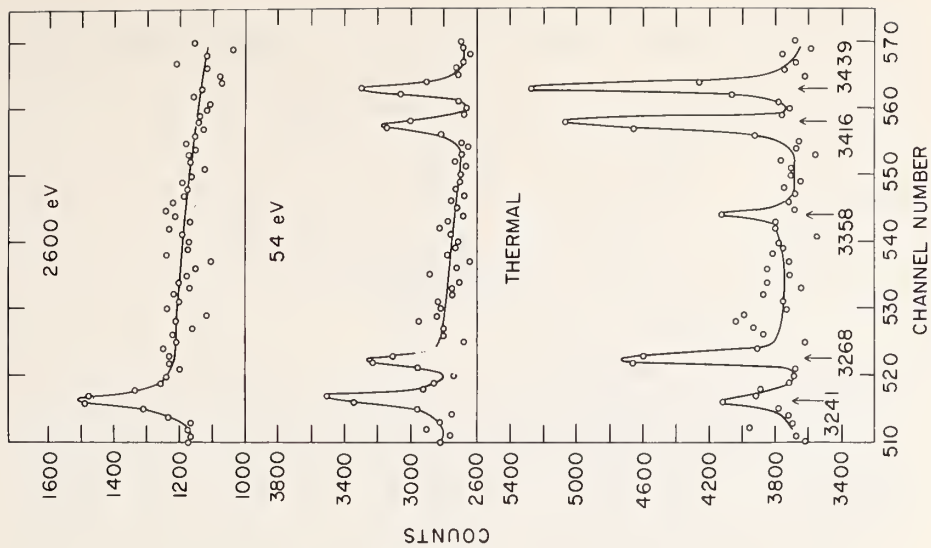


Figure 6. Iron Y-ray spectra.

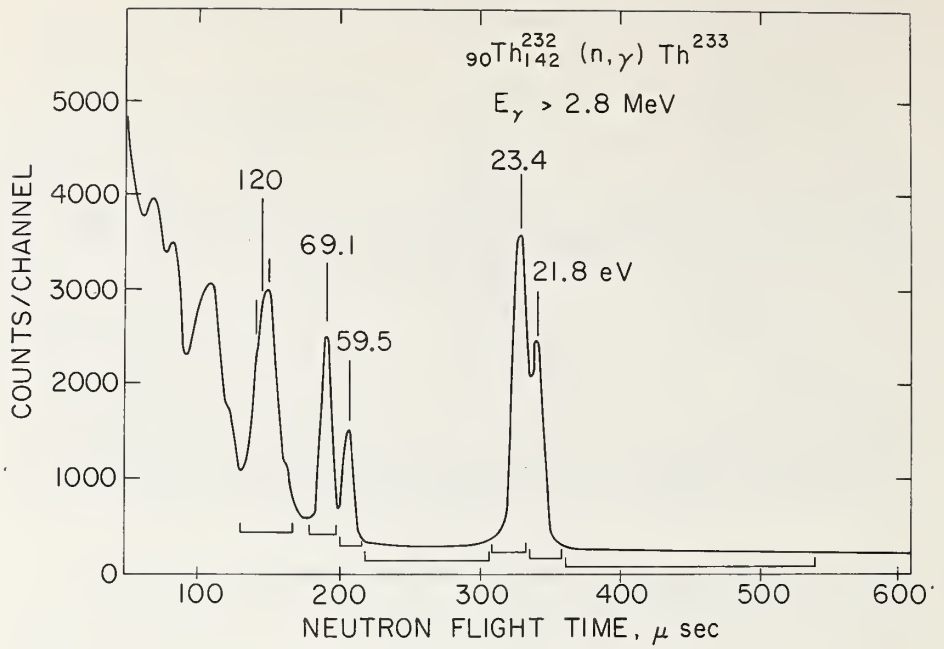


Figure 7. Thorium time-of-flight spectrum.

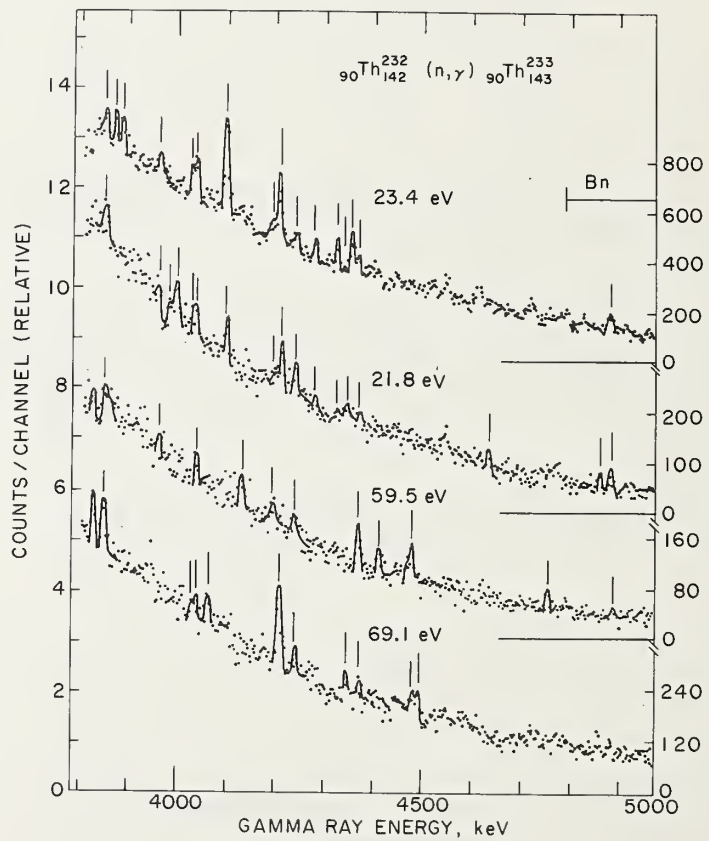


Figure 8. Thorium γ -ray spectra.

TOTAL NEUTRON CROSS SECTION AND RESONANCE PARAMETERS FOR ^{147}Pm

G. J. Kirouac, H. M. Eiland, R. E. Slovacek,

C. A. Conrad and K. W. Seemann

Knolls Atomic Power Laboratory*

Schenectady, New York 12301

ABSTRACT

The total cross section of ^{147}Pm has been determined by transmission measurements on four $^{147}\text{Pm}_2\text{O}_3$ samples over the energy interval 0.008 to 200 eV. The samples contained about 1.6 percent of the decay product ^{147}Sm . The experimental resolution varied from 0.10 μ sec/m at 1.5 eV to about 0.05 μ sec/m at 200 eV. The methods of shape and area analysis were used to obtain the resonance parameters. From these parameters, the following data have been derived: an S-wave level spacing 6.8 ± 1.5 eV, and average S-wave strength function of $(3.1 \pm 0.8) \times 10^{-4}$, and a capture resonance integral of 2300 ± 260 barns.

1. INTRODUCTION

The isotope ^{147}Pm (2.62 years) is formed in the thermal fission of ^{235}U with a yield of about 2.5 percent.[1] Neutron capture in ^{147}Pm leads to the formation of ^{148}Pm (5.4 days) or ^{148m}Pm (41.5 days) with roughly equal probabilities. A large thermal capture cross section (29,000 barns) has been reported for the isomeric state ^{148m}Pm . [2] Subsequent neutron capture produces ^{149}Pm which beta-decays to ^{149}Sm , an important reactor poison (40,000 barns). [3] Thus ^{147}Pm thermal and resonance neutron cross sections are of considerable interest in the design of long-lived reactor power sources.

Previous measurements of the ^{147}Pm thermal cross section are in significant disagreement; published values [3] range from 60 barns to 200 barns. Neutron resonance parameters for ^{147}Pm were previously obtained by Harvey, et al. [4] Due to the presence of considerable amounts of ^{147}Sm and Am in their samples, the analysis only extends to about 50 eV.

In order to remove some of the uncertainty associated with ^{147}Pm cross sections, we have undertaken the measurement of the total cross section from thermal energies up through the resonance region. Resonance

* Operated by the United States Atomic Energy Commission by the General Electric Company, Contract No. W-31-109-Eng.-52.

parameters up to 120 eV have been obtained from the shape and area analysis of transmission data. The capture resonance integral has been calculated from the resonance parameters. Values were also obtained for the average level spacing and the S-wave strength function.

2. EXPERIMENTAL DESCRIPTION

The total cross section measurements for ^{147}Pm were performed in two different experimental arrangements; the initial measurements, covering the resonance region, were performed at the Rensselaer Linear Accelerator and the thermal cross section measurements were made at the Knolls Laboratory about five weeks later.

Four samples containing $^{147}\text{Pm}_2\text{O}_3$ and Al powder were compacted to form targets with dimensions 2.54 cm \times 0.889 cm \times 0.305 cm. The 2.54 cm \times 0.889 cm face was perpendicular to the neutron beam for all measurements. The four samples had ^{147}Pm concentrations of 0.0135, 0.0337, 0.264 and 0.686 atoms/K barn. The two thinner samples were made by depositing Pm_2O_3 on a bulk carrier of finely divided MgO particles. The MgO carrier was then mixed with Al powder and pressed into target compacts. The compacted samples were encapsulated in 0.003 in Cu and sealed by soldering. After leak testing, the copper covered samples were placed in secondary containers made of 0.010 in Al and sealed with an O-ring.

After the transmission measurements were finished, the four samples were dissolved and the ^{147}Pm and ^{147}Sm concentrations were redetermined. Two techniques were employed: liquid scintillation β -counting, and mass spectrographic analysis. The results of the two independent evaluations agreed within 3 percent. Extrapolating to the time of the resonance measurements, a concentration of 1.6 percent was obtained for the ^{147}Sm . This agrees with the area analysis of the 18.4 eV ^{147}Sm resonance which gave 1.7 percent using recommended resonance parameters. [3]

Transmission measurements in the energy range 0.007 eV - 1.5 eV were made at the Knolls Laboratory using a small research reactor. A neutron chopper (14 cm dia. \times 0.1 cm slits) was operated at 20 cps with a 12m flight path. BF_3 tubes, 2 in dia. \times 12 in, were used end-on as neutron detectors. The two thicker ^{147}Pm samples were used back-to-back to provide a target with a thickness 0.950 atoms/K barn. The experimental resolution, $\Delta E/E$, varied from 3.5 percent at 0.008 eV to 50 percent at 1.5 eV.

The thermal transmission measurements were conducted over a total period of three weeks starting about eight weeks after the chemical separation. During the measurement, sample, blank and background runs were alternated every hour. A fission chamber was used as a beam monitor to normalize different runs. Periodic runs were made with a standard Au foil. The Au cross section agreed with published values [3] within 1 percent and no systematic experimental bias was revealed. The final transmission data required a total impurity correction of about 6 percent; most of this correction was due to the Al powder in the sample and the oxygen in Pm_2O_3 .

The measurements in the resonance region were performed at RPI using the linear electron accelerator. The energy range 1.5 eV to 20 eV was sorted into 1024 time channels, 1 μ sec wide; a second analyzer with 0.5 μ sec channels was used from 10 eV to 500 eV. The accelerator was

operated at 240 cps with 0.5 μ sec electron bursts. A tungsten target was used to produce the neutrons which were slowed-down in a thin polyethylene moderator assembly. The flight path was 24.7m long and the neutrons were detected in seven layers of 1 in dia. BF₃ tubes, placed with the tube axis perpendicular to the neutron beam. Separate pre-amps, amplifiers and single-channel pulse-height analyzers were used for each detector layer. Extensive circuitry was employed to add a variable time-delay to the signals from each layer of detectors. The delay was chosen to equate the time of neutron detection in each layer of counters to the time of arrival for neutrons of that energy in the last layer of tubes. Thus the ΔL uncertainty for the seven layers is limited to the ΔL of a single tube. The experimental resolution for various energy ranges is summarized in Table I.

An automatic sample changer permitted the four ¹⁴⁷Pm samples, a blank position and a "notch filter" of Mn, Au and Co to be alternated in the beam every 30 minutes. Individual runs were normalized by means of a thin fission-chamber beam monitor. An exponential function was fitted to the background counting data from the "notch-filter". The background was about 3 percent and was determined to a precision of about 15 percent. Time-delays which determine the triggering of the two time analyzers were calibrated by using the channel locations of resonances observed in the spectrum from a natural Uranium sample. The statistical precision of the final transmission data was about 3 percent.

3. EXPERIMENTAL RESULTS

Transmission data have been obtained from 1.5 eV to 200 eV and neutron resonance parameters have been derived to 120 eV. An additional negative energy resonance has been postulated to explain the magnitude of the thermal capture cross section. Resonances below 10 eV have been analyzed by both shape and area methods. The computer codes developed by Harvey and Atta[5] were used. Above 10 eV only area analysis was used; a constant value of 73 mV for Γ_γ , obtained from the shape analysis of low energy resonances, was assumed. Resonance parameters obtained above 80 eV may be due to multiple unresolved resonances. The resonance parameters for ¹⁴⁷Pm are listed in Table II. The weak resonance observed by Harvey et al.[4] at 1.04 eV has been included in this compilation, although the resonance could not be seen in the present results due to the poor resolution at this energy.

The total cross section for ¹⁴⁷Pm below 1.5 eV is shown in Figure 1. A 2200 m/sec value of 212 ± 9 barns has been obtained from a least squares fit. The non-symmetrical error includes an uncertainty of 3 barns due to an estimated maximum H₂O contamination. The total cross section derived from resonance parameters (including the negative energy resonance) is shown by a solid line in Figure 1.

Transmission data from 1.5 eV to 200 eV are shown in Figure 2. The solid lines were calculated using the resonance parameters of Table II. Dashed lines represent visual fits. Throughout the analysis a value of 8 barns has been assumed for the potential scattering cross section. Of the 19 resonances observed between 1.5 eV and 115 eV, 6 resonances have been assigned to the sample contaminant ¹⁴⁷Sm. Resonances observed above 115 eV cannot be assigned with certainty to ¹⁴⁷Pm. Three of these resonances agree with the reported energies of the three known ¹⁴⁷Sm resonances above 100 eV.[6]

Figure 3 illustrates the graphical determination of the spacing of S-wave resonances and the strength function. These data indicate a level spacing of 6.8 ± 1.5 eV and an average S-wave strength function of $(3.1 \pm 0.8) \times 10^{-4}$.

The resonance parameters of Table II have been used to calculate the absorption resonance integral. The result obtained for a low energy cutoff of 0.5 eV was 2300 ± 260 barns. A contribution of 108 barns for unresolved resonances was calculated from the average neutron parameters. About 72 percent of the resonance integral was due to the 5.36 eV resonance.

4. DISCUSSION

Extensive precautions were taken to prevent H₂O contamination of the samples. The target used for thermal measurements was fired at 925°C, allowed to cool and placed in a desiccator for 24 hours before the double encapsulation. A similar sample, not sealed in Cu and Al, was followed for six weeks to observe any weight change due to H₂O absorption. No change was detected while the sample remained in the desiccator. During a period of six hours when the sample was deliberately exposed to the atmosphere, a weight gain of 2 milligrams occurred. This period was longer than the actual sample was exposed during encapsulation. The observed weight gain was used to calculate a maximum uncertainty of 3 barns in the 2200 m/sec ¹⁴⁷Pm cross section due to H₂O.

Neutron resonances above 120 eV have not yet been analyzed. The energies of levels reported in Table II do not correspond to any known ¹⁴⁷Sm resonances.[6] The level spacing above 115 eV is only slightly more than that observed below 85 eV. This result suggests about four missed levels in the energy interval 85-115 eV. It is possible that moderately strong ¹⁴⁷Pm resonances between 90-105 eV could go unobserved due to the presence of strong ¹⁴⁷Sm resonances at 95 eV and 99 eV in our data. In fact, three of the resonances tentatively assigned to ¹⁴⁷Sm (82.5, 95.4 and 99.5 eV) appear to be too strong to be due to ¹⁴⁷Sm alone. This is true, to a lesser extent, for the 39.9 eV resonance presumed to be due to ¹⁴⁷Sm. The analysis of these levels is continuing.

5. APPENDIX

Chemical separation and extensive chemical and mass spectrometric analyses were performed at the Knolls Laboratory. Initially 5.1 grams of oxide containing 77 percent Pm₂O₃ and 23 percent Sm₂O₃ were obtained from the Oak Ridge Isotope Center. The target preparation consisted of the following steps:

1. Chemical separation of Pm from Sm by a standard ion exchange technique.
2. Conversion of Pm to the oxide Pm₂O₃.
3. Deposition of Pm₂O₃ on MgO for the two thinner samples.
4. Mixing with Al powder and pressing wafers.

The chemical separation was completed three weeks before the transmission measurements in the resonance region were finished. A 2 gram "center-cut fraction" of high purity ¹⁴⁷Pm was obtained. Mass spectrometric analysis of this product indicated less than 3 ppm of ¹⁴⁹Sm, less than 0.05 percent of ¹⁴⁷Sm, and negligible fractions of other rare earths. The material was converted to the oxide by precipitating the oxalate Pm₂(C₂O₄)₃ and firing in O₂ at 925°C.

The deposition of Pm_2O_3 on MgO was performed by dissolving Pm_2O_3 and slurring it with 1 gram of finely divided MgO while simultaneously precipitating the Pm as the hydroxide by adding ammonia. The Pm was absorbed on the MgO particles which act as a bulk carrier of the Pm. The MgO carrier was fired and pulverized, and weighed amounts were mixed with Al powder and pressed into compacts. The two thicker samples were made by mixing Pm_2O_3 directly with Al powder and pressing.

6. REFERENCES

1. E. P. Steinberg and L. W. Glendenin, Proc. Int. Conf. Peaceful Uses Atom. Energy 1955 7, 3 (1956).
2. R. P. Schuman and J. R. Barreth, Nucl. Sci. Engng. 12, 519 (1962).
3. M. D. Goldberg, et al., Neutron Cross Sections, BNL 325, 2nd Ed., Suppl. 2 (1966).
4. J. A. Harvey, R. C. Block, G. G. Slaughter, W. J. Martin and G. W. Parker, Proc. 2nd Int. Conf. Peaceful Uses Atom. Energy 16, 150 (1958).
5. S. E. Atta and J. A. Harvey, Numerical Analysis of Neutron Resonances, ORNL-3205 (1962).
6. E. M. Bowey and J. R. Bird, Nuclear Physics 5, 294 (1957).

TABLE I

SUMMARY OF SAMPLE THICKNESSES AND EXPERIMENTAL RESOLUTION

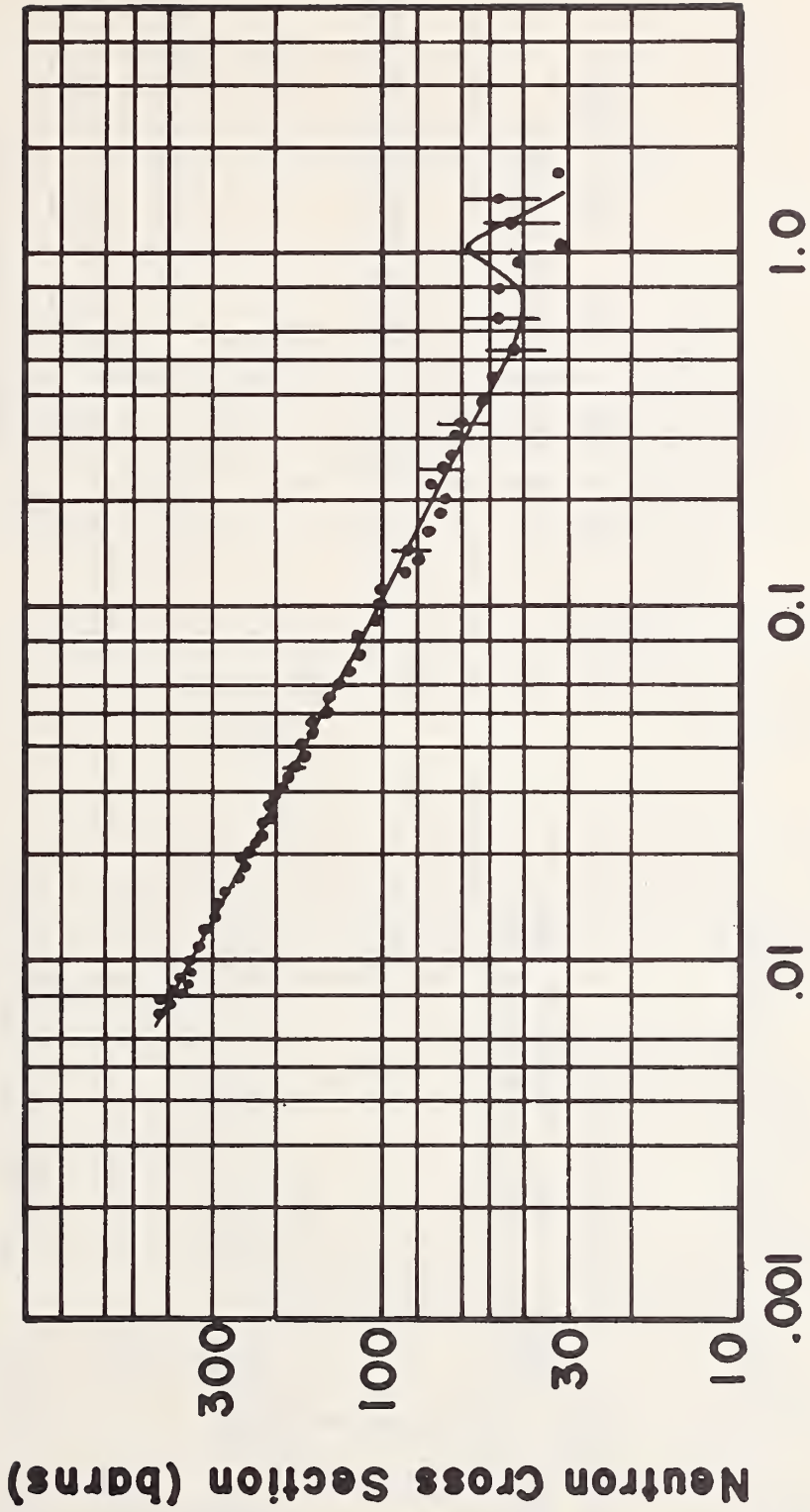
Energy Range (eV)	N (atoms/Kb)	Resolution μ sec/m
0.008 - 1.5	0.950	13
1.5 - 10	0.0135, 0.0337, 0.264	0.10 - 0.07
10 - 20	0.0337, 0.264, 0.686	0.053
20 - 200	0.264, 0.686	0.047

TABLE II

 ^{147}Pm RESONANCE PARAMETERS FROM SHAPE AND AREA ANALYSIS

E_0 (eV)	Shape Analysis		Area Analysis		Average	
	Γ_γ (mV)	$2g\Gamma_n^0$ (mV/eV $^{1/2}$)	Γ_γ (mV)	$2g\Gamma_n^0$ (mV/eV $^{1/2}$)	Γ_γ (mV)	$2g\Gamma_n^0$ (mV/eV $^{1/2}$)
-1.2	73	1.17	-	-	73	1.17
1.04 ^a	-	-	80 ^a	0.0054 ^a	80 ± 25 ^a	0.0054 ± 0.0005 ^a
5.36	67	15.1	67	15.5	67 ± 6	15.2 ± 0.80
6.57	84	0.84	84	0.75	84 ± 8	0.79 ± 0.08
6.92	68	1.95	68	1.81	68 ± 6	1.88 ± 0.14
15.1	-	-	73 ^b	0.37	73	0.37 ± 0.06
19.6	-	-	73 ^b	0.96	73	0.96 ± 0.1
29.2	-	-	73 ^b	0.44	73	0.44 ± 0.07
38.1	-	-	73 ^b	4.3	73	4.3 ± 0.8
45.6	-	-	73 ^b	3.8	73	3.8 ± 0.5
48.2	-	-	73 ^b	3.2	73	3.2 ± 0.5
52.4	-	-	73 ^b	0.26	73	0.26 ± 0.04
65.4	-	-	73 ^b	5.7	73	5.7 ± 0.6
85.5	-	-	73 ^b	3.8	73	3.8 ± .8
115.	-	-	73 ^b	7.5	73	7.5 ± 1.5
131	-	-	-	-	-	-
145	-	-	-	-	-	-
148	-	-	-	-	-	-
154	-	-	-	-	-	-
173	-	-	-	-	-	-
179	-	-	-	-	-	-
189	-	-	-	-	-	-
192	-	-	-	-	-	-

^aData of J. A. Harvey, et al. [4]^b Γ_γ of 73 mV assumed from analysis of 3 low energy levels.^cUncertainties in resonance energies are <1%.



Neutron Energy (eV)

Figure 1

Total Cross Section for ^{147}Pm from .008eV to 1.5eV.

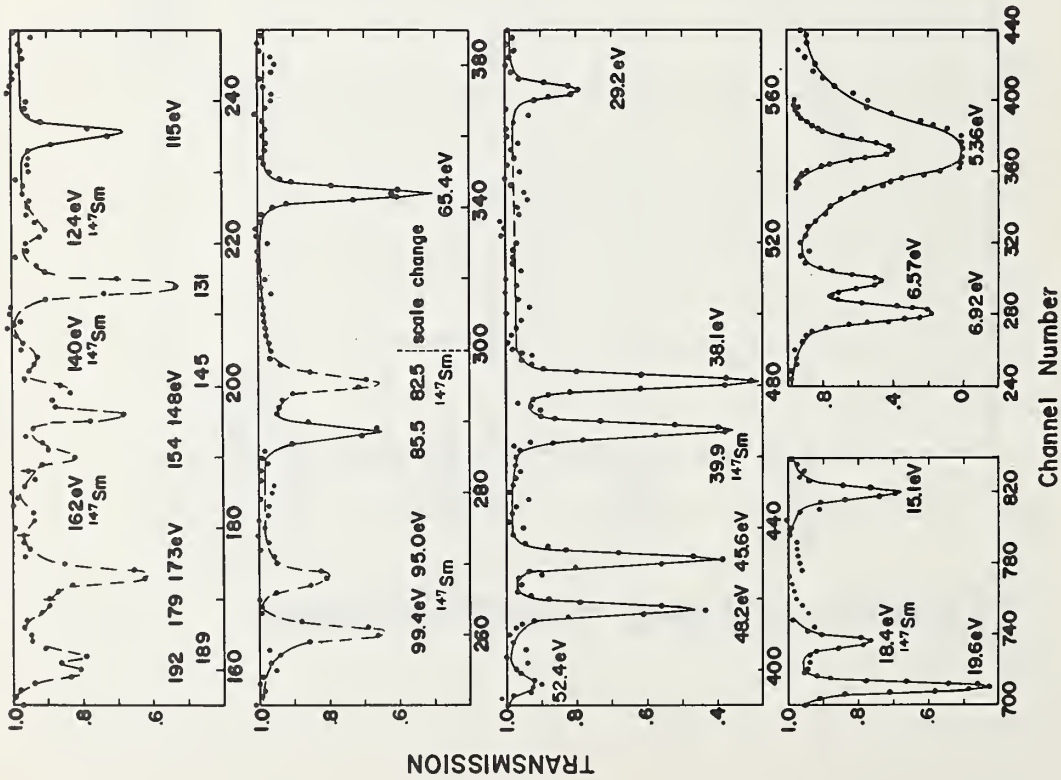


Figure 2

Transmission Data for ^{147}Pm . The solid lines are calculated from resonance parameters. The dashed lines are visual fits

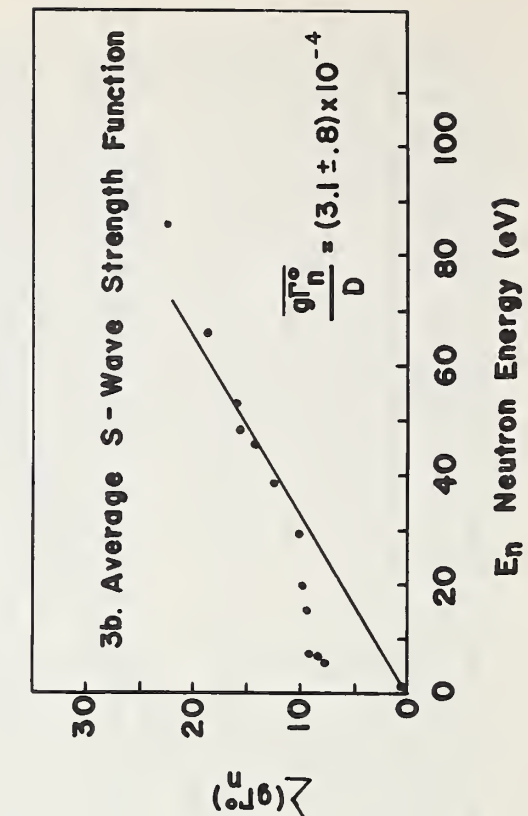
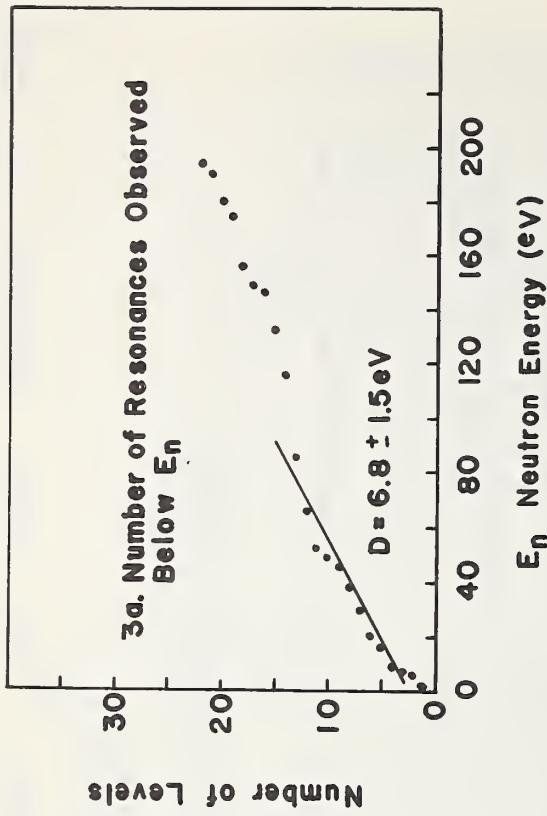


Figure 3

Average Level Spacing and S-Wave Strength Function for ^{147}Pm

S. J. Friesenhahn, W. M. Lopez, F. H. Fröhner,
A. D. Carlson and D. G. Costello

Gulf General Atomic Incorporated
San Diego, California 92101

ABSTRACT

Knowledge of the sodium cross section in the keV region is of prime importance because of its use as a coolant in fast breeder reactors. The total cross section of sodium has been thoroughly investigated; however, with the exception of the thermal region, little data exist on the capture cross section. Recent measurements of the radiation width of the 2.85-keV resonance have led to results that are difficult to reconcile with the thermal capture cross section.

Measurements have been performed at Gulf General Atomic in an attempt to resolve this discrepancy. Preliminary results have yielded the radiation width (0.34 eV) expected from the thermal capture cross section and the capture yield is consistent with that expected from a single level.

Since the neutron width is more than one thousand times larger than the radiation width, this level presents a severe test of the methods used to measure capture areas and to calculate the effects of multiple scattering. The results from the three investigators are compared, and the discrepancies are discussed in an attempt to expedite future capture measurements on very strong levels.

*Work supported by the U. S. Atomic Energy Commission.

1. TECHNICAL DISCUSSION

Recent interest in sodium-cooled, fast breeder reactors has stimulated interest in the sodium capture cross section. The total cross section has been thoroughly investigated by many workers, and the experimental data have been analyzed by Stephenson,⁽¹⁾ employing spin-dependent radii. The cross section below 40 keV is dominated by a single level at 2.85 keV, and the theoretical fit to the total cross section is very satisfactory in the 0 to 40 keV energy region.

The thermal capture cross section has been obtained by a variety of methods, and the value recommended in BNL 325⁽²⁾ is 0.534 barns, with an estimated uncertainty of 1%. This thermal capture cross section can be used to establish an upper limit on the radiation width of the 2.85 keV resonance if one assumes the validity of the single-level formalism. Until the recent measurements at Harwell⁽³⁾ and at Rensselaer Polytechnic Institute,⁽⁴⁾ no direct measurement of the radiation width had been made. Both of these laboratories report anomalous results from their capture measurements, and hence measurements were initiated at the Linear Accelerator Facility of Gulf General Atomic in an attempt to resolve these anomalies.

An 18.59-meter flight path and a 4000-liter liquid scintillator were used to record the time history of the neutron capture events in two metallic sodium samples. The thinner of these samples approximated the sample thickness used by the other two laboratories, thus allowing a direct comparison of the data. The thicker sample was approximately three times as thick as the thin sample, and served as a check on the background and multiple scattering corrections applied to the data. The large scintillator was operated such that a coincidence is demanded between the two halves of the scintillator, thus greatly reducing background events due to single gamma rays.

Since the sodium thermal capture cross section is well known, the neutron flux at 2.85 keV was determined by normalizing the measured relative flux spectrum to yield the correct cross section at 0.0253 eV. This technique eliminates the need for a determination of the detection efficiency of the scintillator for sodium capture events. The relative neutron flux spectrum from 0.01 to 1 eV was determined employing the observed time history of capture in a .01-inch gold sample. The neutron flux was derived using the calculated capture probability in the gold. The accuracy of the calculated capture probability for gold was checked in a separate measurement⁽⁵⁾ employing the detection of capture events in a thick boron slab. The agreement was on the order of 1%. From 1 eV to 3 keV the neutron spectrum was measured with a thin $^{10}\text{BF}_3$ gas proportional counter. The over-all error in the capture area determination due to neutron flux uncertainties is on the order of 5%.

The two samples were prepared by canning pure metallic sodium metal in 0.060-inch wall graphite containers under kerosene at 110°C which was continuously bubbled with nitrogen. The sample weight was determined to an accuracy of 1% by difference weighing and destructive chemical analysis.

In Fig. 1 the measurements on the two samples are compared to calculations using $\Gamma_{\gamma} = 0.34$ eV. The other resonance parameters used in the calculations are those recommended by Stephenson:⁽¹⁾ $E_0 = 2.85$ keV, $\Gamma_n = 410$ eV, $R_+ = 5.85$ F, $\ell = 0$. Since the value of the potential-scattering cross section on the low-energy side of the resonance has an insignificant effect on the capture-area calculation, R_+ was used on both sides of the resonance. The data points exhibit no significant disagreement with the calculated curve, thus tending to confirm the radiation width expected from thermal data, and the hypothesis of a single capturing level.

Since the neutron width is approximately one-thousand times larger than the radiation width, the capture area is almost directly proportional to the radiation width, and hence the uncertainty in the radiation width is directly proportional to the uncertainty in the measured capture area. The radiation widths determined by area analysis of our data along with the results from the other two laboratories are shown in Table 1. The values

Table 1
COMPARISON OF RADIATION WIDTHS (eV)

	<u>Quoted Value</u>	<u>GGA Calculation</u>
RPI	0.60 ± 0.06	0.47 ± 0.05
Harwell	0.60	0.66
GGA	0.34 ± 0.04 0.38 ± 0.08	0.35 ± 0.04

Value expected from thermal capture cross section = .34 eV

obtained in the Gulf General Atomic measurements are in agreement with the value expected from the thermal capture cross section within the experimental errors of the measurements. Also indicated in the figure are the results of area analysis of the data points contained in (3) and (4) using the Gulf General Atomic area analysis code TACASI.⁽⁶⁾ Our analysis of the RPI data from 2 to 4 keV shows better agreement with the expected value than the RPI analysis; however, the result is still significantly high. Our analysis of the Harwell data from 1.5 to 4 keV shows excellent agreement with the expected value; however, since the uncertainties in these data were not specified, the uncertainty in the calculated value is undetermined.

In Fig. 2 the data points from the three laboratories are compared. The agreement in shape between the RPI and GGA data is fair, but the Harwell data exhibit a low-energy tail. Since the natural width of the level is large compared to all of the expected resolution width contributions, the shape of the Harwell curve should not be appreciably affected by resolution broadening. Under this assumption, the Harwell result is difficult to explain.

The discrepancy between the RPI and GGA calculations is illustrated in Fig. 3. As can be seen in the figure the largest discrepancy is on the high energy side of the resonance, where the effects of capture after one or more scattering collisions are most important. The multiple scattering correction factors to the area are 1.5 and 2.0 for the thin and thick GGA

samples respectively, and hence a precise description of multiple scattering effects is very important. The Harwell calculation is in good agreement with the GGA calculation for $\Gamma_{\gamma} = .5 \text{ eV}$.

2. CONCLUSION

The results of the Gulf General Atomic capture measurements are in agreement with calculations based on parameters obtained from total cross-section measurements and from the thermal capture cross section. The shape of the RPI data is in fair agreement with the calculated curve; however, there seems to be an error in normalization and an even larger disagreement in the calculations. The area of the Harwell measurements seems to be in disagreement with calculations and there is a shape anomaly possibly associated with the experimental apparatus.

3. REFERENCES

1. T. E. Stephenson, "The Neutron Cross Section of Sodium Below 40 keV, " BNL 961 (T-401).
2. J. B. Stehn, M. D. Goldberg, B. A. Magurno, and B. Wiernerchasman, BNL 325, Supplement No. 2, Second Edition Z = 1 to 20.
3. M. C. Moxon and N. J. Pattenden, "The Low Energy Cross Section of Sodium, " CN-23/27.
4. E. B. Guerthner, "Linear Accelerator Project Progress Report, October 1966 through December 1966, " pp. 40-48.
5. S. J. Friesenhahn, E. Haddad, F. H. Fröhner and W. M. Lopez "The Neutron Capture Cross Section of the Tungsten Isotopes from 0.01 to 10 Electron Volts, " Nucl. Sci. and Eng., 26, 487-499.
6. F. H. Fröhner, "TACASI - A FORTRAN-IV Code for Least Squares Area Analysis of Neutron Resonance Data, " USAEC Report GA-6906, General Dynamics Corporation, General Atomic Division, August 4, 1966.

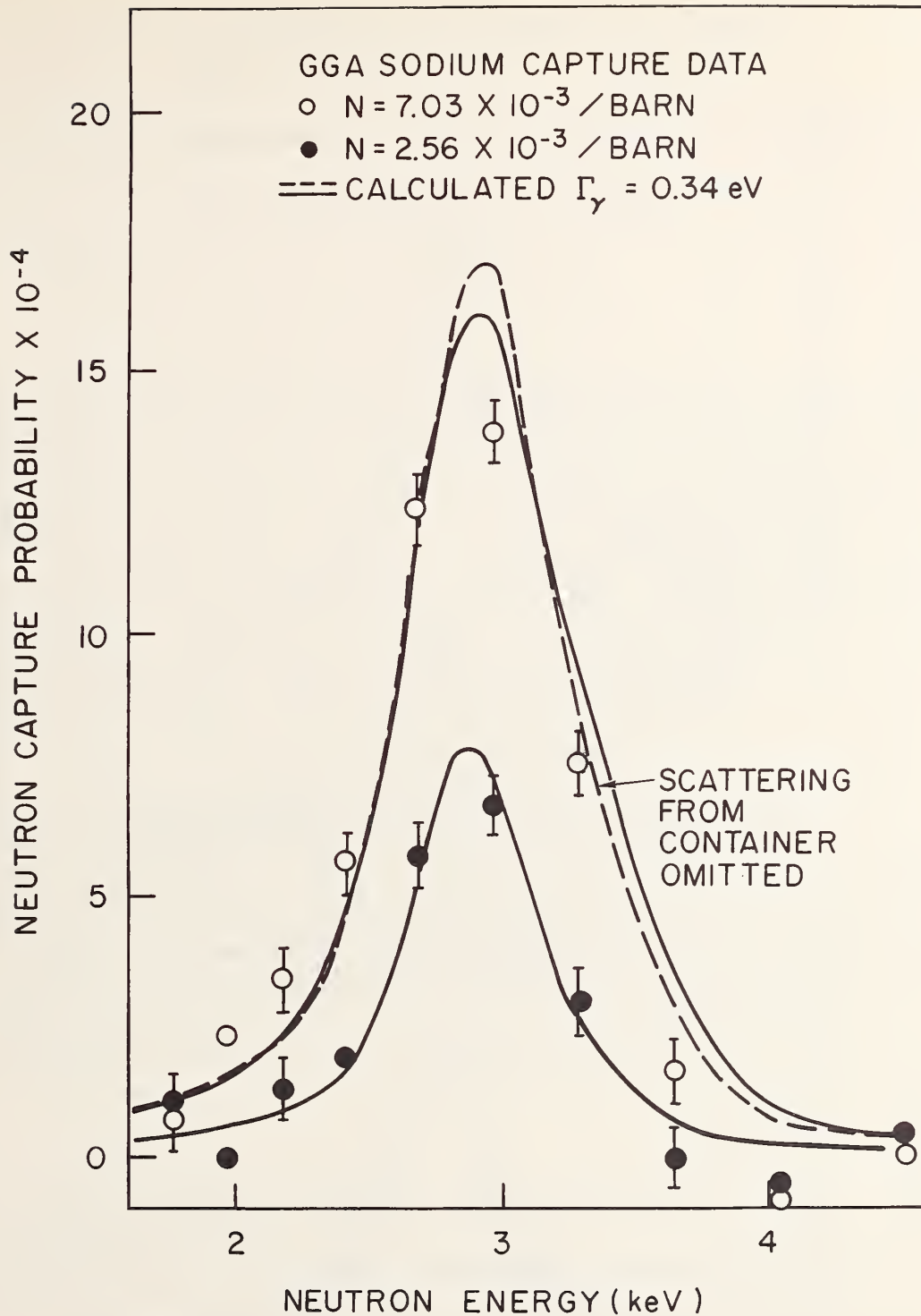


Figure 1. Comparison of calculated vs measured capture probabilities for the two samples used. The effect of omitting the container scattering in the thick sample calculation is also indicated.

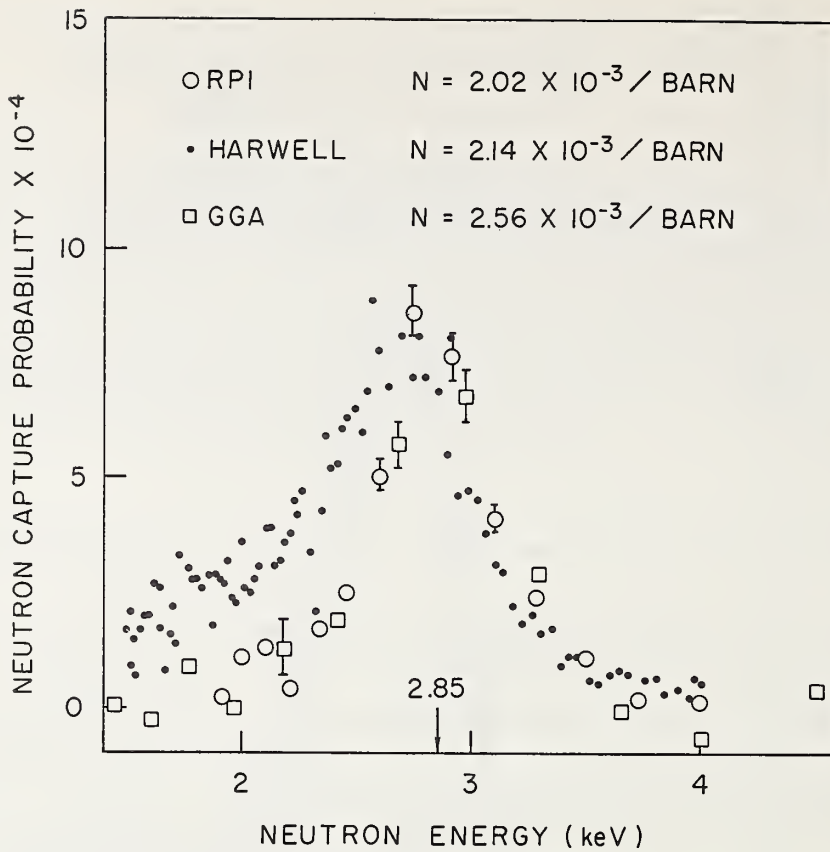


Figure 2. Comparison of capture probabilities measured by the three laboratories for approximately the same sample thickness.

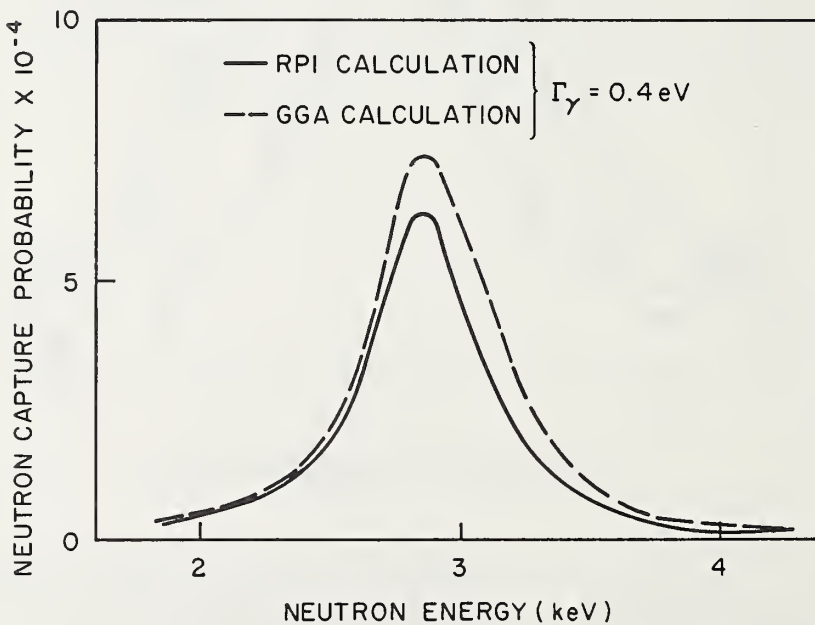


Figure 3. Comparison of RPI vs Gulf General Atomic calculation of the capture probability for a sample thickness of 2.03×10^{-3} nuclei/barn and $\Gamma_{\gamma} = 0.4 \text{ eV}$.

S. A. Cox

Argonne National Laboratory, Argonne, Illinois 60439

ABSTRACT

The status of absolute neutron capture cross sections is reviewed. During the past several years, much of the disparity which had existed between results of various investigations has been eliminated. Recent measurements at low energy (~ 30 keV) are all in good agreement and most of the high energy (~ 200 keV) measurements are in good agreement, but there is a discrepancy of $\sim 15 - 20\%$ in absolute normalization between the two regions. Systematic behavior observed in (n,p), (n, α), and (n,2n) reactions is discussed. Effects due to shell closure have been reported by several authors; however, when recent data are examined and the strong (N-Z) dependence of the cross sections is included, the interpretation in terms of shell structure becomes less clear. Gardner has derived a semi-empirical expression for calculating relative and absolute cross sections for (n,p) and (n, α) reactions. Another empirical expression for (n,p) cross section prediction has been given by Levkovskii. Some interesting systematic behavior is reported for (n,2n) reactions when the cross section corresponding to a bombarding threshold energy difference of 3 MeV are plotted against (N-Z). In the field of fast neutron scattering the vast amount of data which already exists below ~ 1.5 MeV bombarding energy is being supplemented by an ever increasing quantity of data in the region $\sim 1.5 - 10.0$ MeV. Some recent inelastic neutron scattering data obtained by both time-of-flight techniques and by Ge(Li) techniques are discussed. The role of polarization measurements in determining parameters for nuclear models is also briefly discussed. Finally some remarks are made concerning the respective roles of the cross section measurer, the cross section user, and the cross section evaluator.

* This work supported by the U.S. Atomic Energy Commission.

1. INTRODUCTION

When presented with the title of this talk, my first impression was that I was going to make a lot of people unhappy. The field of fast neutron cross sections is a large one with a great many laboratories actively engaged in it. Clearly no one could hope to cover even a small fraction of the field in half an hour. It is thus necessary for me to decide whether to touch on many areas very briefly or to cover a few in some detail. I have chosen the latter course. My choices are based on three considerations; areas of neutron cross sections with which I am somewhat familiar, areas which are of interest to the cross section user, and areas which are not discussed elsewhere in this conference. While I have tried to maintain these three criteria as guide lines throughout this talk, there are occasions where only one or another is operating. This is unavoidable since the cross section measurer and cross section user do not always have common interests or a common evaluation of the importance of the various cross section measurements. In any case, this talk will concentrate on four areas: fast neutron capture; (n,p) , (n,α) , and $(n,2n)$ reactions; fast neutron scattering; and finally a few remarks concerning the relationship between the cross section measurer, the cross section user, and the cross section evaluator.

2. NEUTRON CAPTURE CROSS SECTIONS

I would first like to turn to an area of cross section measurements in which a considerable manpower effort has been expended and in which I have had a long time interest. Just a few years ago the situation in this field was very confused. The mere mention of its name was sufficient to cause mild embarrassment and discomfort to a number of experimental physicists. I refer of course to absolute neutron capture cross section measurements. Measurements in this field have been beset by difficulties for many years, ever since, or so it seems, a measurement of a given cross section was made by more than one experimenter. Very early large discrepancies appeared in the results reported by different workers¹⁻⁵. The $\text{Au}(n,\gamma)$ cross section was the first to fall victim to the proliferation of measurements although this was by no means an isolated case. Agreement between different workers was especially poor in the region below ~ 200 keV neutron energy. In some instances the results at a given energy differed by as much as a factor of two⁵. The more commonly used techniques involved activation measurements²⁻⁵, measurements with large liquid scintillators^{1,3}, spherical shell transmission measurements⁴, and Sb-Be sources. The cross sections were normalized in various ways. In many Sb-Be activation measurements a manganese bath was used for neutron source calibrations. Other activation measurements were based on values of the U^{235} fission cross section, the $n-p$ cross section and the $\text{B}^{10}(n,\alpha)$ cross section. The high energy liquid scintillator results³, i.e., above ~ 200 keV were

based on the U^{235} fission cross section, and the liquid scintillator results below ~ 200 keV were normalized to the spherical shell measurements⁴ which in principle are independent of an absolute neutron flux determination, but the analysis must be carried out with great care. Fortunately I can report that the picture for neutron capture cross sections is not as dark as it was several years ago. A great deal of renormalization, a consistent set of standard cross sections, and re-evaluation of some experiments has resulted in much better agreement.

The situation as it existed several years ago is made clear in Fig. 1 which shows the $Au(n,\gamma)$ cross section plotted against neutron energy and includes only those measurements which were recent at the time². Earlier measurements were left out to emphasize the wide disparity in results in the low energy regions. I am sure that when presented with a picture of cross section data with such widely different results as are depicted here, the cross section user and cross section evaluator are tempted to throw up their hands in despair. However, it must be mentioned that when discrepancies of nearly a factor of two show up as they do in the data for $Au(n,\gamma)$ in the region of 100 keV, the cross section measurer is also somewhat disconcerted. Several features of the rather old data in Fig. 1 are of interest in relation to the recent advances in technique and measurement. All of the data above ~ 200 keV are normalized to the U^{235} fission cross section. Both activation and liquid scintillator results are represented. The differences which do appear in the data are due almost entirely to different choices of the fission cross section used as a standard. When the same fission cross sections are used for all of the data in this region, the differences largely disappear. Below ~ 200 keV the data group into two bands. A number of different approaches were used in determining absolute cross sections. Data were normalized to calibrated Sb-Be sources, the U^{235} fission cross sections, the $B^{10}(n,\alpha)$ cross section, manganese bath measurements and spherical shell transmission measurements. The large disparity evident in the figure has been largely alleviated by three considerations. The highest data points in the graph indicated by the open triangles, were originally based on the shape of the $B^{10}(n,\alpha)$ cross section below 200 keV. Since the data were first reported the $B^{10}(n,\alpha)$ cross section has been re-measured and the earlier data were found to be in error. When the data are corrected to the newer $B^{10}(n,\alpha)$ results, the 30 keV point is reduced $\sim 20\%$. This correction has already been made to the data shown in the slide. Another correction was made necessary when the U^{235} fission cross section was re-measured by P. H. White. This caused a further reduction of $\sim 10\%$ for all the data near 30 keV which had been normalized to the fission cross section. The third factor involved the spherical shell transmission measurements upon which all of the low energy liquid scintillator

measurements were based. Bogart⁷ has re-analyzed the sphere transmission data using Monte-carlo techniques and paying special care to the resonance self-protection correction. His calculations yielded a Au capture cross section at 24 keV which was $\sim 30\%$ higher than that originally reported. All of these considerations combined to effect a marked change in the capture cross section data. The large difference in the shape of the energy dependence which had existed between the low energy liquid scintillator and activation results was removed. The very large disparity in absolute magnitude was reduced to $\sim 20\%$. I have already mentioned that the case of gold is not unique. Before discussing the most recent work in capture cross sections, I would like to demonstrate this point. In Fig. 2, neutron capture cross sections are plotted against neutron energy for six elements⁵. The closed circles and open triangles are respectively activation and large liquid scintillator results both normalized to the U^{235} fission cross section. The open circles are liquid scintillator results normalized to the sphere transmission measurements. It is clear from the figure that the two methods utilizing the fission cross sections for normalization, although quite different in technique, yield data which are in good agreement. The agreement between these two sets of data and that based on the sphere transmission measurements is very poor. This suggests that the cross section differences are due not to differences in technique or to the excentricities of a particular element, but to differences in the standard used for absolute normalization. This was the situation about three years ago. At about that time, Poenitz and co-workers at Karlsruhe began a series of precision capture cross section measurements. The first reported measurements were for the Au capture cross section at 30 and 64 keV⁸. They obtained their absolute normalization in two ways: by measuring the residual activity of the neutron target and by measuring the neutron source strength with the manganese bath method. Their results were in good agreement with the adjusted sphere transmission measurements⁷, i.e., they agree with the low cross section results. Some further interesting results were obtained by Poenitz et al., with their newly developed "grey detector"⁹. This neutron detector has a nearly constant efficiency for a wide range of neutron energy. The small deviations from constant efficiency, which did occur, could be calculated. Using the "grey detector", Poenitz et al. measured the shape of the $Au(n,\gamma)$ cross section from 25-500 keV¹⁰. The curve was then normalized to a best value at 30 keV. The best value was determined by fitting a number of recent determinations at 24 and 30 keV. A comparison of their derived curve with some recent results is shown in Fig. 3. I would like to emphasize several features of the data. The solid curve giving the results of Poenitz et al., is reproduced in the four figures. In the upper left hand figure, the solid curve is in excellent agreement with the data of Harris et al.¹¹, given by the closed circles. The normalization of Harris' data depended only on the measurement of the residual activity of the neutron target. In

the upper right hand figure, the results of Barry² are indicated by closed circles. All of Barry's results lie above the solid curve but agree with the shape. Measurements of Cox⁵ are given in the lower left hand figure and are indicated by crosses. Again the data are higher than the solid curve but agree with the shape. The data of Cox are normalized to the fission cross section measurements of P. H. White¹² and since Barry used the fission detector calibrated by White as his neutron flux monitor, the normalization is essentially the same in both cases. In the lower right hand figure, the data of Vaugn et al.¹³ are given by closed circles. Their data also lie above the solid curve and are also based on the U²³⁵ fission cross section. The conclusion is clear. All of the measurements above 200 keV which are based on the White fission cross sections, are in fairly good agreement and they lie ~ 15% above the data normalized to recent measurements at 30 keV. Poenitz et al.¹⁰ list four ways in which the discrepancies might be reconciled. Certainly none of them would be universally acceptable. They are:

- 1) In the six independent measurements of the capture cross section above ~ 200 keV all measurements of the ratio of the capture cross section to the fission cross section were ~ 15% high.
- 2) The absolute values at low energy obtained by five independent methods are all ~ 15% too low.
- 3) In the energy-region above 200 keV the fission cross section of White is ~ 15% too high.
4. Both the shape measurement of Poenitz and Harris are ~ 15% too low at the higher neutron energies.

None of these possibilities is easy to accept. It is hard to imagine how five or six independent determinations of a given quantity could all err in the same direction and by the same amount. It is equally hard to believe that the U²³⁵ fission cross section is ~ 15% too high above 200 keV. It also seems fortuitous that the two shape measurements of Poenitz and Harris made by such different techniques would agree so well and both be wrong by ~ 15%.

The present status of capture cross sections can be summed up as follows. Recent capture cross section measurements above ~ 200 keV are in good agreement when normalized to the same fission cross section standard. Recent cross section measurements at 24 and 30 keV are also in good agreement but there exists an ~ 15% discrepancy in the normalization of the two regions. This may be something of an over-simplification, however I do believe that the statement represents

a fair appraisal of the current situation for capture cross section measurements. Whether any of the four suggested reasons for cross section discrepancies are really applicable remains to be seen. Although there still remains much to be done in reconciling different cross section measurements, I think it is encouraging that we have at least come this far. A few years ago the situation seemed almost hopeless. Now at least the discrepancies have been reduced to $\sim 15 - 20\%$.

3. (n,p), (n, α), and (n,2n) REACTIONS

Threshold reactions have been widely used as neutron flux integrators and for spectra measurements. For this reason alone it is desirable to have accurate and comprehensive measurements of the cross sections from threshold up to ~ 15 MeV. In addition to the value of the cross section measurement itself an investigation of threshold reactions can shed some light on nuclear structure, e.g., shell model effects and direct interactions. The body of data is too large for me to attempt to catalog it during this brief talk. Rather it seems to me more valuable to review the systematic effects which have been observed in threshold reactions, since these may be employed in estimating previously unmeasured cross sections. For obvious reasons, the bulk of the threshold reaction data have been accumulated in the vicinity of 14 MeV neutron energy¹³⁻²⁷. In addition to the 14 MeV data there is an increasing amount of data available nearer to the reaction thresholds^{28,29}. Most of the measurements of (n,p), (n, α), and (n,2n) cross sections were made with the "activation technique", although there are some exceptions. In one instance the Bi(n,2n) cross section was measured by the Fermi Water Tank Method³⁰. This will be discussed later. The activation method has the advantage that the cross sections of the constituent isotopes of an element can be easily separated. In the high energy region the data includes not only work done at ~ 14 MeV carried out with Cockraft-Walton accelerators but also measurements in the energy range from $\sim 13 \rightarrow 20$ MeV carried out with Van de Graaff accelerators. The T(d,n) reaction was used as the source of neutrons for all measurements in the high energy region.

Some interesting observations of the effects of proton shell closures have been reported by Chatterjee for (n, α) and (n,p) reactions^{31,32}. According to Chatterjee when the (n, α) and (n,p) cross sections are plotted against Z_R , the charge of the residual nucleus, depressions in the cross sections are observed at just those values of Z_R corresponding to proton magic numbers. Figure 4 is taken directly from Chatterjee and gives his plot of the (n, α) cross section against Z_R . The data indicated by closed circles are taken from a number of sources and the errors indicated are those assigned by the various

experimenters. Several features of the figure are of interest. A number of pronounced minima are observed at those values of Z_R which correspond to the proton magic numbers 4, 8, 20, 28, and 50, i.e. at the closure of major proton shells. Additional minima are observed at positions corresponding to the closure of proton sub-shells. These are indicated by the dashed lines. Chatterjee's plot of the (n,p) data is shown in Fig. 5. Again dips in the cross section data indicated by the open circles are observed at values of Z_R corresponding to magic proton numbers. Another interesting feature may be seen in the region between $Z_R = 10$ to 20. The data points have been divided into two groups indicated by the two dashed lines. This is reported to be an example of the odd-even effect which operates in the (n,p) reaction. The upper curve describes the odd proton-even mass residual nuclei and the lower curve describes the behavior for even proton-odd mass residual nuclei. When some more recent data^{14-16,18,23,29} are added, the shell effects are somewhat obscured, especially in the region of $Z = 20$ and 28. One mechanism which would tend to obscure the details of effects due to shell structure is the isotope effect described by Gardner³³ and Levkovskii³⁴. According to Gardner's original description, the cross section for (n,p) reactions for a given nuclear charge Z should differ by a factor of two between neighboring isotopes, the isotope with the higher mass number having the lower cross section. Thus for example the (n,p) cross sections for Ni^{58} and Ni^{60} should differ by a factor of four which is just what is observed^{15,20}. Some examples of the isotope effect for (n,p) reactions are given in Fig. 6. Only (n,p) reactions are included. The isotope effect has also been observed for (n,α) reactions and a description similar to that for (n,p) reaction has been given by Gardner. Returning to the examples given in the figure, we see that for (n,p) reactions the isotope effect is quite evident over a range in Z from 12 to 75. The solid line drawn through each set of points for a given Z follows Gardner's prescription³³. Agreement is quite good for the isotopes of Ni, Ca, S, and Os. The dashed lines are calculations based on the empirical equation of Levkovskii. In contrast to Gardner's rule which gives just the relative cross sections, Levkovskii's expression is normalized to yield absolute cross sections in the mass number range $12 < A < 150$. It is evident from Fig. 6 that the calculated cross sections are in reasonable agreement with experiment.

In a series of recent papers Gardner added some refinements to his calculations. Effects due to level density, Q -value, pairing energy, and the Coulomb barrier were included. Agreement with the experimental data was improved and a semi-empirical expression based on the statistical model was derived. Neither the expressions of Gardner nor Levkovskii contain any explicit shell model dependence. The formulas are primarily functions of A and Z . Their predictions are therefore inconsistent with the shell structure effects reported by Chatterjee

and others. According to Gardner the effects reported by Chatterjee are not true shell model effects. He offered the following explanation. In his plots, Chatterjee included only the cross sections of the most abundant isotope of a given element. In view of the strong (N-Z) dependence of the (n,p) cross section as exhibited in the isotope effect, this must certainly have biased his results. In fact, a plot of (N-Z) against Z_P for the isotopes chosen by Chatterjee does exhibit sharp increases at the magic numbers. This alone might qualitatively account for the observed structure. No recourse to shell model effects on pertinent nuclear parameters such as level density or pairing energy is necessary. Gardner concludes that the reported shell structure effects are only indirectly related to shell closure through the resulting variation of the position of the most abundant isotope relative to the $N = Z$ line and that true shell closure effects, if they exist, are much weaker. Gardner also finds no evidence for the odd-even effect in (n,p) reactions. Similar consideration may well apply to observed shell closure effects for (n, α) and (n,2n) reactions. The present situation with regard to predictions of (n,p) and (n, α) cross sections at 14 MeV is this. Gardner has given explicit expressions for absolute cross sections. His expressions accurately predict the relative cross sections of the isotopes of a given element and give a good representation of the absolute cross section. Levkovskii has given an empirical formula for absolute (n,p) cross sections which in general agrees quite well with experiment. For most isotopes the cross sections calculated from Gardner's formula are in good agreement with those predicted by Levkovskii. However there are a number of isotopes for which there is substantial disagreement. Unfortunately these are just those isotopes for which experimental data are either lacking or not well known. Before a final decision can be made between Levkovskii's and Gardner's formulas, more and better data are needed. The foregoing discussion was concerned with (n, α) and (n,p) cross sections obtained with a neutron energy ~ 14 MeV. A great deal of work has also been devoted to the measurement of the energy dependence of threshold reactions. I will give only one example of each reaction. Figure 7 contains two figures taken from a recent article by Paulsen³⁵. The left hand figure gives the Ni⁶⁰ (n,p) cross section measured from $\sim 6 - 20$ MeV and the right hand figure gives the Cu⁶³ (n, α) cross section measured from 6 - 20 MeV. Both reactions are important since they are used as neutron flux integrators and for spectra measurements; thus it is important to have detailed measurements of the energy dependence. Most of the data points in the figures are those of Paulsen and Liskien.

Returning to 14 MeV measurements we now examine $(n,2n)$ reactions. As with (n,α) and (n,p) reactions some of the systematic behavior observed in $(n,2n)$ reactions will be presented. Effects due to shell closure have also been reported in $(n,2n)$ reactions, although the effect is of a different nature. Borman has analyzed available $(n,2n)$ cross section data in terms of its behavior in the vicinity of magic neutron numbers. Figure 8 gives the data used by Borman for his analysis of even proton target nuclei³⁶. Despite some data points which do not follow the general trend it is apparent that there is anomalous behavior at the magic neutron numbers 28, 50, 82, and 126 ($A \sim 54, 90, 140, \text{ and } 208$). For the two lower magic numbers 28 and 50 the cross section exhibits pronounced minima. However the behavior is just the opposite for the two higher magic numbers where the cross section goes through two maxima. The explanation of the cross section behavior is as follows according to Borman: The thresholds for $(n,2n)$ reactions are generally quite high and, in fact, below $A \sim 40$ they exceed 14 MeV, making the reaction energetically impossible. For most nuclei with mass numbers just above 40 the threshold is just under 14 MeV. Thus the very low cross sections in this region can be explained as a threshold, or Q-value, effect: The few high cross sections near mass number ~ 50 result from $(n,2n)$ reactions with unusually low thresholds. As the mass number increases above $A = 40$, the threshold energy decreases, and so the cross sections rise until in the vicinity of $A = 90$ the thresholds go through another maximum, which results in a depression of the cross section again. Thus the two minima at $N = 28$ and 50 can be explained also as due to the threshold or Q-value effect. In order to explain the maxima in the cross sections at neutron magic number 82 and 126 another mechanism must be invoked. The maxima were finally accounted for by considering the competition between the $(n,2n)$ and $(n,n'\gamma)$ reactions. The level density controlling the $(n,n'\gamma)$ reaction decreases by a much larger fraction at the magic numbers than does the level density controlling the $(n,2n)$ reaction. The branching ratio changes to such an extent that the $(n,2n)$ cross section is enhanced at the magic numbers 82 and 126 ($A \sim 140, 208$). To summarize Borman's results then: At low mass numbers $A \sim 40 - 100$ the $(n,2n)$ cross sections exhibit minima at the position of neutron magic numbers. These minima are ascribed to a shell structure effect on the reaction threshold energy. For the higher mass numbers, the cross sections exhibit maxima at the positions of magic neutron numbers which are explained as due to a sharp reduction, at magic numbers of the cross section of the competing reaction $(n,n'\gamma)$.

Since the $(n,2n)$ cross section does depend strongly on the difference between the bombarding energy and threshold energy two experimenters, Csikai and Peto have argued that more could be learned if this threshold effect were eliminated²². Thus they made a series of measurements with a constant bombarding-threshold energy difference of 3 MeV and observed some interesting effects. Their results are shown

in Figure 9. In the upper figure the cross section data are plotted against $N-Z$, the neutron excess. The solid lines are drawn through data points belonging to nuclides having the same neutron number. It is clear that the cross section for a given neutron number changes markedly as the proton number is varied and in an approximately linear manner. The data group well into a family of lines over a wide range in neutron number. It is more difficult to obtain data to show analogous behavior at constant Z ; however, the data that are available from the work of Csikai and Peto are plotted in the lower figure. Here the cross section data are plotted against N rather than $N-Z$. This was done just to effect a separation of the family of curves for clarity of presentation. The solid lines here connect data belonging to nuclides of the same Z . The data here also group into a family of lines and again the dependence is essentially linear. Csikai and Peto explain the observed $N-Z$ dependence of the cross sections as probably due to the influence of direct neutron inelastic scattering. Strong $N-Z$ dependent effects such as those illustrated in Fig. 9 probably tend to obscure the shell closure effects described previously. When more energy dependent data become available it might be instructive to follow the approach used by Csikai and Peto and re-examine trends in $(n,2n)$ reactions after all cross section data have been adjusted to a constant bombarding-threshold energy difference. In any case, systematic trends in the (n,α) , (n,p) , and $(n,2n)$ cross section data can be of great importance in estimating by interpolation the magnitude of unmeasured cross sections which are of interest to the reactor physicist and engineer.

As mentioned before, the bulk of the (n,x) cross section data have been obtained using the activation technique. This technique has the advantage that it is easy to separate the contributions from the various isotopes of an element. However it does require that the residual nucleus be radioactive and this is not always the case. Recently Fricht and Vonach³⁰ reported using a method for the measurement of $(n,2n)$ cross sections which is sensitive directly to the emitted neutrons and does not depend on induced radioactivity. This method, called the Fermi Water Tank Method, may be described briefly as follows: A hollow sphere of the material to be measured is placed around a T (d,n) neutron source. The sphere and source combination is surrounded by a large water tank. Measurements of the neutron flux are made in the water at various distances from the target. The neutron flux in the water due to evaporation neutrons can be separated from the flux due to the primary 14 MeV neutrons. Then if the total non-elastic cross section is known, the $(n,2n)$ cross section can be calculated. The method also yields the average energy of the evaporation neutron spectrum. Fricht and Vonach obtained a value of $2.25 \pm .25b$ for the Bi $(n,2n)$ cross section in good agreement with other measurements. The average energy of the evaporation neutron spectrum was 2.00 MeV.

4. NEUTRON SCATTERING

I would now like to discuss a more fortunate area of cross section measurement, that of neutron scattering. A vast amount of accurate data has been accumulated during the past several years, especially in the region below ~ 1.5 MeV neutron energy^{37,38}. However, during the last two or three years, there has been a substantial increase in the amount of data in the region from $\sim 1.5 - 10.0$ MeV^{39,42}. There is a twofold purpose in acquiring scattering cross section data. On the one hand there is the value of the cross section data itself. Accurate scattering data is essential to the design of nuclear reactors. On the other hand there is the desire to construct a good nuclear model⁴³. Construction of a nuclear model not only gives better insight into reaction mechanisms, but it also supplies the reactor physicist with a very valuable tool for calculating cross sections. In some cases, the required cross section is difficult to measure. Perhaps the target nuclide is unstable or of very small isotopic abundance. Whatever the reason for the unavailability of the cross section data a reliable nuclear model could be used to obtain the requisite data by interpolation between, or extrapolation from, well measured points. For the purpose of establishing such a model for scattering cross sections a large amount of data is required over the energy range from $\sim .1 - \sim 15$ MeV. In the low energy region below ~ 1.5 MeV the measurements are complicated by the compound nucleus resonance structure. Because many cross sections measured in this energy region exhibit strong cross section fluctuations, the data must be taken in great detail in order to obtain a proper energy average to compare with calculations. Models such as the optical model describe only the average behavior of the cross section energy dependence, not the detailed compound nucleus structure. In the continuum region, above $\sim 4-5$ MeV neutron energy, nuclear properties change only slowly with energy. Only a few widely spaced measurements for each nuclide should suffice to describe the scattering process. The region between ~ 1.5 MeV and $4-5$ MeV is an awkward one. This is the region that in many cases bridges the gap between resonance structure and the continuum. Data in this region must also be taken in some detail.

An example of the detailed resonance structure which is present in the low energy region is given in Fig. 10. The figure is from a report by A. B. Smith⁴⁴ and contains scattering data for Fe. On the left hand side of the figure, the energy dependence of the total elastic scattering cross section is given together with the first three legendre polynomial coefficients obtained from a least squares fit to the angular distribution data. The data were taken at very closely spaced energies in order to faithfully reproduce the detailed resonance structure. On the

right hand side, similar detailed structure is seen in the inelastic scattering cross section corresponding to the 840 keV level in iron. It is clear from an examination of the cross section fluctuations that if measurements had been made at widely spaced and arbitrarily selected energies, the energy-dependent behavior of the cross section would in all likelihood be grossly distorted. Only by taking data at energy intervals smaller than the energy spread of the incident neutron beam can the true average energy dependence of the cross section be obtained. In addition to the structure which arises from the many resonance states of the compound nucleus there is the more controversial phenomenon known as "Intermediate Structure"⁴⁵. This structure is supposed to result from the initial formation of only the simpler types of compound nuclear states, e.g., (2p,1h) states. For intermediate weight elements the resonances arising from such an interaction have spacings of $\sim 200 - 300$ keV and widths of $\sim 50 - 100$ keV. Structure of this type has been observed in the scattering cross sections of many elements so that its existence is not questioned. The interpretation of the structure is another matter and will not be gone into here. Several examples of intermediate structure are given in Fig. 11⁴⁶. The four illustrations contain the scattering cross section and legendre polynomial coefficients for Co, Se, Mn, and Cr. Prominent resonance-like structure is evident in the data for all four elements. An interesting feature of the data is that the indicated resonance spacings and widths change less than a factor of two between the different elements although the compound nucleus level density changes by at least a factor of ~ 15 .

A number of measurements of elastic and inelastic neutron scattering have recently been reported in the energy region from ~ 1.5 to ~ 8.0 MeV. I mention only a few of the more recent data. Kinney⁴⁷ has made extensive measurements of the elastic and inelastic scattering from iron between 4.60 and 7.55 MeV. Some of his results for inelastic scattering to the first excited state are given in Fig. 12. Inelastic scattering angular distributions are given for six incident energies. The pairs of dashed lines near the top and bottom of the figure are to be associated with the 7.55 MeV and 5.0 MeV data respectively. They represent the components of direct interaction and compound nucleus interaction which add together to give the measured inelastic scattering cross section. Kinney reports that the percent contribution of direct interaction to the inelastic scattering cross section increases from $\sim 20\%$ at 4 MeV to $\sim 65\%$ at 7.55 MeV. There are also some recent investigation of the scattering of neutrons in the energy range 4.5 - 8 MeV from S and Zn by Tanaka et al.⁴⁸ Some of their results for Zn are given in Fig. 13. The angular distribution of neutrons inelastically scattered from the first excited state in Zn are given for four incident neutron energies. At all four energies the distributions are strongly peaked forward. The dashed lines are from a Hauser-Feshbach calculation and the solid lines are the result of a DWBA calculation using a non-spherical potential. It is evident that the data agree well with the DWBA calculation, indicating that this particular transition proceeds

mainly via a direct interaction. Their results for inelastic scattering to the second and third excited states however indicate that those two transition proceed mainly via a compound nucleus process. A study of the behavior of optical model parameters as a function of energy was recently reported by Holmquist and Wiedling⁴⁹. They investigated the elastic neutron scattering of neutrons in the energy range 1.5 - 8.0 MeV from Ni, Co, and Cu. The angular distribution data obtained at each bombarding energy were fitted by an optical model calculation in which 5 parameters were varied to obtain the best fit. The best fit for a particular energy was obtained independently of the best fits at other energies. Some of their results for Co and Cu are given in Fig. 14. The five optical model parameters which were varied are plotted against the neutron bombarding energy. The data points are the best fit values for each energy. Reading from top to bottom the parameters are the real potential well depth, the imaginary potential well depth, the diffuseness coefficient for the real well and the value of r_0 for the real and imaginary wells. Except for the two lowest energy points in each case, the data indicate a nearly constant energy dependence over the entire range. The one exception in the data shown here is the radius of the imaginary well for Co which does decrease with increasing energy. The set of optical model parameters obtained by Holmquist and Wiedling gave very good fits to their differential cross section data. It is a point in favor of the optical model that a series of independent fits to scattering data over such a large energy range yields a self consistent set of parameters.

In a recent article Engelbrecht and Fiedelley⁵⁰ described an optical model with energy dependent parameters which gave a satisfactory fit to elastic scattering and polarization data over the neutron energy range $\sim 1 - 155$ MeV. The energy dependence was derived from considerations of the non-local potential. Their parameters were set equal to those of Moldauer in the zero energy limit and fitted at the high energy end to total and reaction cross sections. Their results for the energy dependence of the real and imaginary potential well depth are given in Fig. 15. The real potential depth $V(E)$ is a decreasing function of the energy. The imaginary potential consists of a surface component whose depth is $W(E)$ and a volume component whose depth is $U(E)$. The energy dependence of the two curves for W and V give a good illustration of how the absorption potential changes from a surface absorption potential at low energies to a volume absorption potential at high energies.

A discussion of neutron scattering would not be complete without reference to polarization measurements. Polarization measurements are useful not only in investigation of the spin orbit potential but for other parameters as well. In fact the polarization is quite sensitive to changes in the real potential well depth and radius and to the location of the surface absorption peak. Since any model of neutron scattering must also give a good description of the polarization of

the scattered neutrons it is interesting to determine a set of parameters which give a fit to both the differential scattering and differential polarization data. Considering the number of parameters available in the optical model, it seems essential that both should be fitted at the same time and with the same set of parameters. Figure 16 gives results of just such a fit to some recent polarization data⁵¹. On the left are plotted the differential cross section measurements for Se and Y. On the right are the associated polarization measurements. The dashed and solid curves, which represent two different optical model calculations, illustrate how sensitive the polarization can be to details of the model. The dashed curve is the best fit which could be obtained with the surface absorption peak placed .5 f outside the edge of the real potential well. The solid curve represents the best fit obtained with the surface absorption peak placed at the edge of the real potential well. Quite clearly the solid curve is in much better agreement with the data. Considering the sensitivity of the method, it seems reasonable to expect that polarization measurements combined with elastic and inelastic scattering measurements will afford a better definition of a nuclear model than that which would be obtained from the scattering data alone.

During the last two or three years, the Ge(Li) detector has come into extensive use. Its high resolving power makes it invaluable in the investigation of γ -ray spectra following neutron capture and in the investigation of γ -rays following inelastic neutron scattering. One example of the detector's use in the inelastic neutron scattering studies is given in Fig. 17. These are recent results of Kikuchi et al.⁴⁸ The figure shows the spectrum of γ -rays emitted at 90° following the inelastic scattering of 3.02 MeV neutrons from Zn. Each γ -ray peak is identified by the energy, the isotope from which it is emitted, and the specific transition involved. I would like to call your attention to the three intense γ -rays near channel 400. They arise from transitions between the first excited state and the ground state for the three most abundant isotopes of Zn. This is one example of how the high resolution attainable with a Ge(Li) detector can be employed to obtain data on individual isotopes without the necessity of using separated isotopes. At lower channel numbers, the transition between the 3rd and 1st excited states of Zn^{64} is clearly resolved as is the transition between the 2nd and 1st excited states of Zn^{66} . Certainly with performance characteristics such as are indicated here, the Ge(Li) detector will provide much valuable information concerning the inelastic neutron scattering process. It will be especially useful for measurements close to the inelastic scattering thresholds, a region which is difficult to investigate with conventional T.O.F. techniques.

5. REMARKS CONCERNING CROSS SECTION MEASURERS, USERS, AND EVALUATORS

There is the ever present problem of communication between the cross section measurer and the cross section user. Most cross section measurers are physicists and as such have broader interests than just the measurement of neutron cross sections. The user is interested primarily in obtaining accurate cross section data for his research and the cross section measurer is interested in physics. I would like to make it clear that I am not objecting to the measurer's interest in physics. This is a valid approach to the acquisition of nuclear data. In fact, it may be an essential ingredient. Accurate measurements of nuclear cross sections require a very competent person using the latest experimental techniques. The physicist fits this prescription rather well. It seems to me that the most efficient kind of cross section group would be one in which there was a proper wedding of applied and pure research. The pure physics group by itself would not do the job the users want. Except for certain special instances, their objectives are too far removed from the plain task of acquisition of precise nuclear data. Neither would a group engaged only in applied physics do a satisfactory job. Such a group would in my opinion tend to stagnate. It would become divorced from the mainstream of physics research and as a result, the experimental techniques and even the competence of the experimentalists would suffer. However, it would be of mutual benefit to the cross section measurer and user if the experiments were carried out in a more systematic manner than is often the case today. This could be accomplished by a more efficient utilization of automation in data acquisition and a more widespread use of both on-line and off-line computers in data processing and analysis. This would not only greatly increase the quantity of data available to the user, but also to a large extent would free the experimental physicist from the tedious and time consuming task of data taking.

There is a rather sensitive area I would like to touch on briefly. This involves the respective roles of the cross section measurer and user in the compilation of nuclear data requests. As I implied at the beginning of this talk, the two roles are not always compatible. The measurer has no quarrel with the high precision requested by the user in most cases. The user knows best what precision is needed in a given application. However, some of the requested precisions may be beyond present capabilities of manpower or techniques or both. In these cases the user should be made cognizant of the experimental difficulties, which should be duly taken into account, when he sets his required precision. If after all of these considerations the user decides that he really does need a precision which is beyond present capabilities, then the measurer must do his best to satisfy the request. One example should serve to illustrate the point I am trying to make. Over the past

ten years or so a large number of workers in several laboratories have been engaged in measuring $\bar{\nu}$, the number of neutrons per fission. All of the measurements were normalized to $\bar{\nu}$ for Cf^{252} ; thus a lot of effort has been expended in obtaining accurate measurements of this quantity alone. The total effort comes to more than 100 man-years and the results are still far from satisfactory. The real question then is this. In cases which require a major extrapolation of present techniques or manpower, is the requested precision important enough to justify the expenditure of several calendar years and several times this amount in man years. If the answer is affirmative, then the request is a reasonable one and the all too small community of cross section measurers should do their best to honor it.

In a related area there is the problem of proper data evaluation. This is an important and difficult field. In some cases where objective evaluation has required the assignment of small weight to certain data it is also a rather unrewarding task. Nevertheless, in order to be useful the data must be evaluated. There have been suggestions that the evaluation process should be carried out by computers and not by humans. In spite of the magnitude of developing an evaluation program, there is much to be said for this approach. The character of the problem was nicely stated by K. Parker⁵² at the last Cross Section and Technology Conference when he remarked, "If the operations carried out by hand in evaluating neutron cross sections are logical, then they can be identified and programmed for a computer. If they are not logical, then we should not be doing them at all". Data evaluation is further compounded by the lack of sufficient information in many reports regarding the experimental techniques used and the methods used in assigning errors. There is ample evidence where the disagreement between measurements made at different laboratories is many times the assigned standard deviation. If the man who made the measurements cannot properly estimate his own errors the data evaluator must. Experimental physicists would do the data user and data evaluators a great service by including all pertinent details of the experimental procedure so that intercomparison between data from various sources could be made on an objective basis.

6. CONCLUSION

I hope that I have given a coherent account of at least a small part of the fast neutron cross section field. Much has been left out. Worthy of mention are the programs utilizing linear accelerators. There is a large amount of data being accumulated with these machines; e.g., the radiative capture cross section work at RPI. There are advances in the resolution and precision of total cross section measurements by both conventional and time-of-flight methods. There are also improvements in the precision of standard cross sections, such as that for

the $B^{10}(n,\alpha)$ reaction. A vast amount of data is available for the spectra of γ -rays emitted after neutron capture. All of these areas are very important and show every promise of yielding not only quantities of cross section data but significant information concerning nuclear structure and nuclear reactions. Considering the activity in the field of cross section measurement today, I believe the cross section user can reasonably expect to be presented with a large amount of data within the next 2-3 years. Whether it is exactly the data he wants is another question, and one in which such a conference as this has a degree of responsibility.

7. REFERENCES

1. J. H. Gibbons, R. L. Macklin, P. D. Miller, and J. H. Neiler, Phys. Rev. 122, 182 (1961).
2. J. F. Barry, J. Bunce, and P. H. White, J. Nucl. Energy, 18, 481 (1964).
3. B. C. Diven, J. Terrell, A. Hemendinger, Phys. Rev. 120, 556 (1960).
4. H. W. Schmitt and C. W. Cook, Nuclear Physics, 20, 202 (1960).
5. S. A. Cox, Phys. Rev. 122, 1280 (1961) and Phys. Rev. 133, 378 (1964).
6. R. L. Macklin, N. H. Lazar, and W. S. Lyon, Phys. Rev. 107, 504 (1957).
7. D. Bogart and T. T. Semler, Report NASA TMX-52173 (1966).
8. W. P. Poenitz, J. Nucl. Energy, 20, 825 (1966).
9. W. P. Poenitz, D. Kompe, H. O. Menlove, K. H. Beckurts, Report KFK 635, SM 101/9, EUR 3679 e (1967).
10. W. P. Poenitz, D. Kompe, H. O. Menlove (to be published in J. Nucl. Energy).
11. K. K. Harris, N. A. Grench, R. G. Johnson, F. J. Ferzigen, and R. Sher, Nuclear Physics 69, 37 (1965).
12. P. H. White, J. Nucl. Energy 19, 325 (1965).
13. F. J. Vaugn, K. L. Coop, H. A. Grench, and H. O. Menlove, Bull. Am. Phys. Soc. 11, 5, 753 (1966).
14. J. Csikai and S. Nagy, Nucl. Phys. A91, 222 (1967).
15. Shoji Okumura, Nucl. Phys. A93, 74 (1967).
16. A. Pasquarelli, Nucl. Phys. A93, 218 (1967).
17. Aparesh Chatterjee, Phys. Rev. 134, B374 (1964).
18. B. Mitra and A. M. Ghase, Nucl. Phys. 83, 157 (1966).
19. J. Csikai and S. Nagy, Nucl. Phys. A91, 222 (1967).

20. H. Lishien and A. Paulsen, Nucl. Phys. 63, 393 (1965).
21. M. Bormann, E. Fretwurst, P. Schelka, G. Wrege, H. Biitner, A. Lindner, and H. Meedner, Nucl. Phys. 63, 438 (1965).
22. J. Csikai and G. Peto, Acta Physica Academiae Scientiarum Hungaricae, 23, 87 (1967).
23. H. Liskien and A. Paulsen, J. Nucl. Energy 19, 73 (1965).
24. H. Liskien and A. Paulsen, J. Nucl. Energy 19, 907 (1965).
25. J. Csikai, Atomki Kozlemenezek, 8, 79 (1966).
26. A. Chatterjee, Nucleonics 23, 112 (1965).
27. M. P. Menon and M. Y. Cuyper, Phys. Rev. 156, 1340 (1967).
28. H. Liskien and A. Paulsen, Nukleonik 6, 315 (1966).
29. Proceedings of the Conference on Nuclear Data for Reactors, Paris (October 1966).
30. E. Fricht and H. Vonach, Nukleonik 10, 58 (1967).
31. Aparesh Chatterjee, Nucl. Phys. 60, 273 (1964).
32. Aparesh Chatterjee, Nucl. Phys. 49, 686 (1963).
33. D. G. Gardner, Nucl. Phys. 29, 373 (1962); D. G. Gardner and A. D. Paularikas, Nucl. Phys. 35, 303 (1962); D. G. Gardner and Yu-Wen Yu, Nucl. Phys. 60, 49 (1964); D. G. Gardner and Sheldon Rasenblum, Nucl. Phys. A96, 121 (1967).
34. V. N. Levkouskii, JETP (Soviet Physics) 18, 213 (1964).
35. A. Paulsen, Nukleonik 10, 91 (1967).
36. M. Borman, Nucl. Phys. 65, 257 (1965).
37. A. B. Smith and R. Hayes, Nucl. Phys. A93, 609 (1967).
38. D. Lister, A. B. Smith, and Charles Dunford, Phys. Rev. 162, 1077 (1967).
39. J. A. Cookson, D. Dandy, and John C. Hopkins, Nucl. Phys. A91, 273 (1967).

40. L. Cranberg, T. O. Oliphant, J. Levin, and C. D. Jafiratos, Phys. Rev. 159, 969 (1967).
41. W. B. Gilboy and J. H. Towle, Nucl. Phys. 64, 130 (1965).
42. B. Antolkovic, B. Holmquist, and T. Wiedling, Proceedings of the International Conference on Nuclear Structure with Neutrons, Antwerp, July 19, 1965, Amsterdam (1966).
43. P. A. Modlauer, Rev. Mod. Phys. 36, 1079 (1964).
44. A. B. Smith (private communication)
45. H. Feshbach, A. K. Kerman, and R. H. Lemmer, Ann. Phys. 41, 230 (1967).
46. S. A. Cox, Bull. Am. Phys. Soc. 12, 1, 107 (1967).
47. William F. Kinney, Neutron Elastic and Inelastic Scattering from Fe⁵⁶ from 4.60 - 7.55 MeV (Thesis) University of Tennessee (1967).
48. Shigeya Tanaka (Private communication).
49. B. Holmquist (Private communication).
50. C. A. Engelbrecht and H. Fiedelkey, Ann. Phys. 42, 262 (1967).
51. S. A. Cox and E. E. Dowling Whiting, Bull. Am. Phys. Soc 13, 1, 116 (1968).
52. K. Parker, Conference on Neutron Cross Section Technology, Washington, D. C. (1966).

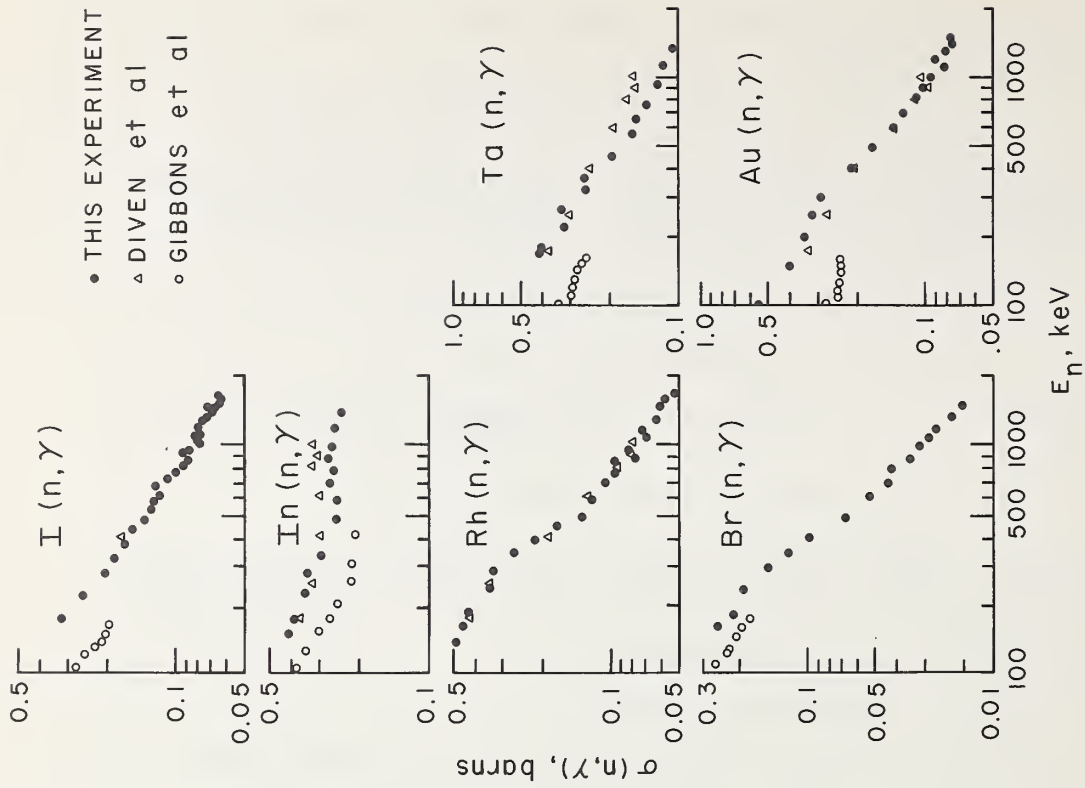


Fig. 2 Comparison of ANL activation measurements with LASL and ORNL large liquid scintillator measurements.

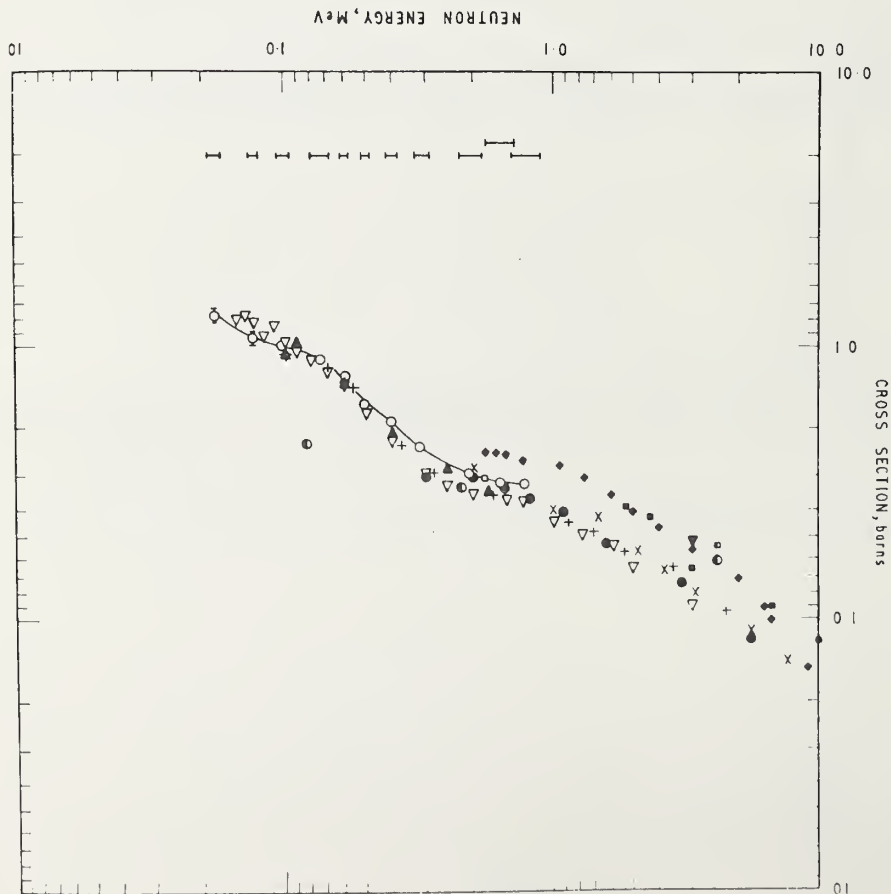


Fig. 1 Discrepancies in the Au(n, γ) cross section as of 1964.

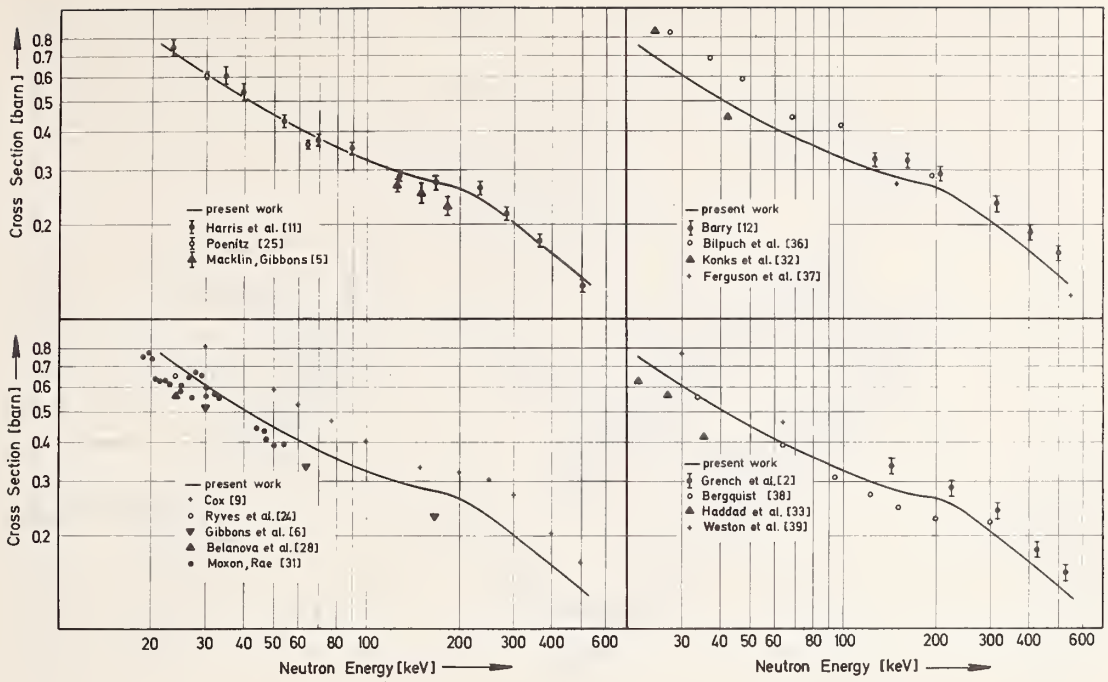
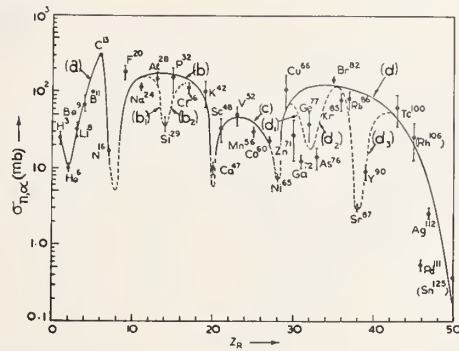
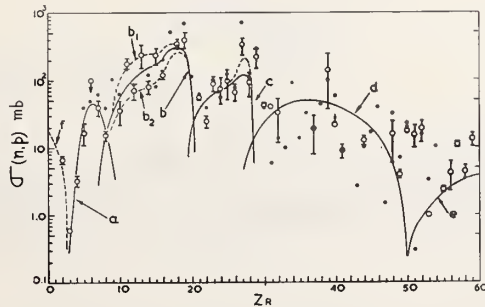


Fig. 3 Recent results of Poenitz et al¹⁰ for the Au(n,γ) cross section compared with other measurements.



4. Effects of shell closure on (n,α) reactions as reported by Chatterjee³².



5. Effects of shell closure on (n,p) reactions as reported by Chatterjee³¹.

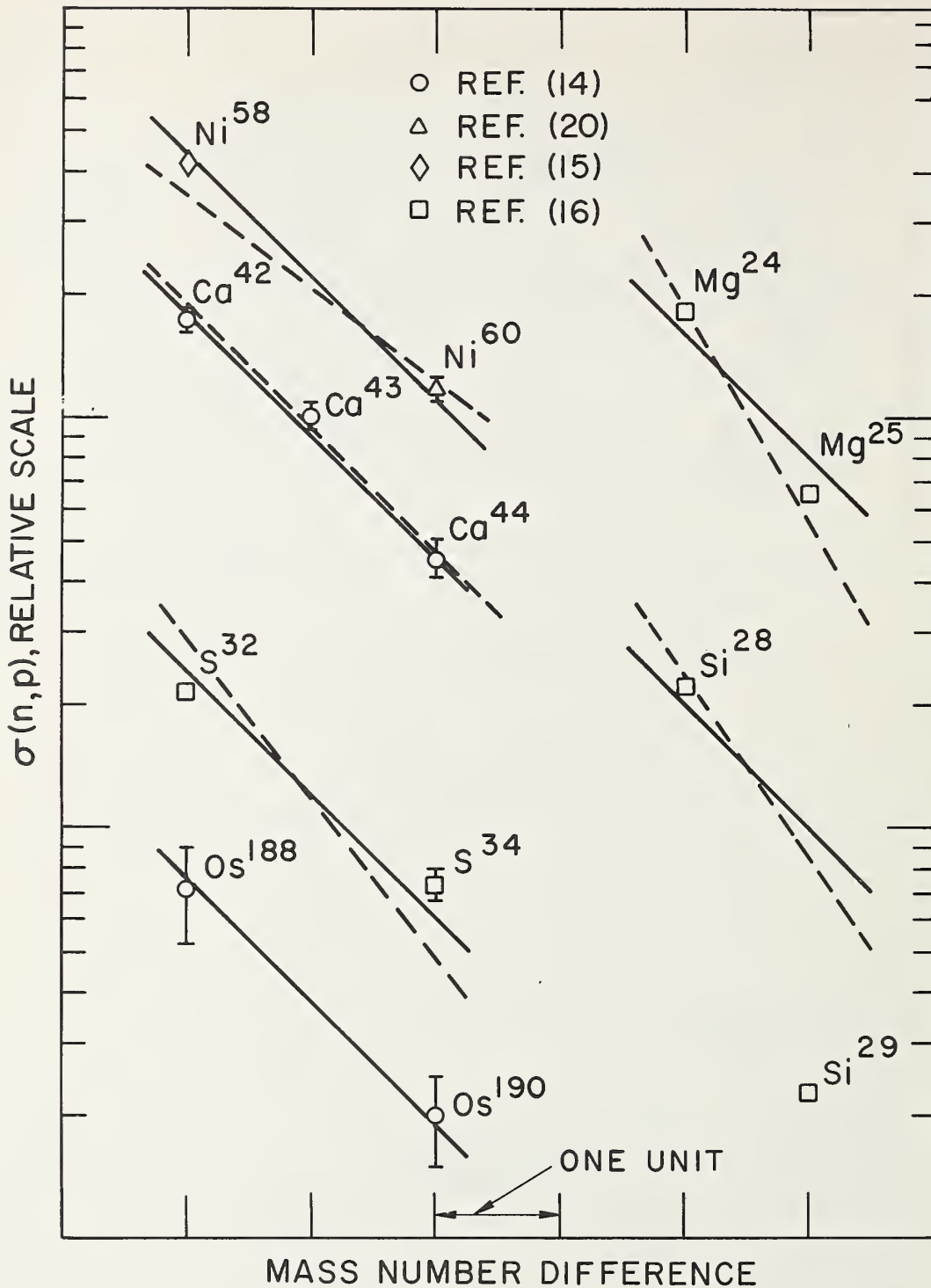
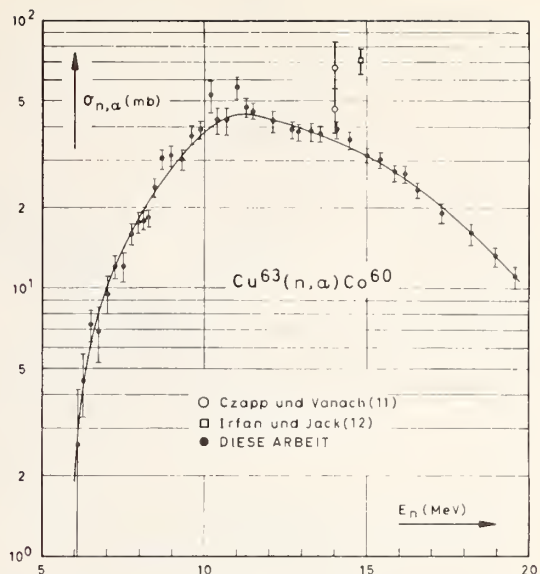
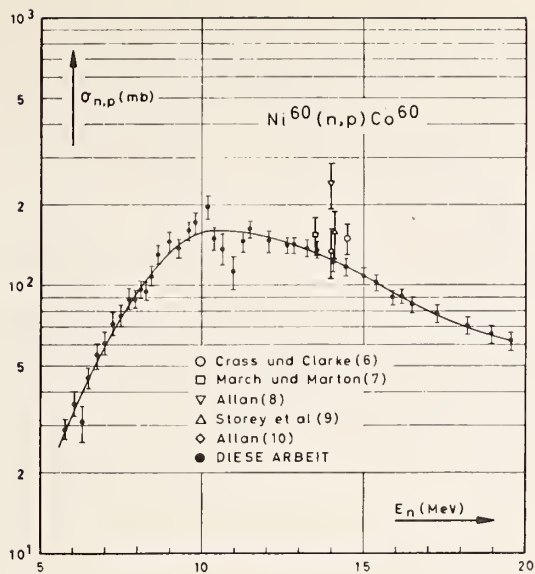
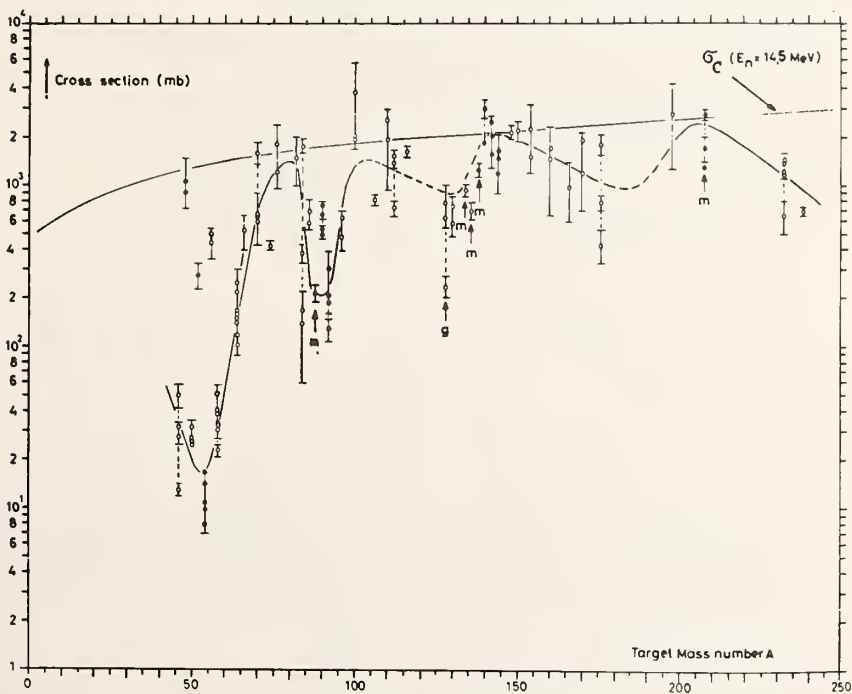


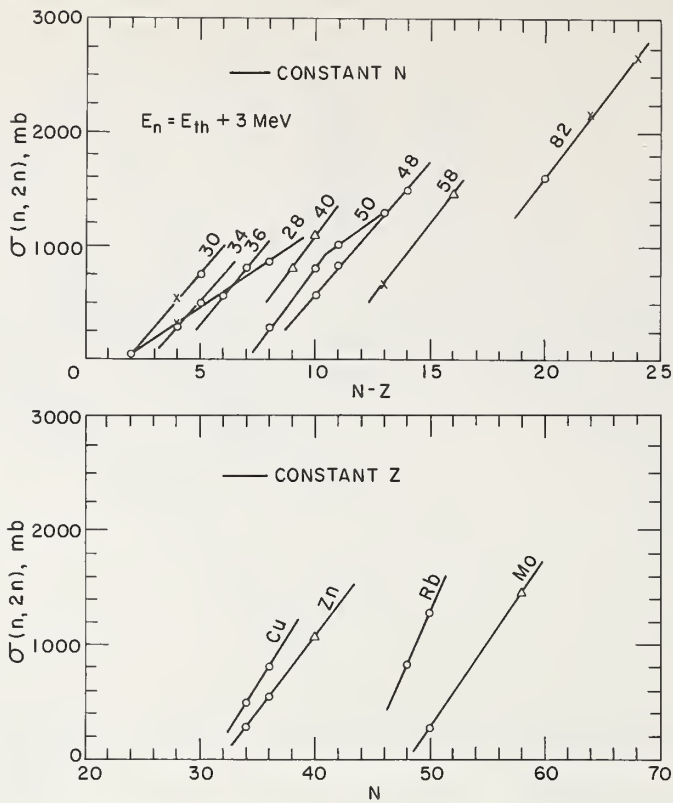
Fig. 6 Isotope effect in (n,p) reactions. The solid lines are from Gardner³³ and the dashed lines are from Levkovskii³⁴.



7. Energy dependence of the $\text{Ni}^{60} \text{ (n,p)}$ and $\text{Cu} \text{ (n,\alpha)}$ reaction³⁵.



8. Anomalous behavior in (n,2n) reaction cross sections at magic neutron numbers as reported by Barmann³⁶.



9. Systematic behavior observed in $(n, 2n)$ reaction cross sections by Csikai and Peto²².

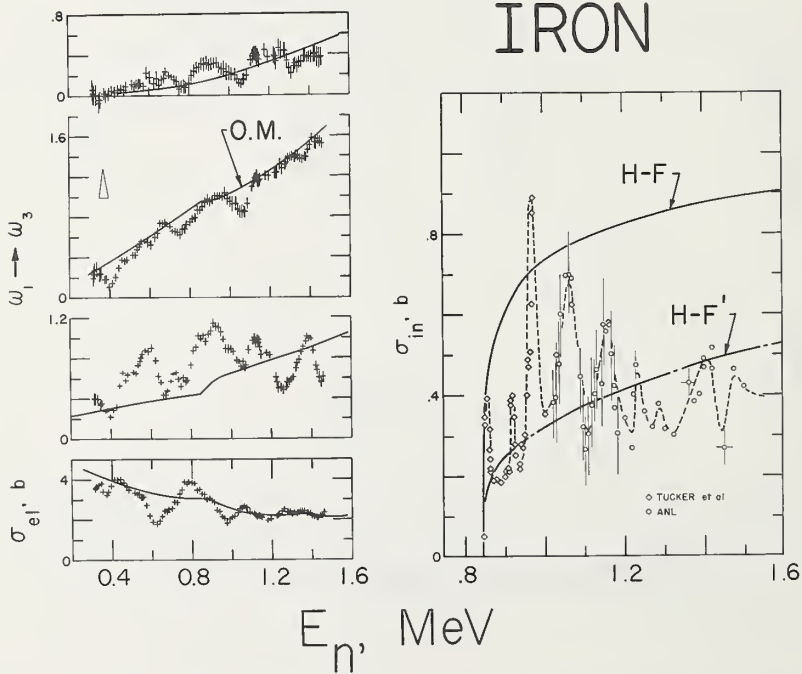


Fig. 10 Resonance structure in the elastic and inelastic scattering cross sections of Fe. The data are from A. B. Smith⁴⁴.

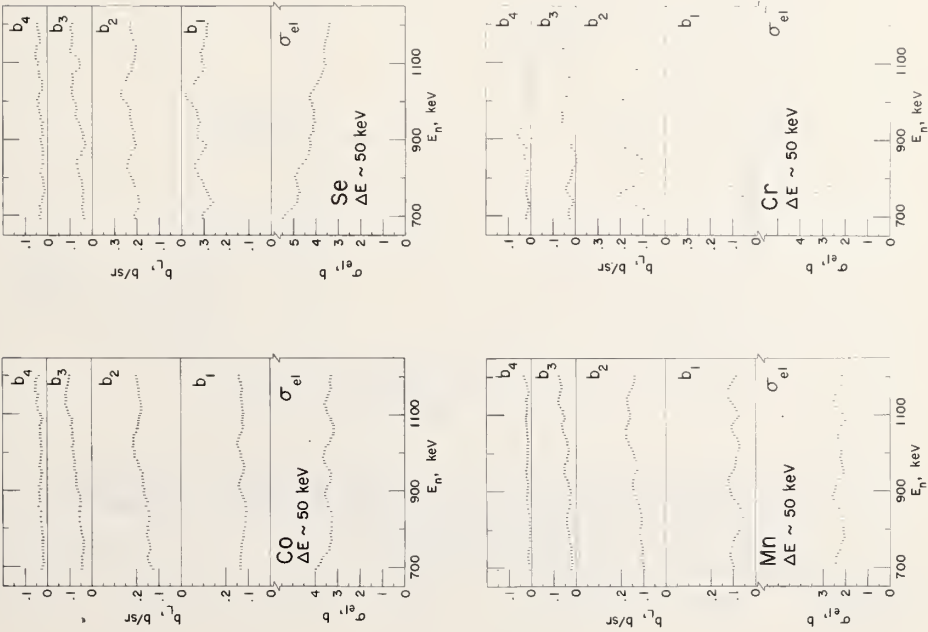


Fig. 11 Examples of observed intermediate structure in elastic neutron scattering from intermediate weight elements reported by S. A. Cox⁴⁶.

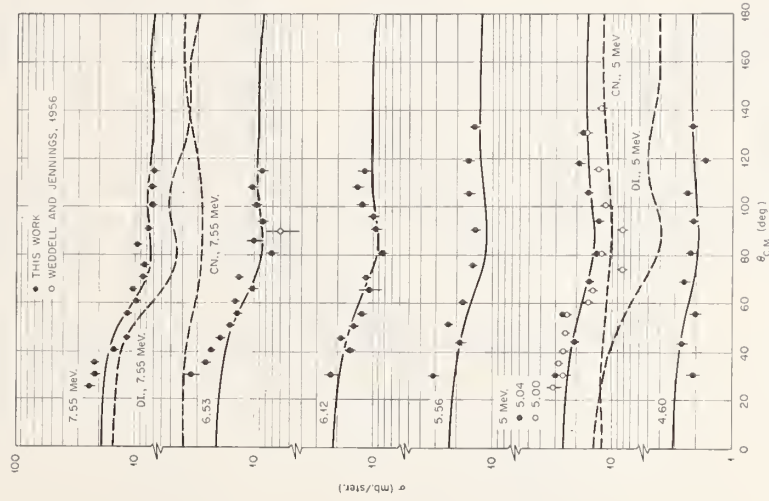


Fig. 12 Inelastic neutron scattering from several excited states in iron reported by Kinney⁴⁷.

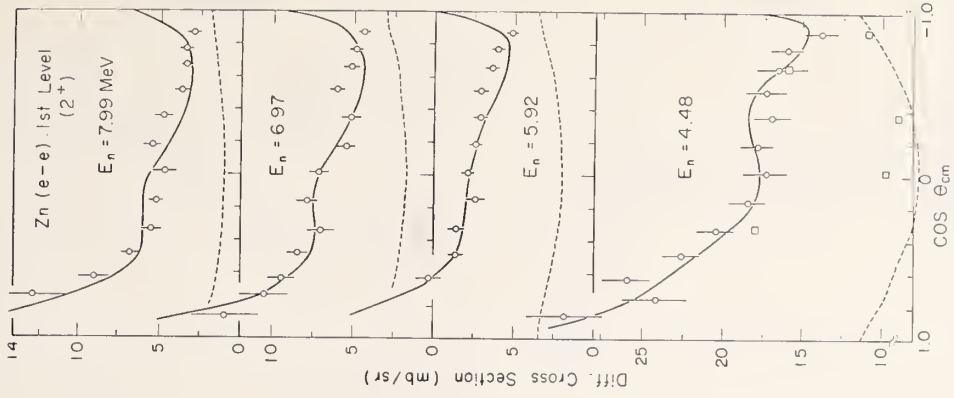


Fig. 13. Inelastic neutron scattering from Zn reported by Tanaka et al.⁴⁸

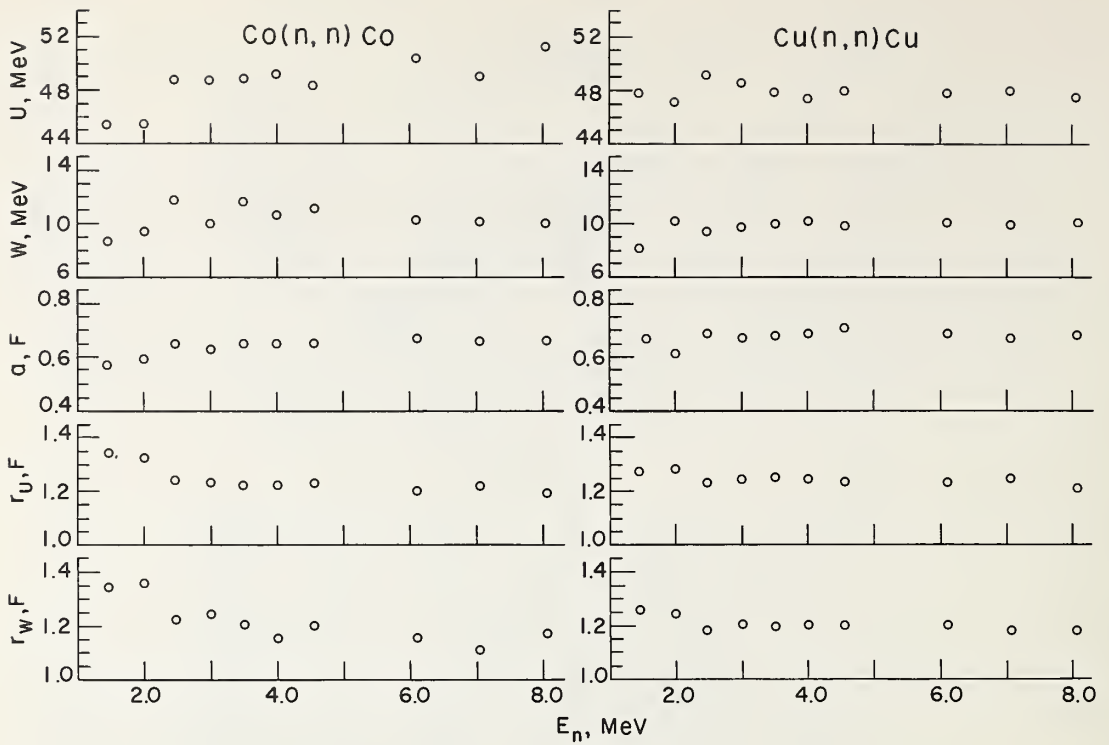


Fig. 14 Results of a 5 parameter optical model fit to scattering data of Holmquist and Wiedling⁴⁹.

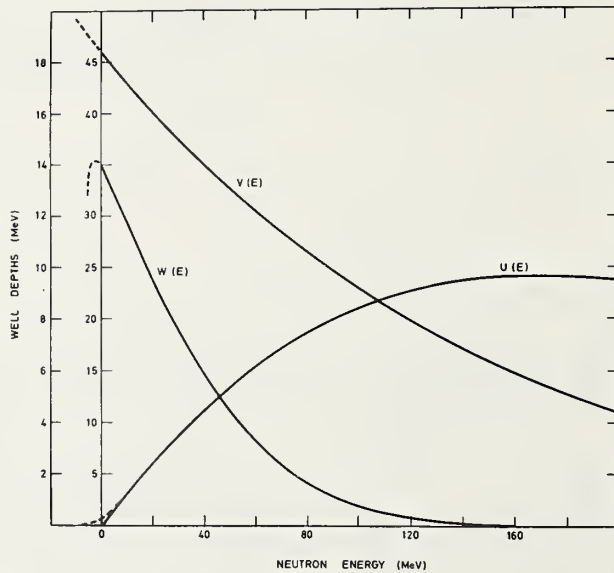


Fig. 15 Energy dependence of optical model parameters obtained by Engelbrecht and Fiedelney⁵⁰ from a fit to low energy scattering data and high energy total and reaction cross section.

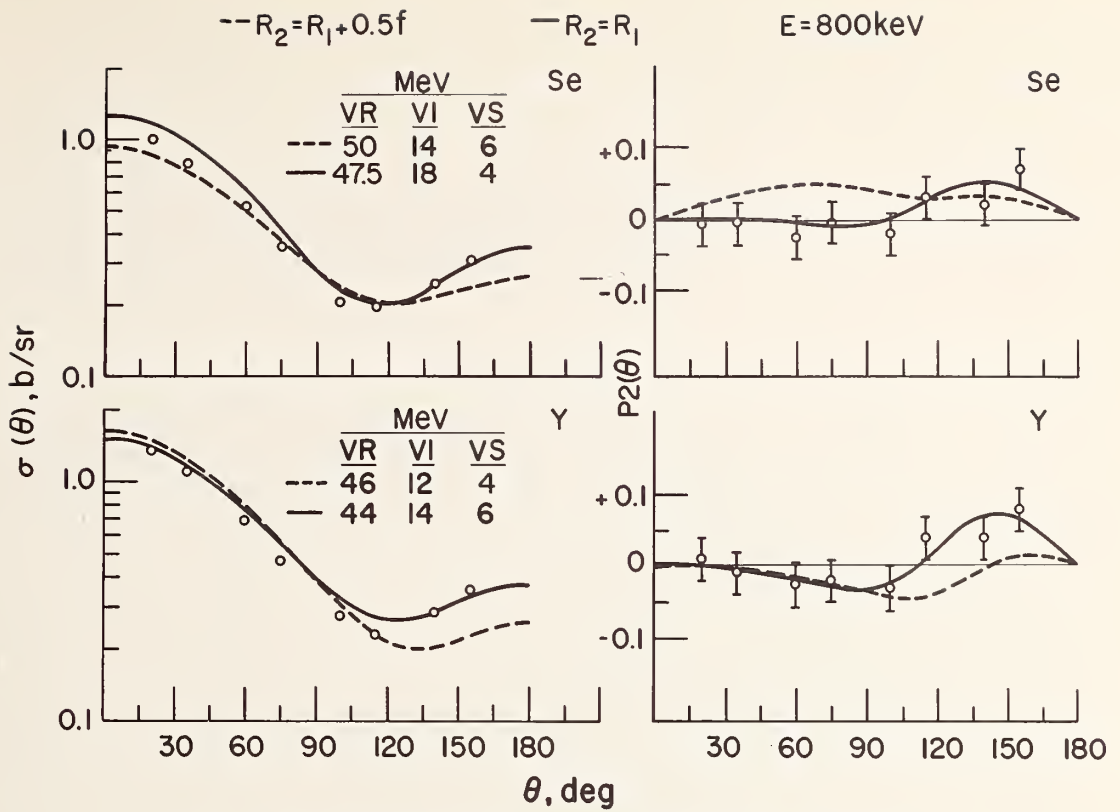


Fig. 16. Optical model fits to recent scattering and polarization data of Cox and Whitting⁵¹.

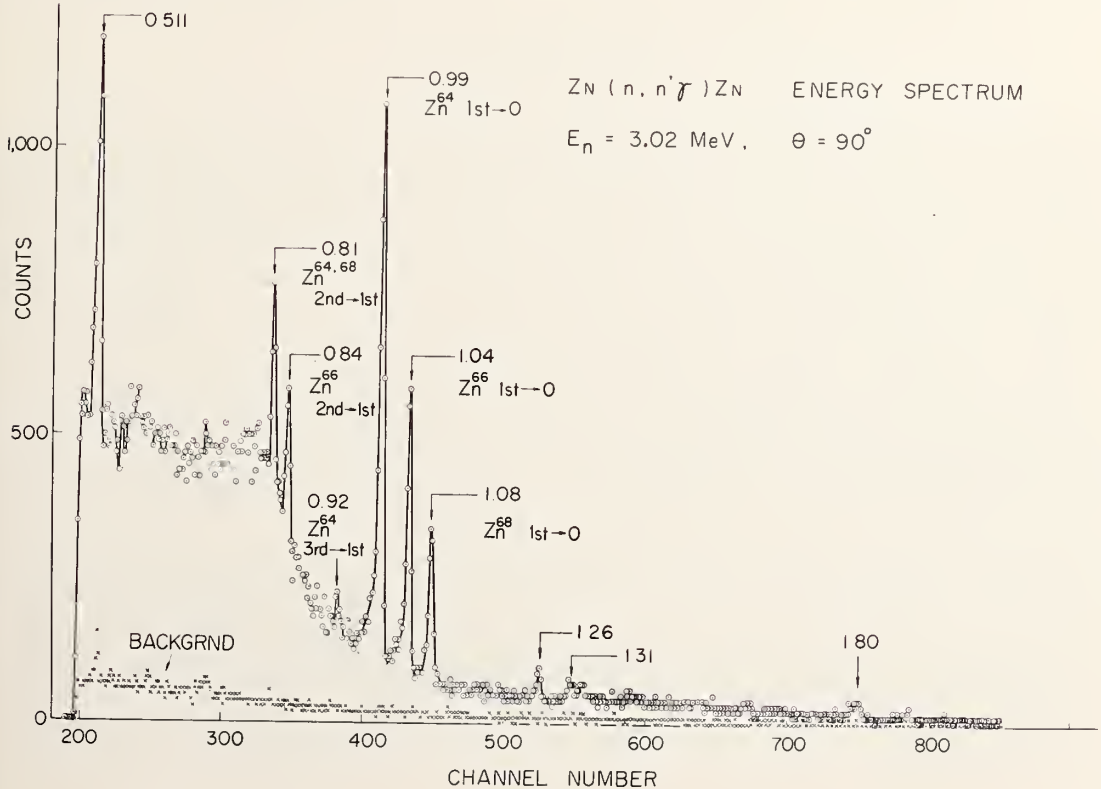


Fig. 17. Example of the use of a high resolution Ge(Li) detector in inelastic neutron scattering studies. Data from Kikuchi et al.⁴⁸

NEUTRON RADIATIVE CAPTURE IN THE KEV REGION*

R. W. Hockenbury, Z. M. Bartolome, W. R. Moyer,
J. R. Tatarczuk and R. C. Block

Division of Nuclear Engineering and Science
Rensselaer Polytechnic Institute
Troy, New York 12180

ABSTRACT

Resonance parameters and resonance capture areas have been obtained for Na, Al, Fe and Ni in the energy range from 200 eV to 300 keV.⁺ Radiation widths were determined for five resonances in Fe, two resonances in Al, two resonances in Na and one resonance in Ni. Where comparisons can be made, the agreement between the present results and other investigations is satisfactory. In Al, the radiation widths are not constant, that of the 35 keV resonance is (2.8 ± 0.3) eV while that of the 5.88 keV resonance is at most 1.0 eV (if g is assumed equal to $1/4$ for the 5.88 keV resonance). For ^{56}Fe and ^{57}Fe , the radiation widths differ by a factor of two to three from resonance to resonance in the same isotope. The weaker resonances in Fe and Ni can be attributed to p-wave neutrons, and from the capture data a p-wave strength function can be determined. In both Ni and Fe the p-wave strength functions are an order of magnitude smaller than those predicted by the optical model.

1. INTRODUCTION

Neutron radiative capture cross section measurements provide information pertinent to nuclear structure and reactor technology. Capture measurements together with total cross section or self-indication measurements enable one to determine resonance parameters including the radiation width, neutron width, spin and resonance energy. Once the resonance parameters are determined over a large energy range, information can be obtained on strength functions and distributions of widths and level spacings. Capture cross sections are also needed for the design of fast reactors since they enter into the calculation of breeding ratios, shielding criteria, critical masses, temperature coefficients and neutron energy spectra. Aluminum, iron and nickel are common structural materials while sodium is used as a coolant in fast reactors.

* Work supported by the U. S. Atomic Energy Commission under Contract AT(30-3)-328.

+ These data were presented in a preliminary form at the 1966 Paris Conference on Nuclear Data and published in Nuclear Data for Reactors, Vol. I, 565 (1967).

In the keV region, neutron scattering is by far the dominant process for s-wave resonances in Na, Al, Fe and Ni. For these resonances, the neutron width is usually known from total cross section measurements and the radiation width is determined from the capture data. In the majority of the resonances observed in the present capture measurements, however, the neutron width is comparable to or less than the radiation width. In these circumstances, the area under the capture resonance gives the quantity $(\theta \Gamma_n \Gamma_\gamma) / (\Gamma_n + \Gamma_\gamma)$. As will be shown later, these "weaker" resonances may be assured to be p-wave resonances and an estimate of the p-wave strength function can be obtained for Fe-56 and Ni-58.

2. EXPERIMENT

The Rensselaer electron linear accelerator was used as the neutron source. Details of the target-moderator geometry may be found in Ref. 1.

A 1.25 meter liquid scintillation detector located at a 25.44 meter flight path was used to detect capture events. Comparisons of the capture data and transmission data (2) show that this capture detector has a sensitivity about 50 times greater than the neutron detectors used in total cross section experiments. An auxiliary experiment was performed to test the prompt neutron sensitivity of the capture detector to scattered neutrons. The results of this experiment show that the prompt sensitivity is about one part in 100,000 at an incident neutron energy of 84 keV. Further details of this capture detector may be found in Ref. 3 and 4.

The relative neutron flux was determined using a $^{10}\text{B}_4\text{C-NaI}$ neutron detector. The normalization to an absolute neutron flux was made by the "saturated" resonance technique (5) using the 5.19 eV Ag resonance. The peak counting rate of the 5.19 eV Ag resonance was compared to the capture area of the 60.2 eV Au resonance in a thin Au foil. This Au foil was then kept in the capture detector during all runs in order to normalize the data to an absolute neutron flux.

3. ANALYSIS AND RESULTS

The capture data were reduced to capture "yield", or fraction of captures per incident neutron, as a function of neutron energy. Typical results are shown in Fig. 1 and 2 for iron and nickel, respectively. Other yield curves for Na, Al, Fe and Ni are shown in Ref. 4. The ordinates are expressed as capture yield divided by sample thickness in units of barns. It is important to note that this is not the true capture cross section since the observed yields include the effects of multiple interactions and resolution broadening.

The resonance capture area, $A_Y = \int (\text{Yield}) dE$, is determined for each resonance for each of several sample thicknesses. For those resonances where the neutron width was known from total cross section measurements, a Monte Carlo code (6) was used to extract the radiation width. Using this Monte Carlo code, it was also determined that the calculated resonance capture area was insensitive to the value of the neutron width within the experimental errors quoted for the neutron width. Table I shows the results obtained for several resonances in Na, Al, Fe and Ni. Note that satisfactory agreement is obtained with other investigators. There are no published values with which to compare the present results for Ni. The variations in radiation widths for Na, Al, Fe-56 and Fe-57 are to be noted. The 5.88 keV Al and 1.15 keV Fe-56 resonances are p-wave resonances while all the others are due to s-wave neutrons.

The majority of the resonances observed in the capture data had not been detected in total cross section measurements. For these resonances, the neutron width is comparable to or less than the radiation width. The complete tables of the resonance parameters obtained from these experiments are too lengthy for this paper and may be found in Ref. 4. If all of these resonances are assumed to be s-wave resonances, then there are far too many small levels to fit a Porter-Thomas distribution of reduced neutron widths. On the other hand, the smallest resonance by itself is large enough to account for the entire d-wave strength function. Therefore, these weaker resonances, previously unobserved in total cross section measurements, are assumed to be p-wave resonances. The further assumption is made that the radiation width is 0.6 eV for all these resonances in Fe-56 and 0.7 eV for those in Ni-58. The p-wave strength function is then calculated for twelve resonances in Fe-56 and ten resonances in Ni-58, covering the energy range from about 1 keV to 60 keV. The value of the p-wave strength function obtained is $(0.10 \pm 0.04) \times 10^{-4}$ for Fe-56 and $(0.04 \pm 0.03) \times 10^{-4}$ for Ni-58. (If the radiation width for Fe-56 is assumed to be equal to 1.0 eV, then the p-wave strength function is found to be $\sim 0.04 \times 10^{-4}$.)

4. SUMMARY

Where comparisons of radiation widths and/or capture areas can be made, the agreement between the present results and those reported in Ref. 2 is generally satisfactory. The data obtained for Fe-56 and Al seem to show a difference between s- and p-wave radiation widths. The radiation widths determined for Fe-57 also show a variation of two to three in magnitude. The neutron capture gamma spectra of Na, Al, Fe and Ni all show a large number of high energy transitions. For these nuclei, there are fewer states available through which the excited nucleus may decay, compared

to a heavier nucleus. Hence the total radiation width may differ from one resonance to another. It is not unreasonable that the s- and p-wave radiation widths may differ since there is a change of parity involved and the E1/M1 transition ratios may vary.

The values obtained for the p-wave strength functions are about an order of magnitude lower than predicted by optical model theory (7). However, Fe-56 and Ni-58 fall at a minimum in the p-wave strength function. A large minimum in the p-wave strength function (8) also occurs at mass ~ 160 and here also the experimental values lie well below theory.

5. REFERENCES

1. R. C. Block, R. W. Hockenbury, Z. M. Bartolome and R. R. Fullwood, Nuclear Data For Reactors, Vol. I. 565 (1967).
2. Neutron Cross Sections, compiled by M. D. Goldberg, et al., BNL 325, 2nd Ed., Suppl. 1, No. 2, Vol. III A.
3. R. C. Block, G. G. Slaughter, L. W. Weston and F. C. Vonderlage, Proc. Symp. on Neutron Time-of-Flight Methods, (J. Saepen, ed.), Euratom, Brussels, 203 (1961).
4. R. W. Hockenbury, "Neutron Capture in Low Absorption Materials", Ph.D. thesis, Rensselaer Polytechnic Institute, August, 1967, to be published.
5. E. R. Rae and E. M. Bowey, J. Nuclear Energy 4, 179 (1957).
6. J. G. Sullivan and G. Werner, Oak Ridge National Laboratory, private communication.
7. C. Slavik, Knolls Atomic Power Laboratory, private communication.
8. B. Buck and F. Perey, Phys. Rev. Letters, Vol. 8, No. 11, 444, (1962).
9. W. M. Good, J. H. Neiler, J. H. Gibbons, Phys. Rev. 109, 926 (1958).
10. J. E. Lynn, F. W. Firk, M. C. Moxon, Nucl. Phys. 5, 603 (1958).
11. J. B. Garg, et al., Conf. on Study of Nuclear Structure with Neutrons, Antwerp, Belgium (1965).
12. M. C. Moxon and N. J. Pattenden, Nuclear Data for Reactors, Vol. I. 129 (1967).

TABLE I.

Some Resonance Parameters of Na, Al, Fe and Ni^a

Isotope	Resonance Energy (keV)	Neutron Width (eV)	g	Radiation Width (this exp.) (eV)	Radiation Width (other workers) (eV)
Na	2.85	410 ^b	3/8	0.61 ± 0.06	0.6 ^b
Na	52.2	700 ^c	3/8	2.60	
			5/8	1.58	
			7/8	1.12	
Al	5.88	20 ^d	3/12	0.95	
			5/12	0.57	
			7/12	0.41	
			9/12	0.32	
Al	35.0	1700 ^d	7/12	2.8 ± 0.3	
Fe-56	1.15	2g $\Gamma_n=0.176\pm 0.028$	0.042	0.6 ^d	2g $\Gamma_n=0.136^e$ 2g $\Gamma_n=0.104^g$
Fe-56	27.7	1670 ^d	1	1.44 ± 0.14	1.5 ± 0.3 ^f 1.3 ^g
Fe-57	3.96	177 ^d	1/4	1.14 ± 0.10	≤ 1.0 ^g
Fe-57	6.21	396 ^d	3/4	1.32 ± 0.12 0.14	≤ 1.7 ^g
Fe-57	29.-	3000 ^d	3/4	4±1	
Ni-62	4.6	1300 ^d	1	0.76 ± 0.12	

a. Note that these are only selected resonances; see Ref. 4 for the complete list.

b. Average value from Ref. 9-12. c. Ref. 11 and 12.

d. Neutron Cross Sections, BNL 325, Vol. I and III A

e. R. C. Block, Phys. Rev. Letters 13, 234 (1964)

f. Macklin, R. L., Plasma, P. J., and Gibbons, J. H. Phys. Rev. 109, 1258 (1958).

g. Moxon, M. C., Int. Conf. on the Study of Nuclear Structure with Neutrons, Antwerp, Belgium, July 19-23 (1965).

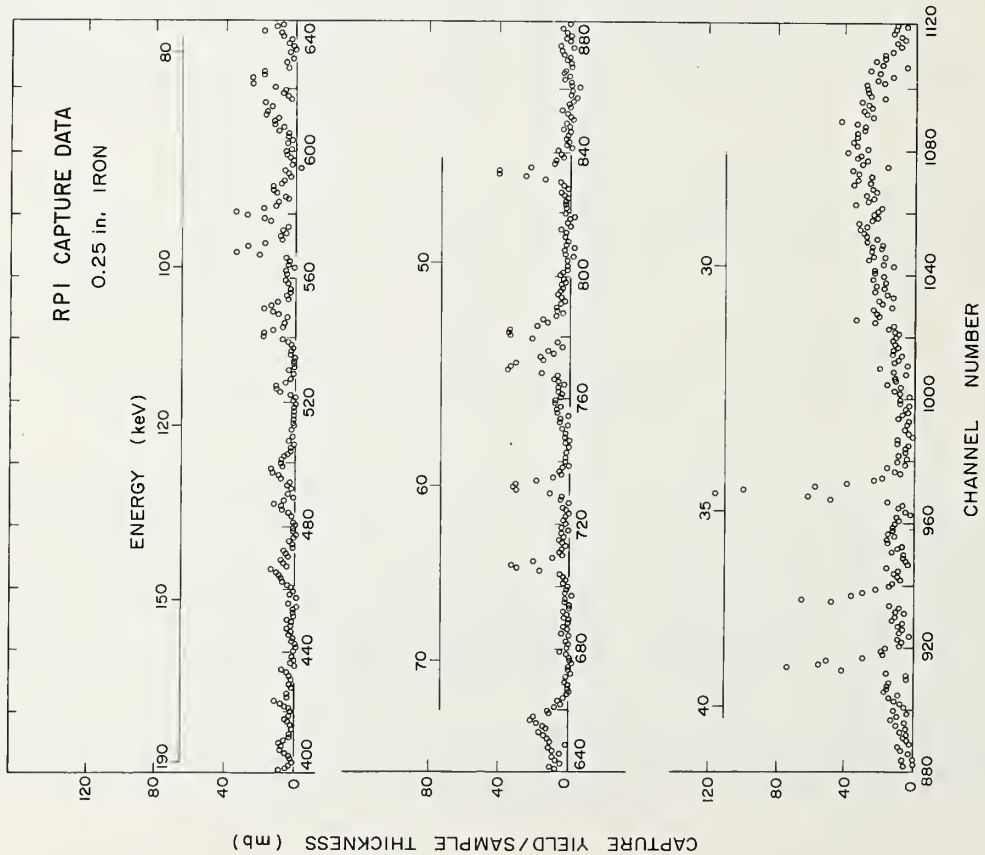


Figure 1 Capture yield divided by sample thickness for iron.

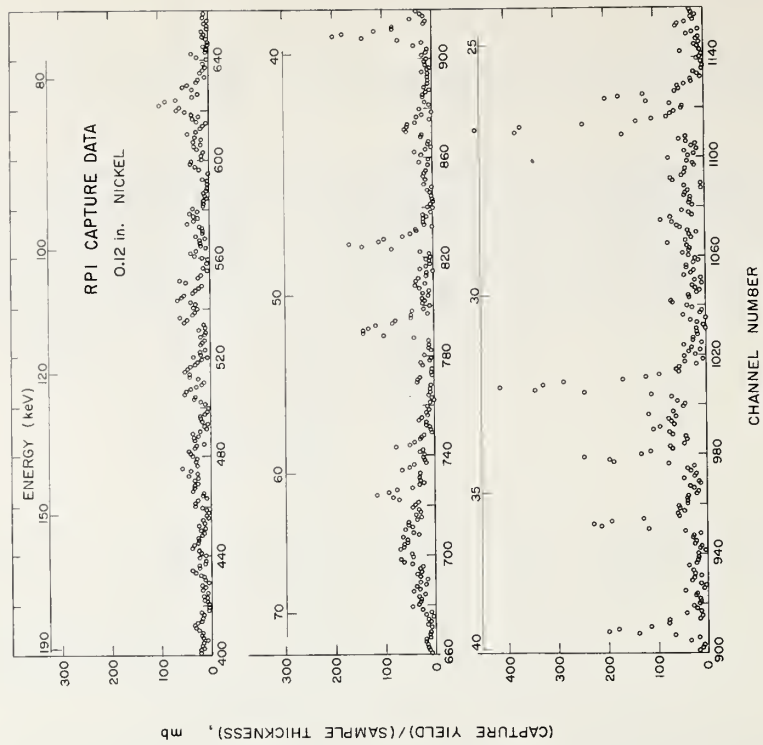


Figure 2 Capture yield divided by sample thickness for nickel.

NEUTRON SCATTERING MEASUREMENTS IN LOW ENERGY
Cd AND Rh RESONANCES*

T. J. King+ and R. C. Block

Rensselaer Polytechnic Institute
Division of Nuclear Engineering and Science
Troy, New York 12180

Scattering measurements have been made using two ${}^6\text{Li}$ glass scintillators as neutron detectors together with a large liquid scintillator anti-coincidence mantle. This system provides (1) high neutron efficiency, (2) fast timing for time-of-flight spectrometry, and (3) greater than 90% rejection of capture background in the ${}^6\text{Li}$ glasses. The high rejection of capture background comes about because of the high efficiency ($>90\%$) for the detection of neutron capture by the large liquid scintillator. This rejection results in an extremely small capture background in the glasses. Measurements were carried out on Rh and Cd from 30 to 1500eV, and six resonances have been analyzed for resonance parameters in Rh. These results together with the results of transmission measurements (which were also made for these samples) yield the spin (J), neutron width (Γ_n) and the total width (Γ) for each resonance.

*Work supported by the U. S. Atomic Energy
Commission under Contract AT(30-3)-328.

+In partial fulfillment of T. J. King's doctoral thesis.

The resonances observed in the low energy neutron cross section of most medium and heavy nuclei are mainly due to s-wave ($l=0$) interaction between the neutron and the nucleus. Each resonance can therefore be described in terms of parameters E_0 , J , Γ_n and Γ (for non-fissile nuclei). In order to determine all of the resonance parameters, it is generally necessary to make a neutron transmission measurement and to measure either neutron scattering (for resonances where $\Gamma_n \ll \Gamma_r$) or neutron capture (for resonances where $\Gamma_n \gg \Gamma_r$).

The conventional methods of measuring resonance neutron scattering are complicated by intense background due to capture, low efficiency, and/or poor timing resolution of the scattering detector. In recent years, the use of ^6Li glass scintillators have been employed at Harwell(1,2,3) to measure scattering cross sections: The use of these glass scintillators has improved both the energy resolution and the neutron detection efficiency. However, a correction for the background had to be done by a subtraction method, thus introducing large statistical uncertainties. A technique has been developed(4) which combines a ^6Li glass neutron detector with a large liquid scintillator anticoincidence mantle. This system has the high neutron efficiency and the good timing resolution of the glass scintillators together with the high efficiency ($> 95\%$) of the liquid scintillator for detecting (and rejecting) capture events. Figure 1 shows the experimental arrangement. Two pieces of 1/2 inch thick by 2 inch diameter ^6Li glass, each mounted on a RCA 6810 PM tube, are located inside the beam port of the scintillator tank. The previous system(4) used only one such detector together with a much simpler logic system. The signals from the glass are added and then sent to two discriminators. The output of each discriminator is fed into the logic system together with the signal from the tank.

If the large scintillator tank were 100% efficient for detecting capture events, then all capture background counts detected in the ^6Li glass would be rejected by operating the ^6Li glass in anticoincidence with the tank. Since the tank is only $\sim 95\%$ efficient, a background correction must be applied to the anticoincidence data. Figure 2 shows a typical pulse height response of ^6Li glass to thermal neutrons and to capture gamma rays. By setting two window discriminators, one on the neutron peak and one on the valley, and then recording these discriminator pulses in coincidence or in anticoincidence with the tank signals, it is possible to determine the number of capture events detected by the ^6Li glass which were not detected by the tank. If we define window 1 as that set on the neutron peak, window 2 as that set on the valley, N as the total number of glass counts in anticoincidence (with the tank) from

discriminator N and β_N as the total number of counts in coincidence from discriminator N then the following equation can be derived:

$$S = \frac{\alpha_1 - \frac{\alpha_2 \beta_1}{\beta_2}}{1 - K \frac{\alpha_2}{\beta_2}} \quad (1)$$

where S is the number of counts due to scattered neutrons. K is determined as the ratio of counts in window 2 to counts in window 1 when only thermal neutrons are incident upon the glass. What this equation shows is that if the detector had not been sensitive to neutrons in the valley ($K=0$), then the correction would simply have been the ratio of β_1 to β_2 times α_2 . Since this is not the case, the extra term ($K \alpha_2 / \beta_2$) must be added to correct for scattered neutrons detected in window 2. Figures 3 and 4 show the four fields of data (corresponding to α_1 , β_1 , α_2 and β_2 respectively) for Rh and Cd. It should be noted that part (a) of each graph (the output of discriminator 1 in anticoincidence with the tank) is mostly due to neutron scattering while part (d) (the output of discriminator 2 in coincidence with the tank) is due to capture. Parts (b) and (c) are combinations of both, due to accidental coincidences, missed capture events, etc. Looking at the 125eV resonance (about channel 250) in Figure 3, one sees that it almost completely disappears in scattering (plot (a)). This indicates that almost all of this resonance is due to capture which agrees with previously published data. Another interesting point to notice is the inversion in the magnitudes of the peaks at 154 and 187eV (about channel 200) in plots (a) and (d). This again is due to different relative contributions of scattering and capture in these resonances. Similar differences can be seen in the Cd data (Figure 4).

The size of the background correction to the scattering data is also an important item to examine. As mentioned before, the rejection of capture background by the system is greater than 95%. For the 154eV resonance in Rh, this correction is about 1% of the scattering data. This is a vast improvement over other systems where the correction could be as much as 50%.

Table 1 gives the results for six analyzed resonances in Rh. The values of the spin state (J), total width (Γ) and $2g \Gamma_n$ are determined by combining the results of transmission data, which were taken separately, and the results of the neutron scattering data. The transmission data were analyzed using the

Harvey-Atta⁽⁶⁾ area analysis code. This code was run on the CDC-6600 computer at New York University by means of the⁽²⁾ telephone link with the IBM-1130 computer at Rensselaer. Area analysis methods were also used on the neutron scattering data. Also given in this table are results quoted by Ribon et. al.⁽⁵⁾ The agreement is good in all cases except for the 435eV resonance. However, the results which are quoted in this paper yields a Γ_γ of 175 meV which is consistent with those for the other resonances in Rh. As of this time, the analysis of the Cd data is not fully completed so that these results are not listed here.

Work is now being done to extend this technique for the fissile elements. Modifications are being made to the tank to allow the use of larger, more efficient ⁶Li detectors so that counting rates can be increased by over an order of magnitude.

REFERENCES

- (1) M. Asghar and F. D. Brooks, Nucl. Inst. and Methods, 39 (1966) 68.
- (2) M. Asghar (1967) EANDC (UK) 70'S.
- (3) M. Asghar et al, Nuclear Physics, 76 (1966) 196.
- (4) T. J. King, R. R. Fullwood and R. C. Block, Nucl. Inst. and Methods, 52 (1967) 321.
- (5) Ribon et al, (1966) Proc. of Antwerp Conf. on Nuclear Structure Studies with Neutrons, Paper 165, North Holland.
- (6) Atta., W. E. and Harvey, J. A., 1962 J. Soc. Indust. Appl. Math. 10, 617.
- (7) W. R. Moyer et al, (1968) Second Conference on Neutron Cross-Sections and Technology, Paper (G-11).

TABLE 1

E_0 (eV)	J	Γ (meV)	$2g \Gamma_n$ (meV)	J^*	Γ^* (meV)	$2g \Gamma_n^*$ (meV)
154.4	0	300	97.5	0	388	97
187	1	180	52	1	210	57
253	1	200	52	1	230	51.9
272	1	280	90	1	252	85.7
319	1	225	135	1	262	146
435	1	350	263	1	431	309

* Ribon et. al⁽⁵⁾

1.25 METER LIQUID SCINTILLATOR DETECTOR
AT 25 METER FLIGHT STATION

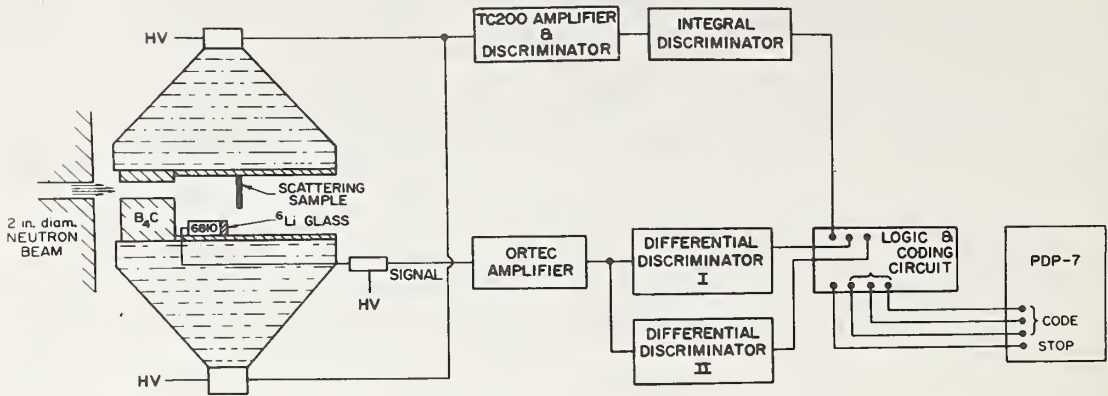


Figure 1 Experimental Arrangement.

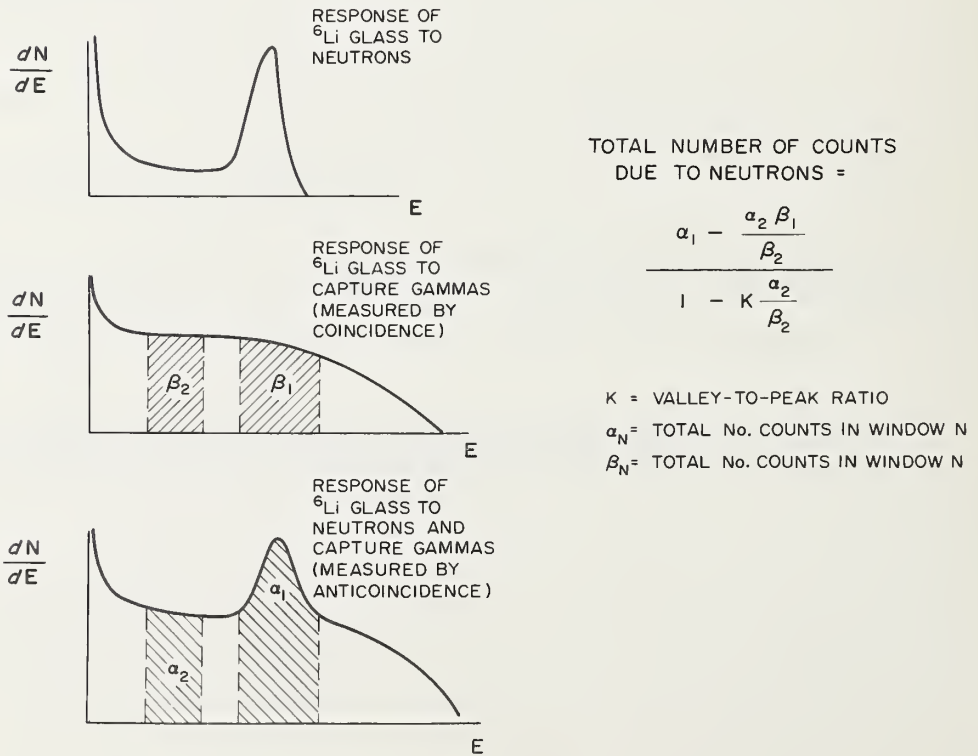


Figure 2 Typical Pulse Height Response of ${}^6\text{Li}$ Glass.

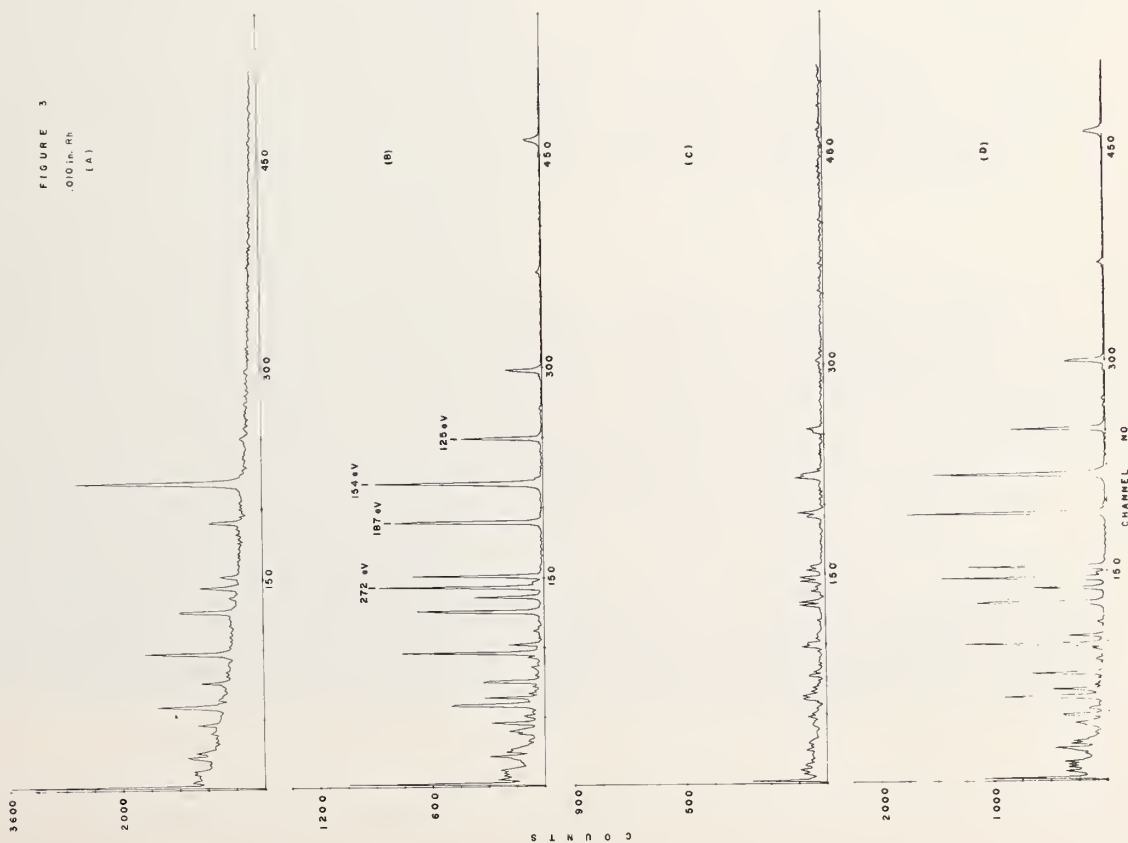


Figure 3 Rhodium Data Plot.

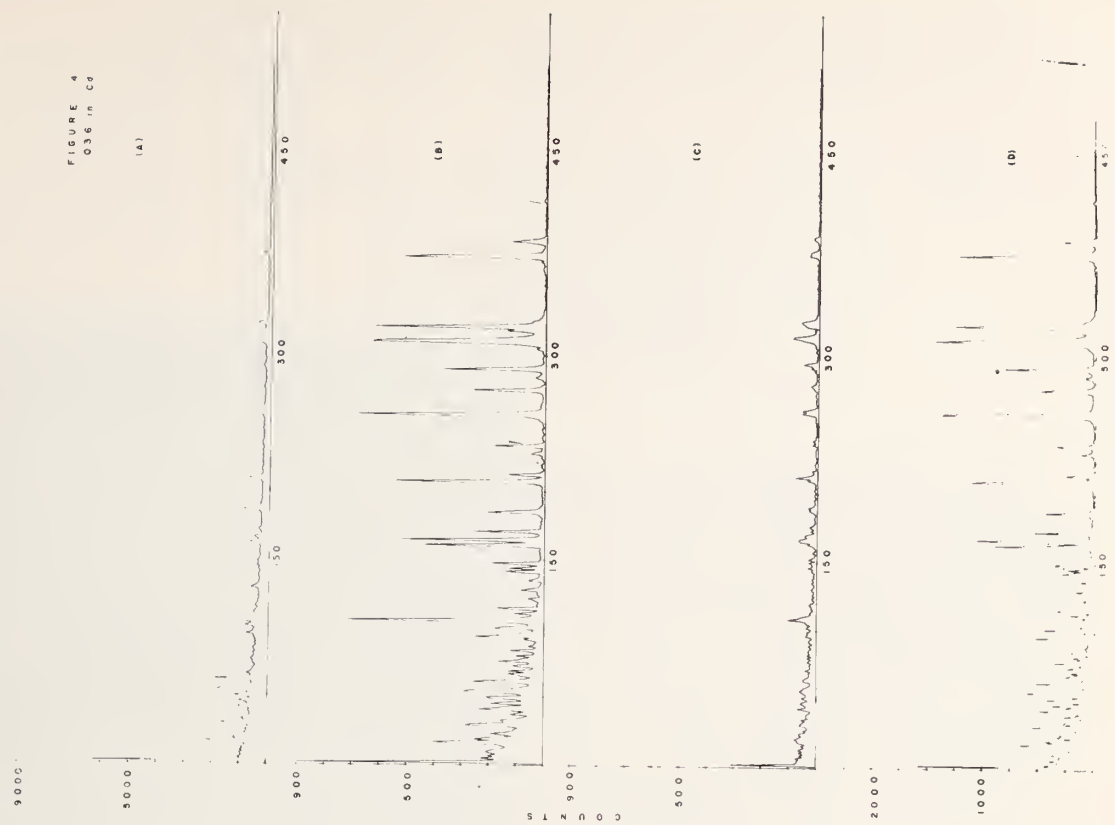


Figure 4 Cadmium Data Plot.

DATE DUE 1 WEEKS FROM DATE
OF RECEIPT

U. S. National Bureau of Standards
Library, Room E01 Admin. Building
Washington, D.C., 20234

PERIODICALS CANNOT BE RENEWED

For Renewal: Call Code 164 X3410
or 921-3410

STOP 3

USCOMM-NBS- DC
(12/68)

High Resolution Total Fast Neutron Cross Sections on Some
Non-Fissile Nuclei in the Energy Range $0.5 \leq E_n \leq 30$ MeV

S. Cierjacks, P. Forti, D. Kopsch, L. Kropp, J. Nebe

Institut für Angewandte Kernphysik

Kernforschungszentrum Karlsruhe

F. R. Germany

Abstract

The spectrometer at the Karlsruhe isochronous cyclotron has been used to measure fast neutron total cross-sections of a number of nuclides ranging from C to Bi. Bursts of 45 MeV (average energy) deuterons of ~ 1 nsec duration striking thick natural uranium targets yield a broad neutron spectrum, capable to obtain useful neutron data between about 0,5 - 30 MeV. Neutrons were analysed by time-of-flight. The analysis system includes a 57 m flight path, a 9 cm diameter x 1 cm thick NE - 213 liquid scintillator in connection with a zero-cross over tunnel-diode time-mark circuit and a digital time analyzer coupled with a CDC-3100 on-line computer as the time recording system. The overall resolution in the present experiments was $\leq 0,03$ ns/m. The high neutron intensity from the cyclotron permits rapid data accumulation. Typically 1% statistical accuracy was obtained in most of the 16000 data points in a 10 - 12h running time.

In the energy dependent cross section significant fluctuations have been observed up to several MeV. In the light elements C, O, Al, Na, S fluctuations outside the statistical uncertainty range up to 10 MeV or more, for the elements Ca and Fe fluctuations up to 6 - 8 MeV and for Bi and Tl up to 3 - 4 MeV were found. In order to investigate the effects of fluctuations a statistical analysis was performed in some cases.

1. Introduction

The objective of the study on high resolution cross-section is the acquisition of a systematic experimental knowledge and the approach of physical understanding of fast neutron scattering phenomena. One of the impulses of such measurements was given from fast reactor design requests and from shielding requirements. On the other hand, studies are chiefly maintained in order to provide a basic physical understanding to allow accurate predictions on unknown data by application of suitable semiempirical non-sophisticated models.

The extremely complicated structure of intermediate and heavy weight nuclei in the fast neutron region is a serious problem to the reactor and nuclear physicist. A microscopic resonance analysis of the resonance structure also in the region of non-overlapping levels

will be possible if at all, only in the lowest energy range covered by the present data. Therefore, other physical interpretations leading to structure information and providing descriptions useful for applied calculations are necessary: useful physical approaches seem to be the concept of intermediate structure in the sense of Ericson ¹⁾ or of Block and Feshbach. ²⁾ In the concept of Block and Feshbach the intermediate configurations represent short lived two-particle, one-hole configurations or more complex 'doorway state' configurations, which should appear as broad peaks in the excitation functions. According to Ericson fluctuations should be present also in the region of strongly overlapping levels as a consequence of the random phase approximation. Other useful concepts are the descriptions of cross sections by average quantities such as the average spacings and average widths of compound nuclear levels.

In section 2 of this paper the high resolution time-of-flight spectrometer employed in this work and some experimental results are described; while in section 3 the analysis and comparisons with calculations based on statistical arguments and compound nuclear theory are outlined.

2. Experiments and results

The experimental procedure required high resolution and sensitivity since all physically meaningful structure should be observed. On the other hand, the measurements required methods capable of the acquisition and processing of a large amount of experimental information. Such requirements are essentially satisfied now by the existing time-of-flight spectrometer and the CDC-3100 on-line data acquisition system at the cyclotron and the extended data processing system of the IBM 7094 computer. The cyclotron provided with a particular 'deflection-bunching' system described elsewhere ³⁾ was used to produce short (~ 1 nsec) intense bursts of neutrons with 20 kc/s repetition rate and a broad neutron spectrum. Neutron production was achieved by (d,nx) reactions in thick natural uranium targets by bombardment with 45 MeV deuterons from the internal beam. By timing of the neutrons over a 57 m flight path a resolution of $\leq 0,03$ nsec/m was obtained. Time-of-flight assignment were made with a digital time-sorter (LABEN UC-KB). Typically 2 x 8000 time channels of 1 nsec channel width were used. The presently used on-line program allows several automatical operations during the measurement (spectrum compatibilisation, dead time observation, etc.) and exerts a great deal of on-line control of the overall-reliability of the time-of-flight apparatus. Unfortunately, however, the maximum input rate of 10^4 c/sec limits the rapid data accumulation at present.

Because of the limited memory capacity of the CDC-3100 the input data are preaccumulated in the memory separately for both sample positions. After each cycle for 'sample in' and 'open beam' position, for which typically a total period of 5 - 8 min was chosen, the information is stored on magnetic tape. Accumulation of the entire information belonging to the same run is accomplished after the measurements.

Total neutron cross-sections of 9 elements, C, O, Na, Al, S, Ca, Fe, Bi and Tl were measured at increasing energy intervals from about 0,5 - 30 MeV. In figures 1 - 5 total neutron cross-sections on C, Na and S are shown in different subintervals. The energy resolution is believed to be ≤ 2 channels at all energies. The statistical uncertainties in most of the data points are between 1 - 3 %. Absolute uncertainties are less than 3%. The data had been compared with selected published data (not shown) from various laboratories 4) - 10). In general, the agreement with published work is good. In several energy regions the data exhibit more structure than was observed in the earlier measurements. The differences in structure can be attributed mainly to the difference in energy resolutions. If our curves are smoothed by using average intervals equivalent to the energy resolution of the previous measurements, the remaining structure agrees with that observed in other laboratories. There are, however, still some discrepancies: Comparing e.g. the data on C in the energy region around 2.8 MeV (fig. 1) with data reported by Willard et. al. 11), there is a discrepancy concerning the sharp resonance of ~ 5 keV (f. w. h. m.) observed in our measurements. This resonance could not be observed by Willard, Bair and Cohn in a 5 keV resolution measurement. We have been unable to identify any error in our data which could be responsible for this disagreement. But the level at 2,817 MeV was observed also in the C 12 (d, p) C 13 reaction 12). So we believe that this is the same resonance as we found in our total neutron cross section measurement.

The sodium data (figures 2 to 4) can be compared mainly with the recent measurements of Langsford et al. 13) which, however, show poorer statistical accuracy than our data. The average cross-sections agree well with these measurements. Over a wide energy range we observed more structure which fact can be attributed to our higher energy resolution. Above 6 MeV we do not agree at all with the details of structure even if the different energy spreads are taken into account. But in this range the Hanford data are in good agreement with our and other data 14).

Similar arguments-i.e. good agreement with other published data 15) 16) was found for comparable energy spreads - applies for the sulfur result. These data are an example for what happens in the MeV region of intermediate weight nuclei. While in the lowest energy region the rapid fluctuations are due to individual levels, these levels start overlapping more and more at increasing energies. At about several MeV the average widths becomes comparable to the average spacings and finally we enter the region of Ericson fluctuations where $\Gamma_J/DJ_\pi \gg 1$. It is this situation where the arguments mentioned earlier, i. e. the need of interpretations leading to structure information and the need of providing descriptions useful for applied calculations, become meaningful.

3. Analysis and Discussion

Causes of fluctuations which were considered are mainly intermediate structure. Additionally Ericson fluctuations and fluctuations of neutron widths and spacings of compound nuclear levels have been included in some cases.

In order to investigate whether a broad structure is present in addition to the fine structure the analysis proposed by Pappalardo ¹⁷⁾ was performed for Al, Na, S, Ca and Fe in the energy regions in which fluctuations were observed. This occurred mostly in the region between 0,8 - 8 MeV. For each element the analysis was performed separately for four quarters of the total range. The correlation functions $C(0, \delta)$ i.e. the unnormalized variance for Al are shown in fig. 6. The sub-intervals over which the data were taken are from 0,8 - 2, 2 - 4, 4 - 6 and 6 - 8 MeV respectively. The error bars are deduced from the finite number of fluctuations.

The presence of a second rise in the variance curves is taken as an evidence that a broader structure exists. From the curves in fig. 6 such a structure must be assumed for aluminum at least in the two lower energy subintervals. Similar results were obtained for the other elements in some energy regions.

To conclude anything about the nature of the structure from these results it is necessary to go into more details. It has been shown by some authors ¹⁸⁾ that intermediate structure can also be explained in terms of statistical fluctuations in the parameters that describe compound nuclear levels, i. e. such structure must not necessarily be interpreted as doorway state structure. We have also considered the possibility of such an interpretation which was done by an analysis similar to the theory of Agodi et al. ¹⁹⁾ Assuming various conventional distributions for level spacings and level widths this theory yields values for the number of levels of given spin and parity that can exist in an average interval and still give rise to the observed intermediate structure. In several cases it is difficult to justify the discrepancy between the number of levels found and the number of levels that would be necessary to explain the observed intermediate structure in terms of level statistics. Although somewhat tenuous, this argument suggests that the broader structure involves the type associated with doorway states. Further evidence for this interpretation comes from a rough calculation of average level distances for two-particle, one-hole states from the shell model which have been made in the cases of Al, Ca and Fe and which gave order of magnitude agreement with the experiment. We would, however, point out that the energy dependence of average distances is in qualitative disagreement. While from the calculation a decrease of the level distances is predicted, the average distances of the broader maxima in the cross section curves seem to increase with increasing energies.

The analysis applied in this work also provides values for the auto-correlations functions which are used in the theory of Ericson fluctuations. This enables us to deduce level densities and average level width if the condition $\Gamma_j / D_{j\pi} \gg 1$ is fulfilled. There is, however, some doubt that this condition holds, especially for the lighter nuclei, even at higher energies.

Nevertheless, it was proved that in various subintervals the calculated curves follow the theoretical dependence of $C(I, \delta)$ on δ if the average is taken over the fine structure only. The values obtained for level

spacings and level widths are largely in agreement with other reported values. 10)

Finally, it should be mentioned that a statistical analysis provides a method to deduce level densities applying the theory of Agodi and Pappalardo 19). The first results which have been obtained up till now are consistent with available estimates of level densities. In the regions of non-strongly overlapping levels it is this method from which most reliable results can be expected.

Summarizing this paper it can be stated: In general individual quantities of compound nuclear levels can not be excepted from MeV neutron experiments except for the lightest nuclei or at lowest energies for some medium weight nuclei. Mainly average quantities can be deduced from high resolution measurements the more accurately the more all physically meaningful structure has been observed. But these quantities will be most important for applied calculations. For reactor requirements it is especially the broader structure in the cross-section curves which is not at all negligible. Therefore, a better understanding of intermediate structure phenomena may be of great importance. Valuable additional information can be obtained from partial cross section measurements. Therefore we try an attack also on this kind of experiments at present.

References

1. T. Ericson, Ann. Phys. 23 (1963), 390
2. H. Feshbach, Ann. Phys. 5, (1958), 353
3. S. Cierjacks, P. Forti, D. Kopsch, L. Kropp, H. Unseld, Conf. 66025 (TID 4500) p. 589
4. J. J. Schmidt, Neutron-Cross Section Evaluation, EANDC-E-35U and References cited there in (1966)
5. D. J. Hughes and R.B. Schwartz, Neutron Cross Sections, BNL-325 (1958) and D. J. Hughes, B. A. Margurno, M. K. Brüssel, Neutron Cross Sections BNL-325, Supplement No. 1, 2nd ed. (1960)
6. A. J. Elwyn, J.E. Monahan, R. O. Lane, A. Langsdorf, Jr., F.P. Mooring, Int. Conf. on the Study on Nucl. Struct. with Neutrons, Antwerp 1965 p. 103
7. D. B. Fosson, R. L. Walter, W. E. Wilson, H. H. Barshall, Phys. Rev. 123, 209 (1961)
8. J. M. Peterson, A. Bratenahl, J. P. Stoering, Phys. Rev. 120 (1960), 521
9. P.F. Yergin, R. C. Martin, E. J. Winhold, H. A. Medicus, W. R. Moyer R.H. Augstson, N. N. Kaushal, Conf. 660 303 p. 690
10. A. D. Carlsson and H. H. Barshall, Phys. Rev. 158 (1967) 1148
11. H. B. Willard, J. K. Bair, H. O. Cohn, ORNL-2501 (1958) p. 18
12. N. J. Mc Gruer, E. K. Warburton, R. S. Bender, Phys. Rev. 100 (1955) 235
13. A. Langsford, P. H. Bowen, G. C. Fox, F. W. K. Firk, D. B. Mc Gonnell, B. Rose, M. J. Saltmarch, Int. Conf. on the Study on Nucl. Struct. with Neutrons, Antwerp, 1965, p. 81
14. D. W. Glasgow, D. G. Foster, H.W-SA-2875, (1963)
15. R. J. Howeston, UCRL-5351
16. U. Fasoli, T. Toniolo, G. Zago, Nuovo Cimento 44, (1966) 455
17. G. Pappalardo, Phys. Lett. 13 (1964), 320
18. P.P. Singh, P. Hoffmann-Pinther, D. W. Lang, Phys. Lett. 13 (1964) 320
19. A. Agodi, G. Pappalardo, Nucl. Phys. 47 (1963), 129

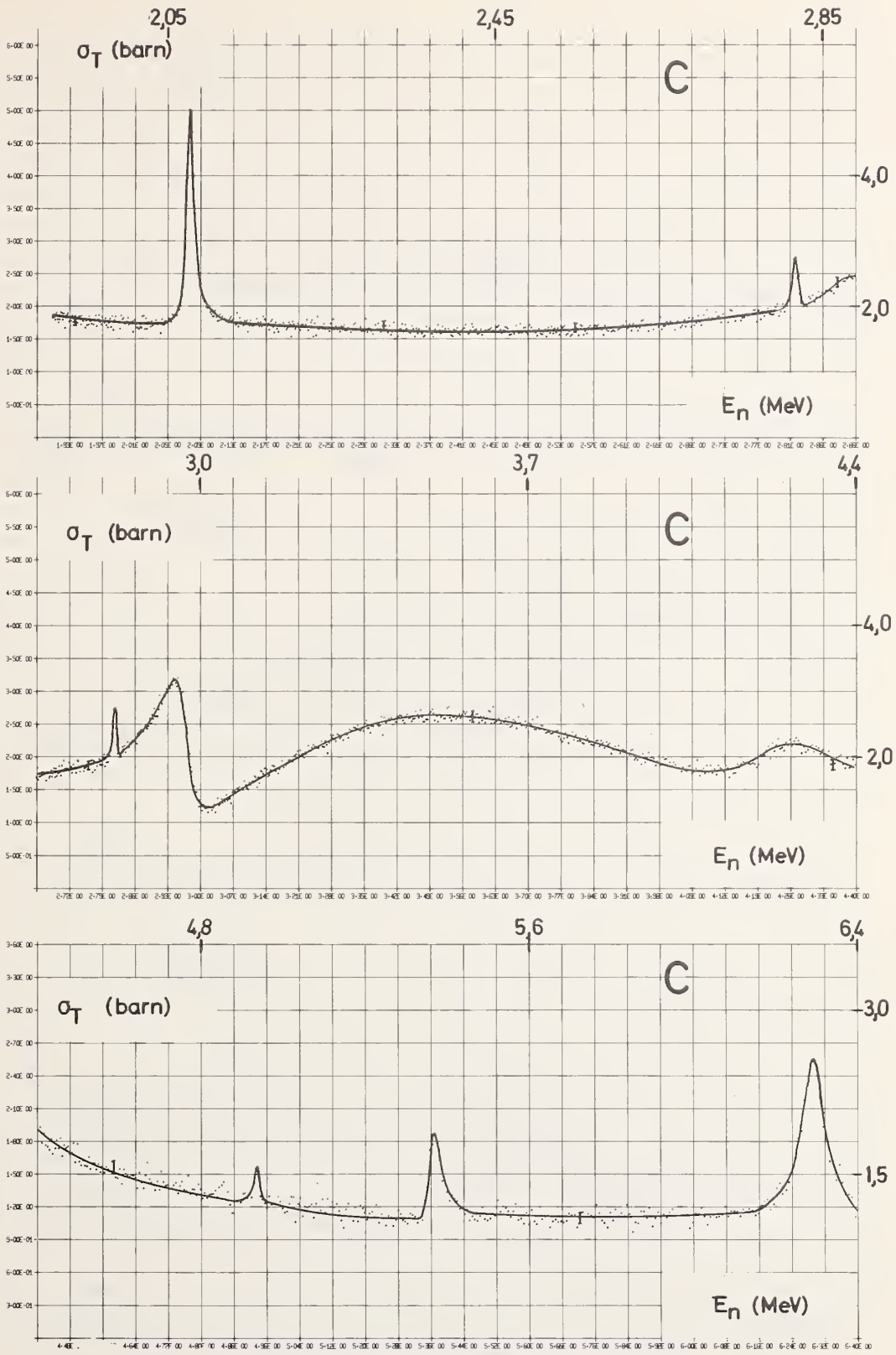


Fig.1 Total neutron cross-section of carbon

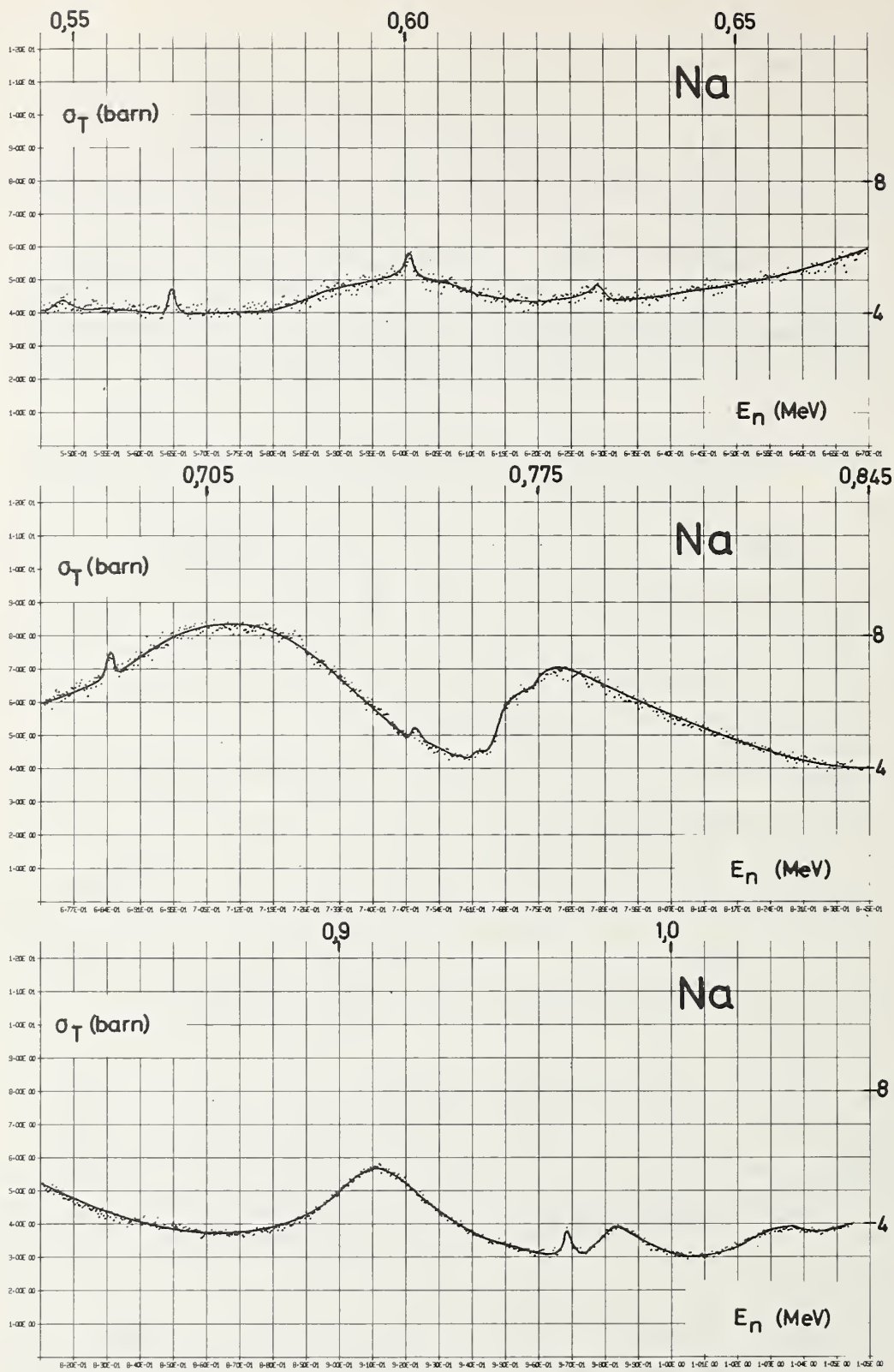


Fig.2 Total neutron cross-section of sodium

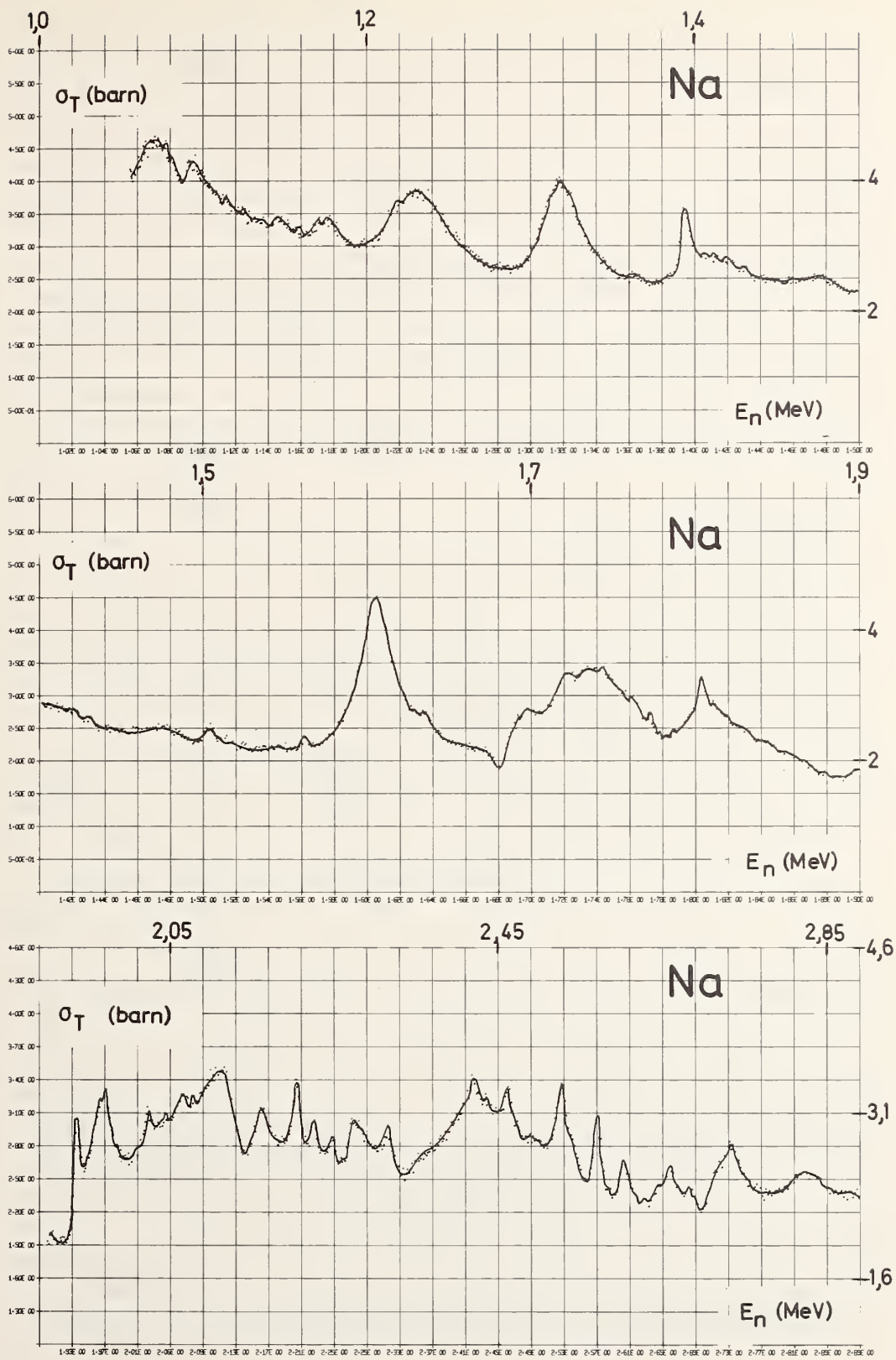


Fig.3 Total neutron cross -section of sodium

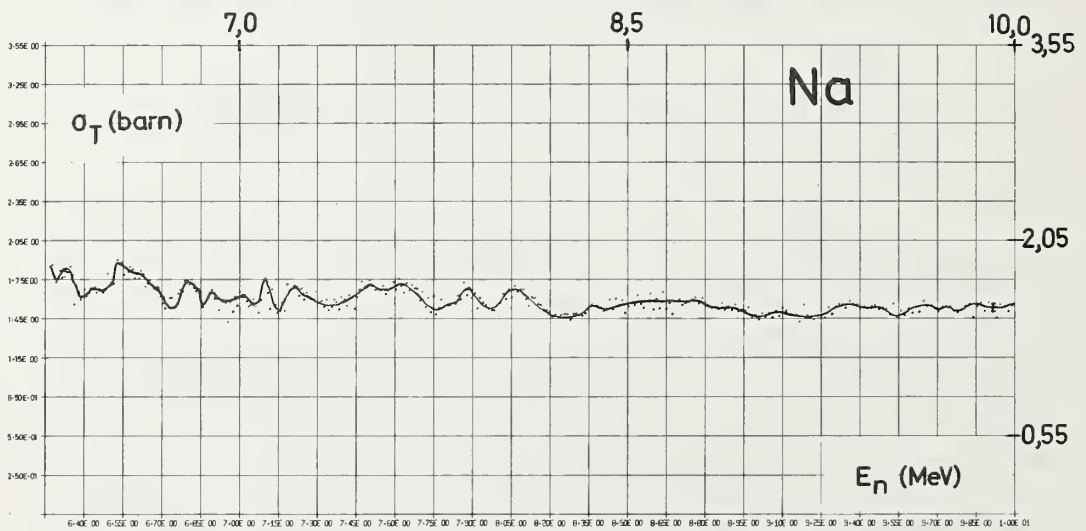
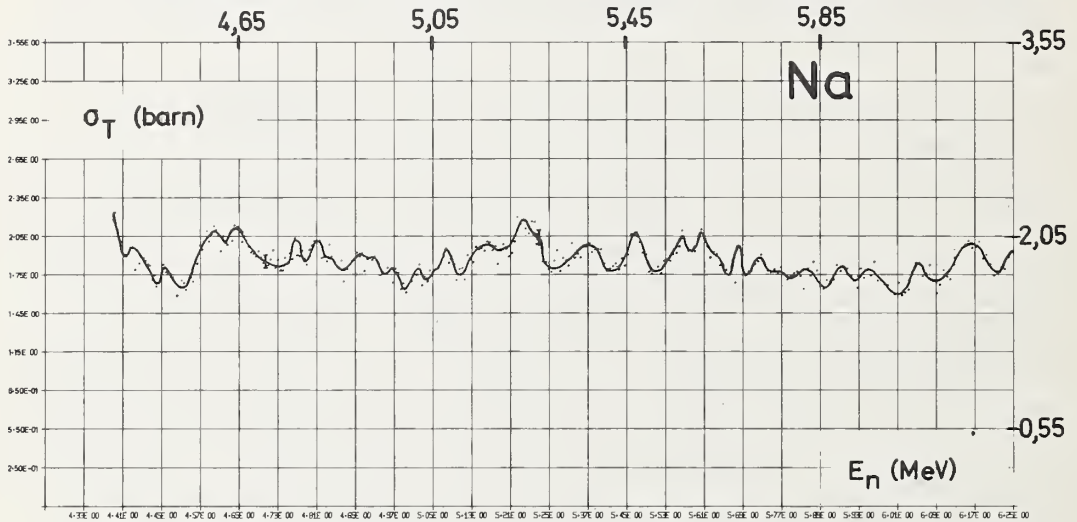
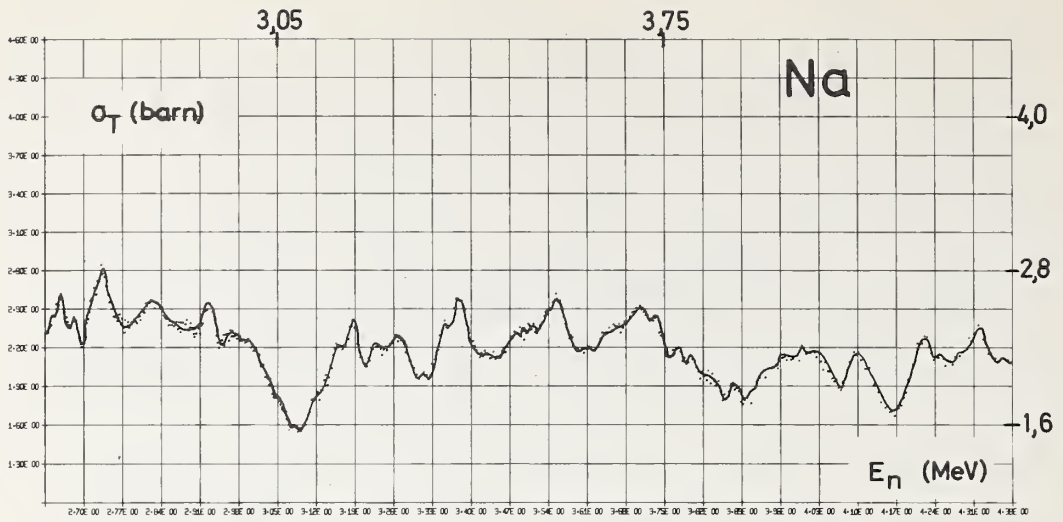


Fig.4 Total neutron cross-section of sodium

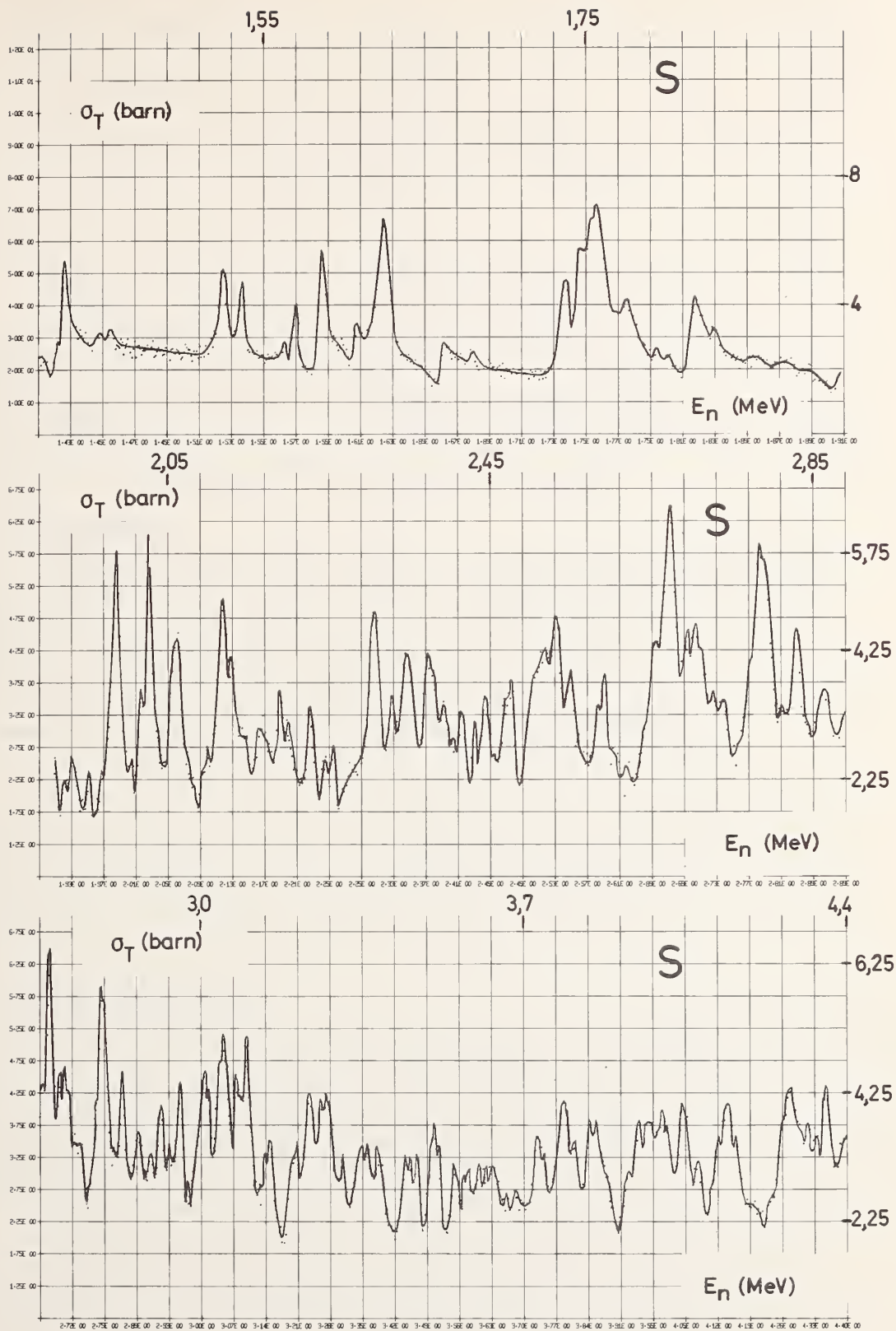


Fig.5 Total neutron cross-section of sulfur

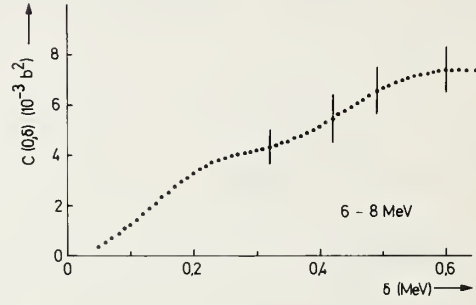
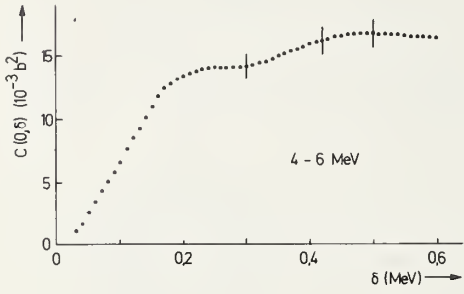
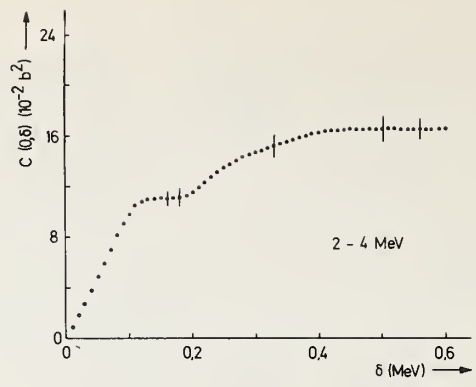
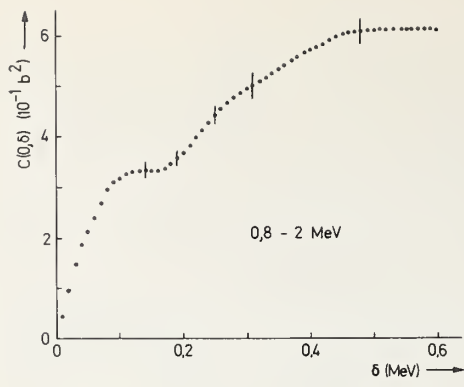


Fig.6 Self-correlation functions for the Al data

Elastic Scattering of Fast Neutrons by Praseodymium and Lanthanum*

D. L. Bernard, G. H. Lenz, and J. D. Reber

University of Virginia

Charlottesville, Virginia 22903

Abstract

The differential cross section for the elastic scattering of fast neutrons by praseodymium and lanthanum has been measured for an incident neutron energy of 8.00 MeV from 25° to 155° in the laboratory system. A pulsed-beam neutron time-of-flight spectrometer was used in conjunction with a Mobley buncher and a 12.7 cm diameter NE102 plastic scintillator. The absolute differential cross section was normalized to the n-p differential cross section at 40° in the laboratory system.

1. Introduction

The study of the elastic scattering of neutrons in the rare-earth region of the periodic table is interesting for reasons which are pertinent both to pure and applied physics. In the realm of pure physics, angular distributions of elastically scattered neutrons can be compared with the theoretical predictions of the optical model. The behavior of the optical model potential parameters can be studied both as a function of incident neutron energy and of scattering mass. Such studies can yield information on the validity of the use of a spherically symmetric optical model of the nucleus to describe distorted rare-earth nuclei.

In the realm of applied physics, in particular, reactor physics, it is necessary to know neutron scattering cross sections of the rare-earths since they are products of fission which contribute to the poisoning of reactor fuel elements. From a knowledge of the total elastic scattering and the total scattering cross sections of neutrons scattered from the rare-earths, the inelastic scattering cross section can be inferred. The present work is directed toward obtaining this information.

2. Experimental Method

The University of Virginia pulsed-beam neutron time-of-flight spectrometer^[1] was used to detect neutrons scattered from samples of praseodymium and lanthanum. A beam of deuterons was chopped in the terminal of the model CN Van de Graaff accelerator and subsequently bunched by a Mobley magnet. The resulting bursts of deuterons of 2 nanosecond duration were incident on a gas cell which contained one atmosphere of deuterium. The deuterium gas was separated from the vacuum system of the Mobley buncher by a $2.286(10^{-4})$ cm Havar^[2] foil.

Samples of praseodymium, lanthanum, and polyethylene were machined to the dimensions shown in Table I. With this sample size neutron flux

* Research supported in part by the National Science Foundation.

¹L. Cranberg, et al, Phys. Rev. 159, 969 (1967).

²Hamilton Watch Company, Lancaster, Pennsylvania. 19104

attenuation and multiple scattering corrections were minimized while still maintaining a substantial yield of scattered neutrons. The samples were

TABLE I

Scattering sample dimensions in centimeters and weights in grams

Sample	I.D.	O.D.	Length	Weight
Praesodymium	0.160	1.588	1.905	23.51
Lanthanum	0.160	1.588	1.727	20.19
Polyethylene	0.160	0.505	1.890	0.31

suspended using thin walled stainless steel tubing (0.102 cm I.D., 0.160 cm O.D.) with their cylindrical axes perpendicular to the incident neutron flux. An automatic sample changer, remotely controlled from the control room of the accelerator was used to position the appropriate sample. A closed circuit television system permitted the samples to be viewed while being positioned. The center of each sample was placed 7.5 cm from the center of the deuterium gas cell in the direction of the incident deuteron beam.

Neutrons were produced from the $D(d,n)He^3$ reaction at a deuteron beam energy chosen to compensate for the beam energy loss in the Havar foil and gas cell. The energy loss in the foil was calculated with a computer program using a range-energy relationship^[3] and the known composition of the Havar material^[2]. The energy loss in the foil and the gas cell was verified experimentally by observing the energy shift of the 6.29 MeV resonance in the C^{12} total neutron cross section. The predictions of the computer calculations differed by 3 per cent from the experimentally determined beam energy loss.

Consequently, the deuteron beam energy necessary to produce monoenergetic neutrons of energy 8.00 MeV was 4.912 MeV. The energy losses in the foil and gas cell were 144 keV and 29 keV, respectively.

The neutrons scattered from the samples were detected with a 12.7 cm diameter by 2.54 cm long NE102 plastic scintillator optically coupled to a 58AVP photomultiplier tube. The detector was placed in a paraffin-lithium carbonate shield assembly which was mounted on an angular distribution carriage whose angular positioning was remotely controlled from the accelerator control room. A copper wedge was used to shield the throat of the tungsten collimator, placed before the detector shield, from the primary neutrons. A schematic diagram of the relative positioning of the target, scatterer, wedge and detector-shield assembly is shown in Figure 1.

A fixed neutron detector was used to monitor the primary neutrons produced at the target. This detector consisted of a 5.08 cm. diameter by 2 mm long NE102 plastic scintillator optically coupled to a 56AVP photomultiplier tube. The detector was placed in a paraffin-lithium carbonate shield supported at 120° from the deuteron beam direction. The

³Publication No. 1133, National Academy of Science, National Research Council, Washington, D. C. (1964).

monitor detector and the deuteron beam were in a vertical plane perpendicular to the plane of the main detector and the beam. A schematic diagram of the electronics used with the monitor and main detectors is shown in Figure 2.

3. Results and Discussion

The relative efficiency of the neutron detector was determined by measuring the neutron yield from the $D(d,n)He^3$ reaction as a function of the laboratory scattering angle for a deuteron energy which yielded 8.00 MeV neutrons at 0° with respect to the beam. In this manner the relative efficiency was determined for neutron energies ranging from 1.70 MeV to 8.00 MeV.

At each angular setting of the neutron detector, the scattered neutron yield was measured for a fixed integrated beam current. A run at each angle was also made with the thin walled stainless steel tubing exposed to the neutron flux and was considered the background run. Neutrons were scattered from the polyethylene sample at 40° in the laboratory system before and after an angular distribution was measured. The yields of neutrons scattered from praseodymium and lanthanum were then normalized to the n-p scattering cross section at 40° in laboratory system.

Figure 3 shows neutron time-of-flight spectra of neutrons elastically scattered by praseodymium measured at 90° in the laboratory system. The flat background neutron spectrum shows the effectiveness of the copper wedge in shielding the primary neutrons from the detector and collimator throat. Shielding the primary neutrons becomes more difficult at forward angles. However, since the primary neutrons are also present in the background spectrum, at forward angles, they can be subtracted from the spectrum accumulated with the sample in place.

No effort has been made to extract inelastic contributions to the elastic neutron group in the time-of-flight spectra taken. Previous work^[4] in this mass region has shown that the shape of the energy spectra of inelastically scattered neutrons show evaporation characteristics and, furthermore, the inelastic neutron region from 0.5 to 2.0 MeV contains more than 70 per cent of the observed inelastic neutrons. This was substantiated in the present work by measuring the elastic neutron spectrum at an angle where the yield of the elastic neutron group was a minimum, i.e., at 80° , and observing the asymmetry of the background yield on either side of elastic peak. No appreciable asymmetry existed and it was assumed that the contribution of the most energetic inelastic neutrons (leaving praseodymium in its 0.140 MeV excited state) to the elastic peak was negligible. Similar results were obtained with the lanthanum scatterer.

The neutron elastic scattering differential cross section was measured as a function of laboratory angle in the angular range from 25° to 155° for lanthanum, and 25° to 160° for praseodymium. Corrections to the data were made for neutron flux attenuation in the samples, multiple scattering within the samples, and angular resolution due to the proximity of the samples to the neutron producing target. The neutron flux attenuation calculations were performed with the aid of existing tables^[5] and amounted to an increase of

⁴ D. B. Thomson, Phys. Rev. 129, 1649 (1963).

⁵ Jules S. Levin, Los Alamos Scientific Laboratory Report No. LA-2177, January, 1959.

the measured differential cross section of 6 per cent for praseodymium and 4 per cent for lanthanum. Multiple scattering and angular resolution corrections were performed with a computer code^[6] rewritten for use with the University of Virginia B5500 Burroughs computer.

The measured and corrected absolute differential cross sections as a function of center of mass angle for elastic scattering of 8.00 MeV neutrons by praseodymium and lanthanum are tabulated in Table II. The uncertainty of the absolute differential cross sections is due mainly to counting statistics and inaccuracy in the relative efficiency of the neutron detector which together amount to about 5%.

TABLE II

Measured and corrected absolute center of mass differential cross section (mb/str) as a function of center of mass angle (degrees) for elastic scattering of 8.00 MeV neutrons by praseodymium and lanthanum. The data is corrected for neutron flux attenuation, multiple scattering and source-sample angular resolution.

$\theta_{c.m.}$	Praseodymium		Lanthanum	
	measured σ_{el}	corrected σ_{el}	measured σ_{el}	corrected σ_{el}
25	1131.8 ⁺ 66.0	1098.8 ⁺ 63.7	1225.9 ⁺ 71.0	1177.7 ⁺ 68.3
30	432.1 ⁺ 25.0	332.3 ⁺ 19.3	507.8 ⁺ 29.0	404.8 ⁺ 23.5
35	148.7 ⁺ 8.6	43.08 ⁺ 2.5	194.3 ⁺ 11.0	80.2 ⁺ 4.7
40	93.8 ⁺ 5.4	46.7 ⁺ 2.7	121.1 ⁺ 7.0	58.2 ⁺ 3.4
45	253.5 ⁺ 14.7	251.2 ⁺ 14.6	169.2 ⁺ 9.8	161.3 ⁺ 9.4
50	344.9 ⁺ 20.0	383.7 ⁺ 22.3	346.4 ⁺ 20.1	374.6 ⁺ 20.6
55	410.3 ⁺ 24.0	461.8 ⁺ 26.8	428.5 ⁺ 25.0	470.6 ⁺ 27.3
60	239.3 ⁺ 14.0	260.2 ⁺ 15.1	289.4 ⁺ 16.8	309.2 ⁺ 17.9
65	138.7 ⁺ 8.0	135.2 ⁺ 7.8	172.0 ⁺ 10.0	169.4 ⁺ 9.8
70	78.2 ⁺ 2.8	30.0 ⁺ 1.7	78.7 ⁺ 4.6	61.3 ⁺ 3.6
80	28.9 ⁺ 1.7	11.3 ⁺ 0.7	36.6 ⁺ 2.1	21.5 ⁺ 1.2
90	64.3 ⁺ 3.7	71.3 ⁺ 4.1	83.5 ⁺ 4.8	88.1 ⁺ 5.1
100	83.8 ⁺ 4.9	89.1 ⁺ 5.2	99.5 ⁺ 5.8	103.2 ⁺ 6.0
120	24.6 ⁺ 1.4	20.5 ⁺ 1.2	46.0 ⁺ 2.7	44.3 ⁺ 2.6
130	37.7 ⁺ 2.2	40.7 ⁺ 2.4	63.0 ⁺ 3.7	63.7 ⁺ 3.7
140	46.7 ⁺ 2.7	48.5 ⁺ 2.8	44.8 ⁺ 2.6	46.2 ⁺ 2.7
150	29.3 ⁺ 1.7	29.1 ⁺ 1.7	34.7 ⁺ 2.0	42.1 ⁺ 2.4
154.5	1.0 ⁺ 2.0	1.0 ⁺ 2.0	1.0 ⁺ 2.0	1.0 ⁺ 2.0
160	1.0 ⁺ 2.0	1.25 ⁺ 2.0		

⁶ J. D. Reber, Ph.D. Thesis, University of Kentucky, 1967.

The data in Table II are plotted in Figures 4 and 5. The solidlines are Legendre polynomial fits to the data. The Legendre polynomial coefficients and their uncertainties are tabulated in Table III.

TABLE III

The Legendre polynomial coefficients and their uncertainties for a best fit to the data plotted in Figures 4 and 5.

Praseodymium	Lanthanum
$A_0 = 238.5 \pm 24.8$	$A_0 = 251.5 \pm 26.4$
$A_1 = 540.7 \pm 71.5$	$A_1 = 584.1 \pm 69.2$
$A_2 = 690.8 \pm 101.3$	$A_2 = 667.5 \pm 111.5$
$A_3 = 795.5 \pm 118.8$	$A_3 = 869.6 \pm 127.6$
$A_4 = 811.8 \pm 124.8$	$A_4 = 767.3 \pm 148.5$
$A_5 = 870.5 \pm 129.6$	$A_5 = 941.5 \pm 133.7$
$A_6 = 841.1 \pm 113.8$	$A_6 = 783.1 \pm 141.1$
$A_7 = 816.2 \pm 99.1$	$A_7 = 833.9 \pm 108.8$
$A_8 = 560.5 \pm 72.7$	$A_8 = 446.9 \pm 91.8$
$A_9 = 197.9 \pm 42.1$	$A_9 = 183.5 \pm 54.8$
	$A_{10} = -67.7 \pm 48.6$

From the Legendre polynomial fits, the total neutron elastic scattering cross sections for the scattering of 8.00 MeV neutrons were determined to be 2.997 ± 0.312 barns for praseodymium and 3.160 ± 0.332 barns for lanthanum.

Conclusion

No effort was made to extract inelastic contributions to the elastic neutron groups as evidence indicates that such contributions are small and within statistical counting uncertainties. The angular distributions of the elastic scattering of 8.00 MeV neutrons by praseodymium and lanthanum exhibit substantial diffraction patterns which were somewhat accentuated after correcting for multiple scattering and source-sample angular resolution. The best Legendre polynomial fits to the data resulted in a determination of the total neutron elastic scattering cross section of 2.997 ± 0.312 barns for praseodymium and 3.160 ± 0.332 barns for lanthanum for an incident neutron energy of 8.00 MeV.

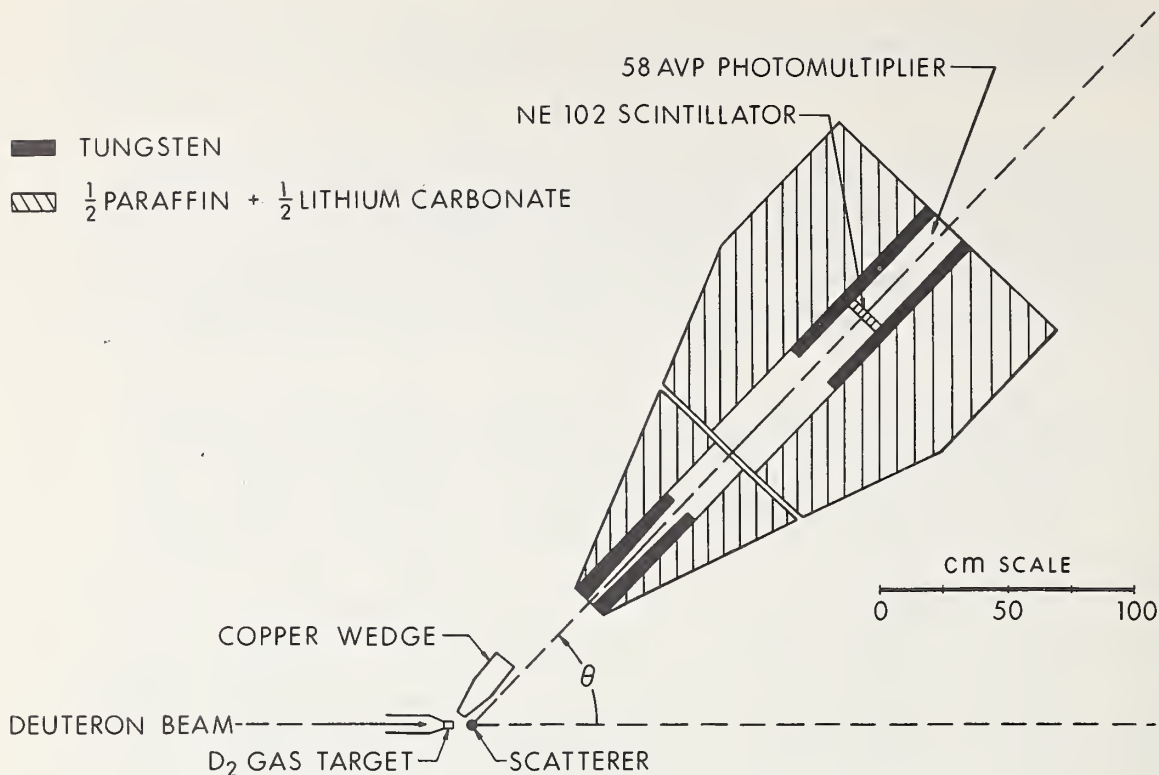


Figure 1. A schematic diagram of the relative positioning of the target, scatterer, wedge and detector-shield assembly.

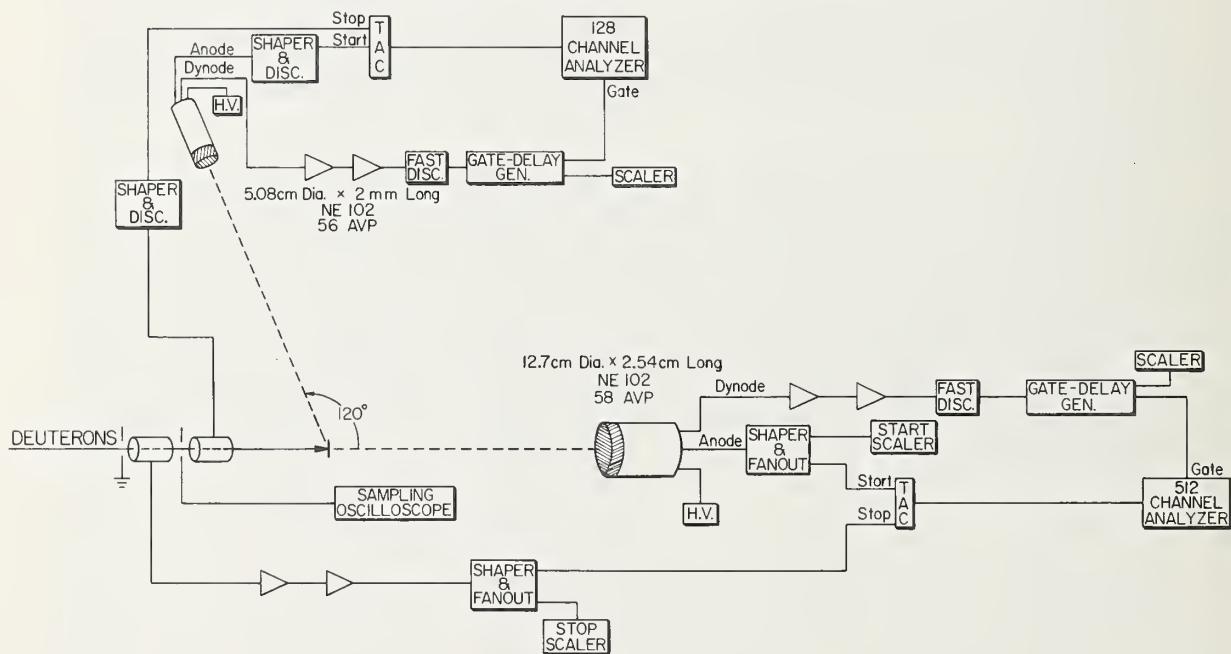


Figure 2. A schematic diagram of the electronics used in this experiment.

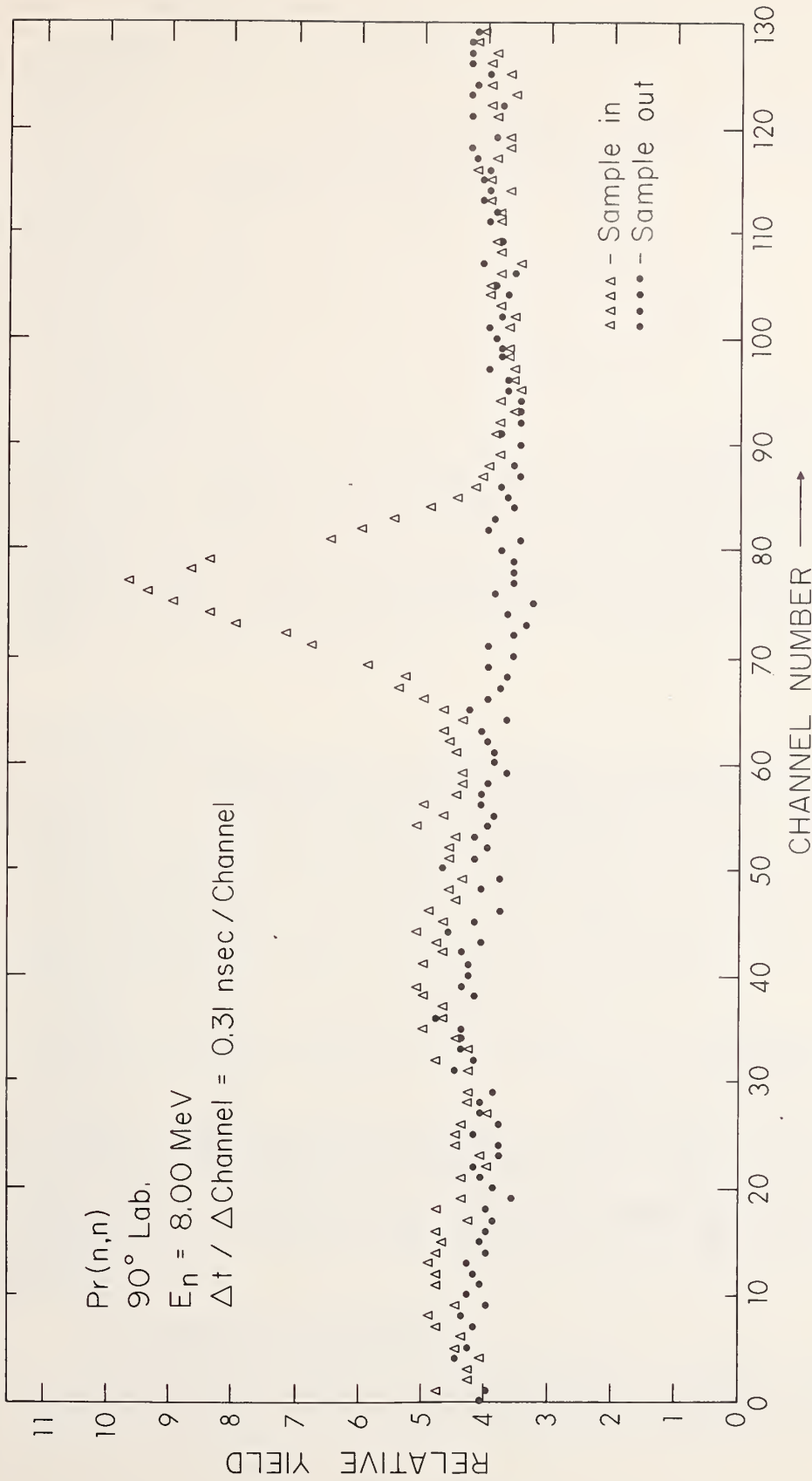


Figure 3. Neutron time-of-flight spectra of 8.00 Mev neutrons elastically scattered by Pr taken with sample in and with sample out. The prompt gamma peak is out of the spectra and to the right. These spectra were taken at 90° in the laboratory system. The neutron energy resolution is about 800 Kev.

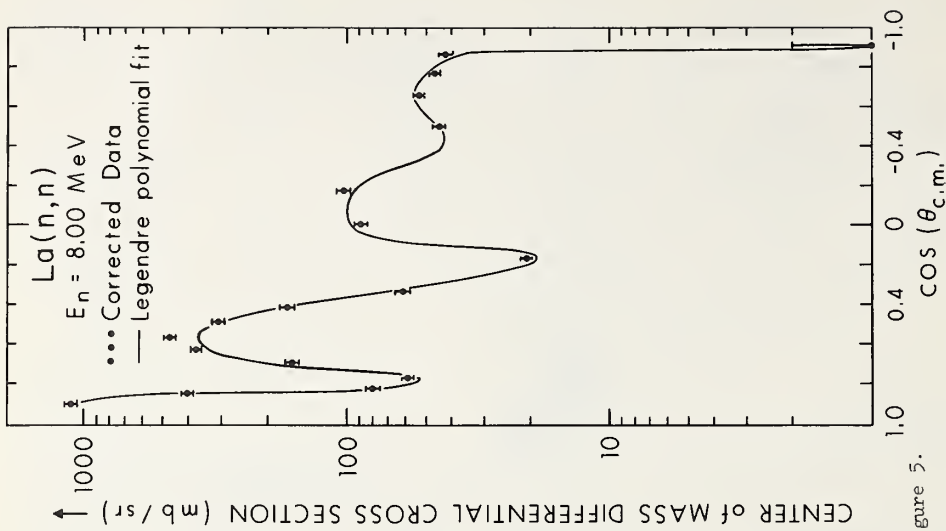


Figure 5.

A plot of absolute center of mass differential cross section as a function of $\cos\theta$ in the center of mass for elastic scattering of 8.00 Mev neutrons by lanthanum. The solid curve through the data points is a Legendre polynomial fit to the data. The differential cross section was normalized to the n-p elastic scattering differential cross section using a tubular polyethylene scatterer.

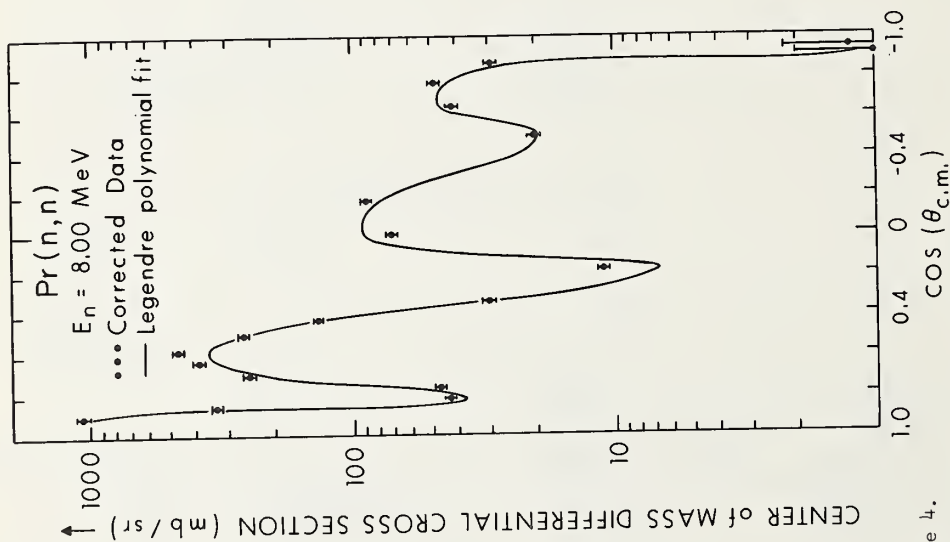


Figure 4.

A plot of absolute center of mass differential cross section as a function of $\cos\theta$ in the center of mass for elastic scattering of 8.00 Mev neutrons by praseodymium. The solid curve through the points is a Legendre polynomial fit to the data. The differential cross section was normalized to the n-p elastic scattering differential cross section using a tubular polyethylene scatterer.

Gamma-Rays from Inelastic Neutron Scattering in Nitrogen

H. Condé and I. Bergqvist
Research Institute of National Defence, Stockholm, Sweden

G. Nyström*
AB Atomenergi, Studsvik, Nyköping, Sweden

Abstract

The gamma-ray production cross section of N has been measured at three different incident neutron energies between 4.5 and 7 MeV. The gamma-ray spectrometer was a 17 ccm Ge(Li)-detector. A time-of-flight technique was employed to suppress the background caused by neutron interactions in the Ge(Li)-detector. The efficiency of the gamma-ray spectrometer was measured with calibrated gamma-ray sources and (p, γ)-reactions. The primary neutron flux was measured with a proton-recoil telescope. Gamma-ray lines of energies from 0.7 to 5.8 MeV were observed with pronounced lines at 0.730, 1.637, 2.315, 5.104 and 5.834 MeV. Differential gamma-ray production cross sections at 55° are given.

1. Introduction

With the main purpose to meet data request for gamma-ray production cross sections in the incident neutron energy region from 4 to 8 MeV an experiment has been set up at the 5.5 MeV Van de Graaff accelerator at Studsvik, Sweden. The gamma-ray detector is a 17 cc true coaxial lithium-drifted germanium detector which is run in a time-of-flight arrangement to reduce the neutron induced background. The aim of the investigation is to measure the spectra as well as the angular distributions of the gamma radiation and to refer the cross sections to the (n,p)-scattering cross section by the use of a proton-recoil telescope.

The experimental arrangements will be described and preliminary gamma-ray production cross sections at 55° are given for the $^{14}\text{N}(n,n'\gamma)$ -reaction at three different incident neutron energies namely 4.5, 6 and 7 MeV.

Gamma radiations from inelastic scattering of fast neutrons in the incident neutron energy interval between 4.7 and 8 MeV in ^{14}N has been studied by Hall and Bonner (1). They used a NaI (Tl) crystal and observed gamma-rays with energies of 1.64, 2.14, 2.31, 4.46 and 5.06 MeV. The cross section at a neutron energy of 7.3 MeV of the $^{14}\text{N}(n,n'\gamma)$ -reaction was reported to be 16.2 mb/sr at 90° with an accuracy of about 30-40 %.

2. Experimental arrangements

The gamma-ray experiment is set up at the 5.5 MeV Van de Graaff accelerator at Studsvik. The accelerator is equipped with a top terminal pulsing system which for the present experiment was adjusted to give about

* Present address: Department of Physics, University of Lund, Lund

10 ns in pulse length with 1 MHz pulse repetition rate. With a post-acceleration beam-sweeping system, the pulses were shortened to about 5 ns in pulse length.

2.1 Neutron source and scattering sample

Neutrons of energies of 4.5, 6 and 7 MeV were produced by the $D(d,n)^3\text{He}$ reaction in a gas target. The gas target had a thin Mo-entrance window and the gas cell was 3 cm in length and 0.8 cm in diameter. The gas pressure was about 1.5 atm and the interior of the gas-cell was covered with a thin gold-layer to reduce the background.

A plastic scintillator (see fig. 1) was used to monitor the output of neutrons from the source. The scintillator was set up in a time-of-flight arrangement to reduce the effect of background pulses in the scintillator caused by gamma-rays and room-scattered neutrons.

About 20 grams of ammoniumazid NH_4N_3 housed in a thin-walled cylindrical holder of plexiglas was used as scattering sample. The sample was mounted at a distance of about 10 cm from the neutron gas target (see fig. 1).

For background measurements an empty holder of the same type as described above was used.

2.2 Gamma-ray detector

As gamma-ray detector a 17 cc true coaxial Ge(Li)-detector was used. It was set up in 55° to the incident neutron beam and at a distance of about 85 cm from the scattering sample. The angle of 55° was used because usually the gamma-ray angular distribution can be represented by an expansion of even-order Legendre polynomials and often the second order terms dominates the expansion. In these cases a good approximation of the integrated cross section is 4π times the 55° differential cross section.

A block diagram of the electronic circuits is shown in fig. 2. The linear pulse-spectrum from the Ge(Li)-detector was recorded on a 4096 channel analyzer. The energy resolution was about 5 keV at 1 MeV of gamma-ray energy.

To reduce the background caused by neutron interactions in the Ge(Li)-detector it was run in a time-of-flight arrangement. Two typical time-of-flight spectra at 4.5 and 7 MeV are shown in fig. 3. The FWHM of the gamma-ray peaks was about 15 ns. The pulses from a single-channel analyzer adjusted to accept pulses in the gamma-ray peak (fig. 3) of the time-of-flight spectra was used to open a gate to the 4096 channel analyzer.

2.3 Proton-recoil telescope

The incident neutron beam-flux was measured with a proton-recoil telescope {Bane et al. (2)}. Four polyethylene radiators with different thicknesses (1.5-18 mg/cm^2) and a blank for background measurements could be used. The protons from the (n,p)-reactions in the radiator were counted with solid-state detectors. A typical spectrum at 7 MeV of incident neutron energy and with a 6.3 mg/cm^2 radiator is shown in fig. 4.

3. Experimental procedure and data handling

3.1 Experimental procedure

Several runs were made at each incident neutron energy both with the scattering sample and with an empty plexiglas-cylinder.

To get a counting statistics of better than 5 % of the pronounced gamma-ray lines the total running time at one neutron energy was about 10-15 hours. The detector efficiency was measured at several energies up to 1.8 MeV and at 2.6 MeV with calibrated gamma-ray sources put in the scattering sample position. At higher energies the efficiency was calculated from a measurement of the gamma-rays from the 992 keV proton resonance of the $^{27}\text{Al}(p,\gamma)^{28}\text{Si}$ -reaction and from the deexcitation scheme given by Azuma et al. (3).

In this way the efficiencies of photo- as well as double-escape events were measured with an accuracy of about 5 % below about 3 MeV of gamma-ray energy and about 20 % above this energy.

3.2 Data handling

When the actual background of a certain gamma-ray energy spectrum had been subtracted the number of counts in each peak was calculated. After applying the efficiency of the Ge(Li)-detector the number of gamma-rays were corrected for attenuation of the gamma-radiation in the ammonium-azide sample.

The attenuation of the gamma-rays in the sample was less than 10 % in the whole energy region of interest. The correction was calculated by using the attenuation coefficients given by Davisson and Evens (4).

The incident neutron flux calculated from the measurement with the proton-recoil detector (see above) was corrected for neutron attenuation and multiple scattering effects using the Monte-Carlo program MULTSCAT {Holmqvist et al. (5)}. The corrections were estimated to be about 5 %.

The energies of the observed gamma-ray lines in the spectrum obtained with the Ge(Li)-detector were estimated by using a linear interpolation between the 846.6 keV line from ^{56}Fe in the background {Chasman (6)} and the 5104 keV line from ^{14}N {Chasman et al. (7)} as references together with the energy-difference of 1022 keV between the photo and double-escape peaks.

4. Results and discussion

A typical gamma-ray spectrum at 7 MeV of incident neutron energy is shown in fig. 5. The given energies of the different gamma-ray lines are in some cases where the half-lives of the excited states are of the order of the flight times of the nitrogen recoils affected by Doppler-broadening and shift. From half-lives values measured by Allen (8) the gamma-ray shifts were estimated to be less than 5 keV in the present measurement.

Table I gives preliminary values of the differential gamma-production cross sections in 55° of the pronounced gamma-ray lines at 4.5, 6 and 7 MeV of incident neutron energies. The cross section for the $^{14}\text{N}(n, n'\gamma)^{14}\text{N}$ reaction including cascades at 7 MeV of neutron energy is 18.0 ± 2.5 mb/sr in good agreement with the value obtained by Hall and Bonner (1).

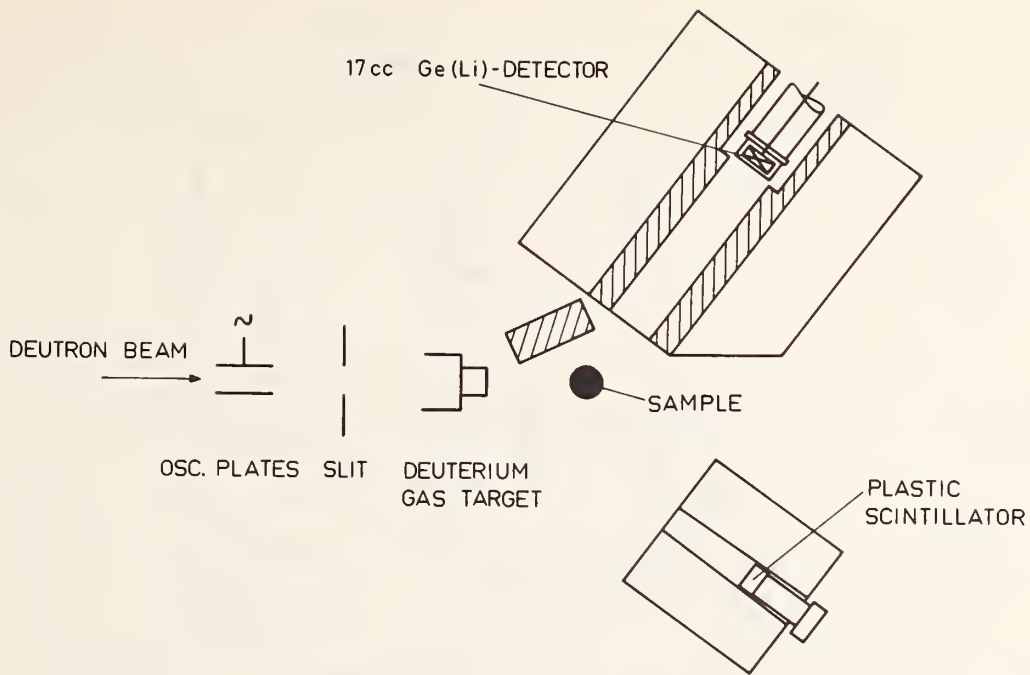
5. References

1. H.E. Hall and T.W. Bonner, Nucl. Phys. 14: 295 (1959/60)
2. S.J. Bame, Jr, E. Haddad, J.E. Perry, Jr, K. Smith and B. Schwarz, Rev. Sci. Instr. 31: 911 (1960)
3. R.E. Azuma, L.E. Carlsson, A.M. Charlesworth, K.P. Jackson, N. Anyas-Weiss and B. Lalović, Can. Jour. of Phys. 44: 3075 (1966)
4. C.M. Davisson and R.D. Evens, Rev. Modern Phys. 24: 79 (1952)
5. B. Holmqvist, B. Gustavsson and T. Wiedling, Arkiv för Fysik 34:5 481 (1967)
6. C. Chasman, Proceedings of the I.A.E.A. Panel on Lithium-Drifted Germanium Detectors, Vienna 1966, page 74
7. C. Chasman, K.W. Jones, R.A. Ristinen and D.E. Alburger, Phys. Rev. 159, 830 (1967)
8. K.W. Allen, Proceedings of the I.A.E.A. Panel on Lithium Drifted Germanium Detectors, Vienna 1966, page 142.

Table I

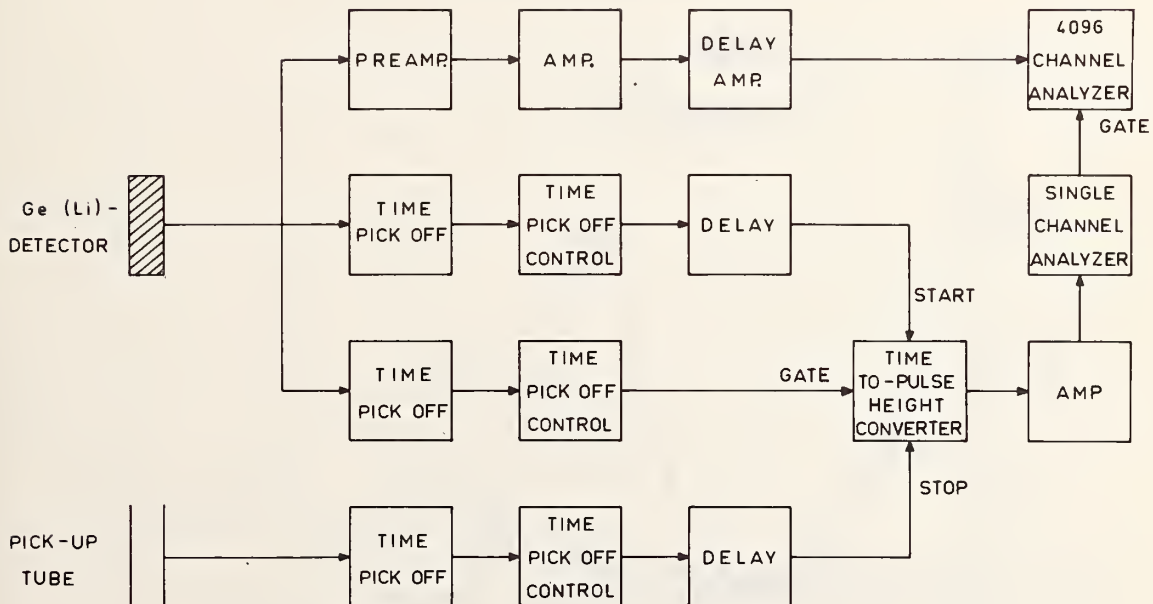
Observed cross sections for gamma-radiations produced by interactions of 4.5, 6 and 7 MeV neutrons with N.

Gamma radiations in keV	Assignement	Cross sections in mb/sr at 55°		
		4.5 MeV	6 MeV	7 MeV
730	$^{14}\text{N}: 5.83 \rightarrow 5.10$			1.3 ± 0.5
1637	$^{14}\text{N}: 3.95 \rightarrow 2.32$	< 1.0	3.1 ± 0.6	4.8 ± 1.0
2140	$^{11}\text{B}: 2.14 \rightarrow 0$	< 1.0	3.9 ± 0.7	2.3 ± 0.5
2315	$^{14}\text{N}: 2.32 \rightarrow 0$	1.0 ± 0.5	4.6 ± 1.0	7.1 ± 1.1
4482	$^{11}\text{B}: 4.48 \rightarrow 0$		< 1.0	3.1 ± 1.0
5104	$^{14}\text{N}: 5.10 \rightarrow 0$		0.9 ± 0.3	3.0 ± 0.5
5707 - 6448				1.8 ± 0.5



EXPERIMENTAL ARRANGEMENTS

Figure 1. A schematic diagram of the relative positioning of the target, scatterer, wedge and detector-shield assembly.



BLOCK DIAGRAM OF THE ELECTRONIC CIRCUITS

Figure 2. A schematic diagram of the electronics used in this experiment.

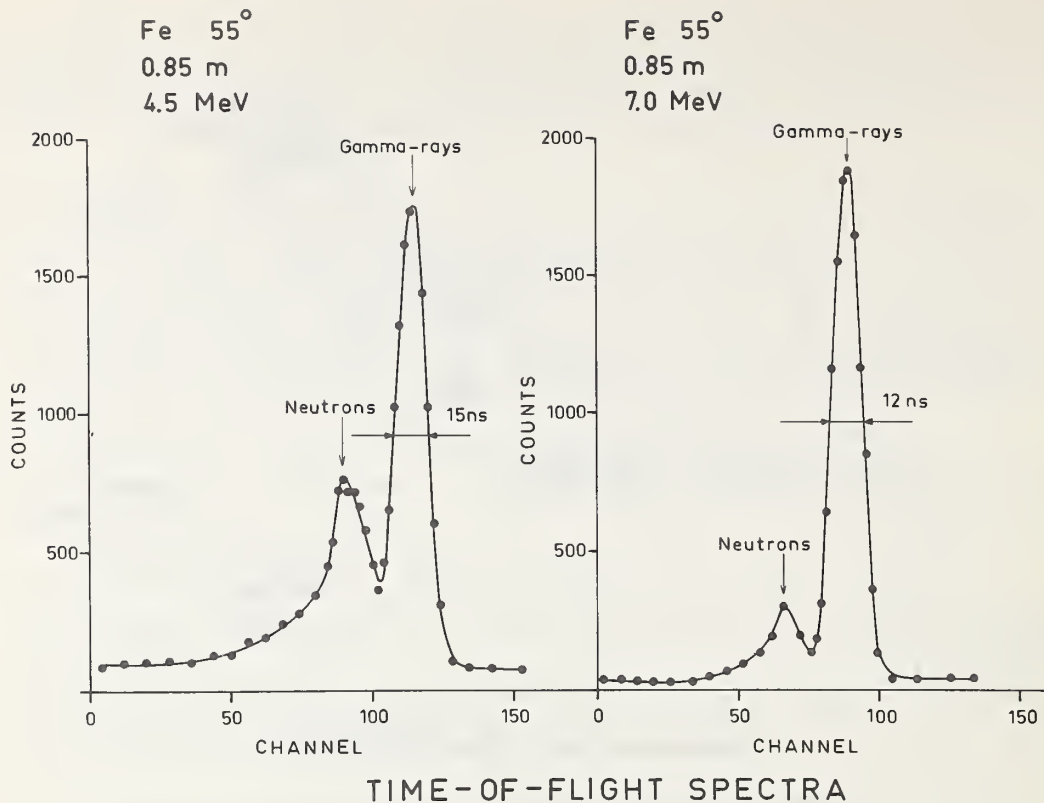


Figure 3. Time-of-flight spectra for the Ge(Li)-detector at 4.5 and 7 MeV of incident neutron energies

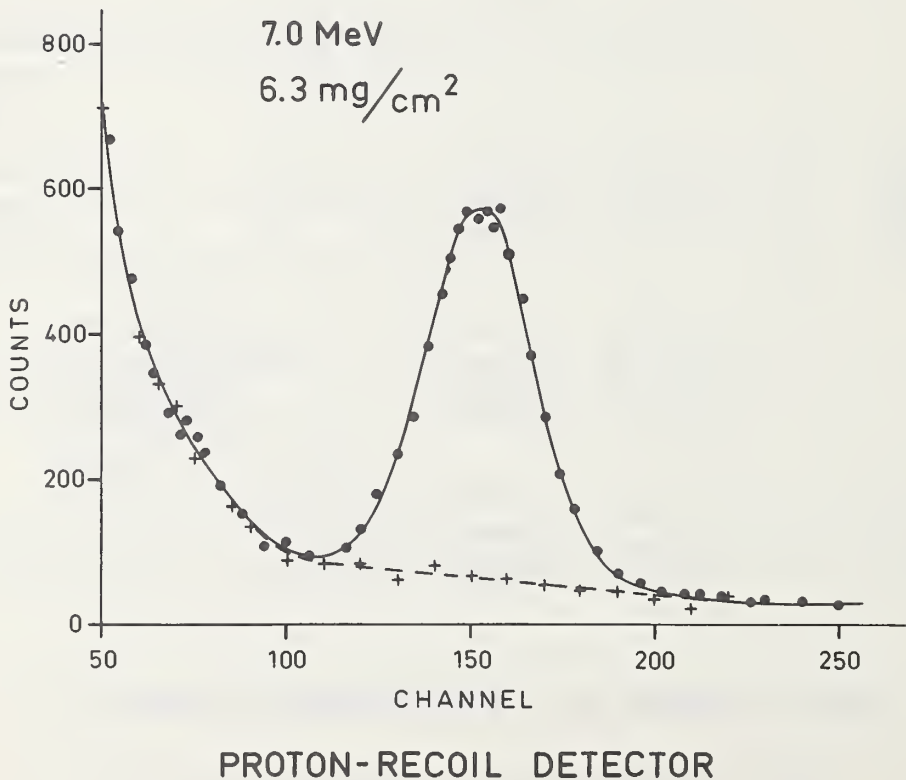


Figure 4. Pulse spectrum for the proton-recoil telescope at 7 MeV of incident neutron energy. Radiator thickness 6.3 mg/cm²

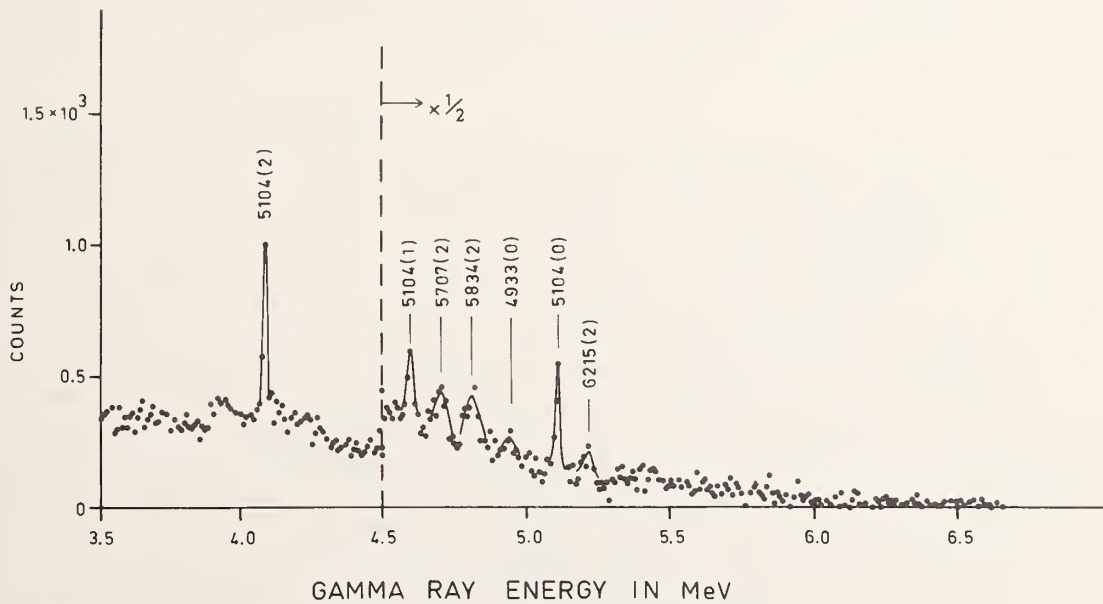
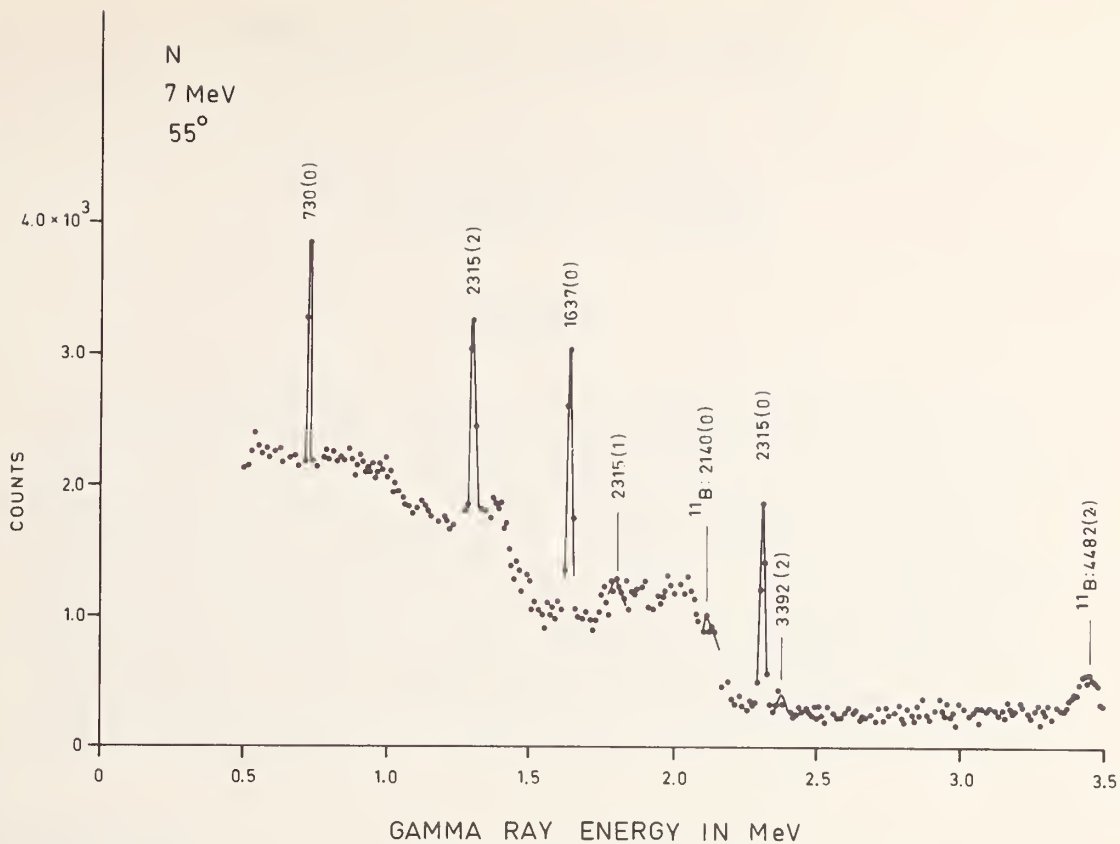


Figure 5. Gamma-ray spectrum of the Ge(Li)-detector at 7 MeV of incident neutron energy

TOTAL NEUTRON CROSS SECTIONS OF CARBON,
IRON, AND LEAD IN THE MeV REGION*

R.B. Schwartz, R.A. Schrack, and H.T. Heaton, II

National Bureau of Standards
Washington, D. C. 20234

ABSTRACT

We have measured the total neutron cross sections of iron and lead in the energy range 0.7 to 4.0 MeV. In addition, as a check on our method, we have also measured the well-known carbon cross section in the same energy range. The neutron time-of-flight method was employed, with the NBS electron linear accelerator as a pulsed neutron source. The neutron energy resolution was 0.3 to 0.16 nsec/m. Our carbon data are in agreement with the earlier results from other laboratories, and our lead data are in good agreement with recent measurements from Saclay and from Wisconsin in the energy regions where we overlap. A detailed comparison of our results with those from other laboratories will be presented.

1. Introduction

In the next ten minutes, I would like to do three things: first, since these are the first cross section data to come from the NBS linac, I want to spend several minutes describing our set-up. Second, I would like to compare critically some of our results with other generally accepted values. Finally, of course, I should like to present some new data.

2. Experimental Arrangement

Figure 1 is a bird's eye view of our target area. We use the pulsed beam of the NBS electron linear accelerator as a source of neutrons. The beam enters from the bottom of the picture, and passes through a secondary emission monitor, which is our first monitor. Since this set-up was designed for both photoneutron spectroscopy as well as neutron cross section measurements, our equipment also includes a dumping magnet. For cross section measurements, the magnet is simply turned off and serves no function. The electron beam emerges from the magnet vacuum chamber into air, and hits our neutron producing target. For the neutron energy range in which we are interested (0.7 to 4 MeV) almost any heavy element will do as a neutron source, provided that it, itself, does not have a great deal of structure in its cross section. We happen to use cadmium, about 3/4" thick, for one very important reason: we had lots of it lying around. Following the neutron source, we have a 931A photomultiplier tube, which furnishes the "start" signal for our time-of-flight measurements. Immediately behind the start photomultiplier is our second monitor - an NBS P-2

*This work was supported in part by the U.S. Defense Atomic Support Agency.

ion chamber^[1] which essentially monitors the shower developed in the cadmium. Behind the P-2 chamber is a pile of lead bricks to serve as a beam dump.

We look at the neutrons coming off at 135° to the electron beam. About $3\frac{1}{2}$ meters downstream from the neutron source we have our sample hanger.

The flight path is 40 m long, most of it evacuated, with iron and masonite collimators strategically placed along its length.

The detector is a liquid scintillator, 13 in. in diameter and 5 in. thick, viewed by three, 58 AVP photomultipliers. The signals from these photomultipliers are processed by more-or-less conventional high-speed modular electronic circuitry [2,3] and furnish the "stop" signal for the time of flight measurements. The timing resolution, and hence the energy resolution, is limited primarily by the beam pulse width, now 3 to 5 nsec, and the transit time of the neutrons in the scintillator, which is 4 nsec. Our overall timing resolution is approximately $6\frac{1}{2}$ nsec, or 0.16 nsec/m (e.g., 25 keV at 3 MeV). Some of the data that I wish to show were, however, taken earlier, with a 10 nsec pulse width, and a resolution of 0.3 nsec/m.

3. Procedure

The total cross sections were measured in the usual way by a transmission experiment. The samples were one to two mean free paths thick.

In these experiments, we made no attempt to determine our energy scale absolutely. Instead, we calibrated our scale in terms of (presumably) well-known levels. Specifically, we fitted our data to the 2.08 and 2.95 MeV levels in carbon, and the peaks at 0.76 and 0.81 MeV in the lead cross section as measured by Cabe, et al. at Saclay [4]. Now, extensive previous testing had shown that our system was quite linear. Hence, it takes only two points to determine the energy scale and our procedure, therefore, overdetermines the scale. Alternatively, we can take the point of view that a straight line fit demonstrates that the Saclay energy scale is consistent, within the quoted errors with the energies recommended for the carbon lines. We estimate that our energy scale is about as accurate as the energies quoted for the reference lines, i.e., 5 keV at the low energy end and 20 keV at the high energy end. We emphasize this point, since, as shall be shown later, there is a discrepancy between our energy assignments in iron and some recent data from Argonne.

The largest correction to the data is the dead-time correction. This is necessarily so when working with a low duty-cycle machine, an electronic system that can only handle one count per pulse, and the desire to finish the experiment in a finite length of time. In fact, we run at rates such that in the open beam, the dead time correction in the last channel (i.e., the lowest energy neutron) is 100 percent. That is, we lose one-half of the events that should fall in the last channel. To first order, however, this correction can be made exactly, in terms of explicitly measured quantities, and, therefore, introduces no error. The first order correction,

however, assumes a constant counting rate, and hence a constant beam current. There is a second order correction if the beam current is not constant. This effect can introduce a one to two percent error at the low energy end. In our later runs the effect was reduced by having the electronics turned off automatically if the beam current varied outside of pre-selected limits, but this was not done in the earlier runs.

No correction was made for inscattering, since the calculated correction [5] was always less than 0.1 percent.

The background, measured by placing an 11" polyethelene block in the sample position, was about 0.1 percent of the open beam rate.

The overall uncertainty on our absolute cross section value is estimated to be two to three percent, based primarily on the count loss correction and possible uncertainties in the monitoring. The statistical accuracy of each point is between one and two percent.

4. Results

4.1. Carbon

Figure 2 shows our carbon data. The region from 2.0 to 3.2 MeV was measured with a resolution of 0.16 nsec/m; outside of this region the resolution was 0.3 nsec/m. We use carbon as an all-purpose check and calibration: the smooth regions below 2 MeV and between the 2 and 3 MeV levels are ideal for checking the magnitude of our cross section values; the 2 and 3 MeV levels, as mentioned earlier, are used for the energy calibration; and the narrow 2 MeV line is used to measure our overall system resolution.

Now, we want to compare our data to other carbon data, and this is a problem. We have something like 1,000 data points in this energy interval and there is probably a comparable number given in the compilation [4]. It is obviously quite impossible to show all these data in one figure. We have, instead, chosen to show all our data points and then simply take the line which is drawn through the data points in the compilation and reproduce this line on our figure. This is the solid line in Figure 2. If one takes the point of view that the compilers drew the line under Divine Guidance, and that it represents the Ultimate Knowable Truth, then this is a reasonable procedure.

In the region below the 2 MeV line, we see that our data are low, by about 3 percent. Since we do not claim an absolute accuracy of better than 2 to 3 percent, we do not consider this to be a serious discrepancy, particularly if one considers the possibility that Divine Guidance may also have some statistical uncertainty associated with it. It is also possible that part of this discrepancy (to the extent that there is a discrepancy) may be due to the second order count loss effect mentioned earlier. We plan to check this point in the near future.

We do not draw the line through the 2 MeV resonance, since we know that our resolution is inadequate to show it in all its natural glory. Our resolution at this energy is about 14 keV, and the resonance width is only 7 keV.

The flat region between the 2 and 3 MeV levels seems to vindicate the Divine Guidance point of view, since the line goes right through our points (or, vice-versa).

Ignoring, for the moment, the level at 2.8 MeV, we note that we do not quite get up to the full peak height of the 3 MeV level. The difference is about 6 percent. We do not consider this a serious discrepancy, however, since the compilation curve at this peak is determined by just one point, which has a 5 percent statistical error [6]. Our resolution (25 keV) is at least as good as any of the other measurements in this region.

Going on to higher energies, our claim is that there is satisfactory agreement between our data and the earlier measurements, keeping in mind the uncertainties in all of the data involved.

Returning to 2.83 MeV, we see a level which seems to have eluded previous workers. Let me remind you that since carbon is 99.9 percent ^{12}C , we are looking at levels in the compound nucleus ^{13}C . This 2.83 MeV level corresponds to an excitation energy of 7.560 ± 0.016 MeV in ^{13}C , and is clearly the same level as the one reported by Young, et al., using the $^{11}\text{B}(^3\text{He}, p)^{13}\text{C}$ reaction, whose energy was given as 7.553 ± 0.007 MeV. This level has also been seen in the $^{12}\text{C}(d, p)^{13}\text{C}$ reaction [7,8].

Assuming that the level is entirely elastic scattering, and that its shape is not greatly distorted by interference, we get the following results for the width, Γ , as a function the spin, J :

J	$\Gamma(\text{keV})$
1/2	1
3/2	0.6
5/2	0.5
7/2	0.4

While it seems highly unlikely that this is an s-wave resonance (i.e., $J = 1/2$), until the spin is explicitly measured we can only state that $\Gamma \lesssim 1$ keV.

4.2. Iron

Our iron data are shown in Figure 3. These data were all measured with a resolution of 0.3 nsec/m. In this case, the line through the points is just that - a line drawn through our points to guide the eye. A very complete, high resolution, set of cross section data exists below 1.5 MeV with which we can compare our results. These are the measurements of Smith, et al., at Argonne. Unfortunately, there is an energy shift between the two sets of data, the Argonne data being systematically higher in energy. This energy shift is only a few keV at 800 keV (which is less than our energy uncertainty), but the shift increases with increasing energy, getting up to 25 keV at 1.4 MeV. I have tried to indicate this for some of the more prominent peaks in Figure 3 by a slanted line going from our peak position, to a short vertical line, indicating the energy of the corresponding peak

as measured by the Argonne group. As mentioned earlier, we do not determine our energy scale absolutely but it is calibrated to be consistent with several other sets of data. It is difficult to see how it can be in error by as much as 25 keV at this energy.

We are not aware of any modern data at all between 1.5 and 2.0 MeV. Above 2.0 MeV, there exist data from Case and from Hanford. We are in general agreement with these results except that our statistical accuracy is much higher and our resolution is better.

4.3. Lead

Our lead data, measured with a resolution of 0.3 nsec/m, are shown in Figure 4. The solid line is, again, just a line drawn through our data points. Below 1.2 MeV, our data are in agreement with those of Cabe, et al. at Saclay. In fact, as mentioned earlier, we use some of the Saclay data to help pin down the low energy end of our energy scale.

We are not aware of any modern data between 1.2 and 2.5 MeV.

Above 2.5 MeV, our data are in good agreement with recent Wisconsin results [9]. We have tried to show this with the dashed line: the points are our data points, the dashed line is the line drawn by Carlson and Barschall through their data points [10]. In view of the fact that both of our energy scales have uncertainties of about 20 keV at these energies, we consider that this is reasonably good agreement. Further, the actual Wisconsin data points deviate from their curve about as much as ours do. In other words, I suggest that while the dashed line is not a spectacularly good fit to our data, the fit to the Wisconsin data, itself, is not tremendously better.

In order to see whether some of the broad peaks at the upper energy end had any fine structure underlying them, we ran the energy region from 2.0 to 3.2 MeV at higher resolution: 0.16 nsec/m. These data are shown in Figure 5. All of the broad peaks seen in the poorer resolution data are now clearly resolved into two or three narrow peaks, with strong suggestions of still finer structure as yet unresolved.

Now, one of the main points of the Carlson and Barschall work was that fluctuations in the cross sections at these energies could be accounted for by fluctuations in the widths and spacings of overlapping levels, or, possibly, by Ericson fluctuations, and that it is not necessary to invoke intermediate structure. Our high resolution data, while covering only a very narrow energy range of just one element, do suggest that in this case at least there is a still simpler explanation: the fluctuations are merely unresolved individual resonances.

5. Conclusion

In addition to providing more data to fill up future editions of BNL 32J, our work has brought to light at least two interesting problems.

First, there is the energy scale problem, as exemplified by the iron data. We have plans for making an absolute energy scale determination for our time-of-flight system, which should help resolve some of these questions.

Second, our high resolution lead data suggest that the explanation of the cross section fluctuations in the MeV energy range may not yet be a completely closed issue.

6. References

- [1] J.S. Pruitt and S.R. Domen, National Bureau of Standards Monograph 48 (June 1962).
- [2] J.K. Whittaker, IEEE Trans. on Nuclear Science NS-13, No. 1, 399 (1966).
- [3] J.K. Whittaker, Nucl. Instr. and Meth. 45, 138 (1966).
- [4] Brookhaven National Laboratory Report BNL 325. Unless otherwise indicated, all neutron cross section data referred to are to be found in this compilation and its various and sundry supplements.
- [5] A. Bratenahl, J.M. Peterson, and J.P. Stoering, Phys. Rev. 110, 927 (1957).
- [6] C.K. Bockelman, D.W. Miller, R.K. Adair, and H.H. Barschall, Phys. Rev. 84, 69 (1951).
- [7] T.E. Young, G.C. Phillips, R.R. Spencer, and D.A.A.S.N. Rao, Phys. Rev. 116, 962 (1959).
- [8] J.N. McGruer, E.K. Warburton, and R.S. Bender, Phys. Rev. 100, 235 (1955).
- [9] A.D. Carlson and H.H. Barschall, Phys. Rev. 158, 1142 (1967).
- [10] See Figure 9 of Ref. 9.

NEUTRON TIME-OF-FLIGHT EXPERIMENTAL AREA

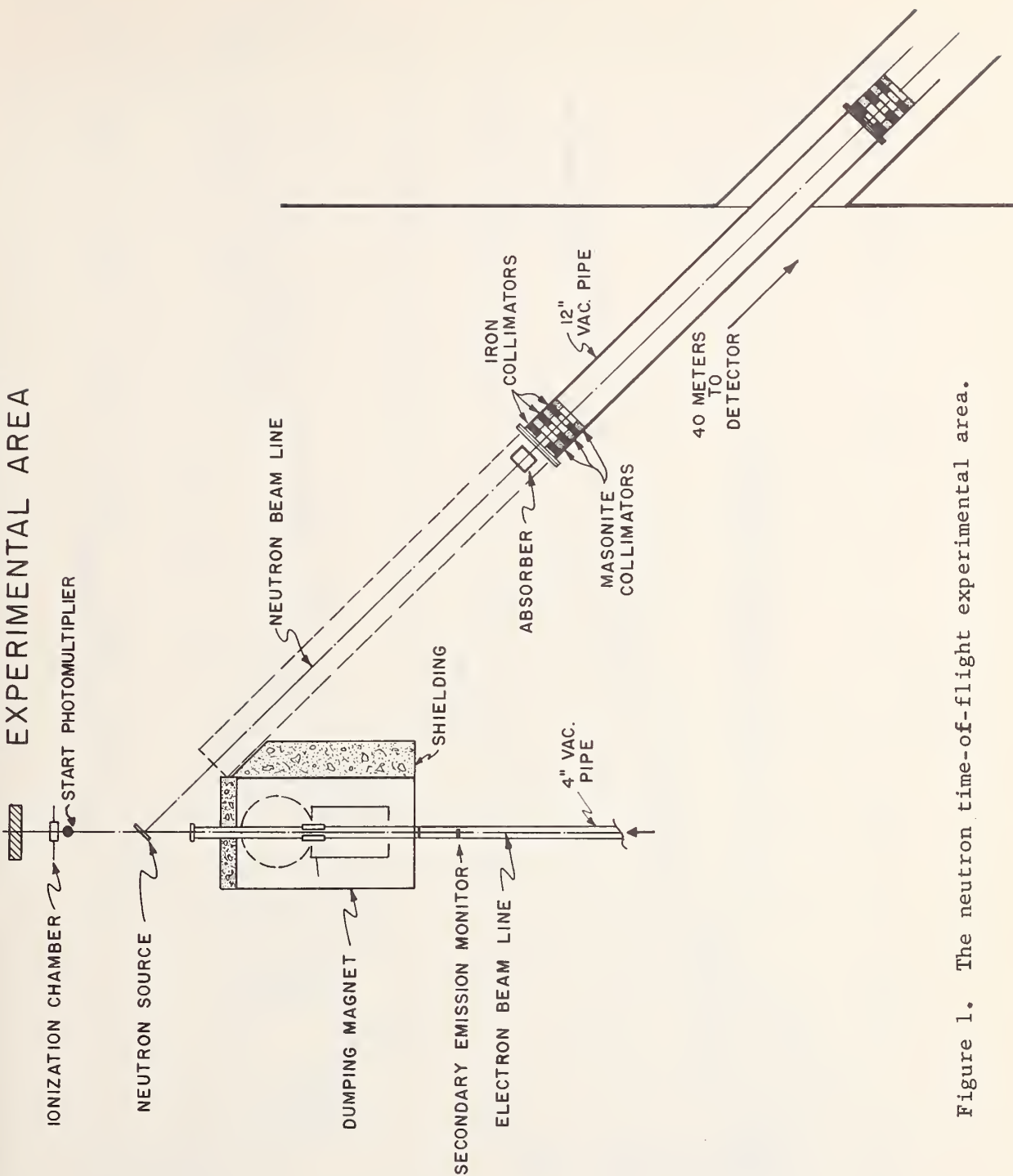


Figure 1. The neutron time-of-flight experimental area.

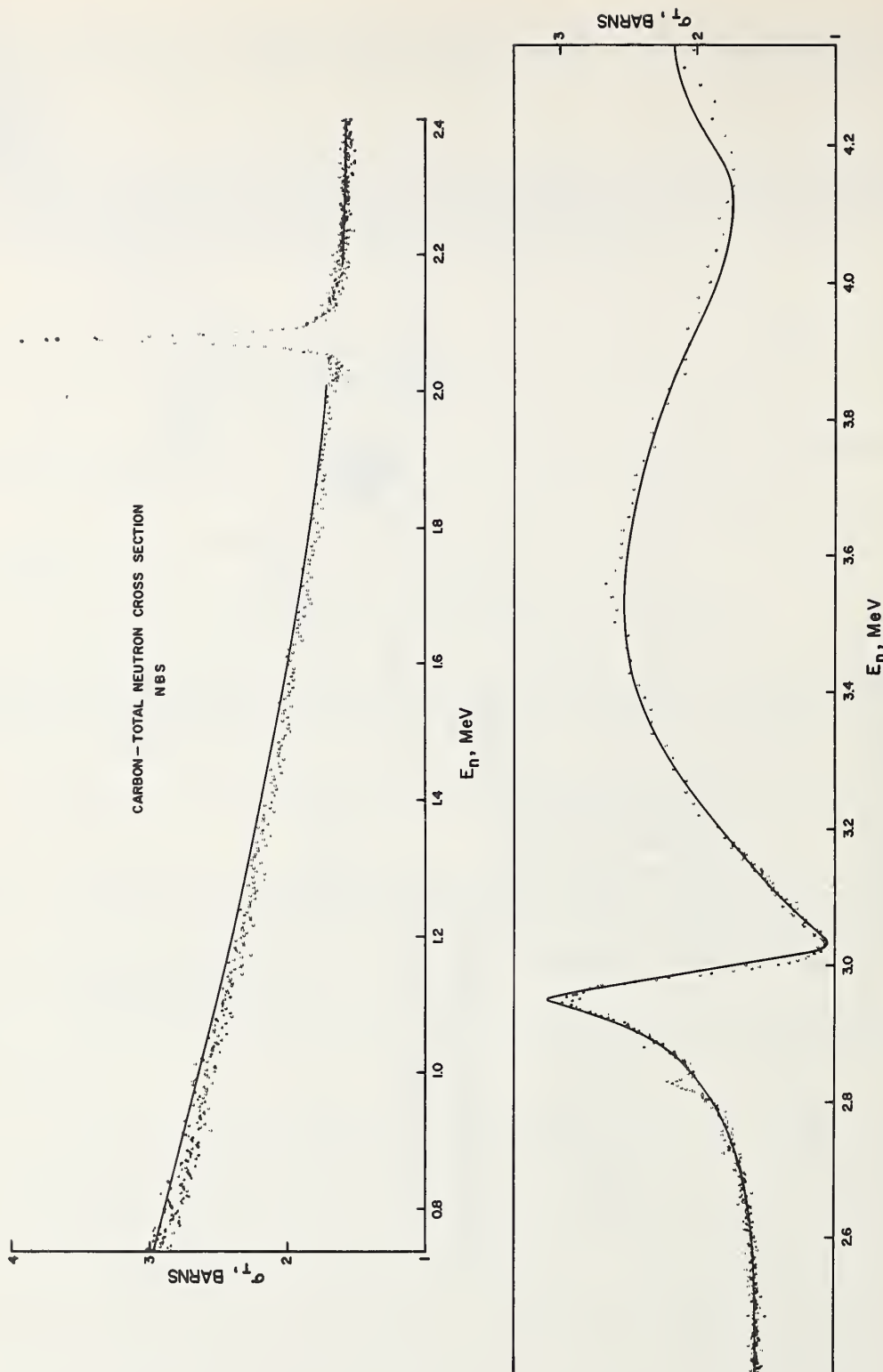


Figure 2. The total neutron cross section of carbon. The region between 2.0 and 3.1 MeV was measured with a resolution of 0.16 nsec/m; outside of this region the resolution was 0.3 nsec/m. The solid line is the curve from the compilation BNL 325.

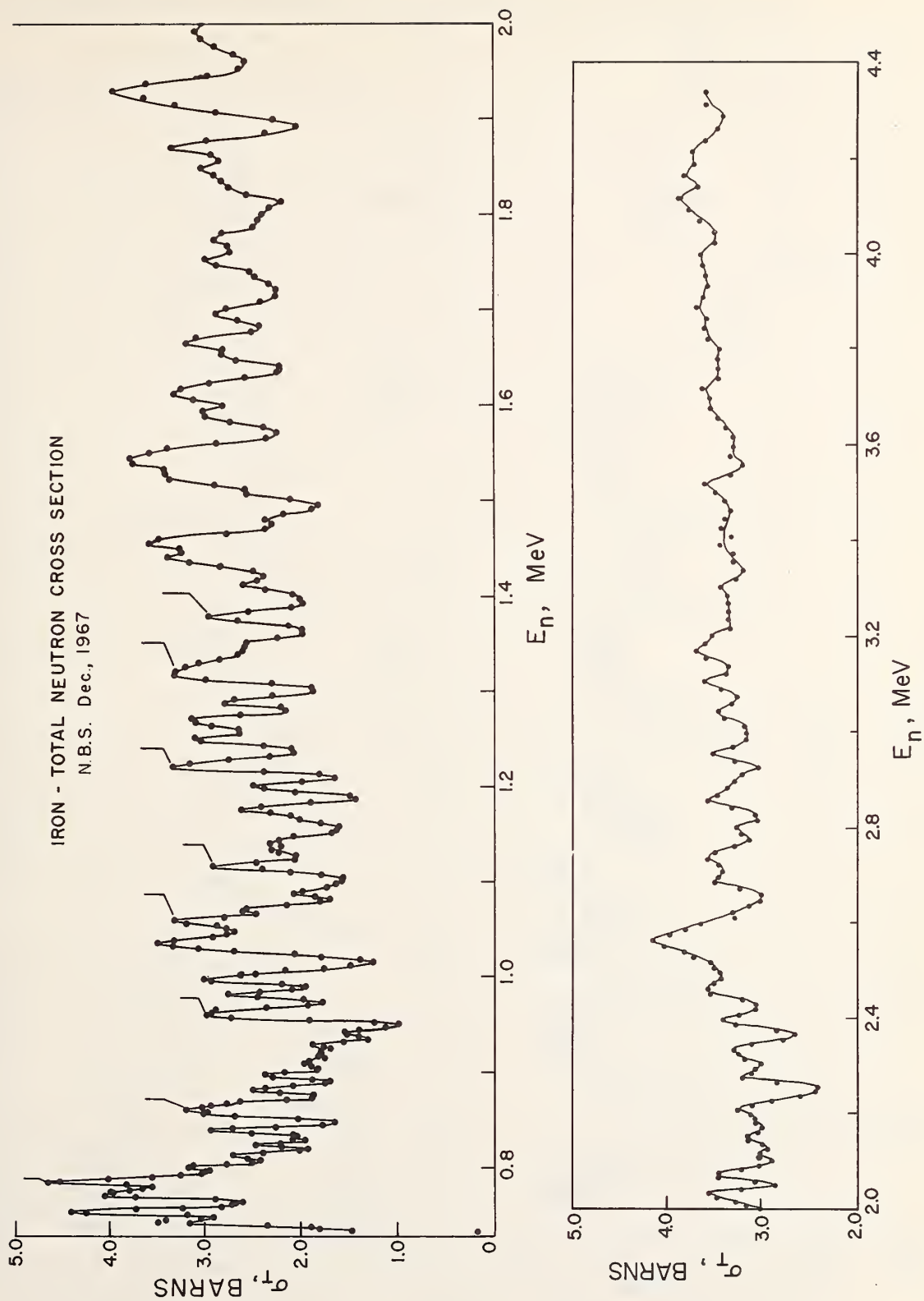


Figure 3. The total neutron cross section of iron, measured with a resolution of 0.3 nsec/m. The short vertical lines indicate the energy shift between our data and the Argonne results.

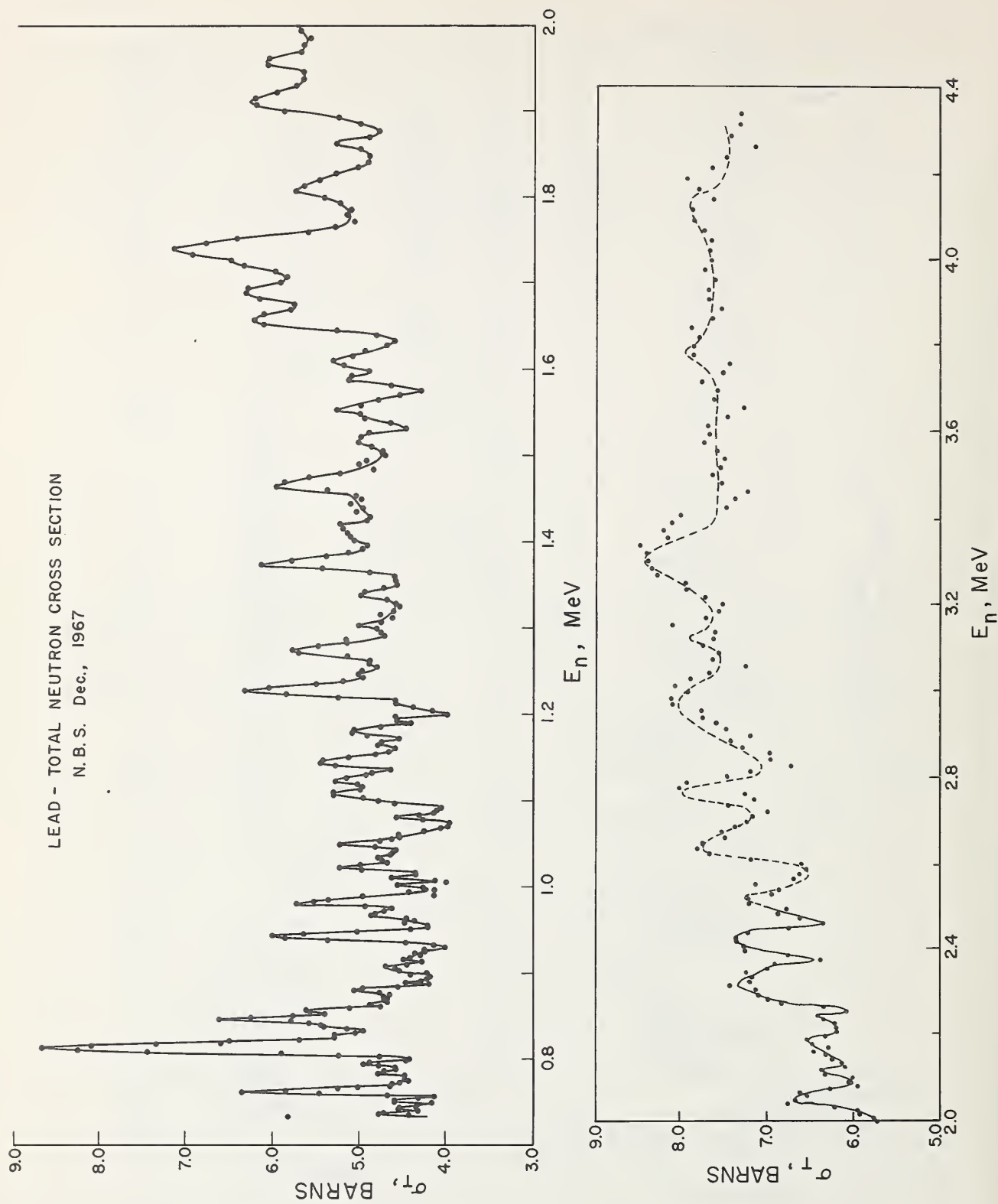


Figure 4. The total neutron cross section of lead measured with a resolution of 0.3 nsec/m. See text for explanation of dashed line.

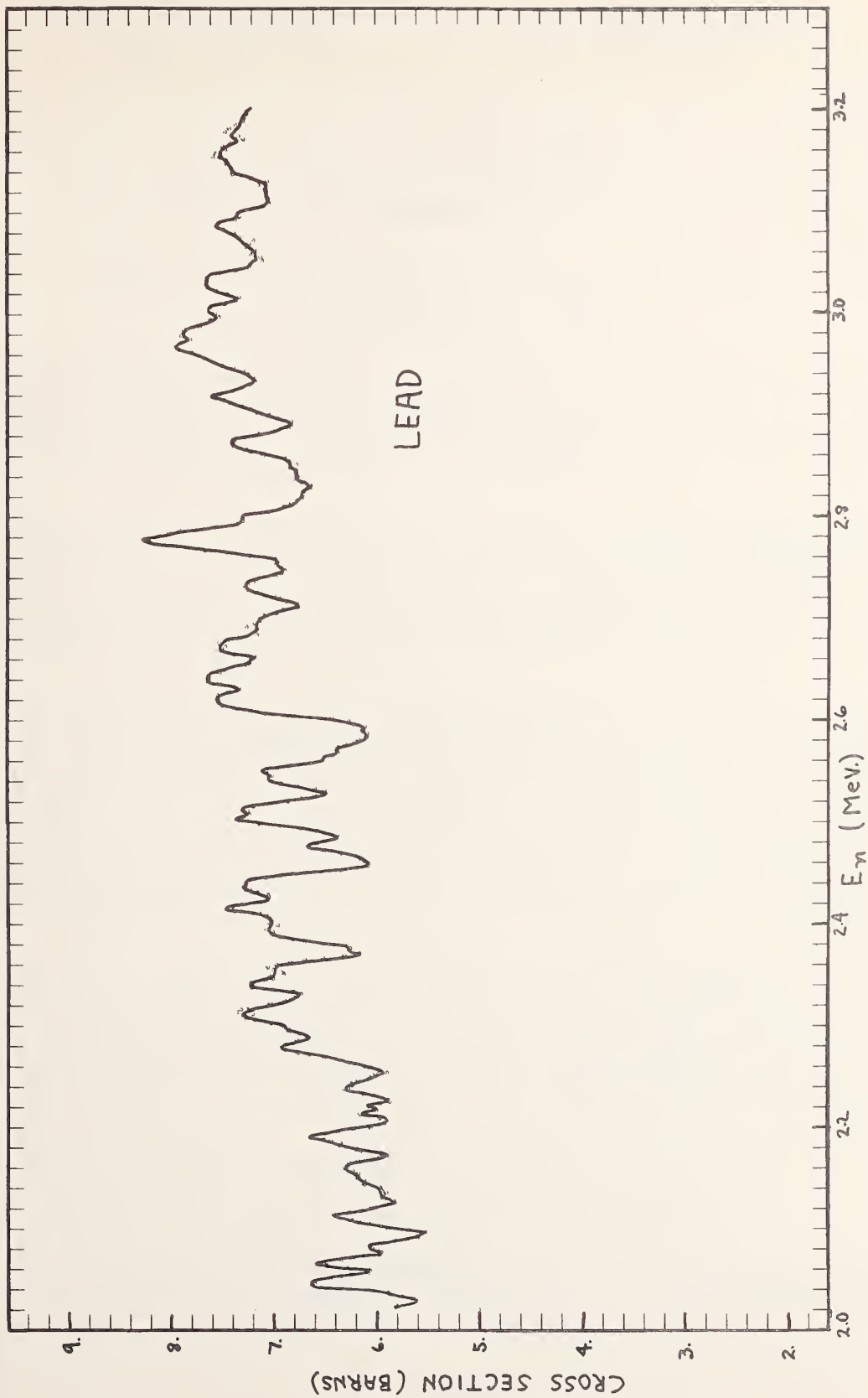


Figure 5. The total neutron cross section of lead, measured with a resolution of 0.16 nsec/m.

NUCLEAR LEVEL SCHEMES FROM RESONANCE NEUTRON CAPTURE

(^{196}Pt , ^{184}W , ^{200}Hg , ^{64}Cu , ^{68}Cu , ^{36}Cl , ^{198}Au , ^{60}Co)

R.N. ALVES*, C. SAMOUR, J.M. KUCHLY**, J. JULIEN
et J. MORGENSTERN.

Center d'Etudes Nucleaires de Saclay, France
91 Gif-sur-Yvette, France

Detailed level schemes can be obtained from gamma ray emission following resonance neutron capture. Such experiments have been performed at the Saclay linear accelerator using time of flight methods, and flight paths of 14 or 28 meters. An 8 cm^3 (Ge Li) detector with 15 keV resolution at 7 MeV was used.

The study of gamma ray spectra from resonance neutron capture presents several advantages with regard to studies of spectra due to thermal neutrons: i) Enhancement of transitions partial width obeys to a Porter Thomas distribution. ii) Spin assignments when many neutron resonances are available. iii) Level schemes can be assigned unambiguously to different isotopes.

We have obtained a detailed level scheme for ^{196}Pt from 22 resonances $J^\pi = 1^-$ and 8 resonances $J^\pi = 0^-$ (1,2). Forty excited states have been identified, 14 levels have spin 1^+ , the corresponding transitions being observed in resonances 1^- and 0^- . Other levels are probably 0^+ or 2^+ . We do not observe the 6803 keV transition to a 2^+ excited state at 1117 keV found by Ikegami and al. The dimensions of our resonance sample and the resolution of Ge(Li) detector would have allowed such a transition to be showed if it existed.

We have also studied the β decay of ^{196}Au , but did not find this excited state (3). Fig. 1 gives the level scheme; levels marked with a broken line are seen only in β decay (3,4), if the ^{196}Pt scheme can be compared with the vibrational harmonic model, when the second excited state 2^+ can be considered as a pure 2-phonon-state, it is evident from fig. 1 that the energy separation

* Nuclear Engineering Institute, Brazil

** Nuclear Research Laboratory, Strasbourg, France

We shall give some particularly illustrative examples. They are discussed in detail in references (1) and (4) and will be published at an early date.

of the 3 excited states 2^+ , 4^+ and 0^+ at 689, 876 and 1137 keV is too high to allow these 3 states to be considered as the 3 components of the 2-phonon-triplet. On the other hand an intermediate state 3^+ appears at 1015 keV and we observe two other levels at 1359 keV ($J=2^+$) and 1400 keV ($J=0^+$ or 2^+). Then the level sequence is better explained by a very anharmonic vibration mode. Similar conclusions are drawn for ^{200}Hg (fig. 2), for which the level scheme was studied from 4 resonances $J^\pi=1^-$ and 1 resonance $J^\pi=0^-$ (130 eV) (5). We found 31 excited states: 16 levels have spin 1^+ and the other states are very probably 0^+ or 2^+ .

^{184}W is a typical example of a deformed nucleus (fig. 3). We have studied 13 resonances 1^- and 4 resonances 0^- (1). We do not observe excited state at 690 keV found in ref. (2). Comparison of our data with fast neutron inelastic scattering allows the assignment of spin 0^+ for the 1004 keV state.

Fig. 4 shows the level scheme of ^{198}Au obtained from 3 resonances 2^+ (5, 60 and 107 eV) and 2 resonances 1^+ (58 and 78 eV) and from thermal spectra (1). We found 63 excited states between 0 and 2320 keV.

Fig. 5 gives the level scheme of ^{60}Co derived from resonance 4^- at 132 eV and thermal spectra (1). We found 65 excited states between 0 and 3820 keV.

Fig. 7 represents the level scheme of ^{64}Cu . Here a few spin values can be given, since we know the spin value of two neutron resonances located at 580 eV and 640 eV. Unfortunately we do not know the spin value of the 220 eV resonance of $^{65}\text{Cu}+n$ and the spin assignment of levels is not possible.

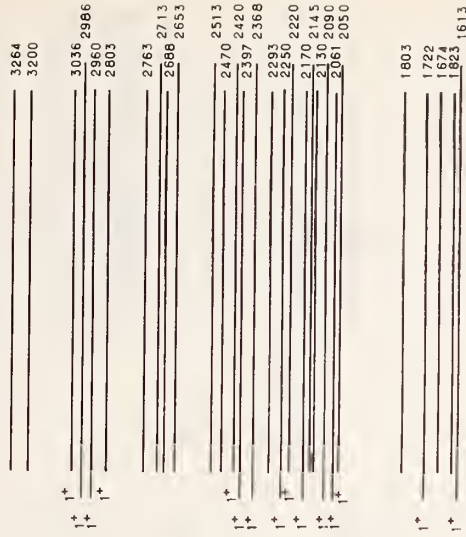
Fig. 8 shows the level scheme for $^{35}\text{Cl}+n$ from thermal and neutron resonance (405 eV) spectra. For this nucleus, we observed strong M1 transitions. All these schemes will be discussed in future publications (6).

References

- (1) C. SAMOUR, Thèse Paris, 1968.
- (2) C. SAMOUR et al., to be published.
- (3) H.E. JACKSON et al., Phys. Letters.
- (4) J.F.W. JANSEN et H. PAUW, Nucl. Phys., A94 (1967) 235.
- (5) R.N. ALVES, Thèse, Paris 1968.
- (6) R.N. ALVES et al., to be published.

183 W+n
0⁺ 7413 kW

199 Hg+n
8033 kW



195 Pt+n
0⁺ 7920 keV

199 Hg+n
8033 kW



183 W+n
0⁺ 7413 kW

199 Hg+n
8033 kW



196 Pt
78

199 Hg+n
8033 kW

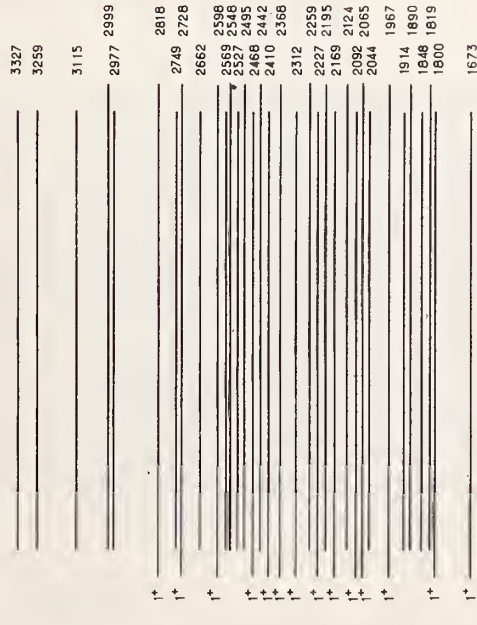


Fig. 3

Fig. 2

Fig. 1

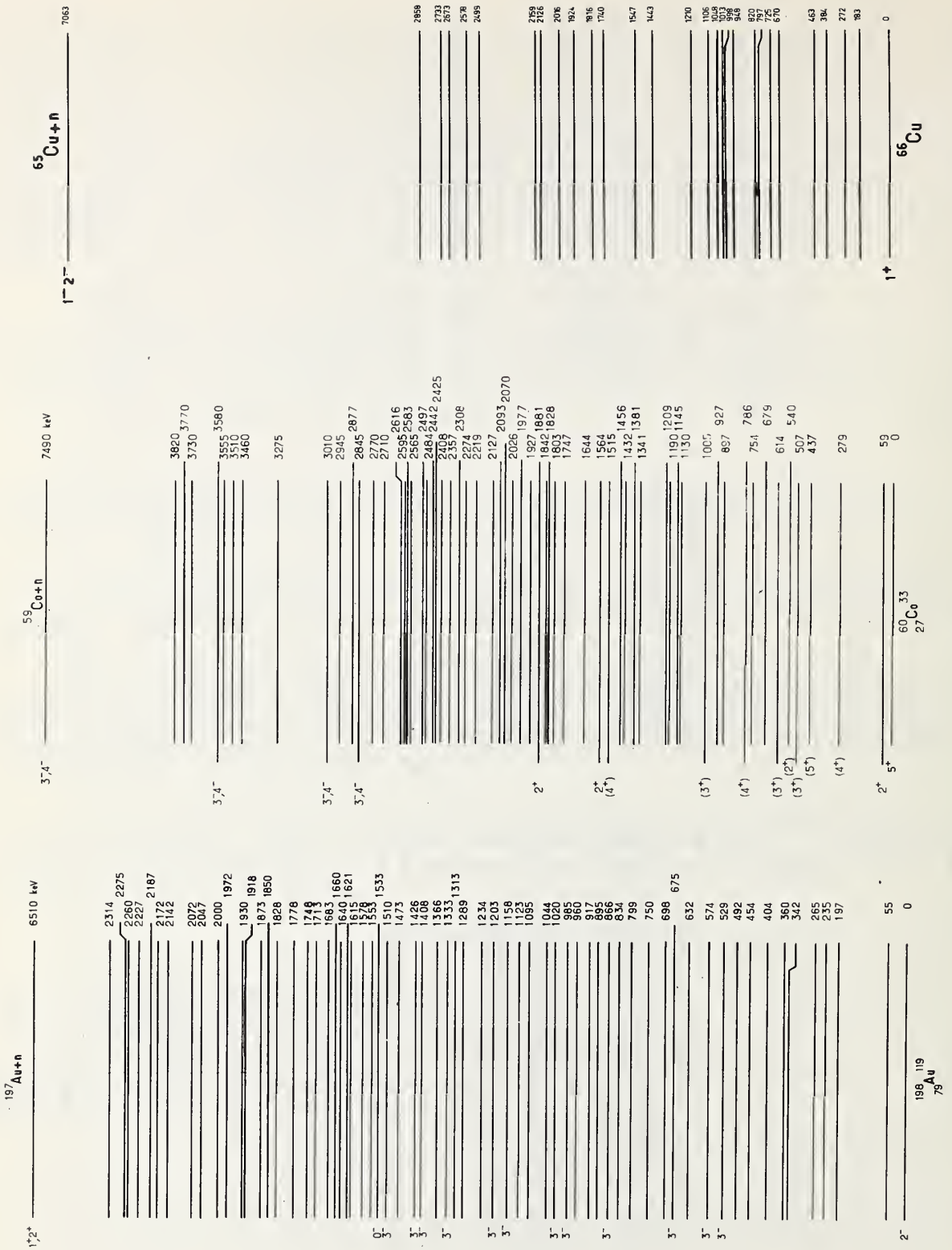


Fig.6

Fig.5

Fig.4

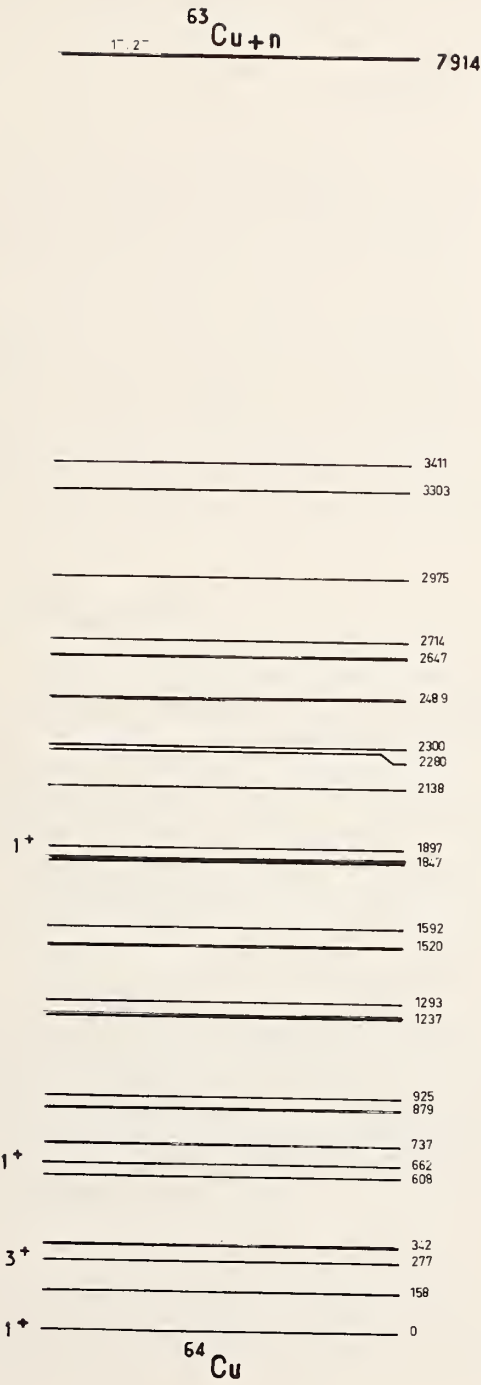


Fig.7

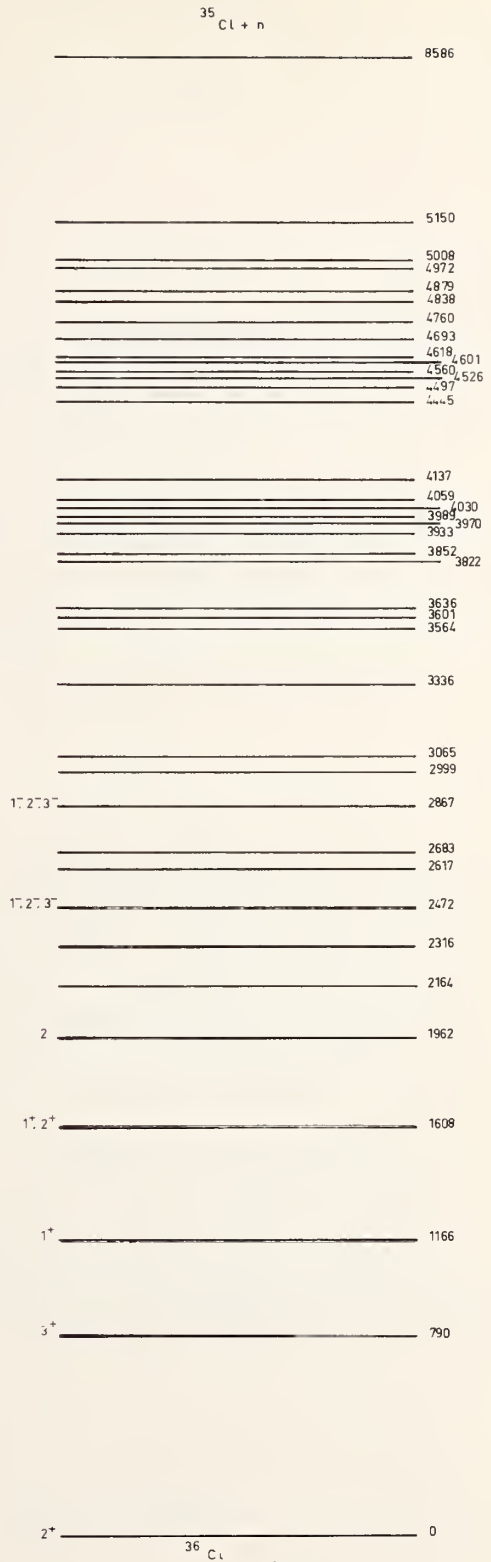


Fig.8

A. Asami*, M. Okubo, Y. Nakajima, and T. Fuketa

Japan Atomic Energy Research Institute,
Tokai-mura, Ibaraki-ken, Japan

ABSTRACT

Transmission measurements on the natural elements of Cd and Sb were carried out with the neutron time-of-flight spectrometer at the JAERI Linac. Metallic samples of different thicknesses, from 0.0047 to 0.306 atoms/barn for Cd and from 0.00085 to 0.183 atoms/barn for Sb, were used. The neutron energy region from a few eV up to several keV was covered with maximum resolution of 10 nsec/m. Transmission measurements with samples at liquid-nitrogen temperature were also made to improve separation of closely spacing resonances. New resonances at relatively low energies were found at 54.3, 59.8 and 62.3 eV in Cd and at 37.9 and 55.2 eV in Sb. The resonance dips in the transmission data have been analysed by the area-analysis method based on the Breit-Wigner single-level formula. The values of the neutron widths and the total widths will be tabulated.

1. INTRODUCTION

Neutron transmission measurements on natural cadmium and antimony were made by the time-of-flight method in the energy range from a few eV to several keV. The samples of several different thicknesses including fairly thick ones were used aiming at improvement of the accuracy in the resonance analysis, at determination of the total widths of the resonances by the thick-thin method, and at finding small resonances in relatively low energy region. In addition to the measurements at room temperature, the measurements were also made with the samples at liquid-nitrogen temperature in order to improve the separation of closely spaced resonances.

The plan of these experiments was also made in an anticipation, when enough number of the resonances are isotopically identified in future, that a detailed systematics will be achieved on the average values of the resonance parameters of nuclides in this mass region, where the s-wave strength function has a minimum and the strength functions of the ten isotopes of tin had been measured (1). While our measurements were under way, the strength functions of four of the cadmium isotopes were reported by Schepkin et al. (2).

*Present address: Nuclear Phys. Div., A.E.R.E., Harwell.

2. MEASUREMENTS

The neutron transmission measurements were made by using the JAERI Linac Time-of-Flight Spectrometer (3) with a 50-m flight-path length. A sample changer and a TMC 4096-channel time analyzer were controlled by a programming circuit, and cyclic measurements of the open-beam, sample-in, and black-resonance-sample-in (for the background measurement) counts were performed automatically with periods determined by the preset monitor counts. The energy ranges of measurements were covered from 12 eV to several keV for Cd and from 1 eV to several keV for Sb with the resolutions ranging from 10 to 60 nsec/m. Five Cd and eight Sb samples of different thickness were prepared, ranging from 0.0047 to 0.306 atoms/barn and from 0.00085 to 0.183 atoms/barn, respectively. The samples were all in the form of metallic plates, except the thinnest two Sb samples which were of metallic powder.

The measurements at liquid-nitrogen temperature were made by using a cryostat (4) which was automatically operated in and out of the neutron beam. An example of comparison of the sample-in spectra between the measurements with samples at room temperature and at liquid-nitrogen temperature is shown in Fig. 1, of which ordinate is rather arbitrary since the spectra of different runs are superposed and normalized at the off-resonance portions. The spacing between the two resonances of Sb in Fig. 1 is only 0.7 eV, where the instrumental resolution is about 0.24 eV and the Doppler width at 90 eV and for mass number of 122 is 0.28 eV at 300° K and about 0.14 eV at 78° K. A tiny dip at 87.72 eV in the spectrum at the liquid-nitrogen temperature looks real, but it is not listed in Table 2.

3. RESULTS AND DISCUSSION

The resonance dips in the transmissions were analysed by an IBM-7044 computer with an area-analysis code (5) which had been modified from the code written by Atta and Harvey (6) based on the Breit-Wigner single-level formula; and besides the neutron widths, the total widths were derived by the thick-thin method with transmissions of several different sample thicknesses in favourable cases.

The preliminary results of the resonance parameters of Cd and Sb are listed in Tables 1 and 2, respectively. In the analyses to obtain the neutron widths, the radiation widths of 110 meV and 90 meV were assumed for Cd and Sb, respectively, excepting the cases that the total widths were determined by the thick-thin method. The data from the thinnest Cd sample at room temperature and from the Cd samples at liquid-nitrogen temperature are not included in Table 1, whereas the data of Sb in Table 2 are almost final ones for that energy region.

The present data agree in general with the other published data except a few minor resonances. The new resonances were found at 54.3, 59.8, 62.3, and 110.2 eV in Cd, although the 110.2-eV resonance is so tiny that there remains uncertainty in its reality. The small resonances at 47.1 and 157.1 eV in the previous Sb data (7) did not come out in the present data even with the thickest sample. In an additional measurement to examine the above discrepancy with a Sb_2O_3 -powder sample of approximately

0.18 atoms/barn in Sb, the resonance dips came out at 47.1 and 92.3 eV very clearly, and these dips were attributed to an arsenic impurity. On the other hand, the new small resonances at 37.9 and 55.2 eV in Sb are not considered as to be resulted from an impurity, because no large resonances at these energies are found in the BNL-325 (8) data. A detailed paper including the average values of the resonance parameters will be reported in near future.

We are grateful to Dr. T. Momota and Dr. H. Takekoshi for their constant encouragement during the course of this work, and also to the operating staffs of the JAERI Linac for their assistances.

4. REFERENCES

- (1) T. Fuketa, F. A. Khan, and J. A. Harvey: ORNL-3425 (1963) 36; and Yu. V. Adamchuk, S. S. Moskalev, H. V. Muradyan: Soviet J. Nuclear Phys. (in Russian) 3 (1966) 801.
- (2) Yu. G. Schepkin, Yu. V. Adamchuk, L. S. Danelyan, and G. V. Muradyan: Nuclear Data for Reactors, Conf. Proceedings, Paris 1966, Vol. 1, IAEA (1967) 93.
- (3) A. Asami, T. Fuketa, Y. Kawarasaki, Y. Nakajima, M. Okubo, T. Sakuta, K. Takahashi, and H. Takekoshi: JAERI 1138 (1967).
- (4) The cryostat was originally prepared to investigate the effect of crystalline binding on the Doppler broadening in neutron resonances. K. Ideno, M. Okubo, and T. Asami: EANDC (J) 7 'L' (1967) 8 (private communication).
- (5) T. Fuketa, A. Asami, M. Okubo, Y. Nakajima, Y. Kawarasaki, and H. Takekoshi: Nuclear Data for Reactors, Conf. Proceedings, Paris 1966, Vol. 1, IAEA (1967) 147.
- (6) S. E. Atta and J. A. Harvey: ORNL-3205 (1961) and its Addendum (1963).
- (7) M. D. Goldberg, S. F. Mughabghab, B. A. Magurno, and V. M. May: BNL-325, Second Ed., Supple. No. 2, Vol. II B (1966).
- (8) D. J. Hughes and R. B. Schwartz: BNL-325, Second Ed. (1958).
- (9) A. Stolovy: Phys. Rev., 155 (1967) 1330.

TABLE I. Parameters of the Neutron Resonances in Cadmium

Resonance Energy, E_0 (eV)	Neutron Width, Γ_n (meV) ^{a)}	Total Width, Γ (meV)	Target Isotope ^{b)}	Spin ^{b)} J
18.34	0.180 ± 0.007	120 ± 20	113	1
27.5	4.1 ± 0.4	170 ± 20	111	1
29.0	$0.004 \pm 0.001^{**}$		111 or 116	
54.3	$0.003 \pm 0.001^{**}$			
56.3	$0.3 \pm 0.1^*$		113	
59.8	$0.006 \pm 0.001^{**}$			
62.3	$0.005 \pm 0.001^{**}$			
63.6	3.1 ± 0.2		113	1
66.7	4.7 ± 0.2	120 ± 10	112	
69.4	$0.2 \pm 0.1^*$		111	
83.2	0.5 ± 0.2		112	
84.8	26 ± 9		113	1
86.2	$3.4 \pm 0.4^*$		111	
89.5	130 ± 20		110	
99.3	12.5 ± 0.7		111	1
102.6	$1.5 \pm 0.7^*$		111	
108.1	8.3 ± 0.6		113	1
110.2				
115.5				
120.0	30 ± 8		114	
137.6	12 ± 1	90 ± 20	111	1
142.7	$5 \pm 1^*$		113	
158.2	$13 \pm 3^*$		113	
163.8	34 ± 5		111	1
192.2	150 ± 50		113	0
214.3	25 ± 3		113	1

a) The value with an asterisk denotes the value of $2g\Gamma_n$, and the value with two asterisks denotes that of $fg\Gamma_n$, where g and f represent the statistical weight factor and the fractional abundance of the isotope, respectively.

b) The isotope assignments and the spin assignments are due to Refs. (2) and (7). The isotope assignments in Refs. (2) and (7) for the 29.0-eV resonance are discrepant each other.

TABLE II. Parameters of the Neutron Resonances in Antimony

Resonance Energy, E_0 (eV)	Neutron Width, ^{a)} $2g\Gamma_n$ (meV)	Total Width, Γ (meV)	Target Isotope ^{b)}	Spin, ^{c)} J
6.233	2.6 ± 0.5	60 ± 10	121	3
15.43	7.5 ± 0.5	100 ± 15	121	2
21.4	30 ± 3	120 ± 20	123	
29.6	5.5 ± 0.3	90 ± 20	121	
37.9	0.019 ± 0.002*			
50.5	2.8 ± 0.2	90 ± 10	123	
53.6	1.9 ± 0.2	95 ± 10	121	
55.2	0.036 ± 0.004*			
64.5	0.65 ± 0.05	90 ± 10	121	
73.8	7.8 ± 0.5	95 ± 10	121	
76.7	5.3 ± 0.4	70 ± 10	123	
89.7	17 ± 4*			
90.4	3.8 ± 1.2*			
104.9	48 ± 5	130 ± 20	123	
111.4	2.8 ± 0.3		121	
126.7	30 ± 3	120 ± 20	121	
131.9	11 ± 1		121	
144.3	15 ± 1.5	100 ± 10	121	
149.9	26 ± 3	100 ± 10	121	
160.7	1.2 ± 0.1		121	
167.1	15 ± 1.5		121	
176.7	0.42 ± 0.04*			
184.8	0.20 ± 0.02*			
186.2	0.20 ± 0.02*			
191.9	24 ± 3	110 ± 10	123	
198.0	0.37 ± 0.04*			
214.0	1.6 ± 0.2*			
218.8	4.3 ± 0.4*			
222.8	5.4 ± 0.5*			
225.1	0.24 ± 0.03*			
230.9	0.9 ± 0.1*			
240.6	17 ± 2*			
246.2	0.25 ± 0.03*			
249.4	0.25 ± 0.03*			

a) The value with an asterisk denotes the value of $4fg\Gamma_n$, and f is nearly equal to 1/2 for antimony isotopes of the mass number 121 and 123.

b) The isotope assignments are due to Ref. (7).

c) The spin assignments are due to A. Stolovy (9).

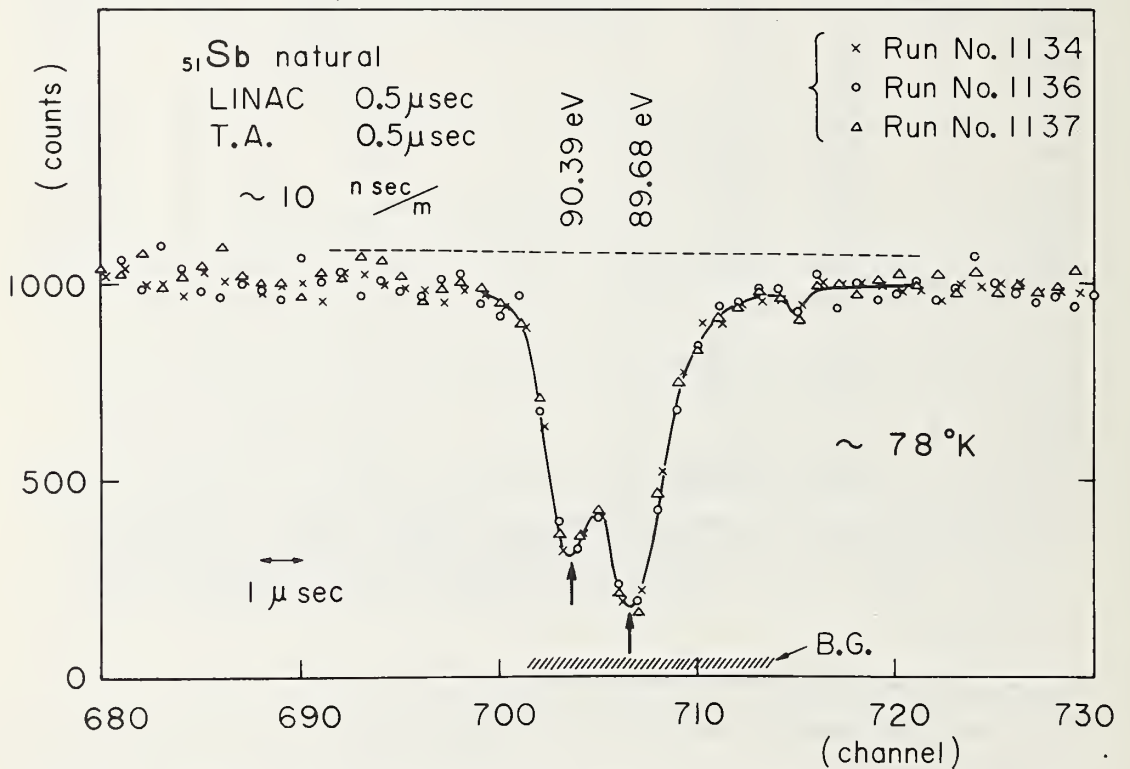
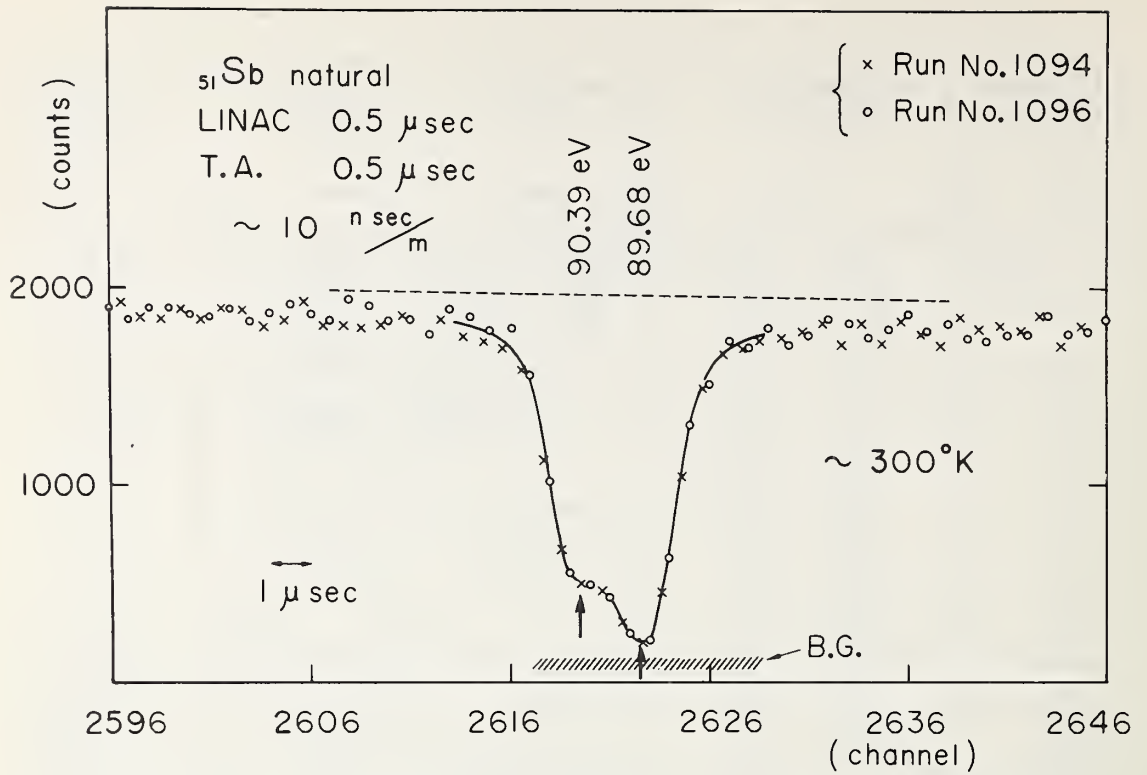


FIG. 1. Comparison of the sample-in spectra between the measurements with samples at the room temperature and at the liquid-nitrogen temperature.

NEUTRON CAPTURE RESONANCES OF TUNGSTEN IN THE RANGE
150 EV TO 100 KEV*

Z. M. Bartolome+, W. R. Moyer, R. W. Hockenbury
J. R. Tatarczuk and R. C. Block

Division of Nuclear Engineering and Science
Rensselaer Polytechnic Institute
Troy, New York 12180

New experimental data on neutron capture in metallic samples of tungsten ^{182}W , ^{184}W , and ^{186}W , have been taken with the 1.25 meter diameter capture tank and a time-of-flight resolution of 2 nsec/meter. Preliminary analysis show that, compared with previous results, (1) at least 9 new prominent resonances are observed in the energy range 225 eV to 4 keV for ^{182}W , 36 new resonances observed in the range 180 eV to 2.6 keV for ^{183}W , 12 observed in the range 145 eV to 4 keV for ^{184}W , and 8 observed in the range 350 eV to 4 keV for ^{186}W . In addition, previously reported single resonances have been resolved in doublets; these are at 3434 eV and 4005 eV in ^{182}W and at 1012 eV, 1402 eV and 1698 eV in ^{183}W . cursory examination of the new data indicates the possibility of analyzing resonances up to approximately 20 keV. The data are in the process of being reduced to yields and Monte Carlo corrections are being applied through the use of the direct link between the NYU CDC-6600 computer and the RPI IBM-1130 computer.

*Worked supported by the U. S. Atomic Energy
Commission under Contract AT(30-3)-328.

+Based in part on the Ph.D. Thesis of Z. M. Bartolome.

1. INTRODUCTION

In order to extend the range of tungsten radiative capture resonance energies hitherto analyzed and reported⁽¹⁾, new measurements have been carried out at the RPI Electron Linear Accelerator Laboratory. Enriched metallic samples of ^{182}W , ^{183}W , ^{184}W , and ^{186}W , whose pertinent characteristics are given in Table I, were supplied by the National Aeronautics and Space Administration.

TABLE I

Isotope	Enrichment	Average Density	Atoms/Barns
^{182}W	93.76%	10.29	.01886
^{183}W	83.75%	9.45	.01327
^{184}W	94.20%	10.50	.02668
^{186}W	97.15%	11.05	.02490

Except for the use of a recently installed flight path, the experimental procedure is similar to that described elsewhere⁽²⁾ and to a paper presented in this conference⁽³⁾. Hence, only a very brief description of the experimental method will be presented.

2. EXPERIMENTAL PROCEDURE

Isotopically enriched metallic tungsten wafers, with a very thin gold foil placed in front of each sample for the purpose of normalization, were positioned in the center of the ORNL 1.25 meter diameter liquid scintillation detector which was located at the 25 meter station. The samples were bombarded with photoneutrons produced from a tantalum target by 60 MeV electrons and moderated by 1-inch thick polyethylene. The 60 MeV electron pulse was of 20 ns duration, and the repetition rate was 400 pulses per second.

For the measurement of the flux, and also for tungsten transmission measurements which were made, a $\text{B}^{10}\text{-NaI}$ scintillation detector was used. This detector was contained in a 4-inch thick lead shield at the 28 meter flight path just behind the neutron capture detector. The shield was thick enough to reduce the natural background in the NaI crystals by approximately a factor of three.

Counts from the capture detector, and alternately from the $\text{B}^{10}\text{-NaI}$ detector, were collected by a PDP-7 on-line computer which was programmed as a 6144 channel time-of-flight

analyzer. The first 4936 channels were set at 31 ns per channel; the remaining 1208 channels were set 1 μ s wide. This arrangement made it possible for observations to be made from 100 keV to approximately 150 eV with a resolution of 2 ns/m at the higher energies; the 1208 channels at 1 μ s per channel afforded a means of extending observations in capture to the 4.96 eV resonance of gold. The time dependent background was ascertained by placing 'resonance' filters between the moderator and the sample under study. The filters used were Al, Na, Mn, and Co which have "black" resonances at 88, 35, 2.85, 0.337, and 0.132 keV.

3. DATA REDUCTION

To facilitate the identification and determination of the energies of the capture resonances, a program was written for the IBM-1130. The raw time-of-flight data was scanned point by point, and any region where two successive data points increased in counts by two or more standard deviations was considered the leading edge of a resonance. The data were further scanned through the peak and to a region where either the counts leveled off or a new resonance began. A gaussian curve was fitted to the data thus scrutinized, and the resonance energy was determined from the center of the fitted curve. The data were then scanned further for successive resonances. The list of computer determined resonances was then compared by visual inspection with plots of the raw counting data in order to eliminate any resonances which were inconsistent with the known resolution and response of the equipment. Over 800 tungsten resonances were resolved and isotopically identified in this experiment, and this represents too lengthy a list of numbers to be reproduced here. However, a listing of these resonance energies can be found in Ref. (4).

The capture data have been reduced to capture yields, i.e. the ratio of neutron captures to neutrons incident upon the sample. These data have been averaged over rather broad energy intervals in the region from 1 keV to 100 keV, and corrections have been applied for resonance self-protection and multiple scattering using the method proposed by Dresner⁽⁵⁾ and the resonance parameters by Block et al⁽¹⁾. This correction, defined as the ratio of the capture cross-section found experimentally to that of an infinitely thin sample, was found for these samples to vary from approximately 30% at 1 keV to about 65% at 10 keV. In figures 1, 2, 3, and 4 are plotted the average capture cross-sections for W-182, W-183, W-184, and W-186 respectively. A complete error analysis has not yet been applied, but an estimated error of 10% has been indicated on these curves. By weighting the isotopic cross-sections by the isotopic abundance occurring in elemental tungsten, a W

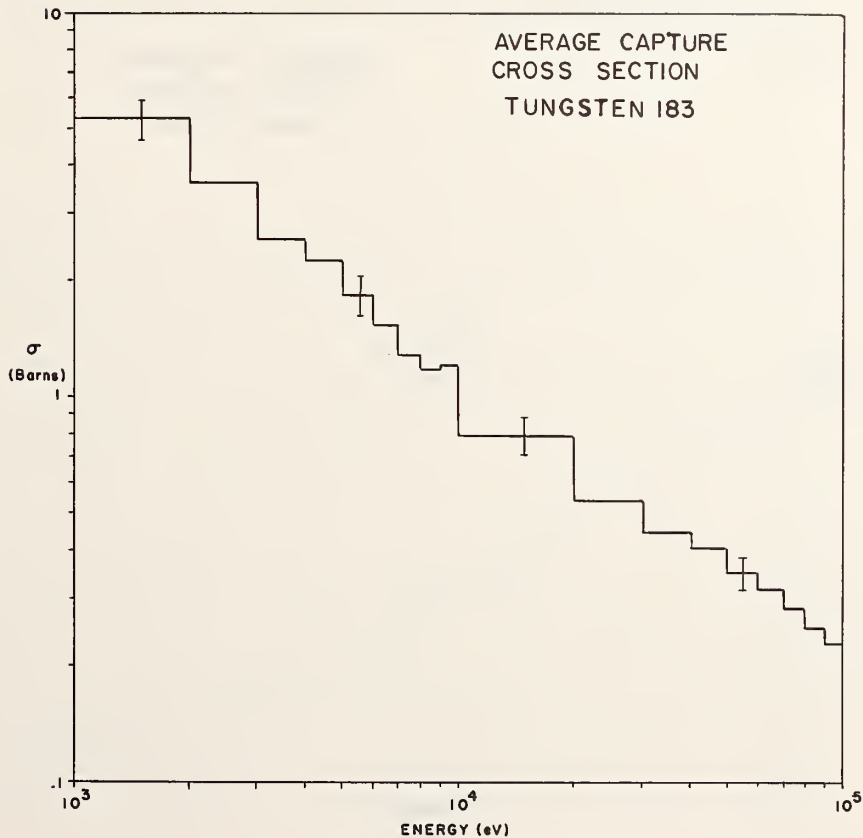
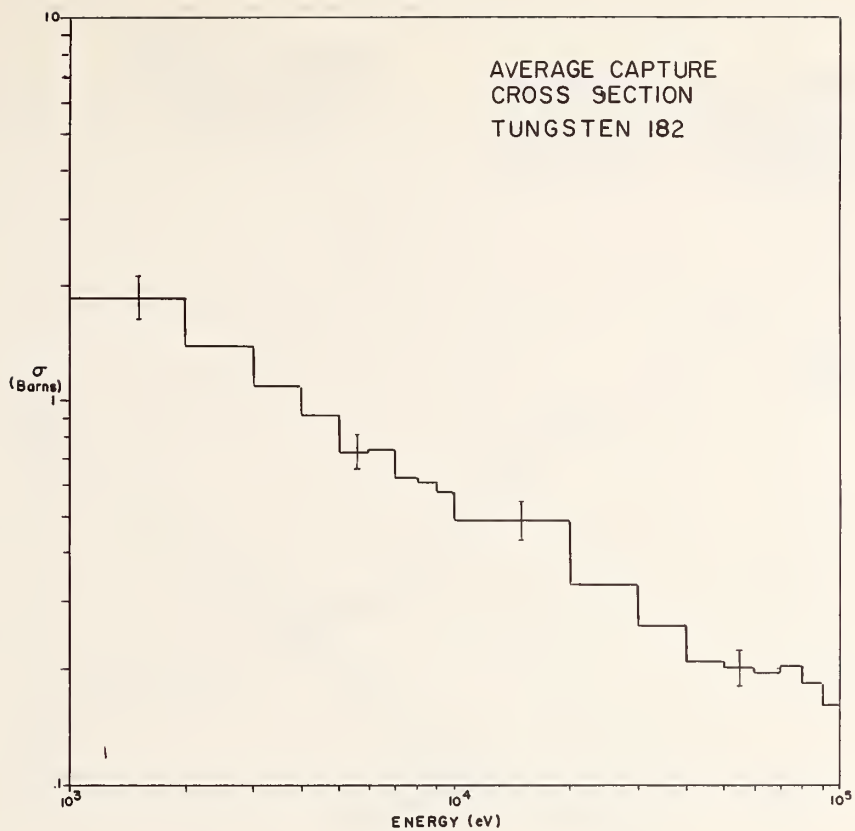
elemental cross-section can be obtained; this is plotted in Figure 5. The figures agree rather well with those given by Dovbenko, et al⁽⁶⁾ and Kapchigashev, et al⁽⁷⁾ for the isotopic average capture cross-sections, and those given by Gibbons, et al⁽⁸⁾ for the average capture cross-section of elemental tungsten.

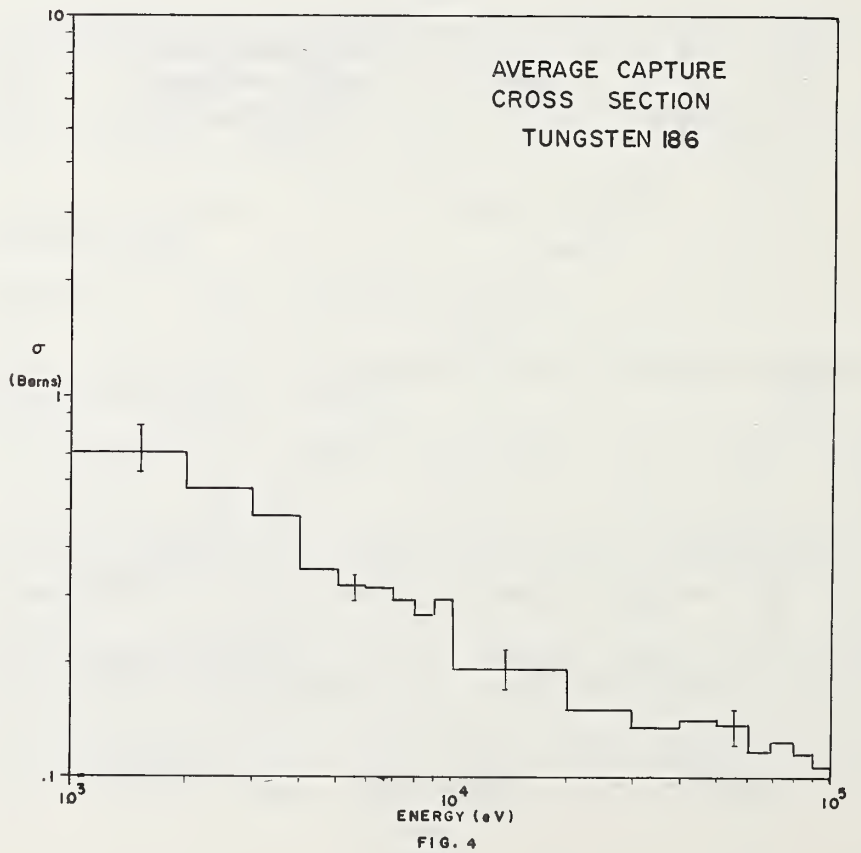
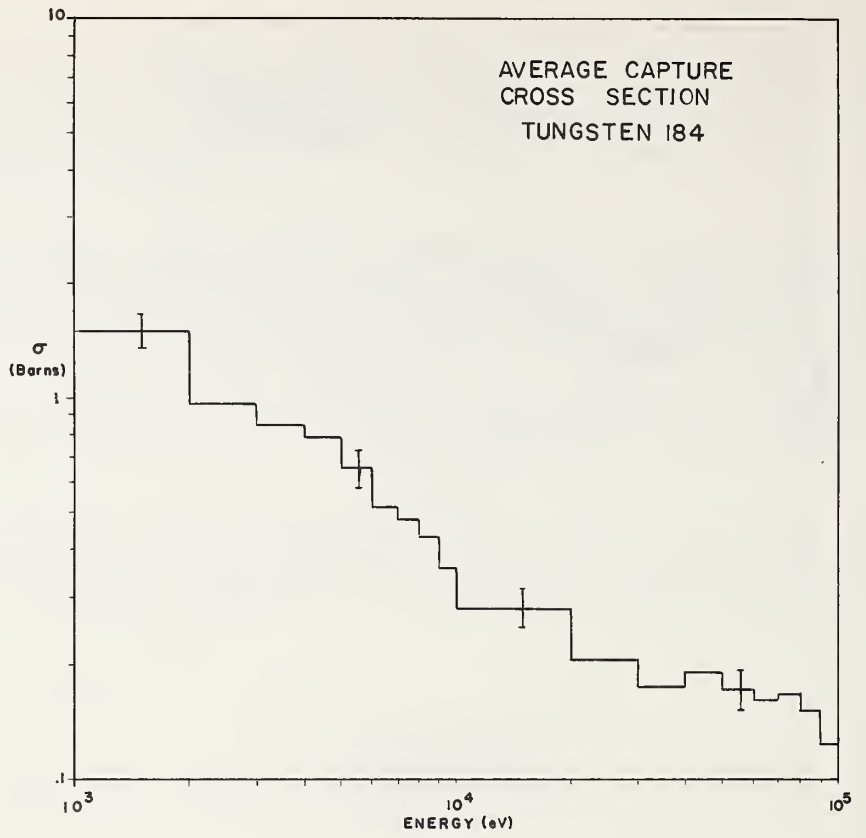
Compared with previous reports⁽¹⁾, at least 9 new prominent resonances have been observed in the energy range 225 eV to 4 keV of ^{182}W , 36 new resonances in the range 180 eV to 2.6 keV for ^{183}W , 12 in the range 145 eV to 4 keV for ^{184}W , and 8 in the range 350 eV to 4 keV for ^{186}W . In addition, previously reported single resonances have been resolved to doublets. These are at 3434 eV and 40005 eV in ^{182}W , and at 1012 eV, 1402 eV and 1698 eV in ^{183}W .

Pertinent resonance parameters are in the process of being extracted from these data and the transmission data, but these results were not completed in time for this paper.

4. REFERENCES

1. R. C. Block, J. E. Russel, and R. W. Hockenbury, Oak Ridge National Laboratory, Phys. Div. Ann. Prog. Report, December 31, 1964, ORNL - 8773, p. 53. Also, R.P.I. Linear Accelerator Project Progress Report, January-March, 1966, p. 14.
2. R. W. Hockenbury, Ph.D. Thesis, R.P.I., 1967 (unpublished).
3. Paper E-7, this conference.
4. R.P.I. Linear Accelerator Project Progress Report, October-December, 1967.
5. L. Dresner, Nucl. Inst. and Meth., 16, 176 (1962).
6. A. G. Dovbenko, V. E. Kolesov, V. N. Kononov, and Yu. Ya. Stavisskii, Conf. on Study of Nuclear Structure with Neutrons, Antwerp, Paper 199 (1965).
7. S. V. Kapchigashev, Yu. P. Popov, and F. L. Shapiro in BNL 325-Second Edition, Supplement No. 2.
8. J. H. Gibbons, R. L. Macklin, P. D. Miller, and J. H. Neiler, Phys. Rev., 122, 556 (1960).





AVERAGE CAPTURE
CROSS SECTION
NATURAL TUNGSTEN

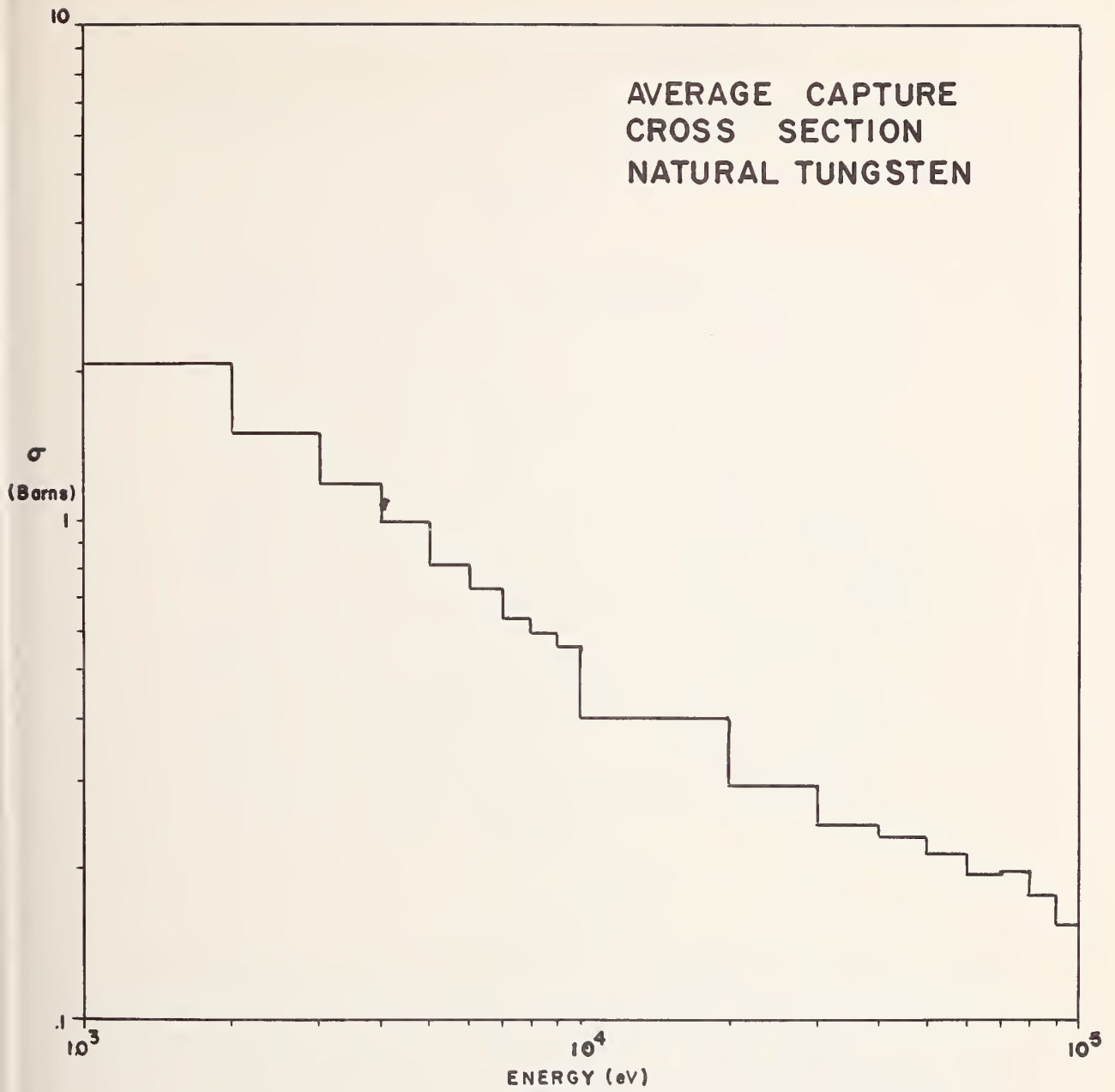


FIG. 5

THE NEUTRON INELASTIC CROSS SECTION FOR THE PRODUCTION OF ^{103m}Rh

J.P. Butler and D.C. Santry, Chalk River Nuclear Laboratories
Chalk River, Ontario

ABSTRACT

The cross section for the threshold reaction $^{103}\text{Rh}(n, n')^{103m}\text{Rh}$ has been measured by the activation method from 0.18 to 14.8 MeV. Neutrons with an energy spread varying from ± 30 to ± 80 keV were obtained from the $\text{T}(p, n)^3\text{He}$, $\text{D}(d, n)^3\text{He}$ and $\text{T}(d, n)^4\text{He}$ reactions using an EN tandem Van de Graaff accelerator and a 2 MeV accelerator. For energies below 5.5 MeV the neutron flux was determined with a calibrated neutron long counter while at higher energies the measurements were made relative to the known cross section for $^{32}\text{S}(n, p)^{32}\text{P}$ reaction. The cross section for $^{103}\text{Rh}(n, n')^{103m}\text{Rh}$ increases rapidly with energy from a value of 25 ± 3 mb at 0.18 MeV to a maximum of 1385 ± 55 mb near 6 MeV. The excitation curve shows distinct discontinuities in slope at about 300, 550 and 800 keV. The decrease in slope at 300 and 800 keV is attributed to the appearance of levels of negative parity which prefer to decay to the ground state, while the increase at 550 keV is caused by levels which decay to the isomeric state. From the excitation curve an effective cross section of 716 ± 40 mb was calculated for a fission-neutron spectrum.

1. INTRODUCTION

The foil activation technique is still the most convenient method for determining fast-neutron fluxes and spectra in nuclear reactors. The (n, p) and (n, α) reactions generally used for these measurements have thresholds greater than 2 MeV and therefore are not suitable for monitoring the neutron flux in the energy region 0.1 to 3 MeV. Although the neutron flux in this region can be calculated or inferred from measurements at higher energies, the environment often produces large perturbations on the flux distribution. Reliable fluxes at these energies can only be obtained by using monitors that are sensitive to these low energy neutrons.

Recently we have measured excitation curves for several (n, n') reactions that produce metastable isomers with convenient half-lives. These reactions should be useful for fast-neutron monitoring in the low energy region since the reactions have low threshold energies, above which the cross sections rise rapidly. Besides being useful for fast-neutron monitoring, precise excitation curves for (n, n') reactions are also of interest from the standpoint of nuclear-reaction theory.

In the present experiment, the activation cross section for the (n, n') reaction on ^{103}Rh has been measured in the neutron energy range 0.18 to 14.8 MeV, by determining the amount of the 57 min $^{103\text{m}}\text{Rh}$ formed at each energy. The reaction has a low threshold energy, 40.4 keV, and therefore should have a good response to neutrons in the energy region 0.1 to 2 MeV.

The reactions $\text{T}(p, n)^3\text{He}$, $\text{D}(d, n)^3\text{He}$ and $\text{T}(d, n)^4\text{He}$ were used to produce monoenergetic neutrons. Activation cross sections were determined relative to the cross section for the $^{32}\text{S}(n, p)^{32}\text{P}$ reaction(1, 2) for neutron energies above 5 MeV and with a calibrated neutron long counter at lower energies. As a check on the accuracy of the measurements both methods were used in the vicinity of 5 MeV.

2. EXPERIMENTAL PROCEDURES

2.1. Neutron Irradiations

Monoenergetic neutrons were produced in the energy region 0.2 to 5.5 MeV by the $\text{T}(p, n)^3\text{He}$ reaction, and from 5.0 to 13.6 MeV by the $\text{D}(d, n)^3\text{He}$ reaction. The experimental arrangement has been described previously(3) and only a brief outline is presented here. Deuterium gas and titanium-tritium (Ti-T) targets were bombarded with deuterons or protons from either the tandem Van de Graaff accelerator or a 2 MeV accelerator. The deuterium target consisted of a 2.7 cm long gas cell filled to about 3-atmospheres pressure. The gas was separated from the accelerator vacuum by 10 mg/cm² tantalum foil. The average neutron energy spread due to target thickness and geometrical effect varied from ± 30 keV at the lower neutron energies to about ± 80 keV at the higher energies. Metal disks of rhodium (3/16 in. diameter and 3-mil thick) were sandwiched between disks of pressed sulfur of the same diameter and 40-mil thick. The samples were irradiated 1.4 cm from the end of the cell at 0° to the collimated deuteron or proton beam. The half angle subtended by the rhodium disks at the average point of origin of the neutrons was 6.5° for the gas cell and 9° for Ti-T target.

In the energy region 13.6 to 14.8 MeV, neutrons were produced from the $\text{T}(d, n)^4\text{He}$ reaction using a Ti-T target and a 150-keV deuteron beam from a Texas Nuclear Neutron Generator. Data were obtained at various energies with samples placed in well defined positions on a circular arc 1.4 cm from the centre of the tritium target. Samples were irradiated at various angles from 0° to 140° on both sides of the beam axis. Any slight misalignment of the beam was corrected by averaging the activities at duplicate angles. Relative cross sections were calculated, using the known angular distributions of neutrons(4) from the $\text{T}(d, n)^4\text{He}$ reaction. These data were then normalized at 14.5 MeV to the value measured at this energy using the $^{32}\text{S}(n, p)^{32}\text{P}$ reaction to measure the neutron flux.

Samples of rhodium and sulfur were also irradiated with the deuterium gas cell evacuated and with titanium-hydrogen targets replacing the ones containing tritium. The observed activities gave a measure of the background contributions. The maximum correction to the $^{103\text{m}}\text{Rh}$ activity for background neutrons from titanium was 14% at a neutron energy of 5.5 MeV. For deuteron bombardments the background contribution varied from 0.6%

at a neutron energy of 8.5 MeV, to 17% at 12.6 MeV. Under the irradiation conditions the activity produced in the samples by scattered neutrons was estimated to be less than 0.04%.

A neutron long counter was used to measure fluctuations in the neutron intensity during irradiations and corrections were made to the saturation activity values for any significant fluctuations.

2.2. Neutron Flux Monitoring

For energies greater than about 5 MeV, the neutron flux was monitored by measuring the amount of ^{32}P produced by the $^{32}\text{S}(n,p)^{32}\text{P}$ reaction so that the cross section values at the higher energies are relative to the known cross section(1,2) for the sulfur (n,p) reaction. Below 4.6 MeV, this reaction is not suitable as a monitor since its cross section does not vary smoothly with neutron energy and its effective threshold is 1.9 MeV.

The neutron flux below 5 MeV was measured with a neutron long counter identical in design to that described by McTaggart(5). It was positioned on the axis of the beam 150 cm from the target. The counter was calibrated with a Chalk River Nuclear Laboratories standard Ra-Be neutron source ($2.86 \pm 0.04 \times 10^6$ neutrons/sec) using a value of 1.09 for the ratio of the response of the counter at 1 MeV to its response to Ra-Be neutrons(6).

To use the neutron long counter as a flux meter in the energy region 0.1 to 5.5 MeV, various corrections were applied to the observed counts. These are outlined here but will be discussed in more detail in a future publication. The corrections took into account: 1. the variation in counter efficiency with neutron energy as reported Allen(6); 2. changes in the effective centre of the counter with energy; 3. room-scattered neutrons; 4. neutrons scattered out of the counter by the presence of the samples; 5. background neutrons produced by the reaction of protons on the titanium in the Ti-T targets; and 6. the difference in half angles subtended by the samples (9°) and the counter (4°) which resulted in the average neutron flux being slightly higher at the counter than at the sample. Many of these corrections varied markedly with energy. The neutron flux as measured with the long counter had an estimated error of ± 4 to 5%.

2.3. Activity Measurements

$^{103\text{m}}\text{Rh}$ decays to the ground state with a half-life of 57.0 min(7) and a transition energy of 40 keV. The 40 keV gamma ray emitted in the transition is almost completely converted(8) ($e/\gamma \approx 500$) with about 79% of the conversions occurring in the L-shell, 9.9% in the K-shell(9,10) and 11% in the M-shell(7). The activity of $^{103\text{m}}\text{Rh}$ can be obtained by measuring either the electrons or the X-rays produced in the conversion of the 40 keV level. After the irradiation, the activities induced in the 3-mil thick rhodium disks were counted in a thin (4 mm x 38 mm) sodium iodide X-ray detector with a thin beryllium window. The $^{103\text{m}}\text{Rh}$ was determined from the intensity of the 20 keV K X-ray. Although $^{103\text{m}}\text{Rh}$ was the main activity observed, there was a small amount of the 40-day ^{103}Ru produced by the (n,p) reaction on ^{103}Rh at neutron energies above 10 MeV. At energies below 1 MeV, the (n, γ) reaction on ^{103}Rh produces a significant amount of the 4.4 min $^{104\text{m}}\text{Rh}$ which also emits rhodium K X-rays. The yield of $^{104\text{m}}\text{Rh}$ however decreases rapidly

with increasing neutron energy. The activity of $^{103\text{m}}\text{Rh}$ at zero time was computed from pulse-height spectra collected over many half-lives.

The efficiency of the detector for the 20 keV K X-rays was measured with a thin source of $^{103\text{m}}\text{Rh}$ on a VYNS film. The disintegration rate of the source was determined by $4\pi e$ -X efficiency tracer technique employing coincidence between the K-conversion electrons and the K X-rays. The efficiency for 4π -counting the conversion electrons (K, L and M conversion electrons have energies of 17, 37 and 39 keV respectively) was varied by placing additional VYNS films on the source. The results obtained were extrapolated to 100% efficiency to give the absolute disintegration rate(11). The initial efficiency of the 4π counter for the 17 keV K-conversion electrons from the VYNS source was 98%. The efficiency of the sodium iodide scintillation counter for the 20 keV X-rays was thus determined to be $3.42 \pm 0.06\%$. This calibration is essentially independent of the conversion factors and the fluorescent yield.

Because of the low energy of the K X-rays there is a large self-absorption correction for the 3-mil thick rhodium disks used in the neutron irradiations. To evaluate this correction rhodium samples from 0.2 to 3 mils in thickness were irradiated with 1 MeV neutrons. The relative activities were plotted against the sample thickness and extrapolated to zero source thickness. From these data it was estimated that only 36.5% of the photons escape from the 3-mil (91 mg/cm^2) thick rhodium foil disks, for our geometry conditions (half angle of 85°). This combined with the measured efficiency for a thin sample gave an overall efficiency of 1.25% for counting $^{103\text{m}}\text{Rh}$ in the metal disks.

The ^{32}P activity induced in the sulfur monitors was measured in a 2π beta proportional counter after ignition of the sulfur. This technique which has been previously discussed(2) leaves $95.5 \pm 0.5\%$ of the ^{32}P activity on the aluminum counting tray as a weightless source. The overall counting efficiency for ^{32}P including the burning efficiency was $49.2 \pm 1.0\%$. The sulfur samples decayed with the accepted half-life of 14.22 days(12).

3. RESULTS AND DISCUSSION

Values of the cross section for the $^{103}\text{Rh}(n, n')^{103\text{m}}\text{Rh}$ reaction were calculated from the activities induced in the rhodium disks and the neutron flux measured either with the sulfur monitors or the neutron long counter. The cross section results obtained are plotted as a function of neutron energy in Fig. 1 and the results obtained with different neutron sources are indicated. The only published cross section for this reaction is a value by Nagel and Aten(13) of $508 \pm 50 \text{ mb}$ at a neutron energy of 14.2 MeV which is in serious disagreement with our results. In the energy region 4.8 to 5.1 MeV ten irradiations were performed and cross sections were calculated relative to both the sulfur monitors and the neutron long counter. The average values agreed within 1% which was well within the accuracy of the two methods. This provided a check on the calibration of the neutron long counter. Above 9.5 MeV the (n, n') cross section decreases sharply, presumably because of competition from the $(n, 2n)$ reaction which has a threshold of 9.42 MeV.

In the energy region 7.7 to 13 MeV, there is a group of low energy or break-up neutrons from the $\text{D}(d, np)\text{D}$ reaction, associated with the

monoenergetic D-D neutrons. The effect of the break-up neutrons on the rhodium samples was calculated from the cross section of the (n,n') reaction on rhodium measured at the lower neutron energies and the number and energy distribution of the break-up neutrons as given by various investigators(14,15,16). The correction to the rhodium activity for these neutrons varies from about 1% at 8.5 MeV to 69% at 12.6 MeV. A detailed description of this correction as applied to the $^{32}\text{S}(n,p)^{32}\text{P}$ reaction has been given previously(2).

Marked discontinuities in the excitation curve for the (n,n') reaction on ^{103}Rh are observed at 300, 550 and 800 keV as shown in Fig. 2. These discontinuities can be explained from a study of the nuclear level structure of ^{103}Rh (17,18) given in Fig. 3. The decrease in slope at 300 keV is caused by the occurrence of the third and fourth levels with spins of $3/2^-$ and $5/2^-$ which prefer to decay to the ground state. This increased competition for the ground state causes the total cross section to the isomeric state to flatten somewhat. The occurrence of the 538 and 650 keV levels of spin $5/2^+$ and $7/2^-$ which feed the isomeric state cause the cross section to increase at 550 keV. A number of levels between 843 and 1043 keV which decay to the ground state cause the curve to flatten again at about 800 keV. Preliminary statistical theory calculations of the cross section in the low energy region, below 0.7 MeV, are in good agreement with the data but final calculations are awaiting more information on the nuclear levels above 650 keV.

A computer program was used to calculate an effective cross section for the $^{103}\text{Rh}(n,n')^{103\text{m}}\text{Rh}$ reaction for a fission-neutron spectrum. The effective cross section, $\bar{\sigma}$, is given by the expression

$$\bar{\sigma} = \int_0^{\infty} N(E) \sigma d E$$

Values for σ were obtained from a smooth curve drawn through our experimental points and the distribution of neutrons in the ^{235}U fission spectrum was taken as that given by Cranberg et al(19).

$$N(E) = k e^{-1.036E} \sinh \sqrt{(2.29E)}$$

where E is the neutron energy and k is a factor normalizing the integral of the spectrum to unity. The calculated value for the (n,n') reaction on rhodium in a fission neutron spectrum is 716 ± 40 mb. The measured value of 403 ± 40 mb reported by Köhler(20) is in serious disagreement with that calculated from the monoenergetic data. Fig. 4 gives the reaction rate, $N(E) \sigma$, of this threshold detector in a fission neutron spectrum from which a mean response energy of 2.23 MeV is calculated. It is also noted that 29% of the yield results from neutrons below 1.5 MeV so the reaction should be useful to monitor fast neutrons in the low energy region of a reactor spectrum.

We wish to thank Mr. J.G.V. Taylor and Mrs. J.S. Merritt for their standardization of the $^{103\text{m}}\text{Rh}$ source and Dr. W.G. Cross for many helpful discussions.

4. REFERENCES

1. L. Allen, Jr., W.A. Biggers, R.J. Prestwood, and R.K. Smith, *Phys. Rev.* 107, 1363 (1957).
2. D.C. Santry, and J.P. Butler, *Can. J. Chem.* 41, 123 (1963).
3. J.P. Butler and D.C. Santry, *Can. J. Chem.* 39, 689 (1961).
4. J.D. Seagrave, *Neutron Source Handbook*, Los Alamos Rept. LAMS-2162 (1957).
5. M.H. McTaggart, A.W.R.E. Report NR/A-1 (1959).
6. W.D. Allen, *Fast Neutron Physics, Part 1*, Edited by J.B. Marion, and J.L. Fowler, Interscience Publishers Inc. New York, pp 365-74 (1960).
7. *Nuclear Data Sheets: compiled by K. Way et al*, National Academy of Sciences, National Research Council, U.S.A. (1961).
8. P. Avignon, A. Michalowicz, and R. Bouchez, *J. Phys. Radium* 16 404, (1955).
9. A. Vuorinen, *Proc. I.A.E.A. Symp. on Standardization of Radio-nuclides*, Vienna, 1966. (International Atomic Energy Agency, Vienna, 1967) p 257.
10. A.M. Bresesti, M. Bresesti and H. Neumann, *J. Inorg. Nucl. Chem.* 29, 15 (1967).
11. P.J. Campion, J.G.V. Taylor, and J.S. Merritt, *Intern. J. Appl. Radiation and Isotopes*, 8, 8 (1960).
12. O.U. Anders, and W.W. Meinke, *Nucleonics* 15, (No. 12) 68 (1957).
13. W. Nagel, and A.H.W. Aten, Jr., *J. Nucl. Energy* 20, 475 (1966).
14. L. Cranberg, A.H. Armstrong, and R.L. Henkel, *Phys. Rev.* 104, 1639 (1956) and L. Cranberg, Private communication.
15. J.D. Anderson, C.C. Gardner, J.W. McClure, M.P. Nakada, and C. Wong, *Livermore Laboratory as listed in ref. 6* pp 97-101.
16. H.W. Lefevre, R.R. Borchers, and C.H. Poppe, *Phys. Rev.* 128 1328 (1962) and R.R. Borchers, Private communication.

17. V.R. Potnis, E.B. Nieschmidt, C.E. Mandeville, L.D. Ellsworth, and G.P. Agin, Phys. Rev. 146, 883 (1966).
18. J.L. Black, Bull. Am. Phys. Soc. 12, 528 (1967) and Private communication.
19. L. Cranberg, G. Frye, N. Nevson, and L. Rosen, Phys. Rev. 103 662 (1956).
20. W. Köhler, FRM-Bericht Nr. 81. Labor. f. Techn. Physik. d. Th, München (1966).

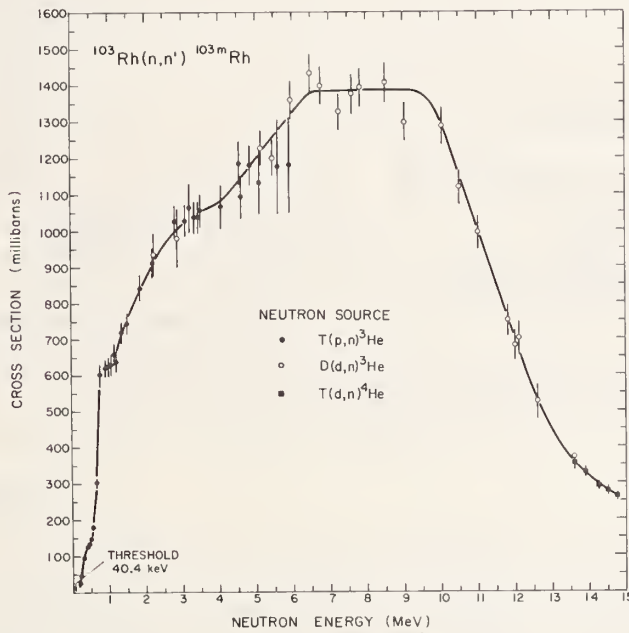


Fig. 1: The $^{103}\text{Rh}(n, n')^{103m}\text{Rh}$ activation cross section

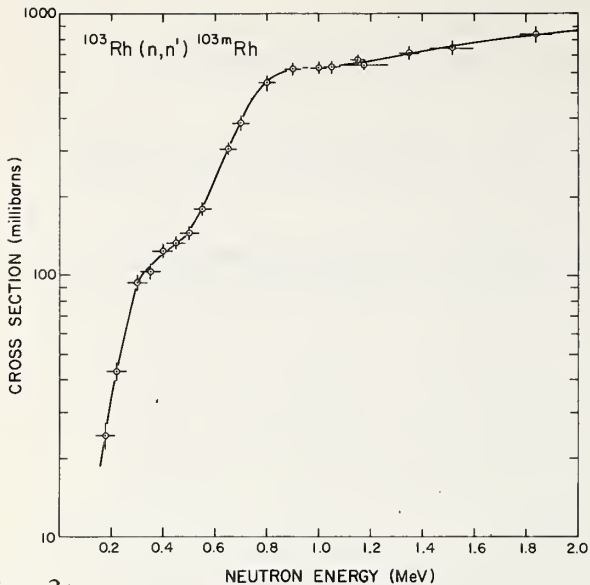


Fig. 2:

A log plot of the cross section for the $^{103}\text{Rh}(n, n')^{103\text{m}}\text{Rh}$ reaction in the low energy region

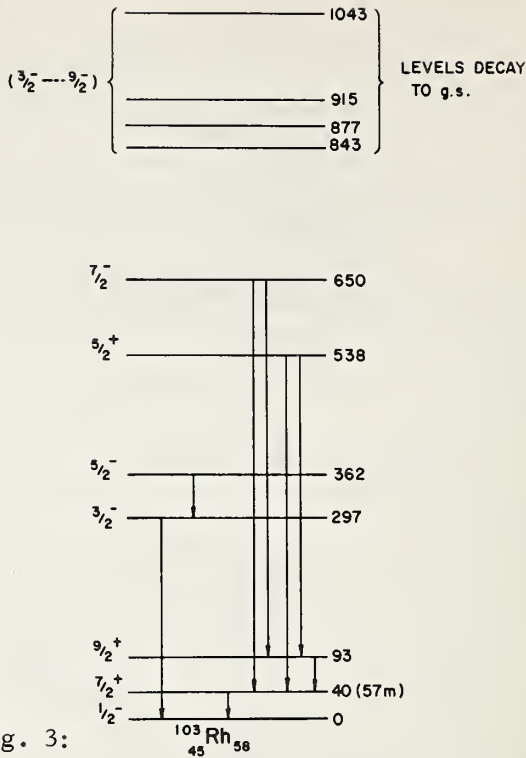


Fig. 3:

The nuclear level structure of ^{103}Rh

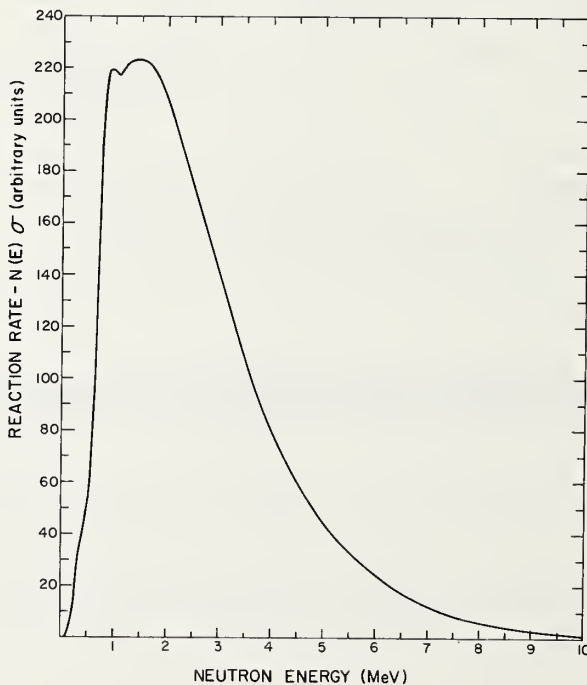


Fig. 4:

The reaction rate for the $^{103}\text{Rh}(n, n')^{103\text{m}}\text{Rh}$ reaction in a ^{235}U fission neutron spectrum

THE $^{14}\text{N}(n, n'\gamma)$ REACTION FOR $5.8 \leq E_n \leq 8.6$ MeV*

J. K. Dickens, E. Eichler, F. G. Perey, P. H. Stelson,
John Ashe,[†] and D. O. Nellis[†]

Oak Ridge National Laboratory
Oak Ridge, Tennessee 37830

Abstract

We have obtained gamma-ray spectra for the reactions $^{14}\text{N}(n, n'\gamma)^{14}\text{N}$, $^{14}\text{N}(n, p\gamma)^{14}\text{C}$ and $^{14}\text{N}(n, \alpha\gamma)^{11}\text{B}$ for incident mean neutron energies $E_n = 5.8, 6.4, 6.9, 7.4, 8.0,$ and 8.6 MeV. The gamma rays were detected using a coaxial Ge(Li) detector of 30 cc active volume. The detector was placed at 55° and 90° with respect to the incident neutron direction, and was 77 cm from the sample; time-of-flight was used with the gamma-ray detector to discriminate against pulses due to neutrons and background gamma radiation. The sample was 100 gm of Be_3N_2 in the form of a right circular cylinder. Data were also obtained using a 75-gm Be sample to provide an estimate of the background. The incident neutron beam was produced by bombarding a deuterium-filled gas cell with the pulsed deuteron beam of appropriate energy from the ORNL 6-MV Van de Graaff. The resulting neutron beam was monitored using a scintillation counter; a time-of-flight spectrum from this detector was recorded simultaneously with the gamma-ray data. These data have been studied to obtain absolute cross sections for production of gamma rays from ^{14}N for the incident neutron energies quoted above.

1. INTRODUCTION

High on the priority list of the tabulation of cross section requests are cross sections relating to gamma-ray production following inelastic neutron scattering.⁽¹⁾ We have set up a system utilizing a large Ge(Li) detector, fast timing, an on-line computer, and a well-pulsed accelerated beam of deuterons, and are studying $(n, n'\gamma)$ reactions. The first sample studied was ^{14}N , principally because of its No. 1 priority.

2. EXPERIMENTAL ARRANGEMENT

The experimental system is shown in the first figure. As indicated in Fig. 1a, the pulsed deuteron beam (~ 1 nsec duration, 2 MHz repetition rate) is detected by a beam pick-off device, and then the beam impinges on the target (deuterium gas at $\sim 1\frac{1}{2}$ atm pressure), producing neutrons. The neutrons interact with the sample, and the resulting gamma rays are

* Research sponsored by the U. S. Atomic Energy Commission under contract with the Union Carbide Corporation.

[†] Texas Nuclear Corporation, Austin, Texas.

detected by the Ge(Li) detector. The sample-to-target distance was between 8 and 11 cm, and the detector-to-sample distance was 77 cm. The electronics system is shown in Fig. 1b. The time interval between the passing of the deuteron beam through the beam pick-off device and the subsequent detection of a gamma ray is used to discriminate between prompt events (i.e., those due to neutron interactions in the sample) and background events. Most of the background events are due to neutrons scattered by the sample (or nearby shielding material) which then interact with the detector or with the shielding near the detector. As a consequence, the time spectrum for a given gamma-ray energy will exhibit two principal peaks. Two such spectra are shown in Fig. 2, one for detected gamma-ray energy ≥ 3.5 MeV and the other for detected gamma-ray energy between 600 and 700 keV. It is apparent from this figure that a clear identification of prompt events can be made provided that the functional dependence of the time response upon gamma-ray energy can be included in the data analysis. We have done this on an event-by-event basis using a programmed on-line computer. As indicated in Fig. 1b, the computer receives two types of information about an event, namely, a pulse whose size is related to the time response of the event and another whose height is related to the energy deposited in the Ge(Li) crystal. The computer correlates these data to separate the prompt from the background gamma rays, and the background-free data are immediately available for further analysis.

3. EXPERIMENTAL PROCEDURE

Data were obtained for six neutron bombarding energies and for two gamma-ray scattering angles. At each of the twelve runs the time response (e.g., Fig. 2) was obtained by bombarding a carbon sample. The empirically determined time response was then inserted into the principal data-taking program.

Spectra were obtained for three samples, carbon, beryllium, and beryllium nitride (Be_3N_2). For each sample three spectra were accumulated (resulting from the division of the time response). The basic spectrum size was 2048 channels, $E_\gamma \sim 7.5$ MeV full scale. The simultaneously recorded background spectra proved to be very valuable in identifying the peaks in the 2048-channel spectrum.

In addition to the gamma-ray spectra, the neutron spectrum from the monitor detector was stored in the computer memory. The neutron energy was determined from time-of-flight, and the shape of the principal peak in this spectrum served as an excellent indicator of accelerator conditions.

The two scattering angles, θ_γ , selected for investigation were $\theta_\gamma = 55^\circ$ and $\theta_\gamma = 90^\circ$. The former was chosen because the Legendre function $P_2(\theta) = 0$ at $\theta = 55^\circ$; hence the cross section for production of a particular gamma ray can be calculated from

$$\sigma(\gamma) = 4\pi \frac{d\sigma}{d\omega} (55^\circ)$$

for most of the gamma transitions studied. The angle $\theta_\gamma = 90^\circ$ was chosen for comparison with data previously obtained for this reaction.⁽²⁾ Chronologically the 55° data were taken at all energies and then the

detector was positioned at 90° . In addition to changing θ_γ , the mean source-to-sample distance was reduced from 9.8 to 8.0 cm. Because of the large sample size used — the Be_3N_2 sample was a cylinder 5.4 cm long and 3.8 cm in diameter — this change somewhat complicated the data reduction.

4. EXPERIMENTAL RESULTS AND DATA REDUCTION

Figure 3 exhibits the spectrum of prompt gamma rays obtained at $E_n = 7.5$ MeV for $\theta_\gamma = 90^\circ$. The energy calibration was obtained from the well-known energies of the principal ^{14}N gamma rays, $E_\gamma = 2.313$ and 5.105 MeV.⁽³⁾ Gamma-ray energies were not determined from our data; rather the energy calibration was used to locate and identify the gamma rays of interest. The identification of several gamma rays in this particular spectrum may seem rather tenuous; however, these are seen clearly at other energies. The broad peaks in Fig. 3, for the most part, correspond to gamma rays emitted from excited nuclear levels with very short half-lives. The identified gamma rays, and their places in the reaction scheme, are summarized in Fig. 4.

The data were reduced to absolute differential cross sections from the general formula

$$\frac{d\sigma(\theta_\gamma)}{d\omega} = \frac{N_\gamma(\theta_\gamma)}{N_n N_s \Delta\Omega_\gamma}$$

where $N_\gamma(\theta_\gamma)$ represents the number of gamma rays emitted into the solid angle $\Delta\Omega_\gamma$ at angle θ_γ , and N_n is the number of neutrons impinging on the N_s nuclei in the sample.

Several parameters had to be determined before absolute values of $d\sigma/d\omega$ could be obtained, and these included the efficiency of the Ge detector, the attenuation of gamma rays in the sample, the effects of the finite sizes of the source and the sample, the neutron attenuation and multiple scattering in the sample, and the efficiency of the monitor system. These are discussed briefly so that the errors on the absolute values of $d\sigma/d\omega$ may be assessed.

The efficiency of the Ge detector was determined absolutely for $E_\gamma \leq 1.84$ MeV using calibrated sources, and relatively for $10.8 \text{ MeV} > E_\gamma \geq 1.63$ MeV, by analyzing a spectrum of the capture process $^{14}\text{N} + n_{\text{thermal}} \rightarrow ^{15}\text{N} + \gamma$. The relative efficiency curve was normalized to the absolute values for $1.6 \text{ MeV} \leq E_\gamma \leq 1.8$ MeV. The error due to uncertainty in efficiency is estimated to be between 5 and 10%.

The attenuation of the gamma rays in the sample was computed from coefficients in the literature and assuming an average gamma-ray path length in the sample of $\pi R/4$, where R is the sample radius. For most of the gamma rays the attenuation is $\sim 10\%$ and so the error to the absolute value from this source is very small. For the 0.728-MeV gamma ray, however, the attenuation is $\sim 30\%$, and the estimated error on $d\sigma/d\omega$ for this line could be 5% from this source.

The efficiency of the monitor detector for neutrons emitted from the source at $\theta_{\text{mon}} \cong 55^\circ$ was calculated using a computer program discussed by Verbinski *et al.*⁽⁴⁾ The calculated efficiencies for the NE-213 monitor detector (2 in. diam by 1 in. deep) are $\approx 13.5\%$ for our neutron energy region, a value which is probably valid to $\pm 10\%$.

The effects of the finite geometry, which included the average neutron intensity in the sample interacting with the average number of sample nuclei, presented more of a challenge. Ideally, one would prefer to work with a relation of the type

$$N_n N_s = \frac{\sigma_{dd}(0^\circ) \Delta\Omega_s e^{-\sigma_1 \bar{N}_s} \bar{N}_s N_m}{\sigma_{dd}(55^\circ) E_m [E_n(55^\circ)] \Delta\Omega_m}$$

where $\sigma_{dd}(\theta_n)$ is the $d(d,n)^3\text{He}$ cross section at angle θ_n (and deuterium) energy E_d), $\Delta\Omega_s$ is the solid angle subtended by the sample with respect to the source, $\exp(-\sigma_1 \bar{N}_s)$ is the average neutron attenuation in the sample, \bar{N}_s is the average number of sample nuclei/cm², N_m is the number of counts registered in the monitor, E_m is the efficiency of the monitor and $\Delta\Omega_m$ is the solid angle subtended by the monitor. To correct for the effect due to the finite geometry the right hand side was multiplied by $(1-\xi)$ where ξ is the (hoped-for small) correction. This factor was calculated using first-order approximations, including approximating $\sigma_{dd}(\theta) = \sigma_{dd}(0^\circ) (1 - k\theta^2)$ where k was chosen to give reasonable values of $\sigma_{dd}(\theta)$ for $\theta < \theta_{max}$, the maximum angle from source to sample. For the Be_3N_2 sample, at $E_n = 8.6$ MeV, $\xi = 18\%$ for the mean source-to-sample distance $D = 9.8$ cm and $\xi = 26\%$ for $D = 8.0$ cm. Although these values are not particularly small, refining the calculation is not expected to alter them by a large amount; we estimate the error on the absolute $d\sigma/d\omega$ to be $< 10\%$ from this source.

Multiple scattering of the neutrons in the sample will have the effect of changing the incident neutron energy by elastic scattering. To obtain the distribution of energy of neutrons at the time of an inelastic collision, a Monte Carlo computation was performed. The energy of the source neutron emitted into angle θ_n was folded into the calculation, and the result for our sample sizes and source-to-sample distances was that the mean energy of the neutron was 75 to 100 keV less than $E_n(0^\circ)$, with a standard deviation of ≈ 100 keV. However, the calculation indicated that some 10% of the inelastic interactions occurred for neutrons of energy less than $E_n(0^\circ) - 500$ keV. The error on the absolute $d\sigma/d\omega$ from this source is difficult to estimate, since it depends upon detailed knowledge of the reaction at energies less than $E_n(0^\circ)$. It seems unlikely, however, that the error should be greater than 10%.

Absolute differential cross sections obtained from the $^{14}\text{N}(n,n'\gamma)^{14}\text{N}$ are summarized in Table 1. Considering all of the sources of error (discussed above) we estimate the overall error to be $< 20\%$ for most of the data.

We extend our appreciation to W. E. Kinney, A. L. Marusak, J. W. McConnell, W. C. White, and J. A. Biggerstaff for their assistance and advice, generously proffered and gratefully accepted, during all phases of the experimental program.

¹A. B. Smith, Compilation of Requests for Nuclear Cross Section Measurements, WASH-1078 [EANDC(US)-103 "U"], June 1967.

²H. E. Hall and T. W. Bonner, Nucl. Phys. 14, 295 (1959).

³C. Chasman et al., Phys. Rev. 159, 830 (1967).

⁴V. V. Verbinski, J. C. Courtney, W. R. Burrus, and T. A. Love (unpublished). R. E. Textor and V. V. Verbinski, ORNL-4160 (1968) (unpublished).

Table 1. Differential Cross Sections (in mb/sr) for Gamma-ray Production from Neutron Interaction with Nitrogen.

Neutron Energy (MeV)	5.80 ± 0.20 ^a		6.35 ± 0.15		6.84 ± 0.15		7.42 ± 0.12		7.95 ± 0.10		8.55 ± 0.10	
	55°	90°	55°	90°	55°	90°	55°	90°	55°	90°	55°	90°
E_γ (MeV)	Residual Nucleus											
0.728			0.13 ^b	0.09 ^d	0.30	0.33	1.00	1.14	1.05	1.30	1.00	1.19
1.622	1.9 ^c	1.9 ^c	2.8	2.7 ^d	3.5	3.0 ^c	3.5	3.3	3.0	3.0	3.2	3.2 ^b
2.313	2.4	2.5	3.5	3.6	4.8	4.6	5.5	5.5	4.6	4.5	5.0	4.6
2.792	0.07 ^c	0.07 ^d	0.25	0.26 ^b	0.30	0.41 ^b	0.51	0.55	0.62	0.63	0.57	0.56 ^b
3.372			0.21 ^b	≤0.19 ^d	0.51 ^b	0.44 ^d	1.0 ^b	1.2	1.3 ^b	1.4	1.3	1.4
4.91	0.21	0.21 ^b	0.74	0.87	0.40 ^b	0.67 ^b	0.48	0.55 ^c	0.54	0.9 ^b	0.11 ^b	0.25 ^d
5.105	0.24	0.27 ^b	0.87	0.80	1.00	1.00	1.9	2.1	2.4	2.5	1.9	1.9
5.685			<0.1		0.10 ^d	0.10 ^d	0.11 ^c	0.12 ^b	0.09 ^c	0.14 ^b	0.15	0.22 ^d
5.832			0.08 ^c	0.09 ^d	0.32 ^b	0.23 ^b	0.32 ^b	0.23 ^b	0.40 ^b	0.39 ^c	0.26 ^b	0.39 ^c
6.44					0.14 ^c	0.21 ^c			0.20 ^b	0.14 ^d	0.32	0.30 ^d
7.03					0.30	0.30	0.30	0.30	0.30	0.42	0.43	0.51
2.13	0.87	0.80	1.0	1.1 ^b	0.81	0.81 ^b	1.2	1.5	1.3	1.4	0.58	0.70 ^b
4.46	0.70 ^d	0.24 ^d	1.0 ^c	0.67 ^c	2.0	1.5	2.6	2.2	3.0	2.6	2.7	2.5
6.09					0.13 ^b	0.06 ^c	0.13 ^b	0.06 ^c	0.18	0.17 ^d	0.38	0.24 ^d
6.72					0.06 ^d	0.15 ^c	0.06 ^d	0.15 ^c	0.11 ^d	0.24 ^d	<0.10	<0.14

^a Spread in neutron energy.

^b ±30%.

^c ±40%.

^d ±50%.

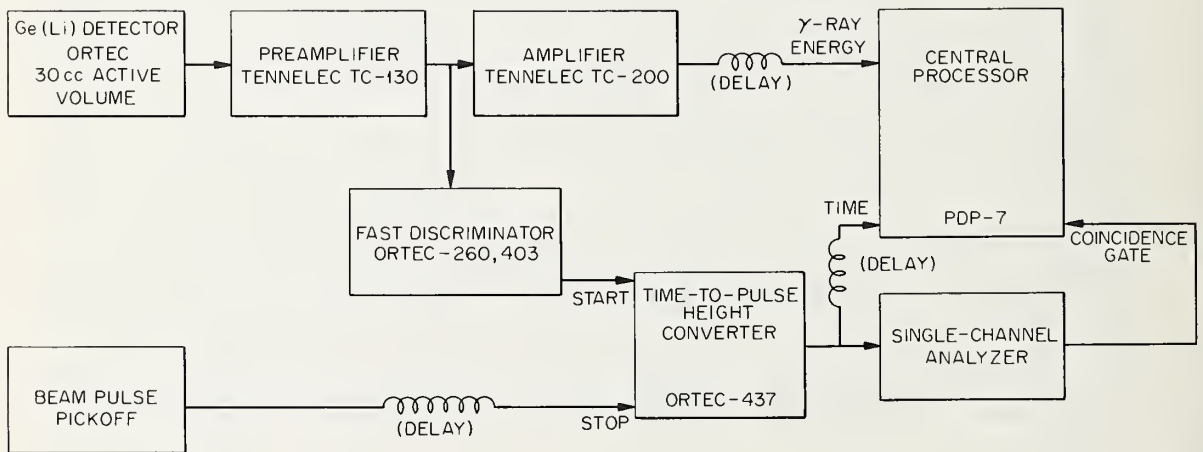
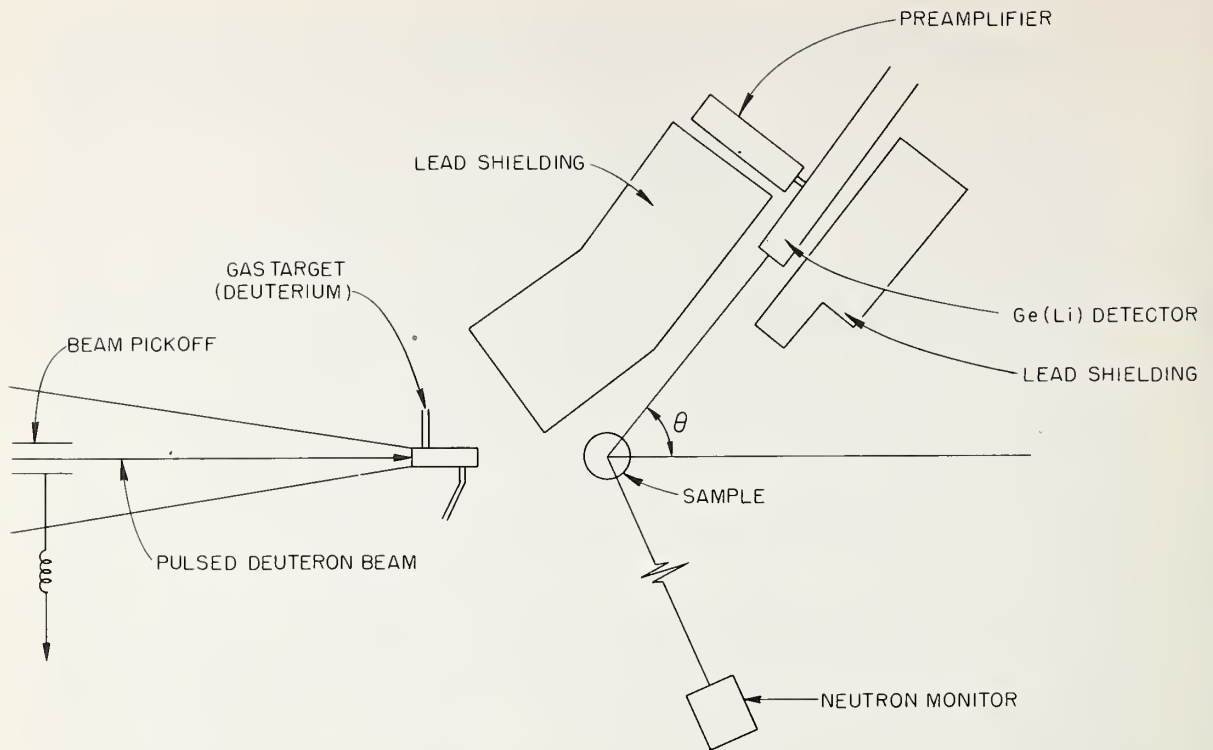
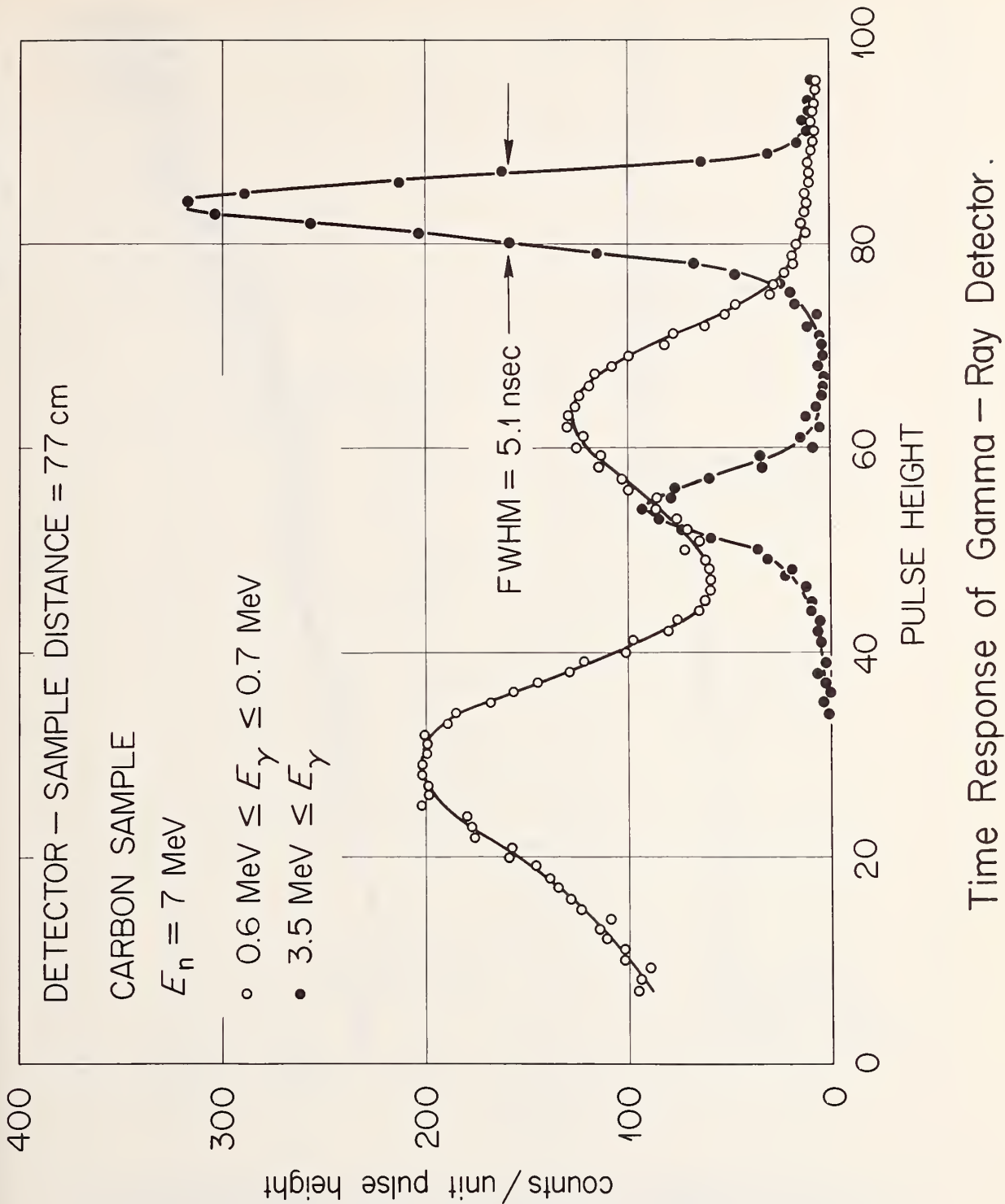


Fig. 1. Experimental Configuration. The upper figure indicated the physical arrangement of the experimental equipment in the bombardment area. The lower figure shows the electronics related to the gamma-ray detector. In addition, the spectrum of neutrons obtained by the monitor counter are stored in computer memory. External scalars monitored (a) the output of the time pick off device, (b) the number of gates to the computer, (c) the deuteron beam monitor.



Time Response of Gamma - Ray Detector .

Fig. 2. Two Time Response Spectra Obtained for 7-MeV Neutrons Exciting ^{12}C . These are 2 of 32 simultaneously obtained spectra, each spectrum for a different gamma-ray energy slice. The right-most peak in each spectrum corresponds to detection of prompt gamma rays produced by scattered neutrons. Each spectrum is divided into three groups, and the division points are stored in memory for the subsequent data runs.

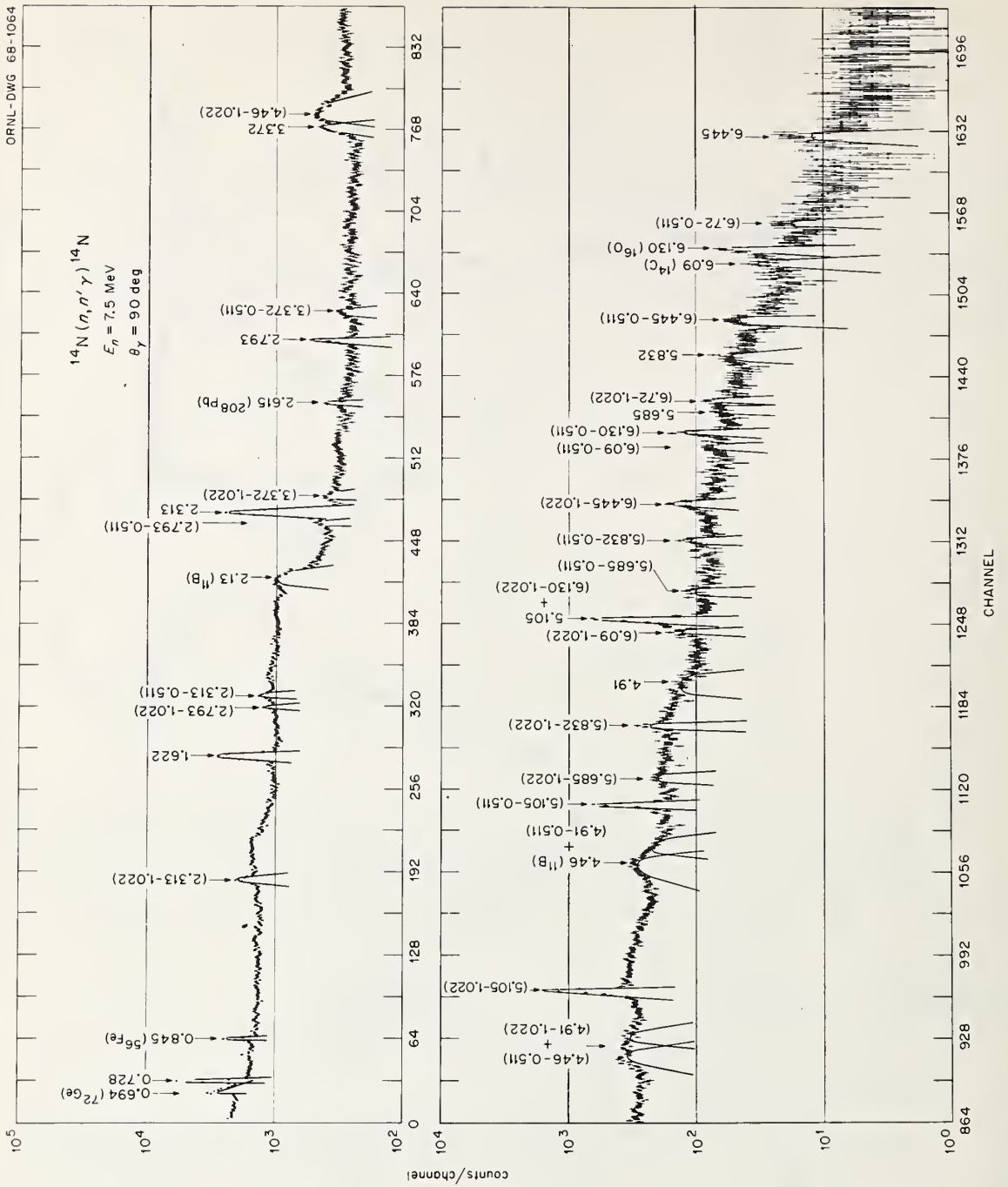
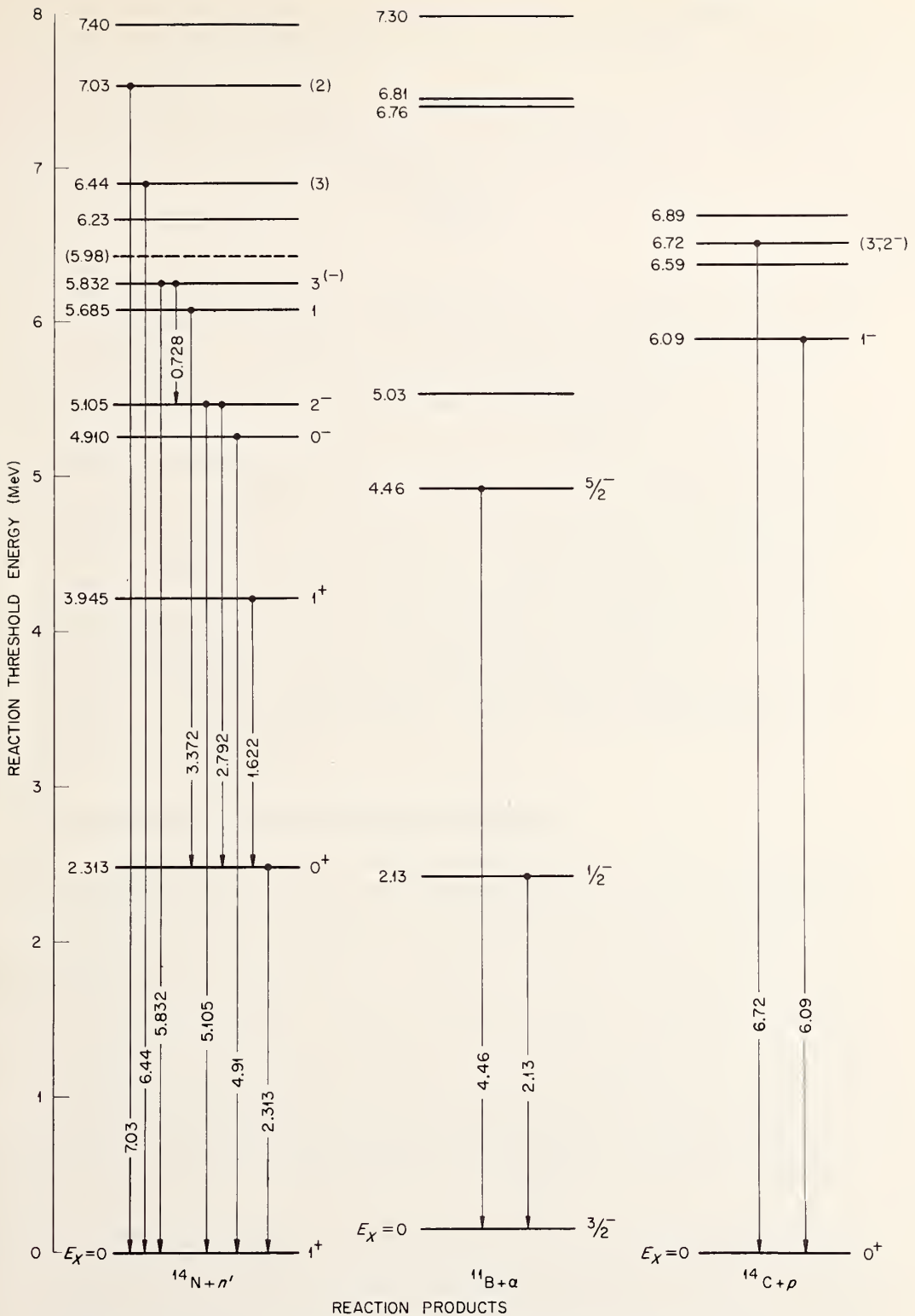


Fig. 3. Spectrum of Gamma Rays for 7.5-MeV Neutron Bombardment of ^{14}N , $\theta_\gamma = 90^\circ$. Peaks are labeled with the energy of the detected gamma ray. Escape peaks are indicated by $(E_\gamma - 0.511)$ and $(E_\gamma - 1.022)$ labels. Isotope symbols indicate gamma radiation emanating from nuclei other than ^{14}N .



Gamma-Rays from Neutron Bombardment of Nitrogen, $6.0 \text{ MeV} \leq E_n \leq 8.6 \text{ MeV}$.

Fig. 4. Summary of Gamma Rays Seen and Identified as Resulting from Nonelastic Neutron Interactions with ^{14}N .

Measurements of Absorption Resonance Integrals for

^{176}Hf , ^{177}Hf , ^{178}Hf , ^{179}Hf , and ^{180}Hf

by R. H. Fulmer, L. J. Esch, F. Feiner, and T. F. Ruane
Knolls Atomic Power Laboratory
Schenectady, New York 12301

ABSTRACT

Absorption resonance integrals have been determined for the major hafnium isotopes by pile oscillator measurements in the KAPL Thermal Test Reactor. The samples were isotopically enriched HfO_2 diluted in Al_2O_3 ceramic pellets. Corrections for self-shielding in the more strongly absorbing samples were made by extrapolating the results of samples with varying dilution to infinite dilution. Measurements were calibrated with gold samples. The gold resonance integral was taken as 1558 b at a cadmium cutoff energy of 0.5 eV. Corrections to the data for variations in cadmium cutoff and deviations in the neutron spectrum from $1/E$ have been made. After these corrections, the resonance integrals are ^{176}Hf , 640 ± 30 b; ^{177}Hf , 7380 ± 500 b; ^{178}Hf , 1950 ± 120 b; ^{179}Hf , 660 ± 30 b; and ^{180}Hf , 43 ± 8 b. From these values the synthesized resonance integral for natural hafnium is 2040 b, in good agreement with a recent measurement of 2125 ± 50 b. These preliminary results may also be compared with values computed from differential measurements with allowance for unresolved resonances. The computed values are ^{176}Hf , 339 b; ^{177}Hf , 7192 b; ^{178}Hf , 1883 b; ^{179}Hf , 497 b; and ^{180}Hf , 36 b.

1. INTRODUCTION AND EXPERIMENTAL PROCEDURE

Absorption resonance integrals for the major hafnium isotopes have been determined from reactivity changes induced by a pile oscillator in the KAPL Thermal Test Reactor. The samples consisted of isotopically enriched hafnium in the form of hafnium oxide diluted to about 1 w/o in aluminum oxide. The hafnium isotopes were enriched to values of 0.74 to 0.95. The samples were in the form of ceramic pellets, of dimensions 0.63 cm diameter and 5 cm total length, enclosed in aluminum capsules. The sample position in the reactor was enclosed by a cylindrical cadmium shield of wall thickness 0.51 mm (20 mils) and diameter 1 cm. The hafnium samples were oscillated, with a thirty second cycle, against a null sample which was similar but contained no hafnium. Corrections were made for the small contributions to the reactivity changes which were due to aluminum or aluminum oxide not compensated in the null sample.

Changes in neutron flux induced by the pile oscillator were monitored by a BF_3 detector. Current from this detector corresponding to changes in the flux was converted to pulse height and stored, as a function of oscillator cycle time, in an RIDL 256 channel analyzer. The 256 channels contained data for the first two cycles of oscillation. The ion chamber currents for subsequent odd cycles were stored in the same channels as for the first cycle, and currents for subsequent even cycles

were stored in the same channels as for the second cycle. After a number of cycles are recorded in this fashion, random effects due to noise tend to add destructively, whereas current changes due to absorptions in the sample add constructively. Typical pulse height data from the multi-channel analyzer are shown in the accompanying figure. The analyzer data are corrected for spurious effects such as reactor drift and are fit to a Fourier sine and cosine series. The amplitude of the first cosine term in the series is proportional to the reactivity change induced by the sample.

The reactivity changes, $\Delta\rho$, of the cadmium covered samples are proportional to absorption cross section and thus to resonance integral:

$$\Delta\rho \propto N \int_{E_{Cd}}^{\infty} \varphi(E) \sigma_a(E) \varphi^*(E) dE \quad (1)$$

where N is the number of atoms in the sample, $\varphi(E)$ the neutron flux at energy E , $\sigma_a(E)$ the microscopic absorption cross section, and $\varphi^*(E)$ the flux adjoint, which serves as a neutron importance function. E_{Cd} is the effective cadmium cutoff energy. If the product $\varphi(E)\varphi^*(E)$ equals $1/E$, then the integral in Equation (1) meets the usual definition of a resonance integral. The reactivity measurements have been calibrated in terms of resonance integral by the use of gold samples. The resonance integral of gold is taken as 1558 b at a cadmium cutoff energy of 0.5 eV.

Self-shielding factors for the samples were in the range 0.7 to approximately 1.0. Corrections to the reactivity values for self-shielding in the more strongly absorbing gold and hafnium samples were made by extrapolating the results for samples of varying dilution to infinite dilution. Two self-shielding models were used in the extrapolation; they were

$$f = [1 - \exp(-\alpha t)] / \alpha t \quad (2)$$

and

$$f = (1 + \alpha t)^{-\frac{1}{2}} \quad (3)$$

where f is the self-shielding, t the sample thickness, and α a parameter which is fit to the data. The results of the extrapolation were insensitive to the choice of the self-shielding model.

2. RESULTS AND DISCUSSION

Resonance integrals measured for the hafnium isotopes are presented in the accompanying table. Column 2 of the table lists the values of isotopic resonance integrals obtained from the calibration with gold. Because each of the five different isotopic enrichments for hafnium used in the oscillator samples contained some fraction of each stable isotope,

the isotopic resonance integrals had to be calculated by accounting for the contribution of each of the five major isotopes to the measurements for each of five isotopic enrichments. Thus five simultaneous equations were solved to obtain the isotopic resonance integrals.

Column (3) of the table lists the correction factor used for each isotope to account for the fact that the product of the episcadmium neutron flux and flux adjoint is not exactly equal to $1/E$. The correction factors are obtained by numerically integrating evaluated differential cross section data for the hafnium isotopes [1] both in a $1/E$ spectrum and in the spectrum calculated for the sample position in the reactor. Column (4) of the table lists factors for each isotope applied to correct the measured data to an effective cadmium cutoff energy of 0.5 eV. These correction factors and the actual cadmium cutoffs were calculated for each isotope by numerical integration using evaluated differential cross section data [1] and the neutron spectrum at the sample position. Possible corrections to the measurements for neutron moderation and for the presence of small amounts of ^{174}Hf in the samples have been evaluated as negligible.

Column (5) of the table lists the experimental values of the isotopic resonance integrals corrected for the two effects mentioned above. These corrected values are compared in column (6) of the table with values computed by J. T. Reynolds et. al. [1] from differential measurements [2] with allowance for unresolved resonances. There is generally good agreement between the values. The synthesized value for the natural hafnium resonance integral, which is listed in Column (5), agrees well with another recent measurement of 2125 ± 50 b [3].

3. References

- [1] J. T. Reynolds, C. R. Lubitz, I. Itkin, and D. R. Harris, "Evaluated Cross Sections for the Hafnium Isotopes", KAPL-3327(ENDF-112), dated August 17, 1967. Values are for $E_{Cd} = 0.625$ eV, temperature 0°K .
- [2] T. Fuketa, ORNL-TM-954 (1964), and T. Fuketa et.al., R.P.I. Lin. Accel. Proj. An. Tech. Report for 1965.
- [3] R. Vidal and F. Roullier, Conf. on Nuclear Data, Paris, Oct. 17-21, 1966, Paper #N-23/73.

Absorption Resonance Integrals for the Major Isotopes of Hafnium

(1) Hf Isotope	(2) Uncorrected Value This Work (barns)	(3) Correction to 1/E Spectrum	(4) Correction to $E_{Cd} = 0.5\text{eV}$	(5) Corrected Value This Work (barns)	(6) Calculation by Ref. 1 (barns)
176	655 ± 27	0.98	1.00	640 ± 30	339
177	7144 ± 300	0.98	1.05	7380 ± 500	7192(7247) ^(c)
178	1969 ± 120	0.99	1.00	1950 ± 120	1883
179	678 ± 28	0.98	1.00	660 ± 30	497
180	45 ± 7	0.94	1.01	43 ± 8	36
natural(a)	2000 ± 80	-----	-----	2040 ± 110	1941(a)

(a) Synthesized value from isotopic resonance integrals.

(b) Computed for $E_{Cd} = 0.625\text{ eV}$, temperature = 0°K .

(c) Value corrected to $E_{Cd} = 0.50\text{ eV}$.

FLUX COMPARISON X 10⁻¹

12

8

4

Oscillation of Hf Sample
Against Null Sample

||||| Odd Cycles
- - - Even Cycles

CHANNEL NOS X 10⁻¹

12

8

4

Changes in neutron flux vs. time (channel number). The flux discontinuity corresponds to the introduction of the Hf absorber. Flux is higher for even cycles due to small upward drift in reactor power.

MEASUREMENTS OF NEUTRON SCATTERING FROM ${}^7\text{Li}$

H. -H. Knitter and M. Coppola

Central Bureau for Nuclear Measurements

EURATOM, Geel, Belgium

Abstract

Angular distributions of neutrons elastically and inelastically scattered by Li-7 were measured at eight incoming energies between 1.12 and 2.30 MeV, using a fast neutron time-of-flight spectrometer. Data were corrected for flux attenuation and multiple scattering in the sample and for effects due to finite geometry. Differential cross section results are expressed in the form of Legendre polynomial expansions. Evaluated total and total inelastic cross sections are presented.

1. Introduction

In the neutron energy range from 1.12 to 2.30 MeV, which was investigated in this work, three types of nuclear reactions may be initiated by neutrons on Li-7, namely the elastic scattering, the inelastic scattering to the first excited state ($Q = -0.478$ MeV) and the Li-7(n, γ)Li-8 process. As far as the (n, γ) reaction is concerned, the experimental results presented in ref. (1) show that the cross section for this reaction is about $6 \mu\text{b}$ at 1 MeV and appears to remain constant in the neighbouring energy region. For this reason, the (n, γ)-process will not be taken into account in our considerations.

Direct study of the inelastic scattering from the 0.478 MeV level of Li-7 was not done up to now in a systematical way, but the existing ($n, n'\gamma$) cross sections were derived from measurements of the γ -radiation accompanying the decay of the level under consideration (2). In fact, apart from the measurement of Batchelor and Towle (3) at 1.5 MeV, the neutrons inelastically scattered from the 0.478 MeV level were not resolved from the elastic ones in the direct neutron measurements previous to the present ones. In those measurement, in order to extract the elastic scattering cross section alone, the inelastic scattering was corrected by subtracting from the observed data an inelastic contribution which was assumed to be isotropic in the centre-of-mass system. The absolute value of the inelastic scattering contribution was derived from the mentioned γ -ray measurements.

All the neutron cross section values in the energy range from 0.001 eV to 15 MeV, existing up to July 1964, are reported in a compilative work of Pendlebury (4). Since then no other measurements of neutron scattering on Li-7 are reported (5) in the energy range of the present experiment.

The aim of the present work was then to give a direct measurement of both the elastic and the inelastic neutron differential scattering cross sections of Li-7 and to compare our direct inelastic results with the ones obtained with the aid of γ -ray measurements.

2. Experimental Procedure

The measurements were performed at the 3 MeV Van de Graaff accelerator of the CBNM using a fast neutron time-of-flight spectrometer. The overall time resolution of the spectrometer was 2.2 ns measured on the γ -peak from the excitation of the 0.478 MeV level of Li-7. A pulsed proton beam with 1 ns burst width, 1 MHz repetition rate, and a mean proton current of $5 \mu\text{A}$ was focussed on an occluded TiT-target. The target was 1 mg/cm^2 thick. The scattering sample was a cylinder of metallic lithium, containing 99.99% of Li-7, with a diameter of $3.68 \pm 0.02 \text{ cm}$, a height of $2.60 \pm 0.02 \text{ cm}$, and a weight of $14.842 \pm 0.002 \text{ g}$. From a radiography it was seen that the Li-7 sample was uniform containing no holes or cavities. This Li-7 cylinder was enclosed in a very thin aluminium container. The neutron scattering contribution due to the container was experimentally subtracted using a dummy can of the same shape and weight. The sample was positioned at 15 cm distance from the beam spot on the target and under zero degree with respect to the direction of motion of the incoming protons. The length of the neutron flight path from the centre of the sample to the detector was chosen in such a way that the inelastically scattered neutron group leaving the Li-7 nucleus in its first excited state ($Q = -0.478 \text{ MeV}$) was always completely resolved from the elastically scattered group. The sample-to-detector distance was chosen between 148.5 cm at the lowest and 237.7 cm at the highest primary neutron energy used in this experiment. A representative time-of-flight spectrum is shown in fig. 1. For the evaluation of the absolute differential neutron scattering cross sections it is necessary to know the relative detector efficiency as a function of the neutron energy. The relative detector efficiency was obtained by comparison of the measured yield of neutrons scattered from hydrogen at several angles between 25° and 67.5° and at a primary neutron energy of 2.3 MeV, with the known n-p differential differential scattering cross sections (6). These data on hydrogen were corrected for attenuation in the sample of the outgoing scattered neutrons. As a scatterer a hollow polyethylene cylinder of 1.00 cm outside diameter, 0.60 cm inside diameter, and 4.00 cm height was used. Its weight was 1.840 g and the hydrogen contents was $14.31 \pm 0.06\%$.

For the absolute calibration of the differential cross sections at each primary neutron energy the neutron scattering from the polyethylene sample was measured at a certain angle. Absolute values of the differential cross sections were then obtained by comparison of the angular distribution results on Li-7 with the $\text{H}(n, n)\text{H}$ differential cross section.

3. Corrections

Several corrections had to be applied to the observed angular distribution data, before deriving from them the final cross section values.

a) Scattering on polyethylene

In this case the following effects were corrected.

- Attenuation of the incoming neutron flux through the scattering sample
- Multiple scattering of neutrons inside the sample
- Attenuation of the scattered neutron flux through the sample
- Intensity variation of the incoming neutron beam due to finite target-to-sample geometry.

These corrections were evaluated in two different ways, using the parallel beam method (7) and the Monte Carlo routine MAGGIE (8). The agreement between the results from the two methods was always excellent (between 0.4 and 1.4%) when in the former calculation a factor was included to allow the correction for the actual divergence of the source neutrons.

b) Scattering on Li-7

Before correcting the effects already mentioned for the case of polyethylene, another correction had to be introduced. In fact, with a light nucleus such as Li-7, multiple scattering can reduce considerably the energies of the elastically scattered neutrons, down to the region of the inelastically scattered ones. By simply adding the peak counts channel by channel, one would then attribute to the inelastic total counting some events which have, instead, elastic origin. To correct automatically this effect an additional part was included in the MAGGIE program. In fig. 1 the histogram obtained from the calculated MAGGIE scores is reproduced, together with the observed time-of-flight spectrum. Being A, B and C the limits for the integrations under the inelastic and elastic peaks respectively, the program automatically normalizes the total score between B and C to the experimentally observed total counting between the same limits. The multiple elastic score added between A and B is then multiplied by the same normalization constant and the result is added to and subtracted from the observed elastic and inelastic countings respectively.

This procedure is automatically repeated for each energy and at each angle and the data for further corrections are prepared.

4. Results

Neutron scattering from Li-7 was measured at ten angles between 22° and 152°, but for two of the angular distributions the maximum scattering angle was reduced to 142 degrees because of geometry limitations at the exit of the accelerator.

Angular distributions of elastically and inelastically ($Q = -0.478$ MeV) scattered neutrons were measured at incident neutron energies of 1.12, 1.37, 1.57, 1.76, 1.87, 2.02, 2.17 and 2.30 MeV, with energy spreads due to target thickness and finite geometry of, 104, 96, 91, 88, 86, 83, 81 and 79 keV respectively. The corrected differential neutron scattering cross section data in the lab. system were fitted with Legendre polynomial expansions of the form

$$\frac{d\sigma}{d\Omega}(\vartheta) = \sum_L B_L P_L(\cos \vartheta).$$

The expansions were limited to six terms in the elastic and to four terms in the inelastic cases. The values of the B_L -coefficients obtained from the least squares fits are presented in table I for the elastic and in table II for the inelastic neutron scattering angular distributions together with their statistical errors. The best fitting curves for the elastic and inelastic neutron scattering from Li-7 are plotted in figs. 2, 3 and 4 together with the corrected experimental points. The evaluated errors of the single experimental points are plotted as bars in the figures.

Fig. 5 shows the total neutron cross sections of Li-7 from other measurements (2, 9) and from the present work, and a total cross section curve recommended by Pendlebury (4). Within the experimental errors this curve is in good agreement with the results of our measurements, although they suggest the slightly different dashed curve drawn in this figure. In fig. 6 the integrated inelastic scattering cross sections from the present experiment are shown together with the $\text{Li-7}(n, n'\gamma)\text{Li-7}$ cross section values of Freeman et al. (2). The two sets of results are in excellent agreement.

The authors wish to thank Dr. J. Spaepen, Director of CBNM, for supporting this work. Special thanks are due to Drs. H. Horstmann and H. Schmid for solving the computing problems connected with the program MAGGIE and for writing the additional part for the automatic correction mentioned earlier. The assistance given by Mr. B. Jay, by the accelerator staff and by the Sample Preparation Group of CBNM is gratefully acknowledged.

5. References

- (1) Hughes D. J. and R. B. Schwartz BNL 325 II (1958)
- (2) Freeman J. M. , A. M. Lane and B. Rose, Phil. Mag. 46, 17 (1955)
- (3) Batchelor R. and J. H. Towle, Nucl. Phys. 47, 385 (1963)
- (4) Pendlebury E. D. , AWRE-report Nr. O-61/64 (1964)
- (5) Neutron data compilation CINDA EANDC 60 "U" (1966) and CINDA EANDC 70 "U" Supplement II
- (6) Gammel J. L. in "Fast Neutron Physics" part II J. Wiley et Sons, New York and London (1963)
- (7) Cranberg L. and J. S. Levin, LA-2177 (1959)
- (8) Parker G. B. , J. H. Towle, D. Sams, W. B. Gilboy, A. D. Purnell and H. J. Stevens, Nucl. Instr. and Meth. 30, 77 (1964)
- (9) Lane R. O. , A. S. Langsdorf, Jr. , J. E. Monahan and A. J. Elwyn, ANL-6172 (1960)

TABLE I

Legendre polynomial coefficients for elastic scattering. Laboratory system.

E_n (MeV)	B_0 $(\frac{mb}{sr})$	B_1 $(\frac{mb}{sr})$	B_2 $(\frac{mb}{sr})$	B_3 $(\frac{mb}{sr})$	B_4 $(\frac{mb}{sr})$	B_5 $(\frac{mb}{sr})$
1.12	109.7+0.5	26.4+0.9	5.7+1.2	-0.6+1.5	0.4+1.7	3.9+2.0
1.37	118.2+0.4	37.5+0.7	24.7+1.0	6.5+1.2	5.8+1.4	-4.2+1.7
1.57	116.5+0.6	44.3+1.2	39.0+1.6	11.0+2.1	1.0+2.3	-1.7+2.7
1.76	121.5+0.9	50.3+1.7	45.1+2.2	14.1+2.9	4.8+3.3	-1.2+3.8
1.87	114.2+0.5	60.5+0.9	50.6+1.2	12.3+1.5	7.6+1.7	-1.6+2.1
2.02	112.6+1.0	65.2+2.0	51.9+2.5	20.0+3.4	15.1+3.7	0.2+4.3
2.17	125.9+0.5	74.7+1.2	56.6+1.6	13.5+2.0	-2.5+2.0	-0.4+2.2
2.30	125.4+2.2	84.1+5.3	75.8+6.9	15.7+8.4	8.2+8.2	-7.4+9.4

TABLE II

Legendre polynomial coefficients for inelastic scattering
($Q = -480$ keV). Laboratory system.

E_n (MeV)	B_0 $(\frac{mb}{sr})$	B_1 $(\frac{mb}{sr})$	B_2 $(\frac{mb}{sr})$	B_3 $(\frac{mb}{sr})$
1.12	14.5+0.4	8.4+0.7	1.0+0.9	-3.7+1.1
1.37	16.9+0.3	6.5+0.5	-1.1+0.7	-0.9+0.9
1.57	16.2+0.4	5.1+0.6	-2.2+0.9	-1.5+1.1
1.76	17.7+0.5	4.3+0.7	0.0+1.0	1.6+1.3
1.87	15.8+0.3	3.3+0.5	-1.0+0.6	-2.4+0.8
2.02	15.8+0.4	5.9+0.7	-0.1+1.0	-0.7+1.3
2.17	16.1+0.4	5.2+0.6	1.8+0.9	-5.1+1.2
2.30	13.0+0.4	1.6+0.7	1.5+1.0	3.8+1.3

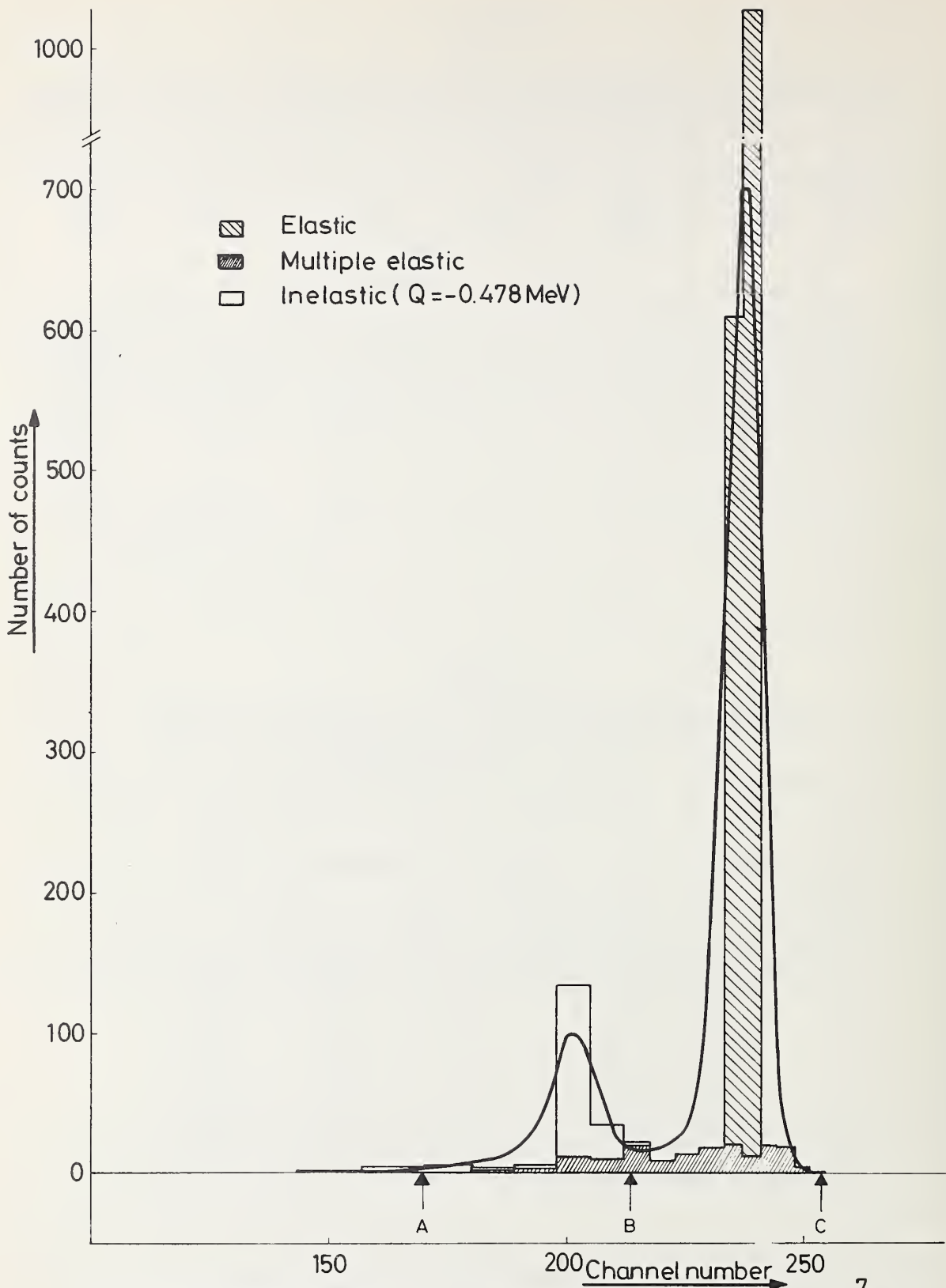


Fig.1 Time-of-flight spectrum of 1.87 MeV neutrons, scattered from ${}^7\text{Li}$ at $\theta = 120^\circ$. The histogram represents the calculated spectrum.

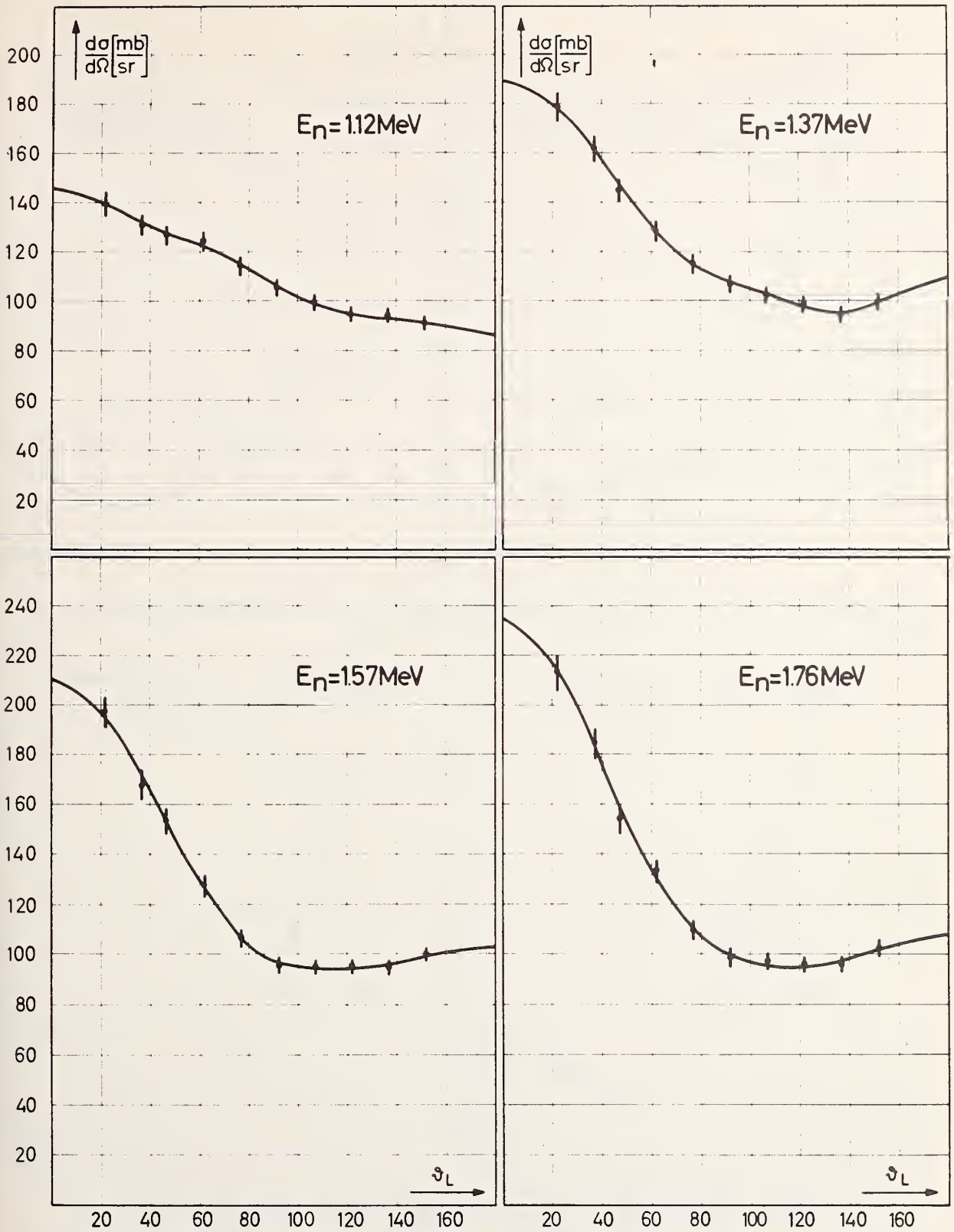


Fig.2 Neutron differential elastic scattering cross sections of ${}^7\text{Li}$ in the lab system. Solid curves are the best fits through the corrected experimental points.

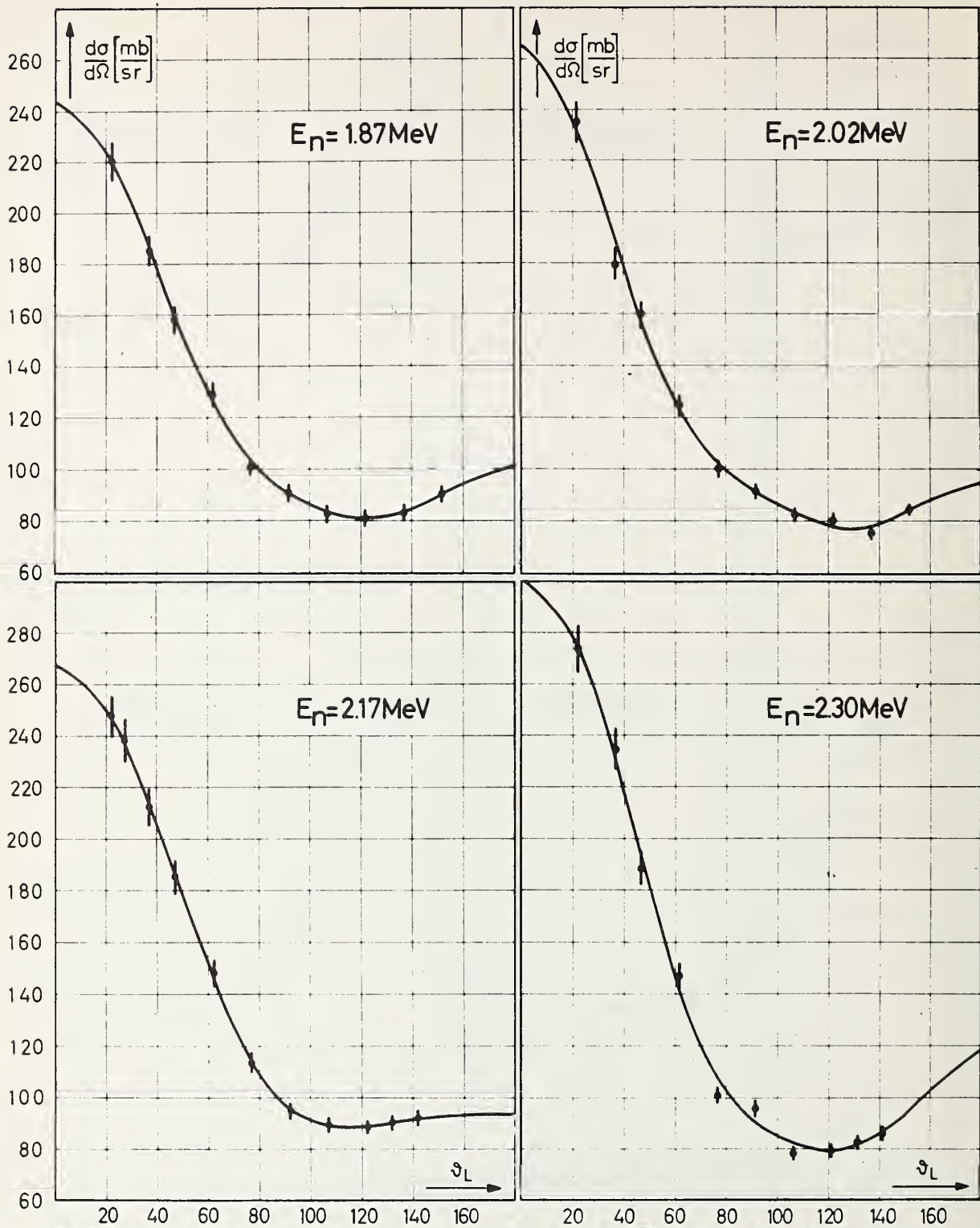


Fig 3 Neutron differential elastic scattering cross sections of ${}^7\text{Li}$ in the lab-system³
 Solid curves are the best fits through the corrected experimental points

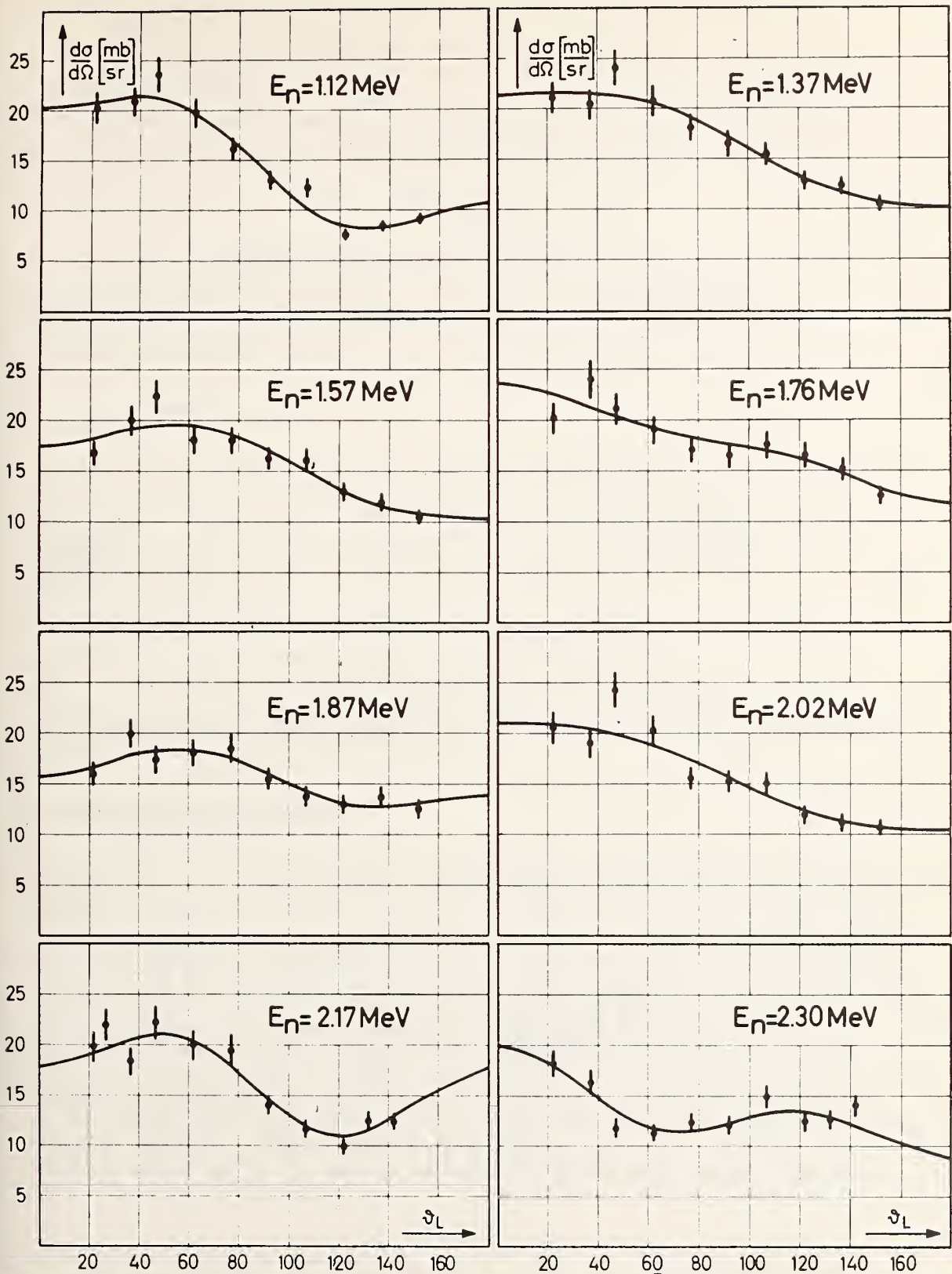


Fig 4 Neutron differential inelastic scattering cross sections of ${}^7\text{Li}$ in the lab-system. $Q = -0.478 \text{ MeV}$. Solid curves are the best fits through the corrected experimental points

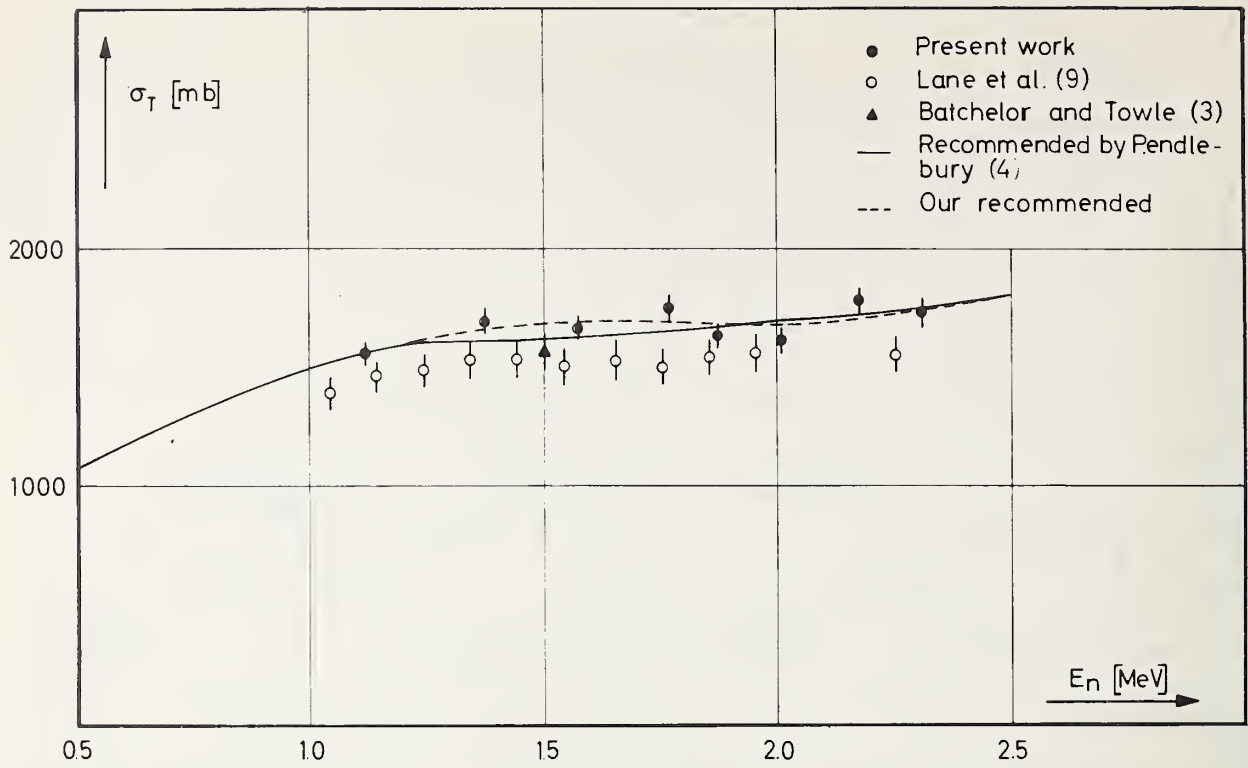


Fig.5 Total neutron cross sections of ${}^7\text{Li}$.

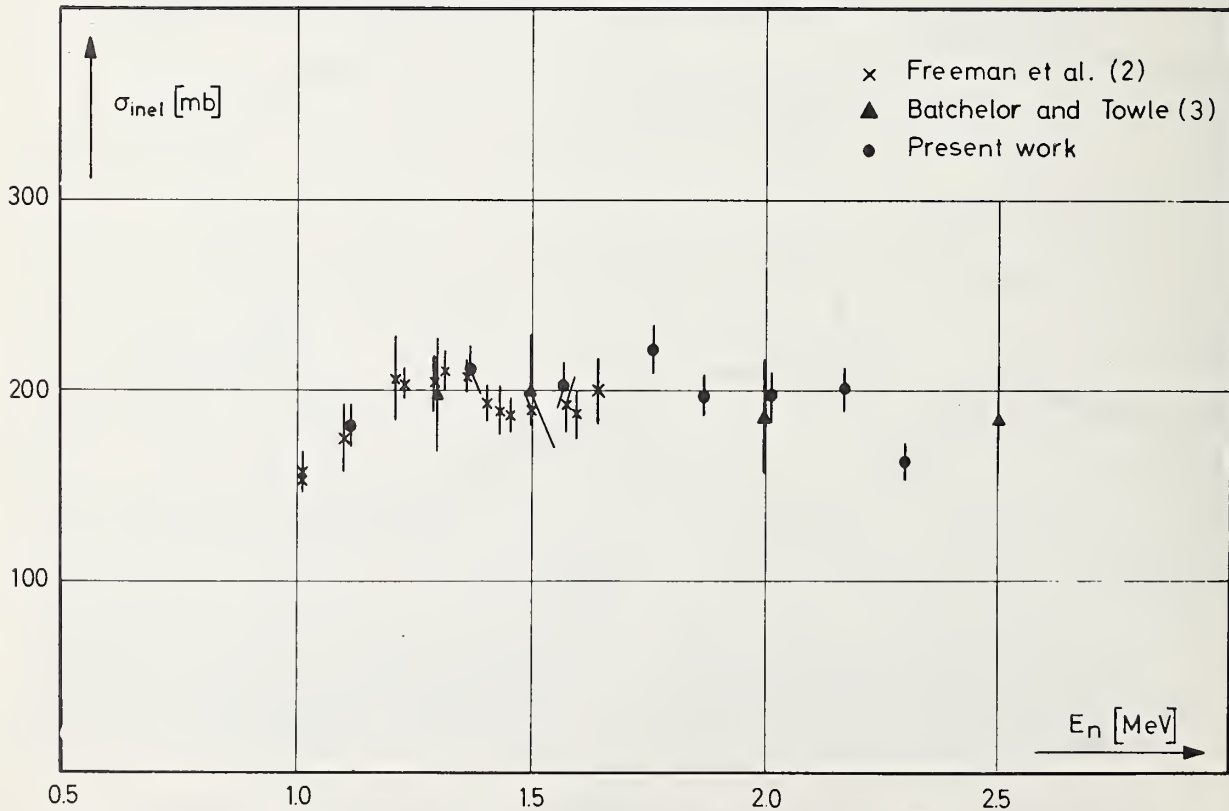


Fig.6 Integrated inelastic neutron scattering cross sections of ${}^7\text{Li}$. $Q=-0.478$ MeV.

Capture Cross Section Measurements for Lu, ^{151}Eu , and ^{153}Eu
and the Total Cross Section of Eu*

M. V. Harlow, A. D. Schelberg, L. D. Tatro, J. H. Warren, N. W. Glass
University of California, Los Alamos Scientific Laboratory
Los Alamos, New Mexico 87544

Abstract

Neutron capture cross sections of Lu, ^{151}Eu , and ^{153}Eu have been measured between 25 and 10,000 eV by time-of-flight techniques with neutrons resulting from the underground detonation of a nuclear device. Experimental details, capture cross section results, and total cross section results derived from these measurements are presented.

1. Introduction

Technological interest [1] in the neutron capture cross sections of lutetium and of the isotopes of europium, ^{151}Eu and ^{153}Eu , has led us to measure these cross sections over a neutron energy range of 25 to 10,000 eV. Of particular interest was to verify earlier results for europium [2] and to resolve the discrepancy in the lutetium cross section around 1000 eV [3, 4, 5].

It was discovered after the data were collected that the beam flux measurements for the two europium samples could be used to derive the total cross section, between 25 and 1500 eV, of an essentially natural isotopic mixture of europium. These results, the details of the experiment, and the normalized capture cross sections (the absolute calculations are in progress) are presented below.

2. Experimental Arrangement

Figure 1 shows a schematic of the geometry and the shielding scheme. Sample foils and the ^6LiF foils of the neutron beam monitors were rigidly mounted to a supporting rack inside the flight tube, an evacuated section of 1.6 mm wall, 10.16 cm diameter aluminum tubing. Placed in extensions to this flight tube were the solid state detectors for each of the beam monitors. A 22.6 mg/cm² nickel foil served as a vacuum seal and entrance window to the flight tube in order to isolate it from the main flight tube system which was also evacuated. The flight path between beam monitor labeled ^6Li (1) and the neutron source, a low yield nuclear device, was 307.2 m. The neutron beam that resulted from the detonation of this device was collimated by a circular aperture, located below ground level, of such a diameter that the beam was 4.0 cm diameter at the monitor ^6Li (1). Neutron energy was determined from the known flight path and the measured time of arrival of the neutrons at a particular target. Source neutrons were moderated by polyethylene.

* Work performed under the auspices of the U. S. Atomic Energy Commission.

The beam intensity was monitored at four positions along the flight path so that sample attenuation could be taken into account in the capture cross section calculations. Each beam monitor consisted of a ${}^6\text{LiF}$ foil, placed at an angle of 45° to the beam axis and centered on it, and a 3 cm^2 diffused junction, silicon detector, located 6 cm from the center of the foil. The detectors had no entrance windows and were operated at sufficient bias voltage to be fully depleted to a depth of 200 microns. The ${}^6\text{LiF}$ foils were $466\ \mu\text{g}/\text{cm}^2$ thick deposits evaporated on $1.13\ \text{mg}/\text{cm}^2$ nickel backings; the foils had a minor axis of 4.75 cm. Upon passage of the neutron beam through the foil, the current produced in the detector by alphas and tritons from the ${}^6\text{Li}(n,\alpha)\text{T}$ reaction was amplified and then recorded as a function of time on recording oscilloscopes. So that the background associated with the nickel backings could be estimated, there was a monitor (labeled BLANK in Fig. 1) that was identical to all the others except that it had no ${}^6\text{LiF}$ deposit.

Capture gamma-ray yields from ${}^{151}\text{Eu}$, ${}^{153}\text{Eu}$, Lu, and Y samples were measured by Moxon-Rae detectors [6, 7] placed 11.59 cm from the center of each sample (see Fig. 1). The detectors had $\text{Bi}_2\text{O}_3+\text{C}$ radiators $7.6 \times 8 \times 0.95\text{ cm}$ thick and totally depleted ($300\ \mu$), diffused junction, solid state detectors for the detection of the conversion electrons. Samples were elliptically shaped with a minor axis of 5.1 cm and a major axis of 7.2 cm, were orientated 45° to the beam, and were centered on the beam axis. The thickness and composition of each is given in Table I. Neutrons scattered by a sample into the solid angle of its gamma detector were attenuated by a 5.8 cm thick block of ${}^6\text{LiH}$. Gamma-ray attenuation of these blocks was accounted for during the calibration of the detectors. Each Moxon-Rae detector was shielded from the gamma radiation of neighboring samples by stacks of lead bricks located between the detector stations. The purpose of the yttrium sample and the corresponding gamma detector was for the assessment of backgrounds in the other Moxon-Rae detectors. Current outputs from the detectors were amplified and fed into recording channels, each of which consisted of an oscilloscope and a drum camera [8].

3. Detector and Electronics Calibration

Calibration of the beam monitors was done by placing each in a well collimated, 2.54 cm diameter, thermal neutron beam coming from the Water Boiler Reactor. The measurement of relative neutron response at thermal neutron energies is valid in the 25 to 10,000 eV range because the energies of particles from the ${}^6\text{Li}(n,\alpha)\text{T}$ reaction are essentially independent of neutron energy over this range. Calibration data were collected as normalized, pulse height spectra. From these spectra the relative neutron response of each monitor was calculated. These calculated responses were all within ± 2 per cent of the average response.

Relative gamma-ray response of the Moxon-Rae detectors was measured in a similar way. For these measurements the detector-target geometry shown in Fig. 1 was simulated, and the yield of gamma radiation from the thermal capture in Lu was measured. Background from neutrons scattered by the Lu was estimated by substituting a Bi sample in place of the Lu. Again, data were collected as pulse height spectra. If one assumes a ± 10 per cent error in the gamma-ray responses calculated from these spectra, then each is within ± 15 per cent of the current responses measured with a 70 Ci ^{60}Co source.

The electronics were calibrated in the field a short time before the experiment. A calibrated current generator was connected to each recording channel, the drum camera was turned to speed, and the current calibration was recorded on film.

4. Data Reduction and Results

Data film records taken for each of the recording channels were digitized by reading them on a digital microprojector which has a punched card output. A computer program converted the film trace coordinates to tables of detector current versus neutron energy. Those tables associated with the beam monitor films were converted to relative neutron beam intensity tables by computer calculations which used the relative sensitivity of each monitor and the known cross section for the $^6\text{Li}(n,\alpha)\text{T}$ reaction. The product of the Moxon-Rae detector sensitivity and the sample mass was divided into the detector current table to calculate the relative gamma ray yield.

Calculation of the capture cross section was carried out by dividing the relative capture gamma-ray yield from a sample by the intensity of the beam incident on the sample. To normalize these cross sections, a normalization factor was derived from the ^{151}Eu data of Konks and Fenin [2] by comparing an integral of that data between 1 and 10 keV to a similar integral of the relative cross section of the present experiment. The normalized capture cross sections that resulted are shown graphically in Figs. 2, 3, and 4; data points have been connected by straight lines. Relative errors in these cross sections are at least ± 8 per cent.

By considering both samples of europium as a single sample and by using beam intensities found at monitors (1) and (3), it was possible to compute the sample transmission, hence total cross section, for a europium sample having a isotopic content of 50 per cent ^{151}Eu and 50 per cent ^{153}Eu . In some applications such a mixture may be considered to be that of natural europium. Corrections to these total cross sections for in-scattering effects, aluminum deposits on the samples, and the nickel backings of the ^6LiF foils were found to be negligible. Results are shown in Fig. 5 as a point plot with points connected by straight lines. The relative error of at least ± 21 barns restricts the useful energy range to 25 - 1500 eV.

5. Conclusions

The most characteristic feature of the cross sections shown in Figs. 2 through 5 are the resonance effects and fluctuations; these effects were also evident on the data film records. If one chooses 1 keV as a point of comparison and averages between 800 and 1200 eV, then one finds that the ratio

$$\langle \sigma_{n,\gamma} \rangle^{153} / \langle \sigma_{n,\gamma} \rangle^{151}$$

has a value of 0.55 ± 12 per cent, which is in agreement with the ratio of 0.68 ($\pm 10\%$ assumed) that is found from the results of Konks and Fenin [2]. As the normalized data stand, our Lu cross sections agree with those found by Block et al [4].

We wish to thank P. Rudnick for his help with the 20 to 1 cameras, L. Black, J. E. Mayer, and R. Showalter for their help in setting up the recording station, and H. A. Grench⁺ for his help with field operations and with the development of the detector calibration techniques. The collaboration of J. R. Neergaard with the computer programming effort is gratefully acknowledged.

6. References

- [1] D. W. Barr and J. J. Devaney, Kilovolt Europium Capture Cross Sections, LA-3643 (U. S. Department of Commerce, Springfield, Virginia) 1966. Also private communication with J. J. Devaney.
- [2] V. A. Konks and Yu. I. Fenin, Conference on Interaction of Neutrons with Nuclei, Dubna, Report No. 1845, (1964) 100.
- [3] V. A. Konks and Yu. I. Fenin, Conference on Study of Nuclear Structure with Neutrons, Antwerp, (1965) Paper 202.
- [4] R. C. Block, G. G. Slaughter, L. W. Weston and F. C. Vonderlage, Neutron Time-of-Flight Methods (Saclay Conference), (1961) 203.
- [5] J. H. Gibbons, R. L. Macklin, P. D. Miller and J. H. Neiler, Phys. Rev. 122 (1961) 182; extrapolation of these results to 1 keV.
- [6] M. C. Moxon and E. R. Rae, Nuc. Instr. and Methods 24 (1963) 445.
- [7] R. L. Macklin, J. H. Gibbons and T. Inada, Nuc. Phys. 43 (1963) 353.
- [8] N. W. Glass, et al., Conference on Neutron Cross Section Technology, CONF-660303 (U. S. Department of Commerce, Springfield, Virginia) (1966) 766-772.

⁺Summer Staff Member, 1966

Table I

Sample	Density (atom/barn)	Isotopic	Content
^{151}Eu	1.43×10^{-3}	96.83%	^{151}Eu
		3.17%	^{153}Eu
^{153}Eu	1.39×10^{-3}	98.7%	^{153}Eu
		1.2%	^{151}Eu
Lu	1.61×10^{-3}	Natural	
Y (Background Sample)	3.80×10^{-3}	Natural	
<p>Note: 1) All samples were self supporting metallic foils.</p> <p>2) The europium foils were coated on both sides with $945 \mu\text{g}/\text{cm}^2$ of Al to retard oxidation and subsequent deterioration. These foils were made by the Isotopes Division of Oak Ridge National Laboratory.</p>			

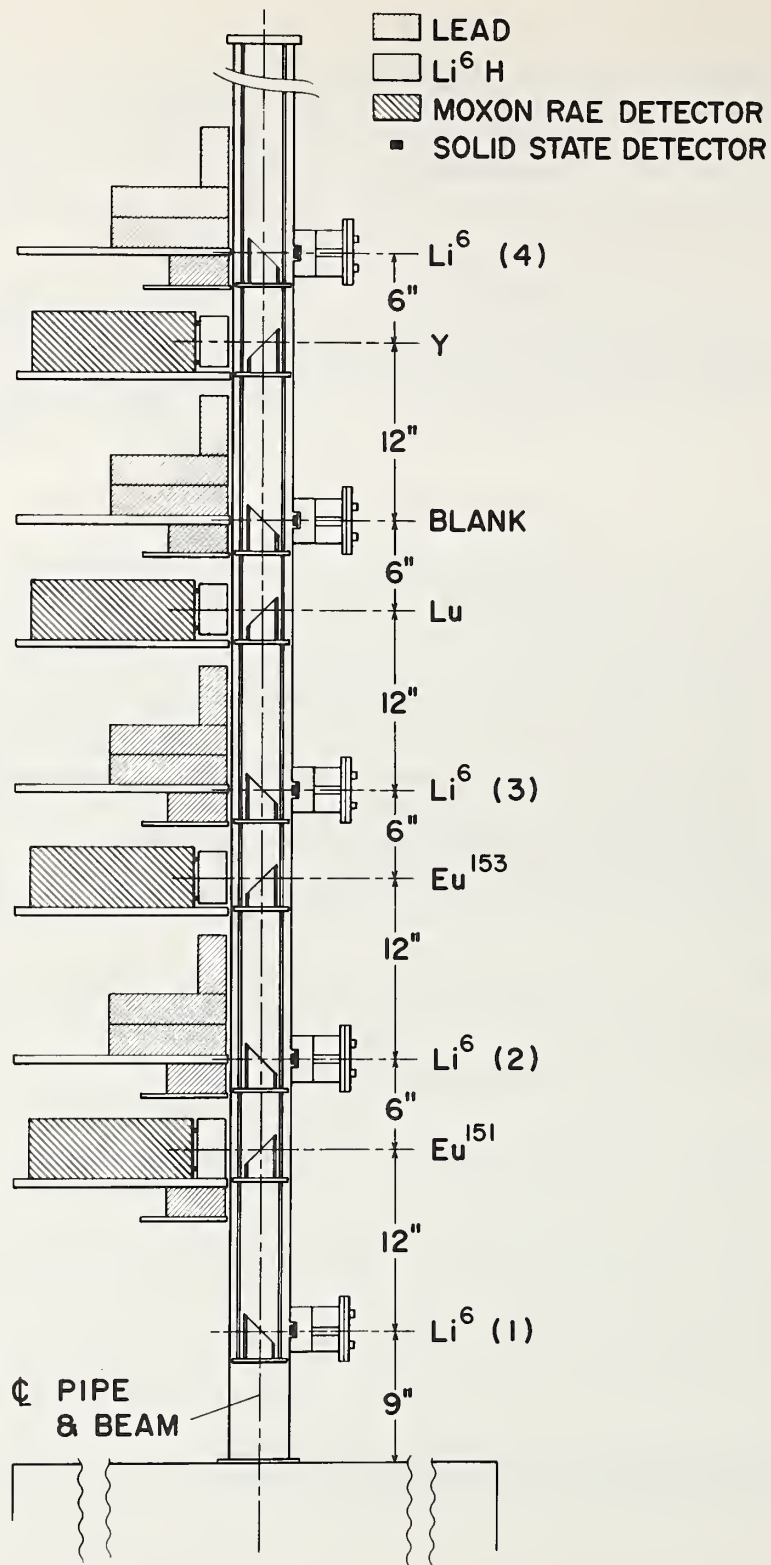


Fig. 1. Experimental geometry and shielding.

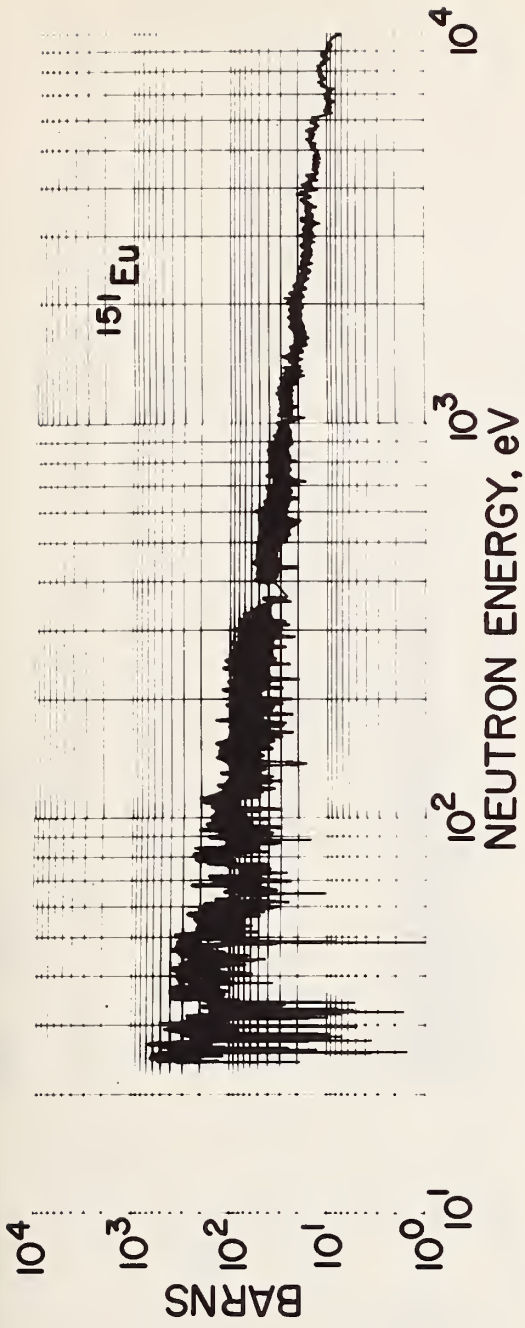


FIG. 2. CAPTURE CROSS SECTION OF ^{151}Eu

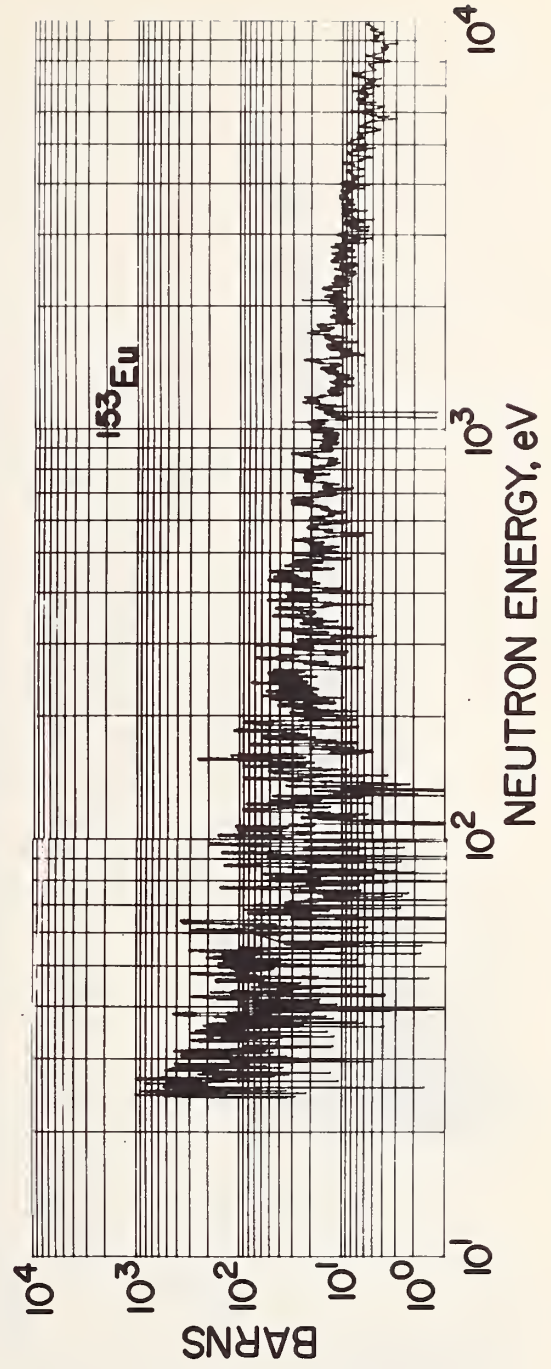


FIG. 3. CAPTURE CROSS SECTION OF ^{153}Eu

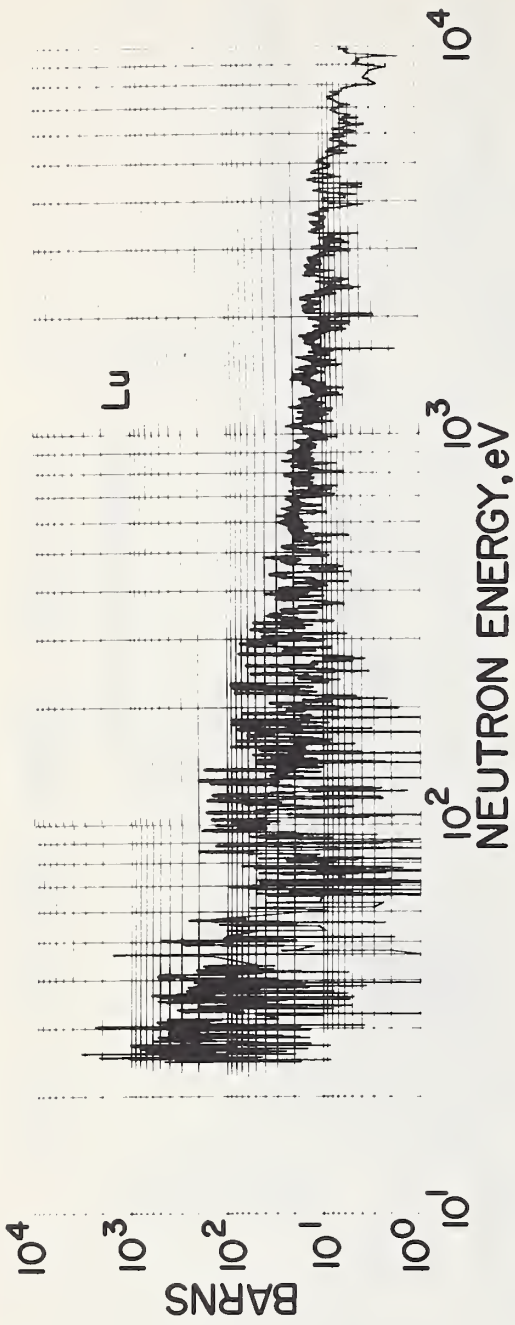


FIG. 4. CAPTURE CROSS SECTION OF Lu

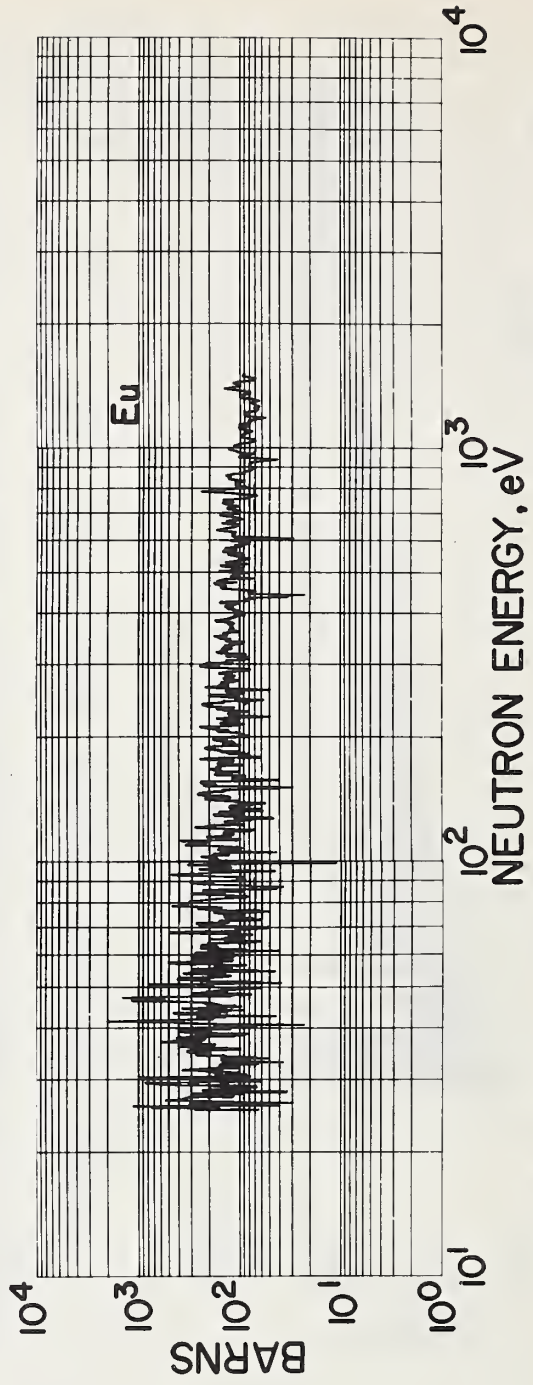


FIG. 5. TOTAL CROSS SECTION FOR A MIXTURE OF 50% ^{151}Eu AND 50% ^{153}Eu .

B. Holmqvist and T. Wiedling

AB Atomenergi, Studsvik, Nyköping, Sweden

ABSTRACT

An experimental study has been done of the angular distributions of elastically scattered neutrons from the elements Al, S, Ca, V, Cr, Mn, Fe, Co, Ni, Cu, Zn, In, and Bi for several energies in the energy interval 1.5 to 8.0 MeV. The results have been compared with optical model calculations. Theoretical distributions have been fitted to the experimental ones by using a diffuse spherical local optical model potential including a spin-orbit interaction term. Optimum fits to the experimental distributions were evaluated in a search routine by varying five optical parameters, i.e. the real and imaginary potential depths, the nuclear radii, and the diffuseness parameter of the real potential. Average parameters were thus obtained for each individual element. The dependence of the real potential depth on the nuclear symmetry parameter $(N-Z)/A$ was also studied at the neutron energies 6, 7, and 8 MeV yielding a value of 50 MeV for the symmetry term.

1. Introduction

The objective of this study was a systematic experimental collection of accurate neutron elastic scattering cross section data for a large number of elements in the energy region 1.5 to 8 MeV. Emphasis was given to elements of general interest in fast reactor design. However, an investigation of this kind and extent and also including some isotopes of not so common use in reactors gives an opportunity for a basic study of the fast neutron scattering process.

The experimental angular distributions have been interpreted within the formalism of the optical model. For a systematic nuclear model study of this character it is quite important to have a large, homogeneous experimental set of material obtained under identical experimental conditions. With the fundamental knowledge of the character of the scattering process at our disposal we are in possession of a tool which allows us to make safer and more reliable calculations and extrapolations into mass and energy regions where little or nothing is known from scattering experiments.

2. Experimental

The measurements were made with the time-of-flight spectrometer at the Studsvik 6 MV pulsed Van de Graaff [1]. The experimental methods are also as described in ref. [1].

The $T(p,n)$ reaction was used for production of neutrons up to 4.6 MeV and the $D(d,n)$ reaction from there on up to 8 MeV. The neutron energy spreads are ± 50 keV and ± 100 keV, respectively.

The differential scattering cross sections were measured relative to the $H(n,n)$ cross sections. The experimental angular distributions have been corrected for the anisotropy of the neutron flux from the source, attenuation of the neutron flux in the scatterer, multiple elastic neutron scattering, and the finite source-sample and sample-detector geometries using a Monte Carlo computer program [2]. The relative errors of the differential cross sections thus obtained are ± 5 per cent.

Differential cross sections for elastic scattering were measured for Al, S, Cr, Mn, Co, Cu, and Zn at 2.5, 3.0, 3.5, 4.0, 4.5, 6.0, 7.0, and 8.0 MeV, for Ca and Bi at 6.0, 7.0, and 8.0 MeV, for Ni and In at 3.0, 3.5, 4.0, 4.5, 7.0, and 8.0, and for Fe at the same last mentioned energies except for 3.5 and 6 MeV. Cross sections for Co and Cu were also measured at 1.5 and 2.0 MeV. The angular distributions were determined in the angular interval 20° to 160° in steps of 10° , but at the higher energies for every 5° in the extreme forward and backward directions of this angular range.

3. Results and Discussion

To get a comprehensive description of the measurements the experimental data were compared with nuclear optical model calculations. The potential is assumed to be of the local optical form

$$-V(r) = Uf(r) + iWg(r) + U_{SO} \left(\frac{\hbar}{\mu c} \right)^2 \frac{1}{r} \frac{d}{dr} |f(r)| \vec{\sigma} \cdot \vec{r}$$

The form factor of the real central potential is of the Saxon-Woods type characterized by the radius, R_U , and diffuseness, a :

$$f(r) = \left[1 + \exp\left(\frac{r-R_U}{a}\right) \right]^{-1}$$

With this form factor the potential is uniform in the nuclear interior in accordance with the short range and saturation properties of the nucleon-nucleon forces. The form factor of the imaginary part of the potential is of the derivative Saxon-Woods type normalized to get $g(r) = 1$ at its maximum and with the radius R_W and width b . The derivative form gives a potential which is peaked at the surface of the nucleus. The spin-orbit part of the potential is of the Thomas type. The radii are defined by the conventional expression $R = r_0 A^{1/3}$ based on the argument of the incompressibility of nuclear matter.

Optical model calculations predict only the elastic scattering cross-sections referring to the shape elastic effect. The process of compound nucleus formation followed by the reemission of the nucleon in the entrance channel is described by the optical model as an absorption process which, however, is experimentally indistinguishable from the

shape elastic scattering. The compound elastic scattering is less bothersome at higher neutron energies since a growing number of channels are then open for the decay of the compound nucleus by different processes and the decay through the entrance channel becomes less probable. The different methods we have used to evaluate the compound elastic cross sections have been discussed in ref. [1]. The compound elastic effect is usually quite small above about 4.5 MeV neutron energy.

The Abacus-2 computer program was used to search for the optical model parameters giving the best fits to the experimental differential cross section data. The goodness of a computed fit was described by the built-in chi-squared test of the Abacus program. The computer code was used for searches at each energy of all the investigated nuclei. The first searches were made by allowing five parameters to vary, i.e. U , W , R_{OU} , R_{OW} , and a . The spin-orbit potential depth U_{SO} and the diffuseness parameter b were kept constant at the values 8 MeV and 0.48 fm, respectively. Some representative angular distributions obtained by such searches are shown in Figure 1 for Al, Co, and In at several energies in the interval 1.5 to 8 MeV. The 8 MeV angular distributions obtained for all the thirteen investigated elements are demonstrated in Figure 2. The solid lines are the optical model fits to the experimental points represented by circles. The optical model descriptions of the experiments are very good. It was observed that the radii R_{OU} and R_{OW} , as well as the diffuseness parameter a , are essentially independent of the energy for each element as are also U and W at least above about 2 MeV neutron energy. (The exceptions are Ca and Ni, the real potentials of which seem to be weakly decreasing functions of the energy.) The results are discussed in detail in ref. [3]. The parameter values have also been studied as functions of the mass number and are plotted for 8 MeV neutron energy in Figure 3. This illustrates the behaviour at lower energies also. The radii and the real diffuseness parameter are essentially independent of the mass number. The real and imaginary potentials, on the other hand, show quite evident mass dependences. There are comparable trends at all the other energies. Because the optical model potential has the character of a mean potential of the constituents of a nucleus there is also a strong motivation to neglect minor individual fluctuations of the calculated values of R_{OU} , R_{OW} , and a and use their mean values in a two parameter search on U and W . This has been performed with the mean values $R_{OU} = 1.21$ fm, $R_{OW} = 1.21$ fm, and $a = 0.66$ fm and gives as a result a somewhat less pronounced scatter in the individual U and W values thus smoothing out the scatter probably caused by experimental inaccuracies but not fluctuations of individual nuclei. The results of these searches at 8 MeV neutron energy are also plotted in Figure 3. The two parameter search gives the same general trend of the mass number dependence of the potentials showing roughly a linear decrease of U with mass number but a somewhat more complicated functionality of W which may reflect collective effects in the target nuclei. The nuclear radii obtained in this investigation are somewhat smaller than those generally found and used in optical model analyses [4]. However, the present experiments are performed with such high accuracy and over a broad range of mass number and neutron energy that the results must be considered quite consistent. There is indeed an indication of somewhat larger radii for the heaviest elements. The value, 0.66, of the diffuseness parameter of the real potential is close to the value, 0.68, usually accepted. As a conclusion we would like to stress that in the energy region investigated the parameters appear to be mainly energy independent but U and W are somewhat mass dependent.

Neutron scattering data have up to now not been of sufficiently great accuracy to demonstrate the need for an isobaric-spin term in the optical potential analyses in the energy range of the present work. Such an effect has been proposed by Lane [5] and can be incorporated in the optical potential as a term proportional to $(N-Z)/A$. The real potential for neutrons would then become $U = U_0 - U_1(N-Z)/4A$. Figure 4 shows U plotted against $(N-Z)/A$ at 6, 7, and 8 MeV indicating $U_1 = (50 \pm 25)$ MeV where the error is the largest deviation from the mean value. This value may be compared with that given by Hodgson [4], i.e. 152 MeV, for a range of nuclei at 96 MeV neutron energy.

The essentially energy independent behaviour of the parameters of the local optical model potential used to describe the elastic scattering of 1.5 to 8 MeV neutrons presented in this paper is of great interest and importance for calculations on those elements used in reactor design.

4. References

1. Antolković, B., Holmqvist, B., Wiedling, T., Angular distributions of neutrons elastically scattered by natural copper in the energy region 1.5 to 4.6 MeV, *Arkiv Fysik* 33 (1966) 297
2. Holmqvist, B., Gustavsson, B., Wiedling, T., A Monte Carlo program for calculation of neutron attenuation and multiple scattering corrections, *Arkiv Fysik* 34 (1967) 481
3. Holmqvist, B., A systematic study of fast neutron elastic scattering in the energy region 1.5 to 8 MeV. (To be published)
4. Hodgson, P.E., Optical model of elastic scattering, Oxford University Press (1963)
5. Lane, A.M., Isobaric spin dependence of the optical potential and quasi-elastic (p,n) reactions, *Nuclear Physics* 35 (1967) 676.

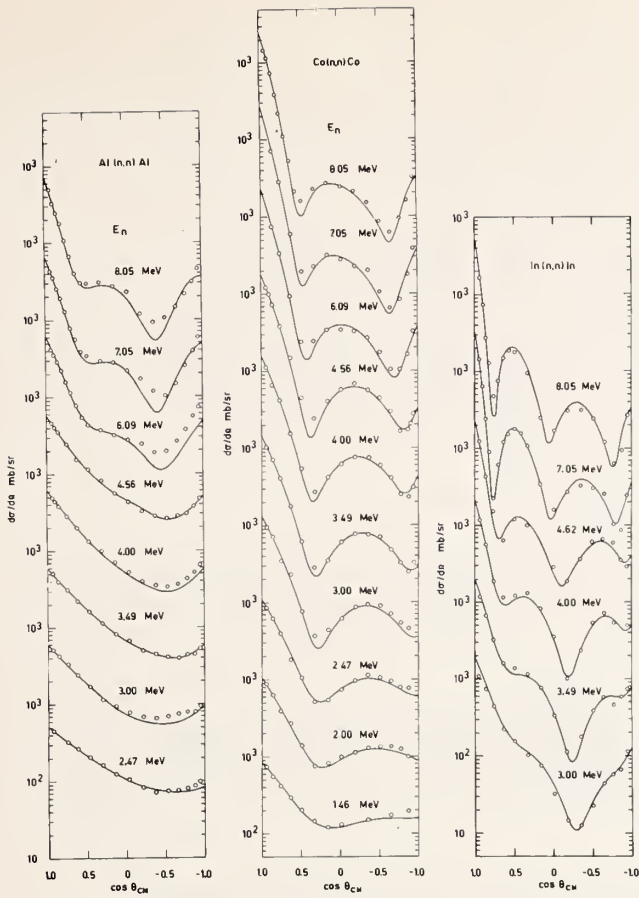
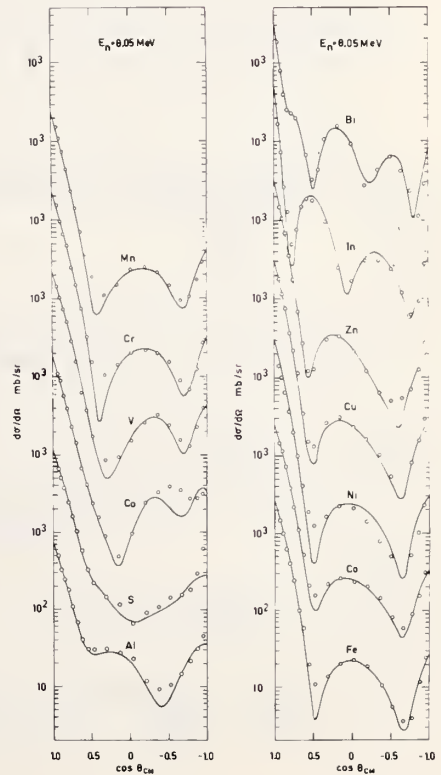


Fig. 1

Experimental (circles) and calculated (solid lines) angular distributions of neutrons elastically scattered by Al, Co, and In.

Fig. 2

Experimental (circles) and calculated (solid lines) angular distributions of 8 MeV neutrons elastically scattered by the investigated elements.



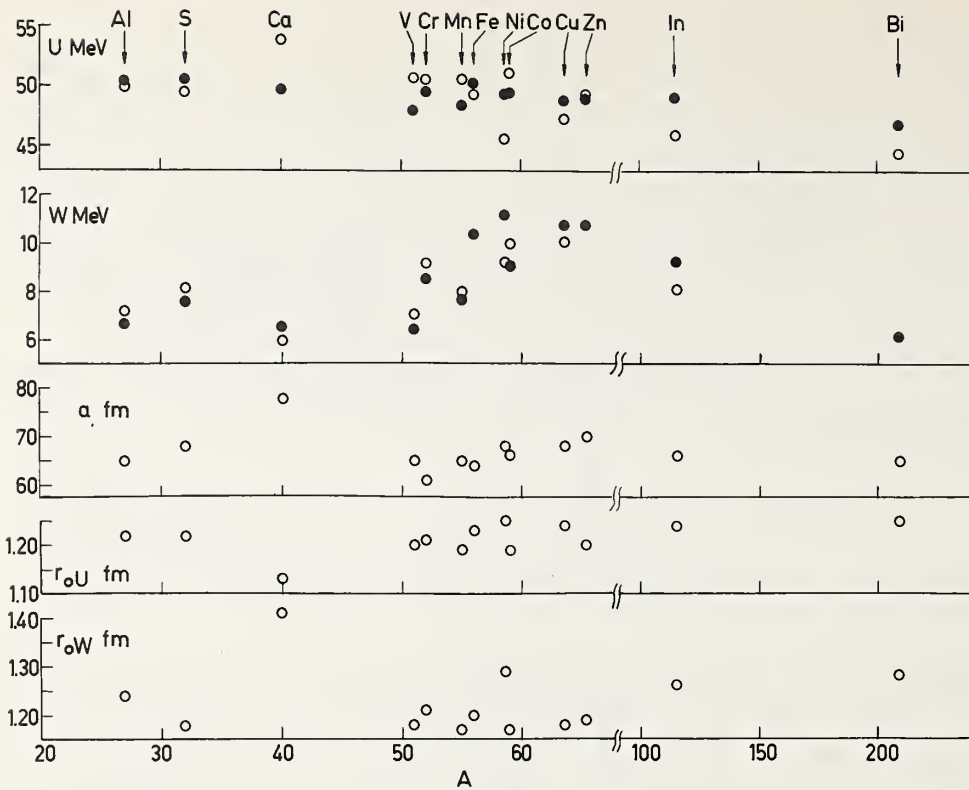


Fig. 3

The optimum values of the five parameter (open circles) and two parameter (filled circles) analyses plotted as functions of the mass number A at 8 MeV.

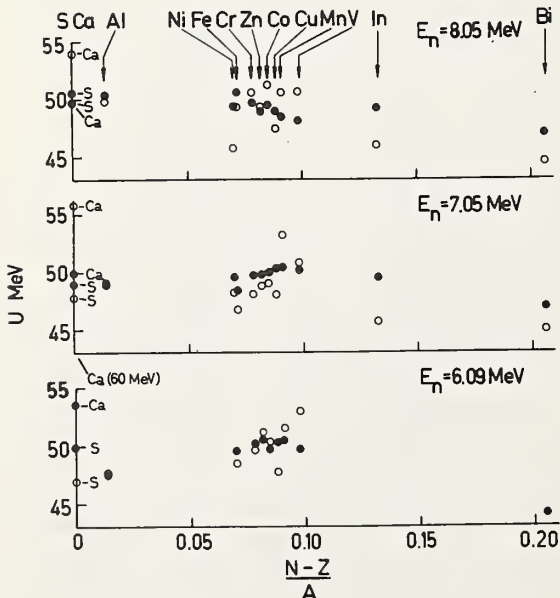


Fig. 4

The real potential depths at 6, 7, and 8 MeV plotted versus the symmetry term $(N-Z)/A$. The open and filled circles are from the five and two parameter analyses, respectively.

TOTAL NEUTRON CROSS SECTIONS OF ^9Be , ^{14}N , AND $^{16}\text{O}^*$

C. H. Johnson, F.X. Haas,⁺ J. L. Fowler, F. D. Martin,⁺⁺
 R. L. Kernell,⁺⁺ and H. O. Cohn
 Oak Ridge National Laboratory
 Oak Ridge, Tennessee 37830

Collected here are total neutron cross sections of some light nuclei measured with sufficient energy resolution to resolve most of the resonances at energies between ~ 1.5 and 5.0 MeV. These include the total cross section of ^9Be from 1.9 MeV to 4.6 MeV with ~ 25 keV resolution, the total cross section of ^{14}N from 2.0 to 4.2 MeV with ~ 5 keV resolution, and the total cross section of ^{16}O from 1.80 MeV to 3.65 MeV with ~ 2 keV resolution.

At the Oak Ridge National Laboratory, in a program of assigning resonance parameters for light nuclei, we measure the scattering of fast neutrons with energy resolution sufficient to draw conclusions with regard to resonance states.⁽¹⁻⁸⁾ Often we have total cross sections with good energy resolution long before we obtain enough other information (angular distributions, for example) to complete the resonance analysis.⁽⁹⁻¹²⁾ While the total cross section curves appear in progress reports, there is sometimes a delay before they are published in the open literature. Since such information is of interest to nuclear technology, we present here earlier unpublished work on σ_T for ^9Be ⁽⁹⁾ and ^{14}N ⁽¹⁰⁾ as well as recent work on ^{16}O ⁽¹¹⁻¹²⁾

Figure 1 shows the total cross section of beryllium from 1.9 to 4.6 MeV.⁽⁹⁾ For this data the $T(p,n)$ reaction, produced by bombarding tritium in a gas cell, served as the source of neutrons. Measurement with a long counter of the rise in the neutron yield at threshold gave the neutron energy spread as 25 keV full width at one half maximum.⁽¹³⁾ The experiment was the standard transmission type⁽¹⁴⁾ with the neutron detector, a 2.5 cm dia 10 cm long propane recoil counter, located along the proton beam direction with its center 38 cm from the center of the gas cell. In separate experiments we used two beryllium samples 2.86 cm dia each positioned midway between the source and the detector. One sample was 1.39 cm and the other 2.38 cm long.

In Fig. 1, the ^9Be total cross section has been corrected for scattered background neutrons, found by removing the direct neutron beam with a lucite attenuator, and for in-scattered neutrons. For this latter correction⁽¹⁴⁾ we used measured differential cross sections.⁽⁹⁾ Since the earlier measurements of Bockelman et al⁽¹⁵⁾ had been corrected for in-scattering under the assumption of isotropic scattering, their results which are replotted in Fig. 1 have been recorrected by use of the differential cross section data.⁽⁹⁾ As is seen, there is good agreement between our data and the corrected data of Bockelman et al.

*Research sponsored by the U. S. Atomic Energy Commission under contract with the Union Carbide Corporation.

⁺ Guest assignee from Monsanto Research Corporation Mound Laboratory (graduate student at University of Cincinnati).

⁺⁺ Graduate student from the University of Tennessee.

Figure 2 gives the total cross section of ^{14}N from 2 to 4.2 MeV.⁽¹⁰⁾ For this case the proton target was tritium absorbed in a thin zirconium layer. It gave a neutron yield with an energy spread of about 5 keV FWHM.⁽¹³⁾ For this experiment also we used open geometry⁽¹⁴⁾ with our neutron detector, a stilbene crystal, 55 cm from the zirconium-tritium target. Pulse shape discrimination suppressed pulses due to gamma rays. Our nitrogen sample, 7.35 gm/cm² of lithium azide⁽²⁾ sealed in a thin walled metal can, was placed half way between the source and the detector. For sample out runs we used a matching blank can which was identical otherwise to that containing the lithium azide. For the in-scattering correction we used the 0° differential cross sections from previous experiments^(2,16) and for the correction for the effect of lithium we used the total cross section of lithium from literature compilation.⁽¹⁷⁾ As in the case of beryllium we evaluated the background due to room scattered neutrons by removing the direct neutrons from the detector with a lucite attenuator.

In order to deduce the J value of the resonances, we need not only the peak height in the total cross section from Fig. 2 but also the reaction cross sections, which in the case of neutrons on nitrogen include the (n, α) and the (n,p) cross sections. These latter cross sections we take from the work of Gabbard, Bichsel, and Bonner.⁽¹⁸⁾ From this information and from previous differential cross section data,^(2,16) we conclude that the 65 keV wide peak at 2.23 MeV is a 3/2-resonance. The 14 keV peak at 2.95 MeV is a J = 5/2 resonance. The 85 keV peak at 3.210 MeV is a J = 3/2 resonance as is also the 30 keV peak at 3.570 MeV. From a qualitative comparison of the angular distributions of the scattered neutrons at 2.950 MeV and at 3.210 MeV⁽¹⁶⁾ with those at resonances at lower energies,⁽²⁾ we make a tentative assignment of positive parities for these latter two resonances.

Figure 3 shows recent data on the total cross section of ^{16}O ^(11,12) obtained from a measurement of the transmission of a beryllium-oxide sample relative to a matching beryllium sample. The procedure was identical to that described above for ^{14}N except that here we used a $^7\text{Li}(p,n)^7\text{Be}$ rather than a $\text{T}(p,n)^3\text{He}$ neutron source. This required a correction of the $^7\text{Li}(p,n)^7\text{Be}^*$ neutron group in addition to the usual corrections for in-scattering and for room scattered background. An unusual technique in the experiment was the use of a thin plating of ^{58}Ni between the lithium target and its platinum backing. This nickel formed a barrier against diffusion of the lithium into the platinum so that we were able to maintain targets with 2-3 keV resolution for many days of operation. The ^{58}Ni isotope was chosen because it has no (p,n) yield at these energies. We measured the ^{16}O cross section with 2 to 3 keV resolution from 1.77 to 3.67 MeV in steps of 2 to 3 keV (except for a small region of 10 keV steps near 1.9 MeV). Data points near the narrower resonances are plotted directly in Fig. 3; however, for most of the region where no narrow resonance was detected, each point is an average of four consecutive cross sections. We also made measurements from 1.116 to 1.162 MeV and from 1.64 to 1.70 MeV, which are not shown here. Previously we had covered the region from 3.35 to 3.73 MeV with 32 keV energy spread and the region from 3.73 to 3.86 MeV with 5 keV energy spread.⁽⁸⁾

We find a resonance at 1.651 MeV⁽¹¹⁾ in good agreement with earlier work of others. Assuming a J = 7/2 assignment, we find $\Gamma = 4$ keV and derive an experimental resolution of 2 keV in good agreement with the

target yield near threshold. This agreement substantiates a previous $J = 7/2$ assignment.⁽¹⁹⁾ Our resonance energies, observed at 1.833, 1.906, and 2.353 MeV, agree with the location of these resonances in earlier work. For the 1.833 MeV resonance we find $\Gamma = 7$ keV, $J = 3/2$. The dip before the resonance indicates interference with d-wave phase shift, suggesting it is a $d_{3/2}$ resonance.⁽¹¹⁾ Our parameters for the 1.906 and 2.353 MeV resonances are consistent with earlier work.

We now turn our attention to several narrow levels which were seen previously only in other reactions. Good resolution measurements⁽²⁰⁾ on the $^{19}\text{F}(d,\alpha)^{17}\text{O}$ spectrum revealed several levels including one we see at 1.689 MeV neutron energy and one at 2.889 MeV. Other good resolution work⁽²¹⁾ on the $^{16}\text{O}(d,p)^{17}\text{O}$ reaction verified the 1.689 MeV resonance. We find the resonances at 1.689 MeV and 2.889 MeV to be less than 1 keV wide. Levels corresponding to the resonances at 3.213 and 3.643 MeV have been observed as resonances in the $^{13}\text{C}(\alpha,n)^{16}\text{O}$ reaction.^(22,23) The resonance at 3.213 which had been identified as a $5/2$ resonance^(22,23) we find has a width of 2 keV. The previously observed neutron resonance at 3.44 MeV we find is a doublet at 3.442 and 3.444 MeV. This possibly invalidates the earlier $J = 5/2$ assignment for a single resonance at 3.44 MeV.

1. References

- ¹H. B. Willard, J. K. Bair, and J. D. Kington, Phys. Rev. 98, 669 (1955).
- ²J. L. Fowler and C. H. Johnson, Phys. Rev. 98, 728 (1955).
- ³H. B. Willard, J. K. Bair, J. D. Kington, and H. O. Cohn, Phys. Rev. 101, 765 (1956).
- ⁴J. L. Fowler and H. O. Cohn, Phys. Rev. 109, 89 (1958).
- ⁵J. E. Wills, Jr., J. K. Bair, H. O. Cohn, and H. B. Willard, Phys. Rev. 109, 891 (1958).
- ⁶H. O. Cohn and J. L. Fowler, Phys. Rev. 114, 194 (1959).
- ⁷M. V. Harlow, R. L. Robinson, and B. B. Kinsey, Nucl. Phys. 67, 249 (1965).
- ⁸C. H. Johnson and J. L. Fowler, Phys. Rev. 162, 890 (1967).
- ⁹J. L. Fowler and H. O. Cohn, Bull. Am. Phys. Soc. 4, 385 (1959).
- ¹⁰F. D. Martin, R. L. Kernell, and J. L. Fowler, Bull. Am. Phys. Soc. 11, 808 (1966).
- ¹¹J. L. Fowler, C. H. Johnson, and F. X. Haas, Bull. Am. Phys. Soc. 12, 1186 (1967).
- ¹²C. H. Johnson, F. X. Haas, and J. L. Fowler, Bull. Am. Phys. Soc. (Washington meeting, April 1968).
- ¹³J. H. Gibbons and H. W. Newson, Fast Neutron Physics, Part I: Techniques, ed. by J. B. Marion and J. L. Fowler, Interscience Publishers, New York-London (1960), p. 133.
- ¹⁴D. W. Miller, Fast Neutron Physics, Part II: Experiments and Theory, ed. by J. B. Marion and J. L. Fowler, Interscience Publishers, New York-London (1963), p. 985.

- 15 C. K. Bockelman, D. W. Miller, R. K. Adair, and H. H. Barschall, Phys. Rev. 84, 69 (1951).
- 16 J. L. Fowler, C. H. Johnson, and R. L. Kernell, Proceedings Conference on Neutron Cross Section Technology (Washington, D. C., 1966), ed. by P. B. Hemming, USAEC Conf. 660303, Book 2, 653 (1966).
- 17 J. R. Stehn, M. D. Goldberg, B. A. Magurno, and R. Wiener-Chasman, BNL-325, Second Edition, Suppl. No. 2, 1964.
- 18 Fletcher Gabbard, H. Bichsel, and T. W. Bonner, Nucl. Phys. 14, 277 (1959/1960).
- 19 F. Ajzenberg-Selove and T. Lauritsen, Nucl. Phys. 11, 1 (1959).
- 20 H. A. Watson and W. W. Buechner, Phys. Rev. 88, 1324 (1952).
- 21 C. P. Browne, Phys. Rev. 108, 1007 (1957).
- 22 R. B. Walton, J. D. Clement, and F. Boreli, Phys. Rev. 107, 1065 (1957).
- 23 M. G. Rusbridge, Proc. Phys. Soc. (London) A69, 830 (1956).

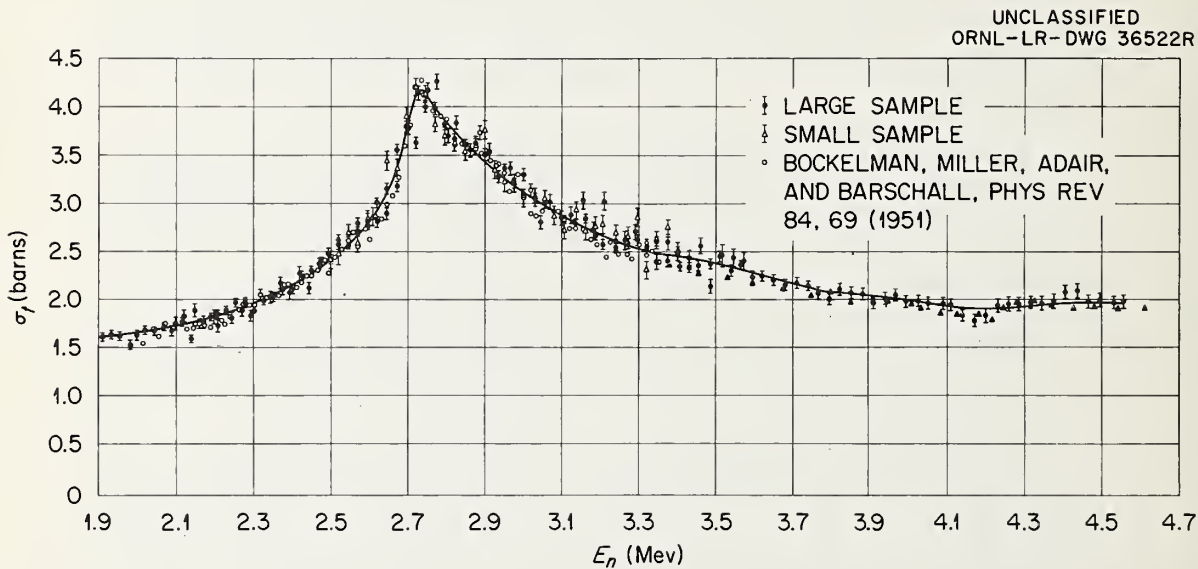


Figure 1
Total Neutron Cross Section of Be in Region 1.9 to 4.5 MeV. Energy Resolution
25 keV

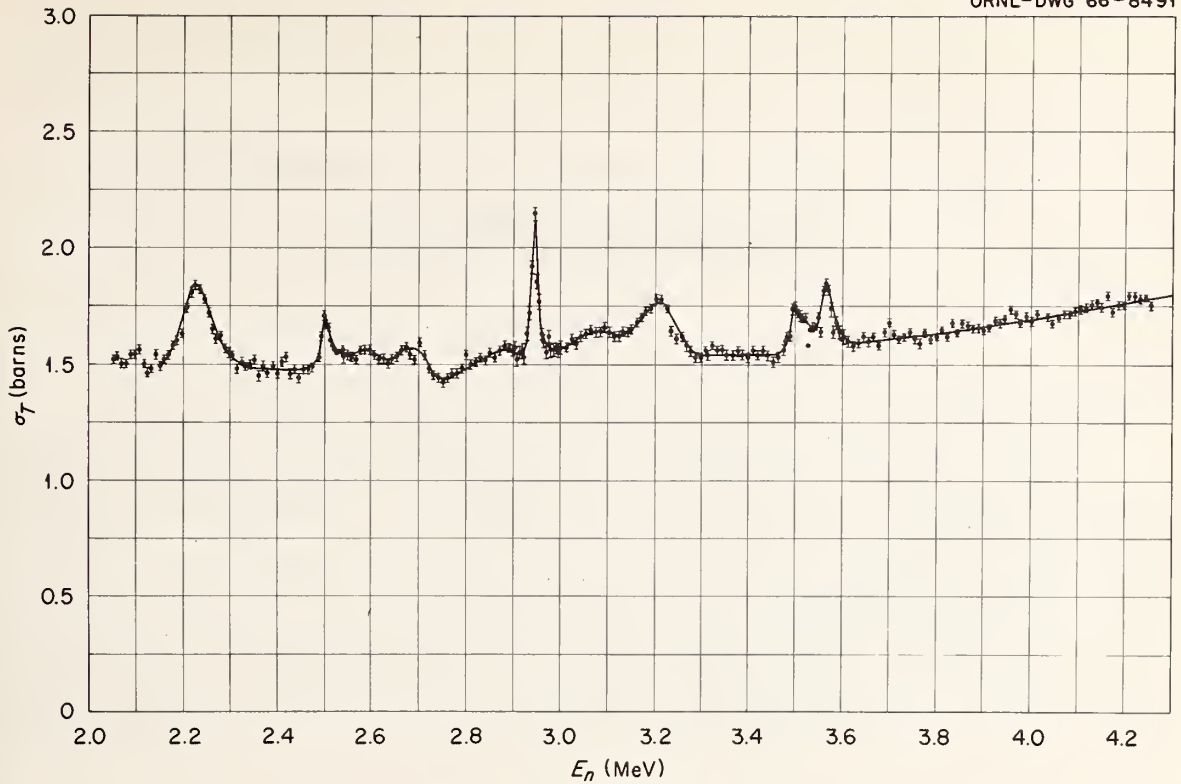


Figure 2

Total Cross Section of ^{14}N from 2.0 to 4.2 MeV. Energy Resolution 5 keV

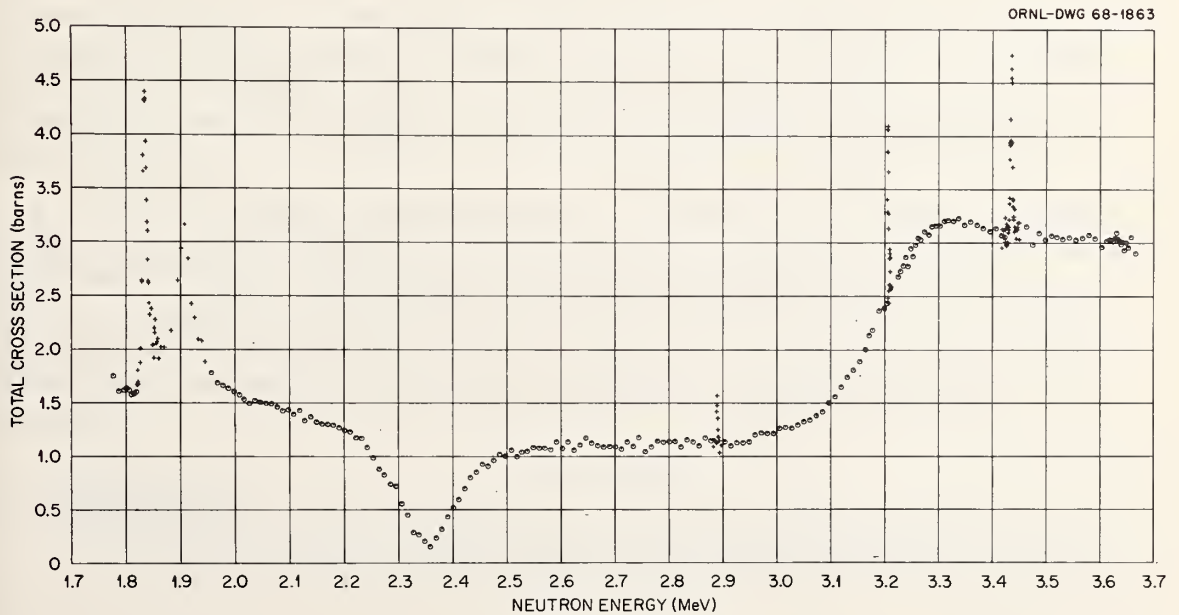


Figure 3

Total Cross Section of ^{16}O . Energy Resolution at Narrow Resonances 2 to 3 keV

Cross Section Measurements of Zirconium*

W. M. Lopez

F. H. Fröhner, S. J. Friesenhahn and A. D. Carlson

Gulf General Atomic Incorporated
San Diego, California 92101

ABSTRACT

Time-of-flight capture, self-indication, and transmission measurements of natural zirconium samples and samples enriched in ^{91}Zr (91%) have been made at the Gulf General Atomic linear accelerator facility. Parameters have been obtained for resonances in ^{91}Zr in the neutron energy range below 4 keV. The radiation width, $\Gamma_{\gamma} = 0.12 \pm 0.03$ eV, obtained in this work for the 292 eV and 681 eV resonances is considerably smaller than previously reported values obtained from transmission measurements. Our value of Γ_{γ} is, however, consistent with previous values deduced from low resolution capture measurements. Low energy (0.01 to 1 eV) capture cross sections for natural zirconium and a table of resonance parameters for ^{91}Zr are presented.

1. INTRODUCTION

Accurate calculations of the neutron absorption properties of zirconium have been hampered by a lack of precise differential cross sections and resonance parameters. Calculated dilute and self-shielded resonance integrals have been $\sim 30\%$ higher than measured values.⁽¹⁾ In the thermal region, the energy dependence of the capture cross section is of interest because the magnitude of the thermal capture cross section must be attributed to the presence of one or more nearby negative energy levels in $^{91}\text{Zr} + n$.⁽¹⁾

Cross section measurements of zirconium have been in progress at Gulf General Atomic as part of a continuing program to improve the precision of cross section information in areas beneficial to the reactor physics community. To this end, the program has pursued methods of measurement and analysis which have optimum sensitivity to the desired parameters and which use as few assumptions and approximations as is practical.

2. MEASUREMENTS

The experimental facility used to obtain neutron capture and self-indication data has been described previously in detail.^(2, 3) It consists

*Work supported by the U. S. Atomic Energy Commission.

of the Gulf General Atomic four-section electron linear accelerator which provides a pulsed neutron source, an 18.6-meter flight path, and a 4000-liter liquid scintillator gamma-ray detector. Capture and self-indication measurements were made concurrently by mechanically cycling a transmission sample in and out of the neutron beam which is incident on a sample located inside the 4π geometry of the capture gamma-ray detector. The timing resolution obtained with this facility is 3 nsec/meter. A one-inch thick polyethylene slab used to moderate the neutron source adds an additional energy spread of about 0.1% due to the neutron slowing-down process. The zirconium samples used in the various measurements are listed in Table 1; the purity of all the samples was 99.8% or higher.

TABLE 1

Sample No.	Sample Thicknesses			
	Thickness (nuclei/barn)	Weight (gms)	Enrichment of ^{91}Zr	Measurement Application
1	$9.3 \cdot 10^{-3}$	159.4	Natural	Self-Indication Ratio (SIR)
2	$4.72 \cdot 10^{-3}$	14.5	"	Capture Area (CA) & SIR
3	$7.73 \cdot 10^{-3}$	62.1	"	CA and SIR
4	0.113	$2.95 \cdot 10^3$	"	Transmission Area (TA)
5	$2.57 \cdot 10^{-4}$	0.786	90.88%	CA
6	$2.15 \cdot 10^{-3}$	6.59	88.5%	CA
7	$1.87 \cdot 10^{-2}$	320	Natural	Thermal Capture

The transmission measurements were made with a thick zirconium metal sample (0.113 nuclei/barn) and four cylindrical gas proportional counters (5 cm diameter by 80 cm long) containing 1 atm of $^{10}\text{BF}_3$ gas. These counters were located at the end of a 240-meter evacuated flight path, and a timing resolution of ~ 16 nsec/meter was obtained.

Figure 1 shows time-of-flight capture data, uncorrected for backgrounds, which were obtained with a thin metal sample enriched in ^{91}Zr (sample No. 6 in Table 1). In these data, six previously unreported weak resonances are observable, which are very likely due to p-wave interactions. Four resonances previously observed by Block⁽⁴⁾ in a capture measurement are also present in these data. A weak resonance at 159 eV previously reported by Block⁽⁴⁾ has also been observed in our capture data (not shown here).

3. ANALYSIS

The methods used to analyze the low-energy (0.01 to 1 eV) capture data have been described by Friesenhahn, et al.⁽⁵⁾ Sample self-shielding and multiple-scattering effects in the data are corrected with the aid of codes written for a UNIVAC 1108 computer. The energy dependence of the neutron flux in the thermal region was inferred from an auxiliary

capture measurement with a thin gold foil (1.53×10^{-3} nuclei/barn), for which the interaction probability is well known. Figure 2 shows capture cross section results deduced from this relative flux spectrum and a capture measurement with sample No. 7 (see Table 1). The data were normalized to the capture area of the 182 eV resonance in ^{91}Zr , using the recommended⁽⁶⁾ value of $2g\Gamma_n = 11 \pm 2$ meV. The capture area of this resonance is insensitive to the assumed radiation width of $\Gamma_\gamma \sim 200 \pm 100$ meV. Consequently, the normalization of the thermal capture cross section in Fig. 2 is known to $\sim \pm 20\%$. Statistical uncertainties in the data are of the order $\pm 5\%$. No evidence for a departure from a $1/v$ behavior is evident in the capture cross section data, shown in Fig. 2, for natural zirconium.

Multisample area analysis of capture, self-indication and transmission data in the resonance region was accomplished with the aid of the computer code TACASI by Fröhner.⁽⁷⁾ This code calculates the observed quantities from single-level Breit-Wigner terms, including the effects of Doppler and resolution broadening, sample self-shielding and multiple scattering. The least squares method is used to find the values of Γ_n and Γ_γ , which produce optimum agreement with up to 20 measured transmission areas, capture areas, and/or self-indication ratios (for example, belonging to different sample thicknesses or taken with different resolutions).

In the analysis of a given s-wave resonance, the resonance energy E_0 and the statistical spin factor, $g_J = (2J+1)/2(2I+1)$, are treated as fixed parameters. In some cases when the ground state spin I of the target nucleus is not large, say $< 5/2$, one can infer the correct compound spin J of the resonance by comparing the "goodness" of fit for the two cases $J = I \pm 1/2$. This is particularly true for strong resonances ($\Gamma_n \gg \Gamma_\gamma$) when one combines a self-indication ratio measurement with a transmission area measurement. Figure 3 illustrates this sensitivity to J by showing the curves in the $(\Gamma_n, \Gamma_\gamma)$ plane defined by the measured transmission area (TA), capture areas (CA), and self-indication ratio (SIR) for the 682 eV resonance. The curves calculated with the code TACASI for both cases $J=2$ and $J=3$, clearly indicate that $J=3$ is the correct spin for this resonance. We note that in this case it is the self-indication ratio which is sensitive to the choice of J , differing by almost a factor of two.

This behavior of the self-indication ratio can be understood if one considers the functional relationship,

$$\text{SIR} = f(E_0, g_J, \Gamma_n, \Gamma_\gamma, n_c, n_t) ,$$

between the self-indication ratio, the resonance parameters (E_0, g_J, Γ_n , and Γ_γ), the capture sample thickness, n_c and the transmission sample thickness n_t . This relationship can be reduced to

$$\frac{g_J \Gamma_n}{\Gamma} = C , \quad (1)$$

if one of the two samples is thin and the other thick. (8) Here C is a known constant, and the parameters on the left side are the unknown quantities we want to determine. Hence, for each of both possible values g^\pm , where \pm indicates $J = I \pm 1/2$, a curve is defined in the $(\Gamma_n, \Gamma_\gamma)$ plane:

$$\Gamma_n^\pm = \frac{C\Gamma_\gamma^\pm}{g^\pm - C} \quad (2)$$

Now let us rewrite Eq. 2 using the true value of C (Eq. 1) in the denominator:

$$\Gamma_n^\pm = \frac{C\Gamma_\gamma^\pm}{g^\pm - g_J \frac{\Gamma_n}{\Gamma}} \quad (3)$$

In this form it becomes obvious that for strong resonances, where $\Gamma_n/\Gamma \approx 1$, the curve defined by Eq. 3 becomes very sensitive to the choice of g^\pm . In fact, if the true value g_J is g^+ and one picks g^- , the value Γ_n^- obtained can become negative. This effect is more noticeable for nuclides with small (nonzero) ground state spins, but it has been sufficiently sensitive to determine spins of $J=3$ for the 293 eV, 682 eV and 1540 eV resonances in ^{91}Zr where $I = 5/2$.

The effects of interference between resonances of the same spin can also be observed in some cases by comparing the behavior of curves in the $(\Gamma_n, \Gamma_\gamma)$ plane defined by self-indication ratios and transmission areas. This is illustrated in Fig. 3-B for the 682 eV resonance. The dashed curves are defined by the observables SIR and TA when the cross section in the region of the 682 eV resonance is treated as a sum over single-level Breit-Wigner terms. For these curves, the potential scattering and potential-resonance interference was calculated with an effective nuclear radius $R = 7.1 \text{ F}$ as measured by Seth, et al. (9) The effects of resonance-resonance interference from the strong levels at 292 eV and 1540 eV on the 682 eV level were taken into account in the solid curves of Fig. 3-B by using a fictitious value R_i of the effective nuclear radius as given by Julien, et al. (10)

$$R_i = R \left[1 + \frac{1}{2R} \sum_{j \neq i} \frac{\chi_j \Gamma_{nj}}{(E_i - E_j)} \right] \quad (4)$$

where χ_j is the neutron wave length at the resonance energy E_j , i labels a given resonance, and j labels adjacent resonances which have the same spin. The resonance scattering cross section is then still described by a sum of single-level Breit-Wigner terms (before Doppler and resolution broadening):

$$\sigma_{nn} = \sum_i \frac{\sigma_{oi}}{1 + x_i} \left(\frac{\Gamma_{ni}}{\Gamma_i} + 2 \frac{R_i}{\lambda_i} x_i \right), \quad (5)$$

where $x = 2(E_i - E)/\Gamma_i$ and σ_{oi} is the peak resonance cross section at the resonance energy E_i . This device was used in order to avoid the necessity of having to include the complete multilevel formalism in our existing analysis codes. Since natural samples were used for the measurements of Fig. 3-B, the potential scattering in the region of the 682 eV resonance was calculated by

$$\sigma_p = 4\pi \sum_m a_m \sin^2(-R_m/\lambda) \quad (6)$$

where a_m is the relative abundance of isotope m . Seth's⁽⁹⁾ value of $R = 7.1 F$ was used for all the isotopes except ^{91}Zr , where we used the value $R = 6.77 F$ as calculated from Eq. 4.

We note that the solid and dashed SIR curves in Fig. 3-B differ by about 6%, whereas the TA curves differ by about 20%. This is understandable since the transmission area from a thick sample (as is the case here) is sensitive to the shape of the resonance in the wings, whereas a self-indication ratio from a thinner sample is more sensitive to the shape at the peak. We also note that the values of Γ_n defined by the solid SIR and TA curves are in much better agreement than those defined by the dashed curves. These results suggest that in some cases area analyses of transmission data alone may be erroneous if multi-level effects are ignored. On the other hand, one must know the level spins to make this correction.

4. RESULTS AND DISCUSSION

Table 2 presents a list of the resonance parameters obtained for ^{91}Zr . As mentioned earlier, the capture measurements are normalized to the recommended value of $2g\Gamma_n = 11 \pm 2$ MeV for the 182 eV resonance in ^{91}Zr .^(6, 11) Consequently, those parameters which are strongly dependent upon a measured capture area, such as $2g\Gamma_n$ for weak levels and $2g\Gamma_y$ for strong levels, have a systematic uncertainty of about $\pm 20\%$. This systematic uncertainty can be removed, in principle, by a more precise transmission or self-indication measurement of the 182 eV resonance.

The most significant differences between the results in Table 2 and earlier results (tabulated in Ref. 6) are found for the total radiation widths Γ_y for the 292 eV and 684 eV resonances. In the present work we obtain $\Gamma_y = 0.12 \pm 0.03$ eV for both resonances with a considerable improvement in precision. Our results agree well with the value 0.13 ± 0.04 eV inferred by Steen and Harris⁽¹⁾ from the low-resolution capture measurements by Kapchigashev.⁽¹²⁾

TABLE 2
Resonance Parameters for $^{91}\text{Zr} + n$

E_o (eV)	Γ_γ (meV)	$2g\Gamma_n$ (meV)	J^π	ℓ
159 ^a				
182.3	$(200 \pm 100)^b$	$(11 \pm 2)^b$		
241	(290 ± 50)	2.5 ± 1		
292	120 ± 30	$\Gamma_n = 635 \pm 40$	3^+	0
448		3.7 ± 1		
632 ^c		1.4 ± 0.5		
682	120 ± 30	$\Gamma_n = 950 \pm 200$	3^+	0
895	(200 ± 100)	43 ± 8		
984 ^c		4.7 ± 1.4		
1195 ^c		4.3 ± 1.4		
1221 ^c		5.4 ± 2		
1395 ^c		2.2 ± 1		
1537	200 ± 60	$\Gamma_n = 8100 \pm 600$	3^+	0
1720 ^c		5.5 ± 2		
1960	$2g\Gamma_\gamma = 260 \pm 70$	(260 ± 80)		
2023	$2g\Gamma_\gamma = 172 \pm 50$	(1500 ± 200)		
2400 ^a				
2484				
2744				
2783 ^a				
3178	$2g\Gamma_\gamma = 180 \pm 50$	(2600 ± 800)		
3664 ^a	$2g\Gamma_\gamma = 230 \pm 70$	$(\Gamma_n \gg \Gamma_\gamma)$		
3890 ^a				

^aPreviously reported by Block⁽⁴⁾

^bQuantities in parentheses were assumed in the analysis. Most of these were obtained from Ref. 6.

^cNew weak levels.

5. REFERENCES

1. N. M. Steen and D. R. Harris, Trans. Am. Nucl. Soc. 10, 265 (1967).
2. E. Haddad, et al., Phys. Rev. 140, B50 (1965).
3. E. Haddad, et al., Nucl. Instr. and Methods, 31, 125 (1964).
4. R. C. Block, WASH 1048, p. 71 (1964).
5. S. J. Friesenhahn, et al., Nucl. Sci. Eng., 26, 487 (1966).
6. M. D. Goldberg, et al., BNL-325, 2nd ed., Supplement No. 2 (1966).
7. F. H. Fröhner, "TACASI, A FORTRAN-IV Computer Program Least Squares Area Analysis of Neutron Resonance Data, USAEC Report GA-6906, General Dynamics Corp., General Atomic Div. (1966).
8. F. H. Fröhner, et al., Book 1 of Conference on Neutron Cross Section Technology, P. B. Hemmig, ed., TID-4500, CONF-660303, Washington, D. C., p. 55 (March 22-24, 1966).
9. K. K. Seth, et al., Phys. Rev. 110, 692 (1958).
10. J. Julien, et al., Nucl. Phys. 76, 391 (1966).
11. R. C. Block, Oak Ridge National Lab Report, ORNL-3425, 32 (1963).
12. S. P. Kapchigashev, Atomnaya Énergiya, 19, 294 (1965).

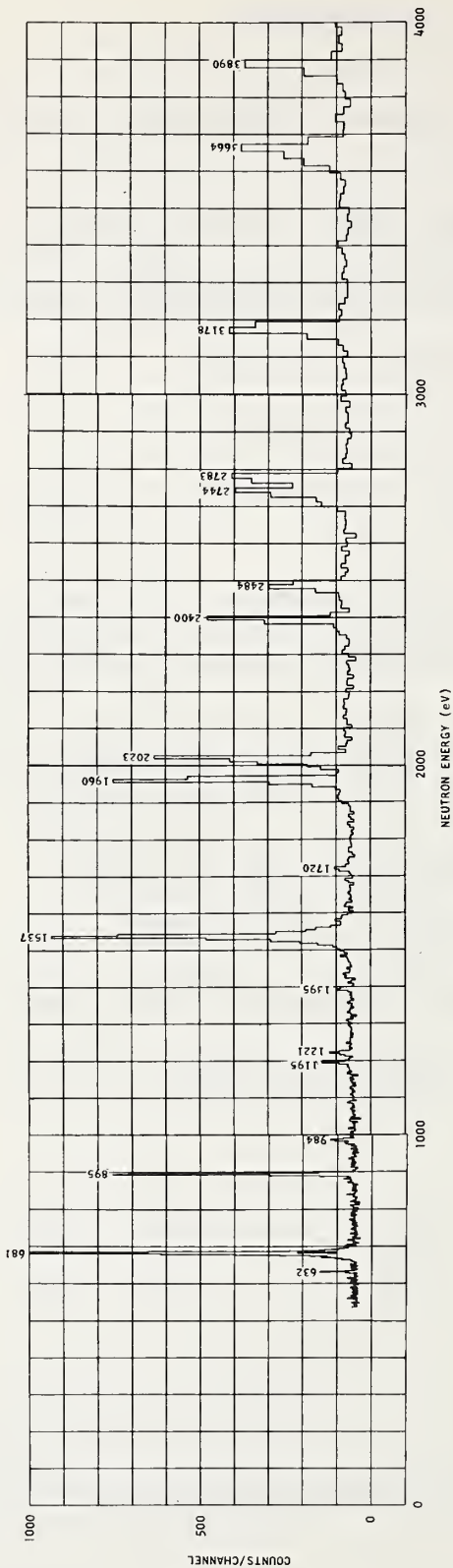


Fig. 1. Time-of-flight capture data obtained with a 6.6 gm zirconium sample ($2.15 \cdot 10^{-3}$ nuclei/barn) enriched to 88.5% in ^{91}Zr . The data were taken with a 50 nsec LINAC burst width, a 62.3 nsec time analyzer channel width, and are not corrected for backgrounds.

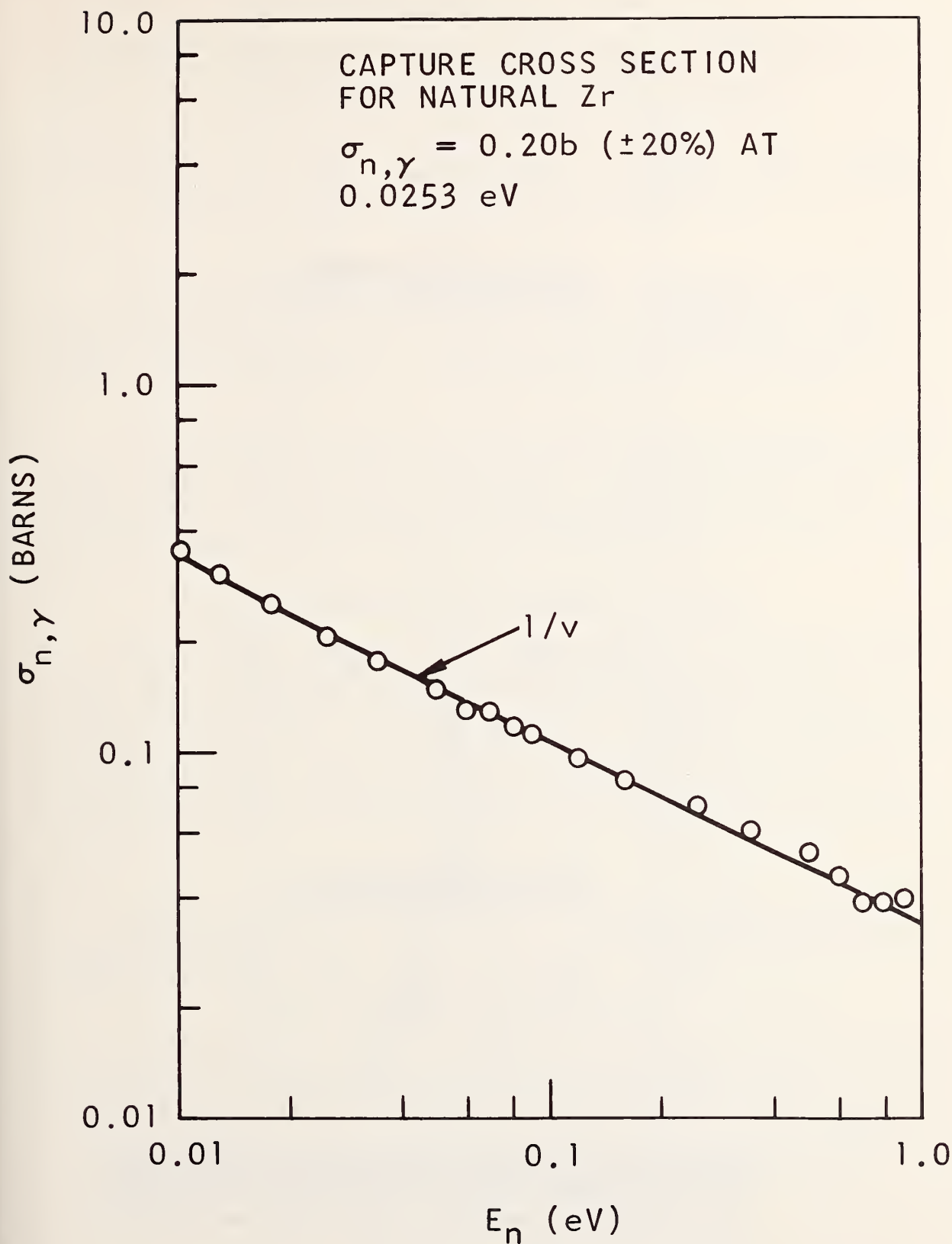


Fig. 2. Low energy capture cross section of natural zirconium.

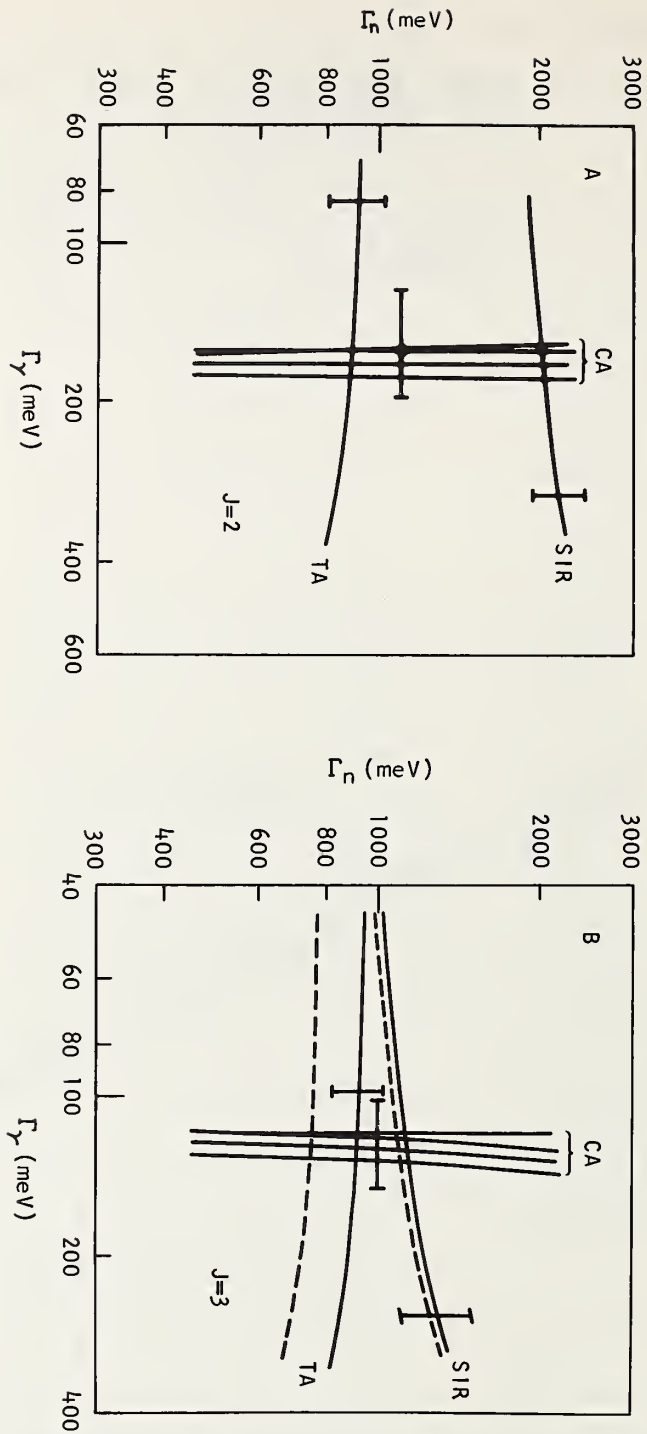


Fig. 3. Calculated curves for the 683 eV resonance in ^{91}Zr which are defined in the $(\Gamma_n, \Gamma_\gamma)$ plane by measured transmission (TA), self-indication (SIR), and capture areas (CA). The two sets of curves illustrate the sensitivity of the calculations to the two possible values of spin: $J=2$ or $J=3$.

THE STRENGTH FUNCTIONS S_0 AND S_1 ,
THE TOTAL RADIATIVE WIDTH Γ_γ AND THE MEAN LEVEL SPACING \bar{D}
AS A FUNCTION OF MASS NUMBER AND SPIN VALUE

J. Morgenstern, R. Alves[†], S. de Barros^{††}, J. Julien and C. Samour
Centre d'Etudes Nucléaires de Saclay, France

The total neutron cross-section has been measured at the Saclay 45 MeV Linac, for about 30 elements from ^{51}V to ^{209}Bi . We have used time of flight methods with two different flight paths: 103 m and 199.3 m. The best resolution was equal to 0.19 ns/m. (1)

The resonance parameters at the potential scattering cross-section were determined by shape analysis of the resonances, (1,2) using single and multilevel formulae. In some cases, p wave resonances were identified by noting the absence of interference (3) between resonant and potential scattering due to the very low value of the p wave potential scattering cross-section.

1. Determination of the strength functions.

The values of S_0 , S_1 and R' obtained with these parameter values are reported in table I. Figure 1 shows the plot versus A of the experimental values of S_0 and the theoretical curve calculated by Jain, (4) using the surface absorption model of Buck and Perey. (5) This model takes into account the deformation for the deformed nuclei, and the coupling with the first 2^+ vibrational state for the even-even spherical nuclei. One can see a fairly good agreement between experimental and theoretical values.

2. Mean level spacing.

Figure 2 shows the variation of the mean spacing values versus A . The curve reported here was calculated by Cameron (6) using Newton's (7) level density formula.

3. Total radiative capture width.

The mean values of Γ_γ for the nuclei studied are presented in table II. Interesting features are the variation of $\langle \Gamma_\gamma \rangle$

† Nuclear Engineering Institute, Rio de Janeiro, Brazil.

†† Nuclear Physics Laboratory, Rio de Janeiro, Brazil.

according to the spin value for the s wave resonances of ^{195}Pt , ^{199}Hg and ^{201}Hg , and the variation of $\langle \Gamma_\gamma \rangle$ with orbital angular momentum for ^{91}Zr and ^{93}Nb .

In figure 3 we have plotted the variation of $\langle \Gamma_\gamma \rangle$ versus A for the values measured in this work and in other laboratories.

4. REFERENCES

1. J. Morgenstern et al., Nucl. Phys., 1967, A102, 602.
2. J. Julien et al., Nucl. Phys., 1966, 76, 391.
3. G. Le Poittevin et al., Nucl. Phys., 1965, 70, 497.
4. A. P. Jain, Nucl. Phys., 1964, 50, 157.
5. B. Buck and F. Perey, Phys. Rev. Letters, 1962, 8, 444.
6. A. G. W. Cameron, Can. J. Phys., 1957, 35, 1021.
7. T. D. Newton, Can. J. Phys., 1956, 34, 804.

TABLE I - STRENGTH FUNCTIONS AND SCATTERING LENGTHS VALUES

TARGET NUCLEI	ENERGY INTERVAL (eV)	$S_0 (10^{-4} eV^{-\frac{1}{2}})$	$R' (\text{fm})$	$S_1 (10^{-4} eV^{-\frac{1}{2}})$
^{51}V	0 - 130 000	$10,6 \begin{matrix} + 4,8 \\ - 2,8 \end{matrix}$	$6,0 \pm 1,0$	$0,43 \begin{matrix} + 0,20 \\ - 0,12 \end{matrix}$
^{55}Mn	0 - 75 000	$4,0 \begin{matrix} + 1,0 \\ - 0,7 \end{matrix}$	$3,6 \pm 0,4$	
^{59}Co	0 - 120 000	$3,8 \begin{matrix} + 1,6 \\ - 1,6 \end{matrix}$	$5,4 \pm 0,4$	$< 0,4$
^{63}Cu	0 - 30 000	$2,4 \begin{matrix} + 0,7 \\ - 0,5 \end{matrix}$	$7,5 \pm 0,4$	
^{65}Cu	0 - 30 000	$1,2 \begin{matrix} + 0,5 \\ - 0,3 \end{matrix}$	$6,9 \pm 0,4$	
^{69}Ga	0 - 2 500	$1,2 \begin{matrix} + 1,2 \\ - 0,4 \end{matrix}$	$6,3 \pm 1$	
^{75}As	0 - 4 000	$1,75 \begin{matrix} + 0,4 \\ - 0,3 \end{matrix}$	$7 \pm 0,0$	
^{77}Se	0 - 1 500	$1,5 \begin{matrix} + 1,0 \\ - 0,5 \end{matrix}$		
$^{79,81}\text{Br}$	0 - 2 000	$1,5 \begin{matrix} + 0,53 \\ - 0,23 \end{matrix}$	$7 \pm 0,8$	
^{89}Y	0 - 30 000	$0,39 \begin{matrix} + 0,27 \\ - 0,12 \end{matrix}$	$6,6 \pm 0,3$	$3,4 \begin{matrix} + 2,0 \\ - 1,2 \end{matrix}$
^{91}Zr	0 - 2 000	$0,8 \begin{matrix} + 1,3 \\ - 0,3 \end{matrix}$	$7,10 \pm 0,3$	$3,8 \begin{matrix} + 7,9 \\ - 2,1 \end{matrix}$
^{93}Nb	0 - 4 100	$0,35 \begin{matrix} + 0,10 \\ - 0,07 \end{matrix}$	$7,1 \pm 0,3$	$3,0 \begin{matrix} + 1,5 \\ - 1,0 \end{matrix}$
^{107}As	0 - 760	$0,37 \begin{matrix} + 0,10 \\ - 0,07 \end{matrix}$		
^{109}As	0 - 760	$0,75 \begin{matrix} + 0,16 \\ - 0,14 \end{matrix}$		
^{135}Ba	0 - 1 350	$0,80 \begin{matrix} + 0,35 \\ - 0,20 \end{matrix}$	$5,8 \pm 0,8$	
^{137}Ba	0 - 1350	$0,30 \begin{matrix} + 0,70 \\ - 0,18 \end{matrix}$	$5,8 \pm 0,8$	

TABLE I. STRENGTH FUNCTIONS AND SCATTERING LENGTHS VALUES

TARGET NUCLEI	ENERGY INTERVAL (eV)	$\beta_0 (10^{-4} \text{eV}^{-\frac{1}{2}})$	$R' (\text{fm})$	$\beta_1 (10^{-4} \text{eV}^{-\frac{1}{2}})$
^{139}La	0 - 10 000	$0,70 \pm 0,20$ $- 0,14$	$4,9 \pm 0,3$	$\leq 0,7$
^{141}Pr	0 - 6 000	$2,04 \pm 0,47$ $- 0,35$	$4,9 \pm 0,5$	
^{143}Nd	0 - 740	$4,1 \pm 2,6$ $- 1,3$	$7,5 \pm 0,8$	
^{145}Nd	0 - 740	$2,9 \pm 1,1$ $- 0,7$	$7,5 \pm 0,8$	
^{169}Tm	0 - 760	$1,50 \pm 0,27$ $- 0,21$	$7,7 \pm 0,8$	
^{192}Pt	0 - 590	$1,7 \pm 1,9$ $- 0,6$	$8,7 \pm 0,5$	
^{194}Pt	0 - 700	$1,4 \pm 2,4$ $- 0,5$	$8,7 \pm 0,5$	
^{195}Pt	0 - 825	$1,70 \pm 0,43$ $- 0,33$	$8,7 \pm 0,5$	
^{197}Au	0 - 1 000	$1,80 \pm 0,39$ $- 0,30$	$8,7 \pm 0,5$	
^{193}Er	0 - 420	$1,5 \pm 2,1$ $- 0,5$	$9,8 \pm 0,7$	
^{199}Er	0 - 700	$2,2 \pm 2,2$ $- 0,7$	$9,8 \pm 0,7$	
^{201}Er	0 - 700	$1,3 \pm 1,3$ $- 0,4$	$9,8 \pm 0,7$	
^{209}Bi	0 - 70 000	$0,65 \pm 0,39$ $- 0,17$	$9,0 \pm 0,4$	$0,25 \pm 0,09$ $- 0,05$

Table 2
Values of $\overline{\Gamma}_\gamma$ for nuclei investigated in this work.

Noyau cible	l	J	$\langle \overline{\Gamma}_\gamma \rangle$ meV	Nombre de résonances	Noyau cible	l	J	$\langle \overline{\Gamma}_\gamma \rangle$ meV	Nombre de résonances
^{56}Fe	(2)	1/2	570 ± 60	1	^{112}Sn	0	1/2	110 ± 20	1
^{63}Cu	0	2	560 ± 50	1	^{116}Sn	0	1/2	43 ± 12	2
^{65}Cu	0		240 ± 20	1	^{117}Sn	0	1	95 ± 15	4
^{64}Zn	0		305 ± 30	1	^{118}Sn	1	3/2	110 ± 10	1
^{66}Zn	0		180 ± 20	1	^{119}Sn	0		45 ± 25	1
^{67}Zn	0	3	350 ± 120	1	^{124}Sn	1	1/2	240 ± 25	1
$^{69,71}\text{Ga}$	0	1,2	300 ± 40	3	^{132}Ba	0	1/2	65 ± 50	1
^{75}As	0	1,2	320 ± 30	6	^{134}Ba	0	1/2	70 ± 20	1
^{74}Se	0	1/2	230 ± 50	2	^{135}Ba	0	1,2	105 ± 5	5
^{76}Se	0	1/2	296 ± 56	1	^{139}La	0	3,4	75 ± 20	1
^{77}Se	0	0 ⁻	280 ± 110	1	^{141}Pr	0	2,3	85 ± 7	4
^{77}Se	0	1 ⁻	440 ± 60	1	^{143}Nd	0	3,4	72 ± 10	4
^{78}Se	0	1/2	300 ± 70	1	^{145}Nd	0	3,4	72 ± 10	3
$^{79,81}\text{Br}$	0	1,2	290 ± 25	7	^{155}Gd	0	1,2	115 ± 20	3
^{91}Zr	0	2,3	110 ± 20	3	^{157}Gd	0	1,2	120 ± 20	1
^{91}Zr	1	1,2,3,4	310 ± 50	3	^{159}Tb	0	1,2	85 ± 5	6
^{96}Zr	0	1/2	220 ± 50	1	^{169}Tm	0	0,1	85 ± 3	8
^{93}Nb	0	4,5	145 ± 20	5	^{183}W	0	0,1	75 ± 3	5
^{93}Nb	1	3,4,5,6	210 ± 40	4	^{192}Pt	0	1/2	52 ± 4	5
^{95}Mo	0	3	120 ± 20	2	^{194}Pt	0	1/2	70 ± 12	3
^{96}Mo	0	1/2	30 ± 20	1	^{195}Pt	0	0	93 ± 10	7
^{97}Mo	0	3 ou 4	130 ± 10	1	^{195}Pt	0	1	118 ± 6	20
^{107}Ag	0	0,1	140 ± 7	6	^{196}Pt	0	1/2	120 ± 18	2
^{109}Ag	0	0,1	132 ± 6	7	^{198}Pt	0	1/2	147 ± 25	1
^{110}Cd	0	1/2	120 ± 40	1	^{197}Au	0	1,2	126 ± 3	16
^{111}Cd	0	0,1	120 ± 15	4	^{198}Hg	0	1/2	130 ± 8	5
^{113}Cd	0	0,1	110 ± 15	4	^{199}Hg	0	0	225 ± 25	3
^{114}Cd			95 ± 25	1	^{199}Hg	0	1	320 ± 35	4
					^{201}Hg	0	1	450 ± 40	3
					^{201}Hg	0	2	320 ± 30	4

Valeurs $\overline{\Gamma}_\gamma$ des noyaux étudiés. Les informations relatives aux conditions expérimentales utilisées se trouvent dans les références 7.6, 7.7, 7.8, 7.10, 7.11, 7.12, 7.13, 7.16, 7.17.

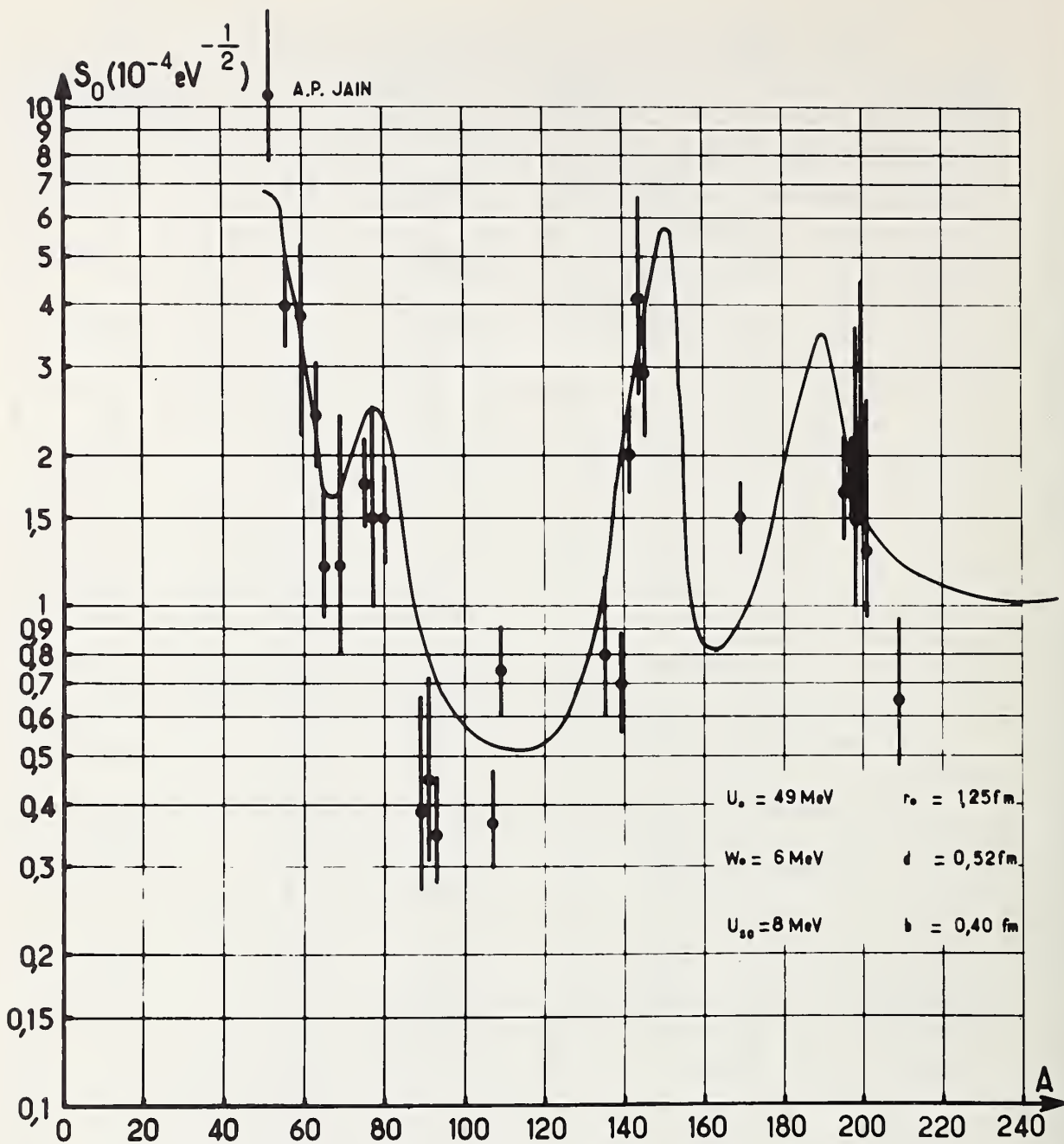


Fig. 1

● Saclay (D. Ph. N.)

Plot of the experimental values of S_0 versus the mass number A and comparison with the theoretical curve calculated by Jain.

Fig. 1

$\frac{D \text{ (eV)}}{\text{état de spin}}$

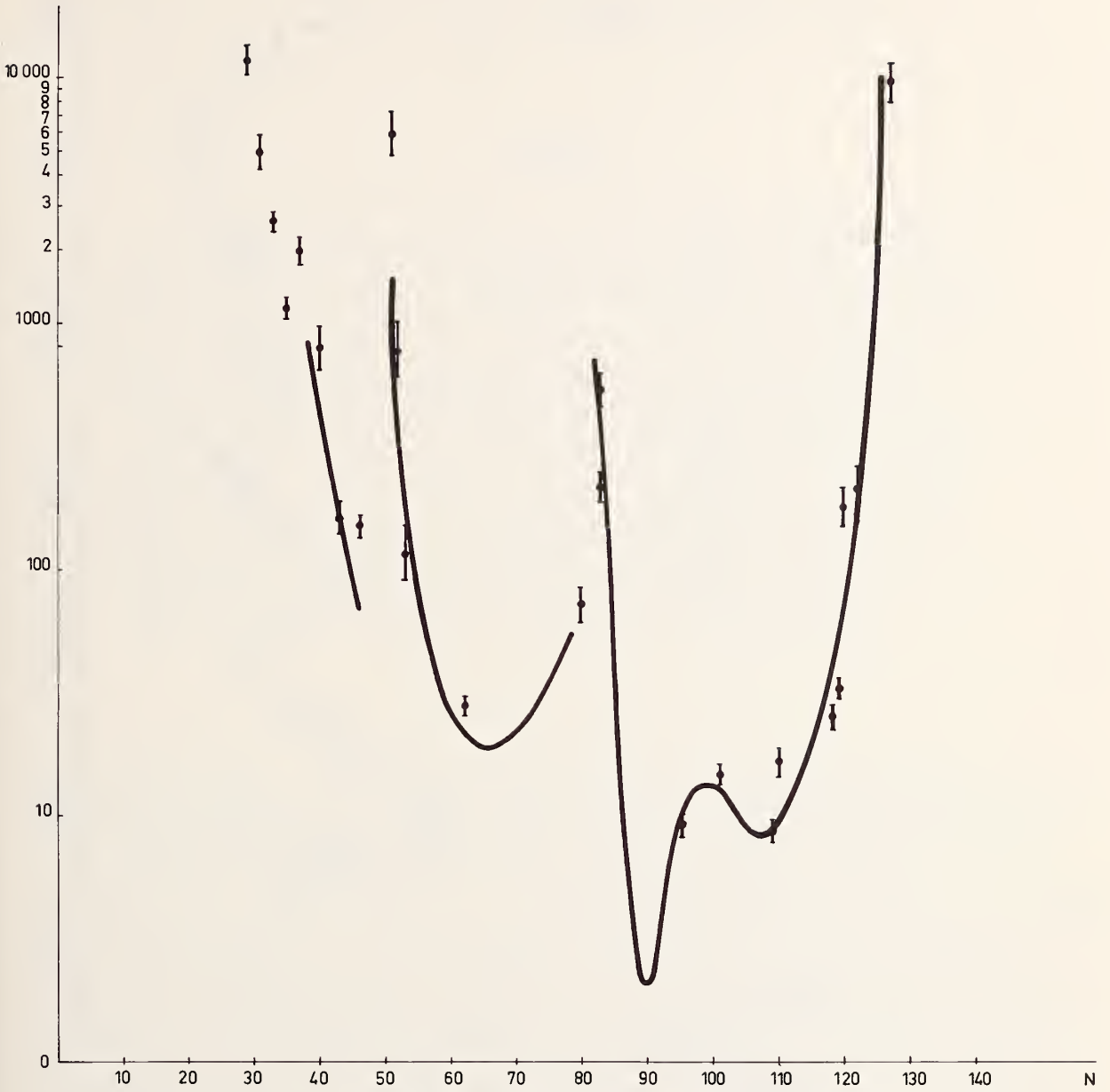


Fig. 2 - Plot of the mean level spacing \bar{D} versus the mass number A . The full curve was calculated by Cameron using Newton's formula.

Fig.2

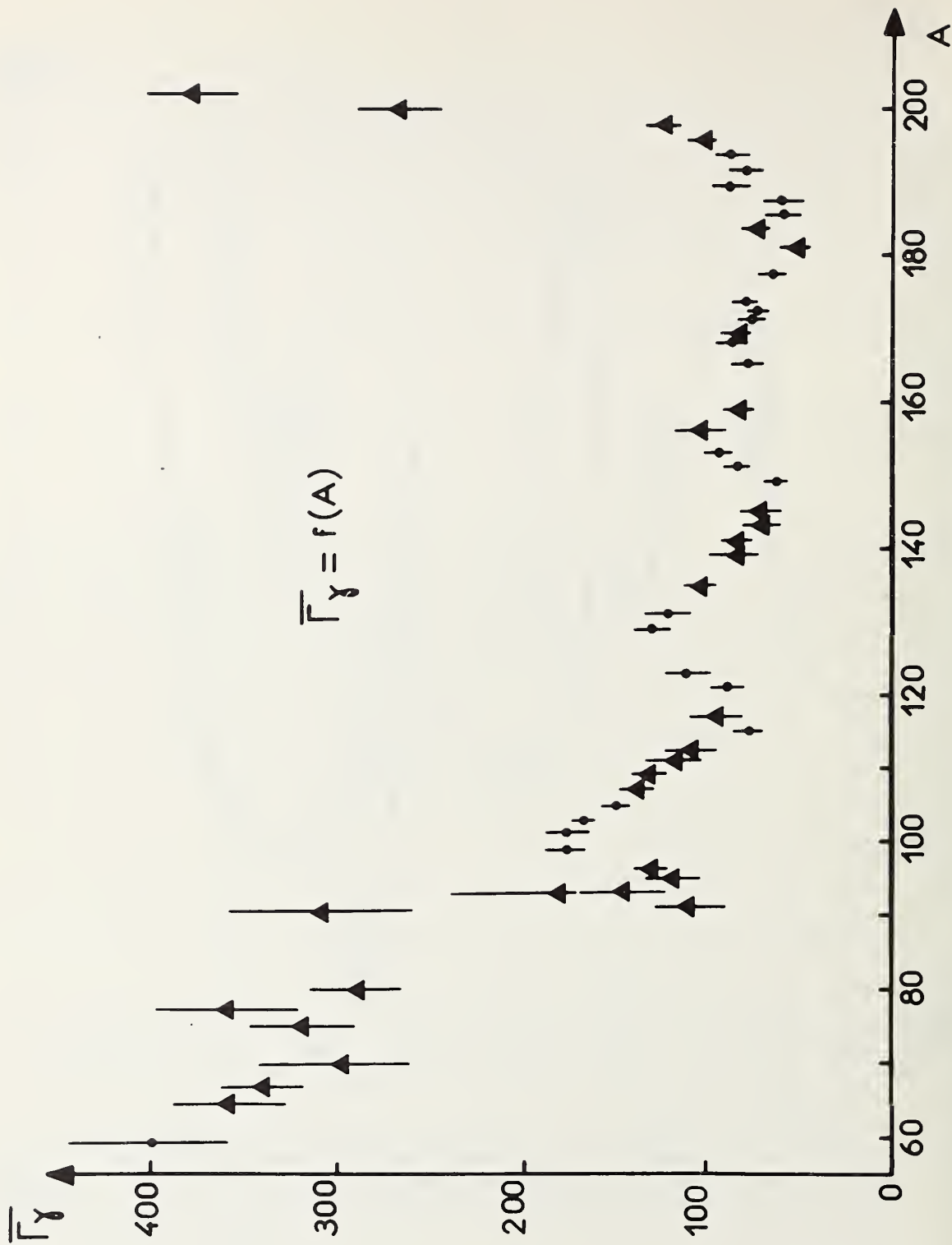


Fig.3

Fig. 3 - Plot of the total radiative width $\bar{\Gamma}_\gamma$ versus the mass number.

THE THERMAL CROSS SECTIONS AND
PARAMAGNETIC SCATTERING CROSS SECTIONS OF THE Yb ISOTOPES*

S. F. Mughabghab and R. E. Chrien
Brookhaven National Laboratory
Upton, New York 11777

ABSTRACT

The total cross sections of oxide samples highly enriched in the Yb isotopes 170, 171, 172, 173, 174, and 176 have been measured at the BNL fast chopper at the BGRR, using 9.9 and 29.74 m flight paths. The total cross sections of the isotopes are found to be 17.0 ± 1.0 b, 57 ± 3 b, 10.2 ± 1.5 b, 28 ± 2 b, 142 ± 5 b, 14.9 ± 1.0 b, respectively. We obtain an average value of 5.2 ± 0.9 b for the paramagnetic scattering cross section of Yb^{+++} at 0.0253 eV, from the measurement on Yb-170, -172, and -176, contrasted with a value of 26.1 ± 2.5 b for Er^{+++} . When the isotopic total cross sections are compounded to form the total cross section of Yb, a value of 67.6 ± 2.0 b is obtained. This is based in part on a thermal value of 3795 ± 760 b for Yb-168 which is calculated from the resonance parameters. Finally, the absorption and the nuclear scattering cross sections of these isotopes at 0.0253 eV will be discussed.

This is part of a program whose main aim is the study of the neutron resonance structure in the rare earth region. During the course of these investigations we became aware of the lack of thermal neutron cross section measurements for the Yb isotopes. For the above reason we decided to extend the energy region of our measurements down to thermal. In order to cover the region from 2.09 to 0.0243 eV, two runs were taken: one with a 512 μsec delay and a 2 μsec channel width; another with a 1024 μsec delay and an 8 μsec channel width, using a 9.90 m flight path and a He^3 detector. Supplementary measurements covering a higher energy region for a study of the resonance parameters were undertaken employing a bank of BF_3 counters at 29.74 meters. Transmission measurements of oxide samples of Yb-170, -171, -172, -173, -174, -176 with respective enrichments of 85.4%, 95.96%, 97.5%, 92.6%, 98.97%, and 97.77% were carried out at the BNL fast chopper facility at the BGRR. The data were collected by an on-line SDS-910 computer.

* Work performed under the auspices of the U.S. Atomic Energy Commission.

Part of the memory was split into two adjacent portions, each with 512 channels: one for storage of the open beam spectrum, the other for the sample-in beam spectrum. The sample holders, 3/4" thick in beam direction, were placed in a slit package at the entrance stator. Because the cyclor is located at the exit stator of the chopper, a special cycling procedure is adopted to take care of proper normalization of the transmission data. For each transmission measurement two runs are taken: one in which the sample is placed in one slit and a dummy in the other; another run in which the sample and dummy are interchanged. The selection of the appropriate slit was determined by a moving stage carrying three 3-inch lucite plugs at the exit stator. The reduction of the raw data to transmission form was carried out on the SDS computer at the termination of the experiment.

In Fig. 1 we show the Yb-173 sample spectrum in the thermal energy region. The type of analysis described earlier was applied to this run. (The background rate in the thermal region is about 1% of the open beam rate.) The final transmission of Yb-173 sample is shown in Fig. 2, in which dead-time corrections were applied to the data. Since these Yb samples are in oxide form and are not 100% isotopically enriched, several corrections had to be applied before the cross section of the isotope was known. These included corrections for oxygen and isotopic impurities. However, during the course of the experiment it became clear to us that these rare-earth oxides absorb water. This necessitated doing a separate experiment to determine the amount of water absorption in these samples.

A sample of natural ytterbium oxide was placed in an aluminum crucible and heated at 800°C under a vacuum. Water absorption for the ytterbium oxide was determined to be 0.19% by weight.

The measured total cross sections at 0.0253 eV are included in the second column of Table I. The first column of Table I shows the natural abundances of the various Yb isotopes in percentages. It is possible to decompose the total cross section into its partial cross sections.

$$\sigma_T = \sigma_a + \sigma_s + \sigma_{pm}$$

where σ_T , σ_a , σ_s , and σ_{pm} are the total, absorption, nuclear scattering, and paramagnetic scattering cross section, respectively. Adopting the resonance parameters of Mughabghab and Chrien [1] and the scattering radii of Chrien, et al. [2], we generated the absorption and nuclear scattering cross sections and absorption resonance integrals for the various isotopes with the aid of the INTTER CODE [3].

For example, assuming that Yb-170 and -172 do not possess bound levels that contribute significantly to the thermal cross section, we get paramagnetic scattering cross sections of 5.0 ± 1.5 b and 5.5 ± 1.7 b. Similarly, adopting an absorption cross section [4] of 5.5 ± 1.0 b for Yb-176, we get $\sigma_{pm} = 5.2 \pm 1.6$ b for Yb-176. Averaging these values, we obtain 5.2 ± 0.9 b for the paramagnetic scattering cross section of Yb⁺⁺⁺ at 0.0253 eV. This is to be contrasted with a value [5] of 26.1 ± 2.5 b for Er⁺⁺⁺. Furthermore, fitting the thermal cross sections of Yb-174 with

$$(\sigma_T - \sigma_{pm}) = \sigma_s + \frac{b}{\sqrt{E}},$$

a nuclear scattering and an absorption cross section of 72.0 ± 5.0 b and 64.8 ± 5.0 b are derived for Yb-174. Similar procedures applied to Yb-171 and Yb-173 indicate that the nuclear scattering cross sections of bound levels for these two isotopes are insignificant. As a result we adopted the calculated values for the nuclear scattering cross sections of these isotopes. This would result, then, in an absorption cross section of 48.4 ± 3.3 b and 19 ± 2 b for Yb-171 and Yb-173, respectively. These values are in good agreement with those of Walker [6], but not of Dobrozemsky, et al. [7].

Compounding all the isotopic cross sections, the following values are obtained for natural Yb: $\sigma_T = 67.6 \pm 2.0$ b, $\sigma_s = 25.6 \pm 3.5$ b, and $\sigma_a = 36.8 \pm 4.1$ b. These are to be compared with previously published values of $\sigma_T = 64 \pm 2$ b [8], $\sigma_s = 30 \pm 3$ b [9], and $\sigma_a = 37.5 \pm 4.0$ b [10].

In Table II we have included the calculated values of the absorption resonance integrals for all the isotopes due to the resolved positive energy levels and from the bound levels. When the various values are compounded to get the absorption resonance integral for the element, we get a value of 174 ± 24 b. The error on this quantity is derived from the errors on Γ_n and Γ_γ . This value is in good agreement with measurements [11] which give 197 ± 20 b for the absorption resonance integral.

References

1. S. F. Mughabghab and R. E. Chrien, Bull. Am. Phys. Soc. 10, 513 (1965). [See also NEUTRON CROSS SECTIONS, BNL 325, 2nd Ed., Suppl. 2 (1966).]
2. R. E. Chrien, S. F. Mughabghab, M.R. Bhat, and A. P. Jain, Phys. Letters 24B, 573 (1967) and private communication.
3. T. E. Stephenson and S. Pearlstein, Nucl. Sci. Eng. (in press) and private communication.
4. D. J. Hughes and R. B. Schwartz, NEUTRON CROSS SECTIONS, BNL 325, 2nd Ed. (1958).
5. S. F. Mughabghab, R. E. Chrien, and M. R. Bhat, Phys. Rev. 162, 1130 (1967).
6. W. H. Walker, Thesis (McMaster University). Quoted by R. Dobrozemsky, et al., below.
7. R. Dobrozemsky, et al., Paper CN 23/82 presented at Conf. on Nuclear Data - Microscopic Cross-Sections and Other Data Basic for Reactors, Paris (1966).
8. R. L. Zimmerman, et al., Nucl. Phys. A95, 683 (1967).
9. M. Atoji, Phys. Rev. 121, 610 (1961).
10. H. Pomerance, Phys. Rev. 83, 641 (1951).
11. J. J. Scoville and J. W. Rogers, Trans. Am. Nucl. Soc. 8, 290 (1965).

TABLE 1
Partial Cross Sections of the Yb Isotopes

	Yb	Yb-168	Yb-170	Yb-171	Yb-172	Yb-173	Yb-174	Yb-176
Natural Abundance		0.135%	3.03%	14.31%	21.82%	16.13%	31.84%	12.71%
σ_T (b)	67.6±2.0	3795 ±760 ^a	17.0±1.0	57 ±3	10.2 ±1.5	28 ±2	142 ±5	14.9±1.0
σ_s (b)	25.6±3.5	13.7±3.7 ^a	2.6±0.5 ^b	3.4±0.9 ^b	4.3 ±0.9 ^b	3.8±0.6 ^b	72 ±5	4.2±0.8 ^b
σ_a (b)	36.8±4.1	3774 ±760 ^a	9.4±0.9 ^b	48.4±3.3	0.38±0.05 ^b	19 ±2	65 ±5	5.5±1.0 ^c
σ_{p_n} (b)	5.2±0.9 ^d	5.2±0.9 ^d	5.0±1.5	5.2±0.9 ^d	5.5 ±1.7	5.2±0.9 ^d	5.2±0.9 ^d	5.2±1.6

^a Values calculated from resonance parameters of V. L. Sailor, et al., Phys. Rev. 96, 1014 (1954). See also Ref. 1.

^b Values calculated from resonance parameters of Ref. 1.

^c Value adopted from Ref. 4.

^d Value is an average value found in present experiment.

TABLE II

Absorption Resonance Integrals of Yb Isotopes

Isotope	Energy Range (eV)	I(+) (b)	I(-) (b)	I(total) (b)
Yb-168	0.597-22.6	30954.1	----	30954.1
Yb-170	8.13 -449	319.1	----	319.1
Yb-171	7.93 -225	287.3	19.2	306.5
Yb-172	139.8 -818	23.5	----	23.5
Yb-173	4.51 -210	379.3	4.5	383.8
Yb-174	345 -910	5.0	28.8	33.8
Yb-176	148.8 -5787	5.3	2.3	7.6

I(+) and I(-) are the contributions to the absorption resonance integrals from positive energy levels and bound levels, respectively. A value of $\langle I_\gamma \rangle = 75 \pm 7$ mV is assumed in the calculation.

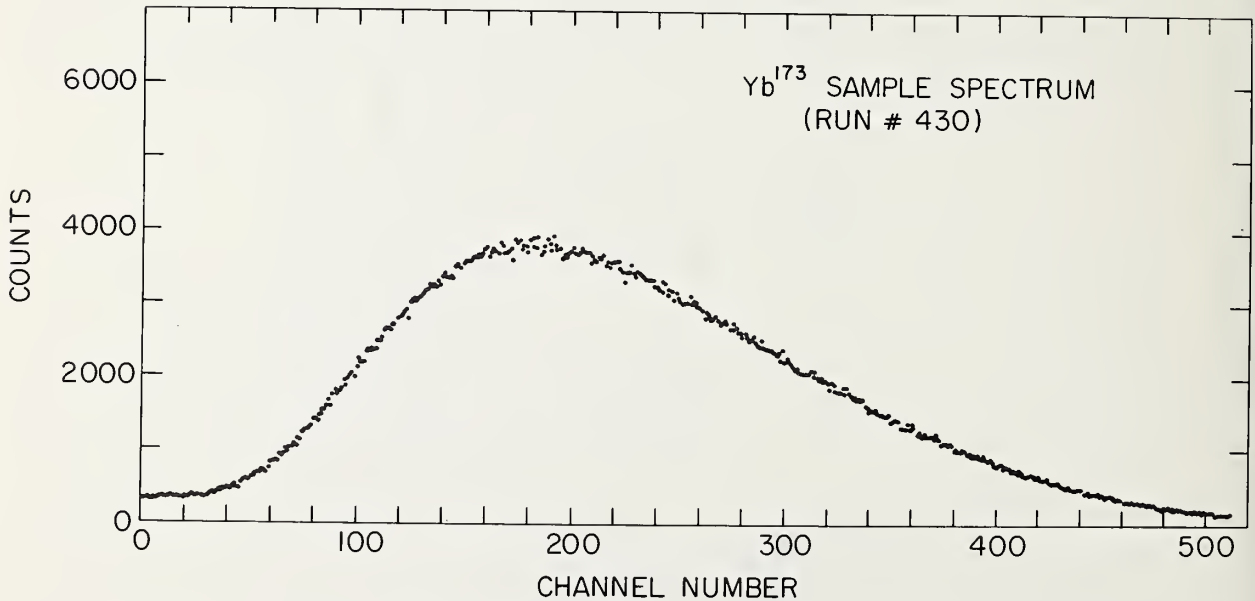


Figure 1. Yb¹⁷³ Sample Spectrum in the Energy Range from 0.506 to 0.0243 eV.

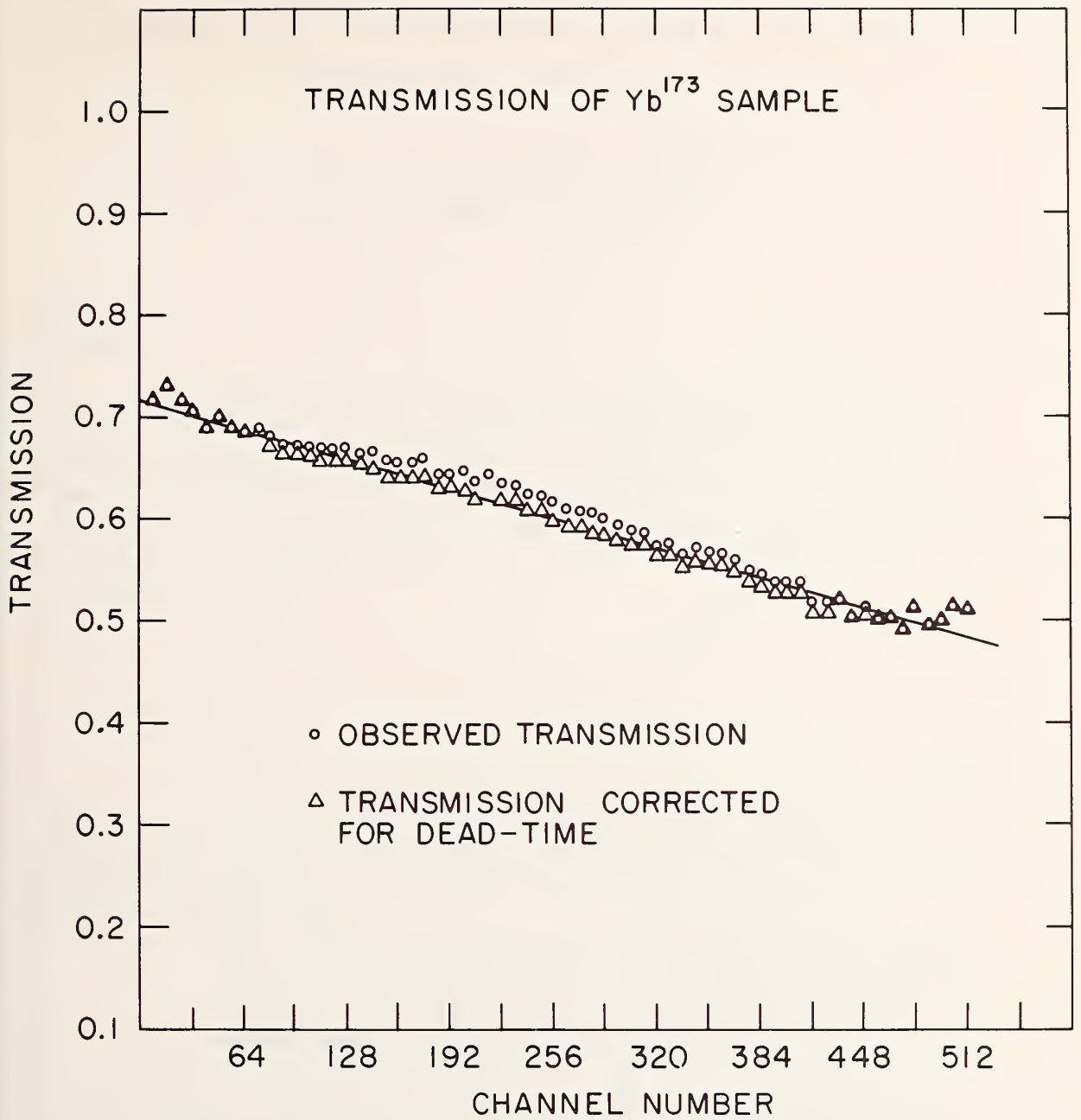


Figure 2. Transmission of Yb¹⁷³ sample in the Energy Range from 0.506 to 0.0243 eV.

CROSS-SECTION MEASUREMENTS FOR THE REACTION $^{152}\text{Eu}(n, \gamma)^{152\text{m}}\text{Eu}$
BETWEEN 0.02 eV and 0.5 eV

F. POORTMANS, A. FABRY, I. GIRLEA ^x
S.C.K. - C.E.N., Mol, Belgium

ABSTRACT

The activation method has been used to measure the cross section for the reaction $^{151}\text{Eu}(n, \gamma)^{152\text{m}}\text{Eu}$ between 0.02 and 0.5 eV. These data are important as ^{151}Eu is used as an activation detector for spectral index measurements in reactors. Monochromatic neutrons were produced with the BR2 crystal spectrometer. Data are given for several neutron energies below 0.5 eV. Isomeric ratios for the resonances at 0.3210 eV and 0.460 eV are deduced.

x

x

x

The main contributions to the neutron cross-sections for ^{151}Eu below 1 eV come from a bound level and two resonances respectively at 0.321 eV and 0.460 eV. In a recent evaluation report [1] the different experimental data which are available are discussed. Our aim was to perform the following experiments.

- 1) Total cross-section measurements between 0.02 eV and 1 eV
- 2) Cross-section measurements for the formation of the 9.3 hr $^{152\text{m}}\text{Eu}$ isomeric state between 0.02 eV and 0.5 eV in order to determine the isomeric ratios for the bound level and the two resonances at 0.321 eV and 0.460 eV.

In this paper, we present our results for the isomeric ratio of the two positive energy resonances and a precise value of the 2 200 m cross-section. Further work is in progress.

The BR2 crystal spectrometer has been used as a monochromatic neutron source. Pb (111) and Be(121) have been used as monochromators respectively below and above 0.1 eV.

^x on leave from Institute of Atomic Physics, Bucarest, Rumania

The following resolutions are obtained :

$$\text{Pb}(111) : \Delta E/E = 2.9 \cdot 10^{-2} \text{ at } 0.1 \text{ eV}$$

$$\text{Be}(121) : \Delta E/E = 1.5 \cdot 10^{-2} \text{ at } 0.46 \text{ eV}$$

The higher order contamination has been determined by the method of Haas and Shore [2] and accurately measured at 0.0976 eV with a Sm filter and 0.654 eV with an Ir filter.

The targets, prepared by CBNM, Euratom, Geel are Eu-Al alloys, containing approximately 5% of Eu. The total amount of Eu is known to better than 1%. The absolute neutron flux is measured by activating thin gold foils and checked for relative values with a BF_3 counter.

The Eu activity is measured with a γ - γ coincidence spectrometer consisting of two 4" x 4" NaI (Tl) crystals. This counting system has been calibrated using a 4π β -counter consisting of two CsI crystals [3]. The precision on the calibration is 2% but improvements are planned for the near future.

Table 1 shows our present results for the total cross-section and the activation cross-section for the formation of the 9.3 hr $^{152\text{m}}\text{Eu}$. After subtracting the contributions from the other resonances at 0.321 eV and 0.460 eV, the isomeric ratios, R, for these two resonances have been deduced. Although these resonances have the same spin 3 [4], the isomeric ratio is quite different as has also been shown by the relative measurements of Wood [5].

Table 1

Experimental cross-sections and isomeric ratios
for the 0.321 eV and 0.460 eV resonances

E (eV)	σ_t (barns) for natural Eu	σ_{act} (barns) for ^{151}Eu	R
0.0253	4601 \pm 70	3003 \pm 80	
0.321	3126 \pm 40	1978 \pm 60	0.35 \pm 0.018
0.460	10989 \pm 130	5788 \pm 190	0.25 \pm 0.009

The authors wish to thank Mrs. De Corte and Mr Cops for assistance during the experiments, Mr Jacquemin for the calibration of the detector, Mr Van Audenhove of CBNM for preparing the targets.

REFERENCES

- [1] P.P. Damle, A. Fabry and H. Van den Broeck, Report BLG-421(1968)
- [2] R. Haas and F.J. Shore, Rev. Scient. Instr., 30 (1959), 17
- [3] This counter has been developed by R. Jacquemin of C.E.N.-Mol
- [4] A. Stolovy, Phys. Rev. 134 (1964) B68
- [5] R.E. Wood, Phys. Rev. 95 (1954) 453

H. K. Vonach, W. G. Vonach, Technische Hochschule München,

H. Münzer, (Universität München) and P. Schramel

(Ges. f. Strahlenforschung, Neuherberg)

German Federal Republic

Abstract

Relative cross-sections for the reactions F^{19} (n,2n), Mg^{24} (n,p), Al^{27} (n, α), Ti^{48} (n,p), V^{51} (n, α), Fe^{56} (n,p), Cu^{65} (n,2n), Ag^{107} (n,2n) Ag^{106m} , In^{115} (n,2n) In^{114m} , Ta^{181} (n,2n) Ta^{180m} and Au^{197} (n,2n) were determined. An overall accuracy (including all sources of systematic errors) of 1% was obtained for the ratios $\sigma(E_n)/\sigma(14.7 \text{ MeV})$. Contrary to earlier measurements, however in agreement with recent results of Bormann very little structure was found in the excitation functions. In addition ratios of the cross-sections to the Al^{27} (n, α) cross-section were determined for 8 of the reactions studied at 14.7 MeV with an overall accuracy of about 2 - 3%.

1. Introduction

Precision measurements of excitation functions of neutron induced reactions were performed for two reasons. Firstly contradictory results have been reported on the existence of Ericson fluctuations in these cross-sections. Strohal, Cindro et al. [1,2] claimed the existence of large fluctuations in the F^{19} (n,2n) and Al (n, α) cross-sections and Csikai [3] found such fluctuations even for reactions involving heavier nuclei up to Tantal. Careful measurements performed by Riehle and Bormann [4] as well as by Thompson and Ferguson [5] on some of the reactions studied in ref. [1] to [3] failed to reproduce the results of these authors and showed very little fine structure of the cross-sections. Although these latter results seem to deserve much more confidence for a number of reasons (see discussion in ref. [4]) additional measurements especially on the reactions not checked in ref. [4] and [5] seemed necessary in order to definitely settle the question of the existence of the claimed cross-section-fluctuations.

Secondly it appeared to the authors that it would be highly desirable to increase the accuracy of excitation function measurements especially for those reactions which are commonly used as cross-section standards, such as the $\text{Al}^{27} (n,\alpha) \text{Na}^{24}$, $\text{Fe}^{56} (n,p) \text{Mn}^{56}$ and $\text{Cu}^{65} (n,2n) \text{Cu}^{64}$ reactions and that a substantial improvement in accuracy could be obtained by a careful analysis and minimization of all possible sources of systematic errors involved in such measurements.

2. Experimental Procedure

The excitation functions were measured in the usual way by means of the activation method. Neutrons are produced in the $\text{T}(d,n)\text{He}^4$ reaction by bombardment of a T - Ti target with 120 keV deuterons produced by the 400 keV van-de-Graaff accelerator of the Gesellschaft für Strahlenforschung. The energy of the emitted neutrons depends on the emission angle due to the center-of-mass motion and the dependence of the neutron flux on emission angle can be calculated easily, as the differential cross-section of the $\text{T}(d,n)\text{He}^4$ reaction is known to be isotropic in the c. m. system at the deuteron energy used. Thus excitation functions could be measured by means of irradiation of samples of the materials to be investigated at different neutron emission angles and comparing the activities formed by the reactions in the various samples. The target assembly used for these irradiations is shown in fig. 1. The samples (high purity metal sheet) were clamped to an aluminum ring of 200 mm diameter centered around the target. Samples were placed in 6 degree intervals corresponding to 30 to 50 keV steps in neutron energy and had themselves an angular extension of 4.5° . The neutron energy spread at any particular angle due to the effects of deuteron energy loss and small-angle scattering in the target is about 100 to 150 keV [4], thus the additional energy spread introduced by the mentioned angular extension of the samples (20-40 keV) did not appreciably deteriorate the energy resolution of the measurements. The target-sample distance of 100 mm was chosen as a compromise between the requirements of intensity and these of minimizing the systematic errors due to the uncertainty in the target-sample distance. As two samples were activated for each energy (one on each side of the ring) possible deviations of the center of the deuteron beam spot from the target center did not introduce errors. Thus the geometrical error is essentially determined by the deviation (in beam direction) of the target plane from the center of the aluminum ring. As this deviation could be kept below 0.15 mm the geometrical errors were kept below 0.6%. The error due to possible excentricities of the ring was smaller than 0.2%. The air-cooled aluminum target assembly was designed to have minimum weight in order to minimize the neutron attenuation and scattering correction to be discussed later. Except for one case, activities formed by the reactions were measured by means of a large (5" x 5") NaJ well crystal. In all cases integral measurements were performed, that is all

γ -pulses exceeding 30 keV were counted. Thus a high detection efficiency and very small sensitivity of the efficiency to electronic drifts was obtained. The absence of interfering activities from other reactions than those studied and from activation of chemical impurities was checked by measuring decay curves for the various samples after preliminary irradiations. The activity of Ta^{180m} formed by the reaction $Ta^{181}(n,2n)Ta^{180m}$ was measured by means of β -counting with a CH_4 flow-counter as only a rather low energy gamma-radiation is emitted in this case.

3. Results

From the specific activities of the samples determined in the described way and the known angular dependence of the neutron flux relative values of the cross-sections were calculated. These values were corrected for the effects of angle-dependent neutron attenuation in the target assembly and for the contribution of elastically scattered neutrons to the activation of the samples. The attenuation corrections simply involved multiplication of the uncorrected cross-sections by a factor $\exp \Sigma_{Al} \cdot d_{Al}(\theta) + \Sigma_{Cu} d_{Cu}(\theta)$, $d_{Al}(\theta)$ and $d_{Cu}(\theta)$ being the thicknesses of aluminum and copper traversed by a neutron produced at the center of the target with emission angle θ . The total macroscopic cross-sections Σ_{Al} and Σ_{Cu} were calculated from the corresponding macroscopic cross-sections $\sigma_{Al} = 1.75$ b and $\sigma_{Cu} = 2.90$ b for 14 MeV neutrons. The amount of the correction was 0.4 to 7.5%. Using the above correction it is assumed that all neutrons interacting with the target assembly are completely absorbed. A large fraction of these neutrons, however, is scattered elastically and thus contributes to the activation of the samples at other angles than those at which they were emitted originally. The intensity of the elastically scattered neutrons (the ratio $\phi_{sc}(\theta)/\phi_{direct}(\theta)$ of the scattered to the direct flux) versus angle θ was determined by means of numerical integration over the contribution of all volume elements of the target assembly and backing to the scattered intensity for a particular angle θ . The legendre polynomial expansion of the differential elastic scattering cross-sections of Al and Cu given by Altamirano [9] was used for these calculations. Fig. 2 shows the results of the calculations. The total scattering contribution as well as the separate contribution of the neutrons scattered by the target backing and by the aluminum target assembly are shown in the figure as a function of the observation angle θ . As the figure shows corrections up to 2.9% have to be applied even for the extremely light-weight set-up used in this experiment and it appears that scattering corrections are absolutely necessary for any high precision measurements of excitation functions. Possibly a large part of the discrepancies observed in previous measurements of excitation functions is due to neglecting these effects. The cross-sections were corrected for the scattering contribution by multiplication with the correction factor $1/(1+\phi_{sc}(\theta)/\phi_{direct}(\theta))$. The corrected excitation functions are shown in figs. 3 to 10. The cross-sections are arbitrarily

normalized to unity at 14.7 MeV, the size of the data points corresponds to the statistical errors (0.2 - 0.75%). The smooth curves are least square fits of first or second degree polynomials except for the $Mg^{24}(n,p)$ and $Al(n,\alpha)$, where definitely fine structure is present and the smooth curves were drawn according to "eye-inspection". Numerical values of these fit-curves describing the relative cross-sections are given in table 1 in 0.2 MeV steps. Also shown in the figures are the excitation functions reported in ref. 1 - 5. Our data definitely support Bormanns conclusion that the large fluctuations found by Strohal and Czikai do not exist and are probably due to systematic errors. Only in the two reactions $Mg^{24}(n,p)$ and $Al(n,\alpha)$ some structure (however completely different from Strohal's results) seems to be definitely present; for all reactions involving nuclei heavier than aluminum no fine structure is detectable within the experimental error about 1%. The error of the individual cross-section values (that is of the ratios $\sigma(E_n)/\sigma(14.7 \text{ MeV})$) is due to both the statistical errors (0.2 - 0.75%) and the following systematic errors:

- 1) The error in the target-sample distance. As discussed earlier, this contributes at most 0.6%.
- 2) The errors of the attenuation correction. This is due to the uncertainty of the total cross-sections used and amounts to about 5% of the correction, that is at most 0.35%.
- 3) The error of the scattering correction. This is predominantly due to the uncertainties of the differential elastic cross-sections and amounts to about 10% of the correction, that is at most 0.3%.
- 4) The error in sample weight. This was smaller than 0.05%.
- 5) The error in the decay corrections due to uncertainties in the half-lives of the activities. This was minimized by measuring each set of samples twice with the sequence of the samples reversed in the second measurement. In this way the error was kept below 0.1% also.
- 6) Errors due to electronic shifts of the detection threshold contributed less than 0.1%.

Combining the effects of these errors it can be shown that the maximum systematic error for the quantity $\sigma(E_n)/\sigma(14.7 \text{ MeV})$ does not exceed 0.9% for all neutron energies and n reactions investigated. This maximum systematic error essentially determines the accuracy of the fit-curves tabulated in table 1 as the influence of the individual data points on the parameters of the fit curves is rather small except for Mg and Al where however the statistical error (0.2%) is small compared to the systematic error anyway. Thus it is believed that the cross-section ratios as given in table 1 do have an overall accuracy of better than 1%. In addition ratios of the cross-sections to the $Al(n,\alpha)$ cross-section were determined for 8 of the reactions investigated at

14.7 MeV. An accuracy of 2 - 3% (including all systematic errors) was obtained by means of careful efficiency calibrations of the well crystal used. The experimentally determined ratios as well as the absolute cross-sections obtained with a value of 111.5 mb for the Al(n, α) cross-section are given in table 2. The value of 111.5 mb was obtained as a weighed average of all measurements previously reported by Nagel [10].

4. References

1. N. Cindro et al. Phys. Letters 6, 205 (1963).
2. P. Strohal et al. Phys. Letters 10, 104 (1964).
3. J. Csikai Proc. Int. Conf. on the Study of Nuclear Structure with Neutrons, Antwerpen 1965.
4. M. Bormann and I. Riehle Z. f. Physik 207, 64 (1967).
5. J. M. Ferguson and I. C. Albergotti Nucl. Phys. A 98, 65 (1967).
6. C. F. Cook and T. W. Bonner Phys. Rev. 94, 651 (1954).
7. J. H. Coon et al. Phys. Rev. 88, 562 (1952).
8. D. Meyer and W. Nyer LA - 1279 (1951).
9. C. P. Altamirano and S. T. Perkins TID 21629 (1964).
10. W. Nagel Thesis Amsterdam 1966.

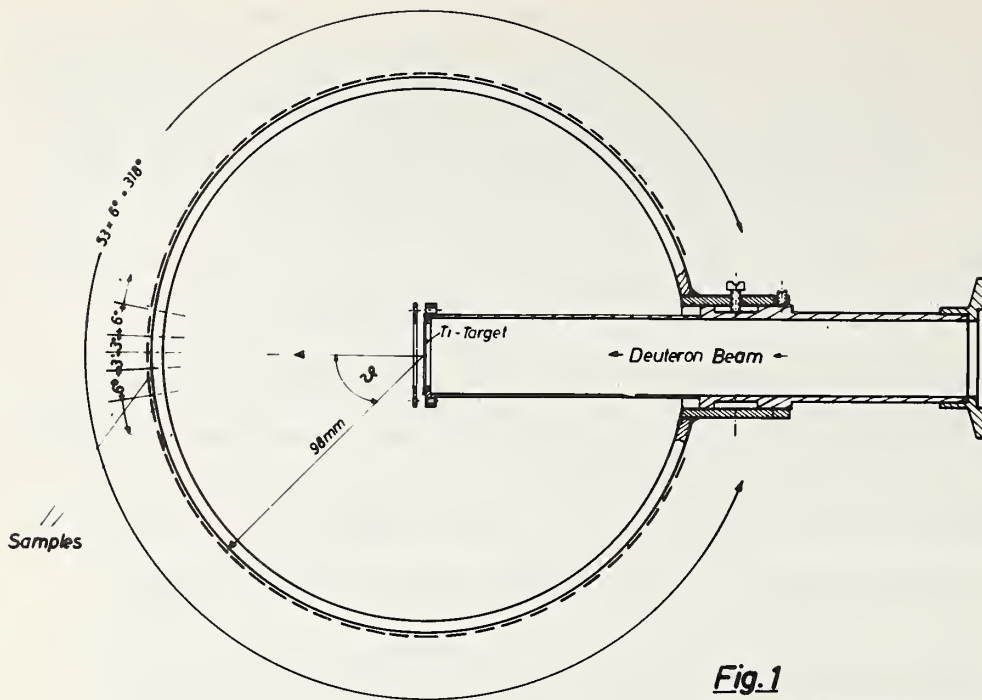


Fig.1
Target Assembly

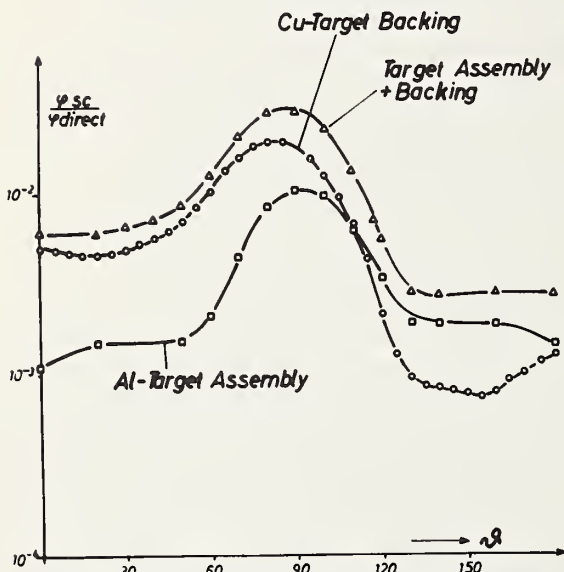


Fig.2 Contribution of the Neutrons Scattered Elastically by the Target Assembly and Backing to the Activation of the Samples.

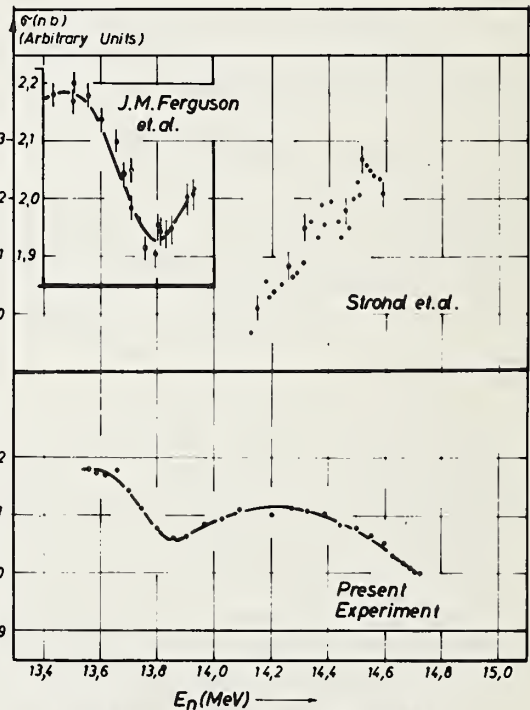


Fig.4 Excitation Function of the Reaction $Mg^{24}(n,p)Na^{24}$

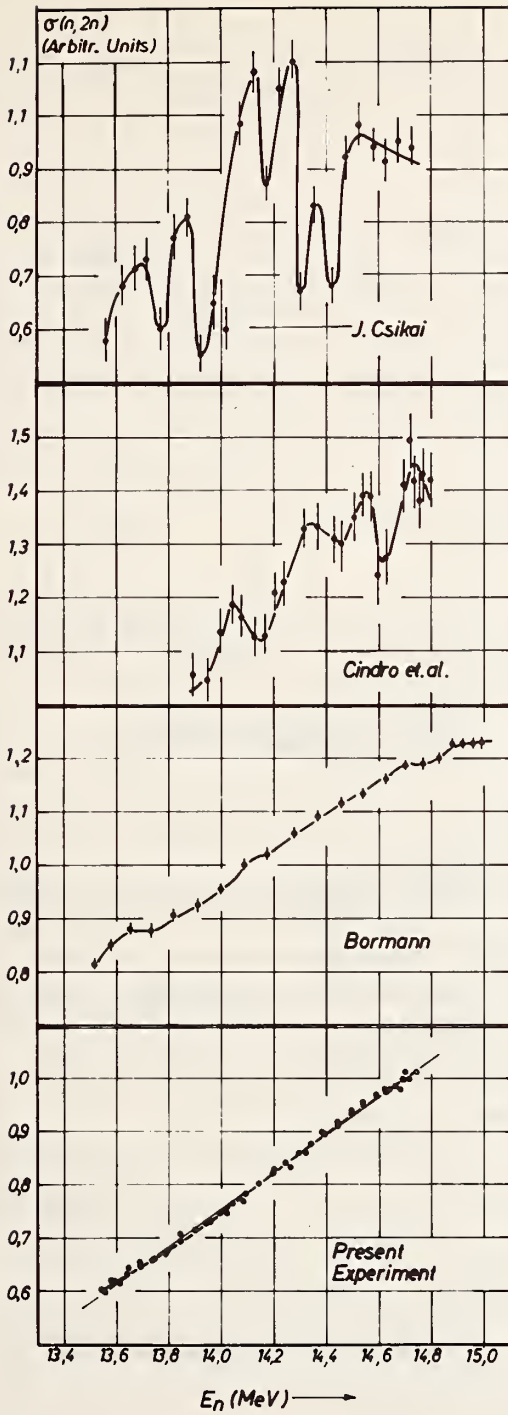


Fig. 3 Excitation Function of the Reaction $F^{19}(n,2n)F^{18}$

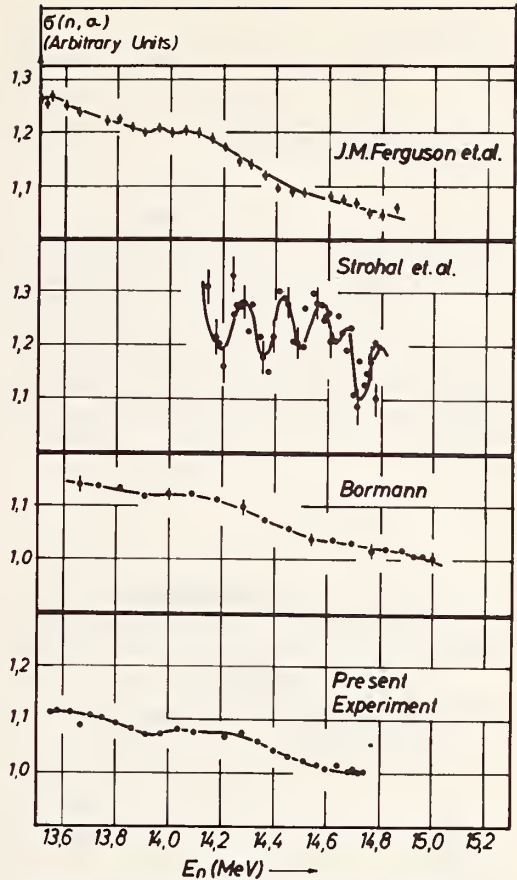


Fig. 5 Excitation Function of the Reaction $Al^{27}(n,\alpha)Na^{24}$

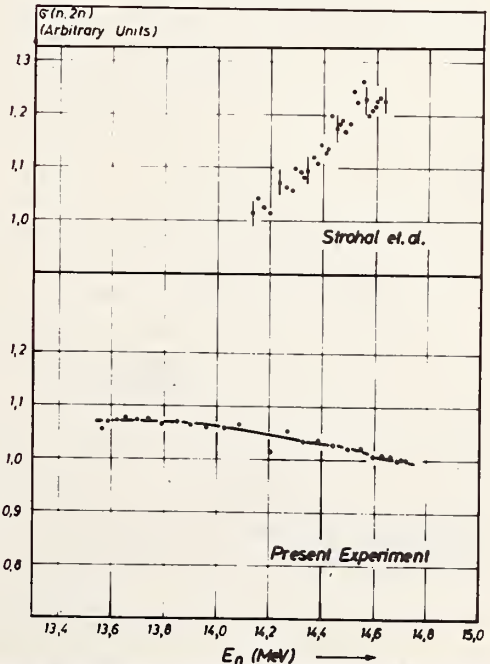


Fig. 6 Excitation Function of the Reaction $Fe^{56}(n,p)Mn^{56}$

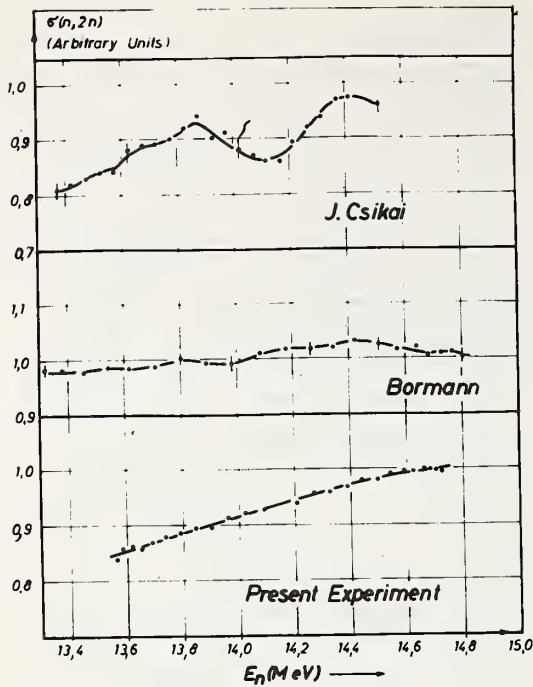


Fig. 7 Excitation Function of the Reaction $\text{Cu}^{65}(n,2n)\text{Cu}^{64}$

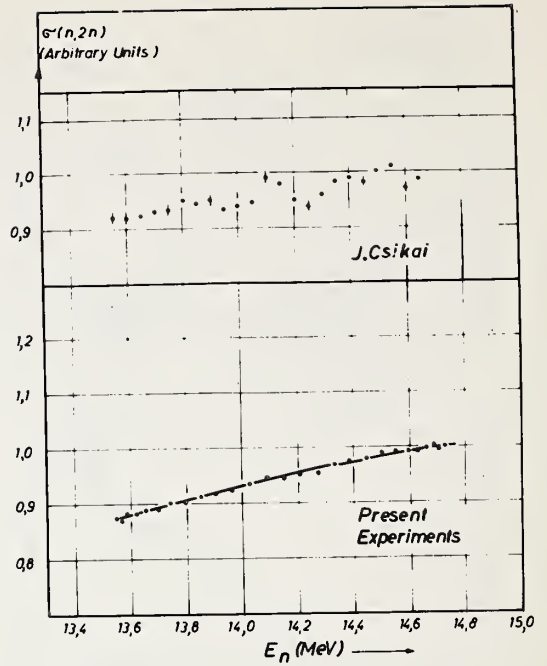


Fig. 8 Excitation Function of the Reaction $\text{Ag}^{107}(n,2n)\text{Ag}^{106m}$

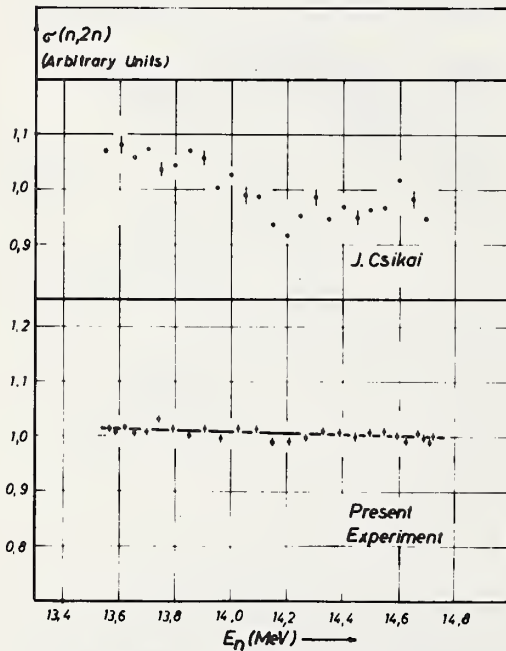


Fig. 9 Excitation Function of the Reaction $\text{Ta}^{181}(n,2n)\text{Ta}^{180m}$

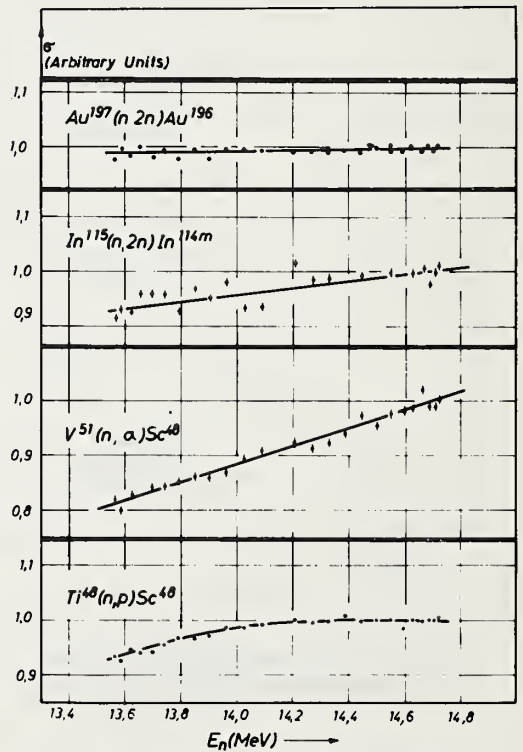


Fig. 10 Excitation Function of the Reactions $\text{In}^{115}(n,2n)\text{In}^{114m}$, $\text{V}^{51}(n,\alpha)\text{Sc}^{48}$, $\text{Ti}^{48}(n,p)\text{Sc}^{48}$, $\text{Au}^{197}(n,2n)\text{Au}^{196}$

T. Watanabe, G. E. Stokes, and R. P. Schuman
Idaho Nuclear Corporation, Box 1845, Idaho Falls, Idaho 83401

Abstract

The total neutron cross section of ^{204}Tl has been measured from 0.2 eV to 1000 eV. The sample was produced by irradiating natural thallium in the Engineering Test Reactor (ETR). The transmission data have been analyzed using the area method to obtain resonance parameters for the two resonances observed, at 122 and 796 eV. Problems associated with taking cross section measurements of a sample produced by neutron irradiation and unseparated from the feed material are discussed.

1. Introduction

The major effort in the Materials Testing Reactor (MTR) fast chopper program is to measure total neutron cross sections of highly radioactive isotopes, including fission products, heavy elements, and isotopes which are produced in reactors for special purposes. The isotope ^{204}Tl , being a pure beta emitter, has a potential application as a radioactive heat source. Since this isotope is produced by irradiating ^{203}Tl with neutrons in reactors, the knowledge of the neutron cross section of ^{204}Tl is of importance in determining the production of the isotope. The resonance parameters of this odd-odd isotope are also of interest in the area of nuclear systematics. For example, in the region of mass number 200, there is considerable difference between the measured average total radiation width and that predicted from theory [1]. The radioactive handling capabilities of the fast chopper were utilized in making the transmission measurements of this isotope. The results of these measurements and the calculated total cross sections are presented from 0.2 eV to 1000 eV.

2. Sample Preparation

One of the major problems of carrying out measurements with any radioactive sample is obtaining an adequate amount of material. For these measurements, the ^{204}Tl was produced by irradiating ^{203}Tl metal in the ETR. Since the ^{204}Tl is an isotope of the feed material, it cannot readily be separated. The irradiated sample was transferred directly to the fast chopper, where transmission measurements were taken and compared to the transmission of an identical but unirradiated sample of the feed material. The ratio of the two transmissions gives the transmission of the sample produced by irradiation. Some problems associated with using samples of this nature are: (1) there is a limit to the accuracy with which one can determine the atom per cent conversion in the irradiation; (2) large resonances in the feed material block out certain regions in the cross section measurements; and (3) in general, the isotope produced may have undergone substantial decay during irradiation which introduces additional contaminants. Figure 1 shows a

* Work performed under the auspices of the U. S. Atomic Energy Commission.

plot of the transmission through the ^{204}Tl and parent matched ^{203}Tl . One can readily see the energy regions which the parent isotope ^{203}Tl blacks out the neutron beam. For these measurements the decay product cross sections were taken to be flat. Since the decay product is ^{204}Pb this is perhaps a good assumption.

The irradiated and unirradiated samples of thallium metal consisted of two rectangular pieces having dimensions 2.022 cm long x .1519 cm wide x 2.78 cm high, and .536 cm long x .1524 cm wide x 2.78 cm high, respectively. Each piece was placed in a special designed aluminum holder. The unirradiated sample which was used as the "open" had an isotopic concentration of 29.5% ^{203}Tl and 70.5% ^{205}Tl . The irradiated sample had an isotopic concentration according to mass analysis at the Idaho Chemical Processing Plant of 3.55% ^{204}Tl , 24.88% ^{203}Tl , 71.57% ^{205}Tl , and 0.9% ^{204}Pb at the end of an irradiation period of 2.3 years.

2. Experimental Details

The MTR fast chopper and special radioactive sample changer, which were used to make the transmission measurements on ^{204}Tl , have been described in the literature [2,3]. Data were obtained at flight paths of 20 meters and 45 meters using BF_3 (96% enriched in ^{10}B) proportional neutron counters of 2.54 cm diameter. Automatic sample changing devices were used to permit counting of the open, sample, and background alternately for a given period of time in order to eliminate the effects of any slow-varying quantity such as the neutron flux from the reactor. The procedure used to determine the background has been described previously [4].

3. Analysis and Result

The transmission data are a composite which include contributions from ^{204}Tl and ^{203}Tl because the unirradiated sample contains more ^{203}Tl than the irradiated sample. Where the ^{203}Tl cross section varies slowly with the energy, the data have been corrected for the ^{203}Tl in a straightforward manner. Where the ^{203}Tl cross section has resonances, the data are not easily corrected for the presence of ^{203}Tl . To make the proper correction for ^{203}Tl , it would be necessary first to obtain ^{203}Tl cross section data that were measured with the same instrument resolution as these data were taken and with the sample thickness corresponding to the difference in the amount of ^{203}Tl between the irradiated and unirradiated sample. In our data the correction for ^{203}Tl is more critical because of the close proximity of ^{203}Tl and ^{204}Tl resonances. This effect is clearly exhibited in Figure 1. Since the required data on ^{203}Tl are not yet available, the data were not corrected in the vicinity of the ^{203}Tl resonances. The remaining contaminants were considered to have a flat cross section in the region of measurement and therefore could be adequately removed from the data.

The corrected transmission data for ^{204}Tl were analyzed for resonance parameters by the area method and the parameters are given in Table I. The 122.8 eV and 796 eV resonance parameters were obtained using the "thick sample" equation [5] relating the area and resonance

parameters. The total cross section data from 0.2 eV to 1000 eV are shown in Figure 2. These data include results of measurements taken at 20 and 45 meter flight paths.

The authors would like to thank R. G. Fluharty, M. S. Moore, and F. B. Simpson for their encouragement and assistance throughout this measurement. We also wish to express appreciation to H. G. Miller, D. B. Hansen, and D. R. Staples for technical aid with the equipment and to A. L. Dittmer for aid in processing the data.

4. References

1. A. G. W. Cameron, "Nuclear Radiation Widths", Can. J. Phys. 35, 666 (1957).
2. R. G. Fluharty, F. B. Simpson, and O. D. Simpson, "Neutron Resonance Measurements of Ag, Ta, and ^{238}U ", Phys. Rev. 103, 1778 (1956).
3. F. B. Simpson and R. P. Schuman, "Cross Section Measurements on Radioactive Samples", in Proceedings of the Symposium on Neutron Time-of-Flight Methods, Saclay, France, July 24-27, 1961, Session II, pp. 85-91 (1961).
4. O. D. Simpson, R. G. Fluharty, M. S. Moore, N. H. Marshall, F. B. Simpson, G. E. Stokes, T. Watanabe, and T. E. Young, "The Determination of Backgrounds for Neutron Time-of-Flight Spectrometers", Nucl. Instr. Methods 30, 293 (1964).
5. E. Melkonian, W. W. Havens, Jr., and L. J. Rainwater, "Slow Neutron Velocity Spectrometer Studies, V: Re, Ta, Ru, Cr, Ga", Phys. Rev. 92, 702 (1953).

Table I

^{204}Tl Resonance Parameters

E_0 (eV)	$\sigma_0 \Gamma^2$ (barns-eV ²)
122.8 eV	6.3×10^4
796.2 eV	16.6×10^4

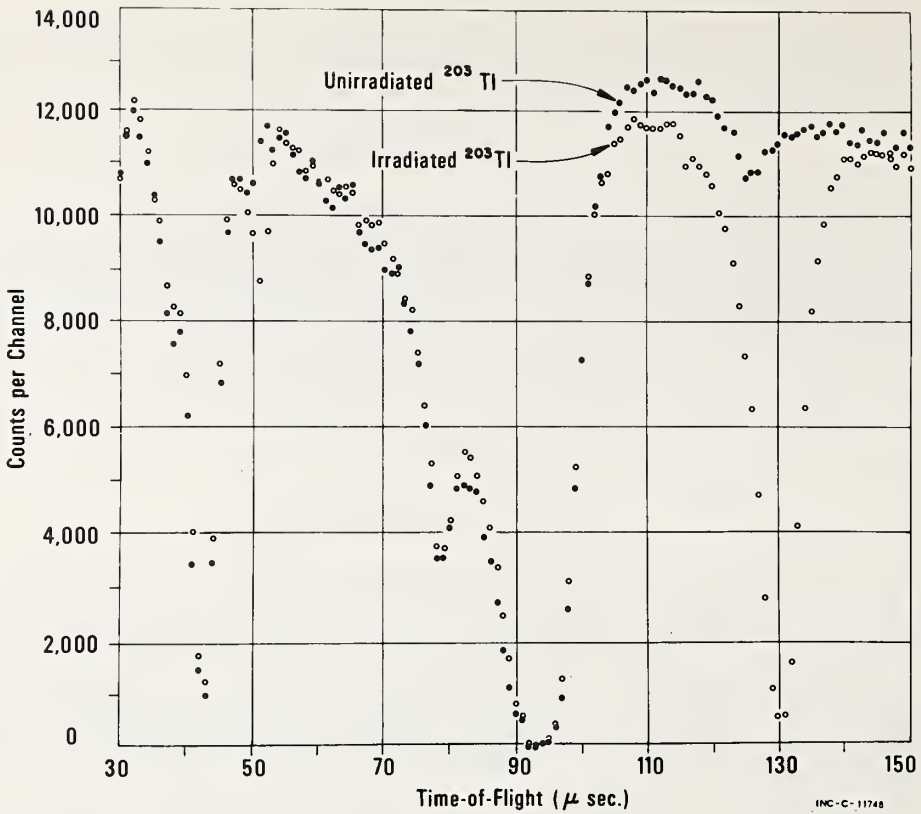


Figure 1 - The transmission data for the ^{204}Tl as a function of time of flight. The solid circles represent accumulated counts for the unirradiated ^{203}Tl , used for the open data; and the open circles represent the corresponding counts for the irradiated sample of ^{203}Tl , used for the sample data of ^{204}Tl .

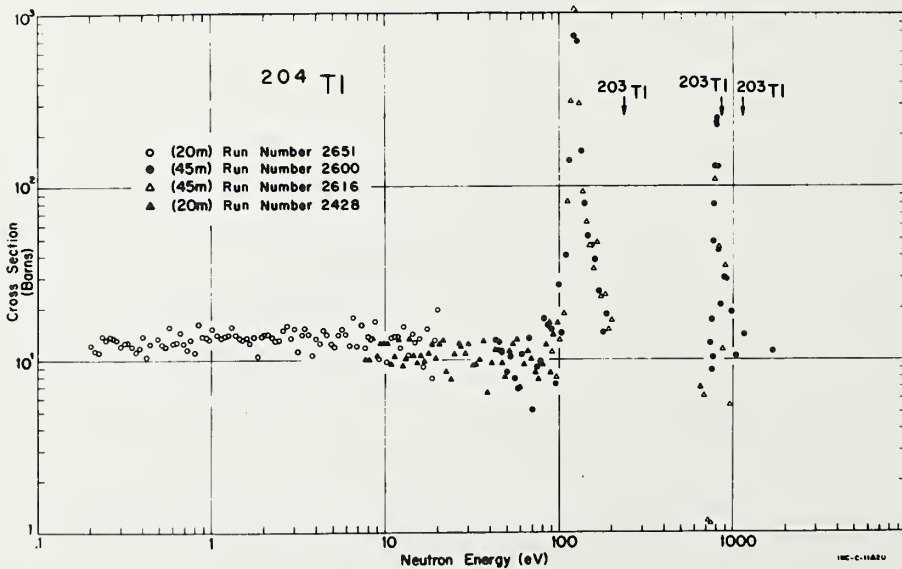


Figure 2 - The total neutron cross section of ^{204}Tl as a function of neutron energy from 0.2 eV to 1000 eV. Location of ^{203}Tl resonances are denoted by arrows.

DETECTION OF A SPIN DEPENDENT EFFECT
IN THE GAMMA SPECTRUM FOLLOWING
NEUTRON CAPTURE

C. Coceva^{*}, F. Corvi^{*}, P. Giacobbe^{*} and G. Carraro^{**}
CBNM Euratom, Geel (Belgium) and CNEN Centro di
Calcolo, Bologna (Italy)

Abstract

The dependence of gamma cascades on the spin of the initial state is exploited to determine the spin of the levels excited by s-wave neutron interaction. The method, based on simultaneous detection of single and coincidence counts by two NaI(Tl) crystals, puts into evidence differences in the general characteristics of gamma cascades such as multiplicity and spectrum shape. The validity of the method is supported by the results of a numerical simulation of the gamma decay process. Results are given for the isotopes: Mo-95, Mo-97, Ru-99, Ru-101, Pd-105 and Hf-177.

1. Introduction

In an effort to find a method of spin assignment of s-wave neutron resonances, the capture γ -ray spectrum was examined in order to see which features of it are dependent on the spin of the initial excited state. Our starting point was the assumption that the multiplicity of the emitted γ -rays is dependent on the spin of the initial state: although such an hypothesis may be supported by some qualitative argument, there is no definite experimental evidence of it.

The simplest way of putting into evidence the multiplicity is to determine the ratio R_J between the count rate S of one gamma detector and the coincidence count rate C of two gamma detectors viewing the capture gamma-ray source. To add more generality to R_J , we introduced in the singles measurements a variable energy threshold E_T^S , while the coincidence threshold was kept fixed at a low value. In case of solid angles of detection small compared to unity and assuming unit intrinsic detection efficiency for γ -rays of energy higher than the thresholds, the ratio R_J has the expression:

$$R_J = \frac{\langle \nu_J^S \rangle}{\langle \nu_J (\nu_J - 1) \rangle} \frac{\Omega_S}{\Omega_C^2}$$

^{*} CNEN, Ispra (Italy)

^{**} CBNM Euratom, Geel (Belgium)

where ν_J is the multiplicity and ν_J^S the number of γ -rays of the generic cascade with energy higher than E_T^S . Brackets indicate an averaging over all the cascades and Ω_S, Ω_C are the solid angles, in 4π units, subtended by the detectors. The ratio R_J , while being obviously independent of the neutron flux and of the resonance parameters, retains a dependence on the multiplicity and on the shape of the capture gamma spectrum.

2. Numerical simulation

To investigate a possible spin dependence of R_J and in case to optimize the effect, a Montecarlo simulation of the gamma decay process was performed on a digital computer(1). Weisskopf and Moszkowsky formulae were assumed for the dependence of electric and magnetic multipole transition probabilities on the energy of the γ -ray. The actual spectrum of excited levels was introduced up to an excitation energy below which energy, spin, parity and branching ratios for gamma decay are experimentally known for every level considered. Above such an energy a continuum of levels was assumed whose density $\rho(E, J)$ is given by the expression deduced from Bethe's free gas model:

$$\rho(E, J) = c(a) \frac{\exp\{2(aU)^{1/2}\}}{U^{5/4}} \frac{2J+1}{\sigma^3} \exp\{-J(J+1)/2\sigma^2\}$$

where $U = E - \Delta$, E being the excitation and Δ the pairing energy. Values for a and Δ and the functional dependence of c on a can be found, for instance, in ref.(2). For the energy dependence of the spin cut-off parameter σ , we used the expression:

$$\sigma^2 = \sigma_0^2 E^{1/2}$$

where σ_0 was chosen so that $\sigma = 4$ at the neutron binding energy. Finally, the two parities were assumed equally probable.

We introduced in the program also a tabulation of the detection efficiency as a function of γ -ray energy and energy thresholds: such a tabulation was calculated for the detectors used in the experiment, namely two 6"x6" NaI (Tl) crystals.

The statistical sample was of 1000 cascades per each of the two possible spin values of the initial state.

The simulation was carried out for the target nuclei Pd-105, Mo-95, Ru-101 and Hf-177. The output of the program gives the estimates of $\langle \nu_J \rangle$, $\langle \nu_J^S \rangle$, R_J with their standard deviations and also the distribution of multiplicity and the primary and total gamma energy spectrum. The distribution of the multiplicity, plotted in fig. 1, confirms our previous assumption, showing a definite dependence on the initial spin. We assume as figure of merit for the effect, or "spin effect index", the difference d between the values of R_J for the two J values, referred to their mean, i. e. :

$$d = 2 (R_{I-1/2} - R_{I+1/2}) / (R_{I-1/2} + R_{I+1/2})$$

In fig. 2 the calculated values of d (open circles) are plotted as a function of the singles energy threshold E_T^S , with their errors as estimated from the finite statistics of the sample. The most striking feature of such a plot

is the general increase of d with E_T^S in all four nuclei. The experimental points (full triangles), determined as described in section 3, are systematically higher than the calculated ones, but they show the same trend with E_T^S . This behaviour is very likely due to the fact that an increase of multiplicity results in a softer γ spectrum. Therefore, for threshold E_T^S high enough, we will have a singles count rate higher for the spin value with lower $\langle \nu_j \rangle$, as it is illustrated in fig. 3 for the case of Hf-177. Of course this effect is directed towards an increase of the spin index d . However the singles threshold should not be set too high, lest Porter-Thomas fluctuations of the limited number of transitions accepted blur the J -dependent effect.

3. Experimental

The experimental work was performed at the 60 MeV electron Linac of CBNM EURATOM, Geel. A neutron flight-path 51.6 m long was used; capture γ -rays were viewed by two 6"x6" NaI(Tl) crystals placed symmetrically at 90° with respect to the neutron beam. To avoid the detection of neutrons scattered from the sample, an appropriate shielding was inserted between sample and crystals. Single and coincidence counts were sent to the two halves of a 4096-channels Intertechnique time-of-flight analyser.

Only samples of natural isotopic composition were used. We looked for a spin effect in the following odd-neutron target nuclei:
 Pd-105, Ru-99, Ru-101, Mo-95, Mo-97 all with $I = 5/2$
 Hf-177, with $I = 7/2$.

All the results given in the following were obtained keeping the energy thresholds respectively at 2.5 MeV for singles and at 0.30 MeV for coincidences detection.

The distribution of the relative R_J values is plotted in fig. 4 for the various target nuclei considered. A strong grouping of the R_J around two different values is evident in each case: as suggested by the numerical simulation, we assign $J = I+1/2$ to the resonances whose R_J belong to the lower group and $J = I-1/2$ to those belonging to the higher group. Correspondingly we call $\langle R_{I+1/2} \rangle$ and $\langle R_{I-1/2} \rangle$ the average values of the two groups. For ease of presentation and comparison, we actually plotted in fig. 4 the relative values:

$$R_J^0 = 2 R_J / (\langle R_{I+1/2} \rangle + \langle R_{I-1/2} \rangle)$$

so that the spin effect index is:

$$d = \langle R_{I-1/2}^0 \rangle - \langle R_{I+1/2}^0 \rangle$$

It has to be noticed that, in the case of Mo and Ru, we plotted together the set of R_J^0 belonging to the two odd isotopes of the same element, because they were found to group around the same average values. Therefore to assign the spin to resonances which are not isotopically identified, it is only necessary to know that they belong to one of the two odd isotopes: this was the case for six unidentified resonances in Mo. For this element the data are much more scattered than in the others, probably because of the presence of p-wave resonances. The dashed squares in the histogram correspond to resonances which are supposed to be excited by p-wave neutrons, because of their strong yield of high energy γ -rays.

The results are summarized in Table 1, where, for each target nucleus of spin I , we give the neutron energy range covered by the present experiment, the number of analysed resonances, the number of spin assignments and the experimental spin effect index d . More detailed results are given in ref.(3).

TABLE 1

Target nucleus	I	En. range (eV)	Nb. of anal. resonances	Spin assignments		d experim.
				$J=I-1/2$	$J=I+1/2$	
^{105}Pd	$5/2$	50-810	50	20	30	0.22
^{99}Ru & ^{101}Ru	$5/2$	24-560	36	16	20	0.20
^{95}Mo & ^{97}Mo	$5/2$	45-1300	38	9	15	0.23
^{177}Hf	$7/2$	1-210	46	21	25	0.12

Table 1 shows that, at least for the class of odd-neutron target nuclei here considered, the spin effect index is mainly dependent on the target spin, while being rather insensitive to the characteristic features of the particular nucleus. The effect seems to decrease with I ; such a trend is confirmed also by preliminary results for Hf-179 with $I = 9/2$.

The validity of the method is supported by the satisfactory agreement between the results of the experiment and those of the numerical simulation, as shown in fig. 2. As a further check, 26 previous spin assignments in Pd-105, Ru-99, Ru-101 and Hf-177 are all confirmed by the present measurement.

4. References

- (1) P. Giacobbe, M. Stefanon and G. Dellacasa "Numerical simulation of the γ -decay of a nucleus from an excited state" CNEN Technical Report in press.
- (2) A. Gilbert and A. G. W. Cameron, Can. J. of Phys. 43 (1965) 1446
- (3) C. Coceva et al. "A method of spin assignment of neutron resonances based on capture gamma-rays detection" to be published.

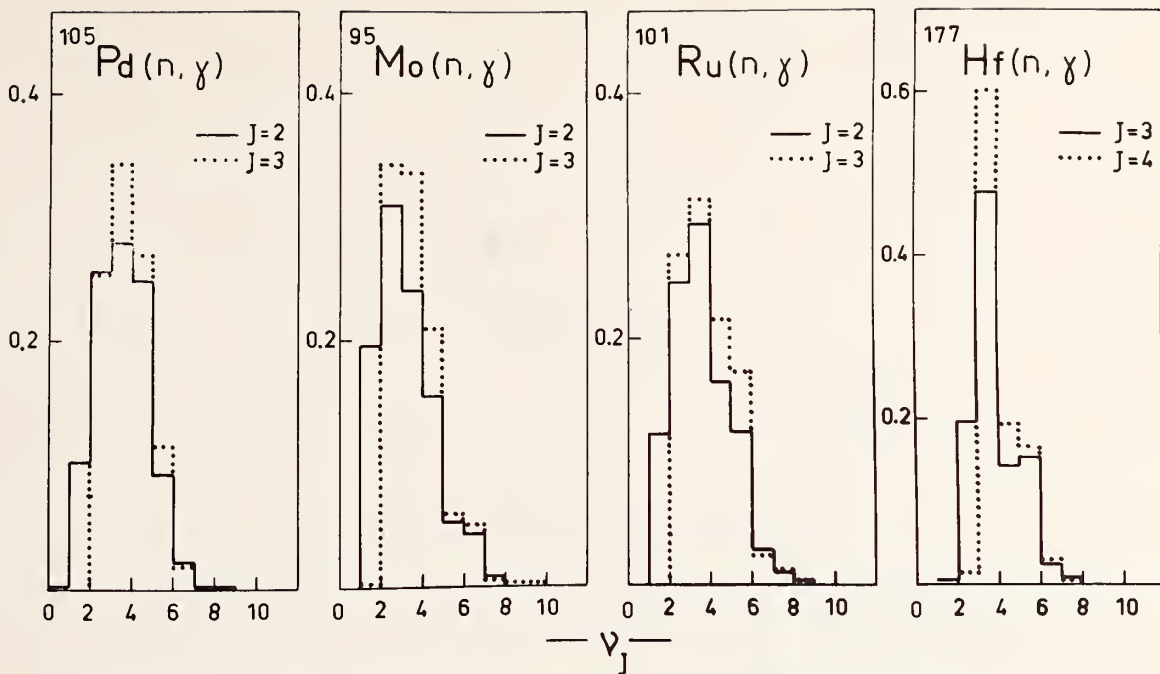


Fig. 1: Calculated frequency distribution of the γ -cascade multiplicity for the two spin values of s-wave resonances in target nuclei Pd-105, Mo-95, Ru-101 and Hf-177.

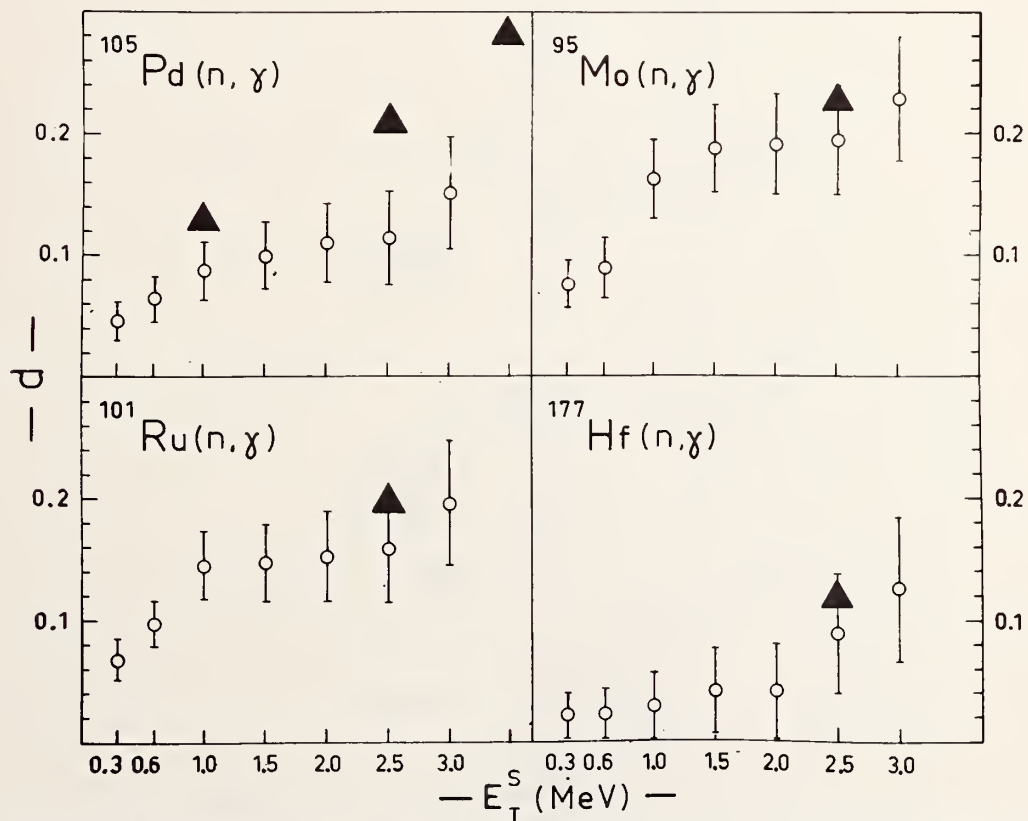


Fig. 2: Calculated (open circles) and experimental (full triangles) values of the spin effect index d as a function of singles energy threshold E_T^S for Pd-105, Mo-95, Ru-101 and Hf-177 target nuclei.

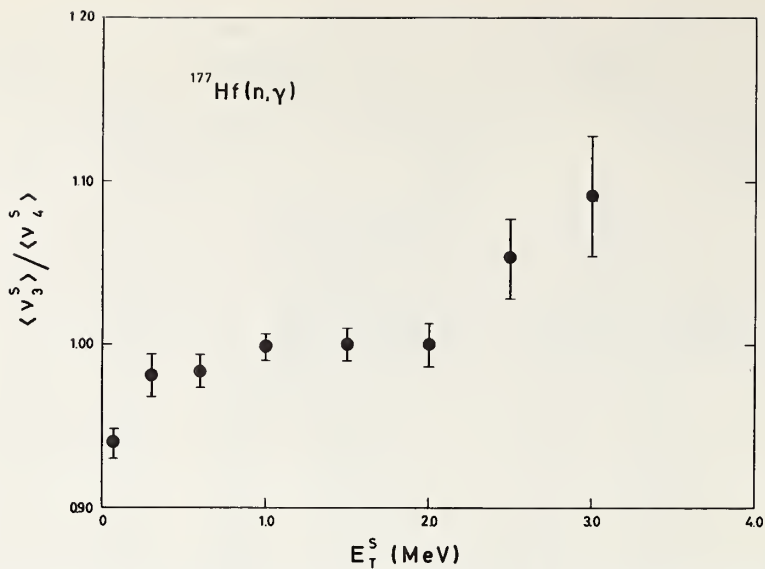


Fig. 3: Calculated ratio of the average number of γ -rays above threshold per neutron capture in levels with $J = 3$ and $J = 4$, as a function of threshold energy E_T^S . The target nucleus is Hf-177.

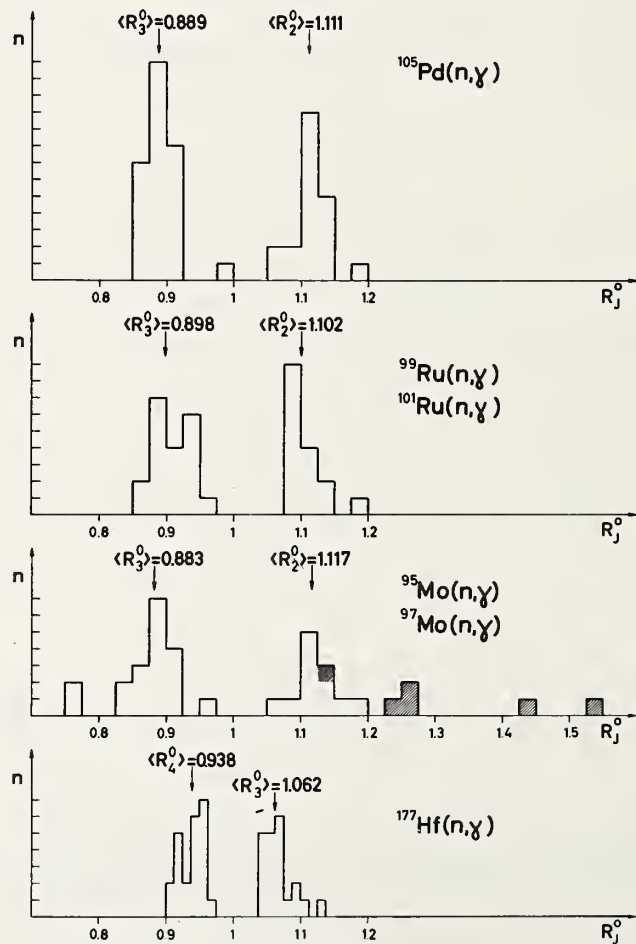


Fig. 4: Distribution of R_J^0 values of resonances belonging to Pd-105, Ru-99 and Ru-101, Mo-95 and Mo-97, Hf-177.

Session F

THE THEORY OF NUCLEAR CROSS SECTIONS
AND THE
ANALYSIS OF NEUTRON INTERACTIONS

Chairman

M. H. KALOS
New York University

by

Erich Vogt

Physics Department, University of British Columbia

Vancouver, B.C. Canada

1. Introduction

The aim of this talk is to describe how we employ our considerable knowledge of nuclear structure to calculate neutron cross sections. Two years ago, at the preceding conference in this series, Perey¹ gave a talk entitled "Filling in Gaps with Cross Sections Calculated from Theory". The present talk will elaborate on the same theme, partly with specific examples of my own and partly with a description of some recent developments which affect the calculation of neutron cross sections. We begin by some general remarks which serve as a framework to relate theory with cross section calculations.

The general behaviour of neutron cross sections is quite complex simply because it arises from the strong interaction of a large assemblage of nucleons. Fig. 1 is intended to remind you that in the neutron bombardment of heavy nuclei we get sharp, closely-spaced resonances at low neutron energies and then much smoother cross sections at higher energies. The processes that go on are usually described by amplitudes corresponding to two extreme pictures: (1) a sum of Breit-Wigner amplitudes corresponding to compound nucleus processes in which the neutron's energy is totally shared among all the target nucleons; (2) a direct reaction amplitude in which the incoming neutron undergoes a single, simple elastic or inelastic scattering event. On the one hand we have sheer random noise, on the other hand beautiful signals with a direct connection to nuclear structure. There are, of course, also many possibilities intermediate between these two extremes.

In the light of the complexity of neutron interactions it is neither possible nor desirable to have a general theory for the calculation of any cross section. You don't want to have one omniscient computer program which can calculate any cross section. Then you couldn't play the games with which this conference deals.

Nuclear theory provides the rules by which the games of cross section calculation are played. Sometimes the rules are straightforward: for example, in the description of resonance structure the Breit-Wigner formula is a constraint on the cross section shape based on very general considerations about the range and strength of the nuclear force. The constraint is a simple formula but its parameters are random numbers.

The game is as simple as roulette. In the direct reactions, and in the average of the resonance cross sections, the cross section behaviour is dominated by the single-particle behaviour of the neutron, that is, by the shell model or the optical model which describes the refraction and absorption of neutron waves. Here everything that we know about nuclear physics comes into play: the average interaction, collective effects, nuclear shapes, effective interactions etc. As our knowledge of nuclear theory builds up, it guides the kind of parameters which we can use in the optical model to calculate neutron cross sections. Here nuclear theory provides us with the good judgment and good taste which shield us from the worst vulgarities of, say, a ten-parameter optical potential. With its combination of rules and proprieties the direct reaction game is rather like cricket.

The cross section calculation games are not only useful but also, often, instructive. They serve as a testing ground for nuclear reaction models and as a tool for learning more about the basic nuclear properties. For example, the imaginary part of the optical potential is almost the only tool we have for measuring the distance which a neutron travels before it is removed from a single-particle orbit inside a nucleus. In the examples which we shall give below we shall see that interaction between theory and cross section calculation goes both ways - theory helps us in the calculations and the calculations add to our theory.

Before leaving Fig. 1 we note that the Breit-Wigner amplitudes give rise to cross section structure even when they overlap very strongly. This structure is called fluctuations and, as Bloch² has emphasized recently, it has many of the features of random noise. The origin of the structure is simply that the square occurs outside the sum. All the Breit-Wigner amplitudes are coherent: we have a square of a sum not a sum of squares. It was only eight years ago that Ericson³ first pointed this out and since then there have been a great number of papers about the structure of the noise. We now know how to deal with it even though its analysis does not tell us a great deal about nuclear structure.

2. The Optical Model

The optical model is concerned with the most basic aspect of nuclear physics - the single-particle motion of nucleons inside atomic nuclei. The neutron cross sections of the optical model are given in terms of the phase shifts, δ_ℓ , of a complex well, $V(r) + iW(r)$ which represents the average interaction of the neutron with a nucleus. The real part, V , of the potential is the potential well of shell model orbits. We know a great deal about it from shell model studies and from the recent great interest in Hartree-Fock orbitals and potentials.⁴ The imaginary part, W , is related to the residual interaction of the shell model which destroys the single-particle motion - or leads to absorption of the neutron. In both the qualitative nature of the optical potential and in the choice of optical model parameters, nuclear theory gives a guide to calculation.

Qualitatively the optical potential has a central term governed by the nuclear radius and surface thickness, a spin-orbit term proportional to the scalar product, $\underline{i} \cdot \underline{\ell}$, of the neutron spin with its orbital angular

momentum, an isotopic-spin term, proportional to the scalar product, $\vec{t} \cdot \vec{T}$, of the isotopic spins of the neutron and the target nucleus, etc. The parameters which are needed to describe all of these may vary with the energy and they may depend on specific nuclear properties such as stability, deformation, etc. As a result there is a large number of parameters which determine the refraction or absorption of neutron waves in nuclei.

Two years ago Perey¹ showed you the great success achieved by the optical model in fitting the elastic scattering of neutrons - particularly when the computer was left free to choose the parameters to fit the data. I will not show you any such fits but instead make a number of comments about things that have been learned recently about the physical facts which establish the rules or the proprieties of the optical game.

a) the shape of the real, central potential. Usually $V(r)$ is chosen to be proportional to $[1 + \exp(r - R)/a]^{-1}$ where R is the nuclear radius and a is the surface thickness. This shape is based on the saturation property of nuclei and on the short-range of the nuclear force. However, if we believe in the independent particle model then the shape should show some oscillations arising from the shell structure. For example, Fig. 2 shows the potential (or the density or charge distributions) which might be appropriate for Ca^{40} which has 4 nucleons in the 1s orbit, 12 in the 1p orbit, 4 in the 2s and 20 in the 1d. Are these oscillations in the shape present and should we use such shapes in cross section calculations in place of the more familiar shape of the Saxon-Woods potential? Some recent work reported at the Chicago meeting⁵ on high energy electron scattering from nuclei finds that these shell oscillations appear to have a much smaller amplitude than might be expected on the basis of the orbits. The explanation most likely is that the short-range repulsion between the nucleons or effective nucleons which travel in the orbits pushes them into the regions where the density of the orbital motion is low. Thus what we have been doing all along is roughly right.

b) the shape of the imaginary, central term. For a decade there has been a comparison of two extreme models, one with volume absorption and another with surface absorption. The correct situation is almost certainly in between these two. The Pauli Exclusion Principle reduces the absorption of neutrons where the density is high so that the absorption is peaked on the surface as shown on Fig. 2. But it is not zero inside. The proprieties of the game suggest that we should always choose a combination of surface and volume absorption. We get away with using only **surface** absorption because in so many problems only a small fraction of the wave penetrates to the interior and because, in three dimensions, the interior is so small compared to the surface region.

c) the spin-orbit term - Much of the information about the spin-orbit term comes from the measurement of polarization of neutrons and protons scattered by nuclei. Recently there has been a great deal of work toward the provision of polarized beams of protons. The resulting measurements of scattering asymmetries may tell us much more about the systematic behaviour of the spin-orbit term. Recent evidence from the analysis of

polarization experiments is that the spin-orbit term is located somewhat inside the real part of the central potential. This finding appears reasonable because of the short-range of the nucleon-nucleon spin-orbit term.

c) the isotopic spin-term. The introduction of a term proportional to $\frac{t \cdot T}{A}$ is not an artifice merely to introduce new parameters into the optical potential. Such a term arises from ordinary central nuclear forces because neutrons and protons separately obey the Pauli principle. The $\frac{t \cdot T}{A}$ term gives rise to (p,n) reactions⁷ in which a proton is elastically scattered and, at the same time changes its charge but leaves the configuration of the remaining nucleons unchanged. The analysis of such (p,n) reactions⁸ yields direct information about the strength and shape of the real part of the isotopic spin term. The strength of the isotopic spin can also be related to the symmetry term (proportional to $(N-Z)/A$) in the Weizäcker formula for nuclear binding energies.

In neutron and proton absorption cross sections the imaginary part of the isotopic spin term plays an important role. For example, if we bombard different isotopes of the same element with neutrons, or protons, $\frac{t \cdot T}{A}$ is proportional to the neutron excess, $(N-Z)$. With higher number of neutrons the absorption cross section increases. Fig. 3 shows some recent Los Alamos measurements⁹ of proton absorption cross sections in which such an increase is observed. Thus the isotopic spin term must be remembered in Hauser-Feshbach calculations of neutron elastic and inelastic scattering, and we should use the guidance obtained from the analysis of (p,n) quasi-elastic scattering. The isotopic spin term is of opposite sign for neutron absorption and proton absorption: it makes neutron absorption smaller. A comparison of the data¹⁰ for neutron and proton absorption displays this effect and suggests, further that the neutrons extend to slightly larger radii than protons.

d) local or non-local potentials. There has been much discussion as to whether or not one should use a local or a non-local potential in the optical model game. By a non-local potential one simply means taking the usual wave equation

$$-\frac{\hbar^2}{2m} \nabla^2 \psi(r) + V(r) \psi(r) = E \psi(r)$$

and replacing the potential term by

$$\int V(r, r') \psi(r') dr'$$

so that the potential at a point \underline{r} affects the wave function at a point \underline{r}' . The many-body theory for nuclei tells us we should use non-local potentials but it does not give us any good guide to the details of the non-local potential.¹ To quite an extent the non-locality can replace the energy dependence of the optical model parameters which are needed with the

ordinary, garden-variety, optical model. On the other hand the energy dependence can be understood from the nuclear physics of the problem. My own inclination is to use a local potential because then one can more easily use nuclear theory to build into the cross section estimates all of the refinements which we discussed and we know sooner when we are doing something that is physically unreasonable. By reverting to non-locality we lose the proprieties of the game: it would be like trying to play cricket in a foreign language.

All of the physical refinements of the optical model are small effects which modify slightly the basic single-particle features of the model. These can be seen most clearly in the absorption cross sections. For neutrons or protons each partial wave, l , has an absorption cross section proportional to a transmission function, T_l ,

$$T_l \equiv 1 - |e^{2i\delta_l}|^2$$

where δ_l is the complex phase shift. At low energies T_l is simply the product of the penetrability and the nucleon strength function,

$$T_l \approx 4\pi P_l S_l$$

The strength function has giant resonances whenever the nucleon energy is near a single-particle level. Fig. 4 shows how the neutron strength functions of the various partial waves vary with atomic weight. Similarly, Fig. 5 shows proton absorption cross sections displaying the giant resonances. The position of the resonances is given by the real central potential, the width by the imaginary central potential and the detailed shape and magnitude by the many refinements from nuclear theory, some of which we discussed above. If we keep all of these facts in mind, the optical model becomes a very powerful and accurate tool in estimating neutron cross sections, not only for elastic scattering but also for direct reactions and compound nucleus processes.

There are limitations to the reliability of optical model predictions. For example, recently I was interested in using the optical model to calculate some reaction rates in the best reactor of all: the interior of a hot star. As shown on Fig. 6 the reactions between charged particles here take place very, very far below the Coulomb barrier - so far that we couldn't think of measuring it. One then asks, why not use the optical model to extrapolate downward from data at higher energies? Such an estimate becomes unreliable because, in these situations, the wave function decays exponentially at a great rate. The absorption cross section becomes sensitive to the exact magnitude of the imaginary potential at distances much beyond the nuclear radius. There is nothing at higher energies that gives us any reliable information about the tail of W . Perhaps, therefore, we will need to measure it with a telescope.

3. Inelastic Neutron Scattering

For years we have had successful models for calculating the direct reactions of neutrons scattered inelastically. For example, if a neutron is scattered from a deformed nucleus it can give rotational energy to the nucleus. The Distorted Wave Born Approximation can be used to calculate the cross section. Analysis of the elastic scattering data (using a suitably deformed optical potential) yields the optical model and hence the distorted waves. From Coulomb excitation studies one knows the matrix element connecting the ground and excited states. Hence the DWBA calculation has no free parameters. As Perey showed two years ago,¹ under such circumstances the cross section predictions for inelastic neutron scattering are about as reliable as for elastic scattering. The magnitude and shape of measured angular distributions and polarizations are fitted remarkably well.

More recently there have been some very interesting attempts to develop microscopic theories¹⁰ which explain the remarkable success of the DWBA models. These microscopic calculations are akin to nuclear structure calculations such as those of the shell model, in that they take account of the two-body interactions between the incoming neutron and the target nucleons. They have thrown some interesting light on why and when the models work and how they might be improved.

In every neutron reaction there is always the possibility that we have inelastic scattering through the compound nucleus rather than through direct reactions. There is no sharp dividing line which tells us which of the two mechanisms is operative. Fortunately we can estimate both types of reactions with considerable accuracy and they have distinctive angular distributions.

To illustrate the calculation of inelastic neutron cross sections proceeding through the compound nucleus I want to use a class of examples for which there are no competing direct reactions, for which the measurements are easy and for which the theory is astonishingly accurate. The class concerns the excitation of isomeric levels. Fig. 7 shows the level structure of In¹¹⁵. The isomeric transition is that from the $\frac{1}{2}^-$ first excited state to the $9/2^+$ ground state. Because of the long lifetime of the isomeric transition we can rule out any contribution from direct reactions. As the figure shows, all the negative parity levels decay by gamma emission to the isomeric state so that the isomeric activity, as a function of neutron energy, is proportional to the sum of the inelastic cross sections to the first four excited states.

Nuclear reaction theory gives us a simple model for calculating the inelastic scattering cross sections averaged over resonance structure or fluctuations. In this model, the Hauser-Feshbach model, the cross section for inelastic scattering is:

$$\bar{\sigma}_{cc'} = \sum_{J\pi} \left[\frac{\pi}{k^2} \frac{c}{S\pi} \sum_{s,l} T_l^{(c)} \right] \left[\frac{\sum_{s',l'} T_{l'}^{(c')}}{\sum_{c''s''l''} T_{l''}^{(c'')}} \right]$$

where the first square bracket is the cross section for compound nucleus formation for a given value of the total angular momentum, J , and parity, π ; the second square bracket is the corresponding branching ratio. This result is like the old evaporation theories, with independent formation and decay of the compound nucleus except for one difference of paramount importance — the Hauser-Feshbach formula forces the compound nucleus to remember that total angular momentum and parity must be conserved. In addition to this restraint from nuclear theory we add to the Hauser-Feshbach formula the transmission functions of the optical model with all their giant resonances or single-particle aspects. Fig. 8 shows the neutron transmission functions for In^{115} calculated with an optical potential which fits the elastic scattering data. We are here in a region where the odd partial waves have large strength functions (transmission functions) and the even partial waves small ones. In using the optical model here we are employing our nuclear physics of the elastic scattering channel to extrapolate to the behaviour of all the inelastic channels. There is a sound physical basis for this. We have no free parameters — the cross section does depend on the detailed spins and parities of the In^{115} levels but these are also known. Fig. 9 shows the result for the cross section for isomeric activity, compared to the experimental data. The fit is remarkably good. There are many cases similar to this in which the cross section can be predicted to within an accuracy of 20% or better. If one wants to do better there are refinements of the average cross section theory — modifications of the Hauser-Feshbach formula — which can be and should be taken into account.

There are two incidental comments which I can't help making with this example. The first is that these measurements of isomeric activity resulting from inelastic scattering are so easy to make that no one has bothered with them for about a decade. Fig. 10 shows a similar agreement between theory and experiment for isomeric activity in Ba^{137} . Here as in the In^{115} case and in several other examples we looked at the data is more than ten years old. Secondly, the isomers by their nature involve a large spin change from the ground state and hence all of the contributing terms in the Hauser-Feshbach formula are from high partial waves. Both Fig. 9 and Fig. 10 show that the predicted cross section is very nearly proportional to the d-wave strength function. This is perhaps the only tool we have for measuring the d-wave strength function. Its measurement would add to our knowledge of the basic optical potential. The d-waves are concentrated in the region of the nuclear surface and are therefore much more sensitive to the surface properties of the potential than the lower partial waves or the total cross section. I wish someone would systematically measure the isomeric activity induced by inelastic neutron scattering for as many isomers as possible.

4. The Thermal Cross Section of U^{235}

As a final example of the use of nuclear theory in estimating cross sections I want to describe a problem associated with the analysis of the neutron cross sections of the fissionable isotopes for thermal cross sections and g-factors (or Maxwellian averages). Everyone knows that the cross section of U^{235} or U^{233} or Pu^{239} are very important and also very

complicated. A decade ago we first found out that nuclear reaction theory could describe the observed cross sections: the gross deviation of the cross section shape from that of the Breit-Wigner formula arose from interference between the broad levels. Subsequent analysis and measurement has shown that there is no unique fit to the cross sections particularly at low energy where resonances below zero neutron energy are important. The full complication of these cross sections was first demonstrated by Lynn¹¹ who showed that in U^{235} , using the widths and spacings extracted roughly from the positive energy resonances one could encounter very unusual cross section shapes and also single narrow peaks arising from the interference of two underlying levels. This led to a most interesting game of generating fictitious cross sections and comparing them to observed cross section shapes. Two years ago Moore and Simpson¹² described this game at the first of these Conferences. I want to describe a similar game which I have played recently in collaboration with G.C. Hanna and D. McPherson of the Chalk River Nuclear Laboratories.¹³

The problem which was posed by Westcott and Hanna was the following: what is the error in thermal cross sections or Maxwellian averages arising from the chance that a small cross section aberration vitiates the standard analysis. In the standard analysis one fits the cross section measurements, say the absorption cross section of U^{235} , by an "eyeball method". This means using the human eyeball to draw a curve through the various sets of data at thermal energies or, alternatively, to use the "eyeball" of a computer to fit the same data with a simple polynomial. Now there are many resonances in U^{235} , some wide, some narrow, some big and some small. What if God or Lynn arranged things so that there was a small narrow resonance or aberration at thermal energies which was never suspected by the eyeball. Then the error in the extracted thermal cross section would be much greater than that deduced from the statistical errors of data.

Nuclear theory is now very nearly sufficient to allow us to assess the contribution to the error from such possible aberrations. Our assessment is based on the following information. First of all, the average value of neutron widths, fission widths, **capture** widths, and level spacings as deduced from the analysis of positive energy resonances in U^{235} . Secondly, the distribution laws for these resonance parameters as determined from a wide range of experience with many neutron resonances and the corresponding theories. We start with the first two positive energy resonances in U^{235} (see Fig. 11) and select resonance parameters for these levels which roughly fit the observed peaks. Having assured that the cross section is roughly right above the thermal region we are then prepared to look at the possible choices of lower lying levels which yield a fit to the thermal data - say from 0.0 eV to 0.15 eV. The lower lying levels are obtained, in our game, by a random selection of each level position and each level width conforming to the known distribution laws. The selection continues to lower energy until the selected resonances no longer influence the thermal region. Occasionally the resonance parameters so chosen may actually provide a fit to the thermal data. If we could find the whole class of fits to the thermal data we could then see how often within this class there was an aberration of the kind we wish to study. Such a **search** for fits to the data, with the resonance parameters chosen from

distribution laws, is too ambitious for present computers - or rather, the data is too good. Only one attempt in about 10^{30} fits the actual data. But the question of small aberrations should be relatively independent of the gross shape of the cross section so we can afford to be less selective. We put three gates on the cross section near thermal energies and obtain a "near-fit" if the computed cross section falls within these gates. We then examine the class of "near-fits" for the presence of small aberrations. I should add that each "near-fit" is calculated with the proper multilevel resonance formula. One such near-fit, with an obvious aberration of the kind sought, is shown on Fig. 11. The level position of this near-fit are also given on Fig. 11.

Even with the broad gates chosen, only rarely does a selected set of resonances yield a cross section which lies within the gates. Using the Chalk River G-20 computer we looked at 92, 923 sets of randomly chosen resonance parameters. Only 269 cases fell within all three gates. In the vast majority of cases the thermal cross section was ten times lower than the observed cross section. This tells us immediately that U^{235} involves some rather strong negative energy resonances.

Of the 269 cases only very few exhibited any kind of aberration of the kind shown. We subjected each case to a polynomial analysis of a kind with which the data of the fissionable isotopes should be treated if one wants to extract g-factors or thermal cross sections. Our tentative conclusion (based on too few cases) is that these catastrophes do not occur with sufficient frequency that they add appreciably to the errors arising from the statistics of the data. The analysis did yield some interesting insights into the proper polynomial analysis of the data¹³. There are many games of this kind in which nuclear theory can assist us in cross section analysis.

5. References

- 1) F.G. Perey, Proceedings of the First Conference on Neutron Cross Sections and Technology, Washington, (1966) - Report - CONF - 660303 (1966).
- 2) C. Bloch, "Statistical Theory of Nuclear Reactions as a Communications Problem", Nuclear Physics (to be published) (1968).
- 3) T. Ericson, Ann. Phys. (N.Y.) 23, 390 (1963).
- 4) G. Ripka, Advances in Nuclear Physics, edited by M. Baranger and E.W. Vogt, Plenum Press, New York (1968).
- 5) R. Hofstadter, Paper AD1 and D.G. Ravenhall, Paper AD4, Bull. Am. Phys. Soc., Series II. Vol. 13, No. 1, (1968).
- 6) G.W. Greenlees and G.J. Pyle, Phys. Rev. 149, 836 (1966),
G.R. Satchler, Nucl. Phys. A92, 273 (1967), L.N. Blumberg, E.E. Gross,
A. van der Woude, A. Zucker and R.H. Bassel, Phys. Rev. 147, 812 (1966).
- 7) J.D. Anderson and C. Wong, Phys. Rev. Letters 7, 250 (1961) 8, 442 (1962).
J.D. Anderson, C. Wong and J.W. McLure, Phys. Rev. 126, 2170 (1962);
129, 2718 (1963).
- 8) G.R. Satchler, R.M. Drisko and R.H. Bassel, Phys. Rev. 136B, 637 (1964).
See also G.R. Satchler in Proceedings of the International Conference
in Nuclear Structure, Gatlinburg Tenn. edited by R. Becker, R. Howard,
P. Stelson and A. Zucker, Academic Press, New York (1967).
- 9) J.F. Dicello, G. Igo and M.L. Roush, Physics Letters, 23, 685 (1966),
Phys. Rev. 157, 1001 (1967).
- 10) G.R. Satchler, Nucl. Phys. A91, 75 (1967).
- 11) J.E. Lynn, Phys. Rev. Letters, 13, 412 (1964).
- 12) M.S. Moore and O.D. Simpson, Proceedings of the First Conference on
Neutron Cross Sections and Technology, Washington, (1964) - Report
CONF - 660303 (1966).
- 13) E.W. Vogt, D. McPherson and G.C. Hanna, to be published (1968).

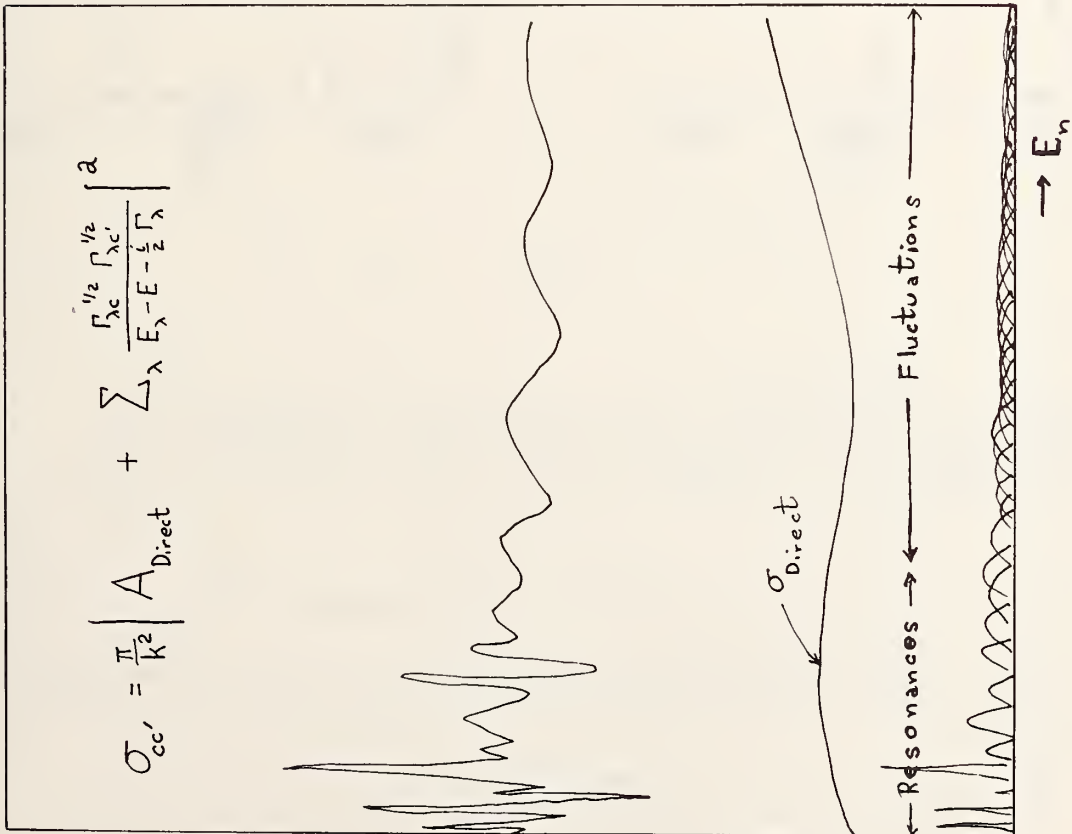


Figure 1 - The qualitative behaviour of neutron cross sections as a function of the neutron energy, E_n . The cross section is a sum of a smooth component from direct reactions and a compound nucleus compound which has individual resonances at low energy and Fluctuations at higher energies. An approximate form for the cross section (ignoring angular momentum sums) is also shown.

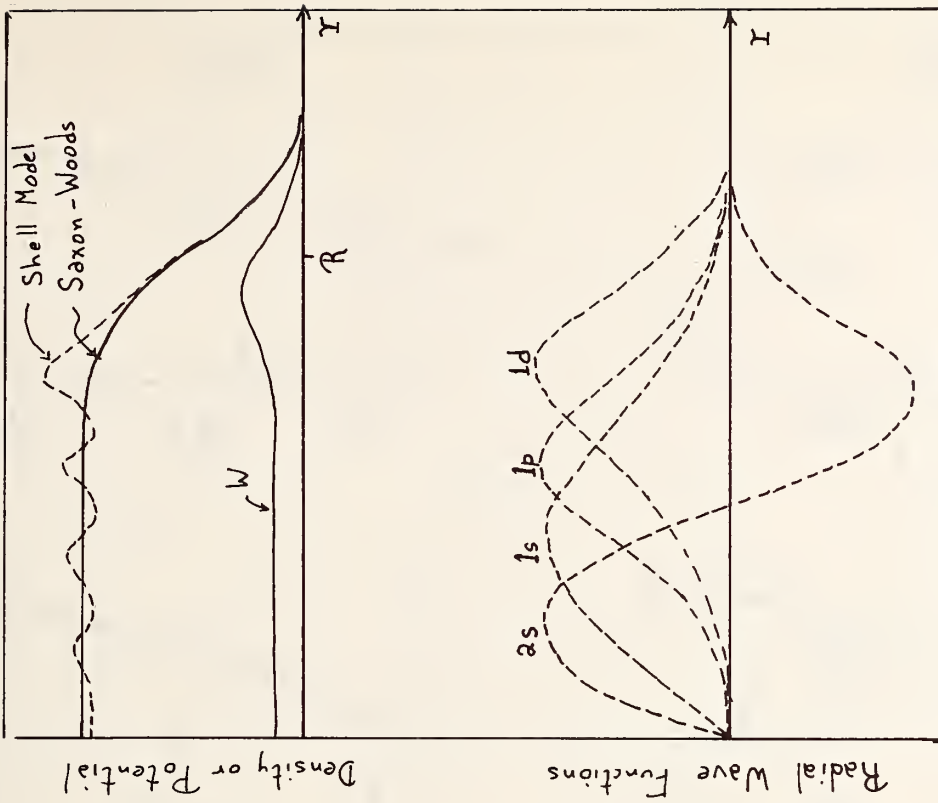


Figure 2 - A qualitative illustration of shell model effects in the nucleon or charge density or in the real part of the optical potential in a nucleus such as C^{14} . The corresponding wave functions are also shown.

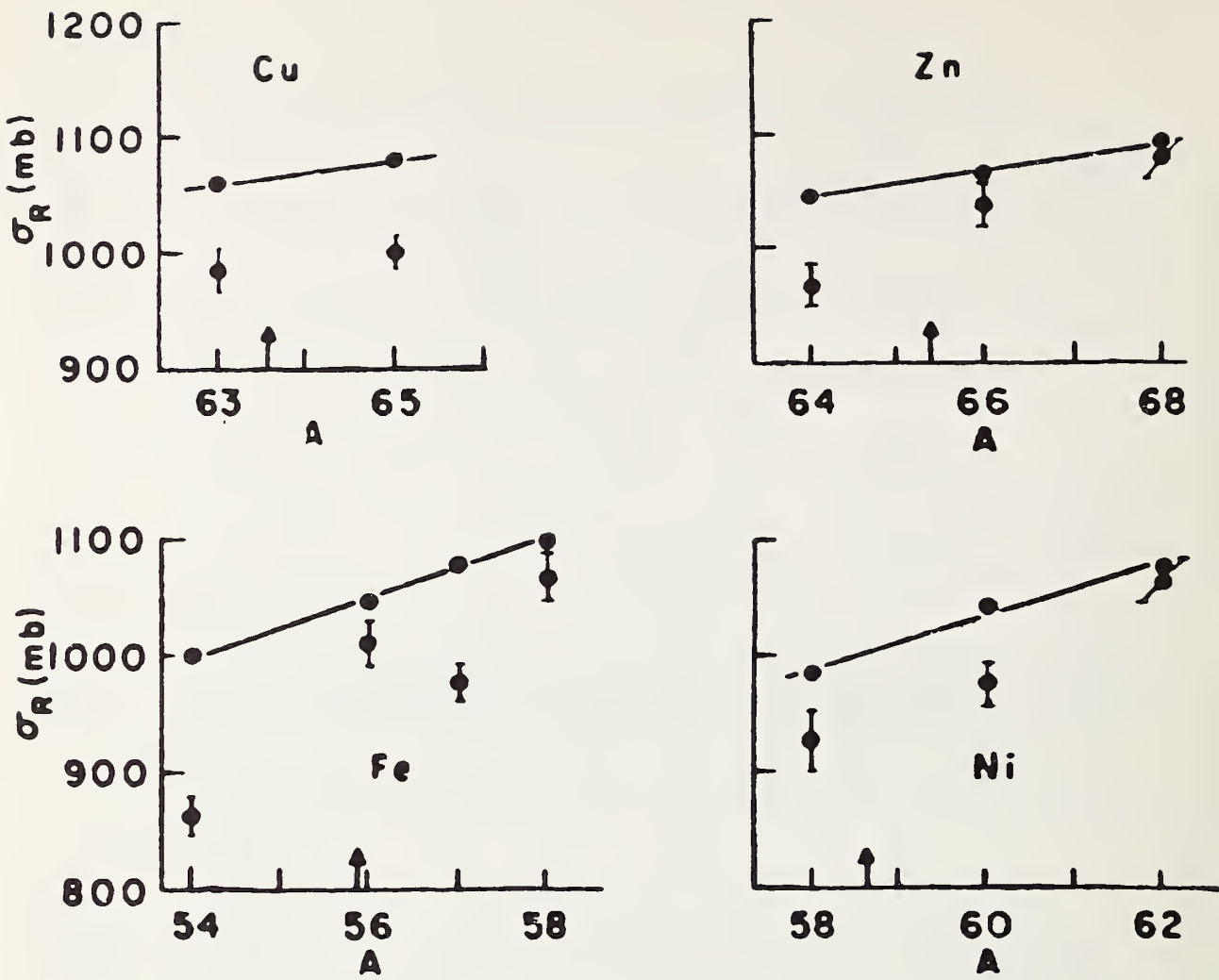


Figure 3 - The measured reaction cross sections (ref. 9) for 14.5 MeV protons on various isotopes of Cu, Zn, Fe and Ni. The solid lines and points without error bars are optical model computations without a symmetry term (proportional to $\frac{t}{A} \cdot \frac{T}{A}$).

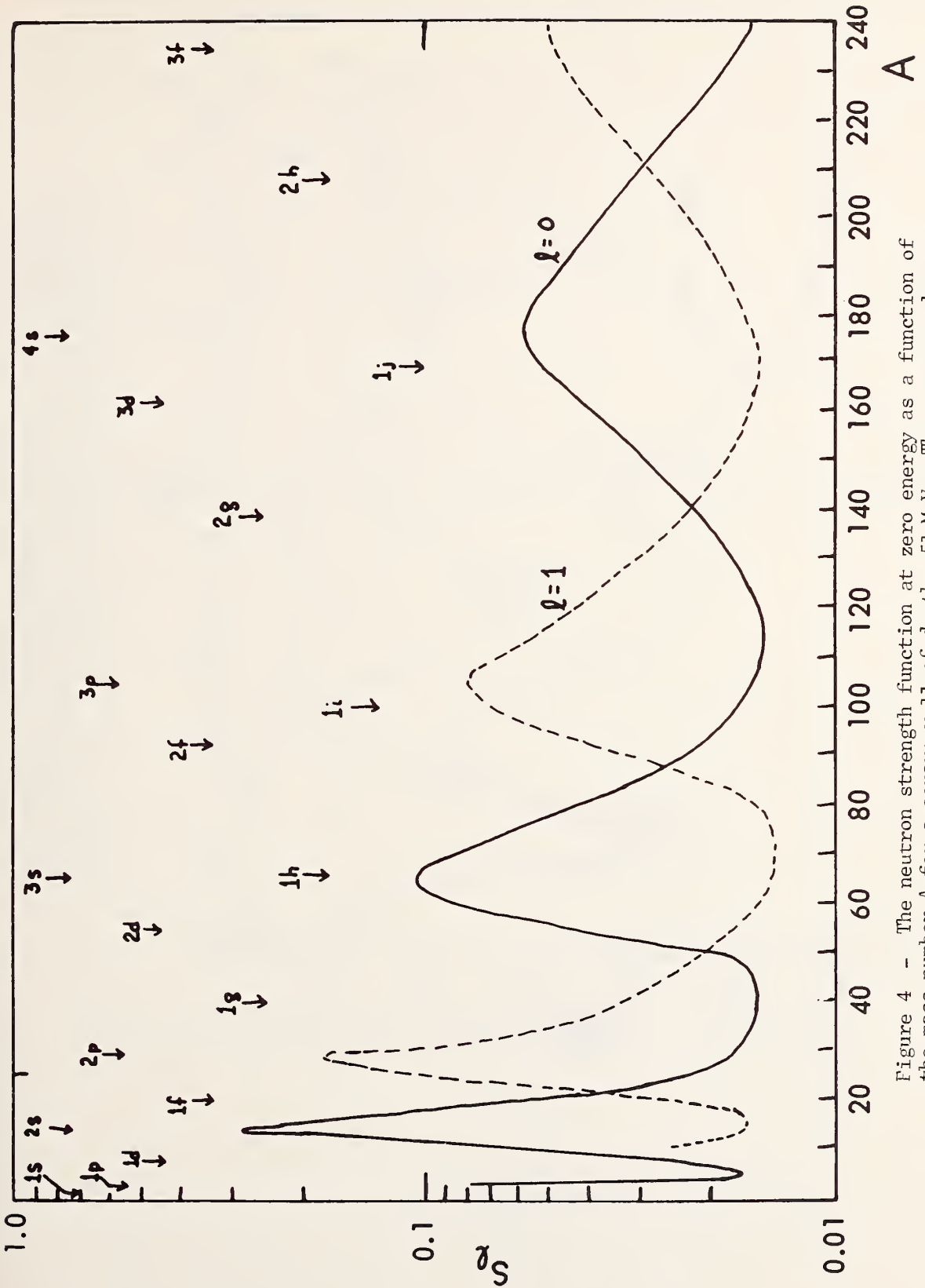


Figure 4 - The neutron strength function at zero energy as a function of the mass number A for a square well of depth -51 MeV. The s-wave and p-wave strength functions are shown, and the positions of the giant resonances of other partial waves is indicated.

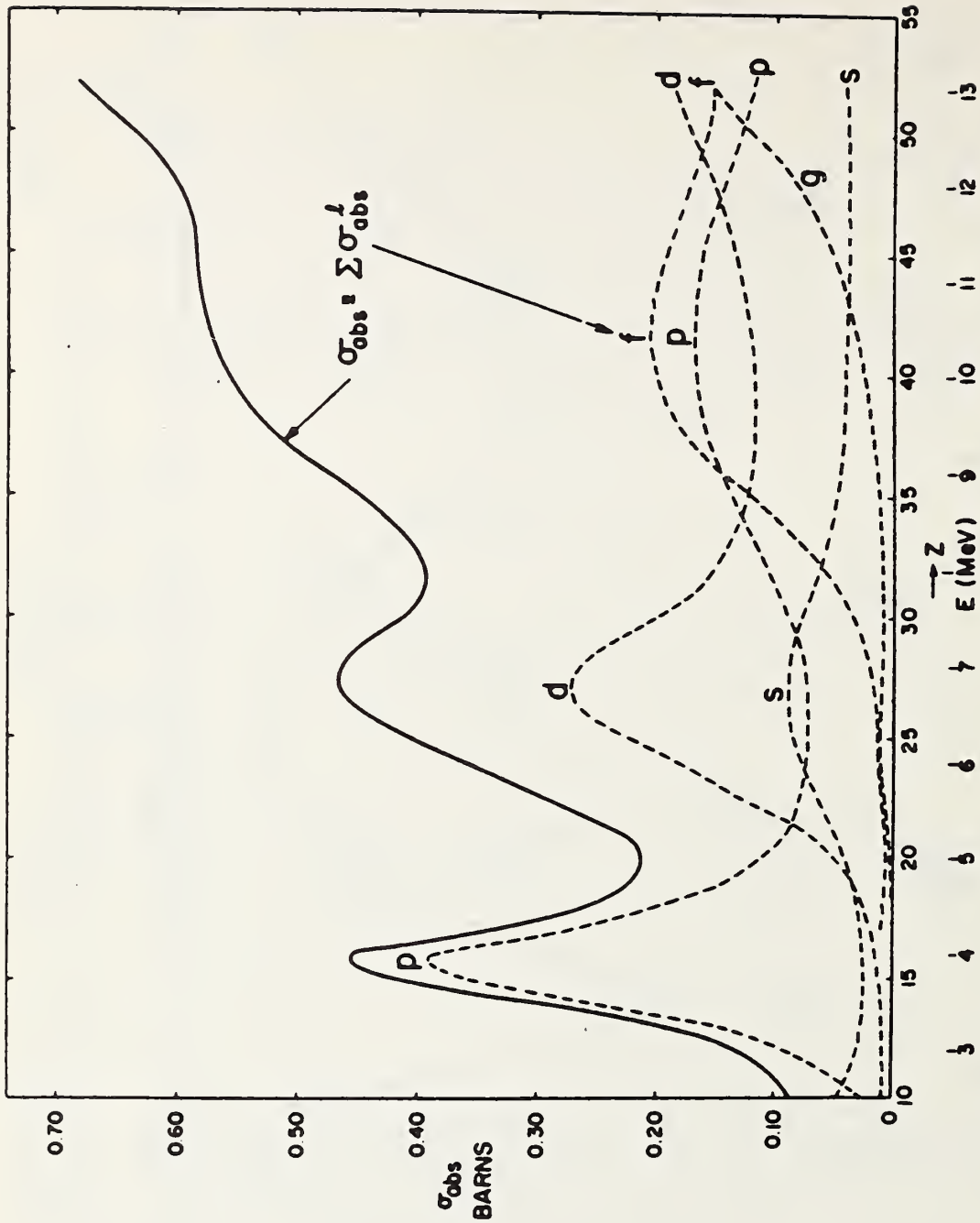


Figure 5 - The proton absorption cross section at the top of the Coulomb barrier (i.e. $E_p = 0.25Z$ MeV) as a function of the atomic number, Z , of the target nucleus, calculated by using a Saxon-Woods potential with $V_0 = -55$ MeV, $R = 1.25A^{1/3}$ fm, $W = -5$ MeV, $a = 0.4$ fm. The contributions from the various partial waves to the total absorption cross section are shown by dashed lines. They clearly exhibit the proton giant resonances.

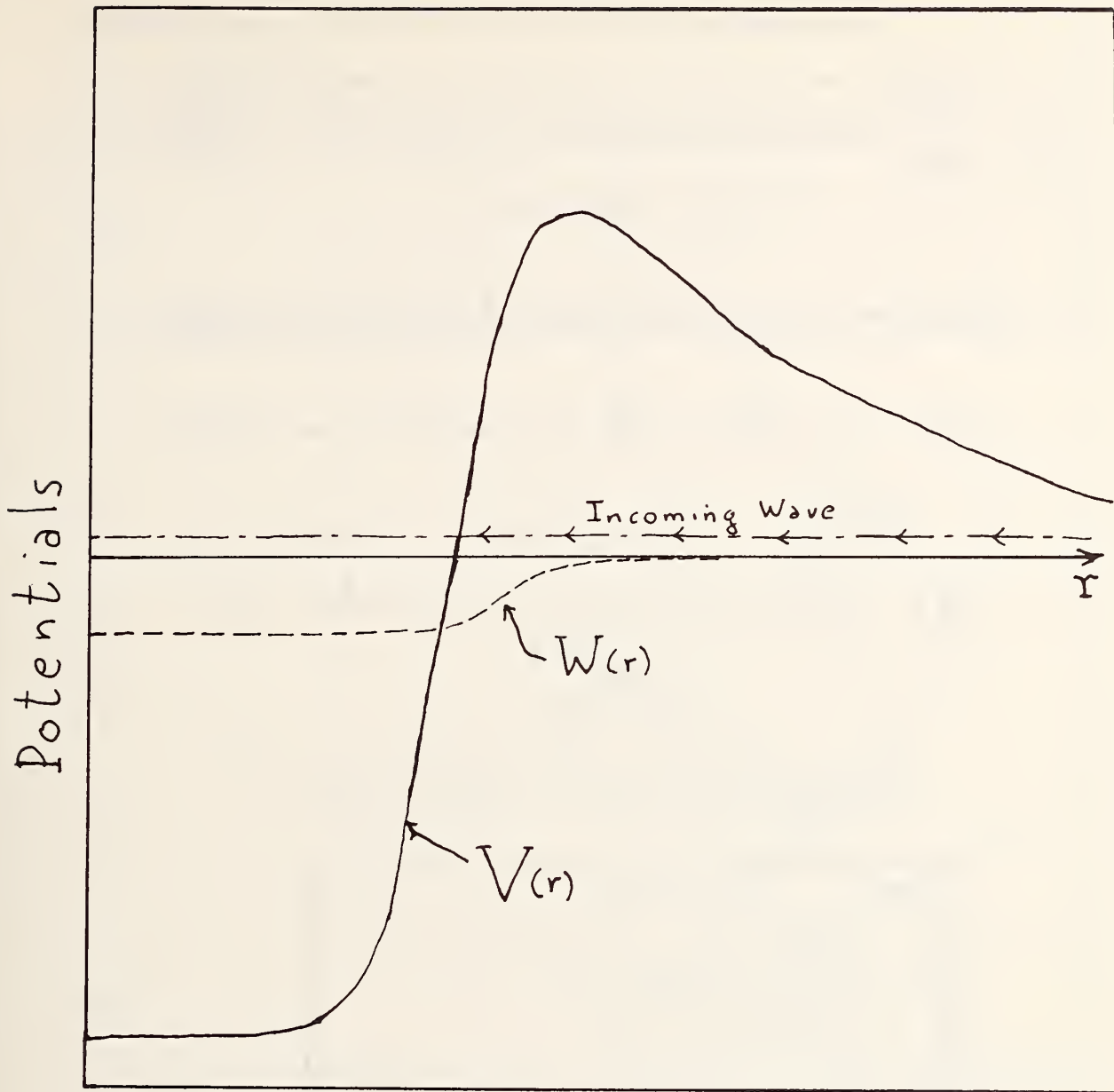


Figure 6 - The optical and Coulomb potentials for low energy reactions with charged particles. At the low energies corresponding to many astrophysical reactions the incoming waves are far below the barrier.

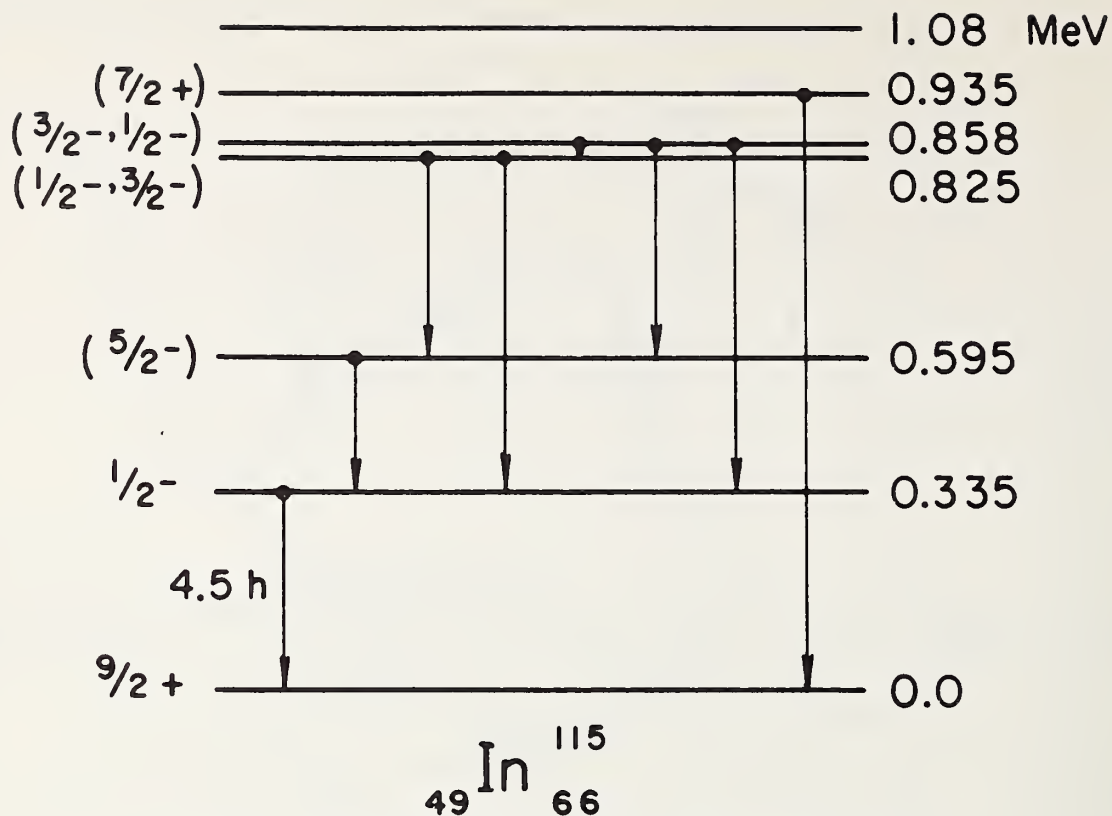


Figure 7 - The low-lying levels of In^{115} and their measured spins and parities. Bracketed spins and parities indicate doubtful assignments. The Hauser-Feshbach calculations clearly indicate a $3/2-$ assignment to the level at 0.595 MeV.

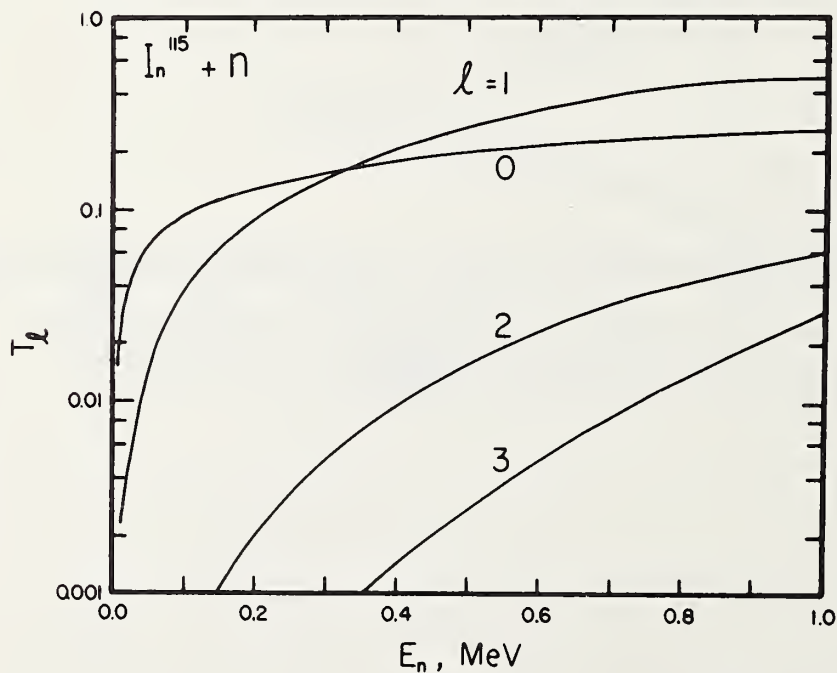


Figure 8 - The neutron transmission functions of In^{115} for various partial waves as a function of the neutron energy.

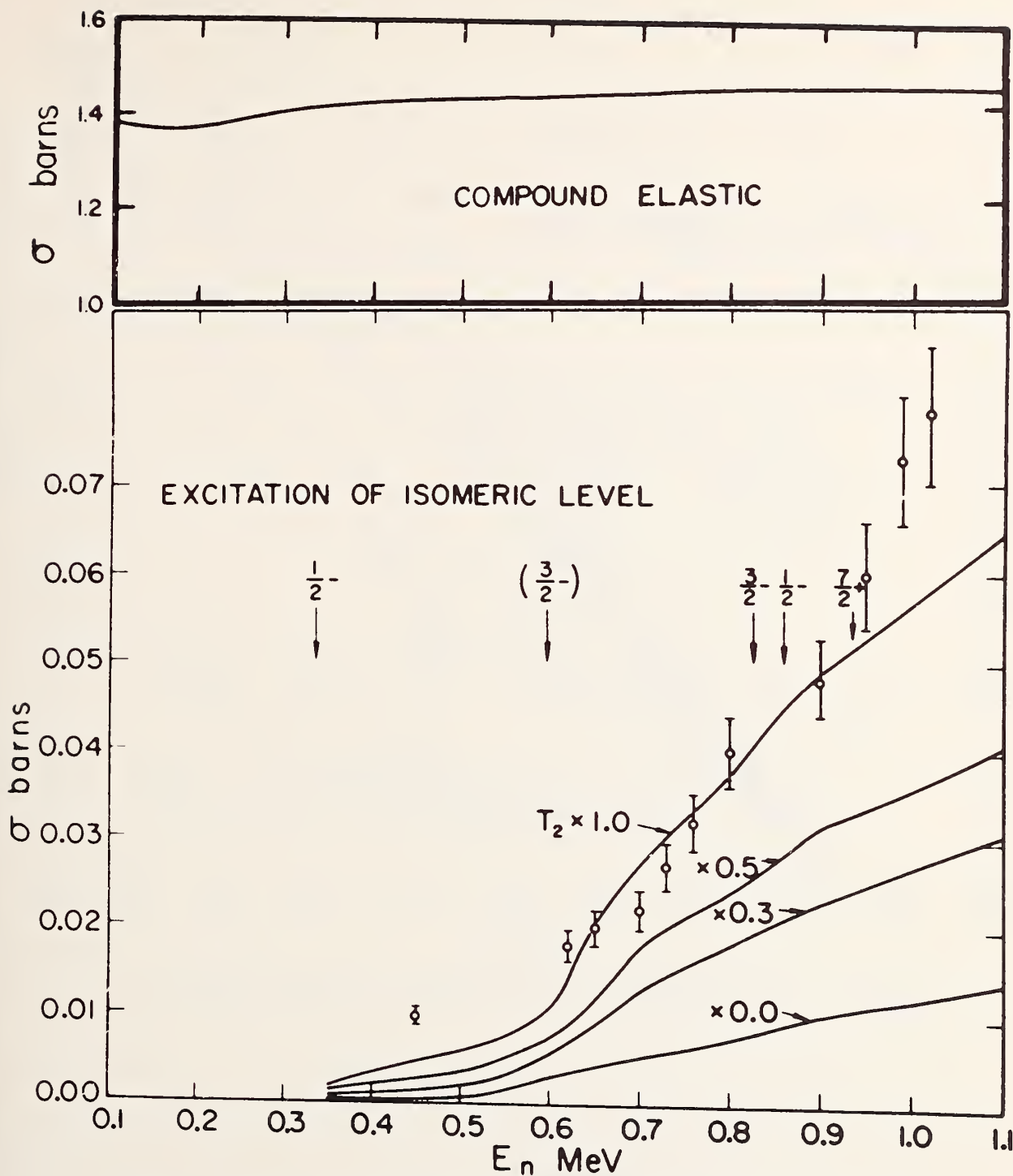


Figure 9 - The cross section for the excitation of the isomeric state in In^{115} by inelastic neutron scattering and for compound elastic scattering in the same nucleus. The data is that of A. Ebel and C. Goodman, *Phys. Rev.* 93, 197 (1954) and the curves are Hauser-Feshbach calculations reported in greater detail by E.W. Vogt, *Phys. Letters* 7, 61 (1963). The direct dependence of the isomeric cross section on the value of the d-wave transmission functions is shown by the variation of the computed curves when only T_2 is varied. The spin, parity and positions of the excited states of ^{115}In are shown in the figure.

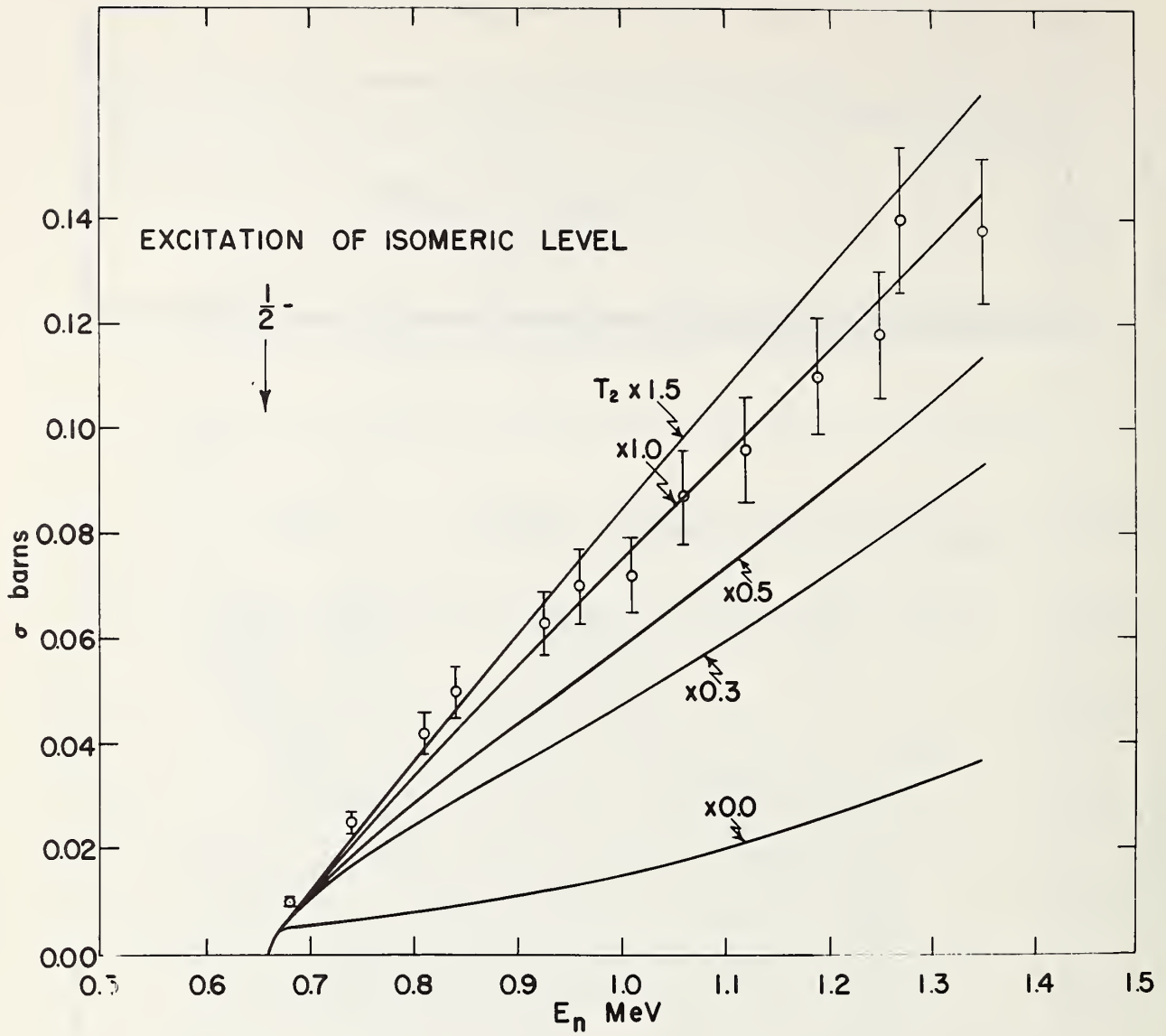


Figure 10 - The cross section for the excitation of isomeric activity in Ba^{137} .

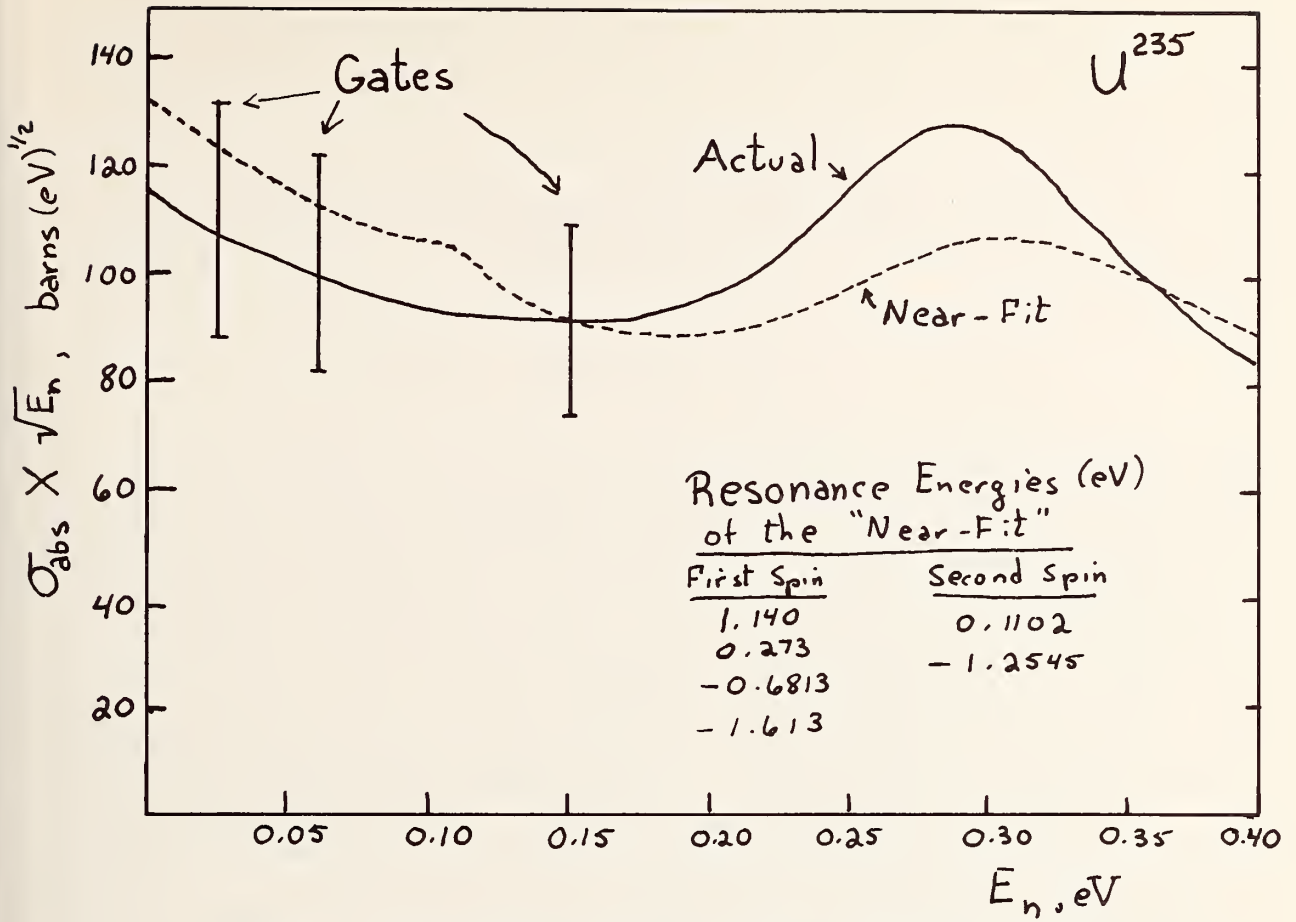


Figure 11 - The absorption cross section of U^{235} at low neutron energies and a randomly-chosen "near-fit", explained in the text, of the kind which might cause difficulty in the analysis of thermal cross sections.

CORRELATIONS IN POSITIONS OF SINGLE-PARTICLE
LEVELS ON COMPLEX NUCLEI

S. I. Sukhoruchkin

Institute for Theoretical and Experimental Physics
Moscow, USSR

ABSTRACT

In the statistical description of complex nuclear spectra the possible shell effects in level spacing distributions are supposed to be small and to be neglected. Positions of low-lying excited states of broad scope of nuclei and strong neutron resonances were analyzed. It appears that even all nuclei being considered simultaneously, in both groups of the data one can see the correlations characterized by a single interval close to 30 keV. Excluding rotational states prominent grouping effect in low-lying states was found by 30, 90, 150, 390, 510 and 780 keV. A small interval can be directly seen in a series of odd-odd nuclei as ground states splittings. Correlational analysis of nucleon binding energies, strong electromagnetic transitions energies and positions of highly excited levels of lead was carried out on computer and an interval of 60 keV was found. Attention was drawn to the fact that two of three most prominent intervals (390, 510 and 780 keV) turn to be close to the mass splitting of elementary particles (511 keV - rest mass of electron, 782 keV - neutron beta-decay energy).

In the statistical description of complex nuclear spectra, possible shell effects in level spacing distributions are supposed to be small. However, some authors have observed a nonstatistical behaviour of level spacing distributions and of positions of strong neutron resonances (1-5). The purpose of this work is to check the systematic character of such deviations from statistical laws. In cases where these effects really exist, in order to get a reliable value of the strength function (an important constant for reactor design), it is necessary that the interval of averaging the neutron widths of individual resonances (or of the measurements themselves) exceed the characteristic energy period of the neutron width modulation. This is related to nonstatistical, or single-particle, effects.

To find trends in relatively simple excitations, we analyzed positions of low-lying excited states (E^*) of a great number of nuclei (excluding the rotational states of deformed nuclei). We have observed a considerable grouping effect in E^* which seemed to be correlated with the variation of the angular momentum of the states, $\Delta J+$. This could be seen from the E^* distribution given previously (7), where the characteristic interval was found to be near 30 keV. Taking the positions of states of all nuclei simultaneously (all ΔJ), we find that the grouping remains. This can be seen in Fig. 1 where the number of low-lying levels in the energy interval $E^* \pm 7.5$ keV is shown (changing E^* by 5 keV steps). All the distribution maxima turn out to be close to the interval number of the period previously obtained (≈ 30 keV). Numbers near the arrows above the most noticeable maxima in Fig. 1, i.e., in the regions where the grouping effect appears, show the ratio of the number of events when the correspondence rule of the even number of periods ($n = E^*:30$ keV) to the even value of variation of $\Delta J+$ is fulfilled, to the number of events when this rule violates, and the same for odd ones. This ratio is almost always greater than unity, which would correspond to the absence of correlations. The grouping in the energies E^* occurs due to systematic identities and multiplicities of intervals between single-particle excited levels of complex nuclei of the order of several hundred keV. They can be described by the spin-orbit terms of the Hamiltonian. Fig. 2 shows examples of the proximity of single-particle splittings in a number of nuclei (e.g., $Z=39$ and $Z=81$) as well as of the multiplicity of their values ($E^* \approx 390$ keV and ≈ 780 keV in Tl^{195} and Tl^{197}). The intervals of the order of 30 keV are superimposed on these large splittings. The smaller interval can be seen directly in a number of odd-odd nuclei as a splitting of the ground state due to the interaction correlated with the spin-spin orientation $\Delta J+=1+$.

Some other examples, for high-lying excited states, are given in Fig. 3. It should be noticed that many of these splittings are of the values that take place in the low-lying states (Fig. 1). In other words, the grouping is of very general (or permanent) character. Even in the case when all the known high-lying levels were analyzed simultaneously, (with $A < 150$ so as not to consider rotational states of deformed nuclei), the grouping remained.

The effect of nonrandom distribution covers also such an energetic nuclear parameter as neutron separation energy, B_n . It was first observed in 1964 during the computer correlation analysis of the binding energies of single-particle states (6). The correlation period found (60.1 keV) turns to be close to the interval of 60 keV that connects the states with even $\Delta J+$ (60 keV = 2×30 keV). Since the neutron resonance position, after the recoil energy correction, is the difference of the E^* -excitation energy of the state and B_n the neutron separation energy for the same nucleus, then from the grouping effect (or more exactly, from the nonstatistical behaviour) of these two values, the presence

of correlations with the same period ≈ 30 keV in the positions of strong neutron resonances automatically follows. These correlations have been discussed before (7). It should be noted that a number of previously found deviations from statistical predictions (1,2,5,8) can be assigned to the groupings in E^* and Bn discussed here.

One of the unexplicable properties of the grouping of low-lying levels is the proximity of distinguishable intervals ≈ 780 keV and 510 keV (see Fig. 1) to charge-mass splittings of nucleon and lepton (782 keV and 511 keV), and the rational relation with the charge splitting of the pion (6).

The multiplicity effect of the distinguishable energetic splittings observed in the more complex excitations in small energy intervals are quite unexpected. However, the same effect is observed in two groups of experimental data: the interval ≈ 5 eV distinguishable in the positions of relatively strong neutron levels. This was pointed out in reference 7, and can be seen even in the positions of all the levels of all the nuclei in the lower right-hand side of Fig. 5. It also appears in the "fine structure" of the level spacing distributions between the levels, D_i . This structure, a strong "statistical fluctuation", was pointed out in the papers by the group from Columbia University in thorium and iodine (3). Arrows in the upper right-hand and left-hand parts of Fig. 5 show the interval 5.5 eV in the D_i distributions. The left-hand part of Fig. 5 gives the total level spacing distributions of a great number of N-even nuclei. The top portion gives the same for the levels with the large reduced neutron width ($\Gamma^n > 1$ mV), i.e., for the levels with relatively large contributions of single-particle states. In the levels with large Γ^n the grouping enhances. Fig. 6 shows the same effect in the D_i distribution of positions of neutron levels of different nuclei, the strongest for each isotope in the interval 0-100 eV with the period marked by an arrow. The confirmation of correlations in such a small scale would be of great interest since it would make possible to investigate fine effects of the shell structure.

The method of comparison of the deviations from the statistical distributions in low-lying and highly excited nuclear states was applied to the energy intervals of several keV (9). Systematic correlations with the same parameters were found in both groups of states. This indicates that the conditions of the statistical model at excitation energies close to the neutron binding energy are in many cases fulfilled incompletely. The model in which these correlations lead to the structure of several electron volts observed in neutron level spacing distributions of heavy N-even target nuclei is discussed in reference 9.

REFERENCES

1. L. A. Toller et al., Phys. Rev. 99, 620 (1955).
2. H. W. Newson et al., Ann. of Phys. 8, 211 (1959).
3. W. W. Havens, Jr., Progress in Fast Neutron Physics, Univ. Chicago Press (1963), p. 215.
4. J. B. Garg et al., Phys. Rev. 134, 985 (1964).
5. W. M. Good et al., Phys. Rev. 1967 (in press).
6. S. I. Sukhoruchkin, Parametric analysis of single-particle energy state, Preprint JINI-1845, Dubna, 1964, p. 39.
7. S. I. Sukhoruchkin, Conference on Nuclear Data for Reactors, IAEA, Vienna, 1967, Vol. 1, p. 159.
8. J. Morgenstern et al., *ibid*, Vol. 1, p. 183.
9. S. I. Sukhoruchkin, Deviations from the Statistical description of the neutron level spacing distributions for intermediate and heavy nuclei. Program and Thesis of the X Annual Conference on Nuclear Spectroscopy and Nuclear Structure, Riga, 1968.
10. W. McLatchie et al., Can. J. Phys. 42, 926 (1964).

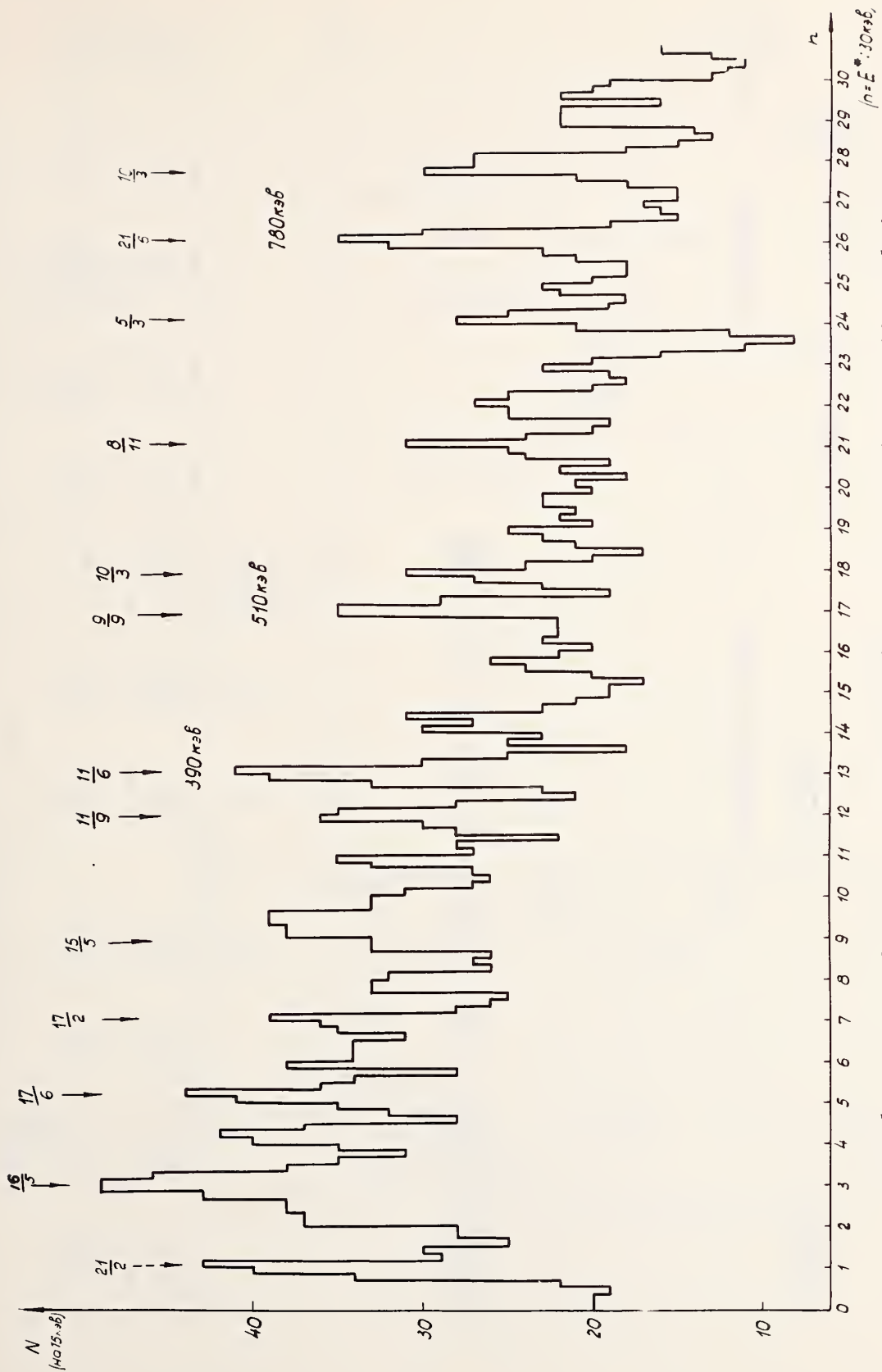


Fig. 1. Distribution of number of low-lying levels of all nuclei.

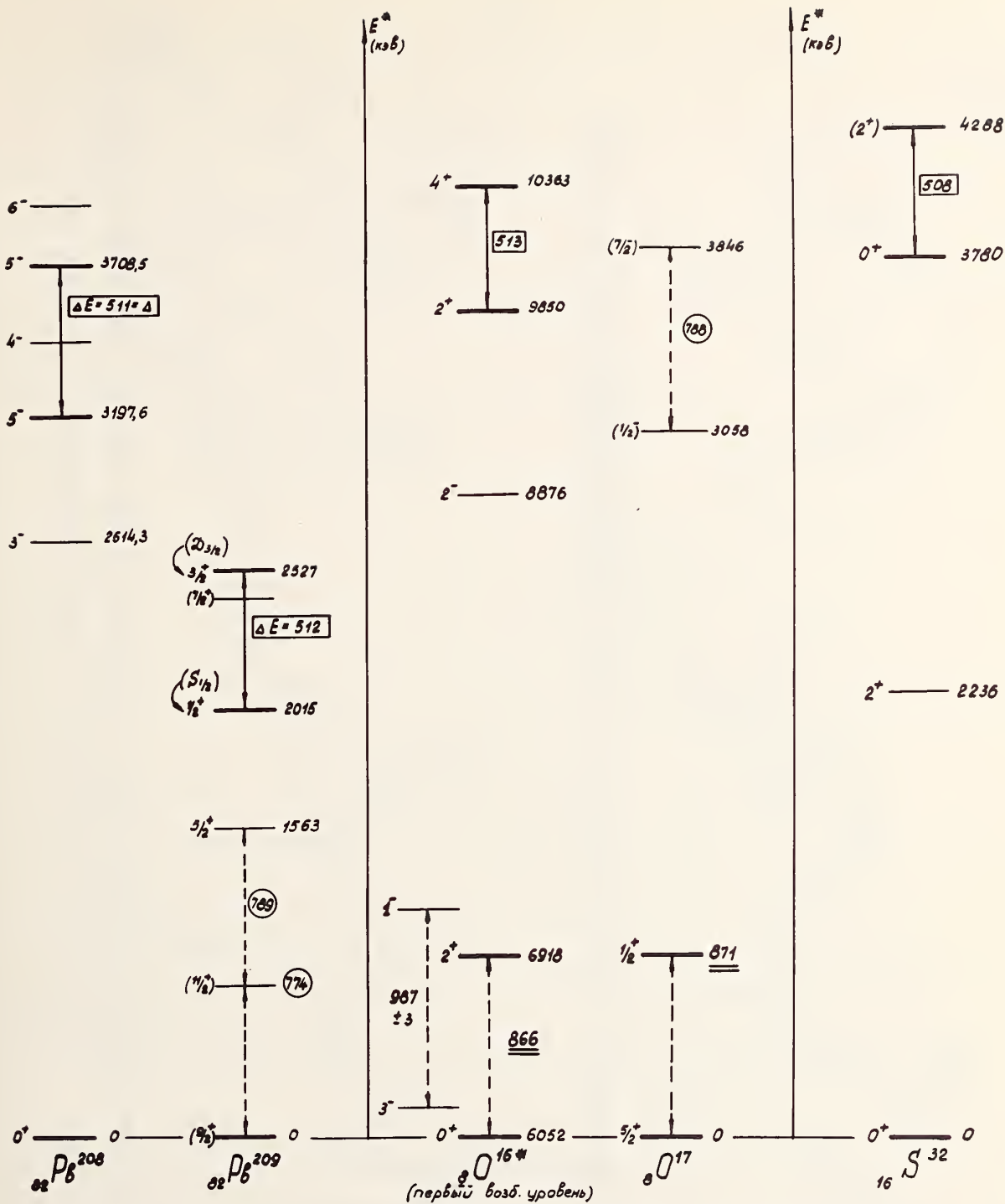


Fig. 3. Energy levels of some neighboring nuclei.

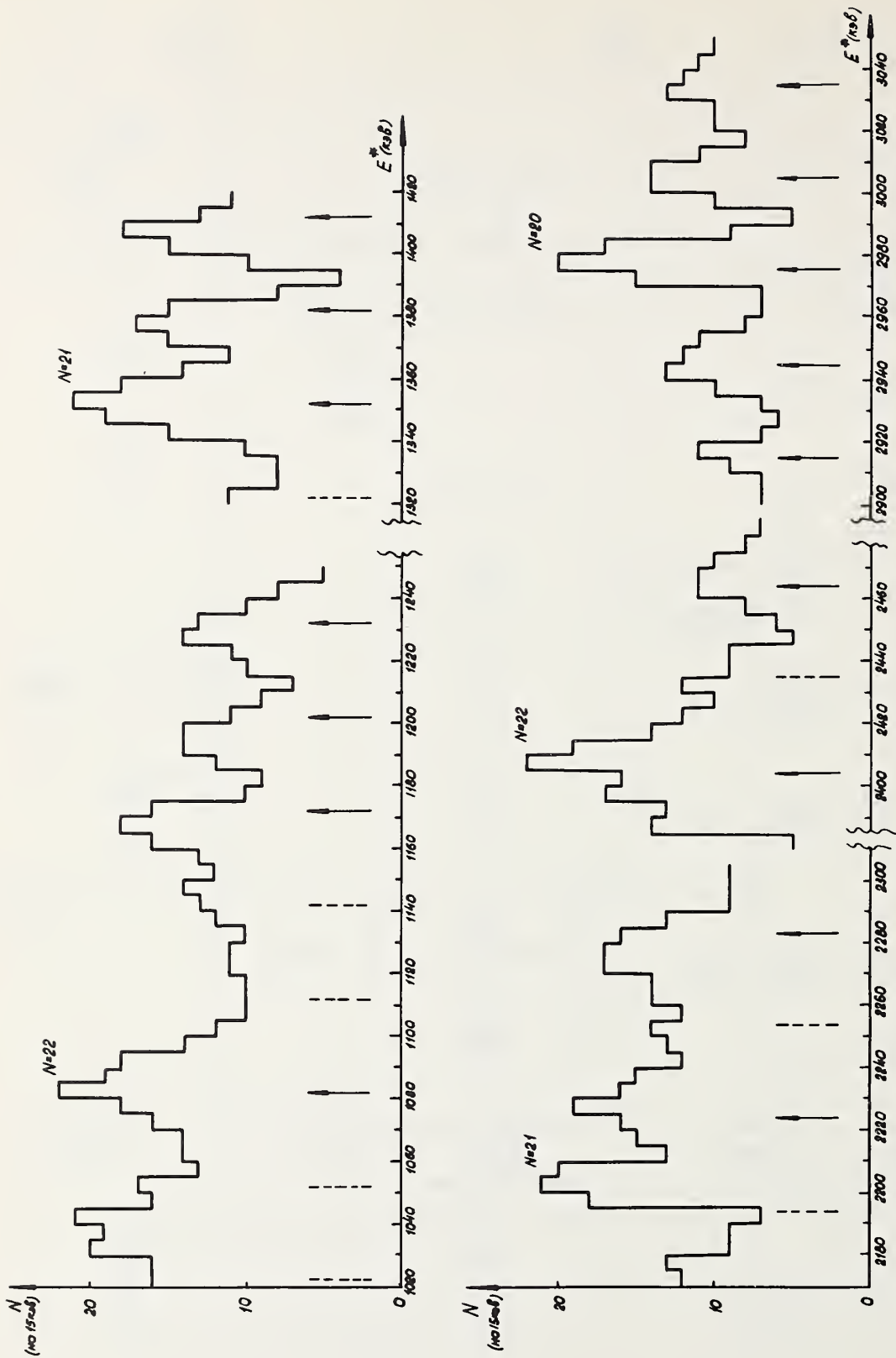


Fig. 4. Distribution of number of high-lying levels of nuclei with $A < 150$.

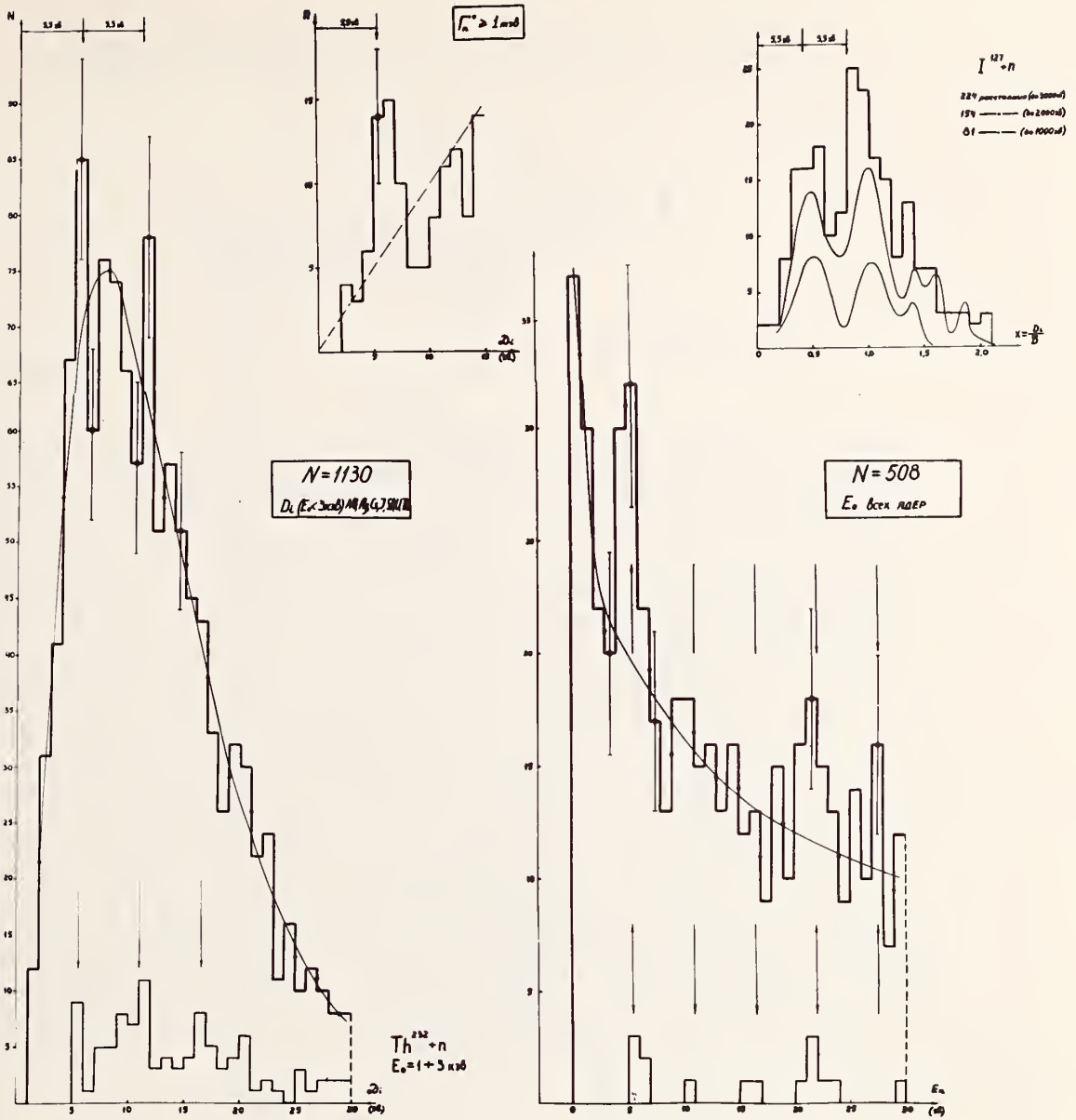


Fig. 5. Distribution of the positions of neutron levels of all nuclei (right) and spacing of levels of N-odd nuclei (left).

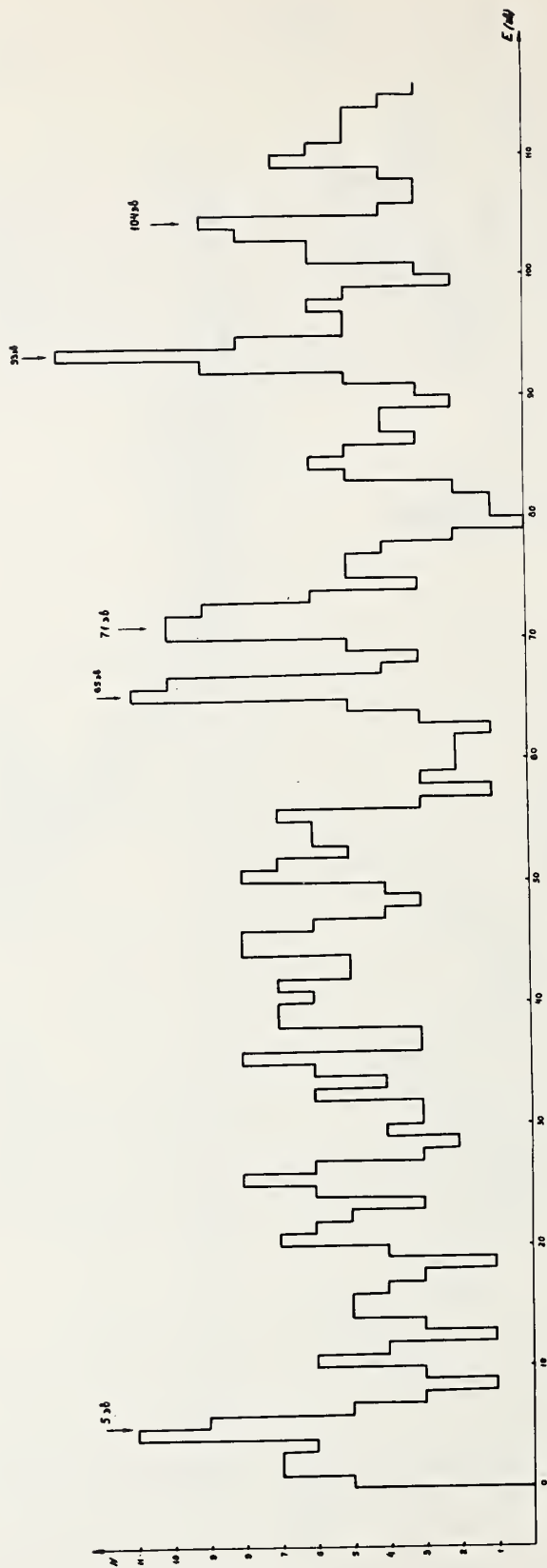


Fig. 6. Distribution of the positions of strong neutron levels.

CALCULATIONS OF ELASTIC SCATTERING AND INELASTIC
DIRECT PROCESSES OF FAST NEUTRONS BY U-238

F. Bühler

Institut für Strahlenphysik
Universität Stuttgart
Stuttgart, Germany

Abstract

Elastic scattering and inelastic direct processes of fast neutrons by U-238 have been studied in the energy range 2.5-14.1 MeV using coupled-equations methods. The target nucleus is described by the collective model. The whole interaction to which the incident neutron is subjected is described by a nonspherical optical-model potential with a spherical spin-orbit-coupling. To overcome the difficulties in fitting the parameters of the optical model, the nuclear form factors are determined by generalizing the equivalent local potential of Perey and Buck [1]. Over the whole energy range a good agreement between theoretical and experimental elastic cross sections is found. The same deformation parameter of the interaction potential was used for all projectile energies. It was compared with the reduced transition probability of Coulomb excitation. The influence of higher rotational states of U-238 on the elastic and inelastic direct scattering has been studied. In case of inelastic scattering, the often used hypothesis that only ground state and first excited state are strongly coupled, is found to be not valid. The influence of the 4^+ and 6^+ states on the potential elastic scattering is unimportant.

1. Introduction and Interaction Model

In this paper we shall report on calculations of the scattering of fast neutrons by the deformed nucleus U-238.

The nucleus is described by using the permanently deformed nucleus model. The interaction potential is assumed to have the form:

$$V(\vec{r}, \zeta) = \sum_{\lambda, \nu} v_{\lambda}(\tau) D_{\nu 0}^{\lambda}(\zeta) Y_{\lambda}^{\nu*}(\vartheta, \varphi) \quad (1)$$

The $D_{\nu_0}^{\lambda}(\zeta)$ are elements of the rotation matrix [2], ζ specifies the orientation of the nuclear symmetry axis (Euler angles), $Y_{\lambda}^{\nu}(\vartheta, \varphi)$ are the spherical harmonics, $\vec{r} = (r, \vartheta, \varphi)$ denotes the coordinates of the incident neutron.

For the axial symmetric problem, the nuclear form factors $v_{\lambda}(r)$ are:

$$v_0(r) = \sqrt{4\pi} V_{opt}(r) \quad (2)$$

$$v_2(r) = -\beta \cdot r \cdot \frac{dV_{opt}(r)}{dr} \quad (3)$$

β is the conventional deformation parameter of the nucleus [3], $V_{opt}(r)$ is the spherical Optical Potential of the form:

$$V_{opt}(r) = \frac{-V_0}{1 + e^{\frac{r-R_v}{a_v}}} - i W_0 \frac{4 \cdot e^{\frac{r-R_w}{a_w}}}{\left(1 + e^{\frac{r-R_w}{a_w}}\right)^2} \quad (4)$$

To the non-spherical Optical Potential (1) we add a spherical spin-orbit coupling [4]:

$$V_{SO} = \gamma \left(\frac{\hbar}{\mu_0 c}\right)^2 \frac{1}{r} \frac{d}{dr} \left(\frac{1}{1 + e^{\frac{r-R_v}{a_v}}} \right) \vec{\sigma} \cdot \vec{l} \quad (5)$$

γ is the depth of the spin-orbit interaction, μ_0 is the mass of the π^0 -Meson.

In $v_2(r)$ we suppress the imaginary part of $V_{opt}(r)$. If we use a potential of the form (1), we have to integrate a series of coupled Schroedinger equations to find the radial part of the wave functions [4, 5, 6, 7, 8]. These calculations require high-speed computing facilities [4, 7]. To overcome the difficulties in fitting the Optical Model parameters in $V_{opt}(r)$, we tried to use the parameters of the equivalent local potential of Perey and Buck [1]. In the potential (1) we only have to fit the deformation parameter β .

In Tab.1 we tabulated the parameters of the equivalent local potential.

Another question is: how many nuclear states are strongly coupled? We studied this question, because in the most papers the hypothesis is used that only the ground state (0^+) and first excited (2^+) are strongly coupled and that the effect of higher excited collective states may be neglected concerning shape elastic scattering and inelastic direct processes to the first excited state [6, 8].

Table 1

Parameters of the equivalent local Optical Potential

E [MeV]	2.5	4.1	7.0	14.1
V_0 [MeV]	46.43	45.97	45.15	43.18
W_0 [MeV]	9.42	9.34	9.18	8.80
R_V [fm]	7.835	7.835	7.835	7.835
R_W [fm]	7.682	7.682	7.680	7.674
γ [MeV]	9.3	8.98	8.52	8.20
a_V [fm]	0.656	0.656	0.656	0.656
a_W [fm]	0.48	0.48	0.48	0.48

2. Results and Discussion

Fig.1 shows the shape elastic scattering cross-section for 2.5 MeV as a function of the deformation parameter β . $\beta = 0$ means that the cross-section is calculated using the equivalent local potential [1].

Comparing with experimental data [9] we see from this figure that the most suitable deformation parameter is $\beta = 0.25$ because we have to add to the theoretical shape elastic scattering cross-section the cross-sections for all direct processes which are within the energy spread due to the final energy resolution of all neutron experiments.

For energies greater than 2 MeV we may neglect cross-sections from compound reactions. From the reduced transition probability $B(E2; 0^+ \rightarrow 2^+)$ of Coulomb excitation we calculated a deformation parameter $\beta = 0.237$. This is in good agreement with our fit.

Fig.2 shows the influence of higher rotational states on the shape elastic scattering. We get one cross-section from coupling only the ground state and first excited rotational state of U-238, the other cross-section was calculated under the assumption that 0^+ , 2^+ and 4^+ states are strongly coupled. For the calculation of all cross-sections we only used quadru-

pol coupling ($\lambda=2$) since an additional coupling with $\lambda=4$ (transitions $0^+ \rightarrow 4^+$) does not appreciably affect the elastic and inelastic direct cross-sections.

Reflecting on the experimental uncertainties we take from this figure that for the calculation of potential elastic scattering the hypothesis of coupling only 0^+ and 2^+ state is valid.

In addition we examined the influence of the third excited state (6^+ -level) on the shape elastic scattering. If we use the coupling of the four states (0^+ , 2^+ , 4^+ , 6^+ ; $\lambda = 2$), the integral shape elastic scattering cross-section changes by approximately 50 mb.

Fig.3 summarizes the inelastic direct cross-sections for different forms of coupling for an energy of 7.0 MeV. In this figure we drew the cross-sections to the 2^+ and 4^+ state of U-238. The solid line gives the cross-section to the 2^+ -state calculated by coupling the 0^+ , 2^+ and 4^+ state, the dashed line is a 2^+ -cross-section calculated by the coupling of the 0^+ , 2^+ state. We see from this plot that the superposition of the first cross-section (solid line) and the corresponding 4^+ -cross-section is approximated by the dashed line of the second cross-section which results from the coupling of the 0^+ and 2^+ states only.

In neutron experiments in the MeV-region the measured elastic scattering cross-section for U-238 is the superposition of shape elastic and direct inelastic cross-sections to the first and mostly to the second excited state. Therefore, if we compare our calculations with experimental data, we may use the coupling of 0^+ and 2^+ state only. If we calculate, however, inelastic direct cross-sections this hypothesis is not valid. As we already mentioned earlier we made the experience that the influence of the 6^+ -state on the inelastic scattering to the first excited state can be neglected.

In Fig.4 we show the calculated elastic scattering cross-section (2.5 MeV) for two deformation parameters.

Fig.5 gives a comparison of theoretical and experimental elastic cross-sections [9, 10] for an energy of 7.0 MeV. The calculation of a cross-section with a complex coupling potential is shown in Fig.6.

Comparing this elastic scattering cross-section with the cross-section plotted in Fig.5 we can conclude that within the experimental uncertainties the absorption part of the coupling potential can be suppressed. Fig.7 summarizes the shape elastic cross-section for different kinds of coupling and in Fig.8 we compared the theoretical elastic scattering cross-section with experimental data [9] for an energy of 14.1 MeV.

3. References

- [1] Perey, F. and B.Buck Nucl.Phys. 32 (1962) 353
- [2] Hecht, K.T. Collective Models.
Selected Topics in Nuclear Spectroscopy (1963).
North-Holland Pub.Comp.Amsterdam (1964).
- [3] Bohr, A., and B.R. Mottelson Dan.Mat.Fys.Medd. 27 (1953) No 16
- [4] Bühler, F. Dissertation, Universität Stuttgart (1967)
- [5] Chase, D.M., L.Wilets and A.R.Edmonds Phys.Rev. 110 (1958) 1080
- [6] Buck, B. Phys.Rev. 130 (1963) 712
- [7] Bühler F., F.Schmidt Contributions to the Calculation of Fast Neutron Scattering by U-238
BMwF-Report K 67-90 (1967)
- [8] Baldoni, B., A.M.Sarius Nuovo Cim. 33 (1964) 1145
- [9] Howerton, R.J. Tabulated Cross Sections (1961)
UCRL 5573
- [10] Batchelor, R., W.B.Gilboy, Nucl.Phys. 65 (1965) 236
and J.H.Towle

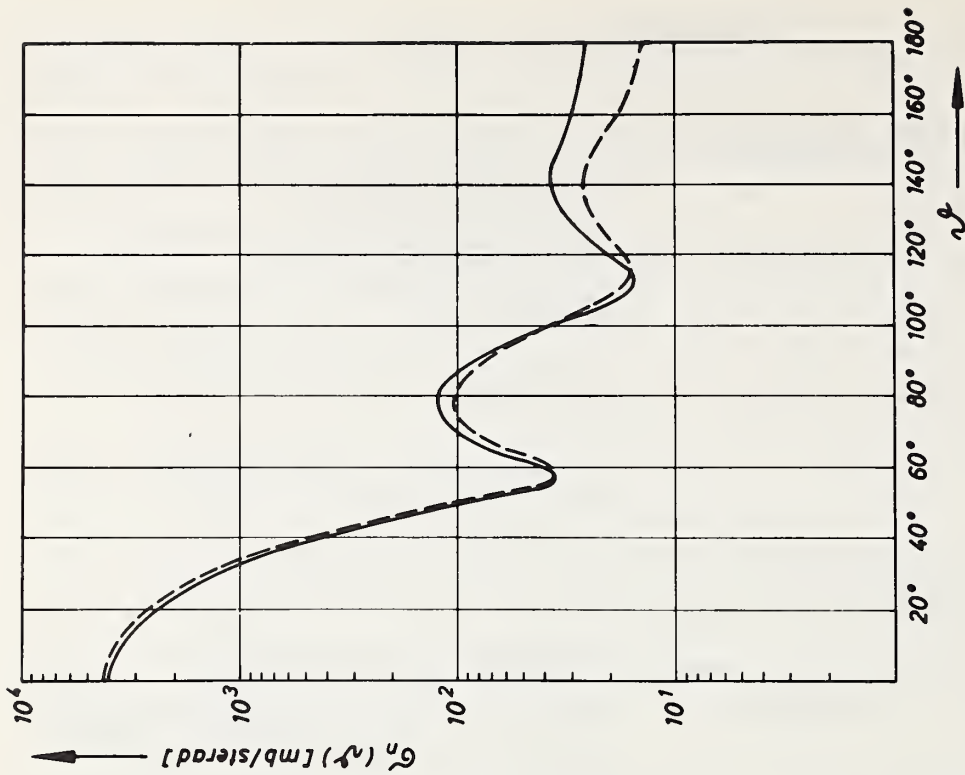


Fig.2: Shape elastic scattering cross-section.

$E = 2.5 \text{ MeV}$

— coupling $O^+, 2^+, 4^+$ ($\lambda = 2$)
 --- coupling $O^+, 2^+$ ($\lambda = 2$)

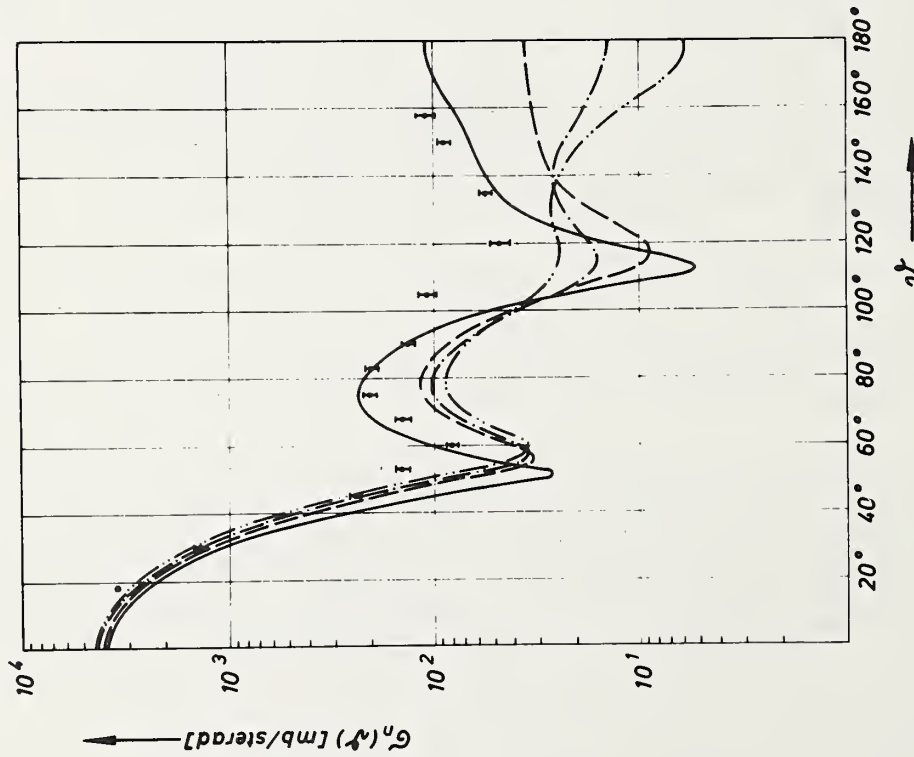


Fig.1: Shape elastic scattering cross-section as a function of the deformation parameter β .

$E = 2.5 \text{ MeV}$

— $\beta = 0$, --- $\beta = 0.2$, -.- $\beta = 0.25$, $\beta = 0.28$

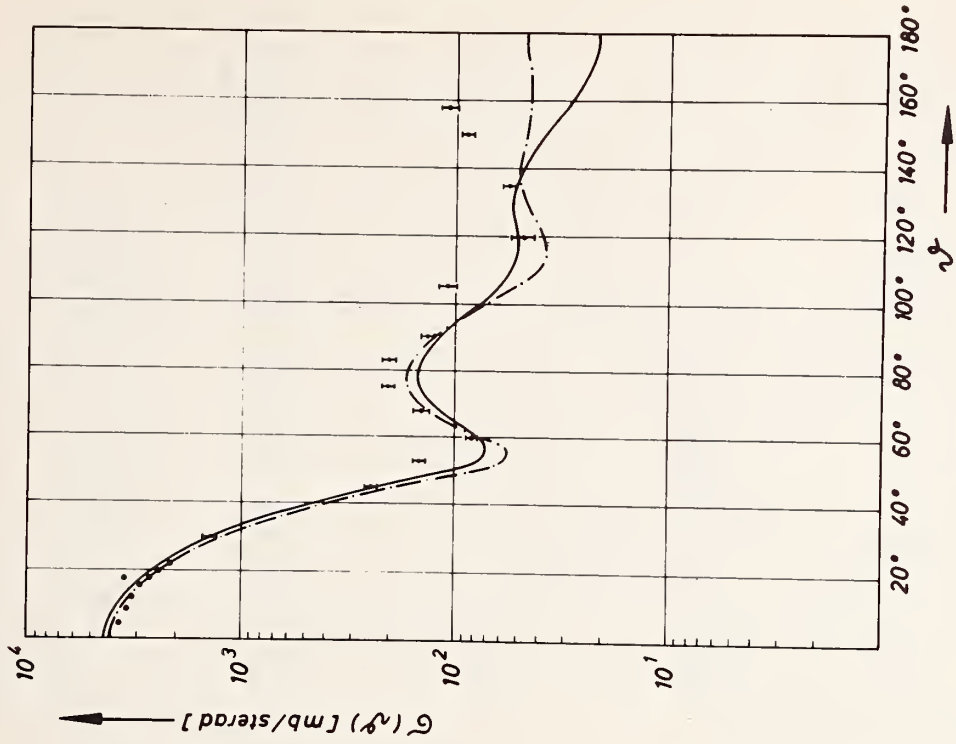


Fig.4: Elastic scattering cross-section.

E = 2.5 MeV

-.-β = 0.2, —β = 0.25

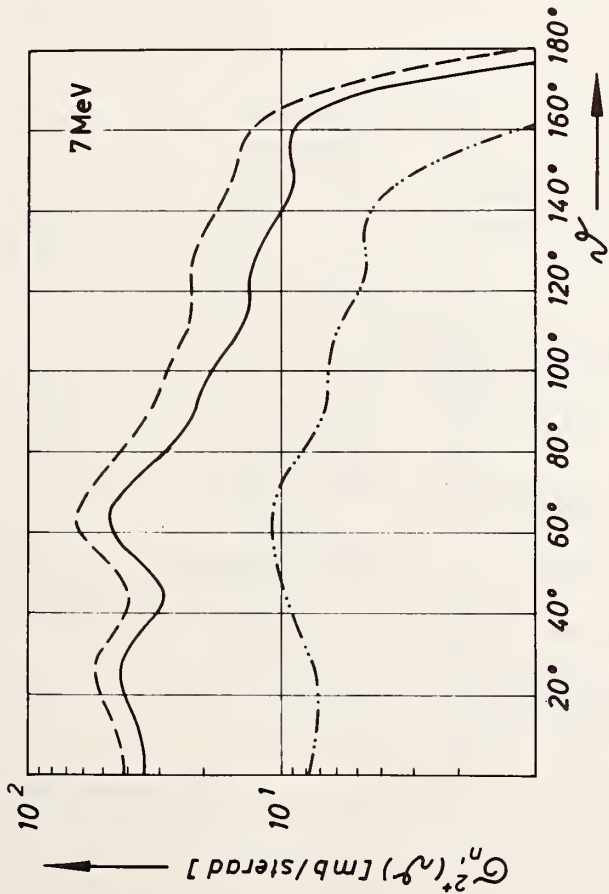


Fig.3: Inelastic direct cross-section to the 2^+ and 4^+ state.

E = 7.0 MeV

--- $\sigma_{n_1}^{2^+}(\beta)$, coupling $0^+, 2^+$

— $\sigma_{n_1}^{2^+}(\beta)$, -.- $\sigma_{n_1}^{4^+}(\beta)$ coupling $0^+, 2^+, 4^+$

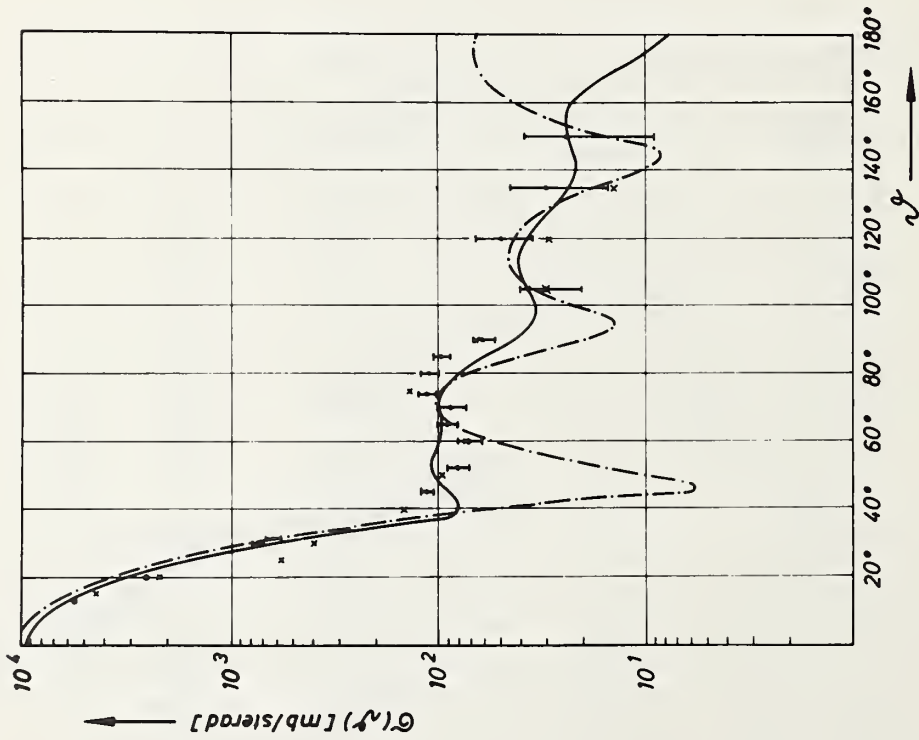


Fig.5: Elastic scattering cross-section.
 $E = 7.0$ MeV
 $-\cdot-\cdot-$ $\beta = 0$, $---$ $\beta = 0.25$

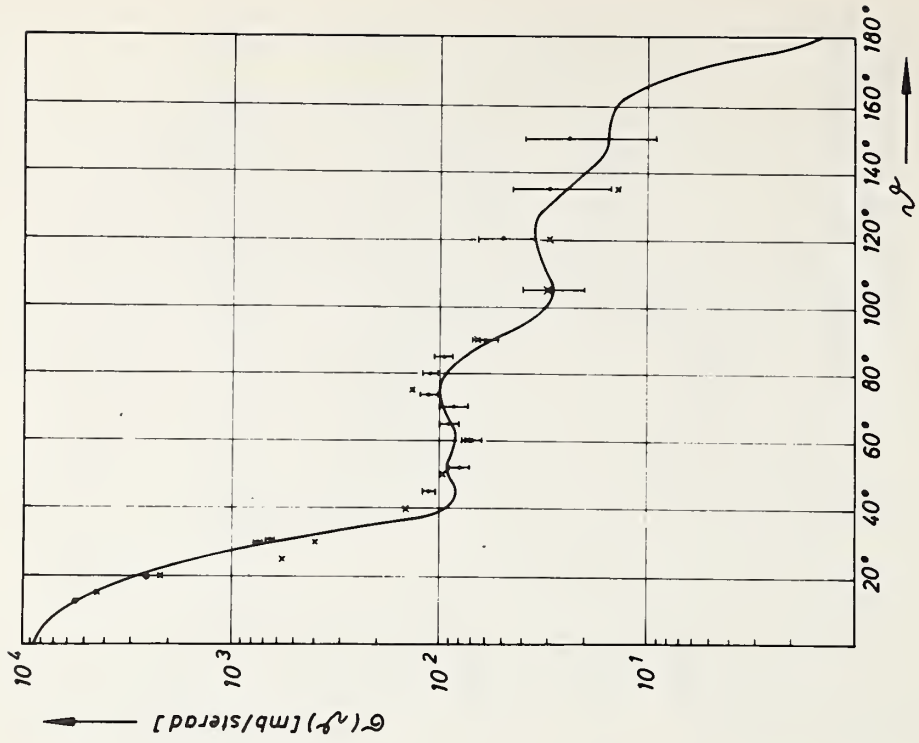


Fig.6: Elastic scattering cross-section calculated
 with complex coupling potential.
 $E = 7.0$ MeV
 $\beta = 0.25$

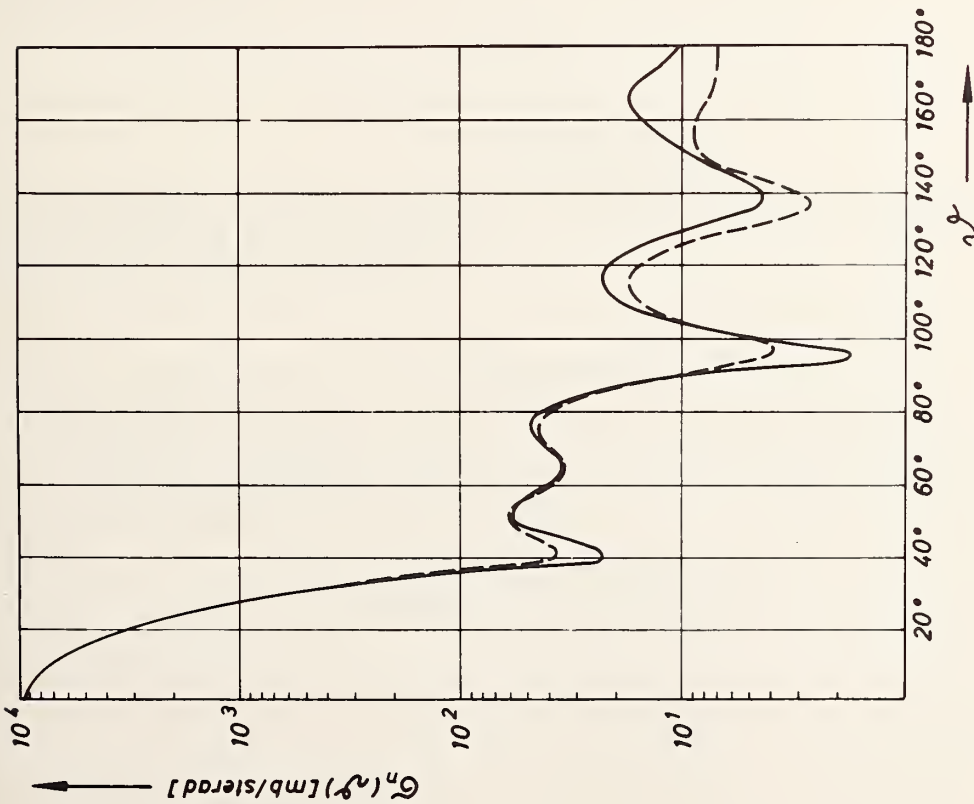


Fig.7: Shape elastic scattering cross-section.

$E = 7.0 \text{ MeV}$

--- coupling of O^+ and 2^+ state

— coupling of O^+ , 2^+ and 4^+ state

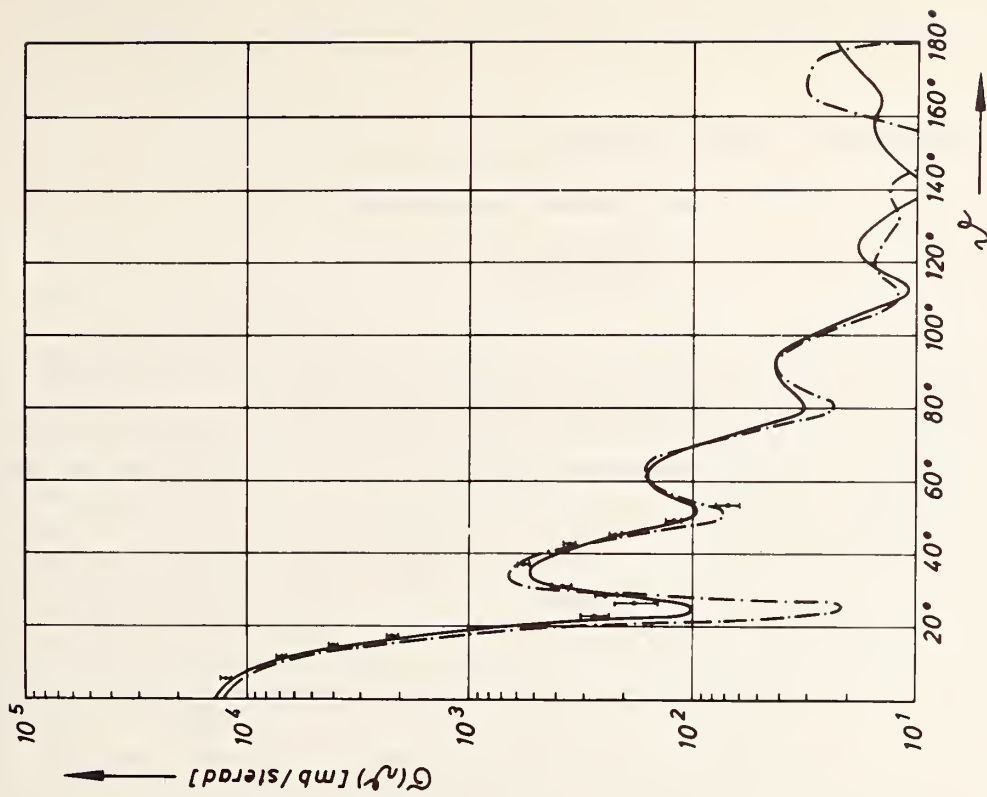


Fig.8: Elastic scattering cross-section.

$E = 14.1 \text{ MeV}$

— $\beta = 0$, --- $\beta = 0.25$

Dr. Nestor Azziz, Westinghouse Atomic Power Divisions

Pittsburgh, Pennsylvania 15230

ABSTRACT

It is known by the theory of Nuclear Matter that the average nuclear potential, i.e., the average potential seen by a nucleon in the nucleus is non-local. With the aim of resolving the bound state problem and/or scattering problems, many non-local potentials have been proposed which more or less account for the actual average potential in nuclear matter. More often, however, a local potential with parameters depending on the energy of the nucleon is used as a tool for nuclear scattering and bound state predictions. The calculations with this local potential are very much simpler than those using a non-local potential since the latter entails the solution of an integral-differential Schrodinger equation. The uncertainty and variety of local parameters is of great concern. The most unfortunate consequence of these uncertainties is the fact that quite often the resulting value of a parameter will disagree with predictions from more fundamental models of the nucleus. We have deduced from first principles the depth of the nuclear potential at the center of the nucleus with energy dependent parameters using the theory of Nuclear Matter^[1].

1. INTRODUCTION

The optical potential may be written as the sum of central, spin-orbit and Coulomb potentials.

$$V = V_c + V_{so} + V_{cou} \quad (1)$$

where for instance, the central potential, V_c , is the sum of a real and imaginary part

$$V_{c \text{ real}} = -V_0 f(r, r_0, a)$$

The radial function $f(r, r_0, a)$ has the usual Saxon-Woods form.

$$f(r, r_0, a) = (1 + \exp(r - R_0)/a)^{-1}$$

We will concentrate our attention on the depth V_0 of the real part of the potential. The energy dependence of this parameter has been obtained by several authors fitting data from various nuclei at several energies. For instance Perey² analyzed 35 proton elastic scattering angular distributions and other data from 9 Mev to 22 Mev for a range of about 40 isotopes from Al up to Au. He expressed $V_0(E)$ as

$$V_0(E) = -53.3 + 0.55E - 0.3 \bar{V}_{\text{cou}} - 27 \frac{(N-Z)}{A} \text{ (Mev)} \quad (2)$$

where \bar{V}_{cou} is an average coulomb potential inside the nucleus. The last term of this equation is the symmetry term which will be discussed later.

Agee and Rosen^[2] have predicted neutron data for about 40 nuclei in the range 0 to 16 Mev. Their optical potential parameters were the same as those obtained by Rosen, Berry, Goldhaber and Auerbach^[2] fitting elastic scattering of polarized protons and 14 Mev neutron elastic scattering data. The latter group found in their last work an energy variation of the potential depth given by

$$V_0 = -49.3 + 0.33 E \text{ (Mev), for neutrons (4-24 Mev)} \quad (3)$$

and

$$V_0 = -53.8 + 0.33 E \text{ (Mev), for protons (7-22 Mev)} \quad (4)$$

Willmore and Hodgson, fitting neutron cross section for Si, S, Ca, Ti, Fe, Ba, Pb and U in the range 1-15 Mev, found a trend for V_0 given by

$$V_0 = -47.01 + 0.267E + 0.00118E^2. \quad (5)$$

These are just a few examples of the many semi-empirical expressions of the optical potential depth that have appeared in the literature.

2. GENERAL CONSIDERATION

Details of our analysis will be given elsewhere. In this section we will summarize the main physical concepts and the results of our work. In the nuclear matter calculations in reference 1, the number of neutrons was assumed to be equal to the number of protons, and protons and neutrons were treated on the same basis. The charge independence assumption of the nuclear forces implies that in the isotopic spin language the total isotopic spin is a good quantum number. The nuclear interaction, nucleon-nucleon or in general nucleon-nucleus, may depend, however, on the scalar product of the isotopic spins of both systems. For the case of nucleon-nucleus interaction this will mean that it will depend on $(N-Z)$, the difference between the total number of neutrons and protons. This term, designated the symmetry term, is determined in the revised nuclear matter calculation assuming that neutrons and protons form two Fermi systems with two different maximum momenta.

Another important concept introduced in this analysis is the rearrangement energy. The optical potential describes the average attraction felt by an external particle which penetrates into the well generated by the nucleons of the nucleus. In general our problem is to resolve the dynamics of the $(A+1)$ particle so we separate the $(A+1)$ Hamiltonian as

$$H_{A+1} = H_A + (E_K) + H_{int}.$$

The ground state of the nucleus A is represented by the Hamiltonian H_A . E_K is the kinetic energy of the incoming particle and the interaction H_{int} is generally assumed to be an optical potential. This optical potential must be such that in case the system $(A+1)$ releases the particle which has penetrated into the nucleus in the same conditions as it was introduced, the nucleus must be left again in its ground state. In other words the optical potential must take into account the average attraction of the particle to the nucleus as the nucleon moves in nuclear matter plus the extra perturbation among the nucleons that this extra nucleon implies. The average

two-body interaction in the many body system (G matrix) is not the same before and after the particle has penetrated. The difference is the rearrangement that the particles will suffer due to the extra particle. Brueckner and Goldman [3] have discussed this concept for the first time in connection with the shell model potential.

3. RESULTS AND DISCUSSION

We write our final result for the optical potential depth as:

$$V_0 = \tilde{V}_0 + (1 - m_R^*) (E - \bar{V}_c) \pm \alpha (N - Z)/A, \text{ Mev.} \quad (6)$$

The constant, \tilde{V}_0 , is given by the binding energy of nuclear matter at the nuclear density $\rho = 0.17 \text{ fm}^{-3}$ multiplied by the reduced mass, plus the kinetic energy of the particle at the surface of the Fermi sea corresponding to $N=Z$. The reduced mass, m_R^* , involves the rearrangement energy caused by the extra particle and represents the effective mass of a nucleon invading the Fermi sea. The average Coulomb potential \bar{V}_c accounts for the slowing down of the protons in nuclear matter which tends to increase its potential depth. \bar{V}_c is zero for neutrons. The negative sign is used for protons and the positive for neutrons.

The symmetry coefficient α has three main contributions: a pure statistical one due to the fact that the neutron and proton actually have different Fermi momenta; a second contribution which comes from the dependency of the two-body interaction in nuclear matter, G matrix, on the Fermi momenta; and a third contribution coming from the difference between the proton and neutron rearrangement energy.

Since \tilde{V}_0 , m_R^* and α are considered independent of energy, the nuclear matter theory leads to a correlation of the form utilized by Perey. Thus correlations of Perey (and others) may be used as a vehicle for comparing experimental data with nuclear matter theory.

In Figure 1 we show our predictions of the proton optical potential depth by crosses. The ordinate indicates the value of the potential depth. On the abscisses we have displayed the mass number A. The open circles indicate the semi-empirical values of Perey and the dashed line corresponds to the formula obtained by Rosen et al. fitting proton polarization data. Each strip corresponds to one incident proton energy. The isotopes are the same as chosen by Perey.

In Figure 2 we show our predictions for the case of neutrons. The semi-empirical value of Rosen et al. and Willmore and Hodgson are indicated with horizontal lines.

Except for the depth of the real part of the potential, V_0 , the uncertainties of the parameters of the semi-empirical formulas for the optical potential could be as much as 20% - 30%. The depth, V_0 , now being analyzed, may have an uncertainty of about 5%.

Because of the good agreement indicated in Figures 1 and 2 and in consideration of the uncertainties in the semi-empirical formulas, we may conclude that optical potential studies could very well be interpreted using a theoretical expression for the depth of the real part of the potential like the one displayed in equation 6. Such a procedure would reduce the arbitrariness in selection of parameters in the fitting of experimental data. Therefore, a more accurate deduction of the values of the remaining parameters relating to the width and shape of the potential may be expected.

4. REFERENCES

1. N. Azziz, Nuclear Physics 85, 15 (1966).
2. F. E. Bjorklund and S. Fernbach, Phys. Rev. 109, 1295, (1958);
F. G. Perey, Phys. Rev. 131, 745 (1963); Rosen, J. G. Berry,
A. S. Goldhaber and H. Auerbach, Ann. Physics (N.Y.) 34, 96 (1965).
Ferme P. Agee and Louis Rosen, Los Alamos Report LA-3538-MS;
D. Willmore and D. E. Hodgson, Nuclear Physics 55, 673 (1964).
3. K. A. Brueckner and D. Goldman, Phys. Rev. 116, 424 (1959).

$$V = 48.6 - 0.30(E - \sqrt{V_c}) + 30(N-Z)/A \quad (\text{MEV})$$

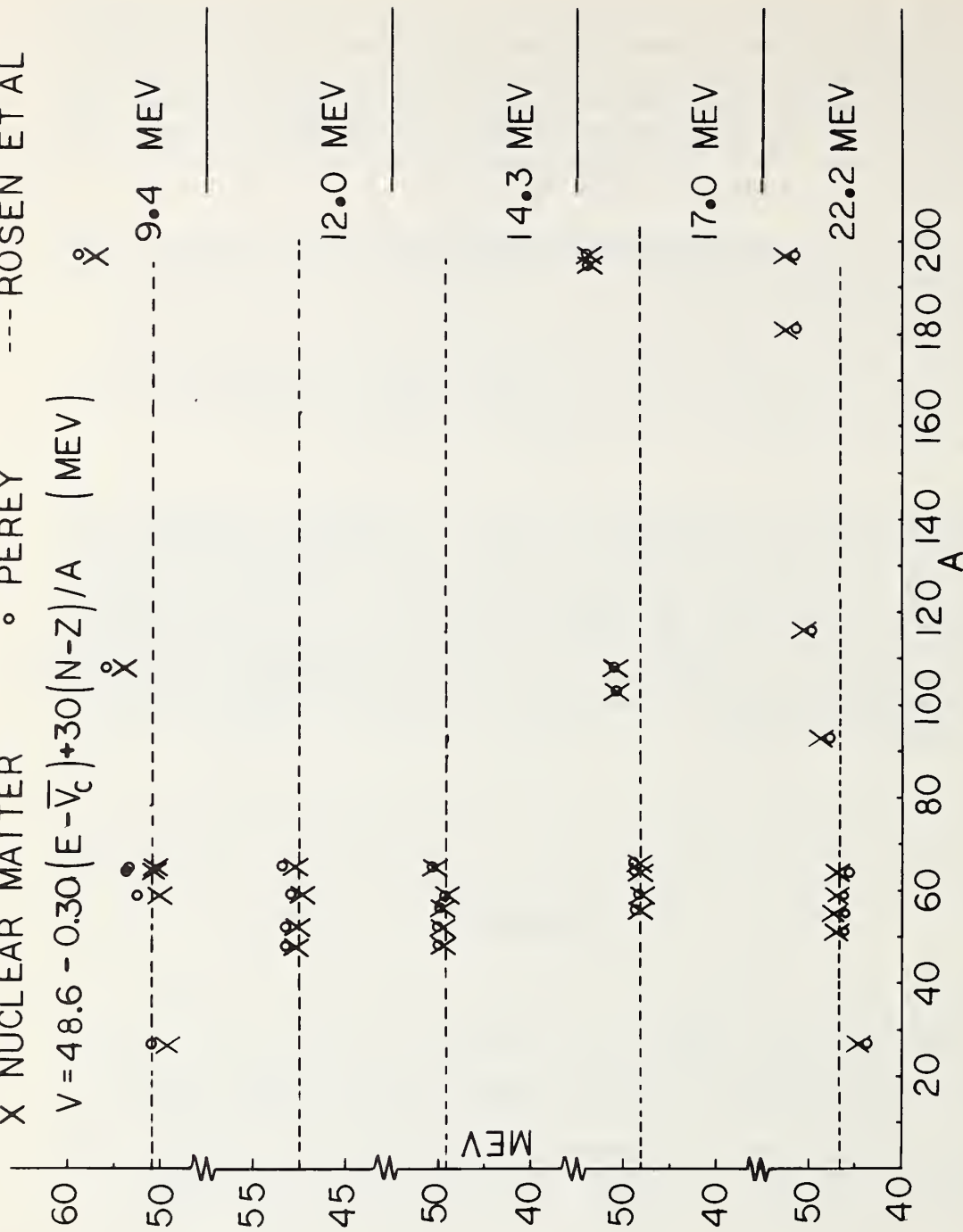


FIGURE 1: Depth of the real part of the optical potential for protons. Comparison between theoretical formula, deduced in this paper and those semi empirical of Perey and Rosen et al. (See reference 2).

$$k_p = 1.35 \text{ fm}^{-1} \quad m_R^* = 0.70 \quad \alpha = 30 \text{ Mev}$$

WILLMORE AND HODGSON — — —
 NUCLEAR MATTER ° $V = 48.6 - 0.30 E - 30 (N-Z)/A$ (MEV)
 ROSEN ET AL — — —

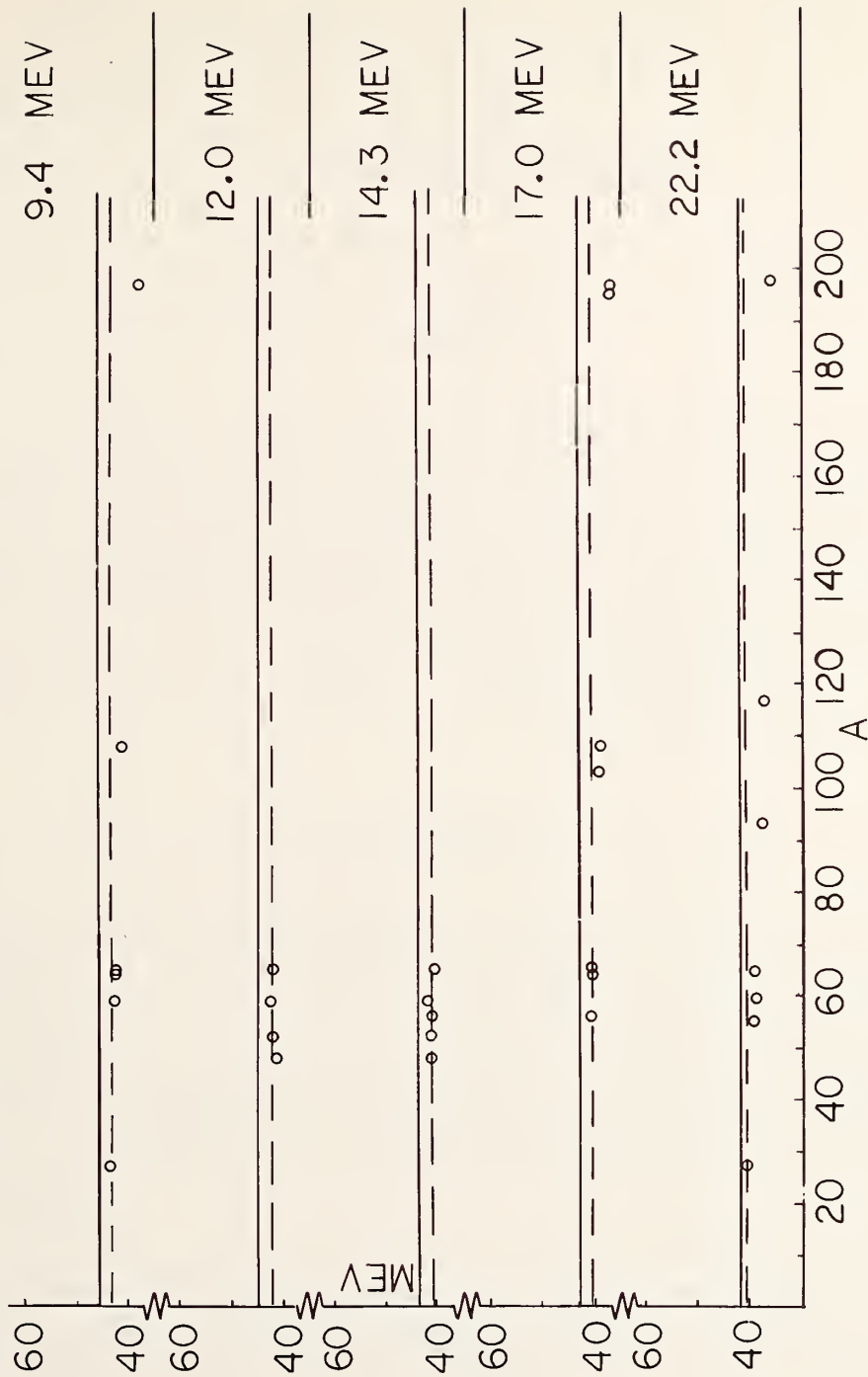


FIGURE 2: Depth of real part of the optical potential for neutrons

$$k_F = 1.35 \text{ fm}^{-1} \quad m_R^* = 0.70 \quad \alpha = 30 \text{ Mev}$$

Comparison between theoretical formula deduced in this paper and those semi-empirical of Willmore and Hodgson and Rosen et al.

THERMAL NEUTRON CROSS SECTIONS AND RESONANCE INTEGRALS
FOR TRANSURANIUM ISOTOPES*

A. Prince
Brookhaven National Laboratory
Upton, New York 11973

ABSTRACT

A systematic procedure for estimating fission and capture thermal cross sections and fission and capture resonance integrals for transuranium isotopes is outlined. The method involves establishing a correlation between the difference of the binding energy and fission threshold ($B_n - E_f$) and the cross sections and resonance integrals. Estimated values for σ_f , σ_γ , I_f , I_γ , $\langle \nu_p \rangle$, α , η , and $\langle E_k \rangle$ (average kinetic energy of fission products) for more than 280 isotopes ranging from $_{88}\text{Ra}^{212}$ to $_{108}\text{X}^{264}$ have been completed. The method of analysis and recommendations are given for possible study and improvements.

1. INTRODUCTION

In considering the transmutation of heavy elements by irradiation in high flux reactors, it is of prime importance to know the magnitudes of the thermal capture and fission cross sections and their respective resonance integrals. A survey of the literature discloses that this type of experimental data for many of the isotopes in the buildup chain are either nonexistent or in drastic disagreement with each other. Similarly, associated data, such as resonance parameters Γ_f , Γ_γ , and Γ_n that could be employed in a Breit-Wigner formalism for calculating σ_f , σ_γ , I_f , and I_γ , are also lacking.

The purpose of this paper is to present a systematic procedure for empirically estimating these quantities without knowledge of resonance parameter data. A technique is also furnished for predicting the average kinetic energies of the fission fragments $\langle E_k \rangle$ and the average number of prompt neutrons $\langle \nu_p \rangle$ emitted per fission.

* This work performed under the auspices of the U.S. Atomic Energy Commission.

2. PROCEDURE

The method consists of establishing a correlation between the parameter of interest and the binding and fission threshold energies. This method was first pointed out by Huizenga, et al. [1], and extended by Vandenbosch and Seaborg [2].

In this analysis the ratio of the thermal neutron fission cross section σ_f and the thermal capture cross section σ_γ is expressed as the ratio of the average fission and capture width

$$\frac{\sigma_f}{\sigma_\gamma} = \frac{\Gamma_f}{\Gamma_\gamma} \quad (1)$$

Extended treatment along similar lines will also produce information on the magnitudes of the fission and capture resonance integrals (beyond Cd cutoff).

2.1 Fission Thresholds

Bohr and Wheeler [3] predicted that the variation of the fission barrier E_f has a strong dependence on the fissility Z^2/A . In an attempt to improve on the various semi-empirical estimates of the fission barriers [2, 4-12] based on this concept, an averaging process of all calculations, coupled with a least-squares analysis of the experimental data, was undertaken. This analysis showed that the simple formula of Vandenbosch and Seaborg was sufficient for isotopes of $Z < 97$. For $Z \geq 97$ the following formula was derived:

$$E_f = -106.247 + 12.99026(Z^2/A) - 0.438185(Z^2/A)^2 + 0.0045383(Z^2/A)^3 + \epsilon, \quad (2)$$

where

$$\epsilon = \begin{cases} 0.0 & \text{for even-even nuclei} \\ 0.47 & \text{for odd A nuclei} \\ 0.72 & \text{for odd-odd nuclei} \end{cases}$$

2.2 Thermal Capture and Fission Cross Sections

The most recent experimental data on σ_γ and σ_f were correlated with $B_n - E_f$ where values of B_n were taken from Mattauch, et al. [13]. Contrary

to the results of Huizenga, et al. [5], the variation of $\ln(\sigma_f/\sigma_\gamma)$ versus $B_n - E_f$ was found to level off as shown in Fig. 1. This deviation may be explained by the channel theory of Hill and Wheeler [14], where the average fission width $\langle \Gamma_f \rangle^{J\pi}$ is related to the average level spacing $\langle D \rangle^{J\pi}$ and the effective number of fission channels $N^{J\pi}$ by

$$\langle \Gamma_f \rangle^{J\pi} = \frac{\langle D \rangle^{J\pi}}{2\pi} N^{J\pi} \quad (3)$$

and $N^{J\pi}$ is dependent upon the penetrability factor P_i by

$$N^{J\pi} = \sum_i P_i \quad (4)$$

with

$$P_i = \frac{1}{1 + \exp \left[\frac{2\pi(E_i^{J\pi} - E)}{\hbar\omega} \right]}, \quad (5)$$

where $E_i^{J\pi}$ is the fission threshold and $\hbar\omega$ the characteristic energy of the barrier curvature. Further analysis showed a qualitative correlation for σ_f and the product $\sigma_f \sigma_\gamma$ which also may be explained in terms of channel theory of fission. Some values obtained for σ_f and σ_γ are tabulated and compared with experimental data in Table I.

2.3 Resonance Integrals

The ratio of experimental values of the fission and capture integrals were also found to have a correlation with $B_n - E_f$ similar to that of σ_f/σ_γ shown in Fig. 1. Investigation of the resonance structure of the compound nucleus disclosed that one half of the capture integral was attained by either the first or third resonance (beyond Cd cutoff) depending on whether the compound nucleus formed was of e-o or e-e (o-o), respectively.

Figures 2 and 3 show the asymptotic growth [15] of the resonance integrals of two of the many isotopes studied. This characteristic feature provided the necessary framework to establish a relationship between the capture resonance integral and $B_n - E_f$ shown in Fig. 4.

Table II provides a comparison of the estimated values of I_f and I_γ with experimental data.

Average Kinetic Energy of Fission Fragments

Since E_f and $\langle E_k \rangle$ have been shown to depend on $Z^2/A^{1/3}$, a functional relationship results in an expression for $\langle E_k \rangle$ given by

$$\langle E_k \rangle = - 466.06158 + 2.159462x - 0.001772276x^2 \quad (6)$$

where

$$x = A^{2/3} [19.0 + \epsilon - E_f]$$

and values of E_f and ϵ are those of Ref. 2.

Equation (6) yielded values better than one percent accurate when compared with existing experimental data (see Table III).

2.4 Average Number of Prompt Neutrons per Fission

A specific form of the variation of the average number of prompt neutrons emitted per fission was analyzed in terms of the energy balance of a fission event. Extending this analysis to the fission threshold and $\langle E_k \rangle$ resulted in the relation

$$\langle \nu_p \rangle = 27.35144 - 0.3530338\langle E_k \rangle + 0.001219425\langle E_k \rangle^2 \quad (7)$$

where $\langle E_k \rangle$ is given by Eq. (6).

Some values of $\langle \nu_p \rangle$ are compared in Table III and are seen to agree within less than one percent with the recommended values.

3. CONCLUSIONS AND RECOMMENDATIONS

The systematic treatment employed here for estimating various nuclear properties of fissioning isotopes has raised several questions which warrant further study. Since the analysis is rather general and deals only with average values, the even-odd (one and three resonance) characteristics of the asymptotic growth of the resonance integrals should be subjected to a more detailed investigation. A possible interpretation of this phenomena might be explicable in terms of a multilevel-multichannel analysis as used by Refs. 16-20. An even more extensive approach and one that has not been tested enough is the recent "quasi-resonance" theory of Lynn [21]. Recent developments in interpreting the n, γ, f process [22-24] and the discrete structure of the fission barrier [25,26] should also be investigated.

Several other parameters that are significant in establishing a more concise correlation must be further refined. Chief among these is the binding energy B_n . In the heavy isotope region the various estimated values of the binding energy might differ by as much as 2 MeV, and since the correlation is highly dependent on $B_n - E_f$, it is obvious that more accuracy in B_n is required. Other relations such as the Γ_γ and $\langle D \rangle$ dependence on the fissility Z^2/A and spin J might also be studied.

Additional analysis should also be applied to Bohr's [27] interpretation of the discrete structure of the fission barrier resulting from the spin and parity of the compound nucleus formed. According to this hypothesis the slow neutron capture by a nucleus of even-odd nature, such as U-235 or Pu-239, leads to two different classes of levels of the compound system, and the fission probabilities Γ_f^+ and Γ_f^- associated with the height of their respective fission barriers E_f^+ and E_f^- will also depend upon the spin.

Following the work on Pu-239 of Northrop, et al. [28], who found two thresholds $E_{f_1} = -1.61$ MeV and $E_{f_2} = -0.72$ MeV below the binding energy B_n , yields an average $\langle B_n - E_f \rangle = 1.16$ MeV. From the systematic approach, this leads to a value of $\sigma_f = 736$ b for Pu-239, which is in excellent agreement with $\sigma_{f_{\text{expt}'}} = 740$ b.

While such agreement might be considered to be somewhat fortuitous, it is felt that more intensive inquiry in this direction, coupled with the other areas of investigation mentioned earlier, should produce even better results.

Estimated values of σ_f , σ_γ , I_f , I_γ , $\langle \nu_p \rangle$, $\langle E_k \rangle$, α , and η for nearly 300 isotopes ranging from ${}_{88}\text{Ra}^{212}$ to ${}_{106}\text{X}^{264}$ are available upon request.

4. REFERENCES

1. J. R. Huizenga and R. B. Duffield, Phys. Rev. 88, 959 (1952).
2. R. Vandenbosch and G. T. Seaborg, Phys. Rev. 110, 507 (1958).
3. N. Bohr and J. A. Wheeler, Phys. Rev. 56, 426 (1939).
4. G. T. Seaborg, Phys. Rev. 88, 1429 (1952).
5. J. R. Huizenga, R. Choudhry, and R. Vandenbosch, Phys. Rev. 126, 210 (1962).
6. W. J. Swiatecki, Phys. Rev. 101, 97 (1956).
7. W. D. Myers and W. J. Swiatecki, Nucl. Phys. 81, 1 (1966).

8. V. E. Viola, Jr. and B. D. Wilkins, Nucl. Phys. 82, 65 (1966).
9. D. W. Dorn, Phys. Rev. 121, 1740 (1961).
10. I. R. Dmitrieva, Reports of the Academy of Sciences of the Beorussian SSR, No. 4 (1966), transl. as BNL-TR-165.
11. S. A. E. Johansson, Nucl. Phys. 22, 529 (1961).
12. V. E. Viola, Jr. and G. T. Seaborg, J. Inorg. Nucl. Chem. 28, 741 (1961).
13. F. Everling, L. A. König, J. H. E. Mattauch, and A. H. Wapstra, Nucl. Phys. 18, 529 (1962).
14. D. L. Hill and J. A. Wheeler, Phys. Rev. 89, 1102 (1953).
15. S. Pearlstein, Brookhaven National Laboratory Report BNL 982 (May 1966).
16. E. Vogt, Phys. Rev. 112, 203 (1958).
17. E. Vogt, Phys. Rev. 118, 724 (1960).
18. M. S. Moore and C. W. Reich, Phys. Rev. 111, 929 (1958).
19. M. S. Moore and C. W. Reich, Phys. Rev. 118, 718 (1960).
20. D. B. Adler and F. T. Adler, Brookhaven National Laboratory Report BNL 50045 (1967).
21. J. E. Lynn, in Proc. International Conf. on the Study of Nuclear Structure with Neutrons, Antwerp (North-Holland Publ. Co., Amsterdam, 1965), p. 125.
22. V. Stavinsky and M. O. Shaker, Nucl. Phys. 62, 667 (1965).
23. J. E. Lynn, Phys. Lett. 18, 31 (1965).
24. R. Vandenbosch, Nucl. Phys. A101, 460 (1967).
25. J. A. Wheeler, Proc. First U.N. International Conf. on Peaceful Uses of Atomic Energy, Geneva, 1955 (United Nations, Geneva, 1955), Paper P/593.
26. P. E. Vorotnikov, Sov. J. Nucl. Phys. 5, 728 (1967).
27. A. Bohr, Proc. First U.N. International Conf. on Peaceful Uses of Atomic Energy, Geneva, 1955 (United Nations, Geneva, 1955), Paper P/911.

28. J. A. Northrop, et al., Phys. Rev. 115, 1277 (1959).
29. E. K. Hyde, et al., The Nuclear Properties of the Heavy Elements (Prentice-Hall, Englewood Cliffs, 1964), Vol. III.
30. J. R. Stehn, et al., "Neutron Cross Sections," Brookhaven National Laboratory Report BNL 325, 2nd Ed., Suppl. 2, Vol. III (1965).
31. C. H. Westcott, et al., Atomic En. Rev. 3, No. 2 (1965).
32. W. R. Cornman, et al., Trans. Am. Nucl. Soc. 10, No. 1 (June 1967).
33. C. H. Ice, Paper DP-MS-66-69 presented at Transplutonium Committee Meeting, Oak Ridge National Laboratory, November 1966.
34. P. R. Fields, et al., Nucl. Phys. A96, 440 (1967).
35. M. K. Drake, Nucleonics 24, 108 (1966).
36. B. W. Stoughton and J. Halperin, Nucl. Sci. Eng. 6, 100 (1959).
37. K. H. Beckurts and K. Wirtz, Neutron Physics (Springer-Verlag, New York, 1964).
38. F. Feiner and L. J. Esch, in Reactor Physics in the Resonance and Thermal Regions, ed. by A. J. Goodjohn and G. C. Pomraning (MIT Press, Cambridge, 1966), Vol. II, p. 299.
39. A. Prince, General Electric Co. Report GEMP 411 (1966).
40. B. M. Gordon and E. V. Weinstock, paper to be presented at American Chemical Society Meeting, San Francisco, April 2, 1968.
41. V. E. Viola, Jr., Nuclear Data, Section A 1, No. 5 (1966).
42. M. Sieger and S. Yiftah, Israel Atomic Energy Commission Report IA-757 (1962).

TABLE I
Thermal Fission and Capture Cross Sections[†]

Target Nucleus	σ_f (b) expt'l.	σ_f (b) estimated	σ_γ (b) expt'l.	σ_γ (b) estimated
$_{88}\text{Ra-226}$	$<1.1 \times 10^{-4}$	3.73×10^{-5}	18.0	28.4
$_{90}\text{Th-230}$	$<10^{-3}$	2.26×10^{-3}	35 ± 10 26 ± 2 22.7 ± 0.6	18.1
$_{92}\text{U-232}$	80 ± 15 77 $\pm 10^a$	24.0	300 ± 200 78 $\pm 4^a$	300.0
U-233	523 ± 4 525 $\pm 2^a$ 527.7 $\pm 2.1^b$	605.0	56 ± 2 49 $\pm 6^a$ 48.6 $\pm 1.5^b$	104.0
U-234	<0.65	0.0074	72 ± 10 95 $\pm 7^a$	40.2
U-235	580 ± 2 577.1 $\pm 0.9^a$ 579.5 $\pm 2.0^b$	781.0	112 ± 10 101 $\pm 2^a$ 100.5 $\pm 1.9^b$	178.0
U-237	$\frac{\sigma_f + \sigma_\gamma}{411}$ $\pm 138^c$	201.0		512.0
U-238	$<5 \times 10^{-4}$	8.54×10^{-4}	2.76 ± 0.06	16.9
$_{93}\text{Np-234}$	900 ± 300	605.0	-----	104.0
$_{94}\text{Pu-238}$	18.2 ± 0.5	19.0	489 ± 3 403 ± 8 500 $\pm 100^a$	278.0
Pu-239	754 ± 9 740.6 $\pm 3.5^a$ 742.4 $\pm 3.5^b$	611.0	287 ± 13 265.7 $\pm 3.7^b$	105.0
Pu-240	0.8 ± 0.7	1.49	250 ± 40 530 ± 50	113.0
Pu-241	1060 ± 210 950 ± 50 950 $\pm 30^a$ 1009 ± 9	787.0	390 ± 80 425 $\pm 40^a$ 382 $\pm 21^b$	185.0

TABLE I (con't)

Target Nucleus	σ_f (b) expt'l.	σ_f (b) estimated	σ_{γ} (b) expt'l.	σ_{γ} (b) estimated
Pu-242	<0.3	0.037	18.6 \pm 0.8 23.0 ^d 18.0 ^d	32.5
^{95}Am -242m (152 yr.)	4600 6000 \pm 500 ^a	797	5500 2000 \pm 600 ^a	219
Am-242g (16 h)	3000 2900 \pm 1000 ^a	797	-----	219
Am-243	<0.072	0.126	73.6 \pm 1.8 84.0 ^d	47.6
^{96}Cm -242	<5	294.0	25	549.0
Cm-243	490 \pm 70 690 \pm 50	1090.0	250 \pm 150	255
Cm-244	-----	170	25 \pm 10 32 20 ^d	485
Cm-245	1880 \pm 150	612.0	135 260 ^d 200 \pm 100	106
Cm-246	0.0	1.92	80 15 \pm 10	124.0
Cm-247	35	634.0	35 180 600 ^d	110.0
^{97}Bk -249	-----	5.59	350 660 ^d	183
^{98}Cf -249	1735 \pm 70	1940.0	270 \pm 100	273.0
Cf-250	<348	699.0	1500 1200 ^d	131.0
Cf-251	3000 \pm 300	143.0	3000 1600 ^d	384.0
Cf-252	-----	81.9	8.5 30 25	424.0

TABLE I (con't)

Target Nucleus	σ_f (b) expt'l.	σ_f (b) estimated	σ_γ (b) expt'l.	σ_γ (b) estimated
${}_{99}\text{Es-253}$	----	713.0	195 351 ^e	332.0

[†] The experimental values of σ_f and σ_γ were taken from Hyde, Ref. 29 unless stated otherwise.

^a Ref. 30.

^b Ref. 31.

^c Ref. 32

^d Ref. 33

^e Ref. 34.

TABLE II

Comparison of Estimated Resonance Integrals with Experiment

Target Nucleus	I_r (b) expt'l.	I_r (b) estimated	I_γ (b) expt'l.	I_γ (b) estimated
${}_{91}\text{Pa-231}$	-----	0.22	480 ^a	633.0
${}_{92}\text{U-233}$	780 ^a	386	137 ^a 150 $\pm 10^b$ 100 $\pm 4^c$ 137 $\pm 7^d$	152.0
U-234	-----	0.8	700 $\pm 100^b$ 661.4 ^c	1000.0
U-235	280 ^a 270 $\pm 50^b$ 264.4 ^c 280 $\pm 11^d$	565.0	140 ^a 100 $\pm 30^b$ 188.3 ^c 140 $\pm 8^d$	302
U-238	-----	0.003	278 ^a 280 $\pm 15^b$ 280 $\pm 10^c$	128
${}_{93}\text{Np-237}$	-----	0.643	$I_r + I_\gamma = 946^a$ 700 $\pm 150^b$ $I_r + I_\gamma = 955^c$	919
${}_{94}\text{Pu-238}$	-----	43.5	3420 ^a 3260 $\pm 280^b$	1500
Pu-239	288 ^a 280.2 ^c 310 $\pm 20^d$	450	134 ^a 181.5 ^c	177
Pu-240	-----	45.0	$I_r + I_\gamma = 8280^a$ 9000 $\pm 1000^b$ 8700 ± 800 9000 ± 3000 } ^c	7990
Pu-241	573 ^a 557 $\pm 33^c$	560	139 ^a	309
${}_{95}\text{Am-243}$	-----	1.46	$I_r + I_\gamma = 2340^a$ 2290 ± 50 } ^c 1374	1280

TABLE II (con't)

Target Nucleus	I_f (b) expt'l.	I_f (b) estimated	I_γ (b) expt'l.	I_γ (b) estimated
$^{96}\text{Cm}-244$	-----	271	$I_f + I_\gamma = 660^e$	498
$^{98}\text{Cf}-252$	-----	79.4	$I_f + I_\gamma < 80^f$	970

^a Ref. 35.

^b Ref. 36.

^c Ref. 37.

^d Ref. 38.

^e Ref. 39.

^f Ref. 40.

TABLE III

Comparison of Estimated Values of $\langle E_k \rangle$, $\langle \nu \rangle$, α , and η with Experiment

Target Nucleus	$\langle E_k \rangle^\dagger$ expt'l.	Ref. 41 $\langle E_k \rangle$	$\langle E_k \rangle$ This Work	$\langle \nu \rangle$ expt'l.	$\langle \nu \rangle$ This Work	$\langle \nu \rangle^{\dagger\dagger}$	α expt'l.	α This Work	η expt'l.	$\eta^{\dagger\dagger\dagger}$ This Work
${}_{90}\text{Th-229}$	159.7 \pm 2.0 165.0 \pm 4	164.0	160.0	2.18 \pm 0.08 ^a	2.09	2.08	-----	1.11 $\times 10^{+3}$	-----	1.88 $\times 10^{-3}$
Th-232	-----	-----	159.0	2.2 \pm 0.4 ^b	2.06	2.04	-----	2.71 $\times 10^4$	-----	7.54 $\times 10^{-5}$
${}_{92}\text{U-232}$	-----	-----	169.0	3.04 \pm 0.05 ^a	2.50	2.48	-----	12.5	-----	0.184
U-233	166.0 \pm 2.0 to 169.6 \pm 2.0	169.6	168.0	2.497 \pm 0.008 ^a	2.48	2.47	0.0926 \pm 0.0023 ^a	0.172	2.292 \pm 0.006 ^a	2.10
U-235	167.0 \pm 2.0 to 172.5 \pm 3.2	169.1	168.0	2.426 \pm 0.006 ^a	2.45	2.43	0.175 \pm 0.002 ^a	0.227	2.078 \pm 0.005 ^a	1.98
${}_{94}\text{Pu-239}$	175.0 \pm 1.7	174.8	175.0	2.892 \pm 0.011 ^a 2.871 \pm 0.014 ^c	2.91	2.89	0.370 \pm 0.006 ^a 0.3580 \pm 0.0054 ^c	0.172	2.116 \pm 0.009 ^a 2.114 \pm 0.010 ^c	2.47
Pu-241	171.0 \pm 4 177.0 \pm 5	174.4	174.0	3.00 \pm 0.04 ^a 2.969 \pm 0.023 ^c	2.88	2.86	0.379 \pm 0.021 ^c	0.235	2.21 \pm 0.07 ^a 2.154 \pm 0.036 ^c	2.31
${}_{95}\text{Am-241}$	-----	-----	178.0	3.09 \pm 0.04 ^d	3.16	3.13	-----	80.3	-----	0.039
${}_{98}\text{Cf-252}$	-----	-----	185.0	3.772 \pm 0.015 ^c	3.76	3.73	-----	5.18	-----	0.604

† References for these experimental values are contained in Ref. 41.

†† Normalized to $\langle \nu \rangle = 2.43$ for U-235.††† Based on $\langle \nu \rangle^{\dagger\dagger}$ ^a Ref. 30.^b Ref. 42.^c Ref. 31.

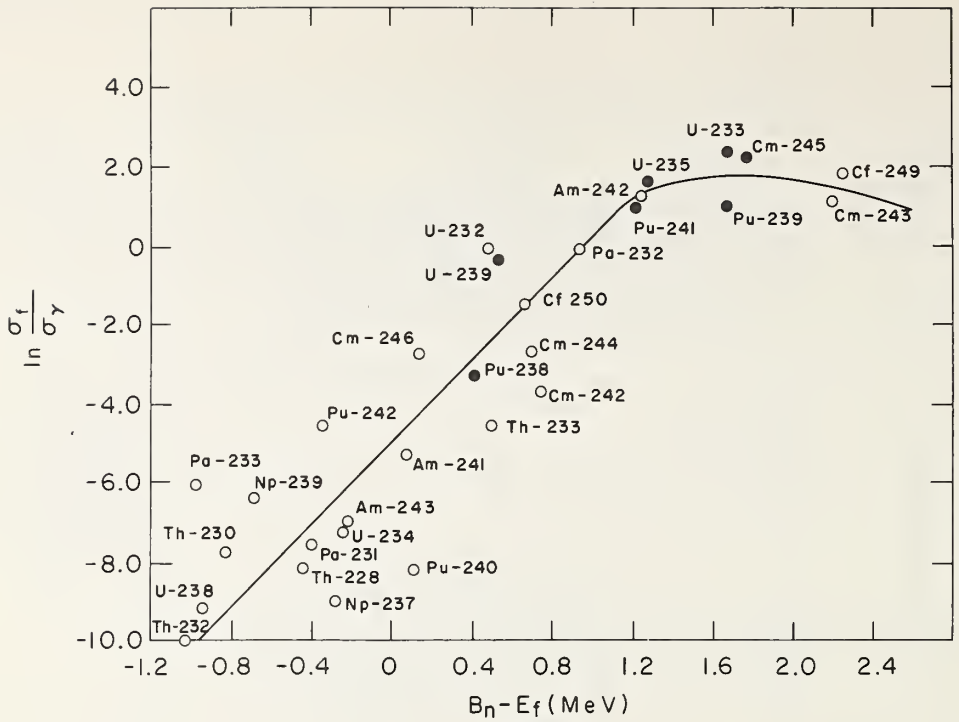


FIGURE 1

CORRELATION OF σ_f/σ_γ WITH THE ENERGY DIFFERENCE ($B_n - E_f$)

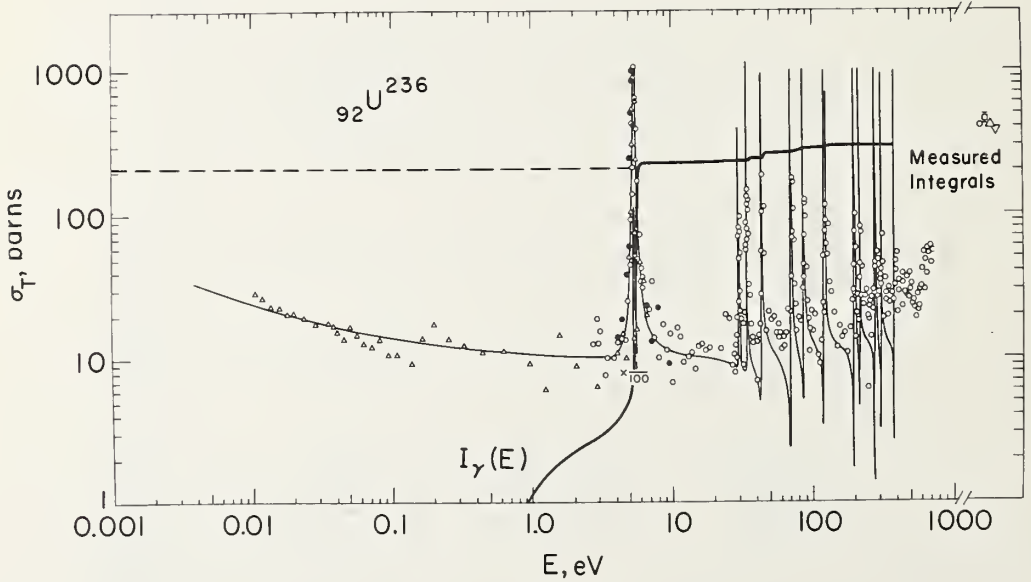


FIGURE 2

ASYMPTOTIC GROWTH OF ^{236}U RESONANCE INTEGRAL

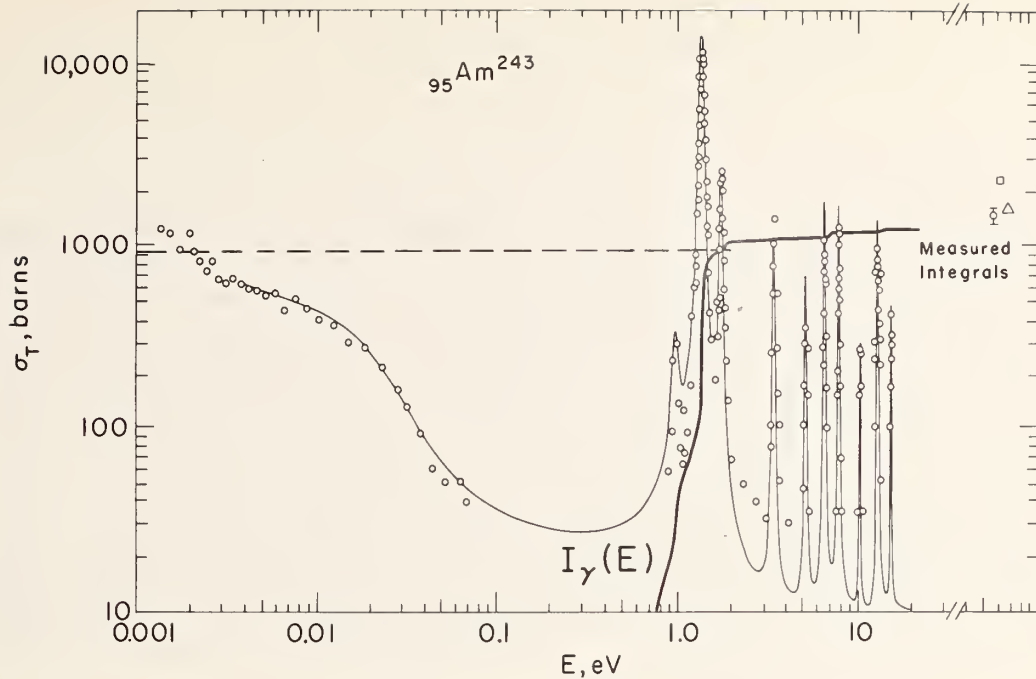


FIGURE 3

ASYMPTOTIC GROWTH OF Am^{243} RESONANCE INTEGRAL

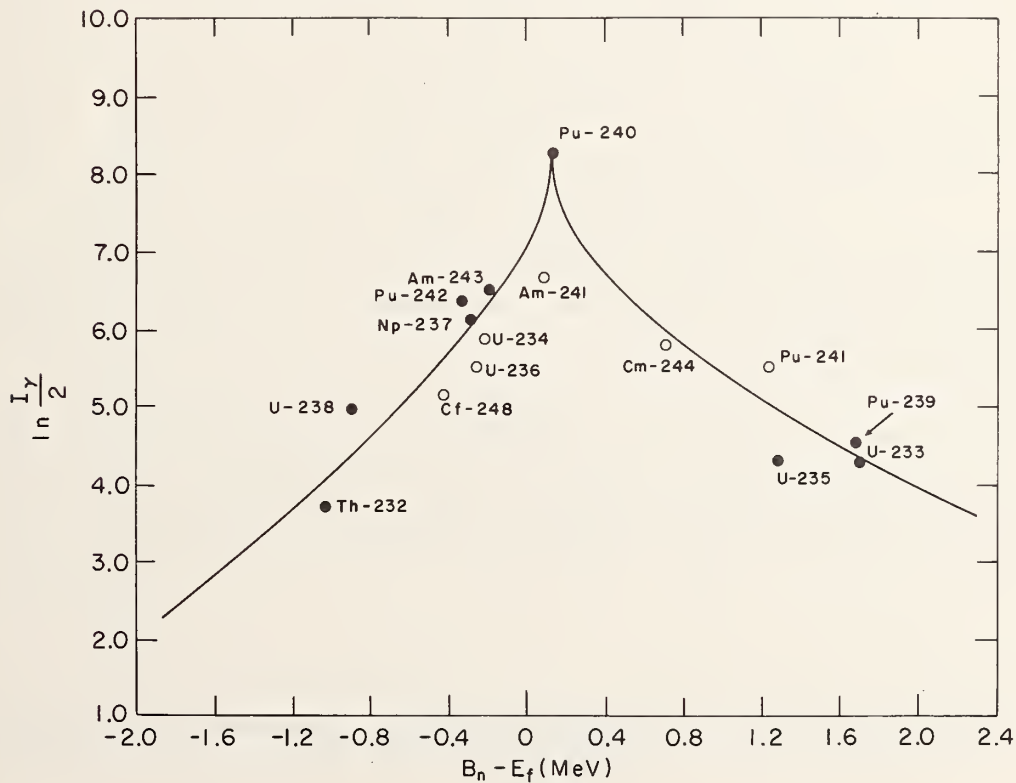


FIGURE 4

CORRELATION OF $I_\gamma/2$ WITH $(B_n - E_f)$
(CUT-OFF ENERGY = 0.5 eV)

Interpretation of the Correlated Analysis of Fission, Total and Capture Cross Section Data*

F. T. Adler and D.B. Adler

Physics Department, University of Illinois, Urbana 61801

A program for the simultaneous analysis of total, fission, and capture cross sections is being developed to provide (a) compatible sets of multi-level parameters useful for reactor applications, and (b) a basis from which further information of more fundamental physical interest can be derived. In particular, by combining results from a triple fit with analytical considerations one can obtain indications for the spin assignments. The success of this technique hinges on the specific J values for the nuclide considered: for Pu-239 this procedure seems feasible while for U-235 the closeness of the J values may not permit this type of analysis. On the other hand, for Pu-239, an analysis of total and fission cross section data alone has already shown that simple perturbation arguments are possible which lead to spin assignments consistent with experimental data. Results of this method will also be presented. For a limited number of levels a perturbation method can be used to establish a correlation with R-matrix parameters.

1. Background

By simultaneous analysis of fission capture and total cross section data, sets of compatible parameters are obtained, which can become useful for practical applications. One of the primary aims of such analysis is the derivation of values for the resonance energies and for the half-widths, constrained to describe at once three independent sets of measurements. Automatized searching procedures in this manner can be made to reach convergence to a higher degree of accuracy than for only one set of data. Similar considerations have been presented elsewhere for the case of the joint fitting of capture and fission data. (1)

Other aspects of this type of analysis are possible, for example the simultaneous analysis of the same type of cross section, measured under different experimental conditions; in particular, measurements at different temperatures and(or) transmission measurements made with different samples.

Results derived from this type of analysis can be utilized also to obtain estimates on the spin assignment, as well as to establish the correlation to other existing methods of analysis. As an illustration of this type of correlation, results obtained from the analysis of fission and total cross section data of Pu-239 are presented in Sections 2 and 3. A brief discussion of the energy dependence of the multilevel parameters is also given in Section 4. The analysis hinges on the multilevel expansions:

*This work was supported in part by the U. S. Atomic Energy Commission under contracts AEC 11-1-1546 and AEC-BNL 150227.

$$\sigma^{(F)}(E) = \frac{C}{\sqrt{E}} \sum_k \left(\frac{GF_k}{v_k} \psi_k + \frac{HF_k}{v_k} \chi_k \right) + \frac{A^F}{\sqrt{E}} \quad (1)$$

$$\sigma^{(T)}(E) = \frac{C}{\sqrt{E}} \sum_k \left[\frac{\alpha_k^0}{v_k} (\psi \cos\omega - \chi_k \sin\omega) + \frac{\beta_k^0}{v_k} (\chi_k \cos\omega + \psi_k \sin\omega) \right] + \sigma_p + \frac{A^T}{\sqrt{E}} \quad (2)$$

where ψ_k and χ_k represent the line shape functions of the k-th resonance, centered around the energy μ_k , with half width v_k ; A^F , A^T represent distant levels contributions, σ_p the potential scattering, ω the hard sphere phase shift, and $C = 6.52 \cdot 10^{5D}$ is a conversion constant in units of barns x eV. (1)

The multilevel parameters of equations (1) and (2) can be compared to parameters obtained with the R-matrix approach. Kapur Peierls-type parameters, equivalent to those of equations (1) and (2) are derivable from the R-matrix parameters. The reciprocal process is also possible, to obtain R-matrix parameters from Kapur-Peierls parameters, however, only for a limited number of channels and levels. The R-matrix parameters are otherwise not uniquely defined, unless specific constraints are imposed on them, or unless a perturbation procedure is practicable, as discussed in Section 4.

2. Correlation of Pu-239 Parameters

In the comparison reported here for Pu-239 and given in Tables I and II, R-matrix parameters have been used to obtain Kapur-Peierls parameters. In particular, the results given in Tables I and II, for the energy range below 40 eV, are obtained from the multilevel (R-matrix) analysis of Vogt (2) and Kirpichnikov (3), and from the work of Bollinger, (4) who used a method equivalent to postulating a diagonal level matrix. Single level analysis has also been performed at Saclay, and the evaluated parameters are given in Schmidt's compilation. (5) In the course of the evaluation of the Bollinger data the η/v values have been also considered, and used as additional information to improve the fitting. In this process some of the multilevel parameters obtained by least squares fitting (listed under C) have been modified (within the least squares variances). The results are given under (D). The details of the η/v analysis have been presented elsewhere. (6)

In view of the large level spacing of Pu-239 it was possible to deduce the parameters of Tables I and II by a perturbation method which has been described before. (6)

In comparing the results it should be noted that Kirpichnikov's analysis is based on the same method used by Vogt, and it includes Vogt's results for the lower energy region. Kirpichnikov made use of the assumption that the capture cross section be rigorously symmetrical, and that interference between levels which are not close be negligible. In the present analysis, this constraint has not been considered necessary, since asymmetries can be expected in general, also in the capture cross section, as an effect of the strong interferences. (7)

From Table I it is apparent that the values for the resonance energies (or, more exactly, the real parts, μ , of the poles of the collision matrix) agree well for all the evaluations considered. An exception is the negative energy level, which has not been considered here, but for its "background" effects. Furthermore, there appears to be an overall good agreement between

the values of α^0 and those of GF. This good agreement can be understood easily because the determination of α^0 and GF requires only the accuracy inherent in an area analysis.

The values of ν show more clearly the variations induced by the different approaches. A simple perturbation treatment shows that, although the interference effects are of the first order for μ , and of the second order for ν , above 7 eV the percentage changes in μ and ν are much larger for ν than they are for μ .

Finally, the parameters β^0 and HF are most sensitive to the interference effects ($\beta^0 = \text{HF} \equiv 0$ for single-level analysis).

Exceptions to the good agreement between the parameters GF or α^0 occur for instance for the fission parameters of the 14.30 eV resonance and for the total cross section parameters of the 14.70 eV level. In the first case, Kirpichnikov's value of GF is too low to match the resonance peak, and it also leads to a disagreement with the value of η/ν measured by Bollinger. For the 14.70 eV resonance the α^0 of Kirpichnikov is larger than the value derived from the least-squares fit. Another discrepancy appears for the asymmetrical parameters β^0 , HF of the 14.30 eV level. It appears that a good fit to the data is obtained if the inequality

$$\frac{\text{HF}}{\text{GF}} > \frac{\beta^0}{\alpha^0} \quad (\text{for the 14.3 eV resonance})$$

is satisfied. This condition also explains qualitatively the negative slope of the η/ν curve around 14.3 eV. With Kirpichnikov's results, HF and β^0 are negative, due to the strong interference postulated between this resonance and the 15.5 eV resonance, which in turn is described as interfering with the 10.9 and 17.6 eV levels. This assumption leads to an erroneous sign for the slope of η/ν .

3. Spin Assignments

In contrast with the R-matrix approach, the data analysis with the multi-level expansion does not require assumptions on the spin state of the resonance levels. A choice for the g value becomes essential only when parameters for the resonance scattering are evaluated from those of the total cross section. The analytical relations connecting one set of parameters to the other are based on elementary dispersion relations.⁽⁸⁾ Thus it is possible in principle to investigate resonance scattering parameters deduced analytically for a given choice of the g value.

The comparison of these results, either to measured data or to values deduced from triple fit of total, capture, and fission cross sections could indicate the spin assignment. For Pu-239, the two g values for s waves (1/4, 3/4) differ enough to make this operation meaningful. For U-235 these values (9/16, 7/16) may instead be too close to obtain significant results with this procedure.

For Pu-239 the comparison with the measurements of Bowman, et al⁽⁹⁾ has indicated compatibility between Bowman's values of the scattering area and the equivalent values deduced analytically from the total cross section parameters. The results of this comparison are shown in Table III.

4. Energy Dependence of Multilevel Parameters

The preceding comparison has been facilitated by the use of a perturbation procedure which is here permissible because of the large level spacing.

The question regarding the energy dependence of the Kapur-Peierls parameters may represent at first a reason of concern, especially in view of using such parameters for practical applications. On one hand, it has been shown that for low-energy resonances (s waves) the energy dependence of the neutron widths can be treated as a perturbation, leading to contributions which are negligible as long as the eigenvalues of the level matrix are distinct, and Γ_n^0 remains smaller than the other partial widths. This is the case for Pu-239 in the region considered here.

The question becomes crucial, on the other hand, for closely spaced resonances: the limiting case, of coalescing eigenvalues of the level matrix, seems to indicate a breakdown of the formulation. It appears, however, that in such a case it is not permissible to neglect the k-dependence of Γ_n , which has the effect of separating the eigenvalues, thus of eliminating the degeneracy. The exact treatment of the eigenvalues of the level matrix with inclusion of the k-dependent terms*, leading to rigorously energy independent poles for the collision matrix leads to results coinciding with those of the well known Humblet Rosenfeld formalism.⁽¹⁰⁾ The formal connection between the channel matrix and the Wigner level matrix⁽¹¹⁾ will suffice to illustrate the point.

Thus it appears justifiable to interpret the parameters of equations (1) and (2) either as an energy independent approximation of the Kapur-Peierls parameters, or as the equivalent of a Humblet-Rosenfeld expansion, having an explicitly prescribed background function.

5. References

1. D. B. Adler. TANDEM: A program for the two-fold least squares analysis of capture and fission cross sections with the multilevel expansion. Report C00 1546-5.
2. E. Vogt, Phys. Rev. 118, 724 (1960).
3. I. V. Kirpichnikov, K. C. Ignatev, S.I. Sukhoruchkin. Journal of Nuclear Energy, Parts A/B 18, 523 (1964).
4. L. M. Bollinger, R. E. Coté, G. T. Thomas. Proceedings, Conference on Peaceful Applications of Atomic Energy, Geneva, Vol. 15, p. 127.
5. J. J. Schmidt. Neutron cross sections for fast reactor materials. Karlsruhe, Germany. Report KFK-120 (EANDC-E-35U).
6. D. B. Adler and F. T. Adler. Multilevel analysis of the Pu-239 cross sections below 40 eV. Report C00 1546-7.
7. D. B. Adler and F. T. Adler. LEMA, a program for calculating neutron cross sections with R-matrix formalism and with the complex pole expansion of the collision matrix. Report C00 1546-4.
8. D. B. Adler and F. T. Adler. Transactions ANS 5, 407 (1962).
9. G. D. Sauter and C. D. Bowman. Phys. Rev. Letters 15, 761 (1965).
10. J. Humblet. S-matrix theory of nuclear resonance reactions, in Fundamentals in Nuclear Theory, Chapter 7, 369-417, IAEA 1967.
11. A. M. Lane and R. J. Thomas. Rev. Modern Phys. 30, 1958 #2.

*

For an approximate numerical treatment of this case, see Reference (7)

TABLE I. MULTILEVEL PARAMETERS AND SELECTED (η/ν) VALUES FOR PU-239 BELOW 20 eV

μ (eV)	ν (eV)	$\alpha^0 10^{-4}$ (eV) $^{\frac{1}{2}}$	$\beta^0 10^{-4}$ (eV) $^{\frac{1}{2}}$	GF 10^{-4} (eV) $^{\frac{1}{2}}$	HF 10^{-4} (eV) $^{\frac{1}{2}}$	g	(η/ν)	$(\eta/\nu)^0$	Source
-.260	.100	.8500	-	.6419	-	(1/4) (xxx)	.80*	.760	A
-.260	.100	.8202	-.0407	.6419	-.0407	1/4	-	.783	C (X)
- 1.1999	.1208	22.5549	-.0764	18.7605	-.0764	3/4	-	.832	B
.296	.0505	2.2314	-	1.3687	-	3/4	.61*	.590	A
.296	.0500	2.2314	.0096	1.3687	.0096	3/4	.63	.590	C (X)
.300	.0501	2.0852	0.0	1.2484	0.0	1/4	-	.599	B
7.830	.0415	4.6637	-	2.3327	-	3/4	.49*	.505	A
7.840	.0379	4.7000	.0734	2.1680	.0734	3/4	.466	.461	B
7.830	.035	4.6670 \pm .140	.2024 \pm .060	2.0732 \pm .10	.0976 \pm .020	3/4	.450	.444	C
7.83	.035	4.5164	.0976	2.1700	.0976	3/4	.485	.480	D
7.82	.0434	4.3284	-	2.3435	-	3/4	-	.505	E
7.82	.043	4.0763 \pm .050	.2979 \pm .015	2.2981 \pm .025	-.0681 \pm .010	3/4	-	.560	F
10.93	.090	8.2576	-	6.7292	-	3/4	.73*	.823	A
10.905	.061	8.3127	-.5863	5.4334	-.5863	3/4	.664	.654	B
10.935	.085	8.6338 \pm .170	-.4049 \pm .050	6.1222 \pm .120	-.4458 \pm .05	3/4	.720	.709	C
10.935	.085	8.6340	-.4049	6.2220	-.4458	3/4	.720	.721	D
10.940	.100	8.5760	-	6.5213	-	3/4	-	.823	E
10.940	.100	8.0580 \pm .080	-.1733 \pm .030	6.4607 \pm .050	-.9122 \pm .020	3/4	-	.802	F
11.90	.0320	4.6227	-	1.6001	-	3/4	.34*	.350	A
11.899	.032	4.7128	.2740	1.6711	.2740	3/4	.371	.355	B
11.90	.025	4.4882 \pm .290	.3078 \pm .030	1.4093 \pm .070	.3625 \pm .030	3/4	.334	.314	C
11.90	.025	4.200	.3078	1.4093	.3625	3/4	.355	.335	D
11.89	.0325	4.3930	-	1.6556	-	3/4	-	.350	E
11.89	.0325	4.4084 \pm .060	.4990 \pm .020	1.5346 \pm .025	.1157 \pm .014	3/4	-	.350	F
14.28	.0504	2.1864	-	1.3070	-	1/2	.60*	-	A
14.306	.0348	2.2505	-.3505	.9014	-.3505	3/4	.425	.401	B
14.290	.0470	2.6107 \pm .250	.1071 \pm .043	1.4166 \pm .147	.2716 \pm .110	3/4	.528	.543	C
14.290	.0450	2.500	.1026	1.4990	.1566	3/4	.585	.600	D
14.31	.0528	2.4580	-	1.8850	-	-	-	.60	E
14.31	.053	2.3780 \pm .065	.2969 \pm .040	1.6270 \pm .100	-.0051 \pm .070	-	-	.68	F

TABLE I. MULTILEVEL PARAMETERS AND SELECTED (η/ν) VALUES FOR PU-239 below 20 eV (continued)

μ (eV)	ν (eV)	$\alpha^0 10^{-4}$ (eV) ^{1/2}	$\beta^0 10^{-4}$ (eV) ^{1/2}	$GF 10^{-4}$ (eV) ^{1/2}	$HF 10^{-4}$ (eV) ^{1/2}	g	(η/ν)	$(\eta/\nu)^0$	Source
14.68	.0397	8.3519	-	3.4712	-	1/4	.45*	-	A
14.70	.0347	8.3500	0.0	2.7672	0.0	1/4	.389	.331	B
14.70	.031	7.6615 ± .500	- .1556 ± .100	3.0265 ± .20	-.2011 ± .120	3/4	.410	.395	C
14.70	.031	7.3950	- .1556	3.2280	-.2320		.456	.437	D
14.69	.0355	7.4600	-	3.3613	-	1/4	-	.452	E
14.69	.0355	6.4460 ± .21	.2129 ± .051	2.8400 ± .15	-.5696 ± .100		-	.440	F
15.50	.4002	3.0353	-	2.8745	-	1/4	.81*	.95	A
15.493	.5240	2.9718	.3336	2.8353	.3336	3/4	.910	.954	B
15.51	.400	2.5489 ± .250	.6232 ± .800	2.0993 ± .210	.1090 ± .200	1/4	.778	.824	C
15.51	.400	2.5489	.1090	2.080	.1090		.813	.816	D
15.42	.3503	2.5591	-	2.4105	-	-	-	.95	E
15.42	.350	2.7050 ± .108	.0927 ± .0920	2.0970 ± .210	.0495 ± .050		-	.775	F
17.60	.0435	5.7208	-	3.0445	-	3/4	.46*	.54	A
17.597	.0345	5.7606	.3288	2.2702	.3288	3/4	.407	.394	B
17.69	.035	6.9055 ± .045	.4038	2.6713	.3408 ± .022	3/4	.391	.387	C
17.64	.035	6.9050	.0826	3.0820	.0300		.424	.446	D
17.66	.0370	6.4249	-	3.0388	-	3/4	-	.542	E
17.66	.0370	5.5471 ± .130	.4842 ± .050	2.4416 ± .13	-.2177 ± .100		-	.440	F

1. The parameters obtained from Michaudon's measurements are preliminary results.
2. (η/ν) values marked with an asterisk* are the experimental values at the resonance energies measured by Bollinger⁴; the other values in this column have been calculated from the resonance parameters using resolution and temperature broadening.
3. $(\eta/\nu)^0$ has been calculated from the resonance parameters without broadening.
4. The following sources of data were used:
 - A. Single level parameters obtained by Bollinger and Coté.^{4/1}
 - B. The R-matrix parameters determined by Vogt and Kirpichnikov.^{2,3/1}
 - C. Multilevel results obtained from the data provided by L. W. Bollinger.
 - D. Adjusted multilevel parameters
 - E. Parameters for the Saclay 1966 measurements, as reported by Schmidt.^{5/1}
 - F. Preliminary multilevel results obtained from the data provided by A. Michaudon.
5. (~~xx~~) Fitted as "neighboring resonances". The value α^0 for the -.26eV level has been adjusted to provide the thermal BNL value of 1024 barns.
6. (xx) Spin assignment of the present analysis

TABLE II. MULTILEVEL PARAMETERS FOR PU-239 BETWEEN 20 and 40 eV

μ (eV)	ν (eV)	$\alpha^0 10^{-4}$ (eV) $^{\frac{1}{2}}$	$\beta^0 10^{-4}$ (eV) $^{\frac{1}{2}}$	GF 10^{-4} (eV) $^{\frac{1}{2}}$	HF 10^{-4} (eV) $^{\frac{1}{2}}$	g	(η/ν)	$(\eta/\nu)^0$	Source
22.20	.0565	7.20	-	4.548	-	1/2	.58 [*] ± .02	.68	A
22.21	.0520	6.485 ± .120	-.4431 ± .100	4.5824 ± .170	-.1633 ± .060	3/4	-	.68	D
23.90	.041	.270	-	.1383	-	1/2	.51 [*] ± .03	-	A
23.90	.038	.226 ± .10	.0835 ± .080	.0756 ± .060	.0720 ± .030	3/4	-	.345 ± .20	C
26.20	.040	4.90	-	2.2846	-	1/2	-	.48 ± .04	A
26.28	.035	4.520 ± .10	.1920 ± .100	2.1719 ± .020	.2679 ± .090	3/4	-	.48	D
27.30	.0215	.380	-	.02651	-	1/2	.07 [*] ± .02	-	A
27.30	.0215	.376 ± .06	.1093 ± .070	.0964 ± .025	-.0439 ± .040	3/4	-	.256	E
32.30	.115	.760	-	.6280	-	1/2	-	.83 ± .02	A
32.30	.105	1.005 ± .140	.003 ± .106	.6368 ± .090	.0114 ± .044	1/4	-	.63 ± .20	C
35.30	.022	.790	-	.0718	-	1/2	.10 [*] ± .02	-	A
35.32	.021	.616 ± .100	-.2220 ± .120	.0704 ± .035	.0164 ± .040	3/4	-	.115 ± .13	C

A. See Source A of Table I

C. See Source C of Table I. (In this case adjustment of α^0 was not needed, since the value of η/ν agrees within the variances of α^0 and GF with Bollinger's value.)

D. α^0 adjusted to reproduce the Bollinger η/ν value, GF not changed.

E. Special case: This resonance appears as a "shoulder" of the 26.2 eV resonance, so that the contribution of the asymmetrical part can alter the η/ν value, if calculated with contributions of other levels and of resolution effects.

TABLE III. COMPARISON OF VALUES FOR g_n^2/Γ WITH BOWMAN'S RESULTS

Resonance Energy (eV)	Bowman's g_n^2/Γ value (mV)	g_n^2/Γ from Bollinger's values (mV)	g_n^2/Γ in a zero order approximation from Kirpichnikov R-matrix parameters (mV)	g_n^2/Γ in a zero order approximation from multilevel parameters (mV)
7.83	$(6.7 \pm 1.9) 10^{-3}$	$6.84 10^{-3}$	$7.61 10^{-3}$	$6.96 10^{-3}$
10.9	$(12.0 \pm 2.4) 10^{-3}$	$13.80 10^{-3}$	$21.08 10^{-3}$	$16.44 10^{-3}$
11.9	$(16.0 \pm 3.1) 10^{-3}$	$13.42 10^{-3}$	$14.15 10^{-3}$	$16.30 10^{-3}$
14.3	$< 4.5 10^{-3}$	$1.71 10^{-3}$	$3.69 10^{-3}$	$3.80 10^{-3}$
14.7	$(40.8 \pm 8.4) 10^{-3}$	$128.98 10^{-3}$	$147.69 10^{-3}$	$49.82 10^{-3}$
15.5	---	$1.78 10^{-3}$	$.84 10^{-3}$	$1.26 10^{-3}$
17.6	$(30.0 \pm 6.6) 10^{-3}$	$22.07 10^{-3}$	$28.45 10^{-3}$	$43.10 10^{-3}$

Gerade - Ungerade Symmetry and the Nuclear Mass Division in Fission

by James J. Griffin, University of Maryland*

College Park, Maryland 20742

The problem of describing the mass division in fission is reviewed. It is proposed that in the first approximation the most probable ratio is the ratio near the saddle point shape of the number of nucleons in gerade orbits, [symmetric under reflection in the plane perpendicular to the nuclear axis] to the number in ungerade orbits. A description of nuclear fission as a process in which deformation proceeds slowly in the early stages and very rapidly between the saddle and scission shapes is suggested as the appropriate basis for the above proposal. The resulting model predicts asymmetric fission for high-Z and symmetric fission for low-Z elements. It provides, in addition, a host of implications for further exploration, some of which are touched upon briefly. It also provides an appropriate context into which shell effects may be considered as a second order influence.

*Work supported in part by the United States Atomic Energy Commission

1. INTRODUCTION

Today I would like to discuss a long standing problem in nuclear physics, perhaps the long standing problem. It first arose at the very discovery of nuclear fission about 30 years ago when Otto Hahn and F. Strassman⁽¹⁾ discovered that Barium occurred among the products of the neutron irradiation of uranium. The conclusion that a fission had occurred of the heavy nucleus into two fragments of approximately half the original mass was a startling revelation. Meitner and Frisch⁽²⁾ recognized at once that the "fission" reaction should release a large energy. Thus was triggered a long history of events which has indeed led us to gather here today. The only point I wish to make is that the Barium which was discovered did not weigh one-half (118) as much as the original fissioning nucleus, but rather weighed (138), so that the mass split first observed was about (1.4/1.0). The discovery experiment on nuclear fission indicated (although perhaps with poor statistics!) already that uranium did not most probably divide into equal parts.

As for the statistics the strong asymmetry of the mass split was very quickly verified,⁽³⁾ and the problem of understanding this experimental fact has been with us ever since.

In Section II we discuss various explanations which have been advanced as possible bases for understanding the fission mass division. In Section III we consider an idealized reflection-symmetry explanation which has recently been advanced and illustrate how finite residual interactions in nuclei, as well as the observed mass-symmetry of low-Z fission, make this view untenable. In Section IV we show how, nonetheless, this symmetry can be incorporated into a model of fission which yields to none of the criticisms advanced against the idealized view of Section III. In Section V we discuss some of the implications of the present model for other aspects of the fission process and some of the questions for which it seems to offer an especially appropriate context for further investigation.

2. POSSIBLE EXPLANATIONS OF FISSION MASS DIVISION

2.1. The Static Liquid Drop Model

Almost immediately after the discovery of fission, Bohr and Wheeler published their celebrated paper⁽⁴⁾ on the liquid drop model of fission. This model provided a description of the distortion process by which a nucleus could break into two large pieces, and organized the relevant energies in such a way as to exhibit the importance of a few MeV of threshold energy in denominating the probability of a process which released 200 MeV. All of this the primitive liquid drop model achieved by means of simple power series calculations, but it did not provide any clue on the explanation of the mass asymmetry.

Nor indeed has subsequent study of the static liquid drop (i.e. of the potential energy of the drop as a function of deformation) improved that situation. S. Frankel and N. Metropolis⁽⁵⁾ utilized an electronic computer to calculate the deformation potential for shapes far from spherical, and W. Swiatecki and his co-workers⁽⁶⁾ have made a beautiful series of analyses of the model by means of both algebraic and digital calculations. But all of these studies leave the situation unchanged from that of 1940: No known property of the static liquid drop model predicts any asymmetric mass division in nuclear fission. In particular, Businaro and Gallone⁽⁷⁾ investigated specifically the questions of the stability of nuclear liquid drops against asymmetric distortions. They found that for fissionabilities^(*) $X < .40$, the liquid drop energy prefers an asymmetric saddle point shape, but such small values of X are irrelevant to experimental nuclear fission as it has been studied so far. Businaro and Gallone also showed that for shapes more distorted than the fission barrier shape, instability towards asymmetry does set in for X values relevant to fissioning nuclei. Answers to such questions as whether in fact a fissioning nucleus would ever reach such shapes, and if it did, what precise effect the instability would have on the mass division were however beyond the reach of these studies. Thus, although offering a possibility of an explanation, it seems fair to say that they, too failed to wring a satisfying prediction from the static liquid drop model.

(*) The fissionability parameter $X = Z^2/A / (Z_c^2/A_c)$, is the dimensionless characterization of the tendency towards fission. In reference (8), the estimate $(Z_c^2/A_c) = 48.4$, is made on the basis of a study of the fission of Th^{201} . Then Cf^{252} , U^{236} , Ra^{226} , and Po^{210} have X -values .79, .74, .71, and .68 respectively.

2.2. The Dynamical Liquid Drop

The dynamical liquid drop model incorporates the effects of kinetic energy as well as the static potential energy effects into the description of liquid drop motion. In particular Hill⁽⁹⁾ and Wheeler⁽¹⁰⁾ suggested that a long but finite cylindrical liquid drop should be unstable against the breaking off of small droplets from^(*) one end or the other, i.e., against a very mass-asymmetric fission. They also calculated the dynamical deformation of nuclear liquid drop (to the limit of the then available digital computing capacity, which was insufficient to allow them to follow the calculation to the actual breaking point) and found a tendency for small asymmetric vibrational amplitudes (inevitably associated e.g. with zero-point oscillations of asymmetric degrees of freedom) to grow as the system evolves dynamically towards scission. Such dynamical instabilities have also been studied for simple cylinder-plus-end cap shapes by Inglis⁽¹¹⁾. He concludes that "the droplet model alone does not provide an adequate explanation of the asymmetry of low energy fission." Thus, to the limited extent to which the dynamical liquid drop has been studied quantitatively, [and one should emphasize that liquid drop dynamics remain largely unexplored^(†) ^(††) by detailed and realistic calculations] it fails also to provide a cogent explanation for fission mass asymmetry.

(*) Reference (10), Figures 50 and 51.

(†) J. R. Nix, reference (12), has recently carried out a dynamical study of fission from saddle point to scission (and beyond) which appears to describe many features of the fission of low-Z nuclei for which the most probable mass division is, however, the symmetric one.

(††) J. N. Lawrence, reference (13), has considered the dynamical liquid drop problem with a view to reducing to a minimum the number of independent variables describing the shape by judicious choice of those variables. Such an approach offers hope that realistic dynamical liquid drop calculations can be made on modern computers with results which are simple enough to provide insight into the process involved.

2.3. The Statistical Theory of Nuclear Fission

Fong⁽¹⁴⁾ has advocated the view that the observed fission mass asymmetry follows from the assumption of statistical equilibrium between the fragments at the scission point. This proposal is again a difficult one to exclude, but it lacks cogency because of the great degree of parametric freedom which is available in the assumed initial situation, i.e. the scission configuration.⁽¹⁵⁾ Nor is it easy to imagine how the number of free parameters can be significantly reduced. There is moreover circumstantial evidence from the successful description of fission fragment angular distributions in terms of fission barrier properties^(*) that the fission process proceeds rapidly from saddle to scission. This evidence is not easy to reconcile with any assumed statistical equilibrium at the scission stage.

2.4. Shell Effects in Fission

Shell effects appear to occur in a variety of detailed aspects of nuclear fission, such as the details of the mass yield curve⁽¹⁷⁾ and the correlation between number of neutrons and fragment mass⁽¹⁸⁾. What the effect might be of incorporating shell corrections into the liquid drop potential and kinetic energies, [for example, by following the method which Swiatecki⁽¹⁹⁾ and Meyers⁽²⁰⁾ have used for the limited range of shapes relevant to the semi-empirical description of stable nuclear masses] is of course an open question in view of the fact that the liquid drop in its simplest form has not yet been fully analyzed. It would be reasonable to assume however that such "dents" as closed shell magic numbers might introduce into the liquid drop potential energy surface would be unable to generate a major qualitative feature like the strong asymmetry of heavy element fission because of the fact that the spherical shape which is required for the nascent heavy fragment, to gain the shell closure energy is so far from the symmetric half-shape which the liquid drop model would seem to prefer. One prefers instead to assume that this feature arises from other causes - and is modified by shell effects which exert essentially a second order influence, and which lead thereby to the phenomenological observed correlations of various details with magic numbers.

(*) E. G. the fact that the average K_0^2 required to fit (d,pf) anisotropies goes to zero near the fission threshold energy. Reference (16). An equilibrium at scission would imply that K_0^2 in this case should be much greater than zero. See also Section V.C.

3. NUCLEONIC REFLECTION SYMMETRY AND NUCLEAR FISSION

3.1. Idealized View

Hill and Wheeler⁽¹⁰⁾ first suggested the possible relevance to mass asymmetry of the symmetry of nucleonic orbits under reflection in a plane perpendicular to the long nuclear axis. They pointed out that independent particle orbits in a reflection-symmetric potential, can be characterized as gerade (even) or ungerade (odd) under this reflection, that under symmetric distortion of this potential to a "necked-in" saddle point configuration the energy of gerade orbits relative to ungerade would rise significantly, and that finally these gerade orbits could be admixed efficiently into the lower energy unfilled ungerade orbits by allowing the potential to become reflection asymmetric. Thus, they concluded that "a quite appreciable effect is at work to factor as asymmetric configuration in the critical form." [See Figure 1.]

More recently Kelson^(*) proposed an explanation for the mass asymmetry of fission based on a more explicit use of the gerade-ungerade symmetry. He also assumes pure independent particle motion for the nucleons in the deforming potential. He then considers a perfectly adiabatic process of deformation from an initial nuclear shape with a given number $N_+(N_-)$ of gerade (ungerade) single particle orbits filled, to a final nuclear potential which describes two separated but reflection-symmetric potentials for the fragments, and in which $N_+(N_-)$ retain their initially prescribed values.

In such a separated configuration it is easy to see that the N^{th} gerade (+) and the N^{th} ungerade (-) orbits are degenerate in energy and that when a degenerate (+-) pair of orbits is filled by identical fermions the wave functions describe a situation in which one nucleon is with certainty in the left (L) portion of the potential and the other is with certainty in the right (R) "pot." A configuration with N_+ (+)- orbits filled and N_- ungerade- orbits filled therefore comes to describe a nucleus with N_- nucleons certainly in each separated pot and $(N_+ - N_-)$ nucleons in (+) orbits to which the corresponding $(N_+ - N_-)$ (-)-orbits are unfilled.

(*) I. Kelson, private communication. The author is grateful to Professor Kelson for supplying a preliminary manuscript on which these comments are based. Professor Kelson informs me that a more critical and quantitative approach is being prepared for publication.

If one were now to measure the number of nucleons in the L-pot [e.g. by measuring the mass of the fragment] he could find quantum mechanically any of the values $N - \langle M_L \rangle N^- + (N^+) - (N^-) = N^+$, since each of the unpaired + orbits yields any amplitude $1/\sqrt{2}$ to be in the L or R- pots. Of all these possibilities, however, only the extreme possibilities $M_L = N^-$ and $M_L = N^+$ can describe a situation in which both pots are unexcited configurations, i.e. contain M_L and M_R nucleons in the lowest orbits. This follows from the fact that the N^{th} (+) orbit has non-zero overlap only with the N^{th} R orbit and the N^{th} L orbit. Thus, although the nucleon in this orbit can go either L or R under the mass measurement it must go into the N^{th} orbit and none other.

To make this more obvious let us assume explicitly that the nucleon $(N^- + 1)^{\text{st}}$ (+) orbit is found under measurement to be in the $(N^- + 1)^{\text{st}}$ L orbit, and suppose that the $(N^- + 2)^{\text{nd}}$ nucleon is found in the $(N+2)^{\text{nd}}$ R orbit. Then the R configuration must have $M_R \geq N^- + 1$, but has no nucleon in the $(N^- + 1)^{\text{st}}$ R orbit, i.e. the R- pot is an excited configuration with a hole in the $(N+1)^{\text{st}}$ orbit. Further adiabatic deformation of such an excited configuration will lead finally to excited fragments. (*) [See Figure 2 .]

Thus, if we assume (a) that the value of N^+/N^- is preserved throughout an adiabatic deformation process and (b) that we must most probably obtain fragments in their ground states, then we conclude that the value of N^+/N^- in the initial nucleus defines the most probable mass ratio in the fission process. This is a remarkably simple relationship and one which, Kelson shows, is well satisfied in the fission of U^{235} and Cf^{252} . It is in fact so simple and so accurate as to remain totally fascinating, even after the bases for it have been undermined (See Part B of this Section).

Kelson, in fact, points out that N^+/N^- varies somewhat with the quadrupole shape of the nucleus and concludes that "the asymmetry in the mass yield distribution is a direct measure of both the magnitude and the sign of the nuclear ground state deformation."

(*) In Appendix I, we estimate the excitation energy associated with each mass unit deviation from the ratio N^+/N^- and conclude that a shift of ten nucleons (i.e. a change in mass ratio from about 1.4 to about 1.2) nucleons is roughly equivalent energetically to the closure of the (50-82) spherical shells.

Kelson exhibits even further phenomenological success in explaining the distribution about the most probable mass (which the energetics of Appendix I might predict to be quite narrow) in terms of the nuclear spin-orbit interaction, which mixes (+) and (-) symmetry in a given orbital and leads in the initial nuclear state to a probability distribution of N_+/N_- values about the most probable value, rather than to a uniquely determined eigenvalue.

3.2 Criticisms of the Idealized View

3.2.1 Effect of Residual Nucleon-Nucleon Interactions

We now turn to the modifications in the preceding discussion which are implied by the existence of residual nucleon-nucleon interactions among the particles in the nucleus. We shall see that such residual interactions entirely upset the logic of the preceding section by guaranteeing that assumption (a) is self-contradictory.

Figure 3 is adapted from a discussion of level crossing given by Hill and Wheeler(*). It exhibits the fact that under an infinitely slow deformation a pair of nucleons e.g. in a doubly degenerate gerade orbital, $a = (++)$, will pass through a level crossing with an ungerade orbital, $b = (--)$, and emerge with the same symmetry only when the Hamiltonian matrix element H_{ab} vanishes identically. Otherwise, a diagonalization of H_{ab} in the neighborhood of the crossover leads to eigenvalues E_{ab}^{low} and E_{ab}^{up} and slow deformation will lead with certainty at large deformation to two particles occupying the orbit $b = (-,-)$ with the symmetry of the lowest energy state.

It follows that in the presence of non-vanishing residual interactions which can scatter a pair of nucleons $(++)$ into orbits $(--)$, the number of gerade states, N_+ , will adjust continually as a slow deformation proceeds, taking always the value which is defined by the lowest energy state of the system.

We note that such residual interactions as we are discussing here do not violate any symmetry normally expected of nuclear interactions. Parity conservation guarantees only that the product of all the independent particle gerade-ungerade signatures be an eigenvalue, and not that each nucleon have a fixed g-u signature. Moreover, we can be certain that interactions do exist in nuclei which effect precisely the scattering we require here: the matrix element H_{ab} is simply the "pairing force" matrix element to which modern nuclear structure theory attributes the ubiquitous even-even stability as compared with odd-even or odd-odd.

(*) Reference 10, Figures 33 through 36.

In fact, if at a large deformation the nucleons are to emerge in the state $a = (++)$, then Hill and Wheeler show that the deformation must proceed extremely rapidly: it is in fact the extreme non-adiabatic situation under which one might expect the system to retain a memory of its initial values of $N+$, $N-$. This observation is central to the alternative description which is proposed in Section IV.

3.2.2 Energetic Barrier to Fission with Fixed $N+/N-$

A second respect in which the maintenance of $N+/N-$ constant from the initial to post-scission configurations fails under close examination is illuminated by considering the effect of the requirement, $N+ = \text{constant}$, on the fission barrier height. In the first place, it is clear that any additional restriction on the wave function leads to an increased fission barrier energy, except when by accident the value imposed happens also to be that realized in the lowest barrier state. One can, by means of statistical considerations outlined in Appendix II conclude that no such accident can be expected in the case at hand and that the reflection-symmetric fission barrier energy will be at least 2.0 MeV greater for a Uranium-like nucleus if one were to require $N+$ to retain a near-spherical value $N+(a_0)$ only four units larger than the value $N+(a_g)$ appropriate for the saddle shape.

Could this $u-g$ symmetry energy be entirely won back by allowing the nuclear threshold to be a reflection-non-symmetric as Hill and Wheeler suggest? If one believes that the liquid drop model describes the lowest energy envelope of the potential surfaces for the myriad of particular nucleonic configurations then the liquid drop studies of Cohen and Swiatecki, which show the symmetric saddle shape to be stable against asymmetric deformations would provide the answer: No! Moreover, if one did find an asymmetric threshold lower than the symmetric liquid drop threshold among the configurations obtained from the initial configuration by a continuous shape deformation process, then an even lower threshold could generally be expected to result from unrestricted search among all possible configurations at the same asymmetric deformation.

The restriction to configurations related continuously to the initial one thus appears bound almost always to slow down the fission process by requiring more energy to be stored in the deformation-potential-energy degrees of freedom, which even at the lowest possible fission barrier already store an improbably large fraction of the available excitation energy. The factor by which the lifetime of the process is increased is therefore expected to be exponential in this energy difference, so that even a small energy difference could allow a weak residual interaction to change the $N+$ value with sufficient probability (this probability increases linear with the lifetime of the state in question, and therefore exponentially in the threshold energy increase) to let more of the fission occur through the lowest energy configuration.

In a sense, this argument is based on the same physics as that of Part 1, since it requires in the end some non-zero residual interaction to allow the initial configuration to be modified. In fact it provides a framework in which to quantify the question of just how strong a residual interaction must be to be effective in modifying one configuration into another whose threshold energy is lower by some specified number of MeV. We have not explored this question (which is complicated even when a framework is available) but rest the case for the present on the exponential increase of the fission lifetime with the threshold energy increase, and on the numerical indications from the reflection symmetric threshold.

3.2.3 Occurrence of Symmetric Fission - An Empirical Contradiction of the Idealized View

We wish finally to point out that the idealized description runs aground on the very simplicity and generality of its prediction that $\frac{N+(\beta_0)}{N-(\beta_0)}$ defines the most probable mass split. Against this prediction must be placed the empirical fact that a drastic change in fission mass asymmetry from most probably asymmetric to most probably symmetric occurs in a narrow region around Radium, whereas no correspondingly dramatic change is occurring in the values of $N+/N-$ for the initial shapes of these nuclei (*). The Idealized Model is therefore in very much the same position as the liquid drop model; whereas the droplet seems (on balance) to predict symmetric fission across the board, the Idealized Model predicts asymmetric fission in all cases, and with even less ambiguity!

Nonetheless, the remarkable simplicity with which the model singles out the mass ratio observed in asymmetric fission, and the automatic way in which a suitable width for the distribution follows from the mere existence of a strong spin-orbit interaction in the nucleus, give the Idealized Model a cogency which makes it difficult to believe that all the physics in it is completely irrelevant. In the next section we outline a specific model which incorporates the effects of gerade-ungerade symmetry naturally into a theory of fission. The connection between this symmetry and the mass asymmetry then emerges not as a fascinating coincidence, but instead as an inevitable consequence of the nucleonic substructure underlying the liquid drop idealization of the nucleus.

(*) Indeed, in this region the nuclei are becoming less prolate, indicating an increase in $N+/N-$ for these nuclei at the ground state shape.

4. G-U SYMMETRY AND "WALK-RUN" FISSION

We first describe a model which allows the incorporation of the gerade-ungerade symmetry in a general way and discuss its relationship to the nuclear liquid drop model. Next the question of the variation of the g-u ratio N^+/N^- with nuclear shape is discussed. And finally the question of stability against reflection non-symmetric shape changes is considered.

The following description emerges:

(1) All nuclei "walk" up the reflection-symmetric hill to the saddle point shape, i.e. their deformation proceeds by a series of many transitions which adjust the nucleonic configurations appropriately to the gradually increasing deformation. This is therefore a "slow" process following approximately the lowest energy envelope of the nucleonic-configurational-potential surfaces. It should be well described by the liquid drop model of fission.

(2) Beyond the fission barrier, all nuclei became unstable against small reflection-asymmetric deformations, but nuclei with $X \geq .70$ are unstable also against major asymmetric deformations. These instabilities occur not in the envelope of the various nucleonic configurations, but in the potential surface of a given configuration. Once a nucleus arrives at such a configuration along the symmetric path, the asymmetry develops very rapidly since the configuration potential no longer binds oscillations along a line of increasing elongation and asymmetry. Thus, the nucleus "runs" to the best asymmetric shape, corresponding to a mass ratio equal to the symmetric N^+/N^- value of the configuration in a nuclear time, and presumably continues its non-adiabatic "run" to scission, - all on a potential surface lying above the liquid drop surface which would be relevant for a slow readjustment of the shape.

4.1 The Nucleonic-Liquid-Drop Model

The connection between the liquid drop model and the properties of independent nucleons in a box has been discussed by Hill and Wheeler^(*). They also provide a very useful asymptotic formula for the density dN/dk single particle eigenstates in a box [i.e. an infinite square well potential] of volume V , surface area S , and integrated mean curvature, C . In Appendix II we show how one can obtain for any reflection-symmetric shape the density of states which have ungerade or gerade symmetry under reflection in the plane containing the area, A_1 , which cuts the shape into two identical halves, (see also Figure 4). Listed there also are the relations among the numbers N^+, N^- , the total energies E^\pm , the maximum wave numbers, k_0^\pm , and the box parameters, V, S , and L . These enable one to calculate the energy of a system of N nucleons as a function of V, S, L , in either of two ways, as follows:

(1) One can allow N_+ and $N_- = N - N_+$ to have the values which yield the lowest total energy for the shape in question. This calculation results in a surface energy (with a curvature correction) which is the microscopic analog^(*) of the surface energy assumed in the liquid drop model. We postulate that this energy, properly treated, will in fact provide, on the average, the empirical liquid drop surface energy^(††). We also assume that the Coulomb energy is not a sensitive function of nucleonic configuration, but can be well estimated by the energy of a uniform charge density Ze/V throughout the box V, S, C . In this way we connect the nucleonic-liquid-drop with the classical liquid drop and place at our disposal the extensive results of Cohen and Swiatecki as those which describe the lowest energy envelope of the nucleonic configurations. This relationship is illustrated in Figure 7, for two typical configurations.

(2) One can also calculate the energy subject to the condition that N_+ remains a constant. This results in an energy rather higher than the liquid drop energy, except in the immediate neighborhood of a surface minimum where this energy is enveloped by the L.D. surface.

These two types of potential surface are relevant to motion on two entirely different time scales. For times too short to allow a nucleon to change orbits the system must follow the configurational potential. If this potential binds the system in the immediate neighborhood of some deformation, then it can move on to another deformation only after one or more nucleons have been scattered by residual interactions into an orbit appropriate to a configuration for a neighboring configurational surface, i.e. in a time long compared to 10^{-22} seconds.

Such changes in deformation, which proceed in fits and starts but proceed slowly on the average, may also be described as adiabatic processes on the enveloping liquid drop potential surface. Non-adiabatic deformations, on the other hand will follow a given configurational potential surface and may occur in a nuclear time of perhaps as little as 10^{-22} seconds.

(*) Hill and Wheeler, reference (10) Figures 11 and 12. But see also the more extensive and critical discussion of reference 20.

(††) We refer to this postulate hereafter as the "Equivalence Postulate." See also Appendix III.

4.2 Simplifications Imposed on the Model

4.2.1 Allowed Shapes

To make the calculations manageable and the discussion intelligible we simplify the nucleonic-liquid drop model by considering only a two dimensional family of shapes. Along one axis we measure a continuous sequence of axially and reflection-symmetric shapes by the relative values, $a = [1 - (R_{\min}/R_0)^2]$, of the difference between cross-sectional area of the figure and that of a sphere of radius, R_0 . In particular, we choose this sequence to be the set of saddle point shapes calculated by Cohen and Swiatecki⁽⁶⁾ and illustrated in Figure 5. The values of a then range from $a = 0$ ($R_{\min} = R_0$, spherical) to $a = 1$ ($R_{\min} = 0$ implies scission). Along the second axis we measure asymmetry in terms of the fractional expansion (contraction) of the half-volume. I.e. at a particular value of the coordinate, δ , a volume $V/2(1 + \delta)$ will be to one side of $Z = 0$ and a volume $V/2(1 - \delta)$ to the other.

The advantage of choosing the Cohen-Swiatecki sequence lie in the beautiful numerical tabulations which these authors provide of the liquid drop properties of these shapes. In particular, $R(\theta)$, including $R(0^\circ) = R_{\max}$ and $R(90^\circ) = R_{\min}$, as well as B_s and B_c (the surface and Coulomb energies relative to their spherical values) are tabulated for $.30 < X < 1.00$ in intervals of $.02$. Although in fact no nucleus is expected to follow precisely this sequence of shapes in the process of fissioning, one shape of the sequence is the appropriate L.D. saddle point shape for every nuclear X -value. Nor is the sequence in any way a grossly unreasonable choice for a calculation which must avoid the complexities involved in defining a distinct sequence of shapes for each and every nucleus.

4.2.2 Calculational Approximations

We note that the statistical analysis of level densities provides algebraic relationships which lead most directly to solutions in terms of series of powers of $(N)^{-1/3}$. In this work, we have calculated only the leading relevant term in such series, unless otherwise specified. Thus, for example, the terms in the energy (Equation (7), Appendix II) involving S^2/V and L are not considered. The omission of such corrections is in fact necessary if the postulate of equivalence between the envelope of the nucleonic potentials and the liquid drop calculations of Cohen and Swiatecki is to be self consistent. The reason is that such terms describe deviations from the simplest liquid drop model and would be equivalent to corrections involving for example a dependence of the surface tension coefficient or surface curvature^(*). Since Cohen and Swiatecki do not include such corrections, neither should a nucleonic model which is postulated to be equivalent to their results.

Finally in order to simplify the statistical level density analysis we calculate for a nucleus which is composed of 240 nucleons, - 60 each of four distinguishable types. Thus the effect of charge on the nucleonic structure is omitted. The Coulomb energy itself is considered to arise from a uniform charge density Ze/V throughout the nuclear volume.

(*) Corrections of this form have also been proposed in other contexts. See e.g. reference (21), (22), and (23).

4.3 The G-U Ratio, N+/N-

In Appendix II, we obtain the following results for the difference between the number of nucleons of each kind occupying gerade orbits and the number in ungerade orbits in the lowest energy configuration [$k_0^{\pm} = k_0$]

$$N+ - N- = \frac{2A_1 k_0^2}{16\pi} - \frac{2C_1 k_0}{8\pi^2} \quad (1)$$

where k_0 is the wave number of the last of the 60 nucleons, A_1 is the area of \circ the circle which divides the reflection-symmetric figure into two equal halves and C_1 is the contribution to the integrated mean curvature of the half-figure from the circular edge which this cut creates (*). The ratio $N+/N-$ which this difference implies is plotted in Figure 6 against the L.D. saddle point shapes corresponding to various fissionabilities, X .

Figure 6 shows that the $N+/N-$ ratio is very nearly equal to 1 at the saddle points of all nuclei with $X \lesssim .67$ and rises to about 1.4 as Z^2/A is increased $X = .70$ to $X = 1.0$. Thus, if it can be shown that the saddle point shape is the relevant determinant of $N+/N-$ at the stage where fission begins to "run" very non-adiabatically, then Figure 6 would predict asymmetric fission and symmetric fission for the X -values where in fact they are observed respectively to occur. It does not, however, predict a value of $N+/N-$ for, say, $X = .74$ as large as the value (1.4) actually observed in U^{236} fission.

4.4 Stability Against Asymmetric Deformation

In Appendix III we consider the question of stability against motion towards finite values of δ and draw two conclusions as follows:

- (a) Asymmetric instabilities in nucleonic configurational potential surfaces can be open to scission (i.e. can reach scission from the osculation point by a path on the surface along which the energy decreases monotonically) only if they osculate the liquid drop at or beyond the saddle point shape.
- (b) Unbounded instabilities in nucleonic configurational potentials occur beyond the saddle point.

Conclusion (a) follows immediately from the equivalence postulate and conclusion (b) demands that $E_s^0(B_s' + 2xB_c')$ be sufficiently negative beyond the barrier. (See Figures 7).

(*) See Figure (4).

We should mention also that the configuration-potential surfaces which become unbounded to scission do not in any way violate the equivalence postulate. In particular, the potential energy everywhere on such surfaces is greater than or equal to the L.D. potential for the same shape. The nucleus will follow such a surface, in spite of the fact that it is by no means the lowest energy surface, because it is able to do so without the delay which nucleonic transitions involve. Thus, we understand in a specific way the weaknesses of arguments based only on final state energetics such as the Idealized View discussed in Section and, indeed, the observation that completely symmetric fission releases more energy than the most probable fission does. We also recognize here the essential role of the nucleonic substructure in distinguishing two time scales in fission. For short times it prevents the nucleus from knowing that any energy other than the configurational potential energy is relevant to its motion. This distinction, becomes overriding as soon as that potential becomes unbounded to scission.

5. IMPLICATIONS FOR OTHER ASPECTS OF FISSION

The specific description of the dynamical processes leading to fission which has unfolded from the incorporation of u-g symmetry into a nucleonic-liquid-drop model offers a new context in which various aspects of the fission process may be re-examined. We mention here some of the features which might emerge from such a re-examination.

5.1 Kinetic Energy vs. Fragment Mass Ratio

According to the present description, asymmetric fission results for nuclei which arrive at the barrier with N^+/N^- values sufficiently different from unity to allow the asymmetric deformation to grow to a significant value. Symmetric fission, on the other hand, results when N^+/N^- is nearly equal to unity at the fission barrier.

In Ra^{226} fission, the balance is evidently very delicate, and the two kinds of fission occur with comparable probabilities. This case therefore provides a test of the most obvious feature of the above picture: that in symmetric fission the nucleus is more elongated when it reaches a nucleonic configuration open to scission than in asymmetric fission. This implies that steady acceleration of the two nascent fragments begins from a configuration of greater relative Coulomb energy in the asymmetric than in symmetric fission. For Ra^{226} , in which both types of fission occur, the word "relative" can be omitted and the inference drawn at once that asymmetric mass divisions in Ra^{226} should exhibit a greater average kinetic energy than mass-symmetric cases. This feature is well verified experimentally (24) (25).

5.2 Impulsive Emission of Light Particles at "Scission"

The present model provides a clear statement that the deformation process proceeds very rapidly from the saddle point to scission. It therefore offers a basis for the non-adiabatic "Sudden-Snap" scission process which has been invoked (26) to explain α -particles [and other light particles, including "pre-scission" neutrons (27) (28)] emitted in fission. Moreover, the successful incorporation of shell effects into the present description seems likely to produce the "Whetstone-Vladimirski" model, (29) (30) which successfully describes (31) certain detailed aspects of the alpha emission (32), as well as certain prominent features of the fission neutron emission (See Section C. below)

5.3 Neutron Emission: Correlation of ν with Fragment Mass

We note the reasonable possibility that the inclusion of shell effects on the potential surface for highly deformed nuclei near scission would obviate a quantitative inadequacy of the present picture, - the prediction of somewhat too small a mass ratio for heavy nuclei. In particular the doubly closed shell at (50,82) should begin seriously to modify the potential energy surface for strongly necked-in shapes near scission, especially those which already prefer a significant asymmetry, (cf. Appendix (I.1) for a rough estimate of the comparative magnitude of shell energies.)

Thus one could expect that upon making the modifications due to such shell effects he would obtain essentially at the "Whetstone-Vladimirski model" which (29) (30) assumes that the nucleus just before scission contains a nearly spherical heavy fragment formed around this 50-82 doubly closed shell. In this way the present picture offers the promise of incorporating into a fundamental description this picture, which was constructed specifically to describe the highly structured correlation observed (*) between fragment mass and number of neutrons emitted.

5.4 Charge Division in Nuclear Fission

It would appear that the extension of the present model to the calculation of charge division is worthy of consideration as a direction for further study. At the outset one could simply consider the effect of enumerating N^p and N^n separately for neutrons and protons to attempt a purely statistical estimate of the most probable charge division. In such a study there will surely come a stage which will require the inclusion of the nuclear symmetry energy for progress to be made. The present model offers an appropriate framework for specifying this problem.

(*) J. Terrell, reference 18, summarizes these observations and cites a variety of references.

5.5 Transition State Properties: Angular Distributions of Fragments

The properties of nuclei near the saddle point appear to determine certain features of nuclear fission, such as angular distributions;⁽³³⁾ ⁽³⁴⁾ quite satisfactorily. This situation is thoroughly consistent with the present model, because of the fact that post-barrier processes are here assumed to occur, on a very short time scale. Thus the assumption ⁽³⁵⁾ in the angular distribution analysis that the nuclear axis does not significantly reorient itself during the time between the barrier and scission is indicated by the present model to be a valid one.

5.6 Resonance Fission

Details of certain of asymmetric fission properties^(*) such as peak mass to valley mass yield ratios⁽³⁶⁾ appear to vary from resonance to resonance in slow neutron fission, indicating a dependence of these properties on the total angular momentum of the fissioning system. Such effects require us to recognize that the single nucleonic configurational surface we have discussed is in fact only the lowest of a multitude of such surfaces, which includes a separate family for every possible value of each of the rigorously conserved quantum numbers (J, π) describing the total angular momentum and the parity (Cf Section G below) of the fissioning system. Then if a nucleus fissions from a state (J, π) the nucleonic surface it reaches at the fission barrier, and on which it then "runs" towards scission, will be different from that it would reach if it has a different value (J', π') . The problem of obtaining a description of such details as depend on (J, π) therefore is in this picture simply the problem of describing the differences among the "open" nucleonic surfaces which depend on these quantum numbers.

(*) The kinetic energy of the fragments also appears to vary in the neighborhood of a resonance. See reference (40) and Section G.

In particular, a reasonable first approximate assumption is that for even-even nuclei, the lowest of these surfaces will throughout the deformation space to be ordered qualitatively as they are in stable even-even nuclei; that is that their energy increases monotonically with angular momentum among states of either parity and that odd-parity states lie higher than even-parity states. For perhaps a semi-quantitative estimate of these differences one might assume that their energy differences correspond to the level structure of the low-lying transition states at the saddle point. For example, one might expect that as regards mass ratio $0+$ states in Pu^{240} run on surfaces lower than $1+$ states and therefore behave with regard to improbable mass-symmetric fission like states of lower excitation than $1+$ states. Thus, $0+$ states would yield less symmetric fission than $1-$ states and the "peak₂₄₀ valley" ratio would be greater for $0+$ than for $1+$ resonances in Pu^{240} , as appears to be the case experimentally⁽³⁷⁾.

5.7 Other Detailed Effects Sensitive to Angular Momentum and Parity

Variations in the parity of fissioning nuclei occur in the region of incoming neutron energy where p-wave capture becomes important. Variations in the average fragment kinetic energy and in the average number, $\bar{\nu}$, of the neutrons emitted from the fragments have been observed to occur under these circumstances^{(38) (39)}. The same estimation used in Section F may be applied here to infer that the spin and parity corresponding to the lower transition state "runs" on the lower nucleonic surface, i.e. the "cooler" one, and leads therefore to lower $\bar{\nu}$ and greater average kinetic energy. This description again agrees with the experimental observations.

5.8 Dependence of Mass Asymmetry on Excitation Energy

In Section VI.F, the known fact that the probability of a symmetric mass division in asymmetric fission increases with excitation energy of the fissioning nucleus was used to obtain a correlation for comparison with resonance fission peak to mass ratios. We wish to point out here that two possibilities may exist in this model which might lead to an increase of this kind.

The first is the recognition that $N+/N- > 1$ is a property of the lowest nucleonic configuration at the fission barrier. Increasing excitation energy might be expected to randomize this ratio systematically towards the value 1; i.e. to favor increasingly symmetric fission with increasing excitation energy.

The second is the possibility that symmetric fission results from a low amplitude "tail" of the wave function well down the valley towards scission, which tail penetrates the potential hill at symmetric, and increases as the vibrational energy in the asymmetric coordinate increases, i.e. with increasing excitation energy.

We have not investigated either possibility. Nor indeed is it clear that they are not simply two ways of describing a single physical feature. Indeed, the whole question of describing the rapid post-barrier motion is one which demands careful study.

5.9 The Width of the Mass Distribution

In Section III A. we mentioned the remarkable description that Kelson (*) had suggested for the width of the asymmetric mass peak; namely, that it arose from the distribution of N^+/N^- about its most probable value as a result of the strong spin-orbit interaction which operates in the nucleus. The question of whether this description could still apply when N^+/N^- is determined by the more deformed saddle point shape is certainly one which deserves attention, as do alternative possibilities which come to mind, such as the vibrational amplitude in the asymmetry coordinate mentioned in Section H.

6. CONCLUSIONS

It would appear that g-u symmetry in the nucleonic liquid drop model provides a cogent explanation of the general features of the observed fission mass asymmetry; in particular the occurrence of most probable asymmetric fission for $X > .70$ and symmetric fission for lower Z nuclei. The magnitude of the most probable mass ratio is not predicted quantitatively in this description. We presume, optimistically, that this must be attributed to some oversight in our simple analysis such as the omission of shell effects rather than to the fundamental irrelevancy of the whole description. In any case its many implications should allow the model expeditiously to be tested and refined or reviewed, as the data might require.

The author wishes to express his gratitude to Drs. S. Cohen and W. J. Swiatecki for their permission to reproduce Figure 5, and to acknowledge helpful discussions with Dr. W. J. Swiatecki, Dr. J. R. Nix and with his colleagues at the University of Maryland.

(*) Cf. footnote Section III A.

A. Deviations of M_H/M_L from the Value $N+/N-$: Energetics

We consider here in somewhat more detail the additional fragment excitation energy which one expects to be associated with the displacement of one nucleon from the heavy fragment to the light fragment, resulting in a mass ratio $(N+/N-)(1 - 2/N) \approx M_H/M_L$ instead of the most probable value of $N+/N-$; i.e. associated with a shift in the mass ratio towards symmetric of ≈ 0.01 .

To make this estimate consider two reflection symmetric potentials just after scission and suppose that $M_H = (N+) - 1$, $M_L = (N-) + 1$, as in the "one particle-one hole" configuration in Figure 5. One can see that in this case if the hole occurs in the a^{th} orbit below the Fermi sea of fragment M_H , then the particle will occur in the b^{th} level above the Fermi sea of fragment M_L , where $a + b = N+ - N-$. If the single particle level density has the value, g , this configuration will have a particle-hole excitation energy of

$$E_{\text{ph}} = (g)^{-1} (N+ - N-) \quad (\text{I.1})$$

in addition to the energy associated in the reflection-symmetric situation with the deviation from constant nuclear density in both fragments. This latter energy will go to zero, however, as the two potentials are adjusted to unequal volumes proportional to M_H and M_L (by allowing them to become asymmetric), whereas the nucleonic excitation energy will adjust not to zero, but to the value

$$\tilde{E}_{\text{ph}} = \frac{a}{g_H} + \frac{b}{g_L} \approx \frac{1}{\tilde{g}} [N+ - N-] \quad (\text{I.2})$$

where \tilde{g} is an appropriate average of g_H and g_L . Taking for \tilde{g} the value $1/10(A/2)(\text{MeV})^{-1}$ we obtain the estimate ($A = 240$)

$$\tilde{E}_{\text{ph}} \approx \frac{20}{A} (N+ - N-) \quad (\text{I.3})$$

or $\approx .8$ MeV per particle transferred for $4(N+ - N-) = 40$. (i.e. for $N+/N- = 1.40$). This energy may be compared with the energy gain of ~ 8 MeV associated with the closure of the 50-82 nuclear shells^(*), to estimate roughly the energetic equivalence of a shift of 10 nucleons near a most probable mass ratio of 1.4 and the energy gained in the formation of a closed shell fragment. This comparison suggests that shell effects may be responsible for significant deviations of the most probable mass ratio observed in real nuclei from that estimated for the average liquid drop nucleus by the statistical methods of Appendix II, and Figure 6. The 10 nucleon shift cited here would correspond to a mass ratio shift from 1.4 to 1.2.

(*) See reference (20).

A. U-G Symmetry and the Nucleonic Liquid Drop

Hill and Wheeler^(*) give the following asymptotic formula for the density of single particle eigenstates⁽⁺⁾ of the wave equation $(\nabla^2 + k^2) \psi = 0$, subject to $\psi = 0$ on the surface of a box of volume V:

$$\frac{dN}{dk} = \frac{V}{2\pi^2} k^2 - \frac{Sk}{8\pi} + \frac{C}{8\pi^2} \quad (\text{II.1})$$

where S is the surface area of the box and C is the integrated mean curvature over the surface of the box.

If the box is reflection symmetric, then each eigenstate exhibits either gerade (+) or ungerade (-) symmetry under the replacement $Z \rightarrow -Z$. We now calculate the state densities, dN^\pm/dk , for these two symmetry classes using equation (II.1). (Cf Figure 4.) Consider the half-box formed by cutting the box into two equal parts joined by the area A_1 . In the half-box, $V/2$, equation (II.1) also described the density of states which satisfy $\psi = 0$ on its surface (including A_1). But this density is precisely the density of (-) states in V, since one and only one (-) state can be constructed from each such state in $V/2$. Thus

$$\frac{dN^-}{dk} = \frac{V}{4\pi^2} k^2 - \frac{k}{8\pi} \left(\frac{S}{2} + A_1 \right) k + \left(\frac{C}{2} + C_1 \right) \cdot \frac{1}{8\pi^2} \quad (\text{II.2})$$

is the density of (-) states in V. [Here C_1 is the increment in the integrated curvature associated with edge formed by the circular perimeter of A_1 .] It follows at once that

$$\frac{dN^+}{dk} = \frac{V}{4\pi^2} k^2 - \frac{1}{8\pi} \left(\frac{S}{2} - A_1 \right) k + \frac{(C - C_1) \cdot 1}{8\pi^2} \quad (\text{II.3})$$

One has thus obtained the basic tool for incorporating u-g symmetry into the nucleonic liquid drop model.

(*) Reference 10, Figure 11. (Cf. also reference 41)

(+) Throughout this Appendix we write formulas for systems of spinless nucleons. A nucleus with 60 of each of the four non-identical nucleons is then described as the sum of four independent systems with $N = 60$.

From equations (II.2) and (II.3) we obtain the total number N_{\pm} of (\pm) states by integration up to the value k_o^{\pm} of the last filled nucleonic state.

$$N_{\pm} = \frac{V}{12\pi^2} (k_o^{\pm})^3 - \frac{1}{16\pi} \left[\frac{S}{2} \mp A_1 \right] (k_o^{\pm})^2 + \frac{1}{96\pi} \left[\frac{C}{2} \mp C_1 \right] k_o^{\pm} \quad (II.4)$$

and the difference ($N_+ - N_-$) given in equation (1) of the text. If we allow N_+ to have the value appropriate to the lowest energy state for given V, S, L , values then $k_o^+ = k_o^- = k_o$ where k_o is given as a power series in $\left(\frac{N}{V}\right)^{1/3} = (\text{density})^{1/3}$ by the expression:

$$k_o = \left(\frac{6\pi^2 N}{V}\right)^{1/3} + \frac{\pi}{8} \frac{S}{V} + \left[\frac{\pi S}{8V}^2 - \frac{L}{4V} \right] \left(\frac{V}{6\pi^2 N}\right)^{1/3} + \dots \quad (II.5)$$

Following Hill and Wheeler one can also obtain the total energy of the system by integration up to k_o :

$$\frac{2M}{\hbar^2} \cdot E = \int_0^{k_o} \hbar^2 k^2 \frac{dN}{dk} = \frac{V}{10\pi^2} k_o^5 - \frac{S}{32\pi} k_o^4 + \frac{Ck_o^3}{24\pi^2} \quad (II.6)$$

and by using (A5) for k_o arrive finally at the following expression for the energy:

$$\begin{aligned} \frac{2ME}{\hbar^2} &= \frac{V}{10\pi^2} \left(\frac{6\pi^2 N}{V}\right)^{5/3} + \frac{S}{32\pi} \left(\frac{6\pi^2 N}{V}\right)^{4/3} \\ &+ \frac{6\pi^2 N}{V} \left[\frac{S^2}{128V} - \frac{L}{12\pi^2} \right] + \dots \end{aligned} \quad (II.7)$$

This energy contains a term proportional to the surface area S , and therefore provides the connection between the nucleons in the potential and the surface energy of the system when it is considered to be a liquid drop. The third and higher terms correspond to corrections to the constant surface tension approximation to the liquid drop. For comparison with a constant surface tension liquid drop models, consistency requires that these terms in the nucleonic energy be omitted.

By means of (II.2) and (II.3) one can write down in a straight forward way analogous expressions for k_o^{\pm} (II.5) and E^{\pm} (II.6). The total energy is

$$E = E^+ + E^-$$

and can be subjected to differentiation with respect to a shape parameter, a , under either of two conditions:

$$(a) \left[dN_+ + dN_- = 0; k_o^+ = k_o^- = k_o \right] \rightarrow \frac{DE}{Da} \quad (II.8)$$

or

$$(b) \left[dN^+ = 0, dN^- = 0. \right] \rightarrow \frac{dE}{da} \quad (II.9)$$

where $a = [1 - (R_{min})^2 / R_0^2]$ parametrizes the Cohen-Swiatecki family of saddle point shapes (*).

Case (II.8) describes the liquid drop derivative which allows the nucleonic configuration to adjust to the lowest energy at the shape in question. It gives the result (in first approximation)

$$\frac{DE}{Da} = h^2 \bar{k}_0^4 R_0^2 B'_s / 4M \dots \quad (II.10)$$

$$\text{where } \bar{k}_0 = (6\pi^2 N/V)^{1/3} \quad (II.11)$$

This same result would also be obtained directly from (II.7). It identifies the constant

$$\frac{h^2 \bar{k}_0^4 R_0^2}{4M} = E_s^0 \quad (II.12)$$

with the surface energy E_s^0 of the spherical drop. [The fact that the infinite square well potential gives a value greater than the empirical surface tension is discussed in Hill and Wheeler(†).] At the shape where, for fixed N^+ , one has $k_0^+ = k_0^-$, the first derivative (II.9) also gives the result (II.10). This property demonstrates the fact that the liquid drop surface osculates each configurational potential surface at that point where its N^+ value gives the lowest energy.

For the second derivatives one obtains

$$\frac{D^2 E}{Da^2} = E_s^0 B''_s + \dots \quad (II.13)$$

and

$$\frac{d^2 E}{da^2} = [B''_s + \frac{2\pi}{3}] E_s^0 + \dots \quad (II.14)$$

Reference 6 shows that B''_s has values

$$0 < B''_s < 1.5 \quad (II.15)$$

for saddle shapes corresponding to $X > .69$. On the other hand, for shapes corresponding to $.50 < X < .69$, one has

$$B_s < -3.0 \quad (II.16)$$

(*) Cf Section IV.B.1. The prime is used throughout this paper to denote derivatives with respect to a .

(†) Reference (10) Figure 11. But see also the more complete discussion of reference (20). We have here chosen simply to identify the constant (II.12) with the empirical nuclear surface energy in order to obtain approximate numerical results. A more realistic estimate would involve the recognition that the nuclear potential is not an infinite square well (in which all the energy is kinetic) but varies over a finite distance near the nuclear surface.

indicating $d^2E/da^2 < 0$. Such nucleonic-potential surfaces are therefore open in this approximation to scission, and one would expect fission to occur with extreme rapidity from the first such configuration which obtains.

We wish to note before closing this section that the variables S = surface area, A_1 = central cross section, and C = integrated mean curvature are obvious candidates for "natural" shape-descriptive variables for the nucleonic liquid drop in the pre-barrier region.

B. Estimate of Symmetric Fission Barrier Energy Increase for Non-Optimal $N+$

With these results it is straight forward to estimate the least cost in energy involved in imposing a value of $N+$ on a system different from the optimal $N+(a)$ value for a given reflection symmetric shape, a . For $N+(a)$ both (+) and (-) orbits are filled to the same value k_o . To shift $(N+ - N-)$ by some specified increment $2\delta N+$ one must empty $\delta N+$ of the uppermost (-) orbits and fill an extra $\delta N+$ of the (+) orbits. The resulting nucleonic energy is thereby increased (in first approximation) by

$$\begin{aligned} \delta E &= \frac{\partial E}{\partial k} \frac{dk}{dN} (2\delta N) = \\ &= \frac{2h^2 \bar{k}_o^2}{M} \cdot \frac{2\pi^2}{V \bar{k}_o^2} \cdot \delta N \\ &= 12\pi E_s^0 (\bar{k}_o R_o)^{-5} = 1/4 \text{ MeV per nucleon} \quad (\text{II.17}) \end{aligned}$$

Where we have used (II.1), (II.12) and the rough estimates: $\bar{k}_o R_o \approx 10$ for 60 nucleons in a Uranium-sized box, and $E_s^0 = 18 (240)^{2/3} (\text{MeV})$. It is on the basis of this estimate that the statement is made in Section III.2 that the rigid imposition of constant $N+(a_o)$ upon a uranium-like case where $(4N+(a_o))$ at the stable shape is at least 8 units greater than $4N+(a_s)$, the lowest energy value at the saddle point, would increase the U^{235} fission barrier by at least 2 MeV.

(*) Clearly, the third derivative is required to specify the nucleonic potential in this situation. But the postulate of equivalence demands that the third derivative be negative (positive) for post-(pre-) barrier shapes. Otherwise the nucleonic potential for this configuration would lie below the L.D. potential for some range of shapes, in contradiction to that postulate.

A. The Equivalence Postulate

In Section IV.A, we stated the Equivalence Postulate: The Liquid Drop potential surface describes the envelope of the lowest energy nucleonic-configurational potential surface. In Appendix II we showed for reflection symmetric families that the shape of a given configurational potential is equal to that of the liquid drop surface at the shape where that configuration is the least energy configuration. This result verifies the postulate for reflection-symmetric shapes, and thereby enhances its credibility as a valid general property of nucleonic liquid drops.

This postulate enables one to make rather efficient use of detailed liquid drop calculations. For example Cohen and Swiatecki⁽⁶⁾ and Nix⁽¹²⁾ show that the nuclear saddle shapes are stable against asymmetric deformations. The equivalence postulate then guarantees that the nucleonic configurational potential at the saddle point is also asymmetry-stable at its minimum (which is the point of osculation for the saddle point), since it must everywhere be higher than the liquid drop surface. One thus concludes that no pre-barrier configuration exists which has an asymmetric threshold lower than the liquid drop threshold, and finally that asymmetric instabilities in nucleonic configurational potentials can be open to scission^(*) only if they osculate the liquid drop at or beyond the saddlepoint shape.

(*) I.e. can reach scission from the osculation point by a path along which the energy decreases monotonically.

B. Asymmetric Instability of Nucleonic-Configuration Away From Osculating Shape

We now consider a nucleonic configuration which osculates the L.D. surface at a shape a_0 . For a shape $a = a_0 + \Delta a$, this nucleonic surface will have an energy

$$E_N(a) = E(a_0) + E'(a_0)\Delta a + 1/2 E''(a_0)(\Delta a)^2 + E_C(a) \quad (\text{III.6})$$

whereas the L.D. energy is

$$E_L(a) = E_S(a_0) + E_{S'S}^0(a)\Delta a_0 + 1/2 E_{S'S}^0(a_0)(\Delta a)^2 + E_C(a) \quad (\text{III.7})$$

where we have assumed the Coulomb energy, $E_C(a)$, depends only on the shape a , of the nucleus, and not at all on the detailed nucleonic configuration. Thus the requirement that $N+ = \text{constant}$ has resulted in an energy increase over the L.D. energy equal to

$$\frac{\pi E_S^0}{6} (\Delta a)^2 \approx \Delta E_{gu} \quad (\text{III.8})$$

according to (II.13) and (II.14).

This energy can of course be regained by a nucleonic rearrangement via residual two particle interactions into the best nucleonic configuration for the shape a . Such a rearrangement will require that $(N+ - N-)$ change by an amount

$$\Delta(N+ - N-) = - \frac{d(N+ - N-)}{da} \Delta a \quad (\text{III.9})$$

and will require a time long compared with the nuclear oscillation time.

We wish to consider instead the effect of breaking the reflection-symmetry by allowing the potential to have a volume $V(1 + \delta)/2$ on one side of the $Z = 0$ plane and a volume $V(1 - \delta)/2$ on the other. To preserve the constant nuclear density, such a configuration must have a proportionate number of nucleons on the corresponding sides of the Z -plane. Since the lowest $N-$ orbits of the (+) and (-) type correspond essentially to $N-$ nucleons in each half and the uppermost $(N+ - N-)$ orbits of the (+) type correspond to nucleons in both halves with amplitude $1/\sqrt{2}$, the change to the reflection asymmetric potential corresponds to shifting $2\delta N$ nucleons from the upper $(N+ - N-)$ (+) orbits into single particle states localized in the large volume, $V/2(1 + \delta)$. Such localized states will obey the boundary condition $\psi = 0$ on the $Z = 0$ plane, and for that reason correspond to orbits of the (-) type as regards their level density properties. We therefore assume (*) that such an asymmetric deformation of the potential leads to a configuration whose g - u symmetry energy corresponds to that of the

(*) This assumption is in fact realized at the scission configuration, as we show in a later publication. (Note added in proof.)

lowest configuration in the reflection-symmetric potential of shape, a . The asymmetric deformation, δ_0 , for this correspondence is given by (*)

$$\delta_0 = -\frac{1}{N} \frac{d(N+ - N-)\Delta a}{da} \quad (\text{III.10})$$

In this way the nucleus can gain back the energy ΔE_{gu} of (III.8) by moving across a continuous potential surface to an asymmetric deformation, δ_0 , given by (III.10). In the process on the other hand its surface and Coulomb energies must increase by an amount (+), $1/2\bar{C}_3\delta_0^2$ according to the liquid drop calculations of reference (6). The question of whether or not the configuration potential is stable at the non-equilibrium shape $a = a_0 + \Delta a$ is therefore answered by the sign of

$$-\frac{\pi E_s^0}{6} + \frac{E_s^0}{2} \bar{C}_3 \left[\frac{1}{N} \frac{d(N+ - N-)}{da} \right]^2 = \kappa_3 \quad (\text{III.11})$$

Since $\left| \frac{1}{N} \frac{d(N+ - N-)}{da} \right| < 1/6$ and $\bar{C}_3 < 4.3$ for all X , $\kappa_3 \sim (-.52 + .06) < 0$,

and there is no marginality in the answer: κ_3 is negative, and the nucleonic configuration is asymmetry-unstable for values of "a" greater than its osculation point.

On the other hand this statement does not answer the crucial question of whether these instabilities are open to scission, i.e. whether or not the instabilities are unbounded. Indeed the nucleus is very unlikely in a given configuration to oscillate very far from its equilibrium shape. All that has been shown here is that at a deformation $\delta_0 \propto \Delta a$, the deviation from the point of osculation, the energy is less than at the symmetric form for the shape, $a_0 + \Delta a = a$. We now turn to the question of when this instability becomes unbounded.

- (*) The fact that δ_0 is linear in Δa is due to the occurrence of a cusp in the nucleonic potential, which occurs along the symmetric line for all $a \neq a_0$. The cusp merely describes the fact the u-g energy is, near symmetric, a linear decreasing function of asymmetry δ .
- (+) The stiffness \bar{C}_3 here is approximately 64/9 times the quantity C_3 tabulated in reference (6). The factor is estimated from the correspondence between the deformations used there which are assumed equivalent to $\alpha_3 P_3(\cos\theta)$, and the fractional volume deformation, δ , used here. If such estimation leads to marginal inequalities, it is dangerous, for reasons discussed in Section (III.4). This does not appear to be the case in equation (III.11).

C. Unbounded Instabilities Occur Beyond the Saddle Point

In Part B we discussed the instability against symmetry which occurs when the given nucleonic configuration oscillates away from its equilibrium point. We now consider the crucial question: Under what circumstances may this instability grow indefinitely? Or, alternatively, under what circumstances may this instability lead to an energy at δ_0 less than the minimum reflection-symmetric energy for the osculation point of the configuration in question?

The answer follows immediately from (III.6) and (II.13):

$$E_N(a, \delta_0) - E_N(a_0, 0) = + [2xE_S^0 B_C' + E_S^0 B_S'] \Delta a + [2xE_S^0 B_C'' + \frac{\pi E_S^0}{6} + \kappa_3] (\Delta a)^2 \quad (\text{III.12})$$

for $\Delta a > 0$. Thus as long as $2xB' + B''$ is positive the instability is bounded. I.e. the energy at (a, δ_0) is greater than the energy at $(a, 0)$. On the other hand when $(2xB' + B'')$ becomes negative (i.e. at the saddle point!) the energy at (a, δ_0) is lower than that at $(a_0, 0)$. Moreover the difference increases with Δa . Then the nucleonic-configuration potential surface is open to ever increasing a -values. The asymmetry, δ_0 , will also grow ($\delta_0 \propto \Delta a$) until $d(N+ - N-)$ become equal to zero, i.e. to an asymmetry, $\frac{1 + \delta_0}{1 - \delta_0}$, equal to $N+/N-$ at the symmetric configuration which first becomes unstable. In this way the nucleus can arrive at an asymmetric scission point in a time short compared to that required for further progress down the symmetric family of shapes.

It is interesting to note that the motion towards asymmetry, once de-stabilized, is accelerated by the term of $O(\Delta a)^2$ in (III.12) because of the $2xB_C''(\Delta a)^2$ term which for $x > .68$ is negative and larger in magnitude than the positive restoring term, $1/2(C_3 \delta^2)$. Careful scrutiny of the zero point oscillations in the bound symmetric configurations, which define the appropriate measure for Δa might even show that this second order term opens configuration potentials even somewhat before the term linear in (Δa) reaches zero, i.e. before the fission barrier.

In any case, this feature guarantees that instability will occur at the latest just beyond the barrier shape, relieving one of any necessity to carefully assess marginal quantitative balances in order to extract the major features of the description.

We also note that in this description it is the fact that $(N+ - N-)$ has already become small at the fission barrier, [so that the upper bound on δ_0 is small] which guarantees that the fission of low Z elements will be nearly symmetric. Thus, it is the u - g symmetry indeed, which dominates the asymmetry, rather than any combination of liquid drop properties.

D. Brief Resume; Cautions

To recapitulate the essential physics of our description we note the following elements:

- (1) Isolation of an extra u-g energy above liquid drop energy associated with requirement that N^+/N^- be kept constant for shapes beyond osculation point a_0 .
- (2) Estimation of asymmetric deformation, δ_0 , which regains this energy, reducing it back to liquid drop value for (a, δ_0) .
- (3) Observation that beyond barrier (a, δ_0) will have lower energy than symmetric point of osculation $(a_0, \delta = 0)$.

We note that if it is impossible to regain all of the u-g energy by going asymmetric, then the asymmetry instability will not obtain until the slope of the liquid drop potential beyond the barrier becomes sufficiently negative. A quantitative estimate of the actual energy gained is in progress and will be reported in a subsequent publication. (*)

We note also that we have greatly simplified the actual complexity of the problem by speaking as though N^+/N^- defined a specific nucleonic-configuration surface, when in fact a multitude of different configurations may correspond to the same value of N^+/N^- : On the other hand, we treat N^+/N^- as a continuous variable, when in fact it must be always a ratio of integers.

Finally one should keep in mind the fact that deformation-potential surfaces are not well defined objects. Except for equilibrium points and cusps (like those which appears in the nucleonic configuration potential for $\delta = 0$ and $a \neq a_0$), their properties may be modified drastically by coordinate re-definition. Only when the deformation space is given a metric can one uniquely define coordinates which exhibit "orthogonality." The metric of the deformation space is defined by the kinetic energy operator for the deformation. Thus the complete dynamical problem becomes coordinate-independent. But the static problem alone does not share this property.

Whenever he omits dynamics, therefore, one is assuming either implicitly or explicitly that the kinetic energy operator will be nearly diagonal in the coordinates he has defined. Like nearly everyone else who has studied nuclear fission, we make this assumption, for the present. When a model appears which seems especially promising, then a dynamical analysis will be recognizably appropriate. Perhaps that the present model will come to fulfill this criterion.

(*) See footnote Appendix III.B. Added in proof.

REFERENCES

- (1) Otto Hahn and F. Strassman, *Naturwiss*, 27 11,89 (1939). (Cf. also H. G. Graetzer, *Am. J. Phys.* 32 9 (1964).
- (2) L. Meitner and O. Frisch, *Nature* 143 239, 471 (1939)
- (3) W. Jentschke and F. Prankl, *Naturwiss*, 27 134 (1939)
- (4) N. Bohr and J. A. Wheeler, *Phys. Rev.* 56 426 (1939).
- (5) S. Frankel and N. Metropolis, *Phys. Rev.* 72 914 (1947)
- (6) W. J. Swiatecki and S. J. Cohen, *Annals of Physics* 22 406 (1963) is part V of this series. Part I - IV are cited therein.
- (7) U. L. Businaro and S. Gallone, *Nuovo Cimento* 5 315 (1957), 1 629 (1955) and 1 1277 (1955)
- (8) D. S. Burnett, et al. *Phys. Rev.* 134 5B 952 (1964)
- (9) D. L. Hill, *Phys. Rev.* 78 197 (1950)
- (10) D. L. Hill and J. A. Wheeler, *Phys. Rev.* 89 1102 (1953)
- (11) D. R. Inglis, *Annals of Physics* 5 106 (1958)
- (12) J. R. Nix, *Nuclear Physics* 71, 1 (1965), and *Ann of Phys.* 41,52 (1967)
- (13) J. N. Lawrence, Ph.D. thesis submitted to Vanderbilt University September, 1967.
- (14) P. Fong, *Phys. Rev.* 89 332 (1953). Also *Phys. Rev.* 102 434 (1956) 122 1542 (1961) and *Phys. Rev. Letters*, 11 375, (1963)
- (15) J. K. Perring and J. S. Storey, *Phys. Rev.* 98 1525 (1955)
- (16) H. Britt et al, *Phys. Rev.* 139, B354 (1965)
- (17) Cf. e.g. A. C. Wahl, *The Physics and Chemistry of Fission*, page 323, Vol. I. [International Atomic Energy Agency, Vienna, 1965].
- (18) Cf. e.g. J. Terrell, *The Physics and Chemistry of Fission*, page 18, Vol. II [International Atomic Energy Agency, Vienna, 1965].

REFERENCES

- (19) W. J. Swiatecki in Proc. Conf. on Nuclidic Masses, Vienna, 1963. ed. by W. H. Johnson, Jr. (Springer Verlag Wien-New York, 1964) page 58.
- (20) W. D. Meyers and W. J. Swiatecki, Nuclear Physics 81, 1 (1966).
- (21) V. M. Strutinskii and A. S. Tyapin, JETP (Soviet Physics) 18, 664 (1964).
- (22) W. J. Swiatecki, Proc. Phys. Soc. A64, 226, (1951).
- (23) Th. A. J. Maris, Phys. Rev. 101, 147 (1956).
- (24) H. C. Britt, H. E. Wegner, and J. C. Gursky, Phys. Rev. 129, 2239 (1963).
- (25) E. Konecny and H. W. Schmitt - to be published.
- (26) I. Halpern, "The Physics and Chemistry of Fission" Vol. II, page 369, [International Atomic Energy Agency, Vienna (1965)]
- (27) H. R. Bowman, J. C. Milton, S. G. Thompson, and W. J. Swiatecki Phys. Rev. 126, 2120 (1962) and 129, 2133 (1963).
- (28) J. C. D. Milton and J. S. Fraser, The Physics and Chemistry of Fission Vol. II, Page 39, [The International Atomic Energy Agency, Vienna, (1965)]
- (29) V. V. Vladimirov, Z. eksp. teor. Fiz. 32, 822 (1957) [English translation: Soviet Physics - JETP 19, 810 (1964)]
- (30) S. L. Whetstone, Phys. Rev. 114, 581 (1959)
- (31) Z. Fraenkel and S. G. Thompson, Phys. Rev. Lett. 13, 438 (1964).
- (32) N. Feather, The Physics and Chemistry of Fission Vol. II, page 387. [International Atomic Energy Agency, Vienna, (1965)].
- (33) J. Griffin, The Physics and Chemistry of Fission Vol. I, page 23 [International Atomic Energy Agency, Vienna, (1965)].
- (34) J. R. Huizenga, The Physics and Chemistry of Fission, Vol. I, page 11 [International Atomic Energy Agency, Vienna, (1965)].
- (35) A. Bohr, Proceedings of the International Conference on the Peaceful Uses of Atomic Energy 2, page 151 (1956).
- (36) G. A. Cowan, A. Turkevich, and C. Browne, Phys. Rev. 122, 1286 (1961).

REFERENCES

- (37) G. A. Cowan, B. P. Bayhurst and R. J. Prestwood, Phys. Rev. 130, 2380 (1963).
- (38) Y. A. Blyumkina, etal. Atomnaya Energiya, 15, 64 (1963).
- (39) V. N. Okolovich and G. N. Smirenkin, Atomnaya Energiya, 15, 250 (1963).
- (40) M. S. Moore and L. G. Miller, the Physics and Chemistry of Fission Vol. I, page 87, [The International Atomic Energy Agency, Vienna (1965)]
- (41) K. C. Hammack, "Topics in Nuclear Structure," Thesis of June, 1951 at Washington University.

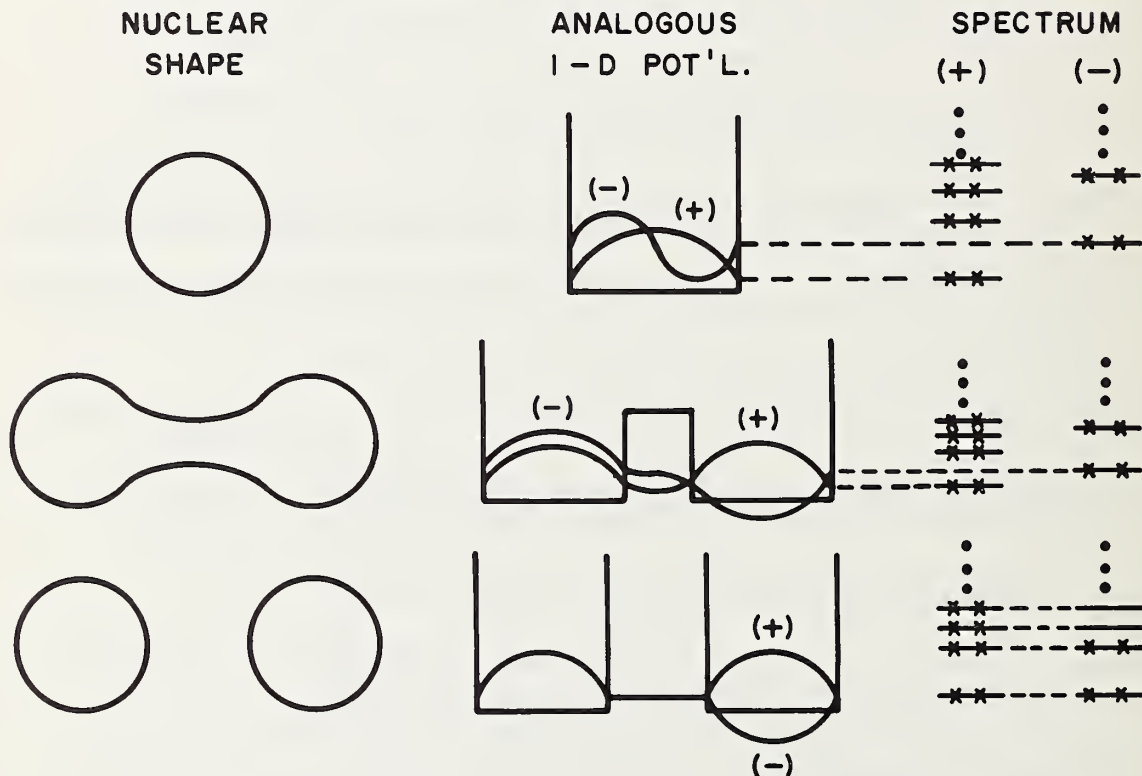


Figure 1. The effect of "necking-in" of a symmetric potential on gerade (+) and ungerade (-) states in that potential is illustrated. As the cross sectional area of the potential at $z = 0$ decreases, the energy difference between the n th gerade state and the n th ungerade state decreases monotonically to zero.

The figure also illustrates the situation which prevails if the shape is changed (in this case from the spherical to the broken configuration) while the values of N_+ and N_- are kept fixed: the energy could be lowered by scattering two (in the simple case shown here) nucleons from (+) to (-) orbits. It is a central proposition of this paper that a reflection asymmetry in the potential can effect such a shift on a shorter time scale than the scattering by residual interactions.

LR COMPONENTS IN A GIVEN (+)-(-) STATE

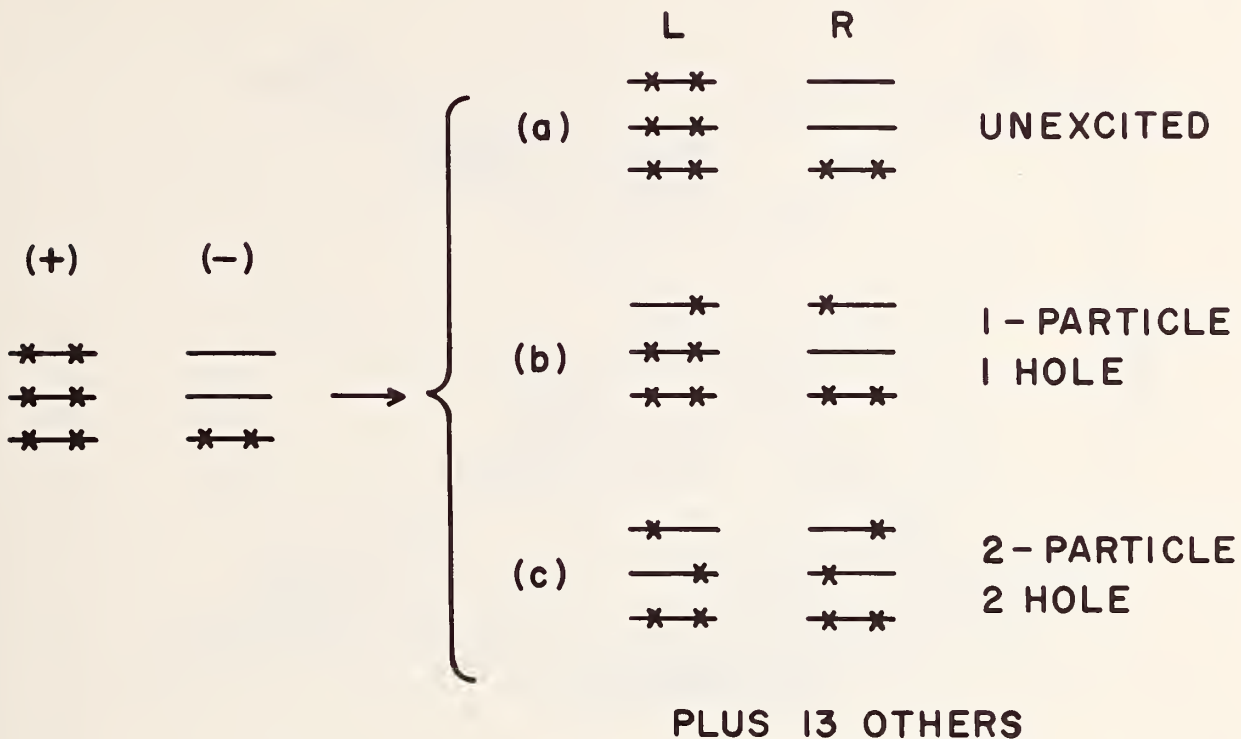
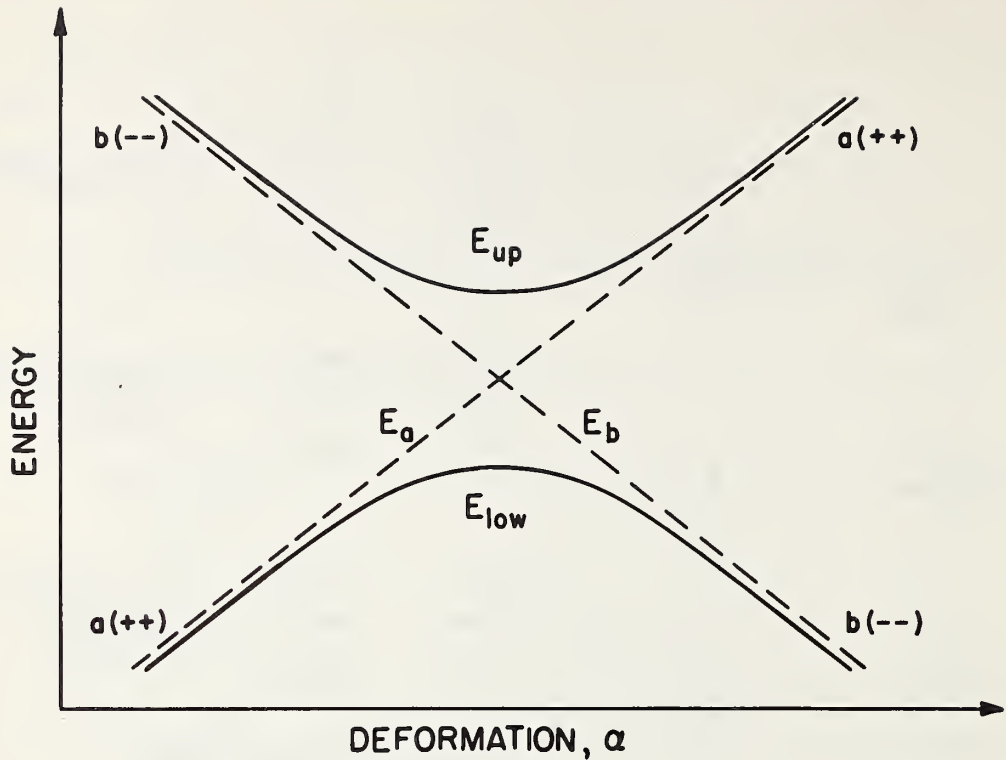
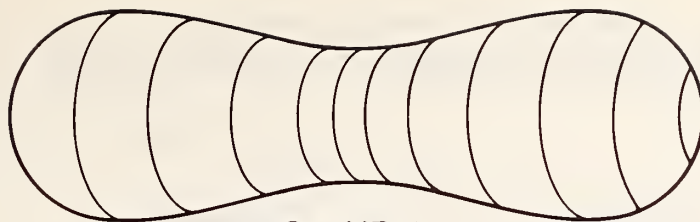


Figure 2. The expansion of a many-body state in a reflection symmetric pair of potentials in terms of the wave functions for particles localized in the Left and Right potentials is illustrated. The "unexcited" configuration has a mass ratio N_+/N_- .

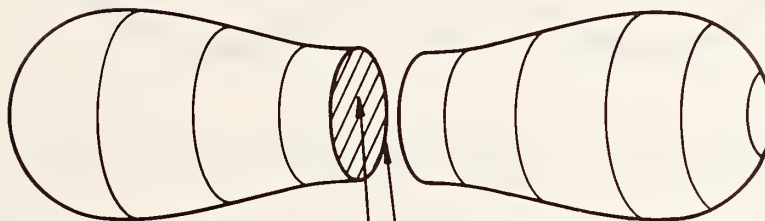


BEHAVIOR OF TWO LEVELS AT A POINT OF NEAR CROSS-OVER.

Figure 3. (After D. L. Hill and J. A. Wheeler, reference 10). A crossing (dotted line) of two levels a, b, considered here as doubly degenerate nucleonic orbits with G-U symmetry as specified, is modified by a residual interaction (e.g. a "Pairing" interaction), which scatters a pair of nucleons in "a" into orbits "b" into the situation described by the solid lines labelled E_{up} and E_{low} . In the adiabatic limit the state (++) at small deformation follows E_{low} and emerges at large deformation as state b(--). Conversely, under very rapid deformation a jump occurs from E_{low} to E_{up} and state a(++) emerges at large deformation with its symmetry character unchanged. Reference 10, Figures 34 and 35 provide a calculation of this situation for a simple case.



VOLUME = V
 SURFACE AREA = S
 INTEGRATED CURVATURE = C

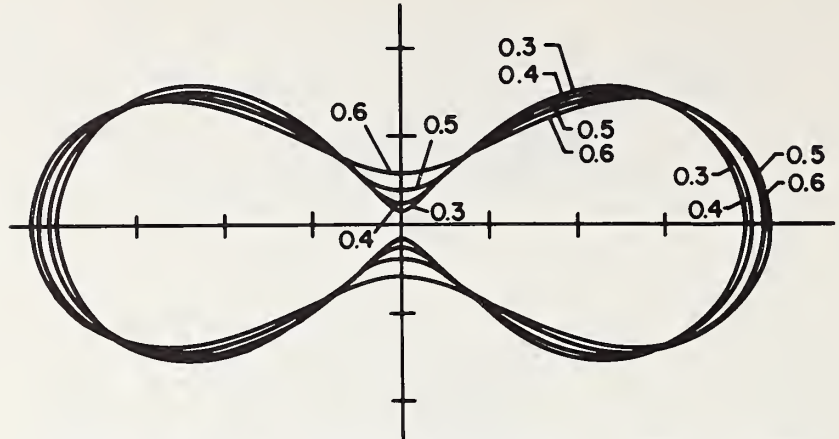


AREA OF FACE = A_1
 CURVATURE OF EDGE = C_1

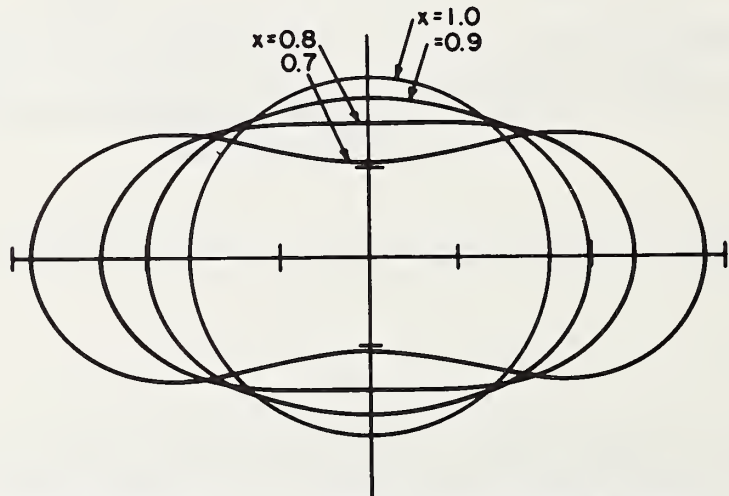
$1/2$ VOLUME = $V/2$
 $1/2$ SURFACE = $S/2 + A_1$
 $1/2$ CURVATURE = $C/2 + C_1$

Figure 4. An illustration of the procedure used in Appendix II to obtain the density of ungerade states for a symmetric figure in terms of the area A_1 and the edge curvature C_1 of the circle which joins the symmetric half-figures.

From S. Cohen and W.J. Swiatecki
DEFORMATION ENERGY OF A CHARGED DROP



COMPARISON OF NECKED-IN SADDLE-POINT SHAPES
 FOR $x \leq 0.6$



COMPARISON OF CYLINDER-LIKE SADDLE-POINT
 SHAPES FOR $x \geq 0.7$

Figure 5. The Cohen-Swiatecki family of saddle-point shapes. We have assumed this sequence of shapes to describe the progress of any nucleus from spherical to scission. This choice guarantees that the liquid drop saddle point shape for any X-value occurs in the family and has correct Liquid Drop threshold energy. It is of course a fiction that a specific nucleus will actually follow this sequence of shapes in motion towards scission.

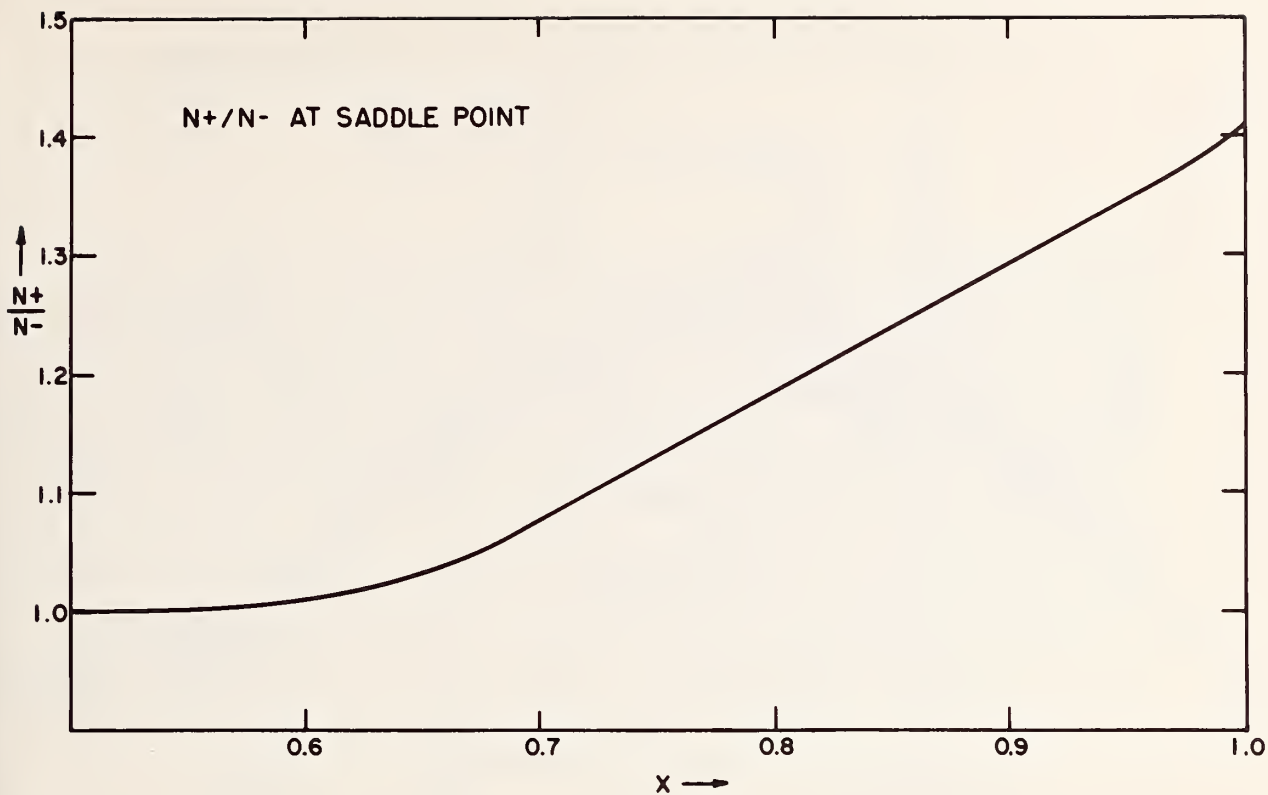


Figure 6. The saddle point values of $N+/N-$. This quantity has been calculated for the lowest energy configuration at each shape in the family illustrated in Figure 5, and plotted against the fissionability parameter for which that shape is the saddle point. The (small) curvature term in Equation (1) was neglected.

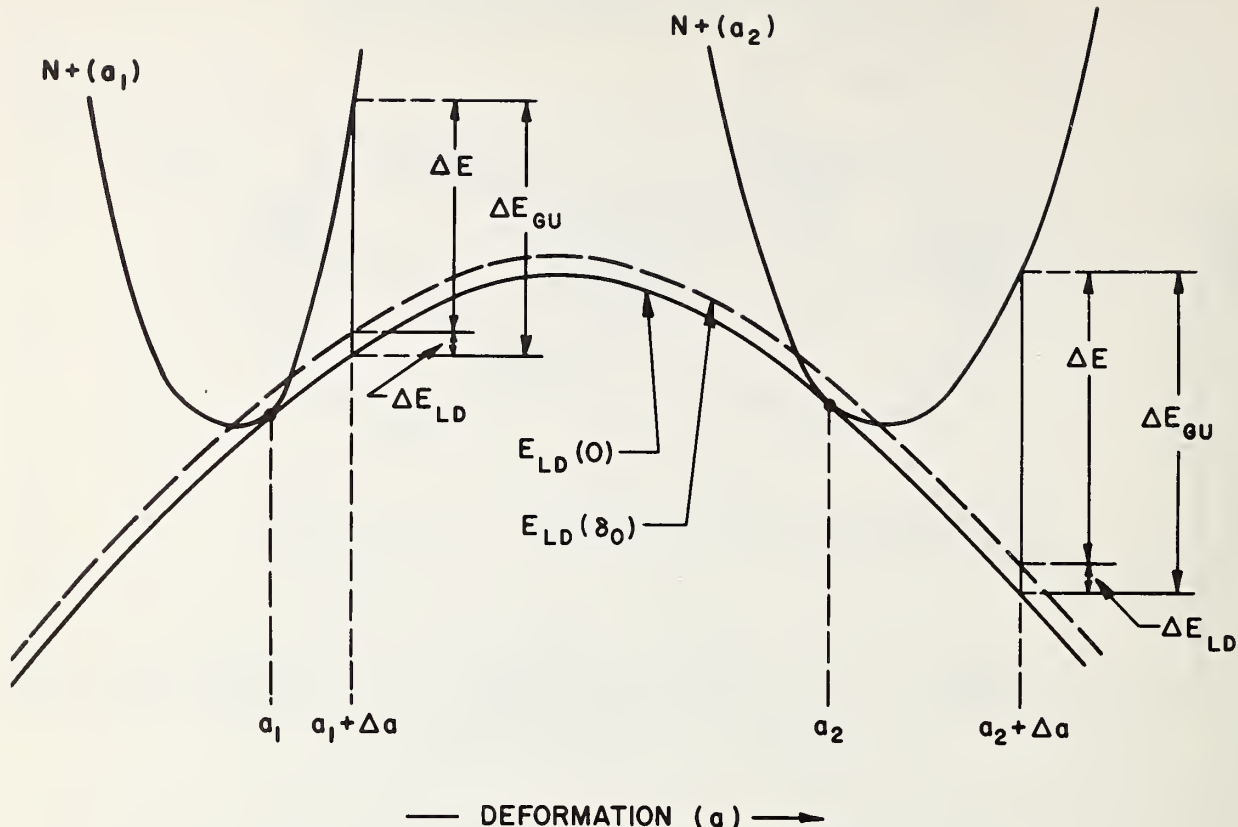


Figure 7. This figure illustrates the energy consideration involved in the proposed explanation of post-barrier asymmetry-instability. The curve $E_{LD}(0)$ portrays the liquid drop energy for a reflection-symmetric nucleus as a function of shape, "a." The dotted curve $E_{LD}(\delta_0)$ describes the liquid drop energy for a figure with asymmetry δ_0 . Also shown are two nucleonic configuration curves labelled by specific values of $N+$ which values are defined by the requirement that they correspond to the lowest energy configuration at the shapes a_1 and a_2 where they osculate $E_{LD}(0)$. In our description the variable $N+$ is treated as continuous variable, so that there corresponds to it a continuous family of nucleonic potential curves, each of which osculates E_{LD} at one particular shape; Postulate of Equivalence. Of this continuous family E_{LD} only two are shown here.

In a shape oscillation away from the osculation point the requirement that $N+$ be held fixed costs an extra energy ΔE_{GU} . This energy arises from the fact that for $\Delta a > 0$, $k_+ > k_-$ and a lower energy results from a shift of nucleons from (+) to (-) orbits. On the assumption that a deviation from reflection symmetry to an asymmetry δ_0 , effects such a shift and regains ΔE_{GU} , one calculates a net gain in energy $\Delta E = \Delta E_{GU} - \Delta E_{LD}$ for the asymmetric shape. The figure illustrates the fact that this gain leads to an energy lower than the energy at the point of osculation only when the slope of E_{LD} is negative; i.e. only beyond the saddle point shape.

CALCULATION OF PHOTON PRODUCTION CROSS SECTIONS
AND SPECTRA FROM 4 TO 15 MEV NEUTRON INDUCED REACTIONS*

R. J. Howerton
Lawrence Radiation Laboratory
Livermore, California 94551

Abstract

Photon production cross sections and spectra resulting from the interaction of neutrons with nuclei are needed for shielding and other calculations. For 4 and ~15 MeV neutrons, as well as at some intermediate energies, cross sections and spectra have been measured for some nuclei. From the 4 and ~15 MeV measurements semi-log plots of $N(E_\gamma)/E_\gamma$ vs. E_γ show a generally linear dependence. The slope of these lines is linearly interpolable on nuclear mass and neutron energy. When the implied differential equation is integrated, an average energy (\bar{E}) may be derived. Likewise, a total photon energy (E_{TOT}) may be obtained from simple considerations of the energetics of the reactions in this neutron energy range. From the quotient of these two quantities, an average multiplicity (M_γ) of photons is obtained. The product of the multiplicity by the sum of the cross sections for the photon producing reactions yields a photon production cross section and the spectrum may be obtained from the normalized spectrum function.

Extensions of the formalism to include fission reactions and anomalous production of single lines will be discussed. Comparisons with experiment show an average deviation ($100 \times (\sigma_{calc} - \sigma_{exp})/\sigma_{exp}$) of 18 percent.

In recent years, the desirability of having an evaluated library of photon production cross sections and spectra, for photons produced by neutron induced reactions as a function of incident neutron energy, has markedly increased. It would be best to base such a library on experimental data or to have a theory sufficient for generating such an evaluated library where there are not adequate data for most isotopes at most neutron energies. Since there are neither sufficient, reliable measurements of the $(n,xy)^1$ cross sections and spectra nor a dependable model which provides calculated cross sections and spectra for most neutron energies, these methods are impossible.

For most isotopes, the (n,γ) reaction is the single photon producing neutron induced reaction below the threshold of the inelastic neutron scattering. The former cross sections have been measured as a function of incident neutron energy for isotopes and elements of major interest. The few measurements, other than thermal, of the spectra of emergent photons of the (n,γ) reaction show that the photon spectra change sharply as a function of neutron energy.⁽¹⁾ While the (n,xy) cross sections and line spectra have been measured for some nuclei for several MeV above the $(n,n'\gamma)$ threshold, measurements at higher energies are relatively scarce.

* Work performed under the auspices of the U.S. Atomic Energy Commission.

¹ The (n,xy) cross section is for production of gamma-rays of any energy level independent of the nuclear process which produced the photon. This should be contrasted with the (n,γ) reaction cross section which is for the absorption of a neutron with de-excitation of the $(A+1)^*$ nucleus only by gamma emission.

This paper presents a formalism for calculating the (n,xy) cross sections and spectra for neutron energies between four and fifteen MeV for target nuclei with mass greater than twenty a.m.u. Note that the method described for calculation is not a theoretical model and is based solely upon observable systematics of relatively few measurements.(2)

Texas Nuclear Corporation experiments (3,4), which determined the (n,xy) cross sections and spectra for 4.1 and 14.8 MeV neutrons, reported line spectra where identifiable and collected "continuum" spectra in energy bins, normally of one-half MeV width. Other experiments(5,6), performed at these energies as well as those between 4 and 14 MeV, can be used to check the interpolative algorithm. All the experiments have been performed with a low energy cut-off which is significantly higher than the low energy cut-off required for photonic calculations. Thus, an extrapolation of the systematics was used in developing the algorithm. When comparing calculations and experiments, one must guard that the photon energy range for integration is the same as the experimental energy limits.

Figure 1 shows the data of Reference 4 for Tungsten for incident neutron energies of 4.1 and 14.8 MeV. Since each data set is well-fit with a straight line of slope $R'(E_n)$, then

$$d \left[\frac{N(E_\gamma)}{E_\gamma} \right] = R'(E_n) dE_\gamma \quad (1)$$

from which

$$N(E_\gamma) = A E_\gamma e^{R'(E_n) E_\gamma} \quad (2)$$

$R'(E_n)$ is intrinsically negative in all reported experiments as expected.

Define $R(E_n) \equiv \left| R'(E_n) \right|$ and obtain² $N(E_\gamma) = A E_\gamma e^{-R(E_n) E_\gamma}$. (3)

An average total photon energy E_{TOT} , neglecting recoil, is then defined as

$$E_{TOT} = \frac{(E_o - \overline{E_n'}) \sigma_{n,n'\gamma} + (E_o - E_T - 2\overline{E_{2n}}) \sigma_{n,2n\gamma} + (E_o - E_T - 3\overline{E_{3n}}) \sigma_{n,3n\gamma}}{\sigma_{n,n'\gamma} + \sigma_{n,2n\gamma} + \sigma_{n,3n\gamma}}$$

where E_o = incident neutron energy

E_T = binding energy threshold for the particular reaction

$\overline{E_{n'}}$ = average energy of neutrons from $(n,n'\gamma)$ reaction

$\overline{E_{2n'}}$ = average energy of neutrons from $(n,2n\gamma)$ reaction

$\overline{E_{3n'}}$ = average energy of neutrons from $(n,3n\gamma)$ reaction

E_{min} = .01 MeV

² Although the form of equation 3 is the same as for a nuclear "temperature model" if $T = 1/R(E_n)$, note again that this result is only from consideration of experimental data.

Clearly, $(n, n'\gamma)$, $(n, 2n\gamma)$ and $(n, 3n\gamma)$ are the only neutron induced reactions considered in this definition of E_{TOT} . However, extension of the definition to include $(n, p\gamma)$, $(n, \alpha\gamma)$ etc. reactions is straightforward.

Now, "A" of equation 3 may be determined from

$$\int_{E_{min}}^{E_{TOT}} E_{\gamma} e^{-R(E_n)E_{\gamma}} dE_{\gamma} = \frac{\sigma_{n,XY}}{A} \quad (4)$$

Define $B = e^{-R E_{min}(R E_{min}+1)} - e^{-R E_{TOT}(R E_{TOT}+1)}$

where $R \equiv R(E_n)$.

Then the normalized spectrum is

$$S(E_{\gamma}) = \frac{R^2 E_{\gamma} e^{-R E_{\gamma}}}{B} \quad (5)$$

The mean energy of the distribution is

$$\bar{E}_{\gamma} = \frac{\frac{R^2}{B} \int_{E_{min}}^{E_{TOT}} E_{\gamma}^2 e^{-R E_{\gamma}} dE_{\gamma}}{\frac{R^2}{B} \int_{E_{min}}^{E_{TOT}} E_{\gamma} e^{-R E_{\gamma}} dE_{\gamma}} \quad (6)$$

In the limiting case with $E_{min} \rightarrow 0$ and $E_{TOT} \rightarrow \infty$, $B \rightarrow 1$,

$$S(E_{\gamma}) \rightarrow R^2 E_{\gamma} e^{-R E_{\gamma}} \quad (7)$$

and

$$\bar{E}_{\gamma} \rightarrow \frac{2}{R} \quad (8)$$

With E_{TOT} and the average photon energy, \bar{E}_{γ} , the average multiplicity of photons is shown to be

$$M_{\gamma} \equiv \frac{E_{TOT}}{\bar{E}_{\gamma}} \quad (9)$$

yielding

$$\sigma_{n,XY} = M_{\gamma} (\sigma_{n,n'\gamma} + \sigma_{n,2n\gamma} + \sigma_{n,3n\gamma}) \quad (10)$$

Figures 2 and 3 present linearly interpolated values for $R(4.1 \text{ MeV})$ and $R(14.8 \text{ MeV})$ for unmeasured elements. For intermediate energies, linear interpolation in energy is used with the resulting equation

$$R(E_n) = .00395 A + .940 + \frac{E_n - 4.1}{14.8 - E_n} (.0019 A - .605) \quad (11)$$

where A is the atomic weight of the nucleus for which photon production cross sections and spectra are desired.

The appropriate average energies of nonelastic neutrons and appropriate thresholds can be procured from Reference 7 and the reaction cross sections from the IRL Evaluated Neutron Cross Section Library. In most cases, these values and a value of $R(E_n)$ from equation 11 are sufficient for the calculation of the (n,xy) cross section and spectrum. There also exists an alteration of the technique for nuclei which always produce a specific discrete gamma-ray in the course of de-excitation. A prime example of such a photon is the 0.845 MeV gamma-ray from Fe^{56} which always appears when $\text{Fe}^{56}(n,n'\gamma)\text{Fe}^{56}$ is the only photon producing reaction. In this case, the energy is subtracted from E_{TOT} and a new multiplicity for the continuum photons is derived as

$$M_c \equiv \frac{E_{\text{TOT}} - E_\gamma^*}{\bar{E}_\gamma} \quad (12)$$

Because one specific discrete photon exists

$$\sigma_{n,xy} = (M_c + 1)(\sigma_{n,n'\gamma}) \quad (13)$$

To account for energy range above the $(n,2n)$ threshold, substitute the ratio $\sigma_{n,n'\gamma} / (\sigma_{n,n'\gamma} + \sigma_{n,2n\gamma} + \sigma_{n,3n\gamma})$ for unity in equation 13 and for the energy of the discrete photon in equation 12, substitute the product of this ratio and the energy. Setting the ratio equal to K equations 12 and 13 become

$$M_c = \frac{E_{\text{TOT}} - K E_\gamma^*}{\bar{E}_\gamma} \quad (12')$$

$$\sigma_{n,xy} = (M_c + K)(\sigma_{n,n'\gamma} + \sigma_{n,2n\gamma} + \sigma_{n,3n\gamma}) \quad (13')$$

Utilizing equations 12' and 13', Fe^{56} at 14.6 MeV neutron energy yields $\sigma_{n,xy} = 4.7$ barns, in complete accord with the values of 4.9 and 4.6 barns, cited in References 5 and 8 for neutrons of 14 MeV.

To obtain a total gamma-ray production cross section and spectrum for fissionable isotopes, the photons accompanying fission must be combined with those of the $(n,n'\gamma)$, $(n,2n\gamma)$, and $(n,3n\gamma)$ reactions. It is further assumed that the multiplicity of fission photons is 7.4 (see Reference 9), and is independent of target isotope and neutron energy. These assumptions should lead to no gross errors, according to the review in Reference 9. A multiplicity of seven gamma-rays per fission and isotropy was assumed by Nellis and

Morgan(10) to find reasonable agreement between their findings and fission and nonelastic cross sections reported in the literature. For the spectrum of fission photons, a single shape is assumed for all energies and fissionable isotopes. According to Reference 9, isotopic independence is a sensible assumption since Kirkbride at Harwell showed no noticeable difference in spectrum shape in the photons resulting from fission of U^{235} , U^{238} , and Pu^{239} by reactor neutrons. The assumption that photon spectral shape is independent of incident neutron energy is not contradicted by experiment.

Therefore, for fissionable isotopes

$$\sigma_{n,xy}(E_n) = M(E_n) \left[\sigma_{n,n'\gamma}(E_n) + \sigma_{n,2n\gamma}(E_n) + \sigma_{n,3n\gamma}(E_n) \right] + 7.4 \sigma_f(E_n) \quad (14)$$

$$N(E_\gamma) = M(E_n) \left[\sigma_{n,n'\gamma}(E_n) + \sigma_{n,2n\gamma}(E_n) + \sigma_{n,3n\gamma}(E_n) \right] \cdot S(E_\gamma) + 7.4 \sigma_f(E_n) \cdot F(E_\gamma) \quad (15)$$

where $S(E_\gamma)$ is defined in equation 5 and $F(E_\gamma)$ is the normalized spectrum of fission photons. After $N(E_\gamma)$ has been calculated, it can be normalized by division by $\sigma_{n,xy}(E)$.

Comparisons of calculations made with the formalism herein described and experiments performed at several laboratories are displayed in Table I.

References

1. R. C. GREENWOOD and J. H. REED, "Prompt Gamma-Rays from Radiative Capture of Thermal Neutrons," IITRI-1193-53, Vol. 1 and 2, Illinois Institute of Technology (1965).
2. N. J. CHAZAN, "Tabulated Neutron-Induced Gamma Production Cross Sections for Primary Neutron Energies of 0.1 to 15 MeV," UCRL-14007 Rev. 1, Lawrence Radiation Laboratory, Livermore (1965).
3. D. O. NELLIS, R. W. BENJAMIN, J. B. ASHE, J. T. PRUD'HOMME, I. L. MORGAN, Summary Technical Report, 22 February 1962, Texas Nuclear Corporation (1962).
4. I. L. MORGAN, R. W. BENJAMIN, O. M. HUDSON, S. C. MATHUR, D. O. NELLIS, C. V. PARKER, W. E. TUCKER, Nuclear Physics Division Annual Progress Report, Texas Nuclear Corporation (1963).
5. J. BENVENISTE, N. J. CHAZAN, A. C. MITCHELL, "Spectra of Continuum Gamma-Rays Resulting from 14 MeV Neutron Interactions with Several Elements," UCID-4619, Lawrence Radiation Laboratory, Livermore (1963).
6. J. L. PERKIN, Nuclear Phys. 60, 561 (1964).
7. R. J. HOWERTON, D. L. BRAFF, W. J. CAHILL, N. J. CHAZAN, "Thresholds for Neutron-Induced Reactions," UCRL-14000, Lawrence Radiation Laboratory, Livermore (1964).
8. V. E. SCHERRER, R. THEUS, W. R. FAUST, Phys. Rev. 89, 1268 (1953).
9. H. GOLDSTEIN, in Reactor Handbook, E. P. Blizzard, Ed., 2nd ed., Vol. III, Part B, pp. 16-62, Interscience Publishers, New York and London (1962).
10. D. O. NELLIS, I. L. MORGAN, "Gamma-Ray Production Cross Sections for U^{235} , U^{238} and Pu^{239} ," ORO-2791-17, Texas Nuclear Corporation (1966).
11. V. E. SCHERRER, R. B. THEUS, W. R. FAUST, Phys. Rev. 91, 1476 (1953).
12. I. L. MORGAN, J. B. ASHE, D. O. NELLIS, R. W. BENJAMIN, S. C. MATHUR, W. E. TUCKER, O. M. HUDSON, JR., P. S. BUCHANAN, Annual Progress Report, Texas Nuclear Corporation (1964).

TABLE I

Nucleus	E_n (MeV)	γ Range (MeV)	$\sigma_{n,x}$ (Exp.) (Barns)	$\sigma_{n,x}$ (Calc.) (Barns)	$\%$ Deviation ^{**}	Ref.
Al ²⁷	4.1	.35 - 2.83	.9	1.3	+ 44	4
Fe	4.1	.5 - 3.75	2.9	3.2	+ 10	4
W	4.1	.5 - 4.0	7.6	5.7	- 25	4
Pb ²⁰⁶	4.1	.64 - 3.5	2.9	} $\overline{3.8^*}$ 2.6	- 32	4
Pb ²⁰⁷	4.1	.57 - 3.5	4.8			
Fe	7.5	1.5 - 6.5	2.3	2.2	- 4	6
Pb	7.5	1.5 - 6.5	3.5	3.8	+ 9	6
W	8.5	1.5 - 6.5	4.5	4.6	+ 2	6
Si	14.8	.5 - 10.0	1.7	2.7	+ 59	6
Fe	14.	not given	4.6	4.7	+ 2	8
Fe	14.	not given	4.9	4.7	- 4	5
Cu	14.	not given	6.3	4.8	- 24	11
W	14.8	.5 - 6.0	9.5	11.2	+ 18	4
Pb ²⁰⁶	14.8	.5 - 7.0	11.7	} $\overline{10.2^*}$ 12.5	+ 22	4
Pb ²⁰⁷	14.8	.5 - 7.0	13.2			
Pb ²⁰⁸	14.8	.5 - 5.5	7.9			
U ²³⁸	14.8	.5 - 7.5	10.7	11.4	+ 6	12
U ²³⁸	14.8	.5 - 6.5	9.9	11.4	+ 15	10
U ²³⁵	14.8	.5 - 6.5	15.1	13.1	- 13	10
Pu ²³⁹	14.8	.5 - 6.5	17.2	13.2	- 23	10

* Calculations were made for natural lead. The experiments were combined for purposes of comparison.

** The percentage deviation is $100(\sigma_{\text{calc}} - \sigma_{\text{exp}}) / \sigma_{\text{exp}}$.

Table I. Comparison of calculated and experimental photon production cross sections. The average deviation is 18 %.

Figure 1

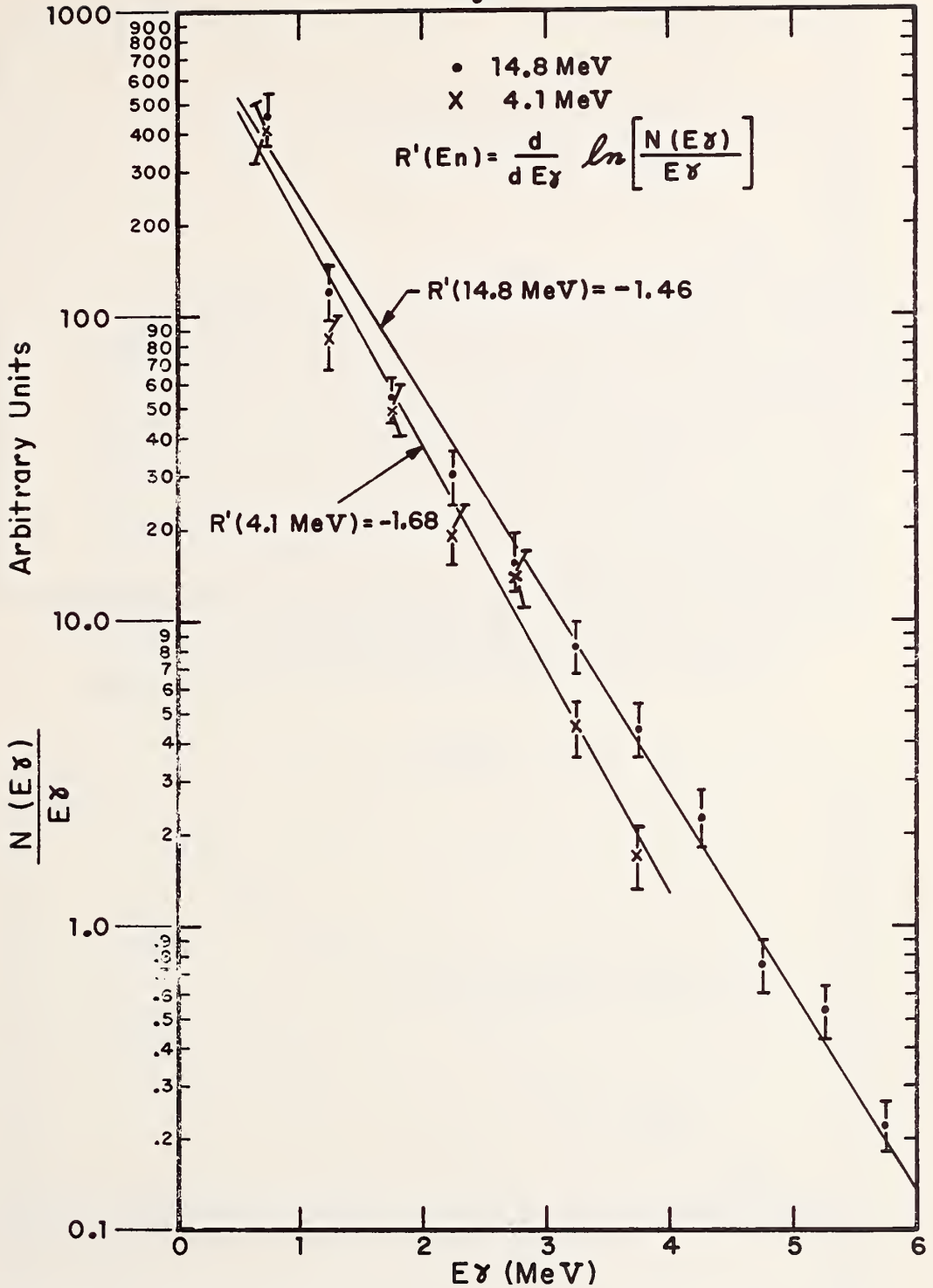


Figure 1. Energy dependence of the number of photons per unit photon energy for incident neutron energies of 4.1 and 14.8 MeV on Tungsten. Data are taken from Reference 4.

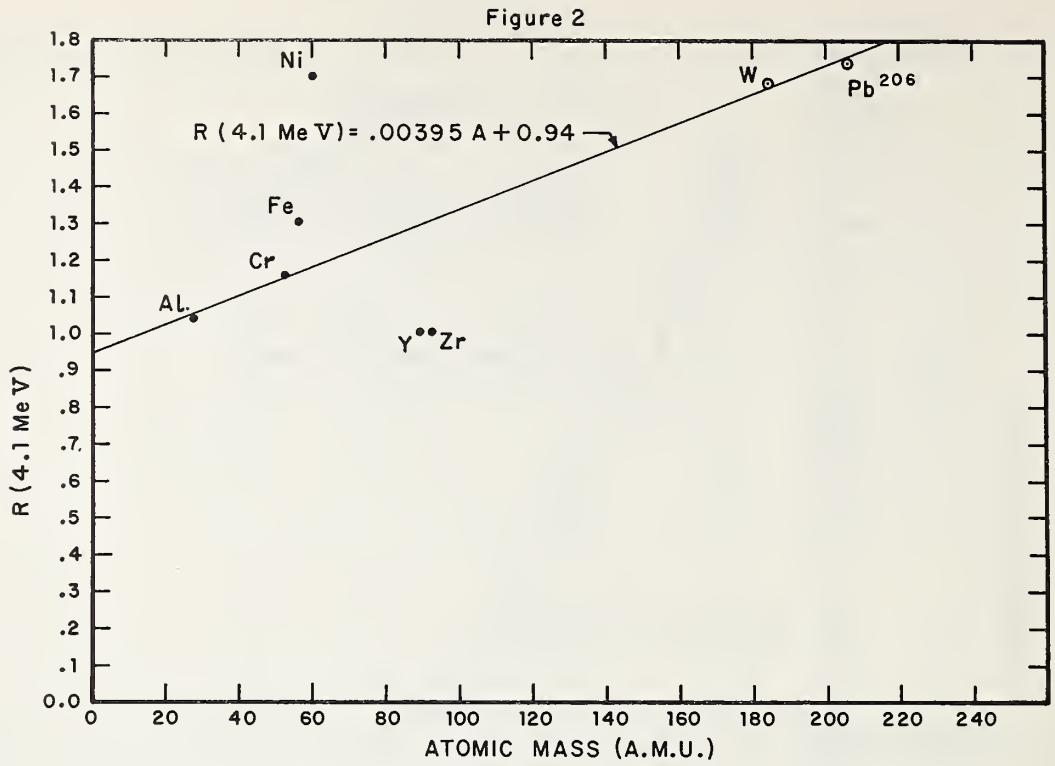


Figure 2. Atomic Mass dependence of R for 4.1 MeV incident neutrons.

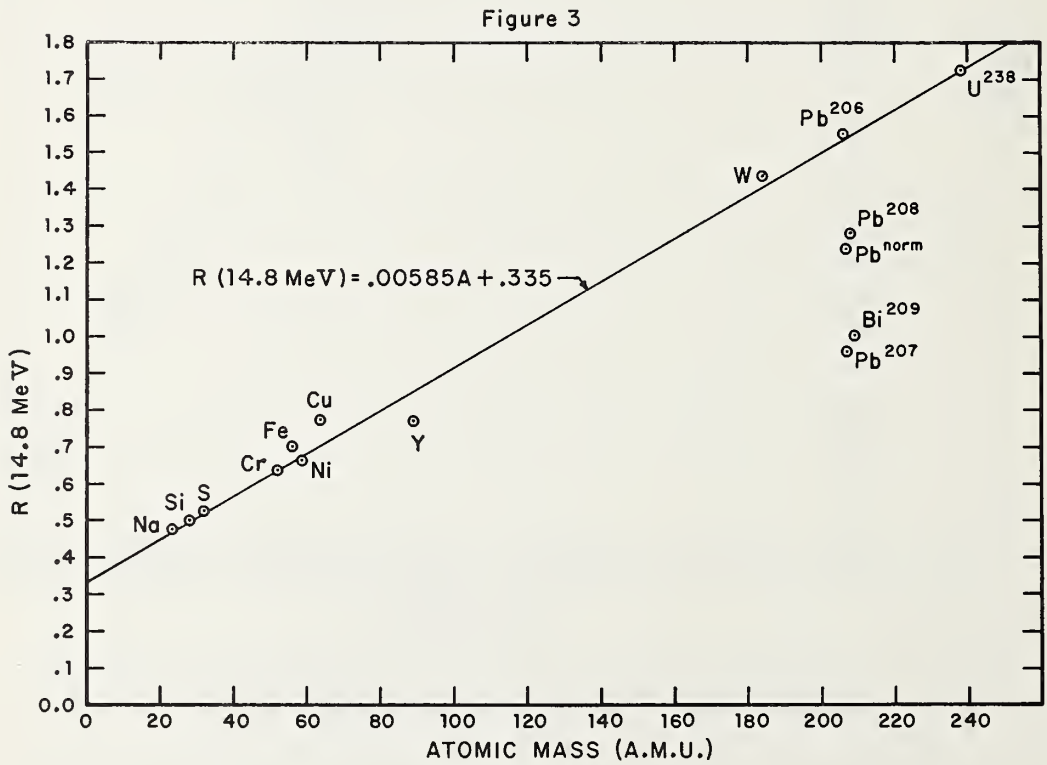


Figure 3. Atomic Mass dependence of R for 14.8 MeV incident neutrons.

THEORY OF DOPPLER BROADENING OF NEUTRON RESONANCES⁺

S. N. Purohit, T. Shea and S. Kang

Division of Nuclear Engineering and Science
Rensselaer Polytechnic Institute
Troy, New York 12181

This paper discusses the Doppler broadening of neutron resonances, using the Van Hove time integral representation of the reaction cross section. This formalism has been applied to study the line shape of the capture, fission, scattering and interference resonances. We have also studied the Doppler broadening of p-wave resonances and the temperature coefficient of the cross section ($T^{d\sigma/\sigma T}$). In addition, the formalism has been extended to obtain the Doppler broadening of multi-level results of the Rosenfeld-Humblet theory. The final expressions involve the multi-level and temperature dependent parameters. All the cross section results have been presented in terms of the ϕ_n integrals, expressible in terms of the resonance line shape functions ψ and χ , using the modified short collision time expansion.

⁺Work supported by the U. S. Atomic Energy Commission under Contract AT(30-3)-328.

1. INTRODUCTION

In this paper we present a theoretical study of the Doppler broadening of neutron resonances. We employ the Van Hove time integral formalism⁽¹⁾, used successfully in the study of thermal neutron scattering by bound atoms. In neutron-nuclear interaction the degree of overlap between nuclear and atomic times depends upon the relative magnitude of the Doppler width with respect to the nuclear width. In the case of wide and well separated resonances the degree of overlap between nuclear and atomic times is very small, therefore, the treatment of the Doppler broadening problem based upon the effective temperature gas model of Lamb⁽²⁾ is justified. However, if the nuclear width is smaller or even comparable to the Doppler width then the degree of overlap is considerable and a detailed treatment is required. At zero thermodynamic temperature, in the absence of binding, the single level Breit-Wigner resonance line shape is a Lorentzian distribution. The increase in temperature distorts this line shape and introduces a temperature dependent asymmetry. At very high temperature this asymmetry disappears. The temperature dependent asymmetry is different from the asymmetries arising from the multi-level effects in fission cross sections, the penetrability factor for p-wave resonances and the energy dependent resonance parameters. It is the objective of this study to emphasize the temperature dependent asymmetry and represent the reaction cross sections in terms of the well known, ψ and χ , the resonance line shape functions.

$$\sigma(E, T) = A(E, T)\psi + B(E, T)\chi + C(E, T) \quad (1)$$

2. REACTION CROSS SECTION AND TIME INTEGRAL

One may represent a nuclear reaction cross section in terms of the Fourier transform of a dynamical correlation function X , with $(E_0 - E)$ as the Fourier transform variable, of time. E and E_0 are neutron and resonance energies in units of $\hbar = 1$.

$$\sigma(E, E_0, T) = \frac{1}{2\pi} \int_{-\infty}^{\infty} \exp i(E_0 - E)t X(E, E_0, T, t) dt \quad (2)$$

In order to determine the X functions for various nuclear reactions one may follow the Heitler formalism⁽³⁾ employed in the study of the Mossbauer effect problems. See Boyle and Hall⁽⁴⁾.

2.1. S-Wave Capture and Fission Resonances

As shown by Lamb⁽²⁾ we can express X as a product of two functions X_{Ns} and X_{As} .

$$X = \left[\frac{\pi \sigma_0 \Gamma}{2} \exp -\frac{\Gamma}{2} |t| \right] \times \left[\langle \exp -i \vec{k} \cdot \vec{r}(t) \exp i \vec{k} \cdot \vec{r}(0) \rangle_T \right] \quad (3)$$

$$= X_{Ns} X_{As}$$

The nuclear function X_{Ns} describes the exponential decay of the compound nucleus with a life time $1/\Gamma$. The atomic function X_{As} is represented by the quantum statistical average $\langle \rangle_T$. It involves the Heisenberg dynamical operator $\vec{r}(t)$ and the neutron wave vector \vec{k} for energy E . The time integral with the above X function was also studied by Nelkin and Parks⁽⁵⁾ and by Singwi and Sjölander⁽⁶⁾.

2.2. P-Wave Resonance

For a p-wave resonance, according to Shea and Purohit⁽⁷⁾.

$$X = \left[\exp i(E-E_0)t \right] X_{Np} \left[1 + iA \frac{d}{dt} \right] \left[X_{As} \exp i(E_0-E)t \right] \quad (4)$$

We have assumed the penetrability factor (See Blatt and Weisskopf⁽⁸⁾).

$$\frac{\gamma_1(E)}{\gamma_1(E_0)} \approx 1 + A(E-E_0) \quad \text{with} \quad A = \frac{1}{(1 + \beta^2 M^{2/3} E_0) E_0} \quad (5)$$

2.3. Scattering Resonance

Following the treatment of Heitler⁽³⁾ we obtain

$$X(E, E', E_0, \mu, t) = \left[\frac{\sigma_0 \Gamma^2}{4} \left(\frac{E'}{E} \right)^{1/2} \exp i(E'-E_0)t \right] \times \quad (6)$$

$$\times \left[\int_0^\infty dt_1 \int_0^\infty dt_2 \exp \left\{ i(E'-E_0)(t_1-t_2) - \frac{\Gamma}{2}(t_1+t_2) \right\} \right]$$

$$\times \sum_{m,n} \langle \exp i \vec{k} \cdot \vec{r}_m(0) \exp i \vec{k} \cdot \vec{r}_m(t_2) \exp i \vec{k} \cdot \vec{r}_n(t+t_1) \exp -i \vec{k} \cdot \vec{r}_n(t) \rangle_T$$

The above expression is an exact result for the scattering resonance case. It involves E' , k' and μ , which represent the scattered neutron energy, the final wave vector and the cosine of the scattering angle respectively. If we assume no coherent scattering ($m=n$) and only elastic scattering ($E'=E$), then we obtain after E' , t_1 , t_2 and μ integrations the same form for X as given by Eq. (2).

2.4. Interference Scattering

In the case of interference between potential and resonance scattering,

$$X(E, E', E_0, \mu, t) = \sigma_0 \Gamma \left(\frac{E'}{E} \right)^{1/2} \mathcal{R} \left[i \exp i(E' - E_0)t \right. \\ \left. \int_0^\infty dt_1 \exp \left\{ -i(E' - E_0)t_1 - \frac{\Gamma}{2}t_1 \right\} \sum_{m,n} \left\langle \exp i\vec{k} \cdot \vec{r}_m(0) \exp -i\vec{k}' \cdot \vec{r}_m(t_1) \exp -i(\vec{k} - \vec{k}') \cdot \vec{r}_n(t) \right\rangle_T \right] \quad (7)$$

For the incoherent elastic scattering ($m=n$ and $E'=E$), after undertaking E' , μ and t integrations one obtains the well known interference term.

3. EVALUATION OF TIME INTEGRAL AND CROSS SECTION

The determination of temperature dependent nuclear reaction cross section involves the evaluation of the temperature dependent quantum statistical average and the time integral. For small values of $(E - E_0)$, the major contribution to the time integral comes from the behaviour of the X function at large times and vice versa. The study of the X functions, given in section 2, for various values of Γ , K , E , E' and E_0 , as a function of time constitutes the basic problem. For the large momentum transfer, the major contribution to the time integral comes from the small time behaviour of the quantum statistical average. If the resonances are wide and the Doppler width $\Delta \ll \Gamma$, then the gas model with an effective temperature is adequate. For $\Delta \gg \Gamma$ the modified short collision time expansion with the gas model as the leading term may well serve the purpose. However, in the case of an extremely narrow resonance there is a very large contribution from the nuclear X_N function at long times. In this case the long time contribution from $\langle \rangle_T$ could also become important. This situation may arise in narrow scattering resonances for the structural materials.

In this paper we limit to the modified short collision time expansion results. We expand X_{As} according to the

Sjölander expansion (9).

$$X_{A_s} = X_{gas} \left[1 + \sum_{n=3}^{\infty} a_n (it)^n \right] \quad (8)$$

a_n are the Sjölander coefficients involving the Placzek moments of the frequency spectrum of lattice vibrations. We present the following cross section results.

3.1. S-Wave Resonance

$$\sigma^S(E) = \sigma(E_0) \left[\Psi + \sum_{n=3}^{\infty} a_n \left(\frac{\sqrt{2}}{\Delta} \right)^n \Phi_n \right] \quad (9)$$

where,

$$\Phi_n = \frac{\xi}{\sqrt{4\pi}} \int_{-\infty}^{+\infty} H_n \left(\frac{\xi}{\sqrt{2}} (x-y) \right) \frac{\exp -\frac{\xi^2}{4} (x-y)^2}{1+y^2} dy \quad (10)$$

$$\chi = 2(E-E_0-R)/\Gamma; \quad \xi = \Gamma/\Delta; \quad \Delta = [4RT_{eff}]^{1/2} \quad (11)$$

3.2. P-Wave Resonance

$$\sigma^P(E) = \sigma(E_0) \left\{ \left(1 + \left[\frac{\chi}{2} - 1 \right] A\Gamma \right) \Psi + \frac{A\Gamma}{2} \chi \right\} + \sum_{n=3}^{\infty} a_n \left[\frac{\sqrt{2}}{\Delta} \right]^n \left\{ \left(1 + \frac{\chi A\Gamma}{2} \right) \Phi_n \right. \quad (12)$$

3.3. Multi-Level Cross Section

$$\left. - \frac{A\Delta}{\sqrt{2}} \Phi_{n+1} - \frac{nA\Delta}{\sqrt{2}} \Phi_{n-1} \right\}$$

Based upon the Humblet-Rosenfeld theory (10), the multi-level cross section is given by the following expression

$$\sigma^m = \sum_j \nu_j \left[\frac{\nu_j G_j + (\mu_j - E) H_j}{(\mu_j - E)^2 + \nu_j^2} \right] \quad (13)$$

Adler and Adler (11) have given the Doppler broadened multi-level cross section based upon the gas model. We present here results for the modified short collision time expansion.

$$\sigma^m = \sum_j \left\{ \left[G_j + (\chi_j - 2) H_j \right] \Psi + H_j \chi \right\} + \delta \sigma_j \quad (14a)$$

and

$$\delta\sigma_{\bar{\gamma}} = \sum_{n=3}^{\infty} a_n \left[\frac{\sqrt{z}}{\Delta} \right]^n \left[(G_{\bar{\gamma}} + \chi_{\bar{\gamma}} H_{\bar{\gamma}}) \Phi_n - \frac{\sqrt{z}}{\xi_{\bar{\gamma}}} H_{\bar{\gamma}} \Phi_{n+1} - \frac{\sqrt{z} n}{\xi_{\bar{\gamma}}} H_{\bar{\gamma}} \Phi_{n-1} \right] \quad (14b)$$

3.4. $T \frac{d\sigma}{dT}$

This quantity is of interest in studying the Doppler effect in reactors. For capture and fission resonances, one obtains

$$T \frac{d\sigma}{dT} = T\sigma(E_0) \left[\frac{C_V}{2} \left(\frac{T}{T_{eff}} \right) \Phi_2 + \sum_{n=3}^{\infty} a_n \left[\frac{\sqrt{z}}{\Delta} \right]^n \left\{ \frac{C_V}{2} \left(\frac{T}{T_{eff}} \right) \Phi_{n+2} + a_n \left[\frac{da_n}{dT} \right] \Phi_n \right\} \right] \quad (15)$$

The leading term corresponds to the gas model. It involves the temperature dependent specific heat $C_V(T)$ and Φ_2 function.

4. DETERMINATION OF Φ_n INTEGRAL

Using the properties of the Hermite polynomials, we can represent

$$\Phi_n(\xi, \chi) = z^{-n/2} \sum_{m=0}^n \left[(-1)^m \binom{n}{m} H_{n-m}(\xi \chi) \right] \sum_{r=0}^{2r \leq m} (2\xi)^{m-2r} \binom{m}{m-2r} (-1)^r I_{m-2r} \quad (16)$$

We define

$$I_{m-2r} = \frac{\xi}{\sqrt{4\pi}} \int_{-\infty}^{+\infty} y^{m-2r} \frac{\exp -\frac{\xi^2}{4} (\chi - y)^2 dy}{1 + y^2} \quad (17)$$

The above integral can be generated using the recurrence relation.

$$I_q = K_{q-2} - I_{q-2} \quad (18)$$

and

$$K_{q-2} = \sum_{p=0}^q \binom{q}{2p} (\xi)^{2p} \frac{(2p)!}{p!} (\chi)^{q-2p} \quad (19)$$

I_0 and I_1 are Ψ and χ functions respectively, therefore, all cross sections can be given by Eq. (1). A Fortran program has been prepared to calculate ϕ_n integrals using the above method. Ψ and χ functions have been calculated using the subroutine developed by Bhat (12). The only binding parameter in the calculation of ϕ_n integrals is the effective temperature given by the following integral.

$$\frac{T_{\text{eff}}}{T} = \int_0^{\infty} \left(\frac{\xi}{2T} \right) f(\xi) \coth \frac{\xi}{2T} d\xi \quad (20)$$

For a monatomic isotropic cubic lattice, the above definition with a given frequency spectrum is justified. However, for the diatomic and triatomic systems, such as UC and UO_2 , an equivalent T_{eff} parameter in terms of the polarisation vectors and eigen frequencies of the normal modes may be defined. In the attached table, we present effective temperatures calculated for $T = 80^\circ$, 300° and 500° K for the materials of interest in fast reactors, as given by Kang and Purohit (13).

Two Fortran programs for calculating s and p-wave neutron resonances have been developed. Preliminary calculations for Fe^{56} resonances have been undertaken. These results predict a temperature dependent asymmetry, which is very pronounced at low temperatures for the case where the Doppler width is greater than the nuclear width. It is these resonances, which influence the temperature dependence of the cross sections and, therefore, the Doppler effect in a reactor. The presence of this asymmetry will also introduce uncertainty in the estimation of resonance parameters.

EFFECTIVE TEMPERATURES FOR STRUCTURAL MATERIALS

Element	Debye Temperature (°K)	EFFECTIVE TEMPERATURES		
		80°K	300°K	500°K
Na	164	96	304	503
Ti	373	151	323	514
V	394	158	325	515
Cr	454	177	333	520
Fe	466	181	335	521
Co	446	175	332	519
Ni	443	174	332	520
Mo	454	177	332	507
Ta	257	117	311	513
W	370	150	321	503

5. REFERENCES

1. L. Van Hove, Phys. Rev. 95, 249 (1954).
2. W. E. Lamb, Jr., Phys. Rev. 55, 190 (1939).
3. A. J. F. Boyle and H. E. Hall, Reports on Progress in Physics 25, 441 (1962).
4. W. Heitler, The Quantum Theory of Radiation, Oxford University Press (1944).
5. K. S. Singwi and A. Sjölander, Phys. Rev. 120, 1093 (1960).
6. M. S. Nelkin and D. E. Parks, Phys. Rev. 119, 1060 (1960).
7. T. E. Shea and S. N. Purohit, submitted for presentation at the American Nuclear Society Meeting, Toronto (1968).
8. J. M. Blatt and V. F. Weisskopf, Theoretical Nuclear Physics, John Wiley & Sons (1952).
9. A. Sjölander, Arkiv för Fysik, 14, 315 (1958).
10. J. Humblet and L. Rosenfeld, Nuclear Physics 26, 529 (1961).
11. F. T. Adler and D. B. Adler, in Reactor Physics in the Resonance and Thermal Regions, ed. A. J. Goodjohn and G. C. Ponraning, MIT Press (1966).
12. M. R. Bhat and G. E. Lee-Whiting, BNL-10337 (1966).
13. S. Kang and S. N. Purohit, R.P.I. Linac Project Progress Report Jan. 1967.

THE NEUTRON CROSS SECTION AND
RESONANCE INTEGRALS OF HOLMIUM*

Thomas E. Stephenson
Brookhaven National Laboratory
Upton, New York 11973

ABSTRACT

Previously reported calculations [1] have been extended. Resonance parameters for 76 resonances of Ho below 500 eV, selected from the literature and from values compiled and recommended in BNL 325 [2], are used as the starting point in fitting the total neutron cross section data [2, 3] to a Breit-Wigner multi-level scattering and single-level absorption formula. The addition of two bound levels, one for each s-wave spin state, yields a calculated ratio of thermal neutron capture cross sections for the two spin states which agrees with experiment ($\sim 60\%$ for $J=3$), as does the calculated value of the thermal capture cross section, 67 b. In addition, the two bound levels enable the fit of the total cross section data to be extended to very low energies (0.2 mV). The energy dependent paramagnetic scattering cross section (23.5 b at 0.0253 eV) and the capture and scattering resonance integrals have also been calculated (~ 672 and 125 b, respectively).

1. INTRODUCTION

In this paper, previously reported calculations [1] of the holmium neutron cross section are extended. Resonance parameters for 76 resonances below 500 eV, selected from the literature and from values compiled and recommended in BNL 325 [2], are used as the starting point in fitting the total neutron cross section data [2, 3] to the Breit-Wigner multi-level scattering and single-level absorption formulae [4]. The calculated cross sections are Doppler-broadened, but are not resolution broadened. Other data used in the fitting procedure include the spin-dependent thermal capture data [2, 5], the low energy coherent [6] and nuclear [5, 7] scattering data, and the energy-dependent paramagnetic scattering data [6]. It is found that two negative energy resonances, one each for $J=3$ and 4 are required to obtain a fit to the data. The parameters of the bound

* This work performed under the auspices of the U.S. Atomic Energy Commission.

levels and the value of the effective scattering radius are given in the next section. The existence of J=3 negative energy levels was previously suggested by Schermer [5].

2. HOLMIUM RESONANCE PARAMETERS

Table I gives the resonance parameters used in this study. The parameters, with the exception of those given for two bound levels, were selected from the literature and from values compiled and recommended in BNL 325 [2]. There are 76 levels listed, and 29 have J-assignments, including the two bound levels. Although the range of the fitting of total cross section data is from 0.2 MeV to 50 eV, the resonance energies of the levels included in the calculation range to about 500 eV. Unfortunately, knowledge of some of the resonance parameters for many of the levels is incomplete. For example, 47 levels have no J-assignments; a statistical weight factor of 1/2 has been assigned to these resonances. The average value (0.072 eV) of the radiation width of the first 16 resonances, excluding the one at 37.24 eV, has been assigned to those levels where the radiation width has not been measured. Although many of the higher energy resonances are not necessary in fitting cross section data below 50 eV, they do contribute to the resonance integrals. It is, therefore, desirable to include as many levels as possible in the calculation of the resonance integrals.

3. FITTING OF THERMAL CAPTURE, AND COHERENT AND NUCLEAR SCATTERING CROSS SECTIONS

The calculated value of the capture cross section at 0.0253 eV, using the parameters of Table I but omitting the bound levels, is 19.9 b. The parameters of the two bound levels, one for each s-wave spin state, have been constructed so that when they are included in the calculation, the calculated value for thermal capture becomes 67 b, in agreement with the recommended value in BNL 325 [2]. The parameters of the bound levels are also constructed to be compatible with Schermer's [5] polarization measurements; when their contribution is included in the calculation, 60.4% of the thermal capture cross section is into the J=3 states (61±2.8% experimental).

Other constraints on the parameters of the bound levels arise from fitting the coherent and nuclear scattering cross sections and from the choice of the effective scattering radius (7.9 f). The coherent scattering cross section, given by

$$\sigma_{coh} = 4\pi \left| R' + \sum_j \frac{g_j \lambda_j \Gamma_{nj}(E)}{2(E-E_j) + i\Gamma_j} \right|^2 ,$$

where the sum is over all resonances, is found to be 9.1 b, in agreement with the measurements of Koehler, et al. [6]. The value of the nuclear scattering cross section deduced from total cross section measurements by Mattos [7] is 7 b. Schermer [5] obtained $\sigma_s < 10$ b from his analysis. The value calculated here is 10.3 b at 0.5 eV.

4. COMPARISON OF THE CALCULATED TOTAL CROSS SECTION WITH EXPERIMENT

Figure 1 presents the calculated partial cross sections between 0.2 mV and 1 eV. The energy-dependent paramagnetic scattering cross section has been calculated using the approximate method described by Koehler, et al. [6] and using parameters based on the low energy angularly dependent differential scattering measurements by these investigators. Figure 2 shows the fit to the data [2, 3] in this same energy region.

Figure 3 compares the calculated total cross section with experimental data [2, 3] between 1 eV and 25 eV, and Fig. 4 covers the region from 25 to 50 eV. The noticeable discrepancy between the calculated and experimental resonance energies in Fig. 4 is due to the use of old cross section data [3], whereas the relevant resonance parameters of Table I are based on results of recent measurements [8, 9]. Cross section data corresponding to the latter have not yet been published.

The resolution of available cross section data above 50 eV is not sufficiently good for meaningful comparisons with calculations.

5. THE RESONANCE INTEGRALS

The resonance integrals for scattering and capture have been calculated by numerical integration of

$$I = \int_{E_1}^{E_2} \sigma(E) \frac{dE}{E} ,$$

where $E_1 = 0.55$ eV is the cadmium cutoff and E_2 is chosen so that all resonances in Table I are included in the calculation.

The calculated values of the scattering and capture integrals are 125 b and 672 b, respectively. No measurement has been reported for the scattering integral. Numerical integration of broad resolution capture cross section data [2] above 500 eV shows that ~ 31 b can be added to the value of the capture integral calculated from the resonance parameters,

giving 703 b. The capture integral has been measured at 860 b by Scoville and Rogers [10]. The 18% discrepancy may be due to unresolved resonances.

Many valuable discussions with Dr. T. J. Krieger during the course of this work are gratefully acknowledged.

6. References

1. T. E. Stephenson and A. M. Ferrer, Bull. Am. Phys. Soc. 12, 650 (1967).
2. M. D. Goldberg, S. F. Mughabghab, S. N. Purohit, B. A. Magurno, and V. M. May, NEUTRON CROSS SECTIONS, Brookhaven National Laboratory Report BNL 325, 2nd Ed., Suppl. No. 2 (1966).
3. D. J. Hughes and R. B. Schwartz, NEUTRON CROSS SECTIONS, Brookhaven National Laboratory Report BNL 325, 2nd Ed. (1958).
4. H. A. Bethe, Rev. Mod. Phys. 9, 115 (1937).
5. R. I. Schermer, Phys. Rev. 136, B1285 (1964).
6. W. C. Koehler, E. O. Wollan, and M. K. Wilkinson, Phys. Rev. 110, 37 (1958).
7. M. C. Mattos, Paper presented at Fifth Rare Earth Research Conf., Ames, Iowa (Aug. 30, 1966 - Sept. 1, 1966).
8. V. P. Alfimenkov, V. I. Lushchikov, V. G. Nikolenko, Yu. V. Taran, and F. L. Shapiro, Sov. J. Nucl. Phys. 3, 39 (1966).
9. V. P. Asghar, M. C. Moxon, and C. M. Chaffey, Conf. on Study of Nuclear Structure with Neutrons, Antwerp (1965), Paper 65; M. C. Moxon, C. M. Chaffey, and V. S. Brown, U.K. Atomic Energy Research Establishment Report AERE-PR/NP 9 (1966).
10. J. J. Scoville and J. W. Rogers, Trans. Am. Nucl. Soc. 8, 290 (1965).

TABLE I
The Resonance Parameters
($R' = 7.9 \text{ f}$)

E_0 (eV)	Γ_n (mV)	Γ_n^0 (mV)	Γ_γ (mV)	J	g	$2g\Gamma_n$ (mV)	Ref.
-8.50		21.95	72.	3	0.4375		a
8.15	0.18		55.	3	0.4375		b
18.2	1.26		69.	3	0.4375		b
35.4	7.4		73.6	3	0.4375		b
37.24	0.75		72.	3	0.4375		c, d
47.63	26.9		90.	3	0.4375		c, d
51.30	50.		84.	3	0.4375		b
54.22	4.2		64.8	3	0.4375		c, d
84.7	7.2		72.	3	0.4375		c, e
85.6	91.50		72.	3	0.4375		b, e
126.6	30.5		96.8	3	0.4375		c, e
128.1	20.7		65.0	3	0.4375		c, e
150.8	42.5		71.7	3	0.4375		c
-1.0		0.0484	72.	4	0.5625		a
3.92	2.2		85.	4	0.5625		b
12.7	13.8		51.	4	0.5625		b
21.1	0.6		84.	4	0.5625		b
39.5	20.		88.	4	0.5625		b
64.9	20.3		70.	4	0.5625		b
71.6	22.0		74.	4	0.5625		b
83.76	11.2		66.7	4	0.5625		c
93.34	87.4		76.7	4	0.5625		c, e
101.7	18.8		75.9	4	0.5625		c, e
106.1	7.5		64.5	4	0.5625		c, e
117.8	12.0		70.3	4	0.5625		c, e
124.7	37.1		74.1	4	0.5625		c, e
169.4	17.7		60.2	4	0.5625		c
201.8	75.6		75.5	4	0.5625		c
239.1	31.2		83.6	4	0.5625		c
68.5			65.		0.5	1.1	b
79.6			53.		0.5	1.4	b
120.5			72.		0.5	6.	b
141.			72.		0.5	1.4	b
149.2			72.		0.5	3.2	b
163.1			72.		0.5	4.8	b
164.			72.		0.5	17.4	b
174.3			72.		0.5	4.0	b
180.6			137	*	0.5	35.0	b, c
188.5			76		0.5	18.4	b

(con't on next page)

TABLE I (con't)

E_0 (eV)	Γ_n (mV)	Γ_n^0 (mV)	Γ_γ (mV)	J	g	$2g\Gamma_n$ (mV)	Ref.
192.4			72.		0.5	7.2	b
195.			72.		0.5	2.6	b
204.7			72.		0.5	10.2	b
214.4			67.		0.5	51.	b
220.2			92.		0.5	32.	b
229.7			72.		0.5	9.6	b
232.5			72.		0.5	7.2	b
254.			144.	*	0.5	140.	b
261.			74.		0.5	34.	b
276.8			72.		0.5	12.2	b
280.8			72.		0.5	17.4	b
287.4			72.		0.5	10.	b
291.4			72.		0.5	28.	b
297.			72.		0.5	26.	b
300.			72.		0.5	100.	b
306.6			72.		0.5	6.6	b
312.8			72.		0.5	14.	b
320.3			72.		0.5	16.6	b
323.4			72.		0.5	38.	b
327.8			72.		0.5	6.2	b
331.8			72.		0.5	68.	b
339.1			72.		0.5	110.	b
341.5			72.		0.5	14.2	b
353.8			72.		0.5	32.	b
358.5			72.		0.5	7.2	b
366.1			72.		0.5	30.	b
374.1			72.		0.5	64.	b
400.5			72.		0.5	16.8	b
404.4			72.		0.5	74.	b
422.4			72.		0.5	24.	b
429.8			72.		0.5	90.	b
442.8			72.		0.5	50.	b
450.2			72.		0.5	76.	b
454.4			72.		0.5	10.4	b
460.8			72.		0.5	11.6	b
485.2			72.		0.5	48.	b
495.			72.		0.5	108.	b

* Probably spin doublet, according to Ref. c (AERE-PR/NP 9).

a) This work.

(con't on next page)

TABLE I (con't)

- b) M. D. Goldberg, S. F. Mughabghab, S. N. Purohit, B. A. Magurno, and V. M. May, NEUTRON CROSS SECTIONS, Brookhaven National Laboratory Report BNL 325, 2nd Ed., Suppl. No. 2 (1966).
- c) M. Asghar, M. C. Moxon, and C. M. Chaffey, Conf. on Study of Nuclear Structure with Neutrons, Antwerp (1965), Paper 65; M. C. Moxon, C. M. Chaffey, and V. S. Brown, U.K. Atomic Energy Research Establishment Report AERE-PR/NP 9 (1966).
- d) V. P. Alfimenkov, V. I. Lushchikov, V. G. Nikolenko, Yu. V. Taran, and F. L. Shapiro, Sov. J. Nucl. Phys. 3, 39 (1966).
- e) V. P. Alfimenkov, V. I. Lushchikov, V. G. Nikolenko, Yu. V. Taran, and F. L. Shapiro, Dubna Preprint P3-3208 (1967).

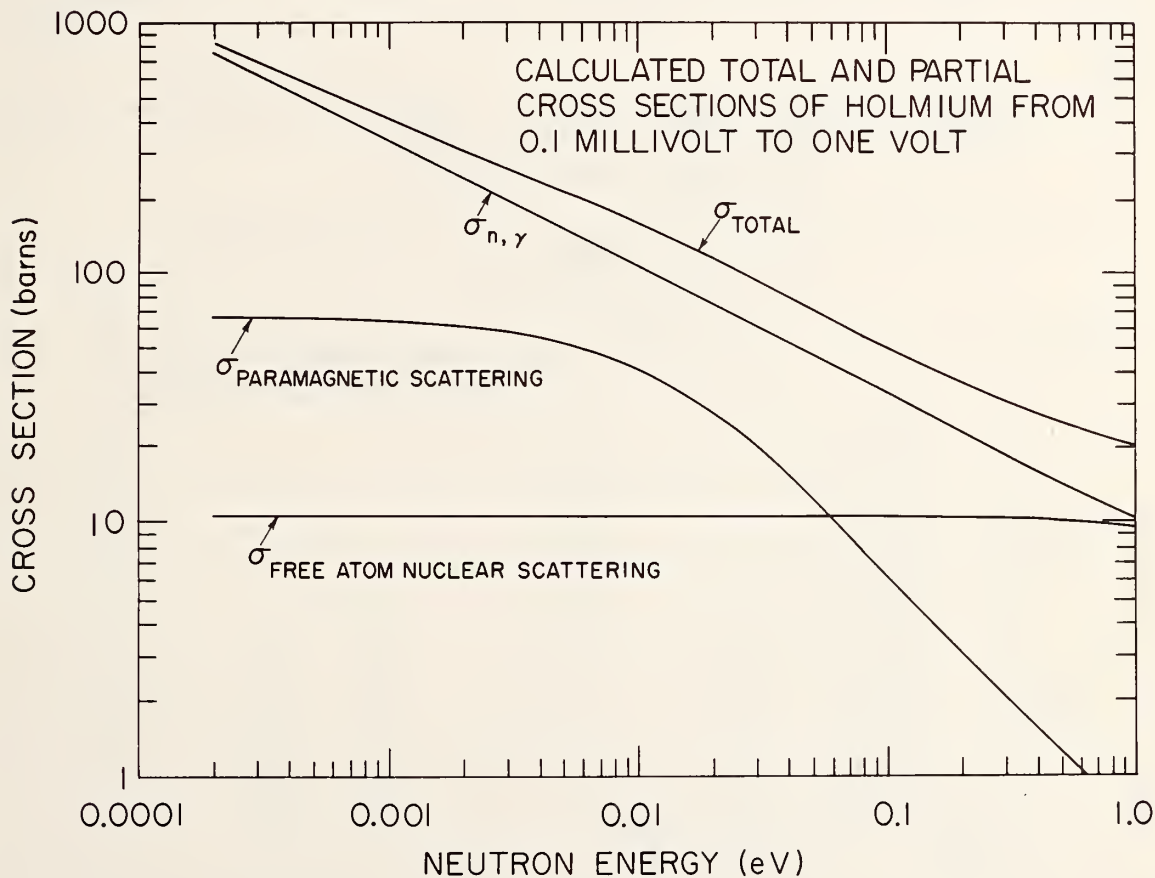


FIGURE 1

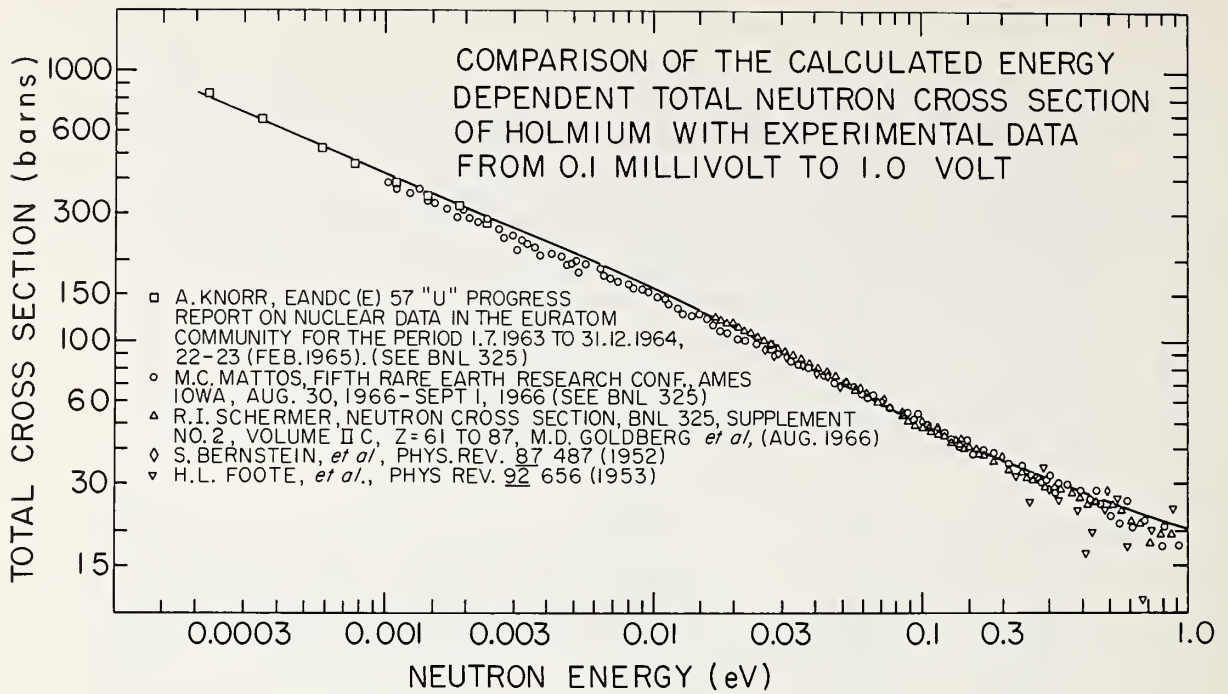


FIGURE 2

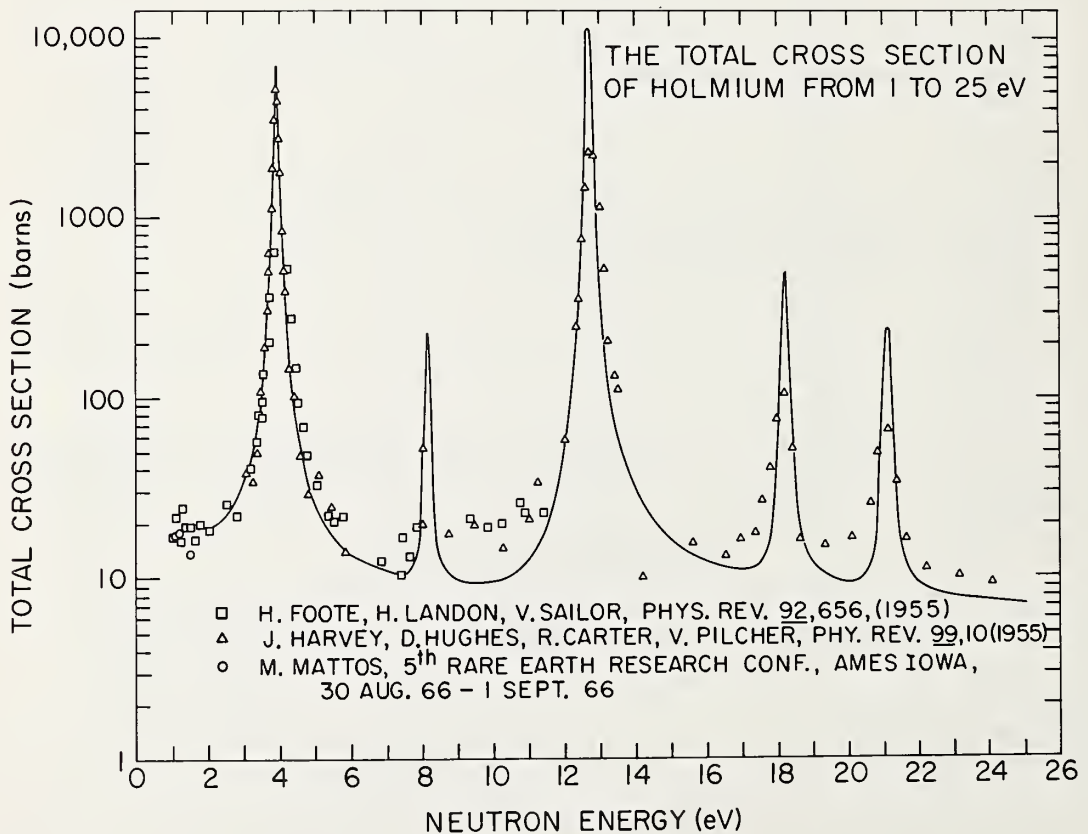


FIGURE 3

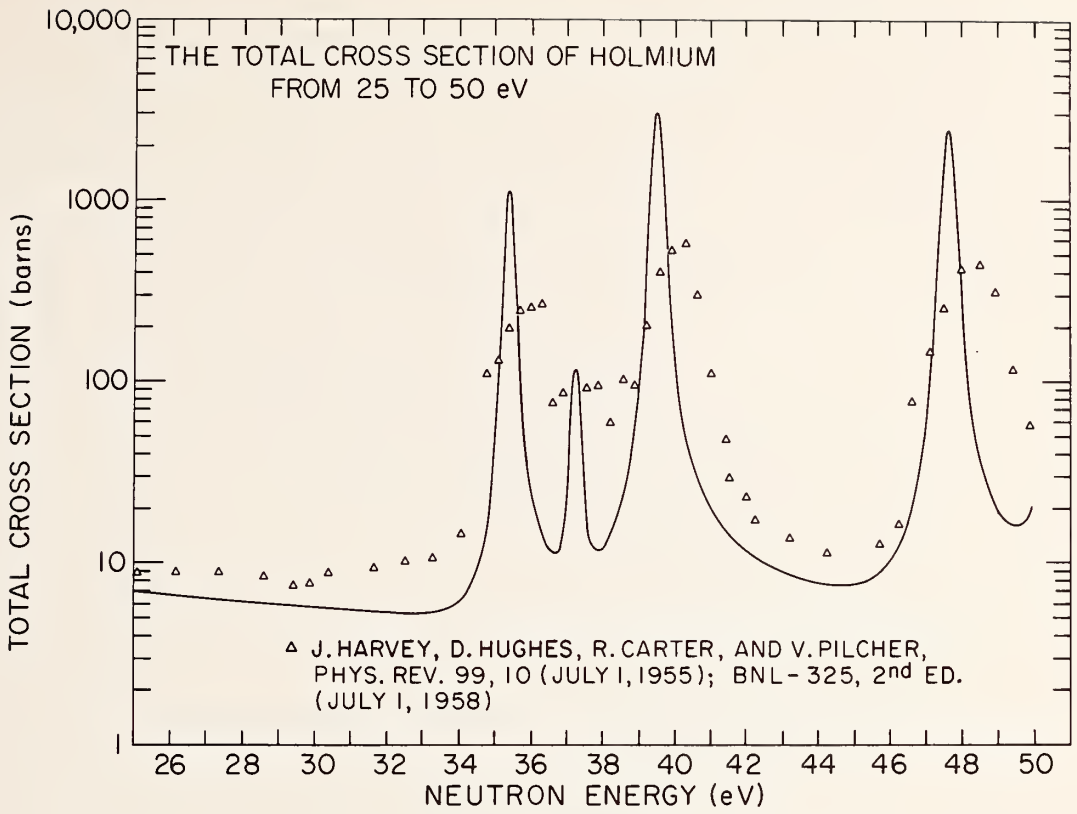


FIGURE 4

Session G

DATA STORAGE, RETRIEVAL,
AND EVALUATION

Chairman

P. HEMMIG

Atomic Energy Commission

RECENT DEVELOPMENTS IN THE AUTOMATED COMPILATION AND
PUBLICATION OF NEUTRON DATA*

S. Pearlstein, Acting Director
National Neutron Cross Section Center
Brookhaven National Laboratory
Upton, New York 11973

ABSTRACT

The National Neutron Cross Section Center at Brookhaven National Laboratory maintains the SCISRS and ENDF Libraries, containing experimental and evaluated neutron data, respectively. Procedures have been developed for the convenient entry and checking of data. Selected portions of the data and associated bibliography are retrieved in the form of listings, punched cards, magnetic tape, and graphic displays. The graphic displays of these data are produced on film or paper with computer selection of appropriate symbols, scales, grids, and labels. These methods are being developed to produce automated ENDF, BNL 325, and BNL 400 publications.

1. INTRODUCTION

In September 1967 the National Neutron Cross Section Center was formed. The new Center merges the Brookhaven compilation and evaluation groups which were formerly funded separately by the Research and the Reactor Development and Technology Divisions of the USAEC. The expanded program of the consolidated group is one example of the importance that the AEC attaches to neutron cross section compilation and evaluation. Concurrently, Brookhaven National Laboratory management appointed an Advisory Committee of six scientists to visit BNL to review the Center's program. The NNCSC services the United States and Canada and has international agreements with the European Nuclear Energy Agency and the International Atomic Energy Agency for the exchange of neutron data.

The NNCSC maintains and develops two large data pools: one for experimental data and one for evaluated data. In the case of experimental data the NNCSC does the following:

* This work performed under the auspices of the U.S. Atomic Energy Commission.

1. Researches all U.S. and Canadian journals, reports, and meetings
2. Places data on tape in the SCISRS [1] system for automated storage and retrieval
3. Issues publications BNL 325 [2] on neutron cross sections and BNL 400 [3] on angular distributions.

In the case of evaluated data the NNCS does the following:

1. Places partial, preliminary, or other data in the ENDF/A [4] format
2. Acts as a secretariat for the Cross Section Evaluation Working Group which fulfills the function of (a) gathering data in the ENDF/B [5] format for use in reactor calculations and (b) making recommendations regarding cross section evaluation procedures in problematic areas.

Another area of Center responsibility, which will not be included in this presentation, is the developing and adopting of new analytic methods and theoretical models for the evaluation of cross sections.

2. EXPERIMENTAL DATA

In 1962, following specifications made by the Sigma Center staff, the SCISRS system was started. Work was completed by the Applied Math Department at BNL in 1964. The input characteristics are shown in Fig. 1. A fixed format was used to provide input information. The types of information that could be supplied, with the exception of comments, were each limited to a definite location and to what could be contained in the 80 columns of an IBM card. Among the items specified are the Z and A of the neutron target, the neutron energy and its uncertainty, the cross section and its uncertainty, the measuring laboratory, the reference, and the date of entry into SCISRS. One card was used to enter each energy point and its associated cross section.

The present size of the library consists of approximately 10^6 data points. The improvement and automation of measuring techniques will increase the size of the cross section library in the next few years. However, the size of the library is expected to stabilize at about 10^7 data points, as some selectivity will then be used in maintaining the files. To quickly examine the contents of the entire data file, it is possible to obtain various edits. Sorting by Z, A, energy range, reference, and laboratory are done routinely. One such retrieval is shown in Fig. 2. Here the sorting was done by Z, A, and reaction type. Comments about the data, the number of data points, etc., appear below each index line. The printout of

needed for publication will be included, such as method, standard, or normalization, and will be linked to the related data by an accession number. Sorting is possible on any field. In Fig. 4, a sort according to reference is shown with the field separators deleted to improve legibility.

For data a similar flexibility in input preparation may be provided. Information common to all data points, such as sample thickness or resolution, can be entered only once. The energy array could be entered by first specifying its identifier, followed by a string of numbers separated by commas. The information contained in the flexible input format would then be converted to a fixed internal format for storage and retrieval.

A Control file would contain all dictionaries and format statements. Redefinitions would need to be made only to the Control file, which would then perform all necessary changes in the input and output routines.

3. EVALUATED DATA

Much useful experience in data file organization and computer graphics has been provided by ENDF/B. Alphanumeric and numerical information are placed on the same tape but in separate sections, as shown in Fig. 5. The building blocks of the library are largely mathematical in nature rather than tailored to accommodate a particular type of data. Consequently, the format is not always efficient but is generally expandable. Some automatic checking of the input is performed. Items such as card sequencing, energy sequencing, and consistency of data points within tables are checked. The latter check is made by interpolation between neighboring points and extrapolation from near neighboring points in order to determine a reasonable region of expectancy for each data point. In addition, it is also determined whether nuclear temperatures are within assigned limits, probability distributions are normalized, and whether Legendre expansions produce negative values of the differential cross sections. Calculations are also performed of the fission spectrum and Maxwellian averaged cross sections and the resonance integrals for comparison with experiment. Further checks of the ENDF/B library are planned.

The contents of the ENDF/B library can be read without knowledge of ENDF/B formats using an edit program. A dictionary is used to identify quantities in an unabbreviated way. Headings clearly identify columns of information, and the scheme for interpolation between numbers is indicated.

4. COMPUTER GRAPHICS

Computer graphics are useful in the checking of large volumes of data and the automation of data publications. Plots may be generated in a fraction

all items may, of course, be arranged according to individual preference. Note that a dictionary has been used to expand the abbreviated entries made in Fig. 1. It is possible to use the edited version shown in Fig. 2 to comprise a keyword made up of the Z, A, reaction type, and reference to extract from the SCISRS library a particular set of data as was entered according to Fig. 1.

Although SCISRS has proved to be extremely useful to BNL and other laboratories, it nevertheless has the following disadvantages:

1. Input format is inflexible, restricting the amounts and kinds of information that can be entered
2. Computer processing of data is hampered by the fact that alphanumeric information is combined with numerical data
3. Title and authors are not available as retrievable items
4. Main SCISRS library programs are written in FAP macro-assembly machine language and are therefore useful mainly to those having compatible equipment.

A new storage and retrieval system, CSISRS [6] is under development by the NNCSC. A tentative proposal has been distributed and comments received. Models of the data files are now being constructed in order to detect whether any basic flaws exist in the concepts being considered. A large scale programming effort will begin in the near future. The characteristics of CSISRS are the following:

1. Separate bibliography and data files linked by accession numbers
2. Flexible input format
3. Expanded range of types of information that can be stored
4. Program language easily transferable to the compilers of most machines
5. Logically linked to automated publication of BNL 325 and BNL 400 and to interactive systems such as SCORE [7].

An example of a flexible input format is shown in Fig. 3. This example is taken from the BIB file presently in use at the NNCSC to store comments pertinent to references. It is an adaptation from the National Bureau of Standards SYX code. It is not as yet computer-linked to the data files but does serve as a working model of the bibliography portion of CSISRS. Separators such as \$, *, and / are used to identify quantities and separate fields. The fields are not restricted in number or in length. The title, for example, may fill one or several cards, the length of field being terminated by the indicator for the next quantity. Eventually, all information

of a second on the face of a cathode-ray tube and recorded by film. Figure 6 was obtained by photographing with 35 mm film angular distribution data generated on a CALCOMP 835 plotter. The experimental points were retrieved from SCISRS and the solid curve from a documented optical model calculation. The data sets including error bars were searched by the computer to determine proper scaling. Data symbols are stored to accommodate several data sets---the first symbol assigned being a blank square. Quality control is important for publication, and much attention is given toward obtaining readable grids, letters, numbers, exponents, etc.

5. CONCLUSIONS

Computers are necessary to handle the vast amount of accumulating data. The use of modern methods of data file organization and computer graphics will improve services to cross section users. Considerable progress has been made towards this objective.

6. References

1. Jerry M. Friedman and Marc Platt, "SCISRS, Sigma Center Information Storage and Retrieval System," Brookhaven National Laboratory Report BNL 883 (July 1964).
2. D. J. Hughes and R. B. Schwartz, "Neutron Cross Sections," Brookhaven National Laboratory Report BNL 325, 2nd Ed. (1958); D. J. Hughes, B. A. Magurno, and M. K. Brussel, "Neutron Cross Sections," Brookhaven National Laboratory Report BNL 325, 2nd Ed., Suppl. No. 1 (1960); M. D. Goldberg, S. F. Mughabghab, S. N. Purohit, B. A. Magurno, and V. M. May, "Neutron Cross Sections," Brookhaven National Laboratory Report BNL 325, 2nd Ed., Suppl. No. 2 (1966).
3. Murrey D. Goldberg, Victoria M. May, and John R. Stehn, "Angular Distributions in Neutron-Induced Reactions," Brookhaven National Laboratory Report BNL 400 (1962).
4. Henry C. Honeck, "ENDF-Evaluated Nuclear Data File and Specifications," Brookhaven National Laboratory Report BNL 8381 (June 1964).
5. Henry C. Honeck, "ENDF/B-Specifications for an Evaluated Nuclear Data File for Reactor Applications," Brookhaven National Laboratory Report BNL 50066 (May 1966).
6. "Proposal for a new Cross Section Information Storage and Retrieval System," National Neutron Cross Section Center Report (Nov. 1967).
7. C. L. Dunford, R. F. Berland, and R. J. Creasy, "SCORE-An Automated Cross Section Evaluation System," Atomic International Report NAA-SR-MEMO-12529 (ENDF 106) (Jan. 1968).

BIB INPUT

```

ADP 16 354 01H1$DP$65J$(14.1MEV)$(ARB.UNITS).
ADP 16 354 * E.GREINER, H.KARGE
ADP 16 354 *// STUDY OF THE NEUTRON-PROTON SCATTERING AT 14.1MEV USING
ADP 16 354 A HIGH PRESSURE DIFFUSION CLOUD CHAMBER. (IN GERMAN)
ADP 16 354 **/C JENA U.
ADP 16 354 ***R J ANN.D.PHYSIK 16 354 (65)
AE 5 565 05B$$SNE$58L$(2.9MEV). 06C$$SNE$58L$(2.9MEV).
AE 5 565 13AL27$$SNE$58L$(2.9MEV). 26FE$$SNE$58L$(2.9MEV).
AE 5 565 28NI$$SNE$58L$(2.9MEV). 29CU$$SNE$58L$(2.9MEV).
AE 5 565 41NB93$$SNE$58L$(2.9MEV). 82PB$$SNE$58L$(2.9MEV).
AE 5 565 * V.I.KUKHTEVICH, B.I.SINITIN, S.G.TSIPIN
AE 5 565 *// REMOVAL CROSS-SECTIONS FOR 2.9 MEV NEUTRONS.
AE 5 565 **/C U.S.S.R.
AE 5 565 ***R J AT.EN.(USSR) .5 565 (58), T J.NUC.ENERGY 11 46 (59)
AE 9 401 81TL205$NG$60K$(25KEV-2.8MEV).
AE 9 401 **/C U.S.S.R.
AE 9 401 ***R J AT.EN.(USSR) .9 401 (60), T SOV.AT.EN 9 942 (61)
AE 9 401 ***R , T J.NUC.ENERGY 16 496 (62)
AE 14 264 52TE122$RES$PAR$63C$(SP). 52TE123$RES$PAR$63C$(23-157EV).
AE 14 264 52TE124$RES$PAR$63C$(SP). 52TE125$RES$PAR$63C$(25-425EV).
AE 14 264 * L.S.DANELYAN, B.V.EFINOV
AE 14 264 *// RADIOACTIVE CAPTURE CROSS SECTIONS OF TELLURIUM ISOTOPES
AE 14 264 AS A FUNCTION OF NEUTRON ENERGIES UP TO 1.5 KEV.
AE 14 264 **/C KURCHATOV
AE 14 264 ***R J AT.EN.(USSR) 14 264 (63), T SOV.AT.EN. 14 258 (64)
AE 20 60 92U238$ALF$66A$(THERMAL).
AE 20 60 * L.N.YUROVA, A.V.BUSHUEV
AE 20 60 **/ USE OF GAMMA SPECTROMETRY TO MEASURE THE RATIO BETWEEN

```

Figure 3. BIB Input.

BIBLIOGRAPHY

```

BAP 10 575 70YB168 RES PAR 65F (GN) (22.56EV). 70YB170 RES PAR 65
F (40-96EV). 70YB171 RES PAR 65F (7-183EV). 70YB172
RES PAR 65F (139-4000EV). 70YB173 RES PAR 65F (17-1
69EV). 70YB174 RES PAR 65F (342-3300EV). 70YB176 RES
PAR 65F (98-3700EV). * J. B. GARG, S. WYNCHANK, W.
W. HAVENS JR, H. CEULEMANS, J. RAINWATER *
IDENTIFICATION OF NEUTRON RESONANCE LEVELS IN YB IS
OTOPES A=171, 172, 173, 174, 176.
COLUMBIA U. S B.AM.PHY.SOC 10 575 (65). PAPER AC2.

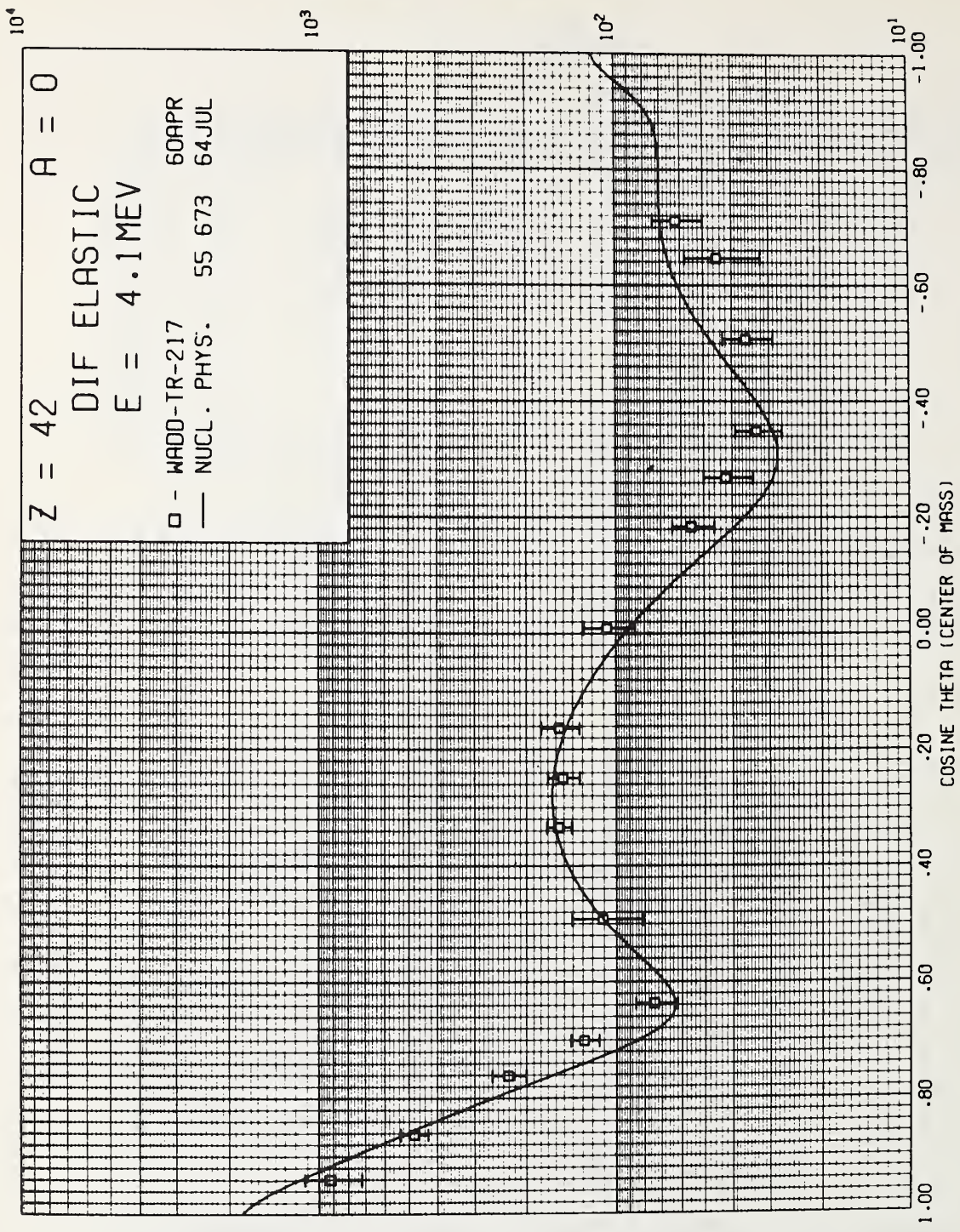
CJP 41 1263 27CO59 RIG 63 (.5EV CUT-OFF). * T. A. EASTWOOD, R. D.
WERNER * THE COBALT RESONANCE CAPTURE INTEGRAL.
CHALK RIVER. J CAN.J.PHYS. 41 1263 (63).

CR 253 635 01H2 DP 61G (14.1MEV). * C. BONNEL, P. LEVY * STUDY OF
THE DEUTERON BREAK-UP REACTION WITH 14.1MEV
NEUTRONS. (IN FRENCH)
FRANCE. J COMPT.REND. 253 635 (61)

CR 265 712 83BI209 N2N 66H (14.5MEV) (TO BI208M). * E. MONNAND, J
.-A. PINSTON * STUDY OF THE ISOMER OF BISMUTH 208.
(IN FRENCH)
GRENOBLE. J COMPT.REND. 265 712 (66).

```

Figure 4. BIB Edit.



(SIGMA)/(OMEGA)-MILLIBARNS/STERADIAN

Figure 5. Computer Graphic of Mo Angular Distribution.

AUTOMATED EVALUATION OF EXPERIMENTAL DATA*

Harry Alter

Atomics International
Div. North American Rockwell Corp.
Canoga Park, Calif. 91303

ABSTRACT

A large fraction of the time required to produce an evaluated cross section library may be classified as nonproductive. A considerable portion of any evaluation is concerned with purely mechanical operations; consequently, not only is there often insufficient time for extensive data evaluation, but there are also long delays between the reporting of measured data and its availability for use in neutronic calculations. To help alleviate some of the problems associated with current data evaluation methods, a comprehensive automated data evaluation system is being developed which will encompass all the operations from the generation of theoretical data to the final evaluated cross section libraries. Such an extensive undertaking has been made possible by major technological advances in the new generation of computers. In particular, these advances are represented by new devices which permit on-line communication between man and a high-speed digital computer.

1. INTRODUCTION

Man-computer interaction is made possible by the freely flowing interchange of information between the man and the computer. This "real time conversation," which takes place between man and computer, has been made possible by advances in the speed and size of the digital computer, by new methods and techniques of programming, and by the development of auxiliary input-output apparatus. The "conversation mode" may be in the form of typed messages, figures and symbols drawn on a television-like display (cathode ray tube), or any other suitable forms which are acceptable to both man and computer.

Communication with a computer has traditionally been limited to punched cards, magnetic or paper tape, and typewriter input, with some kind of printing device being the normal output. Computer graphics, which refers to the concept of man communicating with a computer by means of graphical symbols, such as lines, curves, and dots, as well as by alphanumeric characters, now adds the dimension of sketching and drawing for both input to and output from the computer. The flexibility and high rate of information transfer (as opposed to mere data transfer) presented by such freedom of communication is not likely to be surpassed until it is possible to directly interact with a computer through the spoken word. These new techniques of computer science are being applied to the problems of automating the evaluation of experimental neutron cross section data.

*Based on studies conducted for the U.S. Atomic Energy Commission under Contract AT(04-3)-701

2. THE PROBLEM

For the past several years, there has been an exponential growth in the amount of experimental neutron cross section data. Unfortunately, a parallel growth in the sophistication of evaluation methods has not materialized. Since one cannot realistically forecast an exponential growth in the numbers of data evaluators (an evaluator's lot is not a happy one⁽¹⁾),^[1] one must turn to advances in computers, computer languages, and computer auxiliary devices to meet the evaluation demands brought about by the ever increasing amounts of experimental data produced.

3. A SOLUTION

In an attempt to overcome deficiencies in current evaluation methods,^[2] a comprehensive automated system is being developed which will include all the evaluation steps, from the receipt of new data to the generation of updated neutron cross section libraries.^[3] The structure of this automated evaluation scheme is illustrated in Figure 1. The creation of such a comprehensive calculational system has been made possible by major technological advances in computers, computer languages, and computer auxiliary devices. Of particular interest are the new devices which permit economic on-line communication between man and high-speed digital computers. With such devices, it is possible to insert additional information during the execution of a problem which will influence the final result.

4. DATA STORAGE AND RETRIEVAL

Large amounts of varied information are needed to perform an evaluation. This information consists of all available related experimental data, complete references with detailed description of the experimental technique, errors associated with the measurements, related theoretical information with a detailed account of the methods used to generate this data, and results of previous evaluations. All this information must be immediately available to the evaluator, and constitutes a major information retrieval problem.

The storage and retrieval of reference material presents a formidable problem. At the present time, it does not appear economically feasible to store, as digital data for computer processing, a library of documents relating to cross sections. However, future developments in the area of low cost, rapid access, bulk storage may overcome current objections. One might visualize a more suitable storage system for present applications, in which the CINDA Reference System,^[4] primarily containing recognition information for documents relating to cross sections, is stored as digital information for a computer. In addition, abstracts would be available in digital form for display on an inexpensive auxiliary device when a reference retrieved from CINDA appears to be relevant. Finally, a microcopy of a document may be manually retrieved from a library for use during the evaluation process, when such a document is relevant.

Experimental neutron cross section data is currently stored in a standard digital format for computers by the SCISRS Program.^[5] This system is maintained and updated by the National Neutron Data Center at Brookhaven National Laboratory. An evaluator would have the information contained in the SCISRS system readily accessible to his own digital

(1) With apologies to Gilbert and Sullivan. They had the good sense to pass away before becoming involved with data evaluation.

computer. Theoretical cross section information should also be stored as part of the SCISRS-like system, and thus be available to the evaluator in the same manner as the experimental data. Previously evaluated data, such as the ENDF/B libraries,[6] should be available for retrieval by the evaluation system.

With all the needed information available in digital form on tapes, disks, and/or bulk memory, the evaluator is ready to proceed with the evaluation or to prepare or update a library. The evaluator would operate a display console, directly linked to a high-speed digital computer. A cathode ray tube display device, with light pen, a keyboard, a set of function keys, and microfilm display screen, would be on the console (Figure 2). Stored on disks would be computer routines to perform calculations and other data evaluation functions, which would be activated by the function keys, keyboard, or light pen.

Combinations of operations could be performed by the evaluator at such a console, depending on the nature of the evaluation. For example, consider that new measured values of the U^{238} fast capture cross section have been received in an update of the SCISRS tape. The evaluator could then request a display of the new data against any combination of older measurements and previous evaluations. Related documentation may be retrieved and analyzed. Numerical curve-fitting routines and/or nuclear theory could be used to generate an evaluated set of capture cross sections. The effects of various pieces of data on the final curve could be immediately visualized through the cathode ray tube display. When a newly evaluated cross section curve is determined, programs in the computer would format the information, perform any renormalizations required to other data in the library, and store the new capture cross sections as required. When a new set of evaluated data is produced, there would be an automatic recalculation of a series of standard or benchmark problems. The results of these recalculations would tell both the evaluators and the designers how the new information would affect current reactor safety, design, and economic concepts.

The basic concept which makes an automated cross section evaluation system feasible is the availability of a rapid and convenient conversational mode between the evaluator and the computer. In the past, this conversational capability has been absent, but recent developments in auxiliary computer hardware (namely, the cathode-ray tube console) now provide the conversational mechanism. By making optimum use of the cathode ray tube (CRT) and computer graphics, as both a visual and digital interface between the various components of an evaluation scheme, the evaluator has a flexible and convenient tool for control of the logical flow of computer operations.

A prototype data evaluation system, SCORE,^[7] utilizing interactive computing (or, as it is more commonly known, computer graphics), is currently being developed as a joint research project by Atomic International and the Palo Alto Scientific Center of the International Business Machines Corporation. The system is being developed in support of the ENDF/B national cross section evaluation effort. SCORE is designed to provide a man-computer interactive mode in the evaluation of neutron cross section data for use in nuclear reactor design.

Several new techniques which have been developed for this project include:

- 1) A unique data storage and retrieval system to handle the SCISRS data

- 2) A method for fitting spline curves to nonsmooth data which helps to resolve problems encountered in attempting to fit such data by completely automated methods^[8,9]
- 3) An interactive method for doing Reich-Moore resonance parameter fitting (multilevel resonance theory parameters may be modified by an evaluator until a satisfactory fit is obtained)
- 4) A data overlay module used to overlay evaluated data from the ENDF/B files with data from the SCISRS I experimental data tapes.

The program will retrieve experimental neutron cross section data from a SCISRS I type data file. The methods for storage and retrieval are described in detail in Reference 6. Input data is supplied by the evaluator, who enters this data through a series of active displays on the console. In addition, the evaluator directs the flow of SCORE by means of actions taken at the console, in any desired sequence of operations, which include data sorting, data display in one of several available modes, data correcting, data listing, etc.

The console (Figure 2) used by the evaluator to execute SCORE consists of a CRT on which graphical displays appear, an alphanumeric keyboard which can be used to communicate with the CRT, and a light-sensitive pen used for a similar communication function. The initial display, Figure 3, permits the evaluator to enter such basic identifying information as laboratory, evaluator, date, and problem identification number. In addition, such data as element atomic number, mass number, reaction type, and energy limits, necessary for retrieval of the desired experimental quantities, are supplied. A short line, called a cursor (Figure 3) indicates the position at which a character entered in the keyboard will appear on the screen. This cursor may be moved to any position in the active area of the display by a function key on the keyboard. Thus, the evaluator is completely free to enter and correct any input data on the screen. When all specifications required for retrieval of the desired data are complete, the data is retrieved and displayed. If data for a new nuclide is requested, the data is transferred from tape to an intermediate storage stage on a disk. Once this data has been placed in intermediate storage, any number of subsequent requests relative to that data are satisfied in less than a few seconds. Additional information relating to the data display may also be supplied by the evaluator (Figure 4). The experimental data satisfying the evaluator's request is displayed on the cathode ray tube (Figure 5). The display grid parameters are selected by preset algorithms. Each data point is displayed, using an alphabetic character. References corresponding to these characters appear in the right center of the display. The lower right of the display contains a series of key words which indicate options initiated when that word is detected by the light pen. Several sets of options are currently made available. The various options allow one to modify the grid parameters or the data units, sort the data by reference, correct data (such as those from Reference D), expand the graphical portion of the display to full screen size (Figure 6), and display the data as points and add the error hats (Figure 7).

If any of the data in a display are incorrect (for example, data from Reference D in Figure 5), action may be taken to correct this data. The data points are made sensitive to detection by the light pen. The evaluator detects each point he wishes to correct with the light pen; when this selection procedure is completed, the display shown in Figure 8 appears

on the console screen. When the correction procedure is completed, both the original and corrected data are shown. The result of this correction procedure is illustrated in Figure 9, in which the data from Reference D is shown as having been corrected.

5. CURVE FITTING

Problems which arise in the application of normal curve fitting methods:

- 1) The presence of incorrect data
- 2) Data recorded in incorrect units
- 3) Proper application of weights to data sub-sets

are more rapidly handled in a graphic interactive mode. One type of fitting procedure found useful in data evaluation is the cubic spline. The curve may be uniquely defined by giving the second derivative at a series of nodes (x,y). The second derivative may be calculated for a set of nodes from the continuity conditions at each node.

A simple spline-fitting method has been incorporated in the SCORE system. Nodes are entered through the cathode ray tube, using a light sensitive tracking pattern consisting of three concentric circles (Figure 10). Using the light pen, the tracking pattern may be moved to any location on the display grid. When a node is properly located, it is stored in the computer. The input placement of the nodes should be such as to represent the gross shape of the curve. The spline curve is computed by solving a tri-diagonal matrix equation for the second derivatives at the nodes, the matrix equation being determined by the continuity requirements on the adjoining cubics at the nodes (the curve and its first and second derivatives must be continuous). The computed spline curve is then fitted to the nodes, a residual chi calculated, and the curve displayed upon the cathode ray tube screen (Figure 11), all within a few seconds. The curve may then be adjusted, as desired, by adding, moving, or deleting nodes and recomputing the spline. The adjustment of the nodes has mainly a local effect on the fitted spline curve. It is thus possible to force the spline curve to fit steep peaks or valleys without destroying the fit in other regions (Figures 12 and 13).

Attempts to fit the data illustrated in Figure 10 with a fully automated spline fitting program were less than satisfactory. The program tended to insert too many nodes, thus creating more structure than was justified by the experimental data. However, if an initial set of nodes is given, the automated spline routines can be used to improve the fit. It currently appears that a semi-automated spline fitting technique provides the better results.

6. RESONANCE REGION DATA EVALUATION

The current version of SCORE also contains a resonance region analysis module. A single-level or a two-channel Reich-Moore multilevel calculation has been included, along with methods for resolution and Doppler broadening of the zero degree line shape. That portion of the resonance region module which calculates the zero degree line shape and the resolution and Doppler broadened cross section was supplied by M. S. Moore and N. Marshall of the Idaho Nuclear Corporation. The resonance region line shape is generated from a set of resonance parameters stored on a disk. The display generated, upon completion of the line shape

calculation, compares the experimental cross section values and a curve representing the theoretical line shape (Figure 14). An edit capability has been provided, in order to improve the fit to experimental data from a given set of resonance parameters. One can add or delete resonances, or modify the parameters for an existing resonance data, and then recalculate the line shape for the new set of resonance parameters (Figure 15). In addition, it is possible to display a comparison of the revised line shape, the previously calculated line shape, and the experimental cross sections. A chi value is computed for each curve, in order to provide a numerical comparison of the goodness of the fit of successive curves.

A comparison of single-level and multilevel fits to experimental data is illustrated in Figure 16. Superposed on the measured plutonium-241 fission cross section (dots), is the curve due to a single-level analysis (curve through astericks) and the curve obtained from a multilevel fit. Thus, an evaluator now has the capability for improving sets of resonance parameters, by interacting with his data through the computer and the console. It is readily apparent that a task, which previously required several months to complete, can now be performed in days, and perhaps even in hours. An entirely automated fitting procedure, using numerical parameter fitting methods, can be extremely time consuming, particularly when a multilevel formalism is used. As is the case with spline curve fitting of experimental data, it appears that an interactive system, which combines the numerical parameter fitting with judicious direction of the analysis by the evaluator, would be most economical and useful.

7. COMPARISON OF MEASURED AND EVALUATED DATA

To further aid the data evaluator, the ability to display a comparison between experimental and evaluated data on a console screen has been developed. This mechanism includes the development of a storage system for evaluated neutron cross section data (ENDF/B) which is compatible with the SCORE system, and which utilizes storage methods previously developed for the SCISRS experimental data. To the evaluator, the immediate availability of a display, in which the measured and evaluated data are compared, and with which he is able to interact, can be an extremely useful tool. Figures 17 to 19 represent console screen displays comparing experimental data from the SCISRS tape with ENDF/B evaluated data. In Figure 17, the experimental data is represented by alphabetic entries which correspond to the several sources of information, while the evaluated data from the ENDF/B data file is represented by the curve. In Figure 18, the experimental data from Source B above is compared with the evaluated curve. Data points corresponding to Sources A and C have been deleted. Figure 19 presents an expanded display which compares measured (SCISRS) and evaluated (ENDF/B) data for the sodium total cross section.

8. APPLICATIONS OF SCORE

To the evaluator, an interactive computing system, such as SCORE, can represent a useful tool for the solution to problems of data evaluation and dissemination. In the most simple form, SCORE could be used as an editor for the SCISRS I experimental data tapes. The information stored on these tapes could be visually checked for errors by simply displaying the data. Incorrect data could be selected from the display by the light pen. These entries could be displayed on the cathode ray tube in card image form and edited to correct any errors by entering characters through the alphanumeric keyboard. Corrected data cards would then be produced and merged into the SCISRS library.

Data displays from the SCISRS library could be generated when new experimental information becomes available. "Eye guide" curves can be

rapidly fit to the data with the spline techniques currently in SCORE or with advanced techniques planned for the future. The final displays would be transferred to 35 mm film, via a projected "hard copy" feature. Loose-leaf update pages to data evaluations, such as BNL-325 and BNL-400, could be issued with considerable savings in costs and time.

9. SUMMARY

The introduction of interactive computer graphics has opened a new dimension to the hurried data evaluator. Man-computer interaction during the execution of a data evaluation problem can now be economically accomplished by the use of a graphic display console as a high-speed input-output device. The economy of this mode of operation is based on its time-sharing capability and its convenient output form (namely, graphic displays). The data evaluator, using the input device on a display console, can direct the processing and evaluating of experimental data by monitoring intermediate results. Errors may be corrected easily, before a large amount of computer time is consumed. In addition, the evaluator may inject his analysis of partial results (which otherwise might be very difficult or expensive to approximate, by the computer program) during execution of the program. This interaction can save computer time and turn-around time, and provides insight into the problem being solved.

Many present data evaluation methods can benefit greatly from the inclusion of computer graphics, but the real promise lies in the development of new techniques which make optimal use of its many capabilities.

In preparing this paper, I have profited from many conversations with Charles L. Dunford and Robert F. Berland who, along with Robert J. Creasy of the IBM Palo Alto Scientific Center, are the principal contributors to the development of the Automated (Interactive) Evaluation Computer Program - SCORE.

10. REFERENCES

1. C. Lubitz, "Theory and Experiment in the Construction of Reactor Cross Section Libraries," Conference on Neutron Cross Section Technology, CONF-660303 (1966)
2. K. Parker, "Mechanized Evaluation of Neutron Cross Sections," Conference on Neutron Cross Section Technology, CONF-660303 (1966)
3. H. Alter and C. L. Dunford, "Compilation, Evaluation, and Production of Nuclear Data for Reactor Calculations," NAA-SR-11980, Vol. I (1966)
4. Columbia University and ENEA Neutron Data Compilation Center, "CINDA, An Index to the Literature on Microscopic Neutron Data," EANDC 60 "U" (July 1966) (Also referenced as NYO-72-107 and CCDN-CI/11)
5. J. M. Friedman and M. Platt, "SCISRS, Sigma Center Information Storage and Retrieval System," BNL 883 (T-357) (July 1964)
6. H. C. Honeck, "Specifications for an Evaluated Nuclear Data File for Reactor Applications, ENDF/B," BNL 50066 (T-467) (July 1967)
7. C. L. Dunford, R. F. Berland, and R. J. Creasy, "SCORE, An Automated Cross Section Evaluation System," NAA-SR-MEMO-12529, ENDF 106 (January 1968)

8. A. Horsley, "Computer Evaluation of Neutron Scattering Angular Distribution Data," Conference on Neutron Cross Section Technology, CONF-660303 (1966)
9. R. F. Berland, C. L. Dunford, and R. J. Creasy, "Computer Graphics for Automated Neutron Cross-Section Evaluation," presented at the American Nuclear Society - 1967 Winter Meeting at Chicago, Illinois, November 1967

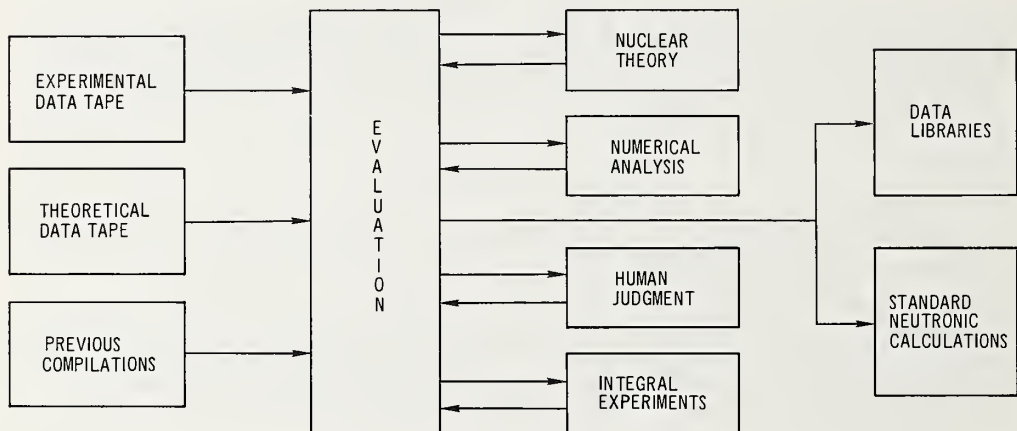


Figure 1. Automated (Interactive) Evaluation Scheme

ODE TO THE DATA EVALUATOR

SCORE is Sympathetic, SCORE is Compassionate

SCORE is Obedient, SCORE is Radiant,

SCORE is Eternal.

Lift up your heads,

ye harried, hounded, and hapless evaluators of data,

SCORE brings you resurrection,

joy, and

uplifting,

Figure 20.

WANTA SEE MORE?



Figure 2. Graphic Display Console

LABORATORY: AI - IBM
 EVALUATOR: C.L.DUNFORD
 DATE: 10/31/67
 PROBLEM I.D.: 1
 ELEMENT: 11
 MASS NUMBER: 23
 REACTION: NA
 MINIMUM ENERGY (MEV): 6.-
 MAXIMUM ENERGY (MEV):
 LEVEL ENERGY (MEV):

PLEASE FILL IN OR CHANGE APPROPRIATE VALUES.
 SIGNAL 'END' WHEN COMPLETE

11-22-67 UNCL

7701-4633

Figure 3. Initial Data Input Display

11 23 NA 6.30000E 00 TO 2.10000E 01 MEV.
 SIGMA MIN = 1.20000E-03 SIGMA MAX = 1.64000E 02

X-AXIS: LOG LIN Y-AXIS: LOG LIN

UNITS

X-AXIS MEV KEV EV LAB CH
 Y-AXIS B MB B/ST MB/ST

X-MIN 6.0E 00 X-MAX 2.1E 01

Y-MIN 1.0E-03 Y-MAX 2.0E 02

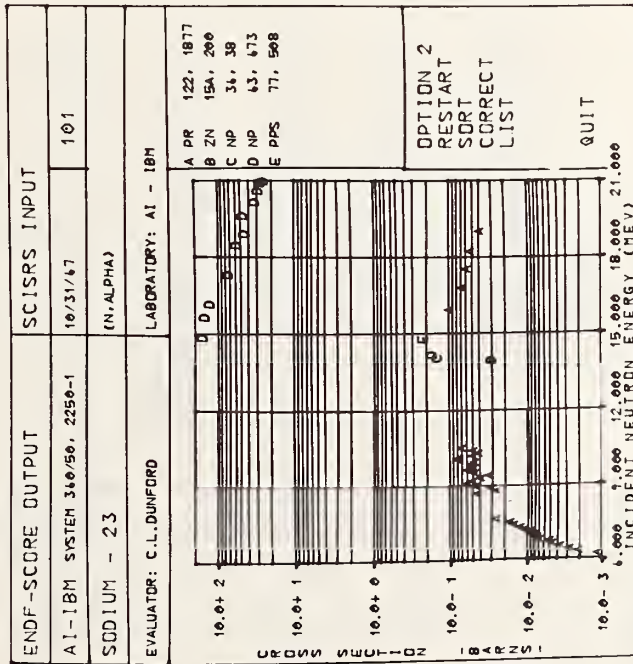
DELTA X 3.0E 00 DELTA Y 3.0E 01

SDRT NDSORT

11-22-67 UNCL

7701-4637

Figure 4. Display of Option Choices
 (Units, Scale, Energy Limits)



7701-4638

Figure 5. Basic Data Display

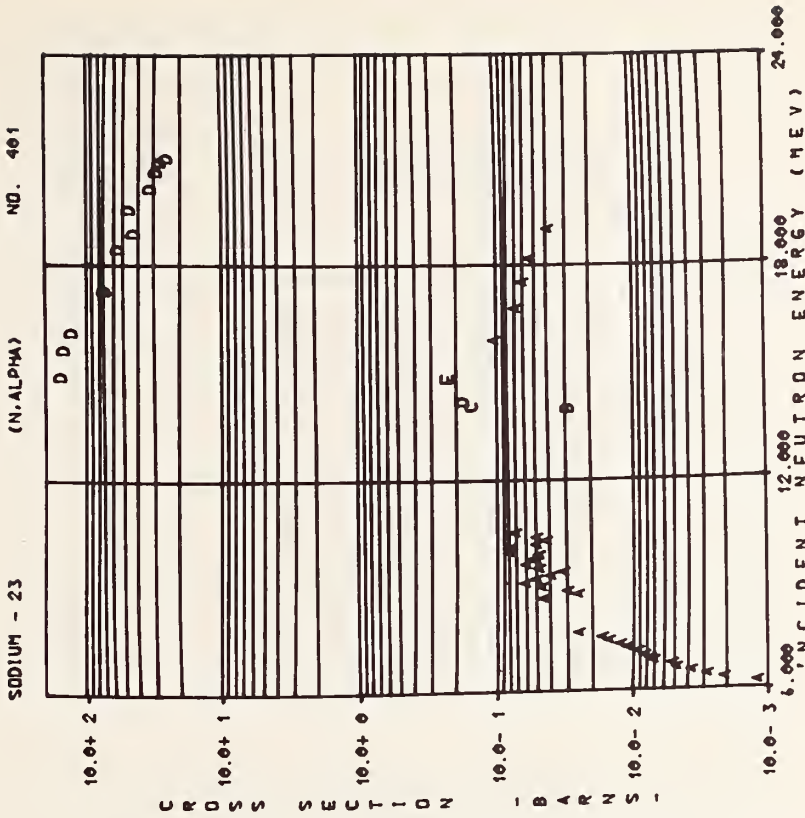


Figure 6. Expanded Display
(Full Screen Size)

SODIUM - 23 (N,ALPHA) ND. 103

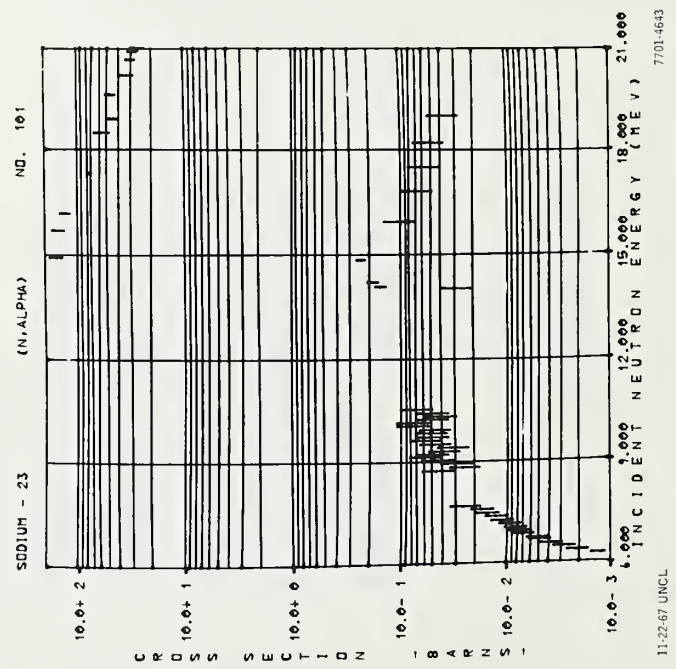
LIGHT PEN DATA TIMES 1.00 -03 PLUS 0.00 +00

INCORRECT DATA		CORRECTED DATA	
ENERGY (MEV)	SIGMA (BARN)	ENERGY (MEV)	SIGMA (BARN)
1.48100E 01	1.49000E 02	1.48100E 01	1.49000E-01
1.56700E 01	1.53000E 02	1.56700E 01	1.53000E-01
1.61500E 01	1.34000E 02	1.61500E 01	1.34000E-01
1.73300E 01	7.55000E 01	1.73300E 01	7.55000E-02
1.84100E 01	6.00000E 01	1.84100E 01	6.00000E-02
1.81200E 01	4.54000E 01	1.81200E 01	4.54000E 01
1.96100E 01	4.90000E 01	1.96100E 01	4.90000E 01
2.01100E 01	3.40000E 01	2.01100E 01	3.40000E 01
2.04300E 01	3.07000E 01	2.04300E 01	3.07000E 01
2.09000E 01	2.90000E 01	2.09000E 01	2.90000E 01
2.10000E 01	2.58000E 01	2.10000E 01	2.58000E 01

7701-4640

11:22:67 UNCL

Figure 8. Display for Data Correction Option



7701-4643

Figure 7. Data Display - Experimental Values with Associated Errors

11:22:67 UNCL

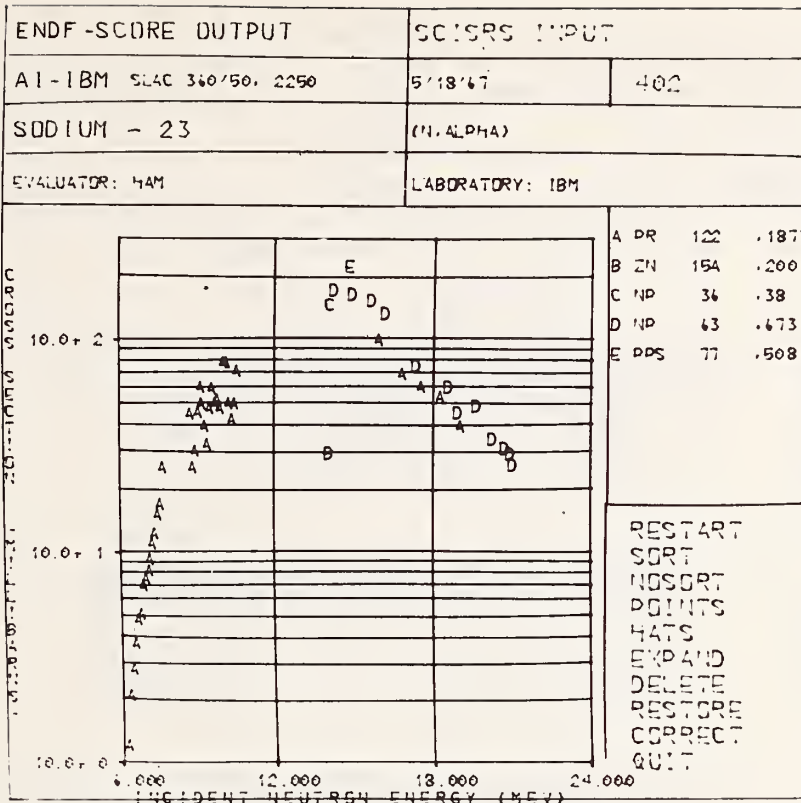


Figure 9. Display with Corrected Reference D Data

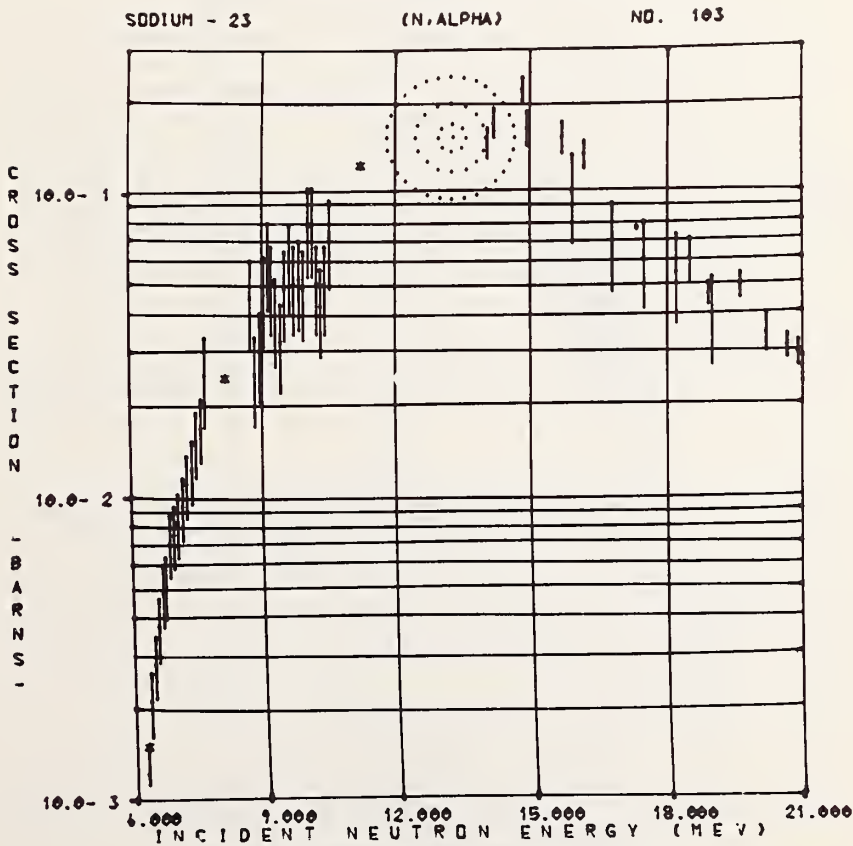


Figure 10. Nodes (*) Entered by Tracking Pattern

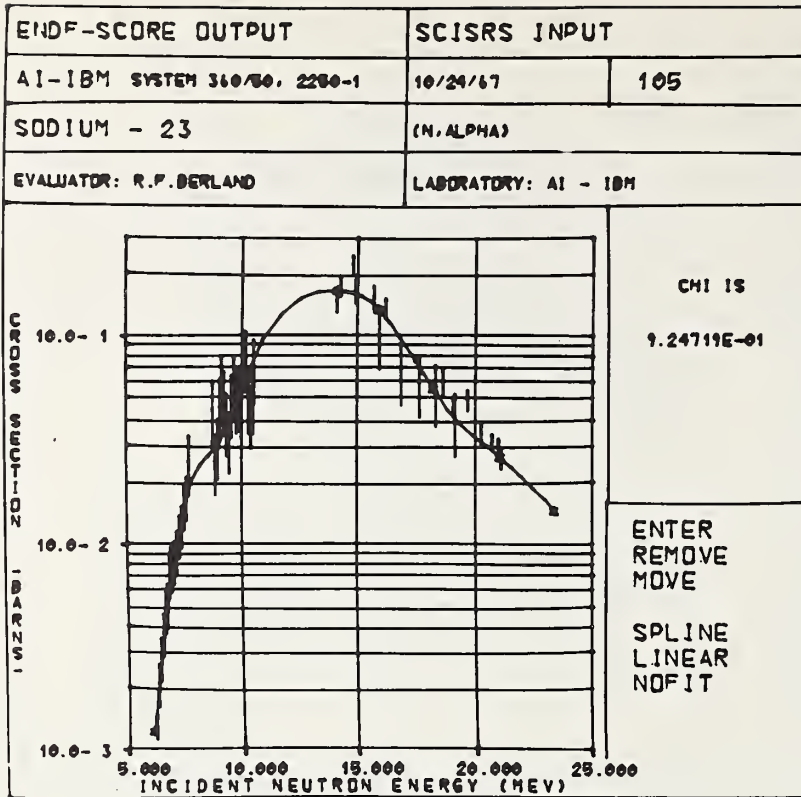


Figure 11. Spline Fit to Experimental Data

SODIUM - 23 (N,ALPHA) NO. 103

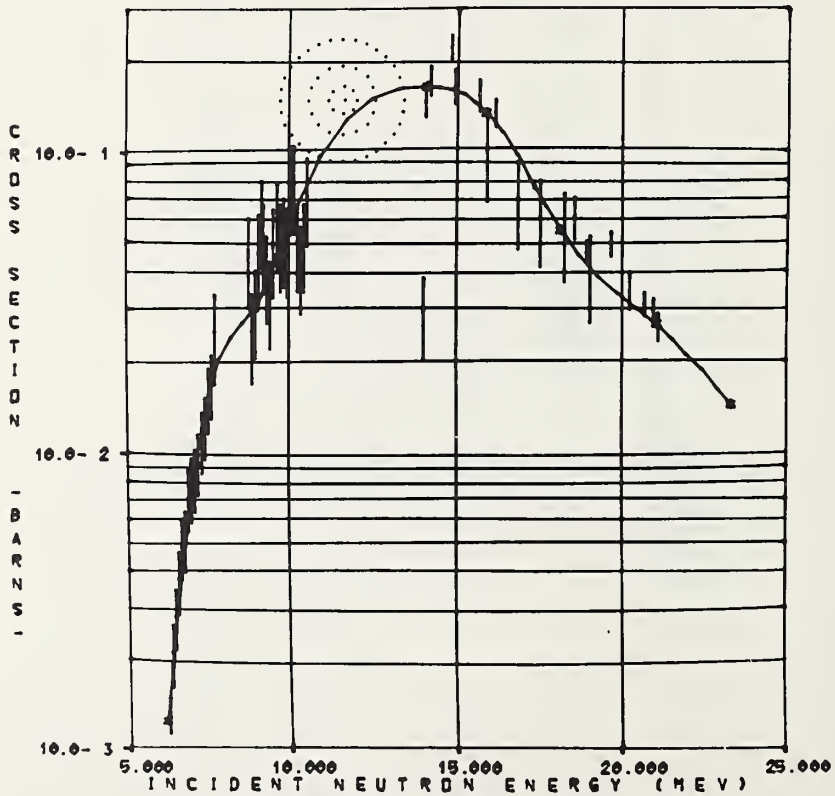


Figure 12. Adjustment of Spline Nodes

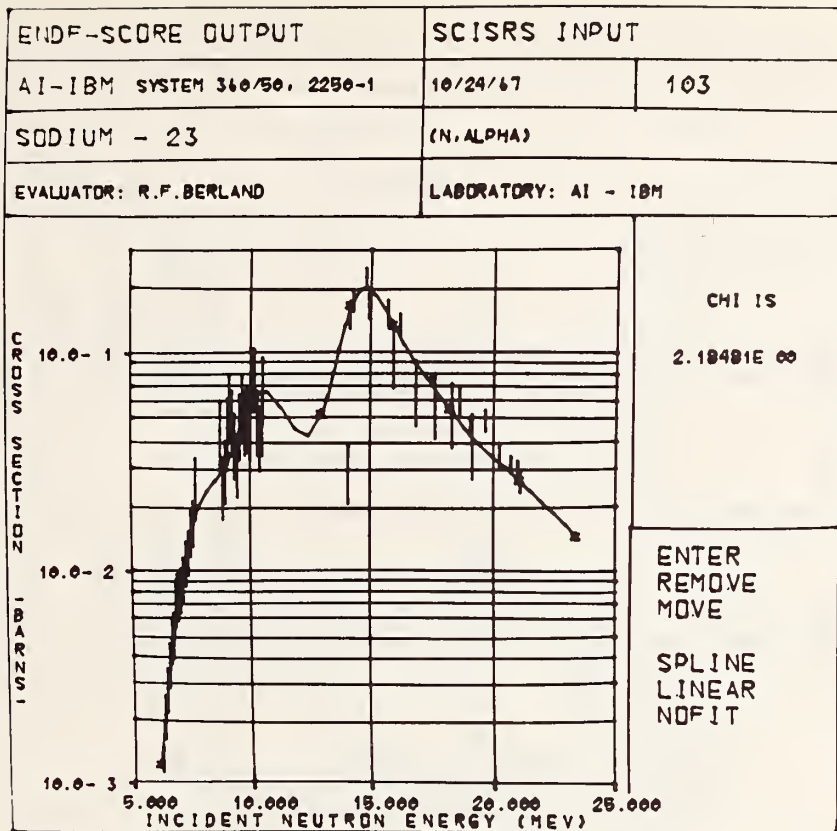


Figure 13. Adjusted Spline Fit

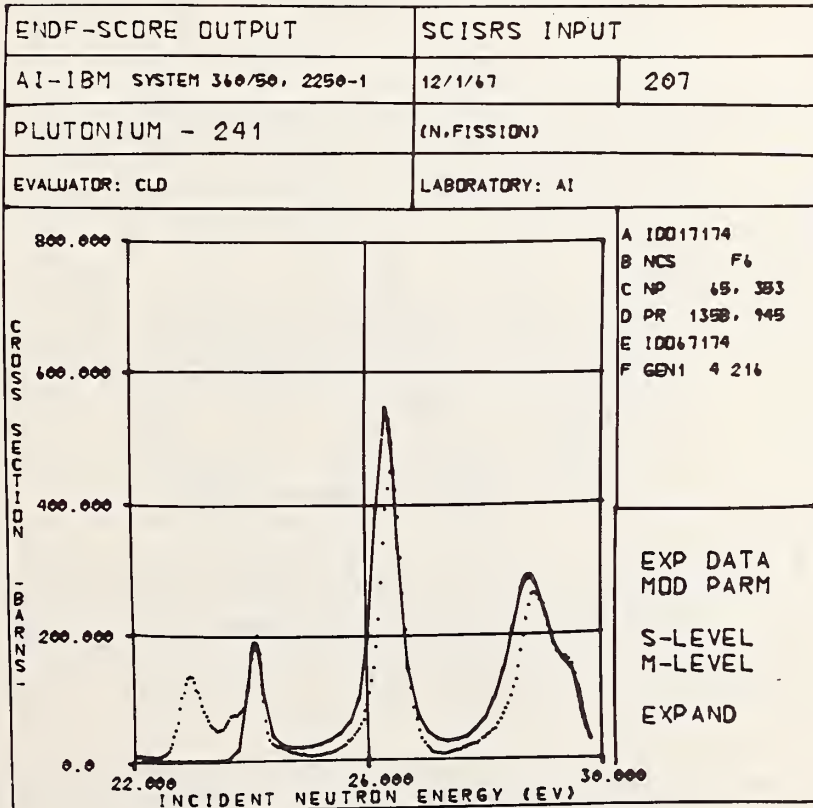


Figure 14. Multilevel Fit with Parameter Set "A"

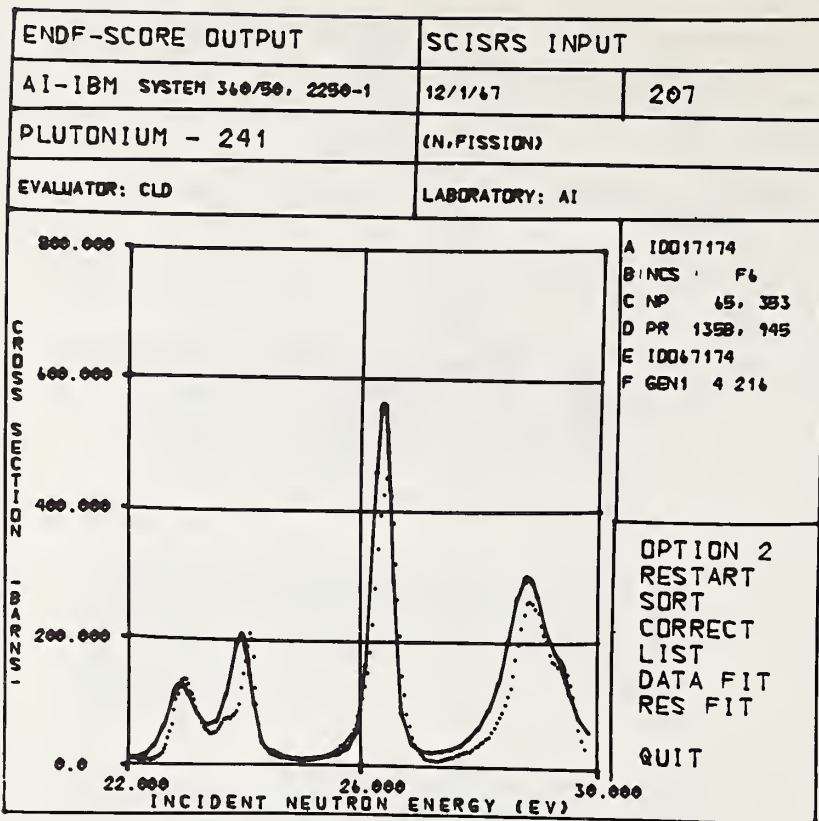


Figure 15. Multilevel Fit with Parameter Set "B"

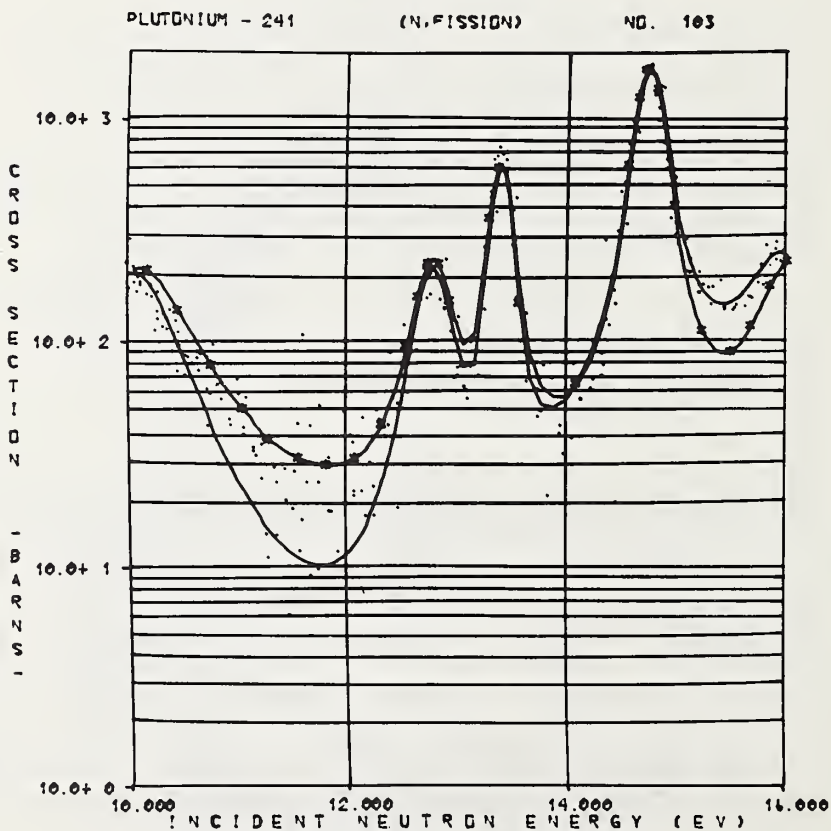


Figure 16. Comparison of Multilevel and Single-Level Fits to Experimental Data

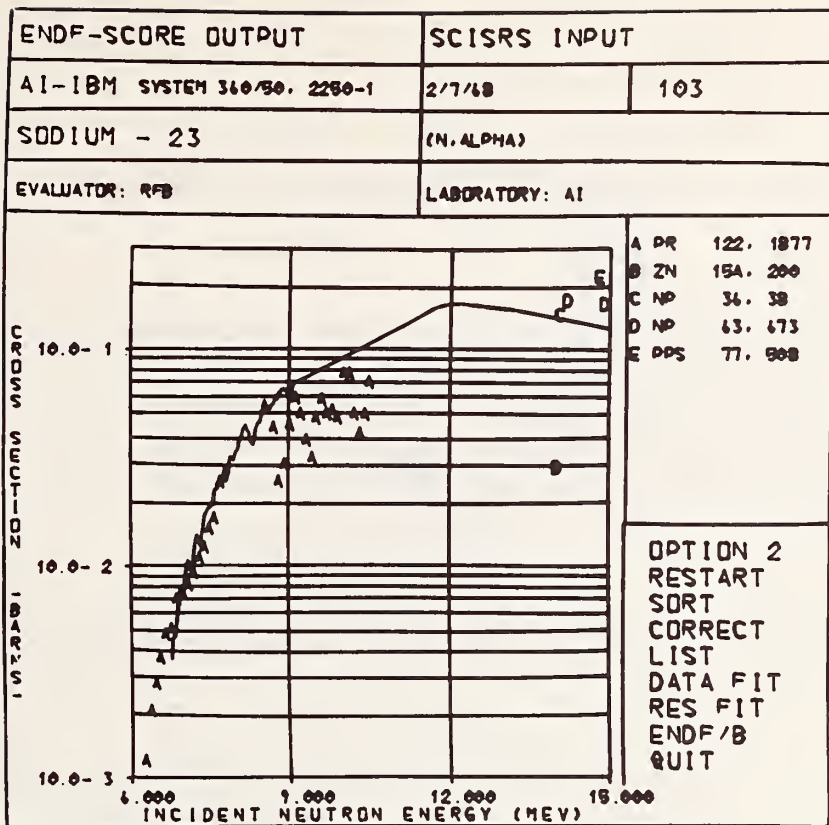


Figure 17. Comparison of ENDF/B Evaluated Data with SCISRS Experimental Data - Sodium (n, alpha)

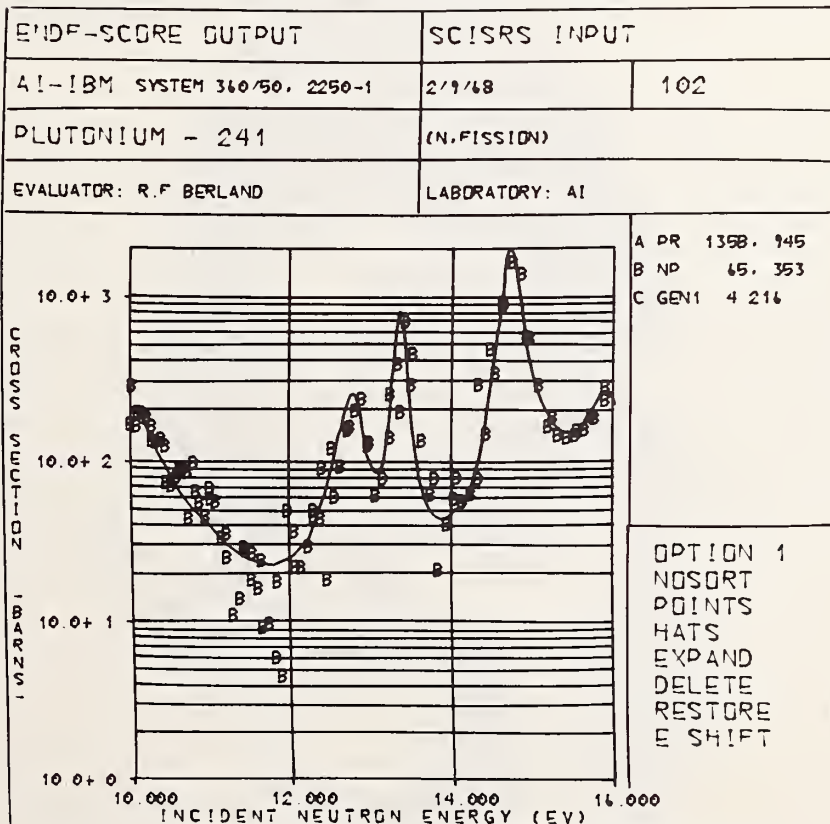


Figure 18. Comparison of ENDF/B Evaluated Data with SCISRS Experimental Data (Reference B only) - Plutonium-241 Fission

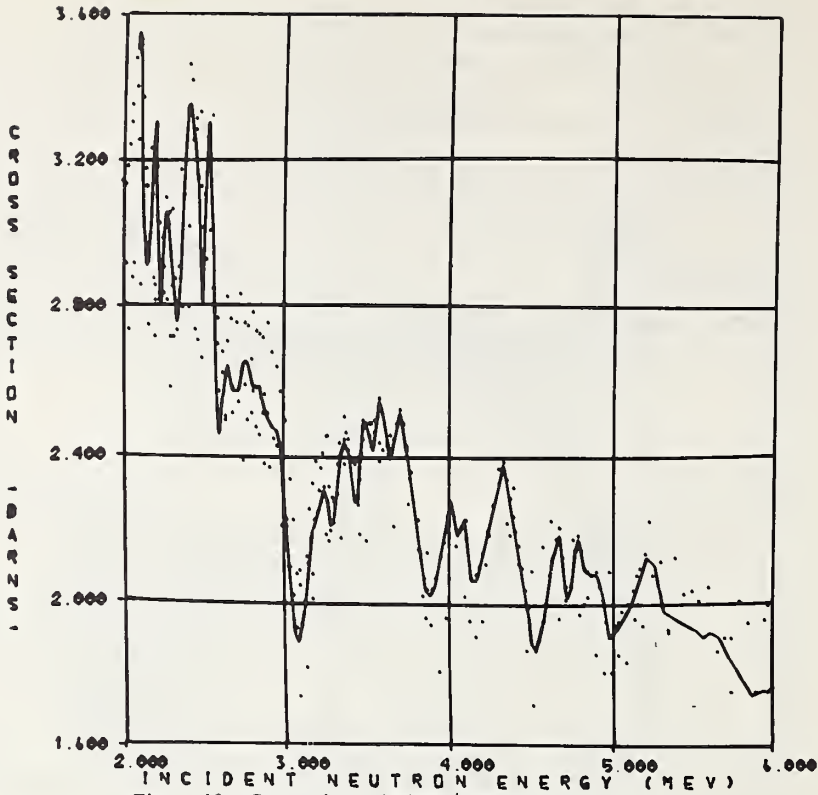


Figure 19. Comparison of ENDF/B Evaluated Data with SCISRS Data - Total Cross Section



Figure 20

PRINCIPLES OF CROSS SECTION EVALUATION

J. J. Schmidt, Institute für Neutronenphysik und
Reaktortechnik, Kernforschungszentrum Karlsruhe

Postfach 6340 German Federal Republic

ABSTRACT

Evaluation consists in the derivation of complete easily interpolable sets of "best" values of microscopic cross sections and parametric data from available experimental and theoretical informations in the energy range 0 to about 15 MeV and the establishment of corresponding computer nuclear data libraries for further use in reactor calculations. Gaps in the experimental information can often be filled successfully by nuclear systematics or parametrization of some nuclear theory or model like statistical reaction theory, optical or evaporation model. The main difficulty in evaluation consists in systematic discrepancies outside experimental error between different experimental data sets, which only sometimes can be resolved by renormalization. Beside the differential experimental data in some cases "clean" integral data which allow unique conclusions to the nuclear data involved are used in the evaluation. The reliability of evaluated nuclear data sets can more and more be assessed by comparison of calculated and measured integral data e.g. from critical facilities. Generally the feedback from these "dirty" integral data to differential data is not unique and therefore a thorough review of the basic microscopic data most probably involved preferred to a computerized data adjustment that may be physically incorrect.

The field of evaluation of neutron cross sections has its origin in the reactor theory. As is well known the reactor theory deals with the solution of the Boltzmann neutron transport equation and of equations derived from it in various approximations in order to describe the neutron physical behavior of nuclear reactors including safety coefficients like the Doppler coefficient. In these equations neutron cross sections enter as continuous functions of neutron energy and angle and other energy dependent data like fission spectra and numbers of prompt fission neutrons, resolved and statistical resonance parameters. As the modern computer capabilities allow and force increasing refinements of the reactor theory methods which have to be considered in parallel with steady refinements of the reactor physics measurement techniques, more and more detailed and reliable values have to be prepared for these nuclear data.

Every evaluation of neutron nuclear data for a given element or isotope today has therefore to fulfill the following general requirements. Reactor neutrons cover energies between about 0 and 15 MeV. In this energy range no reaction the neutrons can undergo from physical grounds, can be left out in an evaluation. Furthermore, as the reactor physicists are interested in the detailed description of thermal as well as intermediate and fast reactors, an evaluation has to consider the subranges of thermal, resonance, and fast neutrons in corresponding similar detail. Therefore the density of the energy and angular mesh points, at which the nuclear data have to be evaluated, has to be as great as to describe the functional dependence of the data in a physically satisfactory almost monochromatic way so as to allow an as simple as possible interpolation between neighboring data points. Linear interpolations on log-log, log-linear or linear-linear scales are most frequently used. In the regions of isolated narrow resonances, where in a double-linear interpolation scheme thousands of data points would be needed for a satisfactory representation of the cross sections, a parabolic interpolation appears to be more appropriate and helps to spare computer storage. Perhaps in the computers of the third generation with their very large storage capacities this restriction can be omitted and the double linear interpolation scheme be adopted throughout. In those special cases in which a cross section or a distribution can be parameterized in a simple and univoque way as e.g. in the case of a pure one level Breit-Wigner cross section, it could suffice to evaluate and store only the parameters. For checking purposes, however, it is advisable to store not only the parameters, but also the data points: group constants for example should come out the same, whether they are calculated from parameters or from data points. According to the different cross section behavior, particularly in the thermal and resonance regions, the energy subdivision will obviously be different for each element or isotope.

In order to fulfill these requirements the evaluation physicist has to consider all available sources of information, to assess critically their reliability and value and to derive, by selection, averaging, inter- or extrapolation or other relevant methods, from the available information a unique set of so called "best" data. The informations which are used in evaluation come from nuclear data measurements, nuclear theories or models and from nuclear systematics. The main basis is the experimental information like measurements of cross sections as a function of the neutron energy, of angular or energy distributions in elastic or inelastic neutron scattering. Likewise theoretical interpretations of measurements like the derivation of resonance parameters from measured resonance cross sections, or the interpretation of measured inelastic scattering distribution in terms of nuclear temperatures are used. In the case of gaps or discrepancies in this basic information recourse must be held to some nuclear theory or model or nuclear systematics

considerations. In the following we shall briefly discuss the principal methods used in the evaluation of neutron cross sections and parametric data in the ranges of thermal, resonance and fast neutrons. For simplicity we shall confine our discussion to medium weight and heavy nuclei.

The thermal energy range, with the exception of the rather complex thermal scattering laws, which we omit from our considerations, presents only minor difficulties in evaluation. To begin with medium weight and nonfissionable heavy nuclei, generally pointwise σ_T data and σ_γ values as averages over thermal reactor spectra mostly reduced to thermal energy (0.025 eV, the most probable neutron energy in a pure Maxwellian neutron spectrum at room temperature) are available from experiment. The remaining data are easily derived in the following way. In many cases the capture cross section in the thermal range follows a pure $1/v$ - law. This $1/v$ - law valid for positive as well as negative energy resonances is easily derived from resonance theory under the conditions that the resonance energies E_r are sufficiently far apart from the thermal range, that the resonance half widths are small compared to E_r , and that many exit channels are available in resonance capture, Γ , which lead to a cancelling of interference terms between different capture resonances and channels. The proportionality constant in the $1/v$ - law is fixed by the "best" value of the capture cross section at thermal energy which can be obtained by weighted averaging of the individual experimental values. If the above first two conditions for a $1/v$ - law are not fulfilled, but still the third one, which is certainly the case for non-magic nuclei, i.e. if the resonances come close to thermal energies, then the cross section in the thermal range can be calculated from one level Breit-Wigner contributions of all known positive s-wave resonances (the contributions of higher l-wave resonances tend to zero for decreasing neutron energy) and of one assumed negative resonance. The neutron width and the position of the negative resonance can be fixed by fitting the cross section contributions of the negative resonance to the best values of the thermal total and capture cross sections. The capture width of the negative resonance can generally be chosen as equal to the average value obtained from the measured Γ of the positive energy resonances, which according to the third condition above obey rather narrow distributions. Best values of $\sigma_T(E)$ are obtained by simple averaging of the experimental values and $\sigma_n(E)$ as the difference $\sigma_T(E) - \sigma_\gamma(E)$.

For the most important fissionable nuclei generally pointwise and thermal experimental values for σ_T , σ_f , α (or η) and occasionally pointwise σ_n values are available, from which one has to construct an internally consistent set of "best" cross sections as a function of the neutron energy. Obviously the evaluation procedure to be chosen depends on the available data types. Most commonly $\sigma_T(E)$ and $\sigma_f(E)$ can be fixed by averaging experimental data, $\sigma_n(E)$ be derived from experimental data or from resonance theory,

$\sigma_f(E)$ be obtained by subtraction and $\alpha(E)$ as the ratio $\sigma_f(E)/\sigma_f^Y(E)$. The quantity η important for the determination of the fuel conversion capability of a reactor can then be calculated from α and best values of $\bar{\nu}$ which in turn can be derived from direct measurements at thermal energies. According to the most accurate available measurement due to Bollinger et al (1) on $\bar{\nu}(E)$ of Pu^{239} at thermal and epithermal energies, $\bar{\nu}$ is constant in this region and equal to the thermal value within experimental limits which are almost comparable with the best precisions of about 1% attainable in modern $\bar{\nu}$ measurements. Thus $\bar{\nu}$ may safely be taken as constant in the thermal and resonance energy ranges. Typical examples of evaluations of "best" thermal cross section values are the works of Westcott et al (2) and of Sher and Felberbaum (3). For evaluations of "best" energy dependent cross sections in the thermal range we refer to the works of Barrington et al (4) and Joanou and Drake (5) as typical examples.

The evaluation of cross sections in the resonance range of neutron energies generally presents much greater difficulties, particularly for fissionable nuclei. Typically transmission and partial cross section measurements of varying energy resolution are available which subdivide the resonance range in two parts, one in which almost all of the neutron resonances are resolved and another one at higher energies in which the experimental overlapping of the resonances, due to the finite energy resolution and/or to the increasing importance of higher l-wave resonances, does not allow the interpretation of the measured cross sections in terms of individual resonances. Because the experimental energy resolution is never exactly monochromatic, the true physical limit between resolvable and overlapping resonances is higher than that attainable by experiment. In typical presently available high resolution transmission measurements resonances can be resolved in medium-weight nuclei up to several 100 KeV (6,7), in heavy nonfissionable nuclei to several KeV (8,9), in fissionable nuclei to a few 100 eV (10,11). Generally partial cross section measurements are more difficult and show worse resolution than transmission measurements. Thus resonance neutron widths derived from transmission measurements are generally known to higher neutron energies than partial reaction widths. The measured resolved resonance cross sections are almost exclusively and successfully interpreted in terms of various approximations to the general R-matrix theory of resonance reactions (12) developed in the past. In the overlapping resonance range only a parametrization of measured cross sections over groups of resonances is possible and concerning the energy dependence of the cross sections one has to rely on fluctuating, often discrepant, experimental results or on statistical theory estimates from average resonance parameters and statistical distributions. We consider these points in more detail below.

In medium-weight nuclei at present the experimentally resolvable resonance range generally ends below the lowest inelastic scattering threshold. The total cross section is almost equal to the scattering cross section, the capture cross

section being only a small component. Thus the σ_T measurement can be described by the R-matrix theory simplified to only one open channel, i.e. the elastic scattering channel, with various subchannels according to different allowed combinations of neutron orbital and resonance total angular momenta (6,13,14). In addition σ_Y measurements are available, which generally reveal more higher l-wave resonances for which Γ_Y is larger than Γ_n . These can generally be interpreted by superposition of single level Breit-Wigner terms.

An evaluation of the nuclear data must specify the resonance parameters including total and partial widths and resonance spins and the energy dependence of σ_T , σ_Y and σ_n . As far as possible resonance parameter and cross section "best" values should be mutually consistent. The σ_T measurements generally agree within experimental error, except mainly for differences introduced by different energy resolutions; for example a better resolved measurement might reveal more resonances than a worse resolved one. The σ_Y measurements, however, often show great differences in resolution and large systematic discrepancies which in the simplest cases are due to wrong normalization or impurity admixtures in the samples; as a typical example we discussed recently various discrepant σ_Y measurements in the keV range on Fe (15). Now most commonly neutron widths corresponding to the analysis of the best resolved σ_T measurement or weighted averages of neutron widths from different, about equally well resolved, σ_T measurements are taken as "best" values and the natural line shape of the scattering cross section is recalculated from these neutron widths. In the case of several measurements this simple procedure obviously is only allowed if the analysis of all these measurements has been done with the same and correct theory. This is not always the case. For example, transmission measurements on medium weight nuclei in the past have often been interpreted by the so called Bethe formula (16) (see e.g. references (17) and discussion in reference (14), section III 1) for which the scattering matrix is not unitary and, which is inadequate to describe the often observed complex interference between different scattering resonances as does the correct one channel multilevel formula. In such a case a reanalysis of the measurement concerned in terms of the correct theoretical description has to be done, before it can be combined with other analyses to "best" data. The difficulties in the evaluation of Γ_n and $\sigma_n(E)$ are generally small compared to those encountered in the evaluation of Γ_Y and $\sigma_Y(E)$. In most cases one can not simply average the existing σ_Y measurements, because the discrepancies due to systematic errors can only rarely be removed. Then one has essentially to select one experimental data set by a critical judgement of the different experiments or by nuclear systematics considerations or just by physical imagination and to take over the Γ_n corresponding to this data set from the experimental analysis or to do oneself this analysis. Then one can calculate $\sigma_Y(E)$ in the natural line shape from these Γ_n and the Γ_Y from the transmission measurements. For those higher resonances, for which only the Γ_n are available and, for which the σ_Y measurements do no more allow a resonance analysis in terms of Γ_Y , the average of the

known Γ_Y for the lower resonances can be taken. In many cases up to recent days the σ_Y measurements were even too crude as to allow an interpretation in terms of resonance Γ_Y . In those cases assuming an infinitely large number of exit channels in capture, and a corresponding constant Γ_Y from resonance to resonance, one could choose measured values of the non- $1/v$ capture resonance integral or of the capture cross section at thermal energy recalculated from resolved resonance contributions or interpolations between known $\bar{\Gamma}_Y$ of neighboring nuclei using the fact of the rather smooth A-dependence of Γ_Y in order to get an estimate of $\bar{\Gamma}_Y$ for a given isotope. As an example we derived $\bar{\Gamma}_Y$ for the main ^{60}Ni isotopes from known isotopic thermal σ_Y values and calculated $\sigma_Y(E)$ from these $\bar{\Gamma}_Y$ and known Γ_Y values up to a few 100 keV (Y14, section III X). We leaveⁿ aside here additional difficulties introduced by the problems of isotopic and spin identification of resonances in elements consisting of several similarly important isotopes.

Heavy nonfissionable nuclei like Th^{232} or U^{238} represent up to a few keV, where p-wave resonances become increasingly important, excellent examples of almost pure s-wave one level Breit-Wigner cross section shapes with very few exceptions in which small distances between neighboring large resonances occur. At epithermal energies, due to the average increase of Γ_Y with \sqrt{E} and the constancy of Γ_n , the capture process dominates, whereas with increasing neutron energy the elastic scattering becomes more and more prominent. Mostly σ_T measurements for various sample thicknesses, allowing an interpretation of the resonance in terms of Γ_n and Γ_Y , and also some σ_Y measurements, which together with the σ_T^n measurements allow a direct determination of Γ_Y , are available. The fact that the resonances are so narrow and far apart explains the rather good agreement in the resonance parameters derived from earlier worse resolved and modern high resolution measurements. Thus best values of resonance parameters are mostly easily obtained (sometimes after rejection of statistical scatter erroneously interpreted as resonances) by weighted averaging of the individual experimental results. Generally Γ_n are determined to much higher energies than Γ_Y . As the measured $\bar{\Gamma}_Y$ correspond to the theoretically expected narrow distributions it is justified to assume the average of the known Γ_Y for those resonances for which Γ_Y is not known. Then $\sigma_n(E)$ and $\sigma_Y(E)$ can be calculated from a superposition of single level Breit-Wigner terms which are the same formulae generally used in the interpretation of the measured cross sections for these nuclei. Only in the vicinity of broad, closely lying resonances level-level interference needs to be taken into account in the scattering cross section. All other cross sections follow by well known formulae from these two.

The evaluation of consistent resonance parameter sets and cross sections for fissionable nuclei represents one of the most difficult, but simultaneously physically most interesting problems

in the evaluation field. This is particularly due to the very complex resonance structure, particularly of σ_f , to the generally very small level distance partly due to the superposition of two s-wave level sequences, to difficulties of spin assignment to resonances of those nuclei like U^{235} with high ground state spin and not very different g-factors. For the main fissionable isotopes many measurement series are available particularly for σ_T and σ_f and more recently also for η , α or σ_γ , and for σ_n . However, unfortunately, neither these measurements nor the resonance parameter sets derived from these measurements are generally in the desirable agreement. The reasons for these discrepancies are manifold: different normalization (e.g. in σ_f measurements), different energy scale, different energy resolution, different statistical accuracy, unsufficiently corrected background effects, etc. They reflect the great experimental difficulties involved particularly in the partial cross section measurements on fissionable nuclei. Furthermore, only very few of the available measurement series yield enough information for the derivation of a complete set of widths and quantum numbers of a given resonance. Finally a whole series of different shape and area resonance analysis methods and various approximations to the many-channel R-matrix theory, ranging from the still most frequently used simple one level formula over the many capture, few fission channel approximations due to Vogt (18) and to Reich and Moore (19,20) to the most sophisticated many-level analyses of Adler and Adler (21). Because of these differences and discrepancies, an evaluation, in a strict sense, would have to go back to the original data, try to understand as much of these discrepancies, to reconcile as far as possible different measurements of the same quantity, select the measurements according to their quality in statistical scatter, resolution, etc., to analyze the selected data sets in terms of one and the same appropriate approximations to the R-matrix theory. Taking into account the different Doppler and energy resolution broadening of the resonances in different measurements, a set of "best" resonance parameters would be derived and the partial and total cross sections be recalculated. The excellent work of Adler and Adler (21) on U^{235} resonances shows how much labor is involved in such a thorough evaluation.

Most of the existing evaluations are based on less sophisticated and laborious methods. They use the fact that the one level interpretation yields resonance half widths not very different from the multilevel results, that most of the experimental resonance analyses use the one level formula and that (particularly with the exception of U^{233} and Pu^{241} resonances) the main part of the resonance fission cross section in the vicinity of the resonance peaks (except in the dips between the resonances, where interference effects become important) can be rather satisfactorily described by the one level formula. Several simple methods, based on extensive applications of the one level formula, for the derivation of complete parameter sets for a given resonance from various carefully preselected

experimental sources are discussed in reference (14), sections IV 1 and IV 3. We consider only one typical example. Given an isolated resonance η in the resonance peak represented by

$$\eta \approx \bar{v} \frac{\sigma_{of}}{\sigma_{o\gamma} + \sigma_{of}} = \bar{v} \frac{\Gamma_f}{\Gamma_\gamma + \Gamma_f} = \bar{v} \frac{\Gamma_f}{\Gamma - \Gamma_n} \quad (1)$$

(σ_{of} , $\sigma_{o\gamma}$ = peak fission and capture cross sections of the resonance considered). σ_{of} and Γ can be determined from a combined area and shape analysis of measured σ_f values. Considering that in the one level approximation

$$\sigma_{of} \Gamma = \sigma_o \Gamma_f = 4\pi \kappa^2 (E_o) \frac{g_j \Gamma_n \Gamma_f}{\Gamma} \quad (2)$$

(E_o = resonance energy, κ = reduced neutron wave length, g_j = statistical weight factor) and inserting Γ_f from equation (1) one gets for Γ_n the following quadratic equation

$$\Gamma_n \left(1 - \frac{\Gamma_n}{\Gamma}\right) = \Gamma_n^1 = \frac{(\sigma_o \Gamma_f) \cdot \bar{v}}{2\pi \kappa^2 (E_o)} \quad (3)$$

where we have set $g_j = 1/2$. Equation (3) is easily solved to give

$$\Gamma_n = \frac{1}{2} \Gamma \left\{1 - \sqrt{1 - 4 \frac{\Gamma_n^1}{\Gamma}}\right\} \quad (3a)$$

Γ_f then follows from equation (1) and Γ_γ from the difference $\Gamma - \Gamma_n - \Gamma_f$. Having established in this way complete one level parameter sets for the available resolved resonances, one can now calculate partial and total cross section, α and η "best" values with the same one level formulae in natural line shape.

We next consider briefly the region of overlapping resonances. In medium weight nuclei "best" σ_T values are usually obtained from the best resolved measurements available which follow most closely the true physical fluctuations of the cross section. For σ_γ some sophisticated average through generally differing experimental data has to be chosen. Also inelastic scattering to the lowest excited levels sets in. We consider the inelastic scattering further below. σ_n is usually obtained by subtraction of the sum of the other partial cross sections from σ_T . For the calculation of energetic self shielding factors for the overlapping

resonances, average (elastic and inelastic) neutron and capture widths, (elastic and inelastic) strength functions and average level spacings for different (ℓ, J) combinations and as functions of the neutron energy must be made use. Here the simplest possible way is to take Γ_γ independent from ℓ, J and E . Appropriate optical potentials to a "best" description of an average through the experimental σ_T values and of measured elastic scattering angular distributions are determined in order to derive the strength functions. The appropriately parameterized Fermi gas model is used for the prediction of the energy and spin dependences of the average level spacing. The average scattering widths are then obtained from strength functions and average level spacings.

In heavy nonfissionable nuclei the overlapping resonance range, in which cross section fluctuations outside statistical error can be observed, covers s- and p-wave neutrons. The cross sections in this range are either directly taken from experiment or calculated from average s- and p-wave resonance parameters and statistical distributions. Generally a statistical theory obtained from averaging single level Breit-Wigner terms is sufficient and average interference terms can usually be neglected as far as the condition $\Gamma/D < 1$ is met ((14), section II 2). The understanding of the usual discrepancies between different σ_γ measurements again represents the main problem here. Average s-wave resonance parameters ($\Gamma_n, \Gamma_\gamma, D$) are generally directly derived from the parameters of the resolved resonances, the p-wave strength function follows from fits of statistical theory expressions to averaged experimental σ_T values in the keV range. The energy dependence of Γ_n is specified by the well known centrifugal barrier penetration factors, the energy and resonance spin dependences of D again by an appropriate Fermi gas model. The parity dependence of D has been shown by Ericson (22) to be very small and is usually neglected. Commonly Γ_γ is assumed to be independent of ℓ and J ; for U^{238} the equality of s- and p-wave capture widths appears to be confirmed within experimental accuracy by the p-wave resonance measurements of Thomas and Bollinger (23). The level spacings for each individual resonance sequence are assumed to obey a Wigner distribution and the reduced neutron widths a Porter-Thomas distribution, assumptions which are well verified by the existing experiments (see, e.g., (24)). For nuclei with a ground state spin $I = 0$ it happens that for certain $\ell > 0$ resonance series the same resonance J value is reached by combinations of ℓ with the two different channel spins $j_\pm = I \pm 1/2$. Under the probably justified assumptions that possible interactions between nuclear and neutron spins are small and can be neglected and, that no correlations exist between $\Gamma_{n j+}^J$ and $\Gamma_{n j-}^J$, the reduced neutron widths

$$\Gamma_n^{(o)\ell j} = \sum_{j=i-1/2}^{i+1/2} \Gamma_{n j}^{(o)\ell j}$$

of such (ℓ, J) resonance series obey a χ^2 distribution with two degrees of freedom (see, e.g., (25)). Interpretation of evaluated resonance capture widths in terms of χ^2 distributions generally yields large numbers of exit channels, typically ranging from 20 to 40 corresponding to rather narrow distributions. Therefore in the calculations one uses almost exclusively constant capture widths in accord with a δ -function distribution. The same parameters from which the average energy dependence of the cross sections is calculated, serve in the calculation of Doppler coefficients and of temperature dependent energetic self shielding factors in the unresolved resonance range.

Whereas for fissionable nuclei almost all what has been said for non-fissionable nuclei remains true, a large additional difficulty is introduced by the fission component. We need only to remember the recent measurements (26-28) strongly deviating from former experiments and the discussions still not completed concerning the energy dependence of α and σ_f for Pu^{239} in the higher eV and lower keV energy range (26,28) in order to demonstrate the difficulties in evaluating "true" $\sigma_f(E)$ and $\alpha_{\bar{f}}(E)$ values in the unresolved resonance range. For estimates of $\bar{\Gamma}_f^{\ell J}(E)$ ($\ell = 0, 1$) several ways are possible. Usually one relies completely on the well known channel theory formula

$$\frac{2\pi \cdot \bar{\Gamma}_f^{\ell J \pi}(E)}{D^{\ell J \pi}(E)} = \sum_i \frac{1}{1 + \exp \left\{ 2\pi \frac{E_i^{\ell J \pi} - E}{\hbar \omega_i^{\ell J \pi}} \right\}} \quad (4)$$

($E_i^{\ell J \pi}$, $\hbar \omega_i^{\ell J \pi}$ = position and width of the i -th saddle point state belonging to the same J, π) valid for saddle point shapes of inverted harmonic oscillators and has then to specify barrier positions and widths from saddle point state systematics (29,30) and/or fission threshold experiments (31,32). Otherwise one uses this procedure only for p-wave neutrons and takes equation (4) for s-wave neutrons with a most probable spin independent barrier width of about 500 keV (see, e.g., (31)) and fixing the saddle point positions by the $\bar{\Gamma}_f$ values calculated from the resolved resonance Γ_f . Also "best" values of $\alpha(E)$ can be used in order to fix $\bar{\Gamma}_f(E)$ with or without specification of the spin dependence ((14), sections IV 1 and IV 3, (33)). Finally combinations of these procedures are possible. In every case, however, one has to assure that on the average statistical theory cross section estimates from the average resonance parameters are or become consistent with the cross section "best" values derived from the experimental data.

Evaluation principles and methods in the fast neutron energy range are generally not as difficult and are well known. So we can be rather brief here. Neutron interactions in medium weight nuclei in addition to those already described before are inelastic

scattering and absorption processes like (n,p) and (n,α) . The inelastic scattering range is subdivided into two subranges. The lower goes from the lowest threshold generally to several MeV, where either measurements of individual level excitation cross sections are available or, where positions, spins and parities of the rest nucleus levels are known and enable rather reliable theoretical predictions of inelastic excitation cross sections by the theory of Hauser and Feshbach (33) with inclusion of the so called statistical fluctuation factors.

In the higher subrange above several MeV inelastic scattering to individual levels can not more be specified experimentally. Only broad energy distributions from inelastic scattering can be measured and interpreted or predicted by an evaporation model. Recent theoretical refinements of the level density expressions and parameters (34) particularly allow more sophisticated interpretations and predictions of "continuous" inelastic scattering spectra than the older evaporation formulae (see e.g. (35)). In the evaluation of the experimental data for σ_n^{exc} one has to pay particular attention to whether the measurements have been corrected for multiple scattering and for neutron attenuation in the sample in order to get no overestimates. We refer here, for example, to an extensive discussion of available σ_n^{exc} measurements on Fe in reference (14), section V 3. The total σ_n in the "continuum" range are generally not directly measured and have therefore to be derived from the difference $\sigma_\chi - \sigma_p - \sigma_\alpha - \sigma_{2n} - \sigma_\gamma - \dots$. As to $\sigma_p(E)$ and $\sigma_\alpha(E)$ one has still to rely as far as possible on experimental data which, however, are often discrepant by different normalization. The statistical theory for these processes, in spite of the progress made (see, e.g., (36)), is apparently still not able to describe measured cross sections within experimental accuracy and thus to make reliable predictions of unknown cross sections (see reference (14), section V). σ_n is generally derived as the difference $\sigma_T - \sigma_\chi$.

Unfortunately the quality and energy resolution of the available measurements for different processes are quite different. In a typical example σ_T might still show physically real fluctuations outside statistical scatter, whereas for a partial cross section or σ_χ at most only a few broadly resolved points are available. This inconsistency between different experimental data sets is also reflected by evaluated data sets--it leads particularly to "local" errors in those data like σ_n which are obtained by subtraction and not from direct experimental information. Unfortunately the refolding of an experimental data set of bad resolution to the good resolution of a transmission measurement is generally either not possible or at least not unique.

For heavy fertile and fissionable nuclei one has in addition to do particularly with $\sigma_f(E)$ and $\bar{\nu}(E)$. For fast energies there is generally much better agreement between different σ_f

measurements than in the keV range. The evaluation of $\bar{\nu}(E)$ for a nuclide presupposes the derivation of basic $\bar{\nu}$ standards from the available experimental data and the renormalization of the experimental $\bar{\nu}$ values to these standards. Concerning the gross structure the available experimental information appears to indicate that the energy dependence of $\bar{\nu}$ can be represented over the whole energy range by a simple second or third degree polynomial in E or by piecewise linear approximations, the free parameters being fixed by a least squares adaptation to the experimental data. However, by this procedure possible fine structures in $\bar{\nu}(E)$ like those observed by Blyumkina et al (37) on U^{235} in the several 100 keV range (but not confirmed by the authors, see (14), section VI 1 g) and attributed to fission channel effects get lost.

Elastic scattering angular distributions in medium weight and heavy nuclei are generally isotropic in the center-of-mass system up to energies of the order of 10 keV where s-wave scattering is predominant. In the resonance range in medium weight nuclei composed of resonances with different ℓ and J values the experimental information on $\sigma_n(E, \theta)$ is still not detailed enough and "best" values of $\sigma_n(E, \theta)$ have to be evaluated from a rather restricted number of measured distributions. In heavy nuclei with the much larger level density $\sigma_n(\theta)$, within the experimentally possible resolutions, is already a rather smooth function of the neutron energy in the keV range. In the MeV range, as is well known, the optical model with appropriate parameterization is able to reproduce the few available $\sigma_n(\theta)$ measurements about within experimental accuracy and can thus be used rather reliably for interpolations and predictions of $\sigma_n(\theta)$.

From the available integral data generally only those rather few which might be called "clean" can directly be used in the evaluation of "best" microscopic data. By "clean" integral data we mean those in which no spatial dependence enters and, in which directly in the experiment and/or afterwards by corrections, the neutron energy spectrum is completely and uniquely specified as a simple function of the neutron energy, and from which one can draw unique conclusions to certain microscopic nuclear data. Typical quantities are the infinite dilute non-1/v capture or activation resonance integral already mentioned above which can be used for the estimate of an average capture width, and measurements of average (n,p) or (n, α) cross sections in a fission spectrum, which can be used for renormalization of $\sigma_p(E)$ or $\sigma_\alpha(E)$ data.

The reliability of evaluated nuclear data sets can more and more be tested by comparison of calculations, in which these data are converted to groups constant sets, and measurements of integral data like spectral indices, prompt neutron decay constants, fission and capture rate traverses, breeding ratios and others in critical facilities (38,39). Particularly the effect of new measurements

of important cross sections, whose results deviate from the evaluated "best" data (44) on the prediction of integral measurements, is studied with "interim" group cross sections sets which differ from the respective "best" sets only in these new data, and yield a test of the reliability of these measurements (39). The results of those integral comparisons and tests give indications as to which microscopic "best" data might be in error and would have to be reinvestigated. Several computer programs have recently been developed (40-43) which allow an adjustment of group constants by fits to sets of measured integral data. However, the feedback from those integral data to differential data or even only to group constants is generally not unequivocal; the adjustment may even lead to physically worse results. This has the consequence that different adjusted data sets are likely to fit a series of critical facility measurements equally well. Furthermore one cannot be sure that such a group cross section set adjusted for critical facility data will allow more correct predictions of the physical properties of large power reactors. Therefore, in order to get better approximations to the physically true cross section shape which, on the nuclear data side of the problem, alone can guarantee throughout correct reactor physics calculations, we would prefer a thorough reevaluation of the basic microscopic data rather than a computerized group cross section adjustment.

REFERENCES

1. L. M. Bollinger, R. E. Cote, G. E. Thomas, Geneva Conf. 1958, P/687; Proceed. Vol. 15, p. 127.
2. C. H. Westcott, K. Ekberg, G. C. Hanna, N. J. Pattenden, S. Sanatani, P. M. Attree, IAEA Atomic Energy Review 3, 1, 1965.
3. R. Sher, J. Felberbaum, BNL - 918 (EANDC(US)-75"U"), 1965.
4. E. P. Barrington, A. L. Pope, J. S. Story, AEEW - R - 351, 1964.
5. G. D. Joanou, M. K. Drake, GA - 5944 (NASA CR - 54263), 1964.
6. C. D. Bowman, E. G. Bilpuch, H. W. Newson, Ann. Phys. (N.Y.) 17, 319, 1962.
7. S. Cierjacks, P. Forti, D. Kopsch, L. Kropp, H. Unseld, IAEA Conf. on Nucl. Data for Reactors, Paris, October 1966, Proceed. Vol. I, p. 444; S. Cierjacks, Ph. D. thesis, unpublished.
8. J. B. Garg, J. Rainwater, J. S. Petersen, W. W. Havens, Jr., Phys. Rev. 134 B, 985, 1964.
9. W. Kolar, K. H. Böckhoff, EANDC(E)-86"AL", 1967.
10. A. Michaudon, H. Derrien, P. Ribon, M. Sanche, Nucl. Phys. 69, 545, 1965.

11. C. A. Uttley, EANDC(UK)-40"L", 1964.
12. A. M. Lane, R. G. Thomas, Rev. Mod. Phys. 30, 257, 1958.
13. G. Rohr, Nucl. Phys. A104, 1, 1967.
14. J. J. Schmidt, KFK-120 {EANDC(E)-35"U"}, part I, 1966.
15. J. J. Schmidt, IAEA Conf. on Nuclear Data for Reactors, Paris, October 1966, Proceed. Vol. II, p. 279.
16. H. A. Bethe, Rev. Mod. Phys. 9, 69, 1937; H. A. Bethe, G. Placzek, Phys. Rev. 51, 450, 1937.
17. C. T. Hibdon, Phys. Rev. 118, 514, 1960; Phys. Rev. 122, 1235; 1961; Phys. Rev. 124, 500, 1961.
18. E. Vogt, Phys. Rev. 112, 203, 1958; Phys. Rev. 118, 724, 1960.
19. C. W. Reich, M. S. Moore, Phys. Rev. 111, 929, 1958.
20. M. S. Moore, C. W. Reich, Phys. Rev. 118, 718, 1960.
21. D. B. Adler, F. T. Adler, ANL - 6792, 695, 1963
Conf. on Neutron Cross Section Technology, Washington,
March 1966, Proceed. Vol. 2, p. 873; final report Sub-
contract AEC - BNL - 006977, 1966.
22. T. Ericson, Advances in Phys. 9, 444, 1960.
23. G. E. Thomas, L. M. Bollinger, EANDC Conf. on the Study of
Nucl. Structure with Neutrons, Antwerp. 1965, P/96.
24. J. J. Schmidt, ANS National Topical Meeting on Reactor
Physics in the Resonance and Thermal Regions, San Diego,
February 1966, Proceed. Vol. II, p. 223.
25. C. E. Porter, R. G. Thomas, Phys. Rev. 104, 483, 1956.
26. P. H. White, J. G. Hodgkinson, G. J. Wall, J. Nucl. En.,
Pts. A/B, Reactor Sci. Techn. 19, 325, 1965.
27. M. G. Schomberg, M. G. Sowerby, F. W. Evans, IAEA Sympos.
on Fast Reactor Physics and Related Safety Problems,
Karlsruhe, November 1966, paper SM-101/41.
28. W. B. Gilboy, G. F. Knoll, IAEA Conf. on Nucl. Data for
Reactors, Paris, October 1966, Proceed. Vol. I, p. 295.
29. J. E. Lynn, IAEA Conf. on Nucl. Data for Reactors, Paris,
October 1966, Proceed. Vol. II, p. 89.
30. J. J. Griffin, IAEA Seminar on the Physics and Chemistry
of Fission, Salzburg, March 1965, Proceed. Vol. I, p. 23.
31. J. A. Northrop, R. H. Stokes, K. Boyer, Phys. Rev. 115,
1277, 1959.

32. H. C. Britt, F. Plasil, Phys. Rev. 144, 1046, 1966.
33. W. Hauser, H. Feshbach, Phys. Rev. 87, 366, 1952.
34. A. Gilbert, A. G. W. Cameron, Can. J. Phys. 43, 1446, 1965.
35. J. M. Blatt, V. F. Weibkopf, Theoretical Nuclear Physics, J. Wiley and Sons, New York, 1952, chapter VIII.
36. H. Büttner, A. Lindner, H. Meldner, Nucl. Phys. 63, 615, 1965.
37. Y. A. Blyumkina et al., At. Energ. 15, 64, 1963; translated in Sov. J. At. En. 15, 725, 1964; Nucl. Phys. 52, 648, 1964.
38. D. Stegemann et al., IAEA Sympos. on Fast Reactor Physics and Related Safety Problems, Karlsruhe, November 1967, paper SM-101/8 (KFK 626, EUR 3670 e).
39. H. Küsters et al., IAEA Sympos. on Fast Reactor Physics and Related Safety Problems, Karlsruhe, November 1967, paper SM-101/12 (KFK 628, EUR 3672 e).
40. P. C. E. Hemment, E. D. Pendlebury, Int. Conf. on Fast Critical Experiments and their Analysis, Argonne, October 1966, ANL-7320, p. 88.
41. A. Pazy, G. Rakavy, Y. Reiss, Y. Yeivin, IAEA Conf. on Nucl. Data for Reactors, Paris, October 1966, Proceed. Vol. II, p. 309.
42. G. Rakavy, Y. Reiss, D. Samoucha, Y. Yeivin, IAEA Sympos. on Fast Reactor Physics and Related Safety Problems, Karlsruhe, November 1967, paper SM-101/41.
43. L. N. Usachev, S. M. Zaritsky, IAEA Conf. on Nucl. Data for Reactors, Paris, October 1966, Proceed. Vol. II, p. 321.
44. W. P. Pönitz, D. Kompe, H. O. Menlove, K. H. Beckurts, IAEA Sympos. on Fast Reactor Physics and Related Safety Problems, Karlsruhe, November 1967, paper SM-101/9 (KFK 635, EUR 3679 e).

Neutron Data Compilation at the
International Atomic Energy Agency

by H. D. Lemmel, P. M. Attree, T. A. Byer*,
W. M. Good, L. Hjaerne**, V. A. Konshin, A. Lorenz

IAEA Nuclear Data Unit
Kaerntnerring 11, A-1010 Vienna, Austria,

ABSTRACT

The paper describes the present status of the neutron data compilation center of the IAEA Nuclear Data Unit, which is now in full operation. An outline is given of the principles and objectives, the working routines, and the services available within the two-fold functions of the Unit:

- a) to promote cooperation and international neutron data exchange between the four major centers at Brookhaven, Saclay, Obninsk and Vienna, which share responsibilities in a geographical distribution of labour;
- b) to collect systematically the neutron data arising from countries in East Europe, Asia, Australia, Africa, South and Central America and to offer certain services to these countries.

A brief description of DASTAR, the DATA STOrAGE AND RETRIEVAL system, and of CINDU, the data CATALOG of the IAEA NUCLEAR DATA UNIT, is given.

* member of the IAEA Nuclear Data Unit since February 1968

** member of the IAEA Nuclear Data Unit since December 1967

Before entering upon a description of the data center activities at IAEA, it is perhaps well to state some views about objectives. These are: (a) that data taken at considerable expense should be made available immediately to the scientific and technical community - by no means should they become inaccessible or lost; (b) that data centers should offer a variety of services, so that various data users can exploit the data files; (c) that the local and regional data centers should be well coordinated within an international data system, in order to furnish greatest access to data with minimum duplication of effort. I should like to give an outline of our activity as a data center at IAEA.

The Nuclear Data Unit of the IAEA was established in 1964 on the recommendation of the International Nuclear Data Committee, to help promote the compilation and distribution of the growing fund of neutron data. In 1965, the IAEA Nuclear Data Unit began to contribute to the bibliographic index CINDA, and in 1966 it started acting as a neutron data center. The world-wide responsibility of data collection and dissemination is now shared between four centers, in a geographical distribution of labour, whereby:

- The NNCSC at Brookhaven services the US and Canada, supplemented by the CINDA operations at DTIE Oak Ridge
- The ENEA Neutron Data Compilation Centre at Saclay (France) services countries in Western Europe and Japan
- The Informacionnyj Centr po Jadernym Dannym (Nuclear Data Information Center) at Obninsk services the USSR
- The IAEA Nuclear Data Unit in Vienna services countries in Eastern Europe, Asia, Africa, South and Central America, Australia and New Zealand (referred to later as the IAEA service area).

This division of the world's neutron data compilation is significant and reasonable, because the problems to solve are specific for each area. These areas differ in their computer equipment, in their scientific interests, in the types of their laboratories and potential data users, and in their geographical and political situation, so that different services are required in each area. On account of these regional differences, it seems evident that it is at present not possible to strive for identical compilation systems in all centers. However, it is both essential and possible to create a common interface for data transfer between the centers.

The responsibilities of the IAEA Nuclear Data Unit have two aspects: (a) to promote data exchange between the four data centers, and (b) to compile and disseminate data within the IAEA assigned service area. First priority has been given so far to the international

exchange and coordination, which the IAEA sought to achieve through consultants' meetings between the four centers. Compilation within the Agency's service area is now being given comparable emphasis. In this area, the number of interested laboratories and the data flow from and to them is increasing.

With our dual responsibility in mind, we developed a data storage and retrieval system, which was designed after studying the experiences of Brookhaven and Saclay, with whom we consulted. I wish now to explain the most significant features of our system, which has been in operation since October 1966.

The system consists essentially of two main files: the data file, DASTAR (= DATA STORAGE AND RETRIEVAL), and a CINDA type index file, called CINDU (= Catalog of the IAEA Nuclear Data Unit). Periodic expanded prints of the index of this dual system provide a computerized publicizing medium for the stored data which is identified by means of accession numbers, called DASTAR-numbers. It is thus possible that scientific papers could not only quote references to, e. g., Atomnaja Energija vol. 20 p. 8, but also to DASTAR-00322 version 2. A reference to a data set in this way is unique; it would, of course, not replace the reference to a printed article, but only supplement it.

The data file DASTAR is characterized by two main features:

- (1) It has a completely flexible format. Thus, we are able to store every piece of data without any loss of information. In general, we store all data in its original format, as we receive it, table by table and unmerged. Format conversions which need manpower and may introduce mistakes, are avoided. However, with each data set the FORTRAN format statement is stored, so that automated data processing, plotting, etc., is possible.
- (2) Numerical data are of little value if they are not accompanied by a minimum of explanatory comments including information on normalization, corrections, definitions, etc. We do not store any data set without such comments.

The CINDU file serves a variety of different functions:

- (1) A printed version of CINDU is published about quarterly as a means of announcing new results. A data compilation is of little value if its contents are not known. The value of this publication is evidenced by the fact that data requests which refer directly to CINDU are increasingly frequent.
- (2) CINDU furnishes a bibliography to each data set. Care is taken that this bibliography is complete. It is possible to retrieve data not

only by a main reference but by any secondary reference as well.

(3) CINDU is the DASTAR retrieval organ. It is a compact source of information upon which retrievals are most commonly made, such as by element, isotope, quantity, energy, date, laboratory, references, authors, etc. It is linked to the data files by accession numbers. This separation of data and index is efficient and eliminates time consuming searches through large data files for single sets of data. Entry is also efficient because an index entry can be made even before data entry is complete. CINDU-6 which was printed November 21, indexes data which were received on November 20.

(4) The data index CINDU allows various specialized data files to be kept, all indexed by accession-numbers. E.g., resonance parameters, thermal scattering data, gamma spectra, etc., seem to require different files but could all be retrieved from the same central index CINDU.

(5) CINDU, perhaps with minor modifications, could be extended to an international index referring to various local data files.

Important though systems and computer operations may be, there are also certain practices which we have also found to be of importance. I want to mention only two:

(1) A most important routine, we find, is to send proof-copies of the data sets to the authors. The purpose is not to relieve the data center from checking responsibility, but to make as sure as possible that everything is correct and nothing has been lost. A by-product of the practice is that authors tend to take increased interest in the data compilation, and higher accuracy is assured. The value of the proof-copy principle is shown by the fact that about one in every eight data sets undergoes correction by the author, sometimes on account of unpublished revisions of the data, sometimes on account of misprints in the printed literature.

(2) Detailed records are maintained to determine the data flow; these records show what data have been sent to whom. This makes it possible to send data revisions automatically to all recipients of the earlier versions. This service, which is of essential interest to both data users and producers, reduces "noise" in the data files, which has been part of the general criticism against data centers.

This was a brief outline of the DASTAR-CINDU system. The entire work, including designing and programming the system, as well as compiling and disseminating over 100,000 data points, preparing plots, etc., was done essentially by two physicists and a part

time programmer within a year. The system is sufficiently flexible that additional features can be added as need arises. In particular, we are considering adding features which might be required for better compatibility between the systems of the various data centers, at the present especially in connection with the new plans at Brookhaven. An essential need for effective exchange between centers at the present time is a joint data index, which could later on be combined with the bibliographical index CINDA. A consultants' meeting took place in Saclay in February 1968 to consider this problem and to recommend compatible formats, definitions, etc.

In summary, our present activities are: to promote the coordination between the four major neutron data centers, and to compile and disseminate data within our geographical service area, using the tools of CINDA, DASTAR and CINDU. These goals will need most of our efforts for the near future. Our experience indicates that services to data users are increasingly becoming obligations of the data center. From this point of view, more emphasis should be given to investigating and analyzing what services to offer. Thus, for example, for the experimenters, the centers from their vantage point should supply various types of transformations of data; for the evaluators, reactor physicists and designers, greater attention should be given to the exchange of evaluated data. In these ways it would be ensured that maximum profit could be drawn from the data on file.

THE ENEA NEUTRON DATA COMPILATION CENTRE

by

Victor J. Bell, Director ENEA Neutron Data Compilation Center
Gif-sur-Yvette, France

The ENEA Neutron Data Compilation Center (better known under its French abbreviation CCDN--Centre de Compilation de Donnees Neutroniques) was created in 1964 as one of two information centers within the Scientific Division of the European Nuclear Energy Agency. According to its Statute and Tasks, the principal objective of the Centre is to improve the collection and dissemination of experimental neutron data produced in Europe and elsewhere, so that the results of the very large effort being devoted in each country to the measurement of neutron cross sections may be made more readily accessible to all interested users.

To meet this objective, the Centre undertook a series of activities:

- a) the maintenance of the bibliographic reference index CINDA and the production and regular distribution of printed editions of this index;
- b) the collection and storage of experimental data in the SCISRS format and the retrieval and dissemination of sections of the data on request;
- c) the collection of evaluated data files to form a central library and the distribution of these files on request;
- d) participation in the development of improved systems for data storage and retrieval; and
- e) the production of Newsletters giving information on the activities of the Centre.

CCDN is financed by 12 European countries and Japan and is situated within the French CEA Research Center at Saclay. The Centre was originally headed by Dr. D. W. Colvin who, during his three-year period of leave from the United Kingdom Atomic Energy Authority, laid the foundations for the successful operation of the Centre. On the return last summer, of Dr. Colvin to the UKAEA, I was transferred from the ENEA Computer Program Library at Ispra to head the Centre, and Dr. S. Schwarz was appointed as Deputy Head of the Centre. At present the Center has an international staff of 17, which includes 5 physicists and 2 senior programmers. In addition, the Center is equipped with its own computer, an IBM 360/30, to enable it to fulfill its tasks, most of which are computer based.

A cooperative arrangement between the U.S. Atomic Energy Commission and the European Nuclear Energy Agency for the exchange of nuclear data provided a basis for the initial activities of the Centre. This resulted in the regular exchange of CINDA entries with the DTIE at Oak Ridge, the exchange of experimental data in the SCISRS format with the Sigma Center, and the exchange of evaluated data files with the evaluated data group at Brookhaven. With the creation at Brookhaven last summer of the National Neutron Cross-Section Centre by the amalgamation of the activities of the Sigma Center and of the evaluated data activities, this exchange has been simplified. The projected inclusion of CINDA under the NNCSC umbrella should eventually complete this picture.

Cooperation was extended beyond the limits of the above agreement by contacts with the International Atomic Energy Agency, which led to arrangements for collaboration between the Agency and the CCDN. This collaboration led to the widening of the exchange of CINDA entries to include contributions from the Obninsk Compilation Centre in the USSR and from the few remaining developed countries not otherwise covered by CCDN or the United States. As a result of this, CINDA 67 was published for the first time in November last year as a worldwide publication. In addition to this, experimental data is also now being exchanged through IAEA on a worldwide basis.

The present work of the Centre continues on the following three activities, which together cover the spectrum of nuclear data exchange. Firstly, the maintenance of the CINDA bibliographic file which contains some 50,000 references to theoretical work, experimental data, and evaluations in the neutron data field. Secondly, the maintenance of the SCISRS experimental data file which contains some 1,000,000 data points from some 10,000 experiments and, thirdly, the distribution of evaluated data files.

In CINDA efforts are being concentrated on the removal of some gaps in the coverage of the main journals and in removing duplicate entries to the same piece of work. This latter program arises because a given experiment is often reported in a variety of publications, from the original private communications, via the report, and journal, to the conference proceedings. These entries have to be grouped so that the most recent publication is the principal entry and previous publications are given as secondary entries.

In data storage a regular system for the compilation of data and for the exchange of update runs has now been established with the National Neutron Cross Section Centre at BNL. At present the latest experimental data within the Centre's area

of responsibility is obtained either by personal contacts or by regular coverage of the literature, so that it may be entered into the data file. To get an idea of the order of magnitude of this activity, the Centre codes about 50 references a month, has a backlog of about 350 references, and entered about 50,000 data points in the last twelve months.

As the services of the Centre have become more well known and the growing usefulness of the Master Data Tape appreciated, the number of requests for data and other information has steadily increased.

The data storage and retrieval activities of the Centre have been based on the development and implementation of the Interim Data Storage and Retrieval System. This System, which attempts to approximate the IBM 7090 SCISRS 1 system on the 360/30 has enabled the Centre to fulfill its data storage requirements and to offer a retrieval service from the data file. However, there are certain operational difficulties in its use, which leads the CCDN to consider alternative programs, and in particular the Centre is engaged in the experimental implementation of the ECSILE system of the Lawrence Radiation Laboratory, Livermore. This program, written in Fortran for IBM 7090, as a successor to SCISRS, merits careful consideration. It is available for distribution at the United States Code Center at Argonne and the ENEA Computer Program Library at Ispra, and CCDN recently received a copy of the version implemented on the CNEN computer installation at Bologna by Dr. Benzi and his team. The modifications made in Bologna enables the program to be implemented on any 7090 installation.

In the field of evaluated data, the library of evaluations has been extended by the release in September 1967 of the ENDF/B category 1 material, which now consists of 57 files.

The capture cross section files for fission products by Professor Benzi of CNEN-Bologna, have recently been amended and extended and the new version was made available in the Centre in January 1968.

The KEDAK files of Dr. J. J. Schmidt, of KFK Karlsruhe have been released and are available in the Centre.

Some new files of fission cross sections from the UK Nuclear Data Library were received from Winfrith. These will be included in the new version of the library which is to be released shortly. The same comment applies to the file on U-238 by Ravier and Vastel and to a new file on Cu, related to the work of Benzi and Haggblom.

The List of Available Evaluations, published as Newsletter No. 5 in April 1967, has been continuously updated and a new list is now in preparation and will be published as Newsletter No. 7 by the end of March. A certain concentration of the present evaluation activities is apparent, and most of the new contributions are related to the UK Nuclear Data Library, the ENDF/B file and the KEDAK library, or are at least produced in a format compatible with one of the above.

A critical survey of the He-3 cross sections was performed by a consultant at the Centre during June and July 1967. The report was published in Newsletter No. 6 in September. It is now, with minor changes, being printed in the journal "Nuclear Data".

Mentioning briefly the future work of CCDN, it is easier to prophesy than to translate these prophesies into achievements. However, in the short term, CCDN is occupied with improving its interim data storage and retrieval situation. In the longer term, it is considering participation in the developments taking place at the NNCSC on a new data storage and retrieval system, and also in the possible evolution of the bibliography CINDA to become the reference file within this new system. In fact, the problem is that of the association of the existing bibliography file with the existing data file in the context of the development of a new system.

In addition, the stage is now set for the worldwide collection and distribution of neutron data. The bibliographic index CINDA is now maintained and distributed on a worldwide basis. Experimental neutron data is being exchanged on a worldwide basis, although there remains the adoption of a common exchange format and the possible adoption of a common storage and retrieval system. The IAEA has so far been able to coordinate and organize this exchange of information, which the regional compilation centres at Brookhaven, Obninsk and Saclay have been able to collect. It is a tribute to the IAEA that so much progress has been made.

AN INTEGRATED SYSTEM FOR PRODUCING
CALCULATIONAL CONSTANTS FOR NEUTRONICS AND PHOTONICS CODES

R. J. Howerton
Lawrence Radiation Laboratory
Livermore, California 94551

Abstract

Input constants for neutronics and photonics calculations are derived from files of evaluated neutron and photon cross sections which are based largely upon compilations of experimental data. Of course, the objective of neutronics and photonics calculations is to obtain reliable values for a spectrum of measurable characteristics of more or less complicated engineered configurations.

The system described here is comprised of a data file of experimental values associated with neutron induced reactions, an evaluated neutron cross section file for 75 isotopes and elements, an evaluated photon cross section file for 87 elements, an evaluated library of light charged particle reactions, and sundry processing codes required for producing calculational constants for Monte Carlo, discrete ordinate, diffusion approximation, and other transport approximation neutronics and photonics codes. In addition, special Monte Carlo codes are used for checking the validity of the evaluated data files.

The compilation of experimental neutron data is linked to its bibliography by arbitrary accession numbers. The components of that part of the system which deals with experimental neutron values include the data compilation, two bibliographic listings, one ordered by alphabetical arrangement of the citation, the other by accession number, an author index, and three indexes or digests of the data compilation.

This is an exposition of the system used at the Lawrence Radiation Laboratory, Livermore, to produce calculational constants required for neutronics and photonics computer codes. We have, at each phase of development, investigated methods and sub-systems developed by others in an attempt to incorporate the best features of each in our own system design. A basic characteristic of a good system is the facility with which changes can be made as more detailed requirements are imposed by improvements in neutronics and photonics calculational techniques. These improvements are usually associated with advances in computer technology which allow better physical approximations in the calculational codes. We attempt to design each part of the system to be adequate for a period of, at least, three to five years with the understanding that major modifications or redesign of some parts of the system will then be necessary.

Figure 1 illustrates the sub-systems and flow of information. The boxes enclosed by solid lines are activities or sub-systems which have been implemented and those enclosed by dotted lines are still in the planning phase. Our major concern is with the data associated with neutron induced reactions and these are the only experimental data which we collect. There are about 450,000 data points currently in the ECSIL [1] (Experimental Cross Section Information Library) system and about 480,000 transmissions stored elsewhere in a similar library. The ECSIL system provides for storage, retrieval and display of the experimental data required to produce semi-empirical¹ cross section information.

The system SECSI deals with semi-empirical cross section information and currently contains values for about 75 isotopes and/or elements. Most of our production of semi-empirical information is done using graphs of experimental data produced on a Cal Comp Plotter which we have found to be adequate for our purposes.

¹ Because so many reaction cross sections and associated data must be estimated to provide the complete sets of values required for calculations, we prefer "semi-empirical" as a label for these values rather than "evaluated."

Apparent contradictions in the data are resolved by examination of the literature description of the experiment, consultation with the authors, if possible, or by judgments made on the basis of past experience.

As shown in Figure 1, some theoretical values such as optical model calculations for applicable energy and mass ranges are used. What is not shown in Figure 1 are two boxes which could be labeled "Systematics" and "Educated Guesses." Most cross sections for most isotopes of interest have not been defined by measurement and there are no reliable theoretical models which will calculate them. For some types of data, such as γ -Ray production cross sections and $n,2n$ reactions, empiricisms or recipes have been developed which are useful in certain ranges of the periodic table and incident neutron energies. These empiricisms are largely formalized systematics while "educated guesses" are usually informal systematics.

From the semi-empirical information, the calculational constants which are the ultimate output of the system are calculated or translated by the computer system SECS POT (Semi-Empirical Cross Section Processing or Translation). Both neutron and photon semi-empirical values are input to SECS POT. The photon information was taken from the work of groups at LRL and National Bureau of Standards, and the current tape library contains information on 87 elements for photon energies from one keV to 100 MeV.

For our own purposes we make Monte Carlo calculations of "k" values for an assortment of critical assemblies and neutron transport for bulk measurements. These calculations cannot tell us that our semi-empirical cross sections are right since compensating errors might result in a correct answer, but they may tell us if we are wrong. As indicated in Figure 1, there is no direct feedback to the semi-empirical information from the critical assembly or bulk measurement calculations. If discrepancies are apparent, a review of the semi-empirical values is instigated. It is emphasized, however, that the semi-empirical information is never adjusted purely on the basis of the calculations.

The bottom line of Figure 1 shows a parallel system to the ECSIL, SECSI, SECS POT chain for charged particles. W. T. Milner of the ORNL Charged Particle Information Center was kind enough to send us their experimental data tapes. We are in the final stages of implementation of a charged particle ECSIL system which has been produced mostly by machine translation of the CPX data tapes.

The system which has been described here was designed, wherever possible, to be relatively computer independent. All programs are written primarily in basic FORTRAN II because compilers for this language are available at most scientific installations. In addition, translation programs are more likely available for going from FORTRAN II to a subsequently developed language than in the other direction. The genesis of the current system has spanned the time interval from 1958 to the present. These ten years of accumulated experience have produced an adequate system for our purposes.

Reference

1. R. J. HOWERTON, W. J. CAHILL, K. L. HILL, D. W. THOMPSON, S. T. PERKINS, "ECSIL: A System for Storage, Retrieval and Display of Experimental Neutron Data," UCRL-50400, Vol. I, Lawrence Radiation Laboratory, Livermore (1968).

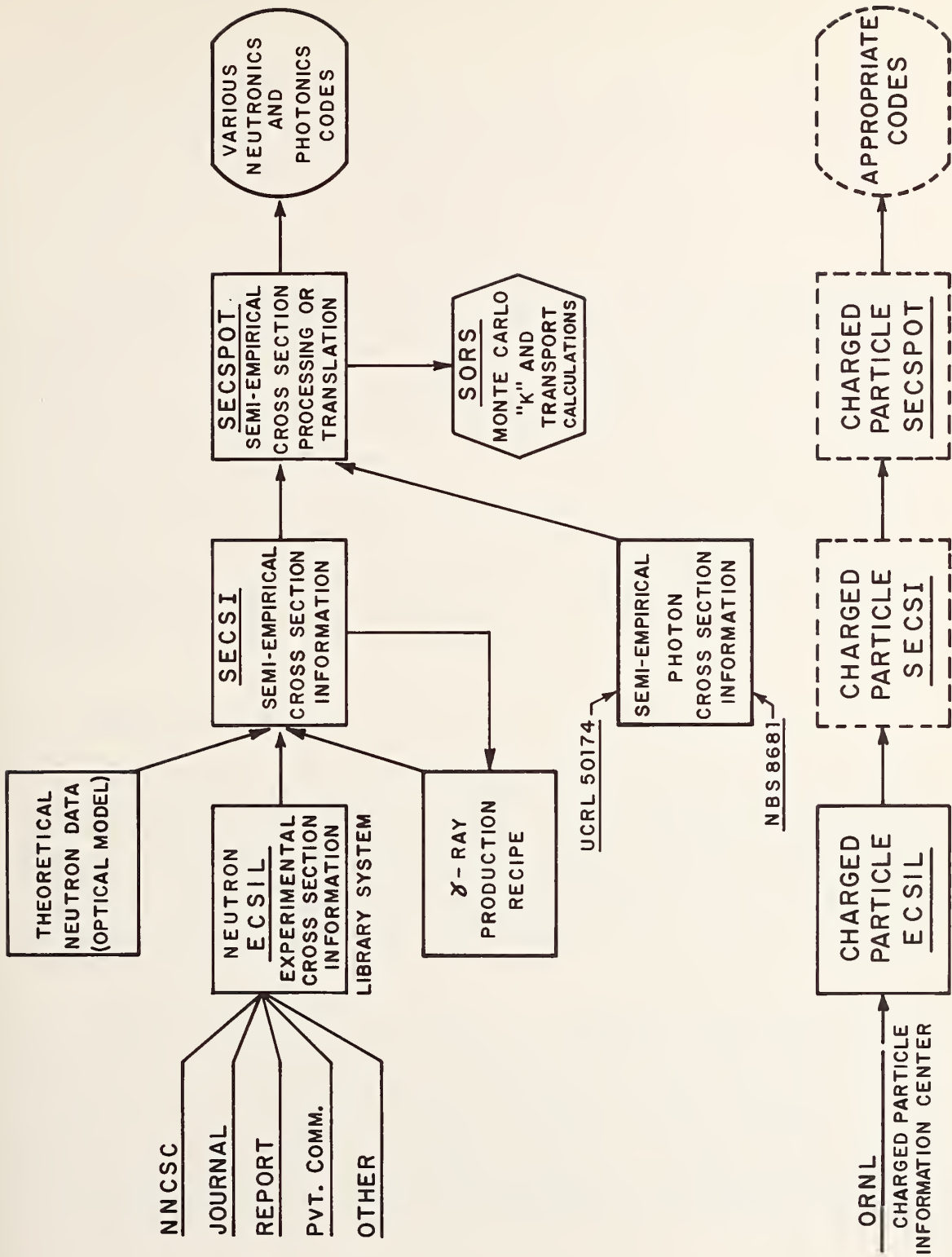


Figure 1 Schematic Outline of the System

T. Fuketa, Y. Nakajima, and K. Okamoto

Japan Atomic Energy Research Institute
Tokai-mura, Ibaraki-ken, Japan

ABSTRACT

A computer programme to make a computer file of resonance data (COMFORD) was prepared. In the COMFORD, the neutron resonance widths, average level spacings, strength functions, and so on are stored in a magnetic tape in order of atomic number. Different blocks of data for the same atomic number are stored in order of publication date and a control number which facilitates the identification of a data block. Symbols, which are equivalent to certain comments, can be attached to the individual numerical data in order to give an idea about the quality of the data, and these symbols may be used to classify the data when they are read out from the COMFORD. The primary purpose of the COMFORD is to use it as an input-data tape for variety of the computer analyses to investigate the statistical property of the neutron resonances; thorough and complete inclusion of all the published data is not intended for the present.

1. INTRODUCTION

Although the neutron resonance parameters are of a kind of the most well accumulated nuclear data, a yet more steady accumulation of the data of wider energy range, higher resolution, and various nuclides is required from the points of view of both reactor technology and nuclear physics. A marked increase in the number of resonances of which parameters are accurately known is requisite for the improvement of the present knowledge of the statistical property of the compound nucleus through the neutron-resonance data.

There are already a vast amount of the neutron-resonance data, and the amount is continuously increasing. Therefore, if those data have to be handled, it is natural to store and retrieve the data by a computer. We have prepared a computer programme "Computer File of Resonance Data (COMFORD)" which stores the neutron-resonance data in a magnetic tape and retrieves the stored data in the form of typed output. Three kinds of data are to be stored in the COMFORD tape: 1) the published data of which storage is started with the data of interest to the persons who want to look into or to make some analysis on those data, 2) the preliminary data,

*The work was performed as a part of the activities of the Japanese Nuclear Data Committee.

and 3) the data which are obtained by making some calculation, correction or averaging for example, on the original data which may have been stored already in the same COMFORD tape. A thorough inclusion of all the published data about the neutron resonances is not intended at present.

The main purpose of the COMFORD is to use the COMFORD tape as an input-data tape for various computer analyses on the resonance data, such as a calculation of the averaged value and an investigation of the distribution or the correlation of the parameters. In writing the COMFORD, no particular survey on the similar programmes were made, although there are apparently more comprehensive programmes or systems such as SCISRS (1) and COSA NOSTRA (2). However, it was the primary matter of concern to make the COMFORD handy for the above purpose, and modification of the COMFORD will be made through the actual experiences of using it with the IBM-7044 computer in the Computer Center of JAERI.

2. GENERAL DESCRIPTION OF THE COMFORD¹⁾

For the sake of conciseness in explanation, an outline of the COMFORD is given by illustrating a typed output of a block of data, without going into the programming flow. Fig. 1 shows the example of a typed output of a block of data. It consists of five items, IDENTIFICATION, COMMENT, AVERAGE LEVEL SPACING, STRENGTH FUNCTION, and INDIVIDUAL RESONANCE PARAMETERS, the output of the last three in the figure being truncated as is seen by the lines where the characters are erased by halves. In the COMFORD tape, the blocks of data are stored in order of the atomic number, and the data blocks of the same atomic number are stored in order of the date of publications; and if the atomic number, the date of publication, and the laboratory name of the different blocks of data coincide, the blocks are stored in order of an ID number which is indicated by arrow with (3) in Fig. 1.

The record of a block of data begins with 'IDENTIFICATION' which contains a symbol of element and an atomic number (1) in the Figure), indexes of contents (2), and ID number (3), the range of energy, the number of resonances in the data block, the reference (4), an abbreviated name of the laboratory, and the date of entry. In the example, the indexes of contents indicate, from left to right, that A = 1 : isotope identification of resonances is given, E = 1 : resonance energies are given, G = 0 : total width of resonance is not given, and so forth. 'NR' (5) gives the number of resonances used to evaluate the average value, and 'x' (6) indicates explicitly that "no data is given" which should be distinguished from "zero" or "blank" in a certain case.

A proviso, which is given by a symbol of a single character (7), can be annexed to each datum. Examples of the symbolic comments are as follows:

¹⁾The FORTRAN IV Programme of the COMFORD was written by T. Mori, IBM Japan; a complete description of the COMFORD will be given elsewhere.

A = there is ambiguity in the datum, ambiguity in the isotope identification for example; or, it means "approximately",
C = see the other comments,
D = the value is dependent on data of other sources,
J = ambiguity in the spin assignment,
L = ambiguity in the neutron angular momentum,
M = the datum is corrected for missed resonances,
S = statistical error only,
Y = the error is not symmetric, and
X = check the original paper, etc.

The symbolic comments can be used in the following manner: the data with a certain symbol which is specified at the input are omitted at the read-out, several symbols specified at the input are regarded as the same proviso in a certain programme which uses the COMFORD tape as an input data tape, and so on.

The comment indicated by ⑧ signifies that there are additional data in a data block with the same atomic number, the date of publication, and the laboratory name, but with an ID number equal to one. Other columns of the Figure may be rather selfexplanatory.

The first two columns of the input-data cards are used to identify the kinds or formats of that cards; the formats of the input-data cards are quite similar to that of the output in Fig. 1, although they are much contracted. The main modes of operations with the COMFORD, which are controlled by the first one of the input-data cards, are storage, revision or correction, and read-out. At the storage mode of operation, if the atomic number, the date, the laboratory name, and the ID number of an input-data block coincide with that of a data block already stored in the COMFORD tape, the storage is not made and an error message is typed out; on the other hand, at the revision mode, the operation is not made unless the above coincidence takes place. At the storage and the revision, the newly-stored data are always printed out.

Six standard modes of read-out are prepared: read-out of

- 1) the whole contents of the tape,
- 2) all the average data,
- 3) all the individual parameters,
- 4) all the data of specified atomic numbers,
- 5) a list of the 'IDENTIFICATIONS' of the whole contents, and
- 6) the blocks of data of which atomic number and the indexes of contents coincide with that specified at the input.

The above list of the 'IDENTIFICATIONS' will provide a tolerably detailed index of the COMFORD tape.

Accumulation of the data in the COMFORD tape enough to evaluate an average execution time by the IBM-7044 has not been achieved. Merits and demerits of the COMFORD should be proved in the actual use of the COMFORD tape as an input-data tape for various computer analyses; at present, computer programmes for those analyses are under preparation.

The authors wish to thank Dr. T. Momota, Dr. R. Nakasima and the members of the Japanese Nuclear Data Committee for their interest and encouragement, and they are also indebted to Dr. K. Moriguchi for his advice on the computer programming.

3. REFERENCES

- (1) J. M. Friedman and M. Platt: BNL-883 (T-357) (1964).
- (2) W. J. Cahill, D. W. Thompson, S. T. Perkins, and R. J. Howerton: UCRL-50132 (1966).

•• C O M F O R O - THE COMPUTER FILE OF RESONANCE DATA ••

PAGE 5

A WORKING GROUP OF THE JAPANESE NUCLEAR DATA COMMITTEE

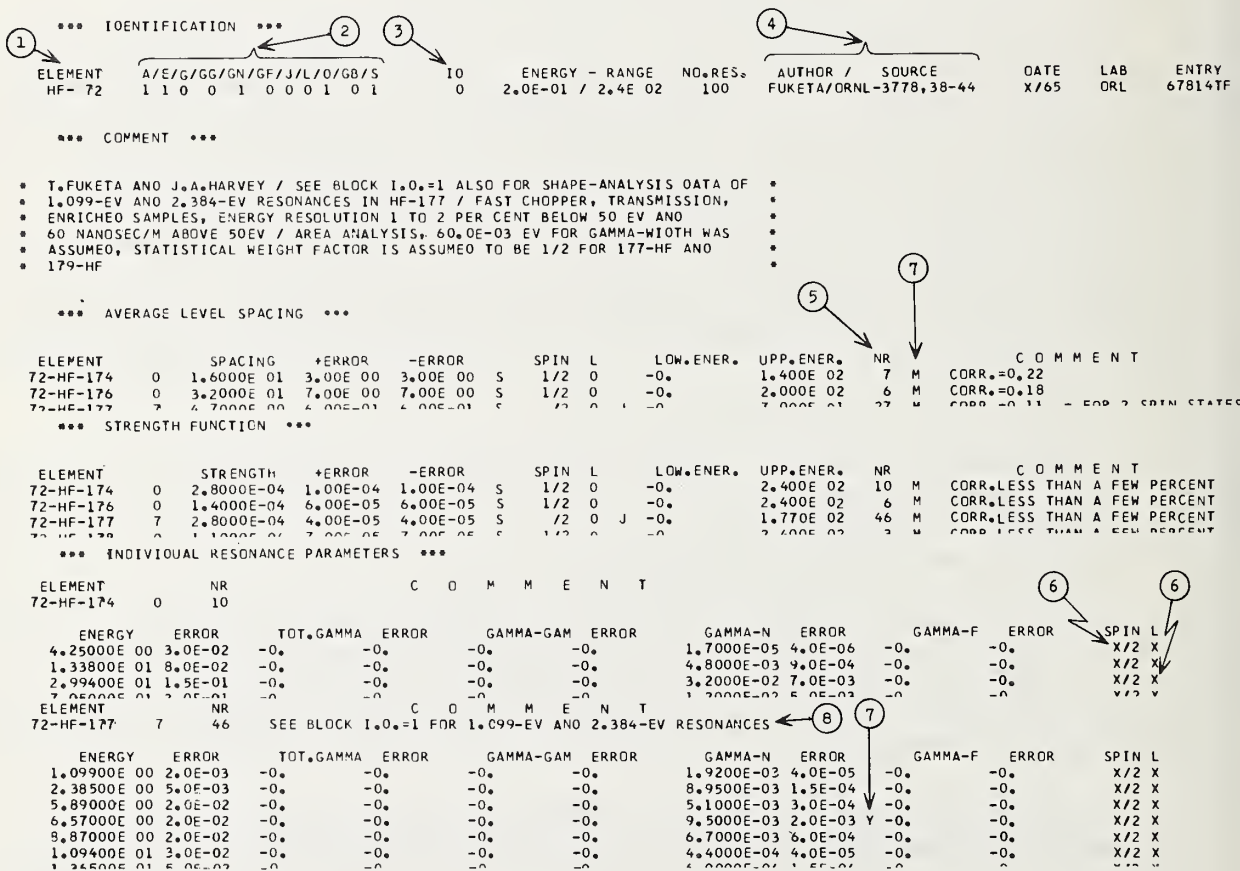


FIG. 1. Example of a typed output from the COMFOR tape.

STORAGE AND RETRIEVAL OF PHOTON PRODUCTION
AND INTERACTION DATA IN THE ENDF/B SYSTEM*

by

Donald J. Dudziak and R. J. LaBauve

University of California
Los Alamos Scientific Laboratory
Los Alamos, New Mexico 87544

ABSTRACT

In order to allow for the storage and convenient subsequent retrieval of data needed in shielding calculations, the ENDF/B format has been extended to include photon production and photon interaction data. Data allowed in the files include: interaction cross sections; atomic form factors for incoherent and coherent scattering; photon (or other secondary radiation) angle, energy, and energy-angle distributions; discrete levels of the nucleus with associated transition probabilities; and photon production multiplicities.

The format is kept as consistent as possible with the existing ENDF/B format and requires no changes in it. A detailed proposal for the format has been approved by the Cross Section Evaluation Working Group (CSEWG). A processing code to put photon production data into forms usable in photon transport codes is being written at the Los Alamos Scientific Laboratory. Data for photon production in sodium have been entered on a test ENDF/B tape for debugging the processing codes, and similar data for magnesium, chlorine, potassium, and calcium are being prepared. Evaluations of these elements by M. K. Drake et al. are being translated from UK to ENDF/B format by a code written at LASL.

*Work done under the auspices of the United States Atomic Energy Commission.

1. INTRODUCTION

The present status of photon production and photon interaction data in the ENDF/B data library, as well as of the associated processing codes, is as follows:

1. A format to store such data has been devised[1] and approved for incorporation in the ENDF/B system. Reaction types have been expanded to include inelastic scattering to 40 discrete levels and to the continuum.
2. Photon production data for sodium[2] have been translated and transmitted to the National Neutron Cross Section Center at BNL. Similar data for magnesium, chlorine, potassium, and calcium are in the process of translation. Photon interaction data for all materials in the file are scheduled to be placed in the ENDF/B system by June 1968. The conversion to ENDF/B format will be done by LRL.
3. A multigroup photon production cross section code, LAPH[3], is being developed by LASL to read the ENDF/B file, construct photon production matrices, and determine spatially dependent source functions for photon transport codes. The translated sodium data are being used by LASL to debug LAPH and by BNL as a test set for extending the data-checking code CHECKER[4]. Later, the ENDF/B processing codes CRECT and DAMMET[4] will need to be modified to operate on the photon data files. A code is being written at the NRDL to reconstruct photon secondary distributions from form factor data. Codes (LATEX and LUTE) have been written[5] to translate the particular extension of the UK data file used by Drake et al. to the ENDF/B format. A more general UK \leftrightarrow ENDF/B translation code will be written at ORNL, incorporating the LATEX and LUTE routines. All codes are written in FORTRAN.

2. DATA STORAGE

The original ENDF/B format[6] provided for the storage of neutron data in files 1 through 7, including such data as resonance parameters, smooth cross sections, angular and energy distributions of secondary neutrons, and thermal scattering laws. To review, a mode 3 card-image tape is arranged by a hierarchy of subdivisions, starting at a material (MAT) and going down through files (MF), sections for reaction types (MT), and finally individual records.

Several modifications of the ENDF/B system were required for its application to shielding technology. Provision for photon interactions and production was needed. Both the neutron interaction data and the photon production data for total neutron inelastic scattering were separated into reaction-type sections for each excited level of the target nucleus. The correspondence between the UK data file and ENDF/B was maintained by assigning the reaction-type numbers shown in Table I. The section for MT = 15 is euphemistically called "inelastic scattering to the continuum," but actually contains all photons not accounted for in the discrete-level sections.

One of the self-imposed guidelines for constructing new formats for photon data was that ease and simplicity of input should be stressed, sometimes at the sacrifice of simple retrieval of the data by the processing codes. Although retrieval routines are completely automated, input is often done manually. The retrieval codes may need to be more elaborate, but input is kept fewer times removed from the basic physics data. Another guideline was that the format should be kept as consistent as possible with both the ENDF/B neutron-data format and the UK data file. Thus, changes in existing processing codes are minimized and coding of UK \leftrightarrow ENDF/B translation routines is simplified.

TABLE I

NEW REACTION-TYPE (MT) NUMBERS FOR INELASTIC SCATTERING

<u>MT NUMBER</u>	<u>DESCRIPTION</u>
<u>5</u> thru <u>14</u>	Inelastic scattering to the <u>1st</u> thru <u>10th</u> levels of the target nucleus
<u>15</u>	Inelastic scattering to the "continuum" (potpourri)
<u>51</u> thru <u>80</u>	Inelastic scattering to the <u>11th</u> thru <u>40th</u> levels of the target nucleus

3. EXTENSIONS OF ENDF/B FORMAT FOR PHOTON PRODUCTION DATA

New files 14, 15, and 16, were created for photon production data (see Table II).

TABLE II

FILES ADDED TO ENDF/B LIBRARY FOR PHOTON PRODUCTION DATA

<u>FILE</u>	<u>DESCRIPTION</u>
14	Photon Angular Distributions
15	Photon Production Multiplicities
16	Photon Energy-Angle Distributions

File 14 is similar to file 4, giving probability densities for the angular distribution of each discrete photon and the continuous spectrum, as either Legendre coefficients or tabulated functions. In addition, the photon file allows for entering an isotropic distribution with a flagging parameter in the HEAD card.

The format for storage of photon multiplicities in file 15 diverges significantly from that of the neutron files. It was deemed advisable to allow for two general categories of photons -- discrete photons from de-excitation of known levels, and photons (discrete or continuum) not associated with a level structure. In the latter case, an option (LO = 1) is provided to present photon energy probability densities, either as tabulated or analytically defined functions. These functions are, in turn, tabulated functions of incident neutron energy, as are the photon yields for each distribution and for the total.

Photon yields for photons at energy E_γ , due to a reaction initiated by a neutron of incident energy E , are given as $y(E_\gamma, E)$ photons/eV-interaction. This multiplicity is subdivided into NK portions, $y_k(E_\gamma, E)$, each portion following a different law or the same law with different parametric representations, as follows:

$$y(E_\gamma, E) = \sum_{k=1}^{NK} y_k(E) f_k(E_\gamma, E).$$

Here the f_k are normalized to unity, while the y_k contain the multiplicities; this scheme is particularly suitable for Monte Carlo calculations. Two common forms for f_k are a tabulated function and a delta function in E_γ . The total photon yield from a neutron interaction, $Y(E)$, is tabulated as a check quantity. The differential photon production cross section can be obtained with the aid of the appropriate cross section, $\sigma(E)$, from file 2 and 3 as

$$\frac{d\sigma(E, E)}{dE_\gamma} = \sigma(E) y(E_\gamma, E),$$

from which multigroup photon production matrices can be constructed.

De-excitation photons from discrete levels can be represented concisely and simply by option 2 (LO = 2). For each level, the only data required other than control parameters are the level energy for the state excited, the nonzero transition probabilities to lower levels, and the energies of those lower levels. Gamma transition conditional probabilities are given only if significant competing processes, such as internal conversion, are present. Data listed for any level include only those for photons originating at the level, not for photons from further cascading. Thus, processing codes must continue searching through data for lower levels, as well as the appropriate cross section in File 3, to construct photon production cross sections. Levels are numbered consecutively by a parameter NS, so that for a transition to a lower level i , the photon energy is determined by $E_{\gamma,i} = ES_{NS} - E_i$. For direct transition probability TP_i , and conditional gamma transition probability GP_i , the associated multiplicity of the photon with energy $E_{\gamma,i}$ is $y(E_{\gamma,i}) = (TP_i)(GP_i)$.

Provision is made for photon energy-angle distributions in file 16, but like file 6, it will probably remain inactive for a while, so the details are not presented here. Energy-angle distributions for continuous photon spectra are specified by a system whereby subsections similar to file 15 (option 1) are used. Either (1) the Legendre coefficients are given as a function of both incident neutron energy and photon energy, with a subsection for each Legendre coefficient; or (2) the photon multiplicities are tabulated as a function of both incident neutron energy and photon energy, with a subsection for each discrete angular cosine value.

4. EXTENSION OF ENDF/B FORMAT FOR PHOTON INTERACTION DATA

New files 23 through 27 were created for photon interaction data (see Table III). Reaction-type (MT) numbers in the 500 and 600 series are assigned to photon interactions in a system somewhat analogous to the 000 and 100 series for neutron reactions; e.g., the pair production cross section is identified by MT = 516, paralleling MT = 16 for (n,2n) reactions.

TABLE III
FILES ADDED TO ENDF/B LIBRARY FOR PHOTON INTERACTION DATA

<u>FILE</u>	<u>DESCRIPTION</u>
23	"Smooth" Cross Sections
24	Secondary Angular Distributions
25	Secondary Energy Distributions
26	Secondary Energy-Angle Distributions
27	Form Factor Data for Incoherent and Coherent Scattering

Files 23 through 26 have, with trivial exceptions, the same structure as files 3 through 6. However, a generalization of their use is provided by allowing angular, energy, and energy-angle distributions of any outgoing particle. Should the need arise, the ambiguity concerning the secondary particle in a photonuclear reaction, such as photofission (γ, f), could be resolved by use of an appropriate flag in existing blank fields of the HEAD record.

A new file especially suited for secondary photon angular distributions is file 27 for atomic form factors. Thus, for incoherent scattering

$$\frac{d\sigma_{inc}}{d\mu} = ZK(q;Z) \frac{d\sigma_c}{d\mu},$$

where $d\sigma_c/d\mu$ is the Klein-Nishina differential cross section, K is the atomic form factor, and q is the momentum of the recoil electron. For coherent scattering,

$$\frac{d\sigma_{coh}}{d\mu} = \pi r_o^2 Z^2 (1 + \mu^2) G(q;Z),$$

where G is now the form factor, q is the recoil momentum of the atom, and r_o is the classical radius of the electron. In either case, the form factor is tabulated as a function of q , and the section structure is similar to that of file 23.

5. DATA RETRIEVAL

For photon production data to be useful in shielding calculations, a photon source term for transport codes must usually be determined. The LAPH code[3] is designed to retrieve data directly from the ENDF/B file, apply a suitable weighting function over N specified neutron groups, and construct a photon production matrix for G specified photon groups. Combined with flux vectors from a neutronics code, such a matrix can directly provide the spatially dependent source term for photon transport calculations. A schematic diagram of the code's operation is shown in Fig. 1, where the left hand side represents data input, and the right hand side depicts operations on the data. Fine-group weighting fluxes, as well as fine-group capture and fission cross sections (σ), are presently obtained from the multigroup constants code MC² [7].

The code's operation can be summarized by considering the major input data and calculations. Considering only one material for simplicity the calculation proceeds as follows for each reaction-type k , photon group g , and neutron fine group ℓ :

$$Y_g^k(E) = \int_{E_g}^{E_{g+1}} dE_Y y^k(E_Y, E) \quad (1)$$

$$\sigma_{g,\ell}^k = (\Delta E_\ell)^{-1} \int_{E_\ell}^{E_{\ell+1}} dE \sigma^k(E) Y_g^k(E), \quad k \neq 18, 102, \quad (2)$$

$$\sigma_{g,\ell}^k = (\Delta E_\ell)^{-1} \sigma_\ell^k \int_{E_\ell}^{E_{\ell+1}} dE Y_g^k(E), \quad k = 18, 102. \quad (3)$$

The $y^k(E_y, E)$ are obtained from file 15, where, in the case of option 2, a subroutine is required to calculate these values (see Appendix B of Ref. 1). Equation 3 is used for capture and fission because of the inadequacy of fine-group weighting fluxes in the resonance region. Let M_n = number of fine groups in broad group n . Then, the operations of Eqs. 1 through 3 are repeated for $g = 1(1)G$, for $\ell = 1(1)M_n$, and for all k for which photon production data are given. For broad group n and weighting fluxes w_ℓ , where $n = 1(1)N$, one can compute the photon production cross section

$$\sigma_{g,n}^k = \left[\sum_{\ell=1}^{M_n} \sigma_{g,\ell}^k w_\ell \right] \left[\sum_{\ell} w_\ell \right]^{-1} \quad (4)$$

The photon production matrix elements are then

$$\sigma_{g,n} = \sum_k \sigma_{g,n}^k \quad (5)$$

For a neutron broad-group flux vector $\phi(\vec{r})$ and an atom number density N of the material, the spatially dependent photon multigroup source vector is given by

$$[S(\vec{r})] = [N\sigma][\phi(\vec{r})]. \quad (6)$$

Presently, such source vectors are being constructed in formats compatible with the QAD and DTF-IV codes[8,9]. Output subroutines for linkage to other photon transport codes can also be written easily, depending upon user's requirements.

Many people helped to devise the format for photon data storage, either by suggestions for storing particular types of data or by commenting on the finished document. Such contributions from M. E. Battat, J. M. Ferguson, D. C. Irving, and R. B. Lazarus are very much appreciated.

6. REFERENCES

1. Donald J. Dudziak (ed.), "ENDF/B Format Requirements for Shielding Applications," LA-3801 (ENDF-111), Los Alamos Scientific Laboratory (1967).
2. M. K. Drake et al., "Neutron and Gamma Ray Production Cross Sections for Sodium, Magnesium, Chlorine, Potassium, and Calcium," NDL-TR-89, U. S. Army Nuclear Defense Laboratory (1967).
3. Alan Marshall and Donald J. Dudziak, "LAPH, a Los Alamos Photon Production Multigroup Cross Section Code for ENDF/B," (to be published).
4. John Felberbaum (ed.), "Description of the ENDF/B Processing Codes CHECKER, CRECT, DAMMET, and Retrieval Subroutines," ENDF-110, Brookhaven National Laboratory (1967).
5. Donald J. Dudziak, "LUTE and LATEX," unpublished UK to ENDF/B format translation codes (1967).

6. Henry C. Honeck, "ENDF/B Specifications for an Evaluated Nuclear Data File for Reactor Applications," BNL-50066 (ENDF-102), Brookhaven National Laboratory (1966; Revised July 1967 by S. Pearlstein, BNL).
7. B. J. Toppel et al., "MC², a Code to Calculate Multigroup Cross Sections," ANL-7318, Argonne National Laboratory (1967).
8. Richard E. Malenfant, "QAD: A Series of Point-Kernel General-Purpose Shielding Programs," LA-3573, Los Alamos Scientific Laboratory (1967).
9. K. D. Lathrop, "DTF-IV, a FORTRAN-IV Program for Solving the Multigroup Transport Equation with Anisotropic Scattering," LA-3373, Los Alamos Scientific Laboratory (1965).

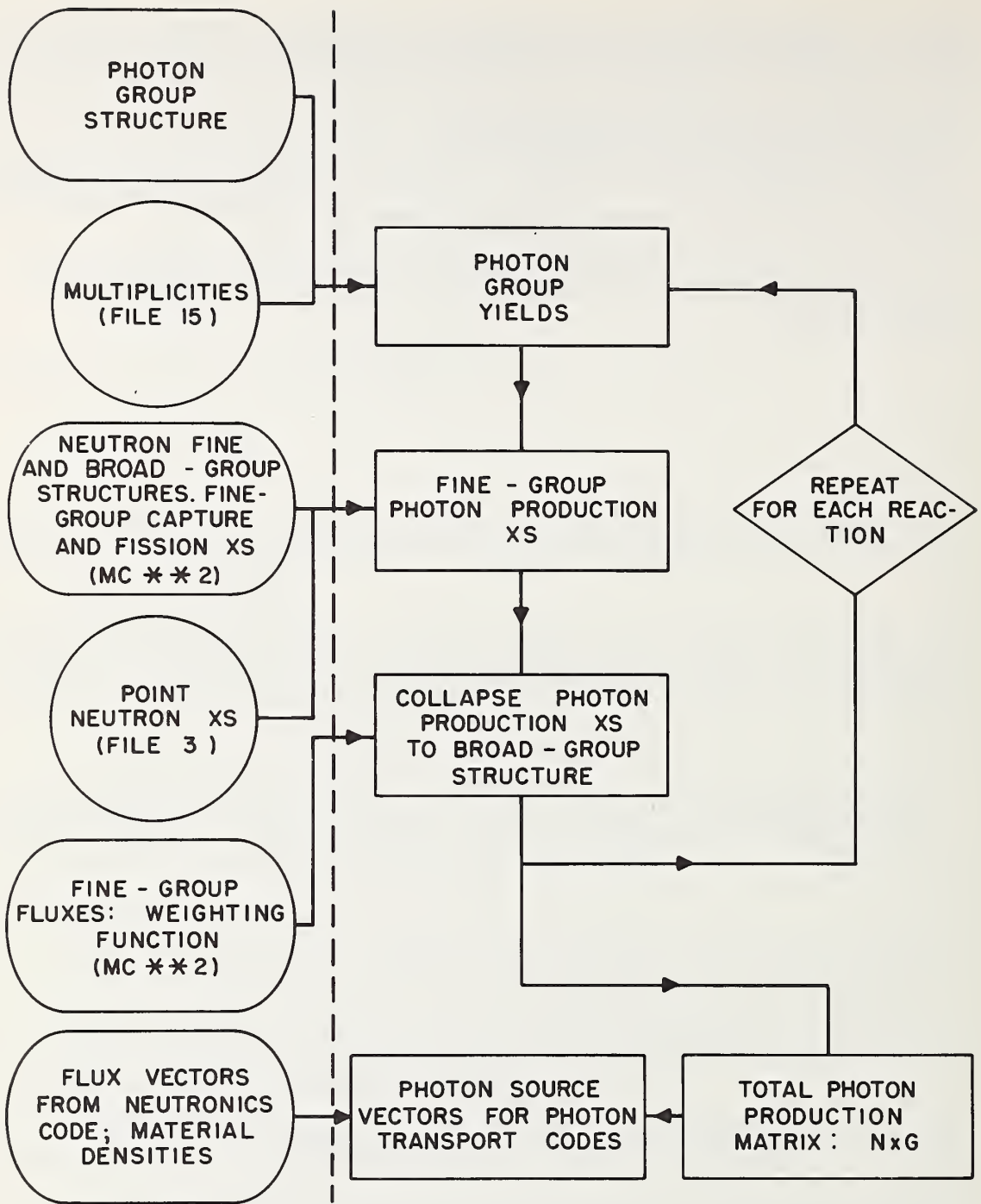


Fig. 1. Schematic Diagram of LAPH Code. Input Data is Shown to Left of Dotted Line.

A MATHEMATICAL SCHEME FOR EVALUATING
CROSS-SECTION DATA ON THE FISSILE ISOTOPES
U-233, U-235, AND Pu-239 IN THE ENERGY RANGE
10 KEV - 10 MEV

P. C. Young and K. B. Cady

Nuclear Reactor Laboratory, Cornell University
Ithaca, New York 14850

ABSTRACT

A mathematical scheme for evaluating simultaneously the experimental data on the three fissile isotopes is being investigated by means of an energy dependent, correlated, non-linear least squares analysis. The scheme correlates the experimental data available for each isotope with the data available as ratio measurements between the isotopes, and incorporates an internal normalizing procedure for data available as relative measurements.

The independent quantities (e.g. σ_f , α , ν) for each isotope are described by energy dependent analytic functions, and from these, the dependent quantities for each isotope (e.g. σ_y , η , σ) and the ratios of quantities between isotopes (e.g. $\sigma_f^{U233}/\sigma_f^{U235}$, $\sigma_f^{Pu239}/\sigma_f^{U235}$) can be generated. Where relative quantities were experimentally measured, the unnormalized data will be used as the input to the scheme; normalizing values will be obtained internally as part of the evaluating procedure. The weight (a measure of the reliability) assigned to each data point will be determined by the quoted standard deviation, augmented, as warranted, by an examination of the individual experiments in regard to the techniques employed and to assumptions applied which may no longer be valid.

It is anticipated that a large part of the discrepancy in the experimental data that is now in evidence may be eliminated by the use of the common normalizing values generated by the scheme.

1. INTRODUCTION

In order to facilitate the analysis, design, and comparison of various reactor systems, the reactor parameters characterizing the system need to be predicted to a high degree of reliability. This required precision in the parameters could be obtained with the available sophisticated reactor analysis codes if the input cross-sections were known with sufficient accuracy. That this is, as yet, not the case, can be seen from examining the requirements placed on the accuracy of the cross-sections by the reactor analysts, and the actual accuracy of the available experimental data^{1,2/}. The precision in the data from an individual experiment often approaches that required by the users, but the spread in data obtained in different experiments does not reflect the desired accuracy.

There exists today a wealth of experimental data on σ_f , α and ν for the three fissile isotopes U-233, U-235 and Pu-239 over most of the energy range 10 Kev to 10 Mev^{3/}. Although only a limited amount of data exists on σ_c , σ_a and η in this range, it will become available in the future as a result of newer experimental techniques, such as that utilizing a liquid scintillation bath. A large percentage of the available data is in the form of ratio measurements (relating a quantity between two isotopes at a given energy; or, for a given isotope, between two energies, thus giving the energy variation of the quantity but not its magnitude) which require a normalization to obtain the absolute quantities.

A plot of the available cross-section data for a particular type isotope reveals values of varying precision scattered about a general trend. A certain amount of spread in the data is to be expected as a result of statistical uncertainties. There exists in some cases, however, as in the fission cross-section of U-235^{4/}, variations greater than the experimental errors would allow. These variations are due to the non-uniform values used for normalization, to differences in energy resolution between experiments, and to systematic effects characteristic of the particular experimental techniques employed. The latter is by far the most difficult to reconcile in that it requires a detailed knowledge of the experimental procedure. Most revisions in the experimental data are due to changes in the original corrections applied to the raw data, brought about by a change in the assumed systematic effects. The reliability of the older data could be enhanced if these systematic effects were examined in view of today's more thorough knowledge of the detectors and experimental techniques that were than employed.

As a consequence of the demand for accurate cross-section sets to be utilized in reactor analysis codes, a much greater interest has recently been taken in regard to the methods of obtaining recommended cross-section values from the expanding wealth of available data. These methods range in complexity from the older method of plotting the data, regardless of energy resolution or normalization, and "eyeballing" a recommended curve, to the latest methods of mechanical evaluation^{5,6/}. Most of the evaluations available today lie between these two extremes; the usual method being that the evaluator critically examines the available data and then bases his recommended cross-sections on only a limited quantity of the data, which in his opinion best reflects the data available at that time. This can and does lead to differences in recommended values, reflecting the individual

evaluator's preference for particular data where conflicts occur. A subsequent revision in the data used or the acquisition of newer, more reliable data could require a revision in the recommended values. These problems and others, as summarized by Schmidt^{1/}, serve to demonstrate the desirability of a mechanical scheme to aid the evaluator in providing a recommended set of evaluated cross-sections.

2. DESCRIPTION OF THE MECHANICAL SCHEME FOR EVALUATION

The development of the mechanical scheme to be described in the following arose as a result of an effort to extend to the energy dependent case the evaluation method used by Westcott et. al.^{2/} to determine recommended 2200 m/sec cross-section values. A modification of the usual Gauss-Newton^{2/} method of weighted non-linear least squares was chosen because it affords the opportunity to simultaneously analyze the data available as absolute and ratio measurements, thus correlating the redundant data between isotopes and reaction cross-sections, and providing an internal means of normalization. The mathematical details describing the present scheme in its most general form are straightforward and are given for completeness in the Appendix.

For each data point used as input to the scheme, the following need to be specified: the type of quantity (i.e., what is it a measure of), the unnormalized numerical value Y_i , the weight $w_i = 1/\sigma_i^2$, and the energy E_i . Because the available data is highly overdetermined, independent quantities $X_k(E, \vec{a})$, sufficient in number to functionalize all the types of input data, and their functional dependence on $\vec{a} = \{a_j\}$, the set of fitting parameters must be chosen. As there is no simple unified theory of nuclear reactions available that is applicable over the range 10 Kev - 10 Mev, this range is to be divided into convenient subranges, chosen in such a manner that the independent quantities can be described as simple analytic functions of the fitting parameters. The fitting function $F_i(\vec{a})$ is specifically, that functional of the independent quantities (and hence of \vec{a}) that explicitly reproduces the type of quantity associated with the data point Y_i . It is a result of the functional form of this quantity that the correlation and normalization of the data takes place. Specification of the independent quantities, X_k , and their functional dependence on \vec{a} determines the functional dependence of the $F_i(\vec{a})$, and hence, of all the matrix elements required in the analysis.

The set of fitting parameters \vec{a} which minimize the functional $Q(\vec{a})$ are determined through an iterative procedure. Initial values \vec{a}_0 are chosen (from a prior investigation of the data for the independent quantities) and the incremental changes Δa_0 are calculated as shown in the Appendix. The matrix elements of T, A and F are then recalculated at the improved estimate of \vec{a} , namely $\vec{a}_1 = \vec{a}_0 + \lambda_0 \Delta a_0$ (where λ_0 is that value of λ which minimizes $Q(\vec{a}_0 + \lambda \Delta a_0)$). The incremental changes $\vec{\Delta a}_1$ are then determined, giving in turn the improved estimate of \vec{a} , $\vec{a}_2 = \vec{a}_1 + \lambda_1 \Delta a_1$. This procedure is repeated until $\Delta a = 0$ (or until a satisfactory convergence criteria is established). The matrix elements of the various matrices evaluated at these final \vec{a} need to be stored, because from these are calculated the covariance matrix of \vec{a} (and hence, the covariance matrix of any functional of \vec{a} , (e.g. the $X_k(\vec{a})$'s), and the first order incremental changes in \vec{a} due to subsequent revision in the input data and/or to the addition of new data.

3. SUMMARY OF FEATURES OF THE EVALUATING SCHEME

The immediate result of the evaluating procedure is a set of fitting parameters $\vec{a} = \{a_j\}$ which define the independent quantities and their variances as functions in energy. These independent quantities and the quantities derived from them form a consistent set of evaluated cross-sections and associated parameters not only for each isotope, but also for the three isotopes taken together. This consistency is a result of analyzing simultaneously the data available for each isotope and the data available as ratio measurements between the isotopes, and is also a result of removing the redundancy in the data by selecting independent quantities. The correlation of the data between isotopes is especially important when comparing reactor systems utilizing different fuels. A more meaningful comparison of the reactor parameters which depend sensitively on the cross-sections (e.g., fuel inventory, doubling time, spectral indices, doppler coefficients, void coefficients, etc.) can be made if the cross-sections used in their derivation are obtained in a common evaluating procedure.

Another feature associated with the simultaneous fitting of ratio and absolute data is the distinct advantage of internal normalization. It is difficult to see from the purely mathematical formulation of the scheme where this normalization occurs; its effect, however, is to normalize the ratio measurements to the "best value" of the normalizing quantity as generated within the scheme. A simple example might help to show this more clearly. Let Y be the experimentally measured ratio of the fission cross-section of U-233 to that of U-235, and let $X_1(\vec{a})$ and $X_2(\vec{a})$ be the independent parameterized functions describing the fission cross-section of U-233 and U-235 respectively. In the present scheme, in order to use directly the reciprocal variance of Y as the weighting factor ($w = 1/\sigma_Y^2$), the fitting function $F(\vec{a})$ to be compared with Y would be $X_1(\vec{a})/X_2(\vec{a})$. The contribution of this data point to the function to be minimized, $Q(\vec{a})$, would be $w (F(\vec{a}) - Y)^2$ and can be rewritten in the following equivalent forms,

$$w \left(\frac{X_1(\vec{a})}{X_2(\vec{a})} - Y \right)^2 = \frac{w}{X_2^2(\vec{a})} \left(X_1(\vec{a}) - X_2(\vec{a}) Y \right)^2 = \frac{1}{X_2^2(\vec{a}) \sigma_Y^2} \left(X_1(\vec{a}) - X_2(\vec{a}) Y \right)^2 \quad (1)$$

From this representation, it is seen that $X_2(\vec{a})$ (the independent quantity representing σ_f U-235) plays the role of the normalizing quantity and that $w/X_2^2(\vec{a}) = 1/X_2^2(\vec{a}) \sigma_Y^2$ is the weight associated with the normalized quantity $X_2(\vec{a}) Y$ (representing a value of σ_f U-233), assuming that $X_2(\vec{a})$, when used as a normalizing quantity, has zero variance.

The individual evaluator still plays an important role in the present scheme, that being i.) The selection of the data and its associated weight to be used as input to the scheme requiring that the evaluator have a thorough knowledge of the available data and the experimental conditions under which this data was obtained, and ii.) The choice of the functional dependence of the independent quantities so as to accurately represent the data over the selected energy subrange. The latter is by no means unique, and reflects the evaluator's "finesse" in fitting the data by either complicated analytic functions (high order polynomials, power functions, physical models, etc.) over large subranges or by relatively simple analytic functions

over smaller subranges. Once these selections are made, however, the mechanical scheme does remove from the evaluator's hands the problems of normalization, consistency and correlation. In addition, the scheme is capable of rapidly making a re-evaluation should the need arise. The effect of a revision in the input data is to change Y and W by incremental amounts. The addition of new data increases N and, thus has the effect of increasing the row dimension of the matrices Y, F and A, the row and column dimensions of W, and the number of terms in the matrix elements in T. The first order changes in \vec{a} resulting from either the revision of the input data or the addition of new data can be expressed directly in terms of these changes and the matrices available from the previous evaluation.

The authors wish to thank Dr. F. Feiner, Knolls Atomic Power Laboratory, visiting professor at Cornell University, for many hours of helpful discussion.

4. APPENDIX

Y_i , unnormalized numerical value of the i th data point $1 \leq i \leq N$.

W_i , weight assigned to Y_i (usually equal to the reciprocal variance of Y_i).

E_i , energy associated with i th data point.

$\vec{a} = \{a_j\}$, set of fitting parameters, $1 \leq j \leq L$.

$\vec{X} = \{X_k(E, \vec{a})\}$, set of independent quantities, $1 \leq k \leq M$.

$F_i(\vec{X}) = F_i(\vec{a})$, fitting function associated with i th data point.

$Q(\vec{a})$, the function to be minimized with respect to the set of fitting parameters \vec{a} .

$$Q(\vec{a}) = \sum_{i=1}^N W_i (F_i(\vec{a}) - Y_i)^2 \quad (A1)$$

the condition expressing that $Q(\vec{a})$ be a minimum is

$$\frac{\partial Q(\vec{a})}{\partial a_j} = 2 \sum_{i=1}^N W_i (F_i(\vec{a}) - Y_i) \frac{\partial F_i(\vec{a})}{\partial a_j} = 0 \quad 1 \leq j \leq L \quad (A2)$$

the expansion of a multivariate function $Z(\vec{a})$, about the point $\vec{a} = \vec{a}_0$, is (to first order)

$$Z(\vec{a}) = Z(\vec{a}_0) + \sum_{j=1}^L \left(\frac{\partial Z(\vec{a})}{\partial a_j} \right)_{\vec{a}_0} \Delta a_{j0} \quad (A3)$$

where

$$\Delta a_{j0} = a_j - a_{j0}$$

Expanding both $F_i(\vec{a})$ and $\frac{\partial F_i(\vec{a})}{\partial a_j}$ according to (A3), substituting into (A2), and keeping only first order terms yields

$$T_0 \Delta a_0 = A_0^T W (Y - F_0) \quad (A4)$$

where

$$Y = [Y_i], \text{ Nx1}$$

$$W = [W_i \delta_{ij}], \text{ NxN (diagonal)}$$

$$F_0 = [F_i(\vec{a}_0)], \text{ Nx1}$$

$$\Delta a_0 = [\Delta a_{j0}], \text{ Lx1}$$

$$A_0 = [\alpha_{ij}(\vec{a}_0)], \text{ NxL} \quad \text{and} \quad \alpha_{ij}(\vec{a}_0) = \left(\frac{\partial F_i(\vec{a})}{\partial a_j} \right)_{\vec{a}_0} \quad (A5)$$

$$T_0 = [t_{ij}(\vec{a}_0)], \text{ LxL} \quad r\beta_{ij}(\vec{a}_0) = \left(\frac{\partial^2 F_r(\vec{a})}{\partial a_i \partial a_j} \right)_{\vec{a}_0}$$

$$t_{ij}(\vec{a}_0) = \sum_{r=1}^N W_r \left(\alpha_{ri}(\vec{a}_0) \alpha_{rj}(\vec{a}_0) + (F_r(\vec{a}_0) - Y_r) r\beta_{ij}(\vec{a}_0) \right)$$

The usual Gauss-Newton method neglects the term $r\beta_{ij}(\vec{a}_0)$ and hence T_0 is simply equal to $A_0^T W A_0$. The method described by Nierenberg^{10/} for minimizing a function of n variables using a paraboloidal fit, when applied to a weighted non-linear least squares problem, is identical with the present method incorporating this modification in the Gauss-Newton method. The retention of this term also resolves the usual difference arising between the covariance matrices of $\Delta \vec{a}$ and \vec{a} .^{11/}

The covariance matrix of \vec{a} , $C_a^{\vec{}}$, is determined in the following manner. Because the Y_i 's are the only quantities that \vec{a} depends on which are assumed to have an error, the expression relating the covariance of a_i and a_j to the covariances of the Y_i 's is, to second order in the deviations of the Y_i 's from their expected values

$$\text{Cov}(a_i, a_j) = \sum_{k=1}^N \sum_{\ell=1}^N \frac{\partial a_i}{\partial Y_k} \text{Cov}(Y_k, Y_\ell) \frac{\partial a_j}{\partial Y_\ell} \quad (\text{A6})$$

or in matrix notation

$$C_{\vec{a}} = S C_Y S^T = S W^{-1} S^T \quad (\text{A7})$$

where

$$C_{\vec{a}} = [C_{ij}], L \times L \quad C_{ij} = \text{Cov}(a_i, a_j)$$

$$S = [s_{ij}], L \times N \quad s_{ij} = \frac{\partial a_i}{\partial Y_j} \quad (\text{A8})$$

$$C_Y = W^{-1}, \text{ since } \text{Cov}(Y_i, Y_j) = \sigma_i^2 \delta_{ij} = \frac{1}{W_i} \delta_{ij}$$

because the Y_i 's are independent.

The matrix element s_{ij} are determined from equation (A2) by differentiating with respect to Y_k and are given as

$$T S = A^T W \quad (\text{A9})$$

Consequently,

$$C_{\vec{a}} = T^{-1} A^T W A T^{-1} \quad (\text{A10})$$

$$= (A^T W A)^{-1} \text{ if the } \beta\text{'s are neglected.}$$

The variances of \vec{a} are, to a multiplicative constant (usually taken as $\theta = Q(\vec{a})/(N-L)$), the diagonal elements of $C_{\vec{a}}$, that is,

$$\sigma_{a_j}^2 = \text{Var}(a_j) = \theta \text{Cov}(a_j, a_j) = \theta C_{jj} \quad (\text{A11})$$

5. REFERENCES

1. Compilation of EANDC Requests, EANDC-55 "U", March, 1966.
2. A. B. Smith (compiler), Compilation of Requests for Nuclear Cross-Section Measurements, WASH-1078, June, 1967.
3. CINDA 67 An Index to the Literature on Microscopic Neutron Data, Part I, EANDC-70 "U", October, 1967.
4. W. P. Poenitz, Measurements of the U-235 Fission Cross-Section in the key Neutron Energy Region, Second Conference on Neutron Cross Sections and Technology, Washington, D. C., March 4-7, 1968, Paper D-5, (these proceedings).
5. K. Parker, Mechanized Evaluation of Neutron Cross-Sections, Topical Conference on Neutron Cross-Section Technology, Washington, D. C., March 22-24, 1966, CONF-660303, p. 247.
6. R. F. Berland, C. L. Dunford and R. I. Creasy, Computer Graphics for Automated Neutron Cross-Section Evaluation, American Nuclear Society Transactions 10: 584, November, 1967.
7. J. J. Schmidt, Principles and Problems in Neutron Nuclear Data Evaluation, KFK-457, October, 1966, (CONF-661014-48).
8. C. H. Westcott, et. al., A Survey of Values of the 2200 m/s Constants for Four Fissile Nuclides, Atomic Energy Review 3: #2, 3, (1965).
9. Hartley, The Modified Gauss-Newton Method for Fitting of Non-Linear Regression Functions by Least Squares, Technometrics 3: 269, (1961).
10. W. A. Nierenberg, A Method for Minimizing a Function of N Variables, UCRL-3816 (Revised), August, 1959.
11. S. L. Piotrowski, Some Remarks on the Weights of Unknowns as Determined by the Method of Differential Corrections, Proceedings of the National Academy of Sciences 34: 23, February, 1948.

On Line Computer System for Cross Section Evaluation

L. E. Beghian and J. Tardelli

Lowell Technological Institute, Lowell, Massachusetts 02139

Abstract

In connection with a program for measuring fast neutron inelastic cross sections by the detection of the de-excitation gamma ray spectrum, using a time-gated Li-Ge detector, the following data acquisition system is used. The output of the detector is fed into a dual 4096 channel ADC interfaced to a PDP-9 computer (Digital Equipment Corp.) on line, equipped with two tape transports. A program has been written to display visually the stored data, compute and subtract background from a peak of interest in the spectrum, and then locate the centroid of the peak. The program can be directed to construct a linear calibration curve from assigned calibration points using a least square fit method, and thus to assign an energy to the peak of interest. The program can be further extended to include spectrum stripping, and thus obtain the intensity as well as the energy of the peak.

Time-gated Li-Ge detectors (1) are more and more commonly used to examine gamma ray spectra emitted by excited nuclei following inelastic neutron scattering. The high energy resolution obtained with these detectors makes it possible to establish a degree of precision not possible in earlier work of this kind performed with NaI (Tl) scintillation spectrometers. By measuring the excitation functions of each gamma ray in the spectrum as a function of primary neutron energy, inelastic cross sections as well as the level scheme of the nucleus of interest can be determined. However, the amount of information which can be obtained with these modern systems in a short time makes it mandatory to use them in conjunction with a correspondingly high speed data acquisition system.

The system to be described consists of a Digital Equipment Corporation PDP-9 computer interfaced with a Technical Measurement Corporation 20 MHz two parameter Input analog to digital converter. The input from the detector is fed into the A.D.C., and thence stored and processed in the computer. The computer itself is equipped with an oscilloscope display, which makes it possible to view the spectrum in the conventional way.

Once relevant "peaks" in the spectrum have been located (i.e. photo and pair peaks) the program described below makes it possible to "strip" off the background and locate the centroid. Thus, an energy calibration curve can be constructed which leads to output in terms of energy for any "peak of interest" or channel. It will also be possible to extend the program to find the area under the peak, i.e. its relative intensity.

1. PROGRAM DESCRIPTION

Software. The software consists of the system operating modes - a data acquisition mode and a data analysis mode - and of a small monitor program. The monitor enables DECTape loading and interchange of the operation modes. It also provides access to the Basic PDP-9 Software system for composing, compiling, and debugging programs.

Monitor. The monitor for this system is based on the DEC FAST-9 program which was written for use in retrieving frequently used programs from DECtape. It has been modified only slightly so as to allow the loading and direct exchange between the two system modes. The software of the modes has been adjusted so that the FAST-9 monitor will respond to console switch commands for mode exchange without paper tape read-in of the monitor.

Data Acquisition Mode. The software of this mode is based on the DEC Multianalyzer Program #2 which provides for a 4096 Channel single parameter data region. The program has been modified to remove some existent faults and to incorporate some subtle changes thought advantageous by the author. In all, however, the program remains essentially the same.

The available commands can be divided into the following categories: Data Accumulation; Data Display; Data Manipulation; Input/Output. Presented below under these headings is a list and short description of each of the commands available in this mode.

Data Accumulation - These commands initiate a data read-in from the analog to digital converter through the systems interface using the supplied machine instructions.

CRA, b, c	set real time clock at a hours, b minutes, c seconds
X	execute data input
S	stop data input

Data input will stop with the S command or when the real time clock reaches its set value, or any one of the 4096 channels overflows.

Data Display - All of the displays are based on the 1024X1024 point raster supplied by the system oscilloscope. The points plotted are referenced by a horizontal base line with appropriate division markings, and by movable vertical upper and lower location bars. There is a static display of the total 4096 channel spectra which is accomplished by averaging every four data points, and there is a dynamic display of any of the 1024 channel quadrants of the total array.

D, xxxx, yyyy	full spectra static display with xxxx and yyyy being the locations of the lower and upper bars respectively
Dd, xxxx, yyyy	dynamic display of quadrant d (=1, 2, 3, 4) where xxxx and yyyy are as above
U [±] xxxx	move the upper location bar [±] xxxx channels
L [±] xxxx	move the lower location bar [±] xxxx channels
F _n	set full scale of plot at 2 ⁿ where n = 9 to 18
E	expand region between upper and lower bars to full 1024 point raster and print out expansion factor
RS	restore display from expanded case to normal

Data Manipulation:

Z	zero the entire data region
I	integrate the total # of counts between the upper and lower location bars and type out the answer

Input/Output - The basic I/O devices are paper tape, teletype, and DECtape.

Paper Tape	PA, xxxx, yyyy	punch ASCII data from channels xxxx to yyyy
	PB, xxxx, yyyy	punch binary data from channels xxxx to yyyy
	RT	read a binary data tape into core
Teletype	W, xxxx, yyyy	write the contents of channels xxxx to yyyy
DECtape	N	record on DECtape the entire data array including title and notes input through the teletype
	ER	erase from the DECtape files a specific experiment recorded with the N command
	RD	read into the data array an experiment previously recorded
	T	type name and notes of the last experiment recorded on or read from DECtape
	P	print a list of all experiments recorded on DECtape reel

Data Analyzer Mode. The software for this mode is based on the DEC Multianalyzer Program #4. Extensive changes have made the current program its distant cousin and similar in a few commands only.

Data input is taken off of DECtape supplied by the data acquisition mode. When this data is read in, however, only 1024 channels of the 4096 are reviewed at one time. This is necessitated by the limited storage of the basic PDP-9 computer. By issuing the command Nn where n = 1 to 7 and following 1024 channels are reviewed:

<u>n</u>	<u>From</u>	<u>Threw</u>
1	1	1024
2	513	1526
3	1025	2048
4	1527	2560
5	2049	3072
6	2561	3584
7	3072	4096

The overlapping allows for investigation of peaks that may be otherwise in the vicinity of "cracks" in the data array. Data also may be input through the papertape reader with the command RTn where n is as above.

The oscilloscope display used in this mode consists of a static 1024 channel matrix with the following commands available for use in examining the data array: D, xxxx, xxxx; L[±]xxx; U[±]xxx; E; RS; Fn. These commands are exactly as in the data acquisition mode, except for the D, xxxx, xxxx command which now displays the selected 1024 channel data array. Beside the examination of data the upper and lower display markers are used for the isolation of portions of the array to be analyzed.

"Peaks of Interest" are isolated in the above manner and analyzed by typing the command LCn where n subscripts the result in a "peaks of interest" array. The data between the markers is corrected for background by the use

of a least squares technique to fit a 3rd order quadratic to the first 15 points after the lower marker and before the upper marker. Solutions to this curve are calculated for all bins between the markers and then subtracted from the proper bins. This can be seen on the display since it uses the same array. A centroid is then located by considering it as being the mean of a probability distribution where:

$$\overline{X} = \sum_i P_i x_i \quad \text{where } P_i = \frac{n_i}{N} \text{ and } N = \sum_i n_i$$

$$\text{so } \overline{X} = \frac{\sum_i n_i x_i}{\sum_i n_i}$$

This location is not necessarily an integer value.

Any of these "peaks of interest" can be flagged by the system operator as a calibration point through the use of the command Ka, b. The a indicates which peak, and the b subscripts the calibration point for later reference. Upon the receipt of this command the system will respond through the teletype with:

```

Calibration Point b
Channel # xxxx.xx
Energy (mev.) =

```

The operator then types in the energy value to be assigned to that point in standard exponential format.

After more than one calibration point is chosen a calibration curve may be constructed by using the command GK. This provides for a linear least squares fit to the points chosen. The system will then type out the equation of this line. The "peaks of interest" and calibration points arrays are not lost when going from one data section to the next. Thus the sections may be reviewed separately and a calibration done for each one, or they may all be reviewed and then calibrated together.

Using the command WEn the indicated "peak of interest" n will be typed out with the calculated value of energy, i.e.

```

Peak #n
Channel #xxxxx.xx
Energy (mev.) = .xxxxxxxxxE+xx

```

Also the command WExxxx,yyyy will cause the values of energy for channels xxxx through yyyy to be typed out.

The various data sections can be output on to DECTape using the command RDn where n refers to which section is being transferred. The various sections are sorted and arranged on one data file so that the tape may then be reviewed by the data acquisition mode for 4096 channel display and printout of the background removed data. A dump of the data sections may also be made on paper tape.

Other commands available to the operator in this mode consist of the previously explained DECTape commands:

T
P
ER

And, the following:

PI	print list of "peaks of interest"
PK	print list of calibration points
ZIn	zero peak n
ZKn	zero calibration point n
EDa,d	print energy difference between peak a and b

The last of these commands is used to locate double escape peaks.

2. REFERENCES

1. L. E. Beghian, F. Hoffman, S. Wilensky. Nuclear Instruments and Methods, 41, 141 (1966).

W. R. Moyer

Division of Nuclear Engineering and Science
Rensselaer Polytechnic Institute
Troy, New York 12181

and

Ronald P. Bianchini and Edi Franceschini

Courant Institute of Mathematical Sciences
New York University 10012

The neutron cross section measurements program at Rensselaer generates several millions of datum points per year. To process and analyze these data requires the services of a large and fast computer. This has been accomplished by linking, via voice grade telephone lines, an IBM-1130 computer at Rensselaer with the CDC-6600 computer at New York University (160 miles away). Communications software developed at the Division of Nuclear Engineering and Science has been tested and is in use exchanging card and printer image records with the CDC-6600 remote batch file at a speed of 2000 bits per second. Remote access to a large computer installation has greatly increased the efficiency of time-of-flight data processing through the reduction in turn-around time.

* Work supported by the U. S. Atomic Energy Commission under Contract AT(30-3)-328.

1. INTRODUCTION

Over the past decade, increased user demand for more detailed cross-section information has resulted in experiments of greatly increased complexity. Transmission measurements by neutron time-of-flight required little more than a 1000 channel time analyzer for the accumulation of results and data reduction by hand was not uncommon. A shift of emphasis to partial cross-section measurements coupled with the demand for even greater accuracy of results has increased the requirements of data storage equipment and experiment control devices. Electronic technology, in the form of small data acquisition computers and mass storage devices, is keeping pace with most data acquisition requirements.

2. PROCESSING REQUIREMENTS

A typical high resolution capture cross-section measurement at the Rensselaer LINAC generates information at the rate of about 1.6×10^5 datum points per week. Of these datum points possibly 35% represent capture data, 12% are background and flux measurement points and the remaining are miscellaneous measurements of detector efficiency and instrument related effects.

In addition to handling these numbers to arrive at raw capture yields, corrections must be applied to account for resonance self protection and multiple scattering. This is done at present with a Monte Carlo code prepared at Oak Ridge National Laboratory by J. G. Sullivan. A set of resonance parameters is assumed, the code computes a capture yield which is compared with the experimental yield, and the parameters are iteratively varied until the two yields are the same. The iterations need to be performed with the experimentalist supplying at each step the revised parameters.

To handle this volume of complex calculations, access to a fast, large memory computer was needed. A research project at New York University (160 miles away) involving batch processing from remote terminals was well under way. Remote processing on the N.Y.U. CDC-6600 from a terminal located at the Rensselaer LINAC was seen as a joint project, profitable to both parties. Data generated at the Rensselaer LINAC could be processed efficiently at the same time the existing void in actual remote terminal batch processing experience could be filled.

The minimum Input/Output configuration for our needs includes a line printer, card reader and punch, paper tape reader, disk storage and a precision curve platter. To be useful, the turn around time on small jobs and compilations via the remote terminal should be less than 15 minutes.

3. COMPUTER VS. HARDWIRED

Two basic terminal philosophies were pursued; the use of a so-called hard-wired telephone terminal and the use of a general purpose computer outfitted with a telephone communications adapter. A survey of available terminal units compatible with the existing N.Y.U. remote batch interface showed the representatives from each philosophy were the Univac DCT-2000 terminal with printer, cord reader and punch versus the IBM 1130 computer with similar peripherals, the computer system costing about twice that of the hardwired system.

The most severe limitation of a typical hardwired terminal system is its restriction of transmission format. Generally these devices transmit one card image at a time, pausing after each record for a line turn-around and acknowledgement from the receiving station. Generally the time used for acknowledgement turnaround is greater than that used for transmitting the card image. When not connected to a central computer, the hard wired device is quite helpless. Most available units can do little more off-line than list or duplicate cards.

The small general purpose computer when used as a terminal becomes an extremely powerful device. Figure 1 diagrams the particular configuration installed at the Rensselaer LINAC. With the exception of the interface to the PDP-7 (under construction), the telephone and some communication software, all items are supplied and serviced by I.B.M. The communications adapter on the 1130 system is rather interesting in that it can converse using either binary synchronous or STR mode. This terminal arrangement is capable of communicating with any present day computer or hardwired terminal (regardless of manufacture) which uses a 201A3 or 201A4 dataset.

Off-line, the Rensselaer terminal becomes a processor capable of some data processing, format changing and production of high quality graphic output under program control.

4. OPERATING EXPERIENCE

After a series of preliminary tests, software was developed at Rensselaer and N.Y.U. to exchange card image and printer image records in the manner of a hardwired unit. These routines take information from the 1442 card reader and transmit it in 8 bit EBCDIC code via the communications adapter. Transmission and reception speed is about 60-70 card or printer records per minute. New communication routines are being written which will organize the information into longer records using sixty bit words coded in CDC-6600 display code. It is expected that communication speeds of 400-600 lines/minute will be achieved.

To date we have gained two months terminal operating experience with an average of about one hour per day. The remote link has shown itself to be highly successful and of unquestionable value to the AEC program at Rensselaer.

The N.Y.U. operating system is particularly convenient for the operation of remote terminals. Large, frequently used programs are stored in source form on a common tape at the N.Y.U. site. Source deck connections and input data are transmitted to N.Y.U. via the link. An N.Y.U. retrieval program, CIMS3, is used to retrieve the source deck and make the corrections before it is compiled and executed. At execution time the user has a choice of output devices so that large amounts of output can be routed to high speed devices at N.Y.U. with samples and summaries being remoted.

Calculations currently being carried out successfully via the terminal include a version of the Harvey-Atta code for analysis of neutron transmission data and the Monte-Carlo code mentioned above. Typical turn-around time for the Harvey-Atta code examining 16 resonances is about 15 minutes. The remote terminal is also being used to expedite the debugging of MC², a program to calculate fast reactor spectra.

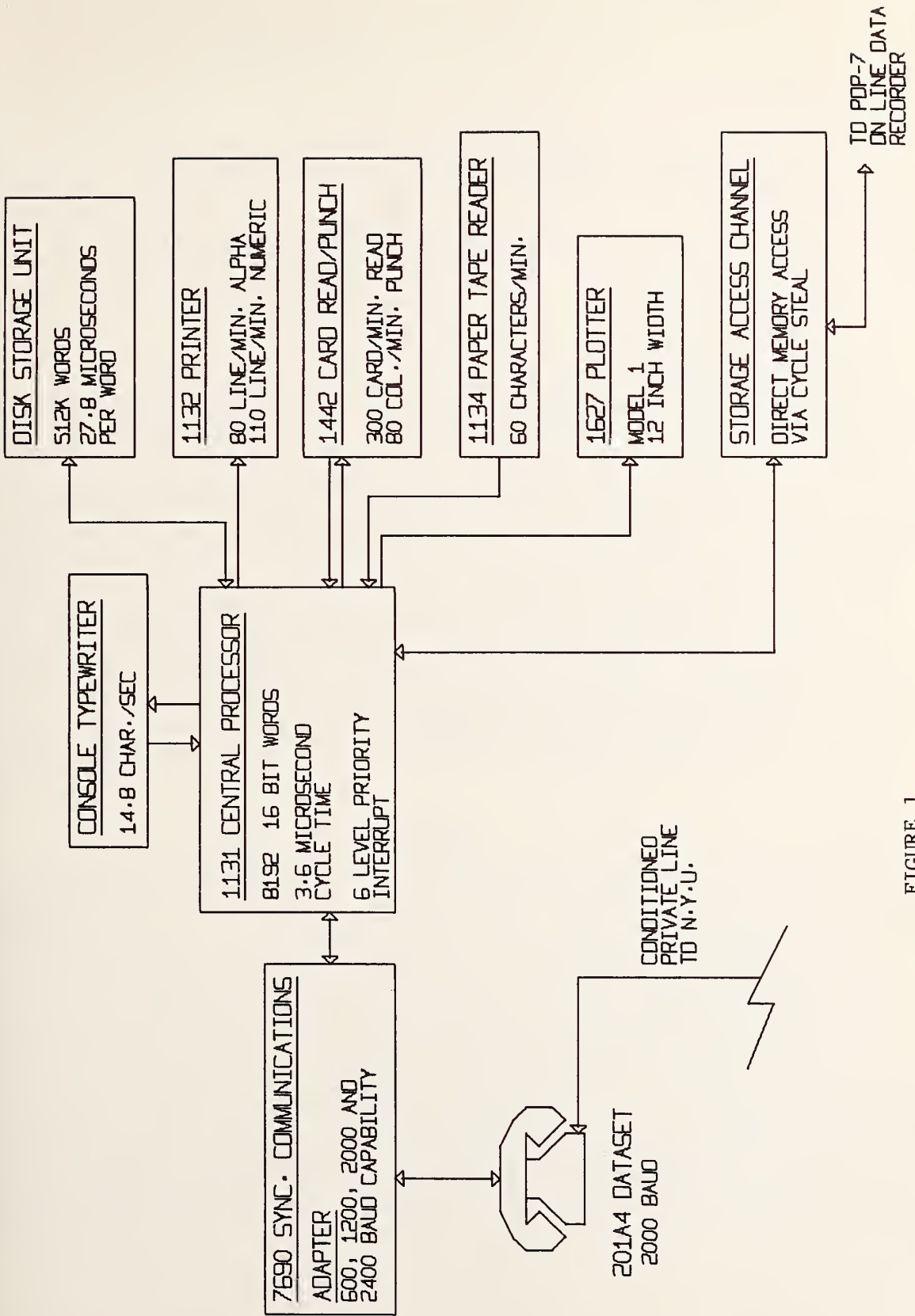


FIGURE 1

LINAC COMPUTER ACCESS TERMINAL

EVALUATION OF URANIUM 238 NEUTRON DATA IN THE
ENERGY RANGE .0001 eV - 15 MeV

by

M. VASTEL, Electricité de France, Paris, France

and

J. RAVIER, Association Euratom - CEA,

Cadarache, France

ABSTRACT

A complete set of neutron cross sections and related quantities has been re-evaluated up to the beginning of 1967 in order to revise the evaluation on Uranium 238 included in 1963 in the United Kingdom Nuclear Data Library. The evaluated parameters have been used in the Breit-Wigner theory in order to calculate the cross sections in the resolved resonances energy range which has been extended up to 3.6 keV. Above 10 keV, this evaluation is mainly characterized by a better determination of the differential elastic scattering up to 1 MeV, an appreciable change in the inelastic cross section in the energy range 0.2 - 0.8 MeV and of the fission cross section between 2 and 4 MeV. No definitive conclusions could be obtained for the capture cross section, because of inconsistencies in both the experimental and theoretical values. A comparison made with evaluations of Uranium 238 data from the KEDAK and ENDF/B Libraries did not reveal large differences but some requests of fast reactor physicists given in the EANDC request list have not been satisfied.

1. INTRODUCTION

This evaluation of U 238 neutron data intends to revise the UKNDL (1) file for this element formerly set up on evaluations made in Winfrith (2) (3) and Aldermaston (4). The literature survey associated with this work is believed to be reasonably complete up to the end of 1966. All other information known to the authors up to the end of 1967 have been considered and the possible disagreements with our evaluation are quoted. The full discussions and all the figures, tables and references relative to this evaluation can be found in two reports (5) (6) to be published very soon. In the next section we summarize the actual situation for the main evaluated quantities we select the outstanding elements of our knowledge either on experimental or theoretical grounds and we draw the attention on the most striking disagreements - in terms of the estimated accuracies reached - between our choices and those of J.J. Schmidt (7) for the KEDAK Library and of W.A. Wittkopf, D.H. Roy, A.Z. Livolsi (8) for the ENDF/B Library (9). In another section we refer to the accuracies

requested by fast reactor physicists, and we come to the conclusion that in some cases our knowledge of the data is not adequate. This knowledge may be improved by properly interpreting fast critical integral experiments.

2. GENERAL STATUS OF THE DATA

The analysis of 214 resolved resonances is now available in the energy range 0 - 3.6 Kev. Two negative energy resonances have been considered in order to reach a thermal value of 2.73 b for $\sigma_{n\gamma}$ and to obtain the shape of the experimental total cross section around 1 ev. Besides the experimental results already considered by J.R. Stehn (10) and also by J.J. Schmidt and W.A. Wittkopf, our evaluation takes also into account the recent Harwell measurements in the energy range 0 - 820 ev (11) which leads us to recommend 23.6 ± 5 mev for $\bar{\Gamma}_\gamma$, value which is 5 % lower than the J.J. Schmidt's one. The calculation of $\bar{\sigma}_T$ with a multilevel Breit-Wigner formalism including Doppler broadening (12) often shows an underestimation of the cross section between the resonances which might be due to some missed p resonances and also to the uncertainty in the distribution of negative energy resonances.

Our evaluated statistical data do not differ very much from those of J.J. Schmidt's though the value of S_0 has been increased ($S_0 = 0.94 + 0.1 \cdot 10^{-4}$) to take into account a possible underestimation (13) of $\bar{\Gamma}_n^0$ above 2 Kev in J.B. Garg's experiments (14). The value of $\bar{\Gamma}_\gamma$ is that obtained from resolved resonances analysis. The use of this data together with the statistical theory gives a higher calculated $\bar{\sigma}_{n\gamma}$ than the recommended one $^{-4}$ which could be better described by using the value $S_1 = 2.10^{-4}$.

The main new information on elastic angular distributions in the energy range .075 - 1.5 Mev has been obtained at Argonne (16) and Harwell (17). For energies greater than 2 Mev, the measurements made in Aldermaston (15) confirm the older ones from Los Alamos (18), (19) and introduce only minor changes. We have extended here (figure 1) to the ENDF/B data of W.A. Wittkopf the comparison made in another report (20) between our evaluation and some others. Apart from the fact that W.A. Wittkopf does not take into account E. Barnard's measurements (17), the main difference is that he follows the experimental results while K. Parker, whose choice has been left unchanged above 2.5 Mev, has considered in addition optical model distribution shapes. For the average cosine of elastic scattering (figure 2) not given in our evaluation but calculated from the evaluated distributions, J.J. Schmidt's choice is almost exclusively based on R.O. Lane's nonelastic angular distributions (2.3) corrected for inelastic

scattering and fission. Around 1.5 Mev we observe the most striking disagreement between the evaluations. It might partly be due to the fact that no coherence is observed between the experimental distributions even when corrections to account for inelastic contributions are performed. J.J. Schmidt's estimation of accuracy on $\bar{\mu}$ is 10 % up to 2 Mev and 5 % above this energy. The total elastic cross section is always obtained by $\sigma_T - \sigma_{ne}$ and an accuracy of 10 to 15 % is estimated for all the energy range.

The Harwell measurements (17) in which the structure of 22 excited levels is set up as far as 1.5 Mev nearly characterized J.J. Schmidt's evaluation (chosen by W.A. Wittkopf & al) and ours at least below 2 Mev. This structure cannot be, around 1 Mev and above, evidently and unambiguously compared to other experiments particularly those obtained by Coulomb excitation (24) (25), (figure 3). Between 1 and 2 Mev, it is not possible to connect the Harwell measurements to those in which values are given for groups of levels (15), (16), (26) (27) but our evaluated inelastic cross section has been nevertheless increased by about 25 % around 1.5 Mev (figure 4). The accuracies relative to each partial inelastic cross section give a total accuracy of about 15 to 20 % below 2 Mev, the maximum error being reached between 1.5 and 2 Mev. Above this energy, the inelastic cross section is taken to be $\sigma_{ne} - \sigma_{nF} - \sigma_{n\gamma} - \sigma_{n2n}$ up to the threshold of (n, 3n) reaction and then based on experimental values around 14 Mev (31), (32), (33). The accuracy which is still around 15 - 20 % up to 6 Mev worsens rapidly above this energy.

Except for statistical shape calculations of S. Pearlstein (37), no new information for (n, 2n) cross section is available and we have kept up the choice of K. Parker based on J.D. Knight's measurements (43) up to 10 Mev (figure 5). These are relative to the effective fission cross section obtained by R.K. Smith (45) i.e. not yet corrected for the low energy component which occurs above 8 Mev in the neutron source reaction D (d, np) D. It seems thus that we must not renormalize to the evaluated σ_{nF} as it is done by J.J. Schmidt whose curve, about 13 % lower than ours around 11 Mev, is taken by W.A. Wittkopf. The estimated accuracy is then about 10 % up to 10 Mev and 20 % above 10 Mev.

The main salient feature for σ_{nF} may be observed in the energy range 1 - 6 Mev (figure 6) where the shape of our curve is mainly based on R.K. Smith's measurements (45) and partly on R.W. Lamphere's (46) which disagree with the former above 2.25 Mev. Using his own evaluation of σ_{nF} (U 235), W.G. Davey (47) removed this inconsistency and obtained a curve, chosen by W.A. Wittkopf which does not practically differ from ours.

J.J. Schmidt's evaluation follows R.W. Lamphere's measurements (below 3 Mev) and is quite similar to K. Parker's. The revision of the absolute measurements of R.K. Smith (48), together with the available new relative measurements of P.H. White (49) and W.E. Stein (50) used with the lowered new evaluations of $\bar{\sigma}_{nF}$ (U 235) - (47), (51) - give a more coherent experimental set mainly around 5 Mev and to a less extent around 2 - 3 Mev. $\bar{\sigma}_{nF}$ should be thus decreased of 15 % from 2 to 6 Mev and of 5 % above 6 Mev, these figures being also characteristic of the accuracy on this quantity.

For the average number of prompt fission neutrons, the accurate relative measurements of I. Asplund-Nilsson (57) and D.S. Mather (58) are limited by the doubtful accuracy on the standard $\bar{\nu}_P^{SP}$ (Cf 252). We have renormalized the experimental values to the IAEA evaluated set of C.H. Westcott (59) and have made a linear fit of the data which gives : $\bar{\nu}_P(E) = (2.32 + 0.03) + (0.152 + 0.006) E$ (Mev), these figures giving an accuracy ranging from 1.5 to 2.5 % from threshold to 15 Mev. This must not be directly compared to J.J. Schmidt's choice, taken by W.A. Wittkopf : $2.358 + 0.156 E$ (Mev) and obtained by renormalizing to the same standards but which includes delayed neutrons.

Our evaluated $\bar{\sigma}_{n\gamma}$ (figure 7) is consistent between 4 and 300 Kev with the evaluation made by T.D. Beynon (60) and the measurements of W.P. Ponitz (from 20 to 100 Kev) (61). Above 300 Kev our evaluation follows J.F. Barry's results (62) as J.J. Schmidt and W.A. Wittkopf do. The actual accuracy on $\bar{\sigma}_{n\gamma}$ ranges from 15 % between 300 Kev and 1 Mev to more than 20 % between 4 Kev and 300 Kev.

3. FAST REACTOR NEEDS

From the Euratom request of EANDC list of June 1967 (63) (64), the requests of J. Ravier, based on a common work with J.Y. Barré (64) on the influence of nuclear data inaccuracies on some characteristic parameters of fast reactors, are not all satisfied in the actual status of the data.

1° - First priority requests

The 5 % accuracy needed on $\bar{\sigma}_{n\gamma}$ is claimed to be reached in some particular recent experiments (61), (62) but a spread much larger than this figure is observed between all the measurements, which implies an identical spread between all the evaluations. Recent measurements (61), (65) and also new adjustment methods of data by interpretation of fast critical integral experiments seem to imply a $\bar{\sigma}_{n\gamma}$ generally lower than the one recommended here of 20 %.

It seems that the 8 % accuracy asked in the energy range 100 Kev - 2.5 Mev on σ_T is just reached in the limited range up to 1.5 Mev. The accuracy reaches 10 % between 1.5 and 2.5 Mev where the total spread of experimental points, large compared with the accuracy of each one may be about 20 %.

The 5 % accuracy needed on the average cosine of elastic scattering between 100 Kev and 2.5 Mev is not reached in so far as we rely on the 10 % estimation made by J.J. Schmidt in this range.

The requested 5 % accuracy on σ_{nn} , from threshold up to 4 Mev is far from being reached according to the actually estimated 15 to 20 % accuracy of our knowledge on this quantity. Concerning the 10 % accuracy needed for excitation cross sections up to 2 Mev, if most of them are known to about 10 to 30 %, this is only up to 1.5 Mev. Higher in energy, the requested 10 % accuracy on nuclear temperature is not reached in consideration of the estimated 10 - 20 % but attention must be drawn on the fact that experimental temperatures are obtained by fitting maxwellian curves on restricted parts of the spectrum and thus do not completely depict the latter.

2° - Priority 2 requests

The knowledge of resonance parameters below 3 Kev allows a good determination of statistical distribution laws though the new results from Los Alamos (65) should imply a strong diminution of $\bar{\gamma}$ down to 19.12 mev. In spite of the above mentioned discrepancy (13 % around 11 Mev) between our choice (taken from K. Parker) and Schmidt's one (taken by W.A. Wittkopf) we think that the 10 % accuracy requested from the threshold up to 10 Mev, is nearly reached though the revision (48) of R.K. Smith's σ_{nF} values should imply a decrease of the relative measurements of J.D. Knight (43) so that σ_{n2n} should be then median between J.J. Schmidt's choice and ours.

As to the 10 % accuracy requested for the fission spectrum below 100 Kev, we do not know of any measurement relative to this part of the observed spectra.

Apart from these requests, the principal hindrance to the 0.5 % accuracy on ν_D (66) is the relative incoherence of the different experimental determinations of the standard ν_P^{SP} (Cf 252).

4. CONCLUSIONS

The positive facts of our actual knowledge of U 238 neutron data are :

1° - a better determination of the differential elastic scattering up to 1 Mev;

2° - an appreciable change of the inelastic cross section around 1.5 Mev which induces proportionnal changes on nonelastic and elastic cross sections, the total cross section being left unchanged.

3° - a better knowledge of the total cross section between 0.2 and 0.8 Mev;

4° - a better definition of the shape of the fission cross section between 2 and 4 Mev.

On the other hand, our evaluations of $\sigma_{n\gamma}$ and σ_{nF} are now too high compared to recent measurements of $\sigma_{n\gamma}$ and σ_{nF} compared to the revision of previous experimental measurements on which σ_{nF} was based; this general trend is consistent with results obtained in interpreting fast critical integral experiments.

Though failing equally about these new information on $\sigma_{n\gamma}$ and σ_{nF} , the evaluations actually contained in ENDF/B, KEDAK and UKNDL do not differ very much except for $\sigma_{n\gamma}$ and σ_{n2n} . But in conclusion, our feeling is that the neutron data for U 238 need further experimental and theoretical attentions in order that the evaluation which could then be done may satisfy the purpose of fast reactor physicists in the actual status of fast reactor theory.

5. REFERENCES

- (1) K. Parker, AWRE O-70/63 (1963)
- (2) H.M. Sumner, AEEW - M 414 (1964)
- (3) E.P. Barrington, A.L. Pope, J.S. Story, AEEW R 351 (1964)
- (4) K. Parker, AWRE O-79/63 (1964)
- (5) J. Ravier, Report DRP/SETR 025 (Feb. 1968 - to be published)
- (6) M. Vastel, EDF Report HX-1/1375 (1968)
- (7) J.J. Schmidt, KFK 120, Part I (1966)
- (8) W.A. Wittkopf, D.H. Roy, A.Z. Livolzi, ENDF 103-BAW 316 (1967)
- (9) H.C. Honeck, BNL 50066-ENDF 102 revised 1967 by S. Pearlstein
- (10) J.R. Stehn & Al, BNL 325 2nd Edition Supplement 2 (1964)
- (11) M. Asghar, C.M. Chaffey, M.C. Moxon, Nucl. Phys. 85 (1966) 305
- (12) J. Ravier et al, REDITE Code, unpublished
- (13) P. Ribon, M. Sanche, H. Derrien, A. Michaudon, Int. Conf. on Study of Nuclear Structure with Neutrons, Antwerp, 1965, paper 166, proceedings p. 565

- (14) J.B. Garg, J. Rainwater, J.S. Peterson, W.W. Havens, jr., Phys. Rev. 134 (1964) B 985
- (15) R. Batchelor, W.B. Gilboy, J.H. Towle, Nucl. Phys. 65 (1965) 236
- (16) A.B. Smith, Nucl. Phys. 47 (1963) 633
- (17) E. Barnard, A.T.G. Ferguson, W.R. Mac Murray, I.J. Van Heerden, Nucl. Phys. 80 (1966) 46
- (18) L. Cranberg, J.S. Levin, LA-2177 (1959)
- (19) M. Walt, J.R. Beyster, R.G. Schrandt, LA-2061 (1956)
- (20) M. Vastel, EDF Report HX-1/1346 (1967)
- (21) E.S. Troubetzkoy & al, UNC-5099 (1964)
- (22) G.D. Joanou, C.A. Stevens, GA-6087 Rev. (1965)
- (23) R.O. Lane, A.S. Langsdorf, jr., J.E. Monahan, A.J. Elwyn, An. of Phys. 12 (1961) 135
- (24) F.S. Stephens, Jr., R.M. Diamond, I. Perlman, Phys. Rev. Lett. 3 (1959) 435
- (25) B. Elbeck, G. Igo, F.S. Stephens, Jr., R.M. Diamond, UCRL-9566 (1960) 25
- (26) R. Batchelor, J.H. Towle, Proc. Phys. Soc. (London) 73 (1959) 193
- (27) L. Cranberg, J.S. Levin, Phys. Rev. 109 (1958) 2063
- (28) R.B. Day, D.A. Lind, unpublished (reported ANL 6132) (1960)
- (29) A. Faessler, W. Greiner, R.D. Sheline, Nucl. Phys. 70 (1965) 33
- (30) C.L. Dunford, IAEA Conf. on Nuclear Data for Reactors, Paris 1966, Paper CN-23/41, Proceedings I, 429 (1967)
- (31) L. Rosen, L. Stewart, LA-2111 (1957)
- (32) R.L. Clarke, Can. J. Phys. 39 (1961) 957
- (33) K.W. Allen, P. Bomyer, J.L. Perkin, J. Nucl. Energ. A/B 14 (1961) 100
- (34) J.S. Levin, L. Cranberg, LADC-2360 (1956)
- (35) C.E. Mandeville, D.L. Kavanagh, CWR-4028 (1958)
- (36) Texas Nuclear Corporation, in WASH-1068 (1966) 194
- (37) S. Pearlstein, BNL-897 (T-365) (1964)
- (38) E.R. Graves, The Reactor Handbook I, AECD-3645
- (39) N.J. Poole, unpublished, quoted in ref. (46)
- (40) J.A. Phillips, AERE-NP/R-2033 (1956) correction made in Ref (46)
- (41) G.P. Antropov, Y.A. Zysin, A.A. Kovrizhnikh, A.A. Lbov, Soviet J. At. Ener. 5 (1958) 456
- (42) E.R. Graves, J.P. Conner, G.P. Ford, B. Warren, unpublished quoted in Ref. ((45)
- (43) J.D. Knight, R.K. Smith, B. Warren, Phys. Rev. 112 (1958) 259
- (44) J.L. Perkin, R.F. Coleman, J. Nucl. Ener. A/B 14 (1961) 69
- (45) R.K. Smith, R.L. Henkel, R.A. Nobles, Bull. Am. Phys. Soc. 2 (1957) 196
- (46) R.W. Lamphere, Phys. Rev. 104 (1956) 1654
- (47) W.G. Davey, Nucl. Sci. & Eng. 26 (1966) 149
- (48) R.K. Smith & al, EANDC Communication (April 1967)
- (49) P.H. White, G.P. Warner, J. Nucl. Ener. 21 (1967) 671
- (50) W.E. Stein, R.K. Smith, J.A. Grundl, Conf. on Neutron Cross Sections & Technology, Washington 1966, Proceedings p 623

- {51} W. Hart, AHSB - (S) - R - 124
- {52} K. Parker, AWRE O-82/63 (1963)
- {53} V. Emma, S. Lo Nigro, C. Milone, R. Ricamo, Nucl. Phys. 63 (1965) 641
- {54} N.D. Allen, A.T.G. Ferguson, Proc. Phys. Soc. A 70 (1957) 573
- {55} F. Netter, CEA Report 1913 (1961)
- {56} V.M. Pankratov, Soviet J. At. Ener. 14 (1963) 167
- {57} I. Asplund-Nilsson, H. Condé, N. Starfelt, Nucl. Sci & Eng. 20, (1964) 527
- {58} D.S. Mather, P. Fieldhouse, A. Moat, Nucl. Phys. 66 (1965) 149
- {59} C.H. Westcott & al., At. Ener. Rev. 3, 2 (1965) 3
- {60} T.D. Beynon, J. Nucl. Ener. (1966, 20) 146
- {61} W.P. Ponitz & al., KFK 635 (1967)
- {62} J.F. Barry & al., J. Nucl. Ener. 18 (1964) 481
- {63} Compilation of requests from Euratom Countries, EANDC (E) 83-U (1967)
- {64} J.Y. Barré, J. Ravier, IAEA Conf. Fast Reactor Physics & Related Safety Problems, Karlsruhe 1967 SM 101/58
- {65} N.W. Glass & al., EANDC Communication (1967)
- {66} A.L. Pope, J.S. STory, EANDC Communication (March 1966)

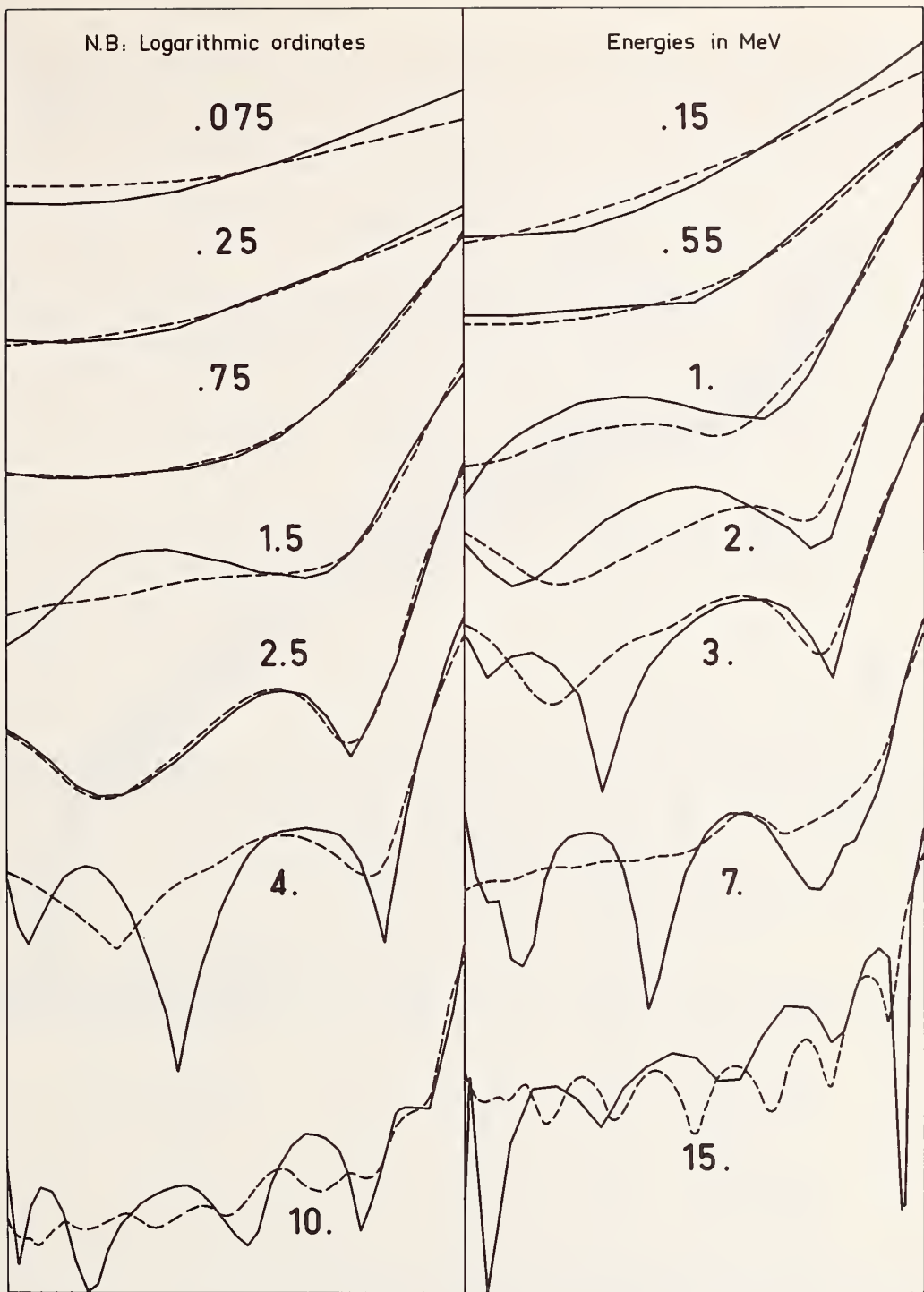


Figure 1: Comparison of our evaluated normalized elastic distributions to those (dotted line) deduced from W.A. Wittkopf & al (8)

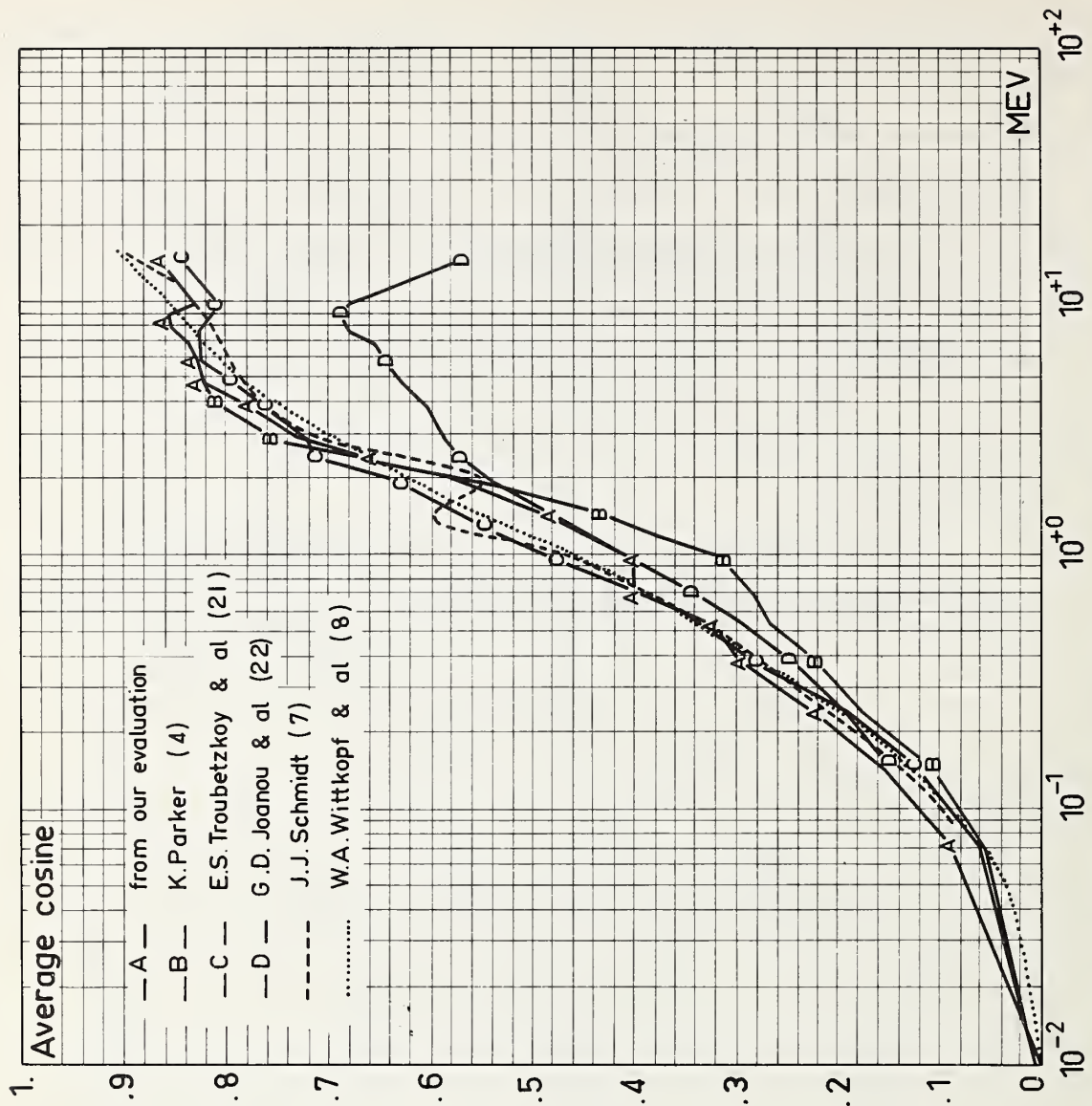


Figure 2: Average cosine of elastic scattering angle

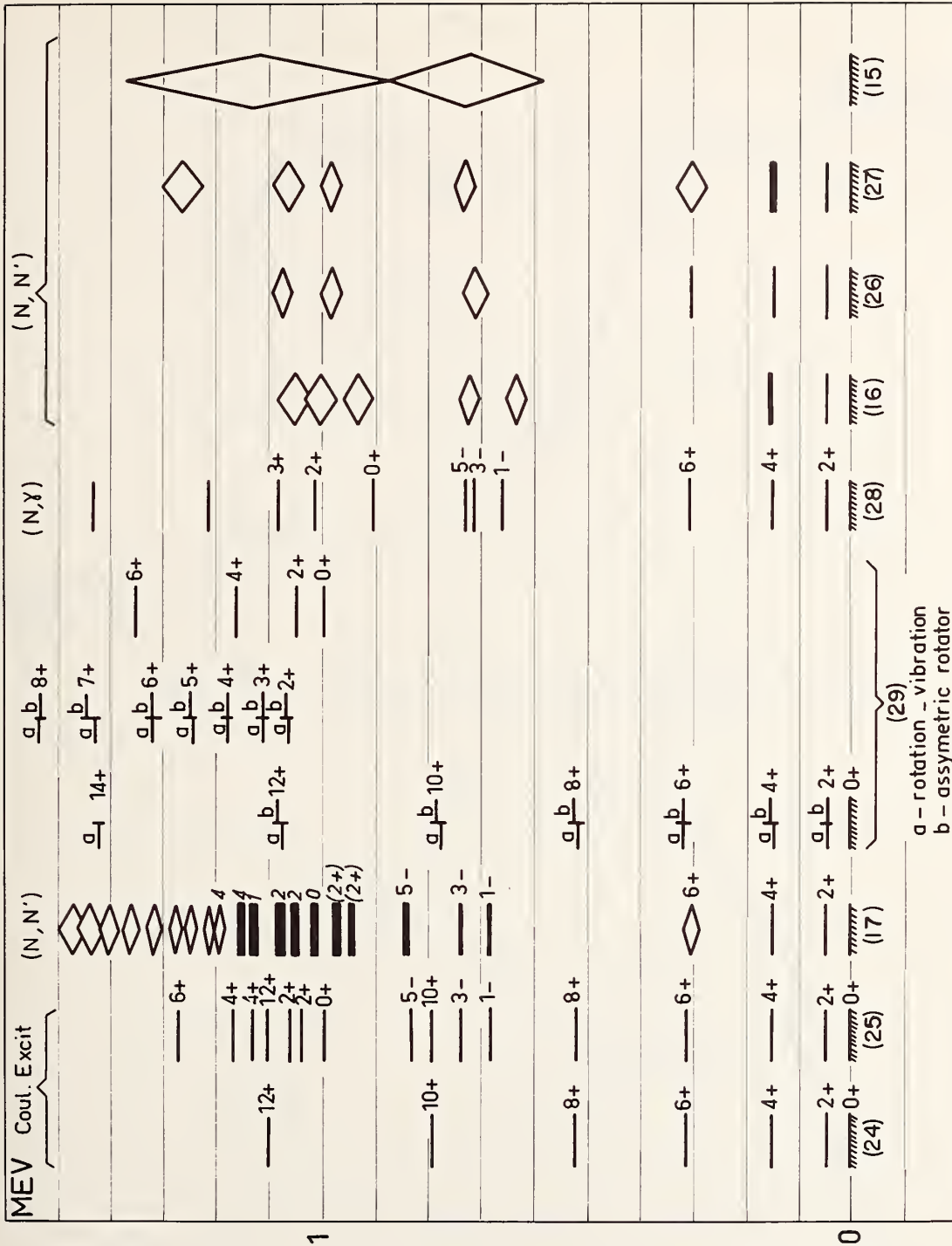


Figure 3: Levels or groups of levels observed or calculated

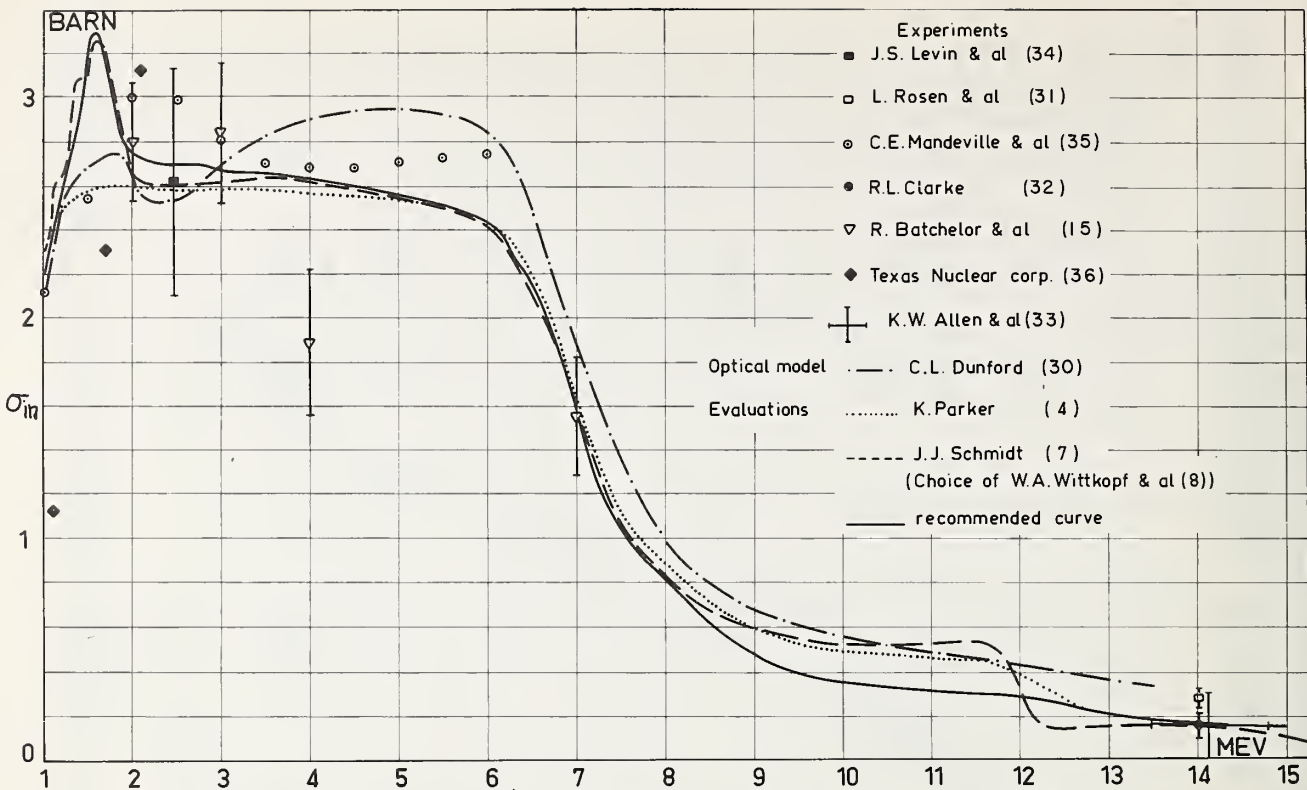


Figure 4: Inelastic cross section from 1 to 15 MeV

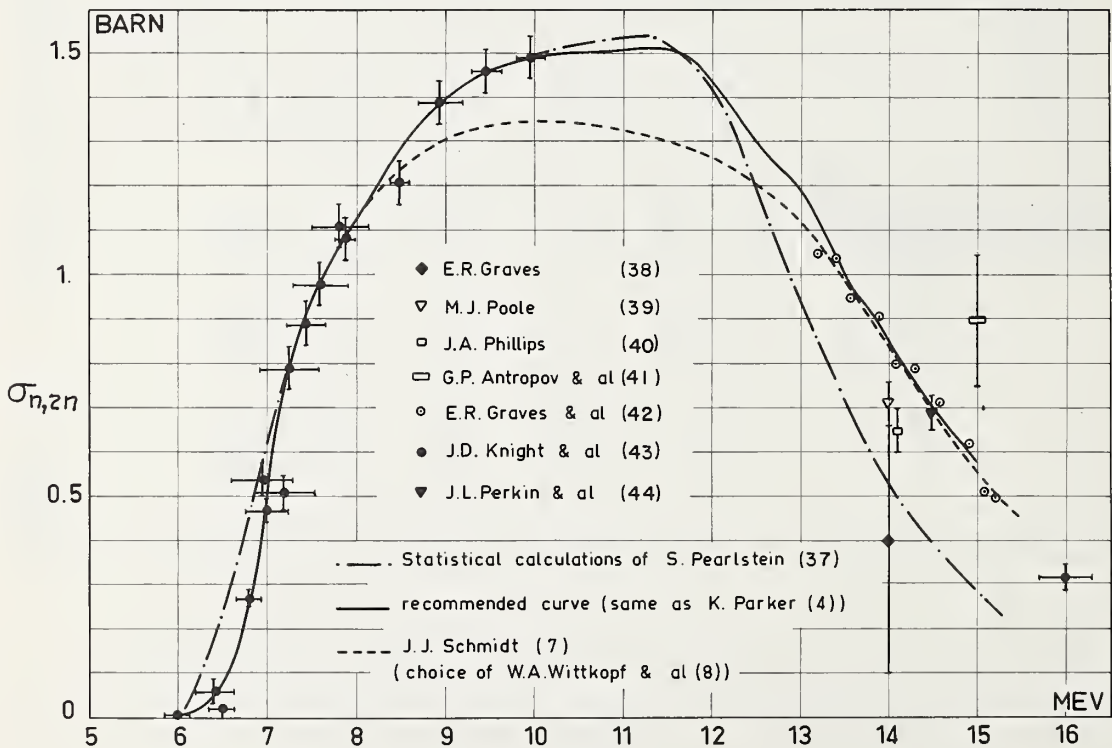


Figure 5 : (n,2n) cross section

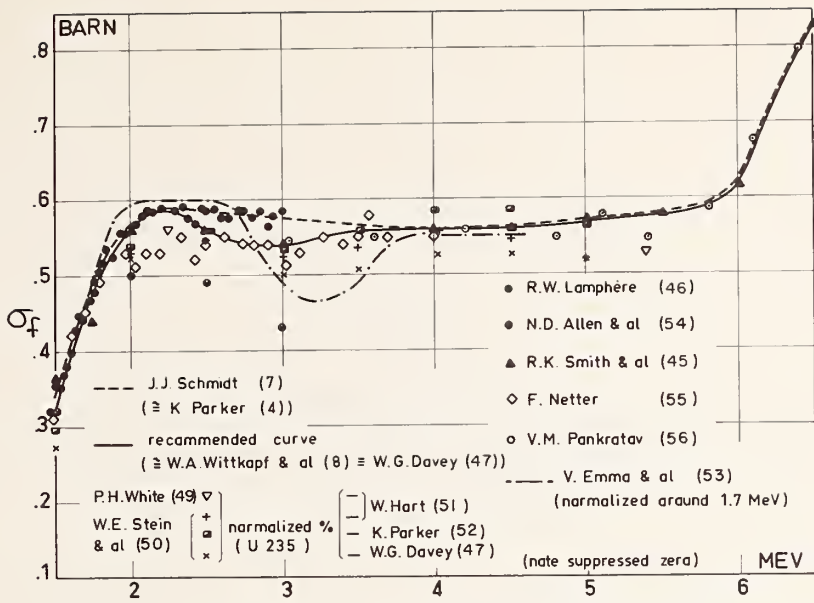


Figure 6 : Fission cross section from 1.5 to 6.5 MeV

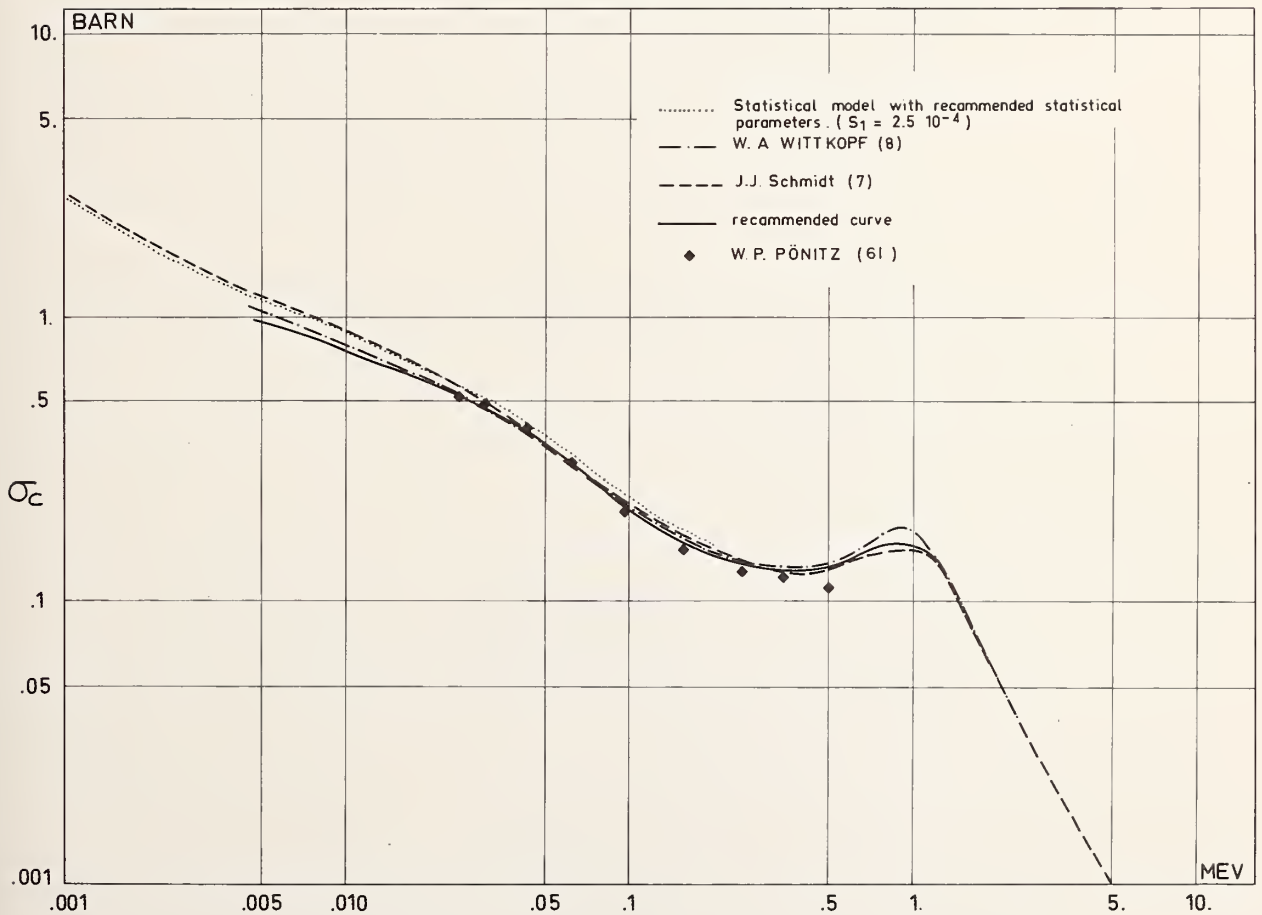


Figure 7: Capture cross section from 1 keV to 10 MeV

Session H

USE OF DIFFERENTIAL DATA IN
ANALYZING INTEGRAL EXPERIMENTS

Chairman

D. BOGART
NASA-Lewis

NEUTRONIC MEASUREMENTS IN NON-CRITICAL MEDIA*

C. A. Stevens

Gulf General Atomic Incorporated
San Diego, California 92112

ABSTRACT

Several types of subcritical experiments, whose purpose is to provide integral checks of cross sections and computational methods in fast reactors and fast neutron shielding, are discussed.

These include studies of the time response to a pulsed neutron source, steady state neutron spectrum measurements, and transmission measurements. The methods which are used to analyze these experiments are described, with the emphasis placed on what cross section information can be extracted from them. A description of how cross section averaging procedures are actually performed in some of the more sophisticated codes designed for this purpose is included.

*Work supported by the U. S. Atomic Energy Commission.

1. INTRODUCTION

In this paper we will discuss a number of experiments on subcritical media, with the emphasis placed on what cross section information can be obtained from the analysis of these experiments. We shall aim our discussion primarily to experiments which support fast reactor development, with some comments about fast neutron shielding.

In an integral experiment it is desirable, but not essential, to measure a quantity which not only can be used to judge the quality of cross sections and computational methods, but which can also be used directly in practical design computations. The resonance integral, diffusion length, diffusion coefficient, neutron age, and prompt neutron decay constant parameters all serve this double purpose in the thermal reactor development program. These parameters are measured by a wide variety of techniques, many of which are well established today. (1) Another integral experiment, namely the measurement of thermal neutron spectra, serves only one of these purposes. The spectra generated in that experiment are generally not used directly in design calculations, but they provide valuable checks on cross sections and computational methods which are so used. It would be most convenient if the integral experiments which have been so well developed for thermal reactors could be used, with only minor modification, to support fast reactor design. In some cases, this is being accomplished - such as in the measurement of spectra by the time-of-flight method - however, there are several reasons why the thermal reactor techniques are not applicable to fast systems. Unlike for thermal reactors, fast reactor analysis tends not to be reducible to one or two equations with coefficients that are simply related to a diffusion length, resonance integral, etc. Hence, fast neutron subcritical integral experiments will serve to provide checks on methods and data, but they will seldom provide constants for direct use in a fast reactor design. Much of the analysis for a thermal system depends on the fact that neutrons can be scattered up in energy as well as down, and furthermore, that there is a simple relation, due to detailed balance, between the kernel for upscattering and that for downscattering. This is the case, for instance, for the diffusion length experiment and the determination of the diffusion coefficient from a pulsed neutron die-away experiment. (2) In fast systems, fission replaces scattering as the mechanism for increasing neutron energy and there is no relation, like that of detailed balance, between "upscattering" and downscattering. This means that some thermal system techniques carry over only to fast multiplying systems and, even then, the analysis of the experiment is more complicated for the fast system.

There are experimental difficulties also. For instance, there are no isotopes, like cadmium or indium for thermal systems, that can absorb almost all neutrons below a fixed high energy while leaving those at still higher energies undisturbed. The measurement of neutron age and the resonance integral, in thermal systems, depends on the use of such filter detectors.

From the above we realize that we cannot use thermal neutron techniques intact to study fast neutron integral experiments. Instead, these techniques have to be modified and new techniques developed. Here we shall discuss some integral experiments which are used for fast neutron systems. These consist of studies of the time response to a pulsed neutron source, neutron spectrum measurements, and transmission measurements. We shall include some discussion of the methods of analyzing these experiments, and a general discussion of the computation of effective cross sections from basic data. The latter pertains to the analysis of integral experiments in general, as well as of more complicated and realistic reactor configurations.

2. PURPOSE OF INTEGRAL EXPERIMENTS

The purpose of the subcritical integral measurements that we discuss here is to provide integral checks on basic cross section data and on computational methods used in the design of complicated systems.

Many integral experiments serve to provide fitted constants to simple phenomenological models of complicated systems. Among these, for instance, are one- and two-point kinetics models of reflected reactor systems, or one-velocity treatments of significantly moderating systems. Such experiments will not be covered here since their analysis provides little or no information about cross sections, although they do serve the role of providing simple models for other uses.

Other integral experiments which will not be discussed are concerned primarily with a direct design application, and cross section information obtained, if any, is only of secondary interest. This is so even though an extensive analysis is required to interpret the experiment properly. The measurement of shutdown reactivity is an example of this type of integral experiment.

A well-conceived integral experiment is sufficiently simple, in geometric arrangement for example, so that it can be analyzed in detail, at reasonable cost, without resorting to approximations of inestimable accuracy. In addition, the experimental results should be fairly sensitive to cross sections and methods being investigated, but they should

not be overly sensitive to uncertainties in cross sections and methods whose importance do not reach beyond the experiment at hand. In fact, the sensitivity, even to cross sections of interest, should not greatly exceed that required for the practical application. The difficulty here, though, is that practical applications vary quite widely and the accuracy requirements for, say, fast reactors and shielding differ very substantially, even from one type of fast reactor to another.

The desired sensitivity of an experiment to a particular cross section can be computed realistically only when the uncertainties in the cross section are well known. Sensitivity calculations for arbitrary cross section changes, on the other hand, are not easily interpreted. In a typical sensitivity test, the cross section for the reaction of interest is changed in some arbitrary manner and the computed estimate of the measured quantity is compared with its value before the cross section change. If the difference is significant, we say that the measurement is sensitive to that particular cross section. There are several difficulties with this approach. The most obvious is that a cross section, especially at high energies, can be changed arbitrarily in a very large number of different ways. At low energies, it is generally much easier to justify changing a cross section by, say, multiplying it by a constant over a specific energy range. The behavior of fast neutron cross sections is sufficiently complicated, so that one is not likely to learn much from such a simple arbitrary change. Secondly, if one cross section is changed, should this be compensated by another cross section change or not? For instance, if we change the inelastic cross section, should we then change the elastic (or capture) cross section so that the total cross section remains unchanged, or should we allow the total cross section to change? To avoid such ambiguities it seems preferable to change some more fundamental quantity such as an optical potential parameter, spin or parity assignment of a nuclear level, or the number of degrees of freedom for a χ^2 distribution used for the unresolved resonance calculation. The sensitivity could then be determined using a new cross section set based upon this change. Such systematic computations would be of considerable help in the final interpretation of experiments but, probably because of large computer expenses involved, they have not yet been carried out.

Sensitivity calculations, in practice, are frequently made by making arbitrary changes in group cross section sets. This is done by necessity and, as seen above, the information obtained about basic cross sections is not without ambiguity. No one has, to this date, made a systematic comparison of sensitivity calculations for a variety of sub-critical experiments.

In some cases, as we shall see, it is possible to use an integral check to judge the cross section for a specific reaction, isotope, and energy range. In general, however, such measurements depend heavily on many reactions over wide energy ranges. For this reason an integral measurement is usually best used as a check on an entire evaluated cross section set rather than on an isolated nuclear cross section. Nevertheless, it is true that some integral experiments place greater emphasis on some cross section and energy ranges than on others. Consequently, a variety of integral measurements is desirable. Later on we shall discuss, more specifically, the details of several such experiments.

3. ANALYSIS OF EXPERIMENTS AND CROSS SECTION UNCERTAINTIES

A discussion of the methods of analysis of experiments can be divided into a discussion of the computation of "effective" cross sections from basic nuclear data and a discussion of methods of solving the transport equation. In keeping with the tone of this conference, we emphasize the former in this discussion, although it is clear that the two are not always easily separable.

Although there is a variety of methods in use to obtain effective cross sections, these are usually used as "group cross sections." These average cross sections are obtained by weighting the basic cross sections with some function, usually an estimate of the scalar flux spectrum at the position of interest, between well-defined energy limits. The uncertainties in the group cross sections accumulate from a lack of basic cross section data, as well as from the approximate nature of the weighting function. Until very recently, these uncertainties have been so large that most users abandoned the task of computing cross sections for their particular application and, instead, used "universal" tabulated group cross section sets.(3) This has been particularly true in fast reactor design. These universal sets were arrived at from whatever sparse data was available, complemented with nuclear model calculations, and then "adjusted" so that as large a range of critical mass and reactivity worth experiments as possible could be reasonably well predicted with their use. These group cross sections, which are still much in use today, usually require very delicate handling. They can often fail to predict the gross properties of systems which differ substantially from those for which the cross sections were adjusted, and they can lead to grossly incorrect predictions of neutron spectra and other important quantities, even in those systems for which the critical mass and reactivity worths were used to make the cross section adjustments. Today, the basic uncertainties are still large enough so that the adjusting procedure is still much in use. In fact, recent work discusses how these

adjustments can be made more systematically with computers, and how more integral data, such as spectrum measurements, can be used to further determine cross section values. (4, 5)

The alternative approach to the cross section problem, which is coming more and more into use, is the calculation of effective cross sections from basic principles. The value of experiments in this case is to check the adequacy of the models used for the cross section evaluation and of the basic data, not to adjust the cross sections themselves.

The cross section analysis, for our purposes, begins with the compiling of the cross section master data files. These consist of a collection of the best available data, presented in very fine energy detail. Any gaps that exist due to a lack of experimental data are filled with suitable interpolations, both by eye and by nuclear model calculations. These data are in a form which could be used directly in a Monte Carlo code having a very fine energy detail capability. Generally, however, a considerable amount of further manipulation is required before these cross sections are suitable for standard multigroup transport and diffusion codes. At present, the ENDF files(6) are becoming the standard source of evaluated data throughout the United States.

The cross section evaluator makes difficult decisions regarding whose experimental data he will use, what nuclear reaction models he will use to interpolate between the measured points, and what computer programs will be used to perform the calculations. As we all know, there are very few isotopes for which cross sections, angular distributions, secondary energies, and other important nuclear parameters can be tabulated accurately over the entire energy range of interest. This situation will remain with us for some time, even with the continuing of the rapid progress which is being made today in cross section measurements, nuclear theory models, and large computer programs.

In addition to uncertainties which arise due to our incomplete knowledge of nuclear cross sections, other uncertainties arise for more mundane reasons. The lengthy data processing, which includes sorting large quantities of data in several ways and preparing several different, but hopefully equivalent, representations of the same data so that it can be of the greatest benefit to cross section users, is subject to errors unless backed up with very extensive checking procedures. For example, the elastic scattering angular distributions are usually tabulated as the coefficients of a Legendre polynomial expansion of the angular distribution. However, the sharply peaked distributions which are typical for heavy nuclei at high energies are not easily represented by a reasonable

number of polynomials. Typically, with only a few polynomials, the angular distributions are not only inaccurate, but can lead to negative cross sections.(7) Similarly, the representation of cross sections as sums of single-level Breit-Wigner cross sections can lead to negative cross sections and other well-known inaccuracies.(8) Many other difficulties of this type can and do occur, but we do not propose to dwell on those here. Suffice it to say that by the time a cross section has been evaluated, there is little reason to use it indiscriminately without some assurance that its use leads to good agreement with integral experiments.

The making up of the evaluated nuclear data file is only the first of many cross section manipulations that are required to compute effective cross sections for most applications. The next step usually transforms the pointwise data to fine (or ultra-fine) multigroup data.

This consists of carrying out integrals of the types:

$$\int \sigma(E) \varphi(E) dE,$$

$$\iint dE' dE \sigma(E' \rightarrow E) \varphi(E'),$$

and

$$\iiint dE' dE d\mu \varphi_n(E') \sigma(E' \rightarrow E, \mu) P_n(\mu)$$

where σ is a cross section or scattering kernel (scattering kernels are in laboratory coordinates), $P_n(\mu)$ a Legendre polynomial, φ is a weighting function which is usually a rough estimate of the flux at the position of interest, and φ_n is an estimate of the n'th Legendre component of the angular flux. The cross sections often vary quite rapidly with energy or angle. Resonances, thresholds, and discontinuities in scattering kernels all must be handled with great care in the integrations. In practice, the very fine mesh which is necessary for accurate evaluation

of some of the integrals is not always feasible within the limits of acceptable computer times, nor is it warranted because of large uncertainties in the pointwise cross sections. A number of codes are used to perform these computations at Gulf General Atomic, (9) and other institutions have similar computer programs.

The results of the integrations serve as the master cross section file for multigroup calculations. These same cross sections are used for almost all reactor design problems. The only exception is when the integrals are very sensitive to the choice of weight function, or when the cross sections depend sensitively on temperature (Doppler broadening). In these cases, the integrals are carried out separately for each application, and use is made of the temperature and a weight function which is more suitable to the immediate application because it includes self-shielding effects.

The next cross section manipulation is performed when a specific problem requires to be solved. Material concentrations, gross leakage, energy and spatial self-shielding are now taken into account in the determination of a more accurate weighting function for those cross sections which are sensitive to the weighting function. In addition, Doppler broadening of cross sections is included. With the help of these refinements, the integrals mentioned previously are once again carried out. For a long time, it was traditional to treat only resonance capture and fission in this manner. Then it became apparent that the wide scattering resonances of intermediate mass nuclei, like aluminum and sodium, also required this additional attention. (10) More recently, integral experiments have indicated a possible need to include self-shielding effects, at high energies, even for the smaller and narrower scattering resonances of heavier nuclei, like tungsten. (11)

A full description of the details by which the corrections mentioned above, particularly self-shielding, are performed is impossible here since they constitute a large portion of what is called reactor physics. Large computer programs, with primary application to fast reactors, have recently become available for computing these cross sections. Among these are MC²(12) and GAF-GAR, (13) which obtain fine group fluxes in the P-1 or B-1 approximation. The effects of spatial heterogeneities, overlapping resonances of the same isotope and of mixtures of isotopes, representation of fissile cross sections by single level or a variety of multilevel, multichannel notations, neutrons of angular momentum $\ell > 0$, and other details of the cross section problem are handled by these codes. Naturally, these contain many approximations whose accuracy is difficult to assess by computation alone.

The last cross section manipulation is usually done immediately after the one described above. It consists of collapsing the fine group cross section data to a coarser group structure. The uncertainties introduced in this step can easily be as large as those in the previous manipulations. Each homogeneous subregion of the actual configuration is first approximated by a bare homogeneous system having the mixture of materials in the subregion. The multigroup neutron balance equations, with space dependence replaced by a buckling, are solved, by the P-N or B-N methods, for the Legendre components of the flux in fine group detail. These are then used as weighting functions to reduce the fine group cross sections to a coarser group structure. This step can be done within the MC² or GAR-GAF codes if only P₀ and P₁ scattering matrices are desired. In many applications, however, it is necessary to use P₃ scattering matrices. Then this last step can be done in the GGC-III, (14) or other similar computer program. GGC-III, in its present form, can obtain P₃ scattering matrices, but it does not have the fine energy mesh capability of the GAF-GAR or MC² programs. There is no widely distributed computer program which computes matrices for P_n scattering for n > 3.

The replacement of each subregion of the true configuration by a bare homogeneous system is not strictly justified, and many practical questions arise from this procedure. These pertain to the value chosen for the buckling, or even if the buckling model is adequate; they pertain to the high energy source used in the neutron energy balance equations, particularly in regions, like a reactor shield and reflector, which do not have a source in the actual configuration. How many coarse groups are needed for the analysis? Is it just a few, as is typical for large homogeneous systems with a distributed source, or are many required, as is the case for a system in which the spectrum varies widely at different positions? Many energy groups will generally be required to predict the correct behavior near an interface between a highly loaded reactor core and a low absorbing reflector, or to predict the penetration through a thick shield. In the latter case, it is also important to have sufficient energy detail to describe the low energy side of scattering resonances in which interference between potential and resonance scattering creates cross section dips through which neutrons can penetrate large distances. (15) Other questions deal with the best way to truncate the Legendre scattering matrices, and how to introduce appropriate transport, or extended transport, cross sections. (16) It is these multigroup cross sections which are finally used in diffusion or transport codes, such as those based on the S_n method, to compute spectra, reactivities, flux profiles and other important integral properties of reactors or nonmultiplying media.

We have reviewed, in a very brief manner, the procedures which are used to transform pointwise cross section data to effective multi-group cross section data. Because this is a cross section conference, we have emphasized the uncertainties in the computation of effective cross sections. There are, of course, a large number of additional uncertainties associated with the solution of the transport equation itself, particularly if the geometry is not one-dimensional.

Causes of uncertainty have been identified in order to both point out the need to carry out "clean" integral experiments and to remind experimenters of the large mixture of effects which they are actually measuring. Specific experiments will now be discussed.

4. TIME-DEPENDENT STUDIES

A comparison of the measurement and analysis of the time response of a fast subcritical assembly to a pulsed source of neutrons offers an integral check of cross sections and computational methods. In addition, the time response is of direct interest in several applications. Among these are the determination of subcritical reactivity and the design of pulsed reactors and accelerator boosters. Here, we shall concentrate only on a discussion of how time-dependent experiments can be used to evaluate cross sections and computational methods.

Probably the most widely performed experiment consists of placing a detector inside, or next to, a fast homogeneous assembly. A pulsed source is used to trigger the assembly, and the resulting time behavior of the detector response is measured with the aid of a multi-channel analyzer. Among the interesting observations to be made on such a system are the response for different detectors, detector positions, and source energies and positions. Of primary interest is a persisting exponential time behavior, particularly if the decay constant is independent of source and detector position. This behavior indicates the presence of a fundamental mode and greatly facilitates the experiment-analysis comparison.

Consider the transport equation in the general form

$$\frac{1}{v} \frac{\partial \phi}{\partial t} = H\phi + S \quad (1)$$

Look for solutions to the homogeneous equation,

$$\frac{1}{v} \frac{\partial \varphi}{\partial t} = H\varphi \quad , \quad (2)$$

which are of the form

$$\varphi(r, E, \Omega, t) = \varphi(r, E, \Omega) e^{-\lambda t} \quad (3)$$

This leads to the equation

$$(H + \frac{\lambda}{v})\varphi(r, E, \Omega) = 0 \quad (4)$$

which may have a finite or infinite number of discrete eigenvalues; there may even be no discrete eigenvalues. (2) In a fast system, we expect to find a fundamental mode only if the system is critical, or not extremely subcritical ($k \gtrsim 0.8$). (17) The measurement of the fundamental decay constant, usually denoted by α , is one of the classic experiments of reactor physics. It can be easily measured and computed in a fast reactor system, either by the Rossi technique, (18) or by the pulsed neutron dieaway technique. (19, 20, 21)

A comparison of the measured and computed values of α serves as an integral check on cross sections and methods. Some insight concerning the relationship between α and the cross sections can be obtained by considering the homogeneous transport equation in the form

$$\frac{1}{v} \frac{\partial \varphi}{\partial t} = -L\varphi + F\varphi$$

where L contains all reactions except for fission which is represented by the operator F ; that is, $H = F - L$. The corresponding eigenvalue equation for α is

$$\left(L - \frac{\alpha}{v}\right)\varphi = F\varphi \quad (5)$$

If there is a real, discrete eigenvalue α , corresponding to a fundamental mode φ - that is, $\varphi = \varphi_{\alpha} e^{-\alpha t}$ - then we can express α as

$$\alpha = \frac{\langle \varphi_{\alpha}^* L \varphi_{\alpha} \rangle - \langle \varphi_{\alpha}^* F \varphi_{\alpha} \rangle}{\langle \varphi_{\alpha}^* \frac{1}{v} \varphi_{\alpha} \rangle} \quad (6)$$

The notation $\langle \rangle$ denotes appropriate integration over the independent variables, and φ_{α}^* is the solution of the adjoint equation

$$\left(L^* - \frac{\alpha}{v} \right) \varphi_{\alpha}^* = F^* \varphi_{\alpha} \quad (7)$$

The prompt decay constant, α , then represents a weighted average of the difference between the operators L and F . The integral check, itself, provides an over-all indication of the capability to compute the balance between processes which create neutrons and those which reduce their population. α is also interpretable as the amount of $1/v$ absorber, homogeneously distributed throughout the system, which must be removed in order to make the system critical. This fact is often put to good use in the calculation of α , but it does not yield much information about cross sections.

The measurement of α provides a number of integral checks because it can be done for a variety of subcritical configurations, including individual components of a geometrically complex system. Critical mass experiments are, on the other hand, limited to configurations for which $k=1$. In addition to this added flexibility of the α measurement, financial advantages, over critical mass experiments, are possible due to the lower fuel inventories required. Furthermore, it is not much more difficult to compute α than it is to compute k with modern computer codes.

Of the integral experiments discussed in this paper, the α measurement probably yields more information about the fission cross section than do the other experiments. This is because it represents a balance between production by fission and loss by other processes and because, unlike the other experiments, it does not depend on the characteristics of an external source.

The α measurement, as was mentioned previously, is applicable only to systems with $k \gtrsim 0.8$. In recent years, the modal analysis has been extended to systems of lower multiplication by the concept of the "pseudo-fundamental mode." This arises in the following way.

The complete solution of Eq. 1 may be represented as

$$\varphi(r, E, \Omega, t) = \sum_{\nu} \varphi_{\nu}(r, E, \Omega) e^{-\lambda_{\nu} t} + \int d\lambda A(\lambda) e^{-\lambda t} \varphi_{\lambda}(r, E, \Omega) \quad (8)$$

where the λ_{ν} are the discrete eigenvalues, φ_{ν} are the corresponding eigenfunctions, and the integral represents the contribution of the continuum eigenvalues. Here we have assumed that the discrete and continuum eigenfunctions form a complete set. The λ_{ν} are fundamental properties of the system, independent of the source, but $A(\lambda)$, which gives the relative abundance of modes in the continuum, does depend, in principle, on the source. If this source dependence is small and if, furthermore, $A(\lambda)$ is highly peaked about some λ , say λ_p , then we say that λ_p is a pseudo-fundamental eigenvalue.

The goal, then, is to isolate such eigenvalues, both experimentally and analytically and use the comparison as an integral check of cross sections and methods.

These methods have been discussed in the literature, (17) but they are still in an early stage of development. Comparison of calculations and measurements have been made on the subcritical facility SUAK, (20) but they are not sufficiently conclusive to be used as referees in choosing cross section sets.

A careful analysis of the "pseudo-eigenvalue" problem requires that the analyst be able to separate true "eigenvalues" from those which are artificially introduced by the multigroup approximation to the continuous energy variable, or by the somewhat arbitrary procedure of neglecting low energy effects. (17) This is not always easy to achieve. Another serious analytical problem arises from the multigroup approximation; the weighting function used for computing the group cross sections, which is usually an estimate of the steady-state spectrum, bears little resemblance to the true spectrum which exists during the decay. Probably the only way around this problem is to use a very fine energy group structure for any "pseudo-fundamental" mode analysis.

In addition to the modal method, there are a number of other ways to analyze a time-dependent pulsed neutron source experiment. We will discuss briefly those which are most useful, or potentially useful, particularly for systems which are highly subcritical.

5. Moments Method

The time moments method was first used by Parks to analyze pulsed neutron experiments in thermal systems. (22) It has also been discussed for higher energy neutrons. (23)

Again consider the transport equation,

$$\frac{1}{v} \frac{\partial \phi}{\partial t} = H\phi + S \quad (1)$$

It is to be understood that ϕ may depend on energy, position, angle and time. We assume that the operator H is independent of ϕ (no feedback), so that the equation is linear. Furthermore, we assume that H does not depend on the time t (constant reactivity).

Multiply by $\frac{1}{n!} t^n$, integrate, and define

$$M_n = \frac{1}{n!} \int_0^{\infty} t^n \phi dt \quad (9a)$$

$$Q_n = \frac{1}{n!} \int_0^{\infty} t^n S dt \quad (9b)$$

to get

$$H M_0 + Q_0 = 0 \quad (10a)$$

and

$$H M_n + Q_n + \frac{M_{n-1}}{v} = 0, \quad n > 0 \quad (10b)$$

It is, of course, necessary, that the integral in Eq. 9 exists, but this is assured if we are subcritical or, if we ignore delayed neutrons, sub-prompt critical.

Equation 10a is the usual steady-state equation for the system. Equation 10b is also a set of steady-state equations with the modified source,

$$Q_n + \frac{M_{n-1}}{\nu} .$$

So, with the recursive use of any available steady-state computer program, Eq. 10 permits the solution of the time moments of the actual distribution. It is possible, in principle, to construct the time dependent pulse shape from the moments, as has been done for thermal neutron assemblies, (24) but this has not been done for fast systems. In practice, the calculated moments can be compared directly with the moments of the measured pulse shape.

The principal advantages of this method are:

1. Existing steady-state codes can be used with, usually, only one modification; namely that the code be capable of accepting and using a source whose anisotropy is as high as that of the flux.
2. The physics of the problem can be represented very accurately. For instance, if an S_n method code, like DTF-IV, (25) is used, all the angular and energy resolution of the flux, as well as the cross section detail which is available in the code can be used to solve the time-dependent problem.
3. Some of the principal characteristics of the system can immediately be deduced from the moments. For instance, the mean emission time and pulse width can be easily obtained from the zeroth, first and second moments. Without much additional effort, the mean time to any reaction of interest, such as the mean time to fission, can be computed.

From Eq. 9a, it is seen that the higher moments give a greater relative weight to long times than do the lower moments. So, in a nonmultiplying medium, the first or

second moments will give information about early times, or high neutron energy cross sections, while higher moments will give greater emphasis to the lower part of the energy spectrum.

4. The method is applicable to nonmultiplying media as well as systems which are just below critical. It does not depend on the existence of separable modes.

The method has some disadvantages as well. (26) The principal one is that it is not easy to reconstruct the complete pulse shape from its moments. Furthermore, the presence of a dominant mode is not easily detectable with the moments method. A dominant mode is normally recognized by an exponential time shape over a substantial time interval and is much more easily noticed from a complete shape of the pulse than from its moments. The results depend sensitively on the space and energy dependence of the external source. Finally, an intense source is required for reasonable statistical precision for the higher moments, which are determined principally by the long time behavior.

6. Measurement and Analysis of Full Time Behavior

Another method of numerical solution is by means of the Monte Carlo method. For example, a Monte Carlo code has been used to compute the time response of blocks of carbon, iron, and copper to pulsed neutron sources of varying energy. (27)

The principal advantage of the Monte Carlo method is that it is possible to make as few approximations as one desires, so that more accurate results can be obtained than with any other method. The main disadvantages are that computer times can be very long and that important physical insight into the problems often is more easily obtained with less accurate, but simpler, methods of computation.

The full time response of a pulsed U^{238} sphere has been measured with detectors of varying energy responses. (28) Recently the time response of a high energy neptunium fission detector was compared with Monte Carlo calculations. (29) The results are in fairly good agreement and, interestingly, they provide a good check of the inelastic scattering cross section of U^{238} . The same technique could probably be used for other materials. Separate calculations have shown that the results are sensitive to arbitrary changes in the inelastic scattering cross sections and rather insensitive to details of the external source. Beghian and

Wilensky have measured the time response of lead slabs of varying thicknesses, (30) but their simplified analysis of the data does not provide an accurate check of cross sections.

A number of investigators have solved the time dependent transport equations, to varying approximations, by direct stepwise integration. The diffusion equation, with the space dependence removed by insertion of a buckling term, has been solved for thermal neutron investigations by this method. (31, 32) It is also feasible to solve the time dependent diffusion equations with space dependence included, if desired. The GAKIN(33) computer program is well suited to such an analysis of a pulsed neutron experiment, but it has not been used for this purpose yet. Its distinguishing feature over other time and space dependent codes, for our application, is the capability of handling many neutron energy groups. Preliminary results on the use of a code which solves the time dependent S_n equations have also been published. (34) This code has been used to study the time response of the Swedish FRO reactor to a pulsed source.

It can be seen, then, that we are approaching the capability of computing the time response to a pulsed neutron source to good accuracy, with the principal uncertainty remaining only in the basic cross sections used for the analysis.

There are other experiments which are designed to give information about the time response of a fast subcritical system. One potentially interesting fast reactor subcritical experiment is the measurement of the detector response to a sinusoidally varying source. Such measurements have been made in thermal system for several years and they offer a number of potential advantages. For instance, one could extract information more easily about the characteristics of a system by studying its response to individually known frequencies than to a very large mixture of frequencies, as is the case for the pulsed neutron source. Perez has discussed the feasibility and application of the method to a fast system. (35) The major difficulty is that of modulating charged particle beams at frequencies of tens of megacycles, as is required for a fast system.

7. FAST SPECTRUM MEASUREMENTS

In recent years experimental techniques have improved to the point where it is feasible to make high resolution measurements of fast neutron spectra. Spectrum measurements of thermal neutron spectra have served very well to establish the adequacy of scattering kernels and other cross sections for reactor calculations. In addition, they have provided excellent guidelines with which to check computational methods.

These experiments are still being very actively pursued, as they continue to provide useful information for reactor and shielding design. There is little question that measured fast spectra will be used just as extensively and profitably to check fast neutron cross sections and computational methods for fast reactors and fast neutron shielding.

There have been essentially two methods used to measure fast spectra. One is the time-of-flight method, used with pulsed neutron sources; the other is with a steady-state energy sensitive detector, the most common of which is probably the proton recoil proportional counter. Each of the techniques has a number of advantages over the other. Advantages of the time-of-flight method are:

1. Resolution can be made as fine as desired by increasing the flight path length. The principal difficulty of the energy sensitive detector technique lies in the poorer resolution which results from having to unfold the spectrum from the detector response.
2. The quantity which is measured by the time-of-flight method is the angular flux. In some shielding situations, the angular flux is of more interest than is the scalar flux. Furthermore, since the angular flux is a more differential quantity than is the scalar flux, a careful analysis of the angular flux permits a more direct indication of the quality of basic cross section data. Of course, this same characteristic of the time-of-flight method is a disadvantage if the quantity of interest is the scalar flux or, more likely, a reaction rate. In this connection, we might mention the "time-of-flight self-indication" experiment which aims to measure reaction rates by the time-of-flight method. Here, the time dependence of gammas resulting from reactions in a material placed at the end of the flight path are measured to deduce a reaction rate in the material. This information, together with a measured flux spectrum, provides a measurement of the reaction cross section. In addition, it provides a direct measurement of the energy dependent reaction rate in a material which is placed in the reactor configuration from which the neutrons are streaming. Such measurements are being seriously considered, but they have not yet been carried out.

Some advantages of the energy sensitive detector are:

1. It is usually placed directly at the position where the flux is desired; thus the $1/r^2$ loss of intensity, which is a characteristic of the time-of-flight method, is not encountered here. This, in turn, permits the use of a lower intensity source.
2. It can be used in a critical configuration, as well as in a subcritical arrangement. The time-of-flight method must be used on a configuration which is sufficiently subcritical so that a large pulse width does not cause poor resolution.
3. The scalar flux is usually of more immediate interest (for reactor physics applications) than is the angular flux. Energy sensitive detectors, if they are isotropic, measure the scalar flux directly. Obtaining an isotropic detector is not easily achieved however.

A very important consideration in both experiments is the perturbation which the detector, on the one hand, or the reentrant hole, on the other, make upon the flux which is being measured. To this date, there exists no accurate estimate of these perturbations for fast systems.

The analysis of a spectrum measurement in a nonmultiplying, or slightly multiplying, medium differs substantially from that in a highly multiplying system. In a nonmultiplying medium the spectrum at high energies depends primarily on the source neutron spectrum while, in a highly multiplying medium, fission neutrons contribute most of the high energy neutrons. In the former, then, it is important to know, to good accuracy, the angle-energy-space dependence of the source. In a highly multiplying medium, on the other hand, we can afford large uncertainties in the source description without hampering the analysis. This is a very significant point because a thorough knowledge of the source is not always easily attainable. For instance, when an electron linear accelerator is used, the neutron source results from deceleration of the electrons in a target material with resulting emission of bremsstrahlung radiation and subsequent production of neutrons by (γ, n) and (γ, f) reactions. An accurate computation of the space-energy-angle production of neutrons resulting from these processes is not practical at this time. Instead, it is common to measure the neutron leakage from an isolated target, and to use it as the source for the true experimental arrangement. This introduces several experimental uncertainties which require attention, such as room return upon the isolated target and production of neutrons by

(γ, n) and (γ, f) processes in the non-target region of the experimental configuration. The proper representation of the source in the calculations also presents a problem. With certain Monte Carlo codes, such as O5R, (36) it is possible to represent the source as a shell source having a diameter equal to the target and having a spectrum and angular distribution equal to the measured leakage from the bare target. This method, which is the most accurate treatment possible, is feasible but it makes the O5R source routine fairly complicated. No existing computer program which uses a deterministic method of solution has this flexibility of source representation. Hence, with these codes it is necessary to approximate the source further, while maintaining the same approximate leakage from the target region. This is not easily accomplished, although it is feasible by trial and error techniques. The accuracy of the source is most critical for the high energy neutron flux. At lower energies, the neutrons have "forgotten" the source details due to having undergone several or more collisions. It is this fact, of course, which permits a very coarse treatment of the high energy source when analyzing thermal nonmultiplying media.

Another difference between the highly multiplying and nonmultiplying media is the relatively slowly varying angular flux in the former and the very anisotropic flux, particularly at high energies, in the latter. This difference is due to the isotropic emission of fission neutrons in the multiplying medium. In the nonmultiplying system the flux at high energies is due primarily to direct streaming from the localized source plus contributions from small angle elastic scattering collisions. At lower energies, the flux becomes less anisotropic because of contributions from large-angle elastic scattering collisions and neutrons resulting from (n, n') , $(n, 2n)$, and $(n, 3n)$ reactions, which tend to emit neutrons isotropically. Of course, the degree of flux anisotropy depends not only on the source and scattering cross sections, which is primarily what we have discussed so far, but also on the amount of absorption, leakage and, of course, fission in the system. It is well to keep in mind, that the analysis of a system in which the flux is anisotropic is more difficult, or at least more expensive, than a system with a slowly varying angular flux.

Another great simplification occurs in a highly multiplying, homogeneous, system. For a critical system, according to the first fundamental theorem of asymptotic reactor theory(37) the scalar flux $\varphi(E, r)$ can be expressed in the separable form

$$\varphi(E, r) = \varphi(E) F(r)$$

where $F(r)$ is the fundamental spatial mode. This permits the replacement of the space variable by a buckling parameter, which greatly simplifies the analysis. Neill, et al., (38, 39) have taken advantage of this simplification when measuring the spectrum in a U^{235} sphere. They measured an angular flux at the center of the sphere by the time-of-flight method; by the symmetry of the system this is the same as the scalar flux. The first fundamental theorem is strictly applicable only for a critical system. When the system is sufficiently subcritical, the presence of higher spatial harmonics can make the analysis much more complicated. However, Neill found that for his system, at $k = 0.96$, measured spectra at different spatial positions differ little, which is justification for neglecting higher harmonic contributions. A similar simplification occurs for highly multiplying subcritical reflected systems. Here it is found that the spectrum computed by a k calculation differs little from that resulting from an exact source calculation, except in the immediate vicinity of the source. (40) This is very useful because most iterative solution methods to the transport equation converge much faster for k calculations than for source calculations, especially for highly multiplying systems. Neill's U^{235} sphere spectrum measurement is shown in Fig. 1. The probable reason for the deviation at low energies is due to deficiencies in the secondary neutron spectrum resulting from inelastic scattering, but this has not yet been confirmed.

The steady-state spectrum is more sensitive to the total absorption cross section than it is to its individual components, including fission. The reason for this is that the fission neutrons merely tend to increase the source, while the absorption and other removal cross sections give structure to the spectrum. It is true, then, that the steady-state spectrum generally provides a sensitive integral check of removal cross sections, but not to the fission cross section. A better integral check on the fission cross section is provided, for instance, by the α measurement discussed previously.

Several fast neutron spectrum measurements, performed by the time-of-flight method, have provided useful information about cross sections. Angular flux spectra at several positions and angles in a U^{238} sphere have been predicted fairly well with the ENDF/B cross section set, which has shown to be somewhat superior to another cross section set based upon earlier evaluation by Joanou and Stevens. (41, 42) The calculation used the GAM-II(43) program to obtain group cross sections, and the DTF-IV code to perform the transport calculations in an S_{32} approximation. Figure 2 shows the comparison, at one position labeled B, of the experimental results compared with the two sets of cross sections. The experimental data is presented with an energy resolution consistent with the calculations in order to provide the most useful comparison. It can

be seen that the differences between the predictions of the two cross section sets are substantial, particularly at lower energies. The significance of this for, say, fast reactor Doppler coefficients is obvious.

Measurements at one angle, namely $\theta = 0$, have also been made in a tungsten sphere. (11) Calculations agreed with the measurements, but not until self-shielding of the high energy scattering resonances of tungsten was included in the analysis. Figure 3 shows the experiment and theoretical predictions. This calculational capability was later incorporated into the GANDY computer program. (44) This self-shielding of the high energy scattering resonances of a heavy nucleus is not usually applied in reactor design calculations. Yet it can be important in some reactor types, such as small thermionic reactors; (45) its consequences on other types of reactors have not been explored. Generally, the effects of scattering self-shielding are most pronounced at high energies (~ 1 MeV) when the neutron width, Γ_n , and the average resonance level spacing are large. The effect, at high energies, is more important in tungsten than in, say, U^{238} , because of the larger spacing in the former. Nevertheless, the effect of scattering resonance self-shielding may well be important at lower energies ($\sim 1-10$ keV) in U^{238} .

Profio has made numerous spectrum measurements in graphite, CH_2 , and other materials, primarily for shielding applications. (46, 47) His experiments and analyses were directed toward a better understanding of the deep penetration problem, which is beyond the scope of this conference, but cross section information was also obtained. For instance, it was found that P_0 to P_3 scattering matrices are sufficient to match experiments. This implies that a very detailed knowledge of the angular distribution for elastic scattering is not required for shielding applications. This is somewhat surprising, however similar conclusions have been reached by others. (48, 49) Better agreement (50) has been obtained with experiment by using graphite cross sections measured at RPI (51) than those used in the ENDF/B evaluation. (52)

Fast spectrum measurements, performed on the experimental fast reactor VERA have been reported. (53) These combine proton-recoil measurements in photographic emulsion (energy range 0.5-5 MeV), proton-recoil measurements in a hydrogen-filled proportional counter (energy range 1 keV - 1 MeV), and time-of-flight measurements using a pulsed neutron source (energy range 10 eV - 50 keV). A similar program to study spectra in breeder reactor cores, by the time-of-flight method, is underway in this country (40) and preliminary measurements have been made in a graphite- U^{235} system essentially equivalent to ZPR-3 Assembly 14. (54) These results are compared with infinite medium calculations, performed with the GAM-II program, in Fig. 4.

Numerous other measurements of fast spectra by the time-of-flight method(19, 55-58) and by proton-recoil spectrometer(59, 60) have now been reported.

The last group of integral measurements we will discuss are transmission measurements.

Verbinski(61) has used small samples of concrete, aluminum, steel, and lithium hydride for an integral check of the cross sections of the constituents of these materials. The experiment is performed by striking the sample with a known spectrum of neutrons from a LINAC target. The spectrum leaving the sample, at a fixed angle, is measured. The O5R Monte Carlo code was used to analyze the experiments. This experiment differs from those described above, in principle, only in that the samples are small. This implies that in Verbinski's experiment, multiple scatters are much fewer than single scatters, which makes his experiment of a less integral nature than the others, although it is certainly not a direct cross section measurement. Because most of the observed spectrum results from single collisions, it is easier to relate the results of Verbinski's measurements to basic cross sections.

At Gulf General Atomic, low resolution transmission measurements through tungsten slabs are presently being performed for varying temperatures. The purpose, here, is to check the adequacy of the strength functions for tungsten, as well as the ability to perform self-shielding computations in the unresolved resonance range.(62)

Transmission measurements through thick samples of several materials have been performed at Oak Ridge.(63) The goal here has been to determine the accuracy of the total cross section, particularly in the valleys that are important for solving deep-penetration problems.

8. SUMMARY

We have discussed a variety of integral experiments whose aims have been to check, primarily, fast neutron cross sections and computational methods used to arrive at effective cross sections from the basic nuclear data. These experiments were all on subcritical media with "clean" geometry. We have seen that these have shed light on important cross section problems.

When the last cross section conference was held here, two years ago, few of the measurements discussed here were being performed. This is particularly true of fast spectrum measurements, and of the

measurement of full time-dependent pulse shapes in fast systems. Since then, we have witnessed a large proliferation of these measurements - we have not been able to mention all of them - and it seems clear that, at this rate, they will soon form an indispensable part of any fast reactor development program.

9. REFERENCES

1. K. H. Beckurts and K. Wirtz, Neutron Physics, Springer-Verlag (1964).
2. M. M. R. Williams, The Slowing Down and Thermalization of Neutrons, North-Holland Publishing (1966).
3. "Reactor Physics Constants, " ANL-5800 (Second Edition), 1963.
4. A. Pazy, et al., "Use of Integral Measurements as Supplementary Data in Neutron Cross-Section Evaluation, " Proc. of the Int. Conf. on Fast Critical Experiments and Their Analysis, " ANL-7320 (1966).
5. Pamela C. E. Hemment and E. D. Pendlebury, "The Optimization of Neutron Cross-Section Data Adjustments to Give Agreement with Experimental Critical Sizes, " Proc. of the Int. Conf. on Fast Critical Experiments and Their Analysis, " ANL-7320 (1966).
6. H. C. Honeck, "ENDF/B, Specifications for an Evaluated Nuclear Data File for Reactor Applications, " BNL-50066.
7. D. C. Irving, et al., "Impossible Legendre Coefficients, " Conf. on Neutron Cross Section Technology (1966).
8. J. M. Otter, "Unicorn - A Program to Calculate Point Cross Sections from Resonance Parameters, " NAA-SR-11980, Vol. VI (1966).
9. M. K. Drake, et al., "Description of Auxiliary Codes Used in the Preparation of Data for the GGC-3 Code. "
10. A. L. Rago and H. H. Hummel, "ELMOE, An IBM-704 Program Treating Elastic Scattering Resonances in Fast Reactors, " ANL-6805 (1964).
11. S. C. Cohen, et al., "The Effect of Heavy Element Scattering Resonances on Fast Spectra and Doppler Coefficients, " Trans. Am. Nucl. Soc. 10, (1967).

12. D. M. O'Shea, et al., "The Automated Preparation of Multigroup Cross Sections for Fast Reactor Analysis Using the MC² Code, " Proc. of the Int. Conference on Fast Critical Experiments and Their Analysis, ANL-7320 (1966).
13. R. T. Shanstrom, C. A. Stevens, et al., "GAF and GAR, New Computer Programs for the Calculation of Neutron Spectra, Treatment of Resonance Effects, and Averaging of Group Cross Sections for Fast Reactor Analysis, " Int. Conference on Utilization of Research Reactors and Reactor Mathematics and Computation, Mexico City (1967).
14. J. Adir and K. D. Lathrop, "Theory and Methods Used in the GGC-3 Multigroup Cross Section Code, " Gulf General Atomic Report GA-7156 (1967).
15. J. Wagschal, et al., "Deep Penetration of Neutrons in Iron, " Trans. Am. Nucl. Soc. 10, (1967), p. 397.
16. G. I. Bell, G. E. Hansen, and H. A. Sandmeier, "Multitable Treatments of Anisotropic Scattering in S_n Multigroup Transport Calculation, " Nucl. Sci. and Eng., 28 (1967).
17. F. Storrer, "Pulsed Neutron Experiments on Fast and Intermediate Systems, " Pulsed Neutron Research, Vol. II, IAEA, Vienna (1965).
18. J. Orndoff, "Prompt Neutron Periods of Metal Critical Assemblies, " Nucl. Sci. Eng. 2 (1957).
19. W. Y. Kato, et al., "Fast-Reactor Physics Parameters, " Pulsed Neutron Research, Vol. II, IAEA, Vienna (1965).
20. M. Kuchle, et al., "Measurements of Neutron Spectra and Decay Constants with the Fast Subcritical Facility SUAK, " Proc. of the Int. Conf. on Fast Critical Experiments and Their Analysis, ANL-7320 (1966).
21. J. W. Weale, et al., "Measurements of the Prompt Neutron Decay Constant of the VERA Reactor Using the Pulsed Source Method, " Pulsed Neutron Research, Vol. II, IAEA (1965).
22. D. E. Parks, J. R. Beyster and N. F. Wikner, "Thermal Neutron Spectra in Graphite, " General Atomic Report GA-2437 (1961).

23. A. E. Profio and J. U. Koppel, "Measurements and Calculations of the Slowing-Down and Migration Time, " Pulsed Neutron Research, Vol. I, IAEA, Vienna (1965).
24. J. U. Koppel, "Time-Dependent Neutron Spectra, " Nucl. Sci. and Eng. 8, 157 (1960).
25. K. D. Lathrop, "DTF-IV, A FORTRAN IV Program for Solving the Multigroup Transport Equation with Anisotropic Scattering, " LA-3373 (1965).
26. T. Gozani, "Experimental Kinetic Studies in Highly Depleted Uranium Sphere, " USAEC Report GA-8465, Gulf General Atomic Incorporated (1968).
27. G. Deconninck, et al., Pulsed Neutron Research, Vol. II, IAEA, Vienna (1965), p. 493.
28. T. Gozani, Trans. Am. Nucl. Soc. 10, (1967) p. 280.
29. T. Gozani and P. d'Oultremont, "Decay of a Neutron Pulse in a Fast Nonmultiplying System as an Integral Check on the High Energy Inelastic Scattering, " this conference.
30. L. Beghian and S. Wilensky, Pulsed Neutron Research, Vol. II, IAEA, Vienna (1965), p. 511.
31. M. J. Ohanian and P. B. Daitch, "Eigenfunction Analysis of Thermal-Neutron Spectra, " Nucl. Sci. and Eng. 19, 343 (1964).
32. A. K. Ghatak and T. J. Krieger, "Neutron Slowing-Down Time and Chemical Binding in Water, " Nucl. Sci. and Eng. 21, 304 (1965).
33. K. F. Hansen and S. Johnson, "GAKIN, A Program for the Solution of One-Dimensional Space-Time Dependent Diffusion Equations, " General Atomic Report GA-7543.
34. A. Bergstrom, et al., Proc. of Int. Conf. on Fast Critical Experiments and Their Analysis, ANL-7320 (1966).
35. R. B. Perez, et al., "The Theory of Fast Reactor Integral Measurements by Propagation Methods, " Proc. Int. Conf. on Fast Critical Experiments and Their Analysis, ANL-7320 (1966).

36. D. C. Irving, et al., "O5R, A General Purpose Monte Carlo Neutron Transport Code, " ORNL-3622 (1965).
37. A. M. Weinberg and E. P. Wigner, The Physical Theory of Neutron Chain Reactors, University of Chicago Press (1958).
38. J. M. Neill, et al., "Spectrum Measurements in a U²³⁵ Sphere, " Informal Session on Reactor Physics at ANS Meeting, Chicago (1967).
39. J. M. Neill, et al., this Conference.
40. C. A. Preskitt and C. A. Stevens, "Fast Reactor Spectrum Measurements, " Gulf General Atomic Report GA-8191 (1967).
41. J. M. Neill, C. A. Stevens, et al., "Position Dependent Neutron Spectra in a Depleted Uranium Sphere, " Informal session on Reactor Physics at ANS Meeting, Chicago (1967).
42. G. D. Joanou and C. A. Stevens, "Neutron Cross Sections for U²³⁸, " NASA Report CR-54290. See also GA-6087 (1965).
43. G. D. Joanou and J. S. Dudek, "GAM-II, A B₃ Code for the Calculation of Fast Neutron Spectra and Associated Multigroup Constants, " General Atomic Division, General Dynamics Corporation GA-4265 (1963).
44. S. C. Cohen and P. K. Koch, "GANDY, A Computer Program for the Evaluation of Effective Cross Sections in the Unresolved Resonance Region, " Gulf General Atomic Report GA-8003 (1967).
45. S. C. Cohen, "Thermionic Critical Experiment Program, " Gulf General Atomic Report GA-8309 (1967).
46. A. E. Profio, et al., "Measurement of the Neutron Angular Flux Spectrum in Graphite, " General Atomic Division, General Dynamics Corporation GA-7470 (1966).
47. A. E. Profio, Air Force Weapons Laboratory Report AFWL-TR-65-193 (1966).
48. K. Shure, "P-3 Multigroup Calculations of Neutron Attenuation, " Nucl. Sci. and Eng. 19, 310 (1964).
49. J. M. Norwood, et al., Air Force Weapons Laboratory Report AFWL-TR-65-209 (1966).

50. A. E. Profio, Gulf General Atomic private communication.
51. P. F. Yergin, et al., "MeV Total Cross Sections with the Rensselaer LINAC," Conf. on Neutron Cross Section Technology (1966).
52. E. L. Slaggie and J. T. Reynolds, Knolls Atomic Power Laboratory Report KAPL-3099.
53. J. W. Weale, et al., "Neutron Spectrum Measurements in the Ten Power Fast Reactor VERA," Reactor Meas. in Nucl. Power (1966), Paper 3.12.
54. J. K. Long, et al., Proc. of the Second U. N. Int. Conf. on the Peaceful Uses of Atomic Energy, 12, 1958, p. 598.
55. D. B. Gayther and P. D. Goode, Pulsed Neutron Research, Vol. II, IAEA (1965).
56. J. L. Russell, Jr., et al., Pulsed Neutron Research, Vol. II, IAEA (1965).
57. E. Greenspan, et al., this Conference.
58. B. K. Malaviya, this Conference.
59. E. F. Bennett, et al., Proc. of Int. Conf. on Fast Critical Experiments, ANL-7320.
60. P. S. Brown, Proc. of Int. Conf. on Fast Critical Experiments, ANL-7320.
61. V. V. Verbinski, et al., "A Method of Evaluating Fast Neutron Differential Scattering Cross Sections with Short Experimental Runs," Nucl. Inst. and Methods, 52, 2 (1967).
62. J. L. Russell, Jr., Gulf General Atomic private communication.
63. C. E. Clifford, et al., "Measurements of the Spectra of Uncollided Fission Neutrons Transmitted Through Thick Samples of Nitrogen, Oxygen, Carbon, and Lead: Investigation of the Minima in Total Cross Sections," Nucl. Sci. and Eng. 27, 299 (1967).

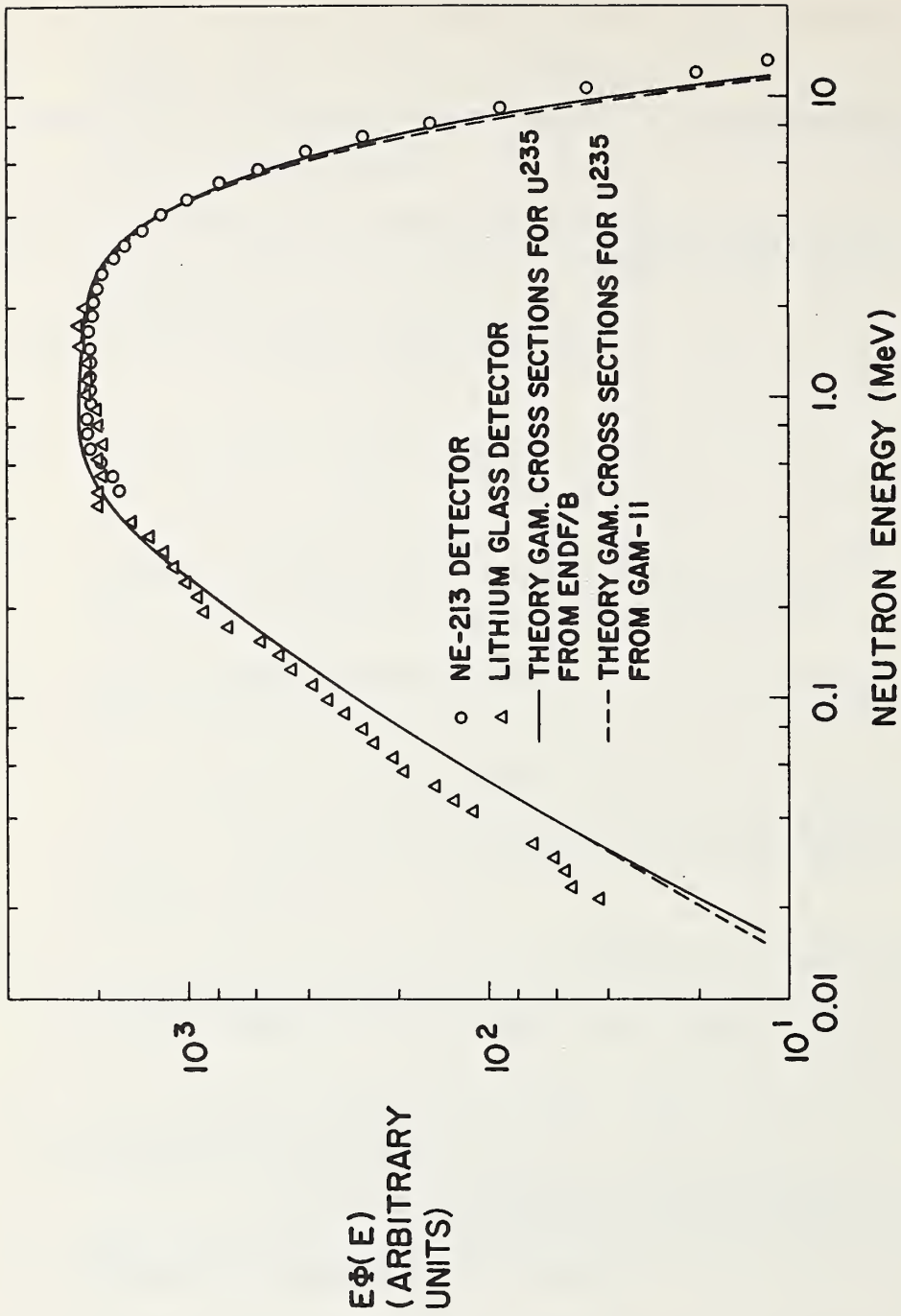


Figure 1. Comparison of calculated and measured neutron spectra at the center of the U²³⁵ sphere.

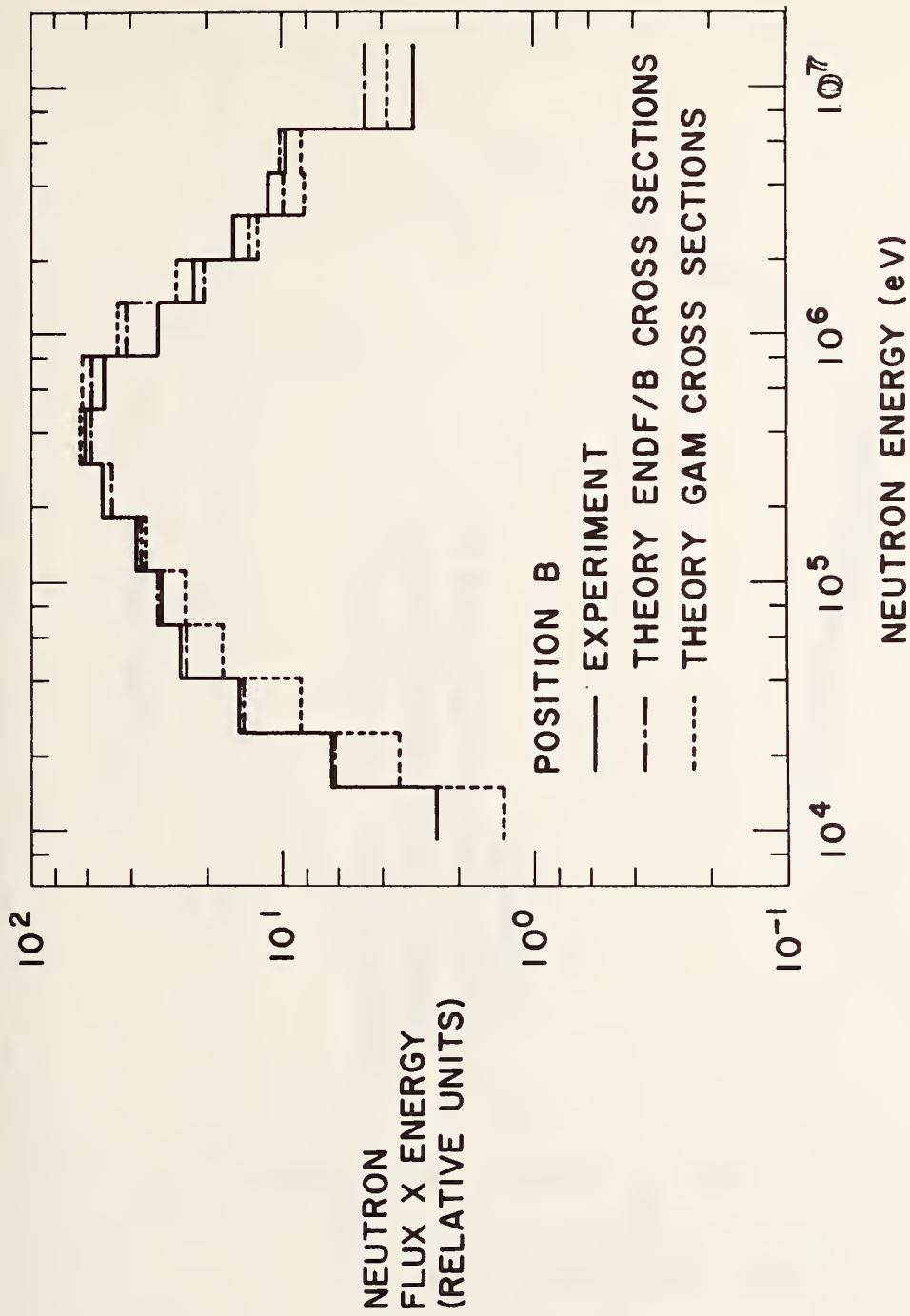


Figure 2. Comparison of theoretical and measured neutron spectra at Position B in the U238 sphere ($R = 6.5$ in., $\mu = 1.000$).

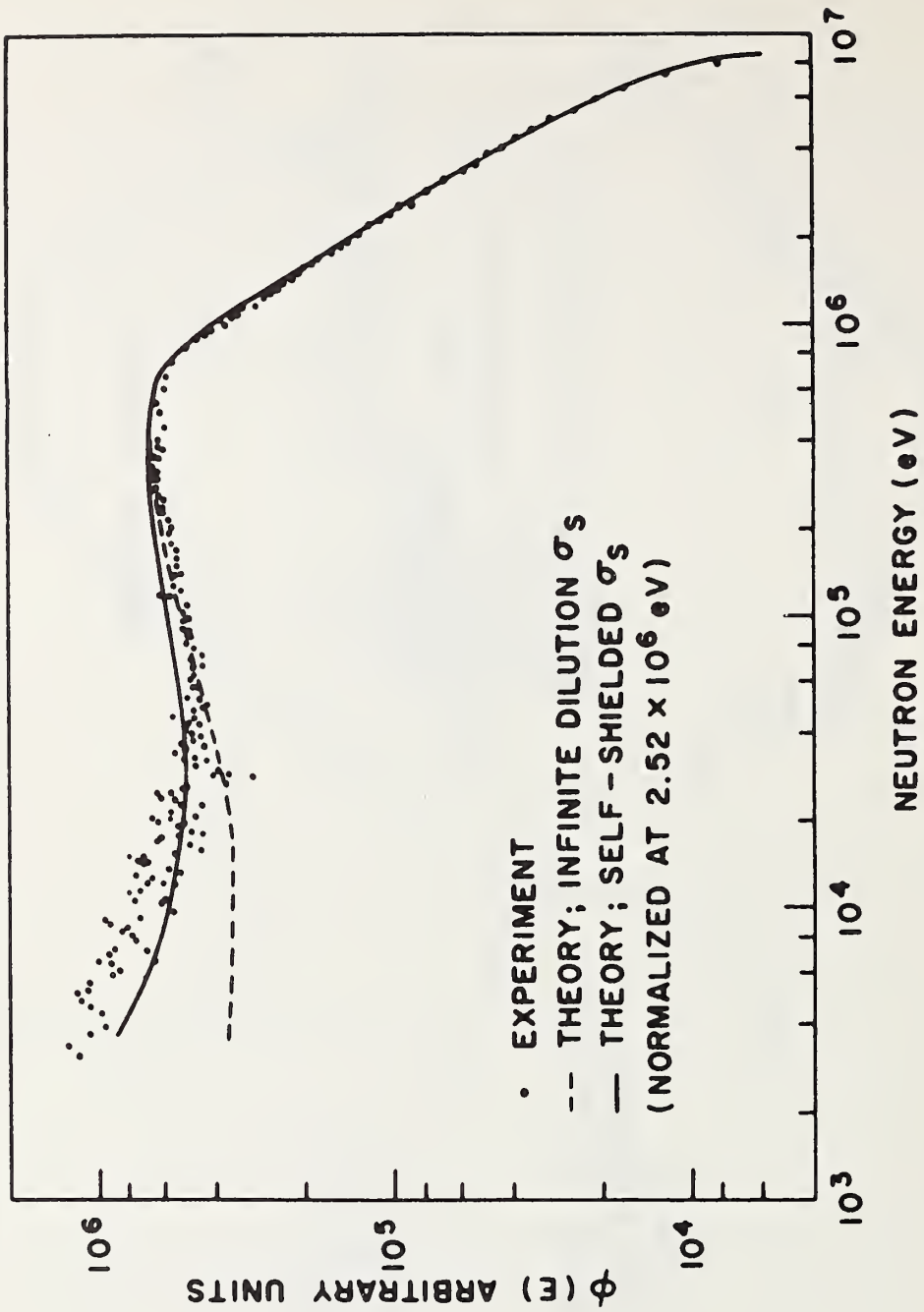


Figure 3. 0° surface spectrum in 25-cm diameter tungsten sphere.

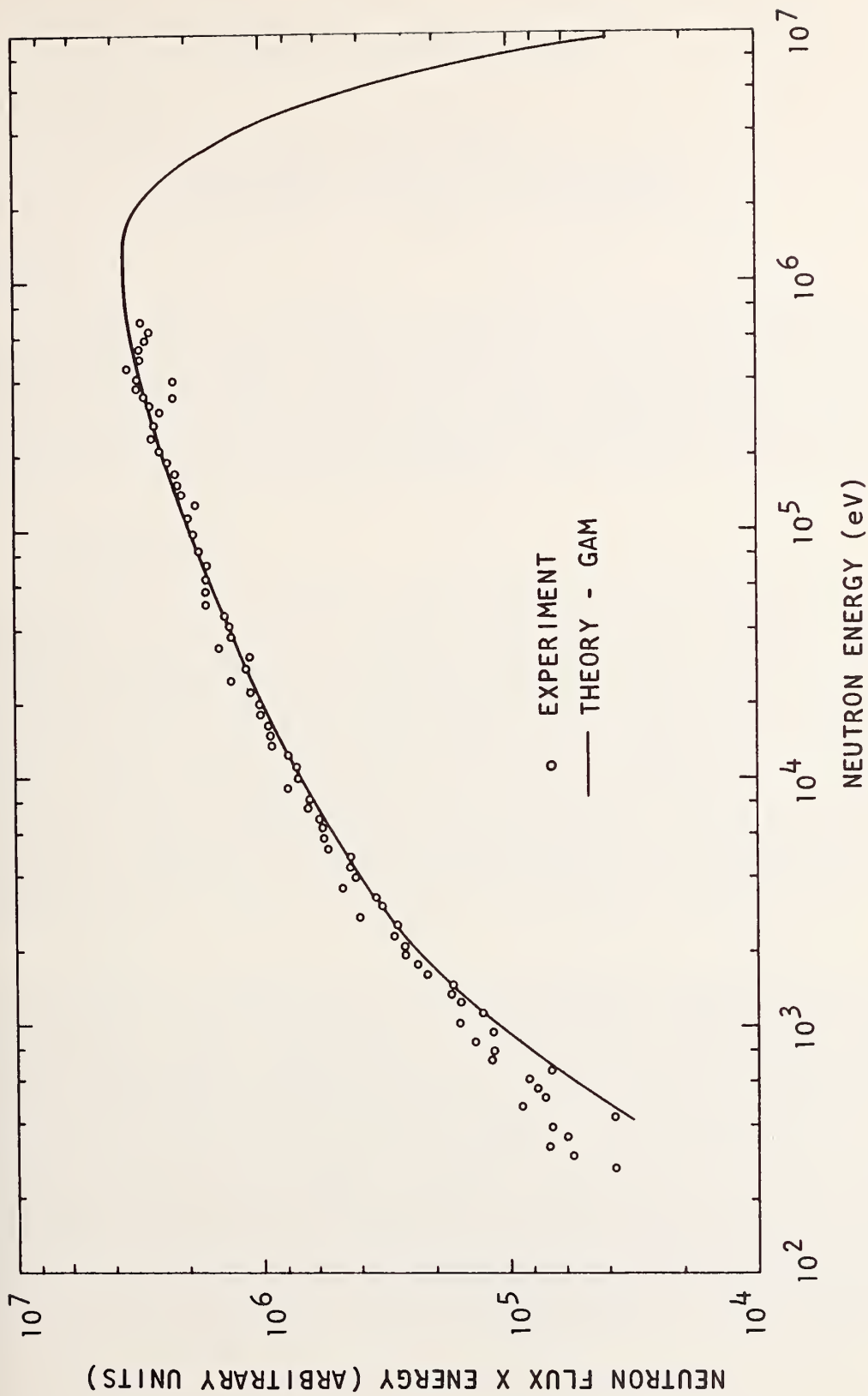


Figure 4. Preliminary spectrum measured in STSF-1.

THE USE OF INTEGRAL SPECTRUM MEASUREMENTS TO IMPROVE
NEUTRON CROSS SECTION DATA

E. D. Pendlebury

Atomic Weapons Research Establishment
Aldermaston, Berks, U.K., England

Abstract

The spectra of emergent neutrons from spherical shells of various materials with a central source of approximately fission spectrum neutrons have been measured at Harwell by M. S. Coates et al. A method which will allow these measurements to be used to improve neutron cross section data is described and some of the outstanding theoretical problems associated with the application of the method are discussed.

1. Introduction

The experiments carried out at Harwell by Coates et al. [1] to measure the spectrum of neutrons emerging in different directions from spherical shells of various materials with a central source of approximately fission spectrum neutrons are potentially very useful for checking and adjusting neutron cross section data. The experiments have the advantages that each system only involves one material (apart from a relatively small amount of natural uranium comprising the neutron source), the geometry is simple, and there are no complications due to heterogeneity. The materials so far studied are natural uranium, iron and sodium and the spectrum from shells of different thicknesses have been measured. Similar measurements have been made at General Atomic by Profio et al. [2] to determine the leakage spectrum from ^{235}U and Tungsten.

A method is described which will enable the results of these experiments to be used in a systematic way to improve the neutron cross section data. The method involves the optimisation of adjustments to the neutron cross section data, bearing in mind their experimental uncertainties, so that they give acceptable agreement with the experimental spectra. This is similar in principle to the methods used by Hemment and Pendlebury [3] and by Pazy et al. [4] to adjust cross section data to make them consistent with experimental critical sizes, and to the method described by Cecchini et al. [5] to adjust cross section data to make them consistent with other integral quantities in critical systems. In practice the adjustment of the cross section data to fit the Harwell spectrum measurements could be carried out on its own or in conjunction with the adjustment to fit experimental

critical sizes where appropriate, as for example in the case of ^{238}U and ^{235}U . For the purpose of this paper it is assumed that the cross section data are being adjusted to fit the spectrum measurements only.

A possible optimisation procedure which can be used in the adjustment of the cross section data is described in Section 2, and the method of calculating, by first order perturbation theory, the required sensitivity of the calculated spectra to changes in the cross section data is indicated in Section 3. In Section 4 some of the work already carried out at Aldermaston in connection with the development of this method is mentioned and some of the outstanding theoretical problems discussed.

2. Optimisation Procedures for the Adjustment of Cross Section Data to give Acceptable Agreement with Measured Spectra

In considering optimisation procedures for the adjustment of cross section data to give acceptable agreement with measured spectra, one needs to distinguish between the cases where both the calculated and experimental spectra can be normalised in a unique way to say a source strength, and where each or both is subject to arbitrary normalisation. In the former case the absolute values of the spectra can be compared whereas in the latter case only the shape of the spectra can be compared. In the case of the Harwell spectrum measurements the results are subject to arbitrary normalisation and so the particular problems associated with this case will be considered.

It is useful to consider the energy range divided up into a number of groups as in multigroup calculations, with both the calculated and experimental spectra represented as flux per group or flux per unit lethargy in each energy group. In this paper consider the spectrum to be specified as flux per group.

Let the experimental flux per unit solid angle about a direction denoted by k in group g from system s be denoted by $Q_{ksg}(\text{exp})$ and let the corresponding calculated value be $Q_{ksg}(\text{calc})$. Due to the arbitrary normalisation of the $Q_{ksg}(\text{exp})$ it is necessary to compare $N_{ks}Q_{ksg}(\text{exp})$ with $Q_{ksg}(\text{calc})$ where N_{ks} is a factor not yet specified. Following reference [3] let x_{mjg} be the percentage increase which has to be made to the group cross section in group g for reaction j in nuclide m in order to give acceptable agreement between the calculated and experimental spectra. It is convenient to exclude the elastic cross section from this and to use the elastic cross section as a dependent variable which is calculated to preserve the balance between the total and partial cross sections. (The total cross section could just as well have been treated as the dependent variable if desired.) Let γ_{ksmjg} be

the change in the calculated flux Q_{ksg} (calc) due to a 1% increase in the group cross section characterized by the subscripts mjg' , with a compensating change made to the elastic cross section. In order to get exact agreement with the experimental values the following equations must be satisfied,

$$Q_{ksg}(\text{calc}) + \sum_{mjg'} \gamma_{ksmjg'} x_{mjg'} = N_{ks} Q_{ksg}(\text{exp}) \quad (1)$$

In view of the uncertainties which exist in the calculations and in the experimental value $Q_{ksg}(\text{exp})$, it is not logical to aim at exact agreement between calculation and experiment. Thus if $N_{ks} q_{ksg}$ represents the residual discrepancy between the calculated values of Q_{ksg} and the re-normalised values $N_{ks} Q_{ksg}$ then

$$Q_{ksg}(\text{calc}) + \sum_{mjg'} \gamma_{ksmjg'} x_{mjg'} = N_{ks} (Q_{ksg}(\text{exp}) + q_{ksg}) \quad (2)$$

The total number of unknowns x_{mjg} and q_{ksg} are obviously very much greater than the number of equations (2), hence, in the absence of any further constraints there are an infinite number of solutions. It is therefore necessary to introduce some criterion which gives a "best" solution. A convenient indication of the goodness of the solution involves the sum of the squares of x_{mjg} and q_{ksg} with appropriate weights given to the various terms according to the experimental uncertainties, and with other additional weights as discussed in reference [3] which allow to some extent for correlations between quantities (x_{mjg} , q_{ksg}) in different energy groups. It is therefore reasonable to aim to minimise such an expression.

Let ξ_{mjg} be the standard deviation of the group cross section typified by mjg and let ζ_{ksg} be the standard deviation of the measured flux in group g in direction k for system s . In view of the above discussion and that in reference [3] (see Section 5 of reference [3]), it is suggested that a suitable function for minimisation is

$$S = \sum_{mj} \frac{1}{G} \sum_{g=1}^G \frac{x_{mjg}^2}{\xi_{mjg}^2} + \sum_k \sum_s \frac{1}{G} \sum_{g=1}^G \frac{q_{ksg}^2}{\zeta_{ksg}^2} \quad (3)$$

The expression S can be minimised with respect to x_{mjg} and q_{ksg} subject to (2) but there are insufficient equations because of the unknown N_{ks} .

The values of N_{ks} could be chosen in many ways. One convenient way might be to choose N_{ks} so that $\sum_g Q_{ksg}(\text{calc}) = N_{ksg} \sum_g Q_{ksg}(\text{exp})$. The disadvantage of this is that the calculated spectrum may not be known over the whole energy range, and would therefore have to be extrapolated, thus leading to another source of error. Alternatively one could choose N_{ks} so that $Q_{ksg^*}(\text{calc}) = N_{ks} Q_{ksg^*}(\text{exp})$ where g^* is the energy group say for which the experimental spectrum in terms of flux per unit lethargy is a maximum, but an improvement on both of these approaches would be to include the N_{ks} in the optimisation procedure and to minimise S with respect to N_{ks} as well as with respect to x_{mjg} and q_{ksg} . This leads to the equations,

$$\frac{x_{mjg}}{\xi_{mjg}^2} + \sum_k \sum_s \sum_{g'} \frac{q_{ksg'}}{\zeta_{ksg'}^2} \frac{1}{N_{ks}} \gamma_{ksmjgg'} = 0 \quad (4)$$

and

$$\sum_g \frac{q_{ksg}}{\zeta_{ksg}^2} (Q_{ksg}(\text{exp}) + q_{ksg}) = 0 \quad (5)$$

which together with equations (2) allow the unknowns x_{mjg} , q_{ksg} and N_{ks} to be calculated. In the case when the N_{ks} are not included in the optimisation procedure equation (5) does not apply. It will be noted that in this latter case the equations are linear in the unknowns whereas when N_{ks} is included in the optimisation, second order terms are introduced through equation (5). This makes a fundamental difference to the way in which the equations can be solved though the non-linearity is not expected to cause any great difficulty.

3. The Calculation of the $\gamma_{ksmjg'g}$

The $\gamma_{ksmjg'g}$ can be calculated from first order perturbation theory using a similar technique to that described in Section 6.2 of reference [6]. For given k and s a separate adjoint calculation has to be carried out for each of the g values with the boundary condition that the adjoint function is unity in the direction denoted by k for each particular g value. The S_n program STRAINT [7] and the perturbation program DUNDEE [8] have been used in preliminary calculations, using a coarse energy group structure, to calculate the sensitivity factors $\gamma_{ksmjg'g}$ for a natural uranium shell, 11.5 cm thick, of the dimensions as one of those used by Coates et al. There are no mathematical difficulties in carrying out these calculations.

4. Discussion

Preliminary calculations have been carried out using the S_n method to give spectra emergent in different directions from shells of natural uranium of the dimensions of those used by Coates et al. for comparison with the measured values. In particular, calculations have been carried out with different data sets for neutrons emergent at 45° from the 11.5 cm thick shell used by Coates et al. Plotted as flux per unit lethargy against lethargy these spectra cover the range from 5 keV to 10 MeV with a maximum in the region of 400 to 500 keV. In the calculations 19 groups cover this energy range. That data used are DFNs 41 and 5 for ^{235}U and ^{238}U in one calculation and the adjusted DFNs 1041 and 1005 [3] in another calculation. In both cases there are too many high energy neutrons and too few low energy neutrons in the calculated spectra. There is a small but noticeable difference between the two calculated spectra though unfortunately the adjusted data give slightly worse agreement with the measured spectrum than the unadjusted data, but it should be emphasized that these are preliminary calculations only.

Before drawing any firm conclusions about the inadequacy of the cross section data based on the comparison of measured and calculated spectra one has first of all to ensure that there are no large systematic errors in the calculated spectra and to this end one has to repeat calculations using different energy group structures, different radial mesh points and different angular meshes. Some check calculations have already been carried out by the Monte Carlo method using the same basic data with a much more detailed representation of the cross sections than in the S_n method, but because of the statistical error in the Monte Carlo calculations one can only usefully compare the spectrum integrated over emergent directions with the corresponding value from the S_n calculations. Comparisons so far obtained have been very satisfactory and consistent with the statistical uncertainty on the Monte Carlo results. Further work is however still necessary to establish the reliability of the direct calculations, and also of the perturbation calculations.

When the reliability of the calculations has been established one can then seriously tackle the problem of trying to explain the differences between calculated and measured spectra in terms of inadequacies in the cross section data. To this end a machine program--a modified and extended version of the present PENICUIK program [3]--needs to be written to solve equations (2), (4) and (5) using the $\gamma_{k\text{smjg},g}$ (on tape) calculated by the perturbation program DUNDEE. It should be noted that there is nothing sacrosanct about the function to be minimised and it may be necessary to investigate alternative forms to that given by equation (2).

From experience gained in adjusting cross section data to fit experimental critical sizes [3] one might anticipate using this method to some extent as a means of establishing the reliability of the experimental results. If the calculated spectra can be made consistent with the measured ones by making acceptable adjustments to the cross section data then this is some indication that there are no large unknown systematic errors in the measured values. If on the other hand the calculated spectra cannot be made consistent with the measured ones this may indicate unknown systematic errors in the measured values.

5. References

- [1] M. S. Coates, D. B. Gayther and P. D. Goode, AERE-R5364 (1968).
- [2] A. E. Profio, J. C. Young, K. L. Crosbie, R. Hackney, H. M. Antunez and J. L. Russell, Jr., International Conference on Fast Critical Experiments and their Analysis, Argonne, October 1966, ANL-7320, p. 524.
- [3] Pamela C. E. Hemment and E. D. Pendlebury, International Conference on Fast Critical Experiments and their Analysis, Argonne, October 1966, ANL-7320, p. 88.
- [4] A. Pazy, G. Rakavy, Y. Reiss and Y. Yeivin, International Conference on Fast Critical Experiments and their Analysis, Argonne, October 1966, ANL-7320, p. 270.
- [5] C. Cecchini, A. Gandini, I. Dal Bono and B. Faleschini, International Conference on Fast Critical Experiments and their Analysis, Argonne, October 1966, ANL-7320, p. 107.
- [6] E. D. Pendlebury, AWRE Report No. 0-32/64 (1964).
- [7] R. D. Wade, AWRE Report No. 0-12/63 (1963).
- [8] Pamela C. E. Hemment, E. D. Pendlebury, M. J. Adams, B. A. Brett and D. Sama, AWRE Report No. 0-40/66.

Fast Neutron Spectra in Multiplying
and Non-Multiplying Media*

J. M. Neill, J. L. Russell, Jr., R. A. Moore, and C. A. Preskitt

Gulf General Atomic Incorporated
San Diego, California 92101

ABSTRACT

Fast neutron spectra have been measured at various positions in spheres of depleted uranium and 93.2% enriched uranium, and these data have been used to provide integral checks on the accuracy of neutron cross sections and computational methods. The data cover the energy range between about 10 keV and 15 MeV and were obtained using three flight path lengths, 45, 50, and 210 meters. The detectors used consisted of a 5-in. diameter NE-213 proton recoil detector for fast neutrons and a 5-in. diameter NE-908 lithium glass detector for intermediate energy neutrons. The pulsed source for the measurements was obtained by impinging the beam from the Gulf General Atomic Linear Electron Accelerator onto tungsten or uranium targets. Several different types of calculation have been compared with the measurements, including multigroup transport theory, and two different sets of cross sections have been used. The measured spectra in the U^{235} sphere are consistently softer than the calculated values. The measured spectra in the U^{238} sphere are accurate enough to permit one to choose the better of the two cross section sets.

*Work supported by the U. S. Atomic Energy Commission.

1. DISCUSSION

Spectrum measurements have been made at various positions inside a 7-in. diameter sphere of enriched uranium and a 20-in. diameter sphere of depleted uranium. These measurements were designed to provide data that would check the accuracy of the appropriate neutron cross sections and the computational methods.

The measurement techniques were similar for both spheres. Each was excited by a pulsed neutron source using the Gulf General Atomic linear electron accelerator. A reentrant hole into each sphere permitted a neutron beam to be extracted, collimated and timed over an evacuated flight path ranging in length from 45 to 210 meters. Two detectors were used in the measurements, an NE-213 proton recoil liquid scintillator⁽¹⁾ to cover the energy range 400 keV to 15 MeV, and a lithium glass scintillator⁽²⁾ to cover the range 200 eV to 1 MeV. The NE-213 detector had been calibrated by means of a monoenergetic neutron source obtained with a Van de Graaff accelerator and by means of Monte Carlo calculations. Its efficiency is known to better than 10% over the energy range 800 keV to 15 MeV. The efficiency of the lithium glass detector has been calculated with certain approximations,⁽²⁾ and these calculations have been supported by more recent computations⁽³⁾ using the O5R Monte Carlo code.⁽⁴⁾ The data were recorded on TMC 201 and 211 1024 channel analyzers and also on an Eldorado analyzer interfaced to an on-line CDC-1700 digital computer.

The 7-in. diameter sphere (APFA-III 93.2% enriched in U^{235}) was studied in a bare near critical configuration ($k_{\text{eff}} \sim 0.96$). Various measurement positions in the sphere were obtained by inserting U^{235} slugs into a 3/4-in. diameter through hole. The control rod configurations were maintained constant throughout the measurements so that the reactivity level changed as the different slugs were inserted. Nevertheless the reactor dieaway time was less than 250 nsecs at all positions. The reactor was excited externally by impinging the electron beam into a 3/8-in. thick disc of tungsten alloy. Both U^{235} sphere and target were air cooled. The reactor and pulsed source intensities were monitored by an externally placed sulphur foil and by room return fission counters.

The 20-in. diameter sphere was excited internally using a spherical 3-in. diameter air cooled target,⁽⁵⁾ also of depleted uranium. This system was designed specially to permit detailed study of the angular flux behavior. The neutrons were extracted in turn from various 1.185-in. diameter reentrant holes normal to the source-LINAC axis. The hole pattern allowed measurements to be made at several angles to five radius

vectors. The neutron source intensity was monitored by means of a 1/4-in. diameter fission counter located in the sphere itself and by means of gold foils.

The measured time-of-flight data from both experiments were corrected for count rate losses, mean emission times and residual backgrounds, and were converted into neutron spectra. Comparisons to the theoretical data were made.

The U^{235} sphere was excited externally, but its high multiplication (~ 30) was believed to permit analysis of the system with a k calculation in an S_n transport theory code. This approach was justified by previous calculations⁽⁶⁾ which had shown that the neutron spectrum in such a reactor was hardly sensitive to the reactivity level between a k_{eff} of 0.93 and 1.00. Also, these calculations indicated that the neutron spectrum was sensitive to the source characteristics only in the immediate vicinity of the source. We have examined the spectrum in detail at the reactor center by comparing it to the results of calculations using the GAM-II⁽⁷⁾ code. GAM-II is an infinite medium code, but it can be used for a bare reactor in the fundamental mode due to the separability of space and energy for such a system. This is useful because more energy detail in the calculated spectrum can be obtained with GAM-II than with space dependent methods. This comparison of theory and measurement is shown in Fig. 1. The agreement is reasonable except below 200 keV where theory is the lower. It is to be noted that the spectrum changes very little when the ENDF/B⁽⁹⁾ cross sections for U^{235} are used instead of those due to Joanou and Drake.⁽⁹⁾

The surface and central measurements of angular spectra are compared in Fig. 2 to the older S_{16} calculations⁽⁶⁾ which were made using the cross sections for U^{235} due to Joanou and Drake.⁽⁹⁾ The measured data have been integrated over the energy intervals used in the theory, and have been normalized as a set to the calculated values. This places reliance on source monitoring, which was considered to have limited reliability since both reactor and external source neutrons were being measured and the reactivity level was changing from one position to another. However, the normalization factor between theory and experiment was remarkably constant for all the positions studied. The discrepancies between theory and experiment are larger at the surface than at the center. The observed spectrum changed very little with position except at the surface. This indicates that the spatial harmonics were small and that a fundamental mode distribution was obtained.

Causes for the observed discrepancies have been postulated:

1. Incorrect inelastic scattering cross sections.

2. Incorrect fission source spectrum
3. Room return neutrons
4. Incorrect detector efficiencies
5. Reentrant hole perturbation.

The short dieaway of the U^{235} sphere coupled to a long flight path provided a significant time separation between the reactor capture and fission gamma rays and the arrival of the fastest neutrons. Since the NE-213 detector is gamma sensitive, it permitted the system dieaway to be studied simultaneously with the time-of-flight measurement. Had the dieaway been larger, similar studies could still have been made by inserting a lithium hydride filter into the flight path.

The experimental data from the U^{238} sphere were reduced using mean emission times based on independent dieaway studies.⁽²⁾ The results from the two detectors were again found to normalize very well together in the overlap energy region. Some typical experimental data from the U^{238} sphere are shown in Fig. 3 and indicate a self-consistent pattern for a constant radius of 6.5 in. Comparative calculations have been performed using the 1DF transport theory code.⁽¹⁰⁾ These calculations used broad group cross sections up to P_3 that were group averaged by the GAM-II code.⁽⁷⁾ The narrow resonance approximation was used to self-shield the absorption cross sections. Two cross section sets for U^{238} were used: Joanou and Stevens'⁽¹¹⁾ and the ENDF/B set.⁽¹²⁾ The source was treated as isotropic and uniformly distributed in a sphere of 1.6 cm in diameter at the center of the system. The source spectrum was taken to be equal to the surface current-spectrum from the bare air-cooled uranium target which was measured in a separate experiment with the same detectors. An S_{32} calculation was performed using Legendre-Gauss quadrature. The high order quadrature was considered necessary to describe the rapid variation of the angular flux which is very highly peaked in the outgoing ($\mu=1$) direction.

For illustrative purposes, we compare in Fig. 4 the measured and calculated angular neutron spectra at Position B. The experimental data have been integrated over the energy intervals of the calculation, but nevertheless remain monitor normalized. Examination of this figure indicates that there is a greater depletion of high energy neutrons than predicted by the theory, no matter which cross section set is used. The measured and calculated angular dependence of the flux in the elastic scattering region (below 49 keV) is shown to be small. This observation could conceivably be used to reduce the order of quadrature at energies less than that value. There are still important differences between theory and experiment but the comparisons given in Fig. 4 and elsewhere⁽¹³⁾ appear to show that the

ENDF/B cross sections provide a better fit. These comparisons already indicate that the theoretical spectra are sensitive to the choice of cross section sets and that the experimental data are of sufficient quality to specify which choice.

The experimental data at other positions are still being examined and compared to further calculations which include:

1. Use of Lobatto⁽¹⁴⁾ quadrature which includes $\mu = 1.000$ direction.
2. Use of a source spectrum adjusted so that the measured and calculated leakage from the bare target are in agreement.

Other items to be investigated include the sensitivity of the spectra to the order of quadrature and the omission of higher order scattering moments. The experimental angular spectra can also be expected to comment on the adequacy of the elastic scattering cross sections for U^{238} .

The two experiments have basic differences: one investigates the response to a given source, the other studies a reactor spectrum which is independent of the exciting source. Since the target source is measured with the same detectors used in the U^{238} sphere studies, that theory experiment comparison is less sensitive to errors in the detector efficiencies. On the other hand, the comparison tests quite severely the calculational methods, particularly the selection of the angular, energy, and spatial meshes. Thus the independence of the U^{235} sphere measurements to the source spectrum will aid in identifying the causes of the observed discrepancies in each experiment whether in theory, in measurement, or both.

2. REFERENCES

1. "Design and Efficiency Calibration of the 5 cm and 13 cm Fast Neutron Detectors," General Atomic Report GA-7483, December 1966.
2. J. R. Beyster, et al., "Integral Neutron Thermalization, Annual Summary Report," USAEC Report GA-8280, General Dynamics Corporation, General Atomic Division, November 1967.
3. D. Huffman, Private Communication, October 1967.
4. D. C. Irving, et al., "O5R, A General Purpose Monte Carlo Neutron Transport Code," USAEC Report ORNL-3622, Oak Ridge National Laboratory, February 1965.

5. A. E. Profio, et al., "Angular Flux Spectrum and Other Characteristics of the 7.62 cm Diameter Uranium Target," General Atomic Report GA-7409, September 1966.
6. J. R. Beyster, et al., "Integral Neutron Thermalization, Annual Summary Report, October 1, 1965 through September 30, 1966," USAEC Report GA-7480, General Dynamics Corporation, General Atomic Division, November 1966.
7. G. D. Joanou and J. S. Dudek, "GAM-II, A B₃ Code for the Calculation of Fast Neutron Spectra and Associated Multigroup Constants," General Atomic Report GA-4265, September 1963.
8. ENDF/B Cross Sections for U²³⁵, KAPL February 1967.
9. G. D. Joanou and M. K. Drake, "Neutron Cross Sections for U²³⁵," NASA Report CR-54263. See also GA-5944, December 1964.
10. Private communication from B. Roos to R. Dahlberg, December 1966. See also K. D. Lathrop, "DTF-IV Code, A FORTRAN-IV Program for Solving the Multigroup Transport Equation with Anisotropic Scattering," USAEC Report LA-3373, Los Alamos Scientific Laboratory, July 1965.
11. G. D. Joanou and C. A. Stevens, "Neutron Cross Sections for U²³⁸," NASA Report CR-54290. See also GA-6087, April 1965.
12. J. J. Schmidt, "Fast Neutron Nuclear Data for U²³⁸ in the Energy Region 4 keV to 10 MeV," KFK 120/Teil I, Abschnitt VI 2, June 1966.
13. J. M. Neill, et al., "Fast Neutron Spectra in Multiplying and Non-Multiplying Media," USAEC Report GA-8551, Gulf General Atomic Incorporated, February 1968.
14. M. Abramowitz and I. Stegun, Handbook of Mathematical Functions, U.S. Government Printing Office, Washington, D. C. (1964). \$6.

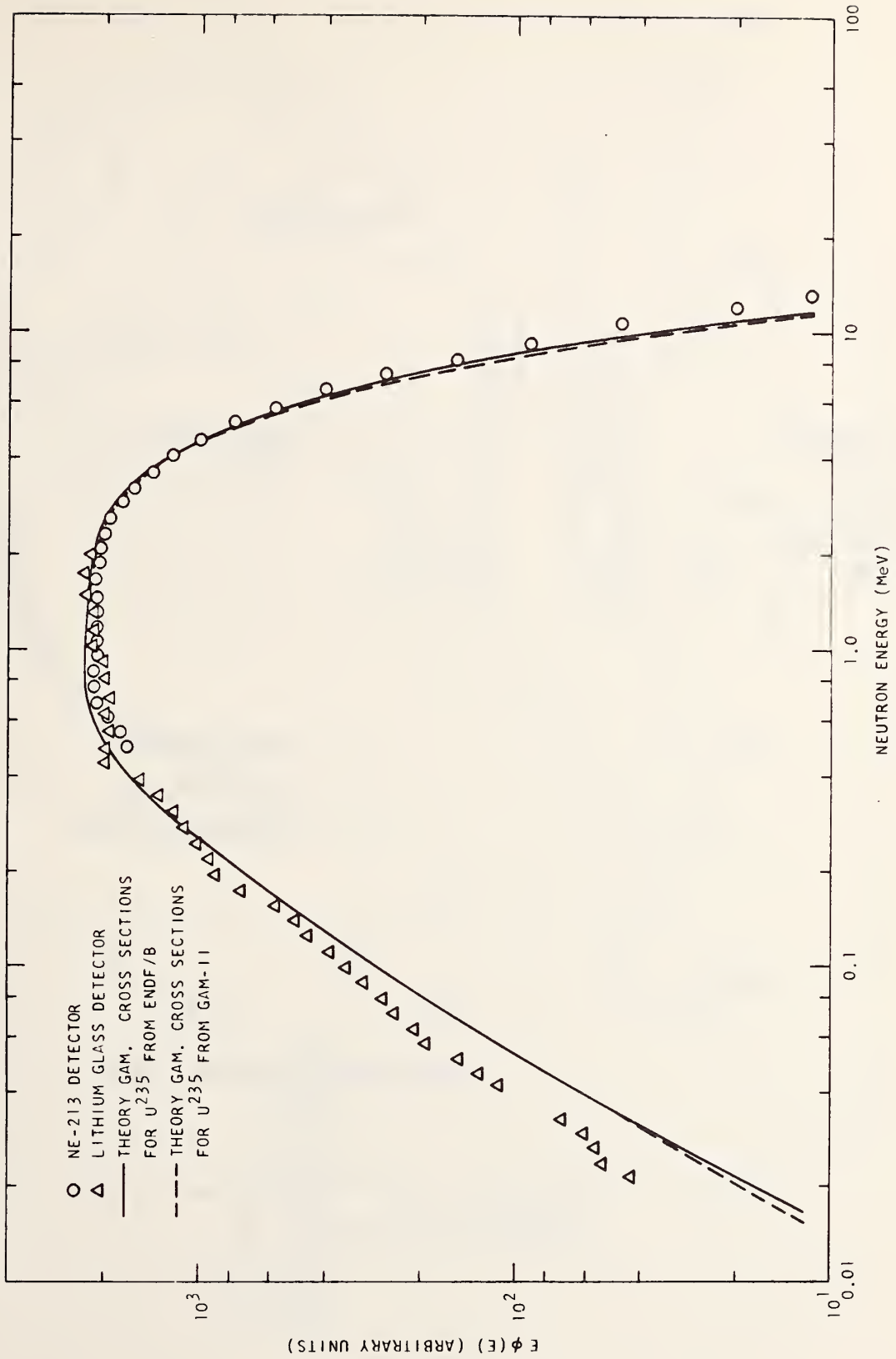


Figure 1. Comparison of calculated and measured neutron spectra at the center of the U²³⁵ sphere.

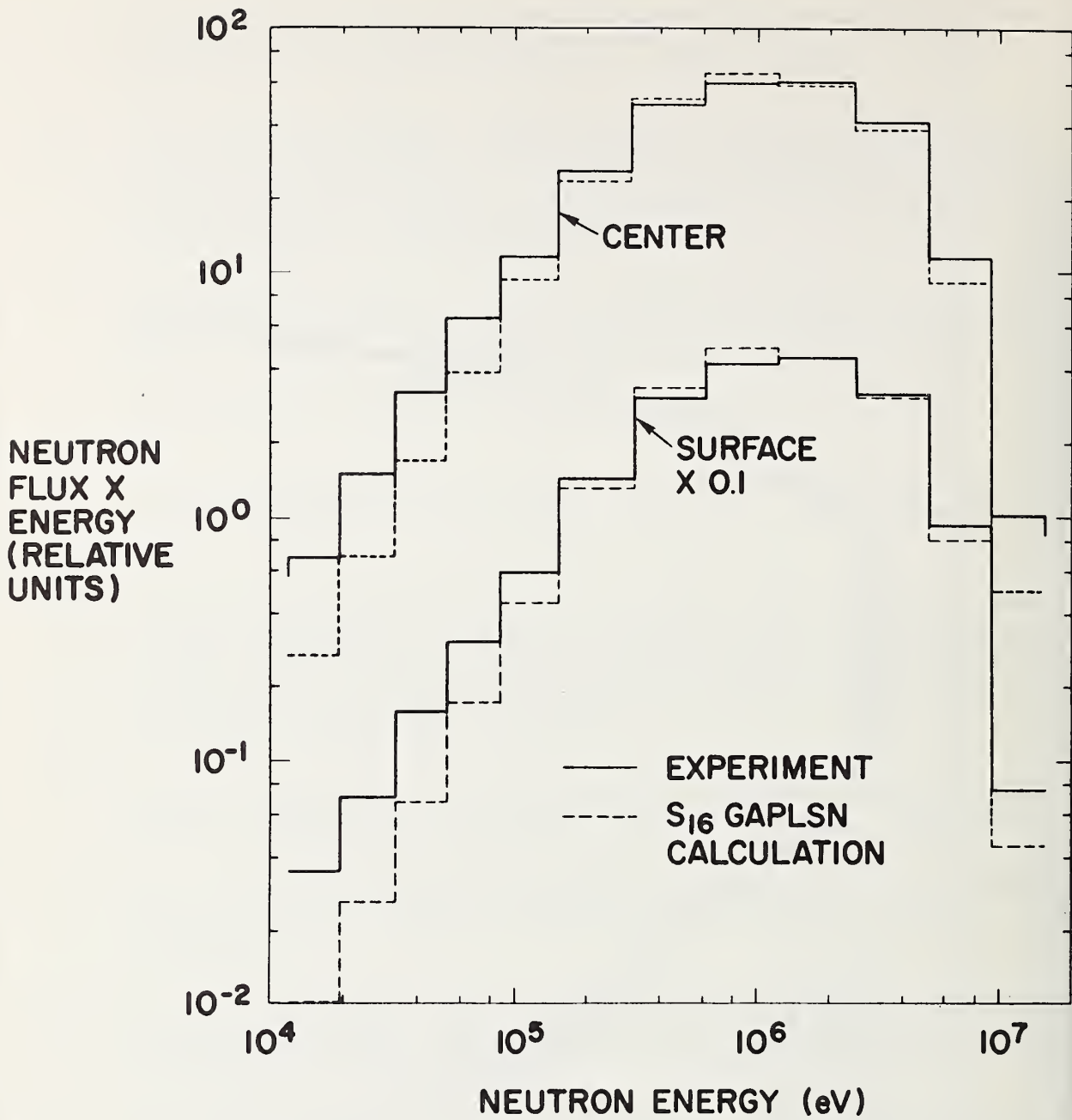


Figure 2. Comparison of U²³⁵ sphere spectra with GAPLSN calculation.

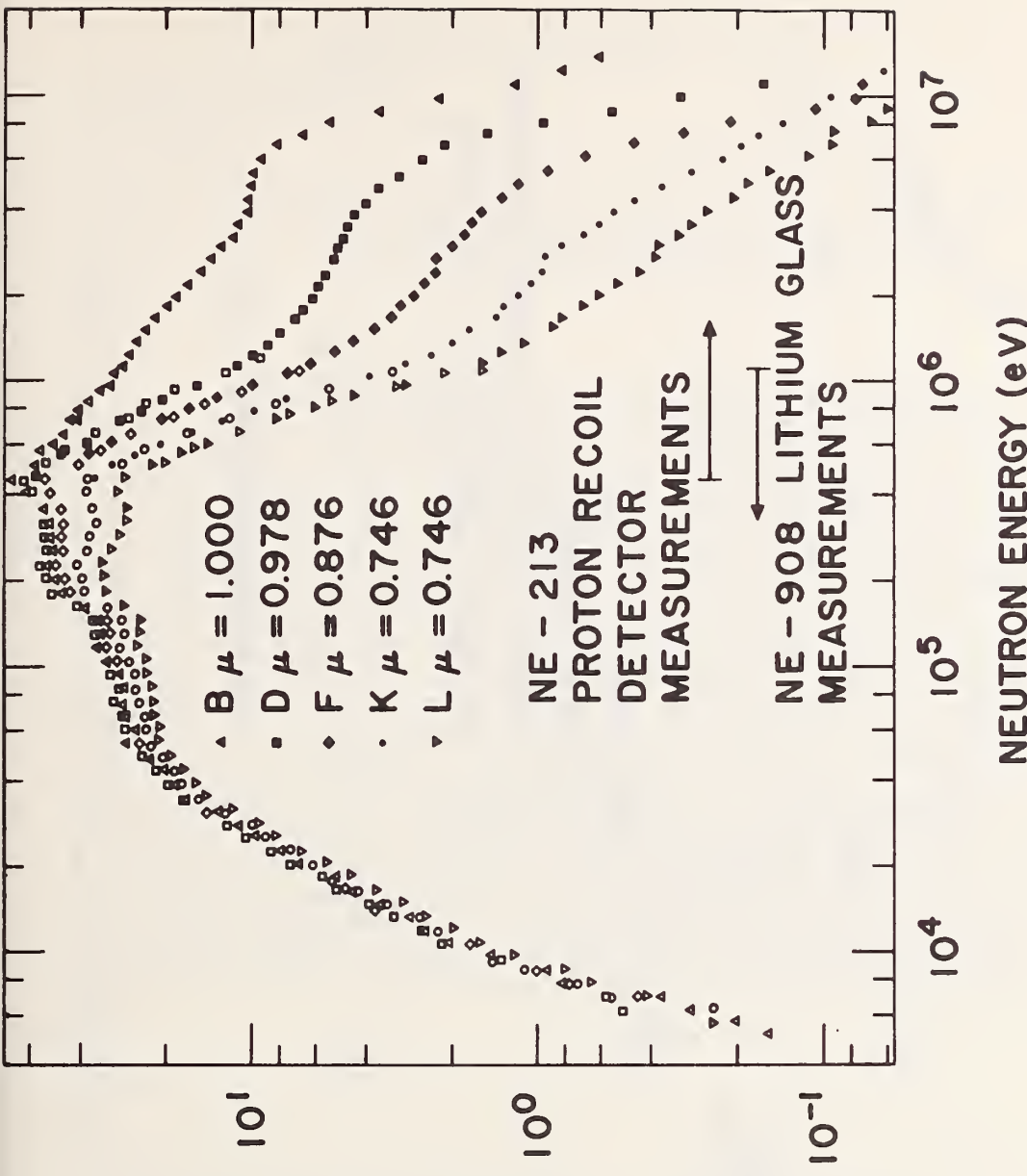


Figure 3. Experimental angular fluxes in the U^{238} sphere at a radius of 6.5 in.

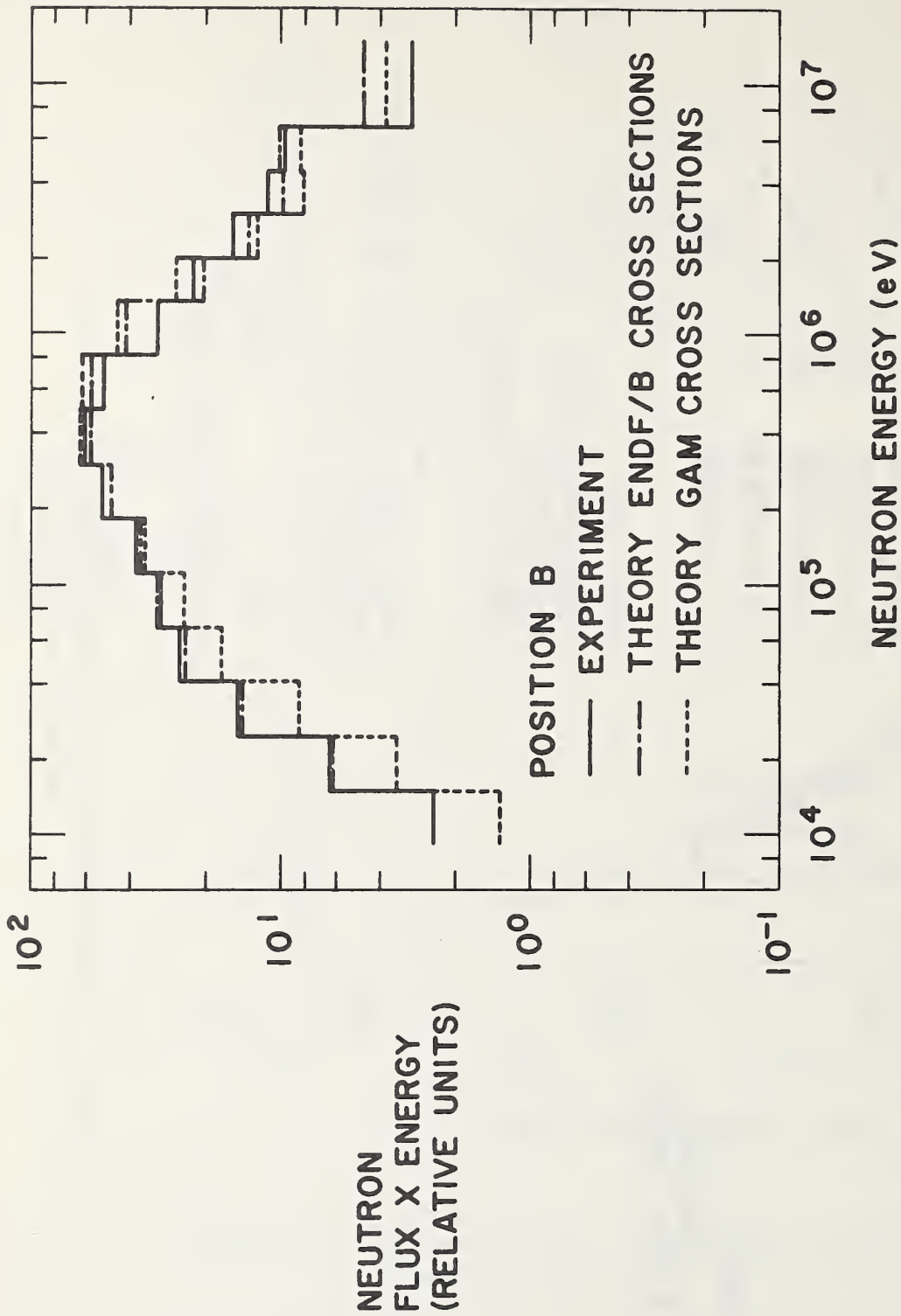


Figure 4. Comparison of theoretical and measured neutron spectra at Position B in the U²³⁸ sphere (R = 6.5 in., $\mu = 1.000$).

STUDIES OF THE ANGULAR DISTRIBUTION OF FAST
NEUTRONS IN DEPLETED URANIUM*

E. Greenspan⁺, B. K. Malaviya, N. N. Kaushal, E. R. Gaerttner
and P. B. Daitch

Division of Nuclear Engineering and Science
Rensselaer Polytechnic Institute
Troy, New York 12181

Fast neutron time-of-flight measurements of position-dependent angular flux from a pulsed depleted uranium assembly have been analyzed to obtain the energy-dependent angular and spatial neutron distributions and to study the relation between anisotropy in the neutron distribution and the differential elastic scattering cross-section. The observed difference between different angular components of the flux indicates a strong anisotropy in the neutron distribution; this anisotropy is a strongly varying function of neutron energy and distance from the source in the assembly. A definite correlation is found between the anisotropy curve and the energy dependence of the differential elastic scattering cross-section of U^{238} . Preliminary transport theory calculations employing the 16-group Los Alamos cross-section set in an S₁₆ approximation show that this cross-section set is inadequate to represent the anisotropic effects of neutron transport in U^{238} .

*Work supported by the U. S. Atomic Energy
Commission under Contract No. AT(30-3)328.

⁺Present address: Negev Nuclear Research Center, Soreq,
Israel.

1. INTRODUCTION

A series of fast neutron spectra has been measured at various positions and angles in a depleted uranium assembly by the time-of-flight technique. A part of these measurements have been analyzed to yield the relative angular and spatial distributions of neutrons in the energy range 0.5 to 10 MeV. Such relative distributions can be obtained without a knowledge of the energy dependent detector efficiency and are especially useful in providing information on the anisotropic effects of neutron transport and checks of the cross-sections used in fast reactor and shielding calculations.

2. DESCRIPTION OF EXPERIMENT

The measurements were made with the time-of-flight method using the RPI Linear Accelerator and 25- and 100-meter flight paths. The over-all experimental arrangement was the same as that described in another paper⁽¹⁾ in these proceedings. The depleted uranium assembly was a 40 in. x 31 in. x 26 in. parallelepiped stacked from 2 in. x 2 in. x 5 in. bricks (made available on loan from Argonne National Laboratory through the courtesy of Dr. W. Kato). The uranium bricks in the seventh layer were arranged so that reentrant holes of different depth and 2 in. x 2 in. cross-section area could be made in five different positions across this layer; the centers of the five transverse channels were located at distances of 8, 14, 18, 22 and 26 inches from one face of the assembly (Fig. 1). A 6 in. x 6 in. x 11 in. recess at the center of the front face of the assembly was provided to allow the placement of an air-cooled target unit. The target consists of a 3.3 in. diameter sphere of lead with a reentrant hole in which air-cooled tantalum plates stop the electron beam and convert it into bremsstrahlung; the photoneutrons produced in the tantalum and lead emerge from the sphere to constitute a nearly isotropic neutron source. The assembly was mounted on a table which could be moved so as to bring different reentrant holes in line with the flight path while maintaining the Linac-assembly geometry unchanged⁽¹⁾. The neutrons emitted from a reentrant hole in the assembly traverse the 100-meter flight path and are detected (for the measurements described here) by a 20-in. diameter, 5-in. thick liquid scintillator; the signals from the detector are time-analyzed by a PDP-7 on-line computer with a minimum channel width of 31.25 nsec.

Time-of-flight measurements have been made, for as many angular components of the neutron flux as possible, for spatial points 6, 10 and 14 inches from the source; the points accessible to the measurement and their designation are shown in Figure 1. Four angular components of the flux can be measured at the 10-in. radial position and six components at a radius of 14 inches; only two components (0° and 90°) are accessible at the 6-in. radius. The measured spectra from different points are normalized to the same total neutron yield; this yield is taken to be proportional to the total charge deposited on the target (measured by a current integrater) times the electron beam energy.

3. ANALYSIS AND DISCUSSION OF RESULTS

From the neutron spectra measured at different positions in the assembly, we can obtain, in addition to the energy distribution of different angular components of the neutron flux at those positions, two other distributions. These are the angular distribution of the neutron flux at certain selected radii (6, 10 and 14 inches) and the space dependence of selected components (0° and 90°) of the angular flux for any neutron energy. These relative distributions are independent of the detector efficiency but require an accurate knowledge of the run-to-run normalization.

The time-of-flight spectra of angular components corresponding to the same radius but different angles in the assembly are found to be significantly different. For example, as shown in Fig. 2, the 0° component has a double peak as compared to the single peak of the 90° component (both at the 10-in. radial position). This difference suggests that there is a strong anisotropy in the measured neutron distribution. The degree of anisotropy as a function of energy in this depleted uranium assembly is shown in Figure 3 which gives the ratio of the 0° angular flux to the 90° angular flux at the 6-, 10- and 14-in. radial positions. A strong energy dependence of the anisotropy is observed. The anisotropy curve is found to follow the shape of the energy dependence of anisotropy in the differential elastic scattering cross-section of natural uranium, shown in Figure 4; this figure gives the probability that a neutron, elastically scattered in natural uranium, will be scattered into a unit solid angle around the 0° direction as compared to that around a 90° direction (evaluated from the data given in reference 2).

The variation of anisotropy with energy depends also on the distance of the point from the source in the assembly as seen from Fig. 3. This figure also shows the comparison of experimental results with transport-theory calculations based on a one-dimensional Sn code DTF-IV⁽³⁾. In these preliminary calculations, the Los Alamos 16-group cross-section set is employed and the uranium assembly with the source is approximated by three concentric spherical regions: the target region, a vacuum shell and uranium region with respective radii of 1.56, 3 and 20 in. The source is assumed to be isotropic and uniform and the source spectrum is taken to be a Maxwellian with $T_{eff} = 0.95$ MeV. These calculations based on the crude 16-group cross-section set do not predict well, the energy variation of anisotropy in depleted uranium.

An example of the variation of the angular flux with direction is shown in Fig. 5 which gives the angular distribution of the neutron density at 14-in. radius in the uranium assembly for selected neutron energies; comparison with DTF-IV calculations is also shown. The measured and calculated distributions are normalized at 90°. For higher energies, calculations are found to overestimate the forward peaking component ($\cos\theta=1$); they underestimate it for lower energies. The over-all agreement is surprisingly good in view of the transport approximation for the angular dependence of the scattering cross-section, employed in the calculations.

4. REFERENCES

- (1) B. K. Malaviya, E. Greenspan and E. R. Gaerttner, "Adequacy of Fast and Intermediate Cross-Section Data from Neutron Spectrum Measurements in Bulk Media", Paper H5, These Proceedings.
- (2) M. D. Goldberg et al, "Angular Distributions in Neutron-Induced Reactions", BNL-400, Vol. 2 (1962).
- (3) K. D. Lathrop, "DTF-IV, A Fortran-IV Program for Solving the Multigroup Transport Equation with Anisotropic Scattering", LA-3373 (1965).
- (4) ANL Staff, "Reactor Physics Constants", ANL-5800, 2nd Ed., P. 568 (1963).

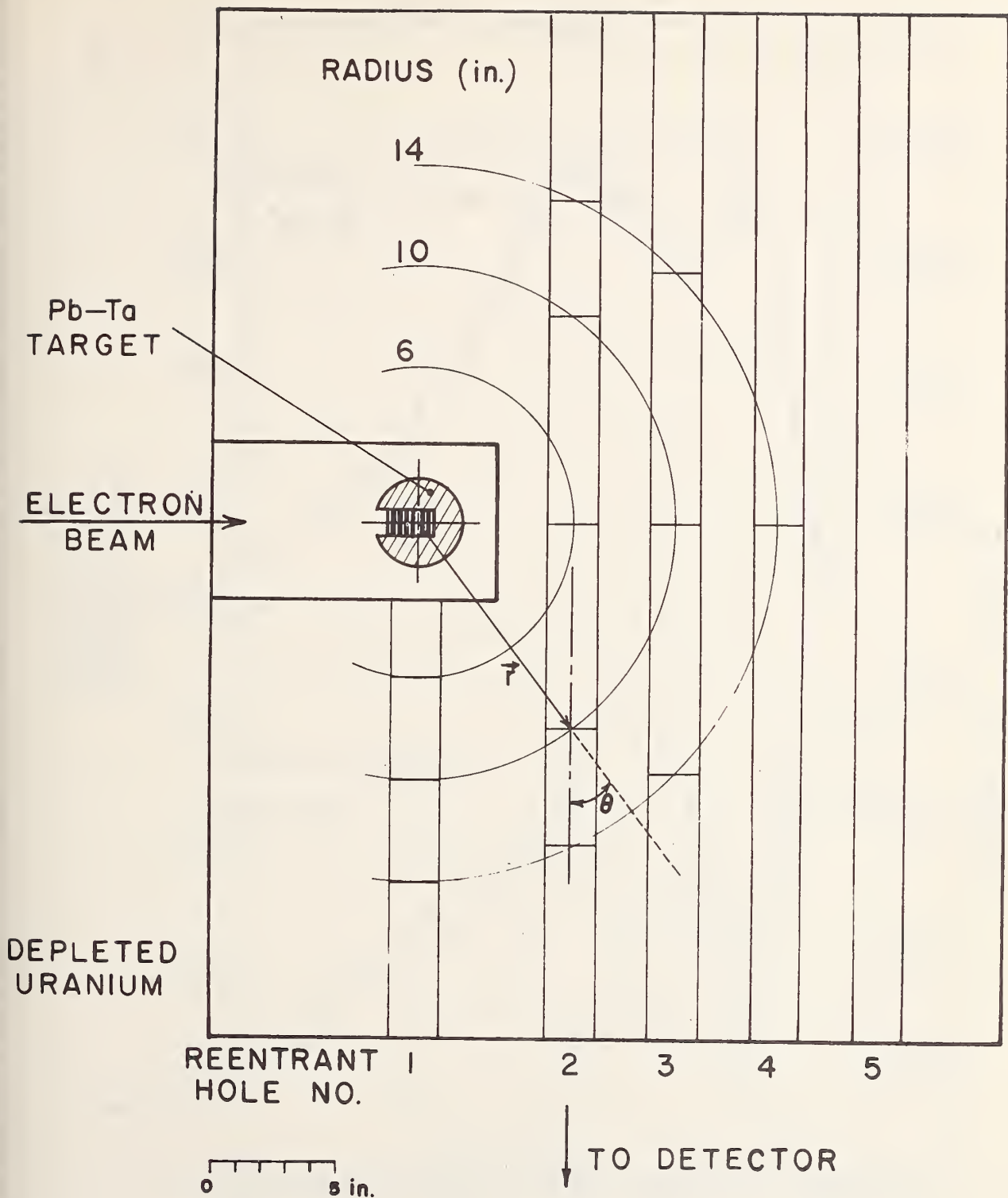


FIGURE 1 The pattern of reentrant holes with respect to the source in the depleted uranium assembly and the designation of experimental points.

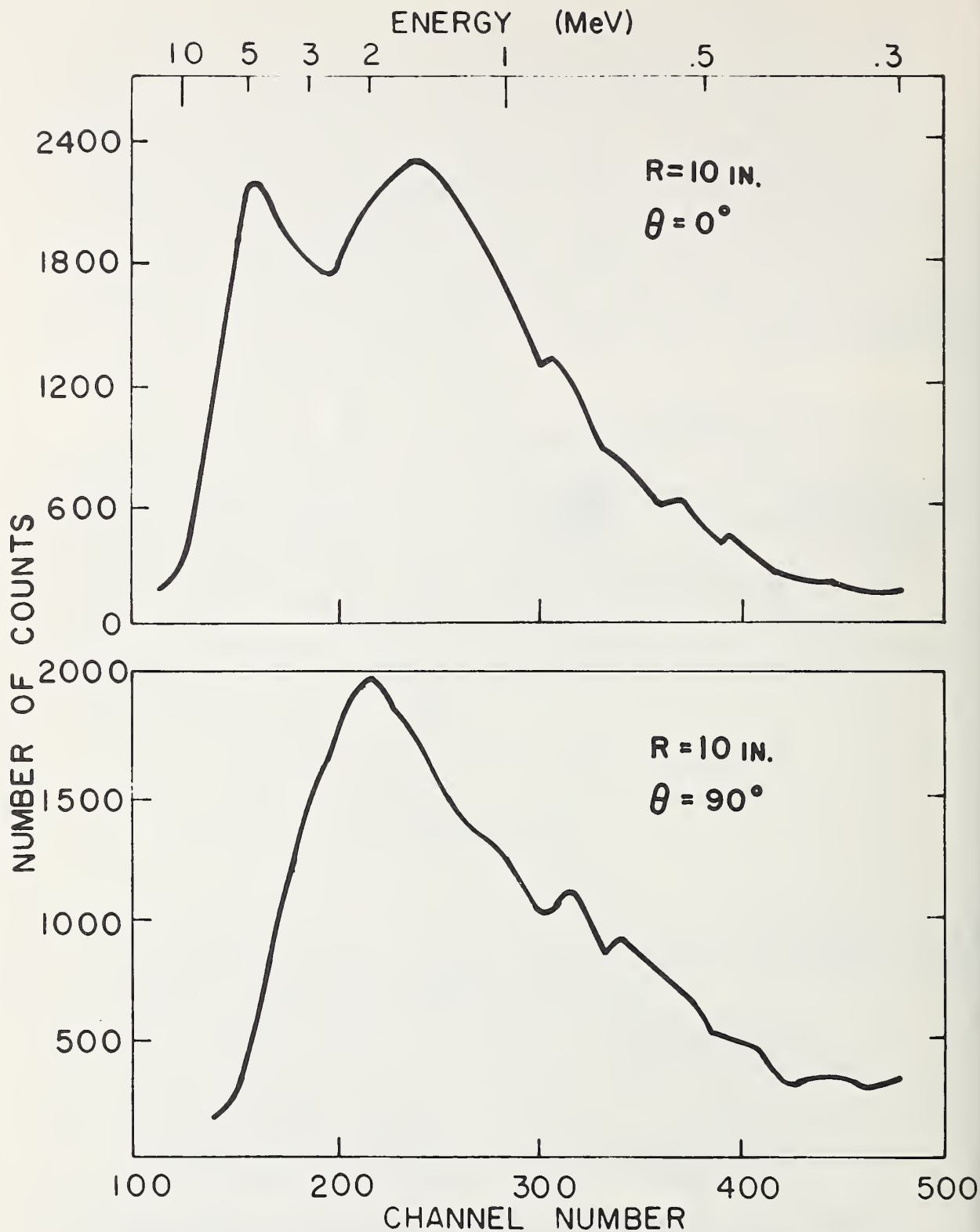


FIGURE 2 Time-of-flight Spectra at the 10-in. radial positions in the 0° and 90° directions.

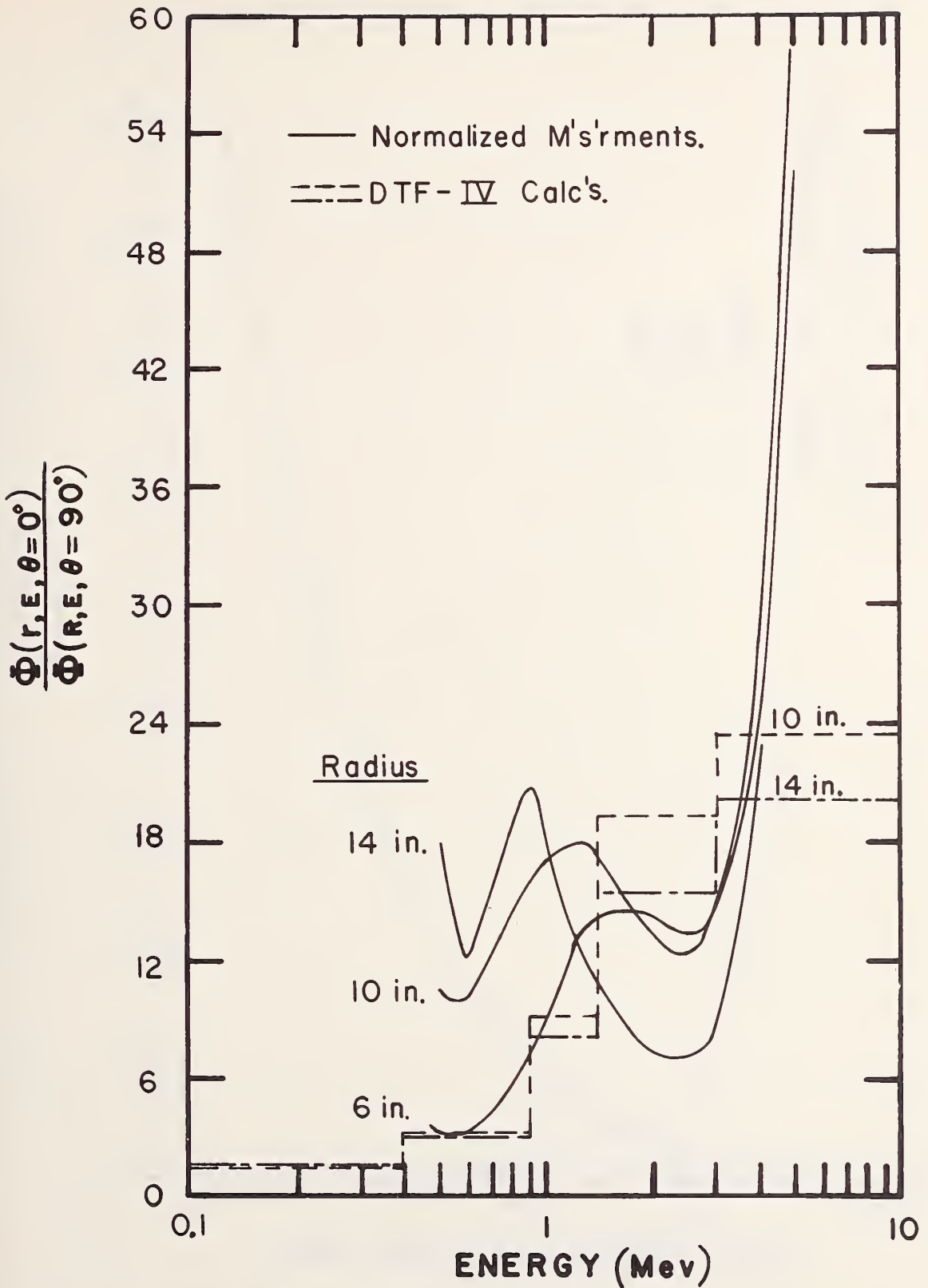


FIGURE 3 Measured and calculated anisotropy ($0^\circ/90^\circ$ components) of the angular flux at different radii in the depleted uranium assembly.

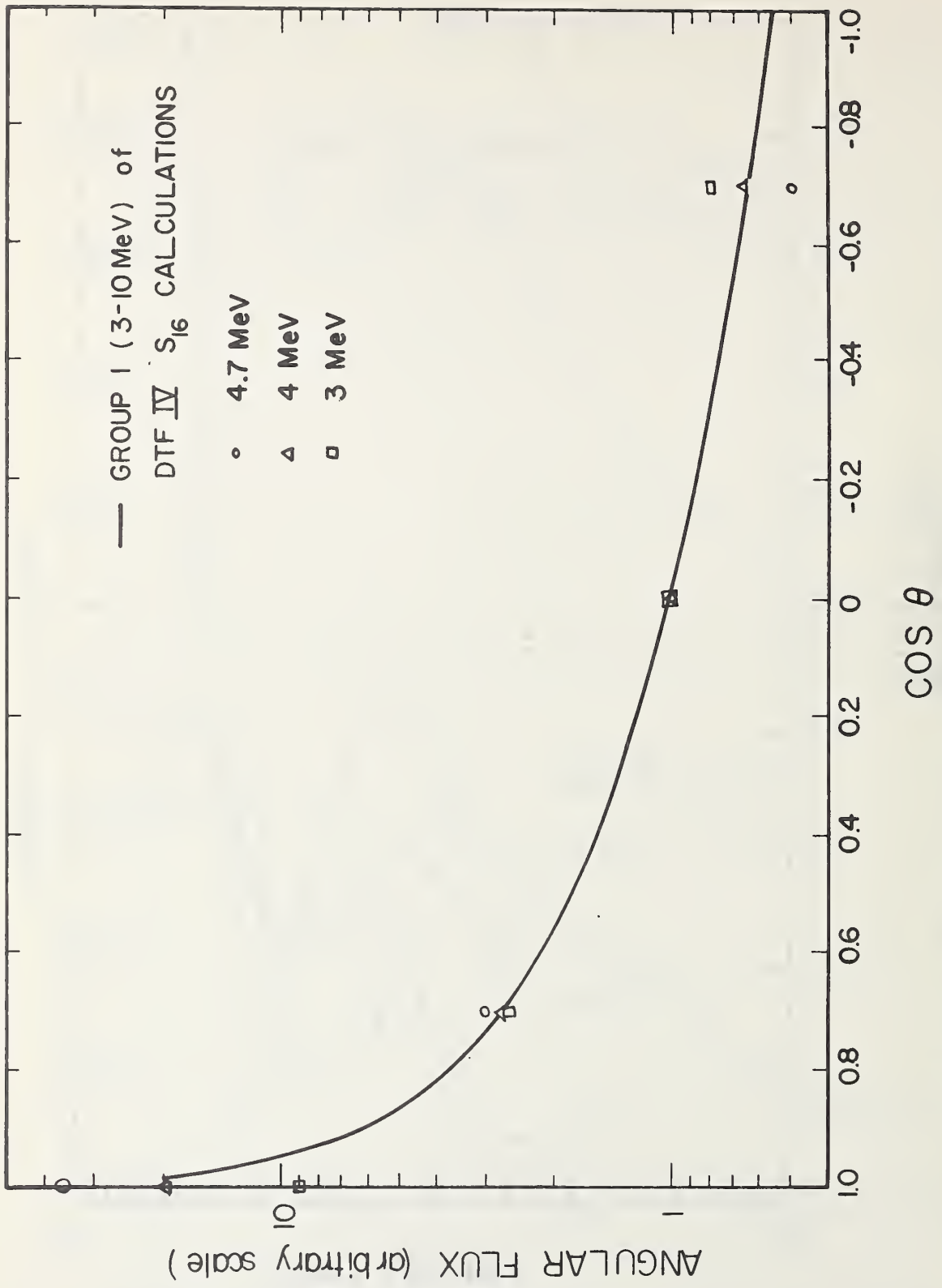


FIGURE 5 Measured and calculated angular flux at 14 in. radius in the depleted uranium assembly for the energy range 3 - 10 MeV.

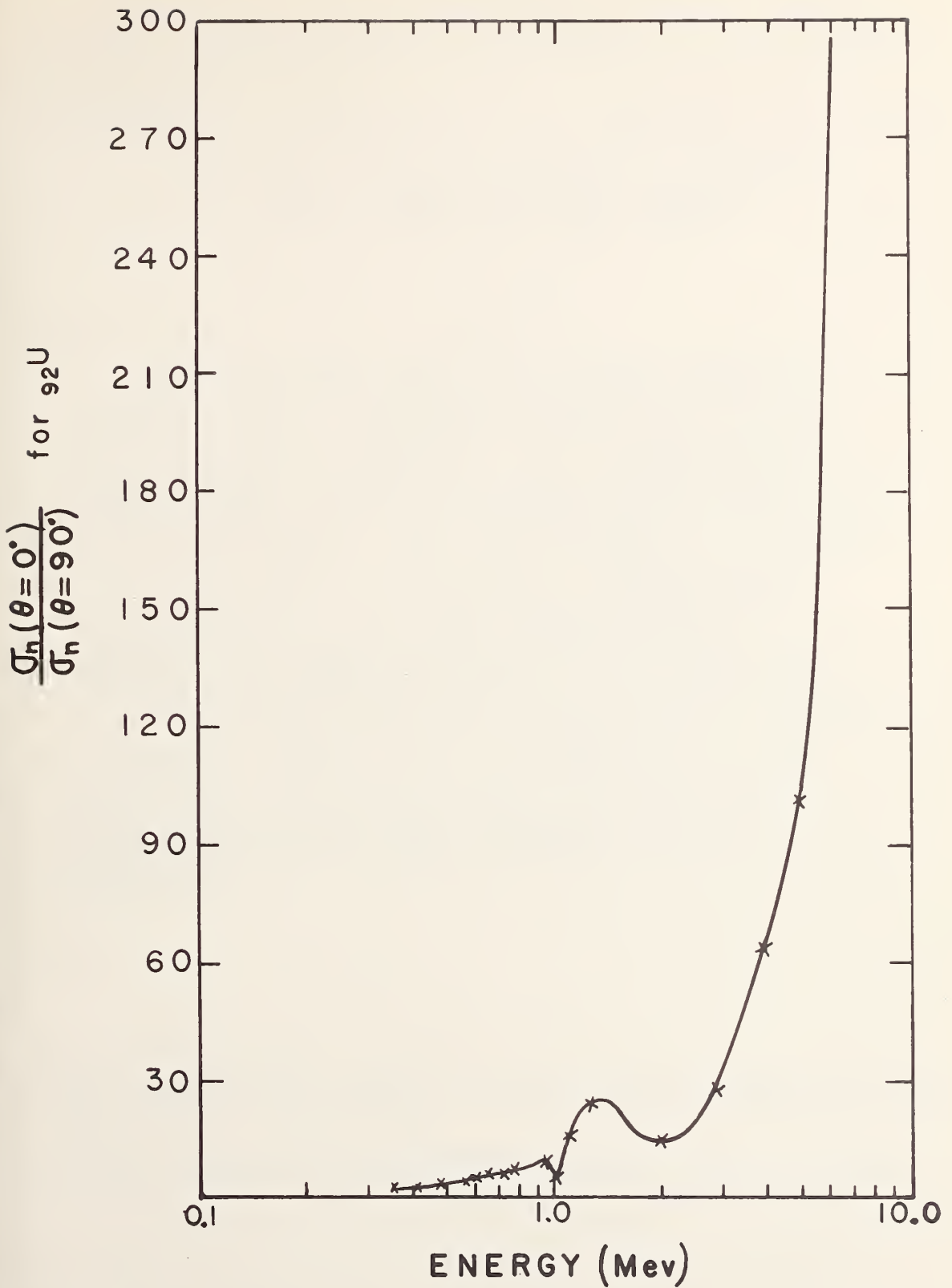


FIGURE 4 Energy dependence of the anisotropy in the differential elastic scattering cross section $\frac{\sigma_n(\theta=0^\circ)}{\sigma_n(\theta=90^\circ)}$ for natural uranium.

ADEQUACY OF FAST AND INTERMEDIATE CROSS - SECTION
DATA FROM NEUTRON SPECTRUM MEASUREMENTS IN BULK MEDIA*

B. K. Malaviya, E. Greenspan⁺, E. R. Gaerttner and A. Mallen

Division of Nuclear Engineering and Science
Rensselaer Polytechnic Institute
Troy, New York 12181

ABSTRACT

The measurement and analysis of intermediate and fast neutron spectra in bulk media provide a valuable means of checking cross-section data and recipes used for the generation of cross-section sets from point-wise data. As an illustration of this approach, position-dependent spectra from a 40-inch cube of iron have been measured by the time-of-flight method, using the RPI LINAC and a set of calibrated detectors to cover the energy range of a few hundred ev to several MeV. The measured spectrum gives a fairly good representation of the resonance structure of iron. The experimental spectra are compared with calculations employing 49 energy groups from the ANL cross-section library and an S₁₆ representation. Although the over-all agreement is good, it is concluded that in order to better represent the fine structure in the spectrum it is necessary to go to a finer energy mesh and to define group boundaries so as to correctly describe the inter-group transfer cross-sections.

* Work supported by the U. S. Atomic Energy Commission under Contract No. At(30-3)328.

+ Present address: Negev Nuclear Research Center, Israel.

1. INTRODUCTION

The fine resolution attainable in fast neutron spectrometry by the pulsed-source, time-of-flight technique makes it possible to study the macroscopic as well as microscopic features of the neutron spectrum in a fast system. The analysis of the measured angular flux is especially instructive for those light and medium-weight materials whose cross-sections have a profuse resonance structure in the keV range; the sharp variations in the spectrum are sensitive to both the cross-section data themselves and to the details of the recipe employed for the generation of cross-section sets. The measurement of intermediate and fast neutron spectra in geometrically simple systems of such pure materials provides a valuable means of checking the cross-section sets used for analytically predicting the microscopic features of the neutron spectrum. To this end, time-of-flight measurements have been made of a series of fast neutron spectra as a function of position and angle inside a 40-inch cube of iron. This paper is mainly concerned with the description of the measurement and analysis of the angular flux in the zero-degree direction.

2. DESCRIPTION OF THE EXPERIMENT

The measurements were made with the time-of-flight techniques using the RPI Linear Accelerator and 27- and 100-meter flight paths. The over-all experimental arrangement is shown in Fig. 1. The electron beam defined by air-cooled aluminum 'strippers' strikes the lead target which is imbedded in the experimental assembly. The 40 in. x 40 in. x 38 in. assembly was stacked from 2 in. x 2 in. x 5 in. bricks of cold-rolled steel (made available on loan from Argonne National Laboratory through the courtesy of Dr. W. Kato). Bricks in the central layer were arranged so that reentrant holes of different depths and 2 in. x 2 in. cross-section area could be made at five different positions across this layer. A 6 in. x 6 in. x 11 in. recess at the center of the front face of the assembly allowed the placement of the target unit. The target⁽¹⁾ consists of a 3.3-in. diameter sphere of lead with a reentrant hole in which air-cooled tantalum plates stop the electron beam and convert it into bremsstrahlung; the photoneutrons produced in tantalum and lead emerge from the sphere to constitute a nearly isotropic fast neutron source.

The assembly rested on a cart which could be moved on rails so as to bring different reentrant holes in line with the neutron flight tube; along with this movement, the electron beam window which is attached to a special expandable bellows section - can also be moved so as to maintain unchanged the over-all geometry for source-neutron production. The neutron beam emerging from the reentrant hole under study, is defined by

1-in. diameter pre-collimators and traverses the evacuated flight tube to 27 and 100-meter stations; a set of post-collimators are placed in the flight tube at about 20 meters to define the beam to a size appropriate to the detector in use. At the 27-meter station, $B_4^{10}C$ -NaI detector is used; this detector is useful for the energy range below about 1 MeV and its efficiency as a function of energy has been determined by calculation^(1,2). At the 100-meter station is located a large (20-in. diameter, 5-in. thick) proton recoil detector (liquid scintillator); this detector covers the energy range above about 0.5 MeV and its efficiency has been determined⁽³⁾ by measurements based on the photonuclear spectrum of deuterium. The signals from the detector are time-analyzed by a PDP-7 on-line data-recording system which is programmed so as to divide the memory into regions of sequentially increasing channel widths starting from a minimum width of 31.25 nsec. The electron beam (55 MeV, 480 pulses per sec.) pulse widths were 10 or 20 nsec. The over-all resolution of the system is 0.3nsec/meter for the 100-meter flight path, not including the mean-emission time. A fission chamber and a target current integrator provide independent means of normalizing the measured spectra.

3. ANALYSIS AND DISCUSSION OF RESULTS

The measured spectra are corrected for dead-time losses, steady-state background, relative detector efficiency and transmission through materials in the flight path. Only the angular flux spectra in the zero-degree direction (reentrant hole no. 1) are considered here. A typical result is shown in Fig. 2 which gives the spectrum at the 12-in. radial position along the zero-degree direction. The measured spectrum fully reflects the resonance structure in the cross section of iron; a resonance peak in the total cross section appears as a dip in the zero-degree spectrum and vice-versa. This is a direct consequence of the role of elastic scattering in the establishment of the neutron flux in the assembly. The "trapping" of neutrons in the energy regions corresponding to the deep valleys in the cross section is most clearly shown by the large peak at 27.9 keV in the spectrum corresponding to the deep interference minimum on the low-energy side of the 29 keV resonance in Fe^{56} . The minimum in the cross section thus acts as a "window" transparent to the neutrons of this energy.

The reduced measured spectra are compared with the results of transport-theory calculations using the one-dimensional S_n code DTF-IV⁽⁴⁾. A 49-group cross-section set covering the energy range 10 keV to 10 MeV has been employed; this set is generated by the Argonne MC² code utilizing the data from an Argonne cross-section library⁽⁵⁾. For the one-dimensional calculation, the geometry of the actual iron assembly with the source is represented by a three-region medium: first a 1.5-in.

radius spherical target region; second a spherical shell of vacuum of outer radius 3 in., followed by a spherical shell of iron of outer radius 20 in. the target region is taken to be void, since lead cross-sections compatible with these calculations were not available. The source is assumed to be isotropic and uniform and the source spectrum is here taken to be a Maxwellian⁽⁶⁾ at $T_{\text{eff}} = 0.95$ MeV.

Typical experiment-theory comparisons are shown in Figures 2, 3 and 4 for the zero-degree angular flux at 12, 4 and 20 inches respectively from the source. The normalization is done arbitrarily at the central region of the spectrum. Only the P_0 component of the elastic scattering matrix was available in the cross-section set and the anisotropy is represented through the transport approximation. The over-all agreement in both the general shape of the spectrum and its "fine structure" is fairly good, although a few points of disagreement are noteworthy. The discrepancies at higher energies, in Figs. 3 and 4 (near the source and the boundary) may be due to an inadequate representation of the source region and the source spectrum or to inaccuracies in the cross section data.

An additional significant observation from the comparison is the slight shift in the measured spectrum with respect to the calculations, especially near sharp variations in the spectrum. This shift cannot entirely be accounted for by the mean-emission time (a correction for which has not been included in reducing the measured spectra) and points up the sensitivity of the fine structure of calculated spectrum to the choice of the group boundaries and group structure employed in the calculation⁽⁷⁾. The effect of these factors is being studied further. The fine resolution in the measured spectrum calls for a larger number of energy groups in the theoretical calculation to achieve a more meaningful experiment-theory comparison. Further calculations of the neutron spectrum in iron will involve finer energy meshes and alternative cross-section sets to better represent the inter-group neutron transfer and will also employ other "raw" cross section data (such as from ENDF/B) as they become available.

4. REFERENCES

- (1) B. K. Malaviya et al, "Fast Neutron Spectrum Program", Linear Accelerator Project Annual Technical Report, RPI-328-100 (1967).
- (2) R. W. Hockenbury et al, RPI Linear Accelerator Project Progress Report for October-December, 1966.
- (3) R. H. Augustson et al., "Calibration of a Large Proton Recoil Detector for Fast Neutron Spectra Measurements", Trans. Am. Nucl. Soc., 9, 2 (1966).
- (4) K. D. Lathrop, "DTF-IV, A Fartran-IV Program for Solving the Multi-group Transport Equation with Anisotropic Scattering", LA-3373 (1965).
- (5) A. Travelli, Private Communication.
- (6) I. B. Bayther and P. D. Goode, Harwell Nuc. Phys. Div. Progress Report AERE-PR/NP9 (1965).
- (7) J. Wagshal, Private Communication.

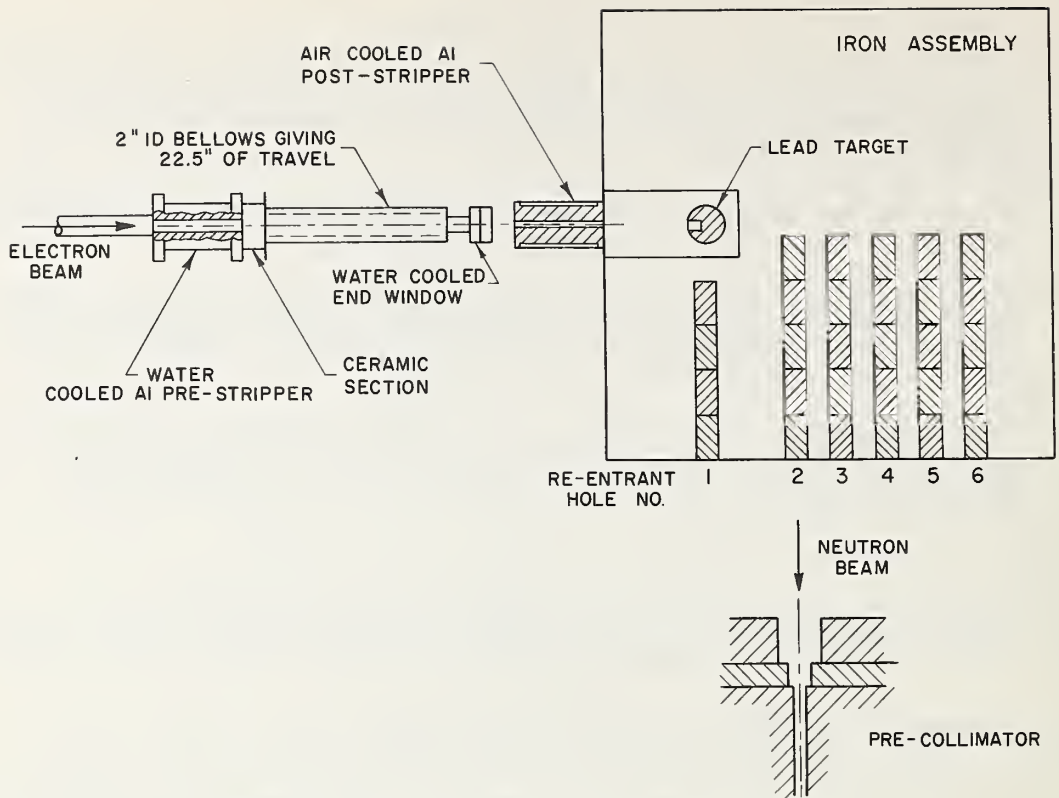


FIGURE 1 General Experimental Arrangement for Time-of-Flight Measurements on Fast Assemblies.

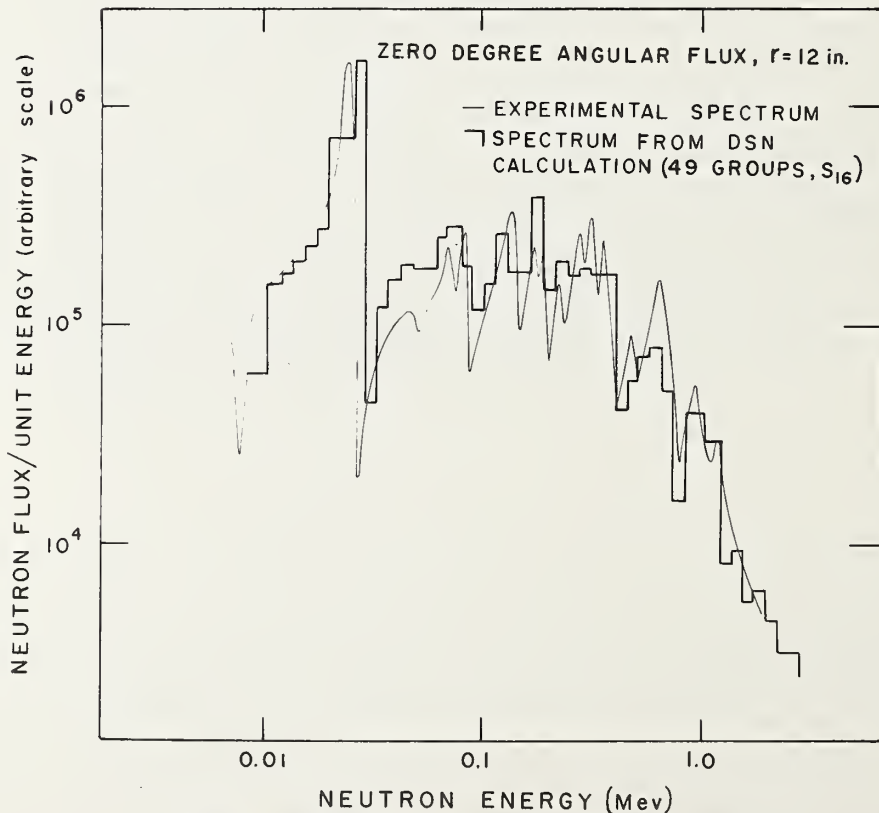


FIGURE 2 Measured and Calculated Zero-Degree Angular Flux at the 12-in. radius in a 40-in. cube of Iron.

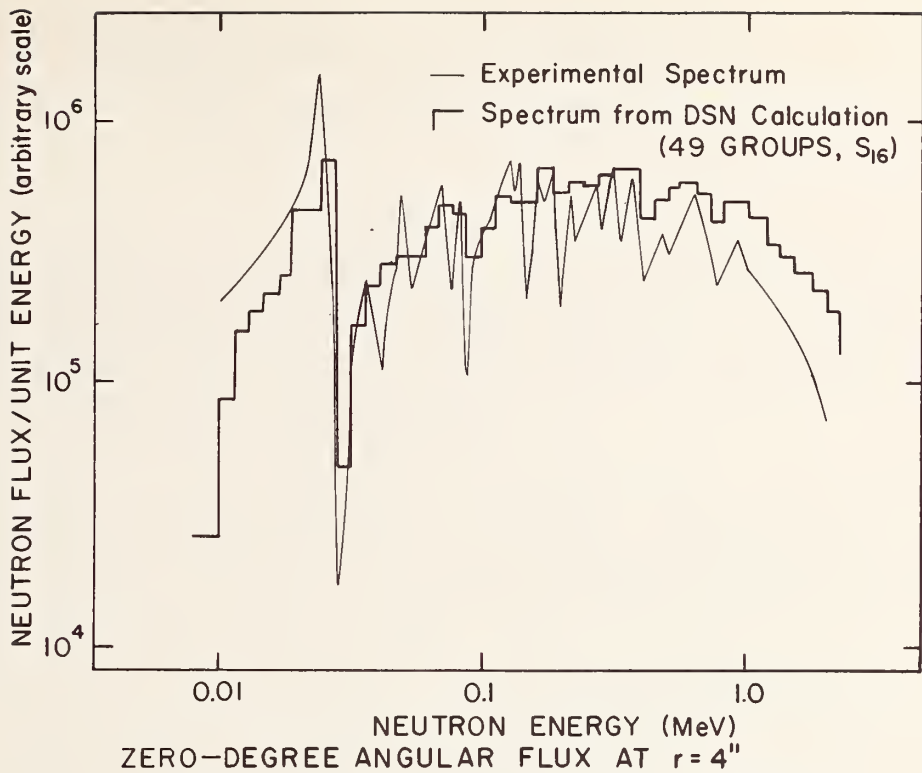


FIGURE 3 Measured and Calculated Zero-Degree Angular Flux at the 4-in. radius in a 40-in. cube of Iron.

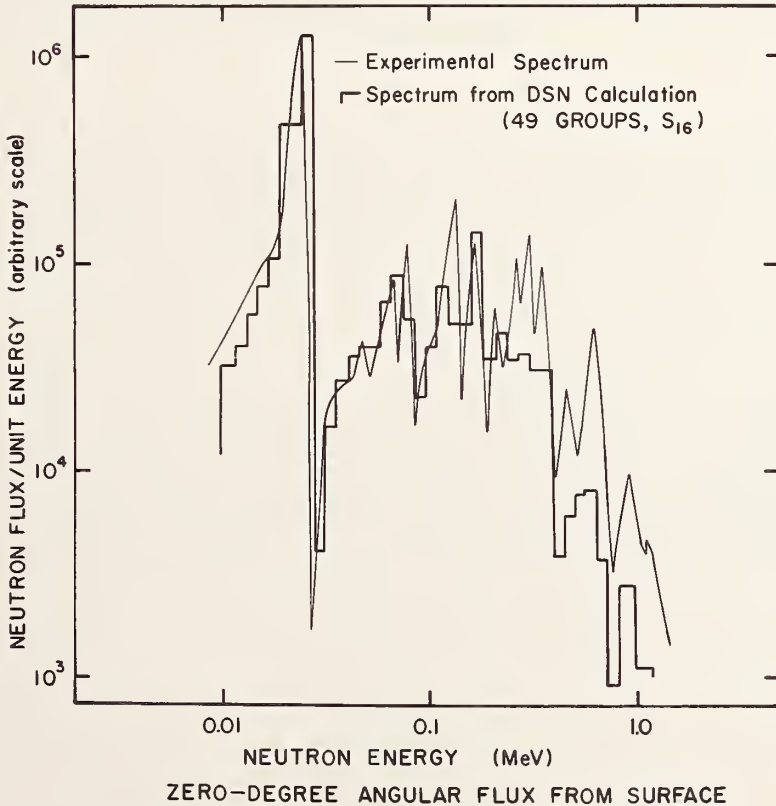


FIGURE 4 Measured and Calculated Zero-Degree Angular Flux at the Surface of a 40-in. cube of Iron.

DIFFERENTIAL DATA AND THE INTERPRETATION OF
LARGE, FAST REACTOR, CRITICAL EXPERIMENTS

W. G. Davey, Argonne National Laboratory
Idaho Falls, Idaho 83401

ABSTRACT

The neutronics of large, plutonium-fueled, fast reactors is studied in critical assemblies where fuel, fertile materials, sodium coolants, and structural materials are used in the form of plates. These are loaded in drawers which are then inserted in a steel matrix. The integral experiments performed measure critical mass, relative reaction rates (principally capture and fission), reactivity effects, the prompt neutron lifetime, and the neutron spectrum.

The interpretation of these measurements involves comparison with the results of multigroup transport and diffusion theory calculations. The group cross sections are constructed from detailed, differential nuclear data by using thousand-group, fundamental-mode, spectra calculated for the particular reactor composition under study. The heterogeneous nature of the reactor lattice is considered in constructing group cross sections in the resonance region.

The complex nature of the calculations makes it difficult to attribute disagreement or agreement between calculated and experimental data to any individual cross section, but the advent of moderately accurate measured spectra promised to improve this situation. However, it is very clear that precise differential measurements of the capture and fission cross sections of the uranium and plutonium isotopes are essential to advancement of our understanding of the complex neutronics of these reactors. These measurements are difficult to perform and the number of precise data obtained in the past five years remains very small, but there can be no substitute for these data in fast reactor analysis.

1. INTRODUCTION

This paper has been written in response to an invitation to evaluate the results of applying existing cross sections to the analysis of fast critical experiments. In particular, an appraisal of the efforts to evolve "consistent" sets of multigroup cross sections using "best" microscopic data was requested in addition to a review of existing discrepancies and remaining problems.

However, a number of difficulties complicate such an evaluation.

First, it is not clear which of the several sets of evaluated microscopic data are best; second, the relationship between multigroup cross sections and the microscopic data from which they are derived can be ambiguous; and third, there are considerable difficulties in computing integral quantities measured in fast critical assemblies. Finally, assuming that these difficulties are overcome, there is the fundamental and difficult problem of deciding the origin of discrepancies between calculated and experimental integral data and establishing a course of corrective action.

As a consequence of the first three difficulties, it is often unclear if one is studying the errors in basic microscopic data or the results of evaluator's prejudices plus the effects of computational uncertainties. Hence, there is no consensus of the true relationship between microscopic data and fast integral data. In addition, there is no consensus upon the best course of action to correct discrepancies between calculated and measured data.

These problems are under intensive study and the purely computational aspects should be largely resolved when computer programs, which are under development, are fully operational. The other problems must still be debated.

In the present paper, I propose to outline the major problem areas of fast critical experimental analysis largely from the point of view of an experimental reactor physicist. I shall discuss the problems of making fast critical experiments as well as analysis problems, and finally, I hope to demonstrate that it is essential that certain nuclear data must be known accurately before there can be any real progress in our understanding of fast reactor physics.

I shall not attempt to cover all the available data and I shall concentrate upon the Argonne studies with which I am most familiar for illustrative purposes.

Most of the information I shall discuss was presented at the Argonne Conference on Fast Critical Experiments and Their Analysis held in October, 1966.⁽¹⁾

2. AREAS OF INVESTIGATION

The problem that we are studying is that of determining the major physics characteristics through the entire lifetime of a plutonium-fueled, sodium-cooled, fast breeder reactor. Both the core and an outer breeder reflector contain U^{238} . The initial fuel charge will contain appreciable quantities of the higher isotopes Pu^{240} , Pu^{241} , and Pu^{242} , in addition to the basic Pu^{239} . During the lifetime of a single charge, approximately 10% of the heavy atoms present in the core will be consumed and significant quantities of Pu^{239} will be formed by neutron capture in the U^{238} . Hence, there will be significant changes due to neutron capture during the lifetime of a single charge of plutonium.

A reactor designer needs to know the major reaction rates in all reactor materials and the reactivity effects of all reactor materials in order to design an efficient, economic, reactor. He must also ensure that the reactor operates in a safe manner. As we have seen, the problem is not only one of ensuring the knowledge of these features during an initial state of the reactor but also one of understanding the behavior of the reactor while it is changing significantly in composition.

Foremost in the thoughts of fast reactor designers at the present time are the problems of ensuring that a large, economic, fast reactor can be designed without a positive power coefficient due to the voiding or reduction in density of the sodium coolant.

The reactivity effect of reduction of sodium density is composed of two parts, (a) a positive component due to the increase in reactivity caused by a hardening of the neutron spectrum or reduction of sodium density, and (b) a negative component associated with increased probability of leakage of neutrons from the reactor core. In a small reactor, the net effect is negative due to the dominance of the leakage component. In a large reactor, the net effect may be positive due to the reduction in leakage from the overall reactor core. A number

of potential designs have been studied to enhance the leakage component from the large core to guarantee a net negative coefficient. Among these are extremely flat, or 'pancaked', cylindrical cores, annular cores, and cores which contain a number of fueled modules within a reflector or breeder region. All of the geometries appear to offer some economic disadvantages in terms of reduction in the breeding gain.

An important phenomenon which is intensively studied because it offers the possibility of compensating for a positive sodium-void coefficient is the Doppler effect. Although the reactivity effects of changing temperature in a fast reactor are generally small except insofar as density changes are produced, the reduction in self-shielding within the resonance region of the neutron spectrum due to increasing temperature (i.e. Doppler broadening) is significant from the viewpoint of safety since it offers a possibility of a prompt negative power coefficient. The reduction in self-shielding within a resonance causes both an increase in capture and fission rates within a given resonance, but in a typical fast reactor core where the U^{238} content may be five to ten times as high as the plutonium content, the net reactivity effect will be negative.

The Doppler effect in particular occurs in the low energy tail of the fast reactor neutron spectrum below approximately 1 to 10 kilovolts. The sodium coefficient is also sensitive to the fraction of low energy flux. Hence, although in general a fast reactor spectrum peaks in the region of several hundred kilovolts, there are important design characteristics related to neutrons which extend from the few tens of electron volts up to the low kilovolt region.

Hence, neutronic knowledge is needed over the entire energy range extending from the upper limit of fission neutrons, approximately 10 MeV, down to the region of a few electron volts. The need to study the neutronics of reactors over this entire energy range places an exceptionally heavy burden upon fast reactor experimental and theoretical physicists. The difficulties faced in both experimental and theoretical fields are greatly eased if precise microscopic cross section data are available.

3. COMPUTATIONAL METHODS

Until comparatively recent years, fast reactor analysis has been conducted using multigroup cross section sets which, although derived ultimately from basic neutron data, have usually been adjusted to give agreement with selected integral parameters such as measured critical masses, fission rates, and reactivity rates. This approach was necessary both because of the lack of precise microscopic cross sections over the entire energy range of interest, and because of the lack of suitable computers and codes which could handle many group, complex geometry, reactor calculations. These methods were moderately successful in explaining the behavior of medium-sized fast reactors where only a negligible number of neutrons lay in the energy region where the resonances in the fissile and the fertile materials were resolved. Above the resolved energy region, the variation in neutron cross sections is not very large, and in general, most cross sections are small so that mean-free paths are moderately large. Under these conditions, few group calculations, with homogenized models of real reactors, were reasonable descriptions of practical cases. This situation was transformed when reactors capable of producing 1000 megawatts of electricity were contemplated, since this was accomplished by increasing the core size, decreasing the fuel enrichment, and consequently degrading the neutron spectrum.

It has now been universally accepted that a much more fundamental and sophisticated approach to reactor computations is essential to design large, fast reactors. Although multigroup cross sections of the older form are still used for some reactor design purposes, the increased availability of accurate microscopic nuclear data plus the need to minimize errors in reducing this data to a form suitable for reactor calculations has led to the development of several automated computer programs which transform the basic data to multigroup form. Examples of this approach are the Galaxy Code, the Atomics International Cross Section Program, and the RBU Code. At Argonne, the efforts in this direction have led to the creation of a multigroup cross section code (MC^2) which generates a multigroup cross section set suitable for fast reactor calculations using an Evaluated Nuclear Data File (ENDF) as input. The ENDF(B) file now being constructed under the chairmanship of the National Neutron Cross Sections Center at Brookhaven National Laboratory will be used for input to MC^2 . The MC^2 code has been described by O'Shea, Toppel and Rago⁽²⁾, and the Atomics International work by Alter⁽³⁾.

MC^2 has been constructed as a modular system of sub-programs which are the control of a simple executive program. The MC^2 program copes with the problems of data retrieval, preliminary averaging, calculation of a weighting spectrum, and final cross section averaging. The procedure is illustrated in Figure 1. Three different types of group structure are incorporated, ultra-fine groups, fine groups, and broad groups. Fine group cross sections are calculated for reactions which vary slowly with energy and ultra-fine group cross sections are constructed for resolved resonance reactions and elastic moderation in light elements. Fine and ultra-fine group fluxes are calculated using a fundamental mode code with a specified input composition. A typical problem might have 22 broad groups, 60 fine groups, each with a lethargy width of 0.25, and 1800 ultra-fine groups with 30 ultra-fine groups per fine group. Inelastic scattering cross sections are computed from excitation functions for individual levels and also by using a nuclear evaporation model above the region of resolved levels. Doppler broadening is also included in the calculations. The heterogeneity of a reactor core can be investigated to some limited degree using MC^2 in that a two-region composition can be incorporated. This approach is possibly adequate for computations of power reactor geometries but is likely to be insufficient to permit the accurate calculation of the plate-type multi-region systems which must be constructed in fast critical experiments. Codes which develop effective multigroup cross sections for heterogeneous systems are under development.

This brief description of computational methods does little justice to the immense effort that has gone into their construction, but is possibly sufficient to show that a considerable degree of sophistication is available. However, it should not be construed that it is possible to make an analysis of critical data using evaluated nuclear data without considerable ambiguity. Apart from the problems of debugging the numerous data reduction and manipulation codes, there are the problems of choice of group structure, mesh size, and the use of diffusion theory, transport theory, or Monte-Carlo calculations for the reactor.

Hopefully, within the next few years, a reliable modular system of computer codes will be available which should be able to handle all the various configurations that are encountered in critical experiments and power reactors with a minimum amount of approximation in data handling.

4. FAST CRITICAL EXPERIMENTAL DATA

To clarify later discussion, I will give a brief description of a fast critical facility and some of the areas of experimental investigation.

A typical fast critical facility is shown in Figure 2. This is Argonne National Laboratory's ZPR-3, a reactor which has supplied the majority of the worlds fast critical information in its twelve years of operation⁽⁴⁾. It consists of two arrays of approximately square stainless steel matrix tubes, one array being stationary and the other mounted on a movable table. Reactor fuel and diluent pieces are loaded in stainless steel drawers which are then inserted in the matrix tubes shown in Figure 2. As in all such split-halves critical assemblies, the reactor is brought to criticality by remotely driving together the two halves and inserting the control rods. The typical drawer containing core materials is shown in Figure 3. The reactor materials are usually constructed in the form of plates of height 2 inches, width 1/8 or 1/4 inches, and of differing lengths. In ZPR-3 and Argonne's other critical facilities, ZPR-6, ZPR-9, and ZPPR, the plates are normally loaded vertically in the drawer as shown. In critical facilities in other countries, alternative arrangements for inserting materials are sometimes used, but a common feature is the use of plate-type materials.

Since any critical facility represents a very large investment in terms of materials, it is essential that the maximum utilization be obtained. Hence, since reactors of many types must be investigated, for example, metallic-, carbide-, and oxide-fueled systems, it is most desirable that each plate contain only a single element. Thus a carbide-fueled reactor can be simulated by the insertion of a metallic-plutonium, metallic-uranium, and graphite plates. A metallic-fueled reactor would be similar but the carbon plates would be omitted, unfortunately oxygen must be inserted in chemical combination with other materials, and iron oxide, uranium oxide, and sodium carbonate are used for this purpose. Sodium, which is the preferred coolant for most fast reactor designs, is inserted in the form of stainless steel clad sodium plates. Hazardous materials such as plutonium are also stainless steel clad.

Since temperature effects in fast systems are very small, the reactor can be operated at nominal room temperature yet simulate the neutronic behavior of a large, fast reactor as long as the material densities in the as-built system correspond to those of the fast power reactor.

The major measurements made in such a critical facility are the critical size, the relative reactivity effects of numerous materials, fission and capture rates (predominantly in the fissile and fertile materials), the prompt neutron lifetime, and the neutron spectrum. Of special importance are measurements of the reactivity effects of reduction of sodium density both in small regions of the reactor core and in large regions. In addition, the Doppler reactivity effects of U^{235} , U^{238} , and plutonium are measured by the use of heated samples. The Doppler effect measurements require very high precision in reactivity measurements.

Very clearly, the heterogeneous nature of the fast critical assembly imposes problems in the measurement of quantities which are sensitive to the resonance region of the neutron spectrum and in the interpretation of such measurements. Ideally, a completely homogeneous experimental arrangement would be used since this is most easily analyzible and corresponds moderately well with the power reactor environment. But economic necessity completely obviates such an approach. Clearly, when the critical mass of large, fast reactors are of the order of three or four tons of fuel, the fissile investment would be prohibitive. The procedure that is adopted is to utilize zones of more homogeneous and power reactor configurations inside the plate-type configuration in order to study and understand the effects of heterogeneity. It should be noted that even though the plate arrangement appears to be exceedingly heterogeneous, most computational studies have shown

that measurements made in such a system can be related with moderate accuracy to the measurements in a power reactor configuration without incurring extreme error. However, the problem is undoubtedly one that requires careful study.

The approach that is being adopted is that of making measurements in configurations which can be described accurately by sophisticated calculations in order to establish the basic quality of fundamental nuclear data. These data may then be used with confidence to compute the characteristics of any fast reactor design. It is believed that the purpose of fast reactor physics studies is to establish fundamentals and not to provide empirical design data. It must be emphasized that this is not a completely academic approach and, in our belief, represents the most economical, and practical, method of providing design data for full-power reactor configurations.

I will now discuss some major experimental measurements and indicate how accurately they may be computed using present data. Many of my illustrations will be taken from papers presented at the Argonne International Conference on Fast Critical Experiments and Their Analysis held in October, 1966⁽¹⁾. I will not attempt to cover the entire field and will limit myself to (a) the critical mass, (b) the sodium-void coefficient, (c) the Doppler coefficient, and (d) the neutron spectrum.

5. THE CRITICAL MASS

The critical mass is the best defined experimental quantity, since it is largely only an accounting problem, to determine the configuration and composition of a self-sustaining reactor system. There are certain complications in reducing the experimental data for heterogeneous, pseudo-cylindrical, critical systems to their homogeneous, regular cylindrical or spherical, equivalents used for most computational tests but, nevertheless, the critical mass remains the most precise measurement that can be made. In many senses, it is also the most fundamental and is a quantity which is sensitive to the fundamental capture and fission cross sections of the fissile and fertile materials and to ν , the number of neutrons per fission.

I shall illustrate the present position by reference to two recent studies.

Baker⁽⁵⁾ has collected the results of calculations of the critical sizes of 38 fast assemblies made with eight different cross section sets. Both U²³⁵ and plutonium-fueled reactors were studied, and the experimental data are predominately of ZPR-3, U²³⁵-fueled reactors. Data from the British ZEBRA and VERA reactors were included. Only five of the 38 assemblies were fueled with plutonium. Unfortunately, most of the cross section sets were constructed an appreciable time ago (generally more than five years) and this study probably does not illustrate the results of calculations that would be obtained today.

A more recent series of studies, although not necessarily a better series, are of the recent ZPR-3 Assembly 48, a plutonium-fueled, simple composition reactor. This reactor was the subject of an international computational study performed to highlight computational problems by comparison with experiment. The specification of the reactor was circulated prior to its construction and the results of the calculations were collected by Davey⁽⁶⁾.

The objective of Baker's study was to attempt to identify the sources of error in eight cross section sets by studying the discrepancies between the

calculated and experimental value (1.000) of the reproduction factor, k , as a function of the reactor composition. The cross section sets used were those of Hansen and Roach in two different forms (HRB, HRC), Yiftah, Okrent, and Modauer, unmodified and modified in three forms (YIFB, YOMD, FDI), ANL Set 800 which is stated to be similar to ANL Set 224, two versions of Russian data (ABBN, Modified ABBN), and a British data set derived largely from the UKAEA data library which leans strongly on the compilations of Parker and others at Aldermaston (FD2).

The k calculations were of homogeneous, spherical models. Transport theory in the S_n approximation (S_4) was used. The results are given in Table 1. Only the last two ZEBRA cases and the last three VERA cases relate to plutonium-fueled reactors.

The mass of data is difficult to digest, but the overall picture is that for several data sets there is good agreement for a very wide range of assemblies, at least for U^{235} -fueled reactors. For example, the most precise set, YOMD, predicts k for all but two U^{235} -fueled reactors to better than 1% accuracy. For plutonium-fueled reactors (VERA 9A, 10A, 11A), there is a systematic error of about 3%. Baker gives an extensive review of the accuracy of fitting and possible sources of error in specific materials, and concludes that, for U^{235} -fueled reactors alone, the standard deviation fit to k ranges from only 0.3% to 0.7%. If plutonium-fueled cases are included, the standard deviations are increased, but not greatly, since there are few such reactors in the series.

This agreement is far better than would be expected from known uncertainties in microscopic basic data, and Baker identifies a number of examples of compensating errors in the data for different isotopes. It is possible that there are also compensating errors in the data for different reactions in the same isotope and in the same reaction over different energy ranges.

This situation is probably a reflection of the fact that a vast amount of data enters into the calculation of the critical mass and, hence, that there must be a degree of statistical compensation for random errors in the input data. Of course, there is an excellent chance for systematic errors propagating, and this appears to be true for the plutonium data in some cross section sets since there are clear systematic errors in the k calculations for these reactors.

By contrast, the ZPR-3 Assembly 48 study represents an extensive, wide-spread, examination of a single reactor of interest.

ZPR-3 Assembly 48 was the first of a series of comparatively simple, plutonium-fueled, critical assemblies which, although not of large critical mass, have spectra broadly similar to those of fast power reactors of several thousand meter core volumes. This was achieved by the use of graphite to moderate the neutron spectrum. One of the major criteria adopted was the maximum simplicity of core design consistent with obtaining suitable neutron spectra and compositions of reactor interests. The preliminary experimental results are given by Broomfield, et al⁽⁷⁾.

The specifications of composition of Assembly 48 were circulated to eleven organizations active in fast reactor field in this country and abroad, and they were requested to calculate a specified series of experimental data prior to the October, 1966, Argonne Conference. The resulting calculated values were collected and compared with experimental data in a paper given by Davey⁽⁶⁾ at the above conference.

The results of the critical mass calculations are given in Table 2.

In Table 2 are given several calculations in both spherical and cylindrical geometry, and homogeneous and heterogeneous compositions, for the as-built composition of Assembly 48. The experimental assembly was a heterogeneous pseudo-cylinder, and hence the direct comparison is between the heterogeneous cylindrical calculation and the experimental value. As can be seen, only some of the establishments calculated the direct case of the heterogeneous cylinder. Some calculated solely the homogeneous spherical case and others solely the homogeneous cylindrical case. Hence, in order to reduce all the calculated values to data which could be directly compared with the experimental value, estimates of the relative critical sizes of spherical and cylindrical reactors (the Shape Factor), and the reactivity effects of heterogeneity, were made. Using these estimates, a best estimate of the heterogeneous cylindrical mass was obtained from each calculation. The last columns in Table 2 show the percentage deviation from the experimental value both in mass and in the multiplication constant k .

Several different basic data sets were used for these calculations, and both diffusion theory and transport theory calculations were performed. Hence, the spread of calculated values represents a composite of a number of different approaches to the problem. It should be emphasized that the calculated values attributed to a given establishment do not necessarily represent the best values obtainable by that establishment. Indeed, it can be seen that certain organizations undertook to use more than one different data set in this study. The significant point, is, therefore, the total spread in data rather than any individual value.

The total spread in predicted critical mass is large, but part of this spread can be attributed to the use of data and methods which have only a certain historical interest in that they have been used in the past for fast reactor studies, and that the spread of calculated critical masses using the best current data would probably be significantly smaller. In certain cases, it can be seen that very accurate predictions of critical mass were possible, and I would particularly direct your attention to the first two sets of calculations in which both an unadjusted and an adjusted value is quoted. The adjustments used in this case were those that have been dictated by comparison of calculations with previous critical experiments, and thus represent a somewhat empirical correction to a calculated critical mass. In this case, it can be seen that past experience in analyzing critical experiments permits a significant reduction in the prediction of a new assembly.

However, it appears that the trend towards significant errors in calculating the critical sizes of plutonium-fueled reactors that were indicated in Baker's work are perhaps borne out by this study. It would appear that the basic data for the plutonium isotopes, particularly Pu^{239} , are appreciably less accurate than those of U^{235} or alternatively, that the chance compensation of errors that appears to occur in U^{235} reactors does not occur here.

An important question that is under intensive study is the use of integral data, such as the critical mass, to correct deficiencies in cross section sets.

Baker indicates that his study of critical masses alone is insufficient to show how data sets should be adjusted, although there can be clear indications of which isotopes are at fault.

However, adjustment of calculations is very widespread. The adjustments may be made in a number of different ways. The simplest and the most direct is that of deriving empirical correction factors to final calculated integral quantities on the

basis of experiments. An alternative method, somewhat less clear in its application, is to adjust either basic microscopic cross sections or multigroup cross sections in order that the actual computed value approaches the experimental value more closely. There is considerable dispute about the value of these different types of adjustment and no consensus of opinion can be given at the present time.

Clearly, it is, in principle, acceptable to select basic microscopic data within the limits of experimental error in order to obtain an improved agreement with experiment. However, the danger in this approach lies in the difficulty of selecting which data in which energy ranges should be adjusted in order to improve agreement. For example, improvement in critical mass could be obtained by adjustment of ν , the number of neutrons per fission, the fission cross section, or the capture cross section of the fuel materials. Hence, unless a correct choice is made, there is great danger in false modification of a data set to improve one integral quantity and, consequently, it is probable that other integral quantities will be incorrectly calculated.

In order to avoid, or to attempt to avoid, errors of subjective judgment, attempts have been made to provide mathematical and computer techniques for adjustment of nuclear data to agree with integral experiments. One of the most extensive of such studies has been conducted by Pendlebury⁽⁸⁾. His study was restricted to improvement of the calculation of critical sizes of both unreflected and reflected U^{235} -fueled systems. Approximately twenty-five systems were selected for study and in all of these, the effect of resonance energy neutrons was negligible. There is no unique way of obtaining adjusted basic cross sections in this manner, but it seems logical to adjust those cross sections to which the critical mass is most sensitive. Despite ambiguities, it is interesting to note that this study did in fact suggest a reduction of the then current U^{235} fission cross sections in the direction and of approximately the same magnitude indicated by White's⁽⁹⁾ later, precise, fission cross section measurements.

Several different approaches to the problem of utilization of critical data have been adopted, but in summary, it is probably fair to state that there is wide agreement that such data as critical masses can and should be used to aid in evaluating nuclear data, but there is equally wide disagreement in the best method for performing this operation.

Of interest to the present audience would be a comparison of the best current microscopic data with the critical mass of Assembly 48. Such a study is being undertaken in connection with ENDF(B), but there is no reason to presume that the data selected for ENDF(B) are superior to those selected by the constructors of the cross section sets used in the current study of Assembly 48.

In point of fact, the deviation in the spread of calculated critical masses for Assembly 48 probably represents the results of different selections from basically the same microscopic data. Hence, no great improvement in the calculation of the most fundamental quantity, the critical mass, can be expected until the most important cross sections of fast reactor fuels and fissile materials are better established than they are at present. However, it should be noted that the use of fast critical experimental data will permit the semi-empirical calculation of the critical masses with reasonably high accuracy as long as experimental data is available for a wide range of critical systems.

6. SODIUM-VOID REACTIVITIES

Fast critical systems are usually constructed of drawers containing plates of various basic materials. The plates are placed in some sequence in a drawer in numbers which give the required composition.

The heterogeneous nature of such a reactor causes variations of sodium-void reactivity values which depend upon the intra-drawer plate configurations. The variations in sodium-void reactivities arise from differences in spatial variations of multigroup fluxes across the drawer, differences in the resonance self-shielding of the higher isotopes in the lower energy regions, and, in some cases, streaming through voided regions.

Because of these variations, the measured sodium-void reactivities do not, in general, correspond exactly to those that would occur in a power reactor (i.e. pin-type fuel elements) configuration of the same average composition. Such exact correspondence is not, of itself, important, but it is necessary that the critical facility measurements be understood and be capable of being computed accurately. When this is true, the same computational methods and cross sections can then be applied to power reactor studies with confidence.

An illuminating calculational study of a series of heterogeneous sodium-void studies has been made by Meneghetti⁽¹⁰⁾. The study was of a series of sodium-void reactivity experiments made in ZPR-6 Assembly 3, a 950 liter, uranium-carbide simulated core, reported by Rusch, Helm, Kato, and Main.⁽¹¹⁾⁽¹²⁾⁽¹³⁾ As a part of the experiments, a cylindrical region approximately 30 cm high and 28 cm in diameter, was voided of sodium by substitution of unfilled, stainless steel cans for sodium-filled cans. The core contained plates of enriched uranium, depleted uranium, graphite, and sodium (in steel cans), and sodium-voiding measurements were made for a series of different local arrangements of these plates. In all cases, the average core composition was the same prior to sodium-voiding. Meneghetti studied eight cases, two of these being with a smaller reduction of sodium fraction than the other six cases. Since the region studied was centrally located, the results would be expected to be sensitive to the effects of changes in capture and fission, but would not be sensitive to leakage effects.

First-order perturbation analyses employing 22-group real and adjoint fluxes from two-dimensional, R-Z geometry, diffusion theory calculations were used to obtain corrections to the reactivity of the reactor for the effects of changes in the resonance-region self-shielding, and the effects of spatial, fine-structure, variations in flux in both the heterogeneous and homogeneous cases. The differences in the reactivity between homogeneous sodium-in and sodium-out cases was obtained by direct two-dimensional calculations.

The cross sections used for this study were obtained from ANL Set 224, a 22-group set in which the cross sections at lower energies are varied to allow for the effects of reactor composition by using effective capture and fission cross sections. These effective cross sections are a function of the potential scattering cross section per absorber atom. For heterogeneous cases, equivalence relationships are used to determine the effective scattering cross sections.

In Set 224, the U^{235} fission cross sections of White⁽⁹⁾ are included, and resonance parameters for U^{238} capture up to 4 keV were derived from the Columbia measurements⁽¹⁴⁾.

The results of Meneghetti's calculations are compared with experiment in Figure 4. The reactivity changes on voiding are presented in In-hours (~ 450 In/ $\%$ in k). The solid bar represents the results of homogeneous voiding calculations (different voiding fractions were used in Cases D and E). The points represent the results of the heterogeneous experiments and calculations.

It can be seen that, in all cases, the reactivity change in the heterogeneous case is significantly larger than the homogeneous case (which is close to the power reactor case). This conclusion is supported by perturbation calculations of Khairallah and Storrer⁽¹⁵⁾ who conclude that this is true for any degree of sodium loss and that differences of 30% to 40% from the homogeneous case may be expected with the plate configuration compared to 6% to 10% deviations from homogeneous for the power reactor case.

Referring to Figure 4, Meneghetti notes that the relatively more negative experimental values in Cases G and H could be due to streaming effects which were not considered in the calculations. Also, the more negative experimental value in Case E could possibly be attributed to experimental error.

Thus, the agreement between the heterogeneous calculations and experiment is remarkably close, but it is completely erroneous to assume that this represents a real situation. Meneghetti emphasizes that the importance of his study lies in the relative correlations between calculated and experimental data, and that the very close agreement in the absolute values is fortuitous.

This is confirmed by a separate study of the ZPR-6 Assembly 3 sodium-void effects made by Helm and Travelli⁽¹⁶⁾ also using ANL Set 224 but using different computational techniques. The Helm and Travelli study was directed to spatial variations of the sodium-void effects and homogeneous, one and two-dimensional, diffusion theory calculations were made. In this case, unlike the Meneghetti study, a detailed flux spectrum was calculated for the sodium-in and sodium-out cases using the fundamental mode code ELMOE, and thus the Set 224 cross sections are not identical to those used by Meneghetti.

The results of the Helm and Travelli work for Assembly 3 are given in Table 3. The second line of this table refers to the experimental cases studied by Meneghetti. Very clearly, the Helm and Travelli central zone calculated reactivity change is approximately twice the experimental value whereas the Meneghetti calculations are in excellent agreement with experiment.

The Helm and Travelli work illustrates a different feature of sodium-void effects, namely, the accuracy of calculation of the spatial variations. In Table 3, four separate types of voiding are illustrated. The "Central Region" set refers to the effects of cylindrical, central regions of differing sizes. The "Slab" set shows the effect of varying axial position, the "Ring" set shows radial variation, and the last value shows the effect of voiding the complete core. Study of Table 3 will show that the agreement with experiment improves as the boundary of the voided region, or the entire voided region, approaches the core boundary, that is, as the effects of neutron leakage become progressively more important. In the case of total core voiding or large region voiding, there is good agreement with experiment, and this perhaps illustrates that the leakage effect calculations are less sensitive to computational method as well as to the quality of cross section data.

Similar studies to those discussed above have been made elsewhere. For example, Adamson, et al.⁽¹⁷⁾ report the results of sodium coefficient studies made on the British fast critical facility, ZEBRA. The case studied, Zebra 6, was plutonium-fueled, and though only of low critical mass ($186 \text{ Kg} \text{ Pu}^{239} + \text{Pu}^{241}$) the neutron spectrum was made similar to that of a larger reactor by the use of both U^{238} and graphite as diluents. As in ZPR-6 Assembly 3, central, non-central, and complete voiding studies were made. In this case, experiments indicated that heterogeneity effects were not very large.

The analysis was made using Set FD2⁽¹⁸⁾, a set based largely on nuclear data evaluation made by Parker and others at Aldermaston in England. The experimental and calculated data are illustrated in Figure 5.

In general, the conclusions were similar to those reached in the ZPR-6 work. The calculated central reactivity effects were in error by about a factor of two, but the leakage (and whole-core voiding) effects were well calculated. Of particular interest were measurements made with plutonium fuels containing different fractions of Pu²⁴⁰. The FD2 data set underestimated the effects of the Pu²⁴⁰ by approximately 25%.

Finally, I would mention a recent paper by Greebler, et al⁽¹⁹⁾ in which the effects of various data changes upon the sodium-void and other effects are discussed.

In summary, with regard to sodium-void effects, we would conclude that:

1. Leakage effects are understood and can be calculated with fair accuracy.
2. As a corollary, the effects of entire core voiding can be calculated, at least for medium-sized and small cores.
3. The mechanisms of the heterogeneity effects are understood, and the relationship between heterogeneous measurements and the homogeneous (and power reactor) cases can be calculated.
4. The central sodium-void effects where the spectrum shift is important cannot be calculated with any degree of confidence. This probably mostly reflects uncertainty in basic nuclear data but computational problems also exist.
5. The discrepancies mentioned above relate to U²³⁵-fueled reactors. Uncertainties in plutonium-fueled cores could be greater since nuclear data for plutonium are less accurately known. Uncertainties could be very large in cores containing appreciable quantities of Pu²⁴⁰ or fission products.

7. DOPPLER COEFFICIENTS

Four methods have been developed for measuring the Doppler Coefficient in fast critical assemblies, (a) the heated sample reactivity method, (b) the cooled sample reactivity method, (c) the heated foil activation method, and (d) the large, heated zone reactivity technique.

Although all of these techniques are practicable, the first, the heated sample reactivity technique, has produced by far the largest quantity of definitive data and appears to be capable of the highest precision. We will, therefore, illustrate the subject of Doppler Coefficients by reference to this technique alone.

The majority of these data have been obtained at Argonne National Laboratory, initially in ZPR-3, and later in ZPR-6 and ZPR-9. Measurements have been made with metallic and oxide samples of natural uranium, U²³⁸-U²³⁵ mixtures, U²³⁸-Pu mixtures, and plutonium alone. These have been made in plutonium-fueled reactor environments at ZPR-3, and uranium-fueled environments at ZPR-6 and 9. The ZPR-3 measurements

are reported by Fischer, Hummel, Folkrod, and Meneley⁽²⁰⁾, Amundson and Gasidlo⁽²¹⁾, Fischer, Meneley, Hwang, Groh, and Till⁽²²⁾ and Gasidlo⁽²³⁾. A recent detailed account of the ZPR-6 Doppler measurements and comparisons with theory is given by Till, Lewis, and Groh⁽²⁴⁾. Measurements at Atomics International are described in recent papers by Carpenter, et al⁽²⁵⁾ and Mountford⁽²⁶⁾.

Here we will not attempt to discuss all of the data and will refer mainly to the work of Fischer, et al⁽²²⁾, Gasidlo⁽²³⁾, and Till, et al⁽²⁴⁾.

Both measurements and calculations are best established for U²³⁸. Expansion effects are not large and are well understood, and experimental precisions are of the order of 1%. Measured data for ZPR-6 Assembly 4Z with and without sodium in the core are shown in Figure 6, for a natural UO₂ sample⁽²⁴⁾. The resonance data for U²³⁸ are moderately well known, and perhaps the greatest uncertainty in the calculation of the U²³⁸ Doppler effect lies in the calculation of the neutron spectrum.

Comparisons of measured and calculated data are shown in Figure 7. The Columbia U²³⁸ resonance data were used⁽¹⁴⁾, and the MC² code and data were used for the calculations. Three calculated curves are shown, MC²-15, -25, and -35, corresponding to 15, 25, and 35 barns of scattering per U²³⁸ atom in the reactor core. Calculations indicate the current best estimate is 33 barns, and thus the calculated values lie about 20% below the experimental data. The experimental variation with the scattering is reproduced quite well.

Similar agreement for U²³⁸ in ZPR-3 Assembly 45 was reached by Fischer, et al⁽²²⁾, and a separate theoretical study by E. A. Fischer (of Karlsruhe)⁽²⁷⁾, gives agreement to about 10% to 15% for calculations and experiments in ZPR-6 Assembly 4Z.

With U²³⁵, both measurements and calculations are more difficult. Expansion effects with highly reactive samples are large, and unless the expansion is constrained, a negative coefficient is obtained. The Doppler coefficient of U²³⁵ is, however, very clearly positive. Figure 8 shows measurements in ZPR-6 Assembly 4Z with constrained and expanding samples which clearly show the effect of the phase change in metallic uranium at about 940°K⁽²⁴⁾. Figure 9 shows the same data after correction for expansion. The agreement is moderately good up to 700°K, but the expansion corrections appear to be less accurate above this temperature. These measurements are compared with calculated data in Figure 10. The measured U²³⁵ Doppler effect is only about 40% of the calculated value although the arbitrarily normalized curve shows reasonable variation with the scattering cross section.

The Doppler effect of U²³⁵-U²³⁸ mixtures in Assembly 4Z is shown in Figure 11⁽²⁴⁾. To good accuracy, the net effect for a mixture is given by prorating the separate U²³⁵ and U²³⁸ contributions.

From the point of view of safety, it should be noted that the effect of sodium voiding in Assembly 4Z is a reduction of only 35% in the U²³⁸ Doppler effect compared to a calculated value of 50%. Also, the power law for the variation of the U²³⁸ Doppler effect with temperature is considered to be insufficiently well known to predict the effects at very high temperatures such as those that might be reached in reactor excursions. High temperature Doppler elements are being developed to stand the temperature range of measurements⁽²⁴⁾.

With Pu²³⁹, there are experimental and analytical problems. These both arise from the fact that the Pu²³⁹ Doppler effect is much smaller than in U²³⁵ and much less than had been appreciated until the fast reactor studies had been made. Because of the smallness of the Doppler effects, expansion corrections are more important and difficult. It now appears that the J=0 and J=1 spin sequences in Pu²³⁹ have appreciably different characteristics and the Doppler effect in a soft, fast reactor spectrum is small, and may be negative. In a hardened spectrum produced by placing a boron sleeve around the Doppler sample, the Doppler effect is positive. Measurements in ZPR-3 Assembly 47 are shown in Figure 11 (Gasidlo⁽²³⁾). They are compared with calculated values of Greebler, et al⁽¹⁹⁾. The calculated values in the normal core are still positive, but are very small. The agreement with calculation for the boron sleeve and disagreement with the normal core should not be overemphasized, since it is probable that expansion corrections must be applied to the experimental data.

Finally, regarding heterogeneity effects, Khairallah and Storrer⁽¹⁵⁾ have shown that heterogeneity effects do not have much effect on the net Doppler coefficient of a reactor (i.e. the net U²³⁸ plus Pu²³⁹ effect) although the magnitude of the effect in the fissile component may be increased in a critical facility composition.

In summary we have:

- (1) The U²³⁸ Doppler effect is well understood and can be calculated to about 20% accuracy. The discrepancy possibly arises because of inaccuracies in the calculated spectrum.
- (2) The decrease in the U²³⁸ Doppler effect in sodium voiding is less than calculated (in a U²³⁵-fueled reactor environment).
- (3) Extrapolation of the U²³⁸ Doppler effect to high temperature is uncertain.
- (4) The U²³⁵ Doppler measurements can be performed with acceptable accuracy. The measured effect is positive but only about 40% of the calculated value.
- (5) The Pu²³⁹ Doppler effect in a soft, fast reactor spectrum is small and possibly negative. The measured reactivity effect is certainly negative, but this may include expansion effects.
- (6) Heterogeneity effects are not of major importance.

8. THE NEUTRON SPECTRUM

It is now possible to make neutron spectrum measurements over the energy range of about 1 keV to a few MeV in fast reactor cores using a proton-recoil spectrometer. Time-of-flight methods can extend these measurements to lower energies, and Li⁶ detectors can extend the data to higher energies, but the value of spectrum data can be illustrated with the proton-recoil technique along.

A single example will be taken. This is the central spectrum measurement in ZPR-3 Assembly 48 made by Bennett, Gold, and Huber⁽²⁸⁾. A detailed spectrum calculation for this core was made by Travelli⁽²⁹⁾ using ANL Set 224. The experimental and calculated data are shown in Figure 12. Two sets of calculated data are given, (a) the fine-group data, and (b) the same data averaged over a Gaussian window to give a direct comparison with the experimental data.

Clearly, the agreement is good over most of the energy range, and at no point is the disagreement more than about 15%.

An alternative way of presenting this data is to average the experimental results over a prescribed group structure and give a numerical comparison with a calculated multigroup flux. This type of comparison with Winfrith (AEEW Fd2), Argonne (ANL), and General Electric (GE) calculations is shown in Table 4 (Davey⁽⁶⁾). Here, the total flux over the range of measurement was normalized to the total calculated flux over the same range. Approximately 20% of the flux lies above, and 4% lies below, the range of measurement.

The data of Table 4 show that in all three cases there is quite good agreement with experiment, almost certainly within the limits of error of the experiment. Yet the three data sets have different origins and thus incorporate different data.

It would, therefore, appear that the neutron spectrum, like the critical mass, depends upon such a large number of nuclear data that some degree of cancellation of errors occurs. Hence, as with the critical mass, the neutron spectrum does not yet enable us to identify sources of cross section errors.

This situation could possibly be strongly changed with the advent of more precise spectral data for systems like Assembly 48 over a wider energy range. However, a more promising approach would perhaps be to measure spectra in a range of systems of simple composition, preferably only fuel plus one diluent, in order to be able to identify in which isotopes the nuclear data are in error.

9. CROSS SECTION UNCERTAINTIES AND FAST REACTOR ANALYSIS

The foregoing discussion has, I believe, shown that in most cases we are able to compute some important integral quantities with quite good accuracy (e.g. critical mass, heterogeneity effects in the sodium-void coefficient, U^{238} Doppler coefficient, spectrum) and that we have a reasonable understanding of the relevant phenomena in the cases where the accuracy of computations is not yet high (absolute sodium-void reactivities, U^{235} Doppler effect, Pu^{239} Doppler effect).

However, it is very clear that since we are dealing with integral quantities which depend upon many different cross section data, it is difficult, or even impossible, to identify a clear correlation between the reactor data and the basic, microscopic cross sections. Indeed, it is probable, that in the cases where calculations are apparently precise (e.g. critical mass), that this is the consequence of accidental cancellation of errors in basic data rather than an indication of accurate nuclear data.

In such a situation, I would contend that it is impossible to understand the complicated field of fast reactor physics without a firm knowledge of certain fundamental cross sections.

These fundamental cross sections are the fission and capture cross sections of the plutonium and uranium isotopes.

In a simple, but very real, sense these are the only vital data for fast reactor studies. They determine the overall neutron economy since coolant and structural absorption is small. The effect of scattering is largely to determine the weighting spectrum for capture and fission reactions. This is exemplified by the spectrum shift contribution of the sodium-void effect.

These simplified arguments ignore the importance of the number of neutrons per fission, ν , and the effect of scattering upon leakage, but I believe that this discussion does not give undue weight to the importance of the capture and fission data.

Here, it should be noted that the primary interest lies in these cross sections in the energy range in which the major portion of the neutron flux lies, that is, above the resolved resonance region (1 to 10 keV). I would like to emphasize this point, since it is possible that the great interest in resonance data is drawing too much attention away from the higher energy measurements.

The situation at these higher energies is illustrated by Figure 13 and 14 (Davey⁽³⁰⁾). Figure 13 shows the clear, and well known, discrepancy between the U²³⁵ fission cross sections of White and the other precise measurements. Figure 14 shows the scattered values of the ratio $\sigma_{\text{F}} \text{Pu}^{239} / \sigma_{\text{F}} \text{U}^{235}$ below about 50 keV. The wide disparity in measured U²³⁸ capture cross sections is shown in Figure 15, taken from the Second Supplement to BNL-325⁽³¹⁾.

These data do not provide a satisfactory basis for fast reactor analysis.

Perhaps the most disturbing feature is the continuing lack of a check upon White's U²³⁵ fission cross sections since these form the basis for most other fast cross sections. However, even if this cross section is well established, an intensive effort would still be needed to establish the other cross sections.

Given precise values for these capture and fission cross sections, it should be possible to utilize the many fast critical data to adjust other cross sections with considerable confidence. Such adjustment techniques, as developed by Pendlebury and others, could then be used to their maximum advantage.

10. REFERENCES

1. Proceedings of the International Conference on Fast Critical Experiments and Their Analysis, Report ANL-7320, October, 1966.
2. D. M. O'Shea, B. J. Toppel and A. L. Rago, The Automated Preparation of Multigroup Cross Sections for Fast Reactor Analysis Using the MC² Code, ANL-7320, 27-32, 1966.
3. Harry Alter, The Atomic International Evaluated Nuclear Data Files and Associated Computer Programs for the Automated Preparation of Multigroup Constants, ANL-7320, 33-46, 1966.
4. B. C. Cerutti, et al, Nucl. Sci. Eng. 1, 126 (1956).
5. Arthur R. Baker, Comparative Studies of the Criticality of Fast Critical Assemblies, ANL-7320, 116-129, 1966.
6. W. G. Davey, Intercomparison of Calculations for a Dilute Plutonium-fueled Fast Critical Assembly (ZPR-3 Assembly 48), ANL-7320, 57-67, 1966.
7. A. M. Broomfield, P. I. Amundson, W. G. Davey, J. M. Gasidlo, A. L. Hess, W. P. Keeney, and J. K. Long, ZPR-3 Assembly 48: Studies of a Dilute Plutonium-fueled Assembly, ANL-7320, 205-215, 1966.
8. Pamela C. E. Hemment and E. D. Pendlebury, The Optimisation of Neutron Cross-section Data Adjustments to Give Agreement with Experimental Critical Sizes, ANL-7320, 88-106, 1966.
9. P. H. White, J. Nucl. Energy, 19, 325, (1965).
10. D. Meneghetti, Calculational Studies of Sodium-void Reactivity Variations Due to Thin Slab Heterogeneities in Fast Critical Assemblies, ANL-7320, 377-385, 1966.
11. G. K. Rusch and F. H. Helm, The Influence of Heterogeneity on the Measured Sodium-void Coefficient in a 950-liter Pancake Fast Core, Transactions American Nuclear Society, 8, 1, 246, (1965).
12. W. Y. Kato, G. K. Rusch, and F. H. Helm, Sodium-void Coefficients, Proceedings on Conference on Safety, Fuels, and Core Design in Large Fast Power Reactors, ANL-7120, 598, (1965).
13. F. H. Helm, W. Y. Kato, G. Main, and G. K. Rusch, Physics Parameters and Sodium-void Coefficients in a 950-liter Pancake Core, Reactor Physics Division Annual Report, July 1, 1964 to June 30, 1965, ANL-7110, (1966).
14. J. B. Garg, J. Rainwater, J. S. Peterson, and W. W. Havens, Jr., Neutron Resonance Spectroscopy. III. Th²³² and U²³⁸, Phys. Rev., 134B, 985, (1964).
15. A. Khairallah and F. Storrer, Calculation of the Sodium-void and Doppler Reactivity Coefficients in Fast Reactors and Critical Assemblies, with Heterogeneity Taken into Account, ANL-7320, 394-402, 1966.

16. F. Helm and A. Travelli, Calculation of the Sodium-void Effect in Large Carbide Cores, ANL-7320, 369-376, 1966.
17. J. Adamson, R. M. Absalom, A. R. Baker, G. Ingram, S. K. I. Pattenden, and J. M. Stevenson, Zebra 6: A Dilute Plutonium-fueled Assembly, ANL-7320, 216-230, 1966.
18. R. W. Smith, J. L. Rowlands, D. Wordleworth, The FD2 Group-Averaged Cross-Section Set for Fast Reactor Calculations, AEEW-R491, (1966).
19. P. Greebler, G. L. Gyorey, B. A. Hutchins, and B. M. Segal, Implications of Recent Fast Critical Experiments on Basic Fast Reactor Design Data and Computational Methods, ANL-7320, 66-79, 1966.
20. G. J. Fischer, H. H. Hummel, J. R. Folkrod, and D. A. Meneley, Nucl. Sci. Eng., 18, 290, (1964).
21. P. I. Amundson, J. M. Gasidlo, Nucl. Sci. Eng., 23, 392, (1965).
22. G. J. Fischer, D. A. Meneley, R. N. Hwang, E. F. Groh, C. E. Till, Nucl. Sci. Eng., 25, 37, (1966).
23. J. M. Gasidlo, Results of Recent Doppler Experiments in ZPR-3, ANL-7320, 345-349, 1966.
24. C. E. Till, R. A. Lewis, and R. N. Hwang, ZPR-6 Doppler Measurements and Comparisons with Theory, ANL-7320, 319-333, 1966.
25. S. G. Carpenter, L. A. Mountford, T. H. Springer, and R. J. Tuttle, Dependence of the Doppler Coefficient of Reactivity for Heavy Elements on Chemical Form, Surface-to-mass Ratio, and Neutron Spectrum, ANL-7320, 334-340, 1966.
26. L. A. Mountford, Doppler Coefficient Measurements in the Cryogenic Temperature Region, ANL-7320, 341-344, 1966.
27. E. A. Fischer, Interpretation of Doppler Coefficient Measurements in Fast Critical Assemblies, ANL-7320, 350-357, 1966.
28. E. F. Bennett, R. Gold, and R. J. Huber, Spectrum Measurements in a Large Dilute Plutonium-fueled Fast Reactor, ANL-7320, 477-480, 1966.
29. A. Travelli, A Comment on the Comparison of Theoretical with Experimental Neutron Spectra in Fast Critical Assemblies, ANL-7320, 481-485, 1966.
30. W. G. Davey, Nucl. Sci. Eng., 26, 149 (1966), also Nucl. Sci. Eng., to be published (1968).
31. Neutron Cross Sections, BNL-325, Supplement 2.

TABLE 1. THE *k* CALCULATIONS IN *S₄* APPROXIMATION USED FOR THE FITS (Baker⁽⁵⁾)

System	Assembly	HRB	HRC	YOMD	YIFB	FD1	ANL-800	ABBN	Modified ABBN	FD2
ZPR-III	2A			1.005		1.021				1.023
	5			1.005		1.025				1.025
	6F			1.003		1.019	1.007			1.021
	9A		0.994	0.998		1.014	1.002			1.011
	10	0.985		0.999		1.008				1.005
	11	0.983	0.986	0.994		1.006		1.011	0.993	0.991
	12	0.999		0.998	1.005	1.011	1.001	1.016	1.002	1.003
	14	1.016	1.020	0.995	1.007	1.006	1.013			1.014
	16	0.995		0.999	1.011	1.012				0.999
	17	1.007		0.998	1.010	1.011				1.009
	20	0.989	0.989	0.992						
	22							0.998		
	23	0.999		1.004	1.016	1.026	1.009	1.026	1.011	1.023
	24	0.981	0.987	0.995		1.007		1.005	0.987	0.981
	25	0.981	0.986	0.991		1.006	0.998	0.999	0.978	0.977
	29	1.001	1.006	1.003		1.024	1.020	1.032	1.017	1.014
	30	1.004	1.005	1.009		1.030		1.039	1.023	1.021
	31	0.995	0.996	1.006		1.026		1.037	1.022	1.018
	32	0.982		1.015	1.030	1.033	1.016	1.034	1.026	1.032
	33	0.988		1.014		1.032	1.019	1.035	1.018	1.033
	34	0.993	0.998	0.997	1.018	1.018	1.014	1.023	1.008	1.007
35			0.994		1.013				1.027	
36	0.982		0.994		1.006	0.998			0.999	
41		0.995	1.002		1.002	1.003			0.994	
Zebra	1	0.979			0.997	1.002				0.987
	2	1.015			0.996	1.006				0.992
	3	0.969			1.023	1.026				0.995
	6A					1.044				1.010
Vera	1B					1.009				1.014
	2A					1.005				1.013
	3A					1.008				1.007
	4A					0.989				0.994
	5A					0.985				0.992
	6A					0.990				0.998
	7A					0.987				0.996
	9A			1.034	1.033	1.032				1.032
	10A			1.026	1.022	1.024				1.022
	11A			1.031	1.030	1.030				1.025

103-11767

TABLE 2. CRITICAL MASS OF ASSEMBLY 48 (kg Pu²³⁹) (Davey⁽⁶⁾)

Organization	Calculated Data				Best Estimate of Heterogeneous Cylindrical Mass	Percentage Deviation from Experiment	
	Sphere		Cylinder			In Mass	In <i>k</i> ^(e)
	Homog.	Hetero.	Homog.	Hetero.			
AEEW FD2			271	250	250 ^(b)	-8.1	-1.2
AEEW Adjusted			292	267	267 ^(b)	-1.8	-0.3
AI	314.1 ^(a)		339.0 ^(a)		314 ^(c)	+15.4	+2.4
ANL				263.3	263.3 ^(b)	-3.2	-0.5
APDA	264 ^(a)		283 ^(a)		258 ^(c)	-5.1	-0.8
BNWL			271		246 ^(c)	-9.6	-1.5
B & W			250		225 ^(c)	-17.3	-2.7
Cadarache (H-R)	286.8		309 ^(e)		284 ^(c)	+4.4	+0.7
Cadarache (USSR)	237.2		256 ^(e)		231 ^(c)	-15.1	-2.3
Cadarache (25GRP)	225.6		243 ^(e)		218 ^(c)	-19.9	-3.1
GE			293	291 ^(f)	268 ^(c)	-1.5	-0.2
Karlsruhe	257 ^(a)	228	277 ^(a)	246 ^(d)	252 ^(c)	-7.4	-1.1
LASL (H-R)	262		283 ^(e)		258 ^(c)	-5.1	-0.8
LASL (USSR)	217		234 ^(e)		209 ^(c)	-23.2	-3.6
W			242		217 ^(e)	-10.2	-3.1

Experiment (Heterogeneous Cylinder)

272

(a) Both AI and Karlsruhe calculate a shape factor of 0.927. APDA calculates 0.930.

(b) Directly calculated.

(c) Subtracting 25 kg from the homogeneous cylindrical mass. This is equivalent to 1.4% in *k*.

(d) Karlsruhe calculates a rather high Δk for heterogeneity of 2.5%.

(e) Using a shape factor of 0.927.

(f) The heterogeneous calculation only allowed for heterogeneity at low energies.

(g) Assuming $(\Delta M/M)/(\Delta k/k) = 6.5$.

103-11765

TABLE 3. SODIUM-VOID COEFFICIENTS IN ASSEMBLY 3 (lh/kg) (Helm & Travelli⁽¹⁶⁾)

Type	Region Boundaries (cm)		Capture + Scatter		Leakage		Total			Total Exp.
	Axial	Radial	DEL 1-dim	PERC 2-dim	DEL 1-dim	PERC 2-dim	DEL 1-dim	PERC 2-dim	k (calc) 1-dim	
Central Region	0-7.62	0-9.342	-1.45	-1.49	-0.44	-0.44	-1.89	-1.93	-1.72	-0.0
Central Region	0-15.24	0-14.27	-1.06	-1.10	-1.57	-1.57	-2.63	-2.67	-2.55	-1.23
Central Region	0-20.32	0-20.66	-0.73	-0.71	-2.54	-2.55	-3.27	-3.26	-3.21	-2.29
Central Region	0-25.4	0-24.91	-0.27	-0.28	-3.52	-3.54	-3.79	-3.82	-3.83	-3.23
Slab	0-7.62	0-14.27	-1.42	-1.42	-0.49	-0.49	-1.91	-1.91	-1.77	-0.18
Slab	7.62-15.24	0-14.27	-0.77	-0.79	-2.64	-2.64	-3.41	-3.43	-3.34	-2.33
Slab	15.24-20.32	0-14.27	+0.30	+0.27	-5.48	-5.48	-5.18	-5.21	-5.15	-5.0
Slab	20.32-25.4	0-14.27	+1.54	+1.48	-7.88	-7.99	-6.34	-6.51	-6.40	-5.82
Ring	0-7.62	25.87-36.45	-1.05	-1.13	-1.12	-1.21	-2.17	-2.34	-2.06	-1.06
Ring	0-7.62	46.30-58.18	-0.53	-0.50	-1.85	-1.89	-2.38	-2.39	-2.33	-2.16
Ring	0-7.62	65.10-69.98 ^(a)	-0.07	-0.05	-2.05	-2.07	-2.12	-2.12	—	-2.25
Ring	0-7.62	72.70-77.86 ^(a)	+0.25	+0.24	-1.98	-2.05	-1.73	-1.81	—	-2.13
Total Core	0-25.4	0-77.86	-0.12	-0.06	-2.61	-2.64	-2.73	-2.70	-2.83	-2.83

^(a) In these regions the one-dimensional perturbation calculations were made in cylindrical geometry.

103-11769

TABLE 4. CALCULATED AND MEASURED CENTRAL SPECTRA IN ASSEMBLY 48, PART 1 (Davey⁽⁶⁾)

Group	AEEW FD2			ANL			GE		
	E_L	ϕ_r	ϕ_E	E_L	ϕ_r	ϕ_E	E_L	ϕ_r	ϕ_E
1	3.68 MeV	1.82		3.68 MeV	1.85		3.70 MeV	1.929	
2	2.23	3.87		2.23	3.53		2.20	3.815	
3	1.35	5.98		1.35	6.04		1.35	6.203	
4	0.821	7.31		0.821	8.55		0.825	8.557	
5	0.498	10.74	10.53	0.498	10.57	10.43	0.50	11.204	10.32
6	0.302	12.11	11.02	0.302	11.76	10.92	0.30	12.141	11.05
7	0.183	11.06	10.53	0.183	10.78	10.43	0.18	10.322	10.52
8	0.111	9.33	10.00	0.111	9.76	9.91	0.11	10.250	9.63
9	67.4 keV	8.57	8.70	67.4 keV	8.28	8.62	67.0 keV	7.985	8.46
10	40.9	7.06	6.92	40.9	6.96	6.85	41.0	6.673	6.66
11	24.8	5.59	5.66	24.8	5.44	5.60	25.0	5.032	5.48
12	15.0	4.64	4.62	15.0	4.65	4.58	15.0	4.689	4.63
13	9.12	3.54	3.74	9.12	3.56	3.71	9.1	3.366	3.69
14	5.53	2.28	2.72	4.31	3.21	3.72	5.5	2.210	2.69
15	3.36	1.68	1.77	2.61	0.83	1.24	3.9	1.159	1.32
16	2.04	0.835	1.23	2.04	0.91	0.70	2.5	0.551	1.01
17	1.23	1.554		1.23	1.39		2.0	0.510	0.64
18	748 eV	0.970		961 eV	0.61		1.3	1.305	
19	454	0.547		583	0.64		800 eV	0.891	
20	275	0.327		275	0.46		502	0.574	
21	167	0.125		101	0.18		310	0.330	
22	101	0.046		29	0.04		150	0.214	
23	61.4	0.012					55.6	0.075	
24	37.3	0.004					Thermal	0.015	

103-11768

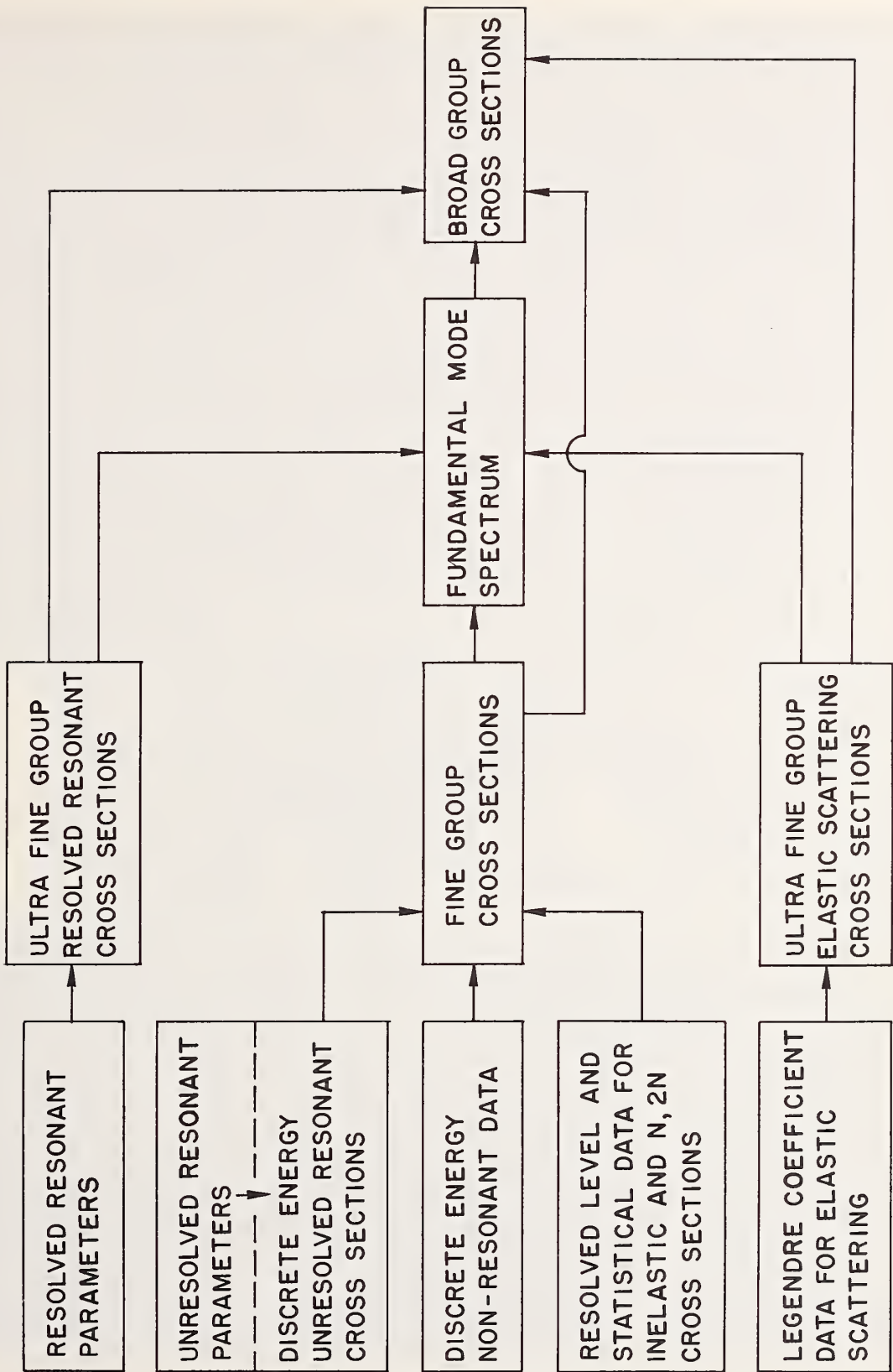


Figure 1. Schematic Diagram of MC² Operation (O'Shea et al.⁽²⁾)

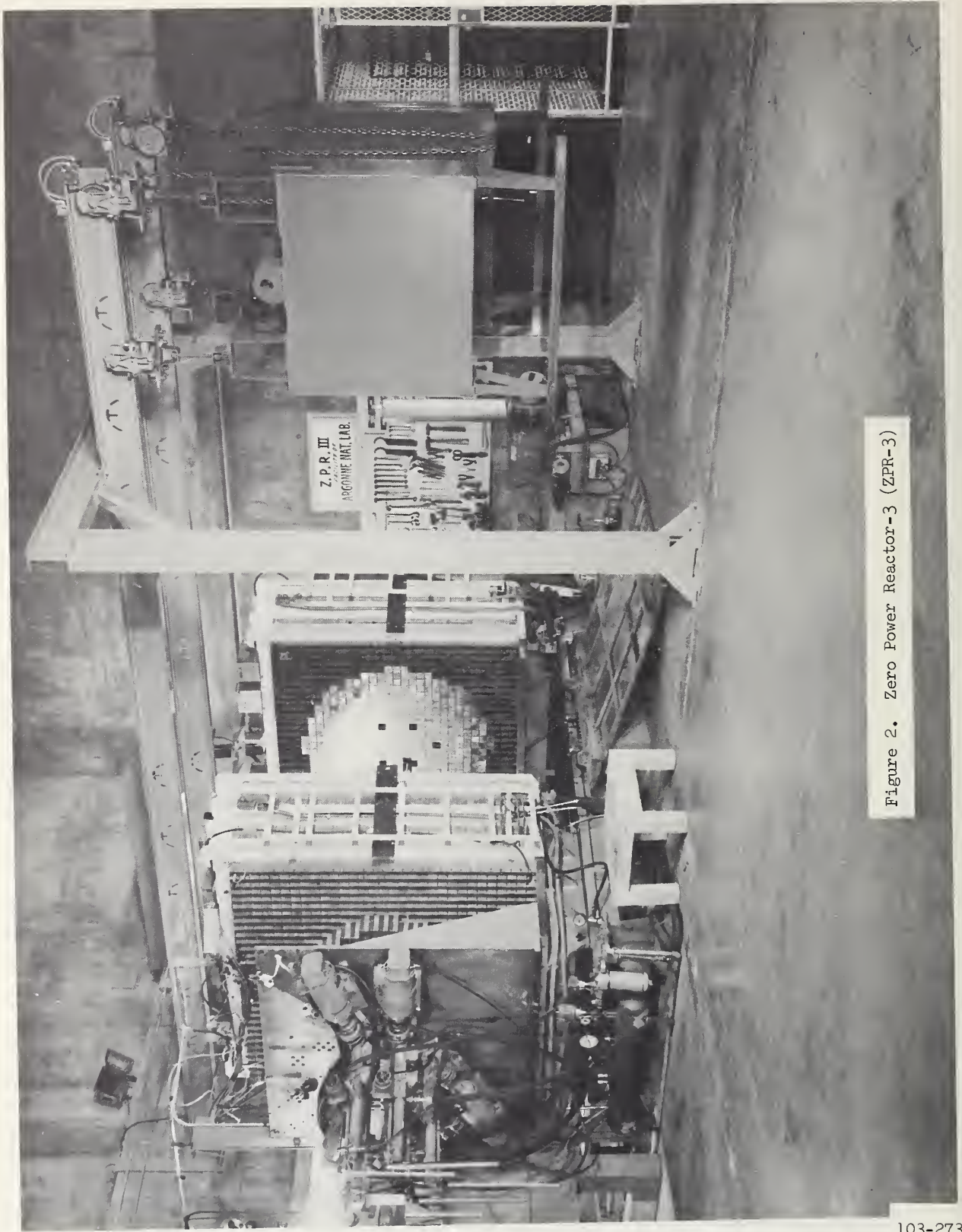


Figure 2. Zero Power Reactor-3 (ZPR-3)

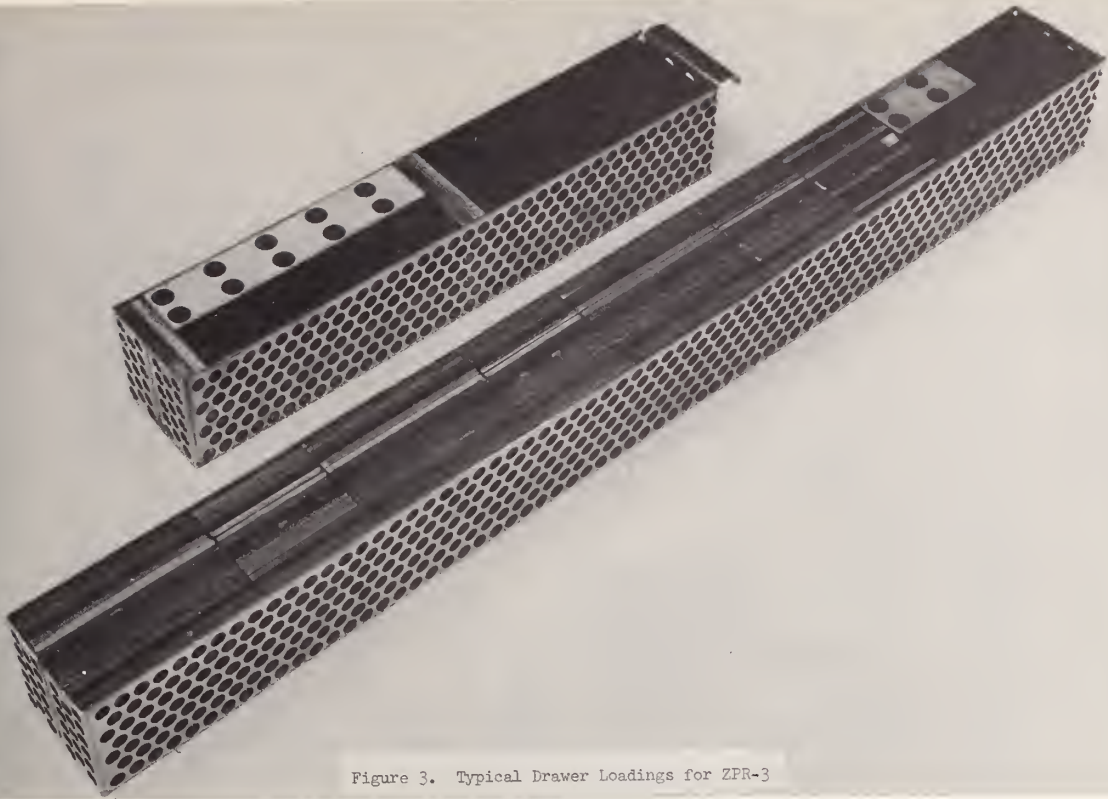


Figure 3. Typical Drawer Loadings for ZPR-3

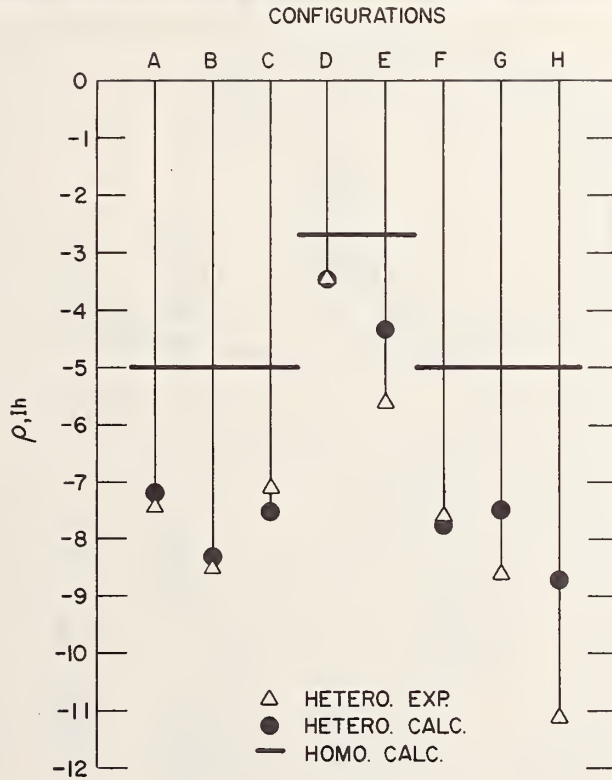
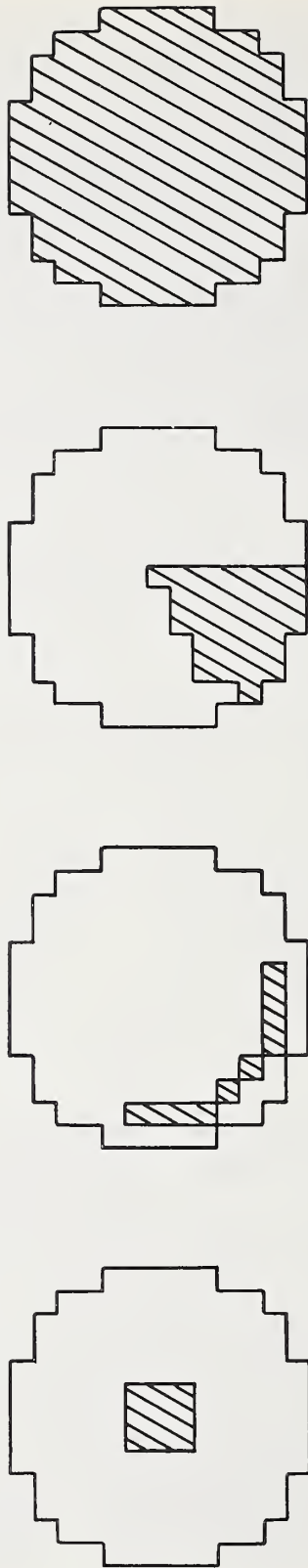



Figure 4. Comparisons of Calculated and Experimental Sodium-void Reactivity Values for Various Intracell Plate Configurations in ZPR-VI, Assembly No. 3 (Meneghetti⁽¹⁰⁾)

112-6949

OUTLINE OF CORE REGION



 SODIUM REMOVED

Voiding experiment:

Normal cell 1.8 ± 0.1
 Double cell 2.0 ± 0.1

2.8 ± 0.1
 3.1 ± 0.1

2.62 ± 0.1

2.63 ± 0.1

Perturbation measurements 2.1 ± 0.1

3.0 ± 0.1

3.0 ± 0.3

3.0 ± 0.3

Calculation: 1.28
 FD 2 data

2.96

2.60

2.60

Figure 5. Measurements of Sodium Reactivity Worth in Units of 10^{-7} dk/k per Gram of Sodium (Adamson et al.⁽¹⁷⁾)

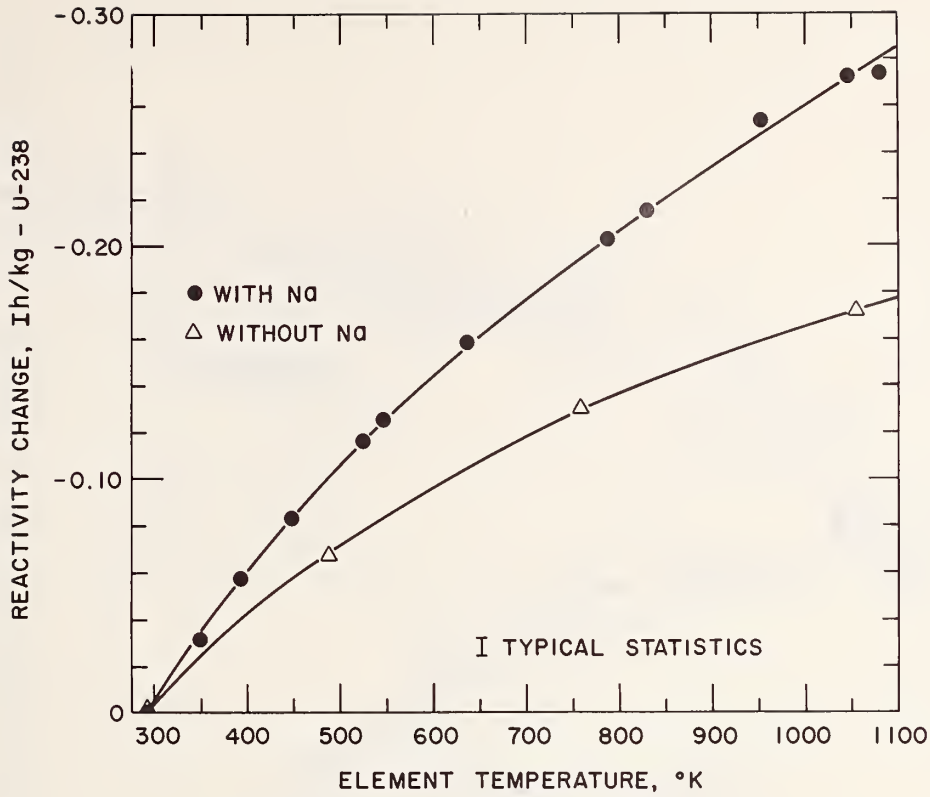


Figure 6. Doppler Effect in Natural UO_2

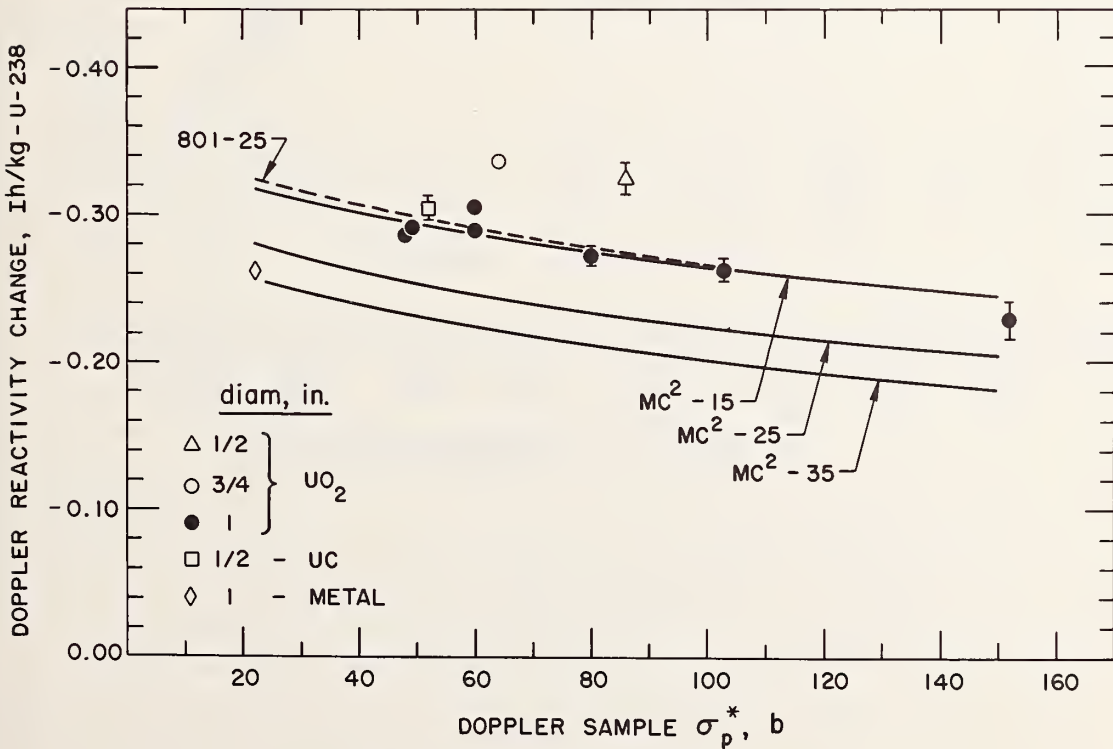


Figure 7. Measured and Calculated U^{238} Doppler Effect in ZPR-6 Assembly 4Z (1100 - 293°K) (Till et al.⁽²⁴⁾)

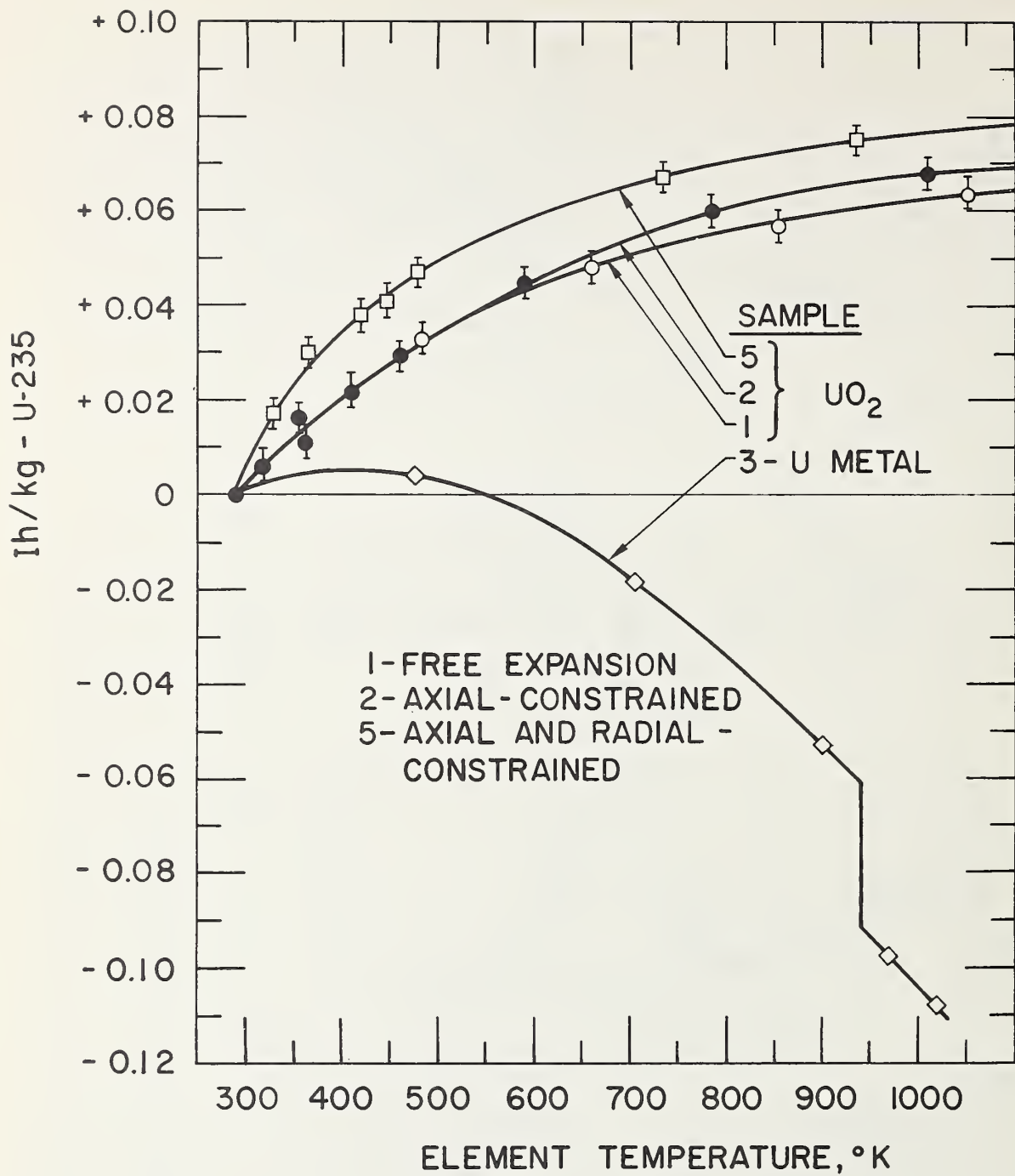


Figure 8. U^{235} Doppler Effect (Till et al⁽²⁴⁾)

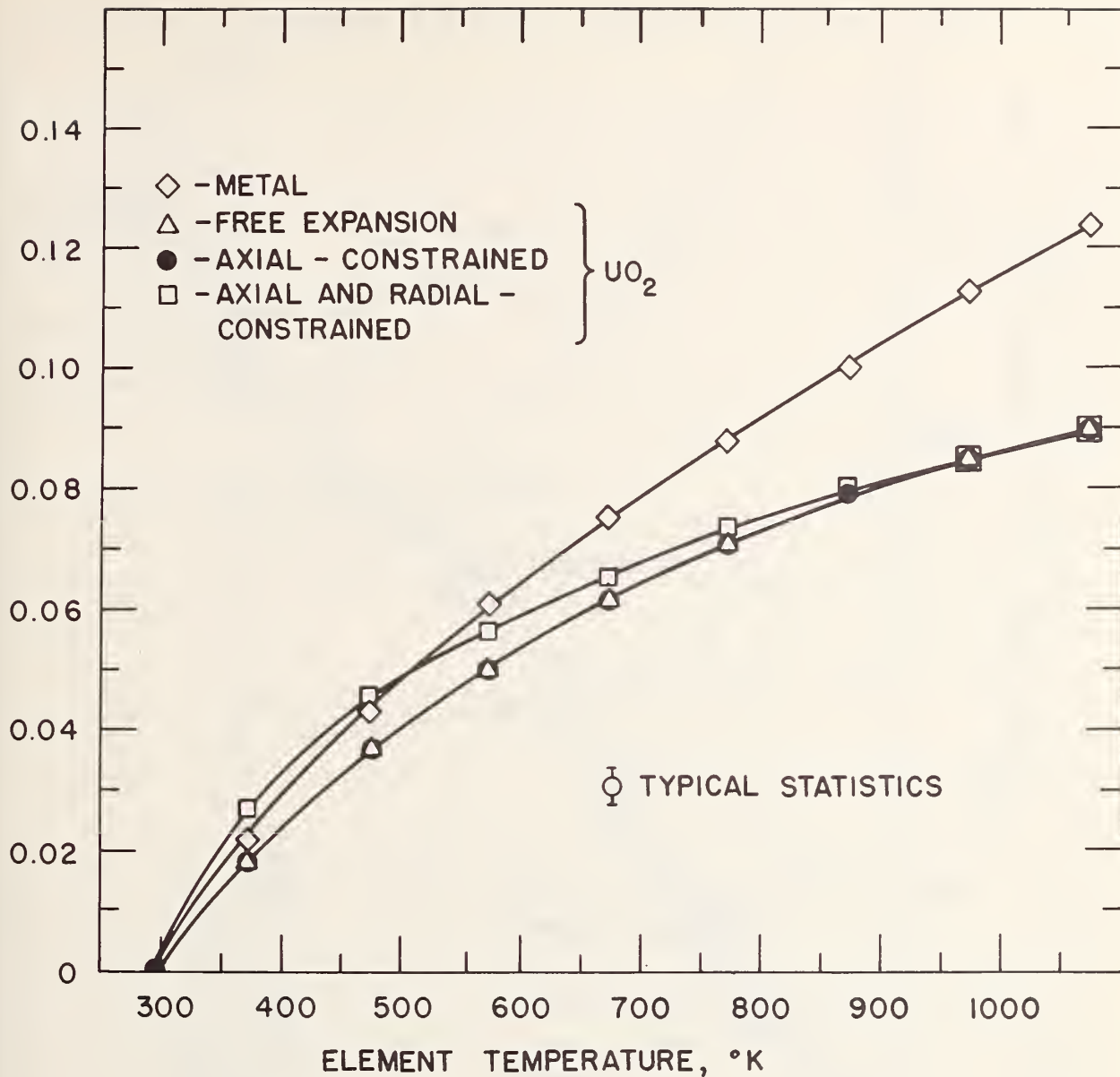


Figure 9. U²³⁵ Doppler Effect Corrected for Expansion (Till et al⁽²⁴⁾)

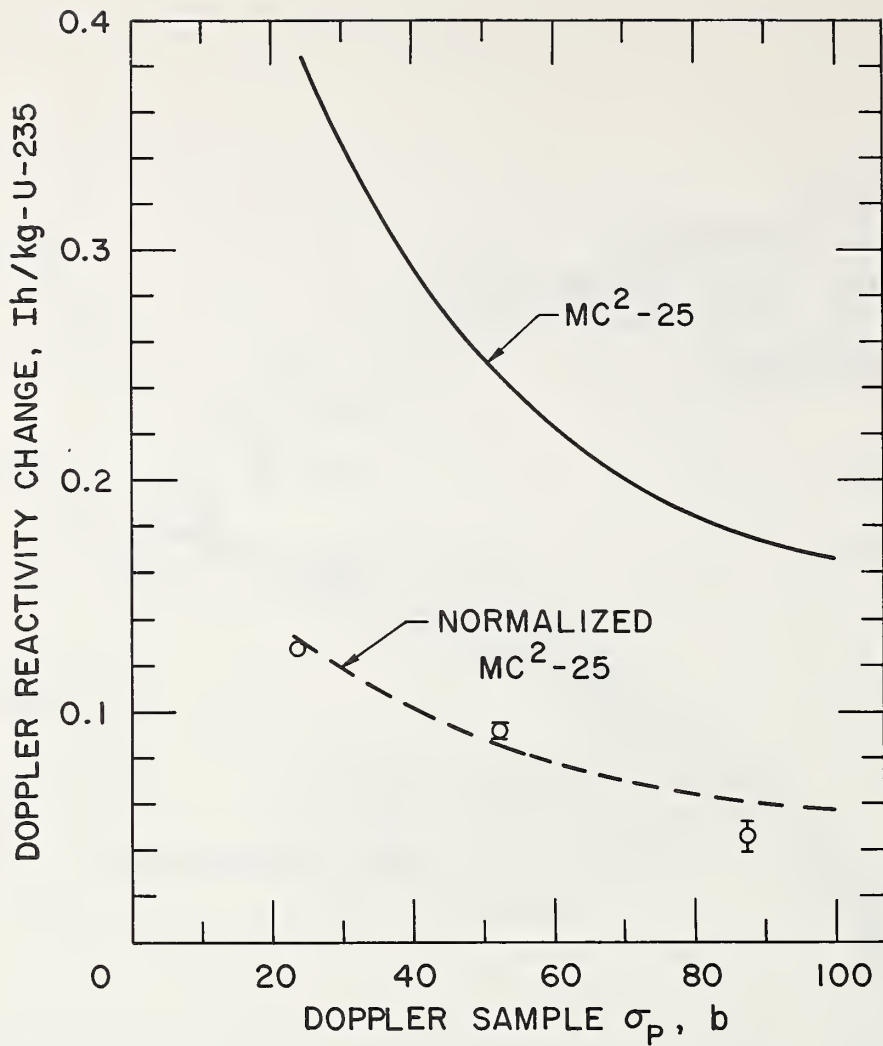


Figure 10

Measured and Calculated U^{235} Doppler Effect in ZPR-6 Assembly 4Z (1100°K - 293°K)

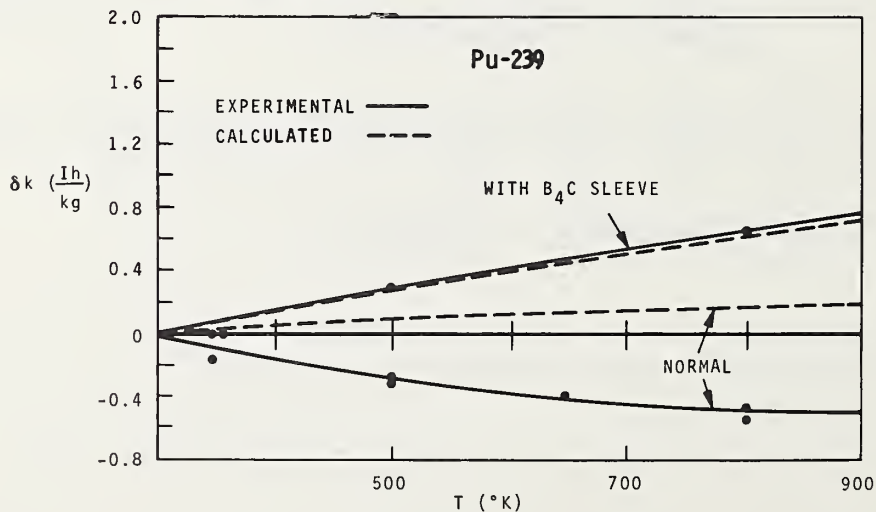


Figure 11. Measured and Calculated Doppler Reactivity Changes in Assembly 47. (Gasidlo⁽²³⁾, Greebler et al⁽¹⁹⁾)

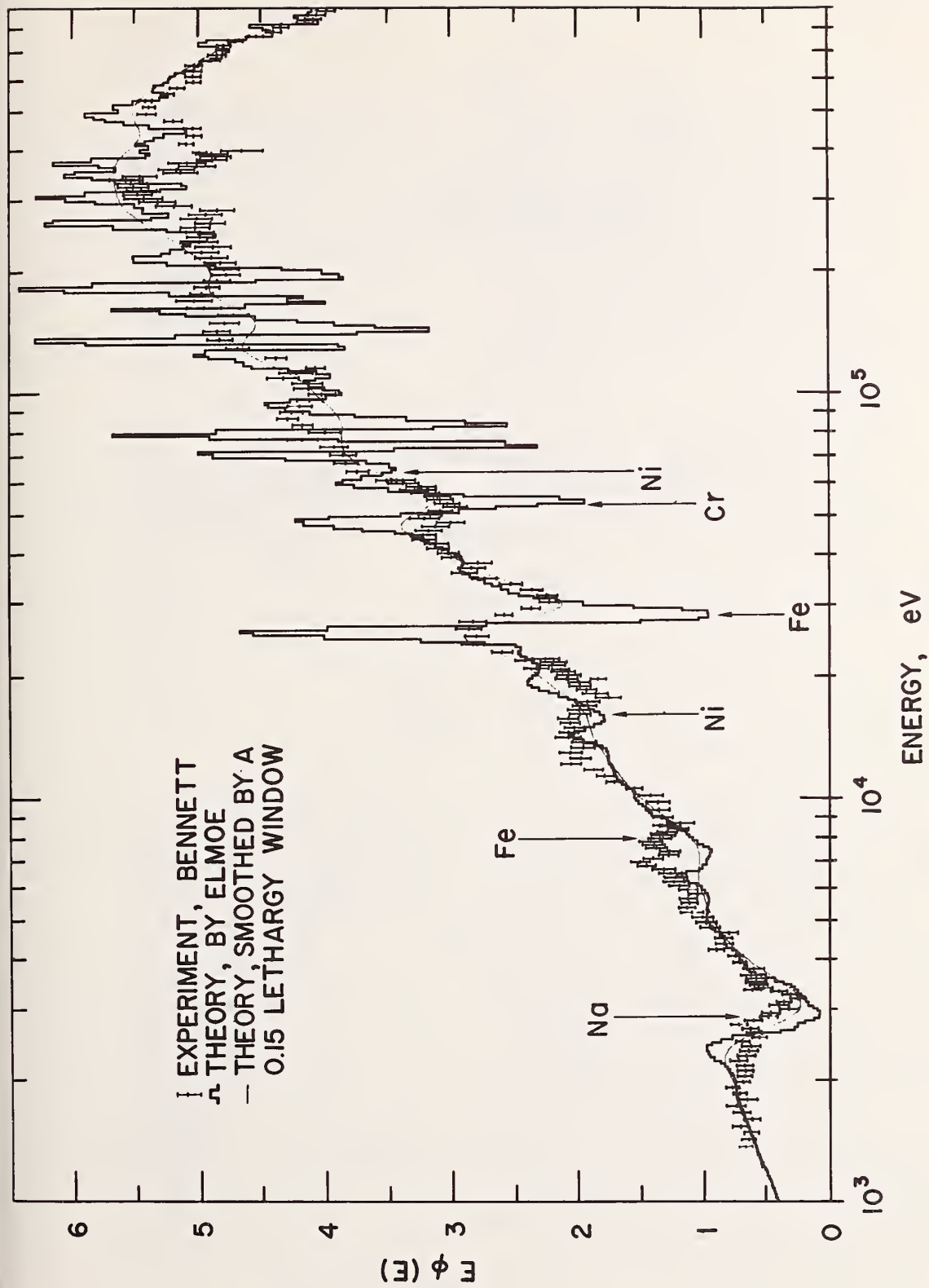


Figure 12. Comparison of Theoretical with Experimental Neutron Spectra in Assembly 48. The histogram gives the result of the ELMOE calculation; the continuous curve shows the same results through a Gaussian window. (Bennett et al (28), Travelli (29))

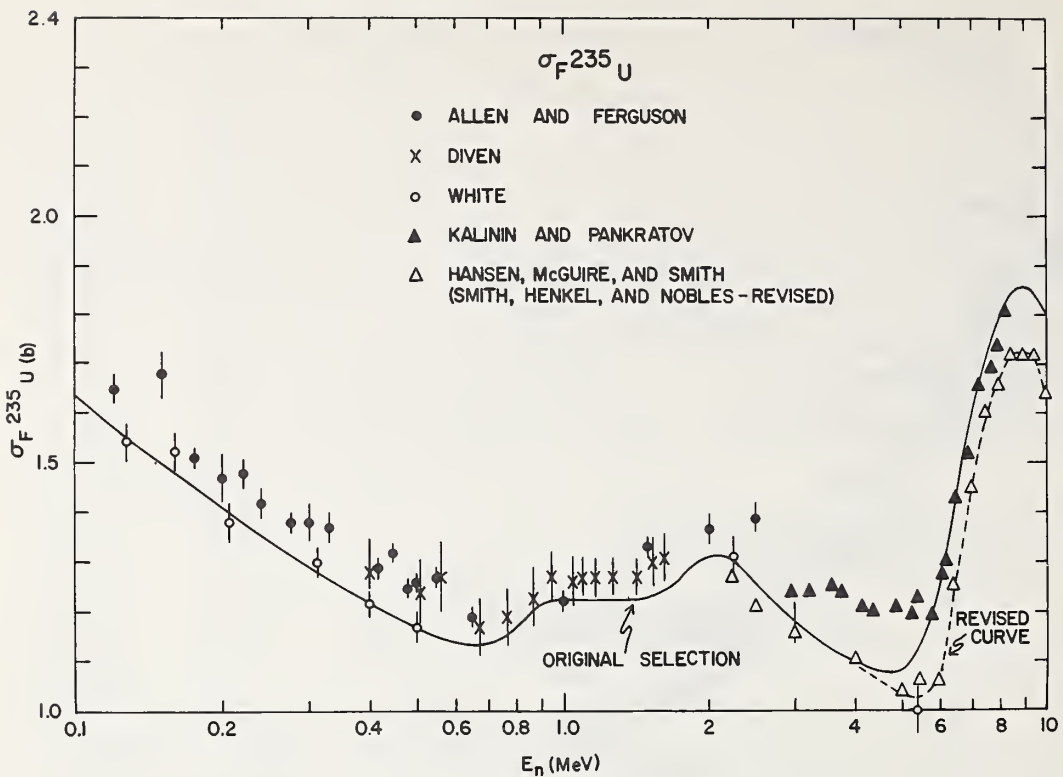


Figure 13. U^{235} Fission Cross Sections (Davey⁽³⁰⁾)

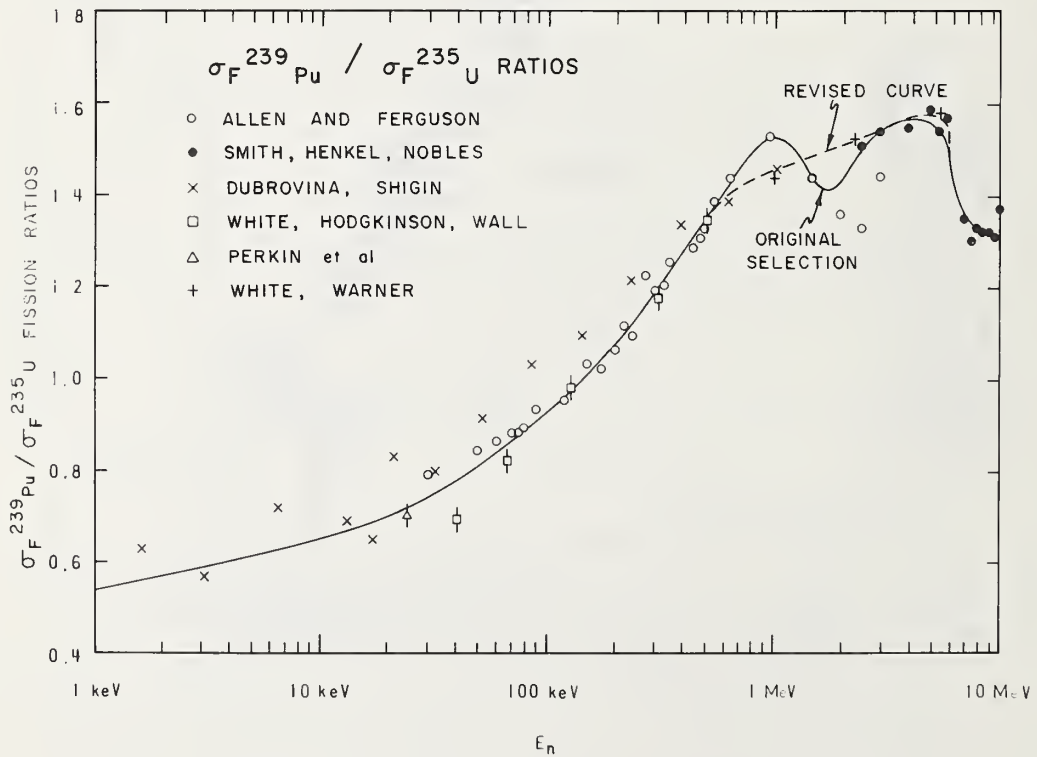


Figure 14. Ratio of Pu^{239} and U^{235} Fission Cross Sections (Davey⁽³⁰⁾)

103-9828

103-9772

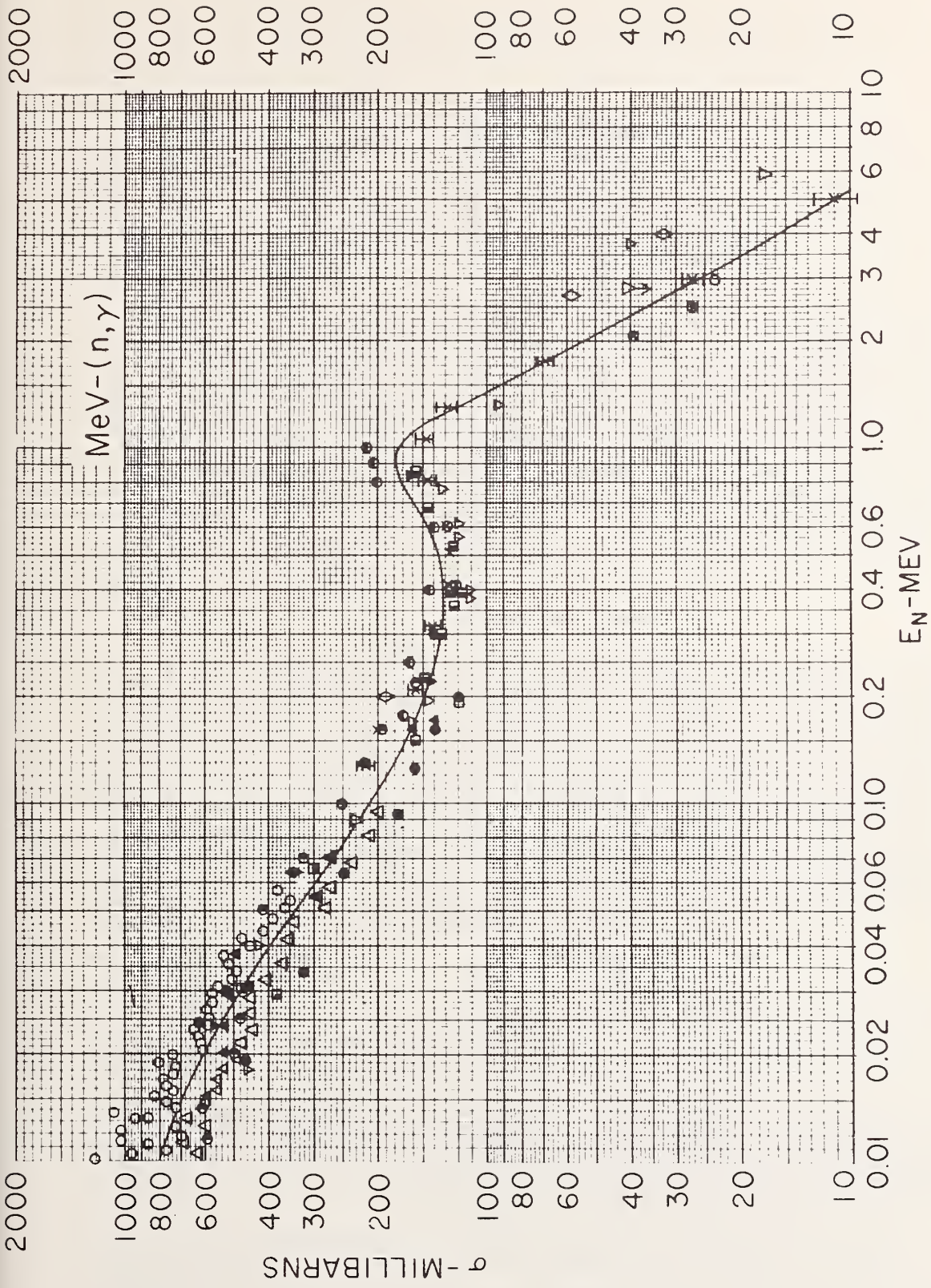


Figure 15. Neutron Capture Cross Sections of ^{238}U from BNL-325, Second Edition, Supplement 2.

CALCULATIONS OF FAST CRITICAL EXPERIMENTS USING ENDF/B DATA
AND A MODIFIED ENDF/B DATA FILE*

by

T. A. Pitterle
E. M. Page
M. Yamamoto +

Atomic Power Development Associates, Inc.
Detroit, Michigan 48226

ABSTRACT

This paper presents calculations of the Pu-239 fueled ZPR-III Assembly 48 and the U-235 fueled ZPR-VI Assembly 2 using two cross section data files - the recently compiled ENDF/B data file and a modified ENDF/B data file. For the modified ENDF/B file, cross sections were re-evaluated as follows: capture and fission for U-235, U-238, Pu-239, and Pu-240; capture for Fe, Cr, Ni, Mo and Na; inelastic scattering for U-238 and Cr; and elastic scattering for the 2.85 kev resonance in Na. Using the MC² code (Multigroup Constants Code), multigroup cross sections are calculated with each data file for the above mentioned assemblies. One and two dimensional diffusion theory calculations are then compared with experiment for criticality, reaction rate ratios, material worths, and sodium void coefficients.

1. INTRODUCTION

Present uncertainties in neutron cross sections impose serious limitations on the accuracy for fast reactor physics calculations particularly for reactivity coefficients such as the sodium void effect. In this paper, the effects of these uncertainties on integral fast reactor measurements are examined by analysis of the Pu-239 fueled ZPR-III Assembly 48 and the U-235 fueled ZPR-VI Assembly 2. A related paper⁽¹⁾ examines Pu-240 cross section uncertainties by analysis of ZPR-III Assembly 48B. Calculations are compared using both the ENDF/B data⁽²⁾ file and a modified ENDF/B data file which has been evaluated as a part of this effort. These modifications to the ENDF/B file emphasize many of the cross sections uncertainties of importance to fast reactor analysis with particular attention placed on evaluation of fission cross section ratio measurements to obtain a consistent set of fission cross sections.

2. DATA EVALUATION

Cross section evaluations for the modified ENDF/B data file are described below. A more detailed description of this evaluation will be published in reference 3.

U-235 Evaluation - The fission cross section below 5 kev and the capture cross section below 3 kev are based on the measurements of DeSaussure⁽⁴⁾ and Michaudon⁽⁵⁾ from 5-21 kev, Perkin⁽⁶⁾ at 24 kev, Knoll⁽⁷⁾ at 30 and 64 kev, and White⁽⁸⁾ from 40 kev to 2.25 Mev. Between 0.5 and 1.6 Mev, the measurements of Diven⁽⁹⁾ were normalized to the White data point at 1.0 Mev to define the energy

*Work Performed Under AEC Contract No. AT(11-1)-865, Project Agreement 18

+Assigned to APDA by Central Research Institute for Electric Power Industry of Japan

dependence between White data points. Above 2.25 Mev, the fission cross section is based on the measurements of Smith, Henkel, and Nobles⁽¹⁰⁾ as corrected for inelastic scattering by Hansen.⁽¹¹⁾

Above 10 kev, alpha values were obtained from measurements of Weston,⁽¹²⁾ DeSaussure,⁽⁴⁾ and Hopkins and Diven.⁽¹³⁾ The mean number of neutrons per fission is given by $\bar{\nu} = 2.43 + 0.088E + 0.0125E^2 - .00062E^3$ (E in Mev) based on a fit to evaluated data of Schmidt.⁽¹⁴⁾ For the fission spectrum, a Watt spectrum with the Cranberg⁽¹⁵⁾ parameters has been used for U-235 fueled systems. The ENDF/B fission spectrum is a simple fission spectrum with a nuclear temperature of 1.27 Mev which is a softer spectrum than the Cranberg spectrum.

U-238 Evaluation - Below 4 kev, the resolved resonance parameters for U-238 were taken from the evaluation of Schmidt.⁽¹⁴⁾ Between 1 and 4 kev, a smooth background capture cross section has been added to the capture cross section calculated from the resolved parameters. The net capture cross section averaged over quarter-lethargy intervals is in agreement with the measurements of Moxon.⁽¹⁶⁾ Above 4 kev, the capture cross section is based on the measurements of Moxon⁽¹⁶⁾ to 30 kev, Ponitz⁽¹⁷⁾ and Moxon to 0.5 Mev and Barry⁽¹⁸⁾ above 0.5 Mev.

The U-238 fission cross section was obtained from the evaluated fission cross section of U-235 and U-238/U-235 fission ratio measurements as follows: Lamphere⁽¹⁹⁾ below 2 Mev, Stein⁽²⁰⁾ from 2.0 to 5.0 Mev, Smith, Henkel and Nobles^(10,11) from 5.0 to 10.0 Mev, and White⁽²¹⁾ at 2.25 and 5.4 Mev. The inelastic scattering cross section was also evaluated in this study using the same energy level scheme as used by Schmidt.⁽¹⁴⁾ This evaluation produces a slightly lower cross section and harder secondary energy distribution than the ENDF/B data.

Pu-239 Evaluation

1. Above 15 Key - The Pu-239 fission cross section above 15 kev is based upon measured Pu-239/U-235 fission cross section ratios as follows: Gilboy⁽²²⁾ (Method A results of author) and Perkins⁽⁶⁾ up to 50 kev; Gilboy,⁽²²⁾ White,⁽⁸⁾ and Allen and Ferguson⁽²³⁾ between 50 and 100 kev; White⁽⁸⁾ and Allen and Ferguson⁽²³⁾ between 0.1 and 0.7 Mev; White and Warner⁽²¹⁾ and Smirenkin⁽²⁴⁾ (Fission ratios from separate fission measurements of Pu-239 and U-235) between 0.7 and 2.5 Mev; and White⁽²¹⁾ and Smith, Henkels, and Noble⁽¹⁰⁾ above 2.5 Mev. Alpha values above 15 kev were obtained from the measurements of DeSaussure⁽⁴⁾ and Hopkins and Diven.⁽¹³⁾ The mean number of neutrons per fission is taken as $\bar{\nu} = 2.892 + 0.1279E + 0.00189E^2 - 0.0001E^3$ (E in Mev) from the evaluation of Schmidt.⁽¹⁴⁾ A Watt fission spectrum is used with an average fission spectrum energy of 2.078 Mev in agreement with the measurement of Bonner⁽²⁵⁾ who fitted the data to a simple fission spectrum with a nuclear temperature of 1.385 Mev.

2. Below 15 Key - The Pu-239 fission cross section below 15 kev has been measured by Cote,⁽²⁶⁾ James,^(27,28) and Shunk.⁽²⁹⁾ Over approximately quarter lethargy averages, these measurements differ by as much as 25% and it is difficult to establish a trend in the data. For this study, averages of the measurements were compared to select a weighted mean with the James⁽²⁸⁾ measurement most heavily weighted.

At the present time, alpha values for Pu-239 below 15 kev have an uncertainty of more than 50%. Values range from about 0.55 as obtained by Kanne⁽³⁰⁾ to greater than unity as obtained in the preliminary measurements reported by Schomberg.⁽³¹⁾ To examine this discrepancy, alpha values were obtained from unresolved resonance

calculations. The fission width of the $\ell=0, J=1$ spin state was adjusted to fit the average evaluated fission cross sections and yield the alpha values. This procedure is equivalent to using experimental total and fission cross sections to extract the alpha value. Parameters held fixed in the calculation were: Uttley's⁽³²⁾ energy dependent s-wave strength functions, $\langle \Gamma_f \rangle$ ($\ell=0, J=0$) = 1.5 ev, $\langle \Gamma_\gamma \rangle$ = 0.04 ev for all spin states, p-wave strength function of $1.75 \times 10^{-4} \text{ ev}^{-1/2}$, and theoretical p-wave fission widths based on estimated fission thresholds summarized by Otter.⁽³³⁾ Results of these calculations are given in Table I where they are compared with experimental, calculated (Sowerby⁽³⁴⁾), and evaluated (ENDF/B evaluation⁽³⁵⁾) alpha values. The sharp drop in experimental alpha values above 20 keV appears to result principally from the increasing contribution of p-wave fission rather than to fission threshold behavior of the $\ell=0, J=1$ state. For lack of better experimental data at this time, calculated alpha values were used below 15 keV in this study.

Pu-240 Evaluation - The Pu-240 evaluation of this study differs principally from the ENDF/B evaluation by the use of a radiation width of 0.020 ev⁽³⁶⁾ to estimate the capture cross section rather than the value of 0.030 ev used in the ENDF/B evaluation.

Na Evaluation - The only change made to the ENDF/B sodium evaluation was to calculate the scattering and capture cross sections for the 2.85 keV resonance with a $J=2$ spin state, $\Gamma_n=285$ ev, and $\Gamma_\gamma=0.293$ ev compared to the $J=1, \Gamma_n=410$ ev and $\Gamma_\gamma=0.336$ incorporated in the ENDF/B evaluation. The $J=2$ spin assignment is based on the measurements of Garg⁽³⁷⁾ with the width of 285 ev obtained as a compromise fit to experimental data. The radiation width of 0.293 ev was obtained by fitting the thermal capture cross section.

Fe, Cr, Ni, Mo Evaluations - For Fe, the capture cross section from 1 to 50 keV is obtained from resolved resonance parameters and measured capture areas. For Cr and Ni, the capture and inelastic scattering cross sections of ENDF/B were modified while for Mo, only the capture cross section was modified. The Cr, Ni, and Mo modifications are based on the same experimental data as the evaluations of Schmidt.⁽¹⁴⁾

3. METHODS OF CALCULATION

In addition to a number of processing routines required primarily to alter cross section data formats, there were basically three codes utilized in the development of the multigroup libraries. The MC² code⁽³⁸⁾ is used for the calculation of multigroup constants for each assembly and data file. A P-1 fundamental mode flux spectrum in the ultrafine group option of MC² with a buckling iterated to criticality is used for averaging the cross sections. In MC², resonance self-shielding is calculated but only one geometrical representation can be used in a single problem. Thus, for the complex plate geometries of ZPR fast critical assemblies the resonance self-shielding calculated in MC² is replaced by values calculated with the IDIOT code⁽³⁹⁾ using different parameters in an equivalence principle for the fertile and fissile isotopes in the composition. The equivalence principle⁽⁴⁰⁾ used is approximately equivalent to separately self-shielding each plate in the assembly followed by a flat flux averaging to define a homogenized cross section. These heterogeneously self-shielded cross sections are used in all criticality calculations and homogeneously self-shielded values are used for reaction rate and material worth calculations. RESPA, an APDA program was used to obtain unresolved resonance parameters for self-shielding calculations by fitting infinite dilution evaluated cross sections.

All calculations reported here are one and two dimensional diffusion theory calculations. Twenty-four groups are used in the one-dimensional calculations to cover the energy range from 8 ev to 10 Mev. The two-dimensional, RZ geometry, calculations were made in 12 groups using a 2/1 group collapse from the 24 groups. The core size used in the calculations are based on the experimental critical mass corrected for control rod effects, irregular core boundary, and the central gap between assembly halves.

4. RESULTS OF CALCULATIONS

ZPR-III Assembly 48 - ZPR-III Assembly 48⁽⁴¹⁾ is a relatively simple, plutonium-fueled assembly with material constituents of plutonium, depleted uranium, sodium (25%), graphite, and stainless steel. Results of multigroup diffusion theory calculations are given in Table 2. Except for moderation (spectral) components of the light element central worths, which are sensitive to the number of groups (inadequately defined at 12 groups), one-dimensional results are essentially identical with two dimensional calculations.

First order perturbation theory calculations of the sodium void measurements with modified ENDF/B data yield values about 50% less than experiment for regions near the core center, where the net void effect is positive. Near the core edges where leakage effects dominate, the experimental results are underestimated by about 15%. The ENDF/B data yields the same leakage contributions as the modified data but predicts negative void effects near the core center where experiment is positive.

ZPR-VI Assembly 2 - ZPR-VI Assembly 2⁽⁴⁴⁾ is a 600 liter, uranium fueled assembly with material constituents of U-235, U-238, carbon, sodium and stainless steel in the core and a depleted uranium blanket. Results of multigroup calculations with both data files are given in Table 3. The central worth measurements were made with rather large samples and sample size effects may be significant particularly for Pu-239, U-238 and B-10. Note also that the value given in the Table is for voiding 1.25 kg of sodium at the core center.

5. DISCUSSION OF RESULTS

Criticality - The modified ENDF/B data yields excellent criticality agreement with experiment for both assemblies analyzed while the ENDF/B data is about 1% under-reactive. Differences in criticality appear to be almost exclusively due to differences between the evaluations for Pu-239, U-235, and U-238 capture and fission cross sections.

Central Worths - In Assembly 48, the most notable difference between the two data sets is the prediction of the moderation components of Na and C central worths. The modified ENDF/B data predicts the correct sign and magnitude of these worths while the ENDF/B data does not adequately predict these worths indicating a probable discrepancy in the calculated adjoint flux spectrum. Both data sets underpredict the B-10 worth (normalized to U-235) by about 10% which tends to indicate an underprediction of the low energy flux. However, the B-10 capture rate with the modified data is about 8% greater than obtained with the ENDF/B data although the B-10 worth is a few per cent lower with the modified data. Thus the difference in B-10 worths appears to be due to the reduced adjoint flux at low energies resulting from the higher Pu-239 alpha values of the modified data.

Central Reaction Rates - The most notable discrepancy with experiment in the reaction rate ratios is the 5% underprediction of the Pu-239/U-235 fission ratio

in Assembly 48 with both data sets. The discrepancy between calculation and experiment appears to be more likely due to uncertainties in the Pu-239 fission cross section than to the calculated flux spectra.

Sodium Void - For Assembly 48 the modified data underestimates the measured void coefficients by about 50% for regions near the core center. However, more careful calculations incorporating heterogeneity and resonance self-shielding effects are necessary to adequately assess the accuracy of the calculations. The ENDF/B data does not predict the experimental positive sodium void effect.

For ZPR-VI Assembly 2, calculated results with both data sets are in good agreement with experiment for a small centrally voided region. The agreement between the two data sets on the void calculations is better than would be expected from a comparative examination of the cross sections.

6. CONCLUSIONS

For the two assemblies analyzed, the modified data file yields better overall agreement with experiment than the ENDF/B data. However, analysis of a greater variety of integral experiments is required to obtain an adequate check on the accuracy of either data file. The importance of the Pu-239 alpha value uncertainty on the sodium void coefficient is clearly demonstrated by the calculations reported in this paper. Alpha values used in the modified ENDF/B data file were calculated and a large uncertainty must be assigned to the calculations. The improved agreement obtained with the high alpha values between calculation and experiment for the sodium void measurements lends inconclusive support to higher alpha values than included in the ENDF/B evaluation.

7. REFERENCES

1. Pitterle, T. A., Yamamoto, M., "A Comparison of Pu-240 Cross Section Evaluations by Calculations of ZPR-III Assemblies 48 and 48B," Session H, these proceedings.
2. Honeck, H. C., "ENDF/B, Specifications for an Evaluated Nuclear Data File for Reactor Applications," BNL-50066(T-467) ENDF 102 (1966).
3. Pitterle, T. A., Page, E. M., Yamamoto, M., "Analysis of Sodium Reactivity Measurements," APDA-216, to be published.
4. DeSaussure, G., et al, IAEA Conference on Nuclear Data, October 1966, Paris and Nuc. Sc. & Eng. 23, 45 (1965)
5. Michaudon, A., et al, J. Phys. Radium 21 (1960) and CEA-2552 (1964)
6. Perkin, J. L., et al, J. Nuc. Energy, 19, 423 (1965)
7. Knoll, G. F., Ponitz, W. P., J. Nuc. Energy, Vol. 21, 643 (1967)
8. White, P. H., et al, "Physics and Chemistry of Fission," IAEA Conf., Salzburg (1965)
9. Diven, B. C., Phy. Rev. 105, 1350 (1957)
10. Smith, R. K., et al, Bull. Am. Phys. Soc. 2, 196 (1951)
11. Hansen, G., McGuire, S., Smith, R. K., "U-235 and U-238 (n,f) Cross Section," WASH-1074, 75 (1967)
12. Weston, L. W., et al, Nuc. Sc. & Eng. 26, 149, (1966)
13. Hopkins, J. C., Diven, B. C., Nuc. Sc. & Eng. 12, 169 (1962)

14. Schmidt, J. J., KFK 120, Part I, 1966
15. Cranberg, L. et al, Phy. Rev. 103, 662 (1956)
16. Rae, E. R., Third Geneva Conf., P/167, Vol. 2 (1964)
17. Ponitz, W. P., et al, KFK-635, 1967
18. Barry, J. F., et al, J. Nuc. Energy 18, 481 (1964)
19. Lamphere, R. W., Phy. Rev. 104, 1654 (1956)
20. Stein, W. E., et al, "Relative Fission Cross Sections of U-238, Np-237, and U-235," Conf. on Neutron Cross Section Technology, CONF-660303, Vol.2 (1966)
21. White, P. H., Warner, G. P., J. Nuc. Energy, Vol. 21, 671 (1967)
22. Gilboy, W. B., Knoll, G. F., CN-23/7, IAEA Conf. on Nuclear Data, Paris (1966)
23. Allen, W. D., Ferguson, A.T.G., Proc. Phys. Soc. A70, 573 (1957)
24. Smirenkin, G. N., et al, At. Energy 13, 366, (1962)
25. Bonner, T. W., Nuc. Phys. 23, 116 (1961)
26. Cote, R. E., et al, Bull. Am. Phy. Soc. II, 1, 187, 1957
27. James, G. D., EANDC-33U, p.14, 1963
28. James, G. D., EANDC(UK)-35L, p.4, 1964
29. Shunk, E. R., et al, "Fission Cross Sections from Petrel," LA-3586, 1966
30. Kanne, W. R., et al, 1955 Geneva Conf., P/595, Vol. 4
31. Schomberg, M.G., et al, SM-101/41, IAEA Symposium on Fast Reactor Physics and Related Safety Problems, Karlsruhe, Germany, October 1967.
32. Uttley, C. A., EANDC(UK)-40L, 1964
33. Otter, J. M., NAA-SR-12515, 1967
34. Sowerby, M. G., Patrick, B. H., unpublished, values given in Reference 1
35. Greebler, P., et al, GEAP-5272, December, 1966
36. Asghar, M., et al, CN-23/31, IAEA Conf. on Nuclear Data, Paris (1966)
37. Garg, J. B., Wynchank, S., et al, Conf. on Study of Nuclear Structure with Neutrons, Antwerp, Belgium (1965)
38. Toppel, B. J., et al, "MC², A Code to Calculate Multigroup Constants," ANL-7318
39. Pitterle, T. A., Green, D. M., "IDIOT, A FORTRAN-IV Code for Calculation of Resonance Averaged Cross Sections and Their Temperature Derivatives," APDA-189 to be published.
40. Pitterle, T. A., Yamamoto, M., APDA-201 (1967)
41. Broomfield, A. M., "ZPR-3 Assembly 48: Studies of a Dilute Plutonium Fueled Assembly," ANL-7320 (1966)
42. Edison, G. E., Bennett, L. L., ANS Trans. Vol. 10, No. 2 (1967)
43. Davey, W. G., "Intercomparison of Calculations for a Dilute Plutonium-Fueled Fast Critical Assembly (ZPR-3 Assembly 48), ANL-7320 (1966)
44. Rusch, G. K., "Investigations of a 600 Liter Uranium Carbide Core (ZPR-VI Assembly No. 2), ANL-7010, p.91 (1964)

TABLE 1 - Comparison of Calculated and Experimental Alpha Values

$\Delta E, \text{ keV}$	Calculated										Estimated Alpha Values				
	With Inelastic ¹					Without Inelastic					Schomburg	(31) DeSaussure	(4) Sowerby	(34) ENDF/B	(35)
	$\bar{E}, \text{ keV}$	$\bar{\sigma}_f$	$S \times 10^4$	Alpha	$\langle \Gamma_f \rangle, \text{ ev}$ $\ell=0, J=1$	$\bar{\sigma}_{in}$	Alpha	$\langle \Gamma_f \rangle, \text{ ev}$ $\ell=0, J=1$	Alpha	Alpha					
.1-.2	.15	19.0	1.15	.83	.051					1.02 ± .3			.62		
.2-.3	.25	18.3	1.54	.81	.047					.87 ± .3			.66		
.3-.4	.35	9.7	1.02	.97	.034					1.5 ± .5			.97		
.4-.5	.45	9.5	0.76	.43	.20					.83 ± .3			.33	.74	
.5-.6	.55	14.5	1.71	.61	.075					.65 ± .2			.27	.72	
.6-.7	.65	4.4	0.80	1.40	.014					2.0 ± .6			1.33	.71	
.7-.8	.75	5.1	0.83	1.01	.030					1.4 ± .4			1.27	.70	
.8-.9	.85	4.8	0.84	1.03	.025					1.1 ± .3			1.28	.69	
.9-1.0	.95	7.4	1.29	.74	.041					.93 ± .3			1.02	.68	
1-2	1.5	4.3	1.00	.91	.029					1.07 ± .3			1.13	.65	
2-3	2.5	2.8	1.06	1.18	.010					1.27 ± .4			.89	.61	
3-4	3.5	2.75	1.07	.90	.019					1.18 ± .4			1.03	.58	
4-6	5.0	2.45	1.06	.78	.023					1.17 ± .4			1.0	.55	
6-8	7.0	2.35	1.05	.62	.035					1.1 ± .4			1.0	.52	
8-10	9.0	2.30	1.05	.51	.050			.057	.52	.9 ± .3			.66	.49	
9.1-11.7	10.4	2.03	1.05	.54	.033			.139	.57					.48	
11.7-15.0	13.4	1.85	1.05	.51	.028			.192	.55					.45	
15.0-19.3	17.2	1.77	1.05	.45	.028			.216	.50	1.02 ± .3				.42	
19.3-24.8	22.1	1.74	1.05	.39	.033			.232	.44	.83 ± .3				.38	
24.8-31.8	28.3	1.69	1.05	.34	.032			.237	.40	.64 ± .2		.39		.34	
31.8-40.9	36.4	1.65	1.05	.30	.030			.243	.36	.45 ± .2		.27		.29	
40.9-52.5	46.7	1.62	1.05	.27	.027			.251	.33			.24		.23	
52.5-67.4	60.0	1.60	1.05	.24	.026			.267	.30			.18		.18	
67.4-86.5	77.0	1.58	1.05	.21	.028			.290	.27			.16		.15	
86.5-111.1	98.8	1.57	1.05	.18	.048			.328	.25					.145	
111.1-142.6	126.9	1.56	1.05	.16	.103			.369	.23						

1. Estimated inelastic scattering widths included in total width.
No statistical averaging was applied to inelastic widths.

TABLE 2 - Comparison of Calculation and Experiment for ZPR-III Assembly 48

k ⁶	Experiment		Modified ENDF/B		ENDF/B	
	1.000 ± 0.001		.9803(.998±0.005) ¹		.9680(.986±0.005) ¹	
Central Worths ⁴						
	ih/kg	σ _p ²	ih/kg ⁵	σ _p	ih/kg ⁵	σ _p
U-235	339 ± 4	2.79	431.0	2.80 *	444.6	2.78
U-238	-24.8 ± 0.5	-0.206	-29.3	-0.192*	-33.0	-0.209
U-238 ³	-20.0 ± 0.2	-0.167	-25.0	-0.164*	-28.3	-0.179
Pu-239	445 ± 4	3.72	560.0	3.69 *	575.6	3.66
Pu-240	81 ± 20	0.681	89.5	0.593	87.8	0.561
			105.5	0.698*	104.6	0.668*
Na	- 6.3 ± 0.3	-0.0051	-6.93	-0.0044*	≈ 0.0	≈ 0.0
C	- 4.5 ± 1.2	-0.0019	-17.2	-0.0057	6.09	0.0019
B-10	-8926 ± 80	-3.13	-10080	-2.78	-10700	-2.85
Fe	-12.3 ± 0.4	-0.0240	-14.9	-0.0229*	-15.8	-0.0235
Cr	- 9.4 ± 0.4	-0.0171	-14.3	-0.0205*	-14.3	-0.0198*
Ni	-18.2 ± 0.2	-0.0374	-20.3	-0.0329*	-19.2	-0.0300
Mn	-21.4 ± 0.4	-0.0413	-53.7	-0.0815	-63.3	-0.0926
Al	-15.7 ± 0.8	-0.0148	-18.5	-0.0137	-15.6	-0.0112
Ox	-6.8 ± 0.9	-0.0038	-12.5	-0.0055	-2.23	-0.0009
Mo	-43.4 ± 0.4	-0.146	-65.4	-0.173*	-107.4	-0.275

Central Reaction Rate Ratios Relative to U-235 Fission

U-238	Fission	0.0307 ± 0.0003	0.0308*	0.0307
Pu-239	Fission	0.976 ± 0.010	0.929 *	0.917
Pu-240	Fission	0.243 ± 0.002	0.234 *	0.225
U-234	Fission	0.204 ± 0.002	0.200	0.1926
U-236	Fission	0.067 ± 0.0006	0.0686	0.0662
U-238	Capture	0.138 ± 0.007	0.134 *	0.140
Na	Capture		0.0010*	0.0095
B-10	Capture		1.337	1.239
Mn	Capture		0.0424	0.0412

* Modified ENDF/B data used in calculations.

1. Eigenvalues in parenthesis include heterogeneity and transport corrections of $1.3 \pm 0.3\% \Delta k^{(42)}$ and $0.5 \pm 0.2\% \Delta k$ respectively.
2. Experimental perturbation cross sections normalized to 2.79b for U-235.
3. Experimental value for 2" x 2" x 2" sample. Calculated with cross sections self-shielded for this sample.
4. Based on 24-group spherical geometry calculations using a calculated shape factor of 0.93.
5. 942 ih = 1% Δk/k
6. Eigenvalue based on two dimensional, RZ geometry Calculations with 12 groups.

TABLE 3 - Comparison of Calculation and Experiment for ZPR-VI Assembly 2

	<u>Experiment</u>		<u>Modified ENDF/B</u>		<u>ENDF/B</u>	
k^6	1.000 ± 0.001		.9913(1.002±0.006) ¹		0.9822(0.993±0.006)	
<u>Central Worths</u> ⁵						
	<u>ih/kg</u>	<u>σ_p^2</u>	<u>ih/kg</u>	<u>σ_p</u>	<u>ih/kg</u>	<u>σ_p</u>
U-235 (273 g) ³	104 ± 2	2.21	119	2.18*	125.0	2.25
U-238 (1154 g)	-6.46 ± 05	-0.139	-7.67	-0.142*	-8.60	-0.156
Pu-239 (93 g)	164 ± 6	3.54	176	3.28*	176.0	3.23
Na (1.25 kg)	1.65 ± 0.5	0.00342	1.78	0.00332*	1.79	0.00329
C	16.9 ± 0.5	0.0183	11.1	0.0104	11.0	0.0101
B-10 (29 g)	-1844 ± 7	-1.669	-2476	-1.93	-2539	-1.95
Fe	-2.87 ± 0.1	-0.0145	-3.97	-0.0172*	-4.07	-0.0174
Cr	-3.13 ± 0.25		-3.74	-0.0151*	-3.80	-0.0151*
Ni			-5.14	-0.0234*	-5.37	-0.0241
Mn			-8.12	-0.0346	-8.30	-0.0349
Al	-1.71 ± 0.44		-2.36	-0.0050	-2.33	-0.0048

Central Reaction Rate Ratios Relative to U-235 Fission

U-238	Fission	0.0358 ± 0.0005 F,S ⁴	0.0339*	0.0320
Pu-239	Fission	1.045 ± 0.02 F 1.09 ± 0.04 S	1.037*	0.999
Pu-240	Fission	0.254 ± 0.005 F	0.276*	
U-234	Fission	0.228 ± 0.005 F 0.236 ± 0.007 S	0.243	0.230
U-236	Fission	0.076 ± 0.004 F	0.078	0.072
U-238	Capture	0.106 R	0.131*	0.136

*Modified ENDF/B data used in calculations.

1. Eigenvalues in parenthesis include heterogeneity and transport corrections of ± 0.7 ± 0.3% Δk and + 0.4 ± 0.3% Δk respectively.
2. Experimental perturbation cross sections normalized to 2.21b for U-235.
3. Weight of sample in grams.
4. F=fission chamber, S=solid state detector, R=radiochemical analysis.
5. 451 ih = 1% Δk/k.
6. Eigenvalues based on two dimensional, RZ geometry calculations with 12 groups.

A COMPARISON OF PU-240 CROSS SECTION EVALUATIONS BY CALCULATIONS
OF ZPR-III ASSEMBLIES 48 AND 48B*

by

T. A. Pitterle
M. Yamamoto +

Atomic Power Development Associates, Inc.
Detroit, Michigan 48226

ABSTRACT

Uncertainties in Pu-240 cross sections have an important influence on fast reactor parameters such as the sodium void and Doppler coefficients, breeding ratio, etc. This paper compares recent evaluations and in particular, two evaluations of the present authors differing primarily by the assumed value of the radiation width. One evaluation is the ENDF/B data which is based on $\Gamma_{\gamma}=30$ mv from the measurements of Bockhoff and Byers while the other evaluation utilizes $\Gamma_{\gamma}=20$ mv from the measurements of Asghar. To assist in evaluating the accuracy of the Pu-240 cross section data, calculations have been made for ZPR-III Assemblies 48 and 48B using both the ENDF/B data file and a modified ENDF/B data file for the critical assembly calculations. The experimental and calculated results are compared to assess the importance of the Pu-240 cross section uncertainties.

1. INTRODUCTION

The plutonium used as fuel in fast reactors is to be obtained as a by-product in thermal reactors and will contain of the order of 20-25% Pu-240. As a result, uncertainties in Pu-240 cross sections have an important influence on fast reactor parameters such as sodium void effects, Doppler coefficients, breeding ratio, etc. In this paper, the Pu-240 capture and fission cross section uncertainties important to sodium cooled fast reactors (cross sections above about 200 ev) are discussed by comparing recent Pu-240 cross section evaluations. Calculations of ZPR-III Assemblies 48 and 48B are compared to assess the effects of these uncertainties. These calculations use both the ENDF/B⁽¹⁾ and a modified ENDF/B⁽²⁾ data file for the criticality calculations. For the modified data file, partial re-evaluations of the ENDF/B data were made for Pu-239, U-235, U-238, Fe, Ni, Cr, Na, and Mo. Included in the calculations are two Pu-240 evaluations of the present authors which are compared in this paper.

2. COMPARISON OF PU-240 EVALUATIONS

Recent evaluations of Pu-240 have been carried out by Yiftah⁽³⁾ and by the present authors⁽⁴⁾ for the ENDF/B data file. As a part of this study, the ENDF/B evaluation has been modified to examine a major uncertainty in the capture cross section. For simplicity, let us designate these evaluations as Pu-240E (ENDF/B), Pu-240M (Modified ENDF/B), and Pu-240Y (Yiftah). These three evaluations are all based on published measurements up to the Paris Conference on Nuclear Data (October 1966). The capture and fission cross sections for the three evaluations are compared in Figure 1. Sources of the discrepancies are discussed below:

*Work Performed Under AEC Contract No. AT(11-1)-865, Project Agreement 18

+Assigned to APDA by Central Research Institute for Electric Power Industry of Japan

1. Fission Cross Section - Above about 10 kev, the differences in the three evaluations of Figure 1 are due principally to differences in normalization and interpolation through the experimental data. These differences are typical of the uncertainties in the available experimental data. The effects of these uncertainties on fast reactor calculations, while larger than desired, are of less importance than the capture cross section uncertainties. Below 20 kev, the fission cross section for the Pu-240E evaluation was calculated from unresolved resonance parameters on the assumption that the threshold fission in Pu-240 is dominantly p-wave with only a small s-wave contribution. The Pu-240M and Pu-240Y evaluations between 700 ev and 10 kev are based on the measurements of Eyers.^(5,6) However, the Pu-240M evaluation represents a smooth curve through the averages in reference 6 while the Pu-240Y evaluation apparently averaged the pointwise data graphed in reference 5.

2. Capture Cross Section - Differences in the capture cross section between Pu-240E and Pu-240Y appear to be due principally in the methods used to obtain unresolved resonance parameters from the preliminary measurements reported by Bockhoff.⁽⁷⁾ A summary of the resonance parameters for the three evaluations is given in Table 1.

In the important low kev energy range, an estimate of the sensitivity of the capture cross section to the unresolved parameters can be obtained by noting that

$$\langle \sigma_{\gamma} \rangle_{\ell=0} = \frac{2\pi^2 \lambda^2 g}{\langle D \rangle} \left\langle \frac{\Gamma_{\gamma} \Gamma_n}{\Gamma} \right\rangle \propto \frac{\langle \Gamma_{\gamma} \rangle}{\langle D \rangle}$$

where the proportionality is approximately correct for s-waves above a few kev where $\Gamma_n \sim \Gamma$. Based on this ratio, the Pu-240Y: Pu-240E: Pu-240M capture ratios would be about 1.3:1.0:0.67. At 3 kev, the ratios from Figure 1 are 1.7:1.0:0.70. The larger than expected capture cross section of Pu-240Y is partly due to the greater p-wave strength function and possibly to the method of calculation. References 3 and 4 should be consulted for additional details of the Pu-240E and Pu-240Y evaluations.

3. ANALYSIS OF ZPR-III ASSEMBLIES 48 and 48B

Assemblies 48 and 48B - ZPR-III Assembly 48⁽¹²⁾ is a relatively simple plutonium-fueled assembly with material constituents of plutonium, depleted uranium, sodium (25%), graphite, and stainless steel. The plutonium content averages about 6% Pu-240. The measured critical mass of the heterogeneous critical cylinder is 272 ± 1.5 kg of Pu-239 with a volume of 417 liters and an L/D ratio of 0.97. Assembly 48B has identical composition as Assembly 48 except for a central core zone, 12 inches high by approximately 15 inches in diameter (8% of the core volume), for which Pu with 22% Pu-240 has been substituted for Pu with 4.5% Pu-240. The average Pu-240 content of the central zone is increased from 6 to 17%. The heterogeneous critical mass of assembly 48B is 282 ± 1.5 kg. Criticality was obtained by adding core material containing approximately 12.2 kg of Pu-239 to the outer radial edge of the cylinder. The total Pu-240 content of the central zone in Assembly 48B is 4.3 kg compared to 1.5 kg for the same volume in Assembly 48. For the analysis, it is important to note that the central zone substitution was achieved by replacing Pu-239 with Pu-240. Therefore, attempts to extract the effects of Pu-240 from the substitution are complicated by the effects of the Pu-239 reduction.

In Assemblies 48 and 48B, the Pu-240 central worth must be extracted from separate measurements of plutonium samples containing 4.5 w/o Pu-240 and 22.28

w/o Pu-240. Experimental uncertainties then lead to large uncertainties in the estimate of the Pu-240 worth. Table 2 indicates typical Pu-240 worths as extracted from annular foil samples measured in assemblies 48 and 48B. Uncertainties assigned to the Pu-240 worths in this table were obtained by combinations of the uncertainties of each of the sample measurements. These experimental uncertainties on the Pu-240 worth are greater than differences in the calculated Pu-240 worths using the Pu-240E and Pu-240M evaluations. Based on an analysis of the results of Table 2, it is estimated that at least a 60% Pu-240 sample is required to achieve an accuracy of 10% on the Pu-240 central worth.

TABLE 2 - Pu-240 Central Worths Extracted from Various Sample Combinations

<u>4.5% Pu-240</u>		<u>22% Pu-240</u>		<u>Pu-240 Worth</u>
<u>Sample</u>	<u>Measured</u>	<u>Sample</u>	<u>Measured</u>	
<u>Thickness, in.</u>	<u>ih/kg</u>	<u>Thickness, in.</u>	<u>ih/kg</u>	<u>ih/kg</u>
<u>Assembly 48</u>				
0.005	422 ± 5	0.005	356 ± 6	81 ± 50
0.010	427 ± 4	0.005	356 ± 6	59 ± 40
0.010	427 ± 4	0.010	366 ± 6	130 ± 80
0.020	430 ± 4	0.020	367 ± 3	105 ± 40
<u>Assembly 48B</u>				
0.010	423 ± 7	0.005	350 ± 6	50 ± 30
0.010	423 ± 7	0.010	356 ± 6	78 ± 50
0.020	428 ± 7	0.020	365 ± 6	103 ± 60
0.005	418 ± 7 ^a	0.005	350 ± 6	66 ± 40

^aSample size not measured. Value estimated from difference between 0.005 and 0.010 samples in Assembly 48.

Methods of Calculation - Details of the methods of calculation are given in reference 2. Basically the calculations are diffusion theory using 24 group cross section sets obtained from MC² (Multigroup Constants Code) problems using an Assembly 48 flux spectrum for averaging the cross section data. Heavy element cross sections were self-shielded for the composition in each zone using an equivalence principle which accounts for the heterogeneity of the material plates in the assembly.

Assembly 48B Calculations - A 12 group two-dimensional, R-Z geometry, diffusion theory calculation of Assembly 48B with modified ENDF/B cross sections (Pu-240M evaluation in the core) gave an eigenvalue of 0.9806. An identical calculation for Assembly 48 gave an eigenvalue of 0.9802.

Based upon the two dimensional analysis, a shape factor of 0.93 was calculated to obtain the core volume of the equivalent sphere. Spherical calculations were then performed using four different cross section combinations. The Pu-240E and Pu-240M evaluations were used in criticality calculations with both the ENDF/B and modified ENDF/B data files. Results of these calculations are given in Table 3. As it is difficult to assess the central zone replacement effects in Assembly 48B from absolute calculated quantities, some results for equivalent spherical calculations of Assembly 48 are given in Table 4. The effects of the central zone substitution can then be examined by comparing differences in discrepancies of calculation and measurement between Assemblies 48 and 48B.

Further, in an attempt to separate the Pu-240 and Pu-239 effects of the central zone substitution, a calculation (see last column of Table 4) was made of Assembly 48B using the Pu-240 atomic density of Assembly 48 in the central zone. The differences between this calculation and Assembly 48 results are attributable to the reduction in the Pu-239 density of the central zone. By comparison of the 48B/48 ratios of the second and fourth columns of Table 4, it is seen that the effects of the Pu-239 and Pu-240 density changes in the 48 to 48B transition tend to offset each other. That is, the decreased Pu-239 density softens the spectrum while the increased Pu-240 density hardens the spectrum. Similar offsetting effects are seen on the sodium and carbon worths. The Pu-239 effects however tend to dominate thereby reducing the sensitivity to Pu-240 cross section data.

First order perturbation calculations of the sodium void measurements were made for the centrally voided regions of Assembly 48B. As in Assembly 48, the calculations (uncorrected for heterogeneity and resonance self-shielding) with the modified ENDF/B data underestimate the measurements by about 50% while ENDF/B calculations predict a negative effect for the measured positive void effect. For voiding the central 1.32 kg of Na and the central 3.08 kg of Na, the experimental 48B/48 ratios are $1.06 \pm .25$ and $1.52 \pm .18$ respectively. Modified ENDF/B calculations with Pu-240M yield 1.09 and 1.30 respectively and with Pu-240E yield about 1.30 and 1.65.

4. DISCUSSION OF RESULTS

Reactivity - Both data sets yield the same eigenvalues for Assembly 48B as their respective calculations for Assembly 48. Therefore the reactivity effects, which are essentially dominated by the relative worth of Pu-239 at the core edge versus that near the core center, offer little assistance in assessing Pu-240 cross sections. The net reactivity difference for Assembly 48B (approximately 19 kg of Pu-240) between Pu-240E and Pu-240M is found to be 0.1% for both data sets.

Central Worths - The only central worths which show a significant sensitivity to the Pu-240 cross sections are Pu-240, Na, and C. However for each of these materials, the experimental uncertainty is of the same order of magnitude as the effects of the Pu-240 cross section uncertainties. In addition, the differences in calculated worths due to the use of different basic cross section sets (Modified ENDF/B and ENDF/B) are generally greater than the differences due to the choice of Pu-240 cross sections (Pu-240M and Pu-240E). Both experiment and calculation indicate no large differences in the central worths between Assemblies 48 and 48B.

Large experimental errors on the central worth measurements of Pu-240 do not permit a confident choice between Pu-240M and Pu-240E. The Pu-240M value may tentatively be preferred as in better agreement with the nominal measured worth in Assembly 48 although both Pu-240M and Pu-240E values lie within the experimental error. However it is estimated the Pu-240Y evaluation would yield a central perturbation cross section in Assembly 48 of about 0.2 to 0.3 barns. This value is well outside the limits of experimental accuracy indicating that the Pu-240Y evaluation greatly overestimates the capture cross section.

Reaction Rates - The relative effects of Pu-240M or Pu-240E cross sections on the reaction rate ratios (except of course the Pu-240 capture rate) are essentially insensitive to the Pu-240 evaluation or the cross section data used in the criticality calculations. A difference of 20% in the Pu-240 capture rate is found between the Pu-240M and Pu-240E evaluations.

Sodium Void Effects - The sodium void measurements for Assemblies 48 and 48B when expressed as 48B/48 ratios lie between the ratios calculated with the Pu-240M and Pu-240E evaluations. Thus these Pu-240 evaluations tend to encompass the effects of Pu-240 on the sodium void coefficient. While this conclusion is informative, it is inconclusive since the Pu-239 density change has a large compensating effect on the sodium coefficient which is subject to considerable uncertainty in the calculations.

The uncertainties in Pu-240 cross sections as represented by the Pu-240M and Pu-240E evaluations have an importance influence on the sodium coefficient. For Assembly 48B, the Pu-240E evaluation relative to Pu-240M results in a 35% increase in the positive moderation component, a net increase of 20% in the central worth, and about a 25% increase in the net void coefficient for the central regions measured.

5. CONCLUSIONS

The present analysis of Assemblies 48 and 48B indicates that the experiments are not sufficiently sensitive to the Pu-240 variations to permit a confident choice between the Pu-240M or Pu-240E evaluations. Only with a low degree of confidence can a slight preference be made to low capture cross sections similar to the Pu-240M evaluation. The Pu-240Y evaluation appears to substantially over estimate the capture cross sections.

Based on the overall analysis, it is felt that the Pu-240M and Pu-240E evaluations represent reasonable lower and upper limits on the Pu-240 capture cross section. However the uncertainties in the capture cross section as represented by these evaluations have been shown by calculation to lead to 25% differences in the sodium void coefficient for small central regions of Assembly 48B.

The present calculations indicate that for the Assembly 48B composition, 40-60% increases in the sodium void effects would be obtained from an experiment wherein the isotopic changes were limited to an increase in the Pu-240 density. This type of experiment, while providing a sensitive estimate of the Pu-240 effects, may not be feasible due to limited void space in the assembly drawers. If this experiment is not feasible, a replacement of U-238 by Pu-240 would be preferable to a replacement of Pu-239. For testing of cross sections, central worth measurements with about 90% Pu-240 samples would be highly desirable when suitable samples can be obtained.

6. REFERENCES

1. Honeck, H. C., "ENDF/B, Specifications for an Evaluated Nuclear Data File for Reactor Applications," BNL-50066 (T-467) ENDF 102 (1966).
2. Pitterle, T. A., et al, "Calculations of Fast Critical Experiments Using ENDF/B Data and a Modified ENDF/B Data File," Session H, of these Proceedings. Also APDA-216 to be published.
3. Yiftah, S., et al, "Basic Nuclear Data for the Higher Plutonium Isotopes," SM-101/21, Symposium on Fast Reactor Physics and Related Safety Problems, Karlsruhe, Germany (November 1967).

4. Pitterle, T. A., Yamamoto, M., "Evaluated Neutron Cross Sections of Pu-240 for the ENDF/B File," APDA-218, to be published. Also APDA Technical Memo No. 43 (January 1967).
5. Byers, D. H., et al, Conference on Neutron Cross Section Technology, Washington, D.C. (CONF-660303, 1966) and Private Communication.
6. Byers, D. H., et al, "Fission Cross Sections from Petrel," LA-3586, p.59 (1966).
7. Bockhoff, K. H., et al, CN-23/89, Paris Conference on Nuclear Data (1966).
8. Asghar, M., Moxon, M. C., Pattendon, N. J., CN-23/31, Paris Conference on Nuclear Data (1966).
9. Leonard, B. R., HW-67219 (1960).
10. Brooks, F. D., Jolly, J. E., IAEA rep. INDSWG-63 (1964).
11. Schmidt, J. J., KFK 120, Part I, 1966.
12. Broomfield, A. M., et al, "ZPR-3 Assembly 48: Studies of a Dilute Plutonium-Fueled Assembly," Proceeding of International Conference on Fast Critical Experiments and Their Analysis, Argonne National Laboratory (October 1966).
13. Edison, G. E., Bennett, L. L., "Discrete - Ordinate Transport Theory Calculations on the Effect of Heterogeneities on Reactivity in ZPR-3 Assembly 48," Trans. Am. Nuc. Soc. Vol. 10, No. 2 (1967).

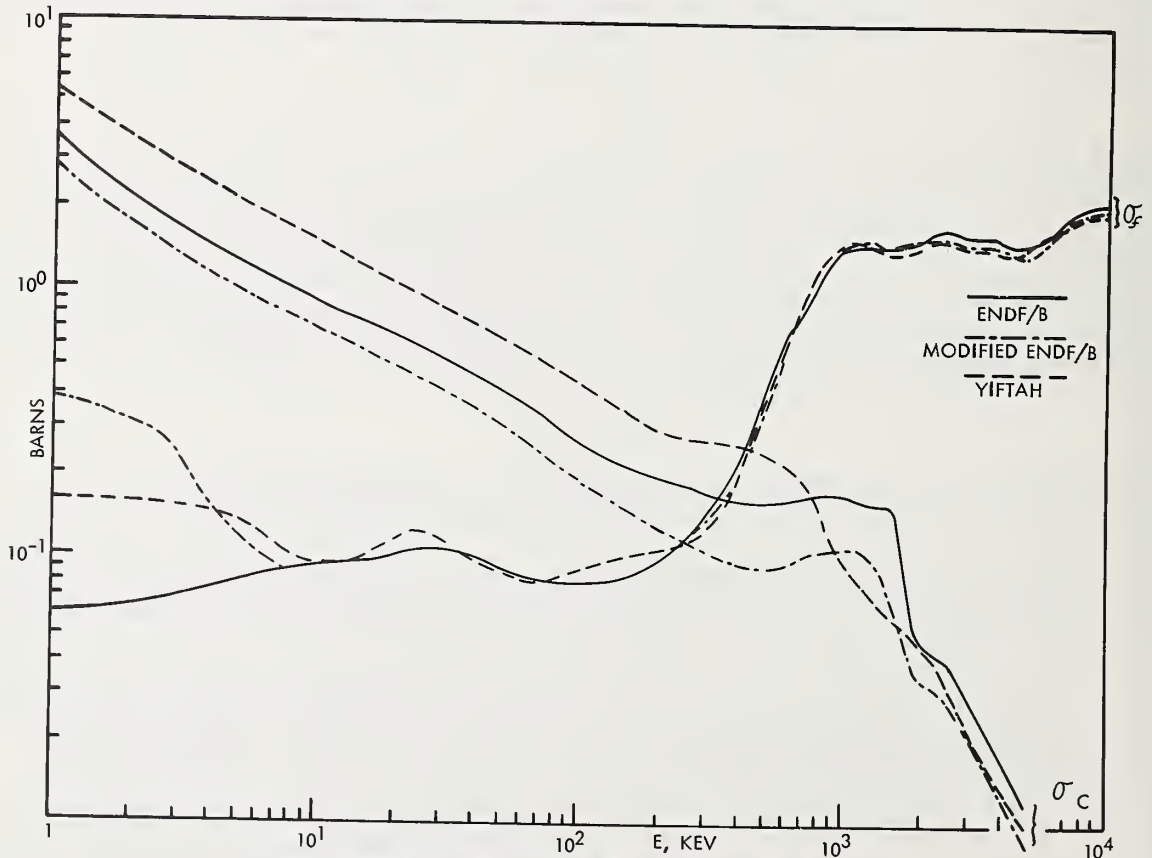


FIG. 1 FISSION AND CAPTURE CROSS SECTION OF Pu-240

TABLE 1 - Summary of Resonance Parameters in Pu-240 Evaluations

Parameters	Pu-240E		Pu-240M		Pu-240Y	
	E range 0-680 ev		E range 0-680 ev		E range 0-680 ev	
<u>Resolved Resonances</u>						
Γ_n	Refs. 7, 8		Refs. 7, 8		Ref. 7	
Γ_γ	Refs. 6, 7 $\langle \Gamma_\gamma \rangle = 0.030$ ev		Ref. 8 $\langle \Gamma_\gamma \rangle = 0.020$ ev		Ref. 7 $\langle \Gamma_\gamma \rangle = 0.032$ ev	
Γ_f	3 resonances - Refs. 5, 6, 9 E > 40 ev - smooth background from unresolved parameters		3 resonances - Refs. 5, 6, 9 E > 40 ev - Ref. 6		E < 120 ev - Ref. 10 E > 120 ev - $\Gamma_f = 0.00023$ ev for all resonances	
<u>Unresolved Parameters</u>						
$\langle \Gamma_\gamma \rangle$	$\langle \Gamma_\gamma \rangle = 0.030$ ev - all J		$\langle \Gamma_\gamma \rangle = 0.020$ ev - all J		$\langle \Gamma_\gamma \rangle = 0.032$ ev - all J	
$\langle D \rangle$ -level spacing	Refs. 6, 7, 8 0-310 ev $\langle D \rangle$ ($\ell=0, J=1/2$) = 16.0 $\langle D \rangle$ ($\ell=1, J=3/2$) = 9.65		All other unresolved parameters as for Pu-240E		Ref. 7 0-200 ev $\langle D \rangle$ ($\ell=0, J=1/2$) = 13.02 $\langle D \rangle$ ($\ell=1, J=3/2$) = 7.65	
Strength Function S_0 ($\ell=0$)	Refs. 7, 8 0-450 ev $S_0 = \frac{\Sigma \Gamma_n^0}{\Delta E} = 1.06 \times 10^{-4}$ ev $^{-1/2}$				Ref. 7 0-555 ev $S_0 = \frac{\langle \Gamma_n^0 \rangle}{\langle D \rangle} = 1.37 \times 10^{-4}$ ev $^{-1/2}$	
S_1 ($\ell=1$)	$S_1 = 1.75 \times 10^{-4}$ ev $^{-1/2}$ based on unresolved parameter fits to U-238 capture cross section				$S_1 = 2.5 \times 10^{-4}$ ev $^{-1/2}$ from U-238 evaluation of Schmidt(11)	
Fission Widths	$\langle \Gamma_f \rangle$ ($\ell=0$) = 0.00019 ev Estimated to fit average of Ref. 5 below 1 keV Typical $\ell=1$ values				$\langle \Gamma_f \rangle$ ($\ell=0$) = 0.00032 ev Fit $\langle \sigma_f \rangle = 0.16$ b at 200 ev Above 1 keV used following values for all J as obtained from fit to $\langle \sigma_f \rangle$.	
	$\frac{E(\text{keV})}{\Gamma(\text{keV})}$	$\frac{J=1/2}{0.010}$ 1.0 0.0060 25.0 0.013 0.0078 50.0 0.015 0.0090	$\ell=1$ values obtained assuming fission is dominantly p-wave. Fission widths obtained from Hill-Wheeler formula as adjusted to fit σ_f above 50 keV.		$\frac{E(\text{keV})}{\langle \Gamma_f \rangle}$ 1.0 0.00023 25.0 0.003 50.0 0.005	
Chi-squared Distributions	$\nu_n = \nu_f = 1$ for all J				$\nu_n = \nu_f = 1$ for all J	

TABLE 3 - Comparison of Calculation and Experiment for Assembly 48B

Experiment	Modified ENDF/B				ENDF/B			
	Pu-240M		Pu-240E		Pu-240M		Pu-240E	
k	ih/kg	σ_p^2	ih/kg	σ_p	ih/kg	σ_p	ih/kg	σ_p
Central Worths ⁴	1.000 ± 0.001		0.9808 (.999) ¹	0.9798 (.998)	0.9690 (.987)		0.9679 (.986)	
U-235	337 ± 4	2.87	418.0	2.884	431.0	2.851	434.0	2.883
U-238	-23.6 ± 0.7	0.203	-29.4	-0.2030	-32.9	-0.2207	-32.7	-0.2200
Pu-239	442 ± 7	3.83	539.0	3.747	542.0	3.715	555.0	3.746
Pu-240 ³	66 ± 40	0.572	96.2	0.671	94.7	0.640	83.6	0.567
Na	-6.3 ± 3.0	-0.0053	-6.89	-0.0046	-8.13	-0.0055	-1.83	-0.0012
C	-7.4 ± 1.8	-0.0032	-16.8	-0.0058	-19.9	-0.0069	-0.160	-0.0001
B-10	-8566 ± 50	-3.150	-9736	-2.834	-9632	-2.813	-10245	-2.899
Fe	-13.2 ± 0.6	-0.0267	-14.6	-0.0237	-14.8	-0.0242	-15.7	-0.0247

Central Reaction Rate Ratios Relative to U-235 Fission

U-238 Fission	0.0297 ± 0.0005	0.0296	0.0297	0.0294	0.0295
Pu-239 Fission	0.964 ± 0.010	0.929	0.930	0.911	0.911
Pu-240 Fission	0.229 ± 0.003	0.228	0.227	0.219	0.219
Pu-240 Capture		0.166	0.216	0.165	0.214
U-238 Capture		0.134	0.134	0.140	0.140

1. Eigenvalues in parenthesis include estimated corrections of 0.013 ± .003 Δk for heterogeneity⁽¹³⁾ and 0.005 ± 0.002 for transport theory corrections to diffusion theory.

2. Normalized to 2.87 for U-235.

3. Experimental worth value corresponds to 0.005 inch samples of 4.5% and 22% Pu-240 based on Assembly 48 sample size measurements.

4. Calculated worths converted to ih/kg using 1% Δk = 942 ih.

TABLE 4 - Comparison of Results for Assemblies 48 and 48B

	Assembly 48				Assembly 48B	
	Experiment		Mod. ENDF/B, Pu-240M		Pu-240 Density of 48	
	Assembly 48	48B/48	Assembly 48	Ratio 48B/48	Mod. ENDF/B, Pu-240M	Ratio Calc/48
k	1.000 ± 0.001	1.000 ± 0.001	0.9803	1.0005	0.9680	0.9999
Central Worths	σ_p		σ_p		σ_p	
U-235	2.79 ± 0.05	0.9943	2.80	0.968	2.78	0.977
U-238	-0.206 ± 0.04	0.952	-0.192	1.002	-0.209	0.993
Pu-239	3.72 ± 0.04	0.993	3.69	0.963	3.66	0.965
Pu-240	0.681 ± 0.20	0.90	0.698	0.913	0.561	0.952
Na ¹	-0.0051 ± 0.0035		-0.0044	0.994	0.0	-0.00246
Na ²	-0.0045 ± 0.0022					
C	-0.0019 ± 0.0005	1.61	-0.0057	0.971	0.0019	-0.0031
B-10	-3.13 ± 0.002	0.960	-2.78	0.967	-2.85	-2.90
Fe	-0.0240 ± 0.008	1.07	-0.0229	0.979	-0.0235	-0.0225

Central Reaction Rate Ratios Relative to U-235 Fission

U-238 Fission	0.0307	0.967	0.0308	0.961	0.0307	0.961
Pu-239 Fission	0.976	0.988	0.929	1.000	0.917	0.993
Pu-240 Fission	0.243	0.942	0.234	0.974	0.225	0.973
Pu-240 Capture			0.171	0.971	0.220	0.973
U-238 Capture	0.138		0.134	1.000	0.140	1.000

1. 0.42 inch diameter cylindrical sample.

2. 2.0 inch cube sample.

3. While experimental errors are not given, a 48B/48 ratio of unity lies within the quoted experimental errors for all measurements except U-238 and B-10.

Integral test of capture cross sections in the energy range

0.1 - 2 MeV

A. FABRY and M. DE COSTER

Centre d'Etude de l'Energie Nucleaire

Mol, Belgium

ABSTRACT

As a first step in a long term applied research programme under consideration in relation with the development of the German fast breeder prototype, capture cross sections averaged over the uranium-235 thermal fission neutron spectrum have been measured by the activation technique for a few nuclides; they most often were found to disagree with earlier similar studies.

The important features of the present method are briefly discussed. Included is a criticism of the uncertainties in the uranium-235 thermal fission spectrum itself, mainly based on recent integral studies and on new measurements of the ^{238}U (n, f) and ^{235}U (n, f) average cross sections using fission track detectors.

The resulting average capture cross sections are compared with evaluated differential data.

Careful integral experiments can offer a helpful supplement in the evaluation of the best microscopic [1] data basic for reactor calculations or for the assessment of nuclear reactions used to test these calculations via neutron spectrometry or spectral indices measurements [2].

In fast assemblies, this becomes particularly true in the upper neutron energy range where the detailed structure of excitation functions does no longer influence the behaviour of the reactor, for instance its reactivity, Doppler effect, neutron lifetimes, and so on.

If integral data such as critical masses [3] or spectral indices [4] are to be taken into consideration as independant contribution to the achievement of the often severe [5] accuracies requested on elementary nuclear parameters by pile designers, the conditions of these integral measurements must be sufficiently clean so that calculational methods are rigorously established.

One dimensional systems are ideal with this respect [1] [3]. Among these lines, a feasibility study of a long term programme [6] is under consideration within the framework of a collaboration between GfK (Karlsruhe), RCN (Petten) and CEN (Mol) for the development of the German breeder prototype. For what concerns nuclear data research, this programme ideally should cover two main goals :

- 1) the generation of a family of intermediate standard neutron spectra, aimed to measure spectral indices by the activation technique as well as the use of fission or α track detectors [7]; that part of the programme is especially directed towards :
 - a) the test of fissile reactions
 - b) the study of some structural materials of which most isotopes can be activated
 - c) the estimation of fission product capture cross sections using the statistical model of nuclear reactions (NEARREX [8] code) and experimental results from activable nuclides with neighbouring atomic masses.
- 2) A renewed application [6] of the spherical shell transmission technique [9] [10] using activation detectors and differential spectrometers, like the Li^6 (n, α) [11] and proton recoil proportional [12] devices : in the high energy range, non elastic group cross sections could be deduced for structural materials, while sophisticated transport calculations on especially selected arrangements are presently being runned to estimate if and to what an accuracy capture group cross sections could be deduced from the measured spectral perturbations.

A small mockup of such a flexible assembly has been realized in a spherical cavity (50 cm diameter) hollowed out of the protruding end of BR1 horizontal thermal column and is described elsewhere [6].

The cavity is now used for the development of techniques and the measurement of fission spectrum averaged cross sections, mainly for the (n, γ) process. The experimental method has been described previously. The main interesting feature remains the same : the reaction rate due to wall return neutrons is experimentally defined from a least square fit analysis of the distribution of the measured reaction rate versus distance to the fission source, using the fact that the wall return contribution presents a flat spatial distribution and that the pure fission spectrum component can be described analytically to a high degree of accuracy. The arrangement has been adapted for this spherical cavity and improved by decreasing to a minimum the amount of material present during the irradiations ; the fission source is now a 19 mm diameter, 2.25 mm thick enriched uranium oxide pellet clad with very thin stainless steel. Transport calculations have been performed in order to deduce the spectrum distortion due to inelastic scattering interactions within the source. The resulting corrections never exceed 3 %. On another hand, the contribution of reactor background neutrons is always negligible.

Figure I displays the physical arrangement. The 200 mg/cm² boron carbide screen is aimed to reduce the wall return contribution down to manageable proportions. Further improvements of the facility are planned. The capture cross sections measurements in that assembly generally disagree seriously with earlier data [14] [15]. In all irradiations, the reaction $^{115}\text{In} (n, n^{\gamma}) ^{115m}\text{In}$ has been used as a monitor [16] for determining the absolute fission flux [13]. Figure 2 illustrates the neutron energy range where most of the reaction rate takes place. The response function is defined here as :

$$I(E_0) = \frac{\int_{E_0}^{\infty} \Phi(E) \sigma(E) dE}{\int_0^{\infty} \Phi(E) \sigma(E) dE}$$

Previous integral measurements suggest that the WATT's [17] and similar analytical descriptions of the ^{235}U thermal fission neutron spectrum could be seriously inadequate below 1 MeV [18]. In order to increase the confidence in our preference for the new multigroup fission spectrum representation tentatively proposed by GRUNDL [18] and supported by our earlier absolute cross section measurements [13], it has been decided to redetermine the ^{238}U (n, f) and ^{235}U (n, f) average fission spectrum cross sections. The number of fission events produced in irradiated detectors has been related through a thermal flux calibration to the number of tracks created by fission fragments in 0.05 mm thick mica foils held tightly against the fission discs. Natural uranium and 90% enriched metallic discs accurately intercompared by mass spectrography (measurements performed at CBNM, Euratom, Geel) have been used in a first series of runs. By additional irradiations of uranium-aluminum alloys (20% weight content of 90% enriched uranium), it has been checked that no surface oxydation effects or variations in the escape probability of fission fragments with their mass distribution introduce systematical errors. All the data points obtained until now are plotted on fig. 3. Black and open circles distinguish the two kinds of fissile discs used in the case of the ^{235}U (n, f) reaction. As compared with the activation monitors, track detectors show poorer statistics; this limits the accuracy of present data, which will be improved by repeated runs. Table I presents our preliminary results. Within the error margin the choice of GRUNDL's multigroup fit is confirmed from the ratio of ^{238}U (n, f) to ^{235}U (n, f) cross sections, but the absolute figure found in the case of ^{238}U is higher than the value measured by LEACHMAN and SCHMITT [20] and supports the evaluated differential cross sections of HART [19]. The GRUNDL's representation has been accepted for the integral tests of capture cross sections, which are illustrated in fig. 4 and table II for some of the reactions studied until now. Again, a thermal flux calibration has been taken as a basis for the determination of reaction rates, in collimated beam as well as isotropic flux geometries, with spectra of known neutron temperature. However, when necessary, the thermal cross sections have been independently studied [21]. This is the case for the reactions ^{175}Lu (n, γ) $^{176\text{m}}\text{Lu}$ and ^{98}Mo (n, γ) ^{99}Mo . No figure was available for the first one while the error margin given in BNL-325 [23] was exceedingly high for the second one, where our result tends to confirm the measurements of CABELL [22]. The fast-slow coincidence technique on ^{239}Np [24] [25] has been applied in the case of the reaction ^{238}U (n, γ) ^{239}U . Only one run has been performed; the accuracy will be improved in the near future. The great discrepancy observed between integral and differential data for dysprosium is not understood presently. It is planned to use our data for a normalization of differential measurements and to compare with theory [8]. Systematic studies on a number of nuclides are in progress.

We would like to thank Mr. F. MOTTE, Head of the CEN-SCK Reactor Study Department, and Mr. J. DEBRUE, Head of the Reactor Physics Section, for their strongly encouraging support to this work.

We are especially indebted to Mr. F. COPS, Mrs. L. DELSA and Mr. D. LANGELA, for their active and continuous assistance during the measurements and interpretations.

It must be stressed in addition that without the help of G. BES, H. BERVOETS, R. BLYAU, R. BRAY and H. VANDERVEE, this work would have been impossible.

We finally thank Mr. V. GRAILET for his nice illustrations.

REFERENCES

- [1] RAKAVY, G., REISS, Y., SAMOUCHA, D. and YEIVIN, Y. : IAEA symposium on "Fast reactor physics and related safety problems", Karlsruhe (1967)
- [2] DAMLE, P.P., FABRY, A. and VAN DEN BROECK, H. : Report BLG-421 (1967)
- [3] GRUNDL, J.A. and HANSEN, G.E. : Nuclear Data for Reactors, Vol I, 321 IAEA (1967)
- [4] CECCHINI, G. and GANDINI, A. : IAEA Conference on "Fast reactor Physics and related safety problems" Karlsruhe (1967) Paper SM-101/31
- [5] SMITH, R.D. : Nuclear Data for Reactors, Vol I, 27 IAEA (1967)
- [6] FABRY, A. and VANDEPLAS, P. : IAEA Conference on "Fast reactor Physics and related safety problems" Karlsruhe (1967) Paper SM-101/25
- [7] MORY, J. : Report CEA-R 2846 (1965)
- [8] MOLDAUER, P.A., ENGELBRECHT, C.A. and DUFFY, G.J. : Report ANL 6978 (1964)
- [9] BETHE, H.A. et al : J. Nucl. En. 3, 207 (1956) ; 3, 273 (1956) ; 4, 3 (1957) 4, 147 (1957)
- [10] DAVEY, W.G. and AMUNDSON, P.I. : Nucl. Sci. Eng. 28, 111-123 (1967)
- [11] DE LEEUW-GIERTS, G. and DE LEEUW, S. : IAEA Conference on "Fast reactor physics and related safety problems" Karlsruhe (1967) Paper SM-101/45
- [12] BENNETT, E.F. : Nucl. Sci. Eng. 27, 16-27 (1967)
- [13] FABRY, A. : Nukleonik, 10 Band, 5, Heft, 280-282 (1967)
- [14] HUGHES, D.J., GARTH, R.C. and LEVIN, J.S. : Phys. Rev. 91, 6 (1953)
- [15] DRUZHININ, A.A., LBOV, A.A. and BILIBIN, L.P. : Soviet J. of Nucl. Phys. 4, 3, 366-368 (1967)
- [16] MENLOVE, H.O., COOP, K.L. and GRENCH, H.A. : Phys. Rev. 163, 1308 (1967)
- [17] WATT, B.E. : Phys. Rev. 87, 1037 (1952)
- [18] GRUNDL, J.A. : Nucl. Sci. and Eng. : 30, 39-53 (1967) and private communications
- [19] HART, W. : Report AHSB (S) R 124 (1967)
- [20] LEACHMAN, R.B. and SCHMITT, H.W. : J. Nucl. Eng. 4, 38-43 (1957)
- [21] FABRY, A. and JACQUEMIN, R. : Work to be published
- [22] CABELL, M.J. : AERE - R 3647 (1961)
- [23] STEHN, J.R. and al : AEC - Report BNL-325, 2d Edit. (1965)
- [24] TUNNICLIFFE, P.R., SKILLINGS, D.J. and CHIDLEY, B.G. : Nucl. Sci. and Eng. 15, 268-283
- [25] SEUFERT, H. and STEGEMANN, D. : Nucl. Sci. and Eng. 28, 277-285 (1967)
- [26] FABRY, A., LANGELA, D. : Private communication
- [27] OFFORD, S.M. and PARKER, K. : AWRE O-63/67
- [28] SCHMIDT, J.J. : Report KFK 120 (1966)
- [29] STUPEGIA, D.C., KEEDY, C.R., SCHMIDT, M. and MADSON, A.A. : IAEA Conference on Nuclear Data for Reactors, I, 520(1967)

Reaction	Average fission spectrum cross sections (mb.)		
	Absolute measurement	Computed from differential cross sections ^[16] ^[19]	
		WATT'S Analytical description	GRUNDL'S Multigroup fit
$^{115}\text{In} (n, n') ^{115m}\text{In}$	200 ± 10 ^[13]	182 ± 15	202 ± 16
$^{235}\text{U} (n, f) \text{ F.P.}$	1335 ± 130	1250 ± 25	1246 ± 25
$^{238}\text{U} (n, f) \text{ F.P.}$	353 ± 30	301 ± 9	336 ± 10

Table I. Further tests on the ^{235}U thermal fission neutron spectrum representations.

Reaction	Basic thermal cross sections (b.)	Average fission spectrum cross sections (mb.)		
		HUGHES ^[14] Renormalized	This work	Computed from differential cross sections*
$^{63}\text{Cu} (n, \gamma) ^{64}\text{Cu}$	4.4 ± 0.1 ^[26]	11.5	10.8 ± 2.5	10.6 ^{[26]**} 11.5 ^{[27]**}
$^{98}\text{Mo} (n, \gamma) ^{99}\text{Mo}$	0.120 ± 0.005 ^[21]	9.6	20 ± 1	28.9 ^{[28]**}
$^{164}\text{Dy} (n, \gamma) ^{165g}\text{Dy}$	2550 ± 75 ^[2]	—	23.3 ± 2.5	93.5 ^{[23]**}
$^{175}\text{Lu} (n, \gamma) ^{176m}\text{Lu}$	16.4 ± 0.9 ^[21]	104	185 ± 10	187 ^{[29]**}
$^{238}\text{U} (n, \gamma) ^{239}\text{U}$	2.73 ± 0.04 ^[23]	—	85 ± 8	75 ^{[23]**} 78 ^{[28]**}

* WEIGHTING SPECTRUM: GRUNDL'S FIT.

** REFERENCES FOR DIFFERENTIAL CROSS SECTIONS.

Table II. Average fission spectrum cross sections for some capture reactions.

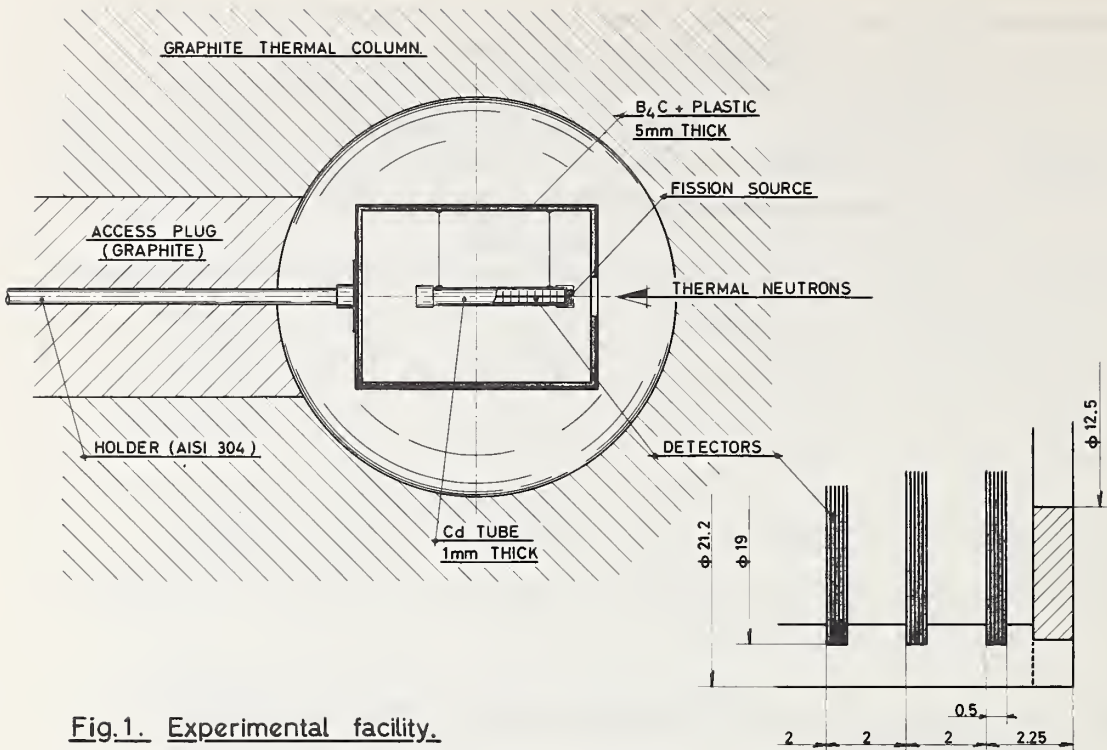


Fig.1. Experimental facility.

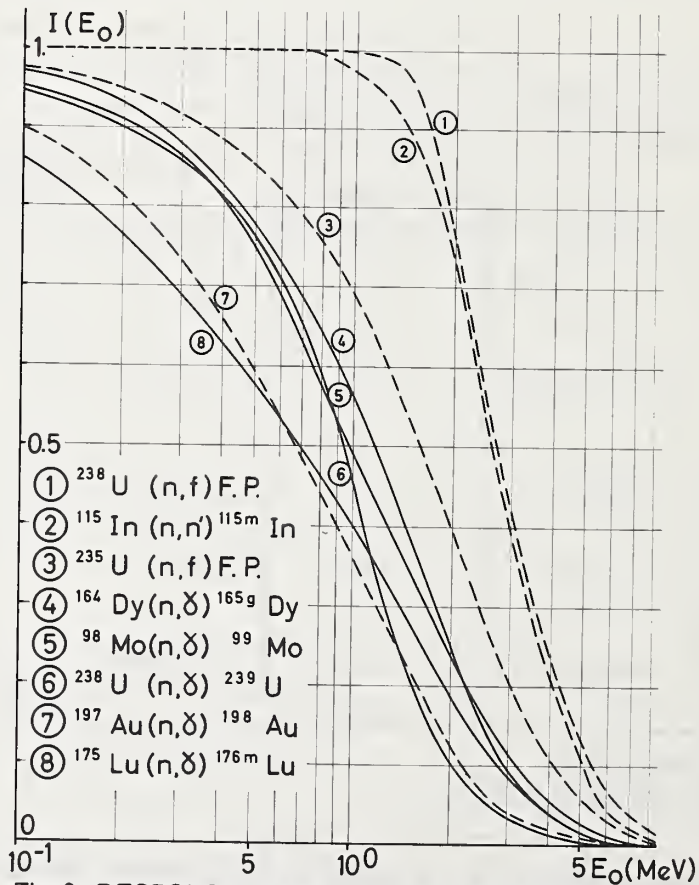


Fig.2. RESPONSE FUNCTIONS IN THE URANIUM-235 THERMAL FISSION NEUTRON SPECTRUM.

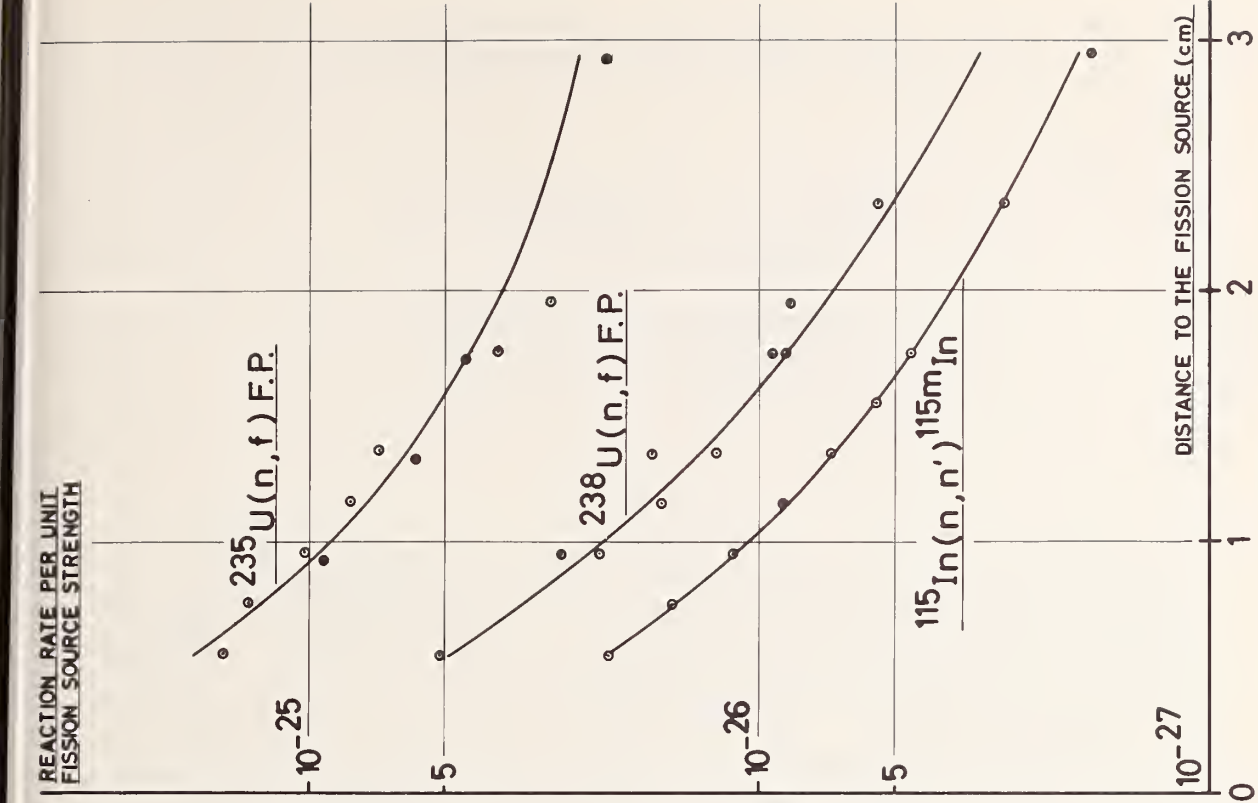


Fig. 3. Test of the ²³⁵U thermal fission neutron spectrum representation.

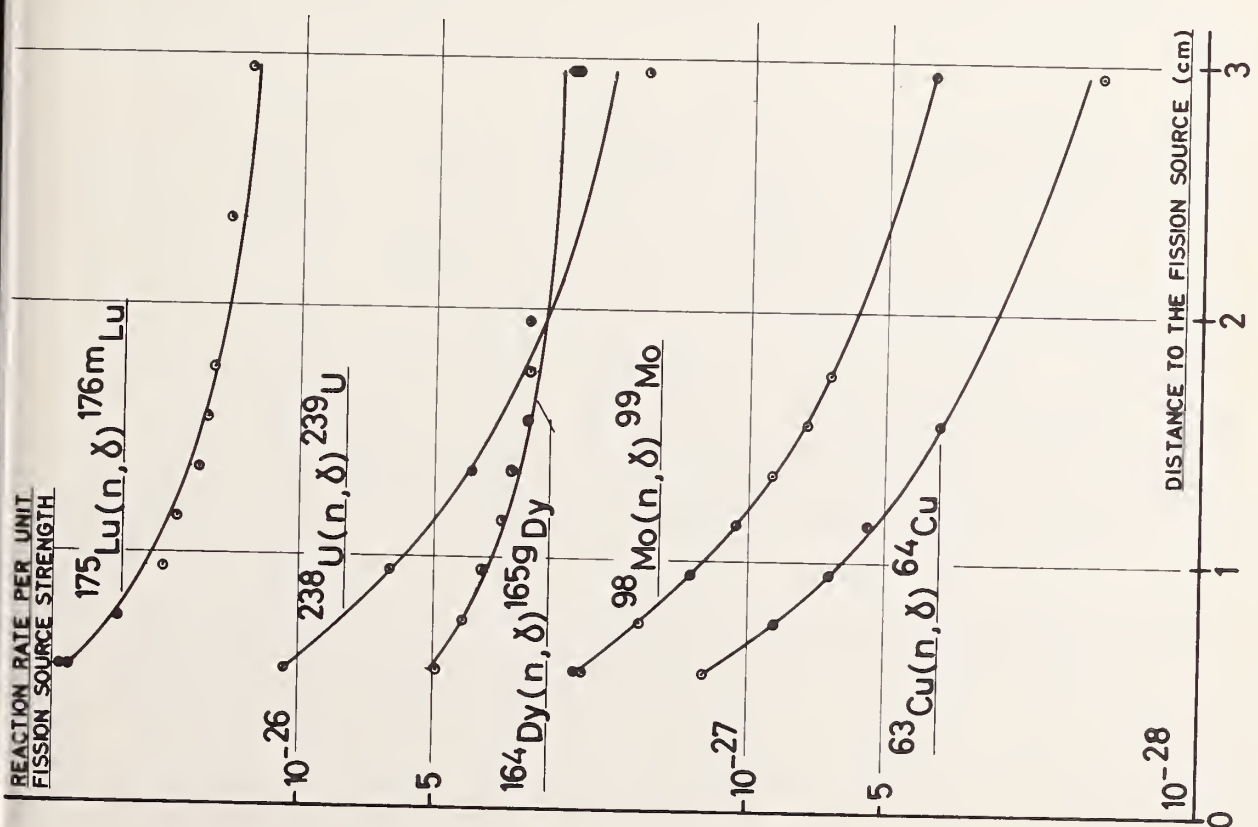


Fig. 4. Measurements of average fission spectrum cross sections.

^{238}Pu PRODUCTION PREDICTIONS
FROM AVAILABLE NEUTRON CROSS SECTIONS*

by

E. J. Hennelly, W. R. Cornman,
and N. P. Baumann

Savannah River Laboratory
E. I. du Pont de Nemours and Co.
Aiken, South Carolina 29801

ABSTRACT

^{238}Pu , a candidate heat source material, is the β -decay product of ^{238}Np ($T_{1/2} = 2.1$ d) that is made by neutron capture in ^{237}Np . ^{237}Np is a relatively stable irradiation byproduct formed in nuclear reactors either by $(n,2n)$ capture in ^{238}U or by successive neutron addition to ^{235}U . A self-consistent set of effective cross sections was derived that, with modern reactor codes, predicts production rates, product isotopic purity, and product yield for a range of thermal reactor spectra. The cross sections are based on existing data that were modified by activation measurements and by analysis of product formation in test sample irradiations.

Cross sections for the respective short-lived decay precursors, ^{237}U ($T_{1/2} = 6.75$ d) and ^{238}Np ($T_{1/2} = 2.1$ d) were measured in high flux test irradiations at Savannah River [$\phi > 10^{15}$ n/(cm²) (sec)]. Effective thermal neutron cross sections of ^{237}Np and ^{238}Pu were established by measuring product formation in test irradiations. Activation measurements with ^{236}U , a target precursor to ^{237}Np , indicated discrepancies in the reported value of the resonance integral. The fission cross section of ^{238}Np was independently verified by fission chamber measurements in a zero power test reactor using samples prepared at high neutron flux. The methods used, in some cases, lead to precise integral cross sections; in others, the results apply best to a particular reactor spectrum.

* The information contained in this article was developed during the course of work under Contract AT(07-2)-1 with the U. S. Atomic Energy Commission.

Lack of a measured absorption cross section for ^{237}U and insufficient knowledge of the ^{238}Np fission cross section prompted us to determine their effective cross sections. The cross section for 6.75 d ^{237}U was obtained [2] by comparing total ^{237}Np formed in two ^{236}U -rich targets simultaneously irradiated (9.3 d) at two known high thermal neutron fluxes [$>10^{15}$ n/(cm²)(sec)]. The ratio of ^{237}Np formed in the two samples was affected by capture in the short-lived isotope, ^{237}U , and an effective absorption cross section of 370 barns was derived. This cross section is relative to the effective fission cross section of ^{235}U of 502 barns and the effective absorption cross section of ^{237}Np of 152 barns. Two-group cross sections for this isotope were not determined.

The effective absorption cross section of ^{238}Np was measured by irradiating purified ^{237}Np samples for about 2 hours at a thermal flux of about 10^{15} n/(cm²)(sec). Losses due to ^{238}Np fission were determined by counting the gamma activity of ^{137}Cs , a fission product. A 6.54% ^{137}Cs fission yield, the average of the neighboring fissionable isotopes, was assumed. Exposure was determined by counting the gamma activity of ^{60}Co produced in calibrated cobalt-aluminum monitors. A capture-to-fission ratio of 0.066 was determined from the isotopic ratio of the resultant plutonium and the gamma activity of ^{137}Cs . The effective absorption cross sections listed in Table I relative to the absorption cross section of ^{237}Np were determined and in total confirmed the published fission cross section of ~1600 barns.

^{235}U fission cross section was chosen as a reference because ^{235}U is the principal fuel in most nuclear reactors. A consistent effective neutron flux can be defined in terms of the ^{235}U fission cross section [3].

$$\phi_{\text{fuel}} = K \cdot \text{megawatts per g } ^{235}\text{U}$$

$$\text{where } K = \frac{3.16 \times 10^{16} \text{ fissions/sec MW}}{(2.56 \times 10^{21} \text{ atoms } ^{235}\text{U/g}) (\sigma_f^{25} \text{ cm}^2/\text{atom } ^{235}\text{U})}$$

HAMMER cell calculations calculated the effective fission cross section of ^{235}U and also related the neutron flux in a target location to that in the fuel. Table I lists the effective cross sections and the best published values for 2200 m/sec cross sections and resonance integrals. The effective cross sections are thermal spectrum (Maxwellian) averages at $T \cong 80^\circ\text{C}$, corrected for resonance capture. Calculations of the ^{238}Pu yield are shown in Figure 1.

To confirm these calculated ^{238}Pu yields, samples of ^{237}Np were irradiated to different total exposures. Plutonium yields were measured by separate determinations of losses due to fissions and losses resulting from neutron capture in ^{238}Pu . Fission losses were determined by counting the gamma activity of ^{137}Cs , and capture losses from isotopic measurements of plutonium. The ^{238}Pu product yield equals the amount of ^{238}Pu divided by the amount of ^{238}Pu plus total losses or the total ^{237}Np burned up. These results are compared in Figure 1 with values calculated with measured fluxes and the effective cross sections in Table I. The good agreement between the calculated and measured ^{238}Pu yield verifies the two somewhat independent techniques and shows how cross sections must be adapted and tested to provide useful information.

The fission cross section for ^{238}Np was also determined from the ratio of ^{238}Np to ^{235}U fissions in a dual ionization chamber placed within the Savannah River Standard Pile (SP), a duplicate of the Thermal Test Reactor. The neptunium target, containing approximately 0.1% of ^{238}Np , was prepared from chemically purified ^{237}Np that was irradiated previously for ~ 8 hours at high flux. The background of residual ^{237}Np fissions was determined after the ^{238}Np ($T_{1/2} = 2.1$ d) had decayed. The alpha activity from ^{238}Pu formed by β decay of ^{238}Np was used to assay the ^{238}Np content of the fission foil at the time of measurement. Fission counts were also determined with combinations of cadmium and boron filters surrounding the ionization chamber to determine the resonance integral. The results are also listed in Table I. The effective cross section of ^{238}Np measured in the SP is quite close to the value derived from assays of irradiated samples, and, coincidentally, the neutron spectra did not differ greatly. The boron filter data suggests a strong resonance below 1 eV. The low value of the resonance integral relative to the thermal cross section suggests a relatively small dependence of the effective cross section with changes in neutron spectrum.

For ^{236}U , the ratio of the resonance integral to the thermal cross section is high (~ 70). Resonance self-shielding effects are important in calculating ^{237}Np production when relatively thick targets are used. Resolution of measured differential cross sections of ^{236}U [4] seems to give a total resonance integral of 300-350 barns from 0.5 to 384 eV, compared to the average

of directly measured total resonance integrals of about 400 barns [4]. A series of experiments was undertaken [5] to determine if the discrepancy could be ascribed to the unresolved energy region above 384 eV or whether it could be assigned to measurement errors in resolving the large resonance at 5.47 eV, which contributes over half of the total resonance integral. For this purpose, the infinite-dilution resonance integral was redetermined by counting the gamma activity of ^{237}U formed by irradiating ^{236}U -rich samples in the SP. Calibrated gold foils served as resonance and thermal neutron flux standards. The resonance integral of 419 ± 25 barns, determined relative to 1550 barns for gold, agreed with the previous average of 400 ± 40 barns. To determine the approximate energy distribution of the remaining difference between the integral and differential measurements, boron-shielded activation measurements were made. The results indicated that approximately 75% of the difference should be added to the measured 231 barns of the first resonance at 5.47 eV, and only 25% can be assigned to energies above 384 eV. The experimental basis for these conclusions is shown in Figure 2. The 18.8-eV resonance of ^{186}W served as a reference and verified the energy scale.

The authors gratefully acknowledge the assistance of C. J. Banick who made the chemical separations and sample analyses.

REFERENCES

1. J. E. Suich and H. C. Honeck, "The HAMMER System, Heterogeneous Analysis by Multigroup Methods of Exponentials and Reactors," DP-1064, E. I. du Pont de Nemours and Co., Savannah River Laboratory (1967).
2. W. R. Cornman, E. J. Hennelly, and C. J. Banick, Nucl. Sci. Eng., 31, 149 (1968).
3. E. J. Hennelly, Nucl. News, 8 (6), 19 (1965).
4. J. R. Stehn, M. D. Goldberg, R. Wiener-Chasman, S. F. Mughabghab, B. A. Magurno, and V. M. May, "Neutron Cross Section," Vol. III, BNL-325, Brookhaven National Laboratory (1966).
5. S. Pearlstein, "Cross Sections for Transuranium Elements Production," BNL-982, Brookhaven National Laboratory (1966).

TABLE I

CROSS SECTIONS FOR ^{238}Pu PRODUCTION

Nuclide	Effective ^(a)		2200 m/sec		Resonance	Integral	
	σ_a	σ_f	σ_a	σ_f	I(Abs)	Fiss/Abs	
	(barns)		(barns)		(barns)		
^{238}U	~12	0	5.6 ^(b)	0	~400 ±40	0.005	
^{237}U	372	2	(480) ^(c)	2	(290) ^(c)	---	
^{237}Np	152	0.02	169	0.02	850	0	
^{238}Np ^(d)	1620 ±100	1520 ±100	---	---	---	---	
	(e)	---	1640 ±150	---	2200 ±200	1500 ±500	1
^{238}Pu	382	12	563	16.3	169	0.14	
^{235}U	502	427	683	577	380	0.67	

(a) Heavy water reactor at 80°C.

(b) 6.0 ±0.4 obtained in resonance integral measurement.

(c) Assumes $\sigma(E)$ same as ^{235}U .

(d) From high-flux irradiations.

(e) From low-flux fission counter. Assumes $\sigma(E)$ dependence same as ^{235}U .

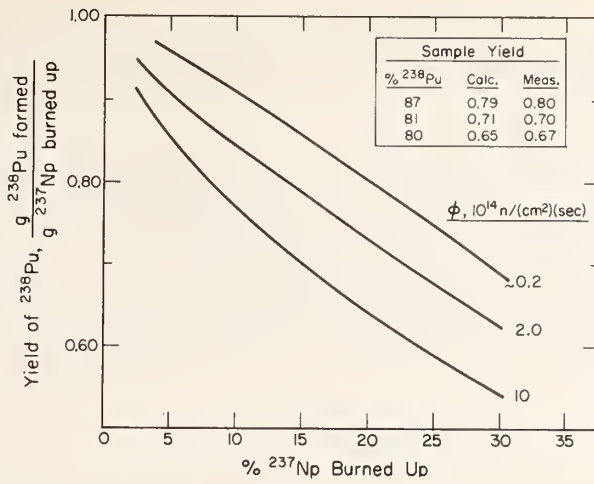


FIGURE 1 YIELD OF ²³⁸Pu

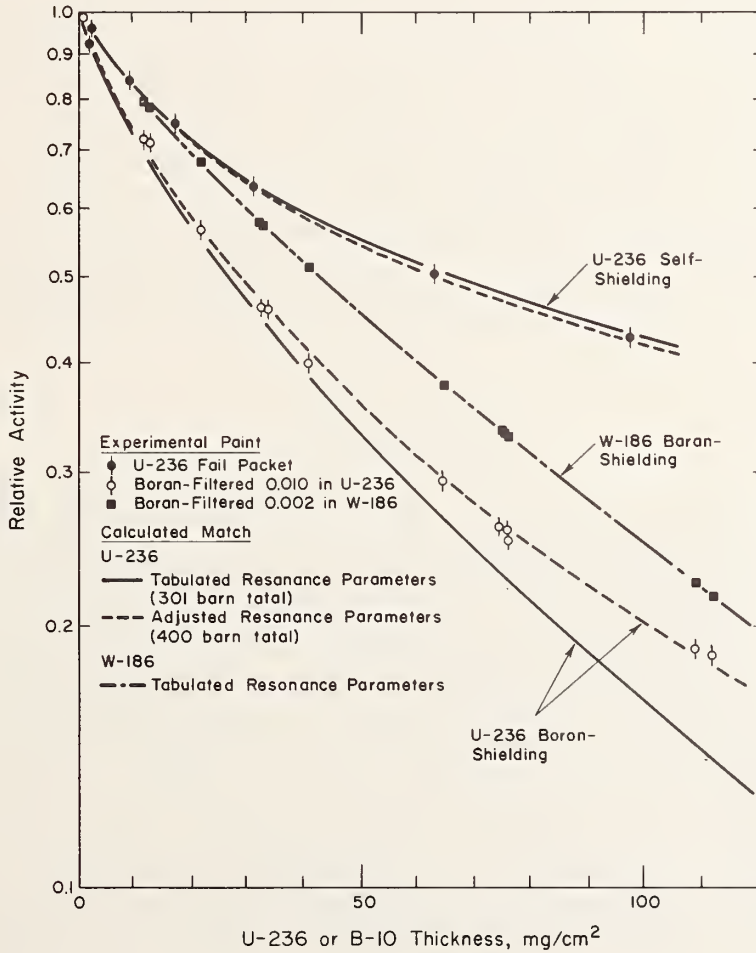


FIGURE 2 DEPRESSION FACTORS IN U-236 FOILS AS FUNCTION OF THICKNESS AND BORON-FILTER THICKNESS

FOIL MEASUREMENTS OF
INTEGRAL CROSS SECTIONS OF HIGHER MASS ACTINIDES*

by

R. L. Folger, J. A. Smith, L. C. Brown,
R. F. Overman, and H. P. Holcomb
Savannah River Laboratory
E. I. du Pont de Nemours and Company
Aiken, South Carolina 29801

ABSTRACT

Thermal and resonance integral capture cross sections were deduced for ^{242}Pu , ^{243}Am , ^{244}Cm , ^{245}Cm , ^{246}Cm , ^{249}Bk , ^{250}Cf , ^{252}Cf , and ^{253}Es from measurements of activation products in unshielded and cadmium-covered thin targets which were irradiated in high-flux charges at Savannah River. Analytical uncertainties in chemical yields were minimized by extensive use of mass spectrometry and alpha pulse energy analysis to determine isotope ratios. The nvt exposures were monitored by the $^{59}\text{Co}(n,\gamma)^{60}\text{Co}$ reaction. The capture cross sections for ^{242}Pu , ^{246}Cm , ^{249}Bk , and ^{252}Cf were used to complete the set of self-consistent cross sections for the chain ^{242}Pu through ^{252}Cf as described in the accompanying paper by J. A. Smith, et al.

1. INTRODUCTION

The high [$>10^{15}$ n/(cm²)(sec)] sustained thermal flux and relatively high [$>10^{14}$ n/(cm²)(sec)] epithermal flux in a heavy water moderated Savannah River reactor made feasible a series of activation experiments using newly available targets of higher mass actinides. Thin targets of several of these actinides were irradiated with and without cadmium covers to determine better thermal and epithermal cross sections for the precursors of ^{252}Cf , because published cross sections for these nuclides [1,2] did not give reliable predictions of yields after extended irradiations. Analysis of actinides and fission products allowed deduction of effective thermal and epithermal cross sections. These were translated to σ_{2200}

* The information contained in this article was developed during the course of work under Contract AT(07-2)-1 with the U. S. Atomic Energy Commission.

and resonance integral values by assuming an idealized spectrum and $1/v$ -behavior of cross sections in the thermal energy range.

2. PREPARATION OF TARGETS AND FLUX MONITORS

Targets were prepared by evaporating nitrate solutions of the purified actinide onto about 1 cm^2 of 0.001-inch-thick aluminum foil backing. 1-2 mg of actinide was deposited for the ^{242}Pu , ^{243}Am , and ^{244}Cm targets; and 1-2 μg for the higher mass targets. The flux monitors were 8-10 mg samples of ~ 0.1 wt % cobalt-aluminum wire wrapped in aluminum foil. The target foils were rolled into cylinders and sealed with the monitors in quartz ampoules, which were, in turn, enclosed in aluminum cylinders. For cadmium-shielded irradiations the aluminum cylinder was lined (sides and ends) with cadmium of thickness (20-125 mils) chosen to maintain thermal blackness throughout the irradiation.

3. IRRADIATIONS AND ANALYSES

The targets were irradiated at thermal fluxes from 1×10^{15} to $3 \times 10^{15} \text{ n}/(\text{cm}^2)(\text{sec})$ for 1 hr to about 1 month.

The irradiated target foils were dissolved in 3 to 6N NaOH and acidified to $\sim 3\text{M}$ with HNO_3 . ^{242}Pu and ^{243}Am were determined by isotope dilution-mass spectrometry. The curium isotopes were determined relative to ^{244}Cm or ^{246}Cm by mass spectrometry; these isotopes were determined by alpha pulse analysis. ^{249}Bk was determined by growth of its α -emitting ^{249}Cf daughter. The californium isotopes were determined relative to ^{252}Cf by mass spectrometry; ^{252}Cf was determined by alpha pulse analysis. The ^{253}Cf yield was measured by growth of its α -emitting ^{253}Es daughter; the yield of $^{254\text{m}}\text{Es}$ was measured by growth of its ^{254}Fm α -emitting daughter. Total fission was determined by gamma energy analysis of ^{137}Cs ; the assumed fission yield was 7% from ^{245}Cm [3] and ^{247}Cm , and 6% from ^{251}Cf .

4. INTERPRETATION OF DATA

Effective average cross sections are found by (1) deriving the equations for transformation by assuming constant flux and cross sections, (2) finding $\sigma\phi t$ values that match measured results, and (3) deducing ϕt values from cobalt monitor activations.

For this analysis, a reactor average, or effective, cross section is defined such that $\bar{\sigma}\phi_{th} = \text{reaction rate per atom}$. The neutron spectrum is assumed to be comprised of a Maxwellian thermal portion plus a $1/E$ epithermal portion (a very good approximation to the spectrum encountered in high flux charges at Savannah River). Cross sections are assumed to vary in the thermal energy range according to a $1/v$ law. Under these assumptions,

$$\bar{\sigma}\phi_{th} = \sqrt{\frac{\pi}{4}} \frac{T_0}{T} \sigma_{2200}\phi_{th} + \frac{1}{\ln E_{max}/E_c} I \phi_{epi},$$

where T is the reactor moderator temperature, and E_{max} (10 MeV) and E_c (0.5-1.0 eV) define the epithermal energy range. Effective cadmium cutoff energies, E_c , were derived from data in Reference [4] by using the mean thickness of cadmium during the irradiation. Self-shielding at resonances in ^{242}Pu , ^{243}Am , and ^{244}Cm was estimated from data in Reference [5].

Cross sections for ^{59}Co were taken as $\sigma_{2200} = 37$ barns and $I = 75$ barns [6]. Half-lives were taken from Reference [7] except for ^{243}Am , where a value of 7370 years [8] was used.

5. RESULTS

A summary of the irradiation histories is given in Table I. Cross sections deduced are listed in Table II. Special considerations involved in deriving some of the cross sections are itemized below.

^{243}Am : The epithermal flux in the shielded irradiation was deduced from the previously measured ^{244}Cm resonance integral because the cobalt flux monitor was defective. To provide a check on the ^{243}Am resonance integral, another value was deduced from yields in the shielded ^{242}Pu irradiation. The respective values were 2180 and 2320 barns.

^{244}Cm : The resonance integral was deduced from burnup in the shielded ^{244}Cm irradiation, while σ_{eff} and σ_{2200} values were deduced from yields in the unshielded ^{243}Am irradiation.

- ^{245}Cm : The capture/absorption ratio for the thermal cross section was estimated at 0.15 from the atom balance in the unshielded ^{243}Am irradiation, after allowing for fission contributions of ^{244}Am and ^{244}Cm . These data were inadequate for an unambiguous determination of σ_a or σ_c .
- ^{246}Cm : The resonance integral was deduced from yields of ^{247}Cm and ^{248}Cm at approximately constant ^{246}Cm concentration in the shielded ^{244}Cm irradiation, while σ_{eff} and σ_{2200} values were deduced from the burnup in the unshielded ^{246}Cm irradiation.
- ^{250}Cf : Cross sections for ^{249}Cf were assumed: $\sigma_a = 1550$ barns, $\sigma_c = 200$ barns in the unshielded ^{252}Cf irradiation, and $I_c \sim 0$ in the shielded ^{252}Cf irradiation.

6. CONCLUSION

The cross sections presented agree fairly well with published values for ^{242}Pu and ^{244}Cm , but differ significantly for ^{243}Am and several of the higher mass actinides. The recent availability of larger quantities of the higher actinides as well as higher fluxes of epithermal neutrons has made possible greater precision in the activation technique. These results are still relatively crude; refined computational techniques and additional activations with separated isotopes should give more precise values. However, the need for an experimentally verified set of cross sections for predicting reactor production of the higher actinides justifies early presentation of the data.

7. REFERENCES

1. S. Pearlstein, "Cross Sections for Transuranium Element Production," BNL-982, Brookhaven National Laboratory (1966).
2. E. K. Hyde, I. Perlman, and G. T. Seaborg, Nuclear Properties of the Heavy Elements, Vol. I, p. 371-3, Prentice-Hall, Inc. (1964).
3. H. R. von Gunter, K. F. Flynn, and L. C. Glendenin, Phys. Rev., 161, 1192 (1967).

4. C. H. Westcott, W. H. Walker, and T. K. Alexander, "Effective Cross Sections and Cadmium Ratios for the Neutron Spectra of Thermal Reactors," Proc. 2nd Intern. Conf. on Peaceful Uses Atomic Energy, Vol. 16, p. 70 (1958).
5. J. C. Stewart and P. F. Zweifel, "A Review of Self-Shielding Effects in the Absorption of Neutrons," Proc. 2nd Intern. Conf. on Peaceful Uses Atomic Energy, Vol. 16, p. 650 (1958).
6. M. K. Drake, Nucleonics, 24(8), 108 (1966).
7. C. M. Lederer, J. M. Hollander, and I. Perlman, Table of Isotopes, 6th Ed., John Wiley and Sons, Inc. (1967).
8. L. C. Brown and R. C. Propst, "A New Determination of the Half Life of ^{243}Am ," accepted for publication in J. Inorg. Nucl. Chem. 1968.

TABLE I

SUMMARY OF IRRADIATIONS

Target	Unshielded		Cd Shielded		E_c (eV)
	Initial Atoms	$\phi_{\text{th}} t$ (n/cm ²)	Initial Atoms	$\phi_{\text{ft}} t$ (n/cm ²)	
^{242}Pu	2.52×10^{18}	1.83×10^{21}	4.15×10^{18}	2.96×10^{20}	0.92
^{243}Am	1.93×10^{18}	4.32×10^{21}	1.99×10^{18}	8.8×10^{20}	0.83
$^{244}\text{Cm}^*$	-	-	4.68×10^{18}	1.02×10^{21}	0.83
^{246}Cm	2.77×10^{15}	1.93×10^{21}	-	-	-
^{249}Bk	2.55×10^{14}	3.65×10^{18}	4.22×10^{14}	5.74×10^{18}	0.55
$^{252}\text{Cf}^{**}$	1.14×10^{15}	1.73×10^{21}	2.30×10^{15}	3.42×10^{20}	0.92
^{253}Es	1.2×10^{13}	6.44×10^{18}	2.5×10^{11}	6.86×10^{18}	0.55

* Isotopic composition, mol % $\frac{244}{93.80}$ $\frac{245}{1.62}$ $\frac{246}{3.20}$ $\frac{247}{0.0566}$ $\frac{248}{0.018}$

** Isotopic composition, mol % $\frac{249}{0.92}$ $\frac{250}{13.72}$ $\frac{251}{3.39}$ $\frac{252}{81.97}$

TABLE IISUMMARY OF EXPERIMENTAL ABSORPTION CROSS SECTIONS
(barns)

<u>Nuclide</u>	<u>σ_{eff}</u>	<u>σ_{2200}</u>	<u>I</u>
^{242}Pu	28	20	1180
^{243}Am	90	78	2250
^{244}Cm	14	8.4	700
^{245}Cm	-	-	260
^{246}Cm	9.3	8.4	260
^{249}Bk	1150	1400	1240
^{250}Cf	1250	1500	5300
^{251}Cf	5300	6600	980
^{252}Cf	7.4	8.6	42
^{253}Es	200	130	3600

Capture/Absorption Ratios

^{244}Cm	0.96 est.	>0.95 est.
^{245}Cm	0.15	~0.5 est.
^{251}Cf	0.1	

REACTOR CROSS SECTIONS FOR ^{242}Pu - ^{252}Cf *

by

J. A. Smith, C. J. Banick, R. L. Folger,
H. P. Holcomb, and I. B. Richter[†]
Savannah River Laboratory
E. I. du Pont de Nemours & Co.
Aiken, South Carolina 29801

ABSTRACT

A self-consistent set of cross sections for nuclides in the chain ^{242}Pu through ^{252}Cf has been deduced from measured contents of ^{242}Pu samples exposed to nvt levels of 4 to 9×10^{22} n/cm² in a highly thermalized neutron spectrum. Some nuclides in the chain exhibit finite cross sections for fission as well as capture, so there are more cross sections to be determined than there are measurements. Independent measurements were used to complete the set.

1. INTRODUCTION

^{242}Pu was irradiated at Savannah River as part of the preparation for the transplutonium program in progress at Oak Ridge National Laboratory [1]. The exposures accumulated, approaching 10^{23} n/cm², were great enough to provide measurable quantities of heavier nuclides up through and in some cases beyond californium. Measured yields were used to deduce a consistent set of cross sections.

2. IRRADIATION

About 270 grams of ^{242}Pu were distributed among eight target slugs (0.94-inch diameter, 6.0 inches long) formed by compacts of PuO_2 and aluminum powders clad in aluminum. The plutonium density in the compact was 0.62 g/cc. The first slug was discharged and analyzed after an exposure of 4×10^{22} n/cm² and the last at 9×10^{22} n/cm². Two other slugs were discharged and analyzed at intermediate exposures.

* The information contained in this article was developed during the course of work under Contract AT(07-2)-1 with the U. S. Atomic Energy Commission.

† Present address: Cooper Union, New York City, New York 10003

The slugs were irradiated in a highly thermalized neutron spectrum, which had a thermal neutron temperature of 120°C and an epithermal-to-thermal flux ratio of 0.35 (the epithermal range is 0.625 eV to 10 MeV). The thermal flux and epithermal-to-thermal flux ratios varied by roughly a factor of 2 from start to end of a fuel cycle. However, constant values equal to the averages were used in analyzing the data because the fuel cycle time was short compared to total irradiation time. The thermal flux level was about 10^{15} n/(cm²)(sec).

3. CHEMICAL ANALYSIS

Four plutonium slugs were sampled by cutting 0.5-inch-thick wafers from the center of the slug. These wafers were measured and weighed, and then dissolved. Contents were analyzed by mass spectrometry and alpha pulse analysis, using the same techniques described in Reference [2].

4. INTERPRETATION OF DATA

A "principal" chain of reactions (Figure 1) was selected for analysis. Other reactions, although present, were not utilized to deduce cross sections either because the quantities involved were too small to permit meaningful measurements (e.g., the lower plutonium isotopes) or because their inclusion would complicate the analysis (e.g., the short-lived isotope at the end of each elemental chain).

In analyzing data, the four measurements of a given nuclide content were used to determine a single cross section by least squares fitting of a curve of content versus exposure. Such a technique allows just one cross section per nuclide to be determined from the data. But two cross sections per nuclide are needed where appreciable fission occurs.

The nvt exposure level of each sample had to be determined experimentally. This quantity can be derived from measured burnup of adjacent fuel plus a calculated target-to-fuel flux ratio. The nvt exposure can be determined more precisely by assuming a cross section for ²⁴²Pu and deducing exposure from ²⁴²Pu burnup. The latter method was used in the present analysis with the calculation from fuel burnup as a check for reasonable values.

The procedure adopted for analysis was to assume values for five cross sections, either from the foil data of Reference [2] or from the literature, and determine the remaining 11 cross sections in the principal chain from the slug data. Cross sections from open literature were used for the lower isotopes of plutonium, americium, curium, and californium that were not included in the principal chain. The beta transitions at ^{243}Pu , ^{244}Am , ^{249}Cm , and ^{250}Bk were assumed instantaneous.

5. CROSS SECTION CONVENTION

The cross section analysis uses an effective thermal cross section defined such that

$$\bar{\sigma} \phi_{\text{th}} = \text{reaction rate per atom.}$$

For the ideal case of a Maxwellian thermal distribution and a $1/E$ epithermal distribution,

$$\bar{\sigma} = \sqrt{\frac{\pi}{4}} \frac{T_0}{T} \sigma_{2200} + \frac{\phi_{\text{epi}}/\phi_{\text{th}}}{\ln E_2/E_1} I,$$

where E_1 and E_2 define the epithermal energy range (0.625 eV to 10 MeV). The average neutron spectrum encountered may be characterized by $T = 393^\circ\text{K}$ and $\phi_{\text{epi}}/\phi_{\text{th}} = 0.35$, although calculations using the HAMMER code [3] indicate some departure from a $1/E$ epithermal distribution, so that

$$\bar{\sigma} = 0.768 \sigma_{2200} + 0.022I.$$

Self-shielding at resonances was included in cases where resonance parameters were known.

6. RESULTS

Measured contents of the samples are itemized in Table I. Exposures (nvt) deduced from ^{242}Pu burnup and those calculated from fuel burnup and target-to-fuel flux ratios are listed in Table II. Cross sections are summarized in Table III, with a distinction being made between assumed and deduced values. Self-shielding at resonances was considered explicitly for those nuclides for which resonance integrals are listed in Table III. One result of this consideration is that some effective thermal cross sections vary with exposure. Another result is that a σ_{2200} value may be deduced from the measurements, if the relationship given in the preceding section is assumed.

This applies to ^{243}Am and ^{244}Cm . A qualitative indication of precision is shown in Figure 2.

7. REFERENCES

1. D. E. Ferguson, Nucl. Sci. Eng., 17, 435 (1963).
2. R. L. Folger, J. A. Smith, L. C. Brown, R. F. Overman, and H. P. Holcomb, "Foil Measurements of Integral Cross Sections of Higher Mass Actinides," presented at Conference on Neutron Cross Sections and Technology, National Bureau of Standards, Washington, D. C., March 4-7, 1968.
3. J. E. Suich and H. C. Honeck, "The HAMMER System, Heterogeneous Analysis by Multigroup Methods of Exponentials and Reactors," DP-1064, E. I. du Pont de Nemours and Co., Savannah River Laboratory (1967).

TABLE I

MEASURED CONTENTS OF ^{242}Pu SLUGS

Nuclide	Atoms at Discharge per Initial Atom of ^{242}Pu				
	Unirradiated	Irradiated Slugs			
		No. 1	No. 2	No. 3	No. 4
Np-237	.5 $\times 10^{-2}$	-	-	-	-
Pu-238	.49 $\times 10^{-2}$	<.3 $\times 10^{-4}$	<.8 $\times 10^{-5}$	-	<.6 $\times 10^{-7}$
239	.39 $\times 10^{-2}$.87 $\times 10^{-4}$.12 $\times 10^{-4}$.22 $\times 10^{-4}$	<.6 $\times 10^{-7}$
240	.184 $\times 10^{-1}$.575 $\times 10^{-3}$.445 $\times 10^{-3}$.112 $\times 10^{-2}$.91 $\times 10^{-3}$
241	.73 $\times 10^{-2}$.118 $\times 10^{-3}$.162 $\times 10^{-3}$.375 $\times 10^{-3}$.270 $\times 10^{-3}$
242	1.00	.511	.402	.276	.194
244	.46 $\times 10^{-3}$.164 $\times 10^{-2}$.202 $\times 10^{-2}$.205 $\times 10^{-2}$.221 $\times 10^{-2}$
Am-243		.127	.115	.086	.061
Cm-242		<.1 $\times 10^{-4}$			
243		.45 $\times 10^{-4}$			
244		.274	.371	.414	.426
245		.163 $\times 10^{-2}$.203 $\times 10^{-2}$.222 $\times 10^{-2}$.226 $\times 10^{-2}$
246		.761 $\times 10^{-2}$.152 $\times 10^{-1}$.250 $\times 10^{-1}$.356 $\times 10^{-1}$
247		.123 $\times 10^{-3}$.273 $\times 10^{-3}$.454 $\times 10^{-3}$.650 $\times 10^{-3}$
248		.614 $\times 10^{-4}$.192 $\times 10^{-3}$.504 $\times 10^{-3}$.954 $\times 10^{-3}$
Bk-249		.345 $\times 10^{-6}$.106 $\times 10^{-5}$.201 $\times 10^{-5}$.342 $\times 10^{-5}$
Cf-249					
250		.289 $\times 10^{-6}$.830 $\times 10^{-6}$.227 $\times 10^{-5}$.395 $\times 10^{-5}$
251		.656 $\times 10^{-7}$.203 $\times 10^{-6}$.485 $\times 10^{-6}$.767 $\times 10^{-6}$
252		.682 $\times 10^{-6}$.290 $\times 10^{-5}$.104 $\times 10^{-4}$.187 $\times 10^{-4}$
253		.821 $\times 10^{-6}$.481 $\times 10^{-7}$.102 $\times 10^{-6}$.317 $\times 10^{-6}$
254		<.4 $\times 10^{-10}$	<.4 $\times 10^{-11}$.15 $\times 10^{-8}$.51 $\times 10^{-8}$
Es-254		.26 $\times 10^{-10}$.71 $\times 10^{-10}$.13 $\times 10^{-9}$.39 $\times 10^{-9}$
255		-	-	.2 $\times 10^{-10}$.8 $\times 10^{-10}$

TABLE II

THERMAL NEUTRON EXPOSURES

Sample	Exposures, 10^{21} n/cm ²	
	²⁴² Pu Burnup(a)	Fuel Burnup(b)
No. 1	36.0	37
No. 2	48.6	53
No. 3	67.9	72
No. 4	85.2	85

(a) Match plutonium burnup assuming $\sigma_{2200} = 20$,
 $I_{\infty} = 1180$ for ²⁴²Pu.

(b) $(nvt)_{\text{target}} = (nvt)_{\text{fuel}} \times (\phi_{\text{target}}/\phi_{\text{fuel}})$.

TABLE III

CROSS SECTIONS(a)
(barns)

Nuclide	σ_{2200}		I_{∞}		$\bar{\sigma}$	
	Abs	Fiss	Abs	Fiss	Abs	Fiss
Np-237					155.	
Pu-238					387.	12.9
239					962.	673.
240					393.	
241					1170.	827.
242	20.		1180.		18.5-20.3 ^(b)	
Am-241					636.	2.4
242					2250.	2250.
242m					6210.	4660.
243	86.6*		1470.		98.6-82.3 ^(b)	
Cm-242					15.5	
243					738.	544.
244	14.5*	1.2	621.		24.7-13.0 ^(b)	0.9
245					2210.*	1880.*
246	8.7		103.		8.9-8.4 ^(b)	
247					457.*	409.*
248					5.4*	
Bk-249					1140.	
Cf-249					1550.	1350.
250					1090.*	
251					4970.*	3550.*
252					7.	
253					165.*	

(a) Asterisks (*) denote cross sections deduced from measurements. Others were assumed.

(b) Range reflects change in resonance self-shielding due to change in atoms/cc.

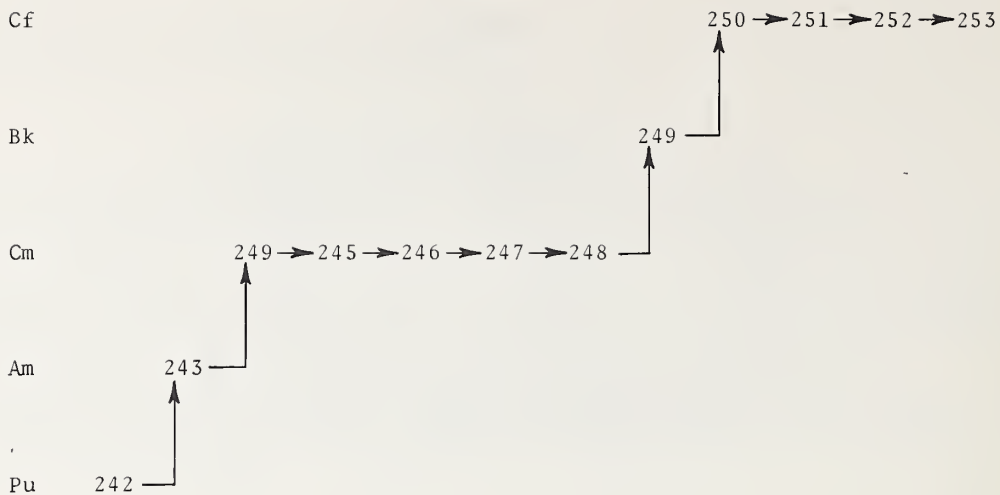


FIGURE 1 PRINCIPAL CHAIN OF REACTIONS ANALYZED

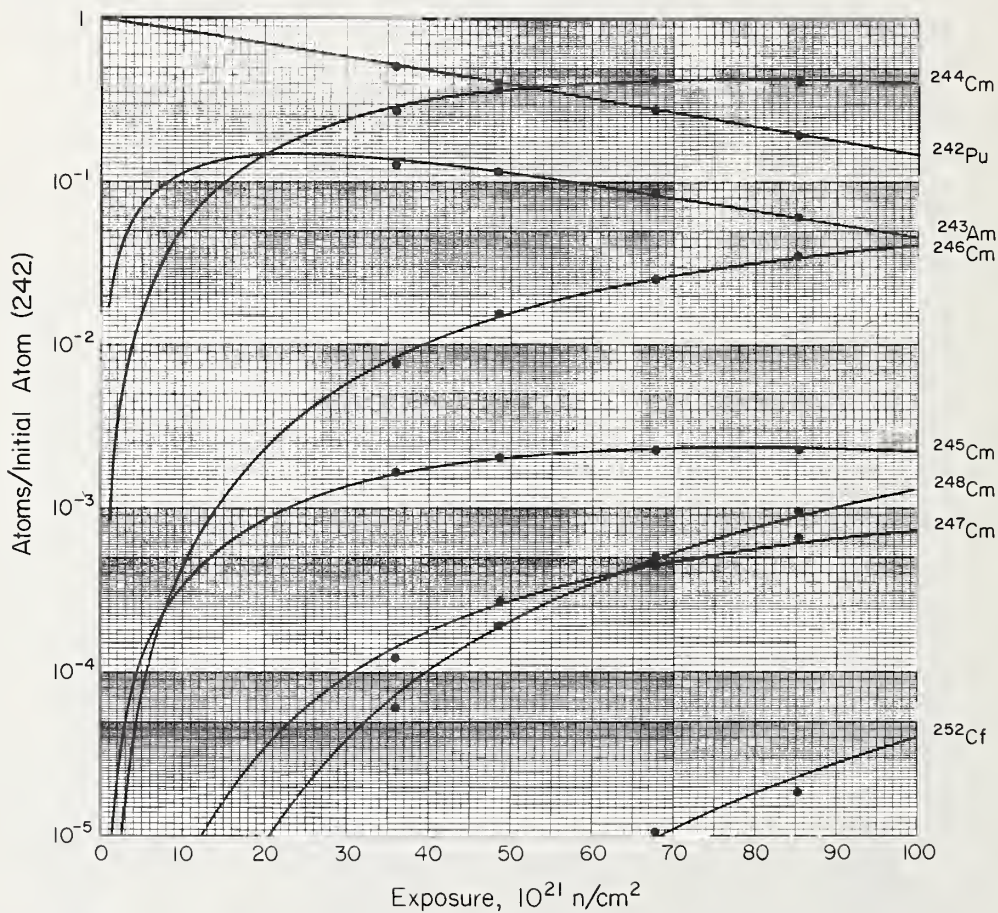


FIGURE 2 COMPARISON OF MEASUREMENTS WITH CONTENTS CALCULATED WITH DEDUCED CROSS SECTIONS

THERMAL REACTOR ABSORPTION
CROSS SECTIONS OF RADIOACTIVE NUCLIDES

R.S. Mowatt, W.H. Walker

Atomic Energy of Canada Limited
Chalk River Nuclear Laboratories
Chalk River, Ontario

A B S T R A C T

A depletion method for measuring absorption cross sections of radioactive fission products is described. For most radioactive fission products the method is capable of accuracies which lead to negligible uncertainties in reactivity calculations. Using this method the effective cross sections for thermal reactor neutrons of Pm-149 and Pm-151 have been determined to be 1000 ± 400 barns and < 700 barns respectively.

1. INTRODUCTION

The extent of neutron absorption by radioactive fission products with half-lives of about a day or greater for which the cross sections are not known is a major source of uncertainty in estimating the effect of fission products on the reactivity of thermal power reactors [1].

Radioactive fission products will only affect absorption significantly if $y\sigma\phi/\lambda$ exceeds some small value determined by the total absorption in the reactor. Here y is the fractional cumulative yield of a radioactive fission product having a cross section σ and decay constant λ . It is apparent that for a given yield the shorter the half-life (larger λ) the larger the cross section will have to be to have a significant effect. Table I lists radioactive fission products with half-lives greater than a day and unknown cross sections. The figure of merit was obtained using the simple criterion above. It is the value of the absorption cross section each requires so that its absorption is equivalent to a change of 0.2 millik in the reactivity of a well-moderated natural uranium reactor with a flux of 5×10^{13} n/cm²sec. For long-lived nuclides which will not come to equilibrium during the lifetime of the fuel in the reactor, the figure of merit is based on their calculated concentrations after an irradiation of 1 neutron/kilobarn. The accuracy of the depletion measurements described here is, like the figure of merit, a function of $\sigma\phi/\lambda$, so that by taking ϕ sufficiently large it is possible to make the uncertainty in the measurement smaller than the figure of merit.

2. DEPLETION MEASUREMENTS

Depletion measurements as a method of determining cross sections have been in use at least since the mid-1940's. In this method the decrease in the amount of nuclide due to irradiation is a measure of its absorption cross section. The method has most frequently been used by mass spectrometrists to measure absorption by stable or long-lived radioactive nuclides.

In the experiments described here we look for a decrease in the saturation γ -ray activity of radioactive nuclides produced by irradiation of naturally-occurring isotopes. Two samples are irradiated in sequence in the high flux irradiation facility in NRU, one for a period that is long compared to the half-life of the activity produced, which gives the saturation level of the activity for that flux, and one for a period short compared to the half-life, which gives the production rate in that flux.

3. THEORY OF ACTIVATION DEPLETION MEASUREMENTS

The equations for the simplified experiment described above can be derived easily. If N atoms of the parent stable nucleus are irradiated for a time t in a flux ϕ the decay rate, $n\lambda$, of the radioactive nucleus at the end of the irradiation is given by

$$n\lambda = N\sigma_p \phi \left(\frac{\lambda}{\lambda + \sigma\phi} \right) \left(1 - \exp(-\lambda t - \sigma\phi t) \right)$$

where it is assumed that σ_p , the stable nuclide cross section, is negligible compared to $\frac{1}{\phi t}$ and λ/ϕ .

Let the subscripts L and S denote the long and short irradiations respectively. If t_S is so short that $(\lambda + \sigma\phi)t_S \ll 1$ then

$$(n\lambda)_S = N\sigma_p \phi \lambda t_S.$$

On the other hand, if $(\lambda + \sigma\phi)t_L \gg 1$, the exponential is negligible and $n\lambda$ has its saturation value,

$$(n\lambda)_L = N\sigma_p \phi \lambda / (\lambda + \sigma\phi)$$

Thus the ratio of the two counting rates, R, for two samples irradiated as above is given by

$$R = (n\lambda)_L / (n\lambda)_S = \frac{(N\bar{\phi})_L}{(N\bar{\phi})_S} \frac{1}{t_S(\lambda + \sigma\bar{\phi}_L)}$$

and

$$\sigma\bar{\phi}_L = \frac{(N\bar{\phi})_L}{(N\bar{\phi})_S} \frac{1}{Rt_S} - \lambda$$

The relative uncertainty in the difference on the right of the equation will decrease as the difference increases, assuming the relative uncertainties in the two terms making up the right-hand side are fixed. Thus an increase in $\bar{\phi}_L$ will permit a more accurate determination of $\sigma\bar{\phi}_L$, and hence of σ .

A number of factors may make it necessary to modify this simple equation. First, the radioactive nuclide of interest may not be formed directly, but by short-lived β -decay of another nuclide which is so produced. The resulting hold-up can have a significant effect on the activity at the end of the short irradiation. It is also possible that the half-life is so long that it is not practical to carry the long irradiation to saturation, or there may be flux perturbations during the long irradiation so that $\bar{\phi}_L$ and $\bar{\phi}_S$ differ. The best method of properly taking these possibilities into account is to use a computer program that evaluates the exact integral equations for the actual condition of the irradiation, and for a range of σ values, and then to read the cross section from a plot of calculated activity ratio versus cross section.

4. MEASUREMENTS WITH ^{149}Pm and ^{151}Pm

These two nuclides were chosen for investigation because of their possible effects on transient fission product absorption following a reactor shut down, and on the accumulation of ^{149}Sm and ^{151}Sm in irradiated samples used for mass spectrometric fission product yield determinations or for reactivity measurements of accumulated fission product absorption. Fig. 1 shows the reactions involved in the irradiation of ^{148}Nd and ^{150}Nd , which yield ^{149}Pm and ^{151}Pm .

Samples - Samples were prepared by sealing from 10 to 100 μg of Nd_2O_3 enriched in ^{148}Nd and ^{150}Nd in quartz tubes about 1 cm long and 1.5 mm OD. These amounts were small enough to avoid significant flux depression in the samples. Relative contents of the capsules were determined by activation. All capsules were irradiated together for 1 minute at 10^{14}n/cm^2 sec and counted with the Ge(Li) diode detector described below.

Irradiations - Irradiations were in the high flux site ($\sim 3 \times 10^{14}\text{n/cm}^2$ sec) of the NRU pneumatic carrier facility. Samples of ^{148}Nd and of ^{150}Nd with a 1% Co in Al wire flux monitor were irradiated for 91.0 hours, followed immediately by a second set irradiated for 2.00 hours. Changes in the reactor flux were monitored from the signals of several ionization chambers installed in the reactor reflector and from the reactor power record.

Counting - An encapsulated Ge(Li) planar diode was used as the γ -ray detector. It is located near the bottom of a Pb shield, 40 cm high with 6 cm walls. Samples are positioned above the detector, and inside the shield by an automatic sample changer.

The resolution of the detector and pre-amplifier is 1.1 keV at 100 keV. Pulses are encoded and then recorded by a PDP-5 computer which also controls the counting cycle and data output.

Counting losses from the total energy peaks due to pulse pile-up in the amplifier were minimized by increasing the distance between sources and detector until dead time counting losses were less than 2%. For the long irradiation samples the earlier counts gave apparent decay rates significantly less than the later counts. These early counts were discarded. The final decay rates correspond to half-lives that are in excellent agreement with the best published values for ^{149}Pm and ^{151}Pm , namely 53.0 hrs and 28.3 hrs respectively. Peak areas were determined by summation over the peak and subtraction of the average background above and below the peak.

5. RESULTS

The flux during the two-hour irradiation was $2.55 \times 10^{14}\text{n/cm}^2$ sec from an ionization chamber comparison of the Co/Al wire activity with known standards and was constant according to the reactor record. From Cd ratio measurements the epithermal index $r\sqrt{T/T_0}$ (Westcott notation [2]) is about 0.004.

The 91 hour irradiation was interrupted by three short shutdowns in the first 45 hours and for this reason the flux ratio, ϕ_L/ϕ_S , is less than unity.

The results are summarized in Table II. All errors shown are standard deviations. The measured ratios of activities corrected to a fixed elapsed time after the end of each irradiation, are 3.108 ± 0.016 for ^{149}Pm and 4.63 ± 0.03 for ^{151}Pm . The calculated ratios for postulated cross sections from 0 to 1500 barns are:

σ (barns)	$R_{\text{calc}} (^{149}\text{Pm})$	$R_{\text{calc}} (^{151}\text{Pm})$
0	3.200	4.678
500	3.152	4.532
1000	3.105	4.473
1500	3.060	4.419

The errors are $\pm 1.0\%$ and 1.2% for the ^{149}Pm and ^{151}Pm calculated ratios, respectively arising mainly from the error in the relative sample size. The cross section corresponding to the measured ratios, and the cross section errors corresponding to errors in the measured and calculated ratios are:

<u>Nuclide</u>	<u>σ(barns)</u>	<u>error from measurement</u> (barns)	<u>error from calculation</u> (barns)
^{149}Pm	960	± 180	± 340
^{151}Pm	150	± 250	± 480

Taking the errors in quadrature and rounding off to the nearest 100 barns the final results are $\sigma(^{149}\text{Pm}) = 1000 \pm 400$ b and $\sigma(^{151}\text{Pm}) < 700$ b. The former is in reasonable agreement with the value of 1700 ± 300 b of Kondurov et al [3] obtained with an activation technique, and published after the present measurements had been started.

6. SUMMARY

A method has been described which permits the measurement of cross sections of radioactive fission products with sufficient accuracy to make negligible the uncertainties in calculating their effect in reactors. It has been used to measure the cross sections of ^{149}Pm and ^{151}Pm , both of which are significantly smaller than their figures of merit, 3000 b and 6600 b (for Pu-239 fuel) respectively, and therefore will not affect reactivity calculations for fluxes less than $\sim 10^{14}$ n/cm²/sec.

About 10 of the 15 cross sections still unknown for fission products with $T_{1/2} \gtrsim 1$ day should be measurable by irradiation of stable isotopes and use of the depletion technique described.

7. REFERENCES

- [1] WALKER, W.H. Proceeding of the Paris Conference on Nuclear Data for Reactors, I, 521 (Oct. 1966)
- [2] WESTCOTT, C.H., WALKER, W.H., and ALEXANDER, T.K., Proc. 2nd ICP UAE 16, 70 (1958)
- [3] KONDUROV, I.A., GRACHEVA, L.M., EGOROV, A.I., KAMINKER, D.M., NIKITIN, A.M. and POPOV, Yu. V. English Translation, J. Nucl. En. 20, 814 (1966)
- [4] RIDER, B.F., PETERSON, J.P., RUIZ, C.P., SMITH, F.R. USAEC report GEAP-4621 (1964)
- [5] HELMER, R.G., McISAAC, L.D., Phys. Rev. 143, 923 (1966)
- [6] BUNNEY, L.R., ABRIAM, J.O., SCADDEN, E.M., J. Inorg. Nucl. Chem. 12, 228 (1960)
- [7] HOFFMAN, D.C., J. Inorg. Nucl. Chem. 25, 1196 (1963).
- [8] ARTNA, A., LAW, M.E., Can. J. Phys. 38, 1577 (1960)
- [9] Nuclear Data Sheet 5-2-19 (1962) Recommended value.

TABLE I

RADIOACTIVE FISSION PRODUCTS WITH UNKNOWN CROSS SECTION

Nuclide	$T_{1/2}$ (days)	Figure ^a of Merit	Nuclide	$T_{1/2}$ (days)	Figure ^a of Merit	Nuclide	$T_{1/2}$ (days)	Figure ^a of Merit
⁹⁵ Zr	65	15	¹²⁵ Sb	950	1000	¹³² Te	3.25	450
⁹⁹ Mo	2.8	370	¹²⁶ Sn	~10 ⁷	300	¹³³ I	0.9	1120
¹⁰³ Ru	40	60	¹²⁷ Sb	3.7	8000	¹⁴⁷ Nd	11.1	270
¹⁰⁷ Pd	~10 ⁹	20 ^b	^{129m} Te	33	600	¹⁵³ Sm	1.96	11000 ^b
¹¹¹ Ag	7.5	5000 ^b	^{131m} Te	1.2	13000	¹⁵⁶ Eu	15	700 ^b

^aFigure of merit is hypothetical cross section in barns required by a particular nuclide to affect the reactivity of a well-moderated reactor fuelled with natural uranium (except where noted) by 0.2 millik in a flux of 5×10^{13} n/cm² sec.

^bFigure of merit applies to ²³⁹Pu fuel.

Table II

EXPERIMENTAL RESULTS AND INPUT DATA FOR RESULTS USED TO OBTAIN COMPUTED RATIOS

Pm-149 and Pm-151 Cross Section Calculation			
<u>Relative sample size</u>	<u>Sample</u>	<u>γ-ray counted</u>	$\frac{N_L}{N_S}$
	Nd-148	285 keV (Pm-149)	7.91 ± .10
		91 keV (Pm-147)	7.85 ± .10
	Nd-150	163, 168 keV (Pm-151)	3.70 ± .04
			7.88 ± .07
<u>Relative flux</u>			
	Co monitors - ion chamber		.943 ± .004
	- Ge(Li) detector		.941 ± .003
	Reactor data		.948 ± .010
			.942 ± .003
<u>Half-lives (hrs)</u>			
	<u>Nd-149</u>	<u>Nd-151</u>	<u>Pm-151</u>
	1.74 ± .01 [4]	0.20 [9]	28.40 ± 0.04 [6]
	1.73 ± .01 [5]		27.8 ± 0.5 [7]
Values used	52.8 ± 0.3 [8]		
	53.0 ± 0.1	0.20	28.3 ± .1
<u>MEASURED RATIOS OF ACTIVITIES</u>			
<u>Sample</u>	<u>γ-ray counted</u>	<u>R_{meas} (long/short)</u>	
Nd-148	285 keV	3.108 ± .016	
Nd-150	163, 168 keV	4.615 ± .035	
	177 keV	4.57 ± .06	
	275 keV	4.65 ± .06	
	340, 345 keV	4.662 ± .035	

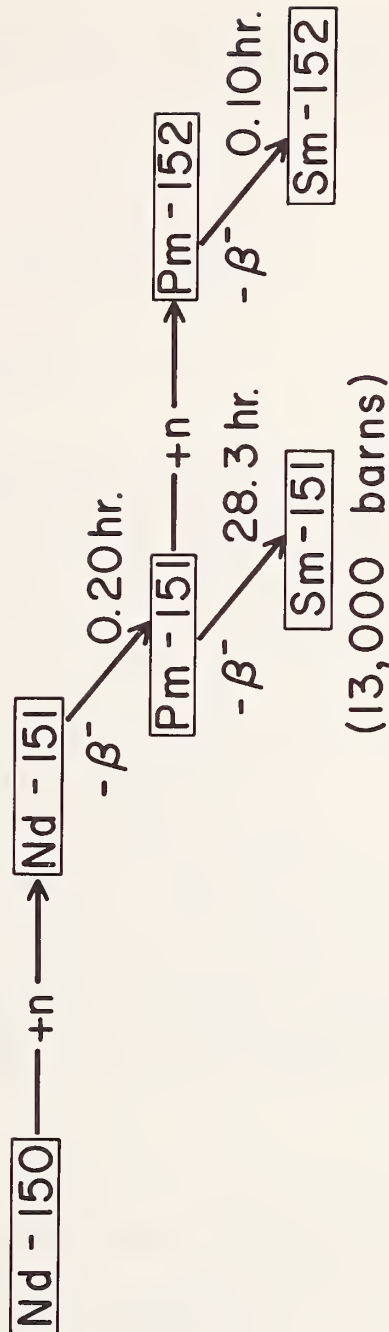
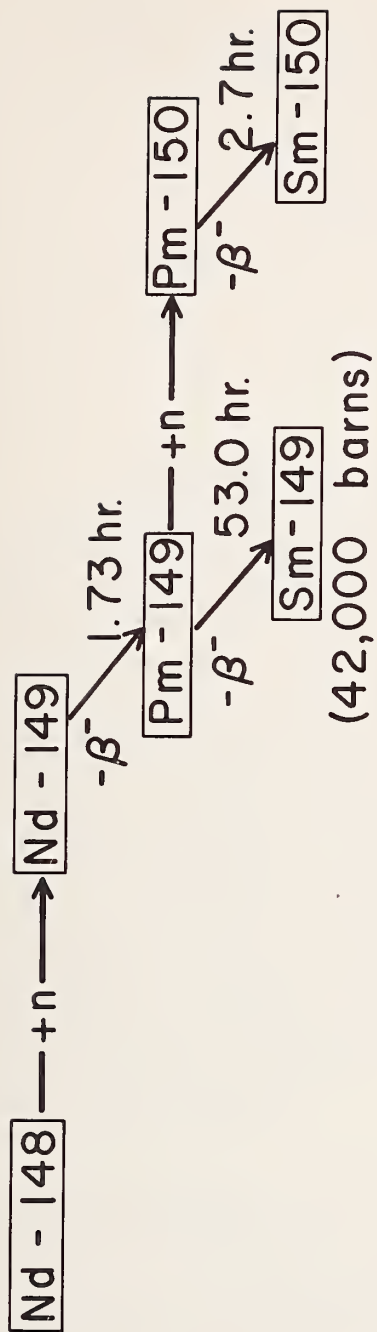


Fig. 1 Nuclear Reactions from Neutron Irradiation of ^{148}Nd and ^{150}Nd

The Decay of a Neutron Pulse in a Fast Nonmultiplying System*
as an Integral Check on the High Energy Inelastic Scattering

Tsahi Gozani and P. d'Oultremont**

Gulf General Atomic Incorporated
San Diego, California 92101

ABSTRACT

The early time behavior of the neutron population in a pulsed sphere of highly depleted uranium (50.8 cm diam) was measured with a neptunium-237 solid-state threshold fission detector. The decay, measured with one nsec time resolution showed an apparent exponential behavior over a relatively large time range. The measured decay was by no means asymptotic, as demonstrated by the fact that the decay constant was $(5.9 \pm 0.2) \times 10^7 \text{ sec}^{-1}$ at $R = 11.7 \text{ cm}$, and $(4.62 \pm 0.15) \times 10^7 \text{ sec}^{-1}$ at $R = 17.8 \text{ cm}$. Furthermore the decay at times longer than 100 nsec loses its exponential feature. A simple multigroup Monte Carlo code, BN-MOC, was used to compute the time response of the detector. Fairly good agreement with the measurement was obtained by using the measured target source, highly anisotropic scattering and the ENDF/B cross sections for ^{238}U . Additional calculations demonstrated the large sensitivity of the decay to variations in the inelastic scattering cross section of ^{238}U . Similar variations had a smaller effect on the steady state spectrum. The experimental and calculational results have shown the feasibility of using these techniques as a sensitive integral check on inelastic scattering in the low MeV energy range.

*This work supported by the U. S. Atomic Energy Commission.

**On leave from Belgo-Nucléaire, Brussels, Belgium.

1. INTRODUCTION

The measurement of the time dependence of the neutron population in a pulsed fast nonmultiplying medium provides means to investigate various types of interactions between neutrons and the medium under study. In many instances a specific interaction dominates over a certain time span. When a strong relationship exists between a particular interaction and the time behavior, the latter can be used as a valuable experimental integral check on the former. Such a relationship exists between the high energy inelastic scattering cross section in ^{238}U and the early time decay of the neutron population in a large ^{238}U assembly. Furthermore if the measurements are confined to the narrow region where the inelastic scattering is dominant e.g., by using proper threshold detectors the sensitivity of the measurements are enhanced. The results of measurements on a sphere of highly depleted uranium using a ^{237}Np threshold detector are described here and compared with a simplified Monte Carlo code.

2. EXPERIMENTAL RESULTS

The high energy neutron population was measured in a 20-in. diam depleted uranium sphere. The experimental details were described in Ref. 1. In essence, the measurements consist in determining the dieaway curve following a narrow neutron pulse (5 to 7 nsec wide) injected into the center of the sphere by the Gulf General Atomic LINAC. The neutron detector was a solid state detector incorporating a ^{237}Np conversion foil and very fast electronics. The ^{237}Np foil has a threshold fission cross section. Its cross section increases rapidly above 0.5 MeV and reaches a plateau value at about 1.1 MeV. Therefore, it is highly suitable for measurements of the inelastic scattering phenomenon in ^{238}U , which has similar large changes in the same energy region.

The time response of the ^{237}Np detector was measured at two locations over a time span of about 200 nsec; at longer time the countrate was extremely low. The time channels which were used, 1.024 nsec per channel, were fine enough to allow careful determination of all pertinent details. The gross features of the decay were determined with a wider channel, 31.166 nsec per channel. Special care was exercised to minimize the γ -flash problem and radio frequency pick-up, which is associated with neutron production by a linear accelerator. (1) Thus the measurements allowed the determination of the neutron buildup during the neutron (and gamma) burst as well as the decay. The results, corrected for small

dead time (due to the "shadowing" effect in the time analyzer) effects, are shown in Fig. 1. This figure and a more careful shape analysis, based on the time dependent logarithmic derivative indicate the existence of an apparent exponential behavior over a substantial part of the decay.

3. DESCRIPTION OF THE CODE

BN-MOC⁽²⁾ is a Monte Carlo code originally written to calculate the time and energy distribution of the leakage fluxes from bare non-multiplying and poorly moderating media which are pulsed by fast mono-energetic neutrons.⁽³⁾ Some recent modifications enable the code to analyze the time, space, and energy dependent scalar flux in cubes or spheres made of a single material. The cross sections and the external source spectrum are supplied according to the multigroup picture. The elastic scattering is treated exactly by using the experimentally available differential cross section. Furthermore, when such scattering takes place the exact energy change within each energy group is computed according to the simple collision theory. The effects of the inelastic scattering are taken into account by the multigroup transfer matrix, assuming that the angular distribution of the scattered neutrons is random and that the resulting velocity is the average velocity of the neutrons within the group; this average is computed assuming an infinite medium spectrum.

The code BN-MOC computes the spectrum of the scalar flux at each "detector" position for each time channel. The code then integrates these time-dependent spectra over the time variable furnishing the steady state spectrum at the different "detector" positions. In order to obtain also the time response of various detectors, the product of the time-dependent spectra, and the energy response of the detector is integrated over energy.

4. COMPARISON OF THE MONTE CARLO CALCULATIONS WITH EXPERIMENT

The GAM-II code was used to generate 20 broad group cross sections. The basic point-wise cross sections were obtained from the ENDF/B tape. The weighting function for the broad group cross sections was the steady-state spectrum in an infinite medium of ²³⁸U. The same weight function was used to generate the broad group fission cross section of ²³⁷Np which is proportional to the efficiency of our detector.

The calculated time response of a spherical ²³⁷Np detector in two locations, R = 11.7 cm and R = 17.84 cm, is compared with the experimental results in Fig. 1. The correct amplitude variation of a point

detector in the two locations is given by multiplying the response at position $R = 17.84$ by 0.33 . This factor is the ratio of the surface area of the spherical shell detectors at $R = 11.7$ cm to that at $R = 17.84$ cm.

All the basic features which are experimentally observed are also reproduced by the calculations.

1. Exponential decay is observed. The graphically fitted decay constant α , at radius 11.7 is $5.5 \times 10^7 \text{ sec}^{-1}$ and is identical to the calculated value. At the position $R = 17.8$ the decay is slower. The fitted α is $4.4 \times 10^7 \text{ sec}^{-1}$, vs the experimental value of $4.7 \times 10^7 \text{ sec}^{-1}$.
2. The shift in the time to reach the peak of the buildup is about 15 nsec between $R = 11.7$ cm and $R = 17.8$. There is good agreement in this value between measurement and calculation.

Careful examination of the Monte Carlo results shows some obvious deficiencies which warrant corrections. It seems that the deviation from the exponential behavior at large radii is less obvious in the calculation than the measurements. This deficiency becomes pronounced when one compares the time dependence of non-threshold detectors like ^{235}U . In that case the Monte Carlo calculation predicts the correct decay up to about 200 nsec and much faster decay at longer times. Furthermore the discrepancy between measurement and calculation increases with the radius.

A plausible explanation for this is the inadequacy in the description of the multiple inelastic scatterings (within the energy group) with small energy loss. These processes, assume higher importance at large distances from the source and at longer times.

5. SENSITIVITY STUDY

It is quite evident on physical grounds, as was argued in the Introduction, that the early time behavior of the neutron population depends on the inelastic scattering. However, the usefulness of the measurement of this decay as an integral check on the inelastic scattering depends to a large extent on the sensitivity of the former to variations in the latter.

It is quite difficult to devise a unique sensitivity check of integral quantity to variations in cross sections in fast reactors. However, in order to have a general idea, we have chosen to calculate the time response of a ^{237}Np detector in various locations in a ^{238}U sphere which

had 20% higher (as compared to ENDF/B) inelastic scattering cross sections, σ_{in} , in all groups. But in order to keep the total collision probability unchanged, the elastic scattering cross sections were reduced by 20%. At the two positions, the calculated decay curves are substantially faster. At $R = 11.7$ cm the fitted decay constant is faster by about 20%, i. e., $\alpha = -6.8 \times 10^7 \text{sec}^{-1}$, whereas at $R = 17.84$ cm, though with poorer statistical precision, it is 10% faster, i. e., $\alpha = -4.8 \times 10^7 \text{sec}^{-1}$.

It is plausible that the sensitivity of the decay to variations in σ_{in} at large distances from the source is reduced as a result of the competition of the elastic scattering.

The calculation elucidates another gratifying fact, namely that the decay, except for the first few nsec, is not affected by details of the energy distribution of the external source. This was shown by comparing a calculation with a monoenergetic source of $E_0 = 1.5$ MeV to other calculations which incorporated the measured distributed U-target source. (6) There is no observable difference in the decay curve apart from the first few channels. The steady state spectrum, on the other hand was strongly modified at the energy region around 1 MeV.

6. CONCLUSIONS

The measurements and the calculations described above demonstrate that the early time decay of the neutron population in the energy region above a few hundred keV is a sensitive integral check on the inelastic scattering of uranium in that region.

The method is basically simple. From the experimental point of view it inherits the simplicity and reliability of the dieaway technique, though care should be exercised to avoid systematic experimental errors. (1)

The Monte Carlo method of calculation used here for comparison is quite general and powerful. Nevertheless, great simplicity is obtained as compared to the more sophisticated Monte Carlo codes such as O5R, (5) if the one-dimensionality and symmetry of the system and a multigroup approach are incorporated in the code. These features make BN-MOC a simple and versatile tool to be used for checking cross sections sets against experimental results.

The calculations have demonstrated the important fact that the decay does not practically depend on the energy distribution of the source. This means that the precise knowledge of the source distribution is not needed for the interpretation of the experimental data.

The calculations and experiments showed the inseparability of space and time in the early time domain and the over-all non-asymptotic feature of the decay. As pointed out in Ref. 3 these facts cast some doubts on the interpretation of some measurements of the decay of a neutron pulse in non-multiplying media^(7, 8) which are based on the concept of buckling and the separability of space and time.

The present method does not make use of any approximation such as the diffusion approximation in the description of the basic processes except for the multigroup approach and simplified treatment of the fission process.

Though the Monte Carlo method furnishes the most detailed comparison with the kinetic experiment, some integral quantities of the latter can be calculated by other means. The most useful integral quantities in this respect are the time moments which can, in principle, be computed with the best available steady state transport codes.⁽¹⁾ The use of time moment necessitates high statistical precision at long times after the neutron burst. At these times the neutron spectrum is strongly degraded and the population is small. It is clear, therefore, that this quantity can specifically be useful for integral studies of the neutron interactions in the unresolved resonance region. This will be investigated later on.

7. REFERENCES

1. T. Gozani, "Experimental Determination of the Kinetic Behavior of Highly Depleted Uranium Sphere," Gulf General Atomic Report GA-8465 (1967).
2. P. d'Oultremont, "BN-MOC, A Simple Monte Carlo Code for Fast Non-Multiplying Systems," unpublished (1965).
3. G. Deconnick, P. d'Oultremont and M. Stievenart, "Contribution to the Study of Fast Neutron Non-Multiplying Assemblies by the Pulsed Neutron Technique," (SM-6414) IAEA Symposium on Pulsed Neutron Research, Vol. II, Vienna 1965.
4. K. D. Lathrop, "DTF-IV, A FORTRAN-IV Program for Solving the Multigroup Transport Equation with Anisotropic Scattering," LASL Report LA-3373 (1965).
5. D. C. Irving, R. M. Freestone, Jr., F. B. K. Kam, "O5R, A General Purpose Monte Carlo Neutron Transport Code," ORNL Report, ORNL-3622 (1965).
6. J. R. Beyster, et al., "Integral Neutron Thermalization, Annual Summary Report, October 1, 1966 through September 30, 1967," USAEC Report GA-8280, Gulf General Atomic Incorporated (1968).

7. L. E. Beghian and S. Wilensky, "The Pulsed Neutron Technique Applied to Fast Non-Multiplying Assemblies," (SM-62/74) IAEA Symposium on Pulsed Neutron Research, Vol. II, Vienna 1965, and L. E. Beghian, *et al.*, *Nucl. Sci. and Eng.* **27**, 80-84 (1967).
8. H. Miessner and E. Arai, "Zur Absolutmessung von Effectiven Neutronen wirkungsquerschnitten im Kev-Gebiet mit einer Schellen gepulsten Anordnung," *Nukleonik*, **8**, 8 (1966).

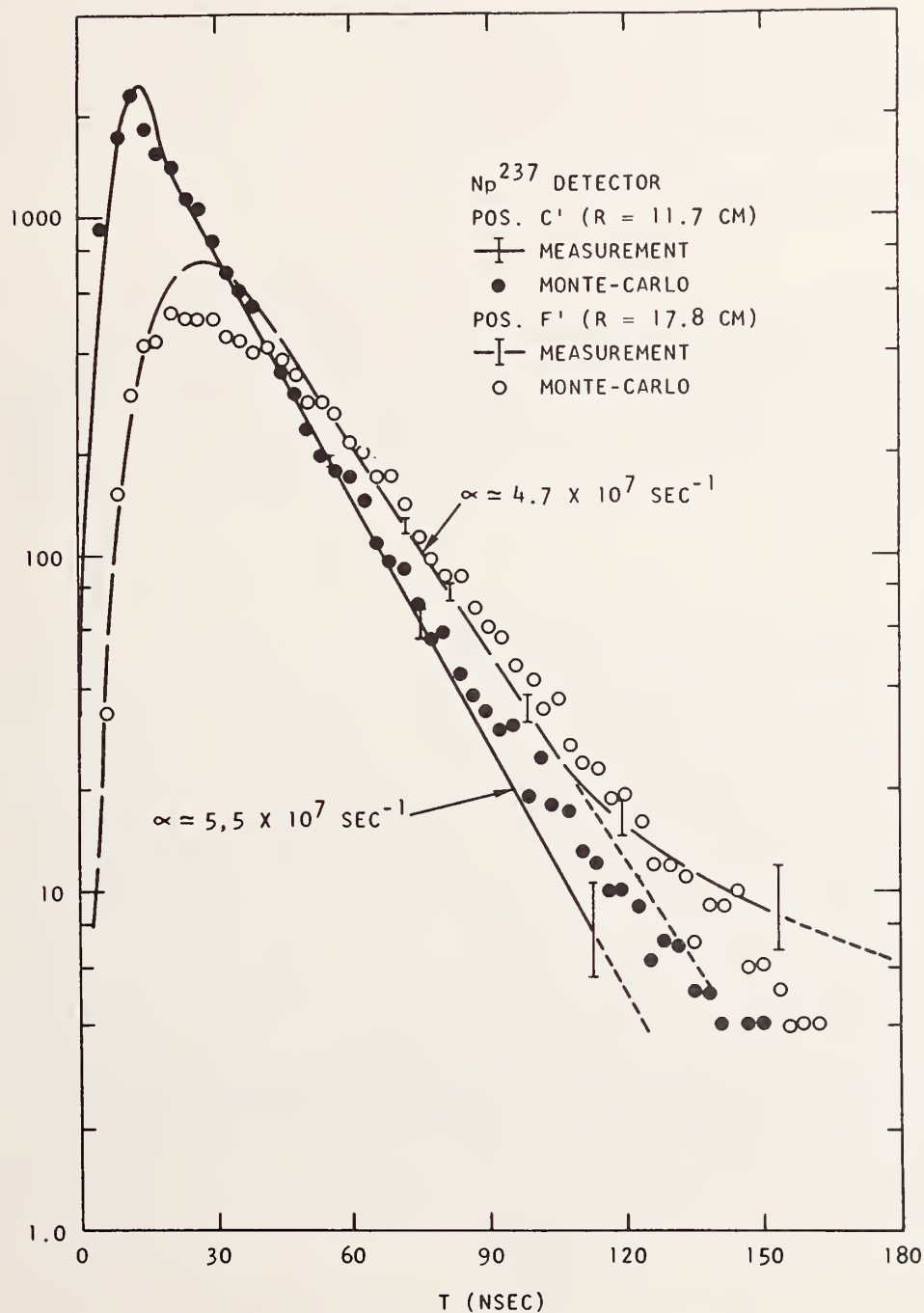


Figure 1. High energy ($E \geq 0.6$ MeV) neutron decay in 20 in. diam ^{238}U sphere.

THE PANEL DISCUSSION SUMMARIZING THE
NEUTRON CROSS SECTIONS AND TECHNOLOGY CONFERENCE

W. W. Havens, Columbia University, Chairman

Participants:

H. Goldstein	Columbia University
H. Kouts	Brookhaven National Laboratory
A. Radkowsky	Naval Reactors Branch, AEC
R. Taschek	Los Alamos Scientific Laboratory

W. W. Havens (Chairman):

"Each Panel Member will review and summarize the highlights of a particular session of the program and then, there will be general comments from the members of the panel about the most significant ideas discussed at the meeting as a whole. After members of the panel have made their comments, there will be comments and questions from the floor. Dr. Taschek will discuss Sessions A and B."

Dr. Taschek:

"Listening to Dr. Fowler's paper on nucleosynthesis, I suddenly realized that it would be a different generation that would be worrying about the cross sections and evaluations for fusion power reactors. Fowler was, after all, talking a little bit about fusion power reactors to produce the neutrons to form his nuclei. We moved very quickly out of that rather esoteric field into more conventional problems which gave an indication of what the remainder of the meeting was to be concerned with. My strongest reaction about cross sections associated with shielding, is that this is one area that stretches beyond Davey's comment (in Session H) of not being interested in the energy region above 1 MeV. Shielding both is concerned with energies up to and above 15 MeV and also provides the major application of our knowledge and interest in the effects of gamma radiation. Though not having been very much exposed to the solid state interest in nuclear reactions, I have realized that this important aspect may become even more so if we ever do develop fusion power reactors, in addition to plutonium

breeders. Although Wechsler developed a very beautiful theory in that area, there is really quite a large discrepancy between the effect, as observed, and the theory. I believe that Wechsler pointed out that there were differences of a factor of two to three in the calculated over what was observed, fortunately in the right direction, namely less damage than expected by a rather large amount. Wechsler suggested that clustering might be a cause of this discrepancy, which indicated an area for further development in this field.

"Session B dealt with cross sections that are used for standards. These cross sections have a large number of other standards associated with them which I will not attempt to discuss, such as the problems of how to make an accurate weighing of the number of fissionable atoms in a foil and so on. The problems here are real and the question kept recurring as to why don't we know these cross sections better? In fact, I think we measurers deserved Davey's criticism when he said that he did indeed need to know cross sections better and in the energy region below 1 MeV, more specifically from 100 kilovolts to 1 keV.

"I want to point out that this is a region in which we have been able to make accurate cross section measurements for only the past few years. The stimulus for this work came from a meeting at Harwell five or six years ago which identified that our worst known region at that time was between 1 and 100 kilovolts and it was largely as a result of that meeting that much work has been done since then as has recently appeared. However, I am afraid that it is necessary to warn people at this moment that the amount of work that is going on in this field which will make improvements in cross sections is dropping precipitously. I understand that the A.W.R.E. people are now reducing their effort and a truly major portion of the very excellent work that has made good cross section values available in that less than 100 kilovolt energy range has come from Aldermaston. Fortunately, the German school as Poenitz reported, has begun to take some interest in this very difficult field. If we really ask for standard cross sections rather than fission cross sections, two subjects which are purposely intermingled, the requirements on some cross sections presently being requested by reactor designers, among others, are very severe indeed. There is a general interest in having, let us say, one fission cross section accurate to about one percent in the whole range up to 1 MeV. That is a very, very difficult thing to do, it's not impossible, but approaching it. You have to remember that the best known measured cross sections, charged particle cross sections, more specifically the total p-p scattering cross section which sort of is a lead pipe cinch, or the total cross sections as a function of neutrons scattered from protons are known only to about half a percent and they may become ultimate standards. I am worried that there are no other new efforts in the offing to perform these exacting

measurements. To demonstrate the need for other measurements of this type, Poenitz' tentative values are really quite different, in the upper end of the energy range, from those that have been accepted for many years. Furthermore, I know of no one who intends to make measurements in the range from 200 keV to 2 MeV. One additional question concerns the interest in fission cross sections. Fission will be one of our secondary standards above 1 MeV and even more particularly, above 3 or 4 MeV, yet the measured values of the cross sections are really discrepant at these energies. There are tremendous spreads; for instance around 5 or 6 MeV there are 50 to 70% differences between different laboratories, and this is a range where there are supposed to be rather straightforward ways of measuring the basic phenomena. I believe that perhaps these ought to be measured in any case whether or not the reactor physicists press us for these measurements. There ought to be at least one cross section that is a true standard covering the full 15 MeV energy range with possibly uranium-235 as that candidate. In addition to absolute standards there is the question of relative cross section measurements. These can be measured more accurately and there is interest in them in many calculations. Finally I tend to agree with Harris who is concerned with the influence of the advent of high resolution detectors such as lithium-germanium counters on cross section measurements. These detectors are so good, at least in measuring gamma rays, that they may be reducing the amount of applied physics work being performed. Reactor people may prefer measurements with poorer resolution and further, the somewhat more limited energy range of these detectors may be in effect reducing the amount of data being acquired which is needed for applied purposes."

Dr. Radkowsky:

"Session C covered the actual needs of the reactor designs for neutron and other fundamental data. The most avid requirements for these cross sections turn out to be in the fast reactor area. The review paper by Greebler and others pointed out that the uncertainties are of a major nature and in fact, the feasibility and desirability of the whole fast reactor development depends on clearing up these uncertainties. Specifically, cost can vary as much as 30 - 50% and there can be a factor of 2 in doubling time. Thus, the direction of the design and the risks that will be taken are going to be strongly affected by the values of the cross sections. The most notable gaps in our knowledge are the ^{239}Pu alpha value below 15 keV, which is by now a cause celebre, the ^{238}U radiative capture cross section, and finally, the average value of ν for ^{239}Pu . Another set of very important quantities was treated in Benzi's paper, "Fission Product Cross Sections and Poisoning in Fast Reactors". Benzi pointed out that very little is known of the energy dependence of the fission product yield or of the variation of the fission product cross sections with

energy. This assumes a very great importance now that the practical designs of fast reactors will turn out to have a larger fraction of the fissions occurring below 1 MeV. In the SIR reactor it was found the loss of reactivity due to fission product poisoning was about twice as much as had been calculated by the best available statistical models of the time. This shows that it is really very important to know these fission product cross sections accurately, especially as we are aiming for high irradiations which means there will be quite large masses of fission products before the fuel is discharged from the reactor. Of course, of immediate concern is the effect of uncertainties upon light water reactors used for commercial power. French, in his paper, pointed out that while the cost may be significantly changed, the actual design or the feasibility is not really going to be affected much by the cross sections. He said that we already seem to be able to calculate the criticality of both plutonium and the ^{235}U fuel system reasonably well as compared with other uncertainties such as those due manufacturing. Furthermore, the progress of these reactors is such that the experience gained with them may outrun the rapidity with which the cross sections are measured so that the differential data will be of less practical use than operating results for the reactor. For example, right now pretty good data up to 10,000 megawatts days per metric ton are available, and while they are designing for 30,000, it may be that by the time that the cross section measurements are made, enough good experience will be available that the measurements would not be of very much help. Another class of phenomena of importance is the effect on the temperature coefficients of cores containing fuels of high plutonium content. This is especially important in plutonium-fueled reactors in determining the extent of the possible use of soluble poison for control. It might be well to determine these higher plutonium cross sections much better, especially with regards to the effects of higher irradiation, since there is the tendency to get a positive temperature coefficient and any region which might lead to instabilities must be avoided. Another example, not mentioned in the Conference, is the Light Water Breeder Reactor. Work is going on rapidly to prepare a demonstration at Shippingport. This is very sensitive to the values of the cross sections since the very success of the project depends on them. Although the breeding ratio starts out with something like 14% to spare, it rapidly decreases due to the accumulation of fission products and in the end of about 2 or 3 years operation, the breeding gain, measured by the fissile inventory ratio, in other words, the amount of additional fissile fuel you may have in the end, is only about 1 or 2% or, just enough to take care of the losses due to reprocessing. A great deal of work using computer programs such as RECAP, a Monte Carlo program which is capable of very fine detail, has been performed to reanalyze the basic Oak Ridge and other experiments to determine the correct value of the

thermal η for ^{233}U . It was found that the original published values were correct although there was some fortunate cancellation of errors in the original analysis. Other fundamental experiments such as the solution criticals of Callahan have also been re-analyzed.

"Perry's paper covered the design of Molten Salt and Graphite reactors. I can't quite agree with him about the fact that the Molten Salt reactors will abound by the time of the second Kennedy Administration, I'd put it about the third or fourth, but he didn't feel they were too sensitive to the values of the cross sections. He analyzed the possible uncertainty in the ^{233}U cross sections, for example, and felt that designers were on safe ground. He did feel that there was some need for cross sections for temperature coefficients, especially in the graphite reactors which have a very small temperature coefficients which can be quite influenced by the values of the cross sections. There doesn't seem to be too much question of feasibility of Space reactors. However, their designers are depending upon a burnable poison for control and since a poison of the proper characteristics is not immediately available, they were surveying the whole field of available isotopes. Since cost is of no consideration in these cases, they can consider the use of separated isotopes for burnable poisons. The design of these reactors could be enormously simplified and their safety assured if a material with the proper cross sections could be located. Another interesting point was the uncertainty in the yield of cesium 137 from plutonium fission and its half life. Since the amount of ^{137}Cs in an irradiated fuel is used as a measurement of the number of fissions which occurred in a given time, the accuracy of a variety of cross sections determined by irradiation in a reactor and compared to the ^{137}Cs yield, must be questioned. In conclusion I would say that the breeder reactor, particularly the fast breeder and the thermal light water breeder, very strongly depend upon cross sections. Their success, their desirability, their economic values, all are going to be very strongly affected by the urgently needed cross sections. Other reactors, such as the commercial light water reactors, don't seem to be so strongly affected, although there still are significant effects, and particularly the space reactors have a special control problem which would be greatly aided if the cross sections were available."

W. W. Havens:

"In my opinion the most significant new information presented at the Session D on cross sections of fission and fertile materials was the demonstration of intermediate structure in sub-threshold fission measurements. Fast neutron physicists have argued for several years about the existence and exploration of intermediate structure. I think that most people now believe it exists. However, this is the first time intermediate structure has been

observed with resonance neutrons and there is no doubt that this intermediate structure, the grouping of the levels, does exist in subthreshold fission. The grouping of levels in the fission cross section may be extremely important for reactor physics because it may give us some knowledge about the way fission cross section averages can be taken. I remember when Bethe used to have to determine average fission cross sections assuming a random distribution of spacings and Γ_n increasing as \sqrt{E} . The averages of cross sections using these assumptions, since shown to be wrong, were the best he could do at the time using the information that was available. The significance of intermediate structure still has to be determined both in subthreshold fission and in above threshold fission. The discovery of level groupings in subthreshold fission will probably lead to a series of experiments to study the level groupings as a function of the fission threshold going down in energy as far as possible and going up as far as possible.

"Especially noteworthy in the cross sections of fissionable isotopes is the fact that there has been an order of magnitude improvement in both the quantity and the quality of data on the fission cross sections. It's very much easier to make a measurement of the total cross section than of the fission cross section. In making total cross section measurements you can use several sample thicknesses and the intensity is sufficient to allow long flight paths to be used. However, in fission cross section measurements the fissionable material is usually very radioactive, and in general only a thin sample can be used as a fission detector, although a thick sample can be used if the neutrons emitted in fission are detected. However, with the very great increases in neutron source intensity and the increase in resolution and the efficiency of detectors, and particularly the bomb-shot work, the total amount of data available on fission cross sections and the quality of the data is now of the same quality as the data on total cross section measurements. Since considerably better resolution can be obtained for total cross section measurements than for fission cross section measurements, it strikes me it's time to remeasure the total cross sections. I think most of the total cross section data that are now used are several years old. The fission cross sections data were so much worse than the total cross section measurements that most scientists have concentrated on measuring fission cross sections.

"The analysis of fission cross section data has also taken a great step forward because of the availability of the large computers and the ability of the large computers to handle many parameters simultaneously. In analysing fission data it cannot be assumed that the single level formula works, and the multi-level formula must be used. It is also very important that the

experimenter look at the cross section between levels to determine the interference between levels, whereas previously the most important energy interval to examine was the cross section near the peak of the level in order to determine the level parameters. The interference dips and the cross section between levels are now probably more significant than the cross sections near the peak of the level. The Los Alamos fission data work certainly is very elegant and impressive with multi-level fits and the demonstrations of different types of levels due to different spin states. I think it has been demonstrated at this Conference that there has been an order of magnitude in the quality and interpretation of the fission data and we had better go back and measure those things that we've taken for granted."

Dr. Goldstein:

"I have received several suggestions about what I should talk on here. Some people who remembered my keynote address at the first of these meetings have suggested that I continue my story of the sex life of the neutron cross section field, or at least tell what's been happening with the marriage that we solemnized at that time. I think I will not, however, go into detail at this time other than to say I have not come to preside over a divorce. Although the immediate financial road ahead may be somewhat rocky, I have great faith that the marriage will hold together. And talking about finances and the way your budgets, or at least the budgets in the U. S., are likely to be in the next year to two, Bob Block asked me to point out to you that in one of the neighboring conventions down the hall there is an excellent exhibit about how to construct tools out of scrap wood and stones.

"But I shall reject these suggestions. Instead I am tempted to begin the same way that Dr. Cox did in his review paper in Session E, when on a much more restricted field and allotted a much longer time, he felt he had to give indeed a very fast talk on fast neutron physics. And I can point out that Session E, which was covering the measurement and analysis of total and partial cross sections for non-fissile material, had about twice as many papers as any other single session in the entire Conference. Perhaps the very length, amounting to some thirty papers, will permit me instead to do a statistical analysis, rather than to give any individual remarks. Certainly it is heartening to observe the burgeoning activity in the field, presumably due to the introduction of new accelerators and neutron sources that have been either constructed in the interim since the last conference or were just then going on the air. One should point to them as I think as the primary reasons for the increase and strong activity in this field. There is the big linear

accelerator at Geel in Belgium, the new linear accelerator right here at the Bureau of Standards, the isochronous cyclotron at Karlsruhe is beginning to turn out some very beautiful work in total cross sections that we saw, and the Linac in Japan is also contributing.

"A second factor has been improvements in instrumentation. In particular in anything to deal with gamma ray production or reactions emitting gamma rays there have been very great advances, mostly because of the development of the germanium-lithium detectors that Taschek alluded to. Statistically, something like two thirds of the papers in this Session referred to or measured something to do with reactions having gamma rays coming out of them--radiative capture cross sections, inelastic scattering or charged particle reactions with accompanying gamma rays. It is my opinion that even from the purely applied viewpoint the results and the information obtained using high resolution detectors are most welcome. To give one example, many of the past discrepancies on the question of probability distributions of partial radiation widths now appear to be clarified. When we go to calculate cross sections in unmeasured regions this will be of great help. It is indeed remarkable how much more information can be obtained about radiative capture cross sections and spectra than could be done in the past. I recall that in iron, which is of particular interest to me, the most that could be offered by the experimentalist only a few years ago was a measurement of the spectra at thermal neutron energies. Now measurements of spectra can be made not only at thermal, not only at many of the resonances observed in the total cross sections, but even between resonances. Further, by means of the new detectors other resonances which were not visible in total cross sections measurements, can be seen. I think all this information, including a flood of data, level schemes and so on, is all grist for the evaluator's mill, and we haven't really begun to digest the benefits coming from there. At the same time I'm glad to see that total cross section measurements are continuing and we're discovering in supposedly well known elements new information as, for example, in iron and carbon. I must regret, to keep up my perennial refrain, there is so little work being done in the high energy region. There were only four papers which dealt with cross sections between 4 and 13 MeV. They were however very good work, and I should like to point especially to the rather extensive set of angular distributions being measured in Sweden. I hope that the next few years, to express again my perennial hope, will see more work in this field.

"Session F, on theory, provided something of a contrast to the burgeoning activity we noted in the experimental field. On the contrary, it seems here that we have reached now a kind of plateau in the theory of reactions. I must emphasize that it's a plateau at a rather rarefied altitude, indicative of a high

level of sophistication that is rather generally dispersed among the workers in the field. We all now apparently handle rather complicated optical model calculations, and the use of multi-level fits in the resonance region (which was just somewhat new in the earlier Conference) has become nearly routine. The very pretty work of the Adlers has shown how far one can go in this direction. We seem to have reached a point now where we're seeking out in the corners for extra little details. It does appear that we have not yet used all the information that can be garnered from such phenomena as polarization or, as Vogt pointed out, the (p,n) type of scattering--quasi-elastic scattering. Until such time as fundamental nuclear theory, i.e. the ability to start from scratch on the bases nucleon properties, can provide us with available and widely based theories, it looks like we have reached something like a plateau. The exception to this judgment is in theory of fission, and those of you who heard Dr. Griffin's enthusiastic adventure into new fields in fission may perhaps in future years remember this Conference primarily by the memory that they were in at the birth of a new theory."

Dr. Kouts:

"Most impressive in Session G was the notable maturing of the nuclear data centers throughout the world that has occurred since the last cross section meeting two years ago, and the growth of the links between these organizations and their supplementing each other's work. We heard about the formation of the National Neutron Cross Section Center at Brookhaven and the improvement in liaison between the compiling and evaluating of data that this union will afford. We have seen in the past two years a growth to maturity in service to the European Community by the Data Center that is sponsored by ENEA at Saclay, and a most remarkable growth in servicing of the world-wide community by the data center at the IAEA. In addition to this, we have initiated a rapid transmission of data between these centers, that I think we can all be proud of. I believe that for the first time we can say that essentially all experimental data are being collected by suitable groups, in such form that they can be easily retrieved by those who need to use them.

"A second thing that impressed me was the growth in automated methods by which these data are treated. These methods only existed in dreams a few years ago. The exploratory work has now almost reached a fruition in automative publishing of compiled data on cross section library tapes. Automatic methods of preparing and publishing the curves that have commonly appeared in the past in, for example, BNL-325, are being worked on at Brookhaven and at Atomics International in this country, at Aldermaston in the United Kingdom, and, as we

have heard, also at the IAEA Data Center. I suspect that hand-drawn curves will not appear in future publications of this kind. The development of data evaluation by automative methods is also remarkable, and I expect all of you are as impressed as I was at seeing the kinds of things that have been possible with Harry Alter's program, SCORE. Yet, I could not help thinking as I listened to Alter, and then later to Schmidt, that although there were many points of similarity in the evaluation being done by machine on one hand, and by man on the other, that there were still many points where the analogy was not complete and where the machine still has a far distance to go. In fact, it could not be said at this time that Alter's machine has replaced J. J. Schmidt. It will be interesting to see to what extent in the future these automated methods can and do evolve to replace the operations that at present the brain, hand, and eye of a human combine to perform the manual evaluation of data.

"In Schmidt's discussion of the bases of data evaluation, I was struck by the extent to which data evaluation that he now does was once done by experimentalists who produced the data. In the past, the measurer was expected to produce numbers which were directly representative of the physical state of the world. This is no longer the case. Experimentalists now commonly publish data whose analysis varies considerably from one case to another. These data can be only partly evaluated; or they can be differential cross sections; perhaps the analysis has progressed to formation of resonance integrals. It might be worth paying a little attention to how much evaluation we can expect the experimentalist to perform. This is a complicated question. To properly reevaluate a cross section in the files, it is sometimes necessary to reevaluate much of the method that was used to transform basic data into cross sections, and to draw inferences on the systematic errors which were present in each of the measurements."

Dr. Radkowsky:

"This was not planned to let Naval Reactors have the last word by summarizing Session H. The outstanding feature in the integral experiments has been the remarkable development of the spectrum measurements which have really attained a much higher accuracy than previously could have been foreseen. In this connection, there were two outstanding review papers which took slightly different points of view on the importance of the spectrum measurements for fast reactor design. Whereas the paper by Stevens emphasized the importance of spectra in being able to resolve differences in evaluated cross section data, Davey felt that it was much more important to measure the capture and fission cross sections as a function of energy, especially from 10 keV to 1 MeV. Of course he is quite correct,

although, as he himself pointed out, Argonne is also continuing to emphasize the measurement of spectra. Notable was the assembly by Davey of a large mass of data showing how far we are from being able to determine the criticality and the critical mass of various fast assemblies to any consistent degree of accuracy and also that criticality is not a good way to determine which cross section set to use. Commenting on the paper by Stevens who pointed out that there has been a great advance in measuring the reactivity or, actually, the decay rate in subcritical assemblies, I believe that one might well be able to learn more from comparing the calculated and measured critical mass, the decay rate, and so on, of measurements made starting from a critical assembly and going to a series of subcritical assemblies of the same composition. I think that one might well be able to learn much from a comparison with integral experiments performed in this kind of consistent manner.

"Other highpoints of the session were the attempts by Pendlebury to use integral spectrum measurements to improve neutron cross section data by optimizing to the data, and the work of Chalk River in measuring the unknown, unstable fission products which still have long enough lifetimes to have a strong effect on the reactivity. (As I pointed out on Session C it is probably even more important for the fast reactor designer to know this data.) Finally, there was the very interesting work on the reactor cross sections of the transplutonium isotopes determined by the analysis of highly irradiated plutonium by J. A. Smith of Savannah River. There are a lot of uncertainties, of course, but it was interesting that for such a large number of nuclei it was possible to get a consistent set of cross sections which reproduced fairly well in the observations."

Dr. Taschek:

"For those people who do measurements and for the people who are on the other end, there is one additional interesting comment. I think you remember that in two or three of the papers on reactors, it was indicated how sensitive, in dollars, reactor capital costs and reactor operating costs were to certain cross sections. Maybe the measurers ought to form a union and present their demands to the users."

Dr. Kouts:

"I would like to comment only briefly on the point Alvin raised, on the need for cross sections. There has been some disagreement in the course of this meeting on how badly improvement in cross sections is needed. Perhaps I can give my own point of view on this.

"I think there are certain areas in the reactor industry in which cross sections are not much used any more. People in these areas have now found how to design the kinds of reactors they are now building. They now build the same reactors over and over, and nothing much ever changes, except little by little, the size of the machine and certain of its minor characteristics. If you are in a position like this, you are likely to develop a rather parochial view of the worth of cross sections to the reactor industry. Of course, if you are then put in the position of having to design something which varies rather markedly from something you have ever designed before, such as perhaps a thermal breeder, then you are suddenly in the soup. You find that you even have to learn the cross sections of the materials in the well-known reactor because you have probably been accounting for them wrongly. I think this is not a very unlikely possibility at all, inasmuch as a number of studies at this time indicate that we may very well use plutonium recycle, at the very least, before fast reactors become an economic necessity in this country."

Dr. Goldstein:

"I would just like to make a remark addressed primarily at the evaluators in connection with Herb Kouts' comments on the man-machine interaction. There is probably no more frustrating experience to the measurer of cross sections who happens to wander over to the other side of the reactor physics center to find that people are making a calculation based on the cross sections or a cross section set that are five or six or more years old, and which take no cognizance of what's happened in between. If you look closely into such instances, you find it is because the particular neutronics code involved has come with a particular library tape welded onto it, and you cannot use that transport code or that reactor code without using that particular library. We are spending a lot of effort on the storage of compiled cross section data, both measured and evaluated, and we must make sure that we ease the route for the entrance of these up-to-date cross sections into our calculations as they are available."

Dr. Radkowsky:

"I think that somehow the only way that we'll ever get the necessary cross sections measured is to dramatize the need for them and I think this is really showing up now in fast reactors. In the question of the other special types of reactors such as the light water breeder, these meetings play a very important part, and I think the reactor physicist may be just remiss in not dramatizing his desperate need for these cross sections in many cases."

LIST OF REGISTRANTS

John L. Abbott
U. S. Naval Weapons Evaluation Facility
Kirtland Air Force Base
New Mexico 87117

Alexander I. Abramov
Institute of Physics and Power
Obninsk, Kaluga Region, U. S. S. R.

D. B. Adler
University of Illinois
Physics Department
Urbana, Illinois 61301

F. T. Adler
University of Illinois
Physics Department
Urbana, Illinois

Irene Aegerter
Swiss Army Medical Service
CBR Section
Reitersts 13,
Berne, Switzerland

Peter G. Aline
General Electric - APED
175 Curtner Avenue
San Jose, California 95125

Harry Alter
Atomics International
8900 DeSoto Avenue
Canoga Park, California 91304

Paul I. Amundson
Argonne National Laboratory
P. O. Box 2528
Idaho Falls, Idaho 83401

Nestor Azziz
Westinghouse - Atomic Power Division
1027 East End Avenue
Pittsburgh, Pennsylvania 15230

William Baer
Westinghouse Electric Corporation
Bettis Laboratory
West Mifflin, Pennsylvania 15122

H. H. Barschall
Department of Physics
University of Wisconsin
Madison, Wisconsin 53706

David M. Barton
Los Alamos Scientific Laboratory
P. O. Box 1663
Los Alamos, New Mexico 87543

R. Batchelor
United Kingdom AEA
A.W.R.E., Aldermaston
Berks, England

Morris E. Battat
Los Alamos Scientific Laboratory
P. O. Box 1663
Los Alamos, New Mexico 87544

Norman P. Baumann
E. I. DuPont - Savannah River
Aiken, South Carolina 29802

K. H. Beckurts
Brookhaven National Laboratory
Department of Physics
Upton, Long Island, New York 11973

Leon E. Beghian
Lowell Technological Institute
1 Textile Avenue
Lowell, Massachusetts 02139

Victor J. Bell
European Nuclear Energy Agency
CCDN, B. P. 9,
91 Gif-sur-Yvette, France

Laurence S. Beller
Argonne National Laboratory
P. O. Box 2528
Idaho Falls, Idaho 83401

Valerio Benzi
C.N.E.N.
Centro di Calcolo
Via Mazzini 2
40138 Bologna, Italy

D. L. Bernard
University of Virginia
Physics Department
Charlottesville, Virginia 22903

J. R. Beyster
Gulf General Atomic
P. O. Box 608
San Diego, California 92101

M. R. Bhat
National Neutron Cross Section Center
Brookhaven National Laboratory
Upton, Long Island, New York 11973

Robert C. Block
Rensselaer Polytechnic Institute
Troy, New York 12180

Karl H. Böckhoff
C.B.N.M. EURATOM
Steenweg, Naar Retie
Geel, Belgium

Donald Bogart
NASA - Lewis Research Center
21000 Brookpark Road
Cleveland, Ohio 44135

Charles D. Bowman
University of California
Lawrence Radiation Laboratory
P. O. Box 808
Livermore, California

Harry L. Brown
Drexel Institute of Technology
Philadelphia, Pennsylvania 19104

Paul S. Brown
University of California
Lawrence Radiation Laboratory
P. O. Box 808
Livermore, California 94550

Ian F. Bubb
University of Manitoba
Fort Charm, Winnipeg,
Canada

Friedrich Bühler
Universität Stuttgart
Institut für Strahlenphysik
Universität Stuttgart, Germany

Danial K. Butler
Argonne National Laboratory
9700 South Cass Avenue
Argonne, Illinois 60439

John P. Butler
Atomic Energy of Canada, Ltd.
Chalk River, Ontario, Canada

Bernard J. Byrne
General Electric Company - KAPL
Schenectady, New York 12301

Robert E. Carter
AFRRI - DASA
National Naval Medical Center
Bethesda, Maryland 20014

Randall S. Caswell
National Bureau of Standards
Washington, D. C. 20234

Charles W. Causey
Office of Naval Research
Washington, D. C. 20360

B. H. Cherry
United Nuclear Corporation
Grasslands Road
Elmsford, New York 10523

Robert Chrien
Brookhaven National Laboratory
Physics Department
Upton, Long Island, New York 11973

Ronald P. Christman
E. I. DuPont - Savannah River Lab.
562 Banks Mill Road
Aiken, South Carolina 29802

S. Gierjacks
Kernforschungszentrum Karlsruhe
Institut für Angewandte Kernphysik
75 Karlsruhe
Postfach 97
German Federal Republic

Marshall R. Cleland
Radiation Dynamics, Inc.
1800 Shames Drive
Westbury, New York 11590

Charles O. Coffey
Douglass United Nuclear
Richland, Washington 99352

H. Conde
Research Institute of National Defense
Stockholm 80,
Sweden

Thomas J. Connolly
Stanford University
Nuclear Engineering Division
Stanford, California 94305

Francesco Corvi
C.N.E.N. (Italy)
% B.C.M.N. EURATOM
Steenweg naar Retie
Geel, Belgium

Samson A. Cox
Argonne National Laboratory
9700 South Cass Avenue
Argonne, Illinois 60439

Hall Crannell
Catholic University
Washington, D. C. 20017

Clyde W. Craven
Oak Ridge National Laboratory
P. O. Box X
Oak Ridge, Tennessee 37830

Charles L. Critchfield
Los Alamos Scientific Laboratory
P. O. Box 1663
Los Alamos, New Mexico 87544

John B. Czirr
Lawrence Radiation Laboratory
L-221, Box 808
Livermore, California 94550

Robert A. Dannels
Westinghouse Atomic Power Divisions
P. O. Box 355
Pittsburgh, Pennsylvania 15230

William G. Davey
Argonne National Laboratory
P. O. Box 2528
Idaho Falls, Idaho 83401

J. C. Davis
University of Wisconsin
Department of Physics, Sterling Hall
Madison, Wisconsin 53706

Achiel J. Deruytter
C.B.N.M. EURATOM
Steenweg naar Retie
Geel, Belgium

Gerard de Saussure
Oak Ridge National Laboratory
P. O. Box X
Oak Ridge, Tennessee 37830

Robert W. Deutsch
Department of Nuclear Science and
Engineering
Catholic University
Washington, D. C. 20017

Joseph J. Devaney
Los Alamos Scientific Laboratory
P. O. Box 1663
Los Alamos, New Mexico 87544

A. DeVolpi
Argonne National Laboratory
9700 South Cass Avenue
Argonne, Illinois 60439

J. K. Dickens
Oak Ridge National Laboratory
Building 5500
P. O. Box X
Oak Ridge, Tennessee 37830

Hermann J. Donnert
State of Kansas
Department of Nuclear Engineering
Kansas State University
Manhattan, Kansas 66502

E. J. Dowdy
Texas A & M University
Nuclear Engineering Department
College Station, Texas 77840

Marvin K. Drake
Gulf General Atomic
P. O. Box 608
San Diego, California 92112

D. W. Drawbaugh
Westinghouse Electric Corporation
Astronuclear Laboratory
Box 10864
Pittsburgh, Pennsylvania 15236

Norman Dudey
Argonne National Laboratory
9700 South Cass Avenue
Argonne, Illinois 60439

Donald J. Dudziak
Los Alamos Scientific Laboratory
P. O. Box 1663
Los Alamos, New Mexico 87544

Charles L. Dunford
Atomics International
P. O. Box 309
Canoga Park, California 91311

Malcolm W. Dyos
Westinghouse - Advanced Reactors Division
Waltz Mill Site
Madison, Pennsylvania 15663

Richard Ehrlich
General Electric Company - KAPL
Knolls Atomic Power Laboratory
Schenectady, New York 12309

Richard W. Enz
Defense Atomic Support Agency
Washington, D. C. 20305

Albert M. Fabry
Centre d'Etude de l'Energie Nucleaire
Boeretang, 200
Mol, Belgium

John A. Farrell
Los Alamos Scientific Laboratory
P. O. Box 1663
Los Alamos, New Mexico 87544

Frank Feiner
Cornell University
Reactor Laboratory
Ithaca, New York 14850

Ronald F. Fleming
University of Michigan
1323 South Forest
Ann Arbor, Michigan 48104

Rex G. Fluharty
Idaho Nuclear Corporation
Idaho Falls, Idaho 83401

Anthony Foderaro
Pennsylvania State University
University Park, Pennsylvania 16802

Preston W. Forbes
U. S. Army
U. S. Military Academy
Department of Physics
West Point, New York 10996

Joseph L. Fowler
Oak Ridge National Laboratory
P. O. Box X
Oak Ridge, Tennessee 37830

William A. Fowler
California Institute of Technology
Kellogg Radiation Laboratory
1201 E. California Boulevard
Pasadena, California 91109

Robert J. French
Westinghouse Electric Corporation
P. O. Box 355
Pittsburgh, Pennsylvania 15230

Martin P. Fricke
Gulf General Atomic, Inc.
P. O. Box 608
San Diego, California 92112

Stanley Friesenhahn
Gulf General Atomics Corporation
P. O. Box 608
San Diego, California 92112

Fritz Fröhner
Gesellschaft f. Kernforschung mbH
75 Karlsruhe
Postfach 3640
German Federal Republic

E. G. Fuller
National Bureau of Standards
Photonuclear Physics Section
Washington, D. C. 20034

Richard H. Fulmer
General Electric Company
Knolls Atomic Power Laboratory
Box 1072
Schenectady, New York 12301

Fletcher Gabbard
University of Kentucky
Department of Physics
Lexington, Kentucky 40506

Arcadio Garcia
Picatinny Arsenal
Dover, New Jersey 07801

Jagadish Garg
State University of New York
Western Avenue
Albany, New York 12203

J. H. Gibbons
Oak Ridge National Laboratory
Oak Ridge, Tennessee 37830

Gunter Gigas
Atomics International
Canoga Park, California 91305

Arnold Gilbert
Lawrence Radiation Laboratory
P. O. Box 808
Livermore, California 94550

Neel W. Glass
Los Alamos Scientific Laboratory
P. O. Box 1663
Los Alamos, New Mexico 87544

Terry F. Godlove
U. S. Naval Research Laboratory
Washington, D. C. 20390

Mark Goldsmith
Bettis Atomic Power Laboratory
West Mifflin, Pennsylvania 15217

Murrey D. Goldberg
Brookhaven National Laboratory
Upton, Long Island, New York 11777

Herbert Goldstein
Columbia University
520 W. 120th Street
New York, New York 10027

Paul Greebler
General Electric Corporation
310 DeGuigne Drive
Sunnyvale, California 95125

Charles Greenhow
Aerospace Corporation
P. O. Box 1308
San Bernardino, California 92402

Herbert Grench
Lockheed Palo Alto Research Laboratory
3251 Hanover Street
Palo Alto, California 94304

James A. Grundl
Los Alamos Scientific Laboratory
P. O. Box 1663
Los Alamos, New Mexico 87544

O. J. Hahn
Mechanical Engineering Department
University of Kentucky
Lexington, Kentucky 40506

William Cornelius Hall
Chemtree Corporation
Chemtree Park
Central Valley, New York 10917

G. C. Hanna
Atomic Energy of Canada, Ltd.
Chalk River, Ontario
Canada

Luisa F. Hansen
Lawrence Radiation Laboratory
P. O. Box 808
Livermore, California 94550

Marvin V. Harlow, Jr.
Los Alamos Scientific Laboratory
P. O. Box 1663
Los Alamos, New Mexico 98544

M. Rafiq Haroon
Georgia Institute of Technology
Nuclear Research Center
Atlanta, Georgia 30332

Donald R. Harris, Jr.
Westinghouse - BAPL
P. O. Box 79
West Mifflin, Pennsylvania 15217

Jay M. Harris
2246 Mohegan Drive
Falls Church, Virginia 22043

W. W. Havens, Jr.
Columbia University
Pegram Nuclear Physics Laboratories
538 W. 120th Street
New York, New York 10027

H. T. Heaton
National Bureau of Standards
Center for Radiation Research
Washington, D. C. 20234

Robert R. Heinrich
Argonne National Laboratory
9700 South Cass Avenue
Argonne, Illinois 60439

Arthur Hemmendinger
Los Alamos Scientific Laboratory
P. O. Box 1663
Los Alamos, New Mexico 87544

Philip B. Hemmig
U. S. Atomic Energy Commission
Washington, D. C. 20545

W. B. Henderson
General Electric Corporation
Evendale, Ohio 45201

E. J. Hennelly
E. I. DuPont - Savannah River Lab.
Aiken, South Carolina 29801

Allen L. Hess
Argonne National Laboratory
P. O. Box 2528
Idaho Falls, Idaho 83401

Carl Hibdon
Argonne National Laboratory
9700 South Cass Avenue
Argonne, Illinois 60439

Chieh Ho
Columbia University
New York, New York 10607

Robert Hockenbury
Rensselaer Polytechnic Institute
Troy, New York 12180

Robert J. Howerton
Lawrence Radiation Laboratory
P. O. Box 808
Livermore, California 94550

John R. Huizenga
University of Rochester
Rochester, New York 14627

Harry H. Hummel
Argonne National Laboratory
9700 South Cass Avenue
Argonne, Illinois 60439

Bruce A. Hutchins
General Electric Corporation-APO
310 deGuigne Avenue
Sunnyvale, California 95125

Karl Ilgen
Institut für Strahlenphysik der
Universität Stuttgart
7 Stuttgart-Vaihingen
Allmandsfr 85
Germany

John S. Ingley
Bellcomm Inc.
1100 17th Street N.W.
Washington, D. C. 20036

David C. Irving
Oak Ridge National Laboratory
P. O. Box X
Oak Ridge, Tennessee 37830

Ivan Itkin
Westinghouse - BAPL
P. O. Box 79
West Mifflin, Pennsylvania 15217

Harold E. Jackson, Jr.
Argonne National Laboratory
9700 South Cass Avenue
Argonne, Illinois 60439

U. P. Jenquin
Battelle Memorial Institute -
Pacific Northwest Laboratory
Richland, Washington 99352

R. L. Joly
C. E. A.
29 Rue de la Federation
Paris (Se), France

Malvin H. Kalos
New York University - CIMS
251 Mercer Street
New York, New York 10012

Vivekananda Kandarpa
Ohio State University Research Foundation
4125 E. 3rd Street, Apt. 4
Dayton, Ohio 45403

Walter Y. Kato
Argonne National Laboratory
9700 South Cass Avenue
Argonne, Illinois 60439

Adolfo Kind
CCR EURATOM
Casella-Postale No. 1
Ispra (Prov. Varese), Italy

John Kirkbride
E. G. & G, Inc.
130 Robin Hill Road
Goleta, California 93107

G. J. Kirouac
Knolls Atomic Power Laboratory
Schenectady, New York 12301

Daniel Klein
Westinghouse - BAPL
P. O. Box 79
West Mifflin, Pennsylvania 15217

W. W. Knowles
Oak Ridge National Laboratory
P. O. Box Y
Oak Ridge, Tennessee 37830

George A. Kolstad
U. S. Atomic Energy Commission
Washington, D. C. 20545

Philip G. Koontz
Los Alamos Scientific Laboratory
P. O. Box 1663
Los Alamos, New Mexico 87544

Herbert Kouts
Brookhaven National Laboratory
Upton, Long Island, New York 11973

Theodore J. Krieger
Brookhaven National Laboratory
Upton, Long Island, New York 11973

Tatsuo Kurosu
CREIEPI
% APDA
1911 First Street
Detroit, Michigan 48226

M. Lachkar
Comm. 1'Energie Atomique
29/33 Rue de la Federation
75 Paris, France

Roger B. Lazarus
Los Alamos Scientific Laboratory
P. O. Box 1663
Los Alamos, New Mexico 87544

Harlan W. Lefevre
University of Oregon
Physics Department
Eugene, Oregon 97403

J. E. Leiss
National Bureau of Standards
Center for Radiation Research
Washington, D. C. 20234

H. Lemel
International Atomic Energy Agency
Kaerntnerring
Vienna 1, Austria

B. E. Leonard
Armed Forces Radiobiology
Research Institute
Bethesda, Maryland 20550

B. R. Leonard, Jr.
Battelle Memorial Institute
Pacific Northwest Laboratory
P. O. Box 999
Richland, Washington 99336

Richard A. Lewis
Argonne National Laboratory
9700 South Cass Avenue
Argonne, Illinois 60439

Daniel Lister
Argonne National Laboratory
9700 South Cass Avenue
Argonne, Illinois 60439

A. Z. Livolsi
Babcock and Wilcox
P. O. Box 1260
Lynchburg, Virginia 24501

Rurik K. Loder
NDL - Edgewood Arsenal
1132 Plaza Circle
Joppatown, Maryland 21085

William M. Lopez
Gulf General Atomic
P. O. Box 608
San Diego, California 92112

C. R. Lubitz
Knolls Atomic Power Laboratory
P. O. Box 1072
Schenectady, New York 12301

R. L. Macklin
Oak Ridge National Laboratory
Oak Ridge, Tennessee 37830

John T. Madell
Argonne National Laboratory
9700 South Cass Avenue
Argonne, Illinois 60439

Benjamin A. Magurno
Brookhaven National Laboratory
Building 197
Upton, Long Island, New York 11973

Fred C. Maienschein
Oak Ridge National Laboratory
P. O. Box X
Oak Ridge, Tennessee 37830

Bimal K. Malaviya
Rensselaer Polytechnic Institute
RPI Linac, Tibbits Avenue
Troy, New York 12181

Sven Malmskog
AB Atomenergi,
Studsvik, Nyköping,
Sweden

Leo P. Mariani
Pennsylvania State University
State College, Pennsylvania 16801

Victoria May
Brookhaven National Laboratory
Upton, Long Island, New York 11973

James H. McCrary
Argonne National Laboratory
9700 South Cass Avenue
Argonne, Illinois 60439

William N. McElroy
Battelle Memorial Institute
Pacific Northwest Laboratory
P. O. Box 999
Richland, Washington 99352

J. D. McGaugh
Westinghouse Atomic Power Divisions
Box 355
Pittsburgh, Pennsylvania 15230

J. H. McNally
Los Alamos Scientific Laboratory
P. O. Box 1663
Los Alamos, New Mexico 87544

James W. Meadows, Jr.
Argonne National Laboratory
9700 South Cass Avenue
Argonne, Illinois 60439

Robert H. Meichle
Douglas United Nuclear Inc.
1760 Building 100 D
P. O. Box 490
Richland, Washington 99352

Howard O. Menlove
Los Alamos Scientific Laboratory
P. O. Box 1663
Los Alamos, New Mexico 87544

George Mertel
ONR-Navy Department
Washington, D. C. 20360

Andre Michaudon
Commissariat Energie Atomique
C.E.N. Saclay
B. P. No. 2
91 Gif-sur-Yvette
France

Emilio Migneco
C.B.N.M. EURATOM
Steenweg naar Retie
Geel, Belgium

Arthur Mittler
University of Kentucky
Physics Department
Lexington, Kentucky 40506

Terus Momota
Japan Atomic Energy Research Institute
Tokai-mura
Ibaraki-ken, Japan

Michael S. Moore
Idaho Nuclear Corporation
Idaho Falls, Idaho 83401

Harry A. Morewitz
Atomics International
5300 Bothwell Road
Tarzana, California 91356

I. L. Morgan
Texas Nuclear
P. O. Box 9267
Austin, Texas 78756

H. T. Motz
Los Alamos Scientific Laboratory
P. O. Box 1663
Los Alamos, New Mexico 87544

M. C. Moxon
U. K. A. E. A.
A.E.R.E., Harwell
Berks, England

C. O. Muehlhause
National Bureau of Standards
Center for Radiation Research
Washington, D. C. 20234

Said Mughabghab
Brookhaven National Laboratory
Upton, Long Island, New York 11973

T. E. Murley
Westinghouse - ARD
Box 158
Madison, Pennsylvania 15663

William M. Murphey
National Bureau of Standards
Center for Radiation Research
Washington, D. C. 20234

Ryuzo Nakasima
Hosei University
Department of Physics
Fujimicho, Chiyodaku
Tokyo, Japan

Arthur Namenson
Naval Research Laboratory
4555 Overlook Avenue, S. W.
Washington, D. C. 20390

D. O. Nellis
Texas Nuclear Corporation
Box 9267
Austin, Texas 78756

M. Neve de Mevergnies
C.E.N. - Mol
Mol, Belgium

H. W. Newson
Duke University
Durham, North Carolina 22706

L. C. Noderer
Combustion Engineering, Inc.
% Nuclear Power Department
P. O. Box 500
Windsor, Connecticut 06095

Hugh Nutley
Seattle Pacific College
Seattle, Washington 98119

Paride A. Ombrellaro
Argonne National Laboratory
9700 South Cass Avenue
Argonne, Illinois 60439

Victor J. Orphan
Gulf General Atomic
P. O. Box 608 - LINAC
San Diego, California 92112

Eric H. Ottewitte
Atomic International
P. O. Box 309
Canoga Park, California 91304

Doran W. Padgett
Office of Naval Research
Washington, D. C. 20360

Earl Page
Atomic Power Development Associates
1911 First Street
Detroit, Michigan 48226

Sol Pearlstein
National Neutron Cross Section Center
Brookhaven National Laboratory
Upton, Long Island, New York 11973

Frances Pecjack
Westinghouse - APD
P. O. Box 355
Pittsburgh, Pennsylvania 15230

E. D. Pendlebury
United Kingdom Atomic Energy Authority
Building E1
A.W.R.E., Aldemaston
Reading, Berks
England

Edwin M. Pennington
Argonne National Laboratory
9700 South Cass Avenue
Argonne, Illinois 60439

Rafael B. Perez
Oak Ridge National Laboratory
P. O. Box X
Oak Ridge, Tennessee 37830

Roland P. Perret
European Nuclear Energy Agency
38 Boulevard Suchet
Paris 16e, France

Alfred M. Perry
Oak Ridge National Laboratory
P. O. Box Y
Oak Ridge, Tennessee 37830

P. J. Persiani
Argonne National Laboratory
9700 South Cass Avenue
Argonne, Illinois 60439

William G. Pettus
Babcock and Wilcox Company
P. O. Box 1260
Lynchburg, Virginia 24505

William Pineo
Duke University
Durham, North Carolina 22706

W. P. Poenitz
Argonne National Laboratory
9700 South Cass Avenue
Argonne, Illinois 60439

Karl G. Porges
Argonne National Laboratory
9700 South Cass Avenue
Argonne, Illinois 60439

Charles A. Preskitt
Gulf General Atomic
P. O. Box 608
San Diego, California 92112

A. Prince
Brookhaven National Laboratory
Upton, Long Island, New York 11973

S. N. Purohit
Rensselaer Polytechnic Institute
Troy, New York 12181

Alvin Radkowsky
Naval Reactors Branch
Department of the Navy
Washington, D. C. 20350

E. R. Rae
U. K. A. E. A.
A.E.R.E., Harwell
Berks, England

Frank Rahn
Columbia University
538 West 120 Street
New York, New York 10027

James H. Ray
United Nuclear Corporation
Research and Engineering Center
Grasslands Road
Elmsford, New York 10523

Robert B. Raziminas
E. I. DuPont - Savannah River Lab.
Aiken, South Carolina 29801

W. C. Redman
Argonne National Laboratory
9700 South Cass Avenue
Argonne, Illinois 60439

J. T. Reynolds
General Electric -
Knolls Atomic Power Laboratory
Schenectady, New York 12308

Pierre Ribon
CEN Saclay
Boite Postale 2
Gif-sur-Yvette
Seine et Oise
France

Allan C. B. Richardson
National Bureau of Standards
Center for Radiation Research
Washington, D. C. 20234

James C. Ritter
Naval Research Laboratories
Washington, D. C. 20390

Jean-Jacques Rollard
Embassy of Switzerland
2900 Cathedral Avenue N. W.
Washington, D. C. 20008

Robert J. Roseberry
Knolls Atomic Power Laboratory
Schenectady, New York 12308

K. I. Roulston
University of Manitoba
Winnipeg 10, Canada

J. W. Rowland
Westinghouse Corp. - Astronuclear
Box 158
Madison, Pennsylvania 15663

Ben C. Rusche
E. I. DuPont - Savannah River Lab.
Aiken, South Carolina 29801

John L. Russell
Gulf General Atomic
P. O. Box 608
San Diego, California 92112

M. Samour
Comm. l'Energie Atomique
29/33 Rue de la Federation
75 Paris, France

Eli Sank
Westinghouse Atomic Power Divisions
P. O. Box 355
Pittsburgh, Pennsylvania 15230

George D. Sauter
Department of Applied Science
University of California
Davis, California 95616

Craig D. Sawyer
General Electric Company - NTPO
P. O. Box 846
Pleasanton, California 94566

Fritz A. R. Schmidt
Institut für Kernenergetik
Universität Stuttgart
Universität Stuttgart, Germany

Josef Johannes Schmidt
Gesellschaft für Kernforschung
75 Karlsruhe
Postfach 3640
German Federal Republic

Martin J. Schneider
Westinghouse Astronuclear Laboratory
Box 19864
Pittsburgh, Pennsylvania 15236

Roald A. Schrack
National Bureau of Standards
Center for Radiation Research
Washington, D. C. 20234

U. Schulze
Brookhaven National Laboratory
Upton, Long Island, New York 11973

Robert B. Schwartz
National Bureau of Standards
Center for Radiation Research
Washington, D. C. 20234

Stephan Schwarz
European Nuclear Energy Agency
CCDN, B.P. 9
91-Gif-sur-Yvette
France

P. A. Seeger
Los Alamos Scientific Laboratory
P. O. Box 1663
Los Alamos, New Mexico 87544

Karl W. Seemann
General Electric - KAPL
P. O. Box 1072
Schenectady, New York 12301

Bal Raj Sehgal
Brookhaven National Laboratory
Upton, Long Island, New York 11973

Wade E. Selph
Radiation Research Association
1506 W. Terrell Avenue
Fort Worth, Texas 76104

Charles Z. Serpan, Jr.
Naval Research Laboratory
Washington, D. C. 20390

Rudolph Sher
Stanford University
Department of Mechanical Engineering
Stanford, California 94305

Harold Sherman
Schlumberger Technology Corporation
Ridgefield, Connecticut 06877

Donald F. Shook
NASA - Lewis Research Laboratory
21000 Brookpark Road
Cleveland, Ohio 44135

Erwin F. Shrader
Case Western Reserve University
Physics Department
University Circle
Cleveland, Ohio 44106

Ernest G. Silver
Oak Ridge National Laboratory
Bldg. 6025, X-10 Area
P. O. Box X
Oak Ridge, Tennessee 37830

Rudolf E. Slovacek
Knolls Atomic Power Laboratory
Schenectady, New York 12305

Alan B. Smith
Argonne National Laboratory
9700 S. Cass Avenue
Argonne, Illinois 60439

J. Richard Smith
Idaho Nuclear Corporation
Box 1845
Idaho Falls, Idaho 83401

James A. Smith
E. I. DuPont - Savannah River Lab.
Aiken, South Carolina 29801

R. K. Smith
Los Alamos Scientific Laboratory
P. O. Box 1663
Los Alamos, New Mexico 87544

Mikhail Sokolov
Science Attache
U.S.S.R. Embassy
1125 - 16th Street N.W.
Washington, D. C. 20036

Maurice Soleilhac
Commissariat a l'Energie Atomique
29033 Rue de la Federation
Parix XV, France

Serge Sonnaert
C. E. A.
29-33 Rue de la Federation
Paris 45e, France

Jozef Spaepen
EURATOM, CBNM
Steenweg naar Retie
Geel, Belgium

Eugene R. Specht
Atomics International
8900 De Soto
Canoga Park, California 91311

Ephraim Stam
North Carolina State University
P. O. Box 5636
Raleigh, North Carolina 27607

Norman M. Steen
Westinghouse Corp. - Bettis Atomic
Power Laboratory
West Mifflin, Pennsylvania 15217

John R. Stehn
Brookhaven National Laboratory
Upton, Long Island, New York 11973

William E. Stein
Los Alamos Scientific Laboratory
P. O. Box 1663
Los Alamos, New Mexico 87544

Thomas E. Stephenson
Brookhaven National Laboratory
Upton, Long Island, New York 11973

Charles A. Stevens
Gulf General Atomic
P. O. Box 608
San Diego, California 92112

H. B. Stewart
Gulf General Atomic
P. O. Box 608
San Diego, California 92112

Leona Stewart
Los Alamos Scientific Laboratory
P. O. Box 1663
Los Alamos, New Mexico 87544

Robert F. Stewart
U. S. Bureau of Mines
P. O. Box 880
Morgantown, West Virginia 26505

Robert W. Stooksberry
Westinghouse Electric Corporation
Bettis Atomic Power Laboratory
Box 79
West Mifflin, Pennsylvania 15217

J. S. Story
U. K. A. E. A.
Atomic Energy Establishment
Winfrith, Dorchester, Dorset
United Kingdom

Lars G. Stromberg
Brookhaven National Laboratory
Upton, Long Island, New York 11973

S. I. Sukhorutchkin
Institute for Theoretical and Experimental
Physics
Moscow, U.S.S.R.

F. P. Szabo
Defence Research Board
C.C.B.R.E.
Ottawa 4, Canada

R. F. Taschek
Los Alamos Scientific Laboratory
P. O. Box 1663
Los Alamos, New Mexico 87544

J. K. Temperley
U. S. Army Nuclear Defense Laboratory
Edgewood Arsenal
Maryland 21010

Paul Thomet
Commissariat Energie Atomique
29-33 Rue de la Federation
Paris 15(e), Paris

Charles E. Till
Argonne National Laboratory
9700 South Cass Avenue
Argonne, Illinois 60439

F. M. Tomnovec
Code 954
U. S. Radiological Defense Laboratory
San Francisco, California 94135

J. W. Truran
Belfer Graduate School of Science
Yeshiva University
601 West 183 rd Street
New York, New York 10033

W. E. Tucker
Texas Nuclear Corporation
P. O. Box 9267
Austin, Texas 78757

W. J. Turner
Australian Atomic Energy Commission
% Atomic Energy of Canada Limited
Sheridan Park, Ontario
Canada

Maurice Pierre Vastel
Electricite de France
Direction des Etudes et Recherches
17 Av. de la Liberation
92 Clamart, France

Ernest R. Venerus
Knolls Atomic Power Laboratory
River Road
Schenectady, New York 12301

Erich Vogt
University of British Columbia
Vancouver 8, B. C.
Canada

H. Vonach
Technische Hochschule Munchen
Physikdepartment,
Experimentelles Tellinstitut Maier-Leibnitz
8 Munchen 2
ArcisstraBe 21
Germany

J. J. Wagschal
Columbia University
287 D. Eng. Terr.
520 W 120th Street
New York, New York 10025

W. H. Walker
Atomic Energy of Canada, Ltd.
Chalk River Nuclear Laboratory
Chalk River, Ontario, Canada

Lars Wallin
Research Institute of National Defence
(FOA)
Stockholm 80, Sweden

O. A. Wasson
Brookhaven National Laboratory
Upton, Long Island, New York 11973

M. S. Wechsler
Oak Ridge National Laboratory
Oak Ridge, Tennessee 37830

Herman Weigmann
C.B.N.M EURATOM
Steenweg naar Retie
Geel, Belgium

Jesse L. Weill
Dept. of Physics and Astronomy
University of Kentucky
Lexington, Kentucky 40506

Peter Weinzierl
Osterreichische Studiengesellschaft
fur Atomenergie Ges. m.b.H.
Wien 8, Lenaugasse 10
Osterreich, Bermany

Jakob Weitman
A. B. Atomenergi
Studsvik, Nyköping
Sweden

C. H. Westcott
Atomic Energy of Canada, Ltd.
Chalk River, Ontario, Canada

L. W. Weston
Oak Ridge National Laboratory
P. O. Box X
Oak Ridge, Tennessee 37830

Lawrence T. Whitehead
Atomic Energy Commission
Oak Ridge, Tennessee 37830

William Whitemore
Gulf General Atomic
Box 608
San Diego, California 92112

Tor Wiedling
Atomic Energy Company
Studsvik, Nyköping
Sweden

Martin Wiener
U. S. Atomic Energy Commission
Germantown, Maryland 20545

Harvey B. Willard
Physics Department
Case Western Reserve University
University Circle
Cleveland, Ohio 44106

T. G. Williamson
University of Virginia
Department of Nuclear Engineering
Charlottesville, Virginia 22901

Robert D. Wilson
University of Virginia
Physics Accelerator Building
Charlottesville, Virginia 22903

Warren A. Wittkopf
Babcock and Wilcox Company
P. O. Box 1260
Lynchburg, Virginia 24505

John J. Woods
Brookhaven National Laboratory
Upton, Long Island, New York 11973

Masaaki Yamamoto
CRIEPI
% APDA
1191 1st Street
Detroit, Michigan 48226

S. Yiftah
Israel Atomic Energy Commission
Soreg Nuclear Research Centre
Yavne, Israel

K. J. Yost
Oak Ridge National Laboratory
P. O. Box X
Oak Ridge, Tennessee 37830

E. Young
High Voltage Engineering Corporation
Burlington, Massachusetts 01803

Paul C. Young
Reactor Laboratory
Cornell University
Ithaca, New York 14850

I. F. Zartman
U. S. Atomic Energy Commission
Washington, D. C. 20545

H. Dieter Zeh
University Heidelberg
16, Philosophenweg
Heidelberg, Germany

AUTHOR INDEX

	Page		Page
Adkins, C.R. -----	337	Coppola, M. -----	827
Adler, D.B. -----	967	Cornman, W.R. -----	1271
Adler, F.T. -----	967	Corvi, F. -----	897
Alter, H.A. -----	1049	Costello, D.G. -----	695
Alves, R.N. ----- 669, 783,	867	Cox, S.A. -----	701
Amiet, J.P. -----	85	Crockett, T.B. -----	235
Anderson, J.D. -----	225		
Asami, A. -----	789	Daitch, P.B. -----	1193
Ashe, J. -----	811	Däverhög, N. -----	125
Attree, P.M. -----	1083	Davey, W.G. -----	1211
Azziz, N. -----	943	Davis, J.C. -----	177
		de Barros, S. -----	867
Banick, C.J. -----	1285	De Coster, M. -----	1263
Barton, D.M. -----	597	de Kruijf, F. -----	201
Bartolome, Z.M. ----- 729,	795	del Marmol, P. -----	611
Batchelor, R. -----	89	Deruytter, A.J. ----- 475,	491
Battat, M.E. -----	407	De Volpi, A. ----- 183,	213
Baumann, N.P. -----	1271	Dickens, J.K. -----	811
Beghian, L.E. -----	1117	d'Oultremont, P. -----	1301
Behkami, A.M. -----	603	Dowdy, E.J. -----	401
Bell, V.I. -----	1089	Doyas, R.J. -----	363
Benzi, V. -----	311	Dudziak, D.J. -----	1101
Berg, S. -----	235	Dyos, M.W. -----	337
Bernard, D.L. -----	755		
Bergqvist, I. -----	763	Eaton, J.R. -----	169
Bhat, M.R. -----	675	Eichler, E. -----	811
Bianchini, R.P. -----	1123	Eiland, H.M. -----	687
Block, R.C. -----635, 729, 735,	795	Esch, L.J. -----	821
Böckhoff, K.H. -----	519		
Bowman, C.D. -----	541	Farrell, J.A. ----- 153,	553
Brown, L.C. -----	1279	Fabry, A. ----- 883,	1263
Brown, P.S. -----	363	Feiner, F. -----	821
Bühler, F. -----	933	Folger, R.L. ----- 1279,	1285
Butler, J.P. -----	803	Forti, P. -----	743
Byer, T.A. -----	1083	Fowler, J.L. -----	851
		Fowler, W.A. -----	1
Cady, K.B. -----	1109	Franceschini, E. -----	1123
Cao, M.G. ----- 481,	513	Friesenhahn, S.J. ----- 695,	857
Carlson, A.D. ----- 139,	695,	French, R.J. -----	259
Carraro, G. -----	897	Fröhner, F.H. ----- 61,	695,
Chrien, R.E. ----- 675,	875	Fuketa, T. ----- 789,	1097
Christensen, D.E. -----	389	Fullwood, R.R. -----	567
Cierjacks, S. -----	743	Fulmer, R.H. -----	821
Coceva, C. -----	897		
Cohn, H.O. -----	851	Gaerttner, E.R. ----- 1193,	1203
Condé, H. -----	763	Garg, J.B. -----	675
Connolly, T.J. -----	201	Giacobbe, P. -----	897
Conrad, C.A. -----	687	Gibbons, J.H. -----	111

	Page		Page
Gigas, G. -----	235	Lemmel, H.D. -----	1083
Girlea, I. -----	883	Lenz, G.H. -----	755
Glass, N.W. -----	573, 837	Lewis, R.A. -----	323
Goldstein, H. -----	37, 1309	Liikala, R.C. -----	389
Good, W.M. -----	1083	Lopez, W.M. -----	695, 857
Gozani, T. -----	1301	Lorenz, A. -----	1083
Greebler, P. -----	291		
Greenspan, E. -----	1193, 1203	Mallen, A. -----	1193, 1203
Griffin, J.J. -----	975	Managan, W.W. -----	247
		Martin, F.D. -----	851
Haas, F.X. -----	851	Matsen, R.P. -----	389
Hansen, L.F. -----	225	Malaviya, B.K. -----	1193, 1203
Harlow, M.V. -----	837	McElroy, W.M. -----	235
Heaton, H.T., II -----	771	McNally, J.H. -----	567
Heeb, C.M. -----	273	Meadows, J.W., Jr. -----	603
Hennelly, E.J. -----	1271	Michaudon, A. -----	427
Hibdon, C.T. -----	159	Migneco, E. -----	481, 513, 527
Hjaerne, L. -----	1083	Moore, R.A. -----	1183
Hockenbury, R.W. -----	729, 795	Mooring, F.P. -----	159
Holcomb, H.P. -----	1279, 1285	Morgenstern, J. -----	669, 783, 867
Holmqvist, B. -----	845	Mowatt, R.S. -----	1291
Hoot, C.G. -----	139	Moxon, M.C. -----	641
Howerton, R.J. -----	1013, 1093	Moyer, W.R. -----	729, 795, 1123
Huizenga, J.R. -----	603	Mughabghab, S.F. -----	875
Hutchins, B.A. -----	291	Munzer, H. -----	885
		Murley, T.E. -----	337
Jackson, H.E. -----	669		
Jenquin, U.P. -----	273	Nakajima, Y. -----	789, 1097
Johnson, C.H. -----	851	Nakasima, R. -----	193
Julien, J. -----	669, 783, 867	Nebe, J. -----	743
		Neill, J.M. -----	1183
Kaiser, W.C. -----	247	Nellis, D.O. -----	811
Kanda, Y. -----	193	Neve De Mevergnies, M. -----	611
Kang, S. -----	1021	Noda, F.T. -----	177
Kaushal, N.N. -----	1193	Nyström, G. -----	763
Kernell, R.L. -----	851		
King, T.J. -----	735	Okamoto, K. -----	1097
Kirouac, G.J. -----	687	Okubo, M. -----	789
Klema, E.D. -----	603	Orphan, V.J. -----	139
Knitter, H.-H. -----	827	Ottewitte, E.H. -----	371, 415
Kohler, W.H. -----	401	Overman, R.F. -----	1279
Kolar, W. -----	519		
Konshin, V.A. -----	1083	Page, E.M. -----	1243
Koontz, P.G. -----	597	Parker, K. -----	315
Kopsch, D. -----	743	Pearlstein, S. -----	1041
Kropp, L. -----	743	Pelfer, P. -----	491
Kuchly, J.M. -----	783	Pendlebury, E.D. -----	315, 1177
		Perey, F.G. -----	811
LaBauve, R.J. -----	407, 1101	Perry, A.M. -----	345
Lane, F.E. -----	381	Perry, R.T. -----	401

	Page		Page
Pineo, W.F.E. -----	153	Tardelli, J. -----	1117
Pitterle, T.A. -----	1243, 1253	Tatarczuk, J.R. -----	729, 795
Poenitz, W.P. -----	503	Tatro, L.D. -----	573, 837
Poortmans, F. -----	883	Theobald, J.P. -----	481, 513, 527
Porges, K.G. -----	213, 247	Till, C.E. -----	323
Poulsen, N.B. -----	401		
Preskitt, C.A. -----	1183	Ulseth, J.A. -----	235
Prezbindowski, D.L. -----	389	Uotinen, V.O. -----	273
Prince, A. -----	951		
Purohit, S.N. -----	1021	Vastel, M. -----	1129
		Vogt, E.W. -----	903
Ravier, J. -----	1129	Vonach, H.K. -----	885
Reber, J.D. -----	755	Vonach, W.G. -----	885
Reeder, S.D. -----	589		
Richter, I.B. -----	1285	Wagemans, C. -----	475
Ruane, T.F. -----	821	Walker, J. -----	169
Russell, J.L., Jr. -----	61, 1183	Walker, W.H. -----	381, 1291
		Warren, J.H. -----	573, 837
Samour, C. -----	669, 783, 867	Wartena, J.A. -----	481, 513
Santry, D.C. -----	803	Wasson, O.A. -----	675
Sauter, G.D. -----	541	Watanabe, T. -----	893
Schelberg, A.D. -----	573, 837	Watts, J.L. -----	363
Schmid, H. -----	533	Wechsler, M.S. -----	67
Schmidt, J.J. -----	1067	Weigmann, H. -----	533
Schneider, M.J. -----	615	Weinstein, S. -----	635
Schrack, R.A. -----	771	Weitman, J. -----	125
Schramel, P. -----	885	Wielding, T. -----	845
Schuman, R.P. -----	893	Winter, J. -----	481, 533
Schwartz, R.B. -----	771	Wolfe, B. -----	291
Seeger, P.A. -----	25	Wong, C. -----	225
Seeman, K.W. -----	687		
Shea, T. -----	1021	Yamamoto, M. -----	1243, 1253
Shepherd, J.P. -----	315	Yost, K.J. -----	53
Sher, R. -----	253	Young, J.C. -----	61
Shunk, E.R. -----	567	Young, P.C. -----	1109
Slovacek, R.E. -----	687		
Smith, H.L. -----	627	Zeh, H.D. -----	85
Smith, J.A. -----	1279, 1285		
Smith, J.R. -----	589		
Smith, R.K. -----	627		
Solomito, M. -----	53		
Spaepen, J. -----	491		
Stanley, P. -----	315		
Stelson, P.H. -----	811		
Stelts, M.L. -----	225		
Stein, W.E. -----	627		
Stephenson, T.E. -----	1031		
Stevens, C.A. -----	1143		
Stokes, G.E. -----	893		
Sukchoruchkin, S.I. -----	923		

